Gondia Education Society's

J. M. PATEL ARTS, COMMERCE & SCIENCE COLLEGE

BHANDARA – 441 904 (M.S.)

●Re-accredited 'B' Grade by NAAC ● Awarded 'College with Potential for Excellence' status (Phase II) by UGC

● R.T.M. Nagpur University recognized 'Centre for Higher Learning & Research'

● Phone No.07184 – 252364, 256883 (R) 252288 **Fax :** 07184 -253268**Email :** principaljmpc@rediffmail.com **website :** www.jmpatelcollege.com

CRITERION – III

RESEARCH, INNOVATION AND EXTENSION

3.2RESEARCH PUBLICATIONS AND AWARDS

3.3.1 Number of research papers published per teacher in the Journals notified on UGC CARE list in 2019-2024

CONTENT

Sr. No.	Year	Number of Research Paper
1	2024	07
2	2023	18
3	2022	10
4	2021	09
5	2020	06

Gondia Education Society's

J. M. PATEL ARTS, COMMERCE & SCIENCE COLLEGE

BHANDARA – 441 904 (M.S.)

●Re-accredited 'B' Grade by NAAC ● Awarded 'College with Potential for Excellence' status (Phase II) by UGC

● R.T.M. Nagpur University recognized 'Centre for Higher Learning & Research'

● Phone No.07184 – 252364, 256883 (R) 252288 **Fax :** 07184 -253268**Email :** principaljmpc@rediffmail.com **website :** www.jmpatelcollege.com

CRITERION – III

RESEARCH, INNOVATION AND EXTENSION

3.2 RESEARCH PUBLICATIONS AND AWARDS

3.3.1 Number of research papers published per teacher in the Journals notified on UGC CARE list in 2019-2024

CONTENT

Research Paper Published in 2024

Sr. No.	Title of Paper	Name of the Authors	Department of teacher	Name of Journal ISSN number	Link to website of Journal	Page No.		
						Research Paper	Journal Homepage	UGC CARE Proof
1.	Role of E-CRM in effectiveness of Strategic Marketing Planning for customer Retention: An Empirical Study	Dr. Anand Muley	Economics	African Journal if Biological Sciences 2663-2187	https://www.afjbs.com/issue-content/role-of-e-crm-in-effectiveness-of-strategic-marketing-planning-for-customer-retention-an-empirical-study-1552	1-10	11-14	15
2.	Perspectives of teachers and Students of Undergraduate Art's Faculty Regarding Internal Assesment	Dr. Bhavana M. Rai	English	Sanshodhak 2394-5990	https://journalsearches.com/ugc-care.php	16-24	Print Only	25
3.	Marathi KavitetilNavpravaah	Mamta Raut	Marathi	Sanshodhak 2394-5990	https://journalsearches.com/ugc-care.php	26-32	Print Only	33

4.	Spectroscopic study of 40K	Rozina Rahaman, Abhijit Bisoi, Ananya Das, Y. Sapkota ,Arkabrata Gupta ,S. Ray, S. Sarkar, Yashraj ,A. Sharma ,Bharti Rohila ,I. Ahmed, **Kaushik Katre**, S. Dutt, S. Kumar, R. P. Singh ,R. Kumar, and S. Muralithar	Physics	PHYSICAL REVIEW C 2469-9985	https://journals.aps.org/prc/	34-46	47	48-49
5.	Disease of Vegetable Crops and their Integrated Management Approaches	Sayeda Parveen Qureshi	Botany	Ajasra 2278-3741	http://ajasra.in/	50-57	58	59
6.	Synthesis, Characterization, In Vitro Anticancer and Antimicrobial Evaluation of Cu(II), Co(II), Zn(II), Mn(II) and Fe(II) Complexes Derived from Dihydralazine and 2- Formyl Thymol	Chaitu N. Bhoi, Rahul T. Bhoi, **Samina K. Tadavi, Ajay M. Ghatole,** Ratnamala S. Bendre	Chemistry	Educational Administration: Theory and Practice 1300-4832	https://kuey.net/index.php/kuey	60-70	71	72
7.	NeocalamitesKanhanesis sp. nov. from Kanhan coal measures of kamthi stage	**Aparna Yadav** and B. B. Kalbande	Botany	Bioinfolet 0976-4755	https://indianjournals.com/Mobile/SearchResult.aspx?query=2#&ui-state=dialog	73-76	77	78-79

Gondia Education Society's

J. M. PATEL ARTS, COMMERCE & SCIENCE COLLEGE

BHANDARA – 441 904 (M.S.)

● Re-accredited 'B' Grade by NAAC ● Awarded 'College with Potential for Excellence' status (Phase II) by UGC

● R.T.M. Nagpur University recognized 'Centre for Higher Learning & Research'

● Phone No.07184 – 252364, 256883 (R) 252288 **Fax :** 07184 -253268**Email :** principaljmpc@rediffmail.com **website :** www.jmpatelcollege.com

CRITERION – III

RESEARCH, INNOVATION AND EXTENSION

3.2 RESEARCH PUBLICATIONS AND AWARDS

3.3.1 Number of research papers published per teacher in the Journals notified on UGC CARE list in 2019-2024

CONTENT

Research Paper Published in 2023

Sr. No.	Title of Paper	Name of the Authors	Department of teacher	Name of Journal ISSN number	Link to website of Journal	Page No.		
						Research Paper	Journal Homepage	UGC CARE Proof
8.	Transition metal complexes of pyridazine-based ligand: synthesis, characterization, biological activities, and molecular docking studies	Smita S. Patil1, **Samina K. Tadavi, Ajay M. Ghatole**, Ratnamala S. Bendre	Chemistry	Journal of the Iranian Chemical Society	https://link.springer.com/journal/13738	**80-94**	**95**	**96**
9.	Analysis of Farmland Soil Samples from Tirora Tehsil of Gondia District in Maharashtra, Central India for its Chemical parameters	**Sangita D. Katre**	Chemistry	Research Journal of Chemistry and Environment	https://www.worldsresearchassociation.com/	**97-101**	**102**	**103**
10.	Imidazole–Thiazole Hybrid: Synthesis, Brain Penetration, Cytochrome P450 Enzyme and Gastrointestinal Absorption Study	Shital M. Dekate, Kishor M. Hatzade, **Dr Ajay M. Ghatole**	Chemistry	Iranian Journal of Science	https://link.springer.com/journal/40995	**104-119**	**120-122**	**123**
11.	Coexisting single-particle excitations and octupole correlations in the transitional nucleus 217Ra	Madhu, A. Y. Deo ,Khamosh Yadav , Dhananjaya Sahoo , Y. Y. Wang, Y. K. Wang, J. Meng ,Saket Suman , S. K. Tandel ,A. Sharma, I. Ahmed , **K. Katre**, K. Rojeeta Devi, S. Dutt, S. Kumar, Yashraj, S. Muralithar, and R. P. Singh	Physics	PHYSICAL REVIEW C	https://journals.aps.org/prc/	**124-138**	**139-140**	**141**

12.	The Healing Power Of Nature In Chitra Banerjee Divakaruni's "The Mistress Of Spices"	**Mr. Bhojraj Pandhari Shrirame&** Dr. Sunil G. Chaudhari	English	Satraachee	http://satraachee.org.in	**142-150**	**151-152**	**153**
13.	The Feminist Reinterpretation of Shashi Deshpande's 'Dark Holds No Terror'	Ajay S. Deokate	English	Satraachee	http://satraachee.org.in	**154-162**	**163-164**	**165**
14.	Metagenome Analysis: A Tool of Multiple Dimensions	**Aparna M. Yadav**, Bipinchandra B. Kalbande, Rajkumar R. Khapekar	Botany	Bioinfolet, 20, (2A):172-176	https://www.indianjournals.com/ijor.aspx	**166-171**	**172**	**173**
15.	Investigation of Structural and Microbial Properties of Samarium-Doped Nickel-Strontium Ferrite Nanoparticles Prepared via the Sol-Gel Route	Rajkanya M. Bhore· Radhakrishnan M. Tigote · Subiya K. Kazi1 · Sanjay R. Chavan · Rahul M. Khobragade · **Girdharilal B. Tiwari**	Chemistry	BioNanoScience, 13, pages1126–1139 (2023)	https://www.springer.com/journal/12668	**175-188**	**189-194**	**195**
16.	Revisiting band structures in 118Xe nucleus via inbeam γ-ray spectroscopy*	A. Pandey, R. Bhushan, A.Rohilla, C. Majumder, H. P. Sharma, S. Chakraborty, R. P. Singh, S. Muralithar, Yashraj, **K. Katre**, B. Rohila, Subodh, A. Kumar, I. M. Govil, S. Jehangir, N. Rather, G. H. Bhati, A. A. Wani, J. A. Sheikh, S. K. Chamoli	Physics	Chinese Physics C	http://cpc.ihep.ac.cn/	**197-213**	**214-215**	**216**
17.	Evidence of transverse wobbling motion in 151Eu	A. Mukherjee, S. Bhattacharya, T. Trivedi, S. Tiwari, R. P. Singh, S. Muralithar, Yashraj, **K. Katre**, R. Kumar, R. Palit, S. Chakraborty, S. Jehangir, Nazira Nazir, S. P. Rouoof, G. H. Bhat, J. A. Sheikh, N. Rather, R. Raut, S. S. Ghugre,S. Ali, S. Rajbanshi, S. Nag, S. S. Tiwary, A. Sharma, S. Kumar, S. Yadav, and A. K. Jain	Physics	PHYSICAL REVIEW C 107, 054310 (2023)	https://journals.aps.org/prc/about	**217-227**	**228-229**	**230**
18.	High-spin spectroscopy in 207At: Evidence of a 29/2+ isomeric state	KhamoshYadav , A. Y. Deo , Madhu, Dhananjaya Sahoo, P. C. Srivastava , Saket Suman , S. K. Tandel, A. Sharma, I. Ahmed , **K. Katre**, K. Rojeeta Devi, Sunil Dutt, Sushil Kumar, Yashraj, S. Muralithar, and R. P.	Physics	PHYSICAL REVIEW C 107, 054303 (2023)	https://journals.aps.org/prc/abstract/10.1103/PhysRevC.107.054303	**232-246**	**247-248**	**249**

		Singh						
19.	An Analysis of Sister of My Heart by Chitra Banerjee Divakaruni: Women's Struggle to find Their Identity	**Bhojraj Pandhari Shrirame,** Sunil G. Chaudhari	English	Bhairavi, Special Volume, April 2023	Print Only	**251-257**	**258**	**259**
20.	"Analysing Virtual and Augmented Reality Applications in Digital Marketing"	**Dr. Anand Muley**	Commerce	European Chemical Bulletin 2023, 12 (S6), 796 - 805	https://www.eurchembull.com/about	**260-269**	**270-271**	**272**
21.	Impact of Hexaconazole on Histo-Architecture of Liver and Intestine of Freshwater African Catfish, Clarias Gariepinus (Burchell, 1822)	**KhomeshHiwrajLanjewar**, Suresh Bapurao Zade, Lankesh Yashwant Bhaisare and Desh Deepak Chaudhary	Zoology	Biochem. Cell. Arch. Vol. 23, No. 1, pp. 639-646, 2023	DocID: https://connectjournals.com/03896.2023.23.639	**273-280**	**281**	**282**
22.	Disenthrallment of Women in Chitra Banerjee Divakaruni's Selected Novels: A Review	**Bhojraj Pandhari Shrirame,** Sunil G. Chaudhari	English	Journal of the Asiatic Society of Mumbai (A UGC - CARE Listed Journal) Volumes I (2) 2023	https://www.asiaticsociety.org.in/journal/	**283-291**	**292-293**	**294**
23.	An Analysis of Impact of Office Automation System on the Quality Improvement of College Admin Staff	Mr. Mangesh P. Wadhi &**Dr. Pravin H. Ghosekar**	Computer Science	Satraachee, Issue 26, Vol. 38, No. 3, Jan-March., 2023	https://satraachee.org.in/	**295-308**	**309-310**	**311**
24.	Impact of Converging Disruptive Technology with Business Strategies for Improved Effectiveness: An Empirical Study	**Dr. Anand Muley**	Commerce	European Chemical Bulletin 2023, 12(Special Issue 4), 13273-13283	https://www.eurchembull.com/search	**312-322**	**323-324**	**325**
25.	Navigating Shifting Identities: Quest for Existence in Bharati Mukherjee's Jasmine	**Dr. Karthik Panicker** and Dr. Sangita Vijay Kongre	English	Mukt Shabd Journal	https://shabdbooks.com/volume-11-issue-10-2022	**326-333**	**334**	**335**

Gondia Education Society's

J. M. PATEL ARTS, COMMERCE & SCIENCE COLLEGE

BHANDARA – 441 904 (M.S.)

● Re-accredited 'B' Grade by NAAC ● Awarded 'College with Potential for Excellence' status (Phase II) by UGC

● R.T.M. Nagpur University recognized 'Centre for Higher Learning & Research'

● Phone No.07184 – 252364, 256883 (R) 252288 **Fax :** 07184 -253268**Email :** principaljmpc@rediffmail.com **website :** www.jmpatelcollege.com

CRITERION – III

RESEARCH, INNOVATION AND EXTENSION

3.2 RESEARCH PUBLICATIONS AND AWARDS

3.3.1 Number of research papers published per teacher in the Journals notified on UGC CARE list in 2019-2024

CONTENT

Research Paper Published in 2022

Sr. No.	Title of Paper	Name of the Authors	Department of teacher	Name of Journal ISSN number	Link to website of Journal	Page No.		
						Research Paper	Journal Homepage	UGC CARE Proof
26.	A Facile Synthesis of Thiazole Derivatives bearing Imidazole Moiety, Schiff Bases and their O-Glucosides	Shital M. Dekate, Kishor M. Hatzade and **Ajay M. Ghatole**	Chemistry	Asian Journal of Chemistry; Vol. 35, No. 1 (2023), 29-38	https://asianjournalofchemistry.co.in/User/SearchArticle.aspx?Volume=&Issue=&Article=&Criteria=Dekate	**336-345**	**346**	**347**
27.	Analysis of Water Quality Using Physico-Chemical Parameters of Chulhardoh Lake in Tumsar Taluka, Bhandara District, Maharashtra, India	Bhageshwari Arvind Thakre, **Sayeda Parveen Qureshi**	Botany	IJFANS ,International Journal of Food and Nutritional Sciences, Journal Volume 11, Iss 12, Dec 2022	https://www.ijfans.org/about	**348-353**	**354**	**355**

28.	Investigation on Endangered Nutritional Medicinal Value Plants o Bhandara District and their Conservation .	**Dr. Sayeda Parveen Qureshi**	Botany	IJFANS International Journal of Food and Nutritional Sciences,Journal Volume 11, Iss 11, Dec 2022	https://www.ijfans.org/about	**356-359**	**360**	**361**
29.	Use and User Study of College Libraries in Bhandara City. (Maharashtra)	**Mona ShambhauYeole&** Dr. Prince Ajaykumar T. Aagashe	Librarian	Journal of the Oriental Institute M.S. University of Baroda, Vol. 71, Issue. 04, No. 10 October - December : 2022	Print Only	**362-371**	**372**	**373**
30.	Entrepreneurial Ecosystem: A Systematic Literature Review	Rahul KrushnajiWadichar ,**Prashant Manusmare** and Mukul AbasahebBurghate	Management	VISION-THE JOURNAL OF BUSINESS PERSPECTIVE 1–14 © 2022 MDI	https://journals.sagepub.com/doi/10.1177/09722629221093866	**374-387**	**388**	**389**
31.	Synthesis of copolymer and its composites with carbon and theirphotoluminescence studies	**Yashpal U. Rathod,** Vikram U. Pandit, Devidas S. Bhagat, Wasudeo B. Gurnule	Chemistry	Materials Today: Proceedings	https://www.scopus.com/sourceid/21100370037	**390-396**	**397-398**	**399**
32.	Thermal degradation studies of 2-hydroxy-4-methoxy acetophenone , guanidine and	Preeti A. Mishra **Yashpal U. Rathod** Vikram U. Pandit Wasudeo B. Gurnule	Chemistry	Materials Today: Proceedings	https://www.scopus.com/sourceid/21100370037	**400**	**401-402**	**403**

	formaldehyde copolymer							
33.	Thiamine hydrochloride (vitamin B1) catalyzed greener synthesis of thiazolidin-4-one derivatives	Devidas S. Bhagat Wasudeo B. Gurnule**Yashpal U. Rathod** Mahipal S. Sankhla Vikram U. Pandit	Chemistry	Materials Today: Proceedings	https://www.scopus.com/sourceid/21100370037	**404**	**405-406**	**407**
34.	Synthesis, characterization and thermal behavior of 2,20-dihydroxybiphenyl-formaldehyde-phenylenediamine copolymer	Santosh P. Chakole **Yashpal U. Rathod** Vikram U. Pandit Wasudeo B. Gurnule	Chemistry	Materials Today: Proceedings	https://www.scopus.com/sourceid/21100370037	**408**	**409-410**	**411**
35.	Non-isothermal decomposition study of copolymer derived from 2-amino 6-nitrobenzothiazole, melamine, and formaldehyde	Punam M Gupta **Yashpal U. Rathod** Vikram U. Pandit Rajesh H. Gupta Wasudeo B. Gurnule	Chemistry	Materials Today: Proceedings	https://www.scopus.com/sourceid/21100370037	**412**	**413-414**	**415**

Gondia Education Society's

J. M. PATEL ARTS, COMMERCE & SCIENCE COLLEGE

BHANDARA – 441 904 (M.S.)

● Re-accredited 'B' Grade by NAAC ● Awarded 'College with Potential for Excellence' status (Phase II) by UGC

● R.T.M. Nagpur University recognized 'Centre for Higher Learning & Research'

● Phone No.07184 – 252364, 256883 (R) 252288 **Fax :** 07184 -253268**Email :** principaljmpc@rediffmail.com **website :** www.jmpatelcollege.com

CRITERION – III

RESEARCH, INNOVATION AND EXTENSION

3.2 RESEARCH PUBLICATIONS AND AWARDS

3.3.1 Number of research papers published per teacher in the Journals notified on UGC CARE list in 2019-2024

CONTENT

Research Paper Published in 2021

Sr. No.	Title of Paper	Name of the Authors	Department of teacher	Name of Journal ISSN number	Link to website of Journal	Page No.		
						Research Paper	Journal Homepage	UGC CARE Proof
36.	In vitro anticancer activity of thiazole based β-amino carbonyl derivatives against HCT116 and H1299 colon cancer cell lines; study of pharmacokinetics, physicochemical, medicinal properties and molecular docking analysis	**Dr. Ajay Ghatole** Dr. Kishor HatzadeDr. Mahesh Gaidhane Dr. Khushal Lanjewar	Chemistry	Indian Journal of Chemistry	https://www.scopus.com/sourceid/24111	**416-433**	**434**	**435**
37.	Butea Monosperma Bark Extract To Its Green Synthesis Of Silver Nanoparticles And Their Antioxidant, Total Flavonoid Content And Antimicrobial Activities	Dr. Gunvant Gadekar Dr. Kalpana Ghoshal **Dr. Ajay Ghatole**	Chemistry	Journal of Applied Biological Sciences	https://mjl.clarivate.com/search-results	**436-446**	**447**	**448**

38.	Issues and challenges of quality education- an indian perspective	Dr. Anand Muley	Commerce	Journal KALA The Journal of Indian Art History Congress	https://ugccare.unipune.ac.in/Apps1/User/WebA/SearchList	**449-454**	**455**	**456**
39.	Studies of chelation ion-exchange properties of copolymer resin derived from 1,5-diaminonaphthalene, 2,4-dihydroxy-propiophenone and formaldehyde	Narayan C. Das **Yashpal U. Rathod** Vikram U. Pandit Wasudeo B. Gurnule	Chemistry	Materials Today: Proceedings	https://www.scopus.com/sourceid/21100370037	**457**	**458**	**459**
40.	An Efficient Carbonized Sugar Catalyzed Entry to 7,8-dihydro-2HChromen-5(6H)-ones	T. Siddiqui P. Kulkarni **G.B.Tiwari** Z. Pudukulathan	Chemistry	JOURNAL OF SCIENTIFIC RESEARCH	https://ugccare.unipune.ac.in/Apps1/User/WebA/ViewDetails?JournalId=101001002&flag=Search	**460**	**461**	**463**
41.	Liquid–liquid extraction of uranium(VI) from weak sodium acetate medium using 2-octylaminopyridine: real sample analysis	Gurupad D. Kore **Sunil B. Zanje** Arjun N. Kokare Vishal J. Suryavanshi Mansing A. Anuse Sanjay S. Kolekar	Chemistry	Journal of Radioanalytical and Nuclear Chemistry	https://www.scopus.com/sourceid/24060	**464**	**465-467**	**468**
42.	The transition metal complexes of Fe(II), Ni(II) and Cu(II) derived from phthalazine based ligands: Synthesis, crystal structures and biological activities	Smita S. Patil **Samina K. Tadavi** Amol Dikundwar Ratnamala S. Bendre	Chemistry	Journal of Molecular Structure	https://www.scopus.com/sourceid/24642	**469**	**470**	**471**

43.	Effect of Selected Pranayama Techniques On Cardiovascular Endurance Of Different College Students of RashtrasantTukadoji Maharaj Nagpur University, Nagpur	**Romi Bisht** Madhavi Mardikar Chandra Mohan Singh	Physical Education	Kalyan Bharati	Print Journal	**472-477**	**478-479**	**480**
44.	Facile extractive separation studies of uranium(VI) assisted by dicyclohexano-18-crown-6 through green approach	Shivaji H. Burungale, **Sunil B. Zanje**	Chemistry	Journal of Radioanalytical and Nuclear Chemistry	https://doi.org/10.1007/s10967-021-07698-9	**481-487**	**488-491**	**492**

Gondia Education Society's

J. M. PATEL ARTS, COMMERCE & SCIENCE COLLEGE

BHANDARA – 441 904 (M.S.)

●Re-accredited 'B' Grade by NAAC ● Awarded 'College with Potential for Excellence' status (Phase II) by UGC

● R.T.M. Nagpur University recognized 'Centre for Higher Learning & Research'

● Phone No.07184 – 252364, 256883 (R) 252288 **Fax :** 07184 -253268**Email :** principaljmpc@rediffmail.com **website :** www.jmpatelcollege.com

CRITERION – III

RESEARCH, INNOVATION AND EXTENSION

3.2 RESEARCH PUBLICATIONS AND AWARDS

3.3.1 Number of research papers published per teacher in the Journals notified on UGC CARE list in 2019-2024

CONTENT

Research Paper Published in 2020

Sr. No.	Title of Paper	Name of the Authors	Department of teacher	Name of Journal ISSN number	Link to website of Journal	Page No.		
						Research Paper	Journal Home page	UGC CARE Proof
45.	Synthesis of Substituted Phenothiazines derivatives, Antioxidant, P-Glycoprotein, Cyp Enzyme Activity, HIA and BBB Prediction	Dr. Mahesh Gaidhane**Dr. Ajay Ghatole**Dr.PravinGaidhane Dr. Gunvant Gadekar Dr. Khushal Lanjewar Dr. MeghashamNarule	Chemistry	Der Pharma Chemica Journal	https://www.scopus.com/sourceid/19700188428	**493-503**	**504-505**	**506**
46.	Innovational combination of hetero-bifunctional N-PEG quinoline scaffolds derivatives with improved anticancer activity against breast and colon cancer cell lines and P-glycoprotein, cytochrome p450 enzyme activity	Dr. Mahesh Gaidhane**Dr. Ajay Ghatole** Dr. Khushal Lanjewar	Chemistry	Turkish Journal of Chemistry	https://www.scopus.com/sourceid/21986	**507-526**	**527-528**	**529**

	prediction							
47.	A facile synthesis of some new pyrimidine-2,4,6-triones analogs and their O-β-D-glucosides P-glycoprotein and antioxidant, antimicrobial study, blood–brain barrier, cytochrome p450 enzyme activity prediction	Dr. Kishor Hatzade**Dr. Ajay Ghatole**Dr.PravinGaidhane Dr. Mahesh Gaidhane Dr. Gunvant Gadekar	Chemistry	Medicinal Chemistry Research	https://www.scopus.com/sourceid/18384	**530-548**	**549-550**	**551**
48.	Digitaria and Setaria species of Subfamily-Panicoideae, Tribe- Paniceae (Poaceae) from Bhandara District of Maharashtra, India	**Dr. Vijay Tiwari** Dr. Chandan Sakharkar	Botany	Tropical Plant Research	https://ugccare.unipune.ac.in/Apps1/User/WebA/SearchList	**552-558**	**559**	**560**
49.	Thermal degradation and antibacterial study of transition metal complexes derived from novel terpolymer ligand.	Wasudeo B. Gurnule, **Yashpal U. Rathod**, Amoli D. Belsare, Narayan C. Das	Chemistry	Materials Today Procedings	Materials Today: Proceedings | Journal | ScienceDirect.com by Elsevier	**561**	**562-563**	**564**
50.	Synthesis, Characterization And Thermal Degradation Study Of Copolymer Resin.	Wasudeo B. Gurnule, Narayan C. Das, Sharad Vajpai, **Yashpal U. Rathod**	Chemistry	Materials Today Procedings	Materials Today: Proceedings | Journal | ScienceDirect.com by Elsevier	**565**	**566-567**	**568**

CRITERION – III

RESEARCH, INNOVATION AND EXTENSION

3.3 RESEARCH PUBLICATIONS AND AWARDS

3.3.1 NUMBER OF RESEARCH PAPERS PUBLISHED PER TEACHER IN THE JOURNALS NOTIFIED ON UGC CARE LIST DURING THE LAST FIVE YEARS

2024

https://doi.org/10.33472/AFJBS.6.6.2024.1600-1609

African Journal of Biological Sciences

Journal homepage: http://www.afjbs.com

Research Paper Open Access

Role of E-CRM in effectiveness of Strategic Marketing Planning for customer Retention: An Empirical Study

Dr Lalit Kumar Sharma,
Professor, School of Business, Galgotias University
lalitks2001@gmail.com
Dr. Meena Rao
Associate Professor Dept. of ECE, Maharaja Surajmal Institute of Technology,
Janakpuri, New Delhi-110058
E-mail id: meenarao81@gmail.com
Dr. Prabu Selvam
Department of Computer Science and Engineering SRM Institute of Science & Technology,
Tiruchirapalli Campus Tiruchirappalli – 621105
Dr. Anand Muley
Assistant Professor, Dept of Commerce, J. M. Patel Arts Commerce and Science College
Bhandara Maharashtra

Volume 6, Issue 6, May 2024

Received: 01 March 2024

Accepted: 7 April 2024

Published: 13 May 2024

doi: 10.33472/AFJBS.6.6.2024.1600-1609

Abstract
In India, strategic marketing strategy for customer retention is more effective when it incorporates Electronic Customer Relationship Management (E-CRM). Businesses can collect and analyze enormous volumes of client data using E-CRM systems, giving them deep insights into the preferences, actions, and buying patterns of their customers. Customer satisfaction and loyalty are raised by the more individualized and focused marketing techniques made possible by this data-driven approach. In the Indian context, E-CRM assists companies in catering to the distinct requirements of different client segments in an extremely competitive and diverse market. Stronger relationships are fostered via E-CRM, which guarantees timely and consistent customer involvement by automating customer interactions and optimising communication channels. By cultivating a devoted clientele, this all-encompassing strategy fosters long-term growth in addition to improving customer retention. E-CRM is therefore essential for strategic marketing strategy targeted at retaining customers in the ever-changing Indian market. A sample of 231 respondents was collected from people in business and marketing sector. The factor that identifies the role of E-CRM in effectiveness of Strategic Marketing Planning for customer Retention are Loyalty Programs and Rewards, Customer Feedback and Engagement, Enhanced Customer Service, and Data-Driven Decision Making.

Keywords: Strategic marketing, Customer retention, Electronic Customer Relationship Management (E-CRM), Data analysis,. Customer satisfaction, Market segmentation, Long-term growth

Introduction

Electronic customer relationship management, or E-CRM, is crucial for strategic marketing planning that is client retention-focused in the competitive and diverse Indian market of today. Businesses may collect and analyse vast volumes of customer data by using E-CRM systems, which enables more targeted and customised marketing efforts that boost customer happiness and loyalty. E-CRM provides valuable insights through data analytics and reporting. Businesses can track key performance indicators (KPIs) related to customer behavior, sales, and marketing effectiveness. E-CRM ensures timely and reliable client involvement by streamlining communication and automating interactions. After "Electronic Customer Relationship Management" (or "E-CRM") technologies were introduced, the strategic marketing plan for customer retention in India significantly improved. Das et al. (2018) showed that the association between effective "Customer Relationship Management" (CRM) tactics and client retention was mediated by customer satisfaction. Thanks to e-CRM systems, businesses were able to gather a vast amount of consumer data, which allowed them to construct customized marketing campaigns based on the preferences of individual customers. This tailored approach improved client satisfaction and fostered loyalty, ensuring long-term retention.

According to Kumar and Mokha (2022), E-CRM systems improved customer satisfaction, which in turn enhanced customer loyalty. The seamless integration of several client touchpoints via E-CRM ensured consistent and customised communication, which was crucial in the competitive banking sector. By leveraging E-CRM data analytics to obtain a more comprehensive insight of customer behaviour and preferences, banks were able to offer tailored financial goods and services. Apart from fulfilling the distinct needs of the customers, this tailored strategy established enduring relationships of trust, both of which were crucial for retaining customers in the banking industry.

Kaur and Kaur (2016) evaluated the competitive advantage that E-CRM provided to the Indian banking sector. They asserted that the effectiveness of E-CRM was significantly increased by this competitive edge, leading to greater client retention results. By automating and streamlining customer contacts, banks were able to reduce operating costs and improve service performance. Because E-CRM systems can react quickly and effectively to consumer inquiries and problems, overall customer happiness has grown. Kaul (2017) elaborated on the wider consequences of CRM in the retail industry, establishing a connection between it and "Customer Lifetime Value" (CLV). Businesses in the retail industry were able to track client preferences and purchase histories thanks to E-CRM systems, which made it possible to launch highly focused marketing campaigns. Retailers improved the shopping experience by providing tailored promos and recommendations, which raised customer satisfaction and loyalty. Retailers were able to improve retention and long-term profitability by using E-CRM to forge closer ties with their customers. As a result, E-CRM was essential to strategic marketing planning for customer retention in India's diverse industries.

Literature Review

Farmania et al. (2021) examined the conversion of CRM operations into "E-CRM" in the context of strategic marketing planning for client retention in India. They emphasized how important it is to use "E-CRM" to boost customer loyalty and promote open innovation by utilizing digital technology. E-CRM systems can manage loyalty programs by tracking customer purchases and rewarding repeat customers with points, discounts, or special offers. In line with the changing market dynamics of India, this transformation signifies a strategic move towards customer relationship management that is more dynamic and flexible. Enterprises can effectively leverage the power of "E-CRM" to customize marketing strategies and activities based on individual consumer preferences and behaviors by fusing traditional CRM techniques with digital technologies. Strategic marketing planning for client retention in the Indian market is critical, and this tailored strategy not only improves consumer happiness but also fortifies long-term loyalty. They also emphasised how adopting "E-CRM" promotes shared consumer interaction, which fosters innovation. Enterprises must consistently innovate to remain competitive and relevant in India's quickly changing market environment, where consumer expectations are ever-changing.

Singh et al. (2023) examined the effect of E-CRM services on customer loyalty in the Indian healthcare sector. It was shown that by boosting client satisfaction and trust, E-CRM services had a favorable impact on customer persistence. The implementation of E-CRM systems allowed healthcare providers to provide individualized care and keep thorough patient data. Patient satisfaction increased and the healthcare provider's credibility was strengthened by this individualized care. In order to keep clients in the healthcare industry, they emphasised the vital role that E-CRM plays in strategic marketing plans.

A customer-centric strategy can be created by examining the idea of "Social E-CRM" (SECRM), as discussed by Naim (2022). For more effective and dynamic client engagement, SECRM combined social media platforms with standard E-CRM procedures. By interacting with customers on social media, firms who used SECRM in India were able to learn a great deal about their preferences and behavior. The efficiency of strategic marketing planning was improved by this method, which also brought value to the customer connection. Businesses could increase customer satisfaction and retention rates by utilizing SECRM to forge closer bonds with their clientele. Mehta and Tajeddini (2016) used the "CRM Magic Quadrant" with the "Readiness Matrix Model" to show how E-CRM systems helped Indian SMEs gather and process customer data efficiently. SMEs were able to create and implement customized marketing plans based on the requirements and preferences of specific customers thanks to this capacity. SME customer satisfaction increased as a result of E-CRM adoption, which guaranteed long-term retention and encouraged loyalty. E-CRM techniques had a major effect on client retention and satisfaction in the insurance business.

Anuradha and Singh (2022) assessed that E-CRM procedures significantly increased customer satisfaction in the Indian insurance sector. Insurance providers were able to deliver prompt, individualized services because E-CRM technologies made communication more effective and reduced procedures. Customers' trust and loyalty were subsequently enhanced by the rapid resolution of their complaints thanks to this personalized service approach. Well-structured loyalty programs can significantly boost customer loyalty and lifetime value. Insurance firms were able to maintain client retention by satisfying their individual needs and provide an exceptional customer experience through the efficient use of E-CRM.

The key to strategic marketing planning's efficacy for client retention in India is "E-CRM". The need of utilising "e-CRM" technologies and tactics to strengthen client relationships in the digital age was highlighted by Joju and Joseph (2016). Businesses may adjust their marketing strategies to suit the changing demands and tastes of Indian consumers by incorporating electronic channels into customer relationship management. Kaur (2016) underlined the value of "electronic-customer relationship marketing (e-CRM)," stressing the platform's capacity to promote tailored interactions and cultivate lifetime client loyalty. A more sophisticated method of comprehending and interacting with clients is provided by "e-CRM" in a nation as diverse as India, where consumer behaviors differ among demographic groups and geographical areas.

The "e-CRM" services offered by service providers were the focus area of Manjunatha and Naidu's (2020) which showed the important success elements that are essential for successful deployment. Companies can customize their "e-CRM" plans to suit the distinct socio-cultural characteristics of the Indian market. Dasgupta and Sahai (2021) showed the significance of "Electronic Customer Relationship Management (eCRM)" in the digital transformation of India's society and economy, highlighting the revolutionary potential of this technology in advancing customer-centric marketing approaches. In order to improve strategic marketing planning and support customer retention initiatives, organizations are turning more and more to digital technology for customer engagement. Analyzing this feedback helps businesses understand customer needs and areas for improvement. Engaging customers by responding to their feedback shows that the company values their opinions, fostering a stronger customer relationship.

Strategic marketing planning for customer retention in India works better when it includes "Electronic Customer Relationship Management," or "E-CRM." In their examination of "E-CRM" in e-commerce, Maxwell and Khan (2018) stressed the role, influence, and advantages of this technology as well as how crucial it is for creating and maintaining customer relationships. Customising marketing techniques according to individual consumer preferences through "E-CRM" enables firms to increase customer satisfaction and extend the duration of their client loyalty. Personalised communication and efficient data management are the means by which this is accomplished. In the competitive and dynamic Indian e-commerce sector, organisations seeking to maintain their clientele may find that carefully implementing "E-CRM" makes all the difference.

According to Mokha and Kumar (2022), the relationship between "E-CRM," customer experience, contentment, and loyalty is extremely important when it comes to strategic marketing planning for client retention in India. They demonstrated the significance of "E-CRM" in generating positive client experiences, which influence satisfaction and foster loyalty. By facilitating seamless interactions across several touchpoints, the deployment of "E-CRM" improves the customer journey and raises satisfaction and retention rates.

Objective

For identifying "Role of E-CRM in effectiveness of Strategic Marketing Planning for customer Retention"

Study's Methodology

231 respondents are considered for this study which was collected from from people in business and marketing sector. Random sampling method was used to collect data and examined by "Explanatory Factor Analysis" for results.

Findings of the Study

Below table shows demographic details of participants it shows that 52.81% are male, and 47.19% are female participants. Regarding age of the respondents, 29.87% are between 26 to 30 years, 35.93% are 30 to 36 years, and 34.20% are above 36 years of age. About Types of Business sector, retail sector is 51.08%, and wholesale sector is 48.92%.

Details of Participants

Variable	Participants	% age
Gender of Participants		
Male	122	52.81%
Female	109	47.19%
Total	**231**	**100**
Age in years		
26 to 30	69	29.87%
30 to 36	83	35.93%
Above 36	79	34.20%

Total	**231**	**100**
Type of Business sector		
Retail sector	118	51.08%
Wholesale sector	113	48.92%
Total	**231**	**100**

"Factor Analysis"

"KMO and Bartlett's Test"

"Kaiser-Meyer-Olkin Measure of Sampling Adequacy"		.769
"Bartlett's Test of Sphericity"	"Approx. Chi-Square"	3647.769
	df	91
	Significance	.000

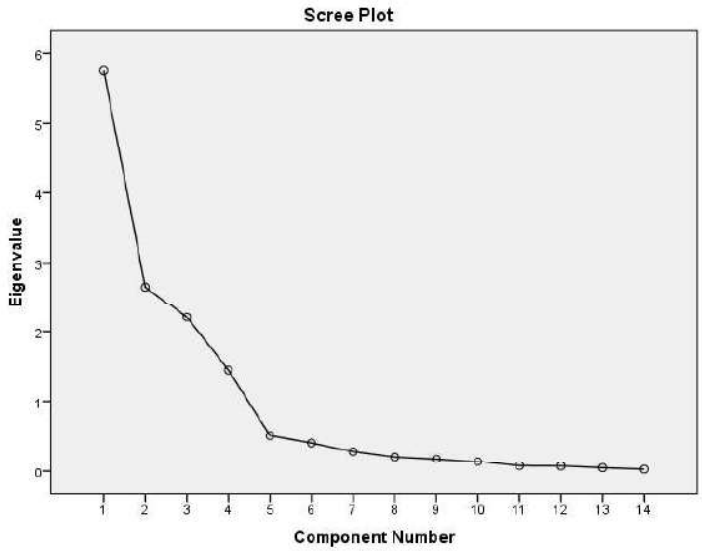
"KMO and Bartlett's Test", value of KMO is .769

"Total Variance Explained"

"Component"	**"Initial Eigenvalues"**			**"Rotation Sums of Squared Loadings"**		
	"Total"	**"% Of Variance"**	**"Cumulative %"**	**"Total"**	**"% Of Variance"**	**"Cumulative %"**
1.	5.759	41.139	41.139	**3.713**	26.523	26.523
2.	2.653	18.947	60.085	**3.665**	26.178	52.701
3.	2.204	15.743	75.829	**2.390**	17.070	69.771
4.	1.447	10.339	86.167	**2.295**	16.396	**86.167**
5.	.511	3.652	89.820			
6.	.407	2.911	92.730			
7.	.283	2.024	94.754			
8.	.205	1.467	96.221			
9.	.176	1.255	97.476			
10.	.136	.971	98.448			
11.	.075	.533	98.980			
12.	.071	.510	99.490			

13.	.046	.328	99.819			
14.	.025	.181	100.000			

All the four factors are making contribution in explaining total 86.167% of variance. The variance explained by Loyalty Programs and Rewards is 26.523%, Customer Feedback and Engagement, is 26.178%, Enhanced Customer Service is 17.070%, and Data-Driven Decision Making is 16.396%.



ScreePlot

"Rotated Component Matrix"

S. No.	Statements	Factor Loading	Factor Reliability
	Loyalty Programs and Rewards		**.972**
1.	E-CRM systems can manage loyalty programs by tracking customer purchases	.955	
2.	It rewards repeat customers with points, discounts, or special offers	.947	
3.	These programs incentivize customers to continue purchasing from the company, enhancing retention	.932	
4.	Loyalty programs can significantly boost customer loyalty and lifetime value	.924	
	Customer Feedback and Engagement		**.955**

1.	It facilitates collection of feedback through surveys, reviews, and social media	.958	
2.	Engaging customers by responding to their feedback shows company values their opinions	.912	
3.	Analyzing feedback helps understand customer needs and areas for improvement	.894	
4.	Engaging customers fosters a stronger customer relationship	.894	
	Enhanced Customer Service		**.868**
1.	Provide tools for improved customer service such as live chat, email, social media	.888	
2.	Prompt and efficient customer support enhances customer satisfaction, and retention	.850	
3.	Customers who receive excellent service are more likely to remain loyal	.807	
	Data-Driven Decision Making		**.830**
1.	Provides valuable insights through data analytics and reporting	.921	
2.	Can track key performance indicators related to customer behavior, sales, and marketing	.906	
3.	Data-driven insights help companies refine their strategic marketing plans	.707	

Factors and the associated variables

The first factor of the study is Loyalty Programs and Rewards, the variables under this factor are E-CRM systems can manage loyalty programs by tracking customer purchases, It rewards repeat customers with points, discounts, or special offers, These programs incentivize customers to continue purchasing from the company, enhancing retention, and Loyalty programs can significantly boost customer loyalty and lifetime value. Second factor is Customer Feedback and Engagement, it includes variables like It facilitates collection of feedback through surveys, reviews, and social media, Engaging customers by responding to their feedback shows company values their opinions, analyzing feedback helps understand customer needs and areas for improvement, and Engaging customers fosters a stronger customer relationship. Enhanced Customer Service is the third factor of the study, it includes variables like Provide tools for improved customer service such as live chat, email, social media, Prompt and efficient customer support enhances customer satisfaction, and retention, and Customers who receive excellent

service are more likely to remain loyal. Last and fourth factor is Data-Driven Decision Making, its variables are Provides valuable insights through data analytics and reporting, can track key performance indicators related to customer behavior, sales, and marketing, and Data-driven insights help companies refine their strategic marketing plans.

"Reliability Statistics"

"Cronbach's Alpha"	"Number of Items"
.879	14

Total reliability of 14 items that includes variables for Role of E-CRM in effectiveness of Strategic Marketing Planning for customer Retention is 0.879

Conclusion

In conclusion, E-CRM (Electronic Customer Relationship Management) plays a "paramount" role in the efficacy of strategic marketing strategy for retaining customers in India. Businesses may better understand their consumers' demands, personalise their interactions with them, and adjust their marketing plans with the help of E-CRM. Stronger ties are fostered by this "personalised" approach, which increases client loyalty and retention. Moreover, E-CRM systems enable companies to monitor consumer behaviour, preferences, and trends by offering insightful data analytics. By anticipating customer demands, addressing concerns proactively, and providing timely answers, organisations can increase customer happiness and loyalty through the use of this "data-driven" approach. Furthermore, E-CRM becomes "indispensable" in a country like India that is quickly changing its digital landscape and seeing an increase in online purchases and digital interactions. Through a variety of digital platforms, including social media, email, and mobile apps, it helps businesses to interact with customers in a seamless and consistent manner. Businesses may maximise ROI, streamline resource allocation, and improve strategic marketing planning procedures by utilising E-CRM successfully. In the end, including E-CRM into strategic marketing planning improves client retention while also fostering competitiveness and sustainable growth in the ever-changing Indian market environment. The factor that identifies the role of E-CRM in effectiveness of Strategic Marketing Planning for customer Retention are Loyalty Programs and Rewards, Customer Feedback and Engagement, Enhanced Customer Service, and Data-Driven Decision Making.

References

1. Das, S., Mishra, M., & Mohanty, P. K. (2018). The impact of customer relationship management (CRM) practices on customer retention and the mediating effect of customer satisfaction. International Journal of Management Studies, 5(1), 4.
2. Kumar, P., & Mokha, A. K. (2022). Electronic customer relationship management (E-CRM) and customer loyalty: The mediating role of customer satisfaction in the banking industry. International Journal of E-Business Research (IJEBR), 18(1), 1-22.
3. Kaur, J., & Kaur, B. (2016). The influence of e-CRM competitive advantage on e-CRM performance in the Indian banking industry. Strategic Change, 25(5), 537-550.
4. Kaul, D. (2017). Customer relationship management (CRM), customer satisfaction and customer lifetime value in retail. Review of Professional Management-A Journal of New Delhi Institute of Management, 55-60.
5. Mehta, A., & Tajeddini, J. (2016). Proposed integrated CRM magic quadrant and readiness matrix model for Indian SMEs. Middle East Journal of Management, 3(3), 179-206.
6. Singh, B., & Anuradha, L. S. (2022). E-CRM practices and customer satisfaction in insurance sector. SAARJ Journal on Banking & Insurance Research, 11(4), 16-23.
7. Naim, A. (2022). Understanding the customer centric approach to add value to social ecrm (SECRM). American Journal of Technology and Applied Sciences, 3, 17-31.
8. Singh, P., Kumar, V., & Kataria, S. (2023). A serial mediation model for investigating the impact of e-CRM services on customer loyalty in the Indian healthcare industry. Journal of Relationship Marketing, 22(1), 62-86.
9. Joju, J., & Joseph, S. (2016). E-Leveraging e-CRM for Future. Indian Journal of Science and Technology.
10. Kaur, P. (2016). Managing relations through electronic-customer relationship marketing [E-CRM]. Asian Journal of Multidimensional Research (AJMR), 5(4), 27-36.
11. Manjunatha, S., & Naidu, G. (2020). Factors of e-CRM services by the service providers and their key success factors–An empirical study. Alochana Chakra Journal, 9(6), 6417-6426.
12. Dasgupta, D., & Sahai, A. K. (2021). Electronic Customer Relationship Management (eCRM). In Digitization of Economy and Society (pp. 293-319). Apple Academic Press.
13. Maxwell, S., & Khan, A. M. (2018). Electronic customer relationship management (E-CRM): A study of its role, influence & benefitsto e-commerce. Management Dynamics, 18(1), 43-51.
14. Mokha, A. K., & Kumar, P. (2022). Examining the interconnections between E-CRM, customer experience, customer satisfaction and customer loyalty: A mediation approach. Journal of Electronic Commerce in Organizations (JECO), 20(1), 1-21.
15. Farmania, A., Elsyah, R. D., & Tuori, M. A. (2021). Transformation of crm activities into e-crm: The generating e-loyalty and open innovation. Journal of Open Innovation: Technology, Market, and Complexity, 7(2), 109.



(https://www.afjbs.com/)

Search for title, author, doi. Search

ISSN : 2663-2187

Chat with us


ISSN: XXXX-XXXX
Vol. 1 Issue 1, Jan 2019
AFJBS
AFRICAN
JOURNAL OF
BIOLOGICAL
SCIENCES
Chat with us
E-Mail: editor@afjbs.com or info@afjbs.com

Website: www.afjbs.com

Effect Of Frequent Exposures Of Mancozeb On Rhynocoris Fuscipes (Hemiptera: Reduviidae) A Natural Enemy Of Groundnut, Arachis Hypogaea Linn. Insect Pests. (Https://Www.Afjbs.Com/Issue-Content/Effect-Of-Frequent-Exposures-Of-Mancozeb-On-Rhynocoris-Fuscipes-Hemiptera-Reduviidae-A-Natural-Enemy-Of-Groundnut-Arachis-Hypogaea-Linn-Insect-Pests-7387)

Volume 6 | Issue -15

Optimizing Strategies For Controlling And Improving Air Quality As An Effort To Minimize The Impact Of Public Health And Climate Change (Case Study : Jakarta City Air Pollution) (Https://Www.Afjbs.Com/Issue-Content/Optimizing-Strategies-For-Controlling-And-Improving-Air-Quality-As-An-Effort-To-Minimize-The-Impact-Of-Public-Health-And-Climate-Change-Case-Study-Jakarta-City-Air-Pollution-7383)

Volume 6 | Issue -15

Evaluation Of Causes Of Hemiplegia/Paraplegia And Effects Of Rehabilitative Services In Patients Admitted In Paraplegic Centers (Https://Www.Afjbs.Com/Issue-Content/Evaluation-Of-Causes-Of-Hemiplegia-Paraplegia-And-Effects-Of-Rehabilitative-Services-In-Patients-Admitted-In-Paraplegic-Centers-7382)

Volume 6 | Issue -15

Phytochemical Study Of Urtica Dioica Extract And Evaluation Of Sun Protection Factor (SPF) (Https://Www.Afjbs.Com/Issue-Content/Phytochemical-Study-Of-Urtica-Dioica-Extract-And-Evaluation-Of-Sun-Protection-Factor-Spf-7381)

Volume 6 | Issue -15

Protective Effect Of Nigella Sativa Oil On Cadmium-Induced Hepato-Nephrotoxicity (Https://Www.Afjbs.Com/Issue-Content/Protective-Effect-Of-Nigella-Sativa-Oil-On-Cadmium-Induced-Hepato-Nephrotoxicity-7380)

Volume 6 | Issue -15

Required files to be uploaded

☐ **Copyright (https://www.scimagojr.com/journalsearch.php?q=21101106407&tip=sid&clean=0)**



(https://www.scimagojr.com/journalsearch.php?q=21101106407&tip=sid&clean=0)

Chat with us

(https://www.scopus.com/sourceid/21101106407)

(http://www.elsevier.com/products/embase/content)

Role of E-CRM in effectiveness of Strategic Marketing Planning for customer Retention: An Empirical Study

PDF (https://www.afjbs.com/uploads/paper/9356b41afe646b56a5e56a0501f0375c.pdf)

Keywords:
Strategic marketing, Customer retention, Electronic Customer Relationship Management (E-CRM), Data analysis,. Customer satisfaction, Market segmentation, Long-term growth

Dr Lalit Kumar Sharma, Dr. Meena Rao, Dr. Prabu Selvam, Dr. Anand Muley

» doi: 10.33472/AFJBS.6.6.2024.1600-1609
(https://www.afjbs.com/./uploads/paper/9356b41afe646b56a5e56a0501f0375c.pdf)

Abstract

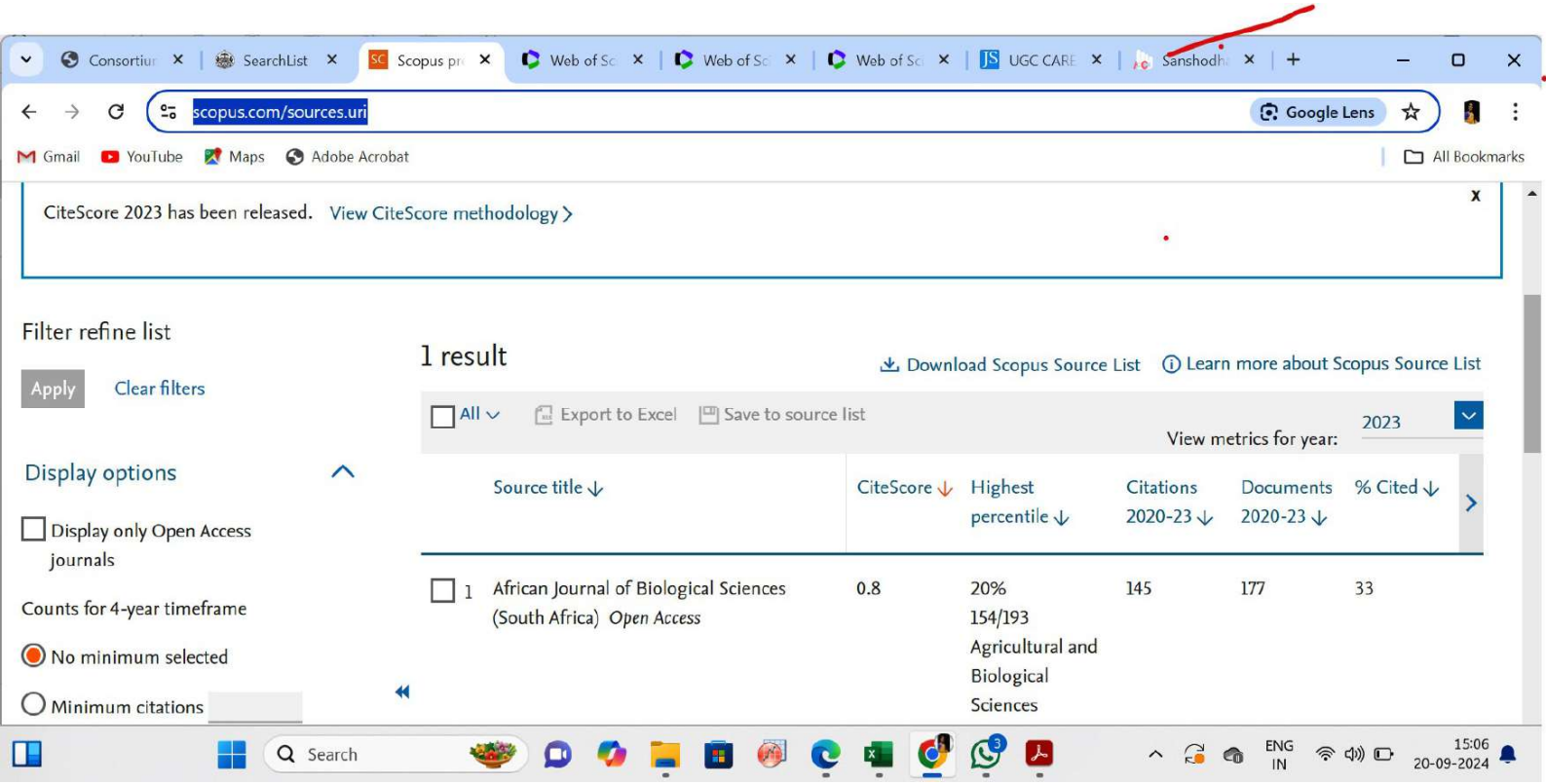
In India, strategic marketing strategy for customer retention is more effective when it incorporates Electronic Customer Relationship Management (E-CRM). Businesses can collect and analyze enormous volumes of client data using E-CRM systems, giving them deep insights into the preferences, actions, and buying patterns of their customers. Customer satisfaction and loyalty are raised by the more individualized and focused marketing techniques made possible by this data-driven approach. In the Indian context, E-CRM assists companies in catering to the distinct requirements of different client segments in an extremely competitive and diverse market. Stronger relationships are fostered via E-CRM, which guarantees timely and consistent customer involvement by automating customer interactions and optimising communication channels. By cultivating a devoted clientele, this all-encompassing strategy fosters long-term growth in addition to improving customer retention. E-CRM is therefore essential for strategic marketing strategy targeted at retaining customers in the ever-changing Indian market. A sample of 231 respondents was collected from people in business and marketing sector. The factor that identifies the role of E-CRM in effectiveness of Strategic Marketing Planning for customer Retention are Loyalty Programs and Rewards, Customer Feedback and Engagement, Enhanced Customer Service, and Data-Driven Decision Making.

Issue

Volume 6 , Issue - 6 (2024)
()

Submit Your Article Here. (https://www.afjbs.com/submit-article)

Chat with us


scopus.com/sources.uri
Google Lens
Gmail
YouTube
Maps
Adobe Acrobat
All Bookmarks
CiteScore 2023 has been released. View CiteScore methodology >
Filter refine list
Apply
Clear filters
Display options
Display only Open Access journals
Counts for 4-year timeframe
No minimum selected
Minimum citations
1 result
Download Scopus Source List
Learn more about Scopus Source List
All
Export to Excel
Save to source list
View metrics for year:
2023
Source title
CiteScore
Highest percentile
Citations 2020-23
Documents 2020-23
% Cited
1 African Journal of Biological Sciences (South Africa) Open Access
0.8
20% 154/193 Agricultural and Biological Sciences
145
177
33
Search
ENG IN
15:06
20-09-2024

UGC CARE LISTED
ISSN No. 2394-5990

इतिहासाचार्य वि. का. राजवाडे मंडळ, धुळे
या संस्थेचे त्रैमासिक

।। संशोधक।।

पुरवणी अंक ४८ – मार्च २०२४ (त्रैमासिक)

- **शके १९४५**
- **वर्ष : ९२**
- **पुरवणी अंक : ४८**

संपादक मंडळ

- प्राचार्य डॉ. सर्जेराव भामरे
- प्राचार्य डॉ. अनिल माणिक बैसाणे
- प्रा. डॉ. मृदुला वर्मा
- प्रा. श्रीपाद नांदेडकर

अतिथी संपादक

- डॉ. अशोक टी. खोब्रागडे
- डॉ. प्रफुल्ल एस. वैराळे
- डॉ. रामचंद्र एम. वासेकर

✷ प्रकाशक ✷

श्री. संजय मुंदडा

कार्याध्यक्ष, इ. वि. का. राजवाडे संशोधन मंडळ, धुळे ४२४००१
दूरध्वनी (०२५६२) २३३८४८, ९४२२२८९४७१, ९४०४५७७०२०
Email ID : rajwademandaldhule1@gmail.com
rajwademandaldhule2@gmail.com

कार्यालयीन वेळ

सकाळी ९.३० ते १.००, सायंकाळी ४.३० ते ८.०० (रविवारी सुट्टी)

सदस्यता वर्गणी : रु. २५००/–

विशेष सूचना : संशोधक त्रैमासिकाची वर्गणी चेक/ड्राफ्टने
'संशोधक त्रैमासिक राजवाडे मंडळ, धुळे' या नावाने पाठवावी.

अक्षरजुळणी : सौ. सीमा शिंत्रे, पुणे.

टीप : या नियतकालिकेतील लेखकांच्या विचारांशी मंडळ व शासन सहमत असेलच असे नाही.

९. **Barrenness of Married life in Indian Society as Depicted in Manju Kapur's *A Married Woman***

- i) Smita Wasudeo Neware, ii) Dr. S.G. Gahane ---------- ४३

१०. **Struggle for Identity as Depicted in the Novel *ChottiMunda and His Arrow***

- i) Archana Sitaramji Rathod, ii) Dr. Dharmapal B. Fulzele ---------- ४६

११. **Unraveling Identity Complexities in *The Shadow Lines***

- i) Prof. Amar Tulshiram Balki, ii) Dr. Priyadarshi V. Meshram ---------- ५२

१२. **Breaking Boundaries: Exploring Innovative Trends in Contemporary Indian Fiction Writing in English**

- Dr. Vaibhao B. Pimpale ---------- ५८

१३. **Utilization of Information and Communication Technology Tools in the Educational Process**

- Atul M Gavaskar ---------- ६३

१४. **Contextualizing Adivasi Literary Discourse in *Bhasha* Literature of India- With Special Reference of Novel Writings In Jharkhand**

- Dr. Manoj Shankarrao Madavi ---------- ६७

१५. **Examining the story *'The Namesake'* by Jhumpa Lahiri: A conceptual leap transcends text**

- Mr. Swapnil P. Dhomane, Prof. Dr. Akshay V. Dhote ---------- ७१

१६. **Perspectives of Teachers And Students of Undergraduate Arts Faculty Regarding Internal Assessment**

- Dr. Bhavana M. Rai ---------- ७७

ISSN No. 2394-5990

PERSPECTIVES OF TEACHERS AND STUDENTS OF UNDERGRADUATE ARTS FACULTY REGARDING INTERNAL ASSESSMENT

Dr. Bhavana M. Rai
Assistant Professor (English)
J. M. Patel Arts,Commerce & Science College,
Bhandara, Maharastra, India
9763633324, *drbhavanarai@gmail.com*

Abstract ;

Assessment is a vital part of successful teaching-learning. The primary function of assessment is to promote teaching and learning in the classroom. It is assumed that the internal assessment marks system gives the opportunity to subject faculty to know students' knowledge both in theory and practical. To know the ground reality of the above assumption, it is essential to know what teachers and students think of internal assessment and how they receive it. The questionnaires were designed to examine teachers' and students' perceptions of internal assessment in the Undergraduate Arts section. This paper will share the data and the findings of the study, which may have some useful implications for other teachers.

Key Words: *Internal Assessment, Tertiary teachers, Undergraduates, Students 'perspective, Assessment methods*

Background of the study:

Assessment is a vital process in teaching-learning, in which internal assessment is assumed to be useful in monitoring the learning of the students. The context of the study is an urban college affiliated to a famous university of Vidarbha, Maharashtra, where internal assessment is recently introduced in the undergraduate courses.

Reasons for selecting the topic:

The present study tries to explore the ground reality of the assumptions that Internal assessment is useful in assessing the knowledge and learning outcomes of the students and to find out how far is internal assessment successful in meeting its very aim and objectives.

Research Question :

What are the perspectives of Tertiary teachers and Undergraduate Arts students regarding internal assessment?

Data Collection Tools :

The data are collected from 20 Tertiary Arts Teachers from both rural and urban colleges of Bhandara district and 50 Undergraduate Arts Students of an urban college of Bhandara district through:

1. Teachers Questionnaire
2. Follow-up Interviews of Teachers
3. Students Questionnaire
4. Follow-up informal discussions with students
5. Personal Journal

Description of the data :

Teachers :

The result of Q1 and 3 indicates that almost all (90%) except 2 teachers reported that they know about the University's objectives for internal assessment. While all (95%) except one said that they are quite aware of the structure of internal assessment prescribed by the university.

Question 4 inquired the reasons why teachers themselves find internal assessment beneficial. The

data received is given in Table No. 1. In response to Q5, 7 teachers reported that it has increased their workload.

Reasons given by teachers	**No. of teachers**
Improves Learning	09
Helps teaching	05
Increases students' marks	07
Better Exam results	12
Increases Students' attention	09

Table No. 1: Why teachers think I.A. is beneficial?

Q.6 inquired about the activities that are carried out in college for internal assessment. The response received is given in the table below.

Name of Activities	**No. of teachers**
Class Test/unit test	10
Home assignment	13
Viva	07
Seminar/presentations	05
Reading tasks	02
Quiz	01

Table No. 2: Activities conducted by teachers in I.A.

In response to Q9, 7 teachers said that they found an excellent performance of their students in internal assessment last year, 8 teachers said it was good and 5 said that it was average. In response to Q 10, 12 teachers said that they think that the internal assessment pattern is successful in meeting aims and objectives. Changes in I.A. suggested by some teachers in response to the last question them are:

- External examiners should come to conduct assessment so that it could be justified and could make students more serious about it.
- The activities for assignment given in the syllabus should be increased.
- More extracurricular activities should be there.

ISSN No. 2394-5990

- Syllabus should be made more interesting so that learning could become an enjoyable process.
- More transparency is required in the process of I.A.

Students' Data :

In the next step of research, the students' questionnaires were filled by 50 undergraduate students pursuing B.A. Degree program in a college of Bhandara district of Maharashtra state of India. In response to the questions all the students (100%) said that they like I.A. and thinks that it is useful. Q3 and Q4 inquired about the reasons for their opinions about I.A. The most important reason given by the students (80%) is that internal assessment helps them to score better marks in their exams. Almost 60 % of students said that it also helps in their personality development.

In response to Q7and Q8, 28 students said that Viva is the most interesting part of I.A. while 18 students said group assignments are the most interesting part. Q9 was an open-ended question which inquired about the kind of activities students want in Internal Assessment.

Activities	No. of Students
Detailed knowledge about subject	08
Innovative activities	06
Group discussion	05
Field works	04
Conversational activities	04

Table No. 3: Activities desired by the students

Data Analysis :

1. <u>Joint appreciation of Internal Assessment by students-teachers:</u>

The data received from both students and teachers indicates that the internal assessment pattern is well received by them and they want it to be continued in future. 85% teachers said that they feel that the internal assessment should be continued in the upcoming sessions while only 10% teachers said that it should be discontinued as it is merely a waste of time and effort.

2. <u>Contradictory responses from teachers</u>

The data received from the teachers through questionnaires and the informal discussion about the reasons why I.A. is conducted in their colleges is quite different from each other. The teachers admitted in informal discussion that the first main reason for conducting an internal assessment is university compulsion but didn't mention it as a major reason in their questionnaire. Both students and teachers reported that I.A. beneficial as it helps in gaining better marks and consequently the better results. But the other benefits given by them differ. Teachers reported it beneficial for assessing various knowledge and skills of the students while students responded that it is useful for personality development (60%) and to create better confidence (40%) and provides a platform for skill building (30%).

3. <u>Opinions of students about the process of I.A.:</u>

54% of students said it is always fair while 34% of students reported it is sometimes fair. Almost 8%

of students said that it is sometimes unfair and only 4% of students said that it is always unfair. At the same time, 78% students reported that the topics and activities are fully taught /discussed while 20% students reported that it is partially taught or discussed.

4. Difference between demand and supply:

There is a considerable difference between what teachers usually do in I.A. and what the students desire. The data received by them shows that there is a demand for more innovative practices in I.A. by the students which are not currently fulfilled or supplied by the teachers. The table below indicates the differences in opinion of teachers and students in this regard.

What Teachers Do?	What Else Students Want?
Unit test/ Class Test	Group Discussion
Seminars/ Presentations	Field Works
Home Assignments/Group Assignments	Innovative activities
Viva	Conversation activities

Table No.4

5. Most popular and least popular activities of I.A. among students:

On the basis of the data received, the most popular part of I.A. according to the students is Viva 56% students and 38% students said the most boring part is individual assignments.

6. Changes needed by students and teachers:

The internal assessment is, however, well received by students and teachers but at the same time they need some changes in it. The most interesting point is that both students and teachers pinpointed each other during the informal discussion for the lack of seriousness from each other. The second most interesting point is that the table clearly indicates that both teachers and students want innovative contents and practices respectively but the students' want was found more prominent than teachers in field observations.

Findings and Conclusions

1. Both teachers and students find Internal Assessment beneficiary for their better results.
2. Students are more enthusiastic for creative and innovative initiatives in the pattern and procedure of internal assessment than their teachers.
3. Both students-teachers are lacking in seriousness for conducting-attempting the internal assessment in the desired way. Interestingly, one thing that both students and teachers expect from each other is to carry out the process more systematically and authentically.

Implications :

1. Internal assessment procedure needs a more serious approach firstly from the teachers.
2. Teachers should plan internal assessment according to the need of the syllabus as well as the inclination and interest of the students.
3. Internal assessment should be different in approach from the other regular assessment.
4. Teachers should constantly research about the new innovative ways to assess and should try to include them in the internal assessment.

ISSN No. 2394-5990

APPENDICES

1. PERCEPTION OF TERTIARY ARTS TEACHERS REGARDING INTERNAL ASSESSMENT

Teachers' Questionnaire

1. Do you know what the university's objectives are for Internal Assessment in Undergraduate Arts classes?

a. Yes ( ) b. No ( ) c. Not sure ( )

2. For what reasons, in your opinion, is Internal Assessment conducted in your college?

.....

.....

.....

.....

3. Are you aware of the structure of internal assessment prescribed by the university?

a. Yes ( ) b. No ( ) c. Not Sure ( )

4. In what ways do you find Internal Assessment beneficial? (Tick the reasons)

a. Improves Learning
b. Helps teaching
c. Increases students' marks
d. Better Exam results
e. Increases Students' attention
f. More seriousness from students
g. Any other

.....

.....

5. Do you feel internal assessment has increased/ decreased your workload?

a. Increased ( ) b. Decreased ( )
c. Partly increased, partly decreased ( ) d. Not Sure ( )

6. What activities are carried out in your College for internal assessment?

.....

.....

.....

.....

7. Do you think that teachers should teach and prepare students for internal assessment? Why?

a. Yes ( ) b. No ( )

.....

.....

8. Do you prepare your students for internal assessment? If yes, how?

.....

.....

9. How do you find your students' performance in Internal Assessment last year?

a. Excellent
b. Good
c. Average
d. Poor

10. Do you think the internal assessment pattern is successful in meeting aims and objectives?

a. Yes ( ) b. No ( ) c. Not sure ( )

11. Do you feel that the internal assessment should continue or be discontinued? Please give reasons.

.....

.....

12. Would you like any changes in the present pattern/ format of Internal Assessment? If yes, please mention what type of changes would you suggest?

a. Yes ( ) b. No ( )

.....

.....

13. Anything Else you would like to mention?

.....

.....

ISSN No. 2394-5990

2. PERCEPTION OF UNDERGRADUATE ARTS STUDENTS REGARDING INTERNAL ASSESSMENT

STUDENTS' QUESTIONNAIRE

1. Do you like internal assessment?
   Yes ( ) No ( )

2. Do you think internal assessment is useful?
   Yes ( ) No ( )

3. If you think that internal assessment is useful, please give reasons for your answer.

……
……

4. If you think that internal assessment is not useful, please give reasons for your answer.

……...
……...

5. What do you think about the process of internal assessment? It is…..

a) Always fair
b) Always unfair
c) Sometimes Fair
d) Sometimes unfair

6. Whether the topics and activities of internal assessment are taught/discussed in the class?

a) Yes, fully discussed/taught
b) Yes, but only few important topics
c) Not at all discussed/taught

7. Which part of the internal assessment did you find dull or boring?

a) Viva
b) Group Assignments
c) Individual Assignments
d) Any other, please mention……..

8. Which part of internal assessment did you like the most?

a) Viva
b) Group Assignments
c) Individual Assignments
d) Any other, please mention……..

9. What kind of activities do you want in Internal Assessment?

……..
……..

10. Do you want an Internal Assessment in your upcoming semesters?

Yes ( ) No ( )

■■■

UGC-CARE List

You searched for "**2394-5990**". Total Journals : **1**

Search:

Sr.No.	Journal Title	Publisher	ISSN	E-ISSN	UGC-CARE coverage years	Details
1	Sanshodhak (print only)	Itihasacharya V. K. Rajwade Sanshodhan Mandal	2394-5990	NA	from April-2021 to July-2024	Discontinued from July 2024

Showing 1 to 1 of 1 entries

Previous 1 Next

Copyright © 2024 Savitribai Phule Pune University. All rights reserved. | Disclaimer

UGC CARE LISTED
ISSN No. 2394-5990

इतिहासाचार्य वि. का. राजवाडे मंडळ, धुळे
या संस्थेचे त्रैमासिक

।। संशोधक।।

पुरवणी अंक ५७ – मार्च २०२४ (त्रैमासिक)

- **शके १९४५**
- **वर्ष : ९२**
- **पुरवणी अंक : ५७**

संपादक मंडळ

- प्राचार्य डॉ. सर्जेराव भामरे
- प्राचार्य डॉ. अनिल माणिक बैसाणे
- प्रा. डॉ. मृदुला वर्मा
- प्रा. श्रीपाद नांदेडकर

अतिथी संपादक

- डॉ. अशोक टी. खोब्रागडे
- डॉ. प्रफुल्ल एस. वैराळे
- डॉ. रामचंद्र एम. वासेकर

✷ प्रकाशक ✷

श्री. संजय मुंदडा

कार्याध्यक्ष, इ. वि. का. राजवाडे संशोधन मंडळ, धुळे ४२४००१
दूरध्वनी (०२५६२) २३३८४८, ९४२२२८९४७१, ९४०४५७७०२०
Email ID : rajwademandaldhule1@gmail.com
rajwademandaldhule2@gmail.com

कार्यालयीन वेळ

सकाळी ९.३० ते १.००, सायंकाळी ४.३० ते ८.०० (रविवारी सुट्टी)

सदस्यता वर्गणी : रु. २५००/–

विशेष सूचना : संशोधक त्रैमासिकाची वर्गणी चेक/ड्राफ्टने
'संशोधक त्रैमासिक राजवाडे मंडळ, धुळे' या नावाने पाठवावी.

अक्षरजुळणी : सौ. सीमा शिंत्रे, पुणे.

टीप : या नियतकालिकेतील लेखकांच्या विचारांशी मंडळ व शासन सहमत असेलच असे नाही.

अनुक्रमणिका

१. **भारतीय आदिवासी कविता**

- डॉ. रामचंद्र मोरेश्वर वासेकर ---------- ५

२. **'एकविसाव्या शतकातील मराठी कादंबरीतील कृषिजन संस्कृतीचे चित्रण'**

- १) कु. चंदा शंकर ढगे, २) डॉ. पदमाकर डिगांबर वानखडे ---------- ८

३. **मराठी आदिवासी साहित्य–एक आकलन**

- प्रा रमेश म धोटे ---------- १२

४. **डॉ. विद्याधर बन्सोड यांच्या कादंबऱ्या – एक परीक्षण**

- अरुण राऊत ---------- १६

५. **अकसिदीचे दाने – ग्रामीण जीवनाचे वास्तव दर्शन**

- १) कु. राखी अशोक मुधोळकर, २) डॉ. विलास आर खुणे ---------- २०

६. **कवयित्री बहिणाबाई यांच्या काव्यातील ग्राम्यदर्शन**

- १) प्रियंका मनोहर बगमारे, २) पदमाकर डिगांबर वानखडे ---------- २६

७. **द. ता. भोसले यांच्या ग्रामीण कथेतील भाषाशैली**

- १) अजिंक्य मोहनराव भांडारकर, २) डॉ. विजय एच. रेवतकर ---------- ३०

८. **नवयुगाची क्रांती ''इवान'' कवितासंग्रह**

- १) कु. विद्या हिरामण देठे, २) डॉ. राजकुमार मुसने ---------- ३५

९. **मराठी कवितेतील नवप्रवाह**

- डॉ.ममता राऊत ---------- ४१

१०. **'झिम्मा' : एक वाङ्मयीन मूल्यमापन**

- १) कु. भारती बालाजी गेडाम, २) डॉ. विलास आर. खुणे ---------- ४६

ISSN No. 2394-5990

मराठी कवितेतील नवप्रवाह

डॉ.ममता राऊत
जे. एम. पटेल कला, वाणिज्य व
विज्ञान महाविद्यालय, भंडारा
मो.नं.८६६८७१८१२७
mamtaraut74@gmail.com

नवकाव्य :

हा अर्वाचिन मराठी काव्याचा नवन्मेषाचा प्रवाह आहे. या प्रवाहात सर्वच दृष्टीकोनातून काव्याचे क्षितीज विस्तारले होते. द्वितीय महायुध्दानंतरच्या परिस्थितीत कमालीची उलथापालथ होऊ लागली. साम्राज्यवाद आणि भांडवलशाहीचे दुष्परीणाम जाणवू लागले. प्रचंड बेकारी दारिद्र्य वाढू लागली. मानवात नैराश्य व वैफल्य निर्माण झाले. भ्रष्टाचार वाढला, दहशतवादामुळे असुरक्षितता निर्माण झाली. स्पर्धेचे युग निर्माण होऊन स्वार्थीवृत्ती, संधीसाधूपणा वाढीस लागला होता व फूटीरतावादी चळवळी जोर धरु लागल्या होत्या.

अशा वातावरणात आशयाचा नवेपणा, अंतदृष्टिचा नवेपणा, वास्तविक जीवन दृष्टिकोन, जीवनातील शाश्वत प्रश्न, भावनानिष्ठ समतानता, नवी प्रतिमासृष्टी, अभिव्यक्ती नाविण्य इत्यादी नव्या जाणिवा, नवे आशय सर्वप्रथम बा.सी. मर्ढेकर यांच्या काव्यात प्रकट झाल्या. महायुध्दोत्तर परिस्थितीत बदलले सामाजिक वास्तविक संदर्भ डोळसपणे कुणी तपासले असतील तर मे मर्ढेकर होत. मराठी कवितेची खरी आंतरिक गरज ओळखून नवयुगाचे आव्हान मर्ढेकरांनी पेलवले. त्यांना राष्ट्रीय व आंतरराष्ट्रीय पातळीची वास्तविक जाणीव अनुभवली होती. त्यामुळे मर्ढेकरांना समाजातील भेसुर वास्तव काव्यात उतरवता आले. मर्ढेकर जीवनातील मुलभूत प्रश्नांना उत्कटतेने मांडतात. समाजकालीन वैफल्य व भयाण भिभत्सपणा ते रेखाटतात. भांडवलशाहीमुळे निर्माण झालेली अर्थशून्यता ते चित्रीत करतात. मर्ढेकरांचे नवे अनुभव, नवी काव्यभाषा, नव्या प्रतिमा, नवी शैली, नवे आशय-अभिव्यक्ती व त्याची प्रयोगशील वृत्ती या सर्व गुणवैशिष्ट्यामुळे मर्ढेकर नवकाव्याचे जनक ठरतात. खऱ्या अर्थाने नवकाव्याची खरी ओळख मर्ढेकरांच्या कवितेने करुन दिली. त्यामुळे केशवसुताप्रमाणेच मर्ढेकरांचेही हे युगप्रवर्तक कार्य मराठी कवितेत उत्तरोत्तर राहिल.

मर्ढेकरांचे समकालीन कवी शरदचंद्र मुक्तिबोध नवकाव्याची धूरा सांभाळणारे आशावादी कवी आहेत. काही प्रमाणात निराशावाद व्यक्त केला तर यांच्या अगदी उलट मुक्तिबोध आशावाद व्यक्त करतात. मुक्तिबोध मार्क्सवादी कवी असून त्यांची कविता सूर्ययुगाचा नवसंदेश घेऊन अवतरते. मुक्तिबोधाच्या काव्यजीवनाला मार्क्सवादाचा प्रभाव असल्यामुळे त्यांचा कवितेत समाजक्रांती आढळते. मुक्तिबोधाना मानवाच्या परिवर्तनाचा, शक्तीचा, उजेडाचा, आशावादाचा ध्यास लागला होता. म्हणून मुक्तिबोध लोक जीवनाशी व भोवतीच्या दु:खाशी समुहातील लाचारी, दु:ख यातनाशी नाते जोडतात व कवितेत क्रांतीचा मार्ग फुलवतात.

मराठी नवकवितेच्या प्रवाहात मुक्तिबोधाची कविता सूर्ययुगाशी नाते जपणारी पहिली कविता आहे. नवकाव्याची धूरा सांभाळणारे आणखी काही महत्त्वपूर्ण नवकवी झालेले आहेत. मर्ढेकर, मुक्तिबोध व पु.शि. रेगे यांनी नवकाव्याची जोमदार सुरुवात करुन दिली. मर्ढेकर मुक्तिबोधानी सामाजिक वास्तविक परिस्थितीची जाणीव करुन दिली. ही जाणीव पुढील नवकवीच्या पिढीत अधिकाधिक वृध्दिंगत झाली. विंदा करंदीकर, वसंत बापट, मंगेश पाडगावकर, सदानंद रेगे हे नवकाव्याचे दुसरे प्रवर्तक आहेत. यापैकी विंदा करंदीकर हे नवकाव्यातील सर्वाधिक प्रयोगशील कवी म्हणून करंदीकरांकडे बघितले जाते. ते मुक्तिबोधाया साम्यवादी परंपरेचे पाईक होते. त्यामुळे त्यांची कविता सभोवतालच्या दाहक वस्तुस्थितीची सतत जाणीव निर्माण करुन देते. आर्थिक विषमतेचे व वर्गसंघर्षाचे भेदक चित्रण करुन करंदीकर जागतिक व अर्थहीन मानवी वैशिष्ट्याचे रुप तितक्याच पोटतिडकीने स्पष्ट करुन देतात. करंदीकराची कविता स्वत:चे वेगळेपण जपत मराठी कवितेला एका साम्यवादी वळणावर घेवून जाते.

वसंत बापट यांच्या कवितेत नवकाव्याची तितकीशी लक्षणे आढळत नाही. त्यांची बहुतांश कविता छंदात्मक असून लावणी व शाहीरीचा बाज त्यांनी सांभाळला आहे. मात्र नव स्वच्छंदवाद व अभिजातवाद त्यांच्या कवितेची सकस बाजू आहे.

मंगेश पाडगावकर हे नवकाव्याच्या दुसऱ्या पिढीचे महत्वाचे कवी आहेत. बालकवी, बोरकर यांच्या निसर्ग जाणिवेची परंपरा पुढे नेणारे निसर्गकवी म्हणूनच त्यांची प्रतिमा मराठी कवितेत आहे. ते स्वत:ला निसर्गकवी म्हणूनच समजतात. त्यांनी तांबे कवीचाही वारसा पुढे नेला आणि नवजाणितेने गीतरचना व भावगीतरचना केली. ती मराठी कवितेत लक्षणीय ठरली आहे. याबरोबरच पाडगावकरांचे संवेदनशील मन, सामाजिक व्यथा-वेदनानी तडफडते. त्यांची कविता सामाजिक वास्तवाबरोबर निसर्ग प्रेमातही तेवढीच हरवून जाते. वेधक प्रतिमासृष्टीमुळे पाडगावकरांच्या कवितेचे मोल मराठी कवितेत आजही तेवढेच आहे.

नवकाव्याच्या दुसऱ्या प्रवाहात चाकोरीबाहेर कविता लिहीणारे कवी म्हणून सदानंद रेगे हे लक्षणीय आहेत. आशयानुभूतीचे वेगळेपण आणि मृत्यूगर्भ कविता यामुळे मराठी कवितेत सदानंद रेगे यांचे स्थान महत्वपूर्ण आहे. दु:खद प्रेमानुभव मृत्यूची स्त्रोत आणि एकाकीपणा हे त्यांच्या काव्यातील स्थायीभाव होय. दु:खाच्या सूरांनी भारावलेली कविता सदानंद रेगे यांनी लिहीली. त्यांची श्रावणगाणी म्हणजे वेदनेतून निसर्गाचा घेतलेला वेध आहे. मृत्यूचे चिंतन करणारा कवी म्हणून रेगे यांची मुद्रा मराठी कवितेत उमटली आहे.

१९६० चा प्रवाह मराठी काव्यप्रवाहात अनेक बाबींकडे लक्ष वेधून घेणारा आहे. या कालखंडात अनेक चळवळीचे आत्मभान जागृत होऊन उदय झाला. अनेक परिवर्तने होऊ लागली. वसाहतदावाचे दुष्परिणाम जाणवू लागले. गरीब-श्रीमंत यातील तफावत वाढली. शहर फुगू लागली तर खेडी ओस पडत चालली. फाळणीचे दुष्परिणामात होऊ लागले. बेकारी, लाचारी, गुन्हेगारी वाढीस लागून शिक्षणाचे अवमुल्यन होत होते. या सर्वांचे परिणाम राजकीय, सामाजिक, धार्मिक व साहित्यिक क्षेत्रातही उमटू लागले. या विघटनकारी घडामोडी मराठी कवितेतील जाणत्या विचारवंताच्या आणि द्रष्टया कलावंताच्या चिंतनाचा भाग बनल्या होत्या.

मार्क्सवादी प्रवाह :

साठोत्तरी मराठी कवितेत विद्रोहाची अनेक रुपे आढळतात. वर्गविषमता, वर्गसंघर्ष, प्रत्यक्ष क्रांती मूल्यसिध्दांताचे विचार, जीवनपरिवर्तनाचे सिध्दांत अशा व्यक्तिवादावर व सामय्वादी विचारावर आधारलेला मार्क्सवादी प्रवाह साठोत्तरी कवितेत उदयास आला. सर्वप्रथम शरदचंद्र मुक्तिबोध, करंदीकर, नारायण सुर्वे यांच्या कवितेवर मार्क्सवादाचा प्रभाव आहे. यानंतर साम्यवादाची प्रखरता शाहीर अमर शेख यांच्या शाहीरी वाङमयात जाणवते. दारिद्र्याचे भयभीत रुप, विषणता, विस्कळीत समाजजीवनाची विष्पण्ण जाणीव, वर्गविहीन समाजरचनेचे स्वप्न इत्यादी जाणीव त्यांच्या काव्यात सर्वत्र दिसतात. अनुभव संपन्नता व कलावंताचा कलंदरपणा अंगात भिनलेला असूनही अमर शेखच्या वाटयाला उपेक्षाच आली. ही मराठी कवितेची शोकांतिकाच आहे. याला कारणीभूत म्हणजे सांप्रदायिक वातावरण.

शाहीर अमर शेख प्रमाणेच अण्णाभाऊ साठे यांच्या कवितेवर मार्क्सवादी प्रभाव आहे. झूंझार व्यक्तिमत्व असलेले अण्णाभाऊ साठे यांची कविता वास्तववादी दृष्टिकोन स्वीकारते, दलित, शोषित, कष्टकरी जीवनाचे प्रतिनिधीत्व करते. तथाकथीत ब्राम्हणी संस्कृतीवर तुटून पडते. जातीभेद व वर्ग जाणीवेची दाहक वेदना व वास्तव त्यांच्या कवितेतून प्रखरतेने प्रकट होते. त्यांच्या वाटयाला उपेक्षा येवूनही ते लोकशाहीर म्हणून मराठी काव्य क्षेत्रात नावारुपाला आले.

दलित प्रवाह :

साठोत्तरी कवितेत वर्ग भेदाची, वर्ग द्वेषाची संतप्त जाणीव व्यक्त करणारा व श्रमिकाच्या अधिकार हक्कासाठी संघर्ष करणारा मार्क्सवादी प्रवाह निर्माण झाल त्याच समरस असणारा दलित कवीचा व्यथागर्भ ज्वलंत जाणिवा व्यक्त करणारा दलित प्रवाह उदयास आला. दलितांच्या वाटयाला आलेल्या पिढयान-पिढयाचा रोष, अमानुषतेची जाणीव, गावकुसाबाहेर उकीरडयाचे जीणे, जाती द्वेषाची हिनभावना, केवळ उपहास, मानवी अधिकार हक्कापासून वंचित, तुच्छता अवहेलना, वाटयाला येणे, शिक्षणापासून वंचित हया सर्व उरी सलत असलेल्या वेदनांचा स्फोट डॉ.बाबासाहेब आंबेडकरांच्या प्रेरणेतून जागृत होऊन त्यांचा ज्वलंत आविष्कार व विद्रोह दलित कविंच्या रुपात बाहेर येतो.

या प्रवाहात दलित कविचे आत्मभान जागृत होऊन मोठी चळवळ उदयाला आली. आणि त्यांच्या वाटयाला आलेले तळागाळातील अनुभवविश्व ते साकारु लागले. यात प्रामुख्याने नामदेव ढसाळ, वामन निंबाळकर, दया पवार, प्रल्हाद चेंदवणकर, यशवंत मनोहर, फ.मु. शिंदे, अर्जुन डांगळे, केशव मेश्राम, त्रयंबक सपकाळे हया कवींचा प्रामुख्याने उल्लेख करावा लागेल.

दलित चळवळीतील कवींच्या मागे फुले, शाहू, आंबेडकरांची प्रेरणा होती. तर पुढे केशवसुत सुर्वे यांचे आदर्श होते. त्यामुळे ही चळवळ म्हणजे सूर्यकुलाचा जाहीरनामाच होती. दलित कवितेच्या रुपानं मराठी कवितेला सूर्यगर्जनेची कविता मिळाली. ही साहित्यिक चळवळ नसून एकूणच सामाजिक शोषणाच्या उद्रेकाची अभिव्यक्ती होती.

१९६० नंतरच्या कवितेत या बदलत्या समाजवादाचा नव्या वाङ् मयीन प्रेरणाचा खोलवर परिणाम दिसून येतो. देशी संस्कृतीपासून

ISSN No. 2394-5990

दुरावलेली मराठी कविता नवनव्या प्रतिमामध्येच अडकून राहते की काय ? अशी भिती निर्माण झाली. ही सर्व परिस्थितीची जाणीव असलेला, साठोत्तरी कवितेच्या नव्या जाणिवा घेऊन नवा प्रवाह उदयास आला. हा प्रवाह कुण्या कवीच्या नावाने ओळखला जात नाही. तर लघुनियतकालिकांचा प्रवाह (Little Magazine) हा प्रवाह आहे. लघुनियतकालिकांमधून कविला लेखन करणारी ही चळवळ प्रामुख्याने प्रस्थापितविरोधी चळवळ म्हणून उदयास आली असून सामाजिक व साहित्यिक देशी परंपरेशी नाते जोडणार चळवळ आहे. नव्याने निर्माण होणाऱ्या चौकट मोडणारी ही चळवळ होती. लघुनियतकालिकांमधून लेखन करणाऱ्या या कवीच्या काव्यातून व्यवस्थेविरुध्द प्रचंड चीड, संताप व्यक्त करीत होती. परात्मतेची भावना, निराशा तर सामाजिक वाङमयीन वास्तव प्रखरतेने प्रकट करीत होती.

अस्तित्ववादी व महानगरीय प्रवाह :

मर्ढेकरानंतर दिलीप चित्रे यांनी मर्ढेकरी परंपरेला एक नवे आयाम मिळवून दिले. मर्ढेकरांची क्रांती, सौंदर्यवादी भूमिका आणि समकालीन अस्तित्ववाद याचे सम्यक दर्शन चित्रे यांच्या कवितेत घडते. सुरुवातीला मर्ढेकरी प्रभावातून निर्माण झालेली दिलीप चित्रे यांची कविता नंतर मात्र मुक्त होवून अस्तित्व शोधाकडे निघाली. जीवनविषयक दृष्टिकोन मांडणारी चित्रे यांची कविता माणसाच्या मुलभूत प्रश्नासाठी विद्रोह करीत असते. मर्ढेकर, करंदीकर यांच्यानंतर महानगरीय संवेदना चित्रे यांच्या कवितेत प्रामुख्याने व्यक्त झाली आहे. स्वानुभवाच्या आधाराने मुंबईतील अस्तित्वाचे ते वेध घेतात.

दिलीप चित्रे यांनी मानवी अस्तित्ववादाचा प्रश्न निर्माण केला. याचा प्रभाव अनेक कवीवर झालेला आढळतो. वसंत आबाजी डहाके यांचीही कविता अस्तित्ववादाचा जोरदार पुरस्कार करते. आत्मजाणीवेकडून सामाजिक जाणीवेपाशी पोहचलेली डहाके यांची कविता व्यवस्थेमुळे मानवी व्यक्तिमत्वाला आलेल्या अवकळेचे, क्षुद्रत्वाचे, हीनगंडाचे दर्शन ते घडवतात. वसाहतवादाचे परीणाम अधिक तीव्रपणे डहाकेच्या कवितेत आढळून येतात. शहर-खेडे यांचे विदारक चित्रण आणि वर्गजाणीव, शहरातील दहशतवाद व मानवाचा सुप्त संघर्ष हे सर्व डहाके यांच्या जाणिवांचे प्रमुख केंद्रे आहेत.

साठोत्तरी कवितेच्या प्रवाहात वसंत आबाजी डहाके यांचे विशेष स्थान आहे. तर दिलीप चित्रे हे साठोत्तरी कविता व लिटील मॅगझीन या प्रवाहाला जोडणारा दुवा आहे. अस्तित्ववादी जीवनदर्शनाचा प्रभाव आणि मानवी जीवनातील अर्थशून्यता व पोकळी यांचे प्रभावी दर्शन चित्रे आणि डहाके यांच्या कवितेतून घडते.

दिलीप चित्रे आणि वसंत आबाजी डहाके यांच्या काव्याचे स्वरुप लघुनियतकालिकामध्ये लेखन करणाऱ्या कवितेपेक्षा थोडे भिन्न होते. प्रस्थापितविरुध्द सर्वस्वी विद्रोही भूमिका या कविची नव्हती. लघुनियतकालिकांद्वारे उदयास आलेल्या या बंडखोर चळवळीत प्रामुख्याने अरुण कोलटकर, बंडू वझे, भालचंद्र नेमाडे, अशोक शहाणे, चंद्रकांत खोत, सतीश काळशेकर, वसंत गुर्जर, प्रदीप नेरुरकर, राजा ढाले, नामदेव ढसाळ, धुरी, मनोहर ओक, तुलसी परब, चंद्रकात पाटील आदि कवी नव्या जाणिवा व नव्या शैलीद्वारे काव्यलेखन करीत होती.

अरुण कोलटकर हे महत्वाचे कवी आहेत. नवकवितेपक्षा अगदी भिन्न स्वरुपाची नवे आशय, नवे तंत्रे अवगत करुन या कवितेत आपले वेगळे कवितेचे स्वरुप साकार केले. महानगरीय संवेदनेचा विद्रोही सूर त्यांच्या काव्यातून प्रकटला आहे. ही महानगरीय संवेदना मर्ढेकरांच्या कवितेपेक्षा अगदी भिन्न आहे. यात समकालीन सद्य जाणिवा आहेत. परंपराभिमान व मानवतावाद यांचा सरळ विरोध कोल्टटकरांची कविता करते.

यंत्रयुगामुळे निर्माण झालेल्या परिस्थितीत बेकारी, गुन्हेगारी मध्यमवर्गीय संवेदना आत्मविनाशाकडे जाणारी प्रवृत्ती, अस्तित्वहीन मूल्यरहित मानवी जीवन, धंदेवाल्यांचा होणारा उपहास हे कोल्हटकरांच्या कवितेचे महत्वाची केंद्रे होत. शहरातील गर्दीचे व तिथल्या उपहासगर्भ जीवनाचे ते जीवंत चित्रण करते व तथाकथित प्रस्थापितावरुध्द विद्रोह करते.

देशीय संस्कृतीला महत्व देणारे निर्भीड वाणीसाठी प्रसिध्द असलेले भालचंद्र नेमाडे हे लघुनियतकालिकात लिहीणारे अग्रेसर कवी आहे. त्यांनी अनुभवलेले ग्रामीण शेतकरी जीवनाची दाहक चटके खेडयातून शहराकडे जाण्याचा कडवट अनुभव, वाटयाला आलेला संघर्ष यामुळे कवितेत केवळ वास्तवानुभूती प्रकट झाली आहे.

जागतिकीकरणामुळे निर्माण झालेल्या भयाण समस्या, मानवी जीवनाची निरर्थकता, महानगरीय संवेदनशिल चिंतनशीलता याद्वारे त्यांच्या कवितेत भावानुभूतीचे दर्शन घडते. भालचंद्र नेमाडे अभिव्यक्ती स्वातंत्र्यप्रिय कवी असल्यामुळे जीवनातील विसंगतीचे ते उपहास गर्भ शब्दांत आपल्या तीव्र भावना व्यक्त करीत असतात. हे त्यांच्या व्यक्तिमत्वाचे लक्षणीय पैलू होय. स्त्रीकडे बघण्याचा स्वतंत्र नैतीक दृष्टिकोन व स्त्री चित्रणाचे महात्म त्यांच्या कवितेत सतत आढळते. खानदेशी बोलीच्या प्रभावामुळे त्यांच्या काही कवितात लोकगीत व ओव्यांसाठी केलेल्या लकबी भाषिक प्रयोग हे त्यांच्या कवितेचे विशेष अंग आहे.

एकीकडे बंडखोरवृत्ती बाळगणारी, नव्या जीवन जाणिवांना स्वीकारणारी, काहीतरी नवे करण्याची महत्वाकांक्षा बाळगणारी, प्रस्थापितांना न जुमानणारी, लघुनियतकालिकांतील कविता फुलत होती. तर दुसरीकडे स्वच्छंदतावादाच्या मुळ उद्दिष्टांना स्वीकारुन सौंदर्यवादी भावलेखन करणारी पिढी आले अनुभवविश्व साकारीत होती. भावतरल व स्पंदनशील व्यक्तिमत्व असलेले हया कवीची काव्यभाषा लयदार असते. सौंदर्याची विविध रुपे न्याहाळणे हया कवीचे छंद असते.

सौंदर्यवादी भावकाव्याचा प्रवाह :

साठोत्तरी मराठी काव्याच्या प्रवाहातील या सौंदर्यवादी भावकाव्याच्या वळणामील पहिल्या पिढीचे प्रमुख कवी म्हणजे मंगेश पाडगावकरांचाही एक समर्थ भावकवी म्हणून याही पिढीत महत्वाचे स्थान आहे. मंगेश पाडगावकरानंतर आपले वेगळेपणाने भावलेखन करणारे सौंदर्यवादी वळणातील ना.धो.महानोर, ग्रेस, म.म. देशपांडे, मधुकर केचे आणि गुरुनाथ धुरी हे प्रमुख कवी आहेत. ना.धो. महानोरांनी लिहीलेल्या 'रानातील कविता' म्हणजे मध्यमवर्गीय जीवनाचा सौंदर्य आविष्कार होय. त्यांच्या 'रानातील कविता' मराठी कवितेला लाभलेली अस्सल व जीवंत कलाकृती आहे. यातील लोकगीतांच्या नैसर्गिक लयीमुळे त्यांनी मध्यमवर्गीय रसिकांना आकर्षित केले. महानोरांच्या कवितेत जणू निसर्ग आणि रान एकरुप होतात. गावरान शृंगाराचे व स्त्रियांच्या लावण्याच्या आशयधन भावछटा महानोरांनी मनमोहक पध्दतीने रंगविले आहे. ना.धो. महानोरांनी रचलेली रानातील लोकगीतांची लयदार घाट मराठी कवितेला लाभलेली अपूर्व देणगी आहे.

मधुकर केचे यांनी आध्यात्माचा पिंड सांभाळत आधुनिक दृष्टिकोन जोपासला आहे. तसेच पाहिले तर मधुकर केचे यांची कविता आधुनिक जीवनाच्या वास्तवापासून आणि संस्कारापासून दूरच राहते. छंदोबध्द रचना अर्थपूर्ण शब्दकळा व नाविण्यपूर्व प्रतिमासृष्टी यामुळे मधुकर केचे यांच्या कवितेला नवस्वच्छंदतावादी प्रवाहात वेगळे स्थान प्राप्त झाले आहे. याच प्रवाहात म.म. देशपांडे कृतज्ञताभाव व्यक्त करणारे समर्थ कवी म्हणून त्यांची ओळख आहे. त्यांनी त्यांच्या भावानुभूती व काव्यानुभूती निसर्ग आणि प्रेम याद्वारेच व्यक्त केलेल्या आहेत. भावानुभव व्यक्त करणारी त्यांची सहज लय त्यांच्या कवितेचे सौंदर्य खुलवित असते.

सौंदर्यवादी भावकाव्याचा प्रवाहात आपले आगळे व वेगळेपण जपणारे कवी म्हणून कवी ग्रेस महत्वपूर्ण स्थान आहे. त्यांच्या 'संध्याकाळच्या कविता' मुळे तर ते गूढवादी संज्ञाप्रवाही कवी म्हणून नावाजले गेले. प्रेम आणि निसर्ग जाणीव दु:खानुभावातून प्रकट करण्याची ग्रेसांची तऱ्हा निराळी आहे. दु:ख जणू त्यांना खूप काही शिकवून जातो आणि संध्याकाळ व्याकुळ करते. ही जाणीव सतत त्यांच्या काव्याद्वारे येते.

नादसुरांची लयबध्द मांडणी, संज्ञाप्रवाही शैली, गुढता कायम ठेवणाऱ्या प्रतिमा, धुक्यातले स्वप्नभास, दु:ख, उदासी, एकाकीपण व मरणाचे अतुट स्मरण, दु:खानुभवातूनच व्यक्त होणारा बोध, शिल्पसौंदर्य, कल्पनाविलास या अमुर्त जाणिवा व्यक्त करणारा ग्रेसासारखा कवी मराठी काव्यसृष्टीत कुणी झालेला नाही. ग्रेसानी संपूर्णपणे आपले वेगळेपण जपले आहे. नाटयमय शब्दकळा मनात रुंजी घालणाऱ्या भावनाची लय, या वेगळया प्रतिमा सामर्थ्यांने ग्रेसांनी त्यांच्या स्मरण अवस्थातील कवितांनी हा प्रवास समृध्दच केला.

१९८० च्या दशकातील सौंदर्यवादी भावकवीच्या प्रवाहात आपली रोमँटीक प्रवृत्तीची लक्षणीय कविता लिहीणारे आत्मलखी व नादलययुक्त कविता कवी आरती प्रभु, सुरेश भट, शंकर रामाणी, तुळशीराम काजे, गजमल माळी, श्रीधर शनवारे, ना.धो. महानोर, आनंद यादव, उ.रा. गिरी, विठ्ठल वाघ, सुधाकर गायधनी, मराठी काव्यसृष्टीला आपल्या वेगळेपणाने समृध्द करणारे महत्वपूर्ण कवी आहेत.

आरती प्रभु हे भावकवीच्या सौंदर्यवादी वळणातील प्रमुख कवी आहेत. त्यांच्या कवितेमधून व्याकुळ भावाचे दर्शन घडते. सुरुवातीला वेदनेभोवती घोटाळणारी त्यांची कविता नंतर प्रेमगीतात मात्र शांत, गाढ प्रीतीचे पत्नीविषयक प्रेमगीतातून शृंगार उत्कट प्रीतीचे दर्शन घडते. निसर्ग त्यांच्या संपूर्ण कवितेत वावरत असतो. असाधारण गेयता व वेधक शब्दरचना यामुळे आरती प्रभू यांच्या कवितेचे विशेष स्थान आहे.

समकालीन समाजाचे दु:ख उरी जपणारी आणि माणसाचे माणूसपण शोधणारी कविता म्हणजे गझलसम्राट सुरेश भट यांची कविता आहे. भटांच्या कवितेवर रसिकांनी भरभरुन प्रेम केले आहे. बहुरसिकप्रिय सुरेश भट हे सामाजिक भान जपणारे कवी आहेत. वेदनेतून जन्माला येणारी सुरेश भटांची कविता सहजच दु:खावर मात करते आणि आशावाद शोधते आणि सामाजिक अन्यायाविरुध्द झुंझार बंड करते. सर्वसामान्य मराठी माणसाला रुचेल अशी अर्थवाही, लाघवी बोली भाषा व ओथंबलेली राष्ट्रभक्ती, प्रयोगशील शैली, विलक्षण आकर्षित करणारी तरल प्रेमभावना यामुळे आजही सुरेश भटांच्या कविता मराठी मनाला अधिक जवळच्या आहेत.

तांब्याच्या गेयतेशी व कुसुमाग्रजांच्या सामाजिक क्रांतीशी त्यांनी नाते जोडलेले आहे. त्यामुळे सुरेश भट सोंदर्यवादी भाव कवीच्या प्रवाहातील प्रचलीत गीतकार आहेत. त्यांच्या भावगीताला लाभलेली नाद-लय-ताल-भावसौंदर्य सहजजेने

ISSN No. 2394-5990

आपलेसे करुन घेणारे आहे. मराठीत मगझलफ हा काव्यप्रकार सुरेश भटांनीच समृध्द व लोकप्रिय केला आहे. त्यामुळे त्यांना गझलसम्राट म्हणून ओळखले जाते. त्यांच्या गझला आजही मनावर राज करतात. या अपार लोकप्रियतेमुळे भट पुढच्या पिढीचे प्रेरणास्थान राहिले आहेत. त्यामुळे मराठी काव्यक्षेत्राला सुरेश भटांची ही मौलिक व समृध्द परंपरा लाभली आहे. याच प्रवाहात तुळशीराम काजे यांची कविता वऱ्हाडी मातीच्या शेतकऱ्यांचे वेदना साकारते. आरंभी उदास व व्याकुळ असणारी त्यांची कविता शेवटी परमेश्वराची आठवण करते. जुन्याच वृत्तीत नवीन आशयाची निर्मिती करुन वेदनेचा शोध घेणारी यांची कविता आहे.

गजमल माळी यांच्या कवितेत सामाजिक व्यथा, वेदनेचे दर्शन घडते. यासोबतच त्या भागात राहणाऱ्या शेतकऱ्यांचे शोषण, कुटूंबाची होणारी दैनावस्था, निसर्गाचे रौंद्ररुप व विषम परिस्थितीचे हृदयद्रावक चित्रण माळी यांची कविता करते. त्यांनी लिहीलेली दीर्घकविता मानवी मूल्यांचा शोध घेते व मानवतावादी दृष्टिकोन प्रस्थापित करते.

उ.रा. गिरी हे तांबे, बोरकर व पाडगावकर यांच्या परंपरेशी नाते जोडणारे कवी आहेत. कवितेचे अनेक वळण आलेत परंतु गिरी यांची कविता त्यांच्या मुख्य स्वरुपापासून दूर गेली नाही. त्यांच्या प्रेम आणि निसर्ग कवितातून ते सामान्य माणसाच्या भावजाणिवा व्यक्त करतात. त्यांच्या काव्याची विशिष्टता म्हणजे त्यांच्या गीताना लाभलेली नैसर्गिक संगीतानुकूलता व नादयुक्तलय होय. उ.रा. गिरी जेवढे गीतावर व संगीतावर प्रेम करत राहिले, तेवढेच ते त्यांच्या कवितेत सौंदर्यप्रेम फुलवत राहिले. आपल्या जगण्याला निसर्गामुळे सौंदर्य प्राप्त झाले अशी त्यांची श्रध्दा असल्यामुळे निसर्ग त्यांना अधिक जवळचा वाटतो. उ.रा. गिरी यांची कविता अनोखा निसर्गप्रेम, तटस्थता व संगीतानुकूलता यामुळे सौंदर्यवादी भावकविच्या प्रवाहात महत्वाचे स्थान निर्माण केलेले आहे.

वऱ्हाडी संस्कृतीशी तिथल्या शेती-मातीशी जीवाभावाचे नाते जपणारी विठ्ठल वाघ यांची कविता लक्षणीय ठरली आहे. वऱ्हाडातील अस्सल जातीवंत निसर्ग पहिल्या प्रथम विठ्ठल वाघांच्याच कवितेत प्रकट झालेला आहे. आकर्षित करुन घेणारी वऱ्हाडी बोलीची लय, काळया मातीची ओढ, शेतकऱ्यांचे कष्ट व अस्सल वैदर्भीय प्रतिमासृष्टी यामुळे विठ्ठल वाघाच्या कवितेने या प्रवाहात आपला ठसा उमटविला आहे.

१९६० नंतरच्या नव्या जाणिवेची, नव्या आधुनिकता व्यक्त करणाऱ्या कवी सुधाकर गायधनी यांचे लक्षणीय स्थान आहे. ही कविता प्रतिमांचा अतिरेक टाळते. समकालीन जीवन प्रवाहाला स्पर्श करीत कवितेचे जुने वाङमयीन मूल्य या कवितेने नाकारले आहे. ती प्रामाणिकपणे जीवन जाणिवा व्यक्त करीत होती. गुळगुळीत शब्दांना तीने बाद केले. ही संपूर्ण वैशिष्टे सुधाकर गायधनी यांच्या ही कवितेत प्रामुख्याने आढळतात.

सुधाकर गायधनी यांची कविता सामाजिक वास्तव प्रकट करतांना भोगवादी सत्तालोलुप वृत्तीवर तुटून पडते. राजकीय जीवघेणी स्पर्धा व सामान्य माणसांचे जीवन याचे चित्रण करते. एक चिंतनशीलता यांच्या कवितेला प्राप्त झाली आहे. या दृष्टीने त्यांची दीर्घ कविता लक्षवेधक आहे.

८० च्या दशकात जागतिकीकरणाचा प्रचंड प्रभाव सामाजावर पडलेला होता. ग्लोबल व्हिलेजमुळे कृषी अर्थव्यवस्था विस्कळीत झाली होती. बेरोजगारीमुळे खेडयाचे अंतर्बाहय विश्व बदलले होते. ग्रामीण जीवनाचे भकास व उदास रुप दिसत होते. राजकीय नेत्यांची मक्तेदारी वाढत होती. भांडवलदारी व्यवस्थेला बळकटी आली होती. कंत्राटदार, ठेकेदार शेतकऱ्यांच्या टाळूवरच लोणी खात होती. जागतिकरणात अस्सल खेडी हरवली होती. त्याबरोबरच माणसं व माणसाची भाषाही बदलली होती. महागाई कौंटुबिक कलह, दुष्काळ, शेतमालाचा घसरता भाव, शिक्षणाच्या समस्या, जाती धर्माचे कलह, गटागटाच घाणेरडं राजकारण, ढोंगी बुवा-बाबांचे अश्लील राजकारण इत्यादी सामाजिक आणि सांस्कृतिक मूल्यांचा ऱ्हास होत चालला होता. अशा वातावरणात मराठी कविता आकारास येत होती व तिचे दालन समृध्द होत होते.

संदर्भ सूची :

१) यशवंत मनोहर : मराठी कविता आणि आधुनिकता, आंबेडकर धम्म प्रकाशन, नागपूर-१९९३

२) ठकार निशिकांत: मराठी कविता स्वरुप आणि विवेचन, स्वाध्याय महाविद्यालय प्रकाशन, नागपूर

३) मल्हार मनोहर - विदर्भ जनजागर, दिवाळी अंक (अतिथी संपादक) दि.०२.१०.२०००

४) सराडकर बबन : भेट मान्यवरांची , तरुण भारत

५) आकोटकर सुरेश : भावचित्रे , लोकत दि. ०१.१२.१९९७

६) जाधव रा.ग. : कविता आणि रसिकता, परिमल प्रकाशन औरंगाबाद

७) सावदेकर आशा : कविता विदर्भाची, विदर्भ साहित्य संघ प्रकाशन नागपूर

८) हेर्लेकर सुलभा : नवे वाङमय नवे विचार, तरुण भारत नागपूर

■■■

Gondia Education Society's

J. M. PATEL ARTS, COMMERCE & SCIENCE COLLEGE

BHANDARA – 441 904 (M.S.)

● Re-accredited 'B' Grade by NAAC ● Awarded 'College with Potential for Excellence' status (Phase II) by UGC

● R.T.M. Nagpur University recognized 'Centre for Higher Learning & Research'

● Phone No.07184 – 252364, 256883 (R) 252288 **Fax :** 07184 -253268 **Email :** principaljmpc@rediffmail.com **website :** www.jmpatelcollege.com

CRITERION – III

RESEARCH, INNOVATION AND EXTENSION

3.3 RESEARCH PUBLICATIONS AND AWARDS

3.3.1 Research Paper

TRANSLATED COPY

Title of Research Paper:	**Emerging Trends in Marathi Poems (Marathi Kavitetil Navpravaaha:मराठी कवितेतील नवप्रवाह)**
Author:	**Dr. Mamata Raut**
Department:	**Marathi**
Affiliated College:	**J. M. Patel Arts, Commerce & Science College, Bhandara**
Name of Journal:	**Sanshodhak (UGC CARE Listed)**
Volume & Year:	**Volume-57 & March - 2024**
Page Number:	**41 to 45**
ISSN Number:	**2394-5990**

J.M. PATEL ARTS, COMM. & SCI. COLLEGE ★ BHANDARA ★

Principal
J.M. Patel Arts, Commerce
& Science College, Bhandara

UGC-CARE List

You searched for "**2394-5990**". Total Journals : **1**

Search:

Sr.No.	Journal Title	Publisher	ISSN	E-ISSN	UGC-CARE coverage years	Details
1	Sanshodhak (print only)	Itihasacharya V. K. Rajwade Sanshodhan Mandal	2394-5990	NA	from April-2021 to July-2024	Discontinued from July 2024

Showing 1 to 1 of 1 entries

Previous 1 Next

Copyright © 2024 Savitribai Phule Pune University. All rights reserved. | Disclaimer

Spectroscopic study of ^{40}K

Rozina Rahaman,[1] Abhijit Bisoi,[1,*] Ananya Das,[2] Y. Sapkota,[3] Arkabrata Gupta,[1] S. Ray,[4] S. Sarkar,[1] Yashraj,[5] A. Sharma,[6] Bharti Rohila,[7] I. Ahmed,[5] Kaushik Katre,[5] S. Dutt,[5] S. Kumar,[5] R. P. Singh,[5] R. Kumar,[5] and S. Muralithar[5]

[1]*Indian Institute of Engineering Science and Technology, Shibpur, Howrah 711103, India*
[2]*Dream Institute of Technology, Samali, Kolkata 700104, India*
[3]*Assam Don Bosco University, Tapesia Campus, Sonapur, Assam 782402, India*
[4]*Amity Institute of Nuclear Science and Technology, Noida, Uttar Pradesh 201313, India*
[5]*Inter-University Accelerator Centre, New Delhi 110067, India*
[6]*Department of Physics, Himachal Pradesh University, Shimla, Himachal Pradesh 171005, India*
[7]*Department of Physics, Panjab University, Chandigarh 160014, India*

(Received 31 August 2023; revised 21 December 2023; accepted 19 January 2024; published 15 February 2024)

High spin states of ^{40}K populated through the ^{27}Al(^{19}F, αnp)^{40}K reaction at 68 MeV beam energy were studied using the Indian National Gamma Array (INGA) facility. Six new levels and fourteen new transitions were added to the existing level scheme. The spins and parities of most of the levels were assigned, modified, or confirmed from $R_{\rm DCO}$, $R_{\rm ADO}$, and linear polarization measurements. The multipole mixing ratios (δ) for most of the transitions were measured. Large-basis shell-model calculations were performed to understand the microscopic origin of the levels. Different particle restrictions in *sd* and *pf* shell orbitals were used to explain the experimental results.

DOI: 10.1103/PhysRevC.109.024318

I. INTRODUCTION

Nuclei in the neighborhood of the doubly closed $N = Z = 20$ region generally show the characteristics of spherical single-particle excitations [1] and their excitation spectra are well explained by the spherical shell model [2–9]. However, in the Nilsson diagram, the low Ω orbitals from the *pf* shell, especially for $1f_{7/2}$, are sharply downsloping for increasing deformation. Therefore, one may expect deformed or superdeformed structures with multihole multiparticle configurations in the *sd* shell nuclei. The advancement of detection and data acquisition systems made it possible to study the spectroscopic properties of light nuclei at high spins. As a result, several deformed, even superdeformed (SD) bands have been observed in nuclei around ^{40}Ca, which has generated new interest in this mass region. Gerace and Green *et al.* [10] explained in their early work about the low-lying levels of ^{40}Ca as a mixture of spherical and deformed states formed by raising particles from the *sd* to the *pf* shell. Later, a superdeformed (SD) band was identified by Ideguchi *et al.* in ^{40}Ca, which is generated by 8p-8h excitation [11]. A weakly deformed ground-state band and highly deformed slightly triaxial sideband in ^{42}Ca were reported in Ref. [12]. SD bands were identified also in a few Ar isotopes, viz. ^{36}Ar [13], ^{38}Ar [14], and ^{40}Ar [15,16]. The origin of the observed SD band in ^{36}Ar was explained by the $(s_{1/2}d_{3/2})^4(pf)^4$ configuration [13]. Shell-model calculation shows that the band in ^{38}Ar was generated from 4p-6h excitations [14]. Similarly, for ^{40}Ar, the origin of the SD band was explained by the mixing of different *m*p-*m*h ($m = 0, 2, 4$) configurations [15,16]. Therefore, this region gives a unique opportunity to investigate experimentally the interplay between single-particle and collective modes of excitations and interpret them theoretically by using microscopic large-basis shell-model calculations.

^{40}K is an odd-odd ($N = 21$, $Z = 19$) nucleus and lies in the lower *pf* shell. In the recent past, we investigated the high-spin structure of a few upper *sd* shell nuclei, viz., ^{33}S [5], ^{34}Cl [6], ^{35}Cl [7], ^{37}Ar [8], and ^{38}K [9]. The low-lying states of these nuclei are primarily generated from single-particle excitations. However, at higher excitation energy, the signature of collective excitation has been found. ^{40}K is the isobaric partner nucleus of ^{40}Ar and ^{40}Ca where the existence of collectivity in terms of deformed and superdeformed bands has already been reported [11,15,16]. So, one may also expect collective excitations at higher excitation energy in ^{40}K, generated from multiparticle multihole excitations.

The ^{40}K nucleus was previously studied by Soderstrom *et al.* [17] through heavy-ion reactions. They extended the level scheme of ^{40}K up to 8 MeV by adding a few new levels and γ's. The spin and parity of all the newly added levels up to 7 MeV were tentative. They assigned them based on the comparison of the branching ratios to the Weisskopf estimates. They added three more levels above 7 MeV but their spins and parities were not assigned. Our primary motivation is, therefore, to investigate the high-spin structure of ^{40}K and search for collective excitations at high excitation energy in ^{40}K. Our preliminary work on ^{40}K was already reported in Ref. [18].

*abhijitbisoi@physics.iiests.ac.in

 ©2024 American Physical Society

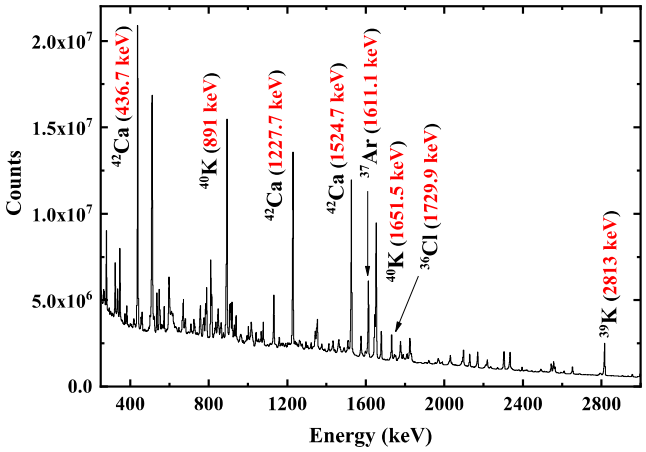


FIG. 1. A total projection spectrum of γ rays emitted from different nuclei populated in the present experiment.

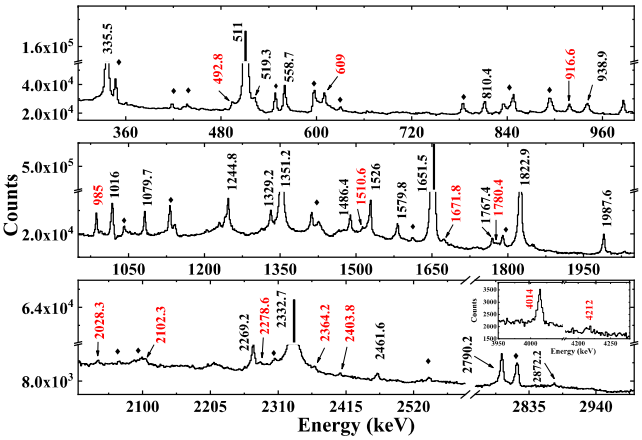


FIG. 2. Background subtracted coincidence spectrum obtained by putting a gate on the 891 keV transition. Newly observed transitions are shown by red color. Transitions marked with ♦ are from contaminants.

II. EXPERIMENTAL DETAILS AND DATA ANALYSIS

High-spin states in ^{40}K were populated through the ^{27}Al(^{19}F, αnp)^{40}K reaction with a 68 MeV ^{19}F beam. The ^{19}F beam was provided by the 15UD Pelletron accelerator at the Inter-University Accelerator Centre (IUAC), New Delhi. The 0.43 mg/cm^2 thick ^{27}Al target was evaporated on 11.4 mg/cm^2 Au backing. A multidetector array (INGA setup), comprising 12 Compton suppressed clover detectors at the time of experiment, was used to detect the γ rays. These twelve detectors were mounted at four different angles, i.e., 148° (4), 90°(4), 57°(1), and 32°(3) with respect to the beam axis. The relevant details of the experimental setup are discussed in Ref. [19]. About 10^8 twofold γ-γ coincidence events were recorded in list mode. The data sorting program, NIASMARS [20], developed at IUAC, was used to generate angle-independent symmetric and angle-dependent asymmetric γ-γ matrices, which were analyzed by INGASORT [21].

Usually, the energy calibration of the clover detectors is performed with ^{152}Eu and ^{66}Ga radioactive sources. The maximum energy emitted from the ^{152}Eu source is 1408 keV. Hence, the ^{66}Ga source, which has γ rays of energies in the range of 833 to 4806 keV, is used for high-energy calibration. Since we have transition energies more than 1.5 MeV, the ^{66}Ga source was prepared through the ^{51}V(^{19}F, $3np$)^{66}Ga reaction at 68 MeV in the same experimental setup. But, ^{66}Ga was not used for energy calibration because we observed energy shifts in a few runs during the experiment. As a result, we did energy calibration of each of the files of all the runs individually using the online γ's, ranging from 300 to 4000 keV. The^{152}Eu source was used for initial energy calibration only. The relative efficiency calibrations of the clovers were performed with ^{152}Eu and ^{66}Ga radioactive sources.

The level scheme of ^{40}K was studied based on the coincidence relationship, relative intensities, the ratio of directional correlation ($R_{\rm DCO}$), the ratio of angular distribution ($R_{\rm ADO}$), and the polarization asymmetry ($\Delta_{\rm IPDCO}$) values of γ rays. A total projection spectrum as well as typical gated spectrum are shown in Figs. 1 and 2, respectively. From PACE4 [22] calculations, the relative cross section of the ^{27}Al(^{19}F, αnp)^{40}K channel was predicted as 11.1% of the total fusion cross section. γ rays from nuclei populated through other dominant channels of the reaction are therefore marked also in Fig. 1.

The spins and parities of most of the levels were not confirmed or assigned in ^{40}K. Therefore, in order to confirm or assign the spins and parities of the levels, the directional correlation of γ rays emitted from excited states (DCO) measurement was carried out. The DCO ratio ($R_{\rm DCO}$) [23] of a γ transition (γ_1) is defined as the ratio of intensities of that γ ray ($I\gamma_1$) for two different angles in coincidence with another γ ray (γ_2) of known multipolarity. It is given by

$$R_{\rm DCO} = \frac{I^{\gamma_1} \text{ observed at angle } \theta, \text{ gated by } \gamma_2 \text{ at } 90^\circ}{I^{\gamma_1} \text{ observed at angle } 90^\circ, \text{ gated by } \gamma_2 \text{ at } \theta}. \quad (1)$$

The $R_{\rm DCO}$ value depends on the multipolarities of these transitions (γ_1 and γ_2), and the angle between the detectors. In the present work, we measured the $R_{\rm DCO}$ for $\theta = 148^\circ$. For stretched transitions of the same multipolarity, the $R_{\rm DCO}$ value is close to unity, and for a stretched dipole (quadrupole) transition gated by a pure quadrupole (dipole) transition, it is nearly 0.5 (2). For a mixed transition, it deviates from the mentioned values. For the assignment of the spins and the γ-ray multipole mixing ratios (δ), the experimental $R_{\rm DCO}$ values were compared with theoretical values calculated using the computer code ANGCOR [23]. Spin alignment parameter $\sigma/J = 0.3$, obtained from a few known $E1$ and $E2$ transitions of ^{37}Ar and ^{42}Ca, was used for this calculation.

The DCO measurement could not be carried out for a few transitions due to their low statistics. So, the angular distribution from oriented nuclei (ADO) measurement was carried out to determine their multipolarities. Two asymmetric matrices were constructed for ADO measurement. In the first matrix, the events from detectors at all angles (except 90°) are stored in the first axis and in the second axis we stored the events from the 90° detectors only. Similarly, in the second matrix, the events from detectors at all angles (except 148°) are stored in the first axis and in the second axis we stored the events from the 148° detectors only. The ADO ratio ($R_{\rm ADO}$) [24] of a

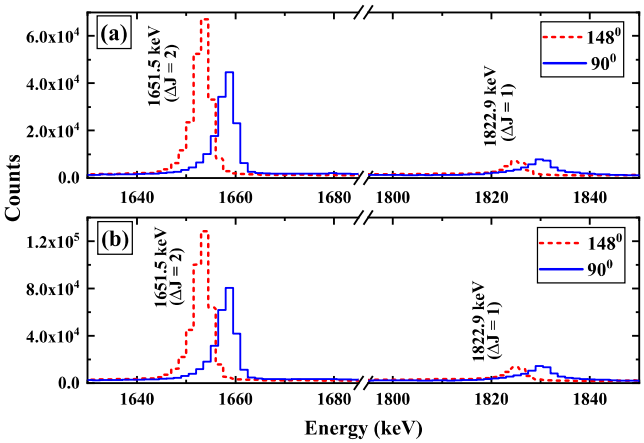


FIG. 3. A schematic representation of (a) DCO and (b) ADO spectra in ^{40}K. These spectra (a) and (b) are generated by putting gate on 891 keV ($\Delta J = 1$) transition. The 90° spectra have been artificially shifted by 5 keV for a clear view.

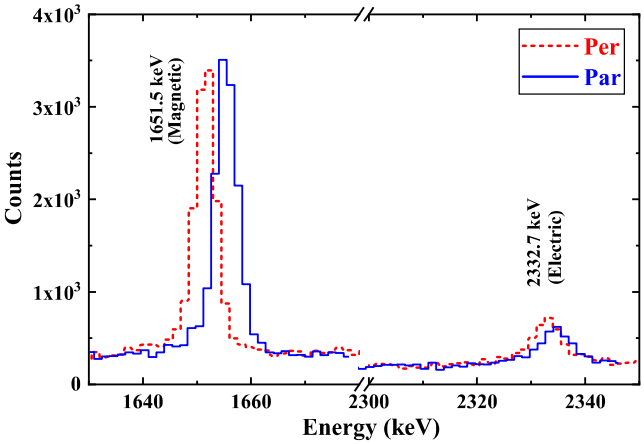


FIG. 4. Spectra generated from perpendicular and parallel matrices indicating the electric (magnetic) nature of 2332.7 keV (1651.5 keV) transition. These spectra are generated by putting gates on 891 keV. The parallel spectrum have been artificially shifted by 5 keV for a clear view.

transition is then defined as

$$R_{\mathrm{ADO}} = \frac{I_{\gamma_1} \text{ measured at } \theta = 148^\circ, \text{ gated by } \gamma_2 \text{ at all angles}}{I_{\gamma_1} \text{ measured at } \theta = 90^\circ, \text{ gated by } \gamma_2 \text{ at all angles}}. \quad (2)$$

For the present setup, R_{ADO} is 0.6 for the pure dipole transition and 1.6 for the pure quadrupole transition and the $\Delta J = 0$ transition. These values are estimated from the measured R_{ADO} values of a few known pure dipole and quadrupole transitions of ^{42}Ca [1]. In the case of mixed transitions, depending on the extent of mixing (δ), R_{ADO} may change from these values. A schematic representation of DCO and ADO spectra is shown in Fig. 3.

The integrated polarization directional correlation of oriented nuclei (IPDCO) [25] measurement was performed to assign the electric or magnetic nature of the transition. Two asymmetric matrices named parallel and perpendicular matrices were therefore constructed for IPDCO measurement. In the parallel (perpendicular) matrix, the simultaneous events detected in the two crystals of 90° clover detectors which are parallel (perpendicular) to the emission plane are recorded in the first axis, and on the second axis the coincident γ-rays detected in any other clover detector are recorded. The polarization asymmetry then expressed as

$$\Delta_{\mathrm{IPDCO}} = \frac{a(E_\gamma)N_\perp - N_\parallel}{a(E_\gamma)N_\perp + N_\parallel}, \quad (3)$$

where $N_\perp$ and $N_\parallel$ are the intensities of full peak observed in the perpendicular and parallel matrices, respectively. The asymmetry correction factor [$a(E_\gamma)$] represents the geometrical asymmetry of the clover detectors placed at 90°. It is defined as

$$a(E_\gamma) = \frac{N_\parallel}{N_\perp}. \quad (4)$$

In the present work, ^{152}Eu and ^{66}Ga radioactive sources were used to extract the asymmetry correction factor $a(E_\gamma)$. In order to measure the Δ_{IPDCO} of the transition, we put a gate on coincident γ's on the second axis and measured the intensities of the transition of interest from the projected parallel and perpendicular spectra. A positive value of Δ_{IPDCO} implies a pure electric transition whereas a negative value indicates pure magnetic transition. For a mixed transition, the value comes close to zero and the sign depends on the amount of mixing. Figure 4 shows the spectra obtained from parallel and perpendicular matrices.

III. RESULT AND DISCUSSION

In the present work, we are not able to extend the level scheme above 8 MeV, but we have modified the existing level scheme based on the coincidence relationship, relative intensities, R_{DCO}, R_{ADO}, and Δ_{IPDCO} values of the γ transitions (Fig. 5). We have added fourteen new γ's and six new levels to the existing level scheme. The relative intensities of most of the transitions were determined from the 891 keV gated spectrum generated from the angle-independent symmetric matrix. Using proper normalization, relative intensities of the 891 keV transition and the transitions parallel to the 891 keV transition were measured from the total projection spectrum. Finally, by considering the intensity of the 891 keV transition to 100, the relative intensities of all the transitions were normalized. They are listed in Table I. We have separately measured the branching ratios of most of the levels, i.e., the gate was put on any transition above the level of interest. They are listed in Table II. In the following sections, we discuss our results in detail.

A. Levels with excitation energy ⩽4 MeV

We did not observe any new transitions below 4 MeV excitation energy. We have only confirmed the spin and parity of a

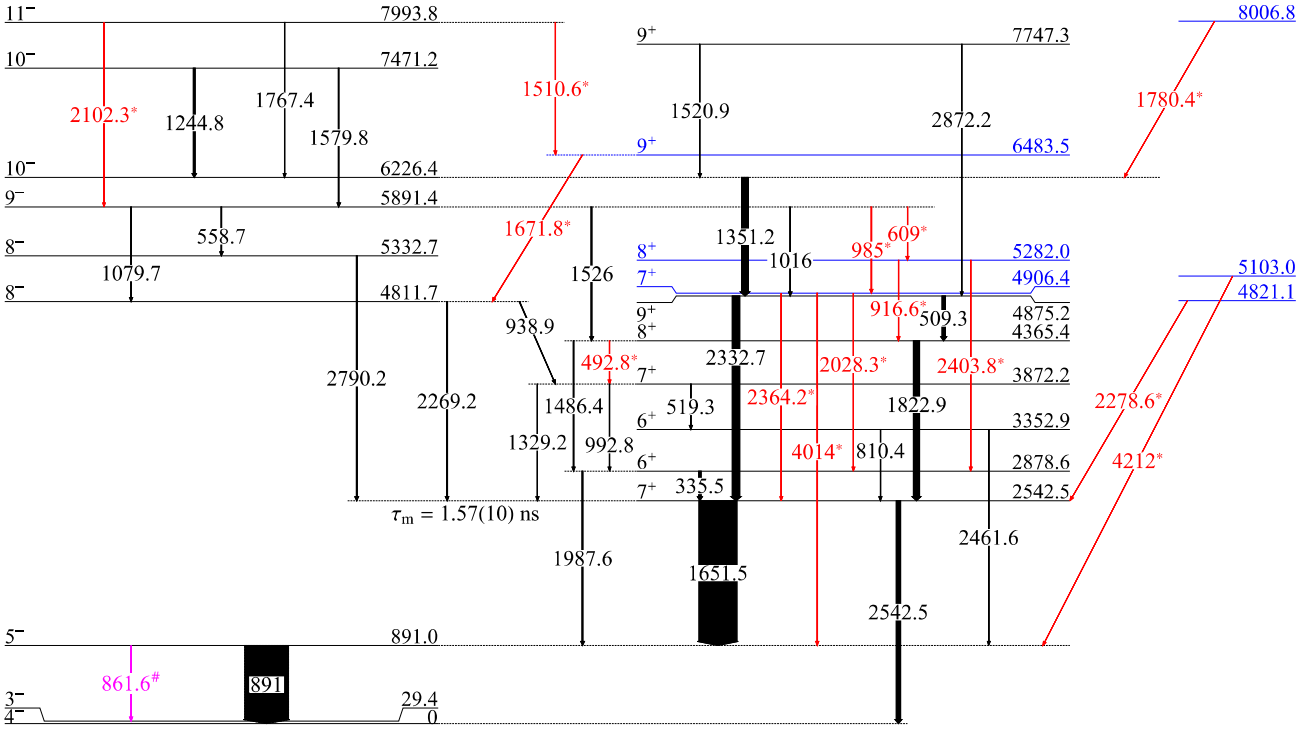


FIG. 5. Partial level scheme of ^{40}K. Energies are given in keV. Newly assigned γ transitions (red) and those already observed in light-ion-induced reactions (magenta) are indicated by * and #, respectively. New levels are indicated by blue lines.

few levels in this energy domain. Earlier, the spin and parity of 3352.9 and 3872.2 keV levels were assigned as (6^+) and (7^+), respectively [17]. In the present work, we measured the $R_{\rm DCO}$, $R_{\rm ADO}$, and $\Delta_{\rm IPDCO}$ values of the decay out transitions from these levels to confirm their J^π assignments. The measured $R_{\rm DCO}$ value of the 810.4 keV transition decaying from the 3352.9 keV level is 0.89(16) and has negative $\Delta_{\rm IPDCO}$. The 810.4 keV is therefore a magnetic dipole transition. Hence, we have confirmed the J^π of 3352.9 keV level as 6^+. The $R_{\rm DCO}$ of the 2461.6 keV transition also supports this assignment. The spin and parity of the 3872.2 keV level is confirmed based on the $R_{\rm DCO}$, $R_{\rm ADO}$, and $\Delta_{\rm IPDCO}$ values of 519.3, 992.8, and 1329.2 keV transitions. The measured $R_{\rm DCO}$ values of 519.3, 992.8, and 1329.2 keV transitions are 0.57(11), 0.96(19), and 1.35(24), respectively. The $\Delta_{\rm IPDCO}$ of 519.3 and 1329.2 keV transitions are negative and positive, respectively. In the case of the $\Delta J = 0$ transition, the positive (negative) $\Delta_{\rm IPDCO}$ value represents the magnetic (electric) nature of the transition [8]. Therefore, the spin and parity of the 3872.2 keV level is confirmed as 7^+.

The spins and parities of all other levels with excitation energy $\leqslant$4 MeV were confirmed in the present work. In this energy range, we extracted the multipole mixing ratios (δ) for ten transitions and compared them with the earlier measurements [1], if available. For extracting the mixing ratios of 891 and 1651.5 keV transitions, we used $R_{\rm DCO}$ value of the 1486.4 keV transition gated by 891 and 1651.5 keV transitions, respectively. Most of the measured multipole mixing ratios (δ) agreed with the earlier measurements (Table I). In our present work, the sign convention proposed by Krane and Steffen is used for mixing ratio (δ) calculation [26].

The 861.6 keV transition, found in the 1651.5 keV gated spectrum, was added to the level scheme (Fig. 5). This transition was previously observed in light-ion induced experiments [1].

B. Levels with excitation energy between 4 and 6 MeV

In this energy range, four new levels (4821.1, 4906.4, 5103, and 5282 keV) and ten new transitions were added to the existing level scheme (Fig. 5). The spin and parity of 4811.7 keV level is examined based on the spectroscopic properties of 938.9 and 2269.2 keV transitions. The measured $R_{\rm DCO}$ and $\Delta_{\rm IPDCO}$ values of 938.9 and 2269.2 keV transitions confirmed their electric dipole nature, which implies a modification of the parity assignment of the 4811.7 keV level from (8^+) to 8^-. The spin and parity of the 5332.7 keV level was previously assigned as (9^+) [17]. The 5332.7 keV level decays to the 2542.5 keV (7^+) level through the 2790.2 keV transition. The $R_{\rm DCO}$ and $\Delta_{\rm IPDCO}$ of 2790.2 keV confirmed its electric dipole nature. We have therefore modified the spin and parity of the 5332.7 keV level from (9^+) to 8^-. The spin and parity of 4365.4, 4875.2, and 5891.4 keV levels were previously assigned as (8^+), 9^+, and (9^-), respectively. In the present work, we have confirmed the earlier assignments based on the $R_{\rm DCO}$, $R_{\rm ADO}$, and $\Delta_{\rm IPDCO}$ values of the decay out transitions of these levels. In the following subsections, we discuss our new findings in detail.

1. 492.8 keV γ decay from 8_1^+ to 7_2^+ level

The 492.8 keV transition is in coincidence with 891, 1329.2, 1351.2, and also with 1651.5 keV [Fig. 6(a)].

TABLE I. Relative intensity ($I_{\rm rel}$), $R_{\rm DCO}$, $R_{\rm ADO}$, $\Delta_{\rm IPDCO}$, and mixing ratio (δ) of the γ transitions in ^{40}K.

E_γ	E_X				$E_{\rm gate}$				$\Delta_{\rm IPDCO}$	Mixing ratio (δ)	
(keV)	(keV)	$I_{\rm rel}$	J_i^π	J_f^π	(keV)	$\Delta J_{\rm gate}$	$R_{\rm DCO}$	$R_{\rm ADO}$	Expt.	Present	Previous [1]
335.5(8)	2878.6(8)	5.3(4)	6_1^+	7_1^+	891	1	0.92(9)	0.93(7)		−0.04(7)	+0.01(2)
492.8(9)	4365.4(9)	0.60(6)	8_1^+	7_2^+	891	1	0.85(16)	1.00(17)		$+0.03^{+0.10}_{-0.12}$	
509.3(7)	4875.2(7)	7.8(14)[a]	9_1^+	8_1^+							
519.3(9)	3872.2(9)	1.13(7)	7_2^+	6_2^+	891	1	0.57(11)	0.55(9)	−0.11(9)	$-0.19^{+0.10}_{-0.13}$	
558.7(7)	5891.4(9)	1.59(10)	9_1^-	8_2^-	891	1	0.84(8)	0.88(8)	−0.11(7)	+0.03(6)	
609.0(9)	5891.4(9)	0.91(11)	9_1^-	8_2^+	891	1	0.70(13)	0.79(12)	+0.08(7)	$-0.08^{+0.10}_{-0.12}$	
810.4(9)	3352.9(9)	0.90(7)	6_2^+	7_1^+	891	1	0.89(16)	0.99(13)	−0.10(8)	$+0.06^{+0.10}_{-0.11}$	
861.6(8)	891.0(8)	0.5(1)	5_1^-	3_1^-	1651.5	2	1.1(4)	1.2(3)			E2
891.0(6)	891.0(8)	100(5)	5_1^-	4_1^-	1651.5	2	0.63 (4)	0.91(5)	−0.07(1)	$+0.14^{+0.12}_{-0.10}$	+0.09(2)
916.6(7)	5282.0(8)	0.74(8)	8_2^+	8_1^+	891	1	1.42(25)	1.32(21)	+0.14(9)	−0.20(37)	
938.9(7)	4811.7(7)	1.11(9)	8_1^-	7_2^+	1329.2	0	0.59(6)	0.75(7)	+0.13(9)	−0.01(6)	
985.0(7)	5891.4(9)	1.15(13)	9_1^-	7_3^+	891	1	1.6(3)	1.56(23)	−0.12(11)	$+0.08^{+0.27}_{-0.24}$	
992.8(9)	3872.2(9)	0.45(4)	7_2^+	6_1^+	891	1	0.96(19)	0.93(15)		$+0.11^{+0.11}_{-0.13}$	
1016.0(7)	5891.4(9)	1.8(2)	9_1^-	9_1^+	891	1	1.46(17)	1.41(14)	−0.06(9)	$-0.15^{+0.35}_{-0.25}$	
1079.7(7)	5891.4(9)	1.26(9)	9_1^-	8_1^-	891	1	0.6(1)	0.71(9)	−0.17(9)	$-0.17^{+0.10}_{-0.13}$	
1244.8(7)	7471.2(7)	3.9(4)	10_2^-	10_1^-	1351.2	1	2.06(23)	1.67(18)	+0.03(5)	$-0.27^{+0.30}_{-0.34}$	+0.13(7)
1329.2(6)	3872.2(9)	1.08(15)	7_2^+	7_1^+	891	1	1.35(24)	1.15(19)	+0.15(8)	−0.28(35)	
1351.2(5)	6226.4(5)	15.6(9)	10_1^-	9_1^+	891	1	0.66(7)	0.76(7)	+0.03(2)	−0.12(5)	−0.07(5)
1486.4(6)	4365.4(9)	1.3(1)	8_1^+	6_1^+	891	1	1.53(25)	1.25(16)	+0.04(12)	$E2$	
1510.6(9)	7993.8(10)	0.45(11)	11_1^-	9_2^+	2269.2	1	1.32 (22)	1.36(17)		$-0.17^{+0.18}_{-0.23}$	
1520.9(8)	7747.3(9)	0.81(13)	9_3^+	10_1^-	1351.2	1	1.00(12)	0.85(9)	+0.09(7)	$+0.17^{+0.18}_{-0.08}$	
1526.0(6)	5891.4(9)	2.5(3)	9_1^-	8_1^+	1822.9	1	0.83(12)	1.06(13)	+0.13(5)	−0.12(9)	
1579.8(7)	7471.2(7)	1.6(1)	10_2^-	9_1^-	2269.2	1	0.77(11)	1.07(11)	−0.10(9)	−0.05(8)	
1651.5(5)	2542.5(7)	87(5)	7_1^+	5_1^-	891	1	1.49(9)	1.6(1)	-0.06(1)	$-0.04^{+0.07}_{-0.09}$	−0.02(3)
1671.8(8)	6483.5(8)	0.66(7)	9_2^+	8_1^-	2269.2	1	0.86(13)	1.00(12)	+0.17(13)	+0.02(10)	
1767.4(6)	7993.8(10)	0.75(9)	11_1^-	10_1^-	1351.2	1	0.51(13)	0.42(6)	−0.14(6)	−0.64(24)	
1780.4(9)	8006.8(9)	0.17(3)									
1822.9(5)	4365.4(9)	14(1)	8_1^+	7_1^+	891	1	0.79(9)	0.87(9)	−0.08(2)	−0.01(6)	
1987.6(6)	2878.6(8)	2.2(2)	6_1^+	5_1^-	891	1	0.66(8)	0.65(7)	+0.13(12)	−0.10(7)	−0.05(4)
2028.3(9)	4906.4(20)	0.34(5)	7_3^+	6_1^+	891	1		1.0(4)			
2102.3(10)	7993.8(10)	0.22(3)									
2269.2(6)	4811.7(7)	1.71(12)	8_1^-	7_1^+	891	1	0.90(16)	0.63(9)	+0.14(10)	+0.11(5)	
2278.6(11)	4821.1(11)	0.12(3)									
2332.7(6)	4875.2(7)	17(1)	9_1^+	7_1^+	891	1	1.47(15)	1.32(12)	+0.08(3)	$E2$	
2364.2(9)	4906.4(20)	0.37(5)	7_3^+	7_1^+	891	1		1.7(4)			
2403.8(8)	5282.0(8)	0.27(4)	8_2^+	6_1^+	891	1		1.8(5)			
2461.6(7)	3352.9(9)	0.62(7)	6_2^+	5_1^-	891	1	0.70(19)	0.81(16)		$-0.07^{+0.14}_{-0.18}$	
2542.5(7)	2542.5(7)	9.8(7)	7_1^+	4_1^-	1351.2	1	2.8(3)	2.4(2)	+0.07(6)	$+0.01^{+0.36}_{-0.29}$	+0.10(7)
2790.2(7)	5332.7(7)	2.6(2)	8_2^-	7_1^+	891	1	0.61(9)	0.79(9)	+0.17(10)	−0.16(9)	
2872.2(9)	7747.3(9)	0.37(6)	9_3^+	9_1^+	891	1		1.4(6)			
4014(2)	4906.4(20)	0.90(8)	7_3^+	5_1^-	891	1	1.23(26)	1.41(19)	−0.11(9)	$-0.30^{+0.25}_{-0.40}$	
4212(2)	5103(2)	0.19(4)									

[a]Intensity is taken from Ref. [17] with proper normalization.

According to the previous level scheme [17], 1329.2 keV was not in coincidence with 1351.2 and 1526 keV transitions. However, we observed 1351.2 and 1526 keV transitions in the 1329.2 keV gated spectrum. Hence, we have placed the 492.8 keV transition in the level scheme (Fig. 5).

2. 4906.4 keV level

The 2028.3, 2364.2, and 4014 keV transitions are in coincidence with the 985 keV transition but not in coincidence with each other [Fig. 6(b)]. On the other hand, these four transitions are also present in the 891 keV gated spectrum (Fig. 2). The 985, 2028.3, and 2364.2 keV transitions are also in coincidence with the 1651.5 keV transition. But the 4014 keV transition is not in coincidence with 1651.5 keV transition [Fig. 6(c)]. Based on the coincidence relationship and the relative intensities, we have placed them by adding a new 4906.4 keV level in the level scheme. The spin and parity of the newly observed 4906.4 keV level is assigned as 7^+, based on the $R_{\rm DCO}$, $R_{\rm ADO}$ and $\Delta_{\rm IPDCO}$ values of 985

TABLE II. Branching ratios of different levels in ^{40}K.

E_X (keV)	E_γ (keV)	Branching ratio
891.0	861.6	0.5(1)
	891.0	99.5(1)
2542.5	1651.5	87(5)
	2542.5	13(5)
2878.6	335.5	65(4)
	1987.6	35(4)
3352.9[a]	810.4	59(5)
	2461.6	41(5)
3872.2	519.3	45.7(28)
	992.8	18.3(16)
	1329.2	36(3)
4365.4	492.8	4(1)
	1486.4	8(1)
	1822.9	88(5)
4811.7	938.9	36(6)
	2269.2	64(6)
4875.2[a]	509.3	31(6)
	2332.7	69(6)
4906.4	2028.3	19.5(16)
	2364.2	24.7(17)
	4014.0	55.8(37)
5282.0	916.6	73(8)
	2403.8	27(8)
5891.4	558.7	21.3(14)
	609.0	11.3(8)
	985.0	12.0(9)
	1016.0	17.2(12)
	1079.7	12.5(9)
	1526.0	25.7(18)
7471.2 [a]	1244.8	71(7)
	1579.8	29(7)
7747.3[a]	1520.9	69(11)
	2872.2	31(11)
7993.8[a]	1510.6	32(8)
	1767.4	53(6)
	2102.3	15(2)

[a]Estimated from relative intensities.

and 4014 keV transitions. Owing to weak statistics, we can only measure the $R_{\rm ADO}$ values of 2028.3 and 2364.2 keV transitions, and the measured $R_{\rm ADO}$'s of these transitions also support the spin assignment of the 4906.4 keV level.

3. 5282 keV level

The 609 and 916.6 keV transitions are in coincidence with each other and also in coincidence with 891, 1651.5, and 1822.9 keV transitions [Figs. 6(d) and 6(e)]. On the other hand, the 2403.8 keV transition is present in the 609 keV gated spectrum [Fig. 6(d)], but not in the 916.6 keV gated spectrum [Fig. 6(e)]. The 2403.8 keV transition is also in coincidence with 335.5, 891, and 1651.5 keV transitions. Based on the coincidence relationship and relative intensities, we have placed the 609 keV transition above the 916.6 and 2403.8 keV transitions and added a new level at 5282 keV. The spin and

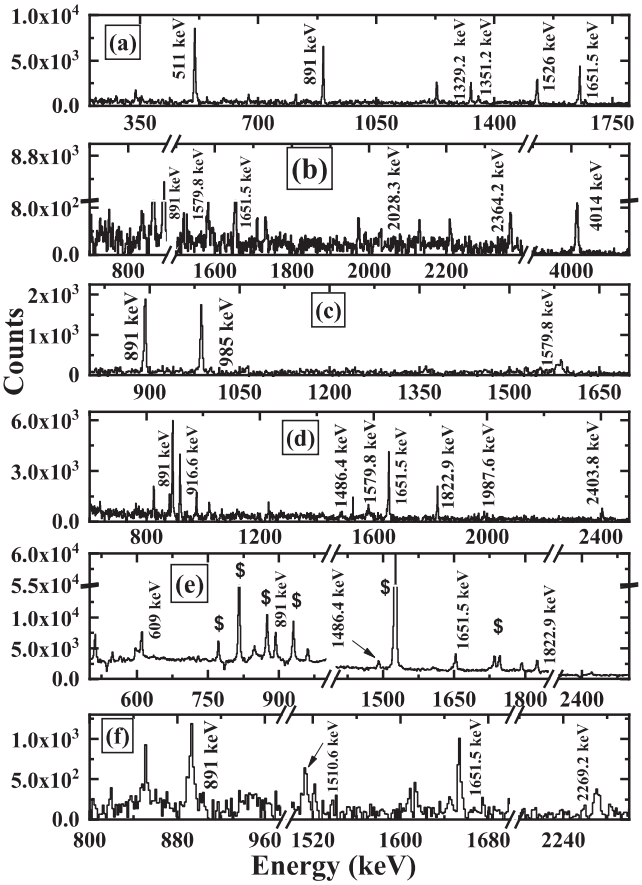


FIG. 6. Background subtracted coincidence spectra obtained by putting gates on (a) 492.8 keV, (b) 985 keV, (c) 4014 keV, (d) 609 keV, (e) 916.6 keV, and (f) 1671.8 keV transitions. In panel (e) the transitions marked with **$** are from ^{42}Ca [27].

parity of the 5282 keV level is assigned as 8^+, based on the $R_{\rm DCO}$, $R_{\rm ADO}$ and $\Delta_{\rm IPDCO}$ values of 916.6 keV.

4. 4821.1 and 5103 keV levels

We have added two more energy levels, 4821.1 and 5103 keV, in this energy domain. However, due to the weak statistics of the decay out 2278.6 and 4212 keV transitions, we are not able to assign their spin and parity in the present work.

In this energy domain, the mixing ratios (δ) of thirteen transitions were measured for the first time (Table I).

C. Levels with excitation energy ⩾6 MeV

In this energy domain, two new levels (6483.5 and 8006.8 keV) and three new transitions (viz. 1510.6, 1671.8, and 2102.3 keV) were added to the existing level scheme (Fig. 5).

1. 6483.5 keV level

The 1510.6 and 1671.8 keV transitions, though in coincidence with each other and also in coincidence with 891, 1651.5, and 2269.2 keV transitions, are not in coincidence

with 1822.9 and 2332.7 keV transitions [Fig. 6(f)]. The relative intensity of the 1671.8 keV transition is greater than that of 1510.6 keV. We have therefore placed 1510.6 keV above the 1671.8 keV transition and added a new level at 6483.5 keV. The spin and parity of the 6483.5 keV level is assigned based on the $R_{\rm DCO}$, $R_{\rm ADO}$ and $\Delta_{\rm IPDCO}$ values of the 1671.8 keV transition (Table I).

2. 1780.4 and 2102.3 keV transitions

In our present study, we have identified the 2102.3 keV transition, which is in coincidence with 558.7, 891, 1651.5, and 2790.2 keV transitions. So, we have placed 2102.3 keV as the decay out transition from the 7993.8 keV level in the current level scheme. A new 1780.4 keV transition decaying from the 8006.8 keV level is observed in the present work. But, due to poor statistics of the 1780.4 keV transition, we could not assign the spin and parity of the 8006.8 keV level.

We have confirmed the spin and parity of the 6226.4 keV level as 10^-. It was earlier assigned as (10^-) [17]. Soderstrom *et al.* [17] reported three new levels, viz., 7471.2, 7747.3, and 7993.8 keV, in their level scheme. But they did not assign the spin and parity of these levels. In the present work, we have assigned the spin and parity of these levels based on the $R_{\rm DCO}$, $R_{\rm ADO}$ and $\Delta_{\rm IPDCO}$ values of the decay out transitions. The 7471.2 keV level decays to the 5891.4 keV level (9^-) through the 1579.8 keV magnetic dipole transition (Table I). We have therefore assigned 10^- as the spin and parity of 7471.2 keV level. The $R_{\rm DCO}$ and $\Delta_{\rm IPDCO}$ values of 1244.8 keV transition also support the present assignment. In a similar way, we have assigned the spin and parity of 7747.3 and 7993.8 keV levels using the $R_{\rm DCO}$ and $\Delta_{\rm IPDCO}$ values of 1520.9 and 1767.4 keV transitions, respectively. In this energy domain, the mixing ratios (δ) of five transitions were measured for the first time (Table I).

The 7033 keV level was placed in the previous level scheme [17]. It decays to the 4812 keV level through the 2220 keV transition. A weak 1142 keV transition was also tentatively assigned between 7033 and 5892 keV levels. In the present work, we could not observe 1142 and 2220 keV decay out transitions from the 7033 keV level (Fig. 7). We therefore removed the 7033 keV level from our present level scheme (Fig. 5).

In the present work, uncertainties quoted in the measured values of intensities, $R_{\rm DCO}$, and $R_{\rm ADO}$ are due to the statistical errors and the errors from the detector efficiency. The uncertainties quoted in the γ energy are extracted from peak fitting and detector calibration errors. Since we did not consider efficiency corrections for polarization measurements, the uncertainties quoted in the $\Delta_{\rm IPDCO}$ measurements are statistical only.

In the following section, we compare our experimental observation with the shell-model results.

IV. THEORETICAL CALCULATION

Large-basis shell-model calculations were performed using the code OXBASH [28] to understand the microscopic origin of each excited state in ^{40}K. The valence space consists of $1d_{5/2}$, $1d_{3/2}$, $2s_{1/2}$, $1f_{7/2}$, $1f_{5/2}$, $2p_{3/2}$, and $2p_{1/2}$ orbitals for both protons and neutrons above the ^{16}O inert core. The number of valence particles (protons + neutrons) in ^{40}K is 24. The sdpfmw interaction [29] (as referred to within the OXBASH [28] code package) was used for the calculation. Other relevant details of the interaction and calculation are discussed in Ref. [3].

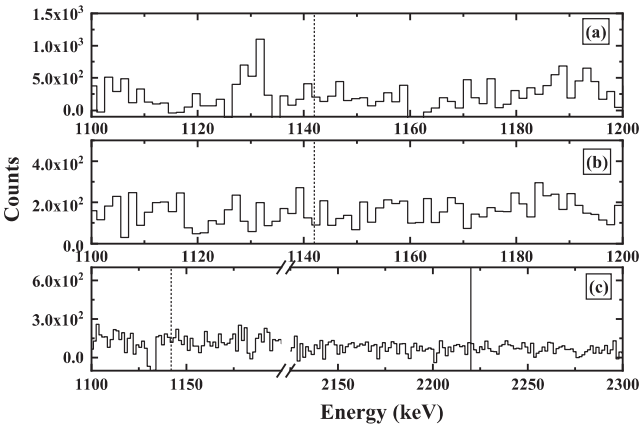


FIG. 7. Background subtracted coincidence spectra obtained by putting gates on (a) 558.7 keV, (b) 2269.2 keV, and (c) 2790.2 keV transitions. The position of 1142 keV transition in panels (a)–(c) is marked by a dotted line. The position for the 2220 keV transition in (c) is marked by a solid line.

Unrestricted calculations for ^{40}K with such a large number of valence particles in the full *sd*-*pf* space are not possible due to the large *m*-scheme basis dimension. Therefore, several particle restrictions in the model space were used in our calculations. During our calculations, we observed that the calculated energies are overpredicted for the positive parity and high spin negative parity states. In these calculations, multiparticle multihole excitations between *sd* and *pf* shells are involved. Therefore, we changed the single-particle energy (SPE) of each of the *pf* orbitals by 600 keV to improve the calculated energies. The results for energy spectra and transition probabilities in ^{40}K with different particle restrictions are discussed in the next sections. For all these calculations, the mass normalization factor, defined as the number of particles up to the *sd* shell, was taken accordingly.

A. Negative parity states

We adopted two different truncation schemes (Theor-N1 and Theor-N2) for the negative parity states.

1. Theor-N1

The particle partition of Theor-N1 is $(sd)^{-1}$-$(pf)^1$. In case of ^{40}K, the maximum possible spin which can be generated in this particle configuration is 5^-. We therefore calculated the excitation energies for 3^-, 4^-, and 5^- levels and compared them with the experimental energies. The comparison shows a very good agreement with experimental values (Fig. 8). In the calculation, the full *sd*-*pf* shell was used and the mass normalization factor was 39.

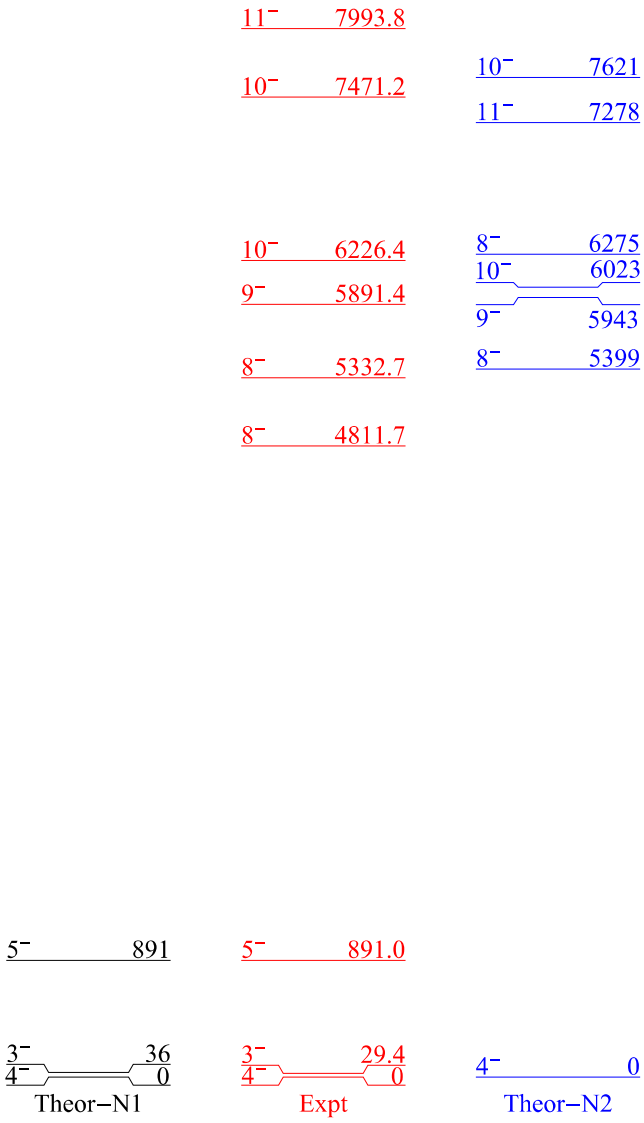


FIG. 8. Comparison of theoretical and experimental level schemes for negative parity states in ^{40}K. All these energies are plotted with respect to the ground state energy (−272.871 MeV) as 0.

2. Theor-N2

We excited two particles [$(sd)^{-3}$-$(pf)^3$ excitation] to the pf orbitals to generate the high spin negative parity states (Theor-N2) of ^{40}K. In the calculation, the full sd-pf shell was used and the mass normalization factor was 37. The results (Fig. 8) show that the calculated energies of 9^-_1, 10^-_1, and 10^-_2 levels agree reasonably well with the experimental energies. However, the 8^-_1 and 8^-_2 states are overpredicted by 587 and 942 keV, respectively. Interestingly, the calculated energy of the 8^-_1 level (5399 keV) is very close to the experimental energy of the 8^-_2 level (5332.7 keV). Since we performed our calculation with a particular configuration i.e. 1p-1h, or 2p-2h, or 3p-3h, etc., the deviation between the experimental and the calculated energy obtained from the shell model may be due to the mixing of different mp-mh configurations. Therefore, both 4811.7 and 5332.7 keV levels are either mixed levels (3p-3h + 5p-5h configuration) or the 5332.7 keV level is generated from pure 3p-3h excitation and only the 4811.7 keV level is a mixed state. Since the full sd-pf model space calculation for 5p-5h excitation is not possible with the present computational facility, the microscopic origins of 4811.7 and 5332.7 keV levels are not confirmed in the present work. It was also noticed that the 11^-_1 state is underpredicted by 716 keV (Fig. 8).

B. Positive parity states

We used one truncation scheme named Theor-P1 to reproduce the positive parity states in ^{40}K. In Theor-P1, only one particle is excited (2h-2p) to the pf shell, and the full sd-pf model space was used to generate the positive parity states. The particle configuration for the truncation is therefore $(sd)^{-2}$-$(pf)^2$. The comparison between experimental and calculated energies is shown in Fig. 9. The figure shows that, except for 7^+_3 and 9^+_2 levels, the experimental and theoretical energies are agreed well. For 7^+_3 (4906.4 keV) and 9^+_2 (6483.5 keV) levels, the calculated energies are underpredicted by ≈650 keV. The mass normalization factor for sd shell two-body matrix elements (TBMEs) for this calculation was 38.

C. Configuration mixing and Collectivity

The decompositions of the wave functions for the positive and negative parity states in ^{40}K are shown in Tables III and IV, respectively. We used the results obtained from Theor-N1 truncation for the low-lying negative parity states. Similarly, for the high spin positive and negative parity states, Theor-P1 and Theor-N2 truncations were used, respectively. The probability and the structure of different partitions having >10% contribution are shown in the tables (Tables III and IV). The partitions are given in terms of occupation numbers of single-particle valence orbits. Here, N_1 is the total number of particle partitions for a particular state, each with contribution >1%, and N_2 gives an estimation of the minimum number of particle partitions, each of which contributes ⩽1% in the state.

Table III shows that the positive-parity states are primarily generated from single-particle excitations. They have a much smaller extent of configuration mixing. For the positive parity states (6^+–9^+), the largest particle partition in their wave function is 67%–93%. Low-lying negative parity states with $(sd)^{-1}$-$(pf)^1$ configuration have 1–3 particle partitions with the largest 99% (Table IV). However, the configuration mixing in terms of single-particle partitions for the high spin negative parity states (8^-–11^-) was increased. It was found that they have 9–12 particle partitions contributing at least 1% with the largest 44%–69% in their wave function. These high spin negative parity states therefore show a considerable amount of configuration mixing in terms of particle partitions. Consequently, these give us a sign of collective excitations at higher excitation energy in ^{40}K.

The reduced transition probabilities [$B(E1)$, $B(M1)$, $B(E2)$, $B(M2)$, and $B(E3)$] for a few transitions were calculated by using the effective charges $e_p = 1.5e$ and $e_n = 0.5e$ and free values of g factors [4,6,7,30–32]. The experimental transition strengths were extracted from the reported level

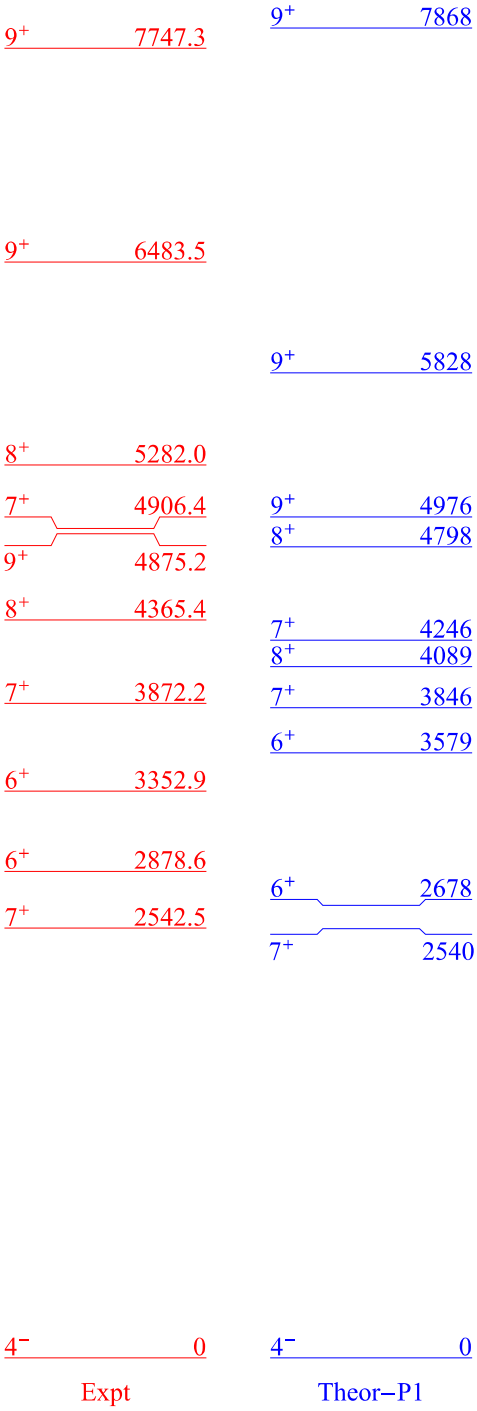


FIG. 9. Comparison of theoretical and experimental level schemes for positive parity states in ^{40}K. All these energies are plotted considering the ground state energy (−272.871 MeV) as 0.

lifetimes [1]. The branching and mixing ratios are taken from the present measurement. The calculated $B(E2)$, $B(M2)$, and $B(E3)$ values show good agreement with the corresponding available experimental data (Table V). The calculated and experimental $B(E1)$ and $B(M1)$ values vary slightly but are of the same order of magnitude. These calculations provide evidence of the reliability of the calculated wave functions.

TABLE III. Structure of the wave functions for the positive parity states in ^{40}K. The partitions are given in terms of occupation numbers of single-particle valence orbits in the following order :$1d_{5/2}$, $1d_{3/2}$, $2s_{1/2}$, $1f_{7/2}$, $1f_{5/2}$, $2p_{3/2}$, and $2p_{1/2}$.

		Energy (MeV)		Wave function			
J_i^π	T	Expt.	Theor.	%	Partition	N_1	N_2
7_1^+	1	2.543	2.540	88	[12,6,4,2,0,0,0]	6	3
6_1^+	1	2.879	2.678	83	[12,6,4,2,0,0,0]	7	3
6_2^+	1	3.353	3.579	69	[12,6,4,2,0,0,0]	7	4
7_2^+	1	3.872	3.846	81	[12,6,4,2,0,0,0]	5	5
8_1^+	1	4.365	4.089	89	[12,6,4,2,0,0,0]	3	3
9_1^+	1	4.875	4.976	93	[12,6,4,2,0,0,0]	3	2
7_3^+	1	4.906	4.246	67	[12,6,4,2,0,0,0]	7	3
				11	[12,7,3,2,0,0,0]		
8_2^+	1	5.282	4.798	79	[12,6,4,2,0,0,0]	7	2
				11	[12,7,3,2,0,0,0]		
9_2^+	1	6.484	5.828	91	[12,6,4,2,0,0,0]	3	1
9_3^+	1	7.747	7.868	88	[12,7,3,2,0,0,0]	4	2

In the present experiment, we used a thick ^{27}Al target with Au backing to populate ^{40}K. We calculated the stopping time [33] of ^{40}K in the ^{27}Al and Au backing using the calculated range and the stopping power of ^{40}K in the target and backing medium [34]. The energy distribution of the recoils (^{40}K) was taken from PACE4 calculation [22]. The estimated stopping time of ^{40}K in the ^{27}Al and Au backing is ≈360 fs. So, we may observe the lineshape of the decay out transitions if the lifetimes of the levels are of the order of the estimated stopping time of ^{40}K. We have not found any lineshape of the decay out transitions in the present experiment. It was also noticed that the reported lifetimes of 2878.6 and 4365.4 keV levels are 0.39(14) and 0.52(20) ps, respectively, which are close to the estimated stopping time of ^{40}K. The calculated lifetimes of a few levels (Table V) are also of the order of the estimated stopping time. However, we have not observed any

TABLE IV. Structure of the wave functions for the negative parity states in ^{40}K. The partitions are given in terms of occupation numbers of single-particle valence orbits in the following order: $1d_{5/2}$, $1d_{3/2}$, $2s_{1/2}$, $1f_{7/2}$, $1f_{5/2}$, $2p_{3/2}$ and $2p_{1/2}$.

		Energy (MeV)		Wave function			
J_i^π	T	Expt.	Theor.	%	Partition	N_1	N_2
4_1^-	1	0	0 (−272.871)	99	[12,7,4,1,0,0,0]	2	1
3_1^-	1	0.029	0.036	96	[12,7,4,1,0,0,0]	3	1
5_1^-	1	0.891	0.891	99	[12,7,4,1,0,0,0]	1	2
8_1^-	1	4.812	5.399	54	[12,5,4,3,0,0,0]	11	9
				16	[12,5,4,2,0,1,0]		
8_2^-	1	5.333	6.275	54	[12,5,4,3,0,0,0]	11	9
9_1^-	1	5.891	5.943	60	[12,5,4,3,0,0,0]	10	7
10_1^-	1	6.226	6.023	64	[12,5,4,3,0,0,0]	10	4
10_2^-	1	7.471	7.621	44	[12,5,4,3,0,0,0]	12	7
				20	[12,5,4,2,0,1,0]		
11_1^-	1	7.994	7.278	69	[12,5,4,3,0,0,0]	9	5

TABLE V. Comparison of experimental and theoretical lifetimes and reduced transition probabilities for different transitions in ^{40}K.

E_X	τ_{mean} (ps)			E_γ		$B(E1)$ ($\times10^{-6}$ e^2fm^2)		$B(M1)$ ($\times10^{-3}\mu_N^2$)		$B(E2)$ (e^2fm^4)		$B(M2)$ (μ_N^2fm^2)		$B(E3)$ (e^2fm^6)	
(keV)	Reported [1]	Theor.	J_i^π	(keV)	J_f^π	Expt.	Theor.	Expt.	Theor.	Expt.	Theor.	Expt.	Theor.	Expt.	Theor.
891.0	1.20(26)	2.3	5_1^-	861.6	3_1^-					$7.1^{+3.8}_{-2.4}$	5.5				
				891.0	4_1^-			65^{+20}_{-14}	34.9						
2542.5	1.57(10) ns	0.72 ns	7_1^+	1651.5	5_1^-							$3.30^{+0.43}_{-0.42}$	7.96		
				2542.5	4_1^-									209^{+77}_{-103}	168
2878.6	0.39(14)	0.24	6_1^+	335.5	7_1^+			2498^{+1642}_{-791}	1204						
				1987.6	5_1^-	71^{+53}_{-25}	264								
3352.9		0.34	6_2^+	810.4	7_1^+				47						
				2461.6	5_1^-		107								
3872.2		0.08	7_2^+	519.3	6_2^+				18.5						
				992.8	6_1^+				12.8						
				1329.2	7_1^+				308						
4365.4	0.52(20)	1.42	8_1^+	492.8	7_2^+			36^{+37}_{-17}	102						
				1486.4	6_1^+					17^{+14}_{-6}	17				
				1822.9	7_1^+			16^{+11}_{-5}	3.2						
4811.7		12.1	8_1^-	938.9	7_2^+		2.00								
				2269.2	7_1^+		4.3								
4875.2	<1.01	0.38	9_1^+	509.3	8_1^+				381						
				2332.7	7_1^+					>8	24.2				
4906.4		0.54	7_3^+	2028.3	6_1^+				11.7						
				2364.2	7_1^+				0.27						
				4014.0	5_1^-								4.7		
5282.0		0.30	8_2^+	916.6	8_1^+				226						
				2403.8	6_1^+						2.34				
5332.7		0.32	8_2^-	2790.2	7_1^+		89								
5891.4		0.59	9_1^-	558.7	8_2^-				226						
				609.0	8_2^+		3								
				985.0	7_3^+								0.25		
				1016.0	9_1^+		14.8								
				1079.7	8_1^-				35.5						
				1526.0	8_1^+		32.5								
6226.4		2.43	10_1^-	1351.2	9_1^+		104								
6483.5		29.7	9_2^+	1671.8	8_1^-		4.5								
7471.2		0.10	10_2^-	1244.8	10_1^-				0.60						
				1579.8	9_1^-				141						
7747.3		0.10	9_3^+	1520.9	10_1^-		31								
				2872.2	9_1^+				24.5						
7993.8		0.16	11_1^-	1510.6	9_2^+								1.06		
				1767.4	10_1^-				40.2						
				2102.3	9_1^-						43.7				

lineshape of the transitions decaying from the levels below 6.5 MeV. This may be due to the presence of long lived states at higher excitation energy, as suggested by the results obtained from shell-model calculations. For the levels above 6.5 MeV, the predicted lifetimes are in the range of 100–160 fs, and they may have lineshapes. But, we could not identify them because of their poor statistics.

D. Two-nucleon transfer spectroscopic factor calculation

It was reported in Ref. [17] that (6_2^+), (7_2^+), (8_1^+), and (9_2^+) levels possess largely the structure of a $T = 0$ and $J = 3$ multiplet coupled to the 6^+ state in ^{42}Ca. On the other hand 6_1^+, 7_1^+, (8_2^+), and 9_1^+ levels possess largely the structure of a $J = 2$ multiplet coupled to the 7^+ state in ^{42}Sc. They predicted these based on their weak-coupling calculations. The yrast 6^+ level of ^{42}Ca is dominated by $\pi(sd)^{12}(fp)^0 \otimes \nu(sd)^{12}(fp)^2$ configuration [27,35]. The particle configuration for the yrast 7^+ level of ^{42}Sc is $\pi(sd)^{12}(fp)^1 \otimes \nu(sd)^{12}(fp)^1$ [36].

The positive parity levels of interest in ^{40}K were generated by exciting one nucleon from sd orbitals to the fp orbitals. In order to investigate the particle configuration in terms of protons and neutrons, LBSM calculations were carried out with SDPFMWPN interaction [29] for the positive parity levels in ^{40}K. The average numbers of protons and neutrons in the sd and pf orbitals for each positive parity level are shown in Table VI. ^{40}K is two nucleons away from ^{42}Ca (^{42}Ca + 1 proton hole +1 neutron hole) and ^{42}Sc (^{42}Sc + 2 proton holes). The results show that for the (6_1^+), (6_2^+), (7_2^+), (7_3^+),

TABLE VI. Average particle occupancies of positive-parity states in ^{40}K.

J^π	E_X (MeV)	$\pi 1d_{5/2}$	$\pi 1d_{3/2}$	$\pi 2s_{1/2}$	$\pi 1f_{7/2}$	$\pi 1f_{5/2}$	$\pi 2p_{3/2}$	$\pi 2p_{1/2}$	$\nu 1d_{5/2}$	$\nu 1d_{3/2}$	$\nu 2s_{1/2}$	$\nu 1f_{7/2}$	$\nu 1f_{5/2}$	$\nu 2p_{3/2}$	$\nu 2p_{1/2}$
7^+_1	2.543	5.9399	2.2015	1.9361	0.9113	0.0094	0.0015	0.0003	5.9874	3.9376	1.9975	1.0449	0.0166	0.0158	0.0002
6^+_1	2.879	5.9408	2.5958	1.9281	0.5174	0.0147	0.0027	0.0005	5.9585	3.5948	1.9820	1.4218	0.0330	0.0089	0.0011
6^+_2	3.353	5.9321	2.6201	1.9485	0.4405	0.0382	0.0160	0.0046	5.9599	3.5781	1.9612	1.3788	0.0517	0.0634	0.0069
7^+_2	3.872	5.9319	2.7371	1.9427	0.3626	0.0226	0.0016	0.0015	5.9680	3.4305	1.9897	1.5304	0.0298	0.0479	0.0036
8^+_1	4.365	5.9386	2.6356	1.9901	0.4117	0.0238	0.0001	0.0001	5.9663	3.4707	1.9987	1.5267	0.0316	0.0060	0.0001
9^+_1	4.875	5.9501	2.2030	1.9661	0.8361	0.0146	0.0001	0.0000	5.9776	3.8732	1.9999	1.1299	0.0193	0.0001	0.0000
7^+_3	4.906	5.9375	2.6704	1.8794	0.4795	0.0278	0.0032	0.0021	5.9609	3.5837	1.9680	1.3364	0.0447	0.1042	0.0021
8^+_2	5.282	5.9458	2.2717	1.8834	0.8813	0.0166	0.0004	0.0008	5.9814	3.9188	1.9989	1.0623	0.0231	0.0150	0.0006
9^+_2	6.484	5.9395	2.8836	1.9994	0.1565	0.0210	0.0001	0.0000	5.9570	3.2206	2.0000	1.7990	0.0232	0.0003	0.0000
9^+_3	7.747	5.9074	3.0730	1.0471	0.9612	0.0100	0.0013	0.0000	5.9767	3.9968	1.9991	1.0053	0.0185	0.0036	0.0000

(8^+_1), and (9^+_2) levels in ^{40}K the average number of neutrons (protons) in the fp shell is close to 2 (0) and the average number of neutrons (protons) in the sd shell is close to 11 (11). Therefore, the structure of these positive parity levels in ^{40}K can be well described by coupling one proton and one neutron hole to the sd shell of ^{42}Ca. On the other hand, for the (7^+_1), (8^+_2), (9^+_1), and (9^+_3) levels, the average number of neutrons (protons) in the fp shell is close to 1 (1) and the average number of neutrons (protons) in the sd shell is close to 12 (10). Therefore, the structure of these positive parity levels in ^{40}K can be well described by coupling two proton holes to the sd shell of ^{42}Sc. We therefore calculated the two-nucleon transfer spectroscopic factor for the positive parity states of interest in ^{40}K in terms of one proton hole + one neutron hole and two proton holes coupled to the sd shell of the low-lying positive parity states in ^{42}Ca and ^{42}Sc, respectively. The details of these calculations are discussed in the next section.

In order to perform the two-nucleon transfer spectroscopic factors calculation to obtain the parentage of the positive parity levels (6^+ to 9^+) in ^{40}K, we have to first calculate the wave function of the states of interest in ^{40}K, ^{42}Ca, and ^{42}Sc. The LBSM calculations were therefore carried out using the code OXBASH to obtain the wave function of states of interest in ^{42}Ca and ^{42}Sc. The SDPFMW effective interaction was used in these calculations. Comparisons between experimental and calculated energies of the levels in ^{42}Ca and ^{42}Sc are shown in Figs. 10 and 11, respectively.

In two-nucleon transfer spectroscopic factor calculations, for a particular state in ^{40}K, the number of contributions from different orbitals for different ΔJ (depending on the core angular momentum and the angular momentum of the level of interest) increases considerably. Therefore, we considered only the contributions having spectroscopic amplitude $\geqslant$0.05. Whenever the maximum contribution is $\leqslant$0.05, we took only the maximum spectroscopic amplitude. The calculated spectroscopic factors, i.e., the square of the spectroscopic amplitude, for the positive parity levels in ^{40}K are shown in Figs. 12 and 13.

The result shows that, among all the positive-parity levels in ^{40}K, 7^+_1, 8^+_2, 9^+_1, and 9^+_3 levels are primarily generated from the yrast 7^+ level of ^{42}Sc. The 6^+_1 level in ^{40}K is primarily generated from the 6^+ $(T = 1)$ level of ^{42}Ca or ^{42}Sc. In the previous work [17], 6^+_1, 7^+_1, (8^+_2), and 9^+_1 levels were identified as coupling of a pair of proton holes with $J = 2$ to the 7^+ state in ^{42}Sc. We found that the 7^+_3, 8^+_1, and 9^+_2 levels are primarily generated from the 6^+ $(T = 1)$ level of ^{42}Ca or ^{42}Sc. In a similar way, 6^+_2 and 7^+_2 levels in ^{40}K are primarily generated from the 4^+ $(T = 1)$ level of ^{42}Ca or ^{42}Sc. Previously, (6^+_2), (7^+_2), (8^+_1), and (9^+_2) levels were identified as the $T = 0$ and $J = 3$ multiplet coupled to the 6^+ state in ^{42}Ca [17].

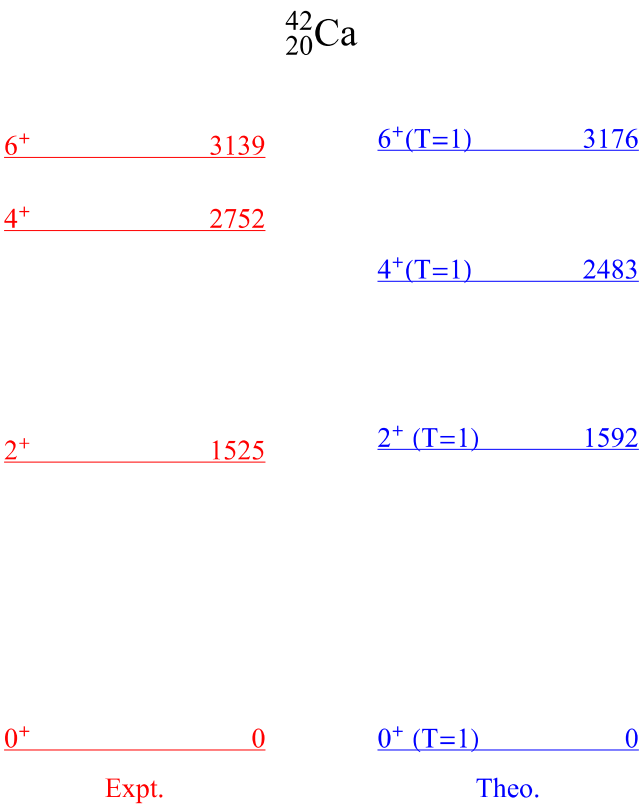


FIG. 10. Comparison of theoretical and experimental positive parity levels in ^{42}Ca. Only the levels of interest are shown in this figure.

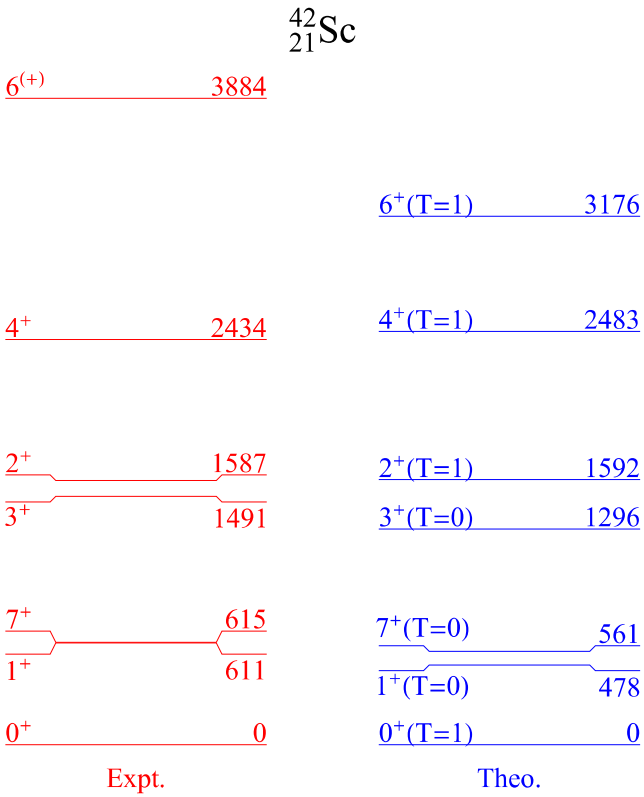


FIG. 11. Comparison of theoretical and experimental positive parity levels in ^{42}Sc. Only the levels of interest are shown in this figure.

V. CONCLUSION

High spin states of ^{40}K populated through the ^{27}Al(^{19}F, αnp)^{40}K reaction with a 68 MeV ^{19}F beam were studied using the Indian National Gamma Array (INGA) facility. Six new levels and fourteen new transitions were added in the existing level scheme. The spins and parities of most the levels were assigned, modified, or confirmed from $R_{\rm DCO}$ and linear polarization measurements. For a few weak transitions, $R_{\rm ADO}$ measurements were carried out to assign their dipole or quadrupole nature. The multipole mixing ratios (δ) of most of the transitions were measured. Large-basis shell-model calculations were performed to understand the microscopic origin of these levels. In our calculations, different particle restrictions in *sd* and *pf* shell orbitals were used to reproduce the experimental level scheme. Collectivity in terms of particle partitions with angular momentum and excitation energy was studied. The experimental transition strengths for a few transitions were compared with the calculated values. Level lifetimes for most of the levels were predicted based on the results obtained from LBSM calculations. Two-nucleon transfer spectroscopic factors were calculated to understand the origin of the low-lying positive parity levels in ^{40}K.

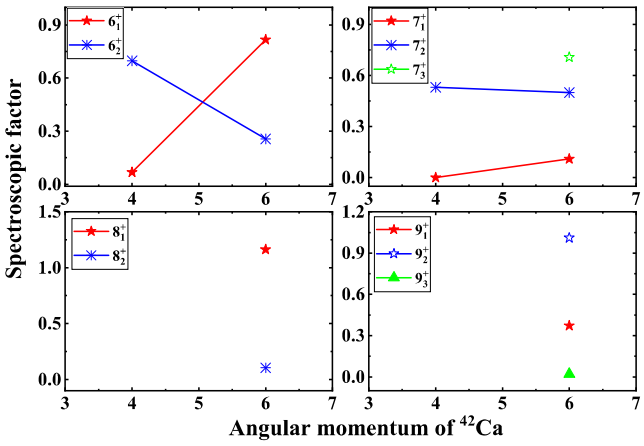


FIG. 12. Calculated spectroscopic factors for the positive-parity states in ^{40}K to estimate the contribution of the low-lying positive-parity states of the core nucleus, ^{42}Ca.

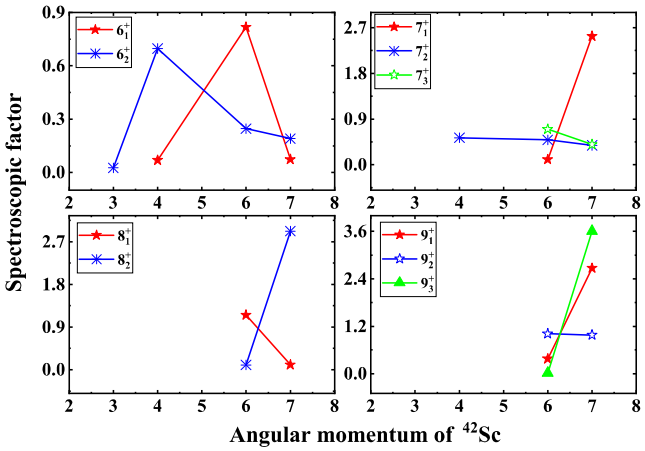


FIG. 13. Calculated spectroscopic factors for the positive-parity states in ^{40}K to estimate the contribution of the low-lying positive-parity states of the core nucleus, ^{42}Sc.

ACKNOWLEDGMENTS

The authors acknowledge the help from all other INGA collaborators and the Pelletron staff of IUAC for their support and cooperation. Special thanks are due to Dr. Debdulal Kabiraj and Abhilash S. R. for their technical help for target preparation and to the Pelletron staff for a nearly uninterrupted beam. One of the authors (R.R.) would like to express her deep gratitude towards Science and Engineering Research Board – Department of Science and Technology (SERB-DST), Government of India (Project No. EMR/2016/006339), for generous financial support. This work was also partially funded by a research grant (Project No. EMR/2016/006339) from SERB-DST, Government of India. The Department of Science and Technology (Grant No. IR/S2/PF-03/2003-III), Government of India, is thankfully acknowledged for supporting the Indian Gamma Array Collaboration.

[1] http://www.nndc.bnl.gov/ensdf/.
[2] F. D. Vedova *et al.*, Phys. Rev. C **75**, 034317 (2007).
[3] R. Kshetri *et al.*, Nucl. Phys. A **781**, 277 (2007).
[4] S. Aydin *et al.*, Phys. Rev. C **86**, 024320 (2012); **89**, 014310 (2014).
[5] A. Bisoi *et al.*, Phys. Rev. C **90**, 024328 (2014).
[6] A. Bisoi *et al.*, Phys. Rev. C **89**, 024303 (2014).
[7] A. Bisoi *et al.*, Phys. Rev. C **88**, 034303 (2013).
[8] A. Das *et al.*, Phys. Rev. C **101**, 044310 (2020).
[9] R. Rahaman *et al.*, Phys. Rev. C **102**, 024315 (2020).
[10] W. J. Gerace and A. M. Green, Nucl. Phys. A **123**, 241 (1969).
[11] E. Ideguchi *et al.*, Phys. Rev. Lett. **87**, 222501 (2001).
[12] K. Hadynska-Klek *et al.*, Phys. Rev. Lett. **117**, 062501 (2016).
[13] C. E. Svensson *et al.*, Phys. Rev. Lett. **85**, 2693 (2000).
[14] D. Rudolph *et al.*, Phys. Rev. C **65**, 034305 (2002).
[15] E. Ideguchi *et al.*, Phys. Lett. B **686**, 18 (2010).
[16] Y.-C. Yang, Y.-X. Liu, Y. Sun, and M. Guidry, Eur. Phys. J. A **54**, 217 (2018).
[17] P.-A. Söderström *et al.*, Phys. Rev. C **86**, 054320 (2012).
[18] R. Rahaman *et al.*, Proc. DAE-BRNS Symp. Nucl. Phys. (India) **66**, 124 (2022).
[19] S. Muralithar *et al.*, Nucl. Instrum. Methods Phys. Res., Sect. A **622**, 281 (2010); S. Ray *et al.*, Proc. DAE-BRNS International Symp. Nucl. Phys. (India) **54**, 56 (2009).
[20] M. Jain, E. T. Subramanian, and S. Chatterjee, Rev. Sci. Instrum. **94**, 013304 (2023).
[21] R. Bhowmick *et al.*, Proc. DAE-BRNS Symp. Nucl. Phys. (India) B **44**, 422 (2001).
[22] A. Gavron, Phys. Rev. C **21**, 230 (1980).
[23] E. S. Macias, W. D. Ruhter, D. C. Camp, and R. G. Lanier, Comput. Phys. Commun. **11**, 75 (1976).
[24] M. Piiparinen, A. Ataç, J. Blomqvist, G. B. Hagemann, B. Herskind, R. Julin, S. Juutinen, A. Lampinen, J. Nyberg, G. Sletten, P. Tikkanen, S. Tormanen, A. Virtanen, and R. Wyss, Nucl. Phys. A **605**, 191 (1996).
[25] K. Starosta *et al.*, Nucl. Instrum. Methods Phys. Res., Sect. A **423**, 16 (1999).
[26] K. S. Krane and R. M. Steffen, Phys. Rev. C **2**, 724 (1970).
[27] M. Lach *et al.*, Eur. Phys. J. A **16**, 309 (2003).
[28] B. A. Brown, A. Etchegoyen, W. D. M. Rae, and N. S. Godwin, MSU-NSCL Report No. 524, 1985 (unpublished).
[29] E. K. Warburton, J. A. Becker, and B. A. Brown, Phys. Rev. C **41**, 1147 (1990).
[30] P. Mason *et al.*, Phys. Rev. C **71**, 014316 (2005).
[31] M. Ionescu-Bujor *et al.*, Phys. Rev. C **73**, 024310 (2006).
[32] M. Ionescu-Bujor *et al.*, Phys. Rev. C **80**, 034314 (2009).
[33] G. F. Knoll, *Radiation Detection and Measurement* (John Wiley and Sons, New York, 1979).
[34] J. F. Ziegler, J. Biersack, and U. Littmark, *The Stopping and Range of Ions in Matter* (Pergamon, Oxford, 1985).
[35] E. K. Warburton, J. J. Kolata, and J. W. Olness, Phys. Rev. C **11**, 700 (1975).
[36] C. J. Chiara *et al.*, Phys. Rev. C **75**, 054305 (2007).

APS (https://www.aps.org/)

PHYSICAL REVIEW C (/PRC/)
covering nuclear physics

Highlights (/prc/highlights) Recent (/prc/recent) Accepted (/prc/accepted) Collections (/prc/collections) Authors (/prc/authors)
Referees (/prc/referees) Search (/search) Press (/press) About (/prc/about) Editorial Team (/prc/staff) (/feeds)

Spectroscopic study of

Rozina Rahaman, Abhijit Bisoi, Ananya Das, Y. Sapkota, Arkabrata Gupta, S. Ray, S. Sarkar, Yashraj, A. Sharma, Bharti Rohila, I. Ahmed, Kaushik Katre, S. Dutt, S. Kumar, R. P. Singh, R. Kumar, and S. Muralithar
Phys. Rev. C **109**, 024318 – Published 15 February 2024

More

Article

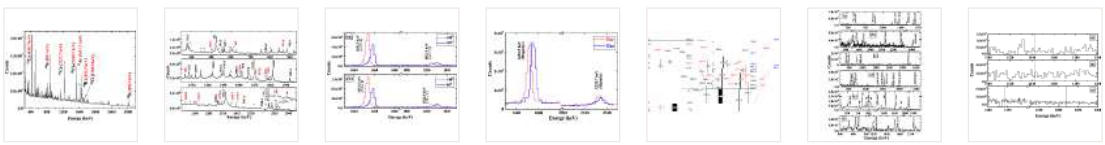
PDF (/prc/pdf/10.1103/PhysRevC.109.024318) HTML (/prc/abstract/10.1103/PhysRevC.109.024318#fulltext)

Export Citation (/prc/export/10.1103/PhysRevC.109.024318)

ABSTRACT
AUTHORS
ARTICLE TEXT
INTRODUCTION
EXPERIMENTAL DETAILS AND DATA ANALYSIS
RESULT AND DISCUSSION
THEORETICAL CALCULATION
CONCLUSION
ACKNOWLEDGMENTS
REFERENCES

ABSTRACT

High spin states of populated through the (2) reaction at 68 MeV beam energy were studied using the Indian National Gamma Array (INGA) facility. Six new levels and fourteen new transitions were added to the existing level scheme. The spins and parities of most of the levels were assigned, modified, or confirmed from , , and linear polarization measurements. The multipole mixing ratios O1 for most of the transitions were measured. Large-basis shell-model calculations were performed to understand the microscopic origin of the levels. Different particle restrictions in and shell orbitals were used to explain the experimental results.



6 More

Received 31 August 2023 Revised 21 December 2023 Accepted 19 January 2024

DOI: https://doi.org/10.1103/PhysRevC.109.024318

©2024 American Physical Society

Physics Subject Headings (PhySH)

This site uses cookies. To find out more, read our Privacy Policy (https://www.aps.org/about/privacy.cfm).

Research Areas

I Agree ()

Already have a manuscript?

Use our Manuscript Matcher to find the best relevant journals!

Find a Match

Refine Your Search Results

2469-9985 Search

Sort By: Title (A-Z)

Search Results

Found 1 results (Page 1) Share These Results

Exact Match Found

PHYSICAL REVIEW C

Publisher:	AMER PHYSICAL SOC , ONE PHYSICS ELLIPSE, COLLEGE PK, USA, MD, 20740-3844
ISSN / eISSN:	2469-9985 / 2469-9993
Web of Science Core Collection:	Science Citation Index Expanded
Additional *Web of Science* Indexes:	Current Contents Electronics & Telecommunications Collection | Current Contents Physical, Chemical & Earth Sciences | Essential Science Indicators

Share This Journal View profile page

** Requires free login.*

Filters Clear All

Web of Science Coverage

Open Access

Category

Country / Region

Language

Frequency

Journal Citation Reports

10

Editorial Disclaimer: As an independent organization, Clarivate does not become involved in and is not responsible for the editorial management of any journal or the business practices of any publisher. Publishers are accountable for their journal performance and compliance with ethical publishing standards. The views and opinions expressed in any journal are those of the author(s) and do not necessarily reflect the views or opinions of Clarivate. Clarivate remains neutral in relation to territorial disputes, and allows journals, publishers, institutes and authors to specify their address and affiliation details including territory.

Criteria for selection of newly submitted titles and re-evaluation of existing titles in the Web of Science are determined by the Web of Science Editors in their sole discretion. If a publisher's editorial policy or business practices negatively impact the quality of a journal, or its role in the surrounding literature of the subject, the Web of Science Editors may decline to include the journal in any Clarivate product or service. The Web of Science Editors, in their sole discretion, may remove titles from coverage at any point if the titles fail to maintain our standard of quality, do not comply with ethical standards, or otherwise do not meet the criteria determined by the Web of Science Editors. If a journal is deselected or removed from coverage, the journal will cease to be indexed in the Web of Science from a date determined by the Web of Science Editors in their sole discretion – articles published after that date will not be indexed. The Web of Science Editors' decision on all matters relating to journal coverage will be final.

Clarivate.™ Accelerating innovation.

© 2024 Clarivate Legal center Privacy notice Cookie policy
Manage cookie preferences Copyright notice Help

5

Diseaseof Vegetable Crops and their Integrated Management Approaches

Sayeda Parveen Qureshi

Associate Professor, P.G. Department of Botany, J.M.Patel College, Bhandara(M.S.)

Abstract

A survey on the prevalence of vegetable diseases was carried out in various regions of the Bhandara district in Maharashtra. The selected plant diseases were selected on the basis of their economic value and plant characteristics. The study included ten different infected Plants. The purpose of this study was to study the impact of various environmental factors and Pathogens against various vegetable diseases and to develop appropriate strategies for the management of vegetable diseases. Infectious plant diseases are caused by various pathogenic organisms like Bacteria, Fungi viruses, Pest and insects. As agriculture has developed, infectious plant diseases are becoming more and more important in terms of crop yield and economic productivity.This research focuses on eco-friendly solutions to tackle these issues, with a focus on prevention, biocontrol and plant extracts.

Keywords-Diseases,Environmental, Infectious,Pathogen.

Introduction

Vegetables are important source of dietary fibers, minerals, antioxidants and vitamins. Vegetable crops are cultivated worldwide for its nutritional benefits and nutraceutical properties. The disease can occur when pathogenic organisms such as fungi, bacteria, viruses and nematodes; soil PH; temperature extremes; changes in the quantity of moisture and humidity in the air; and other elements continuously harm a plant. Plant diseases can have an impact on the growth, function, and structure of plants and crops, affecting the people that rely on them.Epidemiological studies indicate that fruit and vegetables are health-promoting and protective against disease, particularly cardiovascular disease and cancer. Possible plant nutrients providing this protection include antioxidants and dietary fibre. Clinical trials with antioxidant supplements give inconsistent results for protection against lung cancer in smokers, invasive cervical cancer, oesophageal and gastric cancers, colorectal polyps and coronary heart disease. The antioxidants used in trials may be contributing to a more complex system. Antioxidants have differing solubilities which partition across the phases of tissues, cells and macromolecular structures: water-soluble ascorbate, glutathione and urate; lipid-soluble tocopherols and carotenoids, and intermediatory-soluble flavonoids and hydroxycinnamic acids.(M.A.Eastwood,1999).Crucifers are popular temperate vegetables and occupy important place among vegetables in India as well as in the world. India is the second largest producer of crucifers in the world. These crops are affected by many diseases during the growing period which reduce the yield as well as the quality of the produce. Amongst all the diseases, black rot caused by *Xanthomonas campestrispv. campestris* (Pam.) is the most destructive one causing heavy losses. The disease affects primarily above ground parts of the plant at any stage of growth and causes high losses, in yield and quality especially in tropical and subtropical regions during the rainy season.(Gupta M et.al.2013).Phytopathogenic diseases,

however,cause huge losses to vegetables during cultivation, transportation and storage. To protect vegetable losses, various strategies including chemicals and biological practices are used worldwide. Due to the negative health effects of chemical fungicides via food chain, the recent trend is shifting towards safer and more eco-friendly biological alternatives for the control of vegetable diseases.

MATERIAL AND METHODOLOGY:

I.FIELD SURVEY

Bhandara district is one of the administrative districts in the Indian state of Maharashtra. The area of Bhandara district covers 4087 km2 sq. Bhandara district has a latitude of 21.170000 nautical miles (km2) and a longitude of 79.65002 (km2).Bhandara Maharashtra is located in India country under the cities place category. The GPS coordinate of Bhandara is 21*10' 12,0000 N and 79*39' 0.0072 E.The survey was carried out in Bhandara District State of Maharashtra. The areas surveyed were Bela, Gunjepar, Hiwara, Mujbi, Pauni. A sample of infected vegetable plants was collected during the survey. The field study included the distribution of diseases. Some photographs of diseased vegetables were taken during the survey from the field.

II.SAMPLE COLLECTION

The disease was found in the followingvegetable plants -*Abelmoschus esculentus , Capsicum annum L., Solanum lycoperisicum ,Brassica oleracea var botrytis ,Raphanus sativa*, *Solanum melongena, Brassica oleraceaevar.capitata Phaseolus vulgaries Pisum sativum ,Cucurbita*.The samples were collected from various areas of the Bhandara District. The diseases were identified in the laboratory. Six fungal and four bacterial diseases were found on this vegetable crop.

Result and Discussion

Observation Table

S.N	Vernacular name	Botanical Name	Types of disease	Pathogen	Symptoms
1	Bhindi (Okra)	*Abelmoschus esculentus*	Fungal (powdery mildew)	*Erysiphecicho racearum*	Powder-like white spots may appear on the top and bottom surfaces of the leaf and develop rapidly into large spots.
2	Mirchi (Chilli)	*Capsicum annum L.*	Fungal (leaf spot)	*Cercosporaca psici*	On the leaves, brownish circular spots appear with light grey centres and reddish brown edges.

3	Tamatar (Tomato)	*Solanum lycopersicum*	Bacterial fruit canker	*Clavibactermi chiganensis*	Yellow and brown spots appear on fruit surface.Tips of foliage turn crunchy with yellow streaking
4	Fullgobhi (Cauliflowe r)	*Brassica oleraceaevar.botr ytis*	Bacterial (Black rot)	*Xanthomasco mpestris*	Blackflecks or scorched leaf margins appear. Theinfected cauliflower heads often become blackened.
5	Muli (Radish)	*Raphanus sativa*	Fungal (Fusarium wilt)	*Fusariumoxys porum sp.*	Wilting of plants is observed more commonly once flowering commences and yellowing spreads to younger leaves.
6	Vangi (Brinjal)	*Solanum melongenum*	Fungal (leaf spot)	*Cercosporam elongenae*	The leaf spots are characterized by chlorotic lesions, angular to irregular in shape, laterturn grayish brown
7	Pattagobi (Cabbage)	*Brassica oleraceaevar.capi tata*	Fungal (Downy mildew)	*Peronosporap arasitica*	light green-yellow lesions on the upper and lower leaf surface. Later the leaf may become papery and die.
8	French bean	*Phaseolus vulgarise*	Bacteria (Common Blight)	*Xanthomonas campestris pv.phaseoli*	Watersoaked,angular shaped spot on leaves, spots form at the margins and interveinal regions
9	Matar	*Pisum sativum*	Bacteria Bacterial blight	*Pseudomonas syringae PV.pisi*	Small water-soakedspot on leaves stem and pods which coalesce and turn brown and necrotic
10	Pumpkin	*Cucurbita*	Fungus (Black Rot)	*Xanthamonas compestris*	Symptoms on the leaves begin as marginal necrosis followed by large Wedged shaped necrotic area, often with yellow and black hole.







Fig.1-Fungal powdery mildew in Bhindi Fig.2-Fungal (leaf spot) in ChilliFig.3Bacterial fruit canker in Tomato







Fig.4-Fungal wiltin Radish Fig.5- Bacterial Black rot in Cauliflower Fig.6-Fungal leaf spot in Brinjal







Fig.7-BacteriaCommon Blight in French Bean Fig8. Bacterial blight in Pea Fig.9- Black Rot in Pumpkin

Integrated Management

These vegetables are one of the most widely consumed vegetables in Maharashtra due to their availability in local markets, affordability and consumer preference. Vegetable diseases cause a lot of harm to vegetable crops, such as a decrease in growth and yield, a decrease in the quality of the crops, and a decrease in the income of the grower/farmers. Various methods can be used to control vegetable diseases, including (I) cultural practices management, (II) plant nutrient management, and (III) biological control methods.

1.Cultural Practices Management

Cultural practices management includes collection and destruction of diseased plant debris, crop rotation and the use of disease-free seeds to reduce the primary pathogen in the field, wider plant spacing, destruction of weed hosts from the field and the control of vectors, and proper sanitation in the field.

2.Plant Nutrient Management

In order to implement integrated plant nutrient supply (IPNS), it is important to understand and take advantage of the positive interactions between plant nutrients. This will help farmers to increase their yields, soil quality, and the NUE of the nutrients applied.

3.Biomanagement

Biomanagement is the process of using biological materials, especially nonpathogenic soil microbiota,to control the plant pathogens, often referred to as "biological control". The term "biological control" is used to describe the process of using one or several organisms, in isolation or in combination, to eliminate harmful microbes. Bacillus *spp*., Gram positive micro-organism, has been widely used for bio management as a disease suppressor. It is highly adaptable to adverse environmental conditions and is well-suited for the production of endospores for commercial formulations. OtherGram negative micro-organisms have been given special attention as biomass control agents, such as *Pneumoniae spp*.These micro-organisms are highly adaptable to catabolic mode of metabolism, have an excellent root colonizing abilities, and are capable of producing a wide range of antifungal metabolites.

Conclusion

Integrated disease management (IDM) can be thought of as “a tool kit” to control various fungal, bacterial and viral diseases simultaneously. IDM is a sustainable practice that can benefit all types of farmers. It is cost-effective, environmentally friendly and easy to implement. Resistant and tolerant varieties are proven to be more effective than any other method. Chemical methods must not be followed regularly as pathogens can become resistant to them.One of the new but promising approaches for disease control in vegetable crops is the utilization of microbial bio-control agents which are inexpensive and environmentally friendly. The use of these microbial preparations in disease control has been found to be very effective and cost-effective by growers, but more knowledge is needed about the mechanistic basis for disease suppression. There is also a need to raise awareness among growers to increase its use in various agronomic regions and reap the benefits of this low-cost technology for vegetable growers.

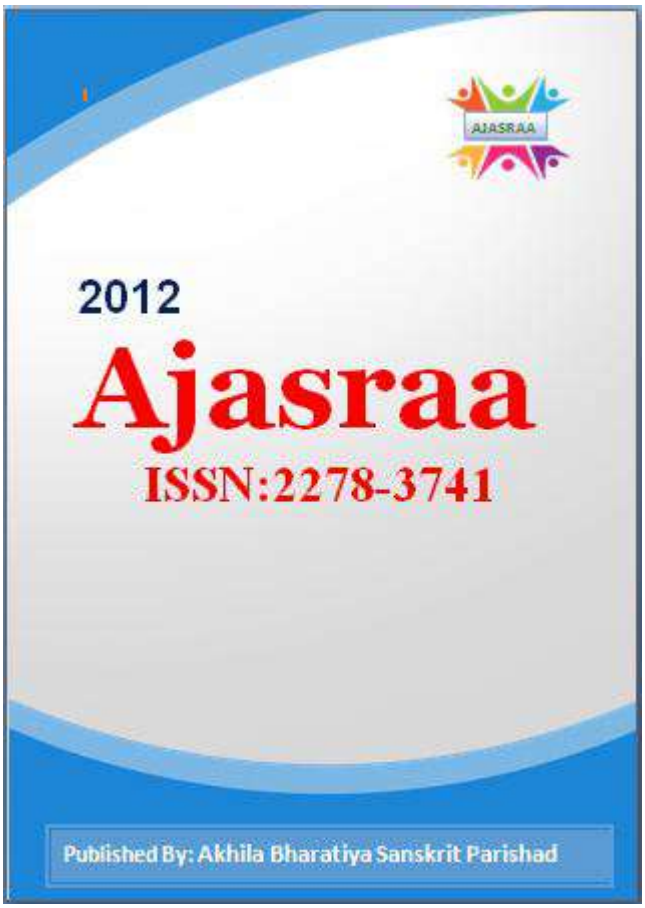
References

- Compendium of Brassica Diseases. American Phytopathological Society Press. Available at http://www.apsnet.org/apsstore/shopapspress/Pages/43443.aspx
- Dhuraj, I.U. et al., (1999). Field evaluation of fungicides against powdery mildew of fengugreek ,J.Mycol.Pl.Pathol.,30 (l):98-99.
- Dhutraj,D.N. (2011). Efficacy of fungicides and bioagents against powdery mildew of Okra J.Pl. Dis. Sci. 6(2):170-172.
- Eigenbrode, S. D. and Trumble, J. T. (1994). Host plant resistance to insects in integrated pest management in vegetable crops. J. Agric. Entomol, 11(3); 201-224(July 1994)
- Etana M.B.et.al (2019) Major onion (*Allium cepa L.*) production challenges in Ethiopia: A review. Journal of Biology, Agriculture and Healthcare. 30;9(7):42-7.
- Gupta ,S. K.andK.R.Shyam ,(1998). Control of powdery mildew and rust of pea by fungicides, Indian Phytopath,51(2):184-186.
- Gupta, M. et.al. (2013). Black rot-A devastating disease of crucifers: a review. Agricultural Reviews, 34(4), 269-278.
- Hidayah ,B.N.et.al(2020) White Rot Disease on Garlic Crop: Identification of the Pathogen and Exploration of the Controlling Strategies .Advances in Biological Sciences Research, volume 14 pg 437-439
- https://www.cabi.org/cpc/datasheet/39723
- Kumar, P., and Poehling, H. M. (2014). Effects of azadirachtin , abamectin , and spinosad on sweet potato whitefly (Homoptera: Aleyrodidae) on tomato plants under laboratory and greenhouse conditions in the humid tropics. Journal of Economic Entomology, 100(2), 411-420.
- Kunkalikar S.R, et.al (2011). Importance and genetic diversity of vegetable-infecting to viruses in India. Phyto pathology. ;101(3):367-76.
- M.A.Eastwood, (1999) .Interaction of dietary antioxidants in vivo: how fruit and vegetables prevent disease?, QJM: An International Journal of Medicine, Volume 92, Issue 9, Pages 527–530, https://doi.org/10.1093/qjmed/92.9.527
- Martínez-dela ParteE et.al.(2013). First report of white mould of beans caused by Sclerotiniasclerotiorum in Cuba. Canadian Journal of plant pathology 27(5), 353-365.

- Mishra R.K.et. al. (2013) Diseases Of Vegetable Crops And Their Integrated Management: A Colour Handbook. New India Publishing Agency.
- Nagendran,K. et.al. (2018) First report of peanut bud necrosis virus infecting bitter gourd (Momordicacharantia L.) in India. Plant Disease. 19;102(3):690.
- Overman, A. J. (1985). Off-season land management, soil solarization and fumigation for tomato. The journal Proceedings-Soil and Crop Science Society of Florida (USA)ISSN: 0096-4522,volume (44)(1985),35-39.
- Peter J.W.et.al (2017) A long-term vegetable crop rotation study to determine effects on soil microbial communities and soilborne diseases of potato and onion. New Zealand Journal of Crop and Horticultural Science 45:1, pages 29-54.
- Plant Disease Management Report: Report No. 4:V060.
- Raid, R. N.(2010) . Evaluation of fungicides for control of downy mildew on broccoli, Spring 2009.
- Shahid,M.et.al. (2017) Recent Advances in Management Strategies of Vegetable Diseases.Microbial Strategies for Vegetable Production,DOI 10.1007/978-3-319-54401-4_9
- Shahnaz,E.et.al. (2021) Postharvest Fungal Diseases in Stone Fruits and Their Management. In Postharvest Handling and Diseases of Horticultural Produce15 (pp. 259-266). 6000 Broken Sound Parkway NW, Suite 300, Boca Raton, FL 33487-2742: CRC Press.
- Sharma, S.et.al. (2017). Integrated disease management of storage rot of ginger (Zingiber officinale) caused by Fusarium sp. in Himachal Pradesh, India. Int. J. Curr. Microbiol. App. Sci, 6(12), 3580-3592.
- Srivastava, S.and Scot Nelson (1982)Cercospora Leaf Spot of Eggplant University of Hawai'I at Mãnoa. College of Tropical Agriculture and Human Resources. Plant Disease 82: 1-5. http://www.ctahr.hawaii.edu/oc/freepubs/pdf/pd-82.pdf
- Stevens,C.et.al (2003). Integration of soil solarization with chemical, biological and cultural control for the management of soilborne diseases of vegetables. Journal of Plant and soil; 253(2), 493-506.
- Vijaya, T., M. et al. (1991). Epidemiology of Cercospora Leaf Spot Disease of Brinjal – Process of Penetration,Environment & Ecology 9.2: 396-98.
- Welles and Colin G. (1922).Cercospora Leaf Spot of Eggplant , Phytopathology Vol.12 No.2.

- Woodward, J. E. et.al (2005). First report of botrytis blight of peanut caused by botrytis cinerea in Georgia. Journal of Plant diseasesn; 89(8), 910-910.
- Yadav,M.et.al (2021). Systemic Resistance in Chilli Pepper against Anthracnose (Caused by Colletotrichum) induced by Trichoderma harzianum, Trichoderma asperellum and Paenibacillusdendritiformis. Journal of Fungi, 7(4), 307.

About the Journal



Kindly email your paper on email: ajasrajournal@gmail.com

Publication from 2012 to 2019 available in Print form only

website: www.ajasra.in , Journal Name: Ajasraa

ISSN: *2278-3741,* *UGC CARE GROUP 1 Journal*

The (Ajasraa ISSN: 2278-3741) publishes original research in English and Hindi language in all subjects. As a comparative education journal, owned by the Akhila Bharatiya Sanskrit Parishad Education Society, we are especially interested in work that is either explicitly or implicitly comparative. Explicitly comparative research includes cross-national studies or studies that compare educational phenomena in a range of countries. Implicitly comparative research typically means single nation case studies that contribute to a larger comparative framework about the topic. Such studies must show how the particular case is theoretically relevant for readers outside the given country.

UGC-CARE List

You searched for "**2278-3741**". Total Journals : **1**

Search:

Sr.No.	Journal Title	Publisher	ISSN	E-ISSN	UGC-CARE coverage years	Details
1	Ajasraa	Akhila Bharatiya Sanskrit Parishad	2278-3741	NA	from January-2022 to Present	View

Showing 1 to 1 of 1 entries

Previous 1 Next

Copyright © 2024 Savitribai Phule Pune University. All rights reserved. | Disclaimer

Educational Administration: Theory and Practice
2024, 30(5), 2345-2355
ISSN: 2148-2403
https://kuey.net/

Research Article

Synthesis, Characterization, In Vitro Anticancer and Antimicrobial Evaluation of Cu(II), Co(II), Zn(II), Mn(II) and Fe(II) Complexes Derived from Dihydralazine and 2-Formyl Thymol

Chaitu N. Bhoi[1], Rahul T. Bhoi[1], Samina K. Tadavi[2], Ajay M. Ghatole[2], Ratnamala S. Bendre[1*]

[1]School of Chemical Sciences, KBC North Maharashtra University, Jalgaon, Maharashtra, 425001, India
[2]Department of Chemistry, J. M. Patel Arts, Commerce and Science College, Bhandara, Maharashtra 441904 India

[*]**Corresponding Author**: Ratnamala S. Bendre
[*]Tel.: +91-9422211435; E-mail addresses: bendrers@gmail.com

Citation: Chaitu N. Bhoi et al. (2024) Synthesis, Characterization, In Vitro Anticancer And Antimicrobial Evaluation Of Cu(II), Co(II), Zn(II), Mn(II) And Fe(II) Complexes Derived From Dihydralazine And 2-Formyl Thymol, *Educational Administration: Theory and Practice*, *30*(5), 2345-2355
Doi: 10.53555/kuey.v30i5.3285

ARTICLE INFO

ABSTRACT

In the present work, we report a new series of Cu(II)(1), Co(II)(2), Zn(II)(3), Mn(II)(4), and Fe(II)(5) complexes of hydrazone ligand (H_2L) synthesized from 2-formyl derivative of thymol and Dihydralazine by environment friendly method. The hydrazone ligand (H_2L) behaves as a dibasic hexadentate ligand and forms dinuclear metal complexes with the general composition $[M_2L(Cl)_m(H_2O)]_n$ (M = Cu(II), Co(II), Zn(II), Mn(II), and Fe(II); m = 1-2 and n = 0-4) by the reaction of hydrazone (H_2L) and metal salts (MCl_2) in the presence of methanol as solvent. The geometry and the nature of bonding of the desired complexes have been presumed from ESI-MS, FTIR, UV-Vis, elemental analyses, TGA, molar conductivity and magnetic susceptibility measurements. The results show that the ligand (H_2L) forms coordinate bonds with central metal ions through nitrogens of phthalazine as well as azomethine (–C=N–) groups and phenolic oxygen atoms. The hydrazone based ligand (H_2L), and its metal complexes were screened for their in vitro anticancer activity against breast cancer cell line (MDA-MB-231); where Cu(II)(1) and Zn(II) (3) complexes were found to have excellent anticancer activity with the GI_{50} value <10 µg/mL and 36.6 µg/mL respectively. All the prepared compounds were also assessed for their antimicrobial and antioxidant activities and were found to be more potent than their parent ligand.

Keywords: Dihydralazine hydrazone, Thymol, Anticancer, Antimicrobial activity, Antioxidant, TGA analysis

1. Introduction

Hydrazones, a significant class of chelating agents, are Schiff bases that are produced when hydrazines condense with carbonyl compounds. In coordination chemistry, heterobinuclear transition metal complexes have emerged as a major area of study in recent years. The primary goals of this class of studies are biological significance research [1,2], electrochemical applications [3,4], chemo sensing [5], or catalysis [6]. Using appropriate polydentate ligands with the ability to hold metals in a rigid arrangement or labile bridging sites to enable binding and potentially activate a variety of molecular species is a common strategy [7, 8]. Hydrazones, which absolutely form stable metal complexes with the majority of transition metal ions, play a significant role in inorganic chemistry [9, 10]. The achievements in the field of bioinorganic chemistry can be attributed to the growing interest in hydrazone complexes, as it is anticipated that a majority of these complexes may serve as representative examples of physiologically significant species [11–13].
The well-known drug molecule Dihydralazine is one of the most significant heterocyclic scaffolds containing a pyridazine ring fused with a benzene ring. Dihydralazine has numerous applications as antihypertensive

Copyright © 2024 by Author/s and Licensed by Kuey. This is an open access article distributed under the Creative Commons Attribution License which permits unrestricted use, distribution, and reproduction in any medium, provided the original work is properly cited.

drug molecule [14]; but it has already stated in terms of idiosyncratic drug reaction [15]. Dihydralazine oxidizes to nitroso and hydroxylamine products which are known to bind to proteins and may cause adverse effects. [16]. Thymol, a naturally occurring monoterpenoid, and prime constituent of Thymus vulgarias has been known for its own biological importance [17, 18]. Derivatization of Thymol with a variety of functions and coordination to various metal ions has been resulted in active antioxidant [19], anticancer [20], and antimicrobial agents [21]. Researchers are quite interested in metal complexes of hydrazones, however the primary mechanism of action of these medications is still unclear and an open issue [22].

In the present study on hydrazones, we have synthesized a newer 6,6'-((1E,1'E)-(2,2'-(phthalazine-1,4-diyl) bis(hydrazin-2-yl-1-ylidene)) bis(methanylylidene)) bis(2-isopropyl-5-methylphenol) (**H_2L**) hexadentate hydrazone ligand, and its Cu(II), Co(II), Cu(II), Zn(II), Fe(II), and Mn(II) complexes. The synthesized ligand and it's metal complexes have been characterized by various physico-chemical and spectroscopic techniques. The study also reveals the biological activities of the synthesized compounds such as anticancer (MDA-MB 231), antioxidant, and antimicrobial.

2. Results and Discussion

2.1 Characterization of the Ligand

The ligand **H_2L** (**Fig. 1**) was synthesized by reacting Dihydralazine and 2-formyl thymol in 1:2 molar ratio respectively. The yellow colored solid was obtained which is soluble in polar aprotic solvents such as DMSO and DMF and polar protic solvents methanol, iso-propanol and ethanol etc. The homogeneity and purity of the organic ligand was primarily analyzed by TLC (Merck, silica gel 60 F254) technique. The structure of the synthesized ligand was confirmed by ^{1}H NMR, ^{13}C NMR, Mass, and FT-IR spectroscopic techniques. Elemental analyses indicated that the ligand has the molecular formula $C_{30}H_{34}N_6O_2$.

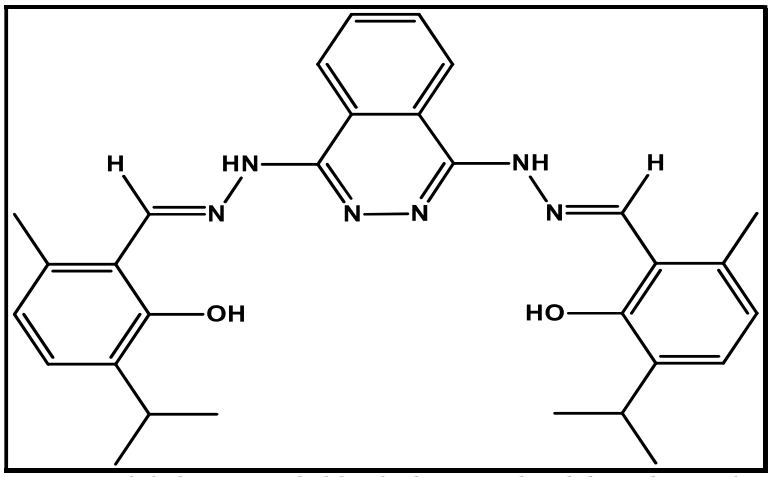


Fig. 1. 6,6'-((1E,1'E)-(2,2'-(phthalazine-1,4-diyl)bis(hydrazin-2-yl-1-ylidene))bis(methanylylidene))bis(2-isopropyl-5-methylphenol) (H_2L)

2.1.1 ^{1}H NMR and ^{13}C NMR spectra

The NMR spectrum was recorded in DMSO-d6 on a Bruker Avance Neo-500 MHz spectrophotometer with TMS as an internal reference standard.

The spectrum of ligand showed two singlet signals in deshielded region at δ 14.10 and δ 12.41 corresponding to the two equivalents –OH protons and two equivalents –NH of two protons respectively. A singlet peak of azomethine group is observed around δ 8.87. A doublet at δ 8.16 (J = 7.65 Hz) and one triplet at δ 9.25–9.29 (J = 7.7 Hz) are corresponding to the aromatic protons of Dihydralazine ring; whereas the two doublets around δ 6.75 (J = 7.7 Hz) and δ 7.39 (J = 7.65 Hz) confirmed the aromatic protons of both thymol rings of ligand; the coupling constants confirmed the adjacent protons of thymol rings. A multiplet around δ 3.29-3.45 is assigned for two sets of protons of isopropyl groups and a singlet appearing at δ 2.50 corresponds to the three protons of methyl group. A doublet of six protons of isopropyl groups appears at around δ 1.20-1.22 (J = 6.9 Hz).

The additional evidence provided by the ^{13}C NMR is the appearance of peaks at δ 19.0, 22.0 and 26.0 clearly indicating the presence of aliphatic carbons of thymol rings in ligand. The peak for the HNC=N carbon of the Dihydralazine scaffold was detected at around δ 155.1 [23]. The overall results of NMR analysis have conveyed the evidences for the structure of synthesized ligand (H_2L).

2.1.2 Mass spectrum

The mass spectrum of the H_2L ligand consists of the molecular ion (M^{+1}) at m/e = 511.5038 amu, with 100 % intensity. Other fragments observed at m/e = 375.57 and 334.57 amu were assigned to $[C_{21}H_{24}N_6O]^+$ and $[C_{19}H_{21}N_5O]^+$ ions, respectively.

2.1.3 IR spectrum

The IR spectrum of the H_2L ligand (Table 3) shows a broad band at 3292 cm^{-1}, assigned to phenolic **ν**(O-H). The spectrum shows also vibrational bands at 1650 and 1564 cm^{-1}, attributed to **ν**(C=C) and **ν**(C=N), respectively [24, 25]. The weak band at 3190 cm^{-1} is characteristic of **ν** (NH) and a sharp peak at 2954 cm^{-1} assignable to **ν**(C-H) group. Whereas the high frequency shift observed at 1138 cm^{-1} is attributed to **ν**(N-N) band which is expected because of the diminished repulsion between the lone pairs of adjacent nitrogen atoms [26].

2.1.4 UV-Visible spectrum

The UV–visible spectrum of the synthesized ligand (H_2L) was recorded in DMF at room temperature. The intense peak at 264 nm could be assigned to π→π* transition of aromatic parts and the band at 287 nm could be due to n→π* transition of azomethine group of the ligand [27].

In the metal complexes moderately intense broad peaks detected in the region, 268–390 nm could be assigned to transitions of ligand based groups, the changes in the position and intensity of n→π* transitions confirm the coordination of ligands to metal. The bands observed around 426-460 nm could be attributed to Ligand to Metal Charge Transfer (LMCT) [28].

Table 1. Physical properties of the ligand H_2L and its metal complexes

Compound Code /(F.wt.)	M.P.	Color	Yield (%)	Elemental analysis, Found / (Cal) %		
				C	H	N
H_2L	>300	Yellow	93	70.12 (70.56)	8.42 (6.71)	15.72 (16.46)
1	>300	Dark Brown	77	54.59 (53.69)	6.75 (6.81)	10.19 (12.52)
2	>300	Army green	75	51.65 (51.67)	7.77 (6.62)	11.01 (12.05)
3	>300	Yellow	72	53.62 (53.39)	7.95 (7.78)	13.50 (12.45)
4	>300	Brown	67	50.54 (50.80)	7.63 (6.83)	9.63 (11.85)
5	>300	Dark brown	63	49.63 (49.63)	8.20 (6.55)	9.35 (11.58)

2.2 Characterization of the metal complexes

The Schiff base hydrazone of 2-formyl thymol and dihydralazine ligand (H_2L) behaves as dibasic hexadentate ligand having an N_4O_2 coordination site. The ligand (H_2L) reacts with chloride salts of Cu(II), Co(II) Zn(II), Mn(II) and Fe(II) through the environment friendly process to yield dinuclear complexes with the general composition $[M_2L(Cl)m(H_2O)]n$ (M = Cu(II), Co(II), Zn(II), Mn(II), and Fe(II); m = 1-2 and n = 0-4) (Fig. 2). Table 2 demonstrates the magnetic moments, UV-VIS absorptions and conductance of the complexes. Table 3 displays the characteristic IR frequencies of the ligand (H_2L) and its metal complexes. The thermal analyses data are presented in Table 4.

2.2.1 Molar conductance data

The conductance values of the metal complexes of **H_2L** were recorded at room temperature for 10^{-3} M solutions of the synthesized metal complexes in DMF solvent and are summarized in Table 2. The conductance values observed in the range 10-19 Ohm^{-1} cm^2 mol^{-1} confirmed the non-electrolytic nature of metal complexes [29]. All the synthesized complexes are non-conducting representing their neutrality and that the divalent metal cations have replaced the hydroxyl and imine protons of ligand molecules. On the basis of above results the suggested structures for the metal complexes are demonstrated in **Fig. 2**.

2.2.2 Magnetic moment

The magnetic moments of synthesized metal complexes inform about the magnetic properties as well as geometry of the metal complexes. The magnetic moment of the Co(II)(2) complex is 3.79 B.M. which shows that the Co(II) ions are present in tetrahedral environment [30]. The magnetic moment of the Mn(II)(4) complex is 5.94 B.M. which corresponds to the high spin octahedral configuration [31]. The magnetic moment of the Fe(II)(5) complex is 4.87 B.M. which indicates the tetrahedral configuration [31].

The tetrahedral geometry of Cu(II) ions in the complex (1) are confirmed by the measured magnetic moment value as 1.5 B.M. The Zn(II) (3) complex is diamagnetic in nature indicating tetrahedral geometry [32, 33]. The μ_{eff} values of metal complexes are displayed in **Table 2.**

Table 2. Magnetic moment, spectral data (nm) and conductance measurements of synthesized metal complexes

Compound	μeff. (B.M.)	π→π* n→π* and LMCT	EC[a] ($\Omega^{-1}mol^{-1}cm^2$)
$C_{30}H_{34}N_6O_2$ (**H_2L**)	---	264, 287	---
$[Cu_2LCl]$ (**1**)	1.5	268, 389, 448	18.80
$[Co_2LCl_2]$ (**2**)	3.79	268, 368, 444	18.12
$[Zn_2LCl]$ (**3**)	Diamagnetic	289, 308, 426	19.42
$[Mn_2LCl(H_2O)]_4$ (**4**)	5.94	267, 351, 461	19.20
$[Fe_2L(Cl)_2].(H_2O)$ (**5**)	4.87	268, 353, 431	19.44

[a] = Electrical Conductance, 10^{-3} M solution in DMF, Ohm^{-1} cm^2 mol^{-1}.

2.2.3 IR spectra of the metal complexes

The broad stretching band due to phenolic -OH group in the IR spectrum of the ligand (H_2L) at 3292 cm^{-1} was found to disappear in the IR spectra of metal complexes (1-5) (Table 3), this confirmed that the proton of phenolic –OH has been deprotonated and has formed coordinate bond with metal ions. In case of spectra of metal complexes, the medium intensity band in the range 3065-3190 cm^{-1} and a strong one at 2954 cm^{-1} respectively can be assigned to ν(N-H) and ν(C-H) stretching frequencies. The spectra of all the complexes showed sharp band at 1610 cm^{-1} and 1558 cm^{-1} attributed to ν(C=C) and ν(C=N) respectively, which have been found to be shifted to lower frequency than that of ligand indicating coordination of ligand through azomethine nitrogen and nitrogens of dihydralazine [34]. All the metal complexes have showed characteristic bands around at 540-560 cm^{-1}, 470 cm^{-1} and 433 cm^{-1} respectively, attributed to the **ν**(M-N), **ν**(M-O) and **ν**(M-Cl) frequencies [26, 35]. The broad band observed around ~3390 cm^{-1} in metal complexes 4 and 5 are assigned to the hydroxyl stretching modes of the coordinated water molecule [36].

Table 3. Characteristic IR bands (cm^{-1}) of the ligand H_2L and its metal complexes

Compound	ν (H_2O)	ν (O-H)	N (N-H)	N (C-H)	ν(C=C)	ν(C=N)	ν (N-N)	ν (M-N)	ν (M-O)	ν (M-Cl)
H_2L	---	3292	3190	2954	1650	1564	1138	---	---	---
1	---	---	3100	2954	1602	1531	1134	540	470	433
2	---	---	3190	2954	1610	1539	1138	559	470	435
3	---	---	3250	2954	1616	1564	1134	558	480	430
4	3385	---	3190	2954	1608	1558	1153	542	470	433
5	3390	---	3190	2954	1610	1558	1150	540	447	418

2.2.4 Thermal Analyses

The outcomes obtained from the TGA-DTA analyses of all the synthesized metal complexes are summarized in Table 4. The results are in good agreement with the formulae proposed from the analytical data (Table 1). A general decomposition pattern was observed, whereby the complexes have been found to decompose in about three stages. In addition to these three decomposition stages, the complexes having coordinated water have exhibited an additional decomposition stage.

Table 4. Thermal analyses data for synthesized metal complexes and ligand H_2L

Code	Formula	MW	Dissociation Stages	Temp range in TG °C	Weight loss Found (Cal.) %	Fragment after Decomposition
H_2L	$C_{30}H_{34}N_6O_2$	510.27	Stage I	124.84-157.05	8.06 (8.04)	$C_{27}H_{28}N_6O_2$
			Stage II	235.10-264.94	15.59 (15.68)	$C_{22}H_{18}N_6O_2$
			Stage III	392.53-438.43	20.74 (21.15)	$C_{17}H_{16}N_6O$
			Stage IV	468.39-485.85	26.13 (25.71)	$C_{11}H_{12}N_6$
1	$C_{30}H_{32}ClCu_2N_6O_2$	669.08	Stage I	211.25-266.25	7.70 (7.72)	$C_{29}H_{30}Cu_2N_6O_2$
			Stage II	360.22-398.94	13.27 (13.28)	$C_{23}H_{18}Cu_2N_6O_2$
			Stage III	499.22-594.95	17.86 (18.01)	$C_{22}H_{17}CuN_6O$
2	$C_{30}H_{32}Cl_2Co_2N_6O_2$	696.06	Stage I	208.32-228.22	10.47 (10.28)	$C_{30}H_{32}Co_2N_6O_2$
			Stage II	283.20-312.28	32.73 (33.16)	$C_{24}H_{22}N_6O_2$
			Stage III	690.73-769.01	27.62 (27.95)	$C_{16}H_{16}N_6O$
3	$C_{30}H_{32}ClN_6O_2Zn_2$	671.08	Stage I	89.73-120.21	4.44 (4.40)	$C_{30}H_{32}N_6O_2Zn_2$
			Stage II	262.92-271.36	22.97 (22.97)	$C_{29}H_{32}N_6O_2$
			Stage III	426.51-458.73	18.10 (17.73)	$C_{22}H_{18}N_6O_2$
			Stage IV	586.61-647.38	10.67 (10.76)	$C_{22}H_{18}N_6$
4	$C_{30}H_{40}ClMn_2N_6O_6$	725.14	Stage I	222.34-307.68	8.67 (8.55)	$C_{30}H_{32}ClMn_2N_6O_2$
			Stage II	450.65-463.19	26.76 (26.87)	$C_{22}H_{17}ClMnN_6O_2$
			Stage III	676.27-794.75	17.98 (17.99)	$C_{22}H_{18}N_6O_2$
5	$C_{30}H_{34}Cl_2Fe_2N_6O_3$	708.07	Stage I	208.50-244.13	4.38 (4.38)	$C_{29}H_{30}Cl_2Fe_2N_6O_2$
			Stage II	421.45-445.67	11.77 (11.81)	$C_{26}H_{24}ClFe_2N_6O_2$
			Stage III	611.59-750.19	16.98 (16.96)	$C_{25}H_{23}FeN_6O_2$

The first decomposition stage for metal complex **5** is the loss of outer sphere water molecule while that of complex **4** is the loss of coordinated water molecules in temperature range 208 °C to 244 °C and 222 °C to 235 °C respectively. The process of decomposition has been found to be in the temperature range 90 °C to 300 °C. Finally, the metal oxides formation occurred in the region 500 °C to 800 °C [37].

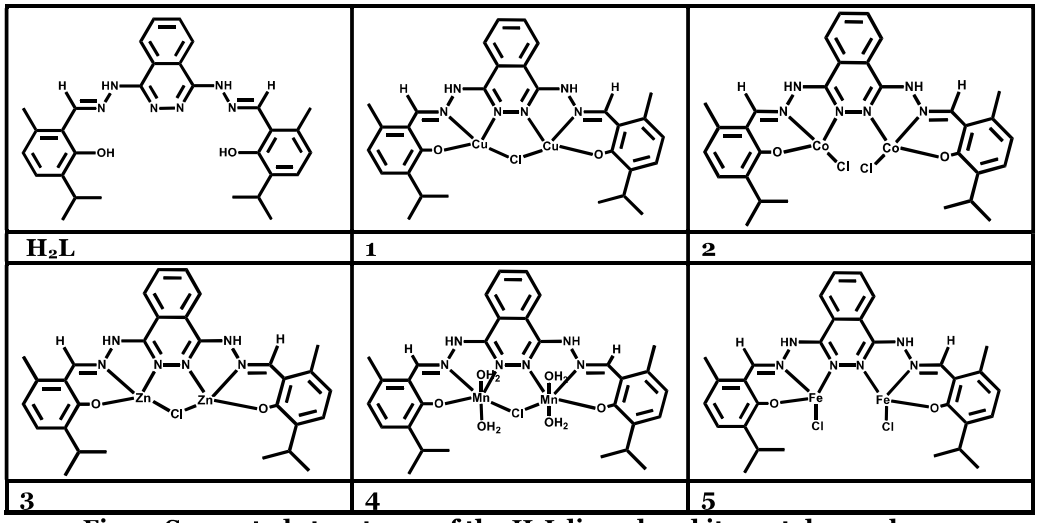


Fig. 2. Suggested structures of the H_2L ligand and its metal complexes

3. Biological appraisal:

3.1 Anticancer activity

The results of the in vitro anticancer screening on breast cancer cell line (MDA-MB 231) are summarized in **Table 5.** The anticancer results exhibit that all the synthesized compounds have moderate inhibitory action on the proliferation of breast cancer cell line (MDA-MB 231). The compound **1** was found to be the most active with the GI_{50} value <10 µg/mL and compound **3** has GI_{50} value 36.6 µg/mL. The outcomes are expressed in the form of graphical representation in Fig**. 3.** as growth curve of human breast cancer cell line (MDA-MB 231) % control growth Vs concentration (µg/mL). **Fig. 4** indicates the effect of synthesized compounds **H_2L**, **1**, **3**, **4** and positive control drug Adriamycin on breast cancer cell line (MDA-MB 231).

Table 5. In vitro cytotoxicity testing of the synthesized compounds against MDA-MB 231 cancer cell line

Compound	Drug concentrations (µg/mL)		
	LC_{50}	TGI	GI_{50}
H_2L	>80	>80	>80
1	>80	53.6	<10
2	NE	NE	>80
3	>80	>80	36.6
4	NE	NE	NE
5	NE	NE	NE
ADR	<10	<10	<10

Where, NE = Non-evaluable data.

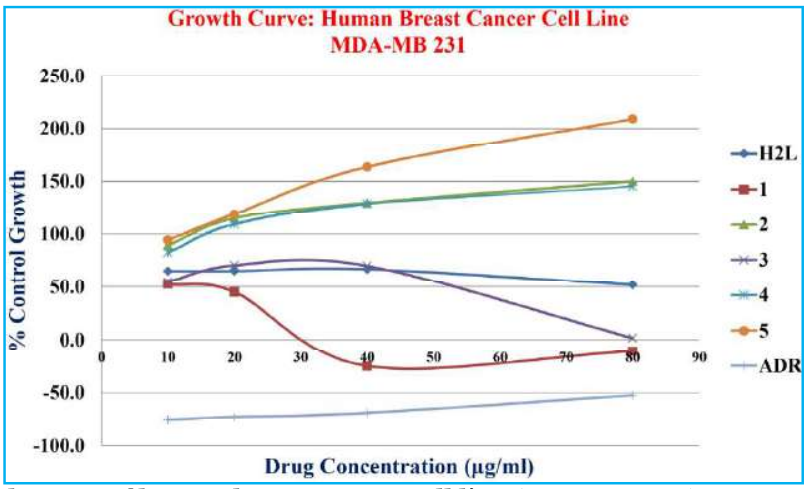


Fig. 3. Growth curve of human breast cancer cell line (MDA-MB 231) % control growth Vs concentration (µg/mL) of synthesized compounds

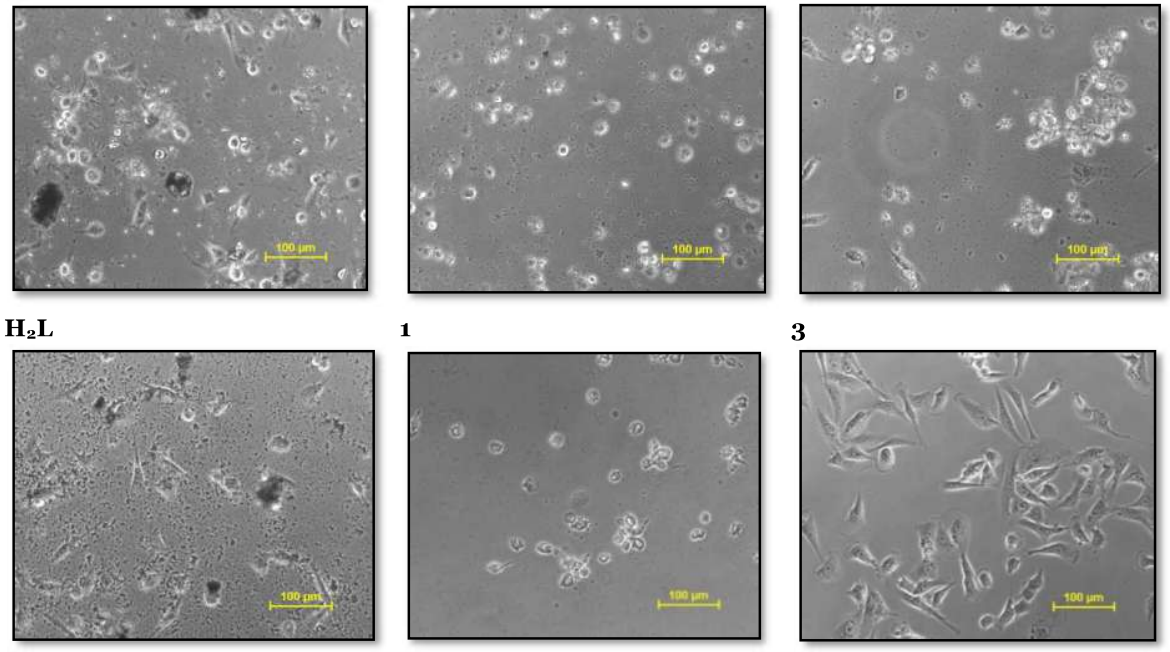


Fig. 4. Effect of synthesized compounds H2L, 1, 3, 4 and positive control drug Adriamycin on breast cancer cell line (MDA-MB 231)

3.2 Antimicrobial activity

The in vitro antibacterial activity of newly synthesized ligand and metal complexes are summarized in **Table 6.** The complexes **1**, **3**, and **5** exhibited excellent activity against the E. coli strain, while the ligand **H_2L** and compound **5** showed very good antibacterial activity against P. aeruginosa strain in comparison with the positive standard Ampicillin and Chloramphenicol. The metal complex **2, 3,** and **4** showed excellent antibacterial potency than positive standard Ampicillin, Chloramphenicol, and Ciprofloxacin against S. aureus strain. The complexes **3** and **5** displayed excellent antibacterial activity against S. pyogenus strain. The overall outcomes revealed that the metal complexes showed enhanced antibacterial potency compared to their parent ligand molecule.

Table 6. In vitro antibacterial potency of synthesized compounds

Compound	Antibacterial activity MIC (µM/mL) [S.D. = ±0.005]			
	E. coli	P. aeruginosa	S. aureus	S. pyogenus
DHPH	0.4411	0.5514	1.1027	0.5514
H_2L	0.2450	**0.1225**	0.1960	0.1960
1	**0.1490**	0.1862	0.3725	0.3725
2	0.3585	0.1792	**0.1434**	0.3585
3	**0.1852**	0.1852	**0.0926**	**0.1852**
4	0.3444	0.1722	**0.1377**	0.3444
5	**0.0883**	**0.1412**	0.1766	**0.1412**
Gentamicin	0.0001	0.0021	0.0005	0.0010
Ampicillin	0.2862	0.2862	0.7155	0.2862
Chloramphenicol	0.1547	0.1547	0.1547	0.1547
Ciprofloxacin	0.0754	0.0754	0.1509	0.1509
Norfloxacin	0.0313	0.0313	0.0313	0.0313

The outcomes of the antifungal activity of newly synthesized compounds are summarized in **Table 7**. The metal complexes **2**, **3**, and **4** have displayed excellent antifungal activity against C. albicans strain while the complex **2** showed very good activity against A. niger and A. clavatus fungal strains as compared to positive standard Griseofulvin. All the remaining synthesized metal complexes and ligand presented low to moderate activity against fungal strains. The microbial activities are clearly indicating that most of the synthesized metal complexes are more potent than the parent ligand (**H_2L**).

Table 7. In vitro antifungal potency of synthesized compounds

Compound	Antifungal activity MIC (µM/mL) [S.D. = ± 0.01]		
	C. albicans	A. niger	A. clavatus
DHPH	2.2055	4.4109	4.4109
H_2L	0.9799	0.9799	1.9597
1	0.7450	0.7450	0.7450
2	**0.1434**	**0.1434**	**0.1434**
3	**0.3705**	0.3705	**0.3705**
4	**0.3444**	0.6887	1.3774
5	1.4124	0.7062	1.4124
Nystatin	0.1080	0.1080	0.1080
Griseofulvin	1.4174	0.2835	0.2835

Bold values indicate significant activities in comparison with standards, S.D. = Standard Deviation*All calculations are performed from graphpad prism (http://www.graphpad.com/scientific-software/prism/)

3.3 Antioxidant activity

The results of DPPH assay of ligand and metal complexes are summarized in **Table 8** and graphically demonstrated in **Fig. 5**. All the metal complexes as well as ligand exhibited very good antioxidant activity in comparison with the positive controls ascorbic acid and α-tocoferol. Among the tested compounds the results of antioxidant activity of metal complexes **4** and **5** showed excellent activity, while remaining compounds exhibited good to moderate anti-oxidant activity.

Table 8. In vitro antioxidant activities of synthesized ligand and metal complexes

Inhibition (%) * Compound	Concentration (µg/mL)				Antioxidant test IC_{50} (µg/mL)
	12.5	25	50	100	
H_2L	42.53±0.034	55.33±0.054	72.42±0.114	83.02±0.043	18.33±0.154
1	43.77±0.116	58.03±0.052	74.97±0.032	86.35±0.112	17.19±0.066
2	39.98±0.027	50.41±0.108	69.94±0.028	79.13±0.063	20.95±0.149
3	45.97±0.054	57.73±0.112	73.97±0.104	85.35±0.048	16.69±0.286
4	45.87±0.038	64.18±0.116	73.37±0.107	81.35±0.103	**15.09±0.186**
5	48.09±0.102	65.47±0.081	72.73±0.112	83.98±0.105	**14.32±0.305**
Ascorbic acid	67.89±0.032	73.88±0.022	82.67±0.031	88.41±0.024	10.45±0.003
α-Tocopherol	56.80±0.015	67.64±0.041	77.14±0.023	86.91±0.012	12.55±0.002

* Mean ± S.D. (n=3)

*All calculations related to IC_{50} are performed from graphpad prism (http://www.graphpad.com/scientific-software/prism/)

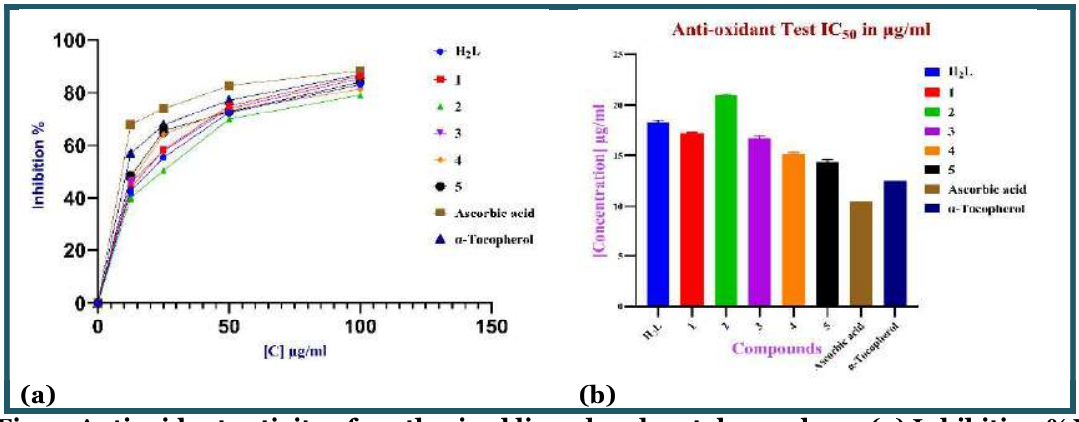


Fig. 5. Antioxidant activity of synthesized ligand and metal complexes (a) Inhibition % Vs concentration (µg/mL); (b) IC_{50} values in µg/mL.

4. Experimental:

4.1 Materials and methods

The chemicals and reagents used for this study were procured from TCI, Sigma-Aldrich, and S. D. fine chemicals and used without further purification. All the solvents were freshly distilled and dehydrated before use. The chemical reactions initially were monitored by TLC (Merck, silica gel 60 F254). The visualization of TLC was achieved in a UV light chamber. The ligand was characterized using ^{1}H NMR, ^{13}C NMR, IR, and mass spectroscopy (Waters, Q-TOF Micromass) whereas the synthesized metal complexes were characterized

by using ESI-MS, FTIR, UV-Vis spectroscopy, elemental analyses, molar conductivity, TGA and magnetic susceptibility. FT-IR spectra were recorded on a Shimadzu FT-IR spectrometer using KBr pellets. The NMR spectra were recorded on a Bruker AC-500 MHz spectrophotometer with TMS as internal standard in DMSO-d_6 solvent.
The magnetic susceptibilities of the metal complexes were measured by the Gouy method at room temperature. The effective magnetic moments were calculated by the formula ($\mu eff = 2.828 (\chi_m T)^{1/2}$ B.M. where χ_m is the molar susceptibility. Electronic spectra of the ligand and complexes were recorded in the range of 200-900 nm on a Shimadzu UV-2450 Spectrophotometer using the 10^{-5} M solution of the compounds in DMF at room temperature (27±2 °C). Molar conductivities of the synthesized metal complexes as 10^{-3} M solutions in DMF were measured on a Systronic Conductivity Bridge with dip type cell. Thermogravimetric analyses measurements were performed in dry nitrogen atmosphere in the temperature range of 30-900 °C at a heating rate of 10 °C/min on a Perkin Elmer Pyris Diamond TG/DTA thermal analyzer. Elemental analysis of ligand and metal complexes were performed on Thermo Fisher elemental analyzer at IIT Bombay.

4.2 Synthesis

4.2.1 Synthesis of the Ligand (H_2L)

The ligand was synthesized in three steps; in first step synthesis of Dihydralazine was performed by the reported method [38], while synthesis of 2-hydroxy-6-isopropyl-3-methylbenzaldehyde was attained via the method reported by our research group [39]. Finally the desired ligand (H_2L) 6,6'-((1E,1'E)-(2,2'-(phthalazine-1,4-diyl)bis(hydrazin-2-yl-1-ylidene))bis(methanylylidene))bis(2-isopropyl-5-methylphenol) was synthesized in the third step.

4.2.1.1 Synthesis of the Dihydralazine (DHPH)

The solution of hydrazine hydrate ($N_2H_4.H_2O$) (12.4 gm, 0.248 mol) in 6.4 mL of 50% aqueous acetic acid was added into the suspension of phthalonitrile (10.24 gm, 0.08 mol) in 20 mL of 1,4-dioxane. The mixture was stirred at 95-100 °C for 4 h. After cooling, the dark orange solid was filtered and crystallized from boiling 3 N HCl solution (50 mL) to isolate DHPH.2HCl in the form of yellow crystals. The free base was obtained by dissolving 5 gm of DHPH.2HCl in 35 mL of water. The solution was filtered to remove undesired impurities and the stoichiometric amount of aqueous KOH solution was added (2 gm, 5 mL) at 20-25 °C. The yellow precipitate was filtered and crystallized from water (70 mL) to isolate crystalline DHPH.

4.2.1.2 Synthesis of the 2-hydroxy-3-isopropyl-6-methylbenzaldehyde

To the solution of thymol (4.5 g, 30 mmol) and NaOH (10 g, 240 mmol) in (12 mL) distilled water, chloroform (7.2 g, 60 mmol) was added in small portions under stirring at 60-65 °C temperature. The reaction mixture was maintained further for 2-3 h at 60-65 °C. The excess chloroform from alkaline solution was removed by steam distillation. The alkaline mass was allowed to cool to 10-15 °C and acidified upto pH 2 by using 0.1 N HCl. The product was extracted using DCM and the oily crude product was isolated after recovery of the solvent.

4.2.1.3 Synthesis of the Ligand (H_2L)

A mixture of dihydralazine (1 mmol), 2-Hydroxy-3-isopropyl-6-methylbenzaldehyde (2 mmol) and acetic acid (0.05 mmol) in ethanol was refluxed for 2 h. The yellow solid obtained was filtered, washed with cold ethanol to remove unreacted starting materials. Finally the resulting product was recrystallized from ethanol. (Yield: 93 %) Anal. Calculated for $C_{30}H_{34}N_6O_2$: C, 70.56; H, 6.71; N, 16.46. Found: C, 70.12; H, 8.42; N, 15.72; Color: Yellow. UV/ vis; λmax (ε): 264 nm, 287 nm. IR (ν_{max}, KBr): 3292 (O-H), 3190 (N-H), 2954 (C-H), 1650 (C=C), 1564 (C=N), 1138 (N-N) cm^{-1};
^{1}H NMR (500 MHz, DMSO-d_6) δ 1.20 (d, J = 6.9 Hz, 6H, -CH(CH_3)$_2$), 2.50 (s, 3H, Ar-CH_3), 3.29-3.45 (m, 1H, -CH(CH_3)$_2$), 6.75 (d, J = 7.7 Hz, 1H, Ar-H), 7.39 (d, J = 7.65 Hz, 1H, Ar-H), 8.16 (d, J = 7.6 Hz, 1H, Ar-H), 8.87 (s, 1H, Ar-CHO), 9.25-9.29 (t, 1H, Ar-H), 12.41 (s, 1H, Ar-NH), 14.10 (s, 1H, Ar-OH); MS m/z calculated $C_{30}H_{34}N_6O_2$: 510.2743, found: 511.5038 $[M^{+1}]^+$.

4.2.2 Synthesis of the metal complexes (1-5)

The metal complexes were synthesized by drop wise addition of methanolic solution of the corresponding metal salt such as $CuCl_2$, $CoCl_2.6H_2O$, $ZnCl_2$, $MnCl_2.4H_2O$, and $FeCl_2$ (0.004 mol in 10 mL methanol) to the methanolic solution of ligand (0.002 mol of **H_2L** in 50 mL methanol) and triethylamine (0.004 mol) with constant stirring under nitrogen atmosphere and refluxing for 2-4 h. The solid complexes formed were filtered and washed with water followed by hot methanol and dried in vacuum desiccators over anhydrous $CaCl_2$.

4.2.2.1 Cu(II)(1) complex

Complex was found to be brown colored, crystalline solid and soluble in DMF and DMSO. (Yield: 77%, F. Wt. 669.08), Anal Calculated for $C_{30}H_{32}ClCu_2N_6O_2$: C, 53.69; H, 6.81; N, 12.52. Found: C, 54.59; H, 6.75; N, 10.19 and m.p; >300 °C. Color: Dark brown. Λm: 18.80 $\Omega^{-1}mol^{-1}cm^2$, μeff: 1.5 B.M., UV/vis; λmax (ε): 268 nm, 389

nm, 448 nm. IR spectrum, **ν**, cm⁻¹: 3100 (N-H), 2954 (C-H), 1602 (C=C), 1531 (C=N), 1134 (N-N), 540 (M-N), 470 (M-O), 433 (M-Cl).

4.2.2.2 Co(II)(2) complex

Complex was found to be army green colored, crystalline solid and soluble in DMF and DMSO. (Yield: 75%, F. Wt. 696.06), Anal Calculated for $C_{30}H_{32}Cl_2Co_2N_6O_2$: C, 51.67; H, 6.62; N, 12.05. Found: C, 51.65; H, 7.77; N, 11.01 and m.p; >300 °C. Color: Army green. Λm: 18.12 $\Omega^{-1}mol^{-1}cm^2$, μeff: 3.79 B.M., UV/vis; λmax (ε): 268 nm, 368 nm, 444 nm. IR spectrum, **ν**, cm⁻¹: 3190 (N-H), 2954 (C-H), 1610 (C=C), 1539 (C=N), 1138 (N-N), 559 (M-N), 470 (M-O), 435 (M-Cl).

4.2.2.3 Zn(II)(3) complex

Complex was found to be yellow colored, crystalline solid and soluble in DMF and DMSO. (Yield: 72%, F. Wt. 671.08), Anal Calculated for $C_{30}H_{32}ClN_6O_2Zn_2$: C, 53.39; H, 7.78; N, 12.45. Found: C, 53.62; H, 7.95; N, 13.50 and m.p; >300 °C. Color: Yellow. Λm: 19.42 $\Omega^{-1}mol^{-1}cm^2$, μeff: diamagnetic, UV/vis; λmax (ε): 289 nm, 308 nm, 426 nm. IR spectrum, **ν**, cm⁻¹: 3250 (N-H), 2954 (C-H), 1616 (C=C), 1564 (C=N), 1134 (N-N), 558 (M-N), 480 (M-O), 430 (M-Cl).

4.2.2.4 Mn(II) (4) complex

Complex was found to be brown colored, crystalline solid and soluble in DMF and DMSO. (Yield: 67%, F. Wt. 725.14), Anal Calculated for $C_{30}H_{40}ClMn_2N_6O_6$: C, 50.80; H, 6.83; N, 11.85. Found: C, 50.54; H, 7.63; N, 9.63 and m.p; >300 °C. Color: Brown. Λm: 19.20 $\Omega^{-1}mol^{-1}cm^2$, μeff: 5.94 B.M., UV/vis; λmax (ε): 267 nm, 351 nm, 461 nm. IR spectrum, **ν**, cm⁻¹: 3385 (Lattice water), 3190 (N-H), 2954 (C-H), 1608 (C=C), 1558 (C=N), 1153 (N-N), 542 (M-N), 470 (M-O), 433 (M-Cl).

4.2.2.5 Fe(II)(5) complex

Complex was found to be dark brown colored, crystalline solid and soluble in DMF and DMSO. (Yield: 63%, F. Wt. 708.07), Anal Calculated for $C_{30}H_{34}Cl_2Fe_2N_6O_3$: C, 49.63; H, 6.55; N, 11.58. Found: C, 49.63; H, 8.20; N, 9.35 and m.p; >300 °C. Color: Dark brown. Λm: 19.44 $\Omega^{-1}mol^{-1}cm^2$, μeff: 4.87 B.M., UV/vis; λmax (ε): 268 nm, 353 nm, 431 nm. IR spectrum, **ν**, cm⁻¹: 3390 (Lattice water), 3190 (N-H), 2954 (C-H), 1610 (C=C), 1558 (C=N), 1150 (N-N), 540 (M-N), 447 (M-O), 418 (M-Cl).

4.3 Anticancer studies

The synthesized ligand (H_2L) and it's metal complexes were screened for their in vitro anticancer activity against MDA-MB 231 cell line using Sulforhodamine B (SRB) assay. The cell lines were grown in appropriate medium containing 2 mM L-glutamine and 10 % fetal bovine serum. For present screening experiment, 5000 cells/well were inoculated into 96 well microtiter plates in 100 μL. After cell inoculation, the microtiter plates were incubated at 37 °C, 5 % CO_2, 95 % air and 100 % relative humidity for 24 h prior to addition of experimental compounds. The solutions of compounds were prepared in DMSO at 100 mg/mL and diluted to 1 mg/mL using water and stored frozen prior to use. At the time of compounds addition, an aliquot of frozen concentrate (1 mg/mL) was thawed and diluted to 100 μg/mL, 200 μg/mL, 400 μg/mL and 800 μg/mL with complete medium containing test article. Aliquots of 10 μl of these different compounds dilutions were added to the appropriate microtiter wells already containing 90 μl of medium, resulting in the required final drug concentrations i.e., 10 μg/mL, 20 μg/mL, 40 μg/ml, 80 μg/mL. After addition of compound, plates were incubated at standard conditions for 48 hours and assay was terminated by the addition of cold TCA. Cells were fixed in situ by the gentle addition of 50 μl of cold 30 % (w/v) TCA (final concentration, 10 % TCA) and incubated for 60 minutes at 4 °C. The supernatant was discarded; the plates were washed five times with tap water and air dried. Sulforhodamine B (SRB) solution (50 μl) at 0.4 % (w/v) in 1 % acetic acid was added to each of the wells, and plates were incubated for 20 minutes at room temperature. After staining, unbound dye was recovered and the residual dye was removed by washing five times with 1 % acetic acid. The plates were air dried. Bound stain was subsequently eluted with 10 mM trizma base, and the absorbance was read on a plate reader at a wavelength of 540 nm with 690 nm reference wavelength [40-43]. Percent growth was calculated on a plate-by-plate basis for test wells relative to control wells. Percent Growth was expressed as the ratio of average absorbance of the test well to the average absorbance of the control wells * 100. Using the six absorbance measurements [time zero (Tz), control growth (C), and test growth in the presence of compound at four concentration levels (Ti)], the percentage growth was calculated at each of the compound concentration levels. Percentage growth inhibition was calculated as: [Ti/C] x 100 %

4.4 Antimicrobial studies

In vitro antimicrobial testing of the ligand and synthesized metal complexes were performed at Microcare Laboratory and TRC, Surat, India as per reported methods [44]. The synthesized compounds were screened for their in vitro antibacterial and antifungal activity against E. coli (MTCC 443), S. aureus (MTCC 96), S. pyogenus (MTCC 442), P. aeruginosa (MTCC 1688) bacterial and A. niger (MTCC 282), C. albicans (MTCC 227), A. clavatus (MTCC 1323) fungal strains respectively by using micro broth dilution method. Chloramphenicol, Ampicillin, Ciprofloxacin, and Gentamycin were used as positive control for antibacterial

activity. Nystatin and Griseofulvin were used as positive control for antifungal activity. The screening results are expressed as minimum inhibitory concentration (MIC). The results of antibacterial testing are indicated in Table 6 with their MIC (µg/mL) values; which revealed that the synthesized compounds have variable inhibitory effects on the growth of bacterial and fungal strains.

4.5 Antioxidant studies

The antioxidant activity test of the synthesized ligand and its metal complexes was performed by DPPH radical scavenging method as per the reported protocol [45]. The stock solution (1 mg/mL) of each compound was prepared in DMSO solvent and for each determination diluted by serial dilution method (100 µg/mL, 50 µg/mL, 25 µg/mL and 12.5 µg/mL). Each aliquot of 0.5 mL was dissolved in 5 mL of 0.06 mM DPPH solution in methanol. The homogeneous mixtures of compounds were incubated at 37 °C in the dark (incubator) for 45 min. The control solution was prepared simultaneously without using the compound. The absorbance of each sample was measured at 517 nm wavelength. All the results were carried out in triplicate and the mean was taken for % inhibition determination. The % inhibition (µg/mL) were calculated by the formula [(Ac–At)/Ac] × 100. Where, Ac = absorbance of the control and At = absorbance of the tested compound. Ascorbic acid and α-Tocopherol were used as reference standards. The antioxidant activity of the compounds relate to their electron or hydrogen radical releasing abilities to DPPH so that they reach stability as diamagnetic moieties. The results are demonstrated in the form of % inhibition and IC_{50} values in µg/mL.

5. Conclusion:

In this study, a new hexadentate hydrazone ligand, 6,6'-((1E,1'E)-(2,2'-(phthalazine-1,4-diyl) bis(hydrazin-2-yl-1-ylidene)) bis(methanylylidene)) bis(2-isopropyl-5-methylphenol) (H_2L) and its metal Cu(II)(1), Co(II)(2), Zn(II)(3), Mn(II)(4), and Fe(II)(5) complexes were synthesized by environment benign method. The properties of the synthesized ligand and its metal complexes were confirmed by various physico-chemical and spectroscopic techniques. The geometries of the complexes have been established by analytical, magnetic and spectral techniques. The $[Mn_2LCl(H_2O)_4]$ complex was found to be having octahedral and the complexes $[Cu_2LCl]$, $[Co_2LCl_2]$, $[Zn_2LCl]$, and $[Fe_2L(Cl)_2].(H_2O)$ were found to have tetrahedral geometry.
In-vitro anticancer screening of the ligand and its metal complexes have been evaluated against MDA-MB 231 breast cancer cell line, the Cu(II)(1) and Zn(II)(3) complexes have exhibited potential activity with GI_{50} values <10 µg/mL and 31.4 µg/mL respectively. The in vitro antimicrobial results revealed that the ligand and metal complexes are more potent antimicrobial agents than the parent compound [DHPH]. The complexes 2, 3, 4 and 5 have shown enhanced antibacterial activity and compounds 2, 3, and 4 have shown potent antifungal potency than the free ligand (H_2L). The compounds 1, 3, 4, and 5 have been found to be very good antioxidant agents than the parent ligand. The chelation of the ligand (H_2L) has been found to result in more potent anticancer, antimicrobial and antioxidant activity.

Declaration of Competing Interest

The authors declare that they have no known competing financial interests or personal relationships that could have appeared to influence the work reported in this paper.

Data availability

We have shared all the data in the attached files

Acknowledgments

The authors are grateful to the UGC, New Delhi, for providing financial assistance through SAP (DSA-I) project Ref. No. F. 4-6/2015/DSA-I (SAP-II).

Funding information

Funding source was not available.

References

1. Patil, S. S., Tadavi, S. K., Dikundwar, A., & Bendre, R. S. (2022). Journal of Molecular Structure, 1247, 131293.
2. Ali, S., Ahmad, A., Banerjee, S., Padhye, S., Dominiak, K., Schaffert, J. M., ... & Sarkar, F. H. (2010). Cancer research, 70(9), 3606-3617.
3. Oiye, É. N., Ribeiro, M. F. M., Katayama, J. M. T., Tadini, M. C., Balbino, M. A., Eleotério, I. C., ... & de Oliveira, M. F. (2019). Critical Reviews in Analytical Chemistry, 49(6), 488-509.
4. Liu, W., & Yin, X. B. (2016). TrAC Trends in Analytical Chemistry, 75, 86-96.
5. Ramdass, A., Sathish, V., Babu, E., Velayudham, M., Thanasekaran, P., & Rajagopal, S. (2017). Coordination Chemistry Reviews, 343, 278-307.
6. Wang, M., Chen, L., & Sun, L. (2012). Energy & Environmental Science, 5(5), 6763-6778.
7. Das Sarma, B., & Bailar Jr, J. C. (1969). Journal of the American Chemical Society, 91(22), 5958-5963.

8. Cieslik, P., Comba, P., Dittmar, B., Ndiaye, D., Tóth, É., Velmurugan, G., & Wadepohl, H. (2022). Angewandte Chemie, 134(10), e202115580.
9. Kendur, U., Chimmalagi, G. H., Patil, S. M., Gudasi, K. B., Frampton, C. S., Mangannavar, C. V., & Muchchandi, I. S. (2018). Journal of Molecular Structure, 1153, 299-310.
10. Holló, B. B., Magyari, J., Armaković, S., Bogdanović, G. A., Rodić, M. V., Armaković, S. J., ... & Szécsényi, K. M. (2016). New Journal of Chemistry, 40(7), 5885-5895.
11. Jayabalakrishnan, C., & Natarajan, K. (2001). Synthesis and Reactivity in Inorganic and Metal-Organic Chemistry, 31(6), 983-995.
12. Mandewale, M. C., Thorat, B., Shelke, D., & Yamgar, R. (2015). Bioinorganic Chemistry and Applications, 2015.
13. Srivastava, A., & Singh, R. (2005). Indian Journal of Chemistry, 44(9), 1868-1875.
14. Stern, H. C., Matthews, J. H., & Belz, G. G. (1984). British heart journal, 52(4), 435.
15. Guengerich, F. P. (2013). In Drug-Induced Liver Disease (pp. 15-33). Academic Press.
16. Bourdi M., Larrey D., Nataf J., Berunau J., Pessayre D., & Iwasaki M. (1990). JClinInvest.85, 1967-1973.
17. Shen, A. Y., Huang, M. H., Liao, L. F., & Wang, T. S. (2005). Drug development research, 64(4), 195-202.
18. He, Lei, H. Mo, Susilowati H., Qureshi, A. A., & Charles E. E.. (1997). The Journal of nutrition 127(5), 668-674.
19. Bendre, R. S., Tadavi, S. K., & Patil, M. M. (2018). Transition Metal Chemistry, 43, 83-89.
20. Bansal, A., Saleh-E-In, M. M., Kar, P., Roy, A., & Sharma, N. R. (2022). Molecules, 27(14), 4597.
21. Tadavi, S. K., Yadav, A. A., & Bendre, R. S. (2018). Journal of Molecular Structure, 1152, 223-231.
22. Kogan, V. A., Levchenkov, S. I., Popov, L. D., & Shcherbakov, I. A. (2009). Russian Journal of General Chemistry, 79, 2767-2775.
23. Bhoi, R. T., Bhoi, C. N., Nikume, S. R., & Bendre, R. S. (2023). Results in Chemistry, 6, 101112.
24. Silverstein, R. M., Basler, G. C., & Morril, T. C. (1991). John Wiley & Sons: New York, 5rd.
25. Fleming, I., & Williams, D. H. (1966). Spectroscopic methods in organic chemistry (p. 94). New York: McGraw-hill.
26. Kumar, K. S., & Aravindakshan, K. K. (2021). Results in Chemistry, 3, 100129.
27. Yeğiner, G., Gülcan, M., Işık, S., Ürüt, G. Ö., Özdemir, S., & Kurtoğlu, M. (2017). Journal of fluorescence, 27, 2239-2251.
28. Pramanik, H. A., Paul, P. C., Mondal, P., & Bhattacharjee, C. R. (2015). Journal of Molecular Structure, 1100, 496-505.
29. Kurtoğlu, M., & Baydemır, S. A. (2007). Journal of Coordination Chemistry, 60(6), 655-665.
30. Chandra, S., & Gupta, L. K. (2005). Spectrochimica Acta Part A: Molecular and Biomolecular Spectroscopy, 61(6), 1181-1188.
31. Al-Saif, F. A., & Refat, M. S. (2012). Journal of Molecular Structure, 1021, 40-52.
32. Casellato, U., Vigato, P. A., & Vidali, M. (1977). Coordination Chemistry Reviews, 23(1), 31-117.
33. Yernale, N. G., Matada, B. S., Vibhutimath, G. B., Biradar, V. D., Karekal, M. R., Udayagiri, M. D., & Mathada, M. H. (2022). Journal of Molecular Structure, 1248, 131410.
34. Adiguzel, R., Esener, H., Ergin, Z., Aktan, E., & Sekerci, M. (2011). Asian Journal of Chemistry, 23(4), 1846.
35. Raj, A., Vinnarasi, J., & Venkataraman, R. (2013). Research Journal of Pharmacy and Technology, 6(10), 1121-1123.
36. Kumar, S., Pandey, P. K., Sinha, N., Chaudhari, S., & Sharma, S. (2018). Journal of Physical Science, 29(3), 1-11.
37. Sarma, B. D., & Bailar Jr, J. C. (1955). 77(21), 5476-5480.
38. Attanasio, D., Dessy, G., & Fares, V. (1985). Inorganica chimica acta, 104(2), 99-107.
39. Bhoi, R. T., Rajput, J. D., & Bendre, R. S. (2022). Research on Chemical Intermediates, 1-22.
40. Vichai, V., & Kirtikara, K. (2006). Nature protocols, 1(3), 1112-1116.
41. Kode, J., Kovvuri, J., Nagaraju, B., Jadhav, S., Barkume, M., Sen, S., ... & Kamal, A. (2020). Bioorganic Chemistry, 105, 104447.
42. Kholiya, F., Chatterjee, S., Bhojani, G., Sen, S., Barkume, M., Kasinathan, N. K., ... & Meena, R. (2020). Carbohydrate polymers, 240, 116282.
43. Skehan, P., Storeng, R., Scudiero, D., Monks, A., McMahon, J., Vistica, D., ... & Boyd, M. R. (1990). JNCI: Journal of the National Cancer Institute, 82(13), 1107-1112.
44. Tille, P. (2015). Bailey & Scott's diagnostic microbiology-E-Book. Elsevier Health Sciences.
45. Bao, J., Cai, Y., Sun, M., Wang, G., & Corke, H. (2005). Journal of Agricultural and Food Chemistry, 53(6), 2327-2332.

Educational Administration: Theory and Practice

(Kuram ve uygulamada eğitim yönetimi)

e-ISSN: 2148-2403 | p-ISSN: 1300-4832 | Frequency 12 Issue Per Year | Nature: Online and Print | Language of Publication: English | Article Processing Charges: 1000 USD

Introduction

The **Educational Administration: Theory and Practice** publishes prominent empirical and conceptual articles focused on timely and critical leadership and policy issues of educational organizations. The journal embraces traditional and emergent research paradigms, methods, and issues. The journal particularly promotes the publication of rigorous and relevant scholarly work that enhances linkages among and utility for educational policy, practice, and research arenas.

The goal of the editorial team and the journal's editorial board is to promote sound scholarship and a clear and continuing dialogue among scholars and practitioners from a broad spectrum of education.

Educational Administration: Theory and Practice presents prominent empirical and conceptual articles focused on timely and critical leadership and policy issues facing educational organizations. As an editorial team, we embrace traditional and emergent theoretical frameworks, research methods, and topics. We particularly promote the publication of rigorous and relevant scholarly work with utility for educational policy, practice, and research.

The journal's primary focus is on studies of educational leadership, organizations, leadership development, and policy as they relate to elementary and secondary levels of education. Examinations of leadership and policy that fall outside K-12 are considered insofar as there are meaningful connections to the K-12 arena (e.g., college pipeline). International comparative investigations are welcome to the extent they have implications for a broad audience.

Basic Journal Information

e-ISSN: 2148-2403 | **p-ISSN:** 1300-4832 **| Frequency Quarterly (12 Issue Per Year) | Nature: Online | Language of Publication: English | Article Processing Charges: 1000 USD**

Coverage Areas: Although the list is not prescriptive, EATP intends to focus on advances in the following sub-domains:

1. Expanded views and sources of educational leadership, including beyond the individual as leader
2. Multiple purposes and outcomes of educational leadership (e.g., instructional, managerial, democratic, inclusive, social justice)
3. diverse analytical/theoretical lenses (e.g., organizational, sociological, sociocultural, distributed, critical)
4. address the influence of leadership and policy on educational practice and outcomes
5. address the impact of diverse forms of leadership preparation and development
6. consider how the organizational structure of districts and schools impacts leadership and improvement processes
7. enrich our understanding of schools as agents of social change
8. examine educational environments that promote equity and social justice for students and faculty

Types of Papers: The Journal accepts the following categories of papers:

- Original research
- Position papers/review papers
- Short-papers (with well-defined ideas, but lacking research results or having preliminary results)
- Technology Discussion/Overview Papers

Peer Review Process: All submitted papers are subjected to a comprehensive blind review process by at least 2 subject area experts, who judge the paper on its relevance, originality, clarity of presentation and significance. The review process is expected to take 8-12 weeks at the end of which the final review decision is communicated to the author. In case of rejection authors will get helpful comments to improve the paper for resubmission to other journals. The journal may accept revised papers as new papers which will go through a new review cycle.

Periodicity: The Journal is published in 12 issues per year.

Citation Analysis: Google Scholar (https://scholar.google.com/citations?hl=en&view_op=list_works&alert_preview_top_rm=2&authuser=4&gmla=AJsN-F5AOTf9koiVb4mMnge1nvlYpBcY7PoFlS7XNtl34c6gRpNSvjK6iA78NYtUld9iVaAUnpjmiryRyjtkMjXvjrimgLnYnL7D17uOcGyvGsP6-pV0C2MOEAx8M27nzeo2qbpjuJo7&user=5biXhQwAAAAJ) | Scopus (https://www.scopus.com/results/results.uri?sort=plf-f&src=s&st1=Educational+Administration+Theory+and+Practice&sid=af17d52d0819bd9cd22cb84add451a96&sot=b&sdt=b&sl=56&s=SRCTITLE%28Ed

Current Issue

Chat with us

Vol. 30 No. 9 (2024): Vol. 30 No. 9 (2024)

Published: 2024-09-02

Scopus Preview

Sources

ISSN | Enter ISSN or ISSNs | Find sources

ISSN: 2148-2403 ×

CiteScore 2023 has been released. View CiteScore methodology >

x

Filter refine list

Apply Clear filters

Display options

- Display only Open Access journals

Counts for 4-year timeframe

- No minimum selected
- Minimum citations
- Minimum documents

Citescore highest quartile

- Show only titles in top 10 percent
- 1st quartile
- 2nd quartile
- 3rd quartile
- 4th quartile

Source type

- Journals
- Book Series
- Conference Proceedings
- Trade Publications

Apply Clear filters

1 result

Download Scopus Source List | Learn more about Scopus Source List

All | Export to Excel | Save to source list

View metrics for year: 2023

	Source title	CiteScore	Highest percentile	Citations 2020-23	Documents 2020-23	% Cited
1	Educational Administration: Theory and Practice	N/A	N/A	N/A	N/A	N/A

Top of page

DOI:10.5958/0976-4755.2024.00071.2
BIOINFOLET 21 (2) : 236 - 239, 2024

NEOCALAMITES KANHANESIS SP. NOV. FROM KANHAN COAL MEASURES OF KAMTHI STAGE

Aparna Yadav and B. B. Kalbande*

Department of Botany, J. M. Patel, College, Bhandara
*Department of Botany, Nabira Mahavidyalaya, Katol

ABSTRACT

Kamthi coalfield one of the major open cast coalfields in Central India, from where the present specimen was collected. The stem was un-branched without leaf sheath, differentiated into nodes and internodes. Internodes long and nodes were narrow. Axis 4 cm to 15 cm long and nodes were also narrow. Internode 1.4 cm to 9 cm long, with conspicuous ridges (24 to 30) and furrows (22 to 25). The ridges were 0.3 to 1 mm broad. Ridges and furrows were continuous from one internode to other, hence identified as *Neocalamites kanhanensis,* which is second record from Kanhan coal field of Kamthi Stage.

Key Words: Kamthi, Nodes, Ridges, Furrows and Leaf sheath

Introduction

Neocalamites commonly found in Triassic and lower Jurassic rocks of Greenland and South Africa as well as throughout Asia and Europe. The axis of *Neocalamites* suggests small calamites with vascular strands that do not alternate at the nodes. The *Asterophyllites* like leaves were found attached to node but not fused at the base. Bractless cones of Equisetum type were borne singly at the end of slender stalk at the node.

Lele (1956) suggest that the *Neocalamites* is known only by its stems, as the leaves, leaf sheaths or the cones are unknown. The stems are generally narrow, but few of them are considerably broad. In India, the genus is represented by only one species i.e. *Neocalamites foxii* (Lele, 1956). Good (1975) has suggested that *Neocalamites* might be considered as intermediate stage between Calamitaceae and Equisetaceae. Waghaye (1995) recorded *Neocalamites foxii* from Satnavari of Kamthi stage, while Talwankar (2001) also recorded it from Kanhan.

Material and Method

The specimen for present study was collected from Kanhan coalfield of Kamthi stage. The material consisted of number of specimens with parts and counterparts. The stem preserved in the form of impression on black carbonaceous shale and specimens were numbered as specimen 1, 2 and 3, and studied with the help of different magnifying lenses and binocular research microscope.

Specimen 1:

It is an impression with part only. It is 6.4 cm long and 1.2 cm broad. It is differentiated into nodes and internodes. The present specimen shows one complete node and internode. The internode is 6.2 cm long. The node is narrow thin, comparatively with the other specimen, it is 1 mm broad. It shows presence of ridges and furrows. In present specimen, ridges are 20 to 24 in number and furrows are 18 to 20 in number. The ridge are broad 0.2 to 0.3 mm while, furrows are thin 0.1 to 0.2 mm broad. The ridges and furrows of node above are not clearly seen. (Plate I-Fig.1; Plate II-Fig.4)

Specimen 2:

In specimen 2, though the counterpart is missing. The impression of the specimen is 4 cm long and 2.4 cm broad. The axis is differentiated into node and internode. In present specimen two nodes and two internodes are present. Each internode is 1.4 to 1.7 cm long and characterized by ridges and furrows. In present specimen 26 to 22 ridges and 22 to 24 furrows are observed. The ridges are broad about 0.4 to 0.5 mm in thickness and furrows are 0.3 to 0.4 mm broad. The ridges and furrows are continuous from one internode to another. (Plate I-Fig.2; Plate II-Fig.5)

Specimen 3:

It is an impression with part and counterpart. The impression is well preserved and shows number of impression of axis overlap or adjacent with each other. The different impression are varies in length and breadth. It ranges from 7 cm to 15 cm. Breadth of different axis ranges from 2 cm to 3.4 cm. Each axis is differentiated into nodes and internodes. All internodes are not equal in length and it ranges from 3 cm to 9 cm. All the nodes almost same in thickness and it ranges from 1 mm to 3 mm broad. All the impression shows characteristic ridges and furrows. The number of ridges and furrows ranges from 24 to 30 and 22 to 25 respectively. The ridges are 0.4 mm to 1 mm broad and furrows are 0.1 mm to 0.7 mm broad. The ridges alternate with the furrows. The ridges and furrows are continuous from one internode to the adjacent internode. (Plate I-Fig.3; Plate II-Fig.6, 7, 8)

Description

Thus, in present specimens the axis ranged from 4 cm to 15 cm in length, while the breadth varied from 1.2 cm to 3.4 cm, but in most of the cases it was 2 cm broad. Each axis was differentiated into nodes and internodes. In all cases nodes were narrow that is from 1 mm to 3 mm thick without leaf sheath, but internodes varied in length from 1.4 cm to 9 cm. In some axis, internode increased gradually in length from one end to other end. The internodes were characterized by the presence of longitudinal ridges and furrows. The number of ridges and furrows were nearly constant and those were between 18 to 30. The ridges were comparatively thick and measured 0.3 to 1 mm broad. The present specimen showed that the ridges and furrows were continuous from one internode to another successive internode.

Comparison

The present specimen was compared with *Phyllotheca* wherein, the aerial stem is branched. The stem is 30 cm long and 1 cm broad having nodes at a distance of 2.5 to 3.5 cm, The nodes are slightly swollen and the longitudinal lines are continuous. But present specimen shows resemblance only in continuous ridges at nodes but differs in internodal distance, swollen node and wider stem as compared to *Phyllotheca brog.*

The comparison was made with *Phyllotheca indica* (Bunbury 1861), which is based upon impression of stem and leaf sheaths. The main stems are without leaves. Internodular surface is ribbed longitudinally, the ribs being convex, somewhat flattened and the furrows narrow. The ribs are continuous over the nodes. The stem bearing the leaf sheath is 7 mm across and the two nodes are at distance of 1 cm. The present specimen differs from *P. indica* in internodal distance and presence of leaf sheath, which were absent in present specimen.

The comparison was also made with *P. sahnii* (Saksena 1962), wherein the stems are faintly ribbed, articulate and swollen at the nodes. Leaf sheath is narrow but spreading above into an open saucer like disc, at least 15 mm in diameter. Thus, differs totally from present specimen.

In case of *Phyllotheca grieibachii,* (Zeiller 1902 and Surange 1956). The stem is biggest, 1.5 cm in diameter with 11 nodes placed at a distance of 1 to 1.3 cm apart and the smallest stem is 0.8 mm across with 16 nodes. The leaf sheath is in the form of a shallow cup with horizontally spreading leaf segments, each supplied by a single median vein. Thus present fossil specimen shows vast difference with P. *griesbachii* in internodal distance and width of stem.

Phyllotheca ampla (Surange and Kulkarni 1967), are stouter stems, strongly ribbed, bearing leafy shoots. The leaf sheaths

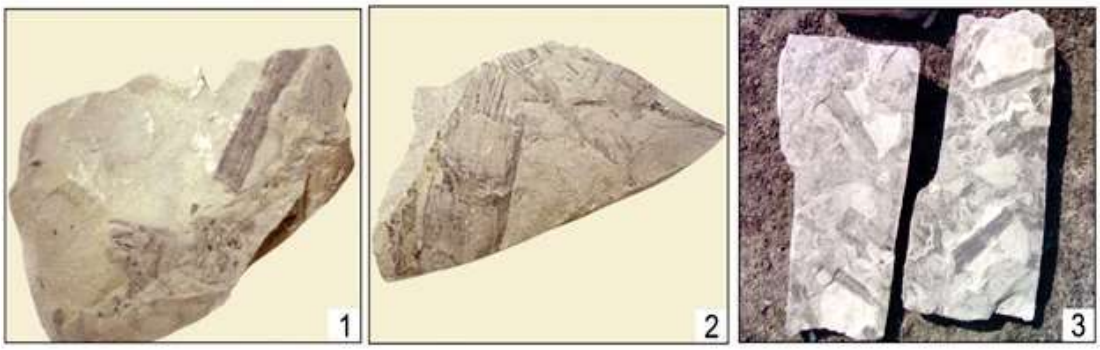
in upper part are about 15 mm broad at lower end tapering to about 5 mm near top. Internodes are 16 mm to 27 mm in length whereas leafy shoots are slender, 3 mm to 8 mm in breadth with internodes 4 to 11 m in length; leaf sheath is cup to saucer shaped 6 to 10 mm in length with 20 free leaflets. Thus *P. ampla* shows dissimilarities with present fossil specimen.

From above discussion it is clear that present fossil specimen can't be compared with *Phyllotheca*. The specimen shows similarity only in continuous ribs and furrows at nodal point, thus comparison is not possible.

Neocalamites is known only for its stem (Lele 1956). The stems are generally narrow, but a few of them were considerably broad and long. A typical specimen measured 18.7 cm long and 3.6 cm broad with only one node. The internodes are fairly long, marked by conspicuous ridges and furrows, which are continuous. On the basis of characters like continuity of ridges and furrows, long internodal distance, broadness of stem and presence of ridges and furrows more than 13 per cm, the present specimen thus shows more affinity to *Neocalamites* than *Phyllotheca* hence it has been kept in the genus *Neocalamites*.

The present specimen resembles *Neocalamites foxii* (Lele 1956), the only described species from India, It is differentiated into node and internodes, broadness of stem which is 3.4 cm but differs in having number of ridges and furrows that is 24 to 30 and 22 to 25 respectively.

The first record of *N. foxii* (Talwankar 2001), from the same locality showed similarities with axis, 6 to 13 cm in length, differentiates into nodes and internodes but differs from present specimen having a narrow stem, 6 mm broad and internode which increases gradually in length from one end to other. Present specimen is also kept in the same genus *Neocalamites,* which is second record from Kanhan. Therefore it is named as *Neocalamites kanhanesis,* the specific name is given after the locality, Kanhan coal field of Kamthi Stage



Diagnosis

The stem is un-branched without leaf sheath, differentiated into nodes and internodes. Internodes long and nodes are narrow. Axis 4 cm to 15 cm long and nodes are narrow. Axis 4 cm to 15 cm long and 2 cm broad. Internode 1.4 cm to 9 cm long, with conspicuous ridges and furrows. Ridges and furrows that is 24 to 30 and 22 to 25 in number respectively. The ridges are comparatively thick 0.3 to 1 mm broad. Ridges and furrows, are continuous from one internode to other, hence identified as *Neocalamites kanhanesis* it is second record from Kanhan coal field of Kamthi Stage.

Holotype: AMY. /N-1. Department of Botany, Institute of Science, Nagpur

Locality: Kanhan coalfield, Nagpur Dist. Maharashtra., India

Horizon: Lower Gondwana of India.

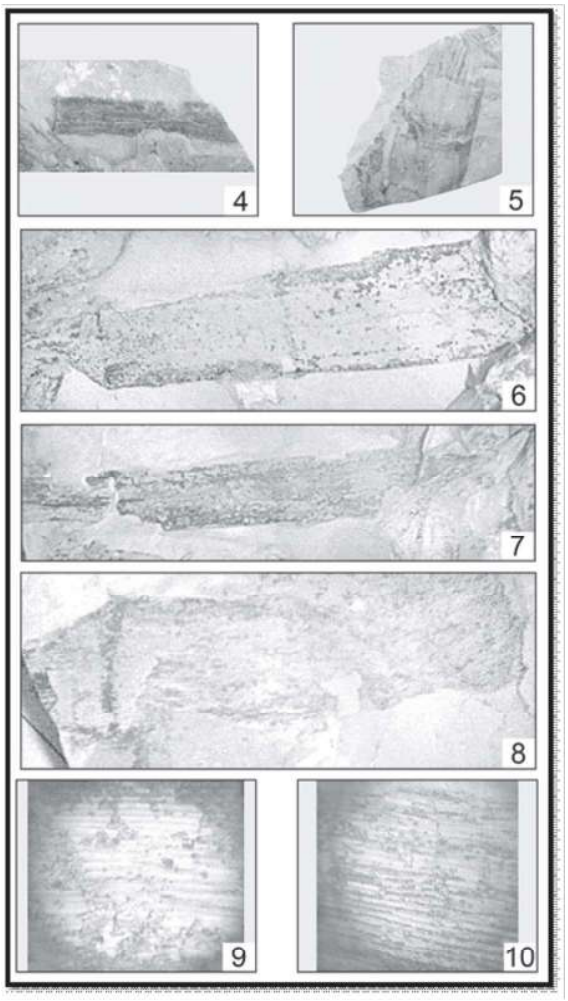
Age: Permotriassic.

References

Bunbury, C.J.F. (1861), *Quart., Journl. Geol. Soc. London,* 17:325.

Good, R.E. (1975), "*Gondwana Geology " Aust, Nat, Univ Press, Canbera,* pp 109-123.
Lele, K.M. (1956), *The Palaeobotanist,* **4**:23.
Saksena, S. (1962), *The Palaeobotanist,* **11**:23.
Surange, K. R. and Kulkarni, M. (1967), *The Palaeobotanist,* **16**:95.
Surange, K.R. (1956), *The Palaeobotanist,* **4**:83.
Talwankar, D. (2001), *"Contribution to the knowledge of lower Gondwana flora from Kamthi Stage of Peninsular India",* Ph. D. Thesis, Nagpur University, Nagpur.
Waghaye, S. M. (1995), "Investigation *of plant fossil of Central India",* Ph. D. Thesis, Nagpur University, Nagpur.
Zeiller, R. (1902), "*Glossopteris indica*, Mem. Geol. Surv of India*", Palaento. Indica,* N.S.2.

Fig.1-3: **Impression of *N. kanhanensis* showing various sizes of stem with node & internode. XN**



Neocalamites vaigyanii sp.nov
Fig. 4-8: A magnified view of *N. kanhanensis* showing various sizes of stem with node & internode. XN
Fig. 9-10 : A magnified view of *N. kanhanensis* showing ridges & furrows. XN

SCISPACE Papers Discover Papers for your research Pricing Sign up

Home / Journals / BIOINFOLET - A Qua...

Overview Publishing trend Papers (632)

Journal • ISSN: 0973-1431

BIOINFOLET - A Quarterly Journal of Life Sciences

Dr. Anil M. Mungikar

About: BIOINFOLET - A Quarterly Journal of Life Sciences is an academic journal. The journal publishes majorly in the area(s): Biology & Population. It has an ISSN identifier of 0973-1431. Over the lifetime, 542 publications have been published receiving 1332 citations.

Topics: Biology, Population, Heritability ...read more

Trace this journal Share

Papers published on a yearly basis

2024	2019	2018	2017
2016	2015	2014	2013
2012	2011	2010	2009

Papers

Search papers Sort by: Citation Count

PDF Open Access Year

Showing all 632 results

Journal Article

Already have a manuscript?

Use our Manuscript Matcher to find the best relevant journals!

Find a Match

Refine Your Search Results

0976-4755 Search

Sort By: Title (A-Z)

Search Results

Found 1 results (Page 1) Share These Results

Exact Match Found

BIOINFOLET

Publisher: **PROF A M MUNGIKAR , MADHUKUNJI, 13 PANNALAL NAGAR, NEW OSMANPURA, AURANGABAD, INDIA, 431 005**

ISSN / eISSN: **0973-1431 / 0976-4755**

Additional *Web of Science* Indexes: **Zoological Record**

Share This Journal View profile page

** Requires free login.*

1 – 1 of 1

Items per page: 10

Filters

Clear All

- *Web of Science* Coverage
- Open Access
- Category
- Country / Region
- Language
- Frequency
- Journal Citation Reports

Editorial Disclaimer: As an independent organization, Clarivate does not become involved in and is not responsible for the editorial management of any journal or the business practices of any publisher. Publishers are accountable for their journal performance and compliance with ethical publishing standards. The views and opinions expressed in any journal are those of the author(s) and do not necessarily reflect the views or opinions of Clarivate. Clarivate remains neutral in relation to territorial disputes, and allows journals, publishers, institutes and authors to specify their address and affiliation details including territory.

Criteria for selection of newly submitted titles and re-evaluation of existing titles in the Web of Science are determined by the Web of Science Editors in their sole discretion. If a publisher's editorial policy or business practices negatively impact the quality of a journal, or its role in the surrounding literature of the subject, the Web of Science Editors may decline to include the journal in any Clarivate product or service. The Web of Science Editors, in their sole discretion, may remove titles from coverage at any point if the titles fail to maintain our standard of quality, do not comply with ethical standards, or otherwise do not meet the criteria determined by the Web of Science Editors. If a journal is deselected or removed from coverage, the journal will cease to be indexed in the Web of Science from a date determined by the Web of Science Editors in their sole discretion – articles published after that date will not be indexed. The Web of Science Editors' decision on all matters relating to journal coverage will be final.

Clarivate.™ Accelerating innovation.

© 2024 Clarivate Legal center Privacy notice Cookie policy
Manage cookie preferences Copyright notice Help

CRITERION – III

RESEARCH, INNOVATION AND EXTENSION

3.3 RESEARCH PUBLICATIONS AND AWARDS

3.3.1 NUMBER OF RESEARCH PAPERS PUBLISHED PER TEACHER IN THE JOURNALS NOTIFIED ON UGC CARE LIST DURING THE LAST FIVE YEARS

2023

Journal of the Iranian Chemical Society
https://doi.org/10.1007/s13738-023-02901-y

ORIGINAL PAPER

Transition metal complexes of pyridazine-based ligand: synthesis, characterization, biological activities, and molecular docking studies

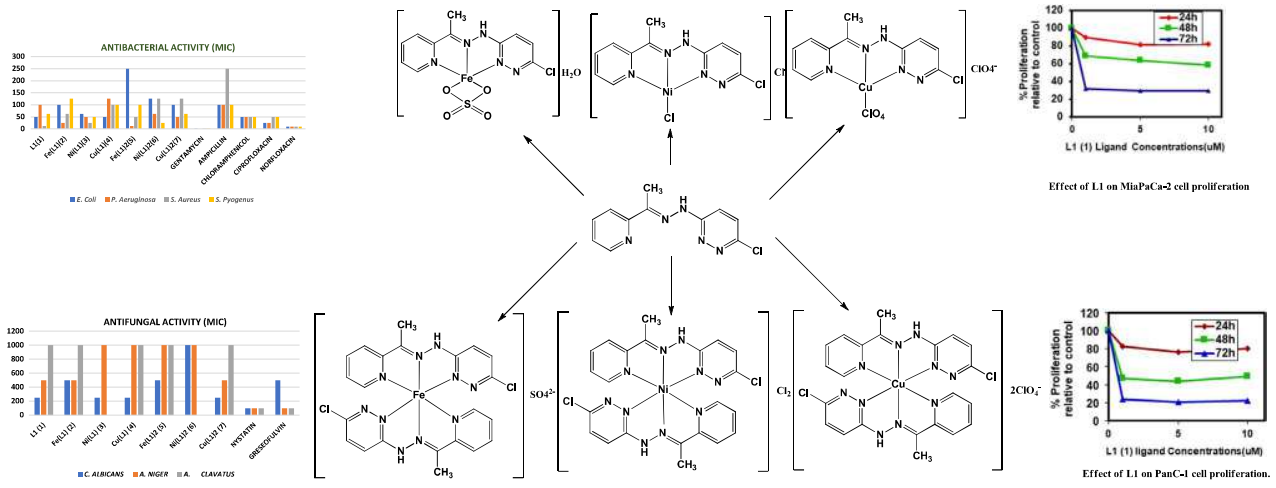
Smita S. Patil[1] · Samina K. Tadavi[2] · Ajay M. Ghatole[2] · Ratnamala S. Bendre[1]

Received: 22 February 2023 / Accepted: 12 September 2023
© Iranian Chemical Society 2023

Abstract

A new class of pyridazine-based six Iron(II), Nickel(II) and Copper(II) metal complexes of *(E)*-2-(6-chloropyridazin-3-yl)-1-(1-(pyridin-2-yl)ethylidene)hydrazine ligand (L1)(1) derived from condensation of 2-(6-chloropyridazin-3-yl)hydrazine and pyridine-2-acetaldehyde were synthesized in 1:1 and 1:2 molar ratio with ligand and characterized by UV–visible, ^{1}H- and ^{13}C-NMR, FT-IR, mass and EPR spectroscopy, elemental analysis and molar conductance. The spectroscopic evidence specifies that the ligands behave as a tridentate ligand through the nitrogen atom of pyridine-2-acetaldehyde, nitrogen atoms of azomethine group and pyridazine ring. The mass spectra demonstrated that the complexes have prepared in 1:1 and 1:2 molar ratio with ligand and suitable metals salts. From the ESR spectroscopy, confirmed that the Cu(L1)(4) complex had the square planar geometry, whereas $Cu(L1)_2$(7) complex had distorted octahedral geometry. The ligand and its six metal complexes were evaluated for their in vitro antibacterial activity against *Staphylococcus aureus* (MTCC 96), *Streptococcus pyogenes* (MTCC 442), *Escherichia coli*(MTCC 443), *Pseudomonas aeruginosa* (MTCC 1688) strains, and in vitro antifungal activity against *Candida albicans* (MTCC 227), *Aspergillus niger* (MTCC 282), and *Aspergillus clavatus* (MTCC 1323) strains by using micro-broth dilution method against standard antibiotics Gentamycin, Ampicillin, Chloramphenicol, Ciprofloxacin, Norfloxacin, and antifungal agents Nystatin and Griseofulvin. Cytotoxicity assays against human colon cancer MiaPaCa-2 and PanC-1 cell lines in vitro were completed for ligand (L1) by 3-(4,5-dimethyl-2-thiazolyl)-2,5-diphenyl-2H-tetrazolium by (MTT) method. Finally, the optimized structures of the ligand and its complexes have been used to accomplish molecular docking studies with receptors of DNA Gyrase (PDB ID-1aj6) enzyme to determine the most preferred mode of interaction.

Graphical abstract



Keywords Pyridazine-based ligand · Metal complexes · Antimicrobial activity · Anticancer activity · Molecular docking studies

Extended author information available on the last page of the article

Published online: 05 October 2023

Introduction

It is well known that many synthetic heterocyclic compounds exhibit various biological behaviours. Important six-membered heterocyclic compounds with adjacent two N-heteroatoms include pyridazine and its derivatives. A significant structural component of many physiologically active chemicals is the pyridazine moiety. Derivatives of pyridazine exhibit a range of pharmacological characteristics [1]. A variety of medications, including cefozopran, cadralazine, minaprine, pipofezine, hydralazine, and cilazapril, as well as a number of herbicides, including credazine, pyridafol, and pyridate, include the common pharmacophore known as the pyridazine structure. Activities usually differ noticeably when the substitution pattern on the pyridazine nucleus is slightly changed. Some well-known drugs have pyridazine moiety in their structure. In medical therapy, levosandane is helpful as a cardiotonic while emorfazone serves as an analgesic and anti-inflammatory [2]. For instance, essential hypertension has long been treated with hydralazine. Hydrazino-pyridazines continue to be a topic of study for improving blood pressure management drugs. Due to its cytotoxic properties, which include significantly reducing blood circulation to tumours, this class of medicine has recently seen a significant increase in therapeutic interest [3]. It has been suggested that pyridazine-based coordination polymers could be useful in medicine and have neuromuscular blocking activity. There is currently a lot of interest in developing strategies for the synthesis of supramolecular polymers that may have potential applications for gas storage, catalysis, and biological activities [4]. The use of pyridazine analogues as ligands for various targets has been demonstrated, and they have been suggested as a "privileged structure for drug discovery". Several compounds with varying substituents on their pyridazine rings have shown a variety of biological functions [5–8]. Moreover, the widespread applications of pyridazine derivatives as dyes and antimicrobial agents have attracted the interest of many investigators [9–13]. After cardiovascular disorders, cancer is the second greatest cause of death among people [14]. Although chemotherapy remains the basis of cancer treatment, the use of existing chemotherapeutics still has significant drawbacks, including a lack of selectivity for cancer tissues, the creation of unwanted side effects, and the development of multiple-drug resistance by cancer cells [15, 16].

Nowadays, pharmaceuticals encompass an analysis of breakthrough molecular effectiveness besides their facility towards obtaining bioactive building blocks. This incorporates cellular, animal, and human quantifiable aspects, all of which are typically overpriced and associated with danger. Lately, computer-assisted review of absorption, distribution, metabolism, and excretion of drugs (ADME) has improved the ability to tackle this issue [17]. Computer models, in especially, enable foreknowledge and trustworthy speedy information, consequently touting analytical methodologies. These computer scientists predict the pharmacokinetic, physicochemical, and pharmacological parameters of small compounds, encouraging lead molecules to proceed to long-acting drugs. SwissADME administered by the Swiss Bioinformatics Foundation is very handy tool for researchers around the globe to produce bioinformatics capabilities and properties, which permits the measurement of ADME parameters to structural-based medicine candidates that produce the data for early threat assessment during the medication design development [18–20]. It also offers the "BOILEDegg" diagnostic [21] and particularly assesses gastrointestinal ingestion (HIA) and P-glycoprotein efflux/preservation (P-gp). Infiltration of the blood–brain barrier (BBB) and substrate restriction of the Cytochrome P450 (CYP) enzyme could also be hypothesized.

In view of the above applications, in this paper we report herewith the synthesis, spectroscopic, antimicrobial, anticancer activities, and molecular docking studies of Iron(II), Nickel(II), and Copper(II) metal complexes of *(E)*-2-(6-chloropyridazin-3-yl)-1-(1-(pyridin-2-yl)ethylidene)hydrazine ligand.

Experimental

Material and methods

Materials such as 3,6-dichloropyridazine (Sigma Aldrich), pyridine-2-acetaldehyde (Sigma Aldrich), and hydrazine hydrate (S D fine) were selected to form the ligand (L1)(1) and its metal complexes.

The solutions of conc. 10^{-3} and 10^{-4}were prepared by dissolving ligand and its metal complexes in DMF at room temperature (30 °C), and the electronic spectra were measured using a Shimadzu UV-2450 Spectrophotometer. The FT-IR spectra of synthesized compounds were recorded as Nujol Mulls in the wave number range 4000–400 cm^{-1} on FT-IR PerkinElmer model Spectrum One Spectrophotometer.

Molar conductivities of metal complexes were measured on a Systronic Conductivity Bridge with dip-type cell, using 10^{-3} M solution of complexes in DMF as a solvent. All the studies mentioned above were carried out at School of Chemical Sciences, Kavayitri Bahinabai Chaudhari North Maharashtra University, Jalgaon (India).

At the Indian Institute of Technology, Bombay, a 410 Prostar Binary LC with 500 MS IT PDA Detectors, Varian Inc., USA, was used to record the mass spectra of the ligands

and the ESI–MS spectra of the metal complexes (India). On a Varian-300 spectrometer, all NMR spectra were measured (at 300 MHz for 1H and 75 MHz for 13C-NMR), with TMS serving as the internal standard and CDCl3 serving as the solvent. At the Indian Institute of Technology, Bombay, ligands and complexes were subjected to elemental analysis using a ThermoFinnigan elemental analyser, and the X-band EPR spectra of copper complexes were captured at liquid nitrogen temperature (77 K) as DMF solutions on a JES-FA200 ESR spectrometer (India).

Procedure for synthesis of ligand (L1)(1): *(E)*-2-(6-chloropyridazin-3-yl)-1-(1-(pyridin-2-yl) ethylidene)hydrazine

Synthesis of 2-(6-chloropyridazin-3-yl)hydrazine

3,6-dichloropyridazine (4 g, 0.0268 mmol) was dissolved in 30 ml of ethanol. To this solution, hydrazine hydrate (4.03 g, 0.0805 mmol) was added dropwise and the mixture was stirred for two hours at ambient temperature. The precipitate was filtered by suction and washed with water so as to remove excess of hydrazine hydrate, followed by cold ethanol and ether to form faint cream coloured, 3.87 g (81.64%) of 2-(6-chloropyridazin-3-yl)hydrazine [22, 23].

Synthesis of *(E)*-2-(6-chloropyridazin-3-yl)-1-(1-(pyridin-2-yl) ethylidene) hydrazine ligandL1(1)

An ethanolic (20 ml) solution of above-prepared hydrazine (3.16 g, 0.0219 mmol) was condensed with pyridine-2-acetaldehyde (2.7 g, 0.0223 mmol) in the presence of catalytic amount of acetic acid, and the reaction mixture was cautiously heated at 40 °C for three hours. The mixture was cooled to room temperature, and precipitate was filtered, washed with cold ethanol and diethyl ether, and dried in vacuum [17, 18]. Ligand (L1)(1) (Brown powder),Yield: 5.27 g(97.21%); IR (Nujol Mulls, cm^{-1}):3182 (–N–H), 1582 –(C=N) azomethine and 1510 (–C=N) aromatic.^{1}H NMR (300 MHz, $CDCl_3$, δ ppm):

2.47 (3H, s, C-8H), 7.26 (1H, t, C-3H), 7.41 (1H, d, C-16H), 7.67–7.73 (2H, m, C-4H, C-15H), 8.08 (1H, d, C-5H), 8.60 (1H, d, C-2H) and 8.77 (1H, s, N-10H).^{13}C NMR (300 MHz, $CDCl_3$, δ ppm): 10.88 (C-8), 116.27 (C-16), 120.08 (C-5), 123.34 (C-3), 129.91 (C-15), 136.13 (C-4), 147.63 (C-14), 148.63 (C-7), 149.25 (C-2), 155.25 (C-6) and 158.45 (C-11).LC–MS (*m/z*)$C_{11}H_{10}N_5Cl = 248.1$ (M^{+1}) found; Calculated for $C_{11}H_{10}N_5Cl = 248.1$. Elemental Analysis Found %: C, 52.44; H, 3.82; N, 27.60; Calcd. For $C_{11}H_{10}N_5Cl$: C, 53.33; H, 4.04; N, 27.60%.UV–Vis (λ_{max}): 239, 315.Molar conductivity ($\Omega^{-1}cm^2\ mol^{-1}$, RT): 6

General procedure for the synthesis of metal complexes of Fe(L1)(2), Ni(L1)(3) and Cu(L1)(4) in 1:1 molar ratio with *(E)*-2-(6-chloropyridazin-3-yl)-1-(1-(pyridin-2-yl) ethylidene)hydrazine ligand (L1)(1)

To a hot solution of *(E)*-2-(6-chloropyridazin-3-yl)-1-(1-(pyridin-2-yl)ethylidene)hydrazine ligand**L1(1)**(0.5 g, 0.002 mmol) in 20 ml ethanol, an ethanolic ($CuCl_2.2H_2O$, $NiCl_2.6H_2O$) or aqueous ($FeSO_4.7H_2O$) solution of metal salt (0.002 mmol, 20 ml) was dropwise added and the reaction mixture was refluxed for eight hours. Brown coloured solution on slow evaporation at room temperature yielded Ni(L1)(3)complex. While in the reaction mixtures of copper and iron complexes saturated solution of sodium perchlorate was added together, the mixture was over again stirred for two hours at ambient temperature to precipitate the complexes. Compounds were filtered, washed out with cold ethanol and diethyl ether, and dried over P_2O_5 in vacuum [24–26].

Complex Fe(L1) (2) (Purple), Yield: 81%; IR (Nujol Mulls, cm^{-1}):1614(–C=N) azomethine and 1592(–C=N) aromatic. LC–MS (*m/z*)[$Fe(C_{11}H_{12}ClN_5O_5S] = 416.96[M^{-1}]$ found; Calculated for [$Fe(C_{11}H_{12}ClN_5O_5S] = 416.1$. UV–Vis ($\lambda_{max}$): 298, 395, 620. Molar conductivity ($\Omega^{-1}cm^2\ mol^{-1}$, RT): 23.

Complex Ni(L1)(3),(Brown), Yield: 74%;IR (Nujol Mulls, cm^{-1}):3190 (–N–H), 1635(–C=N) azomethine and 1593(–C=N) aromatic.LC–MS (*m/z*) [$Ni(C_{11}H_{10}Cl_2N_5)] = 339.97[M^{-2}]$ found; Calculated for [$Ni(C_{11}H_{10}Cl_3N_5)] = 374.94$. UV–Vis ($\lambda_{max}$): 313, 378, 446. Molar conductivity ($\Omega^{-1}cm^2\ mol^{-1}$, RT): 69.

Complex Cu(L1)(4) (Green), Yield: 76%; IR (Nujol Mulls, cm^{-1}):3071 (–N–H), 1633(–C=N) azomethine and 1592(–C=N) aromatic. LC–MS (*m/z*) [$Cu(C_{11}H_{10}Cl_2N_5O_4)] = 408.9$, found; Calculated for [$Cu(C_{11}H_{10}Cl_3N_5O_8)] = 507.89$. UV–Vis ($\lambda_{max}$): 282, 389, 479. Molar conductivity ($\Omega^{-1}cm^2\ mol^{-1}$, RT): 51.

General procedure for synthesis of metal complexes of $Fe(L1)_2$(5), $Ni(L1)_2$(6) and $Cu(L1)_2$(7) in 1:2 molar ratio with*(E)*-2-(6-chloropyridazin-3-yl)-1-(1-(pyridin-2-yl) ethylidene)hydrazine ligand (L1)(1)

Hot solution of ligand (L1)(1)(0.5 g, 0.002 mmol, 30 ml) was added in hot ethanolic ($CuCl_2.2H_2O$, $NiCl_2.6H_2O$) or an aqueous ($FeSO_4.7H_2O$) solution of (0.001 mmol, 20 ml) metal salts. The reaction mixture was refluxed with stirring for eight hours, and then, saturated solution of sodium perchlorate was added up in reaction mixture of copper and

stirred for three hours at room temperature. The products precipitated out at ambient temperature were isolated by filtration and dried over P_2O_5 in vacuum [23–26].

Complex $Fe(L1)_2$(5),(Purple) Yield: 83%; IR (Nujol Mulls, cm^{-1}):1613(-C = N) azomethine and1592(-C = N) aromatic. LC–MS (*m/z*)[$Fe(C_{23}H_{21}Cl_2N_{10})$] = 549.1 ($M^{+2}$) found; Calculated for [$Fe(C_{22}H_{20}Cl_2N_{10}O_4S^{2-})$] = 646.1. UV–Vis ($\lambda_{max}$): 316, 385, 612. Molar conductivity ($\Omega^{-1}cm^2\ mol^{-1}$, RT): 11.

Complex $Ni(L1)_2$(6),(Brown) Yield: 61%;IR (Nujol Mulls, cm^{-1}):3209, 3079(–N–H), 1635(–C=N) azomethine and 1593(–C=N) aromatic. LC–MS (*m/z*) [$Ni(C_{23}H_{23}Cl_4N_{10})]^{2+}$ = 638.7 (M^{-1}) found; Calculated for [$Ni(C_{23}H_{23}Cl_4N_{10})]^{2+}$ = 637.02.UV–Vis (λ_{max}): 274, 408, 468. Molar conductivity ($\Omega^{-1}cm^2\ mol^{-1}$, RT): 131.

Complex $Cu(L1)_2$(7), (Dark green) Yield: 59%; IR (Nujol Mulls, cm^{-1}):3209(–N–H), 1586(–C=N) azomethine and 1463(–C=N) aromatic. LC–MS (*m/z*) [$Cu(C_{22}H_{20}Cl3N_{10}O_4^-]$ = 656.8 (M^{-1}) found; Calculated for [$Cu(C_{22}H_{20}Cl3N_{10}O_4^-]$ = 656.00.UV–Vis (λ_{max}): 279, 323, 400, 477. Molar conductivity ($\Omega^{-1}cm^2\ mol^{-1}$, RT): 60.

Result and discussion

The complexes were prepared by reacting ligand (L1)(1) *(E)*-2-(6-chloropyridazin-3-yl)-1-(1-(pyridin-2-yl)ethylidene) hydrazine with the metal ions of iron, nickel, and copper in 1:1 and 1:2 molar ratio in an ethanolic medium and studied their antimicrobial and anticancer activities.

Elemental analysis

The elemental analysis of the synthesized ligand (L1)(1) corresponded to the calculated percentages of elements and thus confirmed the hydrazone structure.

^{1}H- and ^{13}C-NMR spectra

In the ^{1}H-NMR spectrum, the signal due to ν(N–H) proton seemed as a singlet at 8.77 ppm. Singlet corresponding to methyl protons was observed at 2.47 ppm. Ring protons looked as three doublets at 8.60, 8.01, and 7.41 ppm. The ^{13}C-NMR spectrum provides direct selective information about the carbon skeleton of the synthesized compound. In the ^{13}C-NMR spectrum, the signal due to azomethine carbon appeared at 148.63 ppm. In Supplementary data, ^{1}H and ^{13}C-NMR spectra of ligand clearly confirmed the formation of ligand (L1)(1).

Infrared spectral studies

The IR spectral analysis gives an insight to the structure of the compounds. The characteristic bands of different functional groups provide worthful information of the complexes regarding the coordination of the ligands to the metal. In the IR spectrum of hydrazone ligand (L1)(1), band found around 3182 cm^{-1} can be assigned to ν(–N–H) and strong absorption bands at 1582 cm^{-1} and 1510 cm^{-1}can be assigned to ν(–C=N) azomethine and aromatic ν(–C=N), respectively. The absence of ν(–N–H) absorption in iron complexes confirms binding of ligand (L1)(1) as deprotonated ligands. The shifting of ν(–C=N) azomethine of the ligands to higher wave numbers in the metal complexes indicates the coordination of the azomethine nitrogen with the metal. The other bands observed in the range 1400–1200 cm^{-1} can be attributed to the heteroaromatic rings, which undergo significant alteration upon complexation. Metal complexes $Fe(L1)_2$ (2), Cu(L1)(4), $Cu(L1)_2$(7), and Ni(L1)(3) show a band matching to ν(–O–H) due to water of crystallization.

Electronic spectra

The electronic spectrum of the ligand (L1)(1) illustrious in DMF depicts bands at 239 and 315 nm assignable to $\pi \rightarrow \pi^*$ of aromatic ring and $n \rightarrow \pi^*$ transitions of the azomethine group.

EPR

Each paramagnetic species produces a characteristic EPR signature with well-defined spin Hamiltonian parameters. EPR spectrum gives most useful chemical information which results from nuclear hyperfine structure. Most of the EPR studies are cantered on the copper complexes, because of the presence of unpaired electron. X-band electron paramagnetic resonance spectra of Cu(L1)(4) and $Cu(L1)_2$(7) are shown in Supplementary data. The EPR spectrum of Cu(L1)(4) complex in DMF at liquid nitrogen temperature displays square planar geometry with $g_1 = 2.05$ and $g_2 = 2.24$. The lower g value is near about same that is usually observed in compounds with square planar geometry ($g = 2.04$) [27]. The presence of considerable covalent bonding in the complexes is indicated by the g_{II} values being less than 2.3 [28, 29]. The EPR spectrum of $Cu(L1)_2$(7) complex corresponds to the axial pattern with $g_{II} > g_{\perp}$. Distorted octahedral geometry was obtained for $Cu(L1)_2$(7) complex with $g_{II} = 2.2186$ and $g_{\perp} = 2.047$ values[30] and the signal corresponding to g_{II}appearance hyperfine splitting due to nuclear spin of Cu (I = 3/2) having A_{II} [Cu(II)] = 171 X 10^{-4} cm^{-1}.

Mass spectra

Mass spectral data confirmed the molecular weight corresponding to the expected structure of the ligand as indicated by the molecular ion peak (M^{+1}) comparable to its molecular weight.

In case of most of the metal complexes, the molecular ion peaks match with m/z including or excluding that of counter ions, as shown in Supplementary data (Figs. 1, 2, 3).

Molar conductance

Electric current flow through a substance is characterized by its conductance. Using a 10^{-3} M (DMF) solution of the complexes, molar conductivities of metal complexes were measured on a Systronic Conductivity Bridge with dip-type cell. Electrical conductivity was measured in ohm^{-1} cm^2 mol^{-1}. DMF is having a dielectric constant of 5.4×10^{-3}. The low conductance of ligand and its copper and iron complexes support the non-electrolyte nature, while nickel complexes Ni(L1)(3) and Ni(L1)$_2$(6) are electrolyte in nature due to high conductance values falling in the range for 1:1 and 1:2 electrolytes, respectively.

Assay of antimicrobial activities

In antimicrobial activity, all newly synthesized compounds were evaluated for their *in vitro* antibacterial activity against *Staphylococcus aureus* (MTCC 96), *Streptococcus pyogenes* (MTCC 442), *Escherichia coli* (MTCC 443), *Pseudomonas aeruginosa* (MTCC 1688) strains, and in vitro antifungal activity against *Candida albicans* (MTCC 227), *Aspergillus niger* (MTCC 282), and *Aspergillus clavatus* (MTCC 1323) strains by using micro-broth dilution method. The standard strains used for screening of antibacterial and antifungal activities were secured from Microbial Type Culture Collection (MTCC), Institute of Microbial Technology, Chandigarh. Mueller–Hinton broth was used as the nutrient medium to grow and dilute the drug suspension for the test bacteria.

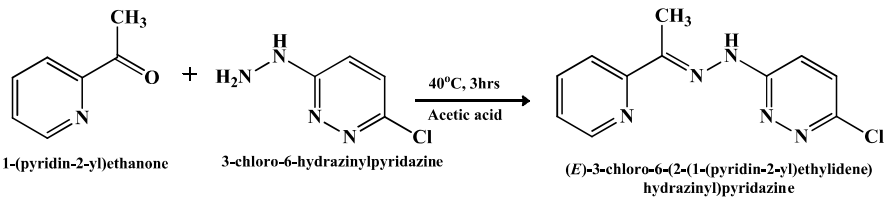


Fig. 1 Reaction scheme for synthesis of (E)-2-(6-chloropyridazin-3-yl)-1-(1-(pyridin-2-yl) ethylidene)hydrazine ligand (L1)(1)

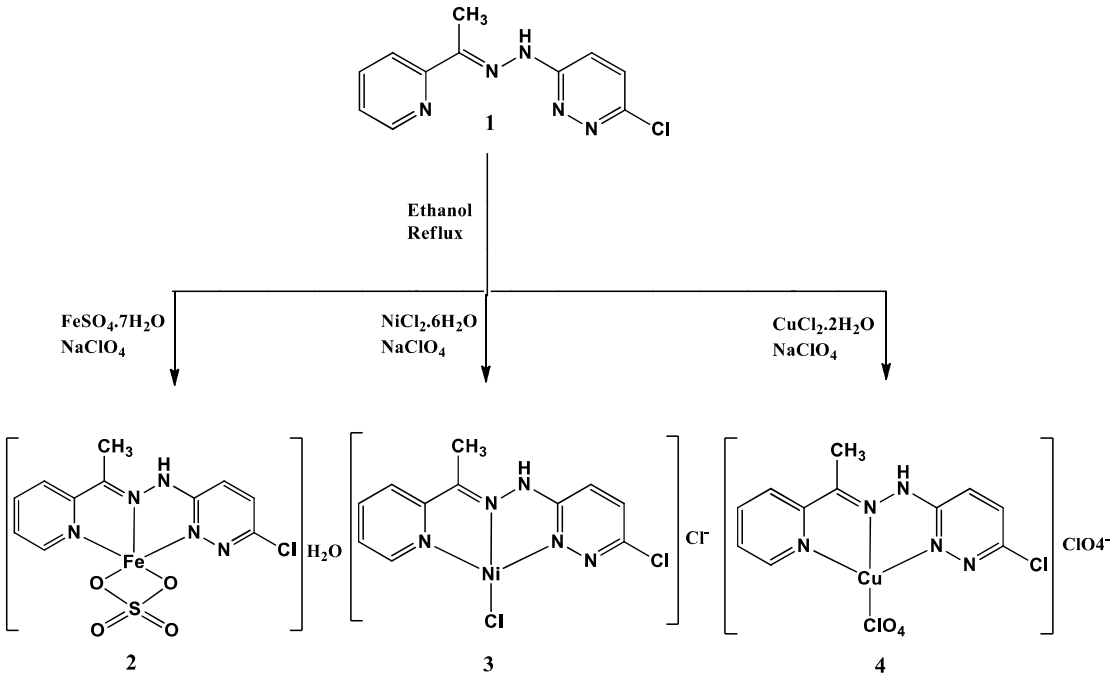


Fig. 2 Reaction scheme for synthesis of metal complexes of ligand (L1)(1) with metals in 1:1 molar ratio

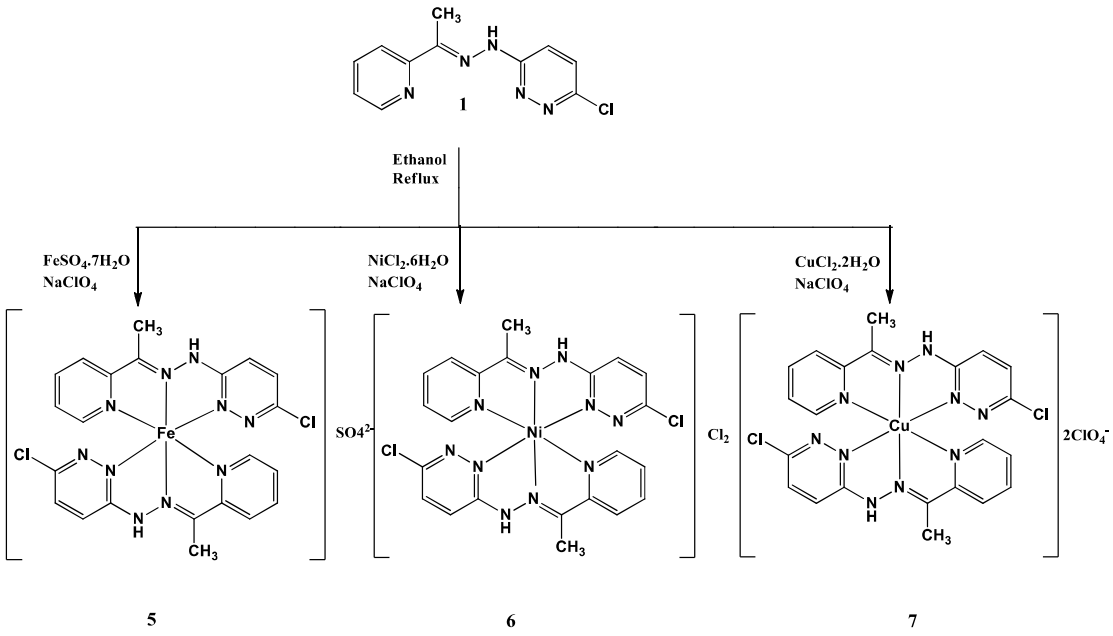


Fig. 3 Reaction scheme for synthesis of metal complexes of ligand (L1)(1) with metals in 1:2 molar ratio

The minimum inhibitory concentration (MIC) measurement was determined as [(Ac–At)/Ac] × 100, where Ac is an average of six replicates of light absorption values of the negative controls, and it was an average of six replicates of light absorption values of the tested compound. The MIC (μg/mL) values for synthesized compounds (1–7) and standard antibiotics Gentamycin, Ampicillin, Chloramphenicol, Ciprofloxacin, Norfloxacin, and antifungal agents Nystatin and Griseofulvin are noted, and the results mentioned in Tables 1 and 2 indicate that synthesized ligand and its metal complexes demonstrated variable inhibitory effects on the growth of bacterial and fungal strains [31–33].

The compounds (1), (4), (3), (2), and (7) showed exceptional antibacterial activity against *Escherichia coli* strain as compared with the positive controls Ampicillin and Chloramphenicol. The compounds (5) and (2) exhibited excellent antibacterial activity against *Pseudomonas aeruginosa* strain as compared with the standards Ampicillin, Chloramphenicol, and Ciprofloxacin [34–36].

Compounds (1), (3), (5), and (2) exhibited very good antibacterial activity against *Staphylococcus aureus* strain

Table 1 Antibacterial activity of (E)-2-(6-chloropyridazin-3-yl)-1-(1-(pyridin-2-yl) ethylidene) hydrazine ligand (L1)(1)and its metal complexes

Antibacterial activity table (minimal inhibition concentration)					
Sr. no	Sample code	*Escherichia coli* (MTCC 443)	*Pseudomonas aeruginosa* (MTCC 1688)	*Staphylococcus aureus* (MTCC 96)	*Streptococcus pyogenes* (MTCC 442)
1	L1(1)	50	100	12.5	62.5
2	Fe(L1)(2)	100	25	62.5	125
3	Ni(L1)(3)	62.5	50	25	50
4	Cu(L1)(4)	50	125	100	100
5	$Fe(L1)_2$(5)	250	12.5	50	100
6	$Ni(L1)_2$(6)	125	62.5	125	25
7	$Cu(L1)_2$(7)	100	50	125	62.5
8	Gentamycin	0.05	1.0	0.25	0.5
9	Ampicillin	100	100	250	100
10	Chloramphenicol	50	50	50	50
11	Ciprofloxacin	25	25	50	50
12	Norfloxacin	10	10	10	10

Table 2 Antifungal activity of(E)-2-(6-chloropyridazin-3-yl)-1-(1-(pyridin-2-yl) ethylidene)hydrazine ligand (L1)(1) and its metal complexes

Antifungal activity table (minimal inhibition concentration)				
Sr. no	Sample code	*Candida Albicans* (MTCC 227)	*Aspergillus Niger* (MTCC 282)	*Aspergillus Clavatus* (MTCC 1323)
1	L1 (1)	250	500	1000
2	Fe(L1) (2)	500	500	1000
3	Ni(L1) (3)	250	1000	> 1000
4	Cu(L1) (4)	250	1000	1000
5	$Fe(L1)_2$(5)	500	1000	1000
6	$Ni(L1)_2$(6)	1000	1000	> 1000
7	$Cu(L1)_2$(7)	250	500	1000
8	NYSTATIN	100	100	100
9	GRESEOFULVIN	500	100	100

as compared with all the standards except Gentamycin and Norfloxacin. Against *Streptococcus pyogenes*, compounds (1) and (7) showed inhibitory action against Ampicillin standard, whereas compound (6) revealed maximum inhibitory action against three Ampicillin, Chloramphenicol, and Ciprofloxacin standards. The antibacterial activities of ligand and its six metal complexes are summarized in Table 1. The antifungal activity of the synthesized ligand and its six metal complexes was studied against three fungal strains, viz. *Candida albicans*, *Aspergillus niger,* and *Aspergillus clavatus*; however, only (1), (3), (4), and (7) showed good results against *Candida albicans* strain, in comparison with the standard drug Griseofulvin. Remaining all the compounds exhibited moderate-to-poor antifungal activities against these three strains. The antifungal activities of ligand and its six metal complexes are summarized in Table 2.

Anticancer activity

Cytotoxicity assays against human colon cancer MiaPaCa-2 and PanC-1 cell lines in vitro were performed for ligand (L1)(1) by 3-(4,5-dimethyl-2-thiazolyl)-2,5-diphenyl-2H-tetrazolium (MTT) method [37]. Doxorubicin was used as a positive control, and IC_{50} values of the tested compounds were calculated from averages of three experiments. IC_{50} is designated as the concentration (in μM) of chemotherapeutic drug L1 that causes 50% inhibition of cancer cell growth. Figures 4 and 5 represent the dose–response curves of MiaPaCa-2 and PanC-1 cells to the ligand (L1)(1) tested. The % proliferation relative to control was determined by MTT method after 24, 48, and 72 h of compound exposures. The ligand (L1)(1) inhibited the proliferation of MiaPaCa-2 and PanC-1 cell line in dose-dependent manner with IC_{50} values around 1 μM indicating that it is a potent anticancer agent against pancreatic cancer cells. Considering that there are very few anticancer agents currently available for treating

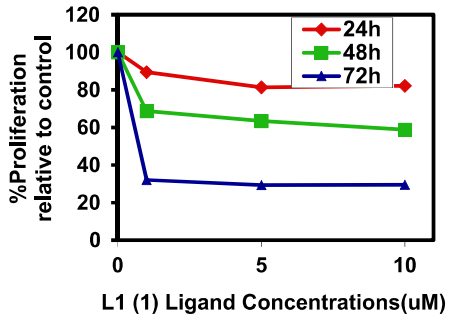


Fig. 4 Effect of L1 on MiaPaCa-2 cell proliferation

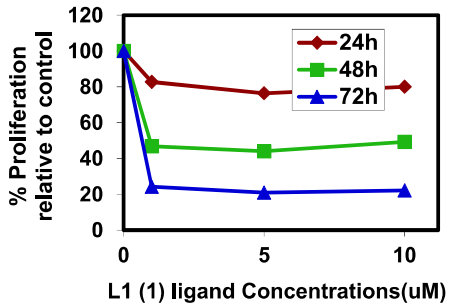


Fig. 5 Effect of L1 on PanC-1 cell proliferation

pancreatic cancer, it would be worthwhile to investigate ligand (L1)(1) for developing it as a potential pancreatic anticancer agent.

Molecular modelling

The molecular docking performed for known standard drugs in the active site of DNA Gyrase (PDB ID-1aj6) enzyme [38–41]. For a better understanding of their activity, a

Table 3 Docking score (kcal/mole) of various standard drugs with DNA Gyrase (PDB ID-1aj6) enzyme

S. no	Ligand	Docking score(kcal/mole)
1	Ampicillin	−7.2
2	Chloramphenicol	−6.9
3	Ciprofloxacin	−7.3
4	Norfloxacin	−7.0

Table 4 Docking score (kcal/mole) of different ligand and synthesized complexes with DNA Gyrase (PDB ID-1aj6) enzyme

S. no	Ligand	Docking score (kcal/mole)
1	Ligand (L1)-(1)	−7.3
2	Complex $Fe(L1)_2$-(5)	−8.1
3	Complex $Ni(L1)_2$-(6)	−7.9
4	Complex $Cu(L1)_2$-(7)	−8.3

comparative investigation of the impacts of known standard Ampicillins, Chloramphenicol, Ciprofloxacin, And Norfloxacin in the DNA Gyrase active site pocket was conducted. Table 3 shows this drug docking score.

Negative binding energies are congruent with the DNA Gyrase selectivity of the antibiotic Ciprofloxacin (−7.3 kcal/mole) as reported in academic papers. The location of the amino acid residue on the active side and the hydrophobic interaction that caused ciprofloxacin to bind to the DNA Gyrase binding pocket were confirmed. Between the hydroxy hydrogen of quinoline with Glu-50 and the carboxylic acid hydrogen of ciprofloxacin, there is a typical hydrogen bond interaction of 2.23 and 3.11 Å. The cyclopropyl ring of Ciprofloxacin exhibits two allylic connections, one with Val-20 at a distance of 4.85 Å and a second with Ile-78 at a distance of 5.11 Å. The quinoline ring of ciprofloxacin, specifically Thr-165 and Ile-78, has a carbon hydrogen bond of 3.54 and 4.62 Å.

The H-bonding or hydrophobic interaction of the docked ligand (L1)(1) with the amino acid residues in the active site, as well as the complexes $Fe(L1)_2$-(5), $Ni(L1)_2$-(6), $Cu(L1)_2$–7, and standard drugs, was used to interpret the complexation of the docked ligand (L1)(1), as well as the complexes with the DNA Gyrase enzyme. Table 4 provides a summary of the findings.

Even for ciprofloxacin, which has the highest negative value (−7.3 kcal/mole), all the synthesized compounds had a comparably high binding score compared to the traditional medication. The copper complex $Cu(L1)_2$-(7), which is synthesized using a 1:2 molar ratio of ligand, has the highest docking score (-8.3 kcal/mole) among the synthetic complexes (Fig. 6, Fig. 7).

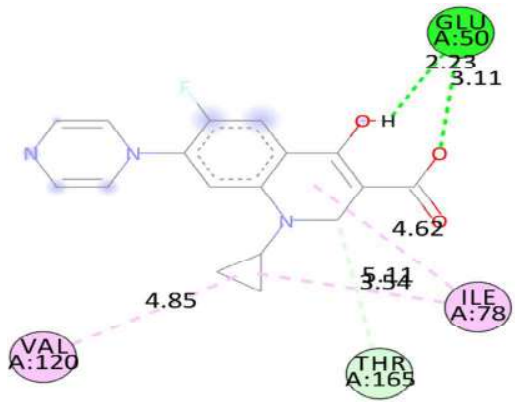


Fig. 6 Docking structure of Ciprofloxacin into the active site of DNA Gyrase enzyme

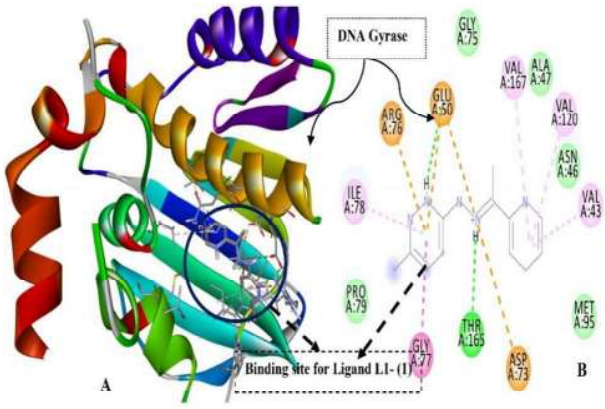


Fig. 7 Docking pose of ligand(E)-2-(6-chloropyridazin-3-yl)-1-(1-(pyridin-2-yl)ethylidene)hydrazine ligand (L1)-(1) into the active site of DNA Gyrase enzyme

Detailed $Cu(L1)_2$-(7) and $Fe(L1)_2$-(5)—DNA Gyrase (PDB ID-1aj6) enzyme interaction having the highest binding score among the other synthesized complexes

The following assignments for protein-inhibitor interaction can be made after taking into account the stereo view of the $Cu(L1)_2$-(7) complex inside the active site canyon of DNA Gyrase and the Discovery Visualizer shown in Fig. 8.

The strong evidence can be used to create more effective heterocyclic compounds. (E)-2-(6-chloropyridazin-3-yl)-1-(1-(pyridin-2-yl)ethylidene)hydrazine Complex $Fe(L1)_2$-(5), ligand shows two types of interaction with Phe-41 (Phenylalanine-41) one through the pyridine ring and another

with the pyridazine molecule, with distances of 5.25 and 4.55 Å. Both Lys-189 (Lysine-189) and Arg-190 (Arginine-189) bind with the same pyridine ring of the same side ligand at distances of 5.26 and 4.18 Å, respectively (Fig. 8).

Within the identical ligand molecule, pyridine and pyridazine molecules engage with the Phe-41 in a Pi-Pi-T configuration with a spacing of 4.99 Å between each. The connection between the pyridine ring of the ligand and Phe-41 also had a Pi–allyl interaction at a distance of 4.40 Å from Arg-190. The binding interaction of ligand $Cu(L1)_2$-(7) with Arg-190 and Phe-41 is inside the pocket of Ile-186, Gly-33, Gly-113, Gly-28, Glu-193, Leu-193, Thr-34, Asp-45, Lys-189, His-116, His-38, His-37, and Ser-112 with interpolated charge ranging from -0.100 to 0.100. The highest donor and acceptor H-bonds from various sites may be seen at Thr-134 and Leu-194. The solvent accessible surface ranges from 10.0 to 28.0, and the hydrophobicity within the pocket ranges from −3.00 to 3.00.

Absorption, distribution, metabolism, and excretion (ADME) investigation of compounds

Pharmacology

The ADME provides the bio-accessibility radar for the molecule to show resemblance as a bioactive suppository [42]. Each vertices in the hexagonal (Fig. 9) graph has the limitations (Table 5) which represent the pharmacology of the compounds.

Drug-likeness

The distorted hexagonal red lines represent the drug-likeness possessions of the synthesized compounds (Fig. 10). Particularly the standard drug-like Ampicillins, Chloramphenicol, Ciprofloxacin, And Norfloxacin fall within parameters

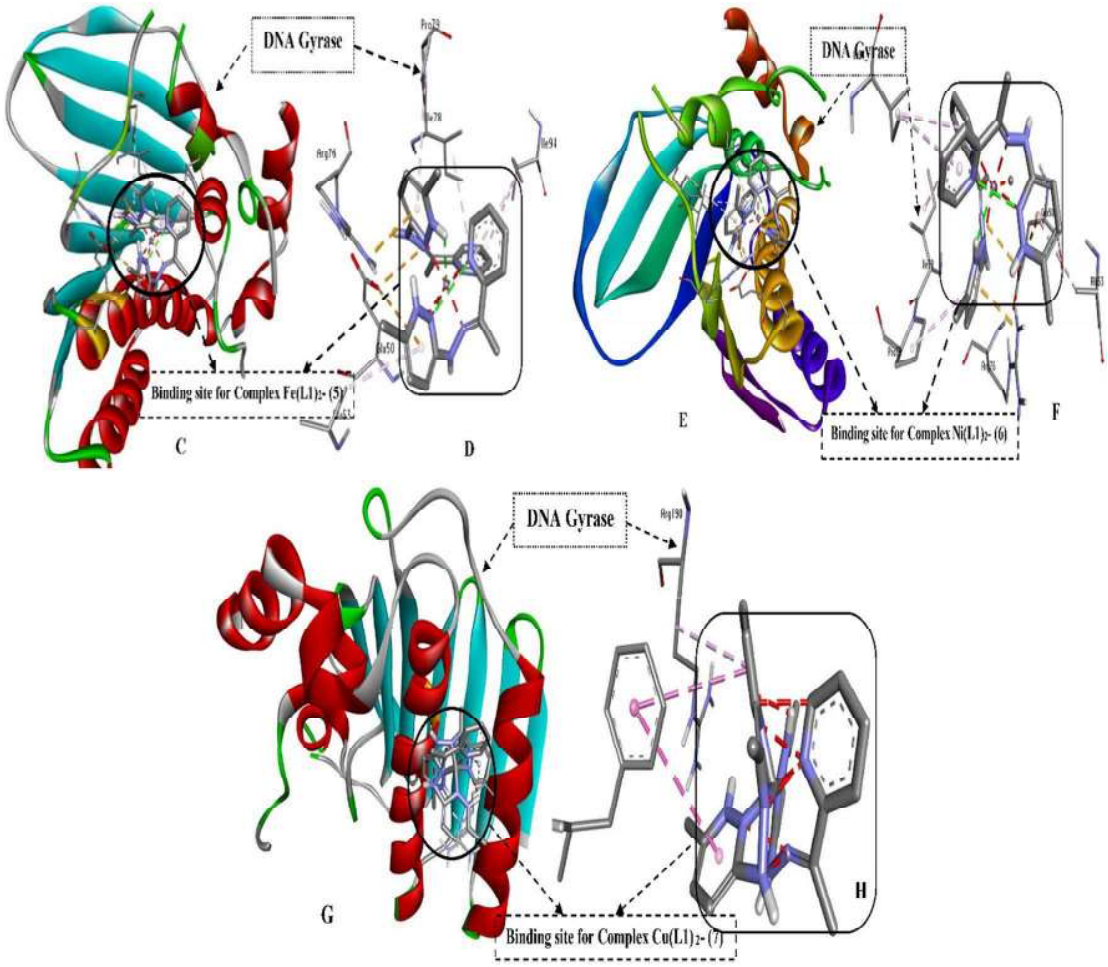


Fig. 8 Docking pose of (C) Complex $Fe(L1)_2$-(5), (E) Complex $Ni(L1)_2$-(6), and (G) Complex $Cu(L1)_2$-(7) with its site of interaction. (D), (F), and (H) Binding mode (stick structure) inside DNA Gyrase enzyme

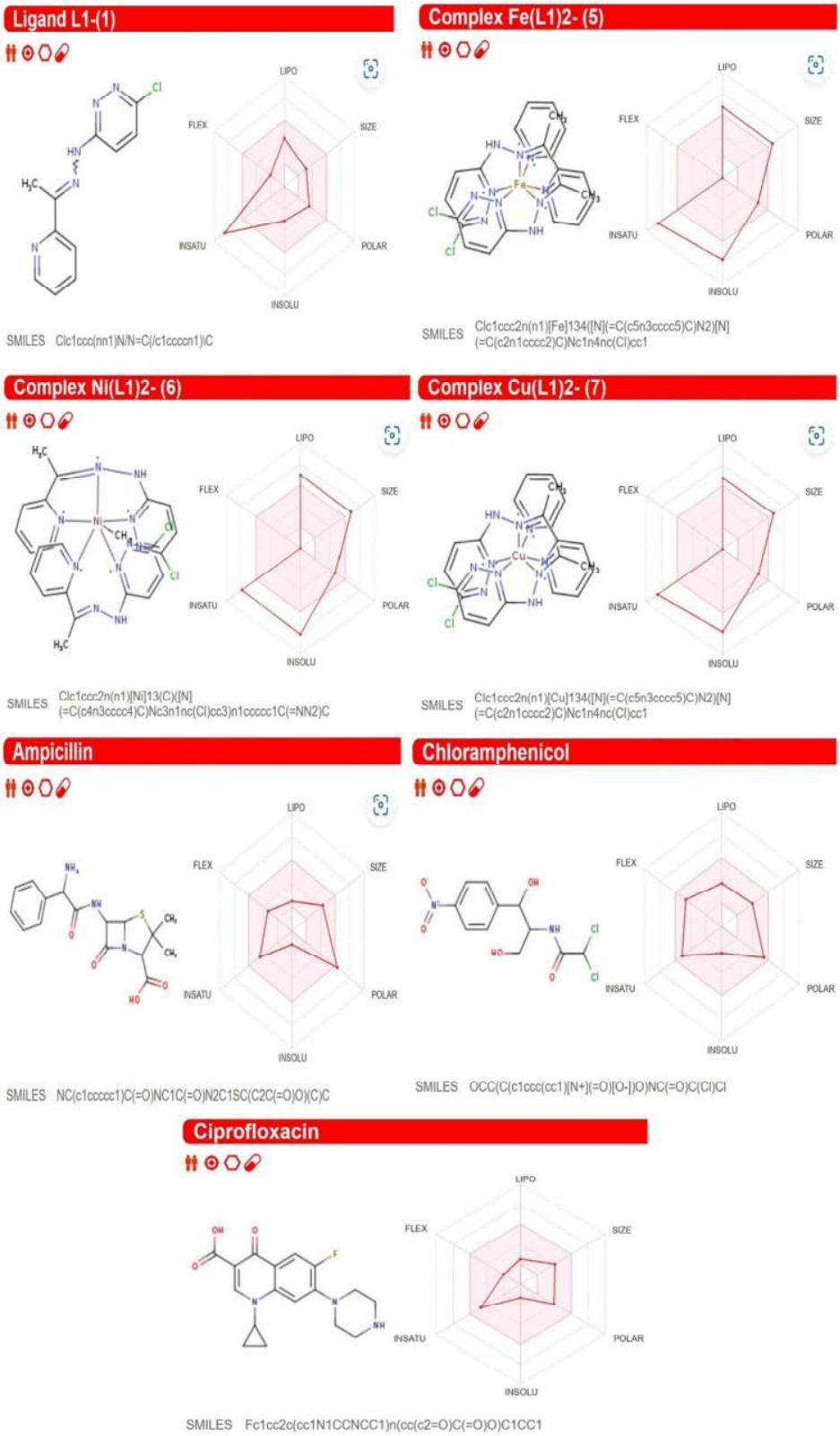


Fig. 9 Bio-availability radar for the synthesized ligand and complexes that to compare with the standard drugs

except for one or two parameters of a bioavailable drug (Tables 6 and 7).

The Ghose [43], Egan [44], Veber [45], and Muegge [46] parameters are used by SwissADME's application for the prediction of medication resemblance when screening small molecules. The Ghose and Veber screening parameters have a scale for the quantitatively depicts of small molecules which are given in Table 8.

The Egan (Pharmacia) [44] screening method is used to predict pill absorption based on a tiny molecule's epithelial absorbency. The Egan method avoids an excess descriptor by holding the polar surface area (PSA) and AlogP98 descriptors in the same model [47]. PSA serves as a benchmark for AlogP98. The dynamic influx and efflux components for small compounds into the human submissive gastrointestinal absorption are portrayed by the Egan computational model (HIA). Molecular targeted absorption into the human intestinal absorption (HIA). Muegge's (Bayer filter) database model helps to discriminate between non-drug-like and drug-like molecules. The database suggests that the molecule with hydroxyl, amine, ketone, and sulfonyl functional groups remarkable has a drug-like molecule. The small molecule to authorize the Muegge model needs the will-described pharmacophore. The Muegge database suggests that the small molecule to act as a drug molecule must contain at least four functional groups that are ketone, hydroxy, sulfonyl, and amine excluding the four functional groups; the molecule with guanidine, carbamate, alcohol, amidine,

Table 5 The appropriate range for each attribute is shown by the pink region within the hexagon

	XLOGP3	MW	TPSA	Solubility (Log S)	Saturation	Flexibility
Range	−0.7 to + 5.0	150 to 500 g/mol	20 to 130 A2	Not higher than 6	0.25 (a section of carbons in the sp3 hybridization)	Near to 9 rotatable bonds

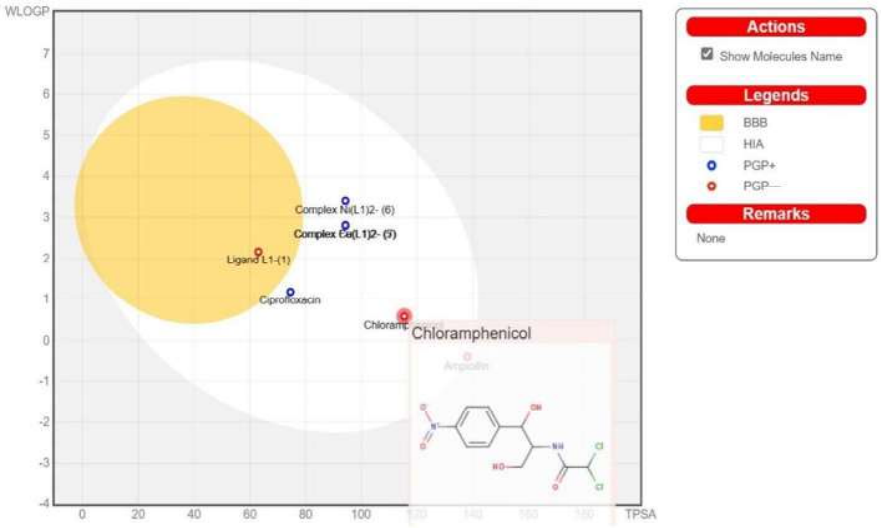


Fig. 10 In the presence of the compounds, the BOILEDEgg enables the measurement of passive gastrointestinal absorption (HIA), brain penetration (BBB), and P-glycoprotein (P-gp)

Table 6 Ligand and complexes and commercial drugs' physicochemical properties

Sr. no	MW	HA	AHA	FCsp3	RTB	HBA	HBD	MR	TPSA
L1-(1)	247.68	17	12	0.09	3	4	1	67.12	63.06
5	551.21	35	24	0.09	0	2	2	146.77	94.28
6	569.1	36	24	0.13	0	3	2	152.63	94.28
7	558.91	35	24	0.09	0	2	2	146.77	94.28
SD1	349.4	24	6	0.44	5	5	3	92.56	138.03
SD2	323.13	20	6	0.36	7	5	3	74.38	115.38
SD3	331.34	24	10	0.41	3	5	2	95.25	74.57

MW molecular weight, *HA*: heavy atoms, *AHA*: aromatic heavy atom, *FCsp3* fraction Csp3, *RTB* rotatable bonds, *HBA* H−bond acceptors, *HBD* H−bond donors, *MR* molar refractivity, *TPSA* total polar surface area; L1−1 ligand (L1)(1), 5 complex Fe(L1)2−(5), 6 complex Ni(L1)2−(6), 7 Complex Cu(L1)2−(7), *SD*1 ampicillin, *SD*2 Chloramphenicol, *SD*3 ciprofloxacin

carboxylic acid, urea, sulfonamide, amide, sulfone, and ester can be acting a drug molecule. The small molecule to be nondrug contains less than four functional groups.

Among all the synthesized molecules ligand (L1)(1), standard Chloramphenicol, and Ciprofloxacin fall within the Lipinski, Ghose, and Veber violation parameters. Veber violation is one of the parameters which follows all the synthesized molecules. In the case of Egan and Muegge, all the compounds have one or more than one violation.

Medicinal chemistry

PAINS, break, and lead-likeness screening

This part of the study helps the medicinal chemist with drug discovery. For the identification of probable problematic fragments, two complementary outline restructuring methods are allowed. The molecules with substructural sections are biologically important in tests regardless of the targeted protein, and these fragments provide misleading biological output. For the molecule to have a potential biological activity, it is analysed on the six orthogonal assays and molecules which are active in two or more assays are fragmented further into 481 fragments that are considered a leading molecule. If such moieties are observed, ADME takes warning. There were no PAINS alerts in the ADME review (Table 9). Brenk et al. [48] develop a method by considering 105 fragments that give the structural alert that is responsible for the poor pharmacokinetics based on highly reactive, metabolically unstable, poisonous, etc. The ADME identifies the problematic fragment by hovering the "question mark" icon with the chemical description. After performing the screening employing the physiochemical filters, Brenk et al. observed that residual molecule gratifies criteria for "lead-likeness". A molecule of this type is accessible to chemical alteration, which will most likely result in an increase in lipophilicity [49]. The screening limits for different parameters set by Brenk are listed in Table 9.

However, Teague and others argue that there are several conceptions that collections combining atoms with MW in the range of 100–350 and ClogP in the range of 13.0 are much superior to those deemed medicines, such as mixtures, and are therefore lead-like [50]. All of the created molecules had two or more Brenk rules, whereas regular Ciprofloxacin, Gentamicin, and Clotrimazole had none, and Sulfacetamide imitated the one Brenk rule (Table 9). When all of the preceding measurements are taken into account,

Table 7 ADME analysis used to investigate the drug-likeness of the title compound compounds

Sr. no	Lipinski #violations	Ghose #violations	Veber #violations	Egan #violations	Muegge #violations
L1-(1)	0	0	0	0	0
5	1	2	0	0	2
6	1	2	0	0	1
7	1	2	0	0	2
SD1	0	0	0	1	0
SD2	0	0	0	0	0
SD3	0	0	0	0	0

L1−1 ligand (L1)(1), 5 complex Fe(L1)2−(5), 6: complex Ni(L1)2−(6), 7 complex Cu(L1)2−(7), *SD*1 ampicillin, *SD*2: chloramphenicol, *SD*3: ciprofloxacin

Table 8 The Ghose and Veber screening range for the ligand molecule

	Ghose screening range				Veber (GSK filter)		
	log P (ClogP)	SW (MW)	MR	NOA	RB	PSA	H-bond (D and A)
Passing range	−0.4 to 5.6	160 to 480	40 to 130	20 to 70 atoms	10 or less	≤ 140 A2	12 or less

SW subatomic weight, *MR* Molar refractivity, *NOA* number of atoms, *RB* rotatable bond, *PSA* polar surface area, *H−bond (D and A)* H−bond (donors and acceptors)

Table 9 Brenk screening limits

Clogp/ClogD	H-bond		Heavy atoms	Rotatable bond	Ring System	Fused ring
Range 0 to 4	Donor Hydrogen < 4	Acceptor Hydrogen < 7	Range 10 to 27	< 8	< 5	No more than two rings

the lead-likeness of all molecules with standard deviations is calculated (Table 10).

P-glycoprotein and CYP enzyme activity prediction

The ADME predicts the molecule can act as a substrate of p-glycoprotein (P-gp) or slow down the cytochrome p450 coenzyme (CYP coenzyme). P-gp is widely distributed and interconnected in the intestinal epithelium, where it pushes xenobiotics—like drug molecules—back into the intestinal lumen and tube endothelial tube, which creates the blood–brain barrier and allows for the passage of drug molecules into capillaries. The biotransformation of the drug molecule is done by the CYP coenzyme. The major factor for the toxicity of the drug molecule is when it gets metabolized via CYP coenzyme and reduces the drug pharmacology. The finding depicts as "Yes" or "No" when the compound under inspection has a large possibility as a substrate or non-substrate of P-gp or non-inhibitor or inhibitor of an assumed CYP, in Table 11.

Table 10 Medicinal chemistry evaluation of the synthesized molecules

Sr. No	PAINS #alerts	Brenk #alerts	Lead-likeness #violations	Synthetic Accessibility
L1-(1)	0	1	1	2.71
5	0	1	2	4.91
6	0	0	2	4.76
7	0	0	2	4.51
SD1	0	0	0	4.16
SD2	0	3	0	2.78
SD3	0	0	0	2.51

L1−1: ligand (L1)(1), 5 complex Fe(L1)2−(5), 6: complex Ni(L1)2−(6), 7: complex Cu(L1)2−(7), *SD*1 ampicillin, *SD*2 chloramphenicol, *SD*3 ciprofloxacin

HIA and BBB prediction

The blood–brain barrier (BBB) and human gastrointestinal absorption (HIA) are related to the P-gp and CYP enzymes. The ADME "BOILEDegg" (Fig. 10) evaluates the HIA by plotting the predictive graph between WLOGP versus TPSA as a function of small molecules. The white region in the BOILEDegg represents the high possibility of gastrointestinal absorption, while the yellow region portrays the brain dispersion. The white and yellow regions are not limited to one. In the red spot, the prediction is for non-substrate of P-gp, while the blue spot is the estimate of effluent by P-gp.

The ADME includes two topological procedures for water solubility of drugs because the HIA and BBB depend upon the water solubility of drugs. The procedures are ESOL [51] model and Ali et al. The AMDE also adopts the third procedure which is Silicos-IT, and all the projected values of molar solubility in water (Log S) are the logarithm decimal.

The ESOL [51] and other criteria [52] were used to measure the water solubility of small compounds, which ranged from weakly soluble (**6a-o**) for standard highly soluble to very soluble (Table 12). All of these compounds have poor solubility in the Ali and Silicos-IT screenings; however, the majority of the combinations are soluble and have poor dissolvability in the ESOL solvency testing (Table 12). Indeed, even common drugs range from highly soluble to poorly soluble to extremely soluble. Continue Log p is the average of all Log *P* values obtained using various lipophilicity criteria (Table 13).

Conclusion

A new hydrazone ligand (L1)(1) and its coordinatively saturated and unsaturated six metal complexes have been prepared in 1:1 and 1:2 ratios by reacting metal salts and ligand, respectively. Spectroscopic information approves the formation of ligand as well as metal complexes. Based

Table 11 Pharmacokinetic evaluation of the synthesized molecules

Sr. no	GI absorption	BBB permeant	P-gp substrate	CYP1A2 inhibitor	CYP2C19 inhibitor	CYP2C9 inhibitor	CYP2D6 inhibitor	CYP3A4 inhibitor
L1-(1)	High	Yes	No	Yes	No	No	No	No
5	High	No	Yes	No	No	No	No	No
6	High	No	Yes	Yes	Yes	No	No	No
7	High	No	Yes	No	No	No	No	No
SD1	Low	No	No	No	No	No	No	No
SD2	High	No	No	No	No	No	No	No
SD3	High	No	Yes	No	No	No	No	No

GI gastrointestinal absorption, *BBB* blood-brain barrier, *CYP* cytochromes, P−gp P−glycoprotein, L1−1 ligand (L1)(1), 5 complex Fe(L1)2−(5), 6 complex Ni(L1)2−(6), 7 complex Cu(L1)2−(7), *SD*1 ampicillin, *SD*2 chloramphenicol, *SD*3 ciprofloxacin

Table 12 Water solubility evaluation of the synthesized molecules

Sr. no	ESOL				Ali				Silicos-IT			
	Log S	Solu. (mg/ml)	Solu. (mol/l)	Class	Log S	Solu. (mg/ml)	Solu. (mol/l)	Class	Log S	Solu. (mg/ml)	Solu. (mol/l)	class
L1-(1)	− 3.11	1.92E-01	7.74E-04	S	− 3.2	1.56E-01	6.31E−04	S	−4.95	2.77E−03	1.12E−05	MS
5	−7.72	1.05E−05	1.90E−08	PS	−8.05	4.94E−06	8.96E−09	PS	−7.11	4.30E−05	7.80E−08	PS
6	−8.12	4.31E−06	7.58E−09	PS	−8.55	1.62E−06	2.84E−09	PS	−7.49	1.86E−05	3.27E−08	PS
7	−7.77	9.51E−06	1.70E−08	PS	−8.05	5.01E−06	8.96E−09	PS	−7.12	4.19E−05	7.50E−08	PS
SD1	−1.15	2.48E + 01	7.09E−02	VS	−1.28	1.85E + 01	5.28E−02	VS	−2.21	2.15E + 00	6.15E−03	S
SD2	−2.32	1.54E + 00	4.77E−03	S	−3.16	2.25E−01	6.96E−04	S	−2.39	1.32E + 00	4.09E−03	S
SD3	−1.32	1.57E + 01	4.74E−02	VS	0	3.34E + 02	1.01E + 00	HS	−3.5	1.04E−01	3.13E−04	S

Solu. solubility, *PS* poorly soluble, *MS* moderately soluble, *S* soluble, *VS* very soluble, *HS* highly soluble, *IS* insoluble, L1−1 ligand (L1)(1), 5: complex Fe(L1)2−(5), 6 complex Ni(L1)2−(6), 7 complex Cu(L1)2−(7), *SD*1 Ampicillin, *SD*2 Chloramphenicol, *SD*3 Ciprofloxacin

Table 13 Lipophilicity evaluation of the synthesized compounds

Sr. No	iLOGP	XLOGP3	WLOGP	MLOGP	Silicos-IT Log P	Consensus Log P
L1-(1)	2.09	2.24	2.17	1.41	2.28	2.04
5	0	6.28	2.81	2.37	−8.77	0.54
6	0	6.76	3.4	2.58	−6.96	1.16
7	0	6.28	2.81	2.37	−8.72	0.55
SD1	1.14	−1.13	−0.39	0.75	0.01	0.08
SD2	0.95	1.14	0.58	0.02	−0.26	0.49
SD3	2.24	−1.08	1.18	1.28	1.9	1.1

L1−1 ligand (L1)(1), 5 complex Fe(L1)2−(5), 6 complex Ni(L1)2−(6), 7 complex Cu(L1)2−(7), *SD*1 ampicillin, *SD*2 chloramphenicol, *SD*3 ciprofloxacin

on the characterization of metal complexes, tetrahedral/square planar and distorted octahedral geometries can be suggested where the ligand behaves as tridentate chelating agent in uninegatively and/or neutral form. In this series, the *in vitro* screenings have been executed for their antibacterial and antifungal activities. The most of compounds exhibited excellent antibacterial against *Escherichia coli*, *Pseudomonas aeruginosa*, *Staphylococcus aureus,* and *Streptococcus pyogenes* as compared to all selected standard drugs, whereas Ligand (L1)(1) and Cu(L1)(4) have good antifungal activity against *Candida albicans*. The result on the anticancer activity of ligand (L1)(1) indicates that there is a good scope for exploration of this class of compounds as anticancer agents against pancreatic cancer.

Acknowledgements Authors are thankful to UGC, New Delhi, for Major Research Project File No. 42-374/2013(SR).

References

1. Mohammad; Open J. Org. Chem. 1, 11–21 (2013).
2. A. Mohammad, A. Singh, J. Pharm. Negat. **2**, 69–72 (2011)
3. A. Sener, Turk. J. Chem. **28**, 39–46 (2004)
4. Y.Q. Xu, J.C. Liu, W.T. Deng, J. Cao, Transit. Met. Chem. **39**, 25–32 (2014)
5. H. Bel Abed, O. Mammoliti, O. Bande, G. Van Lommen, P. Herdewijn, J. Org. Chem. **78**, 7845–7858 (2013)
6. J. Cao, J.C. Liu, W.T. Deng, N.Z. Jin, CrystEngComm **15**, 6359–6367 (2013)
7. K.R. Grunwald, M. Volpe, P. Cias, G. Gescheidt, N.C. Mosch-Zanetti, Inorg. Chem. **50**, 7478–7488 (2011). https://doi.org/10.1021/ic200279g
8. K. R. Grünwald, G. Saischek, M. Volpe, F. Belaj, N. C. Mösch-Zanetti; Eur. J. Inorg. Chem. 2297–2305 (2010).
9. H. Khanmohammadi, M. Darvishpour, Dyes Pigm. **81**, 167–173 (2009)
10. E. Kremer, G. Facchin, E. Estévez, P. Alborés, E.J. Baran, J. Ellena, M.H. Torre, Inorg. Biochem. **100**, 1167–1175 (2006)

11. J. Bouffard, R.F. Eaton, P. Müller, T.M. Swager, J. Org. Chem. **72**, 10166–10180 (2007)
12. P. Bergthaller, R. Stolzenburg, P. Marx, A. G. Agfa Gevaert; U.S. Patent No. 4,767,698. Washington, DC: U.S. Patent and Trademark Office.
13. A. Deeb, F. El-Mariah, M. Hosny, Bioorg. Med. Chem. Lett. **14**, 5013–5017 (2004)
14. U.M. Rafi, D. Mahendiran, A.K. Haleel, R.P. Nankar, M. Doble, A.K. Rahiman, New J. Chem. **40**, 2451–2465 (2016)
15. S. Eckhardt, S. Semin, Diagn. Pathol. **2**, 419–439 (2002). https://doi.org/10.2174/1568011024606389
16. F. Rojo, J. Albanell, A. Rovira, J.M. Corominas, F. Manzarbeitia, Semin. Diagn. Pathol. **25**, 245–261 (2008). https://doi.org/10.1053/j.semdp.2008.08.001
17. K.M. Hatzade, A.M. Ghatole, P.K. Gaidhane, M.K. Gaidhane, G.P. Gadekar, Med. Chem. Res. **30**, 163–181 (2021)
18. M. Gaidhane, A. Ghatole, K. Lanjewar, K. Hatzade, Turk. J. Chem. **44**, 1495–1514 (2020)
19. C.A. Lipinski, F. Lombardo, B.W. Dominy, P.J. Feeney, Adv. Drug Deliv. Rev. **23**, 3–35 (1997)
20. A.M. Ghatole, M.K. Gaidhane, K.R. Lanjewar, K.M. Hatzade, Bulg. J. Sci. Educ. **29**, 206–244 (2020)
21. A. Daina, V. Zoete, Chem. Med. Chem. **11**, 1117–1121 (2016)
22. Schaper K. J., United States Patent, 4997835 (1991).
23. S.S. Patil, S.K. Tadavi, A. Dikundwar, R.S. Bendre, J. Mol. Struct. **1247**, 131293 (2022)
24. J.F. Geldard, F. Lions, Inorg. Chem. **4**, 414–417 (1965)
25. F. Lions, K.V. Martin, Inorg. Chem. **80**, 3858–3865 (1958)
26. R. Bendre, A. Murugkar, S. Padhye, P. Kulkarni, M. Karve, Met.-Based Drugs **5**, 59–66 (1998)
27. B. Hathaway, D.E. Billing, Coord. Chem. Rev. **5**, 143–207 (1970)
28. A.H. Maki, B.R. McGarvey, J. Chem. Phys. **29**, 35–38 (1958)
29. J.R. Wasson, C. Trapp, J. Phys. Chem. **73**, 3763–3772 (1969)
30. S.M. Khalil, J. Coord. Chem. **49**, 45–61 (1999)
31. R.T. Bhoi, J.D. Rajput, R.S. Bendre, Res. Chem. Intermed. **48**, 401–422 (2022)
32. A. Sahraei, H. Kargar, M. Hakimi, M.N. Tahir, J. Mol. Struct. **1149**, 576–584 (2017). https://doi.org/10.1016/j.molstruc.2017.08.022
33. A. Sahraei, H. Kargar, M. Hakimi, M.N. Tahir, Transit. Met. Chem. **42**, 483–489 (2017). https://doi.org/10.1007/s11243-017-0152-x
34. H. Kargar, F. Aghaei-Meybodi, R. Behjatmanesh-Ardakani, M.R. Elahifard, V. Torabi, M. Fallah-Mehrjardi, K.S. Munawar, J. Mol. Struct. **1230**, 129908 (2021)
35. H. Kargar, A.A. Ardakani, M.N. Tahir, M. Ashfaq, K.S. Munawar, J. Mol. Struct. **1233**, 130112 (2021)
36. H. Kargar, F. Aghaei-Meybodi, M.R. Elahifard, M.N. Tahir, M. Ashfaq, K.S. Munawar, J. Coord. Chem. **74**, 9–10 (2021). https://doi.org/10.1080/00958972.2021.1900831
37. N.J. Marshall, C.J. Goodwin, S.J. Holt, Growth Regul. **5**, 69–84 (1995)
38. A.M. Ghatole, M.K. Gaidhane, K.R. Lanjewar, K.M. Hatzade, Indian J. Chem. **60**, 303–320 (2021)
39. A. Jamshidvand, M. Sahihi, V. Mirkhani, M. Moghadam, I. Mohammadpoor-Baltork, S. Tangestaninejad, S. Gharaghani, J. Mol. Liq. **253**(61), 71 (2018). https://doi.org/10.1016/j.molliq.2018.01.029
40. H. Kargar, R. Behjatmanesh-Ardakani, V. Torabi, M. Kashani, Z. Chavoshpour-Natanzi, Z. Kazemi, K.S. Munawar, Polyhedron **195**, 114988 (2021). https://doi.org/10.1016/j.poly.2020.114988
41. H. Kargar, R. Behjatmanesh-Ardakani, V. Torabi, A. Sarvian, Z. Kazemi, Z. Chavoshpour-Natanzi, M. Ashfaq, Inorgan. Chim. Acta **514**, 120004 (2021). https://doi.org/10.1016/j.ica.2020.120004
42. A. Daina, O. Michielin, V. Zoete, Sci. Rep. **7**, 42717 (2017)
43. A. Ghose, V.N. Viswanadhan, J.J. Wendoloski, J. Comb. Chem. **1**, 55–68 (1999)
44. W.J. Egan, K.M. Merz, J.J. Baldwin, J. Med. Chem. **43**, 3867–3877 (2000)
45. D.F. Veber, S.R. Johnson, H.Y. Cheng, B.R. Smith, K.W. Ward, K.D. Kopple, J. Med. Chem. **45**, 2615–2623 (2002)
46. I. Muegge, S.L. Heald, D. Brittelli, J. Med. Chem. **44**, 1841–1846 (2001)
47. A.K. Ghose, V.N. Viswanadhan, J.J. Wendoloski, J. Phys. Chem. **102**, 3762–3772 (1998). https://doi.org/10.1021/jp980230o
48. R. Brenk, A. Schipani, D. James, A. Krasowski, I.H. Gilbert, J. Frearson, P.G. Wyatt, Chem. Med. Chem. **3**, 435–444 (2008)
49. M.M. Hann, G.M. Keseru, Nature Rev. Drug Discov. **11**, 355–365 (2012)
50. S. Teague, A. Davis, P. Leeson, T. Oprea, Angew. Chem. Int. Ed. Engl. **38**, 3743–3748 (1999)
51. J.S. Delaney, J. Chem. Inf. Comput. Sci. **44**, 1000–1005 (2004)
52. J.H. Fagerberg, E. Karlsson, J. Ulander, G. Hanisch, C.A. Bergstrom, Pharm. Res. **32**, 578–589 (2015)

Springer Nature or its licensor (e.g. a society or other partner) holds exclusive rights to this article under a publishing agreement with the author(s) or other rightsholder(s); author self-archiving of the accepted manuscript version of this article is solely governed by the terms of such publishing agreement and applicable law.

Authors and Affiliations

Smita S. Patil[1] · Samina K. Tadavi[2] · Ajay M. Ghatole[2] · Ratnamala S. Bendre[1]

✉ Ratnamala S. Bendre
bendrers@rediffmail.com

[1] School of Chemical Sciences, Kavayitri Bahinabai Chaudhari North Maharashtra University, Jalgaon, Maharashtra 425001, India

[2] Department of Chemistry, J. M. Patel Arts, Commerce and Science College, Bhandara, Maharashtra 441904, India

SPRINGER LINK

Log in

Menu Search Cart

Home Journal of the Iranian Chemical Society



Journal of the Iranian Chemical Society

Publishing model
Hybrid

Submit your manuscript

Editorial board

Aims and scope

Journal updates

Overview

Already have a manuscript?

Use our Manuscript Matcher to find the best relevant journals!

Find a Match

Refine Your Search Results

1735-207X

Search

Sort By: Title (A-Z)

Search Results

Found 1 results (Page 1)

Share These Results

Exact Match Found

JOURNAL OF THE IRANIAN CHEMICAL SOCIETY

Publisher: **SPRINGER , ONE NEW YORK PLAZA, SUITE 4600 , NEW YORK, United States, NY, 10004**

ISSN / eISSN: **1735-207X / 1735-2428**

Web of Science Core Collection: **Science Citation Index Expanded**

Additional *Web of Science* Indexes: **Essential Science Indicators**

Share This Journal

View profile page

** Requires free login.*

Filters Clear All

Web of Science Coverage

Open Access

Category

Country / Region

Language

Frequency

Journal Citation Reports

1 – 1 of 1

Items per page: 10

Analysis of Farmland Soil Samples from Tirora Tehsil of Gondia District in Maharashtra, Central India for its Chemical parameters

Katre Sangita D.
Department of Chemistry, Chhotabhai Javerbhai Patel College, Tirora - 441911, RTM Nagpur University, Nagpur, INDIA
sdkcjpc@yahoo.com

Abstract
Soil analysis is a vital step of nutrient management planning of farmlands that includes fertilizer application, rotational plans, making best use of manures etc. The present research paper investigates the physico-chemical parameters of various soil samples from different villages of Tirora tehsil of Gondia district in Maharashtra state (Central India). An in-depth exploration of the farm soils and crops grown in the area was conducted with the aim to study the morphological and chemical characteristics of the soils.

For this purpose, twenty soil samples were collected in January 2020 from the study area and parameters such as pH, exchangeable cations, electrical conductivity, available nitrogen and potassium, organic carbon, $CaCO_3$ %, base saturation %, cation exchange capacity etc.

Keywords: Chemical analysis, Soil sampling, Kjeldahl's method, Organic carbon, Electrical conductivity.

Introduction

Soil is natural body on which agricultural products grow and it has fragile ecosystem[6,11]. The fertility of the soil depends on the concentration of nutrients like nitrogen, phosphorous, potassium, organic and inorganic materials, conductivity etc. Soil fertility testing is the combination of three discrete but interrelated processes i.e. analysis, interpretation and recommendation[1]. Physicochemical properties such as moisture content, nitrogen, phosphorus and organic matter are taken into account which are essential for the growth of plants. Physical, physico-chemical, morphological and chemical properties of soils play important role in achieving the objectives of various land use, conservation and management programmes, their planning and implementation.

Soil testing helps us to know the nutritional status of the soil to assess the profitability of applying a particular nutrient. Crops may not fully respond to the applied fertilizer, if one of the several productivity factors in the soil becomes a limiting factor. Soil pH is one such important soil characteristics that indicates the availability of plant nutrients. It is a measure of activity of ionized hydrogen(H^+) in the soil solution and is an indicative measurement of the chemical properties of soil. If soil pH is very high, it is of no use to add fertilizers to the crop till excess sodium is removed by gypsum to lower the pH value[8]. If the pH of soil is very low, then the problem can be solved by adding required amount of lime to the acidic soil[7].

Excessive electrical conductance can also lower the efficiency of applied fertilizers. The conductivity is a measure of the total salt content of the soil. Excess of salts in soil which usually accumulate through drainage and seepage from other areas, can hinder the crop growth. Cation exchange capacity is an indicator of nutrient holding capacity of the soil in the exchange sites. It is the measure of the quantity of readily exchangeable cations neutralizing negative charges derived from the isomorphous substitution within the structure of the layer silicate minerals, broken bonds at mineral edges, external surfaces etc.

Material and Methods

Study sight: Tirora tehsil of Gondia district is located in north-western part of Gondia district in Maharashtra (India) with a total geographical area of 617.10 sq. km. It is bound by north latitudes $21^0$13'05'' to $21^0$33'30''and east longitudes $79^0$47'50'' to $80^0$05'00''. Wainganga river flows from north to south in the western part of the tehsil. It forms a major drainage system having the lower elevation ranging from 240 to 280 above MSL whereas the higher elevation is ranging from 350 to 500 above MSL.

Climate: Tirora tehsil has a sub-humid, sub-tropical climate with well-defined summer (from March to May), rainy season (from June to October) and mild winter (from November to February). The mean annual temperature of the study area is 26.4^0C with mean maximum of 29.3^0C and a mean minimum of 24.12^0C. The mean annual precipitation of Tirora tehsil is 1400 mm of which nearly 85% is received during South-West monsoon period (i.e. from June to October).

Physical characteristics of soil in the study area: The particle size distribution shows that majority of the soils in the study area have high amount of clay. Soils developed on shallow weathered pediments, moderately weathered pediments, deeply weathered pediments and aggraded valley fills have high clay content (49.2 to 64.2 %).

Soil sampling: The process of soil sampling should ideally be done keeping in view the basic objectives of soil survey, so that the chemical analysis of the collected soil samples should precisely reflect the characteristics of the field. In the present study, we carried out the analysis of soil samples

collected from different villages of Tirora Tehsil of Gondia District. A spade or khurpi[3] was used to collect the soil in a plastic bucket. For soil sampling, V shaped holes were dug so that a uniform 2 cm thick slice of soil up to a depth of 15cm is obtained. Samples collected were thoroughly mixed by rolling and turning on a piece of clean cloth and air dried in shade.

The soil clods were crushed using wooden pestle and mortar[12]. The entire amount of soil sample then was sieved through 2mm stainless steel sieve. The remaining coarse material left after sieving was re-crushed and re-sieved. The remaining residual matter was discarded. Total 20 soil samples were collected in clean polythene bags and brought to the Laboratory for analysis.

Chemical analysis: The main focus of this study was on those soil quality parameters which influence the movement and retention of water that contribute to store and supply of nutrients. Therefore, some selected physical and chemical parameters were chosen. For the chemical analysis of soil samples[4], soil suspension was prepared in distilled water (1:4 w/v) and allowed the particles to settle down. Analysis of soil samples was carried out for the studies of various parameters like pH, total organic carbon, available nitrogen (N) and potassium (K_2O), electrical conductivity, cation exchange capacity, % $CaCO_3$, base saturation %, exchangeable cations (Na^+, K^+, Ca^{2+}, Mg^{2+}). pH was measured using pH meter. Electrical conductivity was measured using a conductivity meter, organic carbon was measured using Walkley and Black rapid titration method.[9,14] Available potassium was measured using Flame photometer, available nitrogen was estimated by Kjeldahl's method[13], exchangeable sodium and potassium was determined by Flame photometer and exchangeable calcium and magnesium[2] were measured using EDTA complexometric titration method (from ammonium acetate extract of soil).

At pH 10, all exchangeable calcium and magnesium form complex with Versene to a bright blue end point in the presence of Eriochrome Black-T indicator. At pH 12, calcium alone complexes with Versene in the presence of Murexide indicator. The orange-red colour that was initially formed, turns finally into red-violet coloured at end point. The amount of magnesium can be determined by calculating the difference between first and second titrations. % $CaCO_3$ was measured by acid Neutralization method which is a rapid titration method.[10]

Table 1
Chemical characteristics of soils in Tirora tehsil (Weighed means)

Soil series	CEC	pH	EC	% OC	% $CaCO_3$	Available N	Available K	Exchangeable bases				% Base saturation
								Ca^{2+}	Mg^{2+}	Na^+	K^+	
Atri	11.60	6.49	0.043	0.12	0.00	125	188	9.00	0.50	0.22	0.15	85.09
Navegaon khurd	12.80	6.73	0.027	0.09	0.00	113	134	5.50	4.50	0.15	0.12	80.21
Ledada	12.60	6.78	0.023	0.12	0.00	125	161	6.00	3.50	0.22	0.14	78.24
Salebardi	12.40	6.82	0.02	0.12	0.00	125	161	6.00	3.50	0.22	0.12	79.30
Paraswada	11.60	7.06	0.029	0.20	0.00	151	188	6.50	3.00	0.26	0.12	85.14
Wadegaon	10.40	7.9	0.105	0.18	1.48	138	202	8.40	1.60	0.15	0.10	98.60
Silli	20.80	8.1	0.098	0.22	2.34	151	269	12.80	2.60	0.09	0.03	74.58
Bihiriya	24.80	8.14	0.106	0.20	8.10	151	242	18.80	2.00	0.09	0.08	84.53
Kachewani	17.80	8.43	0.1	0.20	7.48	138	202	13.20	2.40	0.09	0.05	88.42
Sarra	18.00	8.65	0.099	0.14	3.07	138	188	11.40	2.60	0.09	0.04	78.47
Boda	16.40	7.3	0.149	0.33	0.00	176	255	9.20	3.40	0.20	0.05	78.33
Paldongari	19.60	7	0.471	0.35	0.00	176	242	9.00	5.50	0.09	0.14	75.14
Khamari	22.80	6.52	0.476	0.35	0.00	176	188	9.50	5.50	0.11	0.05	66.49
Khairbodi	16.80	6.38	0.089	0.49	0.00	188	202	6.50	3.00	0.13	0.05	57.63
Arjuni	10.80	6.42	0.054	0.22	0.00	151	161	4.00	1.50	0.20	0.05	53.21
Bagholi	10.00	6.28	0.025	0.12	0.00	138	148	3.50	1.00	0.20	0.08	47.72
Jamuniya	13.40	4.58	0.116	0.83	0.00	213	228	4.50	3.00	0.09	0.27	58.62
Bopesar	18.00	6.92	0.185	1.21	0.00	238	215	8.00	6.00	0.13	0.19	79.57
Belati khurd	19.80	6.06	0.049	0.41	0.00	163	175	4.50	2.50	0.20	0.10	36.86
Karti bujruk	22.40	5.8	0.072	0.28	0.00	151	161	8.00	2.00	0.20	0.09	45.92

Results and Discussion

Soil analysis provides a snapshot of nutrient availability at a particular time. It provides information which can be used to improve soil fertility through management. Soil analysis should be repeated at regular intervals to identify trends in nutrient availability and adjust nutrient management accordingly. Interpretation of analytical results leads to the detection and monitoring of the changes in the parameters of the soil. Interpretation should take account of the local conditions and crop. Soil analysis also helps to look after important issues like soil health care, proper diagnosis of soil, integrated nutrient management and soil reclamation etc.

In the present study, various chemical parameters of the collected farmland soil samples have shown varying values at different villages of the study area (Table 1). Most of the soils under study are non-calcareous, low in organic carbon and non-saline in nature. The interpretation of analytical data shown in table 1 for these 20 villages can be seen in figure 1 to 5.

Conclusion

We explored some of the basic facts drawn from research and practical experience about soil analysis with a view to make the best use of available information which is important for maximizing nutrient use efficiency and agricultural productivity. The pH values of most soils ranged from 6.06 to 8.7 i.e. slightly acidic to moderately alkaline (Table 1) suitable to grow crops like rice, potato, wheat, tobacco, jowar, tomato etc.

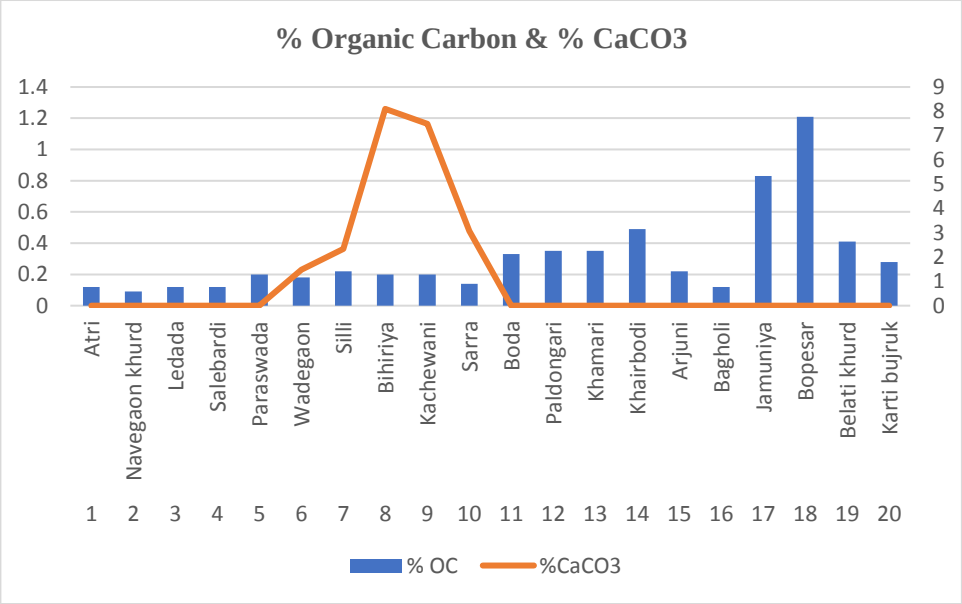


Figure 1: Comparison of Organic carbon and $CaCO_3$ % in 20 soil samples



Figure 2: Comparison of available Nitrogen and Potassium(Kgha^{-1}) in 20 soil samples

https://doi.org/10.25303/2708rjce043047

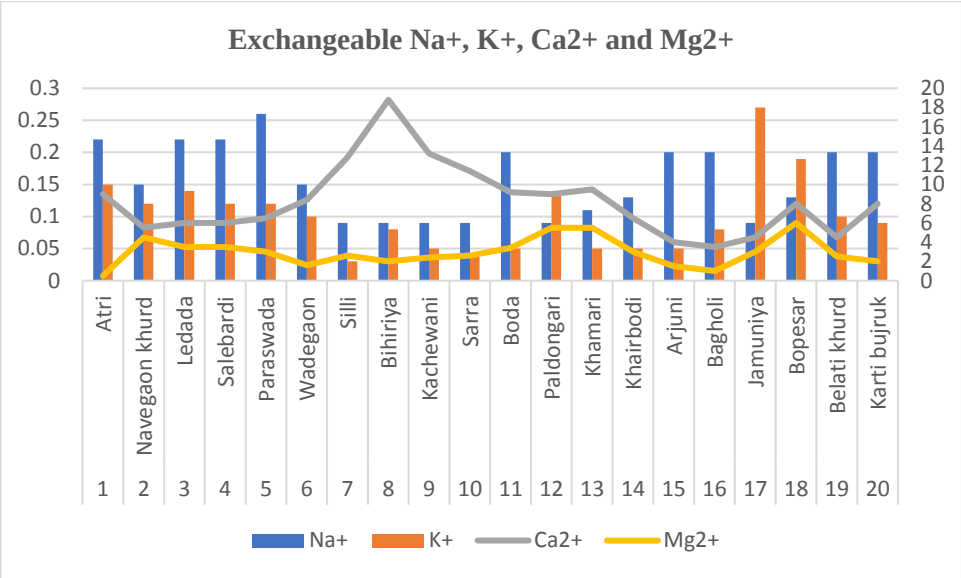


Figure 3: Comparison of Exchangeable Na, K, Ca and Mg in 20 villages soil samples

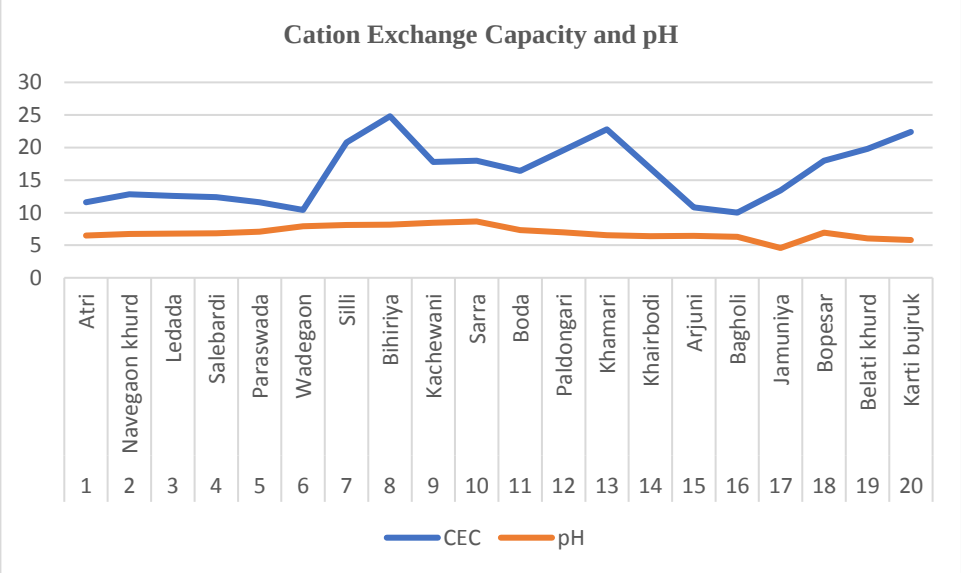


Figure 4: Comparison of CEC and pH of 20 villages soil samples

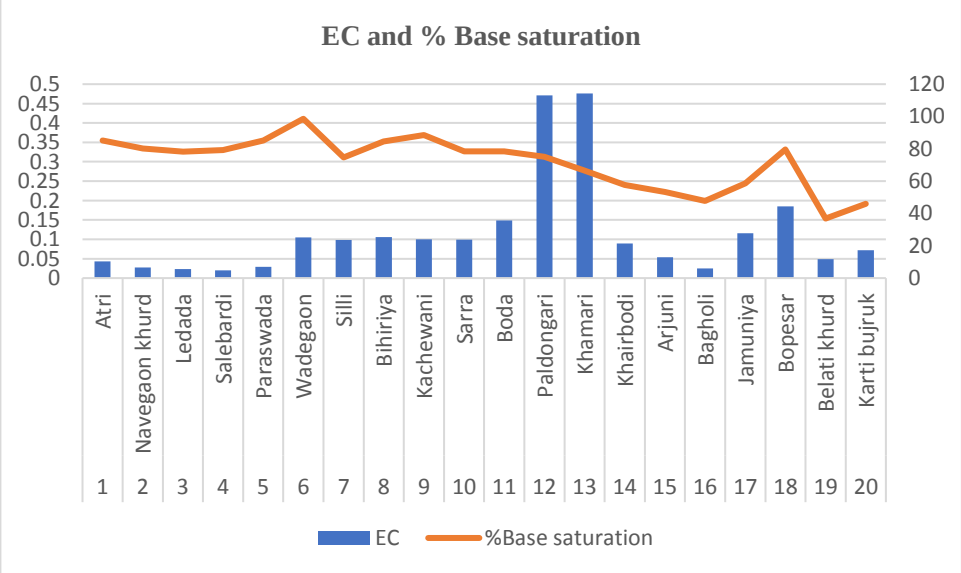


Figure 5: Comparison of EC and Base Saturation % of 20 villages soil samples

https://doi.org/10.25303/2708rjce043047

Cation exchange capacity (CEC) of soils varies from 24.80 to 10.0 c mol (P^+) kg^{-1}. These high values of CEC are attributed to the smectite type of clay minerals and high amounts of clays. Total exchangeable bases (Ca^{2+}, Mg^{2+}, Na^+ and K^+) contribute nearly 90% of CEC of these soils. Presence of these bases in sufficient quantity in the soils is favourable for plant growth. Calcium is the dominant cation followed by magnesium, sodium and potassium. It varied from 3.5 to 18.80 c mol (P^+) kg^{-1}. The dominance of calcium may be due to basaltic parent material, which is the source of high calcium. Magnesium varied from 0.5 to 6.0 c mol (P^+) kg^{-1}. The base saturation ranged from 36.86 to 98.60% (Table 1). The % organic carbon value ranges from 0.09 to 0.49.

Acknowledgement

Author is thankful to Dr. M. V. Singh, Principal, C. J. Patel College, Tirora for providing the necessary facilities for this project. Author also gratefully acknowledges the valuable guidance and suggestions received from Mr. B. S. Rahangdale, Soil and Land Use Survey of India for the analysis of soil samples during this project.

References

1. Beegle D., Interpretation of Soil Testing Result, IN Recommended Soil Testing Procedures for the North-eastern United State, University of Delaware Ag. Experiment Station Bulletin no. 493, 2nd edition UK, 8491 **(1995)**

2. Cheng K.L.L. and Bray R.H., Determination of Calcium and Magnesium in soil and plant material, *Soil Sci.*, **72**, 449-458 **(1951)**

3. Gupta P.K., Soil, Plant, Water and Fertilizer analysis, Agrobios, Jodhpur, India, 2nd edition, 1-5 **(2007)**

4. Jackson M.L., Soil Chemical Analysis, Prantice-Hall of India Pvt. Ltd., New Delhi **(1973)**

5. Katre S.D., Chemical and Morphological Characterization of Agricultural Soil Samples from Tirora Tehsil of Gondia District in Maharashtra, Central India, *Int. J. Sci. Res. Sci. Eng. Technol.*, **9(3),** 222-231 **(2022)**

6. Kaur H., Environmental Chemistry, 2nd Edition, Pragati Prakashan, 416 **(2002)**

7. Lierop W.V., Soil pH and Lime requirement, Chapter 5, Soil Testing and Plant Analysis, Soil Science Society of America Book Series, 3rd edition, 73-126, edited by Westerman R.L. **(1990)**

8. Misra U.K., Acid soil and its management, *Journal of the Indian Society of Soil Science*, **52(4)**, 332-343 **(2004)**

9. Peck T.R. and Soltanpour P.N., The principles of soil testing, Chapter 1, in Soil Testing and Plant Analysis, Soil Science Society of America Book Series, 3rd edition, 1-24, edited by Westerman R.L. **(1990)**

10. Piper C.S., Soil Plant Analysis, Hans Publication, Bombay, 135-136 **(1966)**

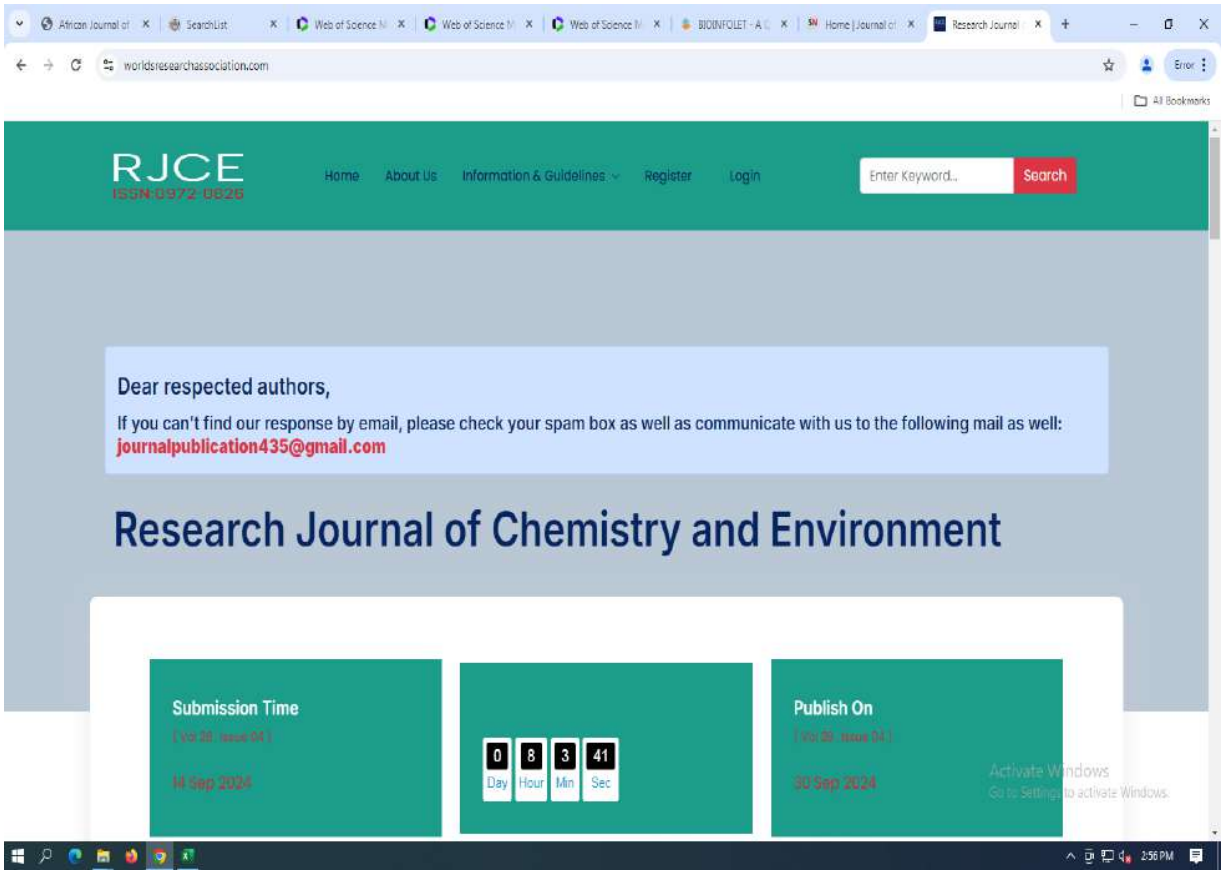
11. Sinha A.K. and Shrivastav, Earth Resource and Environmental issues, 1st edition, ABD publisher Jaipur, India **(2000)**

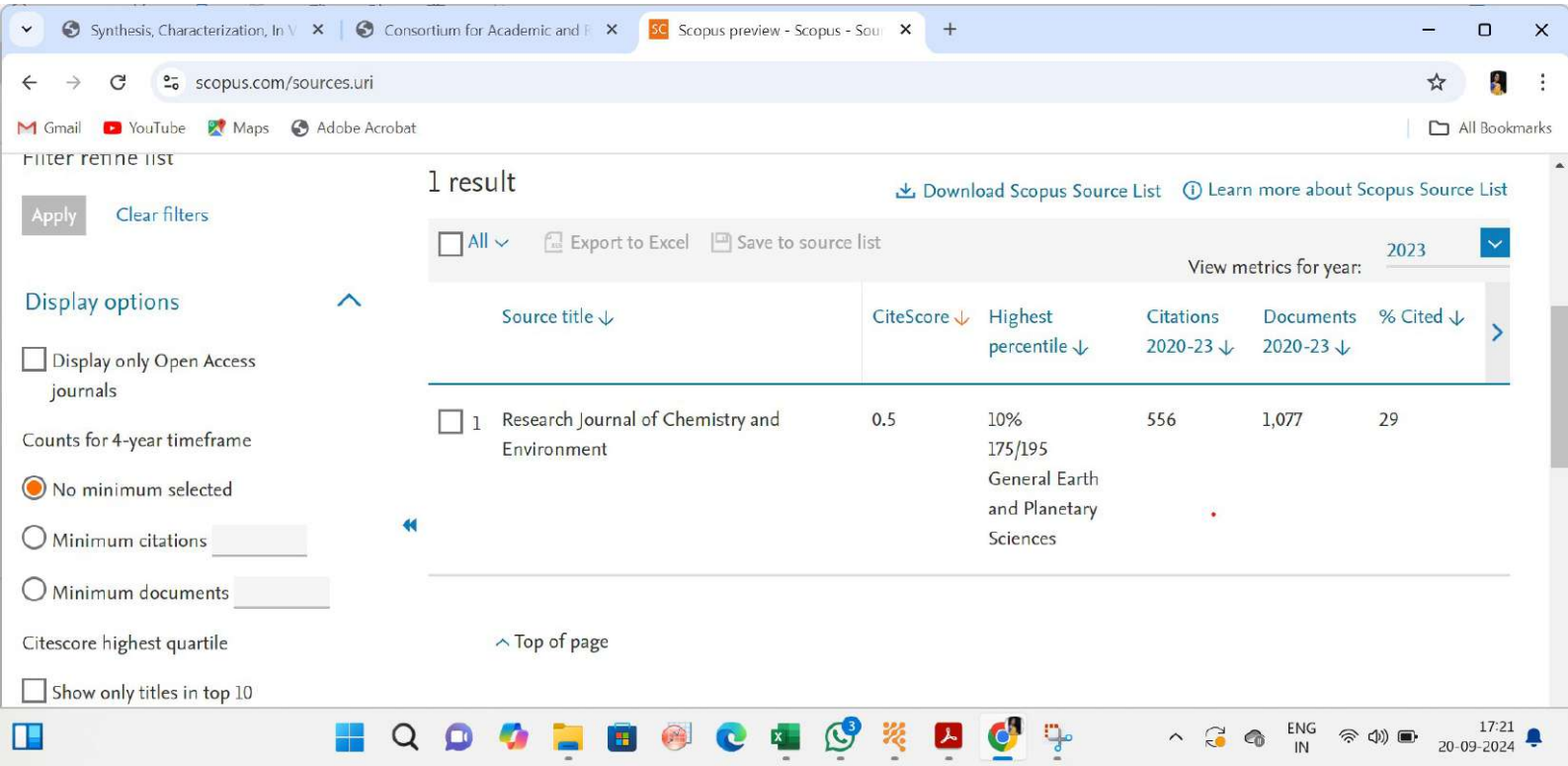
12. Tandon H.L.S., Methods of analysis of Soils, Plants, Water and Fertilizers, 1-48 **(1993)**

13. Treadwell and Hall's modified Kjeldahl method, In association of and Agricultural Chemists, Official and Tentative Methods of Analysis, Washington, 7th Edition **(1950)**

14. Walkley A.J. and Black I.A., Estimation of soil organic carbon by the chromic acid titration method, *Soil Sci.*, **37,** 29-38 **(1934)**.

(Received 30th June 2022, accepted 02nd September 2022)


worldsresearchassociation.com
RJCE
ISSN:0972-0626
Home
About Us
Information & Guidelines
Register
Login
Enter Keyword..
Search
Dear respected authors,
If you can't find our response by email, please check your spam box as well as communicate with us to the following mail as well:
journalpublication435@gmail.com
Research Journal of Chemistry and Environment
Submission Time
14 Sep 2024
0 Day
8 Hour
3 Min
41 Sec
Publish On
30 Sep 2024
Activate Windows
2:56 PM


Synthesis, Characterization, In
Consortium for Academic and
Scopus preview - Scopus - Sou
scopus.com/sources.uri
Gmail
YouTube
Maps
Adobe Acrobat
All Bookmarks
Filter refine list
Apply
Clear filters
Display options
Display only Open Access journals
Counts for 4-year timeframe
No minimum selected
Minimum citations
Minimum documents
Citescore highest quartile
Show only titles in top 10
1 result
Download Scopus Source List
Learn more about Scopus Source List
All
Export to Excel
Save to source list
View metrics for year:
2023
Source title
CiteScore
Highest percentile
Citations 2020-23
Documents 2020-23
% Cited
1
Research Journal of Chemistry and Environment
0.5
10% 175/195 General Earth and Planetary Sciences
556
1,077
29
Top of page
ENG IN
17:21
20-09-2024

Iranian Journal of Science
https://doi.org/10.1007/s40995-023-01496-6

RESEARCH PAPER

Imidazole–Thiazole Hybrid: Synthesis, Brain Penetration, Cytochrome P450 Enzyme and Gastrointestinal Absorption Study

Shital M. Dekate[1] · Kishor M. Hatzade[1] · Ajay M. Ghatole[2]

Received: 27 November 2022 / Accepted: 25 June 2023
© The Author(s), under exclusive licence to Shiraz University 2023

Abstract
Thiazoles, imidazoles, and related derivatives are prominent heterocyclic molecules. Even though the chemistry of imidazole compounds with thiazole moiety has an ancient legacy, the rigorous search for biologically active substances in the imidazole series barely emerged in the last few cascades. The purpose of this communication is to highlight medicinally active substances, while also recent syntheses, which have been reported to still have antimicrobial activities. The present investigation identifies the synthesis and spectroscopic characterization of new 2-amino-4-aryl-1, 3-thiazole-5-carboxaldehydes, their imidazole derivatives, and Schiff bases with various substituted benzaldehydes, including the antimicrobial and antifungal activities among these compounds. The majority of the synthesized compounds are Pgp substrates and CYP3A4 inhibitors, according to the analysis of their pharmacokinetic properties. The overall findings of this study indicated that the molecular to physiologically intriguing imidazole scaffold with varied aromatic substituents was an intriguing methodology for the creation of antibacterial medicines.

Keywords Antimicrobial activity · Bioavailability radar · BOILED-egg · Bioinformatics · Imidazole · Molecular dynamics · Thiazole

1 Introduction

Thiazoles are one of the most explored classes of aromatic heterocycles featuring five members. During the last 2–3 decades, detailed research on the thiazole ring has established that the thiazole scaffold features antibacterial (Satbhaiya and Chourasia 2015), antiviral (Barradas et al. 2011), anti-inflammatory (Geronikaki et al. 2007), antitubercular (Ganesh et al. 2016), antifungal (Tratrat et al. 2018), and anticancer characteristics (Asmaa 2016). Ritonavir was employed to counter novel Coronavirus COVID-19 in the initial phases of the COVID-19 pandemic spread (Zhu et al. 2020). Avafungin is an expansive antifungal agent (Degreef et al. 2006), and sulfathiazoles are organosulfur compounds used as sulfa agents (Mehdi et al. 2008). Thiazofluin is a prospective anticancer therapeutic (Karim et al. 2004), and sulfathiazoles are organosulfur compounds used as sulfa agents (Mehdi et al. 2008). Aside from all this, the thiazole core is a constituent of all extant penicillins, which take transformed bacterial diseases medication (Lambert et al. 1964). Several microbes, fungi, and viruses are being used to design, synthesise, and examine a huge numeral of thiazole molecules incorporating multiple heterocyclic compounds for antibacterial activity. Imidazole-based compounds have been observed anticancer, antihypertensive, antihistaminic, antineurophatic, antihemolytic, cytotoxic, antimycobacterial, antioxidant, and antimicrobial characteristics (Shad et al. 2018). Still, though, imidazole with a thiazole nucleus does have a big amount of potential antimicrobial applications. Schiff bases have been shown to have anticancer,

Biology J. Vatanparast.

✉ Ajay M. Ghatole
ajay.ghatole5@gmail.com
https://jmpatelcollege.com

Shital M. Dekate
snimje04@gmail.com
https://nagpuruniversity.ac.in

Kishor M. Hatzade
kishorhatzade@gmail.com;
https://nagpuruniversity.ac.in

[1] Department of Chemistry, Dhote Bandhu Science College, Gondia, MS 441601, India

[2] Department of Chemistry, J. M. Patel College, Bhandara, MS 441906, India

Published online: 17 July 2023

antituberculosis, antibacterial, antimicrobial, and plant growth inhibitory properties, as well as anti-inflammatory activities (Upadhyay et al. 2020).

The NCI effects, or non-covalent interactions, play a critical role in the recognition and binding between molecules. These interactions are responsible for the stability and selectivity of molecular complexes and are involved in a wide range of biological processes such as protein–protein interactions, enzyme–substrate interactions, and drug-receptor interactions (Trabelsi et al. 2019). Molecular docking calculation is a computational method used to predict the formation of these molecular complexes. It involves the prediction of the binding mode and affinity of a ligand (small molecule) to a receptor (protein) (Issaoui et al. 2017a, b). Molecular docking is a valuable tool in structure-based drug design and is frequently used in the initial stages of drug discovery. The importance of NCI effects and molecular docking calculations lies in their ability to provide insight into the functional mechanisms of molecular systems and their potential relevance to drug discovery (Issaoui et al. 2017a, b). By understanding the underlying mechanisms involved in ligand-receptor binding, researchers can better design drugs that interact with their intended target and avoid off-target effects (Gatfaoui et al. 2017). Moreover, these techniques provide a cost-effective alternative to traditional experimental methods for drug screening. They can efficiently predict the effectiveness of potential drug candidates, which reduces the costs and time associated with experimental drug development (Ghalla et al. 2018). The NCI effects and molecular docking calculations are critical tools in the study of molecular recognition and drug discovery. They provide valuable insights into the mechanisms of ligand-receptor binding and offer efficient, cost-effective solutions for drug screening. These techniques are continually evolving and promise to advance drug discovery efforts in the future (Sagaama and Issaoui 2020).

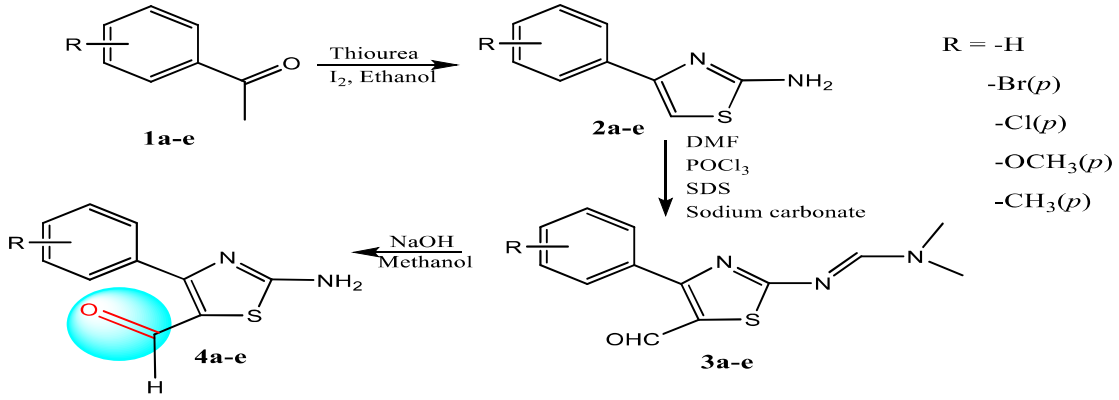
Nowadays, pharmaceuticals encompass an analysis of breakthrough molecular effectiveness besides their facility toward obtaining bioactive building blocks. This incorporates cellular, animal, and human quantifiable aspects, all of which are typically overpriced and associated with danger. Lately, computer-assisted review of absorption, distribution, metabolism, and excretion of drugs (ADME) has improved the ability to tackle this issue (Hatzade et al. 2021). Computer models, in especially, enable foreknowledge and trustworthy speedy information, consequently touting analytical methodologies (Daina et al. 2014). These computer scientists predict the pharmacokinetic, physicochemical, and pharmacological parameters of small compounds, encouraging lead molecules to proceed to long-acting drugs. SwissADME a website administered by the Swiss Bioinformatics Foundation, which is very handy tool for researchers around the globe to produce bioinformatics capabilities and properties. SwissADME permits the measurement of ADME parameters to structural based medicine candidates, that produce the data for early threat assessment during the medication design development. Notably, SwissADME delivers a stage for considering Lipinski's standard of five (Gaidhane et al. 2020), (Lipinski et al. 2001) for detecting oral bioavailability matching. Medication homology is an unintentional combination of chemical compositions and underlying data that establishes whether a surprising substance reflects known drugs. Hydrogen holding appearances, hydrophobicity, electronic distribution, adaptation and molecule size have all been examples of molecular capabilities. SwissADME offers the 'BOILEDegg' diagnostic (Daina and Zoete 2016; Ghatole et al. 2020) particularly assesses human gastrointestinal ingestion (HIA) and P-glycoprotein efflux/preservation (Pgp). Infiltration of the blood–brain barrier (BBB) and substrate-restriction of the Cytochrome P450 (CYP) enzyme could also be hypothesized. Significantly, false promising effects in immunoassay of micro metabolites can be assumed with a high level of confidence (Matlock et al. 2018; Ghatole et al. 2012).

In light of these findings, it was thought that synthesizing new-fangled organic beings integrating the three energetic pharmacophores viz. thiazole, imidazole, in addition, Schiff bases in a sole molecular framework as novel biologically active mixes could be of interest. Thiazole compounds with imidazole moiety and Schiff bases are produced in the current work, and they have numerous biological and pharmacological applications.

2 Result and Discussion

The needed starting chemical 4-aryl-2-aminothiazoles (**2a-e**) were synthesized through a rock-hard segment reaction of thiourea, different acetophenones (**1a-e**), too iodine to achieve desired compound (Taile et al. 2011). The Vilsmeier–Haack reaction of **2a-e**, which yielded 2-Amino-4-(4'-aryl)-1, 3-thiazole-5-carboxaldehydes (**4a-e**) in presence of sodium dodecyl sulphate (SDS), yielded intermediates **3a-e**. The rection time duration was reduced from 4–5 h to 1–1.5 h by utilizing the same quantity of SDS. The Vilsmeier–Haack reaction (Hu et al. 2017), uses SDS, which is a cheap, non-toxic, and easily available micelle. Micelles facilitate reactions by increasing the concentration of reactants within the hydrophilic or hydrophobic micellar areas due to their solubilization capability. They function as microreactors, increasing the rate and selectivity of the reaction. (Scheme 1)

The compound 4-aryl-5-(4-phenyl-1*H*-imidazol-2-yl)-thiazol-2-amines **(5a-e)** (Hatzade et al. 2015) were synthesized by the reaction of phenyl glyoxal, ammonium



Scheme 1 Synthesis of substituted 2-amino-4-aryl-1,3 thiazole-5-carboxaldehydes **(4a-e)**

acetate and glacial acetic acid with 2-amino-4-aryl-1,3 thiazole-5-carboxaldehydes **(4a-e)**. The compounds **6a-o** were synthesized from 4-aryl-5-(4-phenyl-1*H*-imidazol-2-yl)-thiazol-2-amines **(5a-e)** and various benzaldehydes in ethyl alcohol by the catalytic quantity of glacial acetic acid. Structures of all the above-synthesized molecules are confirmed by various spectroscopic analyses. (Scheme 2)

3 Biological Study

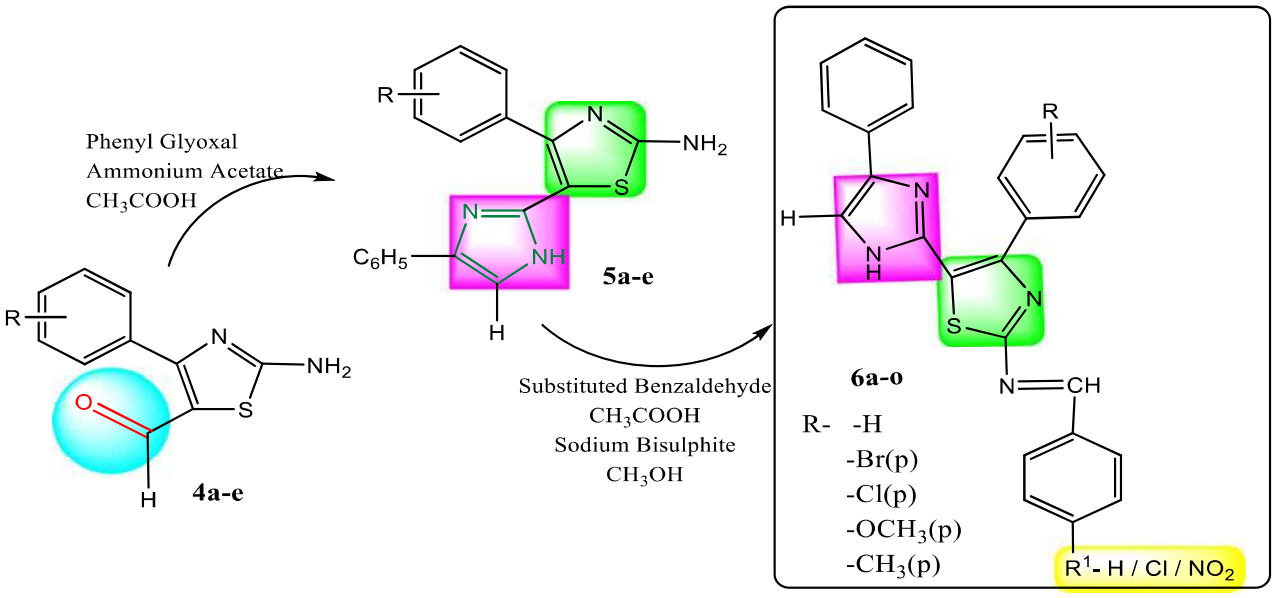
The synthesized compounds were studied for number of biological activities. (Fig. 1)

3.1 Antibacterial Activities

The in vitro antibacterial activity against *Escherichia coli, Klebsiella aerogens, Staphylococcus aureus* and *Bacillus substilis* was tested against the synthesized compounds **4a-e**; **5a-e** & **6a-o** by the cup plate diffusion method. The zone of inhibition was compared between standard drugs Ciprofloxacin, Sulphacetamide and synthesized compounds (100 µg/ml) after 24 h of incubation at 37°.

3.2 Antifungal Activity

Compounds **4a-e**; **5a-e** & **6a-o** were also screened at 100 µg/ml concentration in methanol against *A. niger* and *C. albicans* for their antifungal activity by the cup plate diffusion method. The zone of inhibition after 7 days at 20°



Scheme 2 Synthesis of (imino substituted benzal)-4-aryl-5-(4-phenyl-1H-imidazol-2-yl)-thiazoles

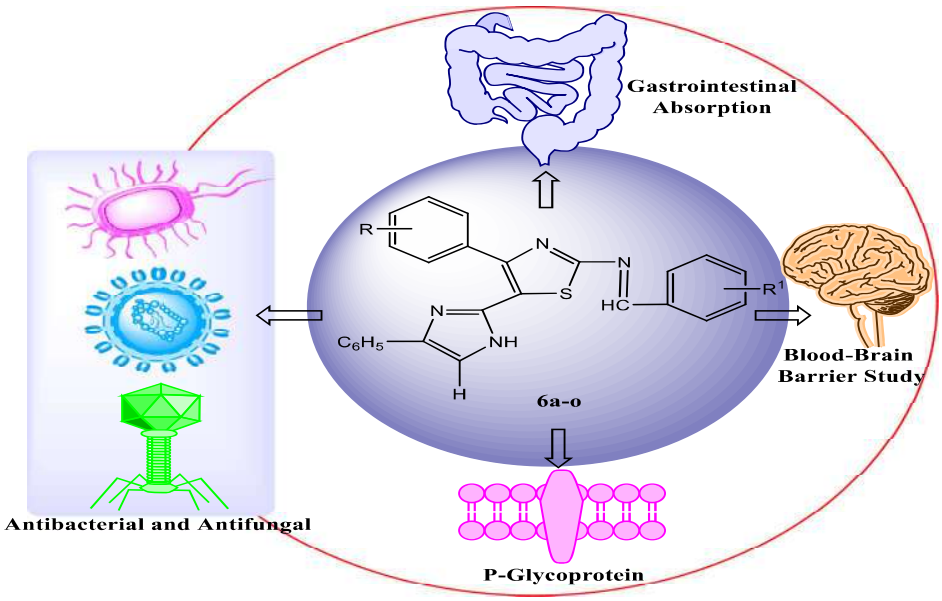


Fig. 1 Biological application of imidazole derivatives

was compared with standard drugs Gentamycin and Clotrimazole (100 μg/ml).

According to Table 1, when compared to its amino counterparts, Schiff bases displayed the best action against Gram +ve, Gram-ve bacteria, and fungi. The results of antibacterial activity showed a little variation in how each Schiff base behaved when tested against bacteria. Similarly, the results of antifungal activity revealed that the Schiff bases had promising antifungal activities against two yeast strains (*C. albicans and A. niger*). These results suggested that Schiff bases had effective and selective antimicrobial activities against both bacteria and fungi. In conclusion, we have synthesized and evaluated in vitro antimicrobial of the newly synthesized Schiff bases. The in vitro results indicated that the new Schiff bases had commonly of greater pharmacological significance than their amino compounds.

4 Absorption, Distribution, Metabolism, and Excretion (ADME) Investigation of Compounds

4.1 Material and Approaches

The client would configure 2D chemical structures by carving or simply describing the simplified molecular-input line-entry system (SMILES) on this website.

4.2 Pharmacology

The SwissADME provides the bio-accessibility radar for the molecule to show resemblance as a bioactive suppository (Daina et al. 2017). Each vertices in the hexagonal (Fig. 2) graph has the limitations (Table 2) which represent the pharmacology of the compounds. (Tables 3, 4)

4.3 Drug-likeness

The distorted hexagonal red lines represent the drug-likeness possessions of the synthesized compounds (Fig. 2). Particularly, synthesized compounds (**6a-o**) and the standard drug-like Sulfacetamide, Gentamicin, and Clotrimazole fall within parameters except for one or two parameters of a bioavailable drug. While the standard drugs like Ciprofloxacin fall within the range Fig. 2.

The prediction of medication resemblance for screening small molecules that the parameters developed by Ghose (1999), Egan (2000), Veber (2002), and Muegee (2001) applied by SwissADME. The Ghose and Veber screening parameters have a scale for the quantitatively depicts of small molecules which are given in Table 5.

The Egan (Pharmacia) (Egan et al. 2000) screening method is used to predict pill absorption based on a tiny molecule's epithelial absorbency. The Egan method avoids an excess descriptor by holding the polar surface area (PSA) and AlogP98 descriptors in the same model (Ghose, Viswanadhan, 1998). PSA serves as a benchmark for AlogP98. The dynamic influx and efflux components for small compounds into the human submissive gastrointestinal absorption are portrayed by the Egan computational model (HIA). Molecular targeted absorption into the human intestine intestinal absorption (HIA). Muegge's (Bayer filter) database model helps to discriminate between nondrug like drug-like molecules. The database suggests

Table 1 Antimicrobial screening results of the compounds **4a–e**, **5a-e** and **6a–o**

Compound no.[a]	Zone of inhibition (mm) (activity index)[std]					
	Antibacterial activity				Antifungal activity	
	Gram-positive		Gram-negative			
	S. aureus	*B. substilis*	*E. coli*	*K. aerogens*	*C. albicans*	*A. niger*
4a	18 (0.56)* (0.60)#	17 (0.60)* (0.65)#	26 (0.76)* (0.93)#	07 (0.32)* (0.33)#	22 (1.04)* (1.00)#	16 (0.67)* (0.69)#
4b	19 (0.59)* (0.63)#	16 (0.57)* (0.61)#	24 (0.70)* (0.56)#	11 (0.50)* (0.52)#	20 (0.95)* (0.91)#	15 (0.62)* (0.65)#
4c	14 (0.43)* (0.46)#	14 (0.50)* (0.54)#	18 (0.53)* (0.64)#	10 (0.45)* (0.48)#	15 (0.71)* (0.68)#	12 (0.50)* (0.52)#
4d	09 (0.28)* (0.30)#	14 (0.50)* (0.54)#	23 (0.67)* (0.82)#	09 (0.41)* (0.43)#	16 (0.76)* (0.72)#	12 (0.50)* (0.52)#
4e	14 (0.43)* (0.46)#	13 (0.46)* (0.50)#	27 (0.79)* (0.96)#	12 (0.55)* (0.57)#	15 (0.71)* (0.68)#	13 (0.54)* (0.56)#
5a	19 (0.59)* (0.63)#	22 (0.78)* (0.84)#	28 (0.82)* (1.00)#	14 (0.64)* (0.67)#	21 (1.00)* (0.95)#	17 (0.71)* (0.74)#
5b	21 (0.65)* (0.70)#	23 (0.82)* (0.88)#	25 (0.73)* (0.89)#	16 (0.72)* (0.76)#	20 (0.95)* (0.91)#	16 (0.67)* (0.69)#
5c	18 (0.56)* (0.60)#	24 (0.85)* (0.92)#	20 (0.59)* (0.71)#	18 (0.82)* (0.86)#	17 (0.81)* (0.77)#	14 (0.58)* (0.61)#
5d	15 (0.47)* (0.50)#	19 (0.67)* (0.73)#	24 (0.70)* (0.86)#	15 (0.68)* (0.71)#	18 (0.86)* (0.82)#	13 (0.54)* (0.56)#
5e	18 (0.56)* (0.06)#	20 (0.71)* (0.77)#	26 (0.76)* (0.93)#	16 (0.72)* (0.76)#	18 (0.86)* (0.82)#	14 (0.58)* (0.61)#
SD1	32	28	34	22	21	24
SD2	30	26	28	21	22	23
6a	21 (0.65)* (0.70)#	21 (0.75)* (0.80)#	19 (0.56)* (0.68)#	20 (0.91)* (0.95)#	17 (0.81)* (0.77)#	19 (0.79)* (0.83)#
6b	26 (0.81)* (0.87)#	22 (0.79)* (0.85)#	18 (0.53)* (0.64)#	17 (0.77)* (0.81)#	15 (0.71)* (0.68)#	20 (0.83)* (0.87)#
6c	24 (0.75)* (0.80)#	23 (0.82)* (0.88)#	17 (0.50)* (0.61)#	18 (0.82)* (0.86)#	19 (0.91)* (0.86)#	19 (0.79)* (0.83)#
6d	23 (0.71)* (0.76)#	21 (0.75)* (0.80)#	19 (0.56)* (0.68)#	19 (0.86)* (0.90)#	18 (0.86)* (0.82)#	18 (0.75)* (0.78)#
6e	24 (0.75)* (0.80)#	22 (0.79)* (0.85)#	20 (0.59)* (0.71)#	18 (0.82)* (0.86)#	15 (0.71)* (0.68)#	18 (0.75)* (0.78)#
6f	32 (1.00)* (1.06)#	27 (0.96)* (1.04)#	25 (0.74)* (0.89)#	19 (0.86)* (0.90)#	22 (1.04)* (1.00)#	20 (0.83)* (0.87)#
6 g	25 (0.78)* (0.83)#	23 (0.82)* (0.88)#	27 (0.79)* (0.97)#	20 (0.91)* (0.95)#	20 (0.95)* (0.91)#	19 (0.79)* (0.83)#
6 h	29 (0.91)* (0.97)#	21 (0.75)* (0.80)#	22 (0.65)* (0.79)#	17 (0.77)* (0.81)#	25 (1.19)* (1.14)#	21 (0.87)* (0.91)#
6i	27 (0.84)* (0.90)#	20 (0.71)* (0.77)#	20 (0.59)* (0.71)#	18 (0.82)* (0.86)#	19 (0.91)* (0.86)#	17 (0.71)* (0.74)#
6j	26 (0.81)* (0.87)#	26 (0.93)* (1.00)#	23 (0.68)* (0.82)#	20 (0.91)* (0.95)#	23 (1.09)* (1.04)#	19 (0.79)* (0.83)#
6 k	25 (0.78)* (0.83)#	24 (0.86)* (0.92)#	21 (0.62)* (0.75)#	19 (0.86)* (0.90)#	24 (1.14)* (1.09)#	18 (0.75)* (0.78)#
6 l	26 (0.81)* (0.87)#	23 (0.82)* (0.88)#	23 (0.68)* (0.82)#	18 (0.82)* (0.86)#	21 (1.00)* (0.95)#	16 (0.67)* (0.70)#
6 m	28 (0.87)* (0.93)#	21 (0.75)* (0.80)#	24 (0.71)* (0.86)#	18 (0.82)* (0.86)#	22 (1.04)* (1.00)#	19 (0.79)* (0.83)#
6n	27 (0.84)* (0.90)#	22 (0.79)* (0.85)#	23 (0.68)* (0.82)#	20 (0.91)* (0.95)#	23 (1.09)* (1.04)#	18 (0.75)* (0.78)#
6o	25 (0.78)* (0.83)#	24 (0.86)* (0.92)#	22 (0.65)* (0.79)#	19 (0.86)* (0.90)#	20 (0.95)* (0.91)#	22 (0.92)* (0.96)#
SD1	32	28	34	22	21	24
SD2	30	26	28	21	22	23

S. aureus = *Staphylococcus aureus, B. substilis* = *Bacillus substilis, E. coli* = *Escherichia coli, K. aerogens* = *Klebsilla aerogens*, *C. albicans* = *Candida albicans, A. niger* = *Aspergillus niger*. (Activity index) = Inhibition zone of the sample/Inhibition zone of the standard

*Activity index against SD1, #Activity index against SD2, For antibacterial activity: SD1 = Ciprofloxacin and SD2 = Sulfacetamide, For antifungal activity: SD1 = Gentamicin and SD2 = Clotrimazole. [a]Concentration of test compounds and standard 100 μg/mL, [b]average zone of inhibition in mm, [std]the standard drug used for the study of antibacterial and antifungal activity

that the molecule with hydroxyl, amine, ketone, and sulfonyl functional groups remarkable has a drug-like molecule. The small molecule to authorize the Muegge model needs the will-described pharmacophore. The Muegge database suggests that the small molecule to act as a drug molecule must contain at least four functional groups that are ketone, hydroxy, sulfonyl and amine excluding the four functional groups the molecule with guanidine, carbamate, alcohol, amidine, carboxylic acid, urea, sulfonamide, amide, sulfone, and ester can be acting a drug molecule. The small molecule to be nondrug contains less than four functional groups.

Among all the synthesized compounds **6a, 6c, 6i-m, 6o,** Ciprofloxacin, and Sulfacetamide within the Lipinski parameters while Ciprofloxacin, and Sulfacetamide fall within the Ghose violation parameters. Veber violation is one of the parameters which follows all the synthesized compound **6a-o** and standard also except Gentamicin as a

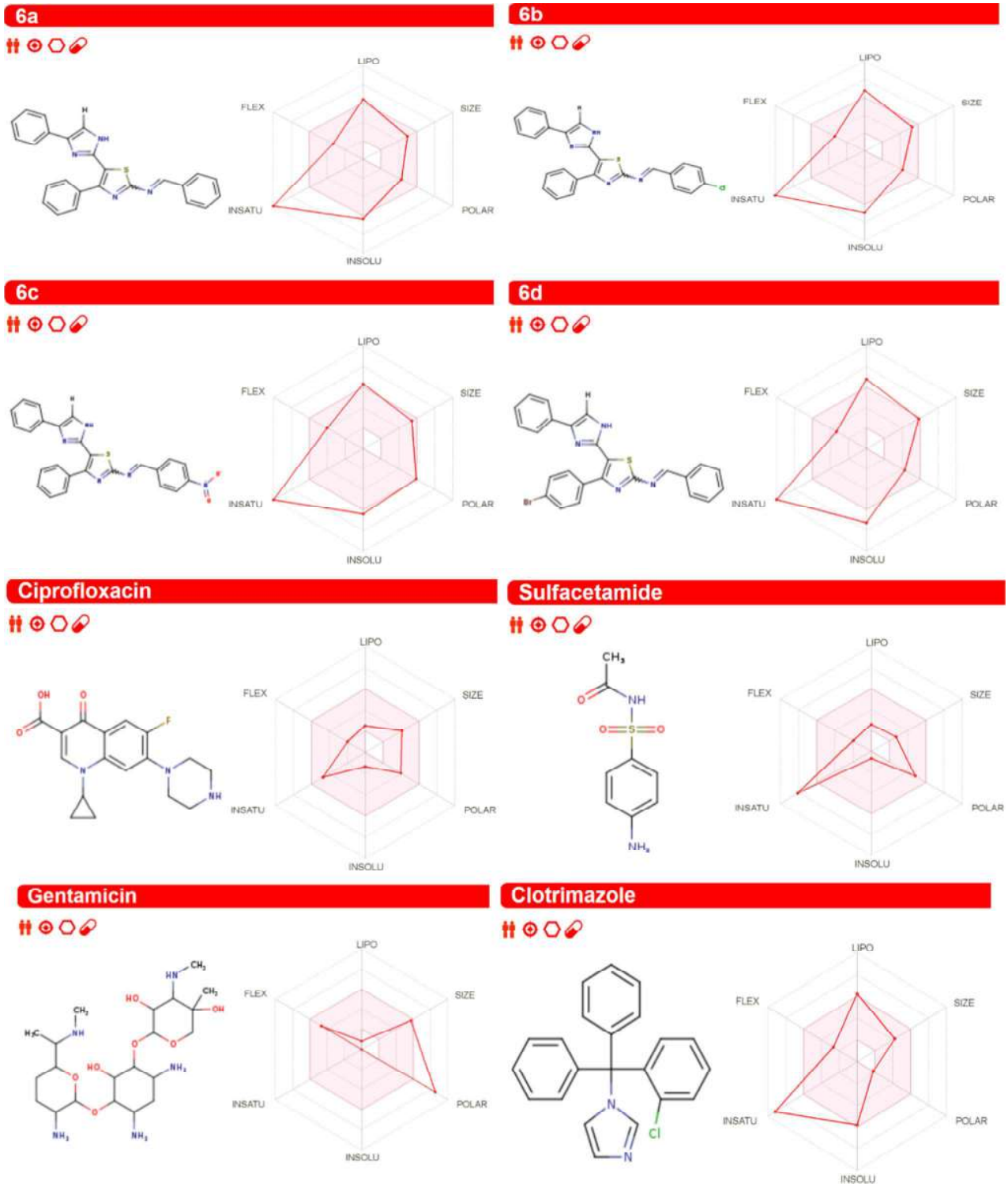


Fig. 2 Bio-avaibility radar for the synthesized imidazole derivatives (**6a-d**) that to compare with the standard drugs

standard drug. In the case of Egan and Muegge, all the compounds have one or more than one violation while the standard Ciprofloxacin and Sulfacetamide follow all the rules.

Table 2 The appropriate range for each attribute is shown by the pink region within the hexagon

	XLOGP3	MW	TPSA	Solubility (Log S)	Saturation	Flexibility
Range	− 0.7 to + 5.0	150–500 g/mol	20–130 A2	Not higher than 6	0.25 (a section of carbons in the sp3 hybridization)	Near to 9 rotatable bonds

Table 3 Synthesized compounds (**6a-o**) and commercial drugs' physicochemical properties

Sr. no.	MW	HA	AHA	FCsp3	RTB	HBA	HBD	MR	TPSA
6a	406.5	30	28	0	5	3	1	124.26	82.17
6b	440.95	31	28	0	5	3	1	129.27	82.17
6c	451.5	33	28	0	6	5	1	133.09	127.99
6d	485.4	31	28	0	5	3	1	131.96	82.17
6e	519.84	32	28	0	5	3	1	136.97	82.17
6f	530.4	34	28	0	6	5	1	140.79	127.99
6 g	440.95	31	28	0	5	3	1	129.27	82.17
6 h	475.39	32	28	0	5	3	1	134.28	82.17
6i	485.94	34	28	0	6	5	1	138.1	127.99
6j	436.53	32	28	0.04	6	4	1	130.76	91.4
6 k	470.97	33	28	0.04	6	4	1	135.77	91.4
6 l	481.53	35	28	0.04	7	6	1	139.58	137.22
6 m	420.53	31	28	0.04	5	3	1	129.23	82.17
6n	454.97	32	28	0.04	5	3	1	134.24	82.17
6o	465.53	34	28	0.04	6	5	1	138.05	127.99
SD1	331.34	24	10	0.41	3	5	2	95.25	74.57
SD2	214.24	14	6	0.12	3	3	2	51.75	97.64
SD3	477.6	33	0	1	7	12	8	118.31	199.73
SD4	344.84	25	23	0.05	4	1	0	101.84	17.82

MW Molecular weight, *HA* heavy atoms, *AHA* aromatic heavy atom, *FCsp*3 fraction Csp3, *RTB* rotatable bonds, *HBA* H-bond acceptors, *HBD* H-bond donors, *MR* molar refractivity, *TPSA* total polar surface area *SD*1 ciprofloxacin, *SD*2 sulfacetamide, *SD*3 gentamicin, *SD*4 clotrimazole

5 Medicinal Chemistry

5.1 PAINS, Break and Leadlikeness Screening

This part of the study helps the medicinal chemist with drug discovery. For the identification of probable problematic fragments, two complementary outline restructuring methods are allowed. According to Baell et al. (Brenk et al. 2008), molecules with substructural sections are biologically important in tests regardless of the targeted protein, and these fragments provide misleading biological output. For the molecule to have a potential biological activity, it is analyzed on the six orthogonal assays and molecules which are active in two or more assays are fragmented further into 481 fragments that are considered a leading molecule. If such moieties are observed swissADME takes warning. There were no PAINS alerts in the SwissADME review (Table 7). Brenk et al. (2008) develop a method by considering 105 fragments that give the structural alert that is responsible for the poor pharmacokinetics based on highly reactive, metabolically unstable, poisonous, etc. The swissADME identifies the problematic fragment by hovering the "question mark" icon with the chemical description. After performing the screening employing the physiochemical filters, Brenk et al. observed that residual molecule gratifies criteria for "lead likeness". Such a molecule is suitable for chemical modification that by most likely to increase lipophilicity (Hann and Keseru 2012). The screening limits for different parameters set by Brenk are listed in Table 6.

However, Teague (Teague et al. 1999) and others argue that there are several conceptions that collections combining atoms with MW in the range of 100–350 and ClogP in the range of 13.0 are much superior to those deemed medicines, such as mixtures, and are therefore lead-like. (Teague et al. 1999). All of the created molecules had two

Table 4 SwissADME was used to investigate the drug-likeness of the title compound (**6a-o**)

Sr. no.	Lipinski #violations	Ghose #violations	Veber #violations	Egan #violations	Muegge #violations
6a	0	1	0	1	1
6b	1	1	0	1	1
6c	0	2	0	1	1
6d	1	3	0	1	1
6e	2	3	0	1	1
6f	1	3	0	1	1
6 g	1	1	0	1	1
6 h	1	2	0	1	1
6i	0	3	0	1	1
6j	0	2	0	1	1
6 k	0	2	0	1	1
6 l	0	3	0	2	1
6 m	0	1	0	1	1
6n	1	2	0	1	1
6o	0	2	0	1	1
SD1	0	0	0	0	0
SD2	0	0	0	0	0
SD3	2	2	1	1	4
SD4	1	0	0	0	1

*SD*1 Ciprofloxacin, *SD*2 sulfacetamide, *SD*3 gentamicin, *SD*4 clotrimazole

Table 5 The Ghose and veber screening range for the small molecule

	Ghose screening range				Veber (GSK filter)		
	log P (ClogP)	SW (MW)	MR	NOA	RB	PSA	H-bond (D & A)
Passing range	− 0.4 to 5.6	160–480	40–130	20–70 atoms	10 or less	≤ 140 A2	12 or less

SW Subatomic weight, *MR* molar refractivity, *NOA* number of atoms, *RB* rotatable bond, *PSA* polar surface area, *H-bond (D & A)* H-bond (donors and acceptors)

Table 6 Brenk screening limits

Clogp/ClogD	H-bond		Heavy atoms	Rotatable bond	Ring system	Fused ring
Range 0–4	Donor hydrogen < 4	Acceptor hydrogen < 7	Range 10–27	< 8	< 5	No more than two rings

or more Brenk rules, whereas regular Ciprofloxacin, Gentamicin, and Clotrimazole had none, and Sulfacetamide imitated the one Brenk rule (Table 7). When all of the preceding measurements are taken into account, the lead likeness of all molecules with standard deviations is calculated.

5.2 P-glycoprotein and CYP Enzyme Activity Prediction

SwissADME predicts the molecule can act as a substrate of p-glycoprotein (P-gp) or slow down the cytochrome p450 coenzyme (CYP coenzyme). P-gp is widely distributed and interconnected in the intestinal epithelium, where it pushes xenobiotics -like drug molecules -back into the intestinal lumen and tube endothelial tube, which creates the blood–

Table 7 Medicinal chemistry evaluation of the synthesized compounds

Sr. no.	PAINS #alerts	Brenk #alerts	Leadlikeness #violations	Synthetic accessibility
6a	0	1	2	3.93
6b	0	1	2	3.92
6c	0	3	2	3.95
6d	0	1	2	3.92
6e	0	1	2	3.91
6f	0	3	2	3.94
6 g	0	1	2	3.91
6 h	0	1	2	3.92
6i	0	3	2	3.94
6j	0	1	2	3.97
6 k	0	1	2	3.96
6 l	0	3	2	4
6 m	0	1	2	4.05
6n	0	1	2	4.04
6o	0	3	2	4.07
SD1	0	0	0	2.51
SD2	0	1	1	1.85
SD3	0	0	1	6.51
SD4	0	0	1	2.7

*SD*1 Ciprofloxacin, *SD*2 sulfacetamide, *SD*3 gentamicin, *SD*4 clotrimazole

brain barrier and allows for the passage of drug molecules into capillaries. The biotransformation of the drug molecule is done by the CYP coenzyme. The major factor for the toxicity of the drug molecule is when it gets metabolized via CYP coenzyme and that reduces the drug pharmacology. The finding depicts as "Yes" or "No" when the compound under inspection has a large possibility as a substrate or non-substrate of P-gp or non-inhibitor or inhibitor of an assumed CYP, Table 8.

5.3 HIA and BBB Prediction

The blood–brain barrier (BBB) and human gastrointestinal absorption (HIA) are related to the P-gp and CYP enzymes. SwissADME 'BOILEDegg' (Fig. 3) evaluate the HIA by plotting the predictive graph between WLOGP-versus-TPSA as a function of small molecules. The white region in the BOILED egg represents the high possibility of gastrointestinal absorption while the yellow region portrays the brain dispersion. The white and yellow regions are not limited to one. In the red spot, the prediction is for non-substrate of p-gp while the blue spot is the estimate of effluent by P-gp.

The swissADME includes two topological procedures for water solubility of drugs because the HIA and BBB depend upon the water solubility of drugs. The procedures are ESOL (Delaney 2004) model and Ali et al. (Fagerberg et al. 2015). SwissAMDE also adopt the third procedure which is SILICOS-IT, all the projected values of molar solubility in water (Log S) are the logarithm decimal.

The ESOL (Delaney 2004) and other criteria (Fagerberg et al. 2015) were used to measure the water solubility of small compounds, which ranged from weakly soluble (**6a-o**) for standard highly soluble to very soluble (Table 9). All of these compounds have poor solubility in the Ali and Silicos IT screenings, however, the majority of the combinations are moderately dissolvable and have poor dissolvability in the ESOL solvency testing (Table 9). Indeed, even common drugs range from highly soluble to poorly soluble to extremely soluble. Continue Log p is the average of all Log P values obtained using various lipophilicity criteria (Table 10).

6 Experimental

Before usage, all solvents were distilled. Melting points of synthesized molecules were obtained uncorrected in an open capillary tube on a liquid paraffin bath. TLC was done on a 60 F254 silica gel (Merck). Merck Chemicals and Himedia provided all reagents and solvents. The Bruker FT-IR spectrometer remained used to capture IR spectra. On a Brucker AC 400 (MHz) apparatus, ^{1}H and ^{13}C NMR spectra were collected. The spectra are presented in parts per million on a scale based on an internal standard

Table 8 Pharmacokinetic evaluation of the synthesized compounds

Sr. no.	GI absorption	BBB permeant	Pgp substrate	CYP1A2 inhibitor	CYP2C19 inhibitor	CYP2C9 inhibitor	CYP2D6 inhibitor	CYP3A4 inhibitor
6a	Low	No	Yes	No	Yes	No	No	Yes
6b	Low	No	Yes	No	Yes	No	No	Yes
6c	Low	No	No	No	No	No	No	Yes
6d	Low	No	Yes	No	No	No	No	Yes
6e	Low	No	Yes	No	No	No	No	Yes
6f	Low	No	No	No	No	No	No	No
6 g	Low	No	Yes	No	Yes	No	No	Yes
6 h	Low	No	Yes	No	No	No	No	Yes
6i	Low	No	No	No	No	No	No	Yes
6j	Low	No	Yes	No	No	Yes	No	Yes
6 k	Low	No	Yes	No	No	No	No	Yes
6 l	Low	No	No	No	No	No	No	Yes
6 m	Low	No	Yes	No	No	No	No	Yes
6n	Low	No	Yes	No	No	No	No	Yes
6o	Low	No	No	No	No	No	No	Yes
SD1	High	No	Yes	No	No	No	No	No
SD2	High	No	No	No	No	No	No	No
SD3	Low	No	Yes	No	No	No	No	No
SD4	High	Yes	Yes	Yes	Yes	Yes	Yes	Yes

GI Gastrointestinal absorption, *BBB* blood–brain barrier, *CYP* cytochromes, *P-gp* P-glycoprotein, *SD*1 ciprofloxacin, *SD*2 sulfacetamide, *SD*3 gentamicin *SD*4 clotrimazole

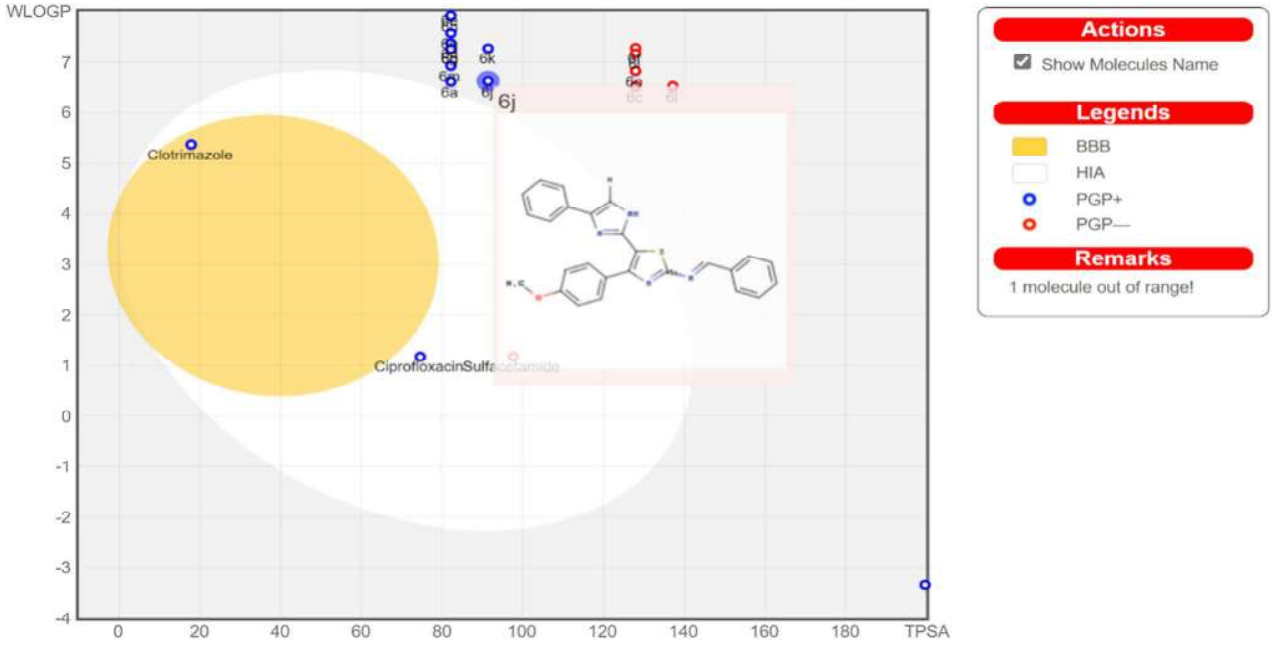


Fig. 3 In the presence of the compound, the BOILED-egg enables the measurement of passive gastrointestinal absorption (HIA), brain penetration (BBB), and P-glycoprotein (P-gp)

Table 9 Water solubility evaluation of the synthesized compounds (**6a-o**)

Sr. no.	ESOL				Ali				Silicos-IT			
	Log S	Solu. (mg/ml)	Solu. (mol/l)	Class	Log S	Solu. (mg/ml)	Solu. (mol/l)	Class	LogS	Solu. (mg/ml)	Solu. (mol/l)	class
6a	− 6.34	1.84E-04	4.53E-07	PS	− 7.24	2.32E-05	5.71E-08	PS	− 10.21	2.51E-08	6.18E-11	IS
6b	− 6.93	5.16E-05	1.17E-07	PS	− 7.9	5.59E-06	1.27E-08	PS	− 10.79	7.10E-09	1.61E-11	IS
6c	− 6.39	1.85E-04	4.11E-07	PS	PS	4.22E-06	9.35E-09	PS	− 9.55	1.28E-07	2.84E-10	PS
6d	− 7.25	2.76E-05	5.69E-08	PS	− 7.96	5.33E-06	1.10E-08	PS	− 10.98	5.05E-09	1.04E-11	IS
6e	− 7.83	7.61E-06	1.46E-08	PS	− 8.61	1.27E-06	2.44E-09	PS	− 11.56	1.43E-09	2.75E-12	IS
6f	− 7.29	2.71E-05	5.11E-08	PS	− 8.75	9.53E-07	1.80E-09	PS	− 10.31	2.59E-08	4.89E-11	IS
6 g	− 6.93	5.16E-05	1.17E-07	PS	− 7.9	5.59E-06	1.27E-08	PS	− 10.79	7.10E-09	1.61E-11	IS
6 h	− 7.51	1.45E-05	3.06E-08	PS	− 8.54	1.37E-06	2.88E-09	PS	− 11.37	2.01E-09	4.23E-12	IS
6i	− 6.97	5.18E-05	1.07E-07	PS	− 8.67	1.03E-06	2.12E-09	PS	− 10.13	3.64E-08	7.48E-11	IS
6j	− 6.4	1.73E-04	3.97E-07	PS	− 7.41	1.71E-05	3.92E-08	PS	− 10.31	2.14E-08	4.91E-11	IS
6 k	− 6.99	4.79E-05	1.02E-07	PS	− 8.06	4.10E-06	8.71E-09	PS	− 10.89	6.07E-09	1.29E-11	IS
6 l	− 6.45	1.70E-04	3.53E-07	PS	− 8.19	3.09E-06	6.43E-09	PS	− 9.64	1.10E-07	2.28E-10	PS
6 m	− 6.63	9.75E-05	2.32E-07	PS	− 7.62	1.02E-05	2.41E-08	PS	− 10.58	1.10E-08	2.61E-11	IS
6n	− 7.22	2.71E-05	5.96E-08	PS	− 8.27	2.44E-06	5.36E-09	PS	− 11.17	3.10E-09	6.82E-12	IS
6o	− 6.68	9.68E-05	2.08E-07	PS	− 8.4	1.84E-06	3.95E-09	PS	− 9.92	5.61E-08	1.21E-10	PS
SD1	− 1.32	1.57E + 01	4.74E-02	VS	0	3.34E + 02	1.01E + 00	HS	− 3.5	1.04E-01	3.13E-04	S
SD2	− 0.68	4.45E + 01	2.08E-01	VS	− 0.61	5.31E + 01	2.48E-01	VS	− 2.36	9.40E-01	4.39E-03	S
SD3	0.24	8.37E + 02	1.75E + 00	HS	0.51	1.54E + 03	3.23E + 00	HS	0.52	1.56E + 03	3.27E + 00	S
SD4	− 5.8	5.43E-04	1.57E-06	MS	− 5.54	9.96E-04	2.89E-06	MS	− 8.59	8.88E-07	2.58E-09	PS

Solu. Solubility, *PS* poorly soluble; *MS* moderately soluble, *S* soluble, *VS* very soluble, *HS* highly soluble, *IS* insoluble, *SD*1 ciprofloxacin, *SD*2 sulfacetamide, *SD*3 gentamicin, *SD*4 clotrimazole

Table 10 Lipophilicity evaluation of the synthesized compounds (**6a-o**)

Sr. no.	iLOGP	XLOGP3	WLOGP	MLOGP	Silicos-IT Log P	Consensus Log P
6a	3.76	5.75	6.62	3.91	7.56	5.52
6b	3.64	6.38	7.27	4.38	8.19	5.97
6c	3.18	5.58	6.53	2.95	5.37	4.72
6d	4.09	6.44	7.38	4.48	8.22	6.12
6e	4.4	7.07	8.03	4.95	8.86	6.66
6f	3.45	6.27	7.29	3.53	6.04	5.32
6 g	3.75	6.38	7.27	4.38	8.19	5.99
6 h	4.28	7	7.92	4.85	8.82	6.57
6i	3.3	6.2	7.18	3.43	6.01	5.22
6j	3.68	5.72	6.63	3.55	7.61	5.44
6 k	4.25	6.35	7.28	4.02	8.24	6.03
6 l	3.48	5.55	6.53	2.64	5.43	4.73
6 m	3.87	6.11	6.93	4.11	8.08	5.82
6n	4	6.74	7.58	4.58	8.71	6.32
6o	3.29	5.94	6.83	3.16	5.89	5.02
SD1	2.24	− 1.08	1.18	1.28	1.9	1.1
SD2	0.5	− 0.96	1.18	− 0.12	− 0.46	0.03
SD3	3.17	− 4.1	− 3.33	− 2.92	− 3.56	− 2.15
SD4	3.07	5.41	5.38	4.38	4.98	4.64

*SD*1 Ciprofloxacin, *SD*2 sulfacetamide, *SD*3 gentamicin, *SD*4 clotrimazole

(trimethylsilane). The Perkin-Elmer 2400 CHN analyzer was used to perform the elemental studies.

6.1 General Procedure for Synthesis of 4-aryl-5-(4-phenyl-1*H*-imidazol-2-yl)-thiazol-2-amines (5a-e)

A mixture of 2-amino-4-aryl-1,3-thiazole-5-carboxaldehydes (5 mmoles), phenyl glyoxal (5 mmoles), ammonium acetate (10 mmoles) and glacial acetic acid (50 mL) was refluxed for 2 h. It was transferred onto ice-cold water (200 mL) and neutralized with NH_4OH. The brown solid obtained was filtered, washed with water and crystallized from alcohol (State- amorphas solid).

6.2 4-Phenyl-5-(4-phenyl-1*H*-imidazole-2-yl)-thiazol-2-amine (5a)

Yield 78% (Yellow), m.p. 283 °C. IR (KBr): 3425–3255 (NH_2 *str*), 3125 (NH *str*), 3075 (CH-arom *str*), 1605 (C=C arom *str*), 1215 (C–S *str*). H^1-NMR δ_H (DMSO-d6, 400 MHz): 13.21 (H, s, -NH), 7.48–8.35(10H, m, Ar–H), 7.46(1H, s, imidazole-H), 7.05 (2H, s, -NH_2). C^{13} NMR δc (DMSO-d6): 173.2 (N=C–S), 157.3 (C=C–N), 143.1 (C=C–N) (imidazole), 133.8 (N=C–NH), 126–134 (aromatic 12C-atom), 121.9 (NH=C–C), 119.5 (C=C–S) (thiazole). Anal. Calcd for $C_{18}H_{14}N_4S$: C, 67.85; H, 4.30; N, 17.55; S, 10.02. Found: C, 67.90; H, 4.43; N, 17.60; S, 10.70 (%).

The compound **5b-e** has 69% (Light Yellow), 76% (Light Red), 77% (Yellow), and 71% (Yellow) yield with 234°, 233°, 283°, 293° C respective melting point.

6.3 General Method for Preparation of 2-(imino substituted benzal)-4-aryl-5-(4-phenyl-1*H*-imidazol-2-yl)-thiazoles 6a-o

A solution of 4-aryl-5-(4-phenyl-1*H*-imidazol-2-yl)-thiazol-2-amines (0.1 mol) and various benzaldehydes (0.1 mol) were dissolved in ethanol using a catalytic amount of glacial acetic acid. The reaction mixture was refluxed with constant stirring at 50–60̊C for 4–5 h. Then, the progress of the reaction is checked by TLC. It was cooled at room temperature and the product was filtered, dried by ether and recrystallized from hot ethanol. To remove excess aldehyde, the product was washed with sodium bisulphite and then washed with chilled ethanol to obtain a pure product (State- amorphas solid).

6.3.1 2-(Iminobenzal)-4-phenyl-5-(4-phenyl-1*H*-imidazol-2-yl)-thiazole 6a

Yield 75% (Yellow), m.p. 143 °C. IR (KBr): 3120 (NH *str*), 3085 (CH-arom *str*), 1610 (C=C arom *str*), 1210 (C–S *str*). H^1-NMR δ_H (DMSO-d6, 400 MHz): 14.02 (H, s, -

NH), 8.38 (H, s, CH), 7.49–8.32 (15H, m, Ar–H), 7.48 (H, s, imidazole-H). C^{13} NMR δc (DMSO-d6): 173.4 (N=C–S), 162.2 (CH=N), 159.5 (C=C–N), 143.1 (C=C–N) (imidazole), 133.8 (N=C–NH), 128.8 (C=C–S) (thiazole), 126–137 (aromatic 18 C-atom), 121.9 (NH=C–C). Anal. Calcd for $C_{25}H_{18}N_4S$: C, 73.87; H, 4.46; N, 13.75; S, 7.86. Found: C, 73.85; H, 4.45; N, 13.70; S, 7.89 (%).

6.3.2 2-(Imino-4-chlorobenzal)-4-phenyl-5-(4-phenyl-1*H*-imidazol-2-yl)-thiazole 6b

Yield 65% (Light Yellow), m.p. 180 °C. IR (KBr): 3130 (NH *str*), 3065 (CH-arom *str*), 1590 (C=C arom *str*), 1350 (C–S *str*). H^1-NMR δ_H (DMSO-d6, 400 MHz): 14.13 (H, s, NH), 8.54 (H, s, CH), 7.53–7.85 (14H, m, Ar–H), 7.51 (H, s, imidazole-H). C^{13} NMR δc (DMSO-d6): 175.3 (N=C–S), 163.2 (CH=N), 161.1 (C=C–N), 143.1 (C=C–N) (imidazole), 133.8 (N=C–NH), 129.2 (C=C–S) (thiazole), 128–136 (aromatic 18C-atom), 114.9 (NH=C–C). Anal. Calcd for $C_{25}H_{17}ClN_4S$: C, 68.25; H, 3.75; Cl, 7.94; N, 12.68; S, 7.08. Found: C, 68.10; H, 3.89; Cl, 8.04; N, 12.71; S, 7.27 (%).

6.3.3 2-(Imino-4-nitrobenzal)-4-phenyl-5-(4-phenyl-1*H*-imidazol-2-yl)-thiazole 6c

Yield 60% (Light Brown), m.p. 154 °C. IR (KBr): 3145 (NH *str*), 3025 (CH-arom *str*), 1580 (C=C arom *str*), 1325 (C–S *str*). H^1-NMR δ_H (DMSO-d6, 400 MHz): 14.02 (H, s, NH), 8.89 (H, s, Ar–H), 8.67 (H, s, CH), 8.35 (2H, d, Ar–H), 8.19 (H, s, imidazole-H), 7.50–7.89 (11H, m, Ar–H). C^{13} NMR δc (DMSO-d6): 172.3 (N=C–S), 165.0 (CH=N), 160.1 (C=C–N), 143.1 (C=C–N) (imidazole), 133.8 (N=C–NH), 127.2 (C=C–S) (thiazole), 123–136 (aromatic 18C-atom), 122.9 (NH=C–C). Anal. Calcd for $C_{25}H_{17}O_2N_5S$: C, 66.50; H, 3.80; O, 7.09; N, 15.51; S, 7.10. Found: C, 66.45; H, 3.75; O, 7.05; N, 15.50; S, 7.08 (%).

6.3.4 2-(Iminobenzal)-4-(4-bromophenyl)-5-(4-phenyl-1*H*-imidazol-2-yl)-thiazole 6d

Yield 74% (Light Yellow), m.p. 156 °C. IR (KBr): 3130 (NH *str*), 3010 (CH-arom *str*), 1595 (C=C arom *str*), 1315 (C–S *str*). H^1-NMR δ_H (DMSO-d6, 400 MHz): 14.16 (H, s, NH), 8.68 (H, s, CH), 7.92 (2H, d, Ar–H), 7.86 (2H, d, Ar–H), 7.78 (H, s, Ar–H), 7.74 (2H, d, Ar–H), 7.55–7.70 (7H, m, Ar–H), 7.50 (H, s, imidazole-H). C^{13} NMR δc (DMSO-d6): 174.4 (N=C–S), 165.4 (CH=N), 160.5 (C=C–N), 143.6 (C=C–N) (imidazole), 132.9 (N=C–NH), 130.8 (C=C–S) (thiazole), 125–138 (aromatic 18C-atom), 122.9 (NH=C–C). Anal. Calcd for $C_{25}H_{17}BrN_4S$: C, 61.65; H, 3.32; Br, 16.50; N, 11.38; S, 6.39. Found: C, 61.86; H, 3.53; Br, 16.42; N, 11.54; S, 6.61 (%).

6.3.5 2-(Imino-4-chlorobenzal)-4-(4-bromophenyl)-5-(4-phenyl-1*H*-imidazol-2-yl)-thiazole 6e

Yield 72% (Brown), m.p. 164 °C. IR (KBr): 3150 (NH *str*), 3015 (CH-arom *str*), 1590 (C=C arom *str*), 1345 (C–S *str*). H^1-NMR δ_H (DMSO-d6, 400 MHz): 14.05 (H, s, NH), 8.59 (H, s, CH), 7.87 (2H, d, Ar–H), 7.78 (2H, d, Ar–H), 7.76 (2H, d, Ar–H), 7.73 (H, s, Ar–H), 7.12–7.98 (6H, m, Ar–H), 7.99 (H, s, imidazole-H). C^{13} NMR δc (DMSO-d6): 171.4 (N=C–S), 164.03 (CH=N), 153.0 (C=C–N), 143.1 (C=C–N) (imidazole), 132.8 (N=C–NH), 128–138 (aromatic 18C-atom), 120.9 (NH=C–C), 119.8(C=C–S) (thiazole). Anal. Calcd for $C_{25}H_{16}BrClN_4S$: C, 57.76; H, 3.10; Br, 15.37; Cl, 6.82; N, 10.78; S, 6.17. Found: C, 57.75; H, 3.08; Br, 15.35; Cl, 6.80; N, 10.75; S, 6.15 (%).

6.3.6 2-(Imino-4-nitrobenzal)-4-(4-bromophenyl)-5-(4-phenyl-1*H*-imidazol-2-yl)-thiazole 6f

Yield 76% (Light Brown), m.p. 189 °C. IR (KBr): 3165 (NH *str*), 3005 (CH-arom *str*), 1605 (C=C arom *str*), 1350 (C–S *str*). H^1-NMR δ_H (DMSO-d6, 400 MHz): 13.54 (H, s, NH), 8.87 (H, s, CH), 8.72 (2H, d, Ar–H), 8.43 (2H, d, Ar–H), 7.89 (2H, d, Ar–H), 7.62 (2H, d, Ar–H), 7.45–8.35 (5H, m, Ar–H), 7.43 (H, s, imidazole-H). C^{13} NMR δc (DMSO-d6): 169.4 (N=C–S), 161.89 (CH=N), 153.5 (C=C–N), 138.1 (C=C–N) (imidazole), 130.8 (N=C–NH), 124–139 (aromatic 18C-atom), 117.9 (NH=C–C), 116.8 (C=C–S) (Thiazole). Anal. Calcd for $C_{25}H_{16}BrN_5O_2S$: C, 56.61; H, 3.04; Br, 15.06; O, 6.03; N, 13.20; S, 6.05. Found: C, 56.60; H, 3.02; Br, 15.03; O, 6.00; N, 13.18; S, 6.03 (%).

6.3.7 2-(Iminobenzal)-4-(4-chlorophenyl)-5-(4-phenyl-1*H*-imidazol-2-yl)-thiazole 6 g

Yield 72% (White), m.p. 186 °C. IR (KBr): 3135 (NH *str*), 3000 (CH-arom *str*), 1600 (C=C arom *str*), 1340 (C–S *str*). H^1-NMR δ_H (DMSO-d6, 400 MHz): 13.65 (H, s, NH), 8.54 (H, s, CH), 7.42–8.12 (10H, m, Ar–H), 7.87 (2H, d, Ar–H), 7.40 (H, s, imidazole-H), 7.38 (2H, d, Ar–H). C^{13} NMR δc (DMSO-d6): 176.0 (CH=N), 172.3 (N=C–S), 160.1 (C=C–N), 146.1 (C=C–N) (imidazole), 142.2 (C=C–S) (thiazole), 135.8 (N=C–NH), 128–135 (aromatic 18C-atom), 124.9 (NH=C–C). Anal. Calcd for $C_{25}H_{17}ClN_4S$: C, 68.10; H, 3.89; Cl, 8.04; N, 12.71; S, 7.27. Found: C, 68.08; H, 3.85; Cl, 8.00; N, 12.70; S, 7.25 (%).

6.3.8 2-(Imino-4-chlorobenzal)-4-(4-chlorophenyl)-5-(4-phenyl-1*H*-imidazol-2-yl)-thiazole 6 h

Yield 70% (Yellow), m.p. 185 °C. IR (KBr): 3135 (NH *str*), 3000 (CH-arom *str*), 1600 (C=C arom *str*), 1340 (C–S *str*). H^1-NMR δ_H (DMSO-d6, 400 MHz): 13.85 (H, s, NH),

8.43 (H, s, CH), 7.95 (2H, d, Ar–H), 7.45–8.12 (5H, m, Ar–H), 7.87 (2H, d, Ar–H), 7.82 (2H, d, Ar–H), 7.79 (2H, d, Ar–H), 7.59 (H, s, imidazole-H). C^{13} NMR δc (DMSO-d6): 176.0 (CH=N), 172.3 (N=C–S), 160.1 (C=C–N), 146.1 (C=C–N) (imidazole), 142.2 (C=C–S) (thiazole), 135.8 (N=C–NH), 128–135 (aromatic 18C-atom), 124.9 (NH=C–C). Anal. Calcd for $C_{25}H_{16}Cl_2N_4S$: C, 63.12; H, 3.35; Cl, 14.88; N, 11.72; S, 6.69. Found: C, 63.16; H, 3.39; Cl, 14.92; N, 11.79; S, 6.74 (%).

6.3.9 2-(Imino-4-nitrobenzal)-4-(4-chlorophenyl)-5-(4-phenyl-1*H*-imidazol-2-yl)-thiazole 6i

Yield 65% (Dark Yellow), m.p. 207 °C. IR (KBr): 3115 (NH *str*), 3010 (CH-arom *str*), 1615 (C=C arom *str*), 1320 (C–S *str*). H^1-NMR δ_H (DMSO-d6, 400 MHz): 14.02 (H, s, NH), 8.97 (H, s, CH), 8.45 (2H, d, Ar–H), 7.51–8.43 (5H, m, Ar–H), 7.87 (2H, d, Ar–H), 7.82 (2H, d, Ar–H), 7.76 (2H, d, Ar–H), 7.50 (H, s, imidazole-H). C^{13} NMR δc (DMSO-d6): 172.3 (N=C–S), 167.65 (CH=N), 157.1 (C=C–N), 143.1 (C=C–N) (imidazole), 130.1 (N=C–NH), 129.2 (C=C–S) (thiazole), 129–150 (aromatic 18C-atom), 123.9 (NH=C–C). Anal. Calcd for $C_{25}H_{16}ClN_5O_2S$: C, 61.75; H, 3.35; Cl, 7.27; N, 14.38; O, 6.61; S, 6.63. Found: C, 61.79; H, 3.32; Cl, 7.30; N, 14.41; O, 6.58; S, 6.60 (%).

6.3.10 2-(Iminobenzal)-4-(4-methoxyphenyl)-5-(4-phenyl-1*H*-imidazol-2-yl)-thiazole 6j

Yield 71% (Milky White), m.p. 210 °C. IR (KBr): 3100 (NH *str*), 3000 (CH-arom *str*), 1604 (C=C arom *str*), 1305 (C–S *str*). H^1-NMR δ_H (DMSO-d6, 400 MHz): 13.98 (H, s, NH), 8.55 (H, s, CH), 8.46 (2H, d, Ar–H), 7.52–8.12 (6H, m, Ar–H), 7.91 (2H, d, Ar–H), 7.80 (2H, d, Ar–H), 7.67 (2H, d, Ar–H), 7.49 (H, s, imidazole-H), 4.01 (3H, s, OCH_3). C^{13} NMR δc (DMSO-d6): 175.3 (N=C–S), 168.0 (CH=N), 160.1 (C=C–N), 146.1(C=C–N) (imidazole), 133.8 (N=C–NH), 129.2 (C=C–S) (thiazole), 124.9 (NH=C–C), 125–137 (aromatic 18C-atom), 55.9 (OCH_3). Anal. Calcd for $C_{26}H_{20}N_4OS$: C, 69.01; H, 4.45; N, 12.38; O, 7.07; S, 7.90. Found: C, 69.00; H, 4.43; N, 12.33; O, 7.09; S, 7.93 (%).

6.3.11 2-(Imino-4-chlorobenzal)-4-(4-methoxyphenyl)-5-(4-phenyl-1*H*-imidazol-2-yl)-thiazole 6 k

Yield 71% (Yellow), m.p. 210 °C. IR (KBr): 3100 (NH *str*), 3000 (CH-arom *str*), 1604 (C=C arom *str*), 1305 (C–S *str*). H^1-NMR δ_H (DMSO-d6, 400 MHz): 13.74 (H, s, NH), 8.87 (H, s, CH), 7.87 (2H, d, Ar–H), 7.72 (H, s, Ar–H), 7.59 (H, s, imidazole-H), 7.33 (2H, d, Ar–H), 7.21–8.35 (6H, m, Ar–H), 7.07 (2H, d, Ar–H), 3.74 (3H, s, OCH_3). C^{13} NMR δc (DMSO-d6): 174.3 (N=C–S), 168.4 (CH=N), 161.1 (C=C–N), 143.1 (C=C–N) (imidazole), 133.8 (N=C–NH), 129.2 (C=C–S) (thiazole), 122.9 (NH=C–C), 114–153 (aromatic 18C-atom), 55.4 (OCH_3). Anal. Calcd for $C_{26}H_{19}ClN_4OS$: C, 66.30; H, 4.07; Cl, 7.53; N, 11.90; O, 3.40; S, 6.81. Found: C, 66.32; H, 4.04; Cl, 7.49; N, 11.84; O, 3.45; S, 6.86 (%).

6.3.12 2-(Imino-4-nitrobenzal)-4-(4-methoxyphenyl)-5-(4-phenyl-1*H*-imidazol-2-yl)-thiazole 6 l

Yield 72% (Dark Yellow), m.p. 235 °C. IR (KBr): 3175 (NH *str*), 3025 (CH-arom *str*), 1600 (C=C arom *str*), 1325 (C–S *str*). H^1-NMR δ_H (DMSO-d6, 400 MHz): 13.89 (H, s, NH), 8.54 (H, s, Ar–H), 8.54 (H, s, CH), 8.12 (2H, d, Ar–H), 7.65–8.10 (6H, m, Ar–H), 7.63 (H, s, imidazole-H), 7.21 (2H, d, Ar–H), 7.09 (2H, d, Ar–H), 3.76 (3H, s, OCH_3). C^{13} NMR δc (DMSO-d6): 172.3 (N=C–S), 162.8 (CH=N), 161.1 (C=C–N), 143.1 (C=C–N) (imidazole), 133.8 (N=C–NH), 122.2 (C=C–S) (thiazole), 120.9 (NH=C–C), 115–143 (aromatic 18C-atom), 53.5 (OCH_3). Anal. Calcd for $C_{26}H_{19}N_5O_3S$: C, 64.85; H, 3.98; N, 14.54; O, 9.97; S, 6.66. Found: C, 64.75; H, 3.99; N, 14.44; O, 9.95; S, 6.64 (%).

6.3.13 2-(Iminobenzal)-4-(4-methylphenyl)-5-(4-phenyl-1*H*-imidazol-2-yl)-thiazole 6 m

Yield 77% (White), m.p. 216 °C. IR (KBr): 3165 (NH *str*), 3014 (CH-arom *str*), 1609 (C=C arom *str*), 1325 (C–S *str*). H^1-NMR δ_H (DMSO-d6, 400 MHz): 13.89 (H, s, NH), 8.36 (H, s, CH), 8.13 (2H, d, Ar–H), 7.49 (H, s, imidazole-H), 7.50–8.17 (10H, m, Ar–H), 7.38 (2H, d, Ar–H), 7.32 (2H, d, Ar–H), 2.43 (3H, s, CH_3). C^{13} NMR δc (DMSO-d6): 175.3 (N=C–S), 162.1 (C=C–N), 160.8 (CH=N), 142.1 (C=C–N) (imidazole), 130.8 (N=C–NH), 125–135 (aromatic 18C atoms), 122.9 (NH=C–C), 121.2 (C=C–S) (thiazole), 22.8 (CH_3). Anal. Calcd for $C_{26}H_{20}N_4S$: C, 74.26; H, 4.79; N, 13.32; S, 7.62. Found: C, 74.10; H, 4.91; N, 13.39; S, 7.65 (%).

6.3.14 2-(Imino-4-chlorobenzal)-4-(4-methylphenyl)-5-(4-phenyl-1*H*-imidazol-2-yl)-thiazole 6n

Yield 75% (White), m.p. 231 °C. IR (KBr): 3132 (NH *str*), 3012 (CH-arom *str*), 1610 (C=C arom *str*), 1345 (C–S *str*). H^1-NMR δ_H (DMSO-d6, 400 MHz): 14.60 (H, s, NH), 8.36 (H, s, CH), 7.79 (2H, d, Ar–H), 7.65 (H, s, imidazole-H), 7.57 (2H, d, Ar–H), 7.54 (2H, d, Ar–H), 7.35 (2H, d, Ar–H), 7.21–8.13 (5H, m, Ar–H), 2.54 (3H, s, CH_3). C^{13} NMR δc (DMSO-d6): 175.4 (N=C–S), 162.8 (CH=N), 155.5 (C=C–N), 142.1 (C=C–N) (imidazole), 133.8 (N=C–NH), 121.9 (NH=C–C), 125–136 (aromatic 18C-atoms), 119.8 (C=C–S) (thiazole), 22.4 (CH_3). Anal. Calcd for

$C_{26}H_{19}ClN_4S$: C, 68.64; H, 4.21; Cl, 7.79; N, 12.31; S, 7.05. Found: C, 68.70; H, 4.15; Cl, 7.72; N, 12.37; S, 7.10 (%).

6.3.15 2-(Imino-4-nitrobenzal)-4-(4-methylphenyl)-5-(4-phenyl-1*H*-imidazol-2-yl)-thiazole 6o

Yield 71% (Brown), m.p. 221 °C. IR (KBr): 3150 (NH *str*), 3015 (CH-arom *str*), 1601 (C=C arom *str*), 1312 (C–S *str*). H^1-NMR δ_H (DMSO-d6, 400 MHz): 13.89 (H, s, NH), 8.76 (2H, d, Ar–H), 8.33 (H, s, CH), 8.07 (2H, d, Ar–H),,7.55 (H, s, imidazole), 7.51–8.34 (5H, m, Ar–H), 7.49 (2H, d, Ar–H), 7.34 (2H, d, Ar–H) 2.76 (3H, s, CH_3). C^{13} NMR δc (DMSO-d6): 174.3 (N=C–S), 163.8 (CH=N), 162.1 (C=C–N), 144.1 (C=C–N) (imidazole), 134.8 (N=C–NH), 127–142 (aromatic 18C-atoms), 123.9 (NH=C–C), 123.2 (C=C–S) (thiazole), 22.7 (CH_3). Anal. Calcd for $C_{26}H_{19}N_5SO_2$: C, 67.08; H, 4.11; N, 15.04; O, 6.87; S, 6.89. Found: C, 67.02; H, 4.15; N, 15.00; O, 6.90; S, 6.90 (%).

7 Conclusion

An efficient new 2-amino-4-aryl-1,3-thiazole-5-carboxaldehydes (**4a-e**), their imidazole derivatives (**5a-e**), and Schiff bases (**6a-o**) with various substituted benzaldehydes. The targeted products were fully characterized using different spectroscopic techniques such as ^{1}H NMR, ^{13}C NMR, IR, Mass Spectroscopy and elemental analysis. The result compound was investigated for their antibacterial activity against Escherichia coli, Klebsiella aerogens, Staphylococcus aureus and Bacillus substilis and antifungal activity against A. niger and C. albicans. The study of the pharmacokinetic parameters of synthesized compounds revealed that most of the compounds are Pgp substrate and CYP3A4 inhibitors. All the synthesized compounds emerged to be non- carcinogenic in nature. The overall results of this study showed that a fascinating protocol for the production of antimicrobial agents was the molecular to biologically interesting imidazole scaffold with diverse aromatic substituent.

Acknowledgements The directors of SAIF in Chandigarh, the head of the department of pharmaceutical sciences at R T M Nagpur University in Nagpur, who supplied vital biological information for the project, and the head of the chemistry department at Dhote Bandhu Science College in Gondia, who provided essential research facility workspaces, are all acknowledged by the authors.

Funding The authors have not disclosed any funding.

Declarations

Conflict of interest The authors declare that they have no known competing financial interests or personal relationships that could have appeared to influence the work reported in this paper. The authors declare the following financial interests/personal relationships which may be considered as potential competing interests.

Ethical approval The work reported in the paper submitted for publication in the Journal is original and has not been submitted for publication elsewhere.

Informed consent All authors have seen and approved this manuscript and consent to having their name in the list of authors, thereby taking responsibility for the results contained in the manuscript.

References

Asmaa S (2016) Synthesis, spectral properties and anti-tumor evaluations of some novel 2-substituted-1, 3-thiazole derivatives. Am Chem Sci J 15(3):1–13

Barradas J, Errea M, D'Accorso N, Sepúlveda C, Damonte E (2011) Imidazo [2,1-b] thiazole carbohydrate derivatives: synthesis and antiviral activity against Junin virus, agent of Argentine hemorrhagic fever. Eur J Med Chem 46(1):259–264

Brenk R, Schipani A, James D, Krasowski A, Gilbert I, Frearson J (2008) Lessons learnt from assembling screening libraries for drug discovery for neglected diseases. Chem Med Chem 3:435–444

Daina A, Zoete V (2016) BOILED-egg to predict gastrointestinal absorption and brain penetration of small molecules. Chem Med Chem 11(11):1117–1121

Daina A, Michielin O, Zoete V (2014) iLOGP: a simple, robust, and efficient description of n-octanol/water partition coefficient for drug design using the GB/SA approach. J Chem Inf Model 54(12):3284–3301

Daina A, Michielin O, Zoete V (2017) SwissADME: a free web tool to evaluate pharmacokinetics, drug-likeness and medicinal chemistry friendliness of small molecules. Sci Rep 7:42717

Degreef H, Heeres J, Borgers M (2006) Antifungal azoles for skin disorders. Expert Opin Ther Pat 16(9):1235–1253

Delaney J (2004) ESOL: estimating aqueous solubility directly from molecular structure. J Chem Inf Comput Sci 44(3):1000–1005

Egan W, Merz K, Baldwin J (2000) Prediction of drug absorption using multivariate statistics. J Med Chem 43(21):3867–3877

Fagerberg J, Karlsson E, Ulander J, Hanisch G, Bergstrom C (2015) Computational prediction of drug solubility in fasted simulated and aspirated human intestinal fluid. Pharm Res 32(2):578–589

Gaidhane M, Ghatole A, Lanjewar K, Hatzade K (2020) Innovational combination of hetero-bifunctional N-PEG quinoline scaffolds derivatives with improved anticancer activity against breast and colon cancer cell lines and P-glycoprotein, cytochrome p450 enzyme activity prediction. Turk J Chem 44(6):1495–1514

Ganesh S, Brindha D, Shalini S, Nikhila M, Perumal Y, Dharmarajan S (2016) Design, synthesis and biological evaluation of imidazo [2,1-b] thiazole and benzo[d]imidazo[2,1-b]thiazole derivatives as Mycobacterium tuberculosis pantothenate synthetase inhibitor. Bioorganic Med Chem 24(6):1298–1307

Gatfaoui S, Issaoui N, Mezni A, Bardak F, Roisnel T, Atac A, Marouani H (2017) Synthesis, structural and spectroscopic features, and investigation of bioactive nature of a novel organic-inorganic hybrid material 1H-1, 2, 4-triazole-4-ium trioxonitrate. J Mol Struct 1150:242–257

Geronikaki A, Hadjipavlou-Litina D, Zablotskaya A, Segal I (2007) Organosilicon-containing thiazole derivatives as potential lipoxygenase inhibitors and anti-inflammatory agents. Bioinorg Chem Appl. https://doi.org/10.1155/2007/92145

Ghalla H, Issaoui N, Bardak F, Atac A (2018) Intermolecular interactions and molecular docking investigations on 4-methoxybenzaldehyde. Comput Mater Sci 149:291–300

Ghatole A, Lanjewar K, Gaidhane M (2012) Syntheses, characterization, antimicrobial activity of copper (II), zinc (II) and cobalt (II) complexes of the bi-dented substituted 2-((E)-2-((2-chloro-6-ethoxyquinolin-3-yl)methyleneamino)thiazol-4-yl)phenol havong ON donor site. J Pharm Res 5(5):2758–2762

Ghatole A, Gaidhane M, Lanjewar K, Hatzade K (2020) Pharmacokinetics, drug-likeness, medicinal properties, molecular docking analysis of substituted β-lactams synthesized via [bmim][PF6]/[Et3NH]+[HSO4]- catalyzed coupling reaction. Chem Bulg J Sci Educ 29(2):206–244

Ghose A, Viswanadhan VWJ (1998) Prediction of hydrophobic (lipophilic) properties of small organic molecules using fragmental methods: an analysis of ALOGP and CLOGP methods. J Phys Chem A 102(21):3762–3772

Ghose A, Viswanadhan V, Wendoloski J (1999) A knowledge-based approach in designing combinatorial or medicinal chemistry libraries for drug discovery. 1. A qualitative and quantitative characterization of known drug databases. J Comb Chem 1(1):55–68

Hann M, Keseru G (2012) Finding the sweet spot: the role of nature and nurture in medicinal chemistry. Nat Rev Drug Discov 11:355–365

Hatzade K, Sheikh J, Taile V, Ghatole A, Ingle V, Genc M, Hadda T (2015) Antimicrobial/antioxidant activity and POM analyses of novel 7-O- -D-Glucopyranosyloxy-3-(4, 5-disubstituted imidazol-2-yl)-4H-chromen-4-ones. Med Chem Res 24:2679–2693

Hatzade K, Ghatole A, Gaidhane P, Gaidhane M, Gadekar G (2021) A facile synthesis of some new pyrimidine-2,4,6-triones analogs and their O-β-D-glucosides P-glycoprotein and antioxidant, antimicrobial study, blood–brain barrier, cytochrome p450 enzyme activity prediction. Med Chem Res 30:163–181

Hu Y, Shen Y, Wu X, Tu X, Wang G (2017) Synthesis and biological evaluation of coumarin derivatives containing imidazole skeleton as potential antibacterial agents. Eur J Med Chem 143:958–969

Issaoui NGH, Brandán S, Bardak F, Flakus H, Atac A, Oujia B (2017a) Experimental FTIR and FT-Raman and theoretical studies on the molecular structures of monomer and dimer of 3-thiopheneacrylic acid. J Mol Struct 135:209–221

Issaoui N, Ghalla H, Bardak F, Karabacak M, Dlala N, Flakus H, Oujia B (2017b) Combined experimental and theoretical studies on the molecular structures, spectroscopy, and inhibitor activity of 3-(2-thienyl) acrylic acid through AIM, NBO, FT-IR, FT-Raman, UV and HOMO-LUMO analyses, and molecular docking. J Mol Struct 1130:659–668

Karim M, Michael S, Kristin W, Beverly S, Daniel G (2004) Effects of the IMP-dehydrogenase inhibitor, Tiazofurin, in bcr-abl positive acute myelogenous leukemia: part I. In vivo studies. Leuk Res 28(11):1125–1136

Lambert C, Wilhelm M, Striebel H, Kradolfer F, Schmidt P (1964) Eine neue gegen Bilharziose und Amoebiase wirksame Verbindung. Kurze Mitteilungen 20:452–453

Lipinski C, Lombardo F, Dominy B, Feeney P (2001) Experimental and computational approaches to estimate solubility and permeability in drug discovery and development settings. Adv Drug Deliv Rev 46(1–3):3–26

Matlock M, Hughes T, Dahlin J, Swamidass S (2018) Modeling small molecule reactivity identifies promiscuous bioactive compounds. J Chem Inf Model 26(5):1483–1500

Mehdi D, Hadi B, Javad B, Nasser L (2008) Theoretical 14N nuclear quadrupole resonance parameters for sulfa drugs: sulfamerazine and sulfathiazole. J Mol Graph Model 27(3):326–331

Muegge I, Heald S, Brittelli D (2001) Simple selection criteria for drug-like chemical matter. J Med Chem 44(12):1841–1846

Sagaama A, Issaoui N (2020) Design, molecular docking analysis of an anti-inflammatory drug, computational analysis and intermolecular interactions energy studies of 1-benzothiophene-2-carboxylic acid. Comput Biol Chem 88:107348

Satbhaiya S, Chourasia O (2015) Syntheses, characterization and antimicrobial activities of 1-(1H-benzo[d][1,2,3]triazol-1-yl)-2-(((3aR,5R)-3-5-disubstituted-3,3a-dihydro-2H-pyrazolo[3,4-d]thiazol-6(5H)-yl)amino)ethanone derivatives. Chem Sci Trans 4(3):819–827

Shad H, Hussain A, Shahzad K, Alam M, Ilyas M, Hussain G, Ahmad K (2018) Multi-component synthesis of novel diazoles: their characterization and biological evaluation. Arch Org Inorg Chem Sci 1(2):52–56

Taile V, Hatzade K, Ingle V (2011) Synthesis of 2-(sulfamoylphenyl)-4'-(iminoaryl/hetroaryl)-4-(4''-hydroxyphenyl)-thiazoles and their O-glucosides. J Heterocycl Chem 48:1428–1433

Teague S, Davis A, Leeson P, Oprea T (1999) The Design of leadlike combinatorial libraries. Angew Chem Int Ed Engl 38(24):3743–3748

Trabelsi S, Issaoui N, Brandán SA, Bardak F, Roisnel T, Atac A, Marouani H (2019) Synthesis and physic-chemical properties of a novel chromate compound with potential biological applications, bis (2-phenylethylammonium) chromate (VI). J Mol Struct 1185:168–182

Tratrat C, Haroun M, Paparisva A, Geronikaki A, Kamoutsis C, Ćirić A, Saxena A (2018) Design, synthesis and biological evaluation of new substituted 5-benzylideno-2-adamantylthiazol[3,2-b][1,2,4]triazol-6(5H)ones. Pharmacophore models for antifungal activity. Arabian J Chem 11(4):573–590

Upadhyay S, Zala R, Bhatt K (2020) Synthesis, characterization and biological screening of schiff bases derived from 4, 6-difluoro-2-amino benzothiazole. Med Anal Chem Int J 4(1):1–7

Veber D, Johnson S, Cheng H, Smith B, Ward KK (2002) Molecular properties that influence the oral bioavailability of drug candidates. J Med Chem 45(12):2615–2623

Zhu Z, Lu Z, Xu T, Chen C, Yang G, Zha T, Xue Y (2020) Arbidol monotherapy is superior to lopinavir/ritonavir in treating COVID-19. J Infect 81(1):e21–e23

Springer Nature or its licensor (e.g. a society or other partner) holds exclusive rights to this article under a publishing agreement with the author(s) or other rightsholder(s); author self-archiving of the accepted manuscript version of this article is solely governed by the terms of such publishing agreement and applicable law.

SPRINGER LINK

Log in

Menu Search Cart



Iranian Journal of Science

Publishing model
Hybrid

Submit your manuscript

Editorial board

Aims and scope

Overview

The Iranian Journal of Science is a multidisciplinary platform for original research articles in Biology, Chemistry, Geology, Mathematics, and Physics.

Special attention to applications of these fields in medical science and multidisciplinary research.
Invites surveys of scientific developments in a subject of current interest.
Divided into five sections: Biology, Chemistry, Geology, Mathematics, and Physics.
Each section considers manuscripts relevant to its specific subjects.

Editor-in-Chief
G. H. Esslamzadeh

Submission to first decision (median)
7 days

Downloads
94,342 (2023)

Societies and partnerships

Shiraz University



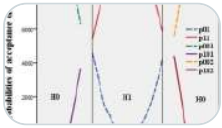
Latest issue

October 2024
Volume 48, Issue 5

View all volumes and issues →

Latest articles

Constrained Bayesian Methods for Union-Intersection and Intersection-Union Hypotheses Testing Problems



View all articles →

This journal has 19 open access articles →

Journal information

Electronic ISSN 2731-8109

Print ISSN 2731-8095

Abstracted and indexed in

BIOSIS
Baidu
CAB Abstracts
CLOCKSS
CNKI
CNPIEC
Dimensions
EBSCO
Google Scholar
INIS Atomindex
INSPIRE
Japanese Science and Technology Agency (JST)
Mathematical Reviews
Naver
OCLC WorldCat Discovery Service
Portico
ProQuest
SCImago
SCOPUS
Science Citation Index Expanded (SCIE)
TD Net Discovery Service
UGC-CARE List (India)
Wanfang
Zoological Record

Copyright information

Rights and permissions

Already have a manuscript?

Use our Manuscript Matcher to find the best relevant journals!

Find a Match

Refine Your Search Results

2731-8095 Search

Sort By: Title (A-Z)

Search Results

Found 1 results (Page 1) Share These Results

Exact Match Found

IRANIAN JOURNAL OF SCIENCE

Publisher:	SPRINGER INT PUBL AG , GEWERBESTRASSE 11, CHAM, SWITZERLAND, CH-6330
ISSN / eISSN:	2731-8095 / 2731-8109
Web of Science Core Collection:	Science Citation Index Expanded
Additional *Web of Science* Indexes:	Biological Abstracts | BIOSIS Previews | Essential Science Indicators | Zoological Record

Share This Journal View profile page

** Requires free login.*

Filters Clear All

Web of Science Coverage

Open Access

Category

Country / Region

Language

Frequency

Journal Citation Reports

Coexisting single-particle excitations and octupole correlations in the transitional nucleus ^{217}Ra

Madhu,[1] A. Y. Deo,[1,*] Khamosh Yadav,[1] Dhananjaya Sahoo,[1] Y. Y. Wang,[2] Y. K. Wang,[3] J. Meng,[3,4] Saket Suman,[5] S. K. Tandel,[5] A. Sharma,[6] I. Ahmed,[7] K. Katre,[7] K. Rojeeta Devi,[7] S. Dutt,[7] S. Kumar,[7] Yashraj,[7] S. Muralithar,[7] and R. P. Singh[7]

[1]*Department of Physics, Indian Institute of Technology Roorkee, Roorkee 247667, India*
[2]*Mathematics and Physics Department, North China Electric Power University, Beijing 102206, China*
[3]*State Key Laboratory of Nuclear Physics and Technology, School of Physics, Peking University, Beijing 100871, China*
[4]*Yukawa Institute for Theoretical Physics, Kyoto University, Kyoto 606-8502, Japan*
[5]*School of Physical Sciences, UM-DAE Centre for Excellence in Basic Sciences, University of Mumbai, Mumbai 400098, India*
[6]*Department of Physics, Himachal Pradesh University, Shimla 171005, India*
[7]*Inter University Accelerator Centre, Aruna Asaf Ali Marg, New Delhi 110067, India*

(Received 3 April 2023; revised 17 May 2023; accepted 27 June 2023; published 6 July 2023)

The level structure of the transitional nucleus ^{217}Ra has been extended with the addition of around 20 new transitions. The discrepancies between the placements of several transitions reported in the earlier studies are resolved. The newly established negative-parity sequence at low excitation energies hints at the expected parity-doublet structures in this nucleus. The properties of the observed simplex bands are compared with that of similar bands in neighboring nuclei. Since the presence of parity-doublet structures reflects octupole correlations, theoretical calculations using reflection-asymmetric triaxial particle rotor model (RAT-PRM) have been performed. A comparison of the observed features of the simplex bands with the predictions of the RAT-PRM calculations suggests that ^{217}Ra exhibits an intermediate behavior between the extremes of spherical and octupole-deformed nuclei. The termination of the simplex bands at intermediate energies and the structures lying above reflect the dominance of the single-particle excitations at higher excitation energies.

DOI: 10.1103/PhysRevC.108.014309

I. INTRODUCTION

The atomic nucleus is a many-body quantal system in which the number of valence nucleons outside the shell closure and the interactions between them mainly govern shape and properties of the system. At the beginning of several major shells, the presence of an opposite-parity intruder orbital in the vicinity of normal-parity orbitals with $\Delta j = \Delta l = 3$ gives rise to long-range octupole correlations between the valence nucleons [1]. Such orbitals are present near the Fermi surface in nuclei with Z or $N \simeq 34$, 56, 88, and 134 where the fingerprints of dynamical or stable reflection asymmetric shapes have been observed [1–3]. The advancements in the experimental facilities with the availability of radioactive ion beams and targets have facilitated the measurements of the $E3$ transition strengths using Coulomb excitation techniques [4–8]. The deduced electric octupole moments, which are a direct measure of the strength of octupole correlations, in the Ra isotopes with $134 \leqslant N \leqslant 138$ (^{222}Ra, ^{224}Ra, ^{226}Ra) have confirmed the stable octupole deformation in these nuclei [4–6,9]. In terms of the level structures, static quadrupole and octupole deformation in the even-even nuclei is characterized by $\Delta I = 2$ sequences of opposite parities connected by enhanced $E1$ transitions. The excitation energies of the states of these $\Delta I = 2$ bands follow the $I(I+1)$ dependence as expected for rotational bands. Also, the negative-parity sequence is expected to be perfectly interleaved with the positive-parity ground state band in the case of static octupole deformation. In addition, the typical $B(E1)/B(E2)$ ratios are of the order of $\approx 10^{-6}$ fm^{-2} for such nuclei [1–3]. For the case of odd-A and doubly odd nuclei where the odd nucleon tilts the total angular momentum with respect to the normal to the symmetry plane, the simplex symmetry is broken [10]. In such nuclei, parity-doublet structures (almost degenerate states of the same spin but opposite parity) are expected [1,10].

As one moves away from the region of stable octupole deformation toward the shell closure, a transitional region is encountered where the interplay between both the single-particle and collective degrees of freedom results in complex structures and the properties mentioned above become less pronounced. The recent high-spin investigations in $N = 130$ isotones (^{218}Ra and ^{220}Th) and ^{219}Th report near-constant transition energies and spin-dependent staggering of $B(E1)/B(E2)$ ratios in these nuclei [11–13]. The almost constant level spacings and angular velocity over a spin range imply that the nucleus does not gain angular momentum by rotating faster. Thus, a new approach in terms of a reflection asymmetric tidal wave running over the nuclear surface has been proposed to interpret the observed properties in these nuclei [14].

It has been noted that the properties of the level structures of nuclei in the transitional region exhibit a significant

*ajay.deo@ph.iitr.ac.in

 ©2023 American Physical Society

dependence on the nucleon number. The low-lying states in ^{216}Ra, with two valence neutrons outside the shell closure, exhibit decreasing level spacing with spin as expected for single-particle $\nu g^2_{9/2}$ excitations [15,16]. On the other hand, spectroscopic studies in ^{218}Ra ($N = 130$) revealed irregular sequences of opposite parity connected by enhanced $E1$ transitions which, in turn, reflect the dominance of octupole correlations over quadrupole deformation in this nucleus [17]. In ^{217}Ra, which lies in between the above mentioned isotopes, three sequences of $E2$ transitions are reported at low excitation energies out of which two are connected by $E1$ transitions [18–21]. Although the alternating parity sequence was qualitatively understood in terms of single-particle neutron excitations, the observed near linear spin dependence of excitation energies and large $B(E1)/B(E2)$ ratios ($\approx 10^{-6}$ fm^{-2}) hint at the contribution of collective degrees of freedom in this nucleus. Thus, the disparate level structure in ^{217}Ra with respect to its neighboring even-even isotopes requires a detailed spectroscopic study of this nucleus to understand how the dominance of underlying degrees of freedom evolves in the transitional region.

Prior to the present work, excited states in ^{217}Ra were established using the in-beam γ-ray and conversion-electron spectroscopy along with the α-decay studies [18–24]. It was observed that the placement and ordering of several transitions were at variance in the in-beam studies and need to be revisited [18–21]. Also, the spin-parities of the excited states above 2.4 MeV energy were reported to be tentative in these studies. It may be noted that the low-lying level structure in ^{217}Ra is observed to be similar to its $N = 129$ isotones [13,25,26]. However, in all the $N = 129$ isotones with $87 \leqslant Z \leqslant 90$ nuclei, except ^{217}Ra, parity-doublet structures have been reported. Therefore, it is imperative to search for similar structures expected in ^{217}Ra and understand the observed properties with the help of the relevant nuclear models. Thus, an extensive γ-ray spectroscopy study of ^{217}Ra has been carried out using the heavy-ion fusion reaction mechanism to investigate high-spin states and the evolution of structure with angular momentum in this nucleus. In the present work, we report an extended level scheme of ^{217}Ra with the addition of around 20 new transitions. We provide the first evidence of a new negative-parity sequence which constitutes the simplex partner band of the already reported ground state alternating parity sequence. Also, the observed level structures in ^{217}Ra reflect the coexistence of single-particle and collective excitations in this transitional nucleus.

II. EXPERIMENTAL DETAILS

High-spin states in ^{217}Ra were populated using the ^{208}Pb(^{12}C, $3n$)^{217}Ra reaction. The ^{12}C beam with 68-, 72-, and 80-MeV energies was provided by the 15UD Pelletron accelerator at the Inter-University Accelerator Centre, New Delhi. The target consisted of an isotopically enriched (99%) and self-supporting ^{208}Pb foil of $\approx$9 mg/cm^2 thickness. The γ rays deexciting the residual nuclei were detected using the Indian National Gamma Array (INGA) [27] comprising 13 Compton suppressed clover detectors and one low-energy photon spectrometer (LEPS). The detectors were placed in five rings at 32°, 57°, 90°, 123°, and 148° with respect to the beam direction. The raw data were collected using a VME based data acquisition system [28], which were then written to a disk in a ROOT [29] Tree format. The energy and efficiency calibration were performed using a standard ^{152}Eu source. The calibrated data were written into another ROOT Tree and various histograms were generated for further analysis. It may be noted that the two- and higher-fold coincidence data collected at the three beam energies were combined to determine the coincidence relationships between the γ rays, multipolarities of the transitions, and lifetime of isomeric states. In addition, single-fold data were also acquired to obtain the intensity information for the strong and noncontaminated γ rays.

The level scheme was constructed on the basis of coincidence relationships between the observed γ rays and the intensity measurements. In order to establish the coincidences between the γ rays, the transitions which were detected within 100 ns with respect to each other were used to construct symmetric two- and three-dimensional prompt histograms. Several *early-delayed* γ-γ matrices within different time windows (ΔT) were generated to search for isomeric states. For such histograms, the transitions which precede (succeed) the coincident γ rays within a certain time interval (ΔT) are placed on the *early* (*delayed*) axis. In the present work, the half-life of the metastable state was extracted using the centroid-shift analysis. It may be noted the lifetimes greater than one-twentieth of the FWHM of prompt distribution can be extracted using the centroid-shift technique [30]. For the current detection setup, the FWHM was found to be around 50 ns for γ rays of $\approx$500 keV energy. For the centroid-shift analysis, histograms of time difference (ΔT) between the γ rays feeding and deexciting the state were generated.

The spin and parities of the states in the level scheme were assigned on the basis of the multipolarities of the γ rays. Since the intensities of the γ rays originating from the oriented nuclear states exhibit a particular angular dependence based on the multipole order of the transitions, the ratios of directional correlations of oriented states ($R_{\rm DCO}$) [31] were measured. An asymmetric γ-γ matrix was generated with the transitions detected at 32° and 148° (θ_1) on the X axis and the coincident transitions detected at 90° (θ_2) on the Y axis. The $R_{\rm DCO}$ value for a given transition is defined as

$$R_{\rm DCO}\,(\gamma_1) = \frac{I_{\gamma_1}\text{ at }\theta_1|\text{gate on }\gamma_2\text{ at }\theta_2}{I_{\gamma_1}\text{ at }\theta_2|\text{gate on }\gamma_2\text{ at }\theta_1}. \tag{1}$$

It was found that for a stretched quadrupole (dipole) gating transition, the $R_{\rm DCO}$ value for a quadrupole (dipole) transition is 1.0 (1.0), whereas the $R_{\rm DCO}$ value for a dipole (quadrupole) γ ray is 0.5 (2.0). Since the $R_{\rm DCO}$ values for the electric and magnetic transitions of a given multipole order are the same, polarization measurements were performed to ascertain the parities of the states.

The polarization asymmetry ($\Delta_{\rm asym}$) [32,33] for a transition of interest is defined as

$$\Delta_{\rm asym} = \frac{a(E_\gamma)N_\perp - N_\parallel}{a(E_\gamma)N_\perp + N_\parallel}, \tag{2}$$

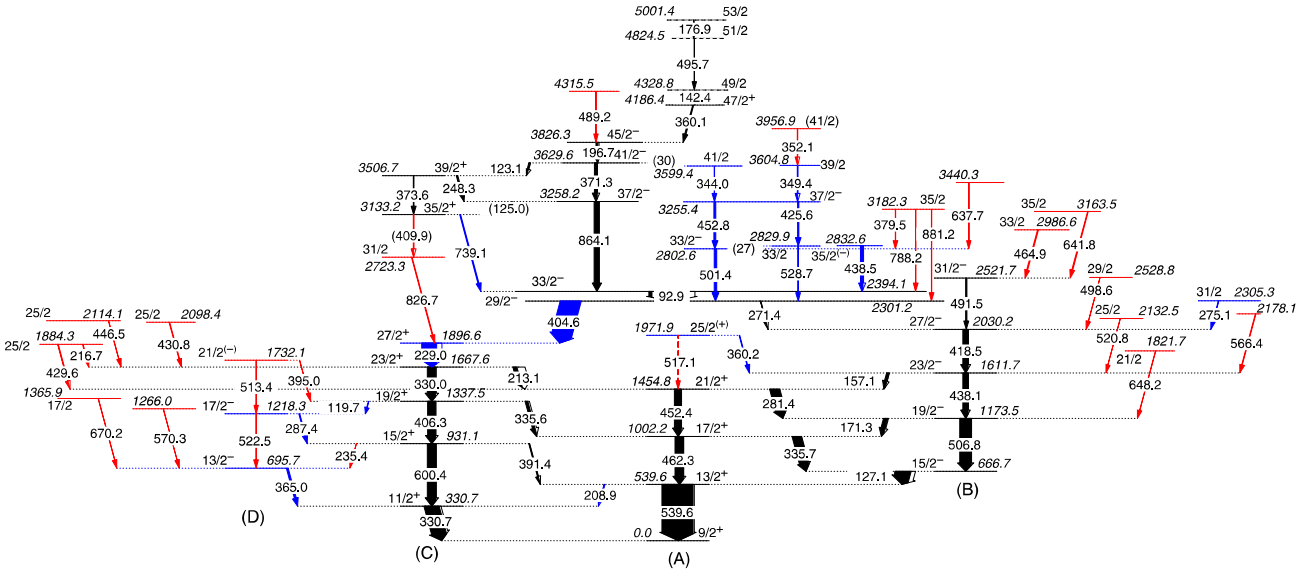


FIG. 1. The level scheme of ^{217}Ra established in the present work. The widths of the closed and open areas of the arrows correspond to the intensity of the γ rays and conversion electrons, respectively. The newly identified γ rays and levels are presented in red color. The transitions whose placements were inconsistent in different studies [18,20,21] or uncertain in Ref. [38] and have been confirmed in the present work are shown in blue color. In addition, the earlier reported γ rays whose ordering has been changed are also shown in blue color.

where $N_\perp$ ($N_\parallel$) denotes the number of Compton-scattered γ rays detected in the direction perpendicular (parallel) with respect to the reaction plane.

The inherent geometrical asymmetry [$a(E_\gamma)$] in the polarization measurements is taken into account by determining the ratio of the parallel to perpendicular counts ($\frac{N_\parallel}{N_\perp}$) for unpolarized gamma rays as a function of energy. For the present detection setup, the value of $a(E_\gamma)$ was found to be 1.02(2). The positive value of polarization asymmetry indicates the electric nature of the transition of interest, whereas the magnetic transitions have negative $\Delta_{\rm asym}$. For the transitions where the measured $\Delta_{\rm asym}$ values are near zero and/or $R_{\rm DCO}$ measurements suggests mixed nature, information on the mixing of different multipoles is required. In order to determine the mixing ratios (δ), theoretical $R_{\rm DCO}$ and linear polarization (P) values were compared with the experimental data points. The theoretical values of $R_{\rm DCO}$ and linear polarization (P) were calculated using the formalism given in Refs. [34–36]. The value of spin alignment parameter was adopted to be 0.3 in the present calculations.

The linear polarization is related to the measured polarization asymmetry as

$$P = \frac{\Delta_{\rm asym}}{Q(E_\gamma)}. \tag{3}$$

The polarization sensitivity [$Q(E_\gamma)$] [33,36], which depends on the geometry of the polarimeter, varies as a function of energy as per the following relation:

$$Q(E_\gamma) = (CE_\gamma + D)Q_0(E_\gamma). \tag{4}$$

Here, $Q_0(E_\gamma)$ is the polarization sensitivity for a point absorber and scatterer and is defined as

$$Q_0(E_\gamma) = \frac{\alpha + 1}{\alpha^2 + \alpha + 1}, \tag{5}$$

with $\alpha = E_\gamma/m_e c^2$, where E_γ is energy of the incident γ-ray photon and $m_e c^2$ is the rest-mass energy of the electron. The coefficients C and D for the polarization sensitivity were taken from Ref. [37].

III. RESULTS

Figure 1 shows the level scheme of ^{217}Ra established in the present study. Apart from a few modifications, the proposed level structure is found to be mostly consistent with that reported in Refs. [18,20]. In addition to the earlier reported transitions, around 20 new γ rays have been placed in the level scheme on the basis of coincidence relationships and intensity measurements. Also, the placements of several known transitions, which were found to be inconsistent in the earlier studies, have been confirmed in the present work. The multipolarities of the observed γ rays, wherever possible, were determined using the $R_{\rm DCO}$ and linear-polarization measurements. Table I lists the energies, relative intensities (I_γ), $R_{\rm DCO}$, and polarization values of the observed γ rays along with the spin-parities and excitation energies of the states. Furthermore, the established level scheme was investigated to search for isomers using *early-delayed* γ-γ matrices. The present analysis does not indicate the presence of any longer-lived [$\tau > 2.5$ ns] state other than the previously reported isomer with $T_{1/2} = 4.62(6)$ ns at an excitation energy of 2.4 MeV [39]. The detailed results are discussed in the following subsections.

A. Revisiting the earlier reported level structures

It has been noted that out of the several transitions which were reported to directly populate the ground state in the recent α-decay study [22], only 540- and 331-keV γ rays are

TABLE I. Table of γ-ray energies, level energies, spin-parity of the initial and final states, and relative γ-ray intensities of the transitions in ^{217}Ra. The $R_{\rm DCO}$ values of the transitions in dipole and quadrupole gates are mentioned along with the linear polarization values and deduced multipolarity of the transitions. The reported errors in the γ-ray energies, relative γ-ray intensities, and $R_{\rm DCO}$ values include contribution from both the systematic and statistical uncertainties. The systematic uncertainty in I_γ is considered to be 5% of the relative γ-ray intensity.

E_γ (keV)	E_i (keV)	I_i^π	I_f^π	I_γ	$R^Q_{\rm DCO}$	$R^D_{\rm DCO}$	P	Multipolarity
92.9(5)	2394.1(5)	$33/2^-$	$29/2^-$	2.1-3.9[a]				
119.7(3)	1337.5(5)	$19/2^+$	$17/2^-$	1.3(3)	0.56(7)	1.16(16)		D
123.1(3)	3629.6(4)	$41/2^-$	$39/2^+$	4.6(2)	0.44(5)			D
(125.0)[b]	3258.2(1)	$37/2^-$	$35/2^+$	–				
127.1(1)	666.7(1)	$15/2^-$	$13/2^+$	49.9(25)	0.67(4)	1.20(7)		$E1$[c]
142.4(4)	4328.8(4)	49/2	$47/2^+$	0.9(1)	0.64(3)			D
157.1(2)	1611.7(3)	$23/2^-$	$21/2^+$	7.4(4)	0.63(4)	1.15(8)		$E1$[c]
171.3(2)	1173.5(2)	$19/2^-$	$17/2^+$	13.4(7)	0.60(3)	1.07(7)		$E1$[c]
176.9(4)	5001.4(4)	53/2	51/2	0.3(1)	0.49(3)			D
196.7(2)	3826.3(2)	$45/2^-$	$41/2^-$	6.2(3)	1.11(9)	2.07(24)		$E2$[c]
208.9(3)	539.6(3)	$13/2^+$	$11/2^+$	1.0(1)				
213.1(2)	1667.6(3)	$23/2^+$	$21/2^+$	13.0(7)	0.49(3)	1.00(6)		D
216.7(3)	1884.3(5)	25/2	$23/2^+$	2.0(1)	0.51(6)	0.94(19)		D
229.0(1)	1896.6(1)	$27/2^+$	$23/2^+$	47.8(24)	1.07(6)	1.94(12)	0.75(11)	$E2$
235.4(4)	931.1(5)	$15/2^+$	$13/2^-$	0.3(1)		0.99(22)		D
248.3(3)	3506.7(4)	$39/2^+$	$37/2^-$	4.5(2)	0.52(4)	0.98(11)		D
271.4(4)	2301.2(5)	$29/2^-$	$27/2^-$	0.9(1)	0.49(5)			D
275.1(3)	2305.3(3)	31/2	$27/2^-$	1.2(1)	1.00(12)			Q
281.4(1)	1454.8(4)	$21/2^+$	$19/2^-$	30.4(15)	0.55(3)	0.98(6)	0.49(8)	$E1$
287.4(3)	1218.3(4)	$17/2^-$	$15/2^+$	2.9(2)	0.53(6)	1.08(17)	0.54(11)	$E1$
330.0(1)	1667.6(3)	$23/2^+$	$19/2^+$	25.9(13)	1.06(6)		0.45(9)	$E2$
330.7(1)	330.7(1)	$11/2^+$	$9/2^+$	46.7(39)		1.45(13)	0.10(5)	$E2(+M1)$[d]
335.6(2)	1337.5(5)	$19/2^+$	$17/2^+$	8.9(5)	0.54(4)		−0.10(3)	$M1$
335.7(1)	1002.2(3)	$17/2^+$	$15/2^-$	28.7(25)		1.00(7)	0.25(5)	$E1$
344.0(3)	3599.4(3)	41/2	$37/2^-$	1.4(1)	0.89(10)			Q
349.4(5)	3604.8(5)	39/2	$37/2^-$	1.3(2)	0.50(7)			D
352.1(4)	3956.9(4)	(41/2)	39/2	1.1(1)	0.75(14)			$D+Q$
360.1(3)	4186.4(3)	$47/2^+$	$45/2^-$	3.6(2)	0.54(4)	0.84(10)	0.37(7)	$E1$
360.2(5)	1971.9(5)	$25/2^{(+)}$	$23/2^-$	2.2(4)		0.85(9)		D
365.0(2)	695.7(2)	$13/2^-$	$11/2^+$	5.7(3)	0.53(8)		0.58(12)	$E1$
371.3(2)	3629.6(4)	$41/2^-$	$37/2^-$	9.4(5)	0.99(7)	1.91(19)	0.64(13)	$E2$
373.6(3)	3506.7(4)	$39/2^+$	$35/2^+$	2.4(1)	1.08(13)		0.56(13)	$E2$
379.5(4)	3182.3(7)	35/2	$33/2^-$	1.0(1)	0.52(7)			D
391.4(3)	931.1(5)	$15/2^+$	$13/2^+$	2.5(1)	0.73(6)			$D+Q$
395.0(4)	1732.1(6)	$21/2^{(-)}$	$19/2^+$	1.0(1)	0.47(5)			D
404.6(1)	2301.2(5)	$29/2^-$	$27/2^+$	63.5(32)	0.51(3)	1.02(6)	0.39(8)	$E1$
406.3(1)	1337.5(5)	$19/2^+$	$15/2^+$	25.7(57)	0.85(10)			Q
(409.9)[b]	3133.2(3)	$35/2^+$	31/2	–				
418.5(1)	2030.2(1)	$27/2^-$	$23/2^-$	17.0(9)	1.03(6)	1.81(15)	0.57(12)	$E2$
425.6(3)	3255.4(4)	$37/2^-$	$33/2^-$	4.1(2)	1.08(11)		0.64(14)	$E2$
429.6(5)	1884.3(5)	25/2	$21/2^+$	0.9(2)	0.86(11)			Q
430.8(5)	2098.4(5)	25/2	$23/2^+$	1.8(1)	0.46(5)			D
438.1(1)	1611.7(3)	$23/2^-$	$19/2^-$	16.8(13)	0.96(5)		0.53(12)	$E2$
438.5(2)	2832.6(2)	$35/2^{(-)}$	$33/2^-$	7.6(4)	0.59(4)	1.05(17)	0.03(3)	$(M1+E2)$
446.5(4)	2114.1(4)	25/2	$23/2^+$	1.0(1)	0.62(7)			D
452.4(1)	1454.8(4)	$21/2^+$	$17/2^+$	21.7(14)	0.99(8)		0.48(12)	$E2$
452.8(2)	3255.4(4)	$37/2^-$	$33/2^-$	5.3(3)	1.15(12)		0.51(13)	$E2$
462.3(1)	1002.2(3)	$17/2^+$	$13/2^+$	27.1(14)	1.04(8)	1.78(14)	0.65(15)	$E2$
464.9(3)	2986.6(3)	33/2	$31/2^-$	3.0(1)	0.49(5)	1.15(15)		D
489.2 (4)	4315.5(4)		$45/2^-$	0.7(1)				
491.5(3)	2521.7(3)	$31/2^-$	$27/2^-$	3.2(2)	1.08(8)		0.87(20)	$E2$
495.7(4)	4824.5(4)	51/2	49/2	0.4(1)	0.47(2)			D
498.6(4)	2528.8(4)	29/2	$27/2^-$	0.7(1)	0.48(6)			D
501.4(2)	2802.6(2)	$33/2^-$	$29/2^-$	8.4(4)	1.07(8)	2.12(22)	0.85(21)	$E2$

TABLE I. (*Continued.*)

E_γ (keV)	E_i (keV)	I_i^π	I_f^π	I_γ	$R_{\rm DCO}^Q$	$R_{\rm DCO}^D$	P	Multipolarity
506.8(1)	1173.5(2)	$19/2^-$	$15/2^-$	37.0(19)	1.04(6)	1.82(10)	0.69(17)	$E2$
513.4(5)	1732.1(6)	$21/2^{(-)}$	$17/2^-$	0.4(1)				
520.8(4)	2132.5(4)	25/2	$23/2^-$	0.7(1)	0.54(3)			D
522.5(3)	1218.3(4)	$17/2^-$	$13/2^-$	1.6(2)		2.06(25)		Q
528.7(4)	2829.9(4)	33/2	$29/2^-$	0.8(1)	0.86(13)			Q
539.6(1)	539.6(3)	$13/2^+$	$9/2^+$	100.0(52)	0.94(5)	1.86(1)	0.49(13)	$E2$
566.4(4)	2178.1(4)		$23/2^-$	2.1(1)				
570.3(4)	1266.0(4)		$13/2^-$	0.8(1)				
600.4(1)	931.1(5)	$15/2^+$	$11/2^+$	28.2(15)	0.90(5)		0.50(14)	$E2$
637.7(4)	3440.3(4)		$33/2^-$	0.9(1)				
641.8(3)	3163.5(3)	35/2	$31/2^-$	1.9(1)	0.89(5)			Q
648.2(4)	1821.7(4)	21/2	$19/2^-$	0.8(1)	0.54(5)			D
670.2(4)	1365.9(4)	17/2	$13/2^-$	1.0(1)		1.78(28)		Q
739.1(3)	3133.2(3)	$35/2^+$	$33/2^-$	3.0(1)	0.51(4)	0.82(9)	0.33(13)	$E1$
788.2(3)	3182.3(7)	35/2	$33/2^-$	1.1(1)	0.57(3)			D
826.7(3)	2723.3(3)	31/2	$27/2^+$	1.4(1)	0.81(10)			Q
864.1(1)	3258.2(1)	$37/2^-$	$33/2^-$	16.4(8)	1.04(6)	1.77(14)	0.93(41)	$E2$
881.2(4)	3182.3(7)	35/2	$29/2^-$	0.8(1)				

[a]Intensity range on the basis of total intensity balance at the $29/2^-$ and $33/2^-$ states assuming the $E2$ multipolarity of the 93-keV transition.
[b]γ-ray energy from the difference of corresponding level energies; centroid of the γ ray could not be unambiguously determined due to strong close lying transitions.
[c]From intensity balance considerations.
[d]$\delta = 6.1(3.6)$; large error in the δ value can be attributed to the contribution of both systematic and statistical uncertainties in the $R_{\rm DCO}$ value.

observed in the present work and previous high-spin studies [18–21]. Figure 2 illustrates the γ rays in coincidence with the 540-keV transition. In addition to the several new transitions, most of the γ rays reported in the previous high-spin studies have been identified in this coincidence spectrum. Furthermore, it was observed that the deduced level structures from the present data are consistent with the reported ground-state "A" and negative-parity "B" sequences [18,20,21]. The level scheme of ^{217}Ra is particularly complex due to presence of several doublets in this nucleus. The 331-keV γ ray is also a doublet and is observed to be in coincidence with its doublet counterpart 330-keV transition. Thus, to determine the multipolarity of the 331-keV transition, the γ rays in a parallel decay path with respect to the 330-keV γ ray were used as the gating transitions. The measured $R_{\rm DCO}$ and polarization values (see Table I) indicate the mixed dipole + quadrupole ($E1 + M2$ or $M1 + E2$) nature of the 331-keV transition. Therefore, to determine the true character of the transition, mixing ratio calculations were performed. As discussed in Sec. II, the mixing ratio for a transition of interest is determined by comparing the theoretical and experimental $R_{\rm DCO}$ and linear-polarization values. The theoretical values of the $R_{\rm DCO}$ and linear polarization were computed as a function of mixing ratio. Here, the theoretical contours were obtained by assuming both the positive and negative parity for the 331-keV state. The experimental point for the 331-keV γ ray is observed to be equidistant to both these contours (see Fig. 3). The comparison of the experimental data point with the contour for the $M1 + E2$ multipolarity suggests a mixing ratio value of 6.1(36), which corresponds to ≈97% $E2$ component in the 331-keV transition. Another possibility is that the 331-keV γ ray is an $E1 + M2$ transition with ≈94% $M2$ component [$\delta = 3.8(8)$]. The Weisskopf estimate for an $E1 + M2$ transition with dominant $M2$ component suggests a half-life of ≈75 ns for the 331-keV state. However, the *early-delayed* analysis does not indicate the isomeric nature of the 331-keV state. Thus, the possibility of the 331-keV γ ray being an $E1 + M2$ transition with a dominant $M2$ component can be excluded. The present analysis suggests a mixed $M1 + E2$ multipolarity for the 331-keV γ ray and, consequently, a spin-parity of $11/2^+$ to the 331-keV state. The deduced spin-parity of the 331-keV state is consistent with the previous

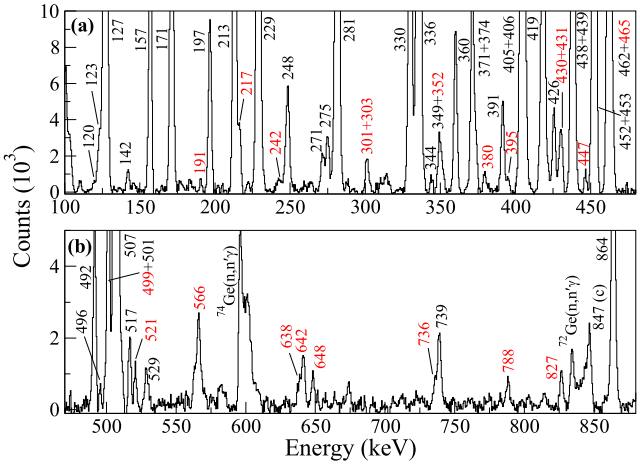


FIG. 2. Coincidence γ-ray spectra illustrating transitions in the gate of the 540-keV γ ray. The new transitions are labeled with red color. The contaminant line marked with (c) is from the reaction of the beam with the Fe target frame.

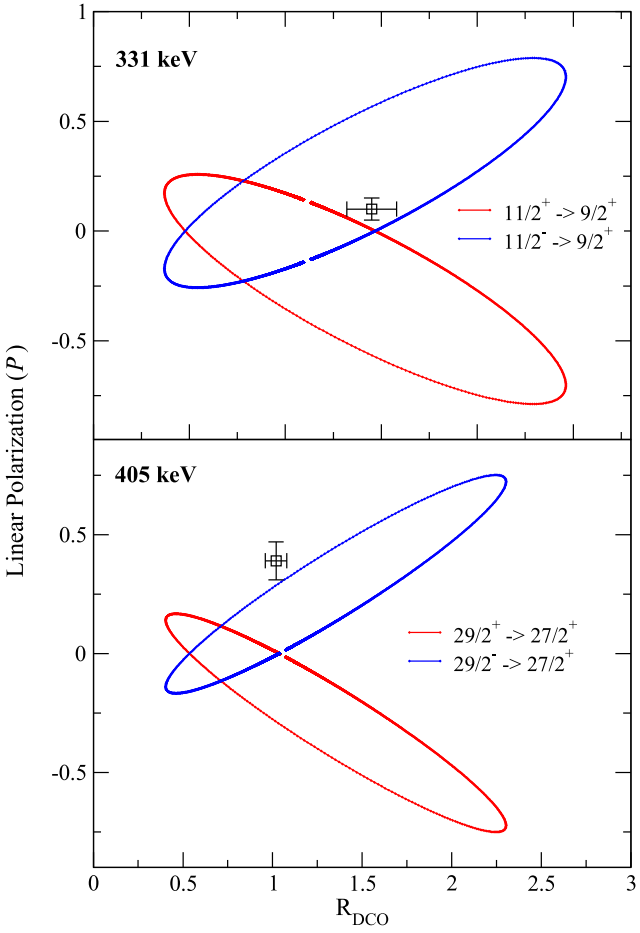


FIG. 3. Theoretical contours illustrating the calculated $R_{\rm DCO}$ and linear-polarization values (P) as a function of mixing ratio (δ), along with the experimental data points, for the 331- and 405-keV transitions.

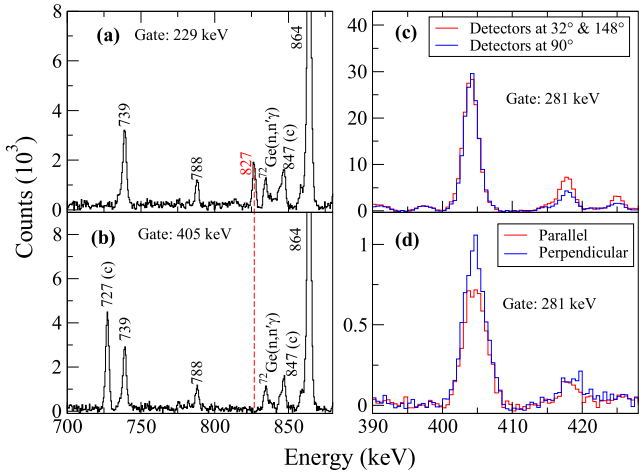


FIG. 4. Evidence for the placement and multipolarity of the 405-keV transition. Panels (a) and (b) illustrate the γ rays in coincidence with the 229- and 405-keV transitions, respectively. The presence/absence of the 827-keV γ ray is indicated. The contaminant peaks marked with (c) are from ^{56}Fe and ^{212}Po. Panel (c) shows a part of the representative gated γ-ray spectrum for the $R_{\rm DCO}$ measurements of the 405-keV γ ray, and panel (d) shows the counts in the parallel and perpendicular crystals of the 90° detectors reflecting the electric nature of the 405-keV transition.

assignments from the γ-ray and conversion-electron spectroscopic studies [18–21]. In addition, Sheline *et al.* [40] had also suggested the same spin-parity for the 331-keV state based on the measured hindrance factors and the reflection-asymmetric model.

Similarly, the states up to $23/2^+$ were established and the observed level structure was found to be in agreement with that reported in the earlier studies. The γ-γ coincidence relationships suggest the presence of 229- and 405-keV transitions above the $23/2^+$ state. However, their relative ordering was found to be inconsistent in Refs. [18,21]. Roy *et al.* [18] placed the 229-keV transition below the 405-keV γ ray on the basis of the presence of a prompt component in the time spectrum of the 229-keV transition. However, the ordering of these two transitions was reversed and a $25/2^+$ state at 2.1 MeV energy was introduced in the level scheme proposed in Ref. [21]. In our work, a new 827-keV γ ray was identified in the gates of all the transitions below the 1668-keV state. A comparison of the gates of the 229- and 405-keV transitions, shown in Figs. 4(a) and 4(b), clearly reflects the coincidence between the 229- and 827-keV transitions. Furthermore, the placement of the 827-keV γ ray is supported by the presence of the 410- and 374-keV γ rays in the gate of the 827-keV transition. Thus, the relative ordering of the 229- and 405-keV transitions and a $27/2^+$ state at 1897 keV were confirmed.

The $R_{\rm DCO}$ values for the 405-keV γ ray in the gate of stretched dipole and quadrupole transitions [see Table I and Fig. 4(c)] unambiguously suggest its $\Delta I = 1$ character, which is also in agreement with the adopted [38] dipole nature of the transition based on the earlier angular distribution measurements [18,19]. Therefore, commensurate with the observed intensity of the 405-keV transition and the underlying reaction mechanism, we assign $I = 29/2$ to the 2301-keV state. Furthermore, the linear-polarization measurements clearly indicate the electric nature of the transition. The deduced $E1$ multipolarity of the 405-keV γ ray is in contrast to its previously assigned $M1 + E2$ character with the dominant $E2$ component [18]. Although the present data unambiguously suggest a $I^\pi = 29/2^-$ to the 2301-keV state, the resulting variance with the previously reported assignments entailed us to further confirm the nature of the 405-keV transition using the mixing ratio calculations. The theoretical $R_{\rm DCO}$ and linear-polarization values were computed by assuming both the positive and negative parity of the 2301-keV state (see Fig. 3). It is apparent that the experimental data point is closer to the theoretical contour corresponding to the $E1 + M2$ multipolarity and the point of intersection of the experimental data point on the contour suggests a near zero δ value. This further corroborates the pure $E1$ nature of the 405-keV γ ray and a spin-parity of $29/2^-$ for the 2301-keV level.

Figures 5(a) and 5(b) illustrate the γ rays in the gate of 864- and 501-keV transitions, respectively. It is evident that both these γ rays are in coincidence with all the transitions below

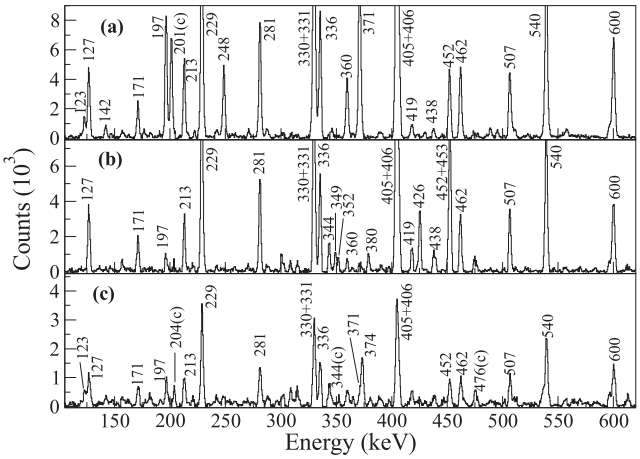


FIG. 5. γ-ray coincidence spectra illustrating transitions in the gate of the (a) 864-, (b) 501-, and (c) 739-keV transitions. The contaminant peaks marked with (c) are mainly from ^{65}Zn and ^{216}Ra.

the $29/2^-$ state. Therefore, the 864- and 501-keV transitions can be placed directly above the $29/2^-$ level. However, an isomeric state [$T_{1/2} = 4.62(6)$ ns] with $I^\pi = 33/2^+$ was identified at 2.4 MeV excitation energy and the 864-keV γ ray was placed above the isomer in the previous studies [18,20,38,39]. Also, it was reported that the $33/2^+$ isomer deexcites via a 93-keV $E2$ transition. Figure 6 shows the coincidence spectra observed in LEPS gated by the γ rays recorded in the clover detectors. The presence of the 93-keV γ ray in the gate of the 864-keV transition [Fig. 6(a)] is in agreement with the previous placement of these transitions. Furthermore, in the earlier work, the 93-keV γ ray was assigned $E2$ character on the basis of conversion-coefficients measurements [18]. Considering the observed intensity (see Fig. 6) and the theoretical conversion-coefficients for the possible multipolarity ($E1$, $M1$, $E2$, $M2\ldots$) of the 93-keV γ ray, the present data also supports its $E2$ multipolarity. Since the present measure-

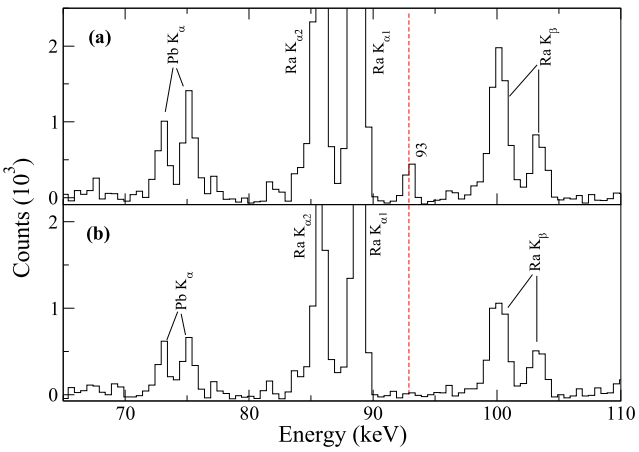


FIG. 6. Coincidence γ-ray spectra observed in the LEPS gated by the (a) 864- and (b) 501-keV γ rays recorded in the clover detectors.

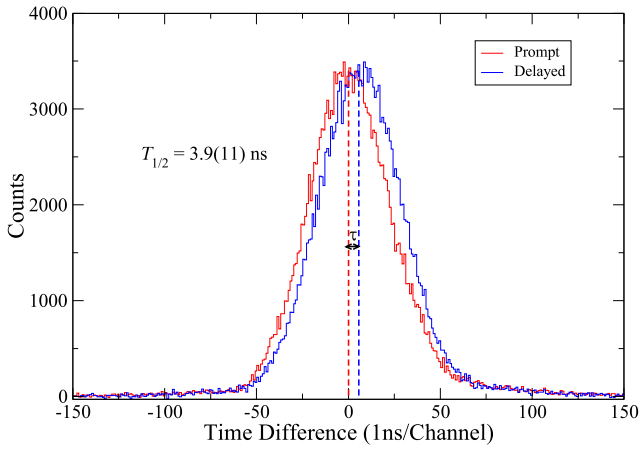


FIG. 7. Centroid-shift analysis to determine the cumulative half-life of the 2301- and 2394-keV states. The blue curve for the time difference between the 864- and 405-keV γ rays is compared with the time difference spectrum obtained using prompt transitions of similar energies. The difference between the centroids of the prompt and delayed distributions gives the cumulative mean life of the states.

ments have assigned the $I^\pi = 29/2^-$ to the 2301-keV state, a spin-parity of $33/2^-$ is deduced for the state at 2394 keV excitation energy.

Furthermore, the half-life of the 2394-keV state has been revisited using the centroid-shift analysis. In our work, the cumulative half-life of the 2301- and 2394-keV states was determined from the time difference between the 864- and 405-keV γ rays. The blue curve in Fig. 7 shows the time difference between the 864- and 405-keV γ rays which is compared with the time difference spectrum (in red color) of prompt transitions with similar energies. It is to be noted that the time difference spectra used for the comparison are generated after taking proper background subtraction into account. The cumulative half-life of the 2301- and 2394-keV states is deduced to be 3.9(11) ns which is found to be consistent with the adopted value of 4.62(6) ns for the 2394 keV state [38]. This suggests that the measured cumulative half-life is mainly due to the half-life of 2394-keV level. The error quoted in the half-life is obtained by adding the systematic and statistical errors in quadrature. The systematic error includes contributions from the discrete binning along the time axis and the uncertainty arising due to shift in the centroid of the prompt distribution of two similar energy transitions.

Furthermore, the placements of the 501- and 739-keV transitions were found to be at variance in Refs. [20,21]. The absence of the 93-keV transition in the gate of the 501-keV γ ray [Fig. 6(b)] confirms the placement of this transition as demonstrated in the present level scheme. Similar method could not be adopted to confirm the placement of the 739-keV γ ray owing to its weak intensity. However, the presence of the 123-, 197-, and 374-keV transitions in Fig. 5(c) confirms the placement of the 739-keV γ ray as shown in the Fig. 1. Similar analysis techniques were employed to confirm the remaining level structures reported in the earlier works.

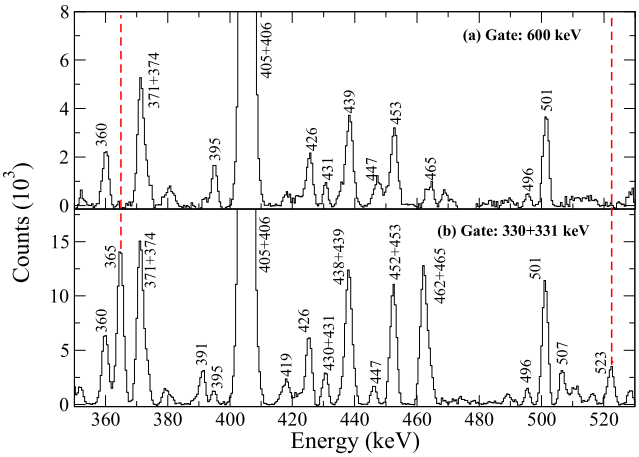


FIG. 8. A part of the coincidence γ-ray spectra in the gate of the (a) 600-keV transition and (b) 330-331 keV doublet. The presence/absence of the 365-keV transition is indicated.

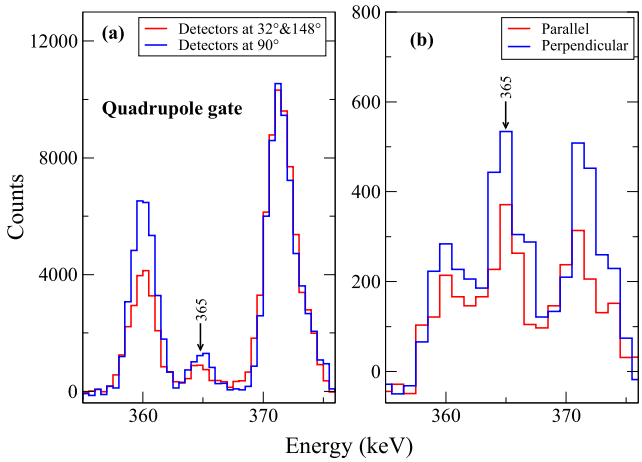


FIG. 10. Representative spectra corresponding to the (a) R_{DCO} and (b) polarization measurements of 365-keV transition.

B. Evidence of parity doublets in ^{217}Ra

Along with the two positive-parity and a negative-parity sequences below the isomer, a 1050-keV state was established on the basis of coincidence between 287- and 119-keV γ rays in the earlier studies [18,20,21]. In addition, a 365-keV transition was tentatively placed above the 1050-keV level in the work of Roy *et al.* [18]. However, in Ref. [21] the 365-keV transition was observed to deexcite the proposed $13/2^+$ state at 696 keV energy. Figure 8 illustrates the coincident transitions in the gates of the 600- and 331-keV transitions. If the placement by Roy *et al.* [18] was correct, then the 600-keV transition should have been in the coincidence with the 365-keV γ ray. However, the absence of the 365-keV γ ray and a newly observed 523-keV transition in Fig. 8(a) clearly suggest that these transitions are parallel to the 600-keV γ ray.

Figure 9 shows the transitions in the gates of the 365- and 523-keV γ rays and confirms the coincidence relationship between these transitions. The placement of the 365- and 523-keV γ rays, as indicated in the Fig. 1, is based on the observed coincidences and intensity considerations. Furthermore, the absence of the 287-keV transition in Fig. 9(a) indicates that the ordering of the 287- and 120-keV transitions as suggested in Refs. [18,20,21] should be reversed. Similar coincidence relationships were utilized to secure the placement of newly identified 395- and 513-keV transitions which, in turn, establishes a state at 1732 keV excitation energy.

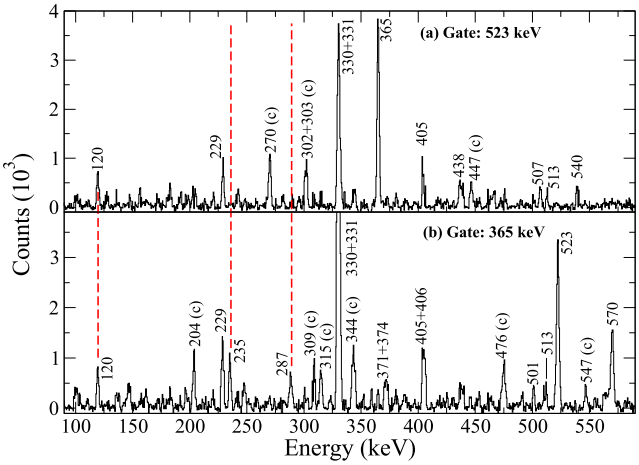


FIG. 9. A part of the coincidence γ-ray spectra illustrating transitions in the gate of the (a) 523- and (b) 365-keV γ rays provide evidence for reordering the 287- and 120-keV transitions. The contaminant peaks marked with (c) are mainly from ^{214}Rn and ^{216}Ra.

Furthermore, the R_{DCO} and linear-polarization values of the observed transitions were utilized to assign the spin-parities to the newly established states. In the gate of the 229-keV γ ray, which is a stretched $\Delta I = 2$ transition, the R_{DCO} value for the 365-keV transition is found to be 0.53(8) (see Fig. 10(a) and Table I). This suggests the dipole character of the 365-keV transition. Figure 10(b) illustrates a part of the representative spectra for the polarization measurements and higher counts in the spectrum corresponding to the perpendicular scatterings with respect to the reaction plane clearly indicates the electric nature of the 365-keV γ ray. Thus, a spin-parity of $13/2^-$ is assigned to the 696-keV state. Furthermore, the measured DCO ratios for the 287- and 523-keV transitions and polarization values for the 287-keV γ ray suggest the spin-parity of $17/2^-$ for the 1218-keV level. Similarly, the R_{DCO} measurements for the 395-keV transition suggests $I = 21/2$ for the 1732-keV state. However, the electric/magnetic character of the transitions depopulating the 1732-keV state could not be determined due to poor statistics. The negative parity of the $21/2$ state is tentatively assigned on the basis of striking similarity in the observed low-lying structures of ^{217}Ra and ^{219}Th [13]. As discussed in Sec. I, parity-doublet structures are a signature of octupole correlations in odd-A and odd-odd nuclei. Thus, the newly established negative-parity sequence provides an experimental evidence of parity doublets in ^{217}Ra and reflects the expected similarity in the structures of the transitional $N = 129$ isotones. Similar analysis techniques were employed to determine the placement and multipolarity of the remaining newly identified γ rays, wherever possible.

The present data also suggest a few unobserved transitions in the level scheme based on the γ-γ coincidences. The coincidence relationships of the 501- and 529-keV γ rays with the 426-keV and other higher-lying transitions indicate the presence of an unobserved 27-keV transition between the 2830- and 2803-keV states. Similarly, the coincidences of the 197- and 360-keV transitions with the γ rays below the 3599-keV state suggest an unobserved 30-keV transition between the $41/2^-$ state and $41/2$ state at 3599 keV energy. Also, the coincidence relationship between the 739- and 371-keV γ rays requires a 125-keV transition, which has been reported in earlier studies [18,20], between the 3258- and 3133-keV states. The centroid and intensity information of the 125-keV transition could not be determined due to the presence of stronger close-lying 123- and 127-keV transitions. Moreover, the 465- and 642-keV transitions are observed to be in coincidence with the 405-keV γ ray and the transitions of sequence "C". This suggests that the $31/2^-$ state deexcites to the the low-lying $29/2^-$ and/or $33/2^-$ states, via weak unobserved transitions.

Several new transitions (viz. 191-, 242-, 301-, 303-, 736-, 859-, 968-keV), which were assigned to ^{217}Ra in the present study, could not be unambiguously placed in the level scheme. These transitions are observed to be in coincidence with all the γ rays below the $29/2^-$ state. However, due to their weak intensities and/or the lack of firm coincidence relationships with the other known γ rays above the $29/2^-$ state, the placement of these transitions could not be ascertained. Furthermore, the present data also suggest a doublet character of the 517-keV transition. One component of the 517-keV doublet is placed between the $25/2^{(+)}$ and $21/2^+$ states, whereas the coincidence relationships suggest the placement of the second 517-keV γ ray above the $29/2^-$ level. In Ref. [20], the 517-keV transition was reported to deexcite the 3259-keV state and populate the 2301-keV level via a 440-keV transition. However, due to absence of a transition at 440 keV and other suitable coincidences of the 517-keV transition above the $29/2^-$ level, the placement of the second 517-keV γ ray remains inconclusive in the present work, similar to the several transitions mentioned above.

C. Intensity measurements

The relative intensities of the observed γ rays were determined using the data collected at 72 MeV beam energy. The data acquired in the single fold were utilized to obtain the intensity information for the strong, noncontaminated (viz. 540-, 229-, 213-, and 462-keV) γ rays. The intensities of all the transitions observed in ^{217}Ra were normalized with respect to that of the 540-keV γ ray, which is assumed to be 100. Due to the presence of several doublets in the level scheme, suitable approaches were employed to determine the relative intensities of the observed γ rays. The 331-keV transition, which directly feeds the ground state, has also been identified as a doublet. Therefore, the intensities of the transitions parallel to the 330-keV ($23/2^+ \rightarrow 19/2^+$) γ ray were obtained in the efficiency corrected summed gate of 540- and 331-keV transitions and normalized with respect to the relative intensity of the 213-keV γ ray. A few transitions, which are in a parallel decay path with respect to the 330-keV γ ray, such as 452-, 438-, and 360-keV, were also identified as doublets. Since the doublet counterparts of these transitions are placed above the isomer and are in coincidence with both the 330- and 331-keV γ rays, their intensities could not be determined in the summed gate of the 540- and 331-keV transitions.

In order to determine the intensities of transitions which are in coincidence with both the γ rays of 330–331 keV doublet, it was important to extract the individual intensity of the 331-keV transition. It may be noted that the 540-keV transition is in coincidence with only the 330-keV γ ray. Therefore, the intensity of the 330-keV transition was determined in the gate of 540-keV γ ray and normalized with respect to the relative intensity of 462-keV γ ray. The relative intensity thus obtained was further corrected for the decay branch of the $19/2^+$ state using the relative intensity of the 395-keV transition. The total intensity of 330–331 keV doublet was determined from the single fold data. Thus, the relative intensity of the 331-keV transition was deduced after subtracting the contribution of the 330-keV γ ray from the summed total relative intensity of the doublet line. Once the relative intensity of the 331-keV γ ray was known, the intensities of the transitions above the $23/2^+$ state were extracted from the efficiency and branching corrected 540-keV gate and normalized with respect to the intensity of the 462-keV γ ray. It may be noted that the relative intensities of the noncontaminated transitions could also be determined in the efficiency corrected summed gate of the 540-, 209-, 365-, and 600-keV γ rays and normalized with respect to that of the 229-keV transition. It was observed that the intensities of the noncontaminated transitions obtained from the above two approaches were consistent with each other.

In order to resolve the doublets, wherever possible, appropriate methods were employed. For example, the total intensity of the 452-453 keV doublet was determined using the singles data. The gate of the 281-keV transition, which is in a parallel decay path with respect to the 452-keV ($21/2^+ \rightarrow 17/2^+$) γ ray, was utilized to find the relative intensity of the 453-keV transition lying above the isomer. The deduced intensity was then normalized with respect to the relative intensity of the 501-keV transition. Further, the intensity of the 452-keV γ ray was extracted by subtracting the contribution of the 453-keV transition from the doublet line. Similarly, suitable coincidence relationships were utilized to determine the intensities of the transitions in the remaining doublets.

The above discussion includes the information on the intensity measurements of all transitions except for the γ rays of the newly established negative-parity sequence. The branching ratio of the 120- and 406-keV γ rays, measured in the gate of the 395-keV transition, was utilized to deduce the relative intensity of the 120-keV transition. Furthermore, the intensity of the 287-keV transition was obtained in the 600-keV gate and normalized with respect to the relative intensity of the 406-keV transition. The branching of the 287- and 523-keV γ rays in the 120-keV gate was determined to extract the intensity of the 523-keV transition. The relative intensities of the 235-, 570- and 670-keV transitions were extracted in the gate of the 365-keV γ ray and were normalized with respect to that of the 523-keV transition. Finally, the intensity of the

365-keV γ ray was obtained in the gate of the 330-331 keV doublet and the relative intensity of the 523-keV γ ray was used for normalization.

IV. DISCUSSION

As discussed in Sec. I, ^{217}Ra with $Z = 88$ and $N = 129$ lies in the transitional region between the spherical and static octupole-deformed nuclei. The earlier reported low-lying sequences starting with $9/2^+$, $11/2^+$, and $15/2^-$ states were qualitatively understood in terms of mainly the shell-model configurations viz. $\nu g^3_{9/2}$, $\nu g^2_{9/2} i_{11/2}$, and $\nu g^2_{9/2} j_{15/2}$, respectively [18]. Although these sequences were reported to terminate at the spins predicted by the above mentioned configurations, the almost constant level spacings observed in the ground-state and negative-parity sequences along with the strong $E1$ connecting transitions reflected the contribution of collective degrees of freedom in this nucleus. In the present work, a new negative-parity sequence has been established along with the above mentioned three sequences. The addition of this newly established negative-parity sequence hints at the parity-doublet structures in ^{217}Ra, which are expected in a odd-A nucleus displaying octupole correlations. Furthermore, the two alternating-parity sequences established in ^{217}Ra are characterized by the simplex quantum number (s) [41]. It is known that for even-A nuclei the sequences $0^{\pm}$, $1^{\mp}$, $2^{\pm}$, $3^{\mp}$, $4^{\pm}$, ... are associated with the $s = \pm 1$ quantum number, respectively. In the case of odd-A nuclei, $s = \pm i$ is assigned to the $1/2^{\pm}$, $3/2^{\mp}$, $5/2^{\pm}$, $7/2^{\mp}$, $9/2^{\pm}$, ... sequences, respectively.

The properties of the observed simplex bands in ^{217}Ra are compared with those of the similar bands in the neighboring nuclei. The energy splitting, which is defined as the difference between the excitation energies of the states of same spin but opposite parity/simplex, indicates the strength of octupole correlations in a given nucleus. Ideally, a near zero splitting is expected in the nuclei with static octupole deformation. In the case of ^{223}Th ($Z = 90$ and $N = 133$), an average energy splitting of $\approx$30 keV is observed which suggests a stable deformation in this nucleus [42]. However, the large average energy splitting ($\approx$190 keV) in ^{217}Ra [see Fig. 11(a)] indicates that the static octupole deformation has not set in this transitional nucleus. Figure 12 illustrates the variation of the initial spin with rotational frequency for the $s = +$ i(+1) band in ^{217}Ra and neighboring nuclei. This relation generally indicates the extent of rotation-like behavior in a nucleus. It may be noted that the $I(\omega)$ pattern for ^{217}Ra is consistent with the almost constant level spacings in the ground-state $E2$ sequence. Also, the similarity in the $I(\omega)$ trend observed in all the $N = 129$ isotones suggests that the addition/removal of a proton in the $h_{9/2}$ orbital does not significantly influence the dependence of excitation energy on the spin. Furthermore, the comparison of the observed $I(\omega)$ for the $N = 129$ and $N = 131$ isotones clearly suggests that the excitation energy of the states better resembles with the behavior expected for typical rotational bands with the increase in neutron number. This, in turn, indicates that the quadrupole deformation in this region is more sensitive to the number of valence neutrons outside the shell closure.

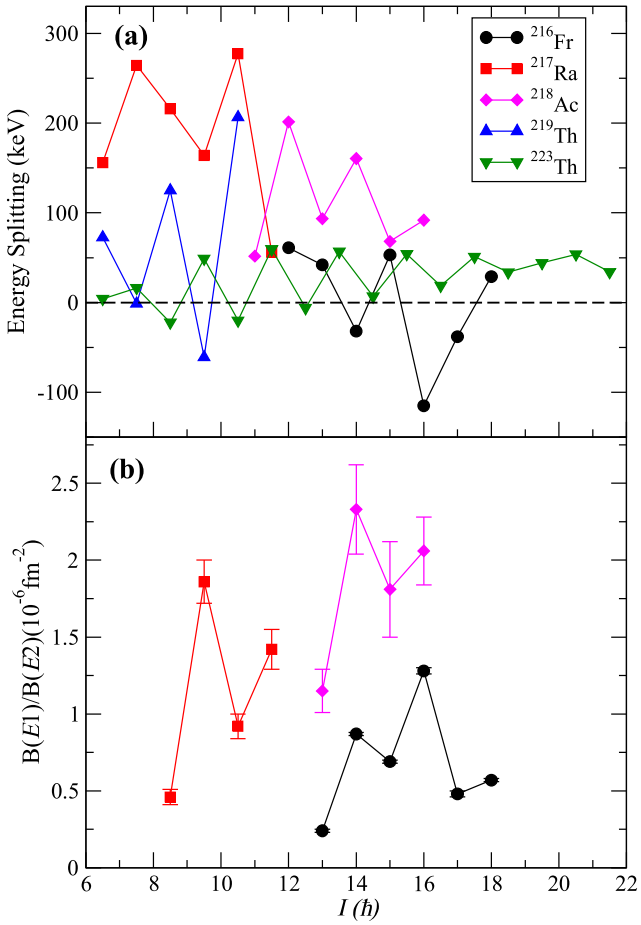


FIG. 11. Comparison of the (a) energy splitting [E(s=$-i$/$-$1)$-$E($s = +i/+1$)] and (b) B($E1$)/B($E2$) ratios versus initial spin for the transitions of $s = +i$ band in ^{217}Ra with $N = 129$ isotones (^{216}Fr, ^{218}Ac, ^{219}Th). The data are taken from Refs. [13,25,26] and the present work.

Furthermore, the experimental B($E1$)/B($E2$) ratios were extracted using the measured γ-ray intensities. The deduced ratios are of the order of $\approx 10^{-6}$ fm^{-2} which are consistent with the benchmark values if octupole correlations are present in a nucleus. It is apparent from Fig. 11(b) that the B($E1$)/B($E2$) ratios for the negative-parity states lie higher than that for the positive-parity states in ^{217}Ra, whereas the converse is true for the odd-odd (^{216}Fr, ^{218}Ac) nuclei. In a stable octupole deformed nucleus, the strengths of the electric dipole transitions [$I^{\pm} \rightarrow (I-1)^{\mp}$] should be independent of the parity of the initial state [14]. However, the $E1$ transitions originating from the positive parity states are forbidden in the framework of a pure vibrational model [14,26]. As the unpaired proton and neutron occupies the $h_{9/2}$ and $g_{9/2}$ orbitals, respectively, the higher ratios for the negative (positive) parity state in odd-A (odd-odd) nuclei are consistent with an intermediate behavior between the extremes discussed above. It is important to note that the staggering in the B($E1$)/B($E2$) ratios can only be related to the staggering in the B($E1$) values if a constant quadrupole deformation is assumed. Therefore, to understand the actual variation of reduced transition

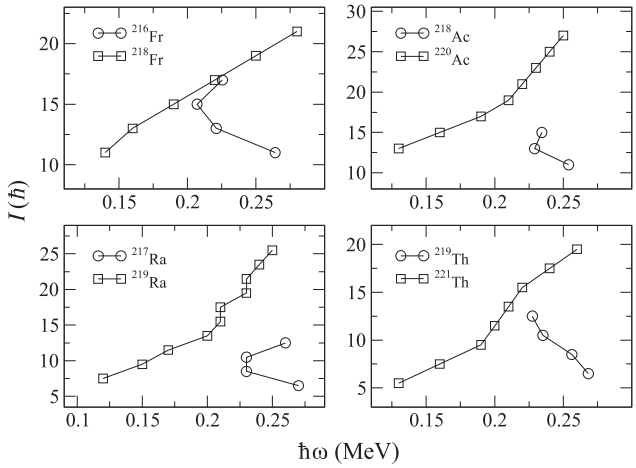


FIG. 12. Systematics of the spin (I) versus rotational frequency [$\hbar\omega(I) = [E(I) - E(I-2)]/2$] for the lowest lying sequence of the $s = +i/+1$ bands in the $N = 129$ and 131 isotones with $87 \leqslant Z \leqslant 90$ [13,25,26,43–46].

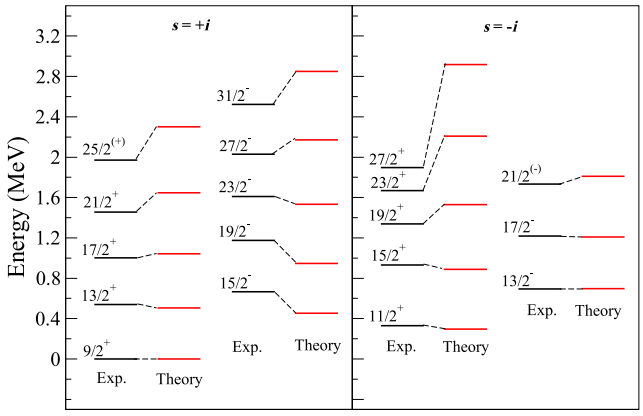


FIG. 13. Comparison of the experimental results with the predictions of the RAT-PRM calculations for the simplex bands in ^{217}Ra.

probabilities and their corresponding ratios with angular momentum, measurements for determining the lifetimes of the states are required.

From the above discussion on the energy splitting, $I(\omega)$, and B($E1$)/B($E2$) ratios, it is evident that the quadrupole and octupole deformations are not fully developed in the ^{217}Ra. However, the newly established parity-doublet structures are a clear indication of octupole correlations in this nucleus. Therefore, for a more quantitative understanding, theoretical calculations including octupole degrees of freedom were performed using reflection-asymmetric triaxial particle rotor model (RAT-PRM) [47]. Recently, RAT-PRM has also been employed to investigate a possibility of coexistence of nuclear chirality and octupole correlations in the form of multiple chiral bands [48–51].

The quadrupole and octupole deformation parameters are taken as input in the RAT-PRM calculations. In the case of ^{217}Ra, the corresponding $\beta_2 = 0.05$ and $\beta_3 = 0.08$ were adopted from the Ref. [52]. With these deformation parameters, the reflection-asymmetric Hamiltonian was solved by expanding the wave function in harmonic oscillator basis [53]. The single-particle space available to the odd nucleon was truncated to include six levels, each above and below the Fermi surface. The pairing correlation was taken into account by an empirical pairing gap formula $\Delta = 12/\sqrt{A}$ MeV. For the core part, a spin-dependent moment of inertia $\mathcal{J}_0 = (3.1 + 1.24I)\ \hbar^2$/MeV and the core parity-splitting parameter E(0^-) = 2.0 MeV were used. Also, the Coriolis attenuation parameters ($\xi^{\pm}$) for the positive and negative parity states were taken to be 0.7 and 1, respectively. In addition, the electromagnetic transition probabilities were calculated by assuming intrinsic dipole moment and quadrupole moments $0.0006{*}AZe\beta_2\beta_3$ and $(3/\sqrt{5\pi})R_0^2Z\beta_2$, respectively [54,55].

The energies calculated from the RAT-PRM calculations for the $s = +i$ and $s = -i$ bands are compared with the experimental excitation energies in Fig. 13. The calculated energies for the positive-and negative-parity states are shifted to coincide with the experimental energy of $9/2^+$ and $13/2^-$ states, respectively. It is observed that the results of the calculations are in good agreement with the experimental energies up to $I^\pi = 21/2^+$ for the positive-parity states and $I^\pi = 27/2^-$ for the negative-parity states. The deviation between the calculated and experimental energies at higher angular momentum may be attributed to the fact that the vibrational effects could not be included in the present RAT-PRM calculations.

Since ^{217}Ra is a odd-N nucleus, the main components of the intrinsic wave functions of the states are dominated by the neutron configurations. As the RAT-PRM calculations include a finite β_3, the intrinsic parity is not a good quantum number and the neutron $g_{9/2}$ and $j_{15/2}$ orbitals mix with each other. The main components of the intrinsic wave functions were expanded in the strong-coupled basis $|IMK\rangle\ \chi^\nu$ (denoted as $|K, \nu\rangle$ for short), where $|IMK\rangle$ is the Wigner function with I, M, and K denoting the quantum numbers of the total angular momentum and its projections along the third axis in the laboratory frame and intrinsic frame, respectively, and χ^ν represents the intrinsic wave function of the neutron single-particle level $|\nu\rangle$. The neutron single-particle levels $|1\rangle$, $|2\rangle$, $|3\rangle$, $|4\rangle$ and $|5\rangle$ predominately involve $g_{9/2}$ orbital with different $\Omega = 9/2, 7/2, 5/2, 3/2$, and $1/2$, respectively (see Table II).

Figures 14 and 15 illustrate the main components of the wave functions for the positive- and negative-parity states of the $s = \pm i$ bands, respectively. It may be noted that the components corresponding to different neutron single-particle levels strongly mix with each other. Furthermore, it is known

TABLE II. The main components $l_{j\Omega}$ of the neutron single-particle levels $|\nu\rangle$ with $\nu = 1, 2, 3, 4$, and 5.

$\|\nu\rangle$	Main components of the neutron single-particle levels
$\|1\rangle$	$0.948\ g_{9/2,9/2} + 0.022\ h_{11/2,9/2} + 0.022\ j_{15/2,9/2} + ..$
$\|2\rangle$	$0.902\ g_{9/2,7/2} + 0.055\ j_{15/2,7/2} + 0.018\ f_{7/2,7/2} + ..$
$\|3\rangle$	$0.878\ g_{9/2,5/2} + 0.076\ j_{15/2,5/2} + 0.010\ i_{13/2,5/2} + ..$
$\|4\rangle$	$0.810\ g_{9/2,3/2} + 0.087\ j_{15/2,3/2} + 0.031\ p_{3/2,3/2} + ..$
$\|5\rangle$	$0.755\ g_{9/2,1/2} + 0.093\ j_{15/2,1/2} + 0.067\ p_{3/2,1/2} + ..$

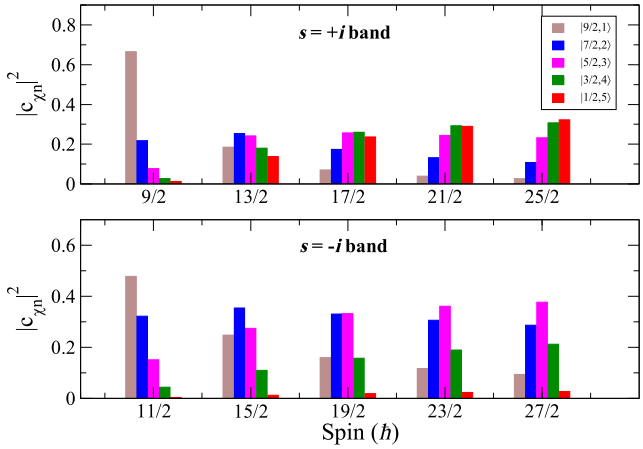


FIG. 14. The probability amplitudes of the main components of the intrinsic wave functions for the positive-parity states of the $s = \pm i$ bands in ^{217}Ra.

that the strong Coriolis effects for the low Ω orbitals result in lowering the energies of the states which have dominant contribution from such orbitals [56]. A comparison of the relative contribution of the single-particle levels with different Ω values in the wave functions of the positive-parity states (see Fig. 14) suggests that the states in $s = +i$ band are more favored than the corresponding states in $s = -i$ band. This is in agreement with the experimental observations and is reflected in the staggering parameters [S(I) = [E(I)-E($I-1$)]/2I] of the positive-parity states in Fig. 16(a). Similarly, it is observed that the single-particle level $|5\rangle$ ($\Omega = 1/2$) significantly contributes to the wave function of all the negative-parity states of $s = +i$ band. However, the negative-parity states of the $s = -i$ band have a dominant contribution from the $\Omega = 5/2$ orbital. The effect of the Coriolis interactions suggests the lowering of energies for the states of the $s = +i$ band, which also agrees with the observed results. The large energy staggering for the negative-parity states is in agreement with the comparatively weak intensity of the newly identified negative-parity sequence.

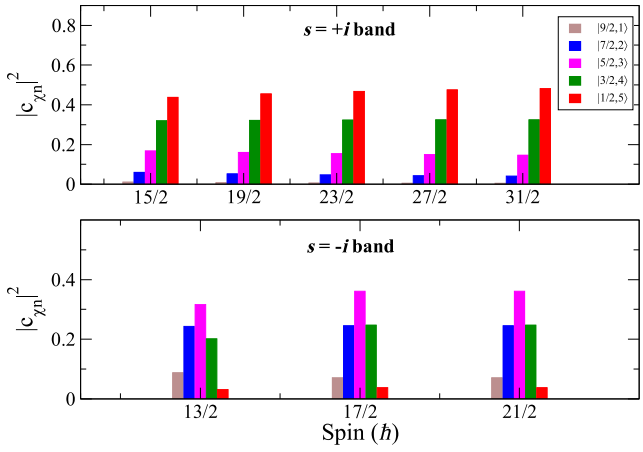


FIG. 15. Same as Fig. 14, but for the negative-parity states.

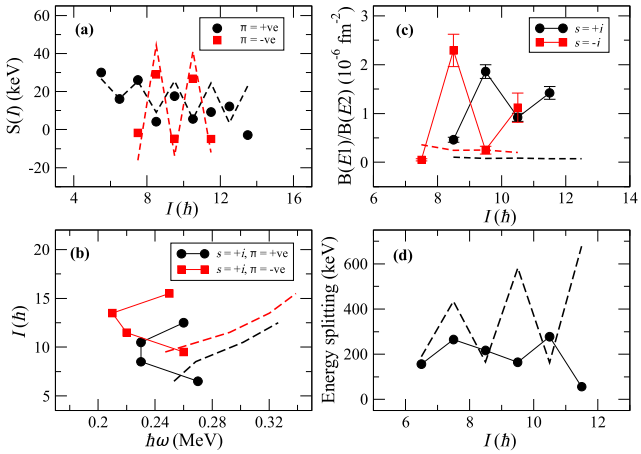


FIG. 16. Comparison of the calculated (a) energy staggering parameters [S(I)], (b) I vs $\hbar\omega$, (c) B($E1$)/B($E2$) ratios, and (d) energy splitting with the experimental results for the simplex bands in ^{217}Ra. The results of the calculations are shown with the dashed lines of the same color.

Figure 16 shows a comparison of the observed features of the simplex partner bands in ^{217}Ra with the results of the RAT-PRM calculations (dashed lines). It is evident from Fig. 16(a) that the RAT-PRM calculations are able to reproduce the phase of staggering for both the positive- and negative-parity states. Also, the calculated values are in excellent agreement with the observed staggering for the negative-parity states, whereas a good agreement is observed for the positive-parity states in the spin range $11/2\ \hbar \leqslant I \leqslant 21/2\ \hbar$. Figure 16(b) illustrates the spin (I) versus rotational frequency ($\hbar\omega$) for the $s = +i$ band. The experimental $I(\omega)$ relation for both the positive- and negative-parity states reflects the almost constant level spacing in these sequences. However, the calculated values exhibit a gradually increasing spacing between the states of the bands. Figure 16(c) shows the variation of the B($E1$)/B($E2$) ratios with spin for both the $s = \pm i$ bands and the calculated results are shown for the comparison. It may be noted that the calculated values are almost constant and significantly underestimated as compared to the observed ratios for both the simplex bands. The absence of spin-dependent staggering in the calculated ratios may be due to the fact that the vibrational effects could not be taken into account in the calculations. Furthermore, the calculated and experimental energy splittings between the states of simplex bands are compared in Fig. 16(d). It is observed that the calculated energy splittings for the parity doublets with $I = 19/2\ \hbar$ and $23/2\ \hbar$ deviate considerably from the measured ones. This is in accordance with the large difference in the calculated excitation energies for the corresponding states of the $s = \pm i$ bands (see Fig. 13). Finally, the comparison of the experimental results with the RAT-PRM predictions further corroborates the fact that the quadrupole and octupole deformation are not fully developed in ^{217}Ra and this transitional nucleus lies between the extremes of spherical and pear shaped nuclei. Also, further improvements to include the vibrational effects in the calculations are needed.

It is interesting to note that the simplex bands observed in ^{217}Ra may also be qualitatively interpreted in terms of the weak coupling of the odd nucleon to the neighboring even-even core nuclei. As discussed earlier, the observed level structures in ^{216}Ra and ^{218}Ra exhibit the dominance of single-particle and octupole degrees of freedom, respectively [15,17]. The level spacings in the ground-state positive-parity sequence "A" of ^{217}Ra exhibit a vibrational like structure which is similar to that observed in ^{218}Ra, whereas the decreasing level spacings in the second positive-parity sequence "C" suggests the coupling of the odd neutron in the $i_{11/2}$ orbital to the low-lying (0^+-8^+) states of ^{216}Ra. The corresponding negative-parity sequences may be understood as arising from the coupling of an octupole phonon to the states of these positive-parity sequences. Similar interpretation has also been employed in understanding the observed structures in ^{219}Th nucleus [13].

Furthermore, it has been pointed out that the negative-parity states in the even-even Ra isotopes ($N \geqslant 126$) reflect how the structure evolves from spherical to octupole deformed regime [58]. The lowest negative-parity state ($I^\pi = 11^-$) in the lighter Ra isotopes (viz. ^{214}Ra and ^{216}Ra) has been identified above 2.3 MeV excitation energy and interpreted as two-quasiparticle proton state arising from the $\pi(h^5_{9/2}i_{13/2})$ configuration [15,57]. On the other hand, the presence of an odd-spin negative-parity $E2$ sequence, interleaved with the ground state positive-parity band, in the heavier isotopes (viz. ^{218}Ra, ^{220}Ra) suggests the onset of octupole collectivity in these nuclei. In ^{218}Ra, a sharp discontinuity at $I^\pi = 11^-$ ($E_x = 2.1$ MeV) is observed in the alignment plot for the negative-parity states [58]. The sudden increase in the alignment above the 11^- state indicates that a band based on the two-quasiparticle proton state (11^-), observed in the lighter isotopes, crosses the yrast negative-parity band originating from octupole vibration. Also, the observed decrease in the B($E1$)/B($E2$) ratios above this state provides further evidence of noncollective effects in the higher-lying levels [58,59]. It may be noted that no features of band crossing at $I^\pi = 11^-$ were reported in ^{220}Ra [58,59]. These observations are consistent with the expected dominance of the collective effects over the single-particle degrees of freedom with the increase in the valence nucleons. Therefore, it may be suggested that the structure above the 11^- and analogous states in the even- and odd-A transitional nuclei, respectively, provide information on the development of octupole collectivity in this region. In ^{217}Ra, the alternating-parity $s = -i$ band is observed to terminate at the $27/2^+$ state and the level structure above this state seems to be dominated by the single-particle excitations. It is interesting to note that a $29/2^-$ state in ^{217}Ra is observed at the similar excitation energies as the 11^- states in ^{216}Ra and ^{218}Ra. Therefore, the $29/2^-$ state may be thought of as originating from the coupling of odd particle (hole) in the $g_{9/2}$ orbital to the 11^- states in ^{216}Ra (^{218}Ra). Furthermore, the observed structural change in ^{217}Ra above the $29/2^-$ level also corroborates the negative parity of the 2301-keV state.

The 11^- state in ^{216}Ra has the $\pi(h^5_{9/2}i_{13/2}) \otimes \nu(g^2_{9/2})$ configuration [15,39]. The addition of an extra neutron in the $g_{9/2}$ orbital results in the $\pi(h^5_{9/2}i_{13/2}) \otimes \nu(g^3_{9/2})$ configuration for the $29/2^-$ state. It may further be noted that the 13^- state in ^{216}Ra [$T_{1/2} = 0.96(20)$ ns] decays via an $E2$ transition of 344 keV to the 11^- level [16,39]. Therefore, the $33/2^-_1$ state in ^{217}Ra at 2394 keV may be realized from the coupling of the odd neutron in the $g_{9/2}$ orbital to the 13^- state in ^{216}Ra. The coupling of an extra $g_{9/2}$ neutron to the dominant configuration of the 13^- level in ^{216}Ra suggests the $\pi(h^6_{9/2}) \otimes \nu(g_{9/2}i_{11/2}j_{15/2})$ configuration for the $33/2^-$ state.

Another possibility is that the $29/2^-$ and $33/2^-$ states in ^{217}Ra originate from the coupling of odd neutron in the $j_{15/2}$ orbital to the 8^+ and 10^+ states in ^{216}Ra, respectively. The 8^+ and 10^+ states in ^{216}Ra are associated with the $\pi(h^6_{9/2}) \otimes \nu(g^2_{9/2})$ and $\pi(h^6_{9/2}) \otimes \nu(g_{9/2}i_{11/2})$ configurations, respectively [15,16]. Thus, the addition of the extra neutron in the $j_{15/2}$ orbital results in the $\pi(h^6_{9/2}) \otimes \nu(g^2_{9/2}j_{15/2})$ and $\pi(h^6_{9/2}) \otimes \nu(g_{9/2}i_{11/2}j_{15/2})$ configurations for the $29/2^-$ and $33/2^-$ states in ^{217}Ra, respectively. Similarly, the coupling of the odd neutron in the $i_{11/2}$ orbital to the 11^- state in ^{216}Ra also results in a $33/2^-$ state in ^{217}Ra with the configuration $\pi(h^5_{9/2}i_{13/2}) \otimes \nu(g^2_{9/2}i_{11/2})$. The sequence of the 864-, 371-, and 197 keV transitions above the isomer exhibits the similar trend of decreasing level spacings as observed in the low-lying sequence based on the $11/2^+$ state. Therefore, the states of this sequence may be understood as originating from the coupling of the $[\pi(h^5_{9/2}i_{13/2})_{11^-} \otimes \nu(g^2_{9/2}i_{11/2})_{11/2^+}]_{33/2^-}$ configuration to the $\nu(g^2_{9/2})_{2^+-6^+}$ neutron excitations.

V. SUMMARY

The level structure of the transitional nucleus ^{217}Ra has been investigated using the ^{208}Pb(^{12}C, $3n$)^{217}Ra reaction. The previously reported level scheme is revisited and the placements of several γ rays, which were found to be inconsistent in the earlier studies, have been confirmed in the present work. The addition of a new negative-parity sequence at low excitation energies provides the experimental evidence of parity-doublet structures in ^{217}Ra, which were earlier reported in all the other $N = 129$ isotones with $87 \leqslant Z \leqslant 90$. Although the level spacings in the $E2$ sequences of the simplex bands do not follow the characteristics of typical rotational bands, the strong $E1$ connecting transitions and parity doublets suggest the presence of octupole correlations in this nucleus. Therefore, theoretical calculations based on the reflection-asymmetric triaxial particle rotor model have been performed to interpret the observed parity-doublet structures. The calculated energies were found to be in reasonable agreement with the experimental results in the spin range $9/2\ \hbar \leqslant I \leqslant 21/2\ \hbar$ for the positive-parity states and $13/2\ \hbar \leqslant I \leqslant 27/2\ \hbar$ for the negative-parity states. The properties [energy splitting, $I(\omega)$ and B($E1$)/B($E2$) ratios] of the simplex bands in ^{217}Ra are also compared with that of the similar bands in neighboring nuclei and the results of the RAT-PRM calculations. The observed structures at low excitation energies reflect an intermediate behavior between the extremes of single-particle excitations and stable octupole deformation. Furthermore, it is observed that the simplex bands in ^{217}Ra terminate at the intermediate excitation energies, unlike ^{218}Ra where the alternating-parity sequence persist up to the

maximum observed spin. Also, the level structures above the $29/2^-$ state in ^{217}Ra appear to be mainly governed by single-particle excitations. Finally, it may be noted that the competing single-particle and collective degrees of freedom govern the structure in different energy regimes of this nucleus.

ACKNOWLEDGMENTS

The authors thank the staff of IUAC target laboratory for facilitating the preparation of the target. The authors gratefully acknowledge the IUAC support staff for their assistance during the experiment. The financial support by DST, India (Grant No. IR/S2/PF-03/2003-III) for the INGA project is acknowledged. The authors also thank INGA collaboration for their help and support. Madhu acknowledges the financial support from DST, India under the INSPIRE fellowship scheme (IF 180082). A.Y.D. and D.S. acknowledge the financial support by SERB (DST) vide Grant No. CRG/2020/002169. K.Y. acknowledges the support from the Ministry of Human Resource Development, India. Y.Y.W., Y.K.W., and J.M. acknowledge the support from the National Natural Science Foundation of China (Grants No. 12141501, No. 12205097, and No. 11935003), and the High-performance Computing Platform of Peking University.

[1] I. Ahmad and P. A. Butler, Annu. Rev. Nucl. Part. Sci. **43**, 71 (1993), and references therein.
[2] P. A. Butler and W. Nazarewicz, Rev. Mod. Phys. **68**, 349 (1996).
[3] S. C. Pancholi, *Pear-Shaped Nuclei* (World Scientific, Singapore, 2020).
[4] H. J. Wollersheim, H. Emling, H. Grein, R. Kulessa, R. S. Simon, C. Fleischmeann, J. de Boer, E. Hauber, C. Lauterbach, C. Schandera, P. A. Butler, and T. Czosnyka, Nucl. Phys. A **556**, 261 (1993).
[5] L. P. Gaffney *et al.*, Nature (London) **497**, 199 (2013).
[6] P. A. Butler, L. P. Gaffney, P. Spagnoletti, K. Abrahams, M. Bowry, J. Cederkäll *et al.*, Phys. Rev. Lett. **124**, 042503 (2020).
[7] B. Bucher, S. Zhu, C. Y. Wu, R. V. F. Janssens, D. Cline, A. B. Hayes *et al.*, Phys. Rev. Lett. **116**, 112503 (2016).
[8] B. Bucher, S. Zhu, C. Y. Wu, R. V. F. Janssens, R. N. Bernard, L. M. Robledo *et al.*, Phys. Rev. Lett. **118**, 152504 (2017).
[9] P. A. Butler, Proc. R. Soc. A **476**, 20200202 (2020).
[10] S. Frauendorf, Rev. Mod. Phys. **73**, 463 (2001).
[11] W. Reviol, C. J. Chiara, M. Montero, D. G. Sarantites, O. L. Pechenaya, M. P. Carpenter, R. V. F. Janssens, T. L. Khoo, T. Lauritsen, C. J. Lister, D. Seweryniak, S. Zhu, and S. G. Frauendorf, Phys. Rev. C **74**, 044305 (2006).
[12] W. Reviol *et al.*, Acta Phys. Pol. B **42**, 671 (2011).
[13] W. Reviol, D. G. Sarantites, C. J. Chiara, M. Montero, R. V. F. Janssens, M. P. Carpenter, T. L. Khoo, T. Lauritsen, C. J. Lister, D. Seweryniak, S. Zhu, O. L. Pechenaya, and S. G. Frauendorf, Phys. Rev. C **80**, 011304(R) (2009).
[14] S. Frauendorf, Phys. Rev. C **77**, 021304(R) (2008).
[15] T. Lönnroth, D. Horn, C. Baktash, and C. J. Lister, and G. R. Young, Phys. Rev. C **27**, 180 (1983).
[16] S. Muralithar, G. Rodrigues, R. P. Singh, R. K. Bhowmik, P. Mukherjee, B. Sethi, and I. Mukherjee, Pramana-J. Phys. **79**, 403 (2012).
[17] N. Schulz, V. Vanin, M. Aïche, A. Chevallier, J. Chevallier, J. C. Sens, Ch. Briançon, S. Cwiok, E. Ruchowska, J. Fernandez-Niello, Ch. Mittag, and J. Dudek, Phys. Rev. Lett. **63**, 2645 (1989).
[18] N. Roy, D. J. Decman, H. Kluge, K. H. Maier, A. Maj, C. Mittag, J. Fernandez-Niello, H. Puchta, and F. Riess, Nucl. Phys. A **426**, 379 (1984).
[19] M. Sugawara, Y. Gono, and Y. Itoh, J. Phys. Soc. Jpn. **53**, 2956 (1984).
[20] M. Sugawara, Y. Gono, T. Kohno, and M. Fukuda, RIKEN Accel. Prog. Rep. **20**, 12 (1986).
[21] S. Muralithar, Ph.D. thesis, Jawaharlal Nehru University, 2011.
[22] E. Parr, J. F. Smith, P. T. Greenlees, K. Auranen, R. Chapman, D. M. Cullen *et al.*, Phys. Rev. C **102**, 054335 (2020), and references therein.
[23] A. Lopez-Martens, K. Hauschild, K. Rezynkina, O. Dorvaux, B. Gall, F. Dechery, H. Faure, A. V. Yeremin, M. L. Chelnokov, V. I. Chepigin, A. V. Isaev, I. N. Izosimov, D. E. Katrasev, A. N. Kuznetsov, A. A. Kuznetsova, O. N. Malyshev, A. G. Popeko, E. A. Sokol, A. I. Svirikhin, J. Piot *et al.*, Eur. Phys. J. A **50**, 132 (2014).
[24] W. Hua, Z. Zhang, L. Ma, Z. Gan, H. Yang, M. Huang, C. Yang, M. Zhang, Y. Tian, X. Zhou, C. Yuan, C. Shen, and L. Zhu, Chin. Phys. C **45**, 044003 (2021).
[25] Pragati, A. Y. Deo, S. K. Tandel, S. S. Bhattacharjee, S. Chakraborty, S. Rai, S. G. Wahid, S. Kumar, S. Muralithar, R. P. Singh, I. Bala, R. Garg, and A. K. Jain, Phys. Rev. C **97**, 044309 (2018).
[26] M. E. Debray, A. J. Kreiner, M. Davidson, J. Davidson, D. Hojman, D. Santos, V. R. Vanin, N. Schulz, M. Aiche, A. Chevallier, J. Chevallier, and J. C. Sens, Nucl. Phys. A **568**, 141 (1994).
[27] S. Muralithar *et al.*, J. Phys.: Conf. Ser. **312**, 052015 (2011).
[28] M. Jain, E. T. Subramaniam, and S. Chatterjee, Rev. Sci. Instrum. **94**, 013304 (2023).
[29] R. Brun and F. Rademakers, Nucl. Instrum. Methods Phys. Res., Sec. A **389**, 81 (1997).
[30] A. Z. Schwarzschild and E. K. Warburton, Annu. Rev. Nucl. Sci. **18**, 265 (1968).
[31] A. Krämer-Flecken, T. Morek, R. M. Lieder, W. Gast, G. Hebbinghaus, H. M. Jäger, and W. Urban, Nucl. Instrum. Methods Phys. Res., Sec. A **275**, 333 (1989).
[32] G. Duchêne, F. A. Beck, P. J. Twin, G. de France, D. Kurien, L. Han, C. W. Beausang, M. A. Bentley, P. J. Nolan, and J. Simpson, Nucl. Instrum. Methods Phys. Res., Sec. A **432**, 90 (1999).
[33] K. Starosta, T. Morek, Ch. Droste, S. G. Rohoziński, J. Srebrny, A. Wierzchucka, M. Bergström, B. Herskind, E. Melby, T. Czosnyka, and P. J. Napiorkowski, Nucl. Instrum. Methods Phys. Res., Sec. A **423**, 16 (1999).
[34] T. Yamazaki, Nucl. Data, Sec. A **3**, 1 (1967).
[35] E. der Mateosian and A. W. Sunyar, At. Data Nucl. Data Tables **13**, 391 (1974).
[36] R. Palit, H. C. Jain, P. K. Joshi, S. Nagaraj, B. V. T. Rao, S. N. Chintalapudi, and S. S. Ghugre, Pramana **54**, 347 (2000).

[37] K. Yadav, A. Y. Deo, Madhu, Pragati, P. C. Srivastava, S. K. Tandel, S. G. Wahid, S. Kumar, S. Muralithar, R. P. Singh, I. Bala, S. S. Bhattacharjee, R. Garg, S. Chakraborty, S. Rai, and A. K. Jain, Phys. Rev. C **105**, 034307 (2022).
[38] F. G. Kondev, E. A. McCutchan, B. Singh, K. Banerjee, S. Bhattacharya, A. Chakraborty, S. Garg, N. Jovancevic, S. Kumar, S. K. Rathi, T. Roy, J. Lee, and R. Shearman, Nucl. Data Sheets **147**, 382 (2018).
[39] G. D. Dracoulis, F. Riess, A. M. Baxter, and A. E. Stuchbery, J. Phys. G: Nucl. Part. Phys. **17**, 1795 (1991).
[40] R. K. Sheline, C. F. Liang, P. Paris, A. Gizon, and V. Barci, Phys. Rev. C **49**, 725 (1994).
[41] W. Nazarewicz, P. Olanders, I. Ragnarsson, J. Dudek, and G. A. Leander, Phys. Rev. Lett. **52**, 1272 (1984).
[42] G. Maquart, L. Augey, L. Chaix, I. Companis, C. Ducoin, J. Dudouet *et al.*, Phys. Rev. C **95**, 034304 (2017).
[43] M. E. Debray, M. A. Cardona, D. Hojman, A. J. Kreiner, M. Davidson, J. Davidson, H. Somacal, G. Levinton, D. R. Napoli, S. Lenzi, G. de Angelis, M. De Poli, A. Gadea, D. Bazzacco, C. Rossi-Alvarez, and N. Medina, Phys. Rev. C **62**, 024304 (2000).
[44] T. C. Hensley, P. D. Cottle, V. Tripathi, B. Abromeit, M. Anastasiou, L. T. Baby, J. S. Baron, D. Caussyn, R. Dungan, K. W. Kemper, R. S. Lubna, S. L. Miller, N. Rijal, M. A. Riley, S. L. Tabor, P.-L. Tai, and K. Villafana, Phys. Rev. C **96**, 034325 (2017).
[45] N. Schulz, V. R. Vanin, A. J. Kreiner, E. Ruchowska, M. Aïche, Ch. Briangon, A. Chevallier, J. Chevallier, M. E. Debray, and J. C. Sens, Z. Phys. A **339**, 325 (1991).
[46] W. Reviol, R. V. F. Janssens, S. Frauendorf, D. G. Sarantites, M. P. Carpenter, X. Chen, C. J. Chiara, D. J. Hartley, K. Hauschild, T. Lauritsen, A. Lopez-Martens, M. Montero, O. L. Pechenaya, D. Seweryniak, J. B. Snyder, and S. Zhu, Phys. Rev. C **90**, 044318 (2014).
[47] Y. Y. Wang, S. Q. Zhang, P. W. Zhao, and J. Meng, Phys. Lett. B **792**, 454 (2019).
[48] Y. P. Wang, Y. Y. Wang, and J. Meng, Phys. Rev. C **102**, 024313 (2020).
[49] Y. Y. Wang and S. Q. Zhang, Phys. Rev. C **102**, 034303 (2020).
[50] Y. Y. Wang, X. H. Wu, S. Q. Zhang, P. W. Zhao, and J. Meng, Sci. Bull. **65**, 2001 (2020).
[51] Y. Y. Wang, Q. B. Chen, and S. Q. Zhang, Phys. Rev. C **105**, 044316 (2022).
[52] P. Möller, R. Bengtsson, B. G. Carlsson, P. Olivius, T. Ichikawa, H. Sagawa, and A. Iwamoto, At. Data Nucl. Data Tables **94**, 758 (2008).
[53] Y. Y. Wang and Z. X. Ren, Sci. China Phys. Mech. Astron. **61**, 082012 (2018).
[54] G. A. Leander, W. Nazarewicz, G. F. Bertsch, and J. Dudek, Nucl. Phys. A **453**, 58 (1986).
[55] P. Ring and P. Schuck, *The Nuclear Many-Body Problem* (Springer-Verlag, Berlin, 1980).
[56] Y. Y. Wang, Phys. Rev. C **104**, 014318 (2021).
[57] A. E. Stuchbery, G. D. Dracoulis, T. Kibédi, A. P. Byrne, B. Fabricius, A. R. Poletti, G. J. Lane, and A. M. Baxter, Nucl. Phys. A **548**, 159 (1992).
[58] J. F. Shriner, Jr., P. D. Cottle, J. F. Ennis, M. Gai, D. A. Bromley, J. W. Olness, E. K. Warburton, L. Hildingsson, M. A. Quader, and D. B. Fossan, Phys. Rev. C **32**, 1888 (1985).
[59] P. D. Cottle, J. F. Shriner, Jr., F. Dellagiacoma, J. F. Ennis, M. Gai, D. A. Bromley, J. W. Olness, E. K. Warburton, L. Hildingsson, M. A. Quader, and D. B. Fossan, Phys. Rev. C **30**, 1768(R) (1984).

APS (https://www.aps.org/)

PHYSICAL REVIEW C (/PRC/)
covering nuclear physics

Highlights (/prc/highlights) Recent (/prc/recent) Accepted (/prc/accepted) Collections (/prc/collections) Authors (/prc/authors)
Referees (/prc/referees) Search (/search) Press (/press) About (/prc/about) Editorial Team (/prc/staff) (/feeds)

Spectroscopic study of

Rozina Rahaman, Abhijit Bisoi, Ananya Das, Y. Sapkota, Arkabrata Gupta, S. Ray, S. Sarkar, Yashraj, A. Sharma, Bharti Rohila, I. Ahmed, Kaushik Katre, S. Dutt, S. Kumar, R. P. Singh, R. Kumar, and S. Muralithar
Phys. Rev. C **109**, 024318 – Published 15 February 2024

More

Article

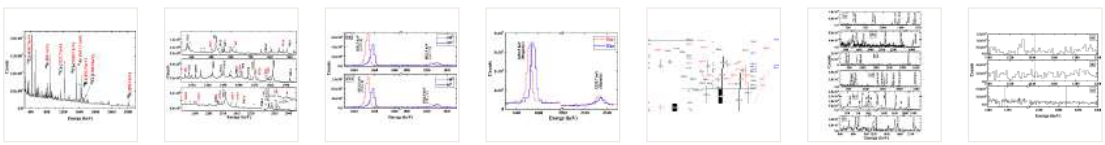
PDF (/prc/pdf/10.1103/PhysRevC.109.024318) HTML (/prc/abstract/10.1103/PhysRevC.109.024318#fulltext)

Export Citation (/prc/export/10.1103/PhysRevC.109.024318)

ABSTRACT
AUTHORS
ARTICLE TEXT
INTRODUCTION
EXPERIMENTAL DETAILS AND DATA ANALYSIS
RESULT AND DISCUSSION
THEORETICAL CALCULATION
CONCLUSION
ACKNOWLEDGMENTS
REFERENCES

ABSTRACT

High spin states of populated through the (2) reaction at 68 MeV beam energy were studied using the Indian National Gamma Array (INGA) facility. Six new levels and fourteen new transitions were added to the existing level scheme. The spins and parities of most of the levels were assigned, modified, or confirmed from , , and linear polarization measurements. The multipole mixing ratios O1 for most of the transitions were measured. Large-basis shell-model calculations were performed to understand the microscopic origin of the levels. Different particle restrictions in and shell orbitals were used to explain the experimental results.



6 More

Received 31 August 2023 Revised 21 December 2023 Accepted 19 January 2024

DOI: https://doi.org/10.1103/PhysRevC.109.024318

©2024 American Physical Society

Physics Subject Headings (PhySH)

This site uses cookies. To find out more, read our Privacy Policy (https://www.aps.org/about/privacy.cfm).

Research Areas

I Agree ()

Sign up to receive regular email alerts from *Physical Review C*

Sign up (https://info.aps.org/journals-emails)

ISSN 2469-9993 (online), 2469-9985 (print). ©2024 American Physical Society. (https://www.aps.org/) All rights reserved. *Physical Review C*™ is a trademark of the American Physical Society, registered in the United States, Canada, European Union, and Japan. The *APS Physics logo* and *Physics logo* are trademarks of the American Physical Society. Information about registration may be found here (/legal). Use of the American Physical Society websites and journals implies that the user has read and agrees to our Terms and Conditions (/info/terms.html) and any applicable Subscription Agreement (https://librarians.aps.org/sitelicense.pdf).

This site uses cookies. To find out more, read our Privacy Policy (https://www.aps.org/about/privacy.cfm).

I Agree ()

Already have a manuscript?

Use our Manuscript Matcher to find the best relevant journals!

Find a Match

Refine Your Search Results

2469-9985 Search

Sort By: Title (A-Z)

Search Results

Found 1 results (Page 1) Share These Results

Exact Match Found

PHYSICAL REVIEW C

Publisher:	AMER PHYSICAL SOC , ONE PHYSICS ELLIPSE, COLLEGE PK, USA, MD, 20740-3844
ISSN / eISSN:	2469-9985 / 2469-9993
Web of Science Core Collection:	Science Citation Index Expanded
Additional *Web of Science* Indexes:	Current Contents Electronics & Telecommunications Collection | Current Contents Physical, Chemical & Earth Sciences | Essential Science Indicators

Share This Journal View profile page

** Requires free login.*

Filters Clear All

Web of Science Coverage

Open Access

Category

Country / Region

Language

Frequency

Journal Citation Reports

The Healing Power Of Nature In Chitra Banerjee Divakaruni's "The Mistress Of Spices"

Mr. Bhojraj Pandhari Shrirame
Assistant Professor (English)
J. M. Patel Arts, Commerce & Science College, Bhandara

Dr. Sunil G. Chaudhari
Associate Professor
N. H. College, Bramhapuri

Abstract:
This research paper explores the theme of the healing power of nature in Chitra Banerjee Divakaruni's novel, "The Mistress of Spices." The protagonist, Tilo, uses spices to heal people's physical and emotional ailments, with each spice having its own unique properties. The paper analyses how the healing power of nature is depicted in the novel and its significance. It examines Tilo's connection to nature, which is depicted as having a profound impact on her emotional well-being, and how she is able to connect with a higher power and help others find emotional and spiritual healing through her work with the spices. The paper concludes that the novel reinforces the idea that nature is an integral part of our lives and that we should strive to connect with it on a deeper level.

Keywords: Nature, Spices, Healing, Emotional, Spiritual

Introduction:

Chitra Banerjee Divakaruni is a highly acclaimed writer of the Indian diaspora, known for her captivating storytelling that often deals with themes of identity, belonging, and the immigrant experience. She was born in Kolkata, India, and later immigrated to the United States, where she currently resides. Divakaruni has written numerous novels, short story collections, poetry collections, and children's books. Her works have received widespread critical acclaim and have been translated into over 29 languages. Some of her notable works include The Mistress of Spices, Sister of My Heart, One Amazing Thing, and Before We Visit the Goddess. In addition to her literary career, Divakaruni is also a professor of writing at the University of Houston.

"The Mistress of Spices" is a novel that expresses the story of Tilottama, which is an Indian name that reflects her cultural heritage. However, when she moves to America, she changes her name to Tilo, her nickname, to better fit in with the culture. The name Tilottama holds significant symbolism, representing a mythological goddess of power, mysticism, and

knowledge from the early Vedic age in India. She has been trained in the art of using spices and has been given magical powers to help people with their problems through the use of spices. Tilo is the mistress of a spice shop in Oakland, California, where she helps people with their physical and emotional ailments by prescribing them specific spices. According to Cheryll Glotfelty, "Ecocriticism is the study of the relationship between literature and physical environment" (Barry, 239). The novel explores the idea that nature can have a profound impact on our physical and emotional health and that we can find solace and healing in the natural world, also the themes of identity, culture, and the immigrant experience. Tilo, who is originally from India, struggles to find a sense of belonging in America, and she must navigate the challenges of living in a new culture while holding onto her traditions and beliefs.

The novel also highlights the power of love and the sacrifices people are willing to make for the ones they love. Tilo falls in love with a man named Raven, but her duty as a Mistress of Spices and her magical powers prevent her from being able to fully engage in a romantic relationship with him. Throughout the novel, her magical powers are threatened by a rival who seeks to take over her spice shop and her customers. She must use all her skills and knowledge to protect her customers and her identity.

Chitra Banerjee Divakaruni's novel "The Mistress of Spices" is a masterful blend of magical realism, romance, and social commentary. The novel explores the challenges of the immigrant experience and the difficulties of reconciling one's cultural identity with the demands of a new culture. The novel's focus on the healing power of nature provides a compelling avenue for analysis. This research paper will examine the significance of this theme and explore how the novel depicts the profound impact that nature can have on emotional well-being and spiritual growth.

The use of spices as a means of healing:

Chitra Banerjee Divakaruni's novel "The Mistress of Spices" presents a unique perspective on the power of spices. The book portrays spices as having mystical and healing properties, with the protagonist, Tilo, possessing magical abilities to utilize them for the benefit of others. As a Mistress of Spices, Tilo is able to heal physical and emotional wounds by skilfully blending different spices, highlighting the potential for nature to provide natural remedies for a range of issues. Tilo introduces "Turmeric" to readers in the second chapter through her dialogue, which goes as "Turmeric the auspicious spice, placed on heads of new borns for luck, sprinkled over coconut at pujas, rubbed into the borders of wedding saris" (TMS 13).

Throughout the novel, Tilo uses various spices to help people with their problems. For example, she uses cinnamon to help a woman who is trying to conceive a child, cloves to help a man with his toothache, and saffron to calm a woman who is anxious and stressed. She believes that each spice has its unique healing properties, and she carefully selects the appropriate spice to address the specific needs of her customers. Moreover, she believes that spices not only have physical healing powers but also possess the ability to heal emotional wounds. She uses spices to help people overcome grief, sadness, and heartbreak. For instance, she uses nutmeg to help a woman get over her lover's death and cardamom to heal a man's broken heart.

In the novel, spices are presented as powerful and magical substances that can heal both the body and soul. The use of spices as a means of healing is deeply rooted in traditional

Indian medicine and Ayurveda, which is an ancient system of medicine that uses natural remedies to treat various illnesses. The use of spices as a means of healing in "The Mistress of Spices" reflects the importance of natural remedies in traditional medicine and the belief that herbs and spices have the power to heal both physical and emotional ailments.

The connection between nature and emotional well-being:

The connection between nature and emotional well-being is supported by scientific research and is also evident in many cultural and spiritual traditions. Spending time in nature has been shown to have a positive impact on mental health and emotional well-being by reducing stress, anxiety, and depression, improving mood, and promoting a sense of connectedness to something larger than oneself. Tilo explains that Kalo Jire has the power to protect and ward off the evil eye, and she expresses this sentiment such as "will split once again tonight kalo jire seeds ofr all who have suffered from America" (TMS 173).

One way that nature can promote emotional well-being is through the restorative effects of exposure to natural environments. Nature has a calming effect on the mind and body, and exposure to natural environments can help to reduce stress and anxiety. Natural environments can also promote feelings of awe and wonder, which can enhance positive emotions and promote a sense of purpose and meaning. In addition, nature can promote physical activity, which has been shown to have positive effects on mental health and emotional well-being. Being physically active in natural environments can enhance mood, reduce stress, and promote feelings of well-being. Moreover, nature can provide a sense of connection to the natural world and to other people. The sense of connectedness can promote social support, which is important for emotional well-being, and can also promote a sense of purpose and belonging. Nature and emotional well-being is an important area of research and has implications for public health and urban planning. Incorporating natural environments into daily life can have positive effects on mental health and emotional well-being and can enhance the overall quality of life.

In "The Mistress of Spices," Tilo's connection to nature is depicted as having a profound impact on her emotional well-being. Tilo is shown to be at her happiest when she is surrounded by plants and nature. She finds solace in her garden, which is filled with herbs and spices from her homeland. The garden is depicted as a place of healing and renewal, a place where Tilo can escape from the stresses of the modern world.

Tilo's connection to nature is also reflected in her interactions with the people she helps. She is able to connect with them on a deep level, understanding their emotional needs and providing them with the healing they need. This reinforces the idea that nature can have a profound impact on our emotional well-being and that we can find solace and healing in the natural world.

The healing power of nature as a means of spiritual growth:

Nature has been regarded as a powerful source of healing and spiritual growth in many cultures and traditions throughout history. The healing power of nature can be attributed to several factors, including its ability to reduce stress, promote physical activity, and provide a sense of connection to something larger than oneself. This connection to nature can be a source of spiritual growth, as it can inspire feelings of wonder and awe, and can lead to a deeper understanding of oneself and the world around us.

One way that nature can promote spiritual growth is through the restorative effects of exposure to natural environments. Being in nature can help to reduce stress and anxiety, and

can promote feelings of relaxation and well-being. This can create an opportunity for introspection and contemplation, which can lead to spiritual insights and growth. In addition, nature can be a source of inspiration and creativity. The beauty and complexity of the natural world can inspire feelings of awe and wonder, which can lead to a deeper appreciation for the world around us. This appreciation can promote spiritual growth by encouraging a sense of interconnectedness with all living things. Moreover, being in nature can provide a sense of perspective and help us to see our place in the world. This can promote humility and a sense of gratitude for the gifts of life, which can be important components of spiritual growth. The healing power of nature can be a powerful means of spiritual growth, and can provide opportunities for introspection, creativity, and connection to the larger world. Incorporating nature into daily life can have positive effects on spiritual growth and enhance the overall quality of life.

In "The Mistress of Spices," the healing power of nature is also depicted as a means of spiritual growth. Tilo is shown to be a deeply spiritual person, and her connection to nature is an important part of her spiritual practice. Through her work with the spices, she is able to connect with a higher power and gain a deeper understanding of the world around her. Tilo's dedication to her customers and to the spices is reflected in her unwavering memory such as "I will chant. I will administer. I will pray to remove sadness and suffering as the old one taught. I will deliver warning" (TMS 7). Tilo's use of the spices is not just about curing physical and emotional ailments; it is also about helping people connect with their inner selves. The spices are a means of unlocking people's hidden emotions and desires, helping them to grow and develop on a spiritual level.

Conclusion:

In conclusion, the healing power of nature is a recurring theme in Chitra Banerjee Divakaruni's "The Mistress of Spices." The novel explores the idea that nature can have a profound impact on our physical and emotional health, and that we can find solace and healing in the natural world. Through her work with the spices, Tilo is able to connect with a higher power, help others find emotional and spiritual healing, and maintain a deep connection to her Indian heritage. The novel reinforces the idea that nature is an integral part of our lives and that we should strive to connect with it on a deeper level.

References:

1. Divakaruni, Chitra Banerjee. The Mistress of Spices. Great Britain: Doubleday. 1997. Print.
2. Barry, Peter, Beginning Theory. New Delhi: Viva Books Private Limited, 2010. Print.
3. Glofelty, Cheryll and Harold Fromm. (ed.) The Ecocriticism Reader: Landmarks in Literary Ecology. Athens: The University of Georgia Press, 1996. Print.
4. Dr. Jayashree Singh and Mrs. Chhavi Goswami. Spices' Action with Internal World- http://ijellh.com/wpcontent/uplods/2015/05/31.-Dr.Jayshree-Singhp paper.pdf
5. The Mistress of Spices by Chitra Banerjee Divakaruni. Vol. No. 3. Issue No. 3 (2015). IJELLH, Web. 25 Feb, 2018, p. 306.
6. M. Fathima Sanjeetha, Dr. S. Mohamed Haneef, 'Nature in Chitra Banerjee Divakaruni's The Mistress of Spices' *International Journal of Research Culture Society* ISSN: 2456-6683 Volume-2, Issue-4, April -2018

An International Registered Peer Reviewed Bilingual Research Journal

SATRAVACHEE

ISSN 2348-8425

सत्रावची

A UGC-CARE Enlisted
Peer Reviewed Research Journal

Special Issue

Year 11, Issue 28,
Vol 40,
July-September, 2023

WOMEN EMPOWERMENT - II

Editor
Anand Bihari

Chief Editor
Kamlesh Verma

ISSN : 2348-8425

SATRAACHEE

UGC Care Enlisted, Peer Reviewed Research Journal

Issue 28, Vol. 40, July-September, 2023

Women Empowerment-II

Editor
Anand Bihari

Chief Editor
Kamlesh Verma

Co-Editor
Archana Gupta
Jay Prakash Singh

Review Editor
Suchita Verma
Ashutosh Partheshwar

Assistant Editor
Guntaj Kour
Shivangi

Advisory Committee and Reviewers

- Prof. Bhupendra Kalsey, Co-Ordinator, Bhartiya Bhasha Vibhag, Nalanda Open University, Patna.
- Dr. Anurag Ambasta, Coordinator, Department of English, St. Xavier's College of Management and Technology, Patna
- Dr. Nutan Kumari, Assistant Director & Associate Professor, Amity, Institute of English Studies & Research, Amity University, Patna
- Dr. Shwet Nisha, Assistant Professor, Dept. of English, Amity University, Patna
- Dr. Pushpalata Kumari, Political Sc., Patna University, Patna.
- Dr. Neera Choudhury, Music, Patna University, Patna.
- Dr. Arvind Kumar, Music, Patna University, Patna.
- Dr. Raju Ranjan Prasad, History, B.B.A.Bihar University, Mujaffarpur

❑❑

सत्राची

मानविकी एवं सामाजिक विज्ञान की पूर्व समीक्षित त्रैमासिक शोध पत्रिका

Pre-Reviewed Quarterly Research Journal of the Humanities and Social Sciences

Price : ₹ **450**

Subscription:

Five Year : Rs. 5000/- (Personal)
: Rs. 10000/- (Institutional)
Life Time : Rs. 12000/- (Personal)
: Rs. 25000/- (Institutional)

The Draft/Cheque may please be made in favour of

'SATRAACHEE FOUNDATION'
C/A No. 40034072172. IFSC : SBIN0006551,
State Bank of India, Boring Canal Rd.-Rajapool,
East Boring Canal Road, Patna, Bihar, Pin: 800001

Google Pay No.: 9661792414

© सर्वाधिकार सुरक्षित (Copyright Reserved)

The editor does not have to agree with the published articles.

Editing/Publishing: Unpaid/ Unprofessional

Publisher: *Satraachee Foundation, Patna*

Editorial Contact:

Anand Bihari
Kala Kunj, Besdide Canara Bank
Bazar Samiti Road, Bahadurpur
Patna-800016

Website : http://satraachee.org.in
E-mail : satraachee@gmail.com
Mob. : 9661792414 (A.Bihari.)
: 9415256226 (Kamlesh Verma.)

❖❖❖

SATRAACHEE

In this Issue...

11 :: Editorial *Anand Bihari*

13 :: Dressing Dissent: Assertion and Resistance through Clothing and Appearance in George Eliot's *Mill on the Floss*
- Ms Garima Nandal, Prof. Sujata Rana

18 :: Daisy in R.K. Narayan's *The Painter of Signs*: A Representative of the Modern Woman
- Dr. Rohini D. Kasar

23 :: Women: An Inspiration to the Inspirers
- Dr. Abhibunnisha Begum, Dr. N. Satyanarayana

27 :: Bankim Chandra's Vision of New India through the Rise of Women in Rajmohan's Wife
- Md. Fajle Alam

31 :: An Ecofeminist Reading of Andrew Marvell's Selected Poems
- Mr Shirsak Ghosh

36 :: Evolution Of Women's Roles In Films
- Shivali K.C.

40 :: Revisiting Socio-Cultural Growth through Women Empowerment
- Dr. Anil B. Patil

45 :: Role of Dr. B. R. Ambedkar in Emancipation of Women in India
- Dr. Maheshkumar B. Bhaisare

49 :: Stifled Enunciates of Females in the Play *Lights Out*
- Vinita Virgandham

54 :: Rejection of Female Identity in *Uchalya* by Laxman Gaikwad
- Mr. Ravindra Ramdas Borse, Dr. Anshu Sharma & Dr. Jitendra Bagul

60 :: An Initiative In The Growth Of Indian Educational System Through Women's Empowerment
- Dr R. Subhashini, Dr S. Chitra

65 :: Women in Ngugi wa Thiongo's Novels: Breaking Gender Barriers
- Dr. Amit. Y. Kapoor

70 :: A Study on National Policy for the Empowerment of Women (2001)
- Dr. Sakshi Jain

75 :: Deeti: A Symbol Of Empowered Women in Amitav Ghosh's *Ibis* Trilogy

- Ms. Pranali Genu Bothe

148 :: Arundhati Roy: The Empowered Indian Woman Writer
- Dr.S.Shanmuga Priya

153 :: Women Empowerment in the Literature of Rashtrasant Tukdoji Maharaj
- Dr. Shravan R. Banasure

157 :: Continuous Learning and Women Empowerment in Rujuta Deshmukh's Poetry
- Dr. Bhagyashree S Gawate

161 :: The Feminist Reinterpretation of Shashi Deshpande's 'Dark Holds No Terror'
- Dr. Ajay Sahebrao Deokate

165 :: The Healing Power Of Nature In Chitra Banerjee Divakaruni's "The Mistress Of Spices"
- Mr. Bhojraj Pandhari Shrirame, Dr. Sunil G. Chaudhari

169 :: Regenerating Womanhood in Bhabhani Bhattacharya's So Many Hungers! and Anita Nair's Ladies Coupe
- Ms. M. Gayathri

173 :: Problems Of Women In Rural India: Reading Of Select Novels Of Shashi Tharoor And Chetan Bhagat
- Dr Hitendra B Dhote

177 :: Be 'You'; Be 'Your Voice': Not Somnolence but Self Consciousness will Ensure Women Empowerment in india
- Dr. Meenakshi Rathore

182 :: Women Empowerment Depicted in the Novels of Chetan Bhagat with Reference to *One Indian Girl* and *Revolution 2020*
- Smt. Leena C. Devre, Dr. Vijay Z. Chaudhari

185 :: Women Empowerment for National Development
- Dr. Prasad R Dagwale

189 :: Women Empowerment in India: A Path to Progress and Equality
- Arjun Namdevrao Khobragade

193 :: Empowerment of Women in Indigenous Badaga Community
- Dr. N. Venugopal

198 :: Problems and Prospects of Indian Women in Manju Kapur's *A Married Woman*
- Dr. S. Florence

203 :: Interpretation of Women Realization with reference to Bai Pan Bhari Deva
- Mr. Milind Subhash Bedse

207 :: The Powerful Voice of Protest and Empowerment in Maya Angelou's

SATRAACHEE, ISSN 2348-8425

आ वो होता जोहवीति सत्त: सत्राचीं रातिं मरुतो गृणान: । य ईवतो वृषणो अस्ति गोपा: सो अद्वयावी हवते व उक्थै: ।। (ऋ. 7.56.18)
उभयं शृणवच्च न इन्द्रो अर्वागिदं वच: । सत्राच्या मधवा सोमपीतये धिया शविष्ठ आ गमत् ।। (ऋ. 8.61.1)

* Editor :

Anand Bihari.
biharidot@ gmail.com
satraachee@gmail.com
09661792414, 09470738162

* Assistant Editor :

1. **Dr. Ankita Kumari**
2. **Mrs. Bhawna Mishra**

सत्राची के अंक











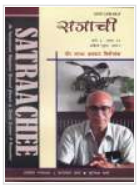


POWERED BY

Advisory Board

- **Prof. Mukteshwar Nath Tiwary.**
  Professor
  Hindi Bhawan, Vishwa Bharti,
  Shanti Niketan. West Bengal
  Mob. 09474765831
- **Dr. Kamlesh Verma.**
  Dept. of Hindi
  Rajkiya Mahila Mahavidyalya,
  Sewapuri,Varanasi, U.P.
  E-mail: kamleshvermajnu@gmail.com
  Mob. 09415256226
- **Dr. Ashutosh Partheshwar**
  Assistant Professor
  Dept. of Hindi
  Oriental College, Patna City.
  Mob. 09934260232
  E-mail: parthdot@gmail.com
- **Dr. Raju Ranjan Prasad.**
  Critic, History & Hindi Lit.
  C-19, Shreenagar,
  Ashiananagar, Patna-25
  Mob. - 08294307626
  E-mail: rajooranjan@gmail.com
- **Dr. Pushpalata Kumari.**
  Assistant Professor & H.O.D
  Political Science
  Patna University, Patna
  E-mail: drpushpalatammc@gmail.com
  Mob. 09431402736
- **Dr. Arvind Kumar.**
  Assistant Professor & H.O.D
  Music





Music

Patna University, Patna

Mob. 09835681230

UGC-CARE List

You searched for "**2348-8425**". Total Journals : **1**

Search:

Sr.No.	Journal Title	Publisher	ISSN	E-ISSN	UGC-CARE coverage years	Details
1	Satraachee	Satraachee Foundation	2348-8425	NA	from July-2022 to October- 2023	Discontinued from Oct. 2023

Showing 1 to 1 of 1 entries

Previous 1 Next

Copyright © 2024 Savitribai Phule Pune University. All rights reserved. | Disclaimer

The Feminist Reinterpretation of Shashi Deshpande's 'Dark Holds No Terror'

Dr. Ajay Sahebrao Deokate
Assistant Professor, Department of English
J. M. Patel Arts, Commerce & Science College, Bhandara. (MS)

Abstract

This research article explores the feminist reinterpretation of Shashi Deshpande's acclaimed novel, "Dark Holds No Terror." Through a close analysis of the text, this study aims to highlight the representation of women characters and their struggle for agency and identity in a patriarchal society. The article examines how Deshpande's narrative challenges traditional gender roles and explores the complexities of female experiences. By employing feminist literary theory, the paper brings to light the novel's themes of self-discovery, autonomy, and empowerment, while also examining the author's portrayal of women's relationships with men and other women. In doing so, this article seeks to shed light on the significance of "Dark Holds No Terror" as a powerful work of feminist literature.

Keywords: Feminism, Patriarchy, Identity, Gender, Discrimination,

Introduction:

Shashi Deshpande's "Dark Holds No Terror" is a thought-provoking novel that delves into the lives of women in a patriarchal society. First published in 1980, the novel revolves around the protagonist Sarita's journey of self-discovery and emancipation from oppressive societal norms. Set against the backdrop of a patriarchal society and the complexities of familial relationships, the novel delves deep into the psyche of its protagonist. Deshpande's eloquent prose captures the intricate nuances of Sarita's emotional turmoil, her internal battles, and her gradual evolution into a woman determined to transcend the constraints placed upon her. "Dark Holds No Terror" is a poignant exploration of the human spirit's resilience and its capacity to overcome even the most daunting challenges. With a keen eye for detail and a deep understanding of human psychology, Deshpande crafts a narrative that resonates universally, inviting readers to contemplate the forces that shape their own lives. This article aims to analyze the feminist reinterpretation of the novel, exploring how Deshpande's narrative serves as a critique of the constraints imposed on women and their quest for liberation.

Objectives:

- To analyze Shashi Deshpande's novel through a feminist lens, examining how its female characters navigate societal expectations and challenge traditional roles.

- To examine the intersection of feminism and literature by critically assessing how the select novel contributes to discussions about women's experiences, revealing the intricate balance between personal liberation and societal limitations.
- To investigate the narrative techniques employed in 'Dark Holds No Terror,' focusing on how they amplify feminist perspectives within the text, and analyze how the narrative structure mirrors gender dynamics.

Research Methodology

The research method involves an in-depth literary analysis of the primary source of select novel. The researcher examines the text's narrative structure, character development, dialogues, and symbolism, with a specific focus on feminist themes. The research relies on, a close reading of, the select novel and secondary sources are closely examined and interpreted in the context of feminist literary theory.

The Representation of Women Characters:

1.1 Sarita - A Quest for Identity:

At the core of the novel is Sarita, who grapples with her identity and self-worth due to society's relentless expectations. She embodies the typical Indian woman, subjected to male dominance and defined by her marital status. The feminist lens reveals how Sarita's journey is emblematic of the struggles faced by women to assert their individuality within a patriarchal framework.

In one instance, Sarita questions her own identity, saying, "Who am I, after all? I am not my father's son, nor my husband's wife. So who am I?" (Deshpande 54). As the narrative unfolds, Sarita's character undergoes a transformation marked by empowerment and self-realization. Her evolution from a young woman eager to break free from constraints to a confident individual who embraces her identity is a powerful testament to the potential for growth and change. Sarita's story becomes a celebration of the capacity of women to shape their own lives and destinies.

1.2 Nalini - Challenging Stereotypes:

Nalini, Sarita's sister, serves as an important counterfoil. As a successful and independent woman, Nalini challenges traditional gender roles. She represents the feminist ideals of self-reliance and the pursuit of professional excellence, illustrating the possibilities of women's empowerment beyond the confines of marriage and domesticity. Nalini expresses her determination to pursue her career, telling Sarita, "I want to make a name for myself in the world, not be known as someone's wife or sister. I want to be Nalini - not just a woman" (Deshpande 87).

Nalini's character is a testament to her eventual assertion of agency and empowerment. As the story progresses, she embarks on a journey of self-discovery, challenging the constraints that society and family have imposed upon her. Her decision to pursue higher education, despite the skepticism and resistance she encounters, demonstrates her determination to reclaim control over her life and define her own path. This evolution from a passive participant to an active agent reflects the novel's overarching exploration of women's autonomy.

Unraveling Patriarchal Norms:

2.1 Subversion of Marital Expectations:

Deshpande uses Sarita's troubled marriage as a lens to examine the institution of marriage itself. The novel exposes the oppressive nature of traditional arranged marriages, where women often find themselves sacrificing their desires and aspirations to fulfill societal

expectations. The feminist perspective dissects the power dynamics within Sarita's marriage, revealing how patriarchal norms dictate her life choices.

Sarita reflects on her feelings of entrapment within her marriage, saying, "I had thought marriage would bring freedom, but it has only given me more chains" (Deshpande 121).

Sarita's character is marked by her rebellion against the constraints that seek to confine her. Her refusal to be subjugated by traditional gender roles and her resistance to conforming to the expected trajectory of marriage and motherhood showcase her complexity. This rebellion is not mere defiance but a manifestation of her deep yearning for a life of purpose and authenticity.

2.2 The Complexities of Motherhood:

Through the character of Ratna, Sarita's mother-in-law, Deshpande explores the multi-faceted role of motherhood. Ratna's character represents the internalized misogyny prevalent among women themselves, perpetuating patriarchal values..Ratna advises Sarita, "Your life's purpose is to be a good wife and mother. Forget about your dreams and ambitions. They are not meant for women like us" (Deshpande 175).

Sarita's character is marked by her rebellion against the constraints that seek to confine her. Her refusal to be subjugated by traditional gender roles and her resistance to conforming to the expected trajectory of marriage and motherhood showcase her complexity. This rebellion is not mere defiance but a manifestation of her deep yearning for a life of purpose and authenticity.

Female Relationships and Solidarity:

3.1 Sisterhood and Support:

The novel emphasizes the significance of female bonds and support networks. Nalini and Sarita's relationship showcases the strength derived from sisterhood. The feminist analysis uncovers the novel's celebration of female friendships as a means of resistance against patriarchy.

In a moment of solidarity, Nalini assures Sarita, "We are in this together, as sisters. We will face the world on our terms" (Deshpande 206).

These siblings embody differing responses to societal expectations, embodying a contrast between tradition and modern aspirations. However, their bond remains unbreakable. Deshpande portrays the complexity of sisterhood, capturing moments of both tension and understanding that underscore the depth of their connection. Their shared experiences and unwavering support reflect the resilience of sisterly relationships in navigating societal pressures.

3.2 Friendships and Rivalries:

Deshpande's portrayal of Sarita's friendships with women like Malini and Leela reflects the complexities of female relationships.

Sarita reflects on her relationships with other women, stating, "I thought women would understand each other, but sometimes we are our own worst enemies" (Deshpande 243).

Female friendships, exemplified by Sarita's close bond with Leela, serve as sources of solace and mutual understanding. Leela becomes a confidante, offering a safe space for candid conversations and emotional release. This portrayal of friendship underscores the significance of companionship in confronting societal expectations and discovering a sense of agency. Deshpande emphasizes how shared experiences and intimate connections create an avenue for women to voice their hopes and fears without reservation.

The Journey to Empowerment:

4.1 Self-Discovery and Autonomy:

The novel's trajectory illustrates Sarita's gradual realization of her own potential and worth. The feminist reading showcases how self-discovery and autonomy are essential elements in empowering women to break free from oppressive structures.

Sarita embraces her newfound independence, declaring, "I am no longer the person I used to be. I have found my own strength, and I will not let anyone take it away from me" (Deshpande 289).

Sarita's journey culminates in a realization of empowerment and autonomy. Her transformation from a young woman constrained by tradition to a self-assured individual willing to embrace her desires and assert her choices underscores the novel's overarching theme of self-discovery. Through Sarita's experiences, Deshpande underscores the potential for women to transcend societal barriers and redefine their identities on their own terms.

4.2 Challenging Beauty Standards:

The novel also addresses societal obsession with beauty standards, which can have detrimental effects on women's self-esteem and confidence. By critiquing such standards, Deshpande champions a feminist discourse on body positivity and self-acceptance.

Sarita challenges society's beauty ideals, stating, "I refuse to be judged by my appearance. I am more than just my looks" (Deshpande 316).

At the core of the narrative is Sarita's bold defiance against traditional ideals of beauty. Her dark complexion, which stands in stark contrast to the prevalent preference for fair skin, becomes a symbol of her rejection of imposed standards. Sarita's rejection of the notion that beauty is confined to physical appearance highlights her willingness to question and challenge prevailing norms.

Conclusion:

Shashi Deshpande's "Dark Holds No Terror" emerges as a remarkable work of feminist literature, offering a powerful critique of patriarchal norms and societal expectations that oppress women. The novel's representation of women characters and their struggles for identity, autonomy, and solidarity resonates with feminist themes, inviting readers to question and challenge prevailing gender norms. As Deshpande's work continues to inspire and engage readers, its feminist re-interpretation remains crucial in promoting gender equality and empowering women in contemporary society.

Works Cited:

- Deshpande, Shashi. Dark Holds No Terror. Penguin Books India, 1980.
- Friedan, Betty. The Feminine Mystique. W.W. Norton & Company, 1963.
- Hooks, Bell. The Feminist Theory: From Margin to Center. South End Press, 1984.
- Mohanty, Chandra Talpade. "Under Western Eyes: Feminist Scholarship and Colonial Discourses." Feminist Review, no. 30, 1988, pp. 61-88.
- Tyson, Lois. Critical Theory Today: A User-Friendly Guide. Routledge, 2014.

An International Registered Peer Reviewed Bilingual Research Journal

SATRAVACHEE

ISSN 2348-8425

सत्रावची

A UGC-CARE Enlisted
Peer Reviewed Research Journal

Special Issue

Year 11, Issue 28,
Vol 40,
July-September, 2023

WOMEN EMPOWERMENT - II

Editor
Anand Bihari

Chief Editor
Kamlesh Verma

ISSN : 2348-8425

SATRAACHEE

UGC Care Enlisted, Peer Reviewed Research Journal

Issue 28, Vol. 40, July-September, 2023

Women Empowerment-II

Editor
Anand Bihari

Chief Editor
Kamlesh Verma

Co-Editor
Archana Gupta
Jay Prakash Singh

Review Editor
Suchita Verma
Ashutosh Partheshwar

Assistant Editor
Guntaj Kour
Shivangi

Advisory Committee and Reviewers

- Prof. Bhupendra Kalsey, Co-Ordinator, Bhartiya Bhasha Vibhag, Nalanda Open University, Patna.
- Dr. Anurag Ambasta, Coordinator, Department of English, St. Xavier's College of Management and Technology, Patna
- Dr. Nutan Kumari, Assistant Director & Associate Professor, Amity, Institute of English Studies & Research, Amity University, Patna
- Dr. Shwet Nisha, Assistant Professor, Dept. of English, Amity University, Patna
- Dr. Pushpalata Kumari, Political Sc., Patna University, Patna.
- Dr. Neera Choudhury, Music, Patna University, Patna.
- Dr. Arvind Kumar, Music, Patna University, Patna.
- Dr. Raju Ranjan Prasad, History, B.B.A.Bihar University, Mujaffarpur

❑❑

सत्राची

मानविकी एवं सामाजिक विज्ञान की पूर्व समीक्षित त्रैमासिक शोध पत्रिका

Pre-Reviewed Quarterly Research Journal of the Humanities and Social Sciences

Price : ₹ **450**

Subscription:

Five Year : Rs. 5000/- (Personal)
: Rs. 10000/- (Institutional)
Life Time : Rs. 12000/- (Personal)
: Rs. 25000/- (Institutional)

The Draft/Cheque may please be made in favour of
'SATRAACHEE FOUNDATION'
C/A No. 40034072172. IFSC : SBIN0006551,
State Bank of India, Boring Canal Rd.-Rajapool,
East Boring Canal Road, Patna, Bihar, Pin: 800001

Google Pay No.: 9661792414

© सर्वाधिकार सुरक्षित (Copyright Reserved)

The editor does not have to agree with the published articles.

Editing/Publishing: Unpaid/ Unprofessional

Publisher: *Satraachee Foundation, Patna*

Editorial Contact:

Anand Bihari
Kala Kunj, Besdide Canara Bank
Bazar Samiti Road, Bahadurpur
Patna-800016

Website : http://satraachee.org.in
E-mail : satraachee@gmail.com
Mob. : 9661792414 (A.Bihari.)
: 9415256226 (Kamlesh Verma.)

❖❖❖

SATRAACHEE

In this Issue...

11 :: Editorial *Anand Bihari*

13 :: Dressing Dissent: Assertion and Resistance through Clothing and Appearance in George Eliot's *Mill on the Floss*
- Ms Garima Nandal, Prof. Sujata Rana

18 :: Daisy in R.K. Narayan's *The Painter of Signs*: A Representative of the Modern Woman
- Dr. Rohini D. Kasar

23 :: Women: An Inspiration to the Inspirers
- Dr. Abhibunnisha Begum, Dr. N. Satyanarayana

27 :: Bankim Chandra's Vision of New India through the Rise of Women in Rajmohan's Wife
- Md. Fajle Alam

31 :: An Ecofeminist Reading of Andrew Marvell's Selected Poems
- Mr Shirsak Ghosh

36 :: Evolution Of Women's Roles In Films
- Shivali K.C.

40 :: Revisiting Socio-Cultural Growth through Women Empowerment
- Dr. Anil B. Patil

45 :: Role of Dr. B. R. Ambedkar in Emancipation of Women in India
- Dr. Maheshkumar B. Bhaisare

49 :: Stifled Enunciates of Females in the Play *Lights Out*
- Vinita Virgandham

54 :: Rejection of Female Identity in *Uchalya* by Laxman Gaikwad
- Mr. Ravindra Ramdas Borse, Dr. Anshu Sharma & Dr. Jitendra Bagul

60 :: An Initiative In The Growth Of Indian Educational System Through Women's Empowerment
- Dr R. Subhashini, Dr S. Chitra

65 :: Women in Ngugi wa Thiongo's Novels: Breaking Gender Barriers
- Dr. Amit. Y. Kapoor

70 :: A Study on National Policy for the Empowerment of Women (2001)
- Dr. Sakshi Jain

75 :: Deeti: A Symbol Of Empowered Women in Amitav Ghosh's *Ibis* Trilogy

- Ms. Pranali Genu Bothe

148 :: Arundhati Roy: The Empowered Indian Woman Writer
- Dr.S.Shanmuga Priya

153 :: Women Empowerment in the Literature of Rashtrasant Tukdoji Maharaj
- Dr. Shravan R. Banasure

157 :: Continuous Learning and Women Empowerment in Rujuta Deshmukh's Poetry
- Dr. Bhagyashree S Gawate

161 :: The Feminist Reinterpretation of Shashi Deshpande's 'Dark Holds No Terror'
- Dr. Ajay Sahebrao Deokate

165 :: The Healing Power Of Nature In Chitra Banerjee Divakaruni's "The Mistress Of Spices"
- Mr. Bhojraj Pandhari Shrirame, Dr. Sunil G. Chaudhari

169 :: Regenerating Womanhood in Bhabhani Bhattacharya's So Many Hungers! and Anita Nair's Ladies Coupe
- Ms. M. Gayathri

173 :: Problems Of Women In Rural India: Reading Of Select Novels Of Shashi Tharoor And Chetan Bhagat
- Dr Hitendra B Dhote

177 :: Be 'You'; Be 'Your Voice': Not Somnolence but Self Consciousness will Ensure Women Empowerment in india
- Dr. Meenakshi Rathore

182 :: Women Empowerment Depicted in the Novels of Chetan Bhagat with Reference to *One Indian Girl* and *Revolution 2020*
- Smt. Leena C. Devre, Dr. Vijay Z. Chaudhari

185 :: Women Empowerment for National Development
- Dr. Prasad R Dagwale

189 :: Women Empowerment in India: A Path to Progress and Equality
- Arjun Namdevrao Khobragade

193 :: Empowerment of Women in Indigenous Badaga Community
- Dr. N. Venugopal

198 :: Problems and Prospects of Indian Women in Manju Kapur's *A Married Woman*
- Dr. S. Florence

203 :: Interpretation of Women Realization with reference to Bai Pan Bhari Deva
- Mr. Milind Subhash Bedse

207 :: The Powerful Voice of Protest and Empowerment in Maya Angelou's

SATRAACHEE, ISSN 2348-8425

आ वो होता जोहवीति सत्त: सत्राचीं रातिं मरुतो गृणान: । य ईवतो वृषणो अस्ति गोपा: सो अद्वयावी हवते व उक्थै: ।। (ऋ. 7.56.18)
उभयं शृणवच्च न इन्द्रो अर्वागिदं वच: । सत्राच्या मधवा सोमपीतये धिया शविष्ठ आ गमत् ।। (ऋ. 8.61.1)

* Editor :

Anand Bihari.
biharidot@ gmail.com
satraachee@gmail.com
09661792414, 09470738162

* Assistant Editor :

1. **Dr. Ankita Kumari**
2. **Mrs. Bhawna Mishra**

सत्राची के अंक











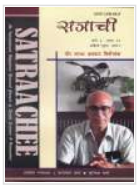


POWERED BY

Advisory Board

- **Prof. Mukteshwar Nath Tiwary.**
  Professor
  Hindi Bhawan, Vishwa Bharti,
  Shanti Niketan. West Bengal
  Mob. 09474765831
- **Dr. Kamlesh Verma.**
  Dept. of Hindi
  Rajkiya Mahila Mahavidyalya,
  Sewapuri,Varanasi, U.P.
  E-mail: kamleshvermajnu@gmail.com
  Mob. 09415256226
- **Dr. Ashutosh Partheshwar**
  Assistant Professor
  Dept. of Hindi
  Oriental College, Patna City.
  Mob. 09934260232
  E-mail: parthdot@gmail.com
- **Dr. Raju Ranjan Prasad.**
  Critic, History & Hindi Lit.
  C-19, Shreenagar,
  Ashiananagar, Patna-25
  Mob. - 08294307626
  E-mail: rajooranjan@gmail.com
- **Dr. Pushpalata Kumari.**
  Assistant Professor & H.O.D
  Political Science
  Patna University, Patna
  E-mail: drpushpalatammc@gmail.com
  Mob. 09431402736
- **Dr. Arvind Kumar.**
  Assistant Professor & H.O.D
  Music





Music
Patna University, Patna
Mob. 09835681230

UGC-CARE List

You searched for **"2348-8425"**. Total Journals : **1**

Search:

Sr.No.	Journal Title	Publisher	ISSN	E-ISSN	UGC-CARE coverage years	Details
1	Satraachee	Satraachee Foundation	2348-8425	NA	from July-2022 to October- 2023	Discontinued from Oct. 2023

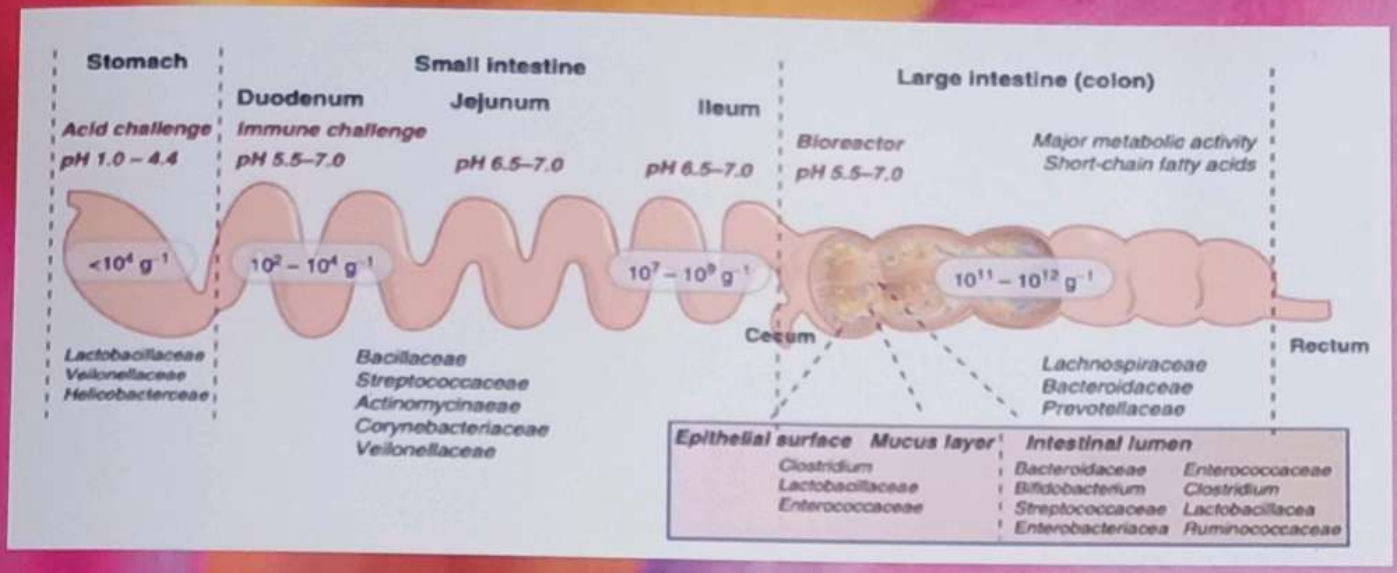
Showing 1 to 1 of 1 entries

Previous 1 Next

Copyright © 2024 Savitribai Phule Pune University. All rights reserved. | Disclaimer

Print ISSN: 0973-1431
Online ISSN: 0976-4755

BIOINFOLET



BL

A Quarterly Journal of Life Sciences

UGC-CARE APPROVED JOURNAL, INDEXED IN WEB OF SCIENCE
CITATION INDEX, EXPANDED.

Vol. 20 2023 No. 2 A

BIOINFOLET 20 (2 A) : 172 - 176, 2023

METAGENOME ANALYSIS : A TOOL OF MULTIPLE DIMENSIONS

Aparna M. Yadav, Bipinchandra B. Kalbande* and Rajkumar R. Khapekar**

Department of Botany, Arts, Commerce and Science College, Bhandara
*Department of Botany, Nabira Mahavidyalaya, Katol.
**Department of Botany, DRB Sindhu Mahavidyalaya, Nagpur.

ABSTRACT

Metagenomics is a rapidly evolving field that enables the study of microbial communities in their natural habitats, through the direct analysis of eDNA. This technique provides a culture-independent approach, to study complex microbial ecosystems. The typical steps involved in metagenome analysis include environmental sample collection, total DNA extraction, preparation of eDNA libraries, library screening by shotgun sequencing or amplicon sequencing, and analysis of sequence data. Metagenomics has found numerous applications in diverse fields, such as environmental monitoring, bioremediation, drug discovery, and human health. Recent advances in sequencing technologies and bioinformatics tools have made metagenomics more accessible and cost-effective, leading to increased adoption and deeper insights into microbial ecology.

Key words: Metagenomics, eDNA, Microbial Ecosystem, Bioremediation, Drug Discovery.

Introduction

Metagenomics is the study of genetic material recovered directly from environmental samples (Handelsman et al., 1998). This method involves analysis of DNA, isolated from microbial communities, which provides information on genetic diversity and metabolic potential of communities (Arumugam et al., 2021; Wang et al., 2021a; Cabello-Yeves et al., 2021).

Metagenomics is a collective study of genomic material obtained from a particular community directly from the field. Metagenomic studies are generally undertaken when the desired organism or a group of organisms can't be isolated from biological system. It is a combination of scientific research and sequencing techniques which allows to study microbial communities without culturing on artificial media (Hu et al., 2021a; Xiong and Yu, 2021; Li et al., 2021 a, b; Zhu et al., 2021a; Kalia and Kumar, 2022).

The first-ever metagenomic attempt was made by Healy et al. (1995). and called it as "zoolibraries". The term "metagenomics" was coined by Handelsman et. al. (1998). It involves several steps, including collection of samples, extraction of DNA, preparation of eDNA libraries screening with the help of shotgun or amplicon sequencing, and analysis of sequence data.

In recent days, Metagenomics is being employed to investigate microbial diversity and their functioning in various environments (Pascoal et al. 2020; Qian et al., 2021). It has been used it to study microbial diversity in wastewater treatment system (Li et al. 2021b), soil environment (Jiang et al. 2022a), marine ecosystems (Cleary et al. 2021), and gut micro-flora (Yuan et al. 2021 & 2022). In addition, it has also been used to identify and characterize antimicrobial resistant genes in environmental samples (Wu et al. 2022) and to study the impact of climate change on microbial communities (Hou et al. 2021). Now a days it has emerged as a powerful tool for studying microbial ecology (Vázquez-Baeza et

al.,2018; Zhu et al., 2019; Zhen et al., 2019; Singh et al., 2021b; Kanika Vasudeva et al., 2023).

Recent advancements in sequencing technologies, particularly next-generation sequencing, have dramatically increased the scale and scope of metagenomic studies and have revolutionized the field of biological sciences (Mardis, 2008; Thomas et al., 2012; Goodwin 2016; Quince et al., 2017; Thompson et al., 2017; Gilbert et al., 2018; Pasolli et al., 2020; Zou et al., 2022). These advances enabled the analysis of complex microbial communities systematically (Nayfach et al., 2016; Pasolli et al., 2019 a and b; Li et al., 2020 a and b; Palleja et al., 2020).

Biodiversity studies undertaken using the technique of metagenomics have revolutionized our understanding of microbial diversity, revealing the presence of new taxa present in diverse environments such as soil, oceans, and human gut (Singh et al., 2021b; Pasolli et al., 2022; Uritskiy et al., 2022; Wang et al., 2022). A set of all genomes belonging to each species, present in a given community can be seen as one metagenome (Ferrer 2016; Liu et al., 2021; Na et al., 2021; Zhang et al., 2021; Fukunaga et al., 2022; Wang et al., 2022). Thus Metagenomic studies can provide more comprehensive view of microbial diversity and their functional capabilities. By allowing culture-independent analysis of microbial flora metagenomics may provide information regarding uncultured microbial counterparts. Several novel organisms have been identified, discovered, and rediscovered in by this concept form surroundings. (Bao et al., 2021; Zhao et al., 2021; Jiang et al., 2022b). Therefore, this novel, relatively quick, and inexpensive survey method could prove valuable information on biodiversity

The concept of molecular phylogenetic approach for classification of prokaryotes was introduced by Woese and Fox (1977), Thereafter 16s rRNA sequencing emerged as a new trend for molecular phylogenetics and identification of microbes. Application of Metagenome sequencing, to environmental data gave encouraging results.

More efficient and accurate sequencing, analysis, and interpretation of complex microbiomes is now possible due to Metagenomics (Pasolli et al. 2019 a and b; Carr et al. 2021). Furthermore, the development of new computational tools has enabled researchers to extract more information from metagenomic datasets and improve taxonomic and functional annotations (Bowers et al. 2020; Forster et al. 2021).

Recent studies have demonstrated the utility of metagenomics in identifying novel bacterial strains and assessing the phylogenetic diversity of microbial communities in various environments, (Fernández-Antúnez et al. 2021; Prakash et al. 2021; Rinke et al. 2021)

Metagenomics plays a crucial role in discovering novel economically important genera having industrial and biotechnological applications, including bioremediation, biodegradation, plastic degradation and bioprocessing. (Lau et al. 2018; Gouda et al. 2019; Ma et al. 2019; Fujimoto et al. 2020; Lee et al. 2020; Kang et al. 2021; Kim et al. 2021; Song et al. 2021; Singh et al. 2021a; Jiang et al. 2021; Meng et al. 2021)

In conclusion, it can be said that metagenomics has revolutionized our understanding of microbial diversity and function in various environments, ranging from the human gut to extreme habitats. The technique has enabled the discovery of new microorganisms and functions that were previously unknown, shedding light on their potential biotechnological applications. Moreover, metagenomics has opened up new avenues for understanding the role of microbial communities in biogeochemical cycles, environmental management, and human health. Despite its limitations, such as the complexity of data analysis and the difficulty in interpreting results, metagenomics remains a powerful tool for studying the microbiome of various ecosystems and has significant potential for future research and applications.

References:

Arumugam, M., Harrington, E.D., Foerstner, K.U., Raes, J., Bork, P., and Hildebrand, F. (2021). *Nucleic Acids*

Research **49**: 75.

Bao, Y., Xie, Q., Li, X., Chen, X., and Hu, W. (2021). *Environmental Science and Pollution Research,* **28(6):** 7269.

Bowers, R. M., Kyrpides, N. C., Stepanauskas, R., Harmon-Smith, M., Doud, D., Reddy, T. B. and Schulz, F. (2020). *Nature Biotechnology,* **38(5):** 525.

Cabello-Yeves, P.J., Zemskaya, T.I., Rosselli, R., Coutinho, F.H., Zakharenko, A.S., Blinov, V.V., Rodriguez-Valera, F., and Logares, R. (2021). *Frontiers in microbiology* **12**: 2437.

Carr, R., Borenstein, E., Képès, F., and Di Camillo, B. (2021). *Briefings in Bioinformatics,* **22(2):** 1122.

Cleary, D. F., Becking, L. E., de Voogd, N. J., Renema, W., de Beer, M., van Soest, R. W., and Kitahara, M. V. (2021). *Environmental microbiology,* **23(2):** 747.

Fernández-Antúnez, C., Molina-Menor, E., and Villalba-Bermell, P. (2021). *Microorganisms,* **9(2):** 345.

Ferrer, M., Golyshina, O. V., Chernikova, T. N., and Golyshin, P. N. (2016). *Biochemical Society Transactions,* **44(3):** 837.

Forster, D., Paszkiewicz, K., Barquist, L., and Langridge, G. C. (2021). *Genome Biology,* **22(1):** 1.

Fujimoto, Z., Ichikawa, M., Akita, Y., Kumasaka, T., and Nakae, T. (2020). *Polymer Degradation and Stability,* **177:** 109.

Fukunaga, Y., Kurata, N., Suzuki, H., and Ohtsubo, Y. (2022). *Scientific Reports,* **12(1):** 1.

Gilbert, J. A., Jansson, J. K., and Knight, R. (2018). *BMC Biology,* **16(1):** 1.

Goodwin S, McPherson, J.D. and McCombie, W.R. (2016). *Nature Reviews Genetics*. **17(6):** 333.

Gouda, S., Banerjee, R., Basu, A., and Gupta, A. (2019). *Sustainable Energy and Fuels*, **3(2):** 264.

Handelsman, J., M. R. Rondon, S. F. Brady, J. Clardy, and R. M. Goodman (1998). *Chemistry and biology,* **5:** 10.

Healy, F. G., R. M. Ray, H. C. Aldrich, A. C. Wilkie, L. O. Ingram, and K. Shanmugam (1995). *Applied microbiology and biotechnology,* **43 (4):** 667.

Hou, J., Liu, L., Zhang, M., Zhang, X., Wang, H., and Chen, X. (2021). *Environmental science and technology,* **55(11):** 7867.

Hu, L., Liu, S., Wang, J., Li, X., Huang, H., Cheng, H. and Li, J. (2021a). *International Journal of Biological Macromolecules,* **183:** 907.

Jiang, C., Zhang, Y., Guo, Y., Wang, Y., Zhang, L., Ma, B., and Wu, J. (2022a). *Forest ecology and management* **507:** 119983.

Jiang, X., Tan, Y., Zhang, L., Chen, S., and Yang, S. (2021). *Journal of Applied Microbiology* **130(2):** 558.

Jiang, Y., Li, B., and Wang, Y. (2022b). *Journal of microbiology and biotechnology,* **32(1):** 1.

Kalia, V., and Kumar, V. (2022). *Biotech* **12 (1):** 1.

Kang, D. W., Lee, J. H., and Roh, H. (2021). *Sci. Rep.* **11:** 2886.

Kanika Vasudeva, Prabhsimran Kaur and Anjana Munshi (2023). High-throughput sequencing technologies in metagenomics, In *"Developments in Applied Microbiology and Biotechnology. Metagenomics to Bioremediation"*, Academic Press, Cambridge, Massachusetts, United States, 685.

Kim, Y. K., Yoon, J. J., and Park, H. D. (2021). *Sci Rep* **11**: 2842.

Lau, S. C. K., Tsoi, M. M. Y., Li, X., Dobretsov, S., Plakhotnikova, I., and Wong, P. K. (2018). *Marine Pollution Bulletin*, **133:** 459.

Lee, D.S., Kim, Y.H., and Hong, M. E. (2020). *Bioresour Technol* **304:** 123.

Li, B., Xie, Y., Zhang, H., Wang, Y., Liu, B., Liu, G., and Wu, J. (2020a). *Microbiome,* **8(1):** 1.

Li, J., Meng, F., Wang, S., Zhang, X., Wang, H., Zhu, X. and Chen, M. (2020b). *Science of The Total Environment*, **722**: 137855.

Li, Y., Li, C., Li, J., and Sun, B. (2021a). *BMC Microbiology*, **21(1):** 111.
Li, Y., Li, Z., Wang, S., Liu, G. and Huang, H. (2021b). *Frontiers in microbiology*, **12:** 706141.
Liu, L., Feng, Y., Zhang, X., and Li, X. (2021). *Journal of Hazardous Materials*, **403:** 123611.
Ma, C., Qin, D., Wang, J., Chen, X., and Han, R. (2019). *Bioresource Technology*, **276**: 158.
Mardis, E. R. (2008). Trends in Genetics, **24(3):** 133.
Meng, Y., Wang, S., Yu, H., Liu, X., Xu, H., Liao, L., and Sun, X. (2021). *Applied Microbiology and Biotechnology*, **105(1):** 101.
Na, J. G., Lee, Y. J., Kim, H. J., Shin, W. J., and Park, D. S. (2021). *Scientific Reports*, **11(1):** 1.
Nayfach, S., Rodriguez-Mueller, B., Garud, N., Pollard, K. S., and Sharpton, T. J. (2016). **26(11):** 1612.
Palleja, A., Mikkelsen, K. H., Forslund, S. K., Kashani, A., Allin, K. H., Nielsen, T. and Pedersen, O. (2020). *Nature Microbiology*, **5(5):** 625.
Pascoal, F., Magalhães, C., Costa, R., and Carvalho, M.F. (2020). *Microorganisms* **8:** 281.
Pasolli, E., Asnicar, F., Manara, S., Zolfo, M., Karcher, N., Armanini, F. and Segata, N. (2019a). *Cell*, **176(3):** 649.
Pasolli, E., Schiffer, L., Manghi, P., Renson, A., Obenchain, V., Truong, D. T. and Segata, N. (2019b). *Nature Methods*, **16(8):** 690.
Pasolli, E., Schiffer, L., Manghi, P., Renson, A., Obenchain, V., Truong, D. T. and Segata, N. (2020). *Nature Methods*, **17(9):** 847.
Pasolli, E., Truong, D. T., Malik, F., Waldron, L., Segata, N., and Huttenhower, C. (2022). *Nature Microbiology*, **7(3):** 370.
Prakash, D., Dhanjal, S., Sharma, S., Vikram, S., Pinnaka, A. K., Shouche, Y. S., and Shukla, P. (2021). Recent advances in metagenomics for exploring microbial diversity in the environment. In *"Microbial Diversity in the Genomic Era"* Springer, Singapore. pp. 221-244
Qian, P.Y., Wang, Y., Lee, O.O., Lau, S.C., Yang, J., Lafi, F.F., Al-Suwailem, A., and Wong, T.Y. (2021). *Microbial ecology* **81:** 92.
Quince, C., Walker, A. W., Simpson, J. T., Loman, N. J., and Segata, N. (2017). *Nature Biotechnology*, **35(9):** 833.
Rinke, C., Chuvochina, M., Mussig, A. J., Chaumeil, P. A., Davín, A. A., Waite, D. W. & and Parks, D. H. (2021). *Nature Communications*, **12(1):** 1.
Singh, R., Nigam, A., and Patel, A. K. (2021a). *Enzyme Microb Technol* **142:** 109717.
Singh, R., Singh, P., and Kaur, P. (2021b). *Journal of basic microbiology* **61:** 493.
Song, W., Xie, S., and Jiang, X. (2021). *Chemosphere* **287:** 132107
Thomas, T., Gilbert, J., and Meyer, F. (2012). *Microbial informatics and experimentation*, **2(1):** 3.
Thompson, L. R., Sanders, J. G., McDonald, D., Amir, A., Ladau, J., Locey, K. J., and Knight, R. (2017). *Nature* **551(7681):** 457.
Uritskiy, G. V., DiRuggiero, J., and Taylor, J. (2022). *mSystems*, **7(1):** e01220.
Vázquez-Baeza, Y., Callewaert, C., Debelius, J., Hyde, E., Marotz, C., Morton, J.T., and Knight, R. (2018). *Annual review of pharmacology and toxicology* **58**: 253.
Wang, H., Li, Y., Zhang, J., Li, H., Li, J., Wang, J., and Liu, B. (2022). *BMC Microbiology*, **22(1):** 1.
Wang, J., Li, Y., Liu, Y., Gao, Y., Huang, B., and Shen, Q. (2021a). *Scientific Reports*, **11(1):** 1.
Woese, C. R. and Fox, G. E. (1977). *Proceedings of the National Academy of Sciences*. **74(11):** 5088.
Wu, X., Liu, Y., Chen, J., Wang, Y., Lin, D., Zhou, Y., and Xie, S. (2022). *Environmental science and pollution research international*, **29(4):** 4592.
Xiong, W., and Yu, X. (2021). *Frontiers in microbiology*, **12:** 685712.
Yuan, J., Yang, Y., Wang, Z., Cheng, Y. and Liu, S. (2022). *Aquaculture* **545:** 737283.
Yuan, X., Yang, Y., Zhang, Y., Zhao, Y., and Li,

J. (2021). *Journal of global antimicrobial resistance*, **26:** 152.

Zhang, L., Yang, J., Hou, W., Zhang, X., and Wu, L. (2021). *Marine Genomics*, **57:** 100843.

Zhao, Q., Cui, Y., Bi, L., Wang, H., and Wu, J. (2021). *International Journal of Environmental Research and Public Health*, **18(18):** 9737.

Zhen, Z., Lu, H., Wang, L., and Yang, Y. (2019). *Frontiers in microbiology* **10:** 2479.

Zhu, C., Zhang, Q., Huang, L., Wang, Q., and Ma, T. (2021a). *Current opinion in biotechnology*, **70:** 94.

Zhu, Y., Li, B., Li, H., Zhang, Y., Li, J., and Dong, X. (2019). *Environmental Science and Pollution Research* **26:** 1089.

Zou, Y., Xue, W., Luo, G., Deng, Z., Qin, P., Guo, R., and Yang, Y. (2022). *Genome Biology*, **23(1):** 1.

SCISPACE Papers Discover Papers for your research Pricing Sign up

Home / Journals / BIOINFOLET - A Qua...

Overview Publishing trend Papers (632)

Journal • ISSN: 0973-1431

BIOINFOLET - A Quarterly Journal of Life Sciences

Dr. Anil M. Mungikar

About: BIOINFOLET - A Quarterly Journal of Life Sciences is an academic journal. The journal publishes majorly in the area(s): Biology & Population. It has an ISSN identifier of 0973-1431. Over the lifetime, 542 publications have been published receiving 1332 citations.

Topics: Biology, Population, Heritability ...read more

Trace this journal Share

Papers published on a yearly basis

2024	2019	2018	2017
2016	2015	2014	2013
2012	2011	2010	2009

Papers

Search papers Sort by: Citation Count

PDF Open Access Year

Showing all 632 results

Journal Article

Already have a manuscript?

Use our Manuscript Matcher to find the best relevant journals!

Find a Match

Refine Your Search Results

0976-4755 Search

Sort By: Title (A-Z)

Search Results

Found 1 results (Page 1) Share These Results

Exact Match Found

BIOINFOLET

Publisher: **PROF A M MUNGIKAR , MADHUKUNJI, 13 PANNALAL NAGAR, NEW OSMANPURA, AURANGABAD, INDIA, 431 005**

ISSN / eISSN: **0973-1431 / 0976-4755**

Additional *Web of Science* Indexes: **Zoological Record**

Share This Journal View profile page

** Requires free login.*

1 – 1 of 1

Items per page: 10

Filters Clear All

Web of Science Coverage

Open Access

Category

Country / Region

Language

Frequency

Journal Citation Reports

Editorial Disclaimer: As an independent organization, Clarivate does not become involved in and is not responsible for the editorial management of any journal or the business practices of any publisher. Publishers are accountable for their journal performance and compliance with ethical publishing standards. The views and opinions expressed in any journal are those of the author(s) and do not necessarily reflect the views or opinions of Clarivate. Clarivate remains neutral in relation to territorial disputes, and allows journals, publishers, institutes and authors to specify their address and affiliation details including territory.

Criteria for selection of newly submitted titles and re-evaluation of existing titles in the Web of Science are determined by the Web of Science Editors in their sole discretion. If a publisher's editorial policy or business practices negatively impact the quality of a journal, or its role in the surrounding literature of the subject, the Web of Science Editors may decline to include the journal in any Clarivate product or service. The Web of Science Editors, in their sole discretion, may remove titles from coverage at any point if the titles fail to maintain our standard of quality, do not comply with ethical standards, or otherwise do not meet the criteria determined by the Web of Science Editors. If a journal is deselected or removed from coverage, the journal will cease to be indexed in the Web of Science from a date determined by the Web of Science Editors in their sole discretion – articles published after that date will not be indexed. The Web of Science Editors' decision on all matters relating to journal coverage will be final.

Clarivate.™ Accelerating innovation.

© 2024 Clarivate Legal center Privacy notice Cookie policy
Manage cookie preferences Copyright notice Help

BioNanoScience
https://doi.org/10.1007/s12668-023-01122-0

Investigation of Structural and Microbial Properties of Samarium-Doped Nickel-Strontium Ferrite Nanoparticles Prepared via the Sol-Gel Route

Rajkanya M. Bhore[1] · Radhakrishnan M. Tigote[1] · Subiya K. Kazi[1] · Sanjay R. Chavan[1] · Rahul M. Khobragade[2] · Girdharilal B. Tiwari[3]

Accepted: 28 April 2023
© The Author(s), under exclusive licence to Springer Science+Business Media, LLC, part of Springer Nature 2023

Abstract
Nickel and samarium-doped strontium ferrite nanoparticles were synthesized using the sol-gel auto-combustion method. The micro-structural characteristics of the ferrite were investigated using X-ray diffraction (XRD) and field-emission scanning electron microscopy (FE-SEM). It was determined that the particle size ranged from 30 to 60 nm, which was confirmed by TEM as well. The vibrating sample magnetometer (VSM) revealed a strong magnetization with paramagnetic behaviour, and the existence of all elements was verified by energy dispersive X-ray spectroscopy (EDS). According to the BET adsorption isotherm, total surface area ranges from 13.77 to 28.49 $m^2\ g^{-1}$. At P/Po (0.99), the total pore volume ranges from 0.02 to 0.04 $cm^3\ g^{-1}$. The average pore width ranged from 3.5 to 6.5 nm, and the isotherm demonstrates type III with an H_3 hysteresis loop. The material shows 84% thermal stability and these synthesized nanoparticles are showing activity against both Gram-positive and Gram-negative bacterial pathogens. These synthesized nanoparticles are showing activity against both Gram-positive, Gram-negative bacteria and fungal pathogens, indicating broad-spectrum activity against microbial pathogens. The increased concentration of compound (0.1) showed antimicrobial activity against all the pathogens, which was measured as the zone of growth inhibition in diameter (mm) and compared with the standard antibiotics, streptomycin and clotrimazole.

Keywords Optical band gap · Magnetic hysteresis · Dielectric loss · Microbial activity

1 Introduction

Recent studies of matter at dimensions ranging from 1 to 100 nanometers, where unique phenomena provide innovative applications towards the physical and chemical characteristics, In nanomaterial's, previous efforts focused on various techniques for synthesizing nanoparticles with controllable size and shape, allowing them to be tailored in terms of their characteristics [1–3]. Many researchers have been drawn to spinel ferrite over the last few decades due to their cubic crystalline structure, greater magnetization, and opto-electric capabilities [4]. The synthesis of nanoparticles reveals high resistivity and reduced eddy current losses; nano-sized ferrites have superior catalytic, electric, and magnetic characteristics. These materials characteristics are extremely sensitive to preparation conditions such as sintering temperature, time, and additive type [5–9]. The addition of a modest number of larger ions, such as rare earth, can result in significant changes in both structural and magnetic characteristics due to the fact that rare-earth ions play a significant role in determining magneto-crystalline anisotropy in 4f–3d intermetallic compounds. Rare earth ions are known to have unpaired 4f electrons, which have the function of causing magnetic anisotropy due to their orbital structure. The impact of several rare earth metal substitutions on ferrites was diverse [10, 11].Rare earth oxides are emerging as interesting additions for improving ferrite characteristics [12,

✉ Radhakrishnan M. Tigote
rmtigote.chemobad@bamu.ac.in

[1] Department of Chemistry, Dr. Babasaheb Ambedkar Marathwada University, Sub campus Osmanabad, Aurangabad, Maharashtra 413 501, India

[2] Department of Microbiology, Dr. Babasaheb Ambedkar Marathwada University, Sub campus Osmanabad, Aurangabad, Maharashtra 413 501, India

[3] J.M. Patel Arts, Commerce and Science College, Research Centre, Dr. Babasaheb Ambedkar Marathwada University, Sub campus Osmanabad, Aurangabad, Maharashtra 413501, India

Published online: 19 June 2023

13]. The electromagnetic features of the nano-spinel structure may be easily adjusted by replacing different cations. Because of its very broad applicability, the doping of rare earth ion-replaced spinel ferrite nanoparticles has achieved a substantial increase in prominence and a remarkable change in the structural, magnetic, and electrical characteristics of ferrite due to rare earth ion substitution, some of which are on La, Gd, Eu, Dy, Er, Tb, Ce, and Y[14–16].

The development of appropriate coating is required to maintain the stability of magnetic iron oxide nanoparticles [17–20]. The essential characteristics of strontium ferrite were improved by doping it with several ions of varying valences. On the one hand, substituting unfamiliar ions for Fe^{3+} ions may alter the magnetic characteristics and phases that are most likely produced [21–24]. Ferrites have also been included in inductors, choke coils, recording heads, and magnetic amplifiers. These properties, together with its high chemical stability and mechanical hardness, make it suitable for electronic industries such as magnetic spin filters, data storage, microwave absorbers, and biomedical areas, where they are very useful for magnetic resonance imaging (MRI), bio-magnetic separation, tumour treatment by hyperthermia, drug delivery and release, catalysis and drug targeting [25–31]. The production of SmO_2 by Sm^{3+} doping lowered the relative density of ferrites. During sintering, this SmO_2 often stimulates grain expansion by replacing rare-earth ions for Fe in ferrite, causing lattice strain and structural disorder and allowing the dielectric and electrical characteristics to be modified. These characteristics can be improved based on the distribution of cations between A- and B-sites, which is significantly influenced by the nature of the ions for their properties [32, 33]. The synthesized methods involve high-temperature calcinations using various techniques to achieve microstructure, crystallography, magnetic, optical, and dielectrical properties, including sol-gel auto-combustion, micro-emulsion method, mechanical and ball-milling, hydrothermal synthesis and co-precipitation, thermal decomposition, citrate-nitrate-assisted, electrospinning, reverse micelle, and ultra-sonication [34, 35].

We focused on the new synthesis of $Ni_{0.8-x}Sm_xSr_{0.2}Fe_2O_4$ (x = 0.02, 0.04, 0.06, 0.08, 0.1) using the sol-gel auto combustion technique, and corresponding studies of various properties such as micro-structural, band energy, size, surface area, magnetic and dielectric constants, dielectric loss, and microbial activities were used to evaluate the resulted synthesis [36–49].

Nanoparticles are playing crucial role in the treatment of various diseases. NPs can attack on the cell membrane of bacterial cells and cause damage, disorganization of cell membrane and death of cell [48]. $Ni_{0.8-x}Sm_xSr_{0.2}Fe_2O_4$ nanoparticles were subjected for antimicrobial activity against different microbial pathogens which includes bacterial and fungal pathogens. Gram-positive *Bacillus subtilis* (ATCC 6633) *Staphylococcus aureus* (ATCC6538), and Gram-negative bacteria *Escherichia coli* (ATCC 8739), and fungal species *Aspergillus niger* ATCC 16404, and *Candida albicans* ATCC 10231 were used for study.

2 Material and Methods

2.1 Materials

The required materials for the preparation of $Ni_{0.8-x}Sm_xSr_{0.2}Fe_2O_4$ are purchased from HI media and used without purification. Nickel nitrate Ni $(NO_3)_2{\cdot}6H_2O$, strontium nitrate $Sr(NO_3)_2$, samarium nitrate Sm $(NO_3)_3{\cdot}6H_2O$, and ferric nitrate Fe $(NO_3)_3{\cdot}9H_2O$ were used as sources of La, A1, Y and Fe, with citric acid as a complexing agent and to maintain neutral condition ammonia is used. All of the chemicals are of A.R. quality

2.2 Synthesis of $Ni_{0.8-x}Sm_xSr_{0.2}Fe_2O_4$ Nanomaterial

For the new synthesis of $Ni_{0.8-x}Sm_xSr_{0.2}Fe_2O_4$ (x = 0.02, 0.04, 0.06, 0.08, 0.1), the nitrates of nickel, strontium, samarium and iron were taken in 20 mL distil water. To this beaker after solubility of all nitrates, citric acid (1:3) portion was added and reaction continued, stirring maintained at temperature 80 °C. For maintaining the neutral condition, the ammonia solution was added in stoichiometric amount. After continuous heating the solution get converted into gel. Again, gel was completely dried within the next 3 h to afford fine powder. This raw powder was calcinated at 1000 °C for 7 h to get pure ferrite nanomaterial.

2.3 Procedure for Antimicrobial Activity

$Ni_{0.8-x}Sm_xSr_{0.2}Fe_2O_4$ nanoparticles were tested against both Gram-negative and Gram-positive and fungal pathogens using agar well diffusion method [49]. The compounds were added in DMSO to reach final concentration 5 mg/mL. Standard antimicrobial drugs used for bacteria and fungi were streptomycin and clotrimazole respectively. Pathogenic cultures were transferred into sterile nutrient broth and incubated at 37 °C for 24 h. These broths containing pathogens were diluted with sterile saline to reach the turbidly to 0.5 McFarland standards. A 200 µL diluted suspension of pathogen was spread inoculated on Mueller Hinton agar plates separately. Wells were created on sterile agar plates and 100 µL of each compound was added in the well separately. One hundred microlitres of DMSO without compound was also added in separate well as negative control. Plates were incubated at 37 °C for 24 h. Plates were observed for zone of growth inhibition; absence of growth surrounding the

well indicates the positive result. The zone of inhibition was recorded in millimetre (mm).

3 Result and Discussion

A series of $Ni_{0.8-x}Sm_xSr_{0.2}Fe_2O_4$ (x = 0.02, 0.04, 0.06, 0.08, 0.1) has been successfully synthesized by employing the sol–gel technique. A UV–visible spectrophotometer is used to determine the absorption peak and band gap of a series. XRD was used to determine particle size, crystal structure, X-ray density, octahedral and tetrahedral sites, and interplanar distance. Field-emission scanning electron microscopy was used to determine structural morphology (FE-SEM). The elemental analysis of a series is provided by energy-dispersive spectroscopy (EDS). Vibrating sample magnetometer was used to investigate the magnetic characteristics (VSM). The average surface area was calculated using BET analysis as well as dielectric and microbial property studies.

3.1 Thermal Analysis

As shown in Fig. 1 the TGA curves from room temperature to 800 °C. At 150 °C the TGA curve was observed due to the weight loss of hydrated water from dried sample. The second portion of temperature range from 200 to 750 °C was associated with the decomposition of metal hydroxides in their respective metal oxide and loss of NH_3 gas. In addition, the larger weight loss in the second portion of peaks tends to show the response of nitrates and citric acid that eventually formed metal oxides. The endothermic peaks from 300 to 750 °C display the decomposition of unreacted citric acid [50]. For the successive formation of synthesized ferrite in spinel phase, the dried product was calcinated for 7 h at 1000 °C. The material shows 16% loss within 2 steps. So, synthesized material is 84% thermally stable. The thermal analysis was taken for a crude product, and the purpose of the analysis was to check the thermal stability of the material [51, 28, 52].

3.2 X-ray Analysis

XRD patterns of $Ni_{0.8-x}Sm_xSr_{0.2}Fe_2O_4$ (x = 0.02, 0.04, 0.06, 0.08, 0.1) ferrites, calcined at 1000 °C for 7 h, are shown in Fig. 2. The reflections from (111), (220), (300), (311), (222), (400), (411), (422), (511), and (440) planes confirmed a spinel cubic unit cell, and (311) plane shows the spinel phase structure [34, 35]. So, these allowed planes confirmed the formation of single-phase having a cubic spinel structure. The crystallite size was found in the range from 30 to 60 nm. The inter planar distance (d), lattice parameter (a), volume (V) and X-ray density (d_x), average particle size (D), hopping lengths 'L_A' and 'L_B' and crystal structure of all the composition have been calculated and are reported in Table 1.

A graph between the lattice parameter and crystalline size with composition is shown in Fig. 3. The crystalline size was calculated by using Debye Scherrer's equation as,

$$D = \frac{0.9\lambda}{\beta \cos\theta}$$

It illustrates the variation of lattice constant with Sm^{3+} content in ferrite. This is attributed to the replacement of smaller ionic radii Fe^{3+} by larger ionic radii Sm^{3+} ions. Figure 4 shows the X-ray density (dx) and unit cell volume (V) with Sm^{3+} concentration. The X-ray density (dx) is depending on the lattice parameter and molecular weight of the sample.

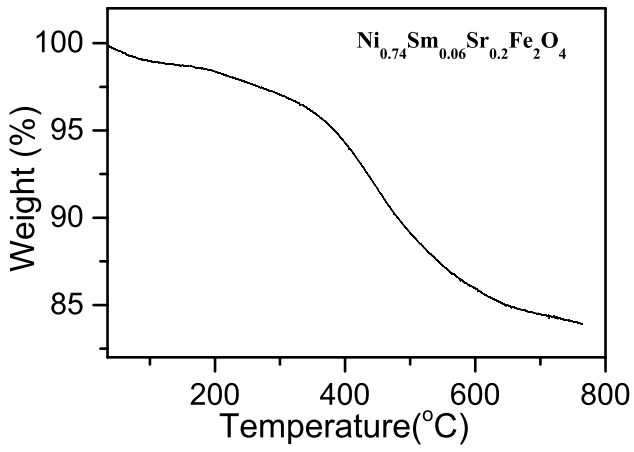


Fig. 1 TGA curve of $Ni_{0.8-x}Sm_xSr_{0.2}Fe_2O_4$

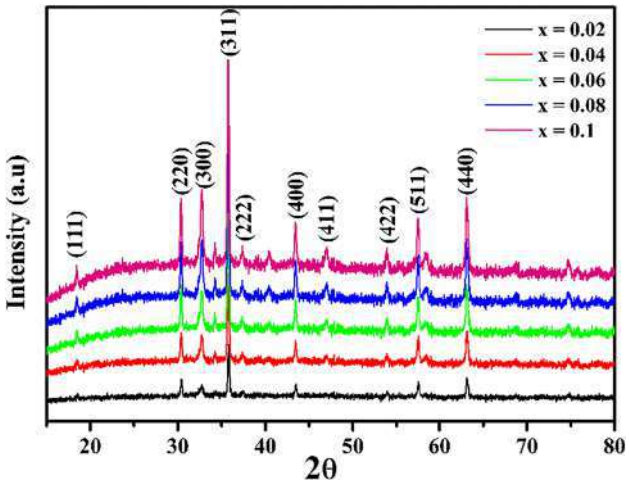


Fig. 2 X-ray pattern of $Ni_{0.8-x}Sm_xSr_{0.2}Fe_2O_4$

Table 1 Inter planar distance (d), lattice constant (a), volume (V) and X-ray density (d_x), average particle size (D), hopping lengths 'L_A' and 'L_B' and crystal structure of $Ni_{0.8-x}Sm_xSr_{0.2}Fe_2O_4$

Sr. No	X	d (Å)	a (Å)	V $(Å)^3$	d_x (g/cm^{-3})	D (nm)	L_A (Å)	L_B (Å)	Crystal structure
1	0.02	2.4679	8.304	572.63	0.0573	61.72	26.726	21.821	FCC
2	0.04	2.4889	8.315	574.89	0.0575	44.17	19.126	15.616	FCC
3	0.06	2.4881	8.311	574.06	0.0576	61.2	26.500	21.637	FCC
4	0.08	2.4329	8.292	570.13	0.0567	41.56	17.996	14.694	FCC
5	0.1	2.4338	8.294	570.54	0.0567	39.31	17.022	13.898	FCC

$$dx = \frac{8M}{NV}$$

Figure 5 depicts the variation in hopping lengths of octahedral and tetrahedral sites with concentration and are calculated by using following formulas,

$$LA = a\frac{\sqrt{3}}{4} \text{ and } LB = a\frac{\sqrt{2}}{4}$$

3.3 Field-Emission Scanning Electron Microscopy and Energy-Dispersive X-ray Spectroscopy

The microstructure and morphology of prepared samples using a field-emission scanning electron microscope (FE-SEM). The SEM images of $Ni_{0.8-x}Sm_xSr_{0.2}Fe_2O_4$ are shown in Fig. 6 (a–e). The microstructure of the sample varies as the concentration of samarium changes. The concentration of samarium increases with a constant concentration of strontium; the nanoparticles are distributed equally and show the cubic structure. Moreover, it is obvious that the particle size is between 40 and 80 nm [34]. Some agglomerates with an irregular shape were also seen. Therefore, the samples reveal multi-domain behaviour [53–56].

Elemental analysis of $Ni_{0.8-x}Sm_xSr_{0.2}Fe_2O_4$ (x = 0.02, 0.04, 0.06, 0.08, and 0.1) was done using the EDS technique shown in Fig. 7 (a–e). All the elements are present, and no extra or impurity peaks are present. The weight percentage and atomic percentage are shown in Tables 2 and 3, respectively. The weight percentage and atomic percentage are equal to 100% which shows the purity of material.

3.4 Transmission Electron Microscopy

Figure 8 (a–e) displays the TEM images of the synthesized materials. TEM analysis was used to verify the size of the particles. The instigated particle size corresponds with the XRD data. The results indicate that the particles are evenly dispersed, as can be seen in the micrographs. This is caused by the sample's strong magnetic properties. It is revealed that the particle size calculated from TEM data is more accurate than the crystallite size calculated from XRD data. The TEM micrograph at high magnetization shows that most of the particles appear to be cuboidal in shape and are agglomerated to some extent. The average grain size of materials is 40 to 80 nm from SEM morphology, which is in good agreement with TEM.

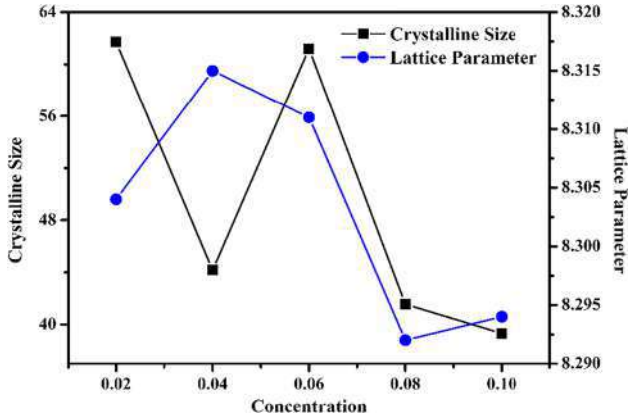


Fig. 3 Disparity of crystalline size and lattice parameter of $Ni_{0.8-x}Sm_xSr_{0.2}Fe_2O_4$

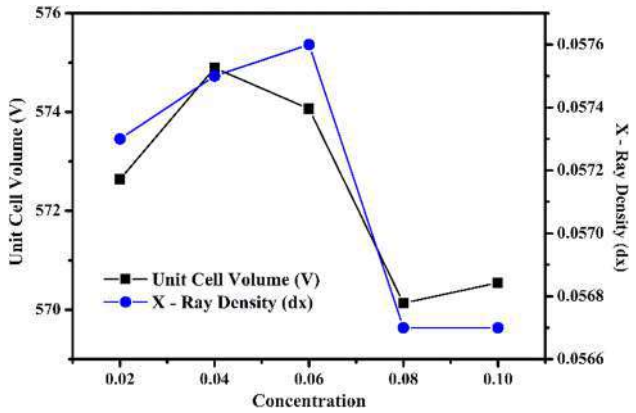


Fig. 4 Distinction of unit cell volume and X-ray density of $Ni_{0.8-x}Sm_xSr_{0.2}Fe_2O_4$

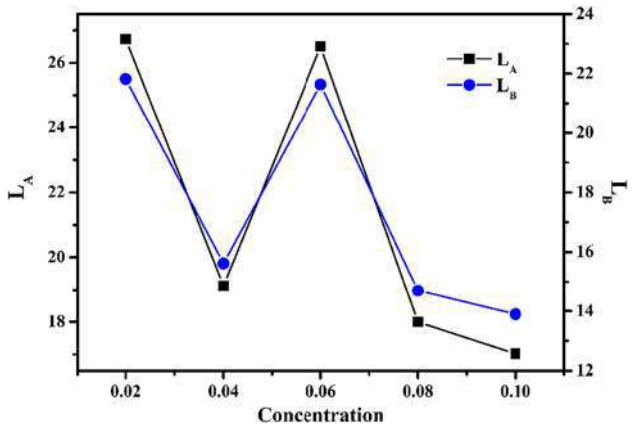


Fig. 5 Discrepancy of hopping length of $Ni_{0.8-x}Sm_xSr_{0.2}Fe_2O_4$

3.5 BET Analysis

The surface area and porosity of the resulted nanomaterials were measured using the Brunauer–Emmett–Teller (BET) equation [57]. Figure 9 (a–e) shows the BET surface area from the N_2 adsorption–desorption isotherm of $Ni_{0.8-x}Sm_xSr_{0.2}Fe_2O_4$; the BET surface area of the particles ranges from 13.77 to 28.29 m g^{-1}. The total pore volume at P/Po (0.99) is between 0.02 and 0.04 cm^3g^{-1}. The surface area, pore volume, and pore diameter of all the concentrations are tabulated in Table 4. The average pore diameter was found to be 3.5 to 6.5 nm. The isotherm represents type III, with an H_3 hysteresis loop, which is a characteristic of mesoporous materials. The surface effects are the result of finite-size scaling of crystallites, which in turn leads to a non-collinearity of magnetic moments on their surfaces.

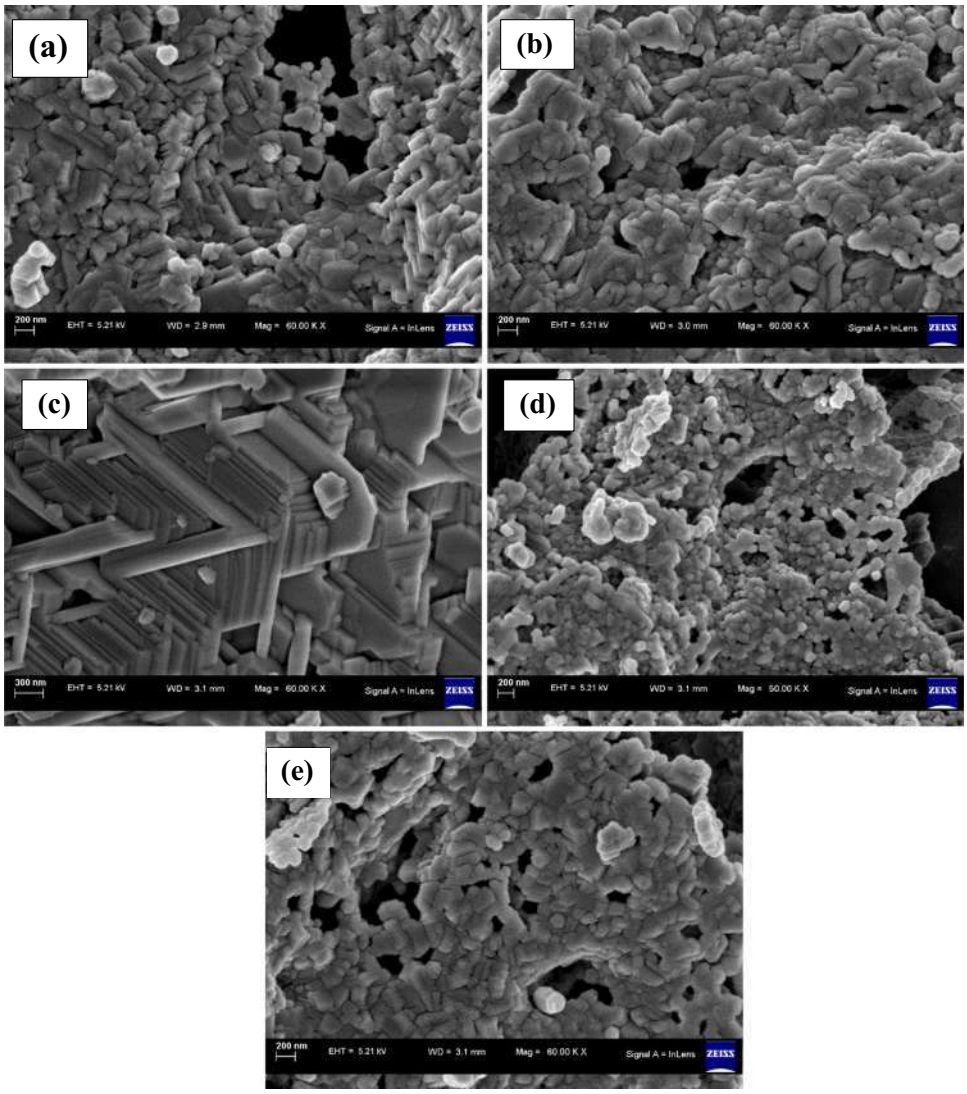


Fig. 6 SEM images of $Ni_{0.8-x}Sm_xSr_{0.2}Fe_2O_4$ (200 nm scale bar for each image) for different atomic weightpercent (**a**) 0.02, (**b**) 0.04, (**c**) 0.06,(**d**) 0.08, and (**e**) 0.1

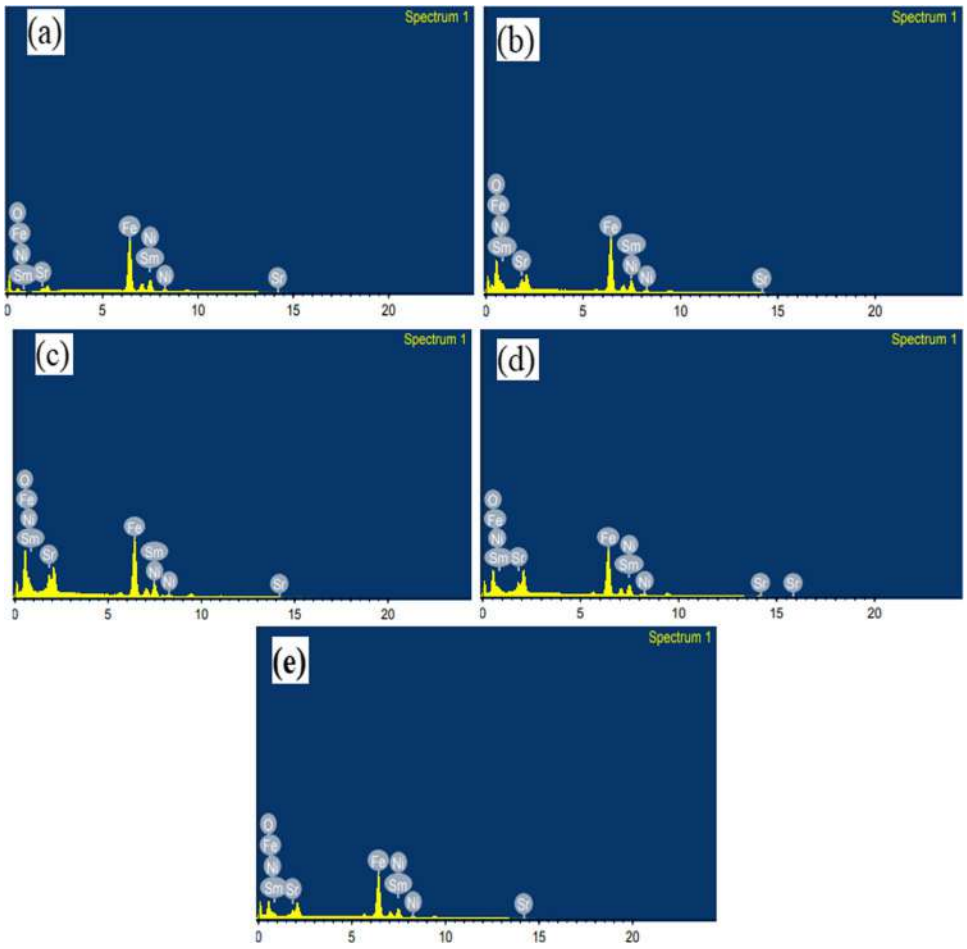


Fig. 7 EDS spectrum of $Ni_{0.8-x}Sm_xSr_{0.2}Fe_2O_4$ for different atomic weightpercent (**a**) 0.02, (**b**) 0.04, (**c**) 0.06,(**d**) 0.08, and (**e**) 0.1

Table 2 The elements of each sample composition $Ni_{0.8-x}Sm_xSr_{0.2}Fe_2O_4$ nanoparticles analysed by (weight %) obtained by EDS

Sr. No	Composition of nanoparticles	Elemental composition (weight %)				
		Ni	Sm	Sr	Fe	O
1	0.02	24.07	1.53	1.89	68.31	4.20
2	0.04	17.28	2.67	3.83	51.24	24.98
3	0.06	14.92	4.02	5.47	45.61	29.97
4	0.08	18.08	4.73	2.70	51.72	22.77
5	0.1	17.39	7.42	2.03	55.04	18.11

Table 3 The elements of each sample composition $Ni_{0.8-x}Sm_xSr_{0.2}Fe_2O_4$ nanoparticles analysed by (Atomic %) obtained by EDS

Sr. No	Composition of nanoparticles	Elemental composition (Atomic %)				
		Ni	Sm	Sr	Fe	O
1	0.02	21.27	0.53	1.12	36.46	13.62
2	0.04	10.38	0.63	1.54	32.37	55.08
3	0.06	8.38	0.88	2.06	26.92	61.76
4	0.08	11.32	1.16	1.13	34.06	52.33
5.	0.1	11.92	1.99	0.93	39.64	45.53

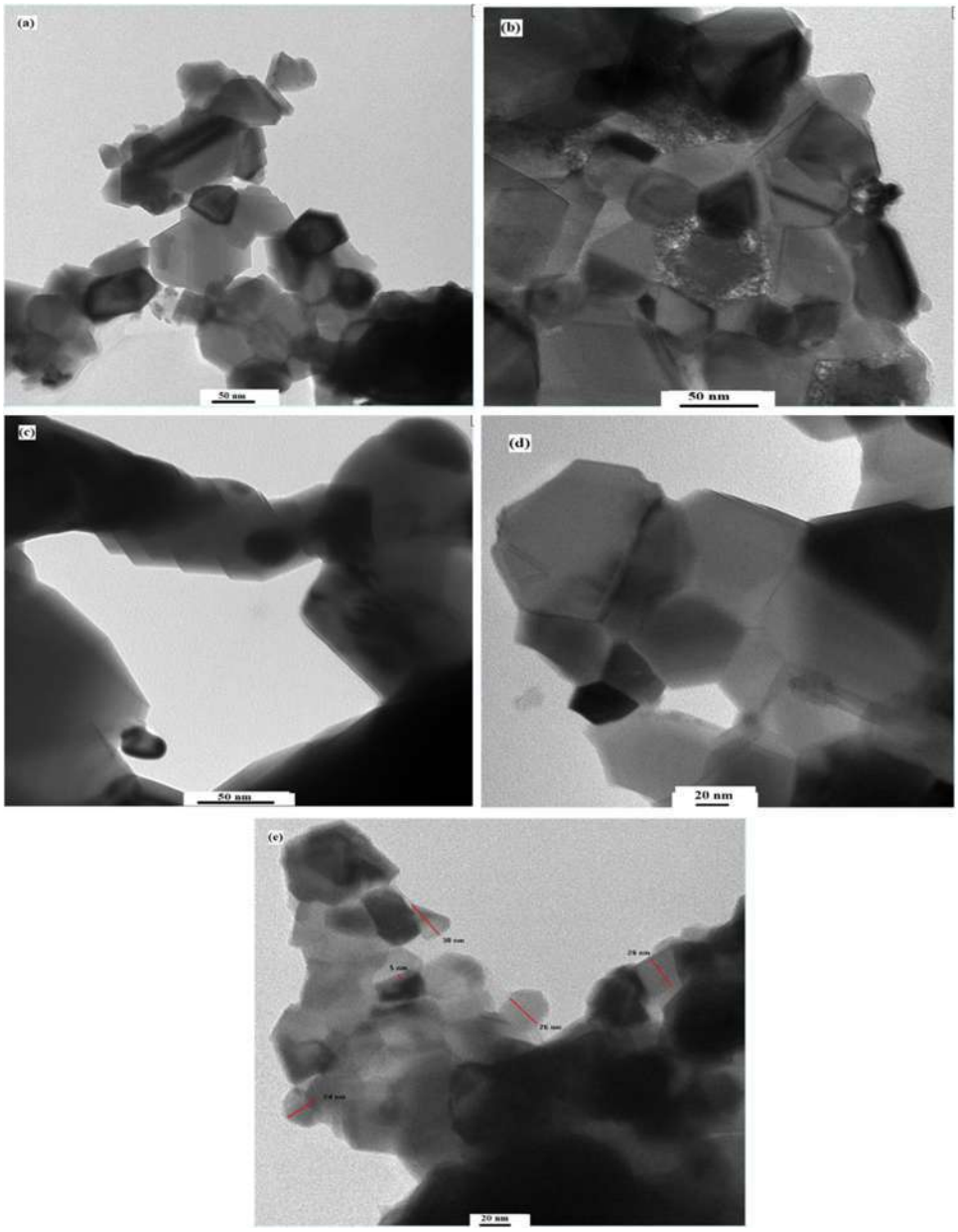


Fig. 8 TEM of $Ni_{0.8-x}Sm_xSr_{0.2}Fe_2O_4$ for different atomic weightpercent (**a**) 0.02, (**b**) 0.04, (**c**) 0.06, (**d**) 0.08, and (**e**) 0.1

3.6 Vibrating Sample Magnetometer

Figure 10 illustrates the M-H loops taken at room temperature for $Ni_{0.8-x}Sm_xSr_{0.2}Fe_2O_4$ (x = 0.02, 0.04, 0.06, 0.08, 0.1) concentration as a function of the applied magnetic field H. Table 5 shows the saturation magnetization (Ms), remanence magnetization (Mr), coercivity (Hc), squareness ratio, Bohr magnetization, and anisotropy constant (K_1) measured from these loops. The enclosure of Hc implies that these materials are soft magnetic. Spinel ferrites can have three different types of interactions: A-B, A-A, and B-B. The A-B interaction represents the most prevalent of the three [4]. The experimental μ_B per formula unit was calculated as follows:

$$\mu_B \frac{\mathrm{M\ x}M_s}{5585}$$

The consequent elevation in Ms and Mr might be attributed to the significant A-B exchange interactions. The squareness ratio has been seen to increase in value. Prepared samples behave as single-domain particles if the squareness ratio is less than 0.5. Hc coercivity is influenced by various parameters such as magnetic domain size, particle shape, grain size, magneto-crystalline anisotropy, and so on. Larger grains have a higher number of domain barriers. As a result, when these domain walls

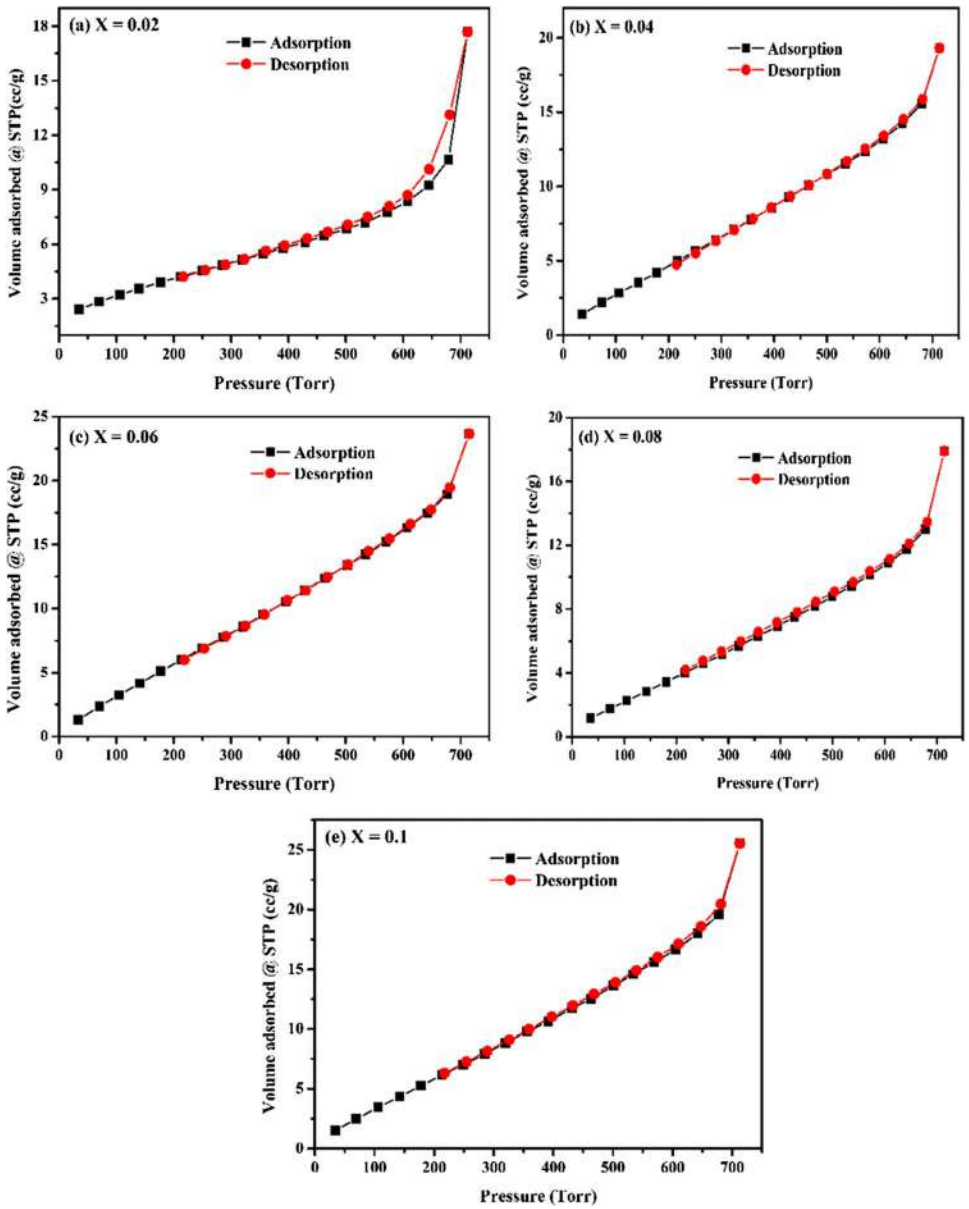


Fig. 9 BET adsorption isotherm of $Ni_{0.8-x}Sm_xSr_{0.2}Fe_2O_4$ for different atomic weightpercent (**a**) 0.02, (**b**) 0.04, (**c**) 0.06, (**d**) 0.08, and (**e**) 0.1

are magnetic or de-magnetized, domain wall movement consumes less energy than domain rotation [14].

Table 4 BET data of $Ni_{0.8-x}Sm_xSr_{0.2}Fe_2O_4$

Sr. No	Concentration	Total surface area (m^2g^{-1})	Pore volume (cm^3g^{-1})	Pore diameter (nm)
1	0.02	13.77	0.0254	3.53
2	0.04	21.54	0.0284	5.56
3	0.06	28.49	0.0354	5.15
4	0.08	17.45	0.0258	6.36
5	0.1	28.29	0.0374	5.49

Figure 11 exhibits an increase in saturation magnetization and remanence magnetization as concentration increases. In contrast to domain rotation's contribution to magnetization or demagnetization, wall movement rises as the number of walls increases with grain size. As a result, samples with larger grains should have lower coercivity, and vice versa. This might explain the compositions' progressive increase and reduction in coercivity. Figure 12 shows more the Bohr magnetization and anisotropy constant increase with increasing samarium concentration. Using the relation, the anisotropic constant K_1 is calculated.

$$K1 = \frac{M_s H_c}{2} \text{x } 104$$

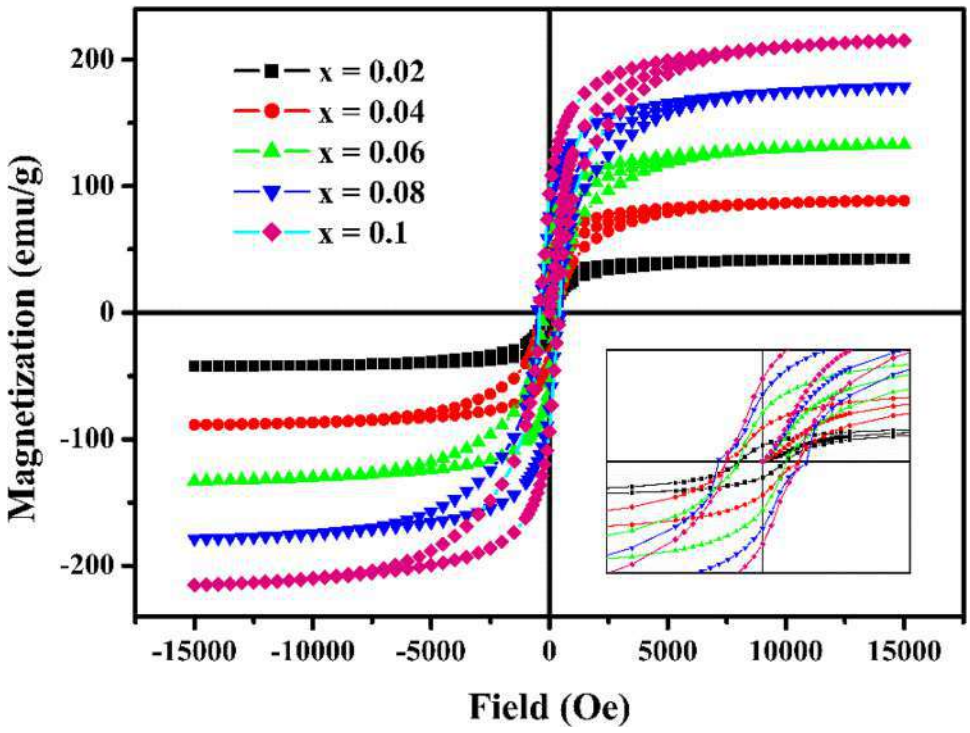


Fig. 10 Magnetic hysteresis loop of $Ni_{0.8-x}Sm_xSr_{0.2}Fe_2O_4$

Table 5 Magnetization data of $Ni_{0.8-x}Sm_xSr_{0.2}Fe_2O_4$

Sr. No.	X	M_S (emu/ gm)	M_r (emu/ gm)	M_r/M_S	Coercivity (H_C) (Oe)	μ_B (Bohr magneton)	$K_1 = \frac{M_s H_c}{2} x\ 10^4$ (erg/cm^3)
1.	0.02	45.23	18.46	0.40	259.05	1.95	5858.41
2.	0.04	89.26	38.89	0.43	412.06	3.89	18390.23
3.	0.06	133.3	56.4	0.42	276.05	5.86	18398.73
4.	0.08	182.84	76.83	0.42	503.86	8.10	46062.88
5.	0.1	215.86	94.34	0.43	429.06	9.63	46308.44

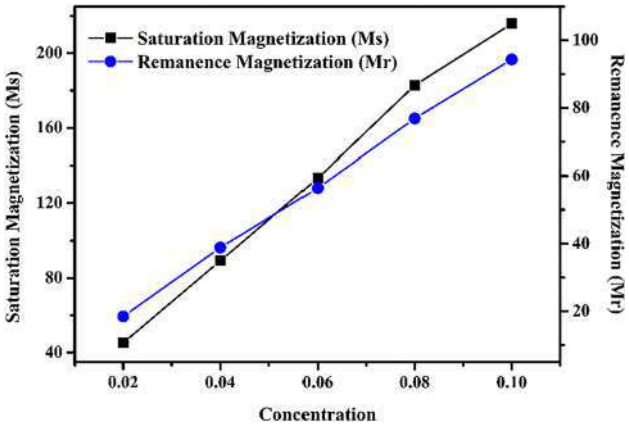


Fig. 11 Variation of Ms and Mr of $Ni_{0.8-x}Sm_xSr_{0.2}Fe_2O_4$

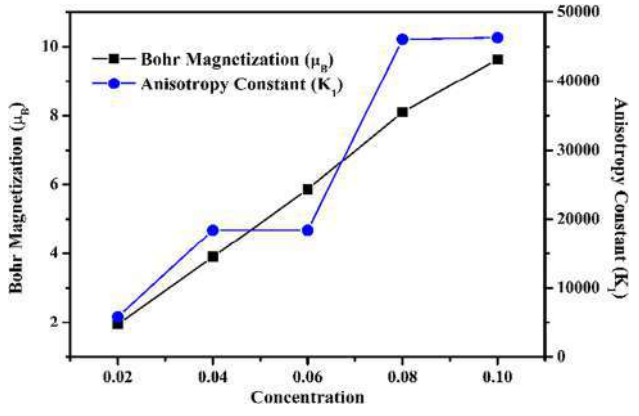


Fig. 12 Variation of μ_B and K_1 of $Ni_{0.8-x}Sm_xSr_{0.2}Fe_2O_4$

Table 6 Optical band gap of $Ni_{0.8-x}Sm_xSr_{0.2}Fe_2O_4$

Sr. No.	Concentration	Optical band gap
1	0.02	3.45
2	0.04	3.64
3	0.06	3.68
4	0.08	3.67
5	0.1	3.70

The anisotropy constant also shows properties of coercivity, i.e., gradual decrease and then increase [58], as all exhibiting data of coercivity as well as Bohr magnetization values containing the paramagnetic behaviour.

3.7 UV–Visible Spectroscopy

The UV–visible spectrophotometer is used to analyse the optical characteristics of a $Ni_{0.8-x}Sm_xSr_{0.2}Fe_2O_4$ (x = 0.02, 0.04, 0.06, 0.08, and 0.1). As a consequence of the experiment, all samples could be analysed using the maximum absorption peaks at 302.34 nm. Table 6 displayed that the band gap of all samples ranged from 3.4 to 3.7 eV. The confirming nickel concentration was decreased by doping of the Sm^{3+} ion, which resulted in a band gap increase due to the ionic size of strontium as well as the samarium composition. The UV–visible spectrum and the band gap spectrum are depicted in Fig. 13(a) and (b).

3.8 Dielectric Study

To examine the dielectric performance, the dielectric constant (ε') and dielectric loss (ε") of the $Ni_{0.8-x}Sm_xSr_{0.2}Fe_2O_4$ nanoparticles as they were synthesized were studied. The decreasing values of the dielectric constant with increasing frequency are shown in Fig. 14(a). According to the Koop's phenomenological theory, this variation in the dielectric constant highlights the dispersion that was caused by Maxwell interfacial polarization. The hopping of electrons between Ni^{2+} and Fe^{3+} ions may be the source of the dielectric constant's dispersion. $Ni_{0.8-x}Sm_xSr_{0.2}Fe_2O_4$ shows high values of the dielectric constant may be explained by the substitution of nickel and samarium for Fe^{3+}, which was predicted to enhance the density of vacancies and the probability of hopping conduction mechanisms. The Koop's model was supported by the first, gradual decline in dielectric constant. Because of the grains and grain boundaries' high dielectric values, variability developed. Figure 14(b) shows the room temperature frequency evolution of the dielectric loss for $Ni_{0.8-x}Sm_xSr_{0.2}Fe_2O_4$ nanoceramics by using dissipative factor (tan δ). It demonstrates that as the frequency rises, the dielectric loss drops significantly. Without a loss peak, the dielectric loss rises for all samples with decreasing frequency.

3.9 Antimicrobial Activity

The concentration of compounds 0.04, 0.06, 0.08 and 0.1 showed activity against the *Bacillus Subtilis* ATCC 6633, *Staphylococcus aureus* (ATCC6538), and *Escherichia coli* (ATCC 8739). NPs can interact with lipid content from the cell membrane and lead to pore formation that leads to cell growth inhibition [50]. The antifungal activity was observed with 0.04, 0.06, and 0.1 samples against fungal pathogens. 0.04 compounds were more active against *Aspergillus niger* ATCC 16404, and *Candida albicans* ATCC 10231. Zone of inhibition was not observed with DMSO. Standard drugs streptomycin and clotrimazole showed antimicrobial activity against all pathogens (Table 7) (Graph 1).

4 Conclusion

The $Ni_{0.8-x}Sm_xSr_{0.2}Fe_2O_4$ nanoparticles were successfully synthesized by using the sol–gel auto combustion method. The material shows 84% thermal stability. The XRD data reveals the cubic spinel structure with particle sizes ranging from 30 to 60 nm. The SEM micrograph shows cubic-shaped granular structure. The elemental analysis shows no extra peaks. So, all elements are present and pure, as well as size and morphology, which are verified by TEM. The BET adsorption isotherm shows total surface area ranging from 13.77 to 28.49 m^2g^{-1}. The total pore volume at P/Po (0.99) is between 0.02 and 0.04 cm^3g^{-1}. The average pore diameter was found to be 3.5 to 6.5 nm. The isotherm represents type III, with an H_3 hysteresis loop. The VSM data shows the synthesized nanoparticles are paramagnetic in nature, with coercivity ranging from 259 to 504 Oe along with Bohr magnetization ranging from 1.95 to 9.63 BM. Their Bohr magneton is enhanced as the anisotropic constant value increases. The band energy range was observed from 3.4 to 3.7 eV at optical density at 302.34 nm. The dielectric loss and dielectric tangent loss show steady loss. These synthesized nanoparticles are showing activity against both Gram-positive and Gram-negative bacterial pathogens *Bacillus Subtilis* ATCC 6633, *Staphylococcus aureus* (ATCC6538), and *Escherichia coli* (ATCC 8739) as well as against fungal pathogens Aspergillus *niger* ATCC 16404, and *Candida albicans* ATCC 10231.

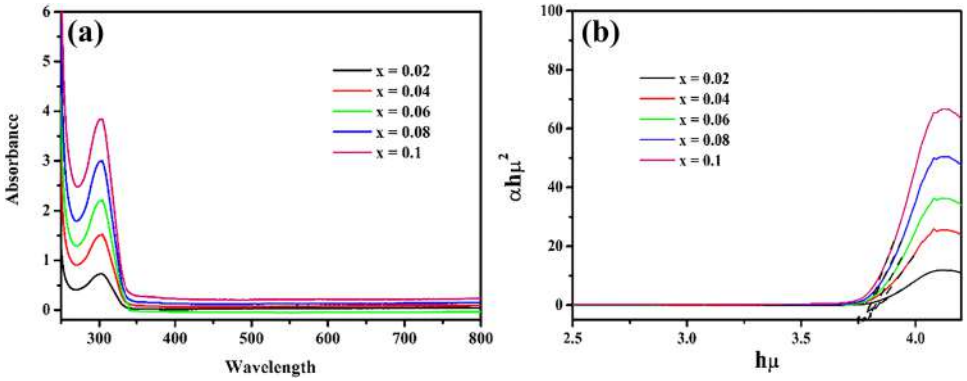


Fig. 13 (**a**) UV–visible spectra of $Ni_{0.8-x}Sm_xSr_{0.2}Fe_2O_4$; (**b**) optical band gap of $Ni_{0.8-x}Sm_xSr_{0.2}Fe_2O_4$

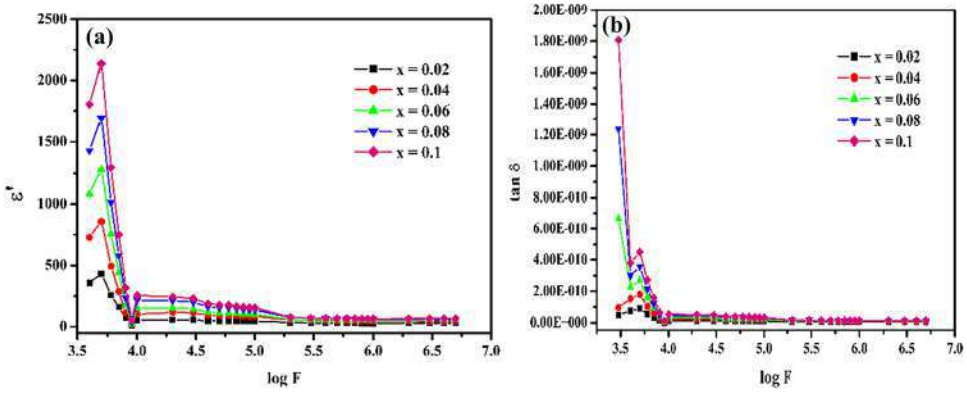


Fig. 14 (**a**) Relationship between dielectric constant and frequency (**b**) Plot of dielectric loss tangent verses frequency

Table 7 Antimicrobial activity of $Ni_{0.8-x}Sm_xSr_{0.2}Fe_2O_4$ nanoparticles against microbial pathogens[a]

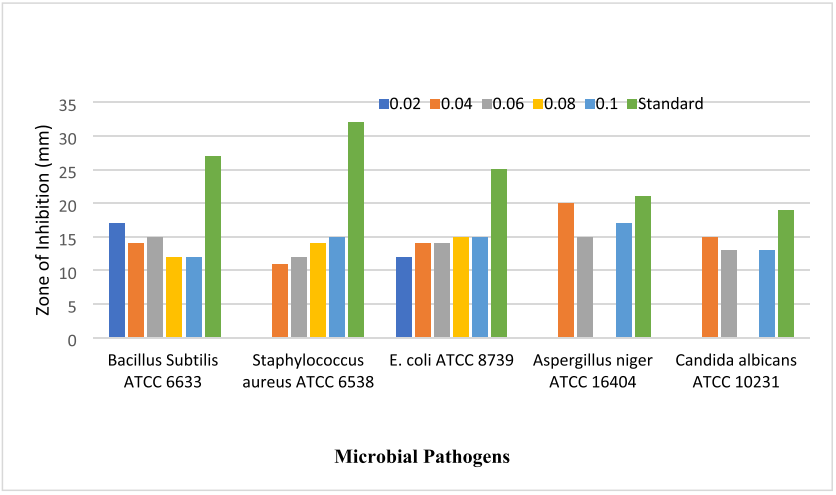
	0.02	0.04	0.06	0.08	0.1	Standard[b]
Bacillus Subtilis ATCC 6633	17	14	15	12	12	27
Staphylococcus aureus ATCC 6538	-	11	12	14	15	32
E. coli ATCC 8739	12	14	14	15	15	25
Aspergillus niger ATCC 16404	-	20	15	-	17	21
Candida albicans ATCC 10231	-	15	13	-	13	19

[a]Zone of growth inhibition in diameter(mm)

[b]Streptomycin and clotrimazole were used as standard antimicrobial drug

"-" indicates negative results

Graph 1 Antimicrobial activity of nanoparticles against different microbial pathogens



Acknowledgements We are thankful to Dr. Babasaheb Ambedkar Marathwada University, Sub-Campus Osmanabad, for performing this study.

Author Contribution Miss. Rajkanya M. Bhore: experimental table work

Dr. Radhakrishnan M. Tigote* (corresponding author): design the new research work and draught the original manuscript

Miss. Subiya K. Kazi: formal analysis

Mr. Sanjay R. Chavan: validation

Dr. Rahul M. Khobragade: study of antimicrobials

Dr. Girdharilal B. Tiwari: methodology

All co-authors have seen and agreed with the contents of the manuscript.

Funding The Chhatrapati Shahu Maharaj Research, Training, and Human Development Institute, Pune, for providing financial support to R. M. Bhore under the SARTHI Fellowship (CSMNRF-2020/2021-22/109).

Data availability All characterised data are available within the manuscript.

Declarations

Consent for Publication All authors have consented to publish.

Conflict of Interest The authors declare no competing interests.

References

1. Mathew, D. S., & Juang, R.-S. (2007). An overview of the structure and magnetism of spinel ferrite nanoparticles and their synthesis in microemulsions. *Chemical Engineering Journal, 129*(1), 51–65. https://doi.org/10.1016/j.cej.2006.11.001
2. Gadkari, A., Shinde, T., & Vasambekar, P. (2010). Influence of rare-earth ions on structural and magnetic properties of $CdFe_2O_4$ ferrites. *Rare Metals, 29*(2), 168–173. https://doi.org/10.1007/s12598-010-0029-z
3. Al-Hilli, M. F., Li, S., & Kassim, K. S. (2012). Structural analysis, magnetic and electrical properties of samarium substituted lithium–nickel mixed ferrites. *Journal of Magnetism and Magnetic Materials, 324*(5), 873–879. https://doi.org/10.1016/j.jmmm.2011.10.005
4. Şabikoğlu, İ., & Parali, L. (2014). FTIR and VSM properties of samarium-doped nickel ferrite. *Functional Materials Letters, 07*. https://doi.org/10.1142/s1793604714500465
5. Bhosale, R. R., Kumar, A., AlMomani, F., Ghosh, U., & Khraisheh, M. (2017). A comparative thermodynamic analysis of samarium and erbium oxide based solar thermochemical water splitting cycles. *International Journal of Hydrogen Energy, 42*(37), 23416–23426. https://doi.org/10.1016/j.ijhydene.2017.03.172
6. Rashmi, S. K., Bhojya Naik, H. S., Jayadevappa, H., Viswanath, R., Patil, S. B., & Madhukara Naik, M. (2017). Solar light responsive Sm-Zn ferrite nanoparticle as efficient photocatalyst. *Materials Science and Engineering: B, 225*, 86–97. https://doi.org/10.1016/j.mseb.2017.08.012
7. Rashmi, S. K., Naik, H. S. B., Jayadevappa, H., Sudhamani, C. N., Patil, S. B., & Naik, M. M. (2017). Influence of Sm^{3+} ions on structural, optical and solar light driven photocatalytic activity of spinel $MnFe_2O_4$ nanoparticles. *Journal of Solid State Chemistry, 255*, 178–192. https://doi.org/10.1016/j.jssc.2017.08.013
8. Samoila, P., Cojocaru, C., Sacarescu, L., Dorneanu, P. P., Domocos, A.-A., & Rotaru, A. (2017). Remarkable catalytic properties of rare-earth doped nickel ferrites synthesized by sol-gel autocombustion with maleic acid as fuel for CWPO of dyes. *Applied Catalysis B: Environmental, 202*, 21–32. https://doi.org/10.1016/j.apcatb.2016.09.012
9. Tahir Farid, H. M., Ahmad, I., Bhatti, K. A., Ali, I., Ramay, S. M., & Mahmood, A. (2017). The effect of praseodymium on cobalt-zinc spinel ferrites. *Ceramics International, 43*(9), 7253–7260. https://doi.org/10.1016/j.ceramint.2017.03.016
10. Almessiere, M. A., Slimani, Y., & Baykal, A. (2018). Structural and magnetic properties of Ce-doped strontium hexaferrite. *Ceramics International, 44*(8), 9000–9008. https://doi.org/10.1016/j.ceramint.2018.02.101
11. Ashraf, G. A., Zhang, L., Abbas, W., & Murtaza, G. (2018). Synthesis and characterizations of Al-Sm substituted Ba-Sr M-type hexagonal ferrite nanoparticles via sol-gel route. *Ceramics International, 44*(15), 18678–18685. https://doi.org/10.1016/j.ceramint.2018.07.096
12. Dahiya, M. S., Tomer, V. K., & Duhan, S. (2018). 31 - Metal–ferrite nanocomposites for targeted drug delivery. In A. A. M. Inamuddin & A. Mohammad (Eds.), *Applications of nanocomposite materials in drug delivery* (pp. 737–760). *Woodhead Publishing*. https://doi.org/10.1016/B978-0-12-813741-3.00032-7
13. Slimani, Y., Güngüneş, H., Nawaz, M., Manikandan, A., El Sayed, H. S., Almessiere, M. A., Sözeri, H., Shirsath, S. E., Ercan, I., & Baykal, A. (2018). Magneto-optical and microstructural properties of spinel cubic copper ferrites with Li-Al co-substitution. *Ceramics International, 44*(12), 14242–14250. https://doi.org/10.1016/j.ceramint.2018.05.028
14. Srinivasamurthy, K. M., Angadi, V. J., Kubrin, S. P., Matteppanavar, S., Kumar, P. M., & Rudraswamy, B. (2018). Evidence of enhanced ferromagnetic nature and hyperfine interaction studies of Ce-Sm doped Co-Ni ferrite nanoparticles for microphone applications. *Ceramics International, 44*(15), 18878–18885. https://doi.org/10.1016/j.ceramint.2018.07.123
15. Tiwari, S., & Vitta, S. (2018). Magnetoelectric and magnetodielectric coupling and microwave resonator characteristics of $Ba_{0.5}Sr_{0.5}Nb_2O_6/CoCr_{0.4}Fe_{1.6}O_4$ multiferroic composite. *Scientific Reports, 8*(1), 11619. https://doi.org/10.1038/s41598-018-30132-2
16. Xie, T., Xu, L., Liu, C., Yang, J., Zhang, X., Tian, M., & Cui, C. (2018). Preparation and magnetic properties of Sm–Co doped strontium ferrite. *Materials Technology, 33*(7), 467–473. https://doi.org/10.1080/10667857.2018.1465746
17. Almessiere, M. A., Slimani, Y., Ali, S., Baykal, A., Ercan, I., & Sozeri, H. (2019). Nd^{3+} ion-substituted $Co_{1-2x}Ni_xMn_xFe_{2-y}Nd_yO_4$ nanoparticles: Structural, morphological, and magnetic investigations. *Journal of Inorganic and Organometallic Polymers and Materials, 29*(3), 783–791. https://doi.org/10.1007/s10904-018-1052-z
18. Almessiere, M. A., Slimani, Y., Güner, S., Baykal, A., & Ercan, I. (2019). Effect of dysprosium substitution on magnetic and structural properties of $NiFe_2O_4$ nanoparticles. *Journal of Rare Earths, 37*(8), 871–878. https://doi.org/10.1016/j.jre.2018.10.009
19. Gajula, G. R., Buddiga, L. R., Chidambara Kumar, K. N., & Dasari, M. (2019). Influence of Sm and Nb on the structural, electric, magnetic and magneto-electric properties of $BaTiO_3$-$Li_{0.5}Fe_{2.5}O_4$ composite ceramics grown by the conventional solid state technique. *Journal of Materials Science: Materials in Electronics, 30*(2), 1262–1274. https://doi.org/10.1007/s10854-018-0394-1
20. Martínez-Pérez, J. P., Bolarín-Miró, A. M., Pedro-García, F., Cortés-Escobedo, C. A., Barba-Pingarrón, A., & Sánchez-De Jesús, F. (2019). Magnetic and dielectric characterization of $_xBiFeO_3$:(1-x) $SrFe_{12}O_{19}$ multiferroic composites. *Journal of Alloys and Compounds, 808*, 151700. https://doi.org/10.1016/j.jallcom.2019.151700
21. Almessiere, M. A., Slimani, Y., Demir Korkmaz, A., Baykal, A., Albetran, H., Saleh, T. A., Sertkol, M., & Ercan, I. (2020). A study

on the spectral, microstructural, and magnetic properties of Eu–Nd double-substituted $Ba_{0.5}Sr_{0.5}Fe_{12}O_{19}$ hexaferrites synthesized by an ultrasonic-assisted approach. *Ultrasonics Sonochemistry, 62*, 104847. https://doi.org/10.1016/j.ultsonch.2019.104847

22. Ashraf, G. A., Rasool, R. T., Hassan, M., & Zhang, L. (2020). Enhanced photo Fenton-like activity by effective and stable Al–Sm M-hexaferrite heterogenous catalyst magnetically detachable for methylene blue degradation. *Journal of Alloys and Compounds, 821*, 153410. https://doi.org/10.1016/j.jallcom.2019.153410
23. Esha, I. N., Munny, K. N., Khan, M. N. I., & Maria, K. H. (2020). $(1-x)BaTi_{0.5}Mn_{0.5}O_3 + (x)Ni_{0.6}Zn_{0.4}Fe_{1.85}Sm_{0.15}O_4$ composite multiferroics: Analyzing the customizing effect on conductive and magnetic properties of $BaTi_{0.5}Mn_{0.5}O_3$ by substituting $Ni_{0.6}Zn_{0.4}Fe_{1.85}Sm_{0.15}O_4$ at different concentrations. *AIP Advances, 10*(12), 125026. https://doi.org/10.1063/5.0028086
24. Meng, X., Wang, Y., Zhao, Y., Zhang, T., Yu, N., Chen, X., Miao, M., & Liu, T. (2020). In-situ exsolution of nanoparticles from Ni substituted $Sr_2Fe_{1.5}Mo_{0.5}O_6$ perovskite oxides with different Ni doping contents. *Electrochimica Acta, 348*, 136351. https://doi.org/10.1016/j.electacta.2020.136351
25. Regulska, E., Breczko, J., Basa, A., & Dubis, A. T. (2020). Rare-earth metals-doped nickel aluminate spinels for photocatalytic degradation of organic pollutants. *Catalysts, 10*(9). https://doi.org/10.3390/catal10091003
26. Shezad, M., Liu, X., Feng, S., Kan, X., Shehzad, T. J., Mudassir, A., Wang, W., & Liu, C. (2020). Investigating the co-substitution impact of yttrium–nickel cations on lattice, morphological and magnetic parameters of SrM based ceramics. *Ceramics International, 46*(7), 8918–8927. https://doi.org/10.1016/j.ceramint.2019.12.138
27. Slimani, Y., Unal, B., Almessiere, M. A., Korkmaz, A. D., Shirsath, S. E., Yasin, G., Trukhanov, A. V., & Baykal, A. (2020). Investigation of structural and physical properties of Eu^{3+} ions substituted $Ni_{0.4}Cu_{0.2}Zn_{0.4}Fe_2O_4$ spinel ferrite nanoparticles prepared via sonochemical approach. *Results in Physics, 17*, 103061. https://doi.org/10.1016/j.rinp.2020.103061
28. Yousaf, M., Akhtar, M. N., Wang, B., & Noor, A. (2020). Preparations, optical, structural, conductive and magnetic evaluations of RE's (Pr, Y, Gd, Ho, Yb) doped spinel nanoferrites. *Ceramics International, 46*(4), 4280–4288. https://doi.org/10.1016/j.ceramint.2019.10.149
29. Abdo, M. A., & El-Daly, A. A. (2021). Sm-substituted copper-cobalt ferrite nanoparticles: Preparation and assessment of structural, magnetic and photocatalytic properties for wastewater treatment applications. *Journal of Alloys and Compounds, 883*, 160796. https://doi.org/10.1016/j.jallcom.2021.160796
30. Almessiere, M. A., Slimani, Y., Algarou, N. A., Gondal, M. A., Wudil, Y. S., Younas, M., Auwal, I. A., Baykal, A., Manikandan, A., Zubar, T. I., Kostishin, V. G., Trukhanov, A. V., & Ercan, I. (2021). Electronic, magnetic, and microwave properties of hard/soft nanocomposites based on hexaferrite $SrNi_{0.02}Zr_{0.02}Fe_{11.96}O_{19}$ with variable spinel phase MFe_2O_4 (M = Mn, Co, Cu, and Zn). *Ceramics International, 47*(24), 35209–35223. https://doi.org/10.1016/j.ceramint.2021.09.064
31. Atta, S., Halder, M., & Meikap, A. (2021). Effect of terbium doping on the optical, electrical and magnetic properties of nanocrystalline nickel ferrite. *Journal of Materials Science: Materials in Electronics, 32*. https://doi.org/10.1007/s10854-021-05407-6
32. Gopal Boda, N. B., Rapolu Sridhar, A., Panasa Reddy, D., & Ravinder. (2021). Thermoelectric power, electrical resistivity and magnetic properties of Ni-Sm nano-particles. *biointerface research in applied. Chemistry, 11*(1), 7835–7846. https://doi.org/10.33263/BRIAC111.78357846
33. Hashim, M., Boda, N., Ahmed, A., Sharma, S. K., Ravinder, D., Sumalatha, E., Ul-Hamid, A., Ismail, M. M., Chaman, M., Shirsath, S. E., Kumar, R., Kumar, S., Meena, S. S., & Nasir, M. (2021). Influence of samarium doping on structural, elastic, magnetic, dielectric, and electrical properties of nanocrystalline cobalt ferrite. *Applied Physics A, 127*(7), 526. https://doi.org/10.1007/s00339-021-04686-4
34. Khan, M., Bisen, S., Shukla, J., Mishra, A., & Sharma, P. (2021). Investigations on the structural and electrical properties of Sm^{3+}-doped nickel ferrite–based ceramics. *Journal of Superconductivity and Novel Magnetism, 34*(3), 763–780. https://doi.org/10.1007/s10948-020-05754-1
35. Selvaraj, S., Gandhi, U., Berchmans, L. J., & Mangalanathan, U. (2021). Effect of magnetic ion substitution on the structure and temperature-dependent magnetic properties of strontium hexaferrite. *Materials Technology, 36*(1), 36–45. https://doi.org/10.1080/10667857.2020.1723832
36. Prodan, A. M., Iconaru, S. L., Chifiriuc, C. M., Bleotu, C., Ciobanu, C. S., Motelica-Heino, M., Sizaret, S., & Predoi, D. (2013). Magnetic properties and biological activity evaluation of iron oxide nanoparticles. *Journal of Nanomaterials, 2013*, 1–7.
37. Barbara Drašler, D. D., Novak, S., Valant, J., Boljte, S., Otrin, L., Rappolt, M., Sartori, B., Iglič, A., Kralj-Iglič, V., Šuštar, V., Makovec, D., Gyergyek, S., Hočevar, M., Godec, M., & Zupanc, J. (2014). Effects of magnetic cobalt ferrite nanoparticles on biological and artificial lipid membranes. *International Journal of Nanomedicine, 9*, 1559–1581. https://doi.org/10.2147/IJN.S57671
38. Pašukonienė, V., Mlynska, A., Steponkienė, S., Poderys, V., Matulionytė, M., Karabanovas, V., Statkutė, U., Purvinienė, R., Kraśko, J. A., Jagminas, A., Kurtinaitienė, M., Strioga, M., & Rotomskis, R. (2014). Accumulation and biological effects of cobalt ferrite nanoparticles in human pancreatic and ovarian cancer cells. *Medicina, 50*(4), 237–244. https://doi.org/10.1016/j.medici.2014.09.009
39. Hanini, A., Massoudi, M. E., Gavard, J., Kacem, K., Ammar, S., & Souilem, O. (2016). Nanotoxicological study of polyol-made cobalt-zinc ferrite nanoparticles in rabbit. *Environmental Toxicology and Pharmacology, 45*, 321–327. https://doi.org/10.1016/j.etap.2016.06.010
40. Montha, W., Maneeprakorn, W., Buatong, N., Tang, I. M., & Pon-On, W. (2016). Synthesis of doxorubicin-PLGA loaded chitosan stabilized (Mn, Zn)Fe_2O_4 nanoparticles: Biological activity and pH-responsive drug release. *Materials Science and Engineering: C, 59*, 235–240. https://doi.org/10.1016/j.msec.2015.09.098
41. Saini, A., Rana, K., Thakur, A., Thakur, P., Mattei, J. L., & Queffelec, P. (2016). Low loss composite nano ferrite with matching permittivity and permeability in UHF band. *Materials Research Bulletin, 76*, 94–99. https://doi.org/10.1016/j.materresbull.2015.12.002
42. Gomes, G. A., Costa, G. L., & Figueiredo, A. B.-H. S. (2018). Synthesis of ferrite nanoparticles $Cu_{1-x}Ag_xFe_2O_4$ and evaluation of potential antibacterial activity. *Journal of Materials Research and Technology, 7*(3), 381–386. https://doi.org/10.1016/j.jmrt.2018.04.021
43. García-Cruz, A., Rincón-Enríquez, G., Ilyina, A., Guízar-González, C., Mtz-Enríquez, A. I., Díaz-Jiménez, L., Quiñones-Aguilar, E. E., Enríquez-Vara, J., Ramos-González, R., & Aguilar-González, C. N. (2019). Bactericidal in-vitro effect of zinc ferrite nanoparticles and the orange wax extracts on three phytopathogen microorganisms. *IEEE Transactions on NanoBioscience, 18*(4), 528–534. https://doi.org/10.1109/tnb.2019.2937840
44. Thakur, A., Sharma, N., Bhatti, M., Sharma, M., Trukhanov, A. V., Trukhanov, S. V., Panina, L. V., Astapovich, K. A., & Thakur, P. (2020). Synthesis of barium ferrite nanoparticles using rhizome extract of Acorus Calamus: Characterization and its efficacy against different plant phytopathogenic fungi. *Nano-Structures & Nano-Objects, 24*, 100599. https://doi.org/10.1016/j.nanoso.2020.100599
45. Rafiq, S., Aadil, M., Warsi, M. F., Yousaf, S., Alotaibi, M. T., El-Bahy, S. M., & Shahid, M. (2022). NiO nanoparticles and their

nanohybrid with flat rGO sheets: As an ideal electroactive material for hybrid capacitor applications. *Ceramics International, 48*(10), 14596–14605. https://doi.org/10.1016/j.ceramint.2022.01.353
46. Rafiq, S., Alanazi, A. K., Bashir, S., Elnaggar, A. Y., Mersal, G. A. M., Ibrahim, M. M., Yousaf, S., & Chaudhary, K. (2022). Optimization studies for nickel oxide/tin oxide (NiO/Xg SnO_2, X: 0.5, 1) based heterostructured composites to design high-performance supercapacitor electrode. *Physica B: Condensed Matter, 638*, 413931. https://doi.org/10.1016/j.physb.2022.413931
47. Yousaf, S., Zulfiqar, S., Somaily, H. H., Warsi, M. F., Rasheed, A., Shahid, M., & Ahmad, I. (2022). An efficient and stable iodine-doped nickel hydroxide electrocatalyst for water oxidation: Synthesis, electrochemical performance, and stability. *RSC Advances, 12*(36), 23454–23465. https://doi.org/10.1039/d2ra03873k
48. Ahmed, S., Ashraf, M., Yousaf, S., Alsafari, I. A., Akhtar, M., Shahid, M., Somaily, H. H., & Warsi, M. F. (2023). High-performance, non-enzymatic glucose sensor based on Fe and Cu doped ZnO/rGO based nanocomposite. *Materials Chemistry and Physics, 297*, 127335. https://doi.org/10.1016/j.matchemphys.2023.127335
49. Mustafa, A., Alsafari, I. A., Somaily, H. H., Yousaf, S., Din, M. I., Rahman, J., Shahid, M., Ashraf, M., & Warsi, M. F. (2023). Fabrication, characterization of NiO–Co_3O_4/rGO based nanohybrid and application in the development of non-enzymatic glucose sensor. *Physica B: Condensed Matter, 648*, 414404. https://doi.org/10.1016/j.physb.2022.414404
50. Jarvin, M., Kumar, S. A., Vinodhkumar, G., Manikandan, E., & Inbanathan, S. S. R. (2021). Enhanced photocatalytic performance of Hausmannite Mn_3O_4-rGO nanocomposite in degrading methylene blue. *Materials Letters, 305*, 130750. https://doi.org/10.1016/j.matlet.2021.130750
51. Warsi, M. F., Iftikhar, A., Yousuf, M. A., Sarwar, M. I., Yousaf, S., Haider, S., Aly Aboud, M. F., Shakir, I., & Zulfiqar, S. (2020). Erbium substituted nickel–cobalt spinel ferrite nanoparticles: Tailoring the structural, magnetic and electrical parameters. *Ceramics International, 46*(15), 24194–24203. https://doi.org/10.1016/j.ceramint.2020.06.199
52. Yousaf, S., Aadil, M., Zulfiqar, S., Warsi, M. F., Agboola, P. O., Aly Aboud, M. F., & Shakir, I. (2020). Hierarchically porous CuO microspheres and their r-GO based nanohybrids for electrochemical supercapacitors applications. *Journal of Materials Research and Technology, 9*(6), 14158–14167. https://doi.org/10.1016/j.jmrt.2020.09.110
53. Iftikhar, A., Yousaf, S., Ahmed Ali, F. A., Haider, S., Ud-Din Khan, S., Shakir, I., Iqbal, F., & Warsi, M. F. (2020). Erbium-substituted $Ni_{0.4}Co_{0.6}Fe_2O_4$ ferrite nanoparticles and their hybrids with reduced graphene oxide as magnetically separable powder photocatalyst. *Ceramics International, 46*(1), 1203–1210. https://doi.org/10.1016/j.ceramint.2019.08.176
54. Yousaf, S., Zulfiqar, S., Shahi, M. N., Warsi, M. F., Al-Khalli, N. F., Aly Aboud, M. F., & Shakir, I. (2020). Tuning the structural, optical and electrical properties of NiO nanoparticles prepared by wet chemical route. *Ceramics International, 46*(3), 3750–3758. https://doi.org/10.1016/j.ceramint.2019.10.097
55. Yousaf, S., Zulfiqar, S., Shahid, M., Jamil, A., Shakir, I., Agboola, P. O., & Warsi, M. F. (2020). Electrochemical energy storage properties studies of $Cu_{0.2}Ni_{0.8}O$-Reduced graphene oxide nanohybrids. *Ceramics International, 46*(9), 14304–14310. https://doi.org/10.1016/j.ceramint.2020.02.115
56. Yousaf, S., Zulfiqar, S., Din, M. I., Agboola, P. O., Aly Aboud, M. F., Warsi, M. F., & Shakir, I. (2021). Solar light irradiated photocatalytic activity of ZnO–NiO/rGO nanocatalyst. *Journal of Materials Research and Technology, 12*, 999–1009. https://doi.org/10.1016/j.jmrt.2021.03.012
57. Hussain, N., Alwan, S., Alshamsi, H., & Sahib, I. (2020). Green synthesis of S- and N-codoped carbon nanospheres and application as adsorbent of Pb (II) from aqueous solution. *International Journal of Chemical Engineering, 2020*, 9068358. https://doi.org/10.1155/2020/9068358
58. Ain, N.-u., Shaheen, W., Bashir, B., Abdelsalam, N. M., Warsi, M. F., Khan, M. A., & Shahid, M. (2016). Electrical, magnetic and photoelectrochemical activity of rGO/$MgFe_2O_4$ nanocomposites under visible light irradiation. *Ceramics International, 42*(10), 12401–12408. https://doi.org/10.1016/j.ceramint.2016.04.179

Publisher's Note Springer Nature remains neutral with regard to jurisdictional claims in published maps and institutional affiliations.

Springer Nature or its licensor (e.g. a society or other partner) holds exclusive rights to this article under a publishing agreement with the author(s) or other rightsholder(s); author self-archiving of the accepted manuscript version of this article is solely governed by the terms of such publishing agreement and applicable law.

SPRINGER LINK

Log in

Menu Search Cart



BioNanoScience

Publishing model

Hybrid

Submit your manuscript

Editorial board

Aims and scope

Overview

BioNanoScience is a peer-reviewed journal publishing topics that include properties and processes of nanoscale phenomena in biological and bio-inspired structures as well as materials for engineered systems.

Covers experimental, theoretical, computational research, and applications in biology and medicine.

Examines fundamental structural and mechanistic analyses of biological processes at the nanoscale and their translation into synthetic applications.

Editor-in-Chief
Victor Erokhin

Journal Impact Factor
3.0 (2023)

5-year Journal Impact Factor
3.1 (2023)

Submission to first decision (median)
8 days

Downloads
163,935 (2023)



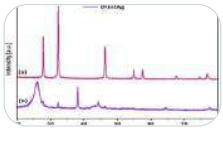
Latest issue

June 2024
Volume 14, Issue 2

View all volumes and issues →

Latest articles

Synergistic Antimicrobial Action of Polymerized Indole-Based Nanocomposites with NfAg on Chemically Reformed Multiple-Layered Carbon Nanotubes



Research | 05 September 2024

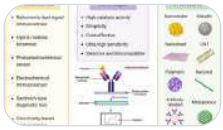
Characterization and Sustainable Applications of Multifunctional, Non-



Genotoxic ZnO-NPs Biofabricated by Organic Biomass Extract of *Nostoc* sp. SI-SN

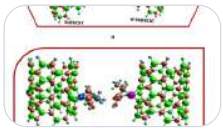
Research | 04 September 2024

Palladium Nanoparticles as a Platform for Cancer Diagnosis and Treatment



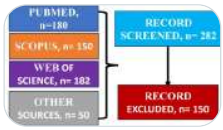
Review | Open access | 02 September 2024

Computational Investigation of Antimony Co-doped with Tungsten (W), Molybdenum (Mo), and Chromium (Cr) on Silicon-carbide Nanotubes: As Dopamine Sensors for the Observation of Neurodegenerative Diseases



Research | 31 August 2024

Eugenol: The Phytocompound's Potential Biological Applications



Review | 31 August 2024

View all articles →

This journal has 37 open access articles →

Journal information

Electronic ISSN 2191-1649

Print ISSN 2191-1630

Abstracted and indexed in

Baidu

CLOCKSS

CNKI
CNPIEC
Dimensions
EBSCO
EI Compendex
EMBASE
Emerging Sources Citation Index
Google Scholar
INSPEC
Japanese Science and Technology Agency (JST)
Naver
OCLC WorldCat Discovery Service
Portico
ProQuest
Reaxys
SCImago
SCOPUS
TD Net Discovery Service
UGC-CARE List (India)
Wanfang

Copyright information

Rights and permissions
Editorial policies

© Springer Science+Business Media, LLC, part of Springer Nature

For authors

Submission guidelines →
Language editing services →
Ethics and disclosures →

How to publish with us →

Open Access fees and funding →

Contact the journal →



Language quality checker

Get your manuscript edited for free →

Use our pre-submission checklist →

Avoid common mistakes on your manuscript.

This journal's calls for papers →

Collections this journal is participating in.

Sign up for alerts →

Get notified when new articles are published.

Explore

Articles →

Volumes and issues →

Collections →

Already have a manuscript?

Use our Manuscript Matcher to find the best relevant journals!

Find a Match

Refine Your Search Results

2191-1649 Search

Sort By: Title (A-Z)

Search Results

Found 1 results (Page 1) Share These Results

Exact Match Found

BIONANOSCIENCE

Publisher: SPRINGER , ONE NEW YORK PLAZA, SUITE 4600 , NEW YORK, United States, NY, 10004

ISSN / eISSN: 2191-1630 / 2191-1649

Web of Science Core Collection: Emerging Sources Citation Index

Share This Journal View profile page

* Requires free login.

Filters Clear All

Web of Science Coverage

Open Access

Category

Country / Region

Language

Frequency

Journal Citation Reports

1 – 1 of 1

Items per page: 10

Editorial Disclaimer: As an independent organization, Clarivate does not become involved in and is not responsible for the editorial management of any journal or the business practices of any publisher. Publishers are accountable for their journal performance and compliance with ethical publishing standards. The views and opinions expressed in any journal are those of the author(s) and do not necessarily reflect the views or opinions of Clarivate. Clarivate remains neutral in relation to territorial disputes, and allows journals, publishers, institutes and authors to specify their address and affiliation details including territory.

Criteria for selection of newly submitted titles and re-evaluation of existing titles in the Web of Science are determined by the Web of Science Editors in their sole discretion. If a publisher's editorial policy or business practices negatively impact the quality of a journal, or its role in the surrounding literature of the subject, the Web of Science Editors may decline to include the journal in any Clarivate product or service. The Web of Science Editors, in their sole discretion, may remove titles from coverage at any point if the titles fail to maintain our standard of quality, do not comply with ethical standards, or otherwise do not meet the criteria determined by the Web of Science Editors. If a journal is deselected or removed from coverage, the journal will cease to be indexed in the Web of Science from a date determined by the Web of Science Editors in their sole discretion – articles published after that date will not be indexed. The Web of Science Editors' decision on all matters relating to journal coverage will be final.

Clarivate.™ Accelerating innovation.

© 2024 Clarivate Legal center Privacy notice Cookie policy
Manage cookie preferences Copyright notice Help

Revisiting band structures in ^{118}Xe nucleus via in-beam γ-ray spectroscopy*

A. Pandey[1] R. Bhushan[1] A. Rohilla[2] C. Majumder[3] H. P. Sharma[4] S. Chakraborty[5] R. P. Singh[6] S. Muralithar[6] Yashraj[6] K. Katre[6] B. Rohila[7] Subodh[7] A. Kumar[7] I. M. Govil[7] S. Jehangir[8] N. Rather[8] G. H. Bhati[9] A. A. Wani[9] J. A. Sheikh[10] S. K. Chamoli[1†]

[1]Department of Physics and Astrophysics, University of Delhi, New Delhi- 110007, India
[2]Institute of Space Sciences, Shandong University, Weihai- 264209, China
[3]Department of Physics, Indian Institute of Technology Bombay, Mumbai- 400076, India
[4]Department of Physics, Institute of Science, Banaras Hindu University, Varanasi- 221005, India
[5]Variable Energy Cyclotron Centre, Kolkata- 700064, India
[6]Inter University Accelerator Centre, Aruna Asaf Ali Marg, New Delhi- 110067, India
[7]Department of Physics, Punjab University, Chandigarh- 160014, India
[8]Department of Physics, Islamic University of Science and Technology, Jammu and Kashmir- 192122, India
[9]Higher Education Department, Government of Jammu and Kashmir, Srinagar, J&K- 180001, India
[10]Department of Physics, University of Kashmir, Srinagar- 190006, India

Abstract: The neutron deficient Xe nuclei with $A \approx 120$ are predicted to have strong octupole correlation at low spins. In the present study, an attempt was made to improve upon the level scheme and also to examine the signatures of octupole correlation in ^{118}Xe via high spin γ-ray spectroscopy. High spin states in ^{118}Xe have been populated via the ^{93}Nb(^{28}Si, $p2n$)^{118}Xe fusion-evaporation reaction at a beam energy of 115 MeV provided by the 15 UD pelletron accelerator facility at IUAC, New Delhi. In the experiment, seven new γ-transitions have been found and placed appropriately in the level scheme. A theoretical study using the triaxial projected shell model (TPSM) approach suggests that the first bandcrossing is due to the alignment of two neutrons, and a parallel band tracking the yrast configuration is the γ-band built on the two-quasiparticle state. Enhanced $E1$ transition rates measured between opposite parity bands involving $\nu h_{11/2}$ and $\nu d_{5/2}$ orbitals having $\Delta j = \Delta l = 3$ indicate the presence of octupole correlation in this nucleus.

Keywords: octupole correlation, γ-ray spectroscopy, TPSM calculations, bandcrossing

DOI: 10.1088/1674-1137/acd83d

I. INTRODUCTION

Nuclei in the $A \approx 120$ region are well suited for studying the effects of shape-driving properties of different quasiparticle configurations. In this region, the Fermi surface for the protons lies close to the low-Ω $h_{11/2}$ orbitals, which drives the nucleus toward a prolate shape, whereas for the neutrons, it is situated among the medium-Ω $h_{11/2}$ orbitals, which induces an oblate deformation [1]. Owing to the conflicting deformation driving properties of protons and neutrons, the nucleus can have a prolate, oblate, or triaxial shape depending on the intrinsic configuration. Additionally, band crossings due to the alignment of $h_{11/2}$ neutrons as well as protons are expected at low rotational frequencies [2]. The presence of octupole driving $h_{11/2}$ and $d_{5/2}$ orbitals near the Fermi surface makes them suitable to exhibit octupole correlation. Octupole correlation in atomic nuclei is due to the interaction between the orbitals of opposite parity having $\Delta j = \Delta l = 3$ near the Fermi level. This situation is found between an intruder orbital and normal parity sub-shell, *i.e.*, for particle number N and/or $Z \approx 34$ ($g_{9/2} \rightarrow p_{3/2}$), 56 ($h_{11/2} \rightarrow d_{5/2}$), 88 ($i_{13/2} \rightarrow f_{7/2}$), and 134 ($j_{15/2} \rightarrow g_{9/2}$) [3, 4]. The nuclei that have their Fermi surface in close proximity to these pairs of orbitals will be particularly susceptible to octupole correlation. Enhanced $E1$ trans-

Received 18 December 2022; Accepted 24 May 2023; Published online 25 May 2023

* The authors are grateful for the pelletron and support staff of IUAC, New Delhi. We would also like to acknowledge the contribution of the INGA collaboration, which is partially funded by the Department of Science and Technology (DST, GoI; project no. IR/S2/PF-03/2003-I) and University Grants Commission (UGC). This work was supported by IUAC, New Delhi (Grant No. IUAC/ XIII/7/UFR-63302). AP wishes to acknowledge financial support from the University Grants Commission (UGC), India. GHB, SJ, JAS, and NR would like to acknowledge the Department of Science and Technology, Govt. of India for providing financial support under Project no. CRG/2019/004960 to carry out a part of the research work. SC acknowledges the financial support received from SERB, INDIA under N-PDF scheme vide reference no. PDF/2022/001829

† E-mail: skchamoli@physics.du.ac.in

©2023 Chinese Physical Society and the Institute of High Energy Physics of the Chinese Academy of Sciences and the Institute of Modern Physics of the Chinese Academy of Sciences and IOP Publishing Ltd

itions between alternate-parity bands, parity doublet structures, and highly collective $E3$ transitions are the experimental fingerprints of octupole correlations. In the $A\approx$ 120 region, octupole correlations in several isotopes of Xe-Cs-Ba having N < 70 have been reported [5–7]. Previously, high-spin γ-ray spectroscopy measurements in ^{118}Xe were reported [8–10], but in almost all the cases, precise data on the polarisation leading to confirmation of parity assignments were missing. In Ref. [10], the issue of octupole collectivity was discussed in relation to the observed interband transitions at 1022 keV ($7^- \rightarrow 6^+$), 846 keV ($9^- \rightarrow 8^+$), 726 keV ($11^- \rightarrow 10^+$), and 924 keV ($8^- \rightarrow 8^+$); however, the quoted $B(E1)$ values have errors in the range of 4% to 28%. Additionally, in Ref. [10], although the transition at 924 keV ($8^- \rightarrow 8^+$), from Band 4 to Band 6, was marked as the $E1$ transition, the parity assignments of Band 4 (negative parity) were based on systematics. In the present work, the excited states in ^{118}Xe were reinvestigated with the following objectives: 1) to update the level scheme with inclusion of more γ transition in the non-yrast bands (if any), 2) to fix the parities (especially of Band 4) with polarisation measurements, and 3) to provide more precise data on the octupole collectivity (transition). We also performed triaxial projected shell model (TPSM) calculations to investigate the observed band structures further.

II. EXPERIMENTAL DETAILS

High spin states in ^{118}Xe nuclei were populated via the ^{93}Nb(^{28}Si, $p2n$) fusion-evaporation reaction at a beam energy of 115 MeV. A monoisotopic Nb target of thickness ~0.9 mg/cm^2 was rolled on a 9.2 mg/cm^2 thick Pb backing foil to form the target [11]. The target was fabricated at the Target Development Laboratory of the Inter-University Accelerator Centre (IUAC), New Delhi [12]. The 115 MeV accelerated beam was provided by the 15 UD pelletron accelerator facility at IUAC [13]. For detecting γ-rays produced in the reaction, the Indian National Gamma Array (INGA) set-up [14] was used. The detectors in the INGA set-up are arranged in five different rings making angles of 32°, 57°, 123°, 148° (having four clover detectors each), and 90° (with eight clover detectors) with the beam direction. At the time of the experiment, only 16 clover detectors (three clover detectors at 32°, one clover detector at 57°, two clover detectors at 123°, four clover detectors at 148°, and six clover detectors at 90°) were available; thus, data were acquired with 16 clover detectors only. For the measurement purpose, the resolution of the clover detectors in the INGA set-up was found to be $\Delta E\sim$ 2.2 – 2.5 (± 0.1%) keV (FWHM at 1332 keV). The energy calibration of the clover detectors (up to a level better than 0.1%) has been done with an ^{152}Eu source following the standard procedure. The data were collected using a CAMAC based high speed distributed analog data acquisition system called CANDLE [15]. Data were collected in the coincidence mode under the condition that at least two clover detectors in the INGA set-up should record γ-rays within the specified time window (coincidence window of 150 ns was set for the real coincidence events).

III. DATA ANALYSIS PROCEDURES

Offline data analysis was carried out using the INGAsort [16] and RADWARE [17] software packages. For the analysis, all the detectors were properly gain-matched using the INGAsort software, and the necessary numbers of symmetric and asymmetric matrices were constructed. To determine the spin of an excited state, the multipolarities of the γ-ray transitions were determined via angular correlation analysis by using the directional correlation of oriented states (DCO) ratio [18]. This method is based on the analysis of the anisotropic distribution of the emitted γ-rays, which depends on the multipolarity of the transition. For the DCO ratio, an asymmetric γ-γ coincidence matrix was constructed using coincidence events registered by detectors placed at 90° and 148° with respect to the beam direction. The anisotropic intensity ratio of two mutually coincident gamma-ray transitions can be evaluated using the formula

$$R_{\rm DCO} = \frac{I_{\gamma_1} \text{ at } 148^\circ \text{ gated by } \gamma_2 \text{ at } 90^\circ}{I_{\gamma_1} \text{ at } 90^\circ \text{ gated by } \gamma_2 \text{ at } 148^\circ} \quad (1)$$

where the numerator denotes the intensity of the γ-ray transition (γ_1) at angle θ_1 = 148° gated by the transition of known multipolarity (γ_2) at angle θ_2 = 90°, and the denominator denotes the intensity of γ_1 at 90° gated by γ_2 at 148°. The DCO ratio depends on the multipolarities of the transition and the geometry of the spectrometer. The $R_{\rm DCO}$ value for stretched γ-ray transitions (γ_1 and γ_2) of the same multipolarity is close to unity. The DCO ratio for pure dipole (quadrupole) transitions gated on stretched quadrupole (dipole) transitions is 0.5 (2.0) in the present work.

Definite parities of the excited states have been deduced from the linear polarization asymmetry ratio ($A_{\rm as}$) extracted from the parallel and perpendicular Compton scattering of the γ-ray photons inside the Clover detectors, *i.e.*, between the Clover germanium crystals [19]. The measured value of $A_{\rm as}$ provides information about the nature of the γ-ray transition *i.e.*, electric or magnetic. The linear polarization asymmetry ratio ($A_{\rm as}$) of the γ-ray transition was calculated using the formula

$$A_{\rm as} = \frac{a(E_\gamma)N_\perp - N_\parallel}{a(E_\gamma)N_\perp + N_\parallel}, \quad (2)$$

where $N_\parallel$ and $N_\perp$ represent the counts for the actual

Compton-scattered γ rays in the directions parallel and perpendicular to the reaction plane, respectively. The correction factor a(E_γ), which was introduced for handling the asymmetry in the response of the segments of the clover detector [20], was estimated using an unpolarized ^{152}Eu source and is evaluated using the relation

$$a(E_\gamma) = \frac{N_\parallel}{N_\perp}. \quad (3)$$

The energy dependence of a(E_γ) is obtained using the equation a(E_γ) = $a + b*E_\gamma$. The fitted plot of a(E_γ) with the value of the coefficients is shown in Fig. 1. A positive value of (A_{as}) indicates the electric (E) nature of the transition, whereas a negative value indicates the magnetic (M) nature. The low energy limit for the polarization measurement was approximately 200 keV in the present work. The linear polarization analysis of the 676 keV γ ray transition in ^{118}Xe is shown in Fig. 2.

IV. RESULTS

The level scheme of ^{118}Xe has been modified in the present work by placing seven new γ-transitions based on the γ-γ coincidence and intensity relationship, as shown in Fig. 3. Most of the γ-transitions presented in this level scheme were reported in Ref. [10]. This study revisits all the excited states populated, and all the previous placements were either confirmed or updated according to the γ-γ coincidence and intensity relationship. The experimental results obtained in the present work are summarized in Table 1. The measured relative intensities of the γ rays from the single-gated spectra were normalized for the 337-keV transition. Relevant energy gated spectra in support of the present γ-transition placement are presented in Figs. 4, 5, and 6. These spectra show the previously reported γ rays in ^{118}Xe [8–10] along with the newly observed γ rays. All the new γ rays belonging to ^{118}Xe have been observed in the low lying 473 keV energy gated spectrum shown in Fig. 4. Moreover, observation of these γ rays in all other coincidence γ-spectra shown in Figs. 5(a)–(e), confirms the placement. Figure 6 shows the self-gated 429 keV spectra, which support our tentative placement of the transition in the level-scheme.

In this work, the spin-parity of most of the states has been assigned firmly on the basis of the DCO ratio and (A_{as}) values of the transitions. The DCO ratio for some transitions (those absent from Table 1 could not be evaluated, owing to the low statistics observed for those transitions in the present work. The observed level sequences have been numbered in accordance with the previous study [10], to avoid confusion while comparing the previous work and the present review. This work revisits all the γ-transitions reported in the previous work [10], adding some important information based on spectroscopic measurements, as summarized in Table 1. While some new transitions and decay paths have been found in the present work, our level scheme is consistent with that proposed earlier [9, 10].

1) In the previous work [10], the yrast band transition, *i.e.*, $12^+ \rightarrow 10^+$, was assigned E_γ = 775.9 keV, but in the present work, the $12^+ \rightarrow 10^+$ transition was observed to have E_γ = 775.1 keV, which was confirmed using the 256 keV gated spectra, as shown in Fig. 7(b). The close-lying $14^+ \rightarrow 12^+$ transition could not be resolved in the present work. Therefore, we adopted E_γ = 775 keV for the $14^+ \rightarrow 12^+$ transition. The relative intensities, DCO, and A_{as} measurements are reported for the composite peak because individual peaks cannot be resolved unambiguously. The presence of two close-lying transitions has been confirmed using the 787 keV gated spectra, as shown in Fig. 7(a).

2) In the present study, spin and parity assignments in the yrast band/band 6 are updated to the 20^+ state supported by angular correlation analysis.

3) Band 4 has been tentatively suggested to have negative parity according to systematic behavior observed in

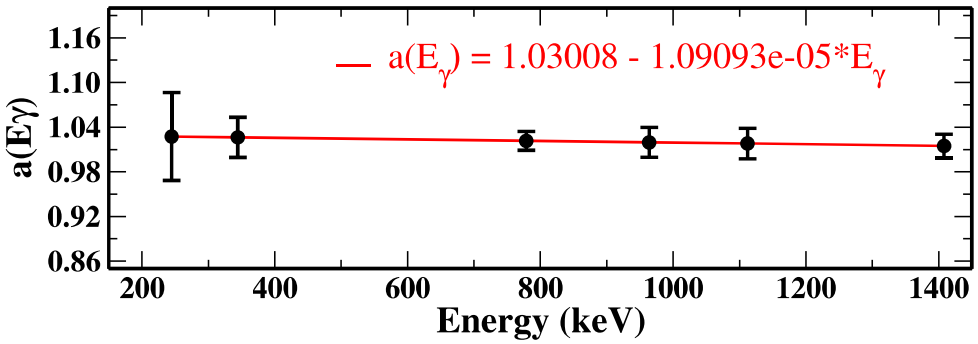


Fig. 1. (color online) Plot of the correction factor a(E_γ) vs. E_γ obtained with an unpolarized ^{152}Eu source. The solid red line represents the linear fit of the data. The errors in the correction factor values are approximately 5%–10%.

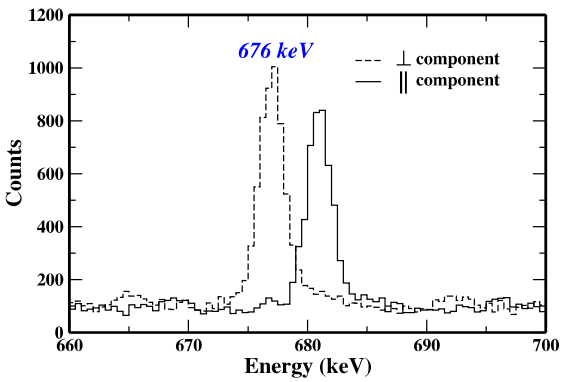


Fig. 2. (color online) Perpendicular (dashed line) and parallel (solid line) components of the 676 keV γ ray in ^{118}Xe, obtained from the linear polarization analysis in the present work. The parallel component is deliberately shifted (5 keV energy to the right) to give a clearer view and aid understanding.

heavier even Xe nuclei [10]. The parity of band 4 depends on the electric/magnetic nature of the decaying 924/1144 keV transition. In the present work, the A_{as} of the 924 keV transition, *i.e.*, $8^- \rightarrow 8^+$, has been found to be positive, confirming the electric nature of the transition. This confirms the parity of band 4 to be negative. Spin and parity assignments in this band are supported up to the 14^- state by angular correlation analysis.

4) In the present study, the spin and parity assignments in the band 11 are updated to the 11^+ state supported by angular correlation analysis. Two newly found interlinking transitions, i.e., 1136 ($11^+ \rightarrow 10^+$) and 1084 ($(13^+) \rightarrow 12^+$) keV have been placed in the level scheme.

V. DISCUSSION

In this section, the experimental results are discussed first by comparison with the neighboring isotopes and from general considerations and then by using the theor-

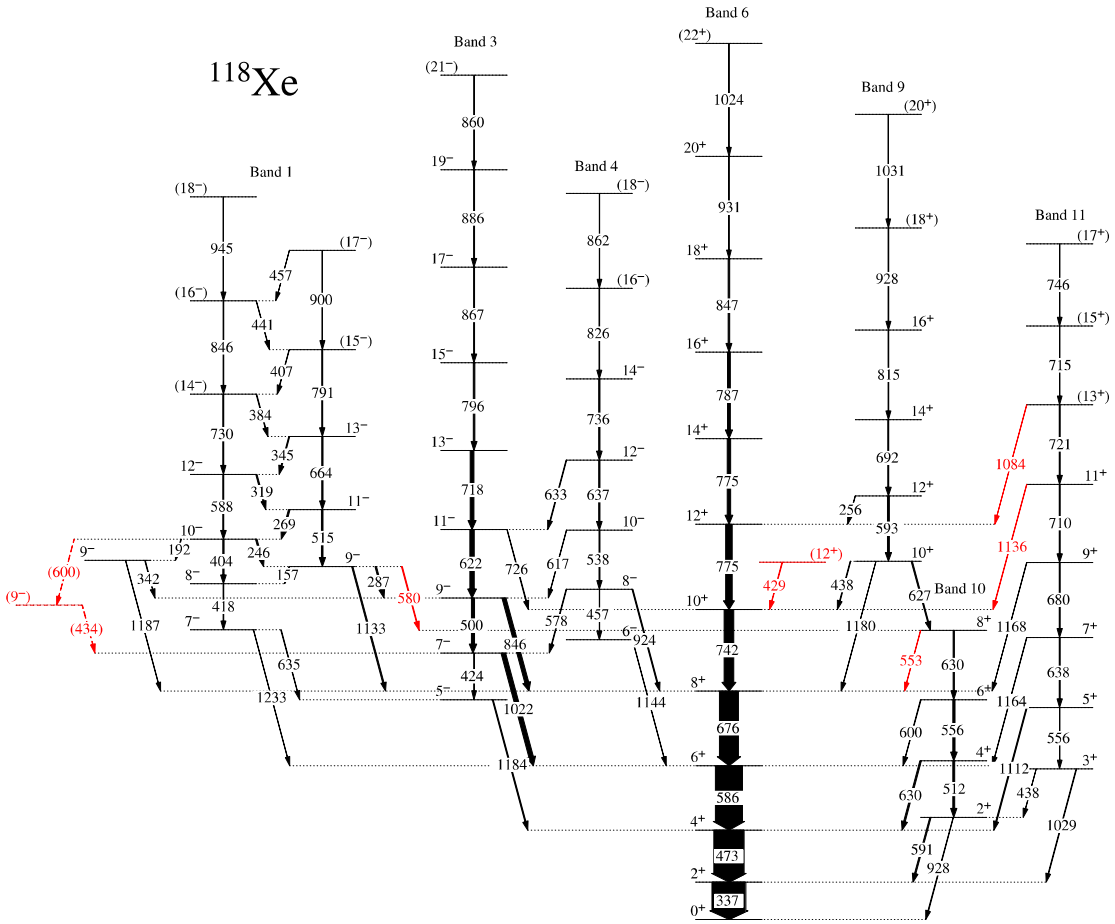


Fig. 3. (color online) Level scheme of ^{118}Xe deduced in the present work. Newly identified γ-rays are marked in red. Other peaks shown here were previously reported in [10]. Only bands that were reproduced in the present work are shown and discussed in the text.

Table 1. Gamma-ray energies, initial level energies, relative intensities, DCO ratio, polarisation asymmetry parameter, multipolarity, and band number assigned to the transitions in ^{118}Xe.

E_γ /keV	E_i	I_γ [b]	$R_{\rm DCO}$ [c]	$A_{\rm as}$	$I_i \to I_f$	Multipolarity	Band
156.8(7)	3205	8.3(7)			$9^- \to 8^-$	$M1/E2$	1
191.7(5)	3452	15.6(10)	0.67(17)		$10^- \to 9^-$	$M1/E2$	1→
246.5(5)	3452	41.6(30)	0.83(12)		$10^- \to 9^-$	$M1/E2$	1
255.6(5)	3845	11.5(13)	0.99(26)		$12^+ \to 12^+$	$M1/E2$	9→6
268.7(5)	3721	39.8(31)	0.79(14)		$11^- \to 10^-$	$M1/E2$	1
286.9(5)	3205	39.0(32)	1.26(14)		$9^- \to 9^-$	$M1/E2$	1→3
319.4(5)	4040	29.0(23)	0.73(17)		$12^- \to 11^-$	$M1/E2$	1
337.4(1)	338	1000	1.00	0.13(5)	$2^+ \to 0^+$	$E2$	6
341.6(5)	3260	13.4(14)			$9^- \to 9^-$	$M1/E2$	→3
344.9(5)	4385	22.2(19)	0.57(6)		$13^- \to 12^-$	$M1/E2$	1
384.3(5)	4770	21.6(22)			$(14^-) \to 13^-$	$(M1/E2)$	1
403.7(5)	3452	37.0(34)	1.03(11)		$10^- \to 8^-$	$E2$	1
406.6(5)	5176	12.7(18)			$(15^- \to 14^-)$	$(M1/E2)$	1
418.5(5)	3048	21.5(14)			$8^- \to 7^-$	$M1/E2$	1
423.5(5)	2418	10.1(7)	1.18(29)		$7^- \to 5^-$	$E2$	3
429.1(5)	3244	13.1(17)	0.99(20)		$(12^+) \to 10^+$	$(E2)$	→6
434.5(5)	2852	12.5(16)	1.10(19)		$(9^-) \to 7^-$	$(E2)$	→3
437.9(7)	1366	7.7(12)			$3^+ \to 2^+$	$M1/E2$	11→10
438.1(5)	3253	18.7(13)	1.01(15)		$10^+ \to 10^+$	$M1/E2$	9→6
441.1(7)	5617	8.6(13)			$(16^- \to 15^-)$	$(M1/E2)$	1
456.9(7)	6074	3.8(9)			$(17^- \to 16^-)$	$(M1/E2)$	1
457.3(5)	2997	14.6(16)	1.03(9)		$8^- \to 6^-$	$E2$	4
472.7(1)	810	910.0(463)	1.02(2)	0.12(4)	$4^+ \to 2^+$	$E2$	6
500.4(5)	2918	89.2(58)	0.98(9)	0.18(14)	$9^- \to 7^-$	$E2$	3
512.3(5)	1440	57.6(35)	1.05(17)		$4^+ \to 2^+$	$E2$	10
515.2(5)	3721	50.0(33)	1.26(10)		$11^- \to 9^-$	$E2$	1
538.5(5)	3535	24.9(24)	1.35(20)		$10^- \to 8^-$	$E2$	4
553.1(5)	2626	10.1(10)	0.84(11)		$8^+ \to 8^+$	$M1/E2$	10→6
555.8(5)	1996	65.2(31)	1.10(15)[e]		$6^+ \to 4^+$	$E2$	10
556.0(5)	1922	11.5(14)	1.10(15)[e]		$5^+ \to 3^+$	$E2$	11
577.8(5)	2997	14.3(24)			$8^- \to 7^-$	$M1/E2$	4→3
579.6(5)	3205	19.4(27)	0.60(7)		$9^- \to 8^+$	$E1$	1→10
586.3(1)	1397	814.9(487)	0.97(3)	0.13(3)	$6^+ \to 4^+$	$E2$	6
588.2(5)	4040	32.5(69)			$12^- \to 10^-$	$E2$	1
590.6(5)	928	45.2(37)			$2^+ \to 2^+$	$M1/E2$	10→6
592.6(5)	3845	51.0(42)	1.12(13)		$12^+ \to 10^+$	$E2$	9
599.6(5)	1996	17.4(15)			$6^+ \to 6^+$	$M1/E2$	10
599.8(7)	3452	8.6(12)			$10^- \to (9^-)$	$(M1/E2)$	1→
617.2(5)	3535	16.1(13)			$10^- \to 9^-$	$M1/E2$	4→3
622.1(3)	3541	131.4(76)	1.08(11)	0.16(9)	$11^- \to 9^-$	$E2$	3

Continued on next page

Table 1-continued from previous page

E_γ/keV	E_i	I_γ [b]	R_{DCO} [c]	A_{as}	$I_i \rightarrow I_f$	Multipolarity	Band
627.2(5)	3253	33.3(23)	1.17(16)		$10^+ \rightarrow 8^+$	$E2$	9→10
629.9[d]	2626,1440				$8^+ \rightarrow 6^+$, $4^+ \rightarrow 4^+$	$E2$,$M1/E2$	10,10→6
635.1(5)	2630	12.7(11)			$7^- \rightarrow 5^-$	$E2$	1→3
637.2(5)	4173	35.3(21)	1.14(12)		$12^- \rightarrow 10^-$	$E2$	4
638.1(5)	2560	20.2(18)	1.06(14)		$7^+ \rightarrow 5^+$	$E2$	11
664.4(5)	4385	33.1(37)	1.35(11)		$13^- \rightarrow 11^-$	$E2$	1
676.2(1)	2073	567.6(335)	0.96(4)	0.11(4)	$8^+ \rightarrow 6^+$	$E2$	6
680.2(5)	3241	33.8(37)	0.85(18)		$9^+ \rightarrow 7^+$	$E2$	11
691.9(5)	4537	31.8(37)	0.95(10)		$14^+ \rightarrow 12^+$	$E2$	9
709.6(5)	3951	27.2(18)	0.91(12)		$11^+ \rightarrow 9^+$	$E2$	11
715.4(5)	5388	12.7(8)			$(15^+ \rightarrow 13^+)$	$(E2)$	11
718.2(3)	4259	105.8(61)	0.81(11)	0.17(7)	$13^- \rightarrow 11^-$	$E2$	3
721.3(5)	4673	28.1(19)			$(13^+) \rightarrow 11^+$	$(E2)$	11
725.9(5)	3541	17.3(12)			$11^- \rightarrow 10^+$	$E1$	3→6
729.6(5)	4770	29.0(19)			$(14^-) \rightarrow 12^-$	$(E2)$	1
736.2(5)	4909	39.6(35)	0.89(19)		$14^- \rightarrow 12^-$	$E2$	4
742.0(1)	2815	296.3(206)	1.04(6)	0.09(7)	$10^+ \rightarrow 8^+$	$E2$	6
745.7(5)	6134	11.4(15)			$(17^+ \rightarrow 15^+)$	$(E2)$	11
775	4365,	298.9(220)[e]	1.09(5)[e]	0.10(12)[e]	$14^+ \rightarrow 12^+$,	$E2$,	6,
775.1(3)	3589				$12^+ \rightarrow 10^+$	$E2$	6
787.0(5)	5152	79.5(87)	0.81(20)	0.16(17)	$16^+ \rightarrow 14^+$	$E2$	6
790.7(5)	5176	26.5(39)			$(15^-) \rightarrow 13^-$	$(E2)$	1
795.6(5)	5054	45.8(46)	0.80(20)		$15^- \rightarrow 13^-$	$E2$	3
814.9(5)	5352	20.3(27)	0.95(15)		$16^+ \rightarrow 14^+$	$E2$	9
825.5(5)	5734	19.2(26)			$(16^-) \rightarrow 14^-$	$(E2)$	4
845.9(3)	2918	116.6(129)	0.54(8)	0.13(13)	$9^- \rightarrow 8^+$	$E1$	3→6
846.4(5)	5617	21.9(57)			$(16^- \rightarrow 14^-)$	$(E2)$	1
846.7(5)	5998	48.5(54)	0.91(36)		$18^+ \rightarrow 16^+$	$E2$	6
859.7(5)	7667	9.9(17)			$(21^-) \rightarrow 19^-$	$(E2)$	3
862.5(7)	6597	7.5(16)			$(18^-) \rightarrow (16^-)$	$(E2)$	4
866.9(5)	5921	31.0(35)	0.91(11)		$17^- \rightarrow 15^-$	$E2$	3
886.1(5)	6807	21.9(30)	1.11(14)		$19^- \rightarrow 17^-$	$E2$	3
899.5(5)	6074	12.3(10)			$(17^-) \rightarrow (15^-)$	$(E2)$	1
924.4(5)	2997	25.3(17)	0.86(27)	0.09(14)	$8^- \rightarrow 8^+$	$E1$	4
928.3(5)	928	15.4(10)			$2^+ \rightarrow 0^+$	$E2$	10
928.5(5)	6280	14.2(3)			$(18^+) \rightarrow 16^+$	$(E2)$	9
931.4(7)	6930	8.9(7)	1.06(19)		$20^+ \rightarrow 18^+$	$E2$	6
945.4(5)	6562	12.7 (16)			$(18^-) \rightarrow (16^-)$	$(E2)$	1
1021.7(3)	2418	131.5(76)	0.51(4)	0.12(8)	$7^- \rightarrow 6^+$	$E1$	3→6
1024.0(7)	7954	5.5(5)			$(22^+) \rightarrow (20^+)$	$(E2)$	6
1028.7(5)	1366	15.1(14)	0.58(7)		$3^+ \rightarrow 2^+$	$M1/E2$	11→6

Continued on next page

Table 1-continued from previous page

E_γ/keV	E_i	I_γ [b]	R_{DCO} [c]	A_{as}	$I_i \rightarrow I_f$	Multipolarity	Band
1031.1(7)	7311	9.0(7)			$(20^+)\rightarrow(18^+)$	($E2$)	9
1084.0(7)	4673				$(13^+)\rightarrow 12^+$		11→6
1111.7(5)	1922	26.9(27)	0.54(6)		$5^+\rightarrow 4^+$	$M1/E2$	11→6
1132.6(5)	3205	34.6(32)	0.51(4)		$9^-\rightarrow 8^+$	$E1$	1→6
1136.3(5)	3951	10.0(15)			$11^+\rightarrow 10^+$	$M1/E2$	11→6
1143.5(5)	2540	12.2(17)	1.15(29)		$6^-\rightarrow 6^+$	$E1$	4→6
1163.6(7)	2560	8.5(7)			$7^+\rightarrow 6^+$	$M1/E2$	11→6
1168.4(7)	3241	5.3(5)			$9^+\rightarrow 8^+$	$M1/E2$	11→6
1180.0(7)	3253	6.0(11)			$10^+\rightarrow 8^+$	$E2$	9→6
1184.4(5)	1995	29.8(20)	0.51(16)		$5^-\rightarrow 4^+$	$E1$	3→6
1187.3(5)	3260	11.2(9)	0.55(12)		$9^-\rightarrow 8^+$	$E1$	→6
1232.9(5)	2630	10.3(14)	0.47(5)		$7^-\rightarrow 6^+$	$E1$	1→6

[b] Intensity uncertainties does include the errors due to the uncertainty in the efficiency correction. [c] Gated on 473 keV stretched quadrupole gamma-ray transition. [d] Represents doublet γ-energy peaks which cannot be resolved. [e] I_γ, R_{DCO} and A_{as} reported for composite peaks because individual peaks cannot be resolved unambiguously. Note: The intensities (I_γ) of the doublet peaks were estimated by choosing the appropriate gating conditions. For example, 599.8 keV ($10^-\rightarrow 9^-$) γ-ray transition, the total intensity was evaluated by putting a gate on 1022 keV ($7^-\rightarrow 6^+$) γ-ray transition, while for 599.6 keV ($6^-\rightarrow 6^+$) γ-ray transition, the intensity was evaluated by subtracting the intensity of the 599.8 keV γ-ray transition from the total intensity of the doublet peak evaluated from the spectrum gated on the 337 keV γ-ray transition.

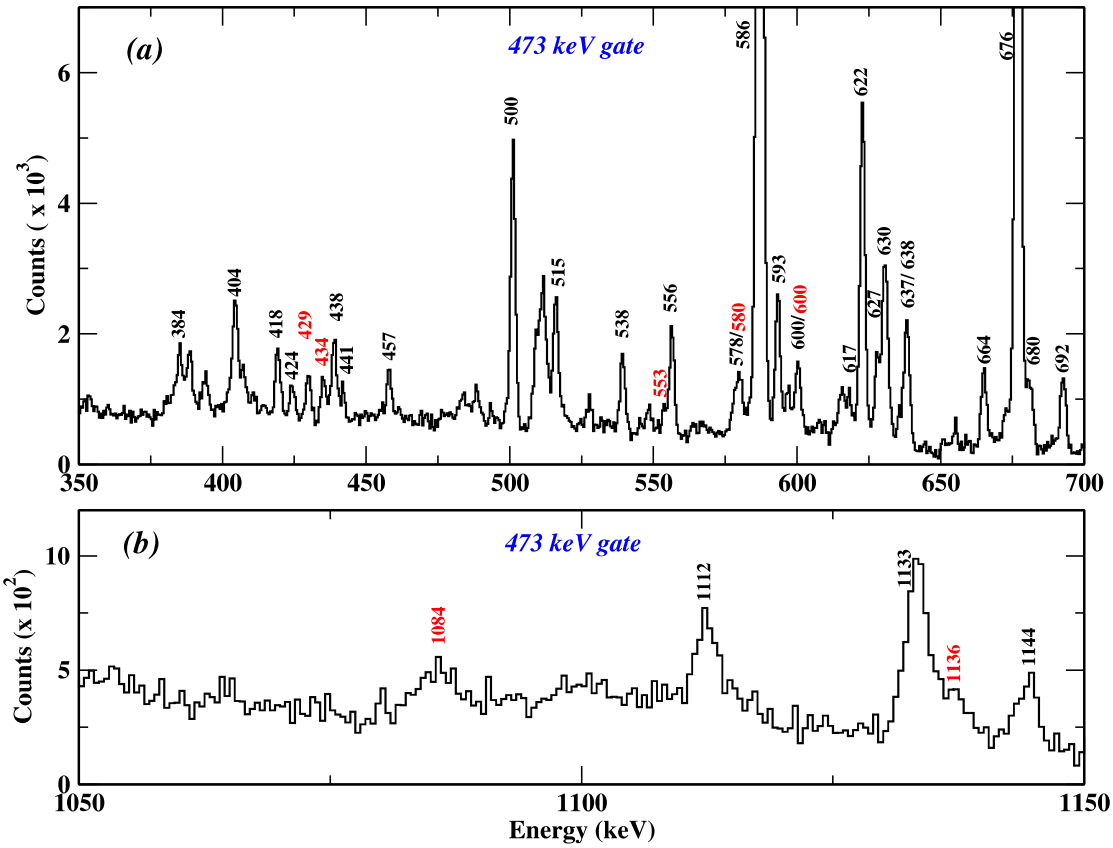


Fig. 4. (color online) Prompt $\gamma-\gamma$ coincidence spectra showing (a) 350 to 700 keV γ-ray transitions and (b) 1050 to 1150 keV γ-ray transitions, gated by the 473 keV gamma transition of the yrast band in ^{118}Xe. Newly observed transitions are marked in red. Only transitions of present interest are shown in keV. One channel at the x-axis corresponds to 0.5 keV.

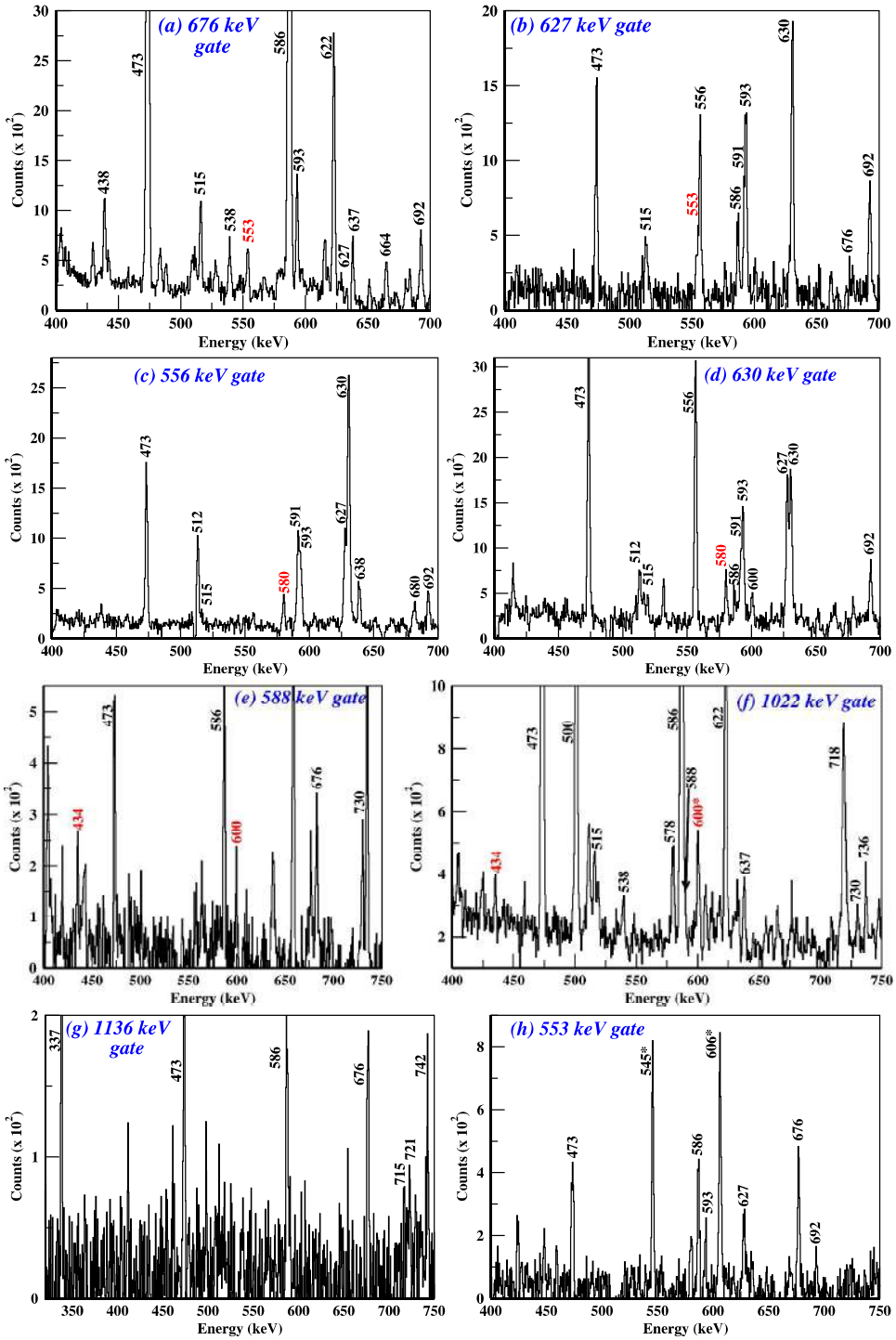


Fig. 5. (color online) Prompt $\gamma-\gamma$ coincidence spectra, with gates at (top left to bottom) (a) 676 keV, (b) 627 keV, (c) 556 keV, (d) 630 keV, (e) 588 keV, (f) 1022 keV, (g) 1136 keV, and (h) 553 keV, in support of the placement of all the newly found transitions. The γ-ray transition peaks marked with an asterisk in Fig. 5(h) are the contaminant peaks from the other channel. The 600 keV transition in Fig. 5(f) is marked with an asterisk to denote the contribution of the contaminant peak (601 keV, $4^+ \rightarrow 2^+$) from the other populated channel (^{118}Te) [21], which accounts for the unexpected high statistics under the peak. One channel at the x-axis corresponds to 0.5 keV.

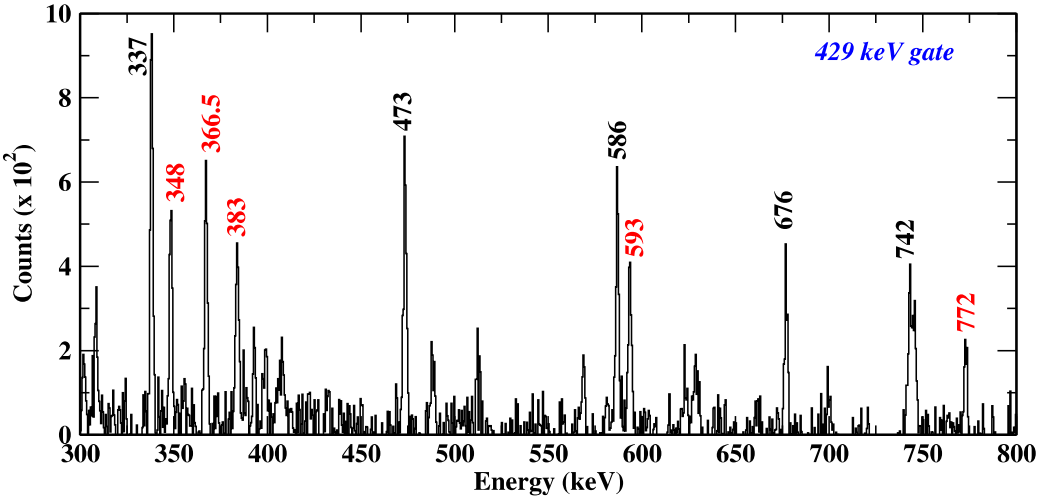


Fig. 6. (color online) Prompt $\gamma-\gamma$ coincidence spectra, gated by the 429 keV ($(12^+) \rightarrow 10^+$) γ-ray transition (decaying into yrast band) to justify the tentative placement of the 429 keV transition. Unknown transitions suggested to be coming from other populated channels are marked with red color. One channel at the x-axis corresponds to 0.5 keV.

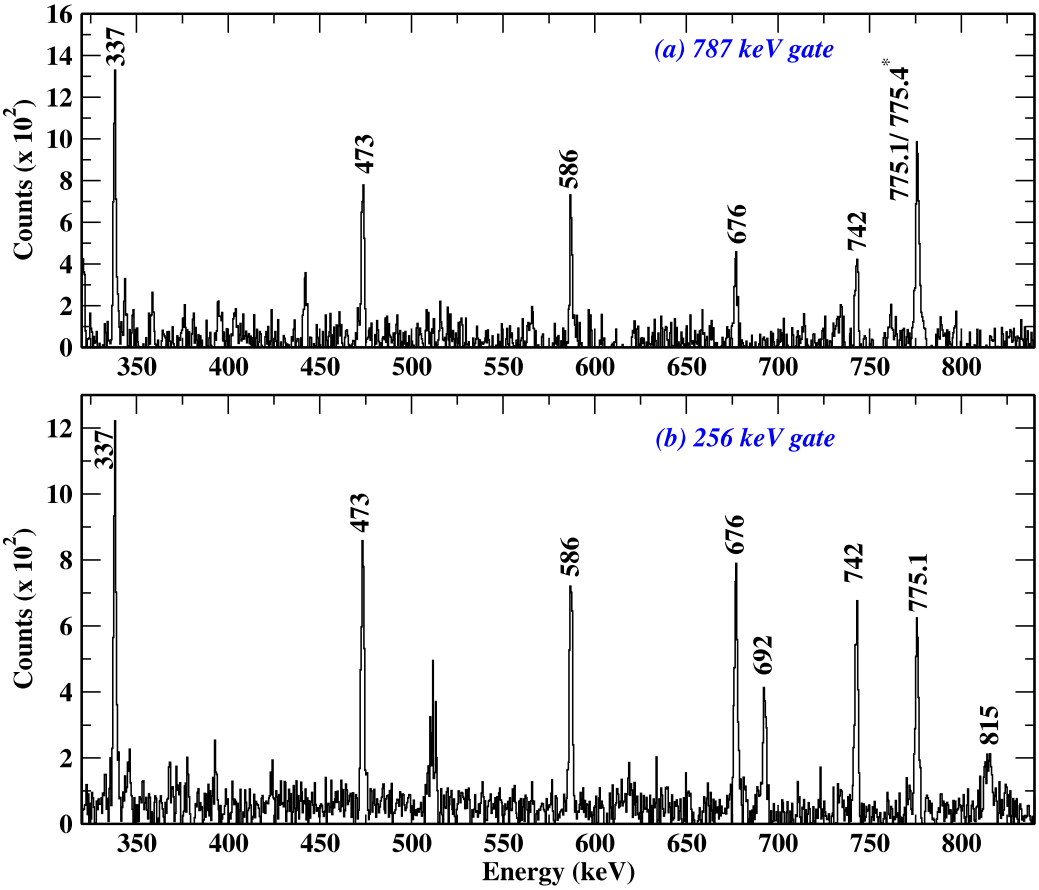


Fig. 7. (color online) Prompt $\gamma-\gamma$ coincidence spectra: (a) gated by the 787 keV ($16^+ \rightarrow 14^+$) γ-transition of the yrast band in ^{118}Xe confirming the presence of two close-lying peaks at 775 keV; (b) gated by the 256 keV ($12^+ \rightarrow 12^+$) interlinking γ-transition between bands 9 and 6 to support the placement of the 775.1 keV transition. The tentative value of the 775.4 keV transition is denoted by an asterisk. One channel at the x-axis corresponds to 0.5 keV.

etical framework of the TPSM approach.

A. Comparison with neighboring isotopes

All the bands (level structure) observed in the present work will be briefly discussed in this section. In Refs. [9, 10], the alignment plot of the yrast band is compared with the neighboring even Ba-nuclei (see Fig. 10 (a) [9] and Fig. 10 (c) [10]). Two conflicting interpretations of the first alignment in the yrast band have been proposed in Refs. [8, 9]. The first alignment in the yrast band in ^{118}Xe at ω_1 = 0.39 MeV/$\hbar$ was attributed to $h_{11/2}$ protons [10], while in heavier Xe nuclei, the first alignment is attributed to $h_{11/2}$ neutrons. In order to resolve this ambiguity, triaxial projected shell model (TPSM) calculations have been carried out (discussed in the next section). On the basis of TPSM calculations, the ground state band in ^{118}Xe is understood to be crossed at ω_1 by the aligned two quasiparticle $(\nu h_{11/2})^2$ configuration. Band 10 originating at lower excitation energies is interpreted as an even-spin quasirotational γ-band [22]. Band 10 is crossed at a frequency of ω = 0.31 MeV/$\hbar$ by band 9, which also crosses the extrapolated yrast band at a frequency near 0.41 MeV/$\hbar$. Band 9 in ^{118}Xe was identified as an aligned two quasi-particle (qp) $(\nu h_{11/2})^2$ band on the basis of the observed alignment pattern and extracted crossing frequencies (see Fig. 11 (b) [10]). Band 11 has been extended up to 11^+ on the basis of angular correlation analysis in the present work. In Ref. [10], the alignment (i_x) plot as a function of the rotational frequency ($\hbar\omega$) for band 11 (Fig. 12 [10]) exhibits an increase at the frequency ω_1, which is attributed to $h_{11/2}$ neutrons. The experimental energy staggering plot, *i.e.*, S(J) vs. J, in the quasirotational γ-band for the range of even isotopes in Xe nuclei, *i.e.*, $^{116-128}$Xe, is shown in Fig. 2 (a) of Ref. [23]. The energy staggering parameter S(J) is considered as a key signature of the γ-dependence of the potential. The comparison of ^{118}Xe with other even isotopes reveals strong staggering with negative S(J) values at even J and positive S(J) values at odd J, which is associated with a γ-independent potential having a deformed γ-soft/γ-unstable structure. Additionally, the magnitude of staggering (see Fig. 2 (a) [23]) is observed to increase with the decreasing neutron number in the Xe nuclei. In Ref. [9], the alignment i_x calculated for the strongly coupled negative-parity band (band 1) in ^{118}Xe is shown (see Fig. 13 (a) [9]). According to a comparison of the $B(M1)/B(E2)$ ratios with theoretical predictions (see Fig. 18 (a) [10]) and the observed alignment behavior, band 1 in ^{118}Xe was assigned to the $\pi[(g_{9/2})^{-1}\ h_{11/2}]$ configuration. In Ref. [10], a similar alignment pattern extracted for the observed low-lying decoupled negative-parity bands (see Fig. 14 [10]) and the interconnection of these two decoupled bands due to weak interlinking transitions of mixed ΔI = 1, $M1/E2$ character suggest that bands 3 and 4 are the signature partner bands based on the two-quasiproton $\pi[h_{11/2}g_{7/2}]$ configuration. Bands 3 and 4 decay to the positive parity yrast band via several interlinking transitions. The observation of the interlinking $E1$ transition between opposite parity bands is assumed to be indicative of octupole correlations. Keeping this in mind, observed interlinking transitions with ΔI = 1, i.e., $E\gamma$ = 1184, 1022, 846, 726 keV have been confirmed to have an electric nature in the present study, which is in agreement with the previous studies [9, 10]. One such interlinking transition (924 keV) was confirmed to have $E1$ multipolarity for the first time on the basis of angular correlation and A_{as} measurements. Enhanced $E1$ strength is one of the spectroscopic measures of octupole correlation in the nuclei. The enhancement of the $E1$ strength can be deduced from the ratio of the reduced transition probabilities of the electric dipole $B(E1;\ \mathrm{I} \rightarrow \mathrm{I\text{-}1})$ and electric quadrupole $B(E2;\ \mathrm{I} \rightarrow \mathrm{I\text{-}2})$ transitions using the following relation:

$$\frac{B(E1)}{B(E2)} = \frac{E_\gamma^5(E2) * I_\gamma(E1)}{1.3 * 10^6 * E_\gamma^3(E1) * I_\gamma(E2)}\,\mathrm{fm}^{-2} \qquad (4)$$

where E_γ is in MeV and $B(E1)/B(E2)$ is in fm^{-2}. The $B(E1)/B(E2)$ ratios estimated using this relation are presented in Table 2. To give a more clearer view of the present data, a comparison of the *B(E1)* values with those obtained in the previous work [10] is shown in Fig. 8. Except for I = 7 $\hbar$, the observed $B(E1)$ values are found to be lower than the *B(E1)* values reported by Sears *et al.*

Table 2. $B(E1)/B(E2)$ ratios and a comparison of the reduced transition probabilities, *i.e.*, $B(E1)$, from the present work and those reported in Ref. [10] in ^{118}Xe.

Band	Q_0[a] (e b)	$I_i^\pi \rightarrow I_f^\pi$	$B(E1)/B(E2)$ (10^{-7} fm^{-2})	$B(E1)$ (10^{-4}e^2 fm^2)	$B(E1)$(10^{-4}e^2 fm^2) Sears *et al.*	D_0 (e fm)
3	3.55	$7^- \rightarrow 6^+, 7^- \rightarrow 5^-$	1.48(23)	5.93(95)	3.50(14)	0.076(6)
		$9^- \rightarrow 8^+, 9^- \rightarrow 7^-$	0.61(1)	2.53(6)	3.42(16)	0.048(1)
		$11^- \rightarrow 10^+, 11^- \rightarrow 9^-$	0.13(1)	0.57(3)	1.79(51)	0.023(1)
4		$8^- \rightarrow 8^+, 8^- \rightarrow 6^-$	0.23(2)	0.88(7)	1.69(27)	0.029(3)

[a] Q_0 is taken from the previous study [10].

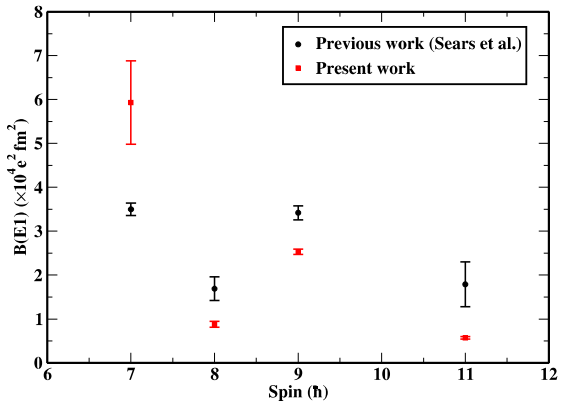


Fig. 8. (color online) $B(E1)$ transition strengths obtained in the present work compared with those reported in the previous work [10]. More precise data on $B(E1)$ values are presented in the present work barring the $B(E1)$ value at $I = 7\hbar$.

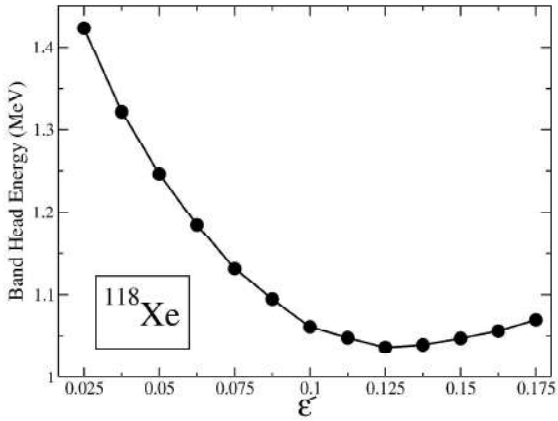


Fig. 9. Variation of the ground-state projected energy surfaces as a function of triaxiality ϵ' for the ^{118}Xe nucleus.

[10]. The reduction in the $B(E1)$ values in the present work is found to be due to the observed low intensity of the interband transition relative to the corresponding intraband transition, as a different reaction is chosen to populate high spin states. The present $B(E1)$ values are clearly more precise than the earlier work, except for $I = 7\hbar$, which has a large fitting error solely due to the low statistics of the 424 keV $(7^- \rightarrow 5^-)$ transition. The observed transition rates are comparable to those found in ^{114}Xe [24] and ^{118}Ba [6] and are understood as evidence for octupole correlations related to the $vh_{11/2}$ and $vd_{5/2}$ orbitals. The intrinsic electric dipole moment D_0 has been estimated using the following relation:

$$D_0 = Q_0 * \left[\frac{5}{16} * \frac{B(E1)}{B(E2)}\right]^{1/2} \text{efm} \tag{5}$$

where Q_0 represents the intrinsic quadrupole moment.

B. Triaxial projected shell model (TPSM) analysis

In order to provide a microscopic description of the observed band structures, we performed a TPSM [25] study of ^{118}Xe. TPSM works in several stages, and in the first stage, the triaxial basis is generated by solving the deformed Nilsson potential with the deformation parameters of ϵ=0.225 and $\epsilon' = 0.13$. The axial deformation parameter ϵ has been chosen by slightly adjusting the tabulated value given in Ref. [26]. This re-ajustment of the tabulated values is required as the nuclear model employed in the present analysis differs from that used in Ref. [26]. The nonaxial deformation ϵ' is fixed in such a way that the bandhead of the γ-bands is reproduced; this procedure was adopted in most of the previous studies [27–29]. The non-axial deformation value is consistent with the value obtained from the minimum of the potential energy surface shown in Fig. 9. In this figure, the projected ground-state energy is drawn as a function of the triaxial parameter with the axial deformation parameter fixed. It needs to be emphasised that these deformation parameters are used to solve the triaxial potential from which the deformed basis space of the TPSM is constructed. In principle, the final results should be independent of the deformation used in constructing the basis space. However, in practice, a limited basis space is employed, and the final results are dependent on the basis deformation. It is, therefore, important to choose optimum deformation values. The pairing interaction parameters employed in the present work are those used in Refs. [30, 31].

In the second stage of the TPSM study, the projected states are generated by using the three-dimensional angular-momentum projection technique. In the third and final stage, the projected basis is used to diagonalise the shell model Hamiltonian consisting of pairing plus quadrupole-quadrupole interaction terms. Details on the technical aspects of the model can be found in our previous publications [32–35]

For this system, high-spin states have been observed up to I=36, and in order to interpret such high-spin states, it is essential to include 4-neutron and 4-proton quasiparticle (qp) configurations in addition to 2-neutron and 2-proton excitations. In the present work, the TPSM basis is composed of 0-qp (qp vacuum), two-proton, two-neutron, 4-qp, 4 neutron, and 4 proton configurations, *i.e.*,

$$\begin{aligned}
&\hat{P}^I_{MK}|\Phi\rangle;\\
&\hat{P}^I_{MK}\, a^\dagger_{p_1} a^\dagger_{p_2}|\Phi\rangle;\\
&\hat{P}^I_{MK}\, a^\dagger_{n_1} a^\dagger_{n_2}|\Phi\rangle;\\
&\hat{P}^I_{MK}\, a^\dagger_{p_1} a^\dagger_{p_2} a^\dagger_{n_1} a^\dagger_{n_2}|\Phi\rangle;\\
&\hat{P}^I_{MK}\, a^\dagger_{n_1} a^\dagger_{n_2} a^\dagger_{n_3} a^\dagger_{n_4}|\Phi\rangle;\\
&\hat{P}^I_{MK}\, a^\dagger_{p_1} a^\dagger_{p_2} a^\dagger_{p_3} a^\dagger_{p_4}|\Phi\rangle,
\end{aligned} \tag{6}$$

where $|\Phi\rangle$ represents the vacuum state, and the three-dimensional angular-momentum projection operator [36] is given by

$$\hat{P}^I_{MK} = \frac{2I+1}{8\pi^2}\int \mathrm{d}\Omega D^I_{MK}(\Omega)\hat{R}(\Omega), \tag{7}$$

with $\hat{R}(\Omega)$ being the rotation operator in terms of Euler angles. The $|\Phi\rangle$ in the TPSM approach is the triaxial quasiparticle vacuum state, and the angular-momentum projection operator in Eq. (7) projects not only the good angular-momentum but also states having good K-values.

TPSM calculations for positive parity states have been performed by considering both neutrons and protons occupying the three major oscillator shells of $N = 3$, 4, and 5. The projected bands from the intrinsic Nilsson + Bardeen–Cooper–Schrieffer (BCS) states in the vicinity of the Fermi surface are depicted in Fig. 10. It is noted from Fig. 10 that the ground state band having $K = 0$ is crossed by the two-neutron aligned configuration with $K = 1$ at I=12. More interestingly, the K=3 two-quasiparticle band, having the same intrinsic wave function as the K=1 band, also crosses the ground state band at spin I = 16 ħ. It is therefore expected that apart from the K=1 s-band that becomes yrast after the crossing at I=12, a parallel s-band, which is a γ-band built on the two-quasiparticle band, will track the yrast band. The normal γ-band based on the ground-state band with K=2 is located at an excitation energy of approximately 0.9 MeV from the ground-state. The two-proton configurations are noted to be quite high in energy and do not appear to become yrast up to quite a high-spin.

The projected bands from four-neutron and four-proton quasiparticle configurations are also plotted in Fig. 10, and the band structures obtained from these states lie

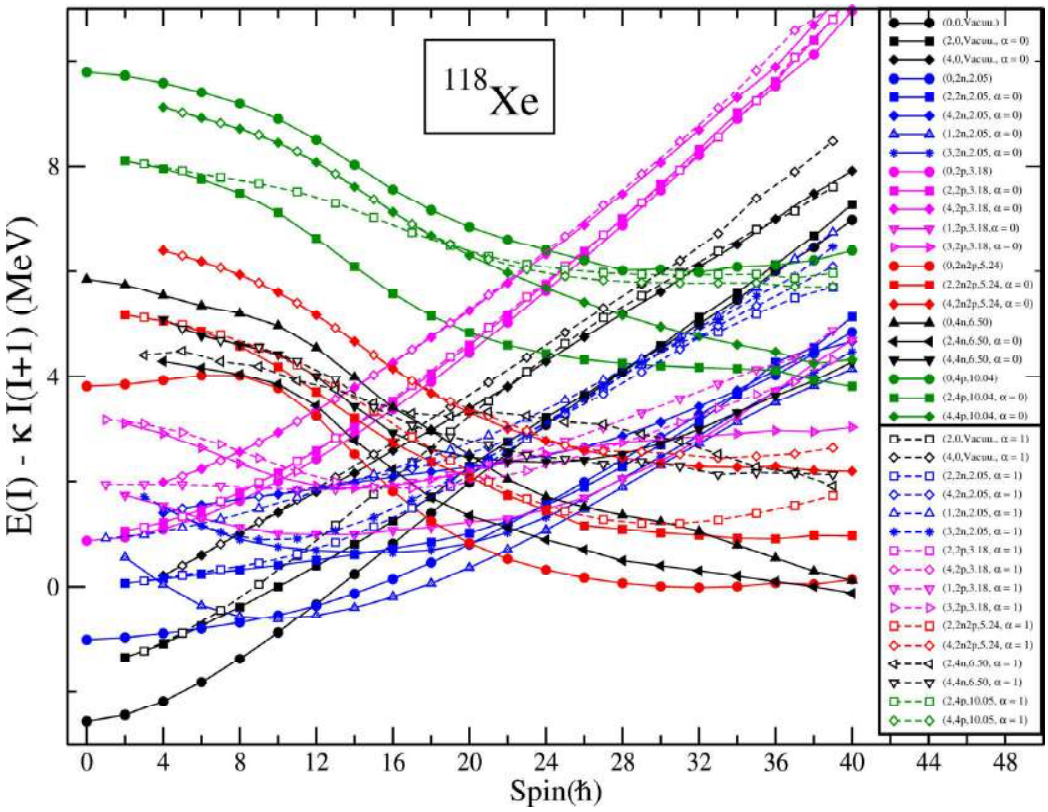


Fig. 10. (color online) Band diagram for the ^{118}Xe nucleus. The labels (0,0,Vacuu.), (2,0,Vacuu.), (4,0,Vacuu.), (1,2n), (3,2n), (1,2p), (3,2p), (0,2n2p), (2,2n2p), and (4,2n2p) correspond to the ground state band and the following bands: γ, 2γ, two neutron-aligned, γ-band on this two neutron-aligned state, two proton-aligned, γ-band on this two proton-aligned state, two-neutron plus two-proton aligned, and $\gamma-$ and $\gamma\gamma-$ bands built on this four-quasiparticle state. The excited K=0 bands resulting from the projection of two-quasineutrons and two-quasiprotons are denoted by (0,2n) and (0,2p), respectively. Some bands having large signature splitting are separated into even-spin (labeled as $\alpha = 0$) and odd-spin states (labeled as $\alpha = 1$). The first crossing at I=12 is due to the 2n K=1 aligned configuration that forms the S-band configuration. The second and third crossings at approximately I=22 and 36 are due to the aligning 2n2p and 4n configurations.

at a higher excitation energy than the two-neutron+ two-proton quasiparticle bands. It is noted that the $\alpha = 0$ component of the four-neutron quasiparticle state, having K=2, crosses the yrast-state band at I=34. The projected band from the K=4 component of the four-neutron state also crosses the ground-state at a higher spin value. In contrast, the $\alpha = 1$ branch of this configuration and the four-proton quasiparticle band structures lie at higher excitation energies.

The obtained band structures after diagonalization of the shell model Hamiltonian are compared with the experimental data in Fig. 11. It is evident from Fig. 11 that the TPSM approach reproduces the experimental data reasonably well. The calculated band structures have been plotted using the wavefunction analysis shown in Fig. 12, as was done for ^{156}Dy [34].

We would like to add that there has been some controversy regarding the nature of the bandcrossings in ^{118,120}Xe isotopes [9, 10]. It has been argued based on the systematics of the bandcrossings in the neighboring isotopes, in particular, to those of ^{120,122}Ba, that the first bandcrossing should be due to the alignment of two-protons [10]. However, the cranked shell model analysis predicts the first crossing to be due to neutrons, as for heavier isotopes [10]. It is evident from the present TPSM study that the first bandcrossing is also due to the alignment of two neutrons, as can be seen from Fig. 10. In order to further investigate the bandcrossing properties of the yrast band, we have extracted the aligned angular-momentum from the calculated quantities and the results are plotted in Fig. 13 as a function of the rotational frequency. It can be noted from Fig. 13 that the bandcrossing frequency as well as the gain in the alignment is well reproduced by the TPSM calculations. We would like to add that in the earlier study [8], the bandcrossing due to neutrons was disregarded, as the experimentally deduced gain in the alignment was smaller than that predicted by the cranked shell model approach. In the present analysis using the TPSM approach, three band crossing frequencies and the gain in the alignment are reproduced. The first crossing is inferred to be due to the alignment of two neutrons, the second results from a four-quasiparticle

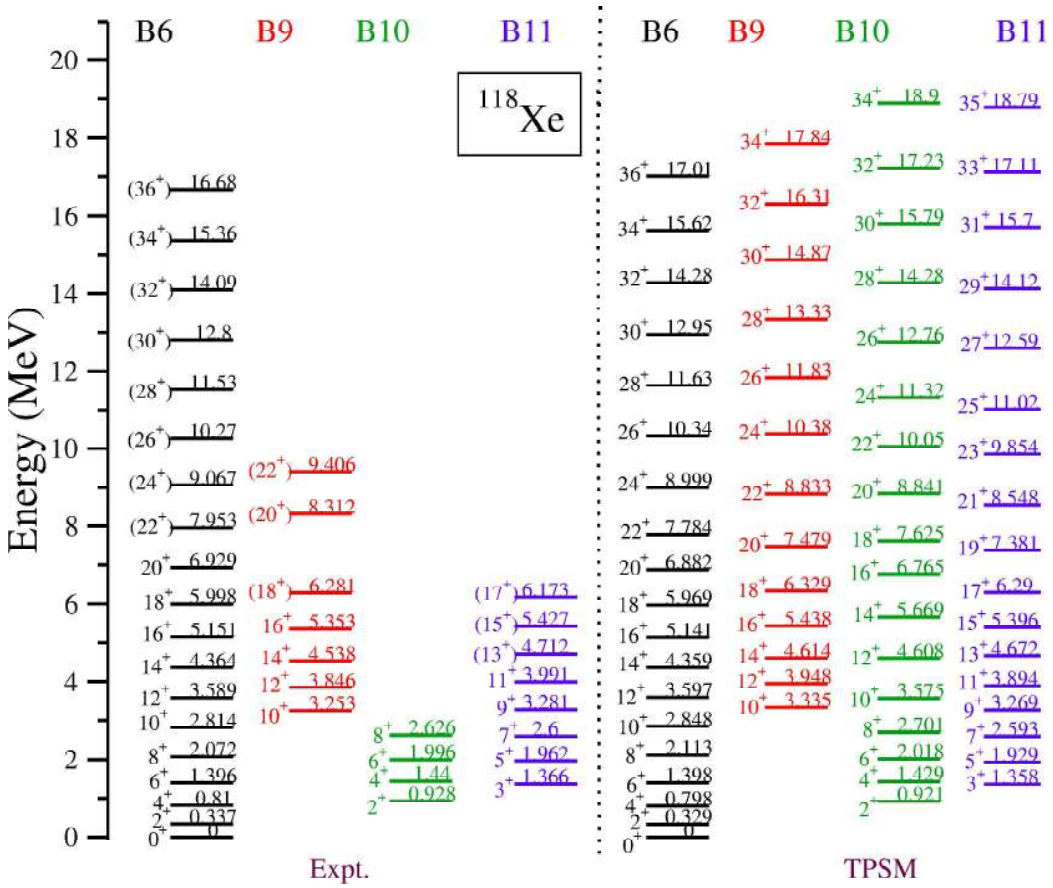


Fig. 11. (color online) Comparison of the calculated positive parity band energies with present experimental data (bands B6, B9, B10, and B11) for ^{118}Xe.

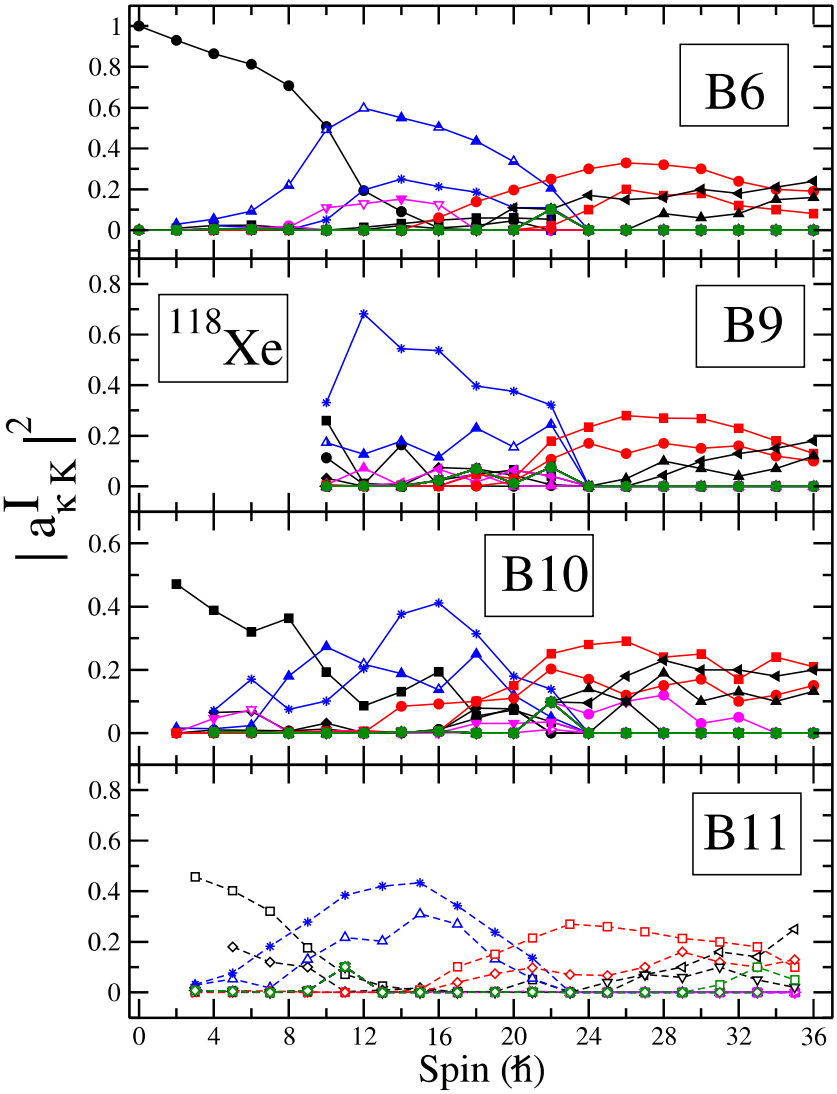


Fig. 12. (color online) Probabilities of various projected K-configurations in the wavefunctions of the observed postive parity bands for ^{118}Xe. For clarity, only the lowest projected K-configurations in the wavefunctions of bands are shown. In the numerical calculations, projection has been performed from 44 intrinsic states. The probabilities $|a^I_{K}|^2$ of various bands are labeled as in Fig. 10.

configuration, and the third results from a four-neutron configuration.

We also performed the TPSM investigation of the negative parity bands observed in ^{118}Xe with the same parameters used to describe the positive parity states. In order to generate the negative parity yrast states in an even-even system, which are basically two-quasiparticle states, where one neutron is in the N=4 shell and the second neutron of the two-quasiparticle state in the N=5 shell. Normal two-neutron and two-proton configurations are also constructed based on the basic two-quasiparticle configuration, and the details shall be provided in a separate study [37]. The TPSM results for the negative parity bands are compared with the experimental data in Fig. 14, and the results are noted to be in good agreement with the data. As is evident from Fig. 15, which provides the probabilities of various configurations in the wavefunctions, band B1 is dominated by a two-neutron state having quasiparticle energy of 0.907 MeV and projected to K=3 and 7 configurations.

We would like to add that the TPSM approach conserves the parity quantum number at the mean-field level, as octupole correlations are not considered. The enhanced $E1$ transitions observed in the experimental study, which indicate the possible presence of the octupole correlations, cannot be studied using the present version of

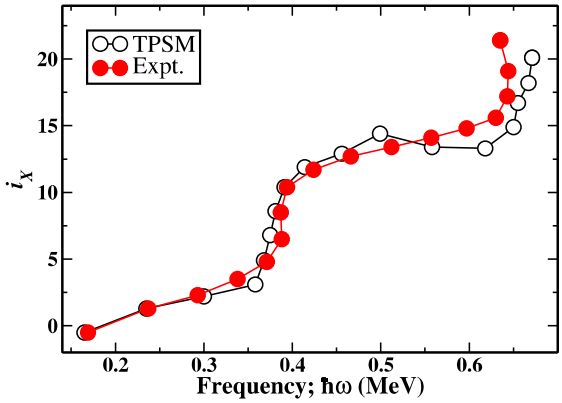


Fig. 13. (color online) Comparison of the aligned angular momentum, $i_x = I_x(\omega) - I_{x,\mathrm{ref}}(\omega)$, where $\hbar\omega = \frac{E_\gamma}{I^I_x(\omega) - I^I_x(\omega)}$, $I_x(\omega) = \sqrt{I(I+1)-K^2}$, and $I_{x,\mathrm{ref}}(\omega) = \omega(J_0 + \omega^2 J_1)$. The reference band Harris parameters used are J_0=23 and J_1=90, which are obtained from the measured positive parity energy levels, as well as those calculated from the TPSM results, for the ^{118}Xe nucleus.

the TPSM approach. We are in the process of generalizing the model to incorporate the octupole-octupole interaction, and the $E1$ transitions observed shall be investigated in future.

Furthermore, inspired by the recent experimental data [38], we extend the TPSM calculations to study the low spin yrast and γ-band transitional probabilities. Electric quadrupole transition probabilities are calculated using the eigenfunctions obtained from the diagonalization of the Hamiltonian [34] within the chosen set of the TPSM basis. The reduced electric quadrupole transition probability $B(E2)$ from an initial state (σ_i, I_i) to a final state (σ_f, I_f) is given by

$$B(E2, I_i \to I_f) = \frac{\mathrm{e}^2}{2I_i+1} |<\sigma_f, I_f||\hat{Q}_2||\sigma_i, I_i>|^2. \quad (8)$$

where $\hat{Q}_2$ is related to the quadrupole operator [34]. As in our earlier publications [35, 37], we have used the effective charges of 1.5e for protons and 0.5e for neutrons. The

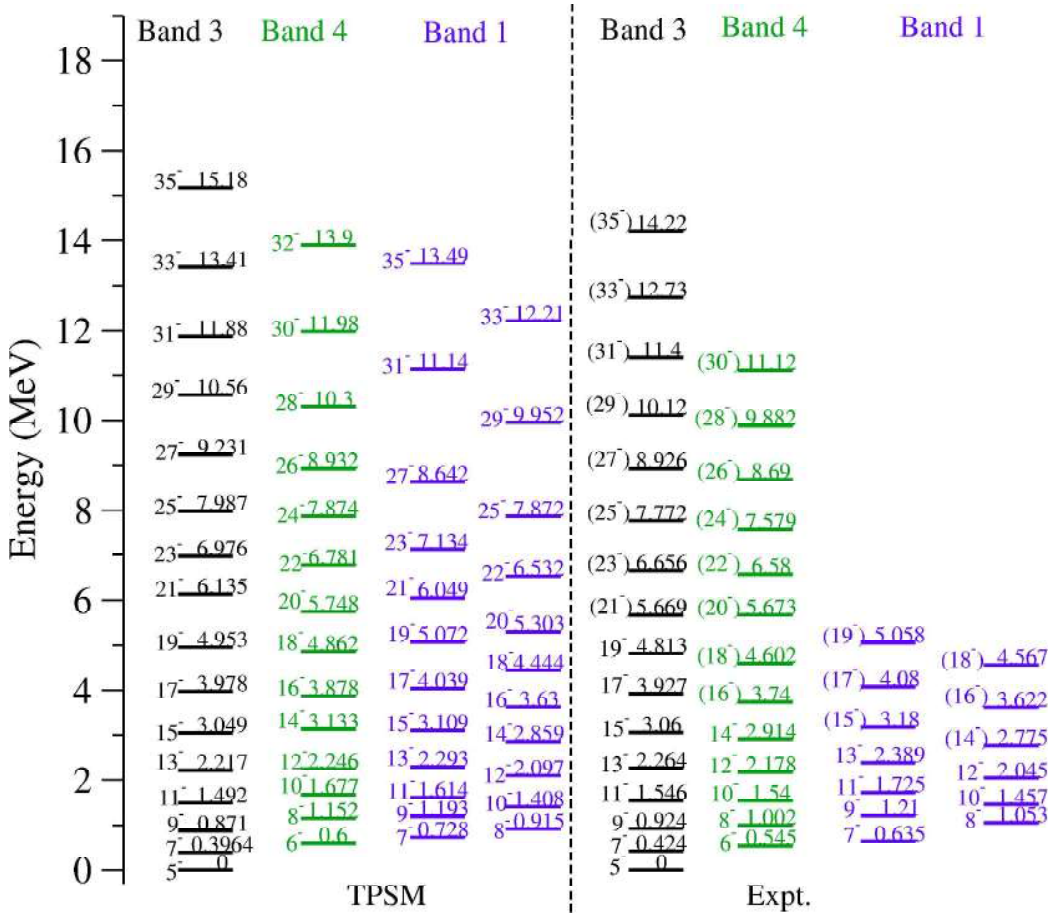


Fig. 14. (color online) Comparison of the calculated negative parity band energies with present experimental data (bands B3, B4, and B1) for ^{118}Xe.

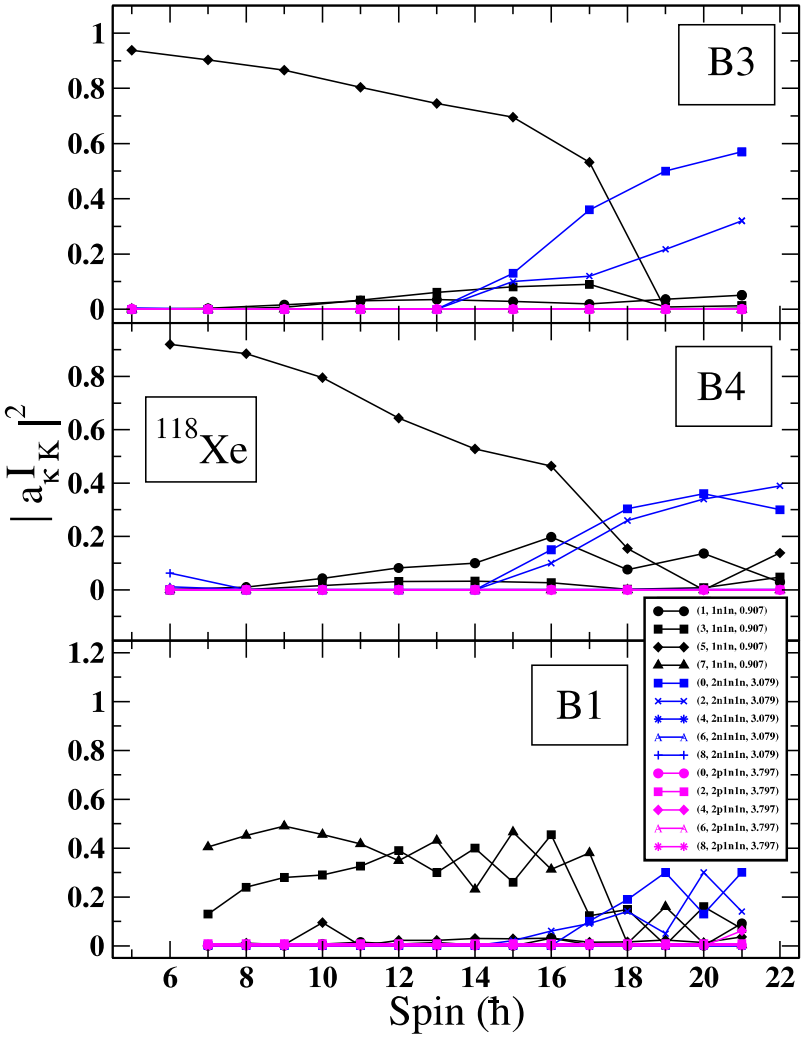


Fig. 15. (color online) Probabilities of various projected K-configurations in the wavefunctions of the observed negative parity bands for ^{118}Xe. For clarity, only the lowest projected K-configurations in the wavefunctions of bands are shown, and in the numerical calculations, the projection has been performed from 44 intrinsic states.

effective charges are employed instead of the bare charges, as the core is used in the TPSM, and valence particles occupy only three major oscillator shells. The major emphasis here is to introduce transitional probabilities to elucidate the recent measurement of the lifetimes of ^{118}Xe along the yrast line [38]. The data depict a rapid variation of the $B(E2)$ transition probabilities along the yrast band with probabilities showing an increasing trend for low-spin states and dropping for high-spin states. In Fig. 16, the TPSM calculated $B(E2)$ transition probabilities are compared with the available theoretical and experimental results [38]. It is noted from the figure that the TPSM results reproduce the experimental trend for the known values reasonably well and are also in good agreement with those predicted by IBM calculations with fitted parameters [38].

In particular, the increasing trend of $B(E2)$ values for low-spin states up to 6^+ and the drop for the $8^+ \to 6^+$ transition are well described by the TPSM calculations. This decreasing trend can be traced to the crossing of the 2-qp neutron configuration with the ground-state band. The transition probabilities in the band-crossing region are reduced as the states are mixed in the this region.

Table 3 compares the experimental reduced $E2$ transitional probabilities for the γ-band (in-band, inter-band) with the ones calculated using the TPSM wavefunctions. The experimental data on transition strengths and the results of the IBM calculations in \tablename 2 are from Ref. [38]. It is evident that TPSM calculations reproduce these transitions quite well compared with the corresponding

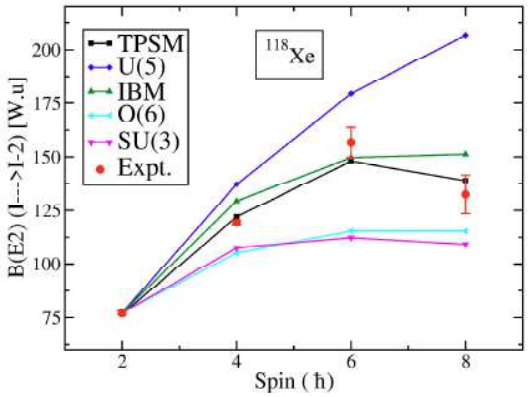


Fig. 16. (color online) Comparison of $E2$ transition probabilities (in W.u) for the yrast band in ^{118}Xe with TPSM and IBM calculations. The experimental data for the transition strengths and the results of the IBM calculations are from Ref. [38].

IBM results.

VI. SUMMARY

High spin states in ^{118}Xe have been investigated via the ^{93}Nb(^{28}Si, $p2n$)^{118}Xe reaction deploying an INGA detector set-up at IUAC, New Delhi. In the present study, we were successful in 1) adding seven new γ-transitions to the previously existing level structure, 2) fixing the negative parity of band 4 through polarisation measurement of its γ-ray transition and hence confirming the electric nature of the 924 keV ($8^- \rightarrow 8^+$) transition for the first time, and 3) providing more precise data (errors in the range of 4% − 18%) for the $B(E1)$ values except for $I = 7$ ħ. Enhanced $B(E1)/B(E2)$ ratios for the transitions from $I^\pi = 7^-$, 9^-, 11^-, and 8^- support the existence of octupole correlation between $vh_{11/2}$ and $vd_{5/2}$ bands having $\Delta j = \Delta l = 3$ in ^{118}Xe. However, there is a need to examine low lying interlinking transitions of $E1$ character with lifetime measurement techniques in neutron deficient (Xe-Cs-Ba) nuclei having $A \leq 120$ ($Z \leq 56$) to establish the octupole correlation in this mass region.

Table 3. Comparison of $E2$ transition probabilities (in W.u) for the quasi-γ band in ^{118}Xe with TPSM and IBM calculations. The experimental data for the transition strengths and results of the IBM calculations are taken from Ref. [38].

I_i^π	I_f^π	$B(E2)$ Expt.	$B(E2)$ TPSM	$B(E2)$ IBM
$2_\gamma^+ \rightarrow$	2_g^+	36(12)	40.700	4
	0_g^+	1	1.142	1
$3_\gamma^+ \rightarrow$	2_γ^+	49(13)	59.19	11
	2_g^+	1	2.574	1
$4_\gamma^+ \rightarrow$	2_γ^+	2.4(5)	3.808	3.8
	4_g^+	1	3.275	1
$5_\gamma^+ \rightarrow$	3_γ^+	27(9)	33.981	10
	4_g^+	1	2.918	1
$6_\gamma^+ \rightarrow$	4_γ^+	4.6(10)	7.685	12.5
	6_g^+	1	2.129	1

References

[1] Y. Liang *et al.*, Phys. Rev. C **45**, 1041 (1992)
[2] S. Juutinen, *et al.*, Z. Phys. A **338**, 365 (1991)
[3] P. Butler, *et al.*, Rev. Mod. Phys. **68**, 349 (1996)
[4] I. Ahmad, *et al.*, Annu. Rev. Nucl. Part. Sci. **43**, 71 (1993)
[5] K. Selvakumar, *et al.*, Phys. Rev. C **92**, 064307 (2015)
[6] J. Smith, *et al.*, Phys. Rev. C **57**, R1037 (1998)
[7] P. Mason, *et al.*, Phys. Rev. C **72**, 064315 (2005)
[8] E. Paul, *et al.*, Phys. Rev. C **51**, R2857 (1995)
[9] S. Törmänen, *et al.*, Nuclear Physics A **572**, 417 (1994)
[10] J. M. Sears *et al.*, Phys. Rev. C **57**, 2991 (1998)
[11] A. Pandey, *et al.*, Nucl. Instrum. Meth. Phys. Res. A **985**, 164667 (2021)
[12] S. Abhilash, *et al.*, J. Radio. Nucl. Chem. **305**, 749 (2015)
[13] G. K. Mehta, *et al.*, Nucl. Instrum. Meth. Phys. Res. A **268**, 334 (1988)
[14] S. Muralithar, *et al.*, Nucl. Instrum. Meth. Phys. Res. A **622**, 281 (2010)
[15] B.Ajith*et al.*,http://www.iuac.res.in/iuacoldwebsite/research/np/inga/candle-DAE-Vol.44B_2001_390.pdf
[16] R. K. Bhowmik *et al.*, http://www.iuac.res.in/iuacoldwebsite/research/np/inga/ingasort-DAE-Vol.44B_2001_422.pdf
[17] D. Radford, Nucl. Instrum. Meth. Phys. Res. A **361**, 297 (1995)
[18] A. Kramer-Flecken, *et al.*, Nucl. Instrum. Meth. Phys. Res. A **275**, 333 (1989)
[19] K. Starosta, *et al.*, Nucl. Instrum. Meth. Phys. Res. A **423**, 16 (1999)
[20] S. Chakraborty *et al.*, Braz. J. Phys., 406-410 (2017)
[21] K. Kitao, Nucl. Data Sheets **75**, 99 (1995)
[22] J. Genevey-Rivier *et al.*, Nucl. Phys. A **283**, 45 (1977)
[23] E. A. McCutchan *et al.*, Phys. Rev. C **76**, 024306 (2007)
[24] S. Rugari, *et al.*, Phys. Rev. C **48**, 2078 (1993)
[25] J. A. Sheikh, K. Hara, Phys. Rev. Lett. **82**, 3968 (1999)
[26] P. Möller, J. R. Nix, At. Data Nucl. Tables **59**, 185 (1995)
[27] J. A. Sheikh, *et al.*, Phys. Rev. C **84**, 054314 (2011)
[28] G. H. Bhat, *et al.*, Phys. Rev. C **86**, 047307 (2012)
[29] C. L. Zhang, *et al.*, Phys. Rev. C **92**, 034307 (2015)
[30] J. A. Sheikh, *et al.*, Nucl. Phys. A **824**, 58 (2009)
[31] G. H. Bhat, *et al.*, Phys. Lett. B **707**, 250 (2012)
[32] G. H. Bhat, *et al.*, Phys. Rev. C **89**, 014328 (2014)
[33] J. A. Sheikh, *et al.*, Phys. Rev. C **77**, 034313 (2008)
[34] S. Jehangir *et al.*, Phys. Rev. C **97**, 014310 (2018)
[35] J. A. Sheikh, *et al.*, Phys. Scr. **91**, 063015 (2016)
[36] K. Hara, Y. Sun, Int. J. Mod. Phys. E **04**(04), 637-785 (1995)
[37] S. Jehangir *et al.* (in preparation)
[38] C. Müller-Gatermann, *et al.*, Phys. Rev. C **102**, 064318 (2020)

APS (https://www.aps.org/)

PHYSICAL REVIEW C (/PRC/)
covering nuclear physics

Highlights (/prc/highlights) Recent (/prc/recent) Accepted (/prc/accepted) Collections (/prc/collections) Authors (/prc/authors)
Referees (/prc/referees) Search (/search) Press (/press) About (/prc/about) Editorial Team (/prc/staff) (/feeds)

Spectroscopic study of

Rozina Rahaman, Abhijit Bisoi, Ananya Das, Y. Sapkota, Arkabrata Gupta, S. Ray, S. Sarkar, Yashraj, A. Sharma, Bharti Rohila, I. Ahmed, Kaushik Katre, S. Dutt, S. Kumar, R. P. Singh, R. Kumar, and S. Muralithar
Phys. Rev. C **109**, 024318 – Published 15 February 2024

More

Article

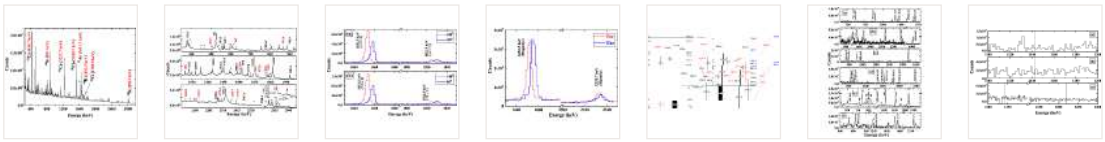
PDF (/prc/pdf/10.1103/PhysRevC.109.024318) **HTML (/prc/abstract/10.1103/PhysRevC.109.024318#fulltext)**

Export Citation (/prc/export/10.1103/PhysRevC.109.024318)

ABSTRACT
AUTHORS
ARTICLE TEXT
INTRODUCTION
EXPERIMENTAL DETAILS AND DATA ANALYSIS
RESULT AND DISCUSSION
THEORETICAL CALCULATION
CONCLUSION
ACKNOWLEDGMENTS
REFERENCES

ABSTRACT

High spin states of populated through the (2) reaction at 68 MeV beam energy were studied using the Indian National Gamma Array (INGA) facility. Six new levels and fourteen new transitions were added to the existing level scheme. The spins and parities of most of the levels were assigned, modified, or confirmed from , , and linear polarization measurements. The multipole mixing ratios O1 for most of the transitions were measured. Large-basis shell-model calculations were performed to understand the microscopic origin of the levels. Different particle restrictions in and shell orbitals were used to explain the experimental results.



6 More

Received 31 August 2023 Revised 21 December 2023 Accepted 19 January 2024

DOI: https://doi.org/10.1103/PhysRevC.109.024318

©2024 American Physical Society

Physics Subject Headings (PhySH)

Research Areas

This site uses cookies. To find out more, read our Privacy Policy (https://www.aps.org/about/privacy.cfm).

I Agree ()

Sign up to receive regular email alerts from *Physical Review C*

Sign up (https://info.aps.org/journals-emails)

ISSN 2469-9993 (online), 2469-9985 (print). ©2024 American Physical Society. (https://www.aps.org/) All rights reserved. *Physical Review C*™ is a trademark of the American Physical Society, registered in the United States, Canada, European Union, and Japan. The *APS Physics logo* and *Physics logo* are trademarks of the American Physical Society. Information about registration may be found here (/legal). Use of the American Physical Society websites and journals implies that the user has read and agrees to our Terms and Conditions (/info/terms.html) and any applicable Subscription Agreement (https://librarians.aps.org/sitelicense.pdf).

This site uses cookies. To find out more, read our Privacy Policy (https://www.aps.org/about/privacy.cfm).

I Agree ()

Already have a manuscript?

Use our Manuscript Matcher to find the best relevant journals!

Find a Match

Refine Your Search Results

2469-9985 Search

Sort By: Title (A-Z)

Search Results

Found 1 results (Page 1) Share These Results

Exact Match Found

PHYSICAL REVIEW C

Publisher:	AMER PHYSICAL SOC , ONE PHYSICS ELLIPSE, COLLEGE PK, USA, MD, 20740-3844
ISSN / eISSN:	2469-9985 / 2469-9993
Web of Science Core Collection:	Science Citation Index Expanded
Additional *Web of Science* Indexes:	Current Contents Electronics & Telecommunications Collection | Current Contents Physical, Chemical & Earth Sciences | Essential Science Indicators

Share This Journal View profile page

** Requires free login.*

Filters Clear All

Web of Science Coverage

Open Access

Category

Country / Region

Language

Frequency

Journal Citation Reports

Evidence of transverse wobbling motion in ^{151}Eu

A. Mukherjee,[1] S. Bhattacharya,[2] T. Trivedi,[1,3,*] S. Tiwari,[3] R. P. Singh,[4] S. Muralithar,[4] Yashraj,[4] K. Katre,[4] R. Kumar,[4] R. Palit,[5] S. Chakraborty,[6] S. Jehangir,[7,8] Nazira Nazir,[7,9] S. P. Rouoof,[8] G. H. Bhat,[7] J. A. Sheikh,[9] N. Rather,[8] R. Raut,[10] S. S. Ghugre,[10] S. Ali,[11] S. Rajbanshi,[12] S. Nag,[13] S. S. Tiwary,[14] A. Sharma,[15] S. Kumar,[16] S. Yadav,[17] and A. K. Jain[2]

[1]*Department of Pure & Applied Physics, Guru Ghasidas Vishwavidyalaya, Koni, Bilaspur-495009, India*
[2]*Amity Institute of Nuclear Science & Technology, Amity University U.P., Noida-201313, India*
[3]*Department of Physics, University of Allahabad, Prayagraj- 211002, India*
[4]*Inter University Accelerator Centre, Aruna Asaf Ali Marg, New Delhi-110067, India*
[5]*Department of Nuclear and Atomic Physics,Tata Institute of Fundamental Research, Mumbai-400005, India*
[6]*Variable Energy Cyclotron Centre, Kolkata-700064, India*
[7]*Department of Physics, S.P. College, Srinagar, Jammu and Kashmir, 190 001, India*
[8]*Department of Physics, Islamic University of Science and Technology, Jammu and Kashmir, 192 122, India*
[9]*Department of Physics, University of Kashmir, Hazratbal, Srinagar, 190 006, India*
[10]*UGC-DAE Consortium for Scientific Research Centre, Kolkata-700106, India*
[11]*Government General Degree College at Pedong, Kalimpong-734311, India*
[12]*Department of Physics, Presidency University, Kolkata-700073, India*
[13]*Department of Physics, IIT(BHU), Varanasi-221005, India*
[14]*Department of Physics, Manipal university Jaipur, Rajasthan-303007, India*
[15]*Department of Physics, Himachal Pradesh University, Shimla 171005, India*
[16]*Department of Physics and Astrophysics, University of Delhi, Delhi-110007, India*
[17]*Department of Physics, Panjab University, Chandigarh-160014, India*

(Received 21 December 2022; revised 22 January 2023; accepted 8 May 2023; published 22 May 2023)

Transverse wobbling was investigated in the ^{151}Eu nucleus by populating the excited states using ^{148}Nd(^{7}Li, 4n) ^{151}Eu at a beam energy of 30 MeV. Three new interconnecting transitions have been placed between the two negative parity bands. The $M1/E2$ character of the interconnecting $\Delta I = 1$ transitions between the negative parity bands was extracted from the mixing ratios using the $R_{\rm DCO}$ and linear polarization method. The spin and parity of the states of different bands have also been assigned. The dominant $E2$ character of the interlinking transitions between the yrast and first phonon wobbling band and the dominant $M1$ character between the yrast band and its signature partner band indicate the presence of transverse wobbling in the ^{151}Eu nucleus. It is further demonstrated that the triaxial projected shell model approach describes the observed experimental properties.

DOI: 10.1103/PhysRevC.107.054310

I. INTRODUCTION

The nonaxial or triaxial nucleus with uneven density distribution along its three principal axes, medium (m), long (l), and short (s) axes, is energetically favored to rotate around the principal axis having the largest moment of inertia (MoI), i.e., $J_m \geqslant J_l \neq J_s$, respectively. The characteristic feature of such a triaxial nucleus is the presence of chiral rotation or wobbling motion. Initially, the wobbling motion of the even-even triaxially deformed nucleus was described by Bohr and Mottelson [1] without the inclusion of the intrinsic angular momentum. In case of the odd A nucleus, wobbling excitations can be induced from the alignment of high-j particles as explained by Hamamoto [2]. Further, Frauendorf and Dönau classified the wobbling motion of the triaxial nuclei into two categories viz. *longitudinal and transverse* wobbling [3]. The change in the pattern of wobbling energy ($E_{\rm wobb}$) as a function of increasing spin is the primary criterion to distinguish between the two wobbling modes. The wobbling energy decreases (increases) with increasing spin for the transverse (longitudinal) wobbling mode. A triaxial nucleus showcases transverse wobbling motion when the quasiparticle (hole) emerging from the bottom (top) of a deformed shell aligns its angular momentum j with the s axis (l axis), whereas in the case of a longitudinal wobbler, the angular momentum of the odd particle aligns with the axis having the largest moment of inertia, i.e., the medium axis (m) [4].

The first experimental evidence of wobbling motion in the nucleus was observed in the ^{163}Lu isotope [5], which arises from the excitation of the wobbling phonon ($n_\omega = 1$) built on the aligned proton $i_{13/2}$ orbital. Following this breakthrough observation, one and (or) two phonon wobbling bands were simultaneously observed in the chain of odd mass Lu isotopes [6–9], ^{167}Ta [10], ^{135}Pr [11,12], ^{133}La [13], ^{127}Xe [14], ^{133}Ba [15], ^{183,187}Au [4,16], and ^{105}Pd [17] nuclei. Apart from these odd mass nuclei, ^{130}Ba [18,19] and ^{136}Nd [20,21] are the only two even-even nuclei in which wobbling motion was

*ttrivedi1@gmail.com

 ©2023 American Physical Society

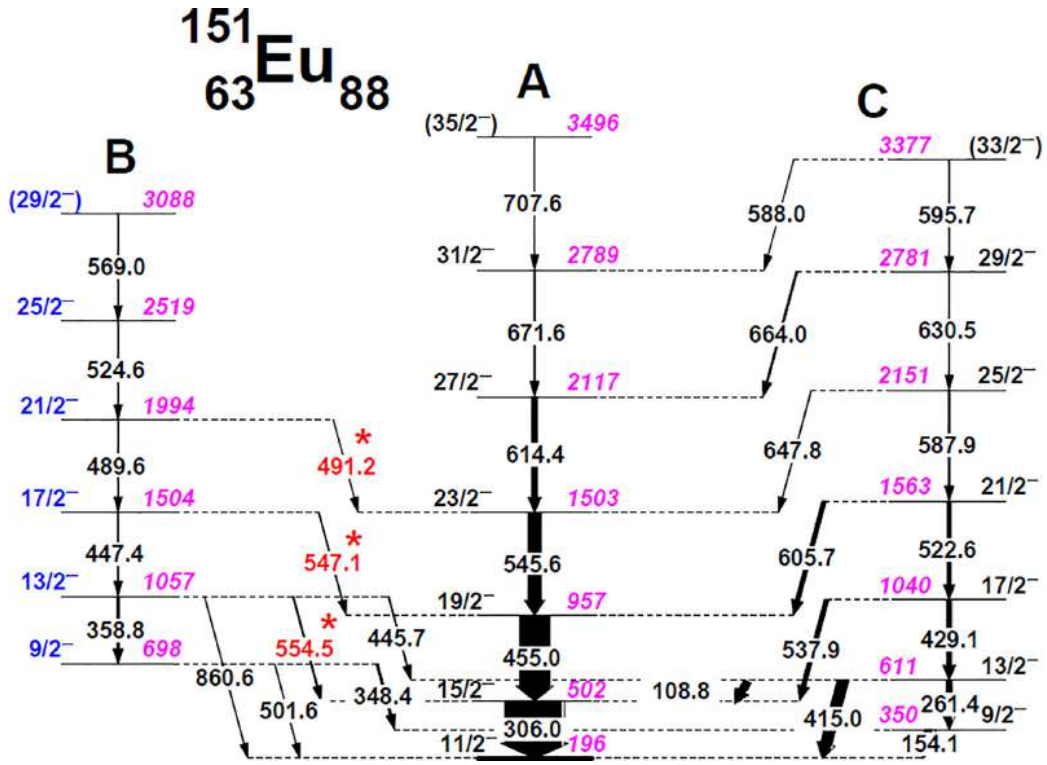


FIG. 1. Partial level scheme of ^{151}Eu based on the present work and the previous studies [31–34]. The newly observed transitions in the present work (labeled in red font) are marked by asterisks, while the spin states labeled in blue font are modified in the present study. The thick solid black line representing the $11/2^-$ state is an isomeric state with $\tau_{1/2} = 58.9(5)$ μs. The transition energies are in keV. The level energies are rounded off to the nearest keV.

observed to date. Among these nuclei, ^{127}Xe, ^{133}Ba, ^{133}La, and ^{187}Au fall into the category of longitudinal wobbling (LW), while the rest of them show the transverse mode of wobbling motion (TW). The wobbling phonon excitation with decaying $\Delta I = 1$ transitions between the strongly deformed bands are observed at a high spin range in Lu and Ta isotopes, whereas in other nuclei, these interlinking transitions are observed between two normal deformed bands lying within a spin range of 15–20$\hbar$. So far, multiphonon wobbling bands have been observed in ^{183}Au [16], ^{127}Xe [14], ^{135}Pr [12], and ^{133}Ba [15] nuclei where the wobbling excitations of the first three candidates is associated with particlelike behavior of the quasiparticles while the later showcases the observation of wobbling excitations from a holelike quasiparticle. Contemporarily, various theoretical interpretations have been made to evaluate the presence of wobbling motion in these nuclei [19,20,22–28]. On the one hand, the two-dimensional plots of the probability distributions of the spin coherent states (SCS) have been used to generalize the classification of the collective excitations of the quantum states of the particle coupled to a triaxial rotor (PTR) model as transverse and longitudinal wobbling modes [25]. On the other hand, another terminology called "tilted precession" (TiP) was proposed to interpret and classify the deformed bands observed in these triaxial nuclei [23]. However, based on different studies, the wobbling motion in some of the suggested wobblers is still under debate [23,27,29]. Recently, the theoretical prediction of wobbling excitation based on adiabatic and configuration-fixed constrained triaxial CDFT calculations in $^{57-62}$Ni isotopes opens up $A \approx 60$ mass region for studying the presence of wobbling phenomenon [30].

Although the wobbling motion of a nucleus was studied in the ∼130 and 180 mass region, such evidence is yet to be observed in the ∼150 mass region. The collective structures of the nuclei lying in the ∼150 mass region have been rigorously studied in the past decades. For instance, Jongman *et al.* had established the reflection asymmetric structure of the ^{151}Eu isotope by observing enhanced *E1* transitions between its positive and negative parity bands [32]. The previous study of ^{151}Eu has also reported the presence of strong interband $\Delta I = 1$ transitions which are interpreted to arise from the rotation of the triaxial shape [32]. The theoretical particle rotor calculation with the odd proton in deformed potential points towards the triaxial shape of the nucleus with $\epsilon_2 \sim 0.19$ at $\gamma = 20°$; however, because of the limitation of the model, the calculated level energies were not much sensitive to the chosen deformation parameters [33]. Further, the similarity between the ratio of transition strength compared with the neighboring triaxial ^{150}Ho, also indicates its nonaxial structure [32], however, concrete evidence is yet to be found supporting such a triaxial structure.

In the present work, we have studied the triaxial structure of ^{151}Eu by performing detailed in beam γ-ray spectroscopic measurement. The band built on the unfavored sequence of the yrast band in the ^{151}Eu nucleus is predicted to arise because of the one-phonon wobbling excitation along with the

identification of the signature partner (SP) band for the first time in ∼150 mass region. The ambiguity in spin and the parity of the signature partner band was removed on the basis of the directional correlation of oriented nuclei ratio and polarization measurement. The nature of the mixed interlinking transitions has also been established using these methods to determine the dominant $M1/E2$ character of the transitions. Further, the triaxial projected shell model (TPSM) analysis was performed to interpret the experimental results.

II. EXPERIMENTAL DETAILS

The excited states of ^{151}Eu were studied using the ^{148}Nd(^{7}Li, 4n)^{151}Eu fusion evaporation reaction and Indian National Gamma Array (INGA) [35] at IUAC, New Delhi. The 30-MeV energetic beam of ^{7}Li, provided by 15 UD pelletron was bombarded on ^{148}Nd target of thickness 750 μg backed with 12 mg/cm^2 of ^{197}Au. The decaying γ rays were detected using 16 Compton suppressed clover detectors placed at 32°, 57°, 90°, 123°, and 148° along with two ancillary LEPS detectors at 61° and 119°, respectively. The relative efficiency and energy calibration of the detection system were performed with the two radioactive sources ^{152}Eu and ^{133}Ba by placing them at the target position. The coincidence data was sorted in different symmetric and angle-dependent asymmetric $\gamma-\gamma$ matrices using the INGASORT program [36]. The $\gamma-\gamma$ matrices were analyzed using the RADWARE [37,38] and ROOT [39] software packages. Further, an asymmetric matrix consisting of events detected by the clover detectors at 148° on one axis and 90° on the other axis was constructed to assign the multipolarities of the γ rays based on the directional correlation of oriented nuclei (DCO) ratio measurements. A total of 5.2×10^8 γ-γ coincidence events were collected in event-by-event mode.

III. DATA ANALYSIS

A. Level scheme

The partial level scheme of ^{151}Eu nucleus relevant to the present study is shown in Fig. 1. The negative parity yrast band A emerges from an isomer, having lifetime $\tau_{1/2}=58.9(5)$ μs, at $11/2^-$ state [32] and was observed up to the $(35/2^-)$ state at level energy 3496 keV. The band C was observed up to the $33/2^-$ state at an excitation energy of 3377 keV. The spin and parity of the negative parity bands A and C are consistent with the previous studies [32,33]. The ambiguity in the spin and parity of band B in the previous work [32] was removed in the present work by performing the $R_{\rm DCO}$ and polarization measurements. The previously reported $7/2^-$ state at 243-keV excitation energy in band B with $\tau_{1/2}=0.36(2)$ ns [34] is not observed in the present study. The band B was observed up to the $(29/2^-)$ state, and three new interconnecting γ-ray transitions with energies 554.5, 547.1, and 491.2 keV have been identified and placed between bands A and B. The representative gated spectra at 306.0- and 524.6-keV transitions are shown in Figs. 2 and 3, respectively, to support the placement of these interlinking transitions. The intensities of the observed transitions in bands A, B, and C are measured with respect to the 306.0-keV transition, as listed in Table I. The intensity uncertainties include systematic errors which are estimated to be 5% for $200\leqslant E_\gamma\leqslant1000$ keV and 10% for energies outside of this range.

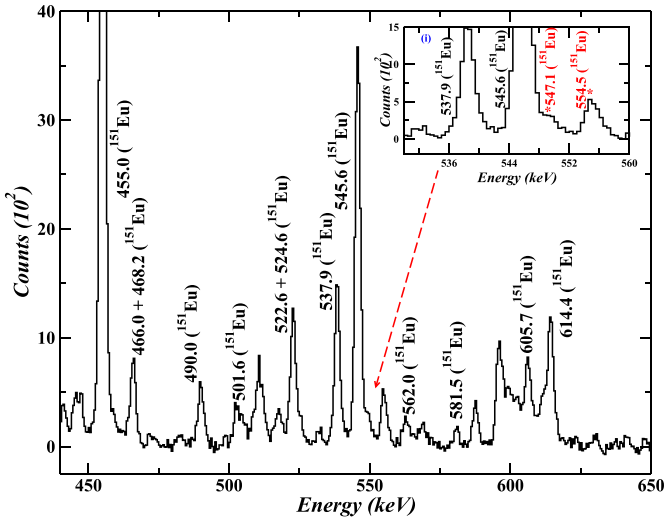


FIG. 2. A portion of the background subtracted spectrum obtained by gating on 306.0-keV transition of band A in ^{151}Eu. The red colored asterisk marked energies denote the newly placed transitions in the level scheme.

B. Angular correlation and polarization measurements

The assignment of the spin and parity of the γ-ray transitions was done using the directional correlation of oriented states (DCO) ratio, and linear polarization measurements, respectively. In the present study, the DCO ratio is defined as

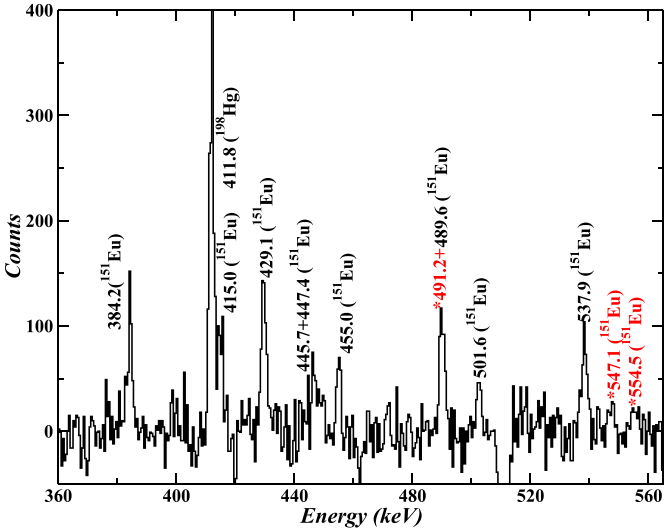


FIG. 3. A portion of the background subtracted spectrum obtained by gating on 524.6-keV transition of band B in ^{151}Eu. The red colored asterisk marked energies denote the newly placed transitions in the level scheme. The 411.8-keV transition originates from the ^{198}Hg nucleus as it was populated because of the reaction of the ^{7}Li beam on ^{197}Au backing.

TABLE I. Excitation energies (E_i) of levels, spin-parity assignments for the initial (I_i^π) and final (I_f^π) state, γ-ray transition energies ($E\gamma$), relative intensities ($I\gamma$), DCO ratios ($R_{\rm DCO}$), polarization asymmetries ($\triangle$), mixing ratios (δ), and multipolarities of the γ rays observed in the decay of ^{151}Eu.

E_i(keV)	$(I_i^\pi) \rightarrow (I_f^\pi)$	E_γ(keV)[a]	I_γ	$R_{\rm DCO}$	$\triangle$	δ[b]	δ[c]	δ_{av}	Assignment
350	$9/2^- \rightarrow 11/2^-$	154.1	13.8(7)	0.65(12)	–	–	–	–	$(M1/E2)$
502	$15/2^- \rightarrow 11/2^-$	306.0	100	0.97(11)	0.160(24)	–	–	–	$E2$
611	$13/2^- \rightarrow 15/2^-$	108.8	10.5(6)	0.68(10)	–	–	–	–	$(M1/E2)$
611	$13/2^- \rightarrow 9/2^-$	261.4	9.5(5)	0.98(16)	–	–	–	–	$(E2)$
611	$13/2^- \rightarrow 11/2^-$	415.0	19.3(10)	0.44(7)	0.038(35)	-3.3^{+9}_{-14}	-3.3^{+13}_{-30}	-3.3^{+15}_{-33}	$M1/E2$
698	$9/2^- \rightarrow 11/2^-$	501.6	1.0(1)	0.61(11)	–	–	–	–	$(M1/E2)$
698	$9/2^- \rightarrow 9/2^-$	348.4	3.7(3)	–	–	–	–	–	–
957	$19/2^- \rightarrow 15/2^-$	455.0	52.8(27)	1.02(11)	0.222(20)	–	–	–	$E2$
1040	$17/2^- \rightarrow 13/2^-$	429.1	8.9(7)	0.97(15)	0.227(55)	–	–	–	$E2$
1040	$17/2^- \rightarrow 15/2^-$	537.9	7.9(5)	0.54(9)	0.024(15)	-6.2^{+25}_{-88}	-6.3^{+33}_{-88}[d]	-6.3^{+41}_{-88}	$M1/E2$
1057	$13/2^- \rightarrow 9/2^-$	359.0	1.6(1)	0.96(17)	–	–	–	–	$(E2)$
1057	$13/2^- \rightarrow 13/2^-$	445.7	1.7(1)	0.84(18)	–	–	–	–	$\Delta I = 0, M1/E2$
1057	$13/2^- \rightarrow 15/2^-$	554.5	2.4(3)	0.68(10)	−0.079(28)	-0.08^{+10}_{-9}	-0.10^{+2}_{-11}	-0.09^{+11}_{-14}	$M1/E2$
1057	$13/2^- \rightarrow 11/2^-$	860.6	0.9(1)	–	–	–	–	–	–
1503	$23/2^- \rightarrow 19/2^-$	545.6	22.6(13)	1.02(12)	0.200(36)	–	–	–	$E2$
1504	$17/2^- \rightarrow 13/2^-$	447.4	1.5(1)	1.05(17)	–	–	–	–	$(E2)$
1504	$17/2^- \rightarrow 19/2^-$	547.1	1.5(1)	–	–	–	–	–	–
1563	$21/2^- \rightarrow 17/2^-$	522.6	6.9(5)	0.92(13)	–	–	–	–	$(E2)$
1563	$21/2^- \rightarrow 19/2^-$	605.7	7.5(5)	0.56(11)	–	–	–	–	$(M1/E2)$
1994	$21/2^- \rightarrow 17/2^-$	489.6	1.2(1)	0.96(13)	–	–	–	–	$(E2)$
1994	$21/2^- \rightarrow 23/2^-$	491.2	<0.5	–	–	–	–	–	–
2117	$27/2^- \rightarrow 23/2^-$	614.4	10.0(6)	0.95(14)	–	–	–	–	$(E2)$
2151	$25/2^- \rightarrow 21/2^-$	587.9	2.8(2)	0.95(18)	–	–	–	–	$(E2)$
2151	$25/2^- \rightarrow 23/2^-$	647.8	1.2(1)	–	–	–	–	–	–
2519	$25/2^- \rightarrow 21/2^-$	524.6	1.1(1)	0.91(25)	–	–	–	–	$(E2)$
2781	$29/2^- \rightarrow 27/2^-$	664.0	2.6(2)	0.59(10)	–	–	–	–	$(M1/E2)$
2781	$29/2^- \rightarrow 25/2^-$	630.5	<0.5	–	–	–	–	–	–
2789	$31/2^- \rightarrow 27/2^-$	671.6	2.5(2)	1.06(22)	–	–	–	–	$(E2)$
3088	$(29/2^-) \rightarrow 25/2^-$	569.0	0.7(1)	–	–	–	–	–	–
3377	$(33/2^-) \rightarrow 29/2^-$	595.7	1.6(2)	–	–	–	–	–	–
3377	$(33/2^-) \rightarrow 31/2^-$	588.0	< 0.1	–	–	–	–	–	–
3496	$(35/2^-) \rightarrow 31/2^-$	707.6	< 0.1	–	–	–	–	–	–

[a]The uncertainty in the E_γ values is 0.5 keV.
[b]mixing ratio obtained from R_{DCO} method in the present study.
[c]mixing ratio obtained from R_{DCO}-polarization method in the present study.
[d]The maximum probable negative uncertainty is mentioned for 537.9 keV.

[40]

$$R_{\rm DCO} = \frac{I_{\gamma 1} \text{ observed at } 148^\circ \text{ gated on } \gamma_2 \text{ at } 90^\circ}{I_{\gamma 2} \text{ observed at } 90^\circ \text{ gated on } \gamma_2 \text{ at } 148^\circ}, \quad (1)$$

where the I_γ denotes the intensity of the γ rays. The value of $R_{\rm DCO}$ depends on the detector geometry as well as the substate population width (σ/j) of the fusion evaporation reaction which is derived from the experimentally observed pure $E2$ and $E1$ transitions. In the present experimental setup, the $R_{\rm DCO}$ values of stretched $E1$ transitions (384.2, 466.0, 587.2 keV) from the residual nuclei (^{151}Eu and ^{198}Hg) were compared with the theoretically calculated $R_{\rm DCO}$ for different values of σ/j using the ANGCOR [41] program. The comparison between the theoretical and experimentally observed $R_{\rm DCO}$ estimates the average value of $\sigma/j \approx 0.35$. Thus, for the present geometrical setup $R_{\rm DCO} \approx 1$ for stretched quadrupole transitions and $R_{\rm DCO} \approx 0.6$ for stretched dipole transitions when the gate is on the stretched quadrupole transition, whereas the $R_{\rm DCO}$ for mixed transitions differ from these values depending on their mixing ratios (δ). The $R_{\rm DCO}$ values obtained in the present study are listed in Table I. The spin assignment of the states in signature partner band B with band head at 698-keV level energy was ambiguous in the previous study [32]. In the present work, the spin of these states was confirmed and modified on the basis of the $R_{\rm DCO}$ values of the corresponding deexciting transitions. The spin of the state with the 698-keV-level energy was changed to $9/2^-$ from $(11/2^-)$ [32] based on the $R_{\rm DCO} = 0.61(11)$ of the decaying 501.6-keV transition, interlinking band B with the $h_{11/2}$ band A. Further, the $R_{\rm DCO} = 0.68(10)$ of 554.5 keV shows the dipole nature of the transition confirming the $13/2^-$ spin state of 1057-keV-level energy. The quadrupole nature of intraband 359.0-keV transition in band B with $R_{\rm DCO} = 0.96(17)$ further supports the assignment of the $9/2^-$ and $13/2^-$ spins to 698- and 1057-keV-level energies, respectively. Moreover, the $R_{\rm DCO} = 1.05(17)$, 0.96(13), and 0.91(25) of the

TABLE II. The deduced polarization [$P(\theta)$], measured polarization asymmetries ($\triangle$), and calculated polarization sensitivity (Q) of the gamma rays produced in the experiment. The angular distribution coefficients (a_2 and a_4) were taken from Refs. [45,31] for ^{198}Hg and ^{151}Eu, respectively.

Nucleus	E_γ(keV)	a_2	a_4	$P(\theta)$	$\triangle$	Q
^{198}Hg	411.8	0.23(2)	−0.05(2)	0.36(3)	0.131(9)	0.36(3)
^{151}Eu	455.3	0.37(8)	−0.04(6)	0.66(7)	0.222(20)	0.34(7)
^{198}Hg	587.2	−0.20(3)	−0.05(3)	0.27(4)	0.080(26)	0.29(5)
^{198}Hg	636.6	0.24(2)	−0.03(2)	0.39(3)	0.094(8)	0.24(3)
^{198}Hg	767.3	0.26(3)	−0.08(4)	0.40(5)	0.079(29)	0.20(6)

intraband 447.4-, 489.6-, and 524.6-keV transitions, respectively, in band B also indicate their quadrupole nature. Apart from this, the measured $R_{\rm DCO} = 0.44(7)$, 0.54(9), 0.56(11), and 0.59(10) values of the interconnecting 415.0-, 537.9-, 605.7-, and 664.0-keV transitions respectively, between the wobbling band C and yrast band A show their mixed dipole nature.

The assignment of the parity to the states was carried out using linear polarization measurements. The clover detectors placed at 90° angle act as a Compton polarimeter and are used to deduce the polarization asymmetry of the transitions. The polarization asymmetry ($\triangle$) is measured using the following formula:

$$\triangle = \frac{a(E_\gamma)N_\perp - N_\parallel}{a(E_\gamma)N_\perp + N_\parallel}, \tag{2}$$

where $N_\perp$ ($N_\parallel$) is the number of counts of γ-ray transitions lying perpendicular (parallel) to the plane formed by the beam direction and the direction of emission of gamma ray. The 1.03(7) value of the correction factor $a(E_\gamma)$ was measured using the decay data of the ^{152}Eu radioactive source in the present experimental setup. To determine the experimental asymmetry, two asymmetric matrices were constructed with coincidence events corresponding to parallel and perpendicular segments of the clover detectors (with respect to the emission plane) along one axis and coincident events corresponding to all the detectors of the array on the other axis [40,42]. Further, the polarization asymmetry ($\triangle$) is used along with the polarization sensitivity (Q) to determine the linear polarization of the γ- rays using the following formula [42,43]:

$$P(\theta) = \frac{\triangle}{Q}. \tag{3}$$

The polarization sensitivity Q is a measure to characterize a Compton polarimeter and is calculated using pure transitions from different residual nuclei populated in the present reaction. The sensitivity parameter was determined using Eq. (3), where the polarization asymmetry of the pure quadrupole and dipole transitions was obtained from the present analysis, as presented in Table II. The linear polarization $P(\theta)$ measurement was carried out using the Klein-Nishina formula [44] in which the angular distribution coefficients a_2 and a_4 parameters were taken from Refs. [31,45] for ^{198}Hg and ^{151}Eu, respectively. Figure 4 represents the fitted curve of the Q parameter using the following relation [43]:

$$Q = Q_0(a + b \times E_\gamma), \tag{4}$$

where Q_0 represents the polarization sensitivity of an ideal Compton polarimeter and is defined as

$$Q_0 = \frac{1+\alpha}{1+\alpha+\alpha^2}, \tag{5}$$

with $\alpha = \frac{E_\gamma(\text{keV})}{511}$. The parameters a and b having the values of 0.626(125) and $-3.22(23) \times 10^{-4}$ are obtained from the least square-fitting method. A positive value of the linear polarization indicates the electric nature of the transition, while a negative value indicates the magnetic nature.

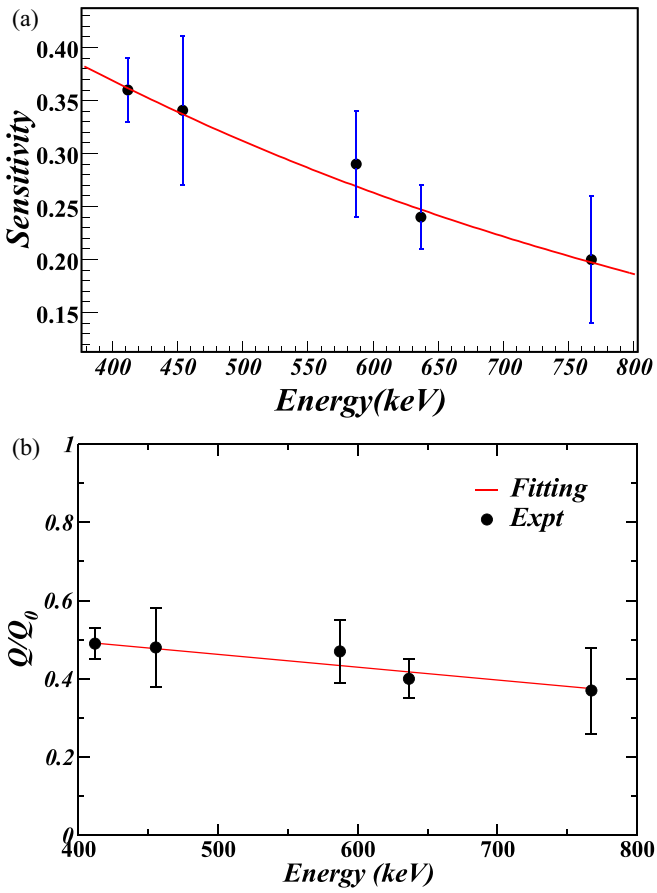


FIG. 4. (a) Polarization sensitivity of the clover detectors placed at 90° of the INGA array used in the experiment. (b) The variation of Q/Q_0 as a function of energy (in keV). The solid line represents the fitted curve of the experimental data points.

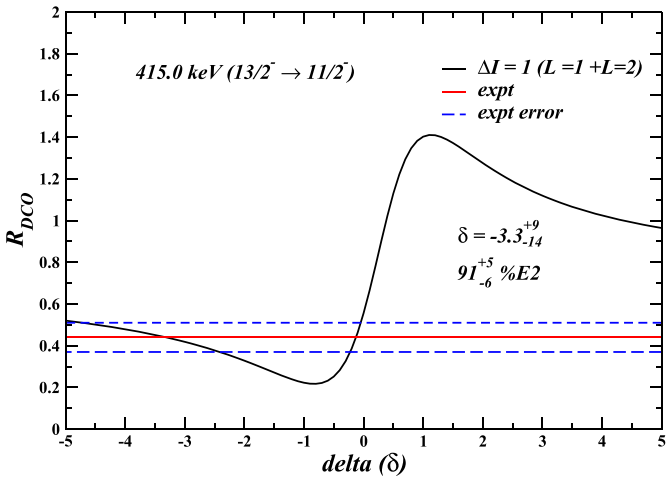


FIG. 5. The variation of $R_{\rm DCO}$ as a function of mixing ratio (δ) for 415.0-keV transition in ^{151}Eu giving two values of $\delta = -3.3^{+9}_{-14}$ and -0.12^{+8}_{-10}. The higher value of δ is mentioned in the plot as it is also supported by the polarization measurement.

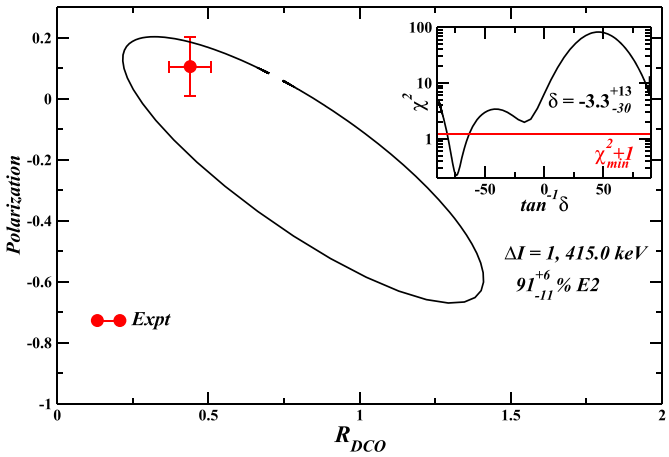


FIG. 6. The variation of $R_{\rm DCO}$ as a function of the polarization at different mixing ratio (δ) for 415.0-keV transition in ^{151}Eu in which the inset shows the minimum of the χ^2 versus $\tan^{-1}\delta$ plot giving mixing ratio $\delta = -3.3^{+13}_{-30}$.

In the present study, the tentative parity of band B has now been confirmed using polarization values. Table I shows the polarization asymmetry values of the γ-ray transitions. The negative parity was assigned to band B based on the polarization asymmetry of the new interlinking 554.5-keV transition between bands B and A. The negative value of $\triangle = -0.079(28)$ of 554.5-keV transition shows its dominant magnetic nature. While the positive values of $\triangle = 0.038(35)$ and 0.024(15) of the mixed $\Delta I = 1$ interconnecting transitions 415.0 and 537.9 keV between bands C and A indicate its dominant electric nature. The errors in linear polarization measurement have been determined from the error propagation method [42,46].

Further, the mixing ratios of the $\Delta I = 1$, $M1/E2$ interconnecting transitions have been extracted from the comparison of experimental and theoretical $R_{\rm DCO}$ values and the $R_{\rm DCO}$-polarization method. Figure 5 shows the theoretical $R_{\rm DCO}$ versus mixing ratio (δ) plot for 415.0-keV transition decaying from the $13/2^- \rightarrow 11/2^-$. The comparison of experimental $R_{\rm DCO}$ value of 415.0 keV gives two values of $\delta = -3.3^{+9}_{-14}$ and -0.12^{+8}_{-10}. The linear polarization supports the higher value of the mixing ratio. As shown in Fig. 6, the value of δ obtained from the $R_{\rm DCO}$-polarization method gives $\delta = -3.3^{+13}_{-30}$. Thus the average value of the mixing ratio for 415.0-keV transition obtained from both the methods is $\delta_{\rm av} = -3.3^{+15}_{-33}$. Notably, the experimental $\delta_{\rm av}$ value lies close to the $\delta = -5.6 \pm 26$, which is obtained from the angular distribution coefficients a_2 and a_4 taken from Ref. [31]. Similarly, the average mixing ratio $\Delta I = 1$, 537.9-keV transition, obtained using both $R_{\rm DCO}$ and the $R_{\rm DCO}$-polarization method (as shown in Figs. 7 and 8, respectively) is $\delta_{av} = -6.3^{+41}_{-88}$. The higher mixing ratio values suggest that the interlinking $\Delta I = 1$, 415.0-, and 537.9-keV transitions between bands A and C have dominant $E2$ characters. On the other hand, the $\delta_{\rm av} = -0.09^{+11}_{-14}$ of 554.5-keV transition between bands A and B (as obtained from Figs. 9 and 10) shows its dominant $M1$ character. The reduced χ^2 minimization, with three degrees of freedom, for the experimental $R_{\rm DCO}$ and polarization was determined using the formula mentioned in Ref. [47]. The uncertainty in the mixing ratio for the $R_{\rm DCO}$-polarization method was calculated by finding the range of $\tan^{-1}\delta$ for which the $\chi^2_{\rm min} + 1$ value is reached [42,48]. The values of the mixing ratio (δ) of the interconnecting transitions are tabulated in Table I.

IV. DISCUSSION

The $n_\omega = 0$ and 1 bands

As the Introduction points out, the wobbling motion in odd-A triaxial deformed nucleus occurs when the angular momentum (j) of the odd particle aligns with either of the principal axes of the triaxial core. When j of the odd quasiparticle is perpendicular (parallel) to the m axis, having the largest MoI, a transverse (longitudinal) mode of wobbling

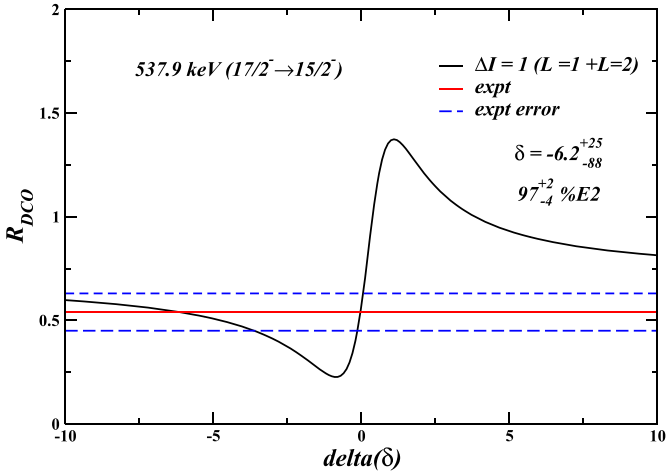


FIG. 7. The variation of $R_{\rm DCO}$ as a function of mixing ratio (δ) for 537.9-keV transition in ^{151}Eu giving two values of $\delta = -6.2^{+25}_{-88}$ and -0.04^{+9}_{-10}. The higher value of δ is mentioned in the plot as it is also supported by the polarization measurement.

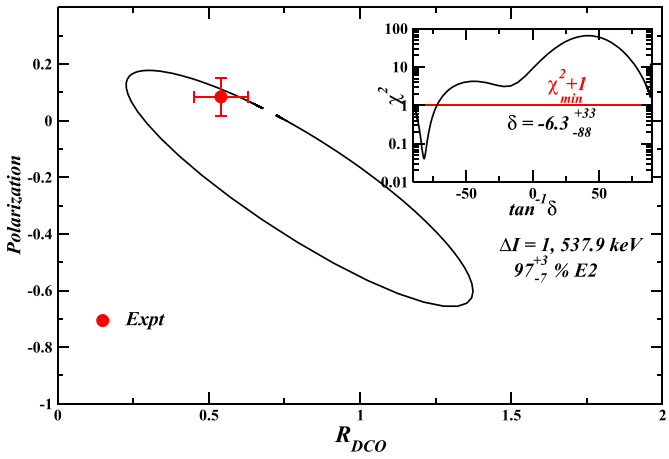


FIG. 8. The variation of R_{DCO} as a function of the polarization at different mixing ratio (δ) for 537.9-keV transition in ^{151}Eu in which the inset shows the minimum of the χ^2 versus $\tan^{-1}\delta$ plot giving mixing ratio $\delta = -6.3^{+33}_{-88}$. Here, the quoted negative uncertainty for δ is maximum probable uncertainty.

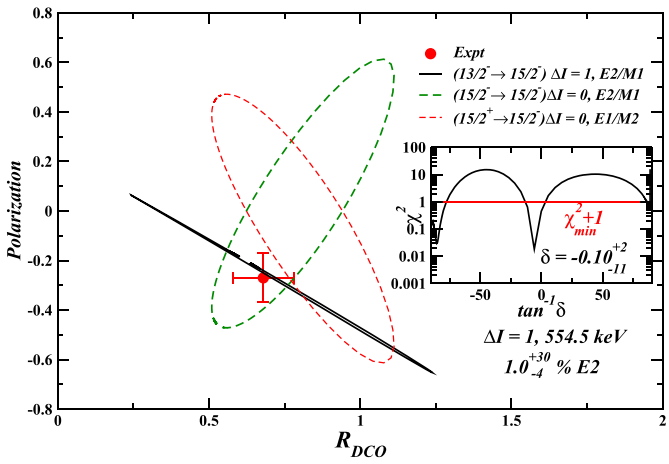


FIG. 10. The variation of R_{DCO} as a function of the polarization at different mixing ratio (δ) for 554.5-keV transition in ^{151}Eu in which the inset shows the minimum of the χ^2 versus $\tan^{-1}\delta$ plot giving mixing ratio $\delta = -0.10^{+2}_{-11}$.

motion is induced. The qualitative difference between the two modes of wobbling motion is given by the wobbling energy (E_{wobb}) defined as follows:

$$E_{\mathrm{wobb}} = E(I, n_\omega = 1) - \frac{E(I+1, n_\omega = 0) + E(I-1, n_\omega = 0)}{2}, \quad (6)$$

where n_ω is the wobbling phonon number and $E(I, n_\omega)$ is the excitation energy of the respective bands. The precession cone, defined by the rotor-, odd particle-, and total angular momenta, revolves around the m axis, which increases the wobbling energy E_{wobb} with increasing spin I in the case of the longitudinal wobbler. On the other hand, in the case of a transverse wobbler, the E_{wobb} decreases with an increase in I because of the revolution of the precession cone around the s (or l) axis, having smaller MoI relative to the m axis

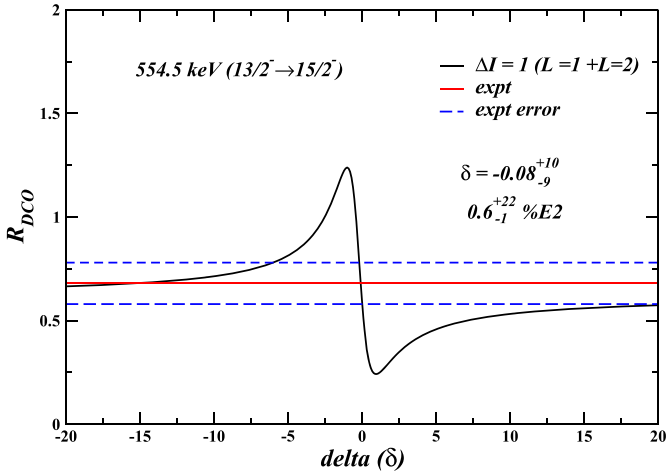


FIG. 9. The variation of R_{DCO} as a function of mixing ratio (δ) for 554.5-keV transition in ^{151}Eu giving $\delta = -0.08^{+10}_{-9}$.

[4]. Figure 11 shows the comparison of wobbling energy of ^{151}Eu nuclei with ^{135}Pr [11], ^{133}Ba [15],^{133}La [13], ^{127}Xe [14], and ^{183,187}Au [4,16] nuclei where wobbling motion was established experimentally. As shown in Fig. 11(a), the wobbling energy gradually decreases with an increase in energy for ^{135}Pr, ^{133}Ba, and ^{183}Au isotopes showing the characteristics of transverse wobbling. In the case of the ^{135}Pr nucleus, the j of the quasiproton particle in the $h_{11/2}$ and in ^{183}Au the j of the quasiproton particle in the $i_{13/2}$ orbital aligns with the s axis of the triaxial core to produce the transverse mode of wobbling excitation. The contradictory increasing pattern of the wobbling energy for the positive parity band in ^{183}Au nucleus was suggested to be the initial part of the transverse wobbling band similar to the ^{163}Lu nucleus [16]. In the ^{133}Ba nucleus, the j of the quasineutron hole in the $h_{11/2}$ orbital aligns with the l axis to maximize its overlap with the triaxial core and behaves as a transverse wobbler. Similar to these established transverse wobblers, the wobbling energy of ^{151}Eu also decreases with increasing spin, indicating the presence of transverse wobbling in this nucleus. The j of the quasiparticle seems to align with the axis of the triaxial core to minimize the energy of its attractive short-range interaction leading to the occurrence of transverse wobbling motion. While in Fig. 11(b), the increasing wobbling energy as a function of spin (I) in ^{133}La, ^{127}Xe, and ^{187}Au shows the longitudinal wobbling motion of these isotopes. The alignment of j of the quasineutron particle in the $h_{11/2}$ orbital of ^{127}Xe and the quasiproton particle in the $i_{13/2}$ orbital of ^{187}Au with the m axis of the triaxial core causes the longitudinal mode of wobbling. Further, the theoretical comparison of wobbling motion in the ^{151}Eu nucleus with these established wobblers is discussed in terms of TPSM calculations in the next section.

One of the primary characteristics of wobbling motion is the appearance of rotational $E2$ bands from the excitation of the wobbling phonons n_ω, connected by strong $\Delta I = 1$ transitions having predominantly $E2$ character. In ^{151}Eu, the two rotational bands A and C are interconnected by $\Delta I = 1$

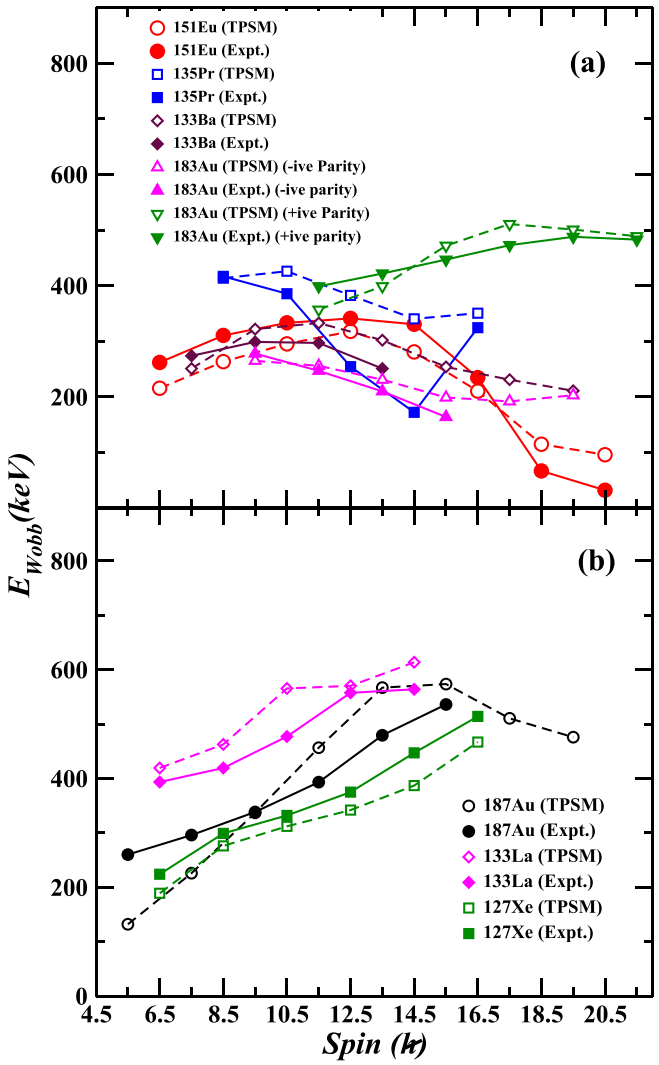


FIG. 11. Comparison of wobbling excitation energy for $n_\omega = 1$ band in ^{151}Eu with (a) transverse wobblers ^{135}Pr [11], ^{133}Ba [15], and ^{183}Au [16], and (b) longitudinal wobblers ^{187}Au [4],^{133}La [13], and ^{127}Xe [14].

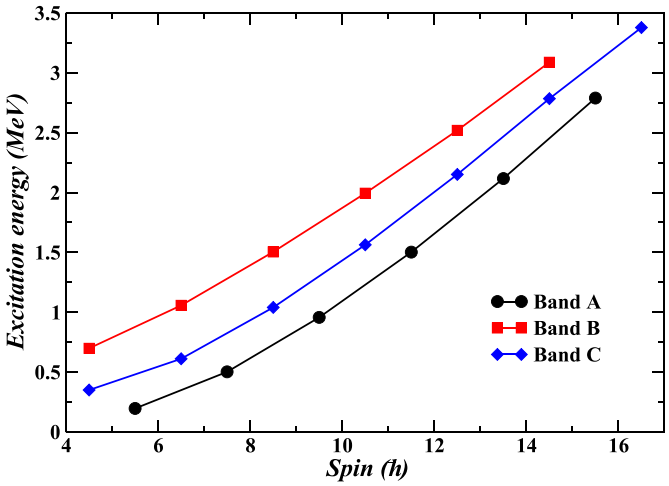


FIG. 12. The variation of excitation energy as a function of spin $I(\hbar)$ for bands A, B, and C of the ^{151}Eu isotope.

transitions. To determine the dominant $M1/E2$ character of these interlinking transitions $R_{\rm DCO}$ and linear polarization measurements have been carried out. The average mixing ratio $\delta_{\rm av} = -3.3^{+15}_{-33}$ for 415.0-keV transition, decaying from $13/2^- \rightarrow 11/2^-$, shows $91^{+7}_{-15}\%$ of its $E2$ character. Whereas, $\delta_{\rm av} = -6.3^{+41}_{-88}$ for 537.9-keV transition, decaying from $17/2^- \rightarrow 15/2^-$, shows $97^{+3}_{-15}\%$ of its $E2$ character. The comparison of calculated B(λL) ratios in ^{151}Eu with their corresponding counterparts in different triaxial nuclei showing wobbling motion is tabulated in Table III. The B($E2_{\rm out}$)/B($E2_{\rm in}$) in ^{105}Pd, ^{135}Pr, and ^{133}Ba is larger than the B($M1_{\rm out}$)/B($E2_{\rm in}$) for the $\Delta I = 1$ interconnecting transitions between the $n_\omega = 0$ and 1 bands, establishing their enhanced $E2$ character. Similarly, in the ^{151}Eu isotope, the higher values of B($E2_{\rm out}$)/B($E2_{\rm in}$) for 415.0 and 537.9 keV supports band C as the wobbling band built from the excitation of $n_\omega = 1$ on the aligned $h_{11/2}$ proton configuration yrast band A (with $n_\omega = 0$). Moreover, the increase in the % of the $E2$ character with spin is observed in ^{151}Eu similar to other wobbling nuclei as shown in Table III.

Another required characteristic to establish wobbling motion is the presence of the signature partner band of the $n_\omega = 0$ band connected by $\Delta I = 1$ transitions. It is essential to identify the signature partner band of the yrast $n_\omega = 0$ band to ensure that the band identified as the wobbler band is not misinterpreted as the signature partner band. Unlike the wobbling phonon band, the interband transitions between the zero phonon band and its signature partner should have a dominant $M1$ character. In the present study, three new interlinking transitions (554.5, 547.1, and 491.2 keV) have been placed between bands A and B in ^{151}Eu. The $\delta_{\rm av} = -0.09^{+11}_{-14}$ for 554.5-keV transition shows its dominant $M1$ character with only $0.8^{+42}_{-1}\%$ $E2$ mixing. Similar to the signature partner bands of other wobbler nuclei, the higher value of ($M1_{\rm out}$)/B($E2_{\rm in}$) for 554.5-keV transition in ^{151}Eu, supports band B as the unfavored signature partner (SP)of the $n_\omega = 0$ band A, as tabulated in Table III. Additionally, patterns of higher excitation energy and weak population in comparison to the $n_\omega = 1$ band are expected for the unfavored signature partner of the $n_\omega = 0$ bands. From the variation of excitation energy as a function of spin, shown in Fig. 12, it is noted that the excitation energy of band B is higher than that of band C, although both bands B and C are built on the $9/2^-$ state having similar spin sequence. Such observations further justify band B to be the signature partner of $n_\omega = 0$ band A.

V. TRIAXIAL PROJECTED SHELL MODEL ANALYSIS

In this section, we shall compare the experimental band structures and transition rates of ^{151}Eu with the numerical results obtained using the TPSM approach. The details of this formalism for odd-A nuclei can be found in Ref. [49], and the model was shown to be successful in describing the high spin states in ^{103,105}Rh [50], $^{125-137}$Pr, and $^{127-139}$Pm nuclei [51]. In the present case of ^{151}Eu, we have followed

TABLE III. The experimental mixing ratio (δ), $E2$ fractions, and experimentally obtained transition probability ratios $B(E2_{in})/B(E2_{out})$ and $B(M1_{in})/B(E2_{out})$, of various nuclei in comparison with the data for the ^{151}Eu nucleus.

Nucleus	E_γ(keV)	$I_i^\pi \rightarrow I_f^\pi$	δ[a]	E2%	$\frac{B(E2_{out})}{B(E2_{in})}$	$\frac{B(M1_{out})}{B(E2_{in})}(\mu_N^2/e^2b^2)$
$n_\omega = 1$ wobbling band						
^{151}Eu	415.0	$13/2^- \rightarrow 11/2^-$	-3.3^{+15}_{-33}	91^{+7}_{-15}	0.1836^{+124}_{-304}	0.0020^{+37}_{-15}
	537.9	$17/2^- \rightarrow 15/2^-$	-6.3^{+41}_{-88}[b]	97^{+3}_{-15}	0.2795^{+58}_{-420}	0.0014^{+85}_{-12}
^{105}Pd [17]	991	$17/2^- \rightarrow 15/2^-$	1.8 ± 5	76 ± 13	0.66 ± 18	$0.16\ 2\pm 97$
	1034	$21/2^- \rightarrow 19/2^-$	2.3 ± 3	84 ± 4	0.60 ± 9	0.089 ± 26
	994	$25/2^- \rightarrow 23/2^-$	2.7 ± 6	87 ± 6	0.34 ± 7	0.029 ± 16
^{135}Pr [11]	812.8	$21/2^- \rightarrow 19/2^-$	-1.54 ± 9	70.3 ± 24	0.843 ± 32	0.164 ± 14
	754.6	$25/2^- \rightarrow 23/2^-$	-2.38 ± 37	85.0 ± 40	0.500 ± 25	0.035 ± 9
^{133}Ba [15]	743.4	$17/2^- \rightarrow 15/2^-$	-2.10 ± 19	81.51 ± 273	2.94 ± 18	0.26 ± 4
	812.0	$21/2^- \rightarrow 19/2^-$	-1.95 ± 16	79.18 ± 271	2.36 ± 20	0.28 ± 4
Signature partner band						
^{151}Eu	554.5	$13/2^- \rightarrow 15/2^-$	-0.09^{+11}_{-14}	0.8^{+42}_{-1}	0.0014^{+72}_{-13}	0.0362^{+3}_{-15}
^{135}Pr [11]	593.9	$13/2^- \rightarrow 11/2^-$	-0.16 ± 4	2.5 ± 12	–	–
^{133}Ba [15]	1067.0	$13/2^- \rightarrow 11/2^-$	-0.15 ± 2	2.20 ± 57	–	–

[a]The average value of δ has been taken for the ^{151}Eu nucleus.
[b]The maximum probable negative uncertainty is mentioned for 537.9 keV.

the same approach with one proton quasiparticle state generated by solving the triaxial Nilsson potential and pairing the Hamiltonian solution obtained in the BCS approximation. The Nilsson potential with the deformation parameters ϵ and ϵ', listed in Table IV, have been used for ^{151}Eu and for other odd-A nuclei where wobbling motion has been identified. The axial deformation parameter ϵ is normally chosen from the measured quadrupole moment of the system, wherever available, otherwise the tabulated values using the phenomenological potential models are employed [4,13,16,17,52,53]. The value of ϵ' is, preferably, chosen from the minimum of the potential energy surface (PES) of the nucleus. However, for some nuclei, PES does not depict minimum, and for these nuclei the value of ϵ' that reproduces the wobbling band-head energy is adopted because it is known that this band-head energy is very sensitive to nonaxial deformation.

The intrinsic states obtained from the solution of the triaxial Nilsson potential with these deformation parameters are projected onto good angular-momentum states. For each state, about 40 to 50 intrinsic states are selected around the Fermi surface for which the angular-momentum projection is performed. These projected bands (basis states) were then employed to diagonalize the shell model Hamiltonian consisting of pairing and quadrupole-quadrupole interaction terms. The interaction strengths used in the present calculations are the same as those used in the previous studies [51]. The energies for the three bands, after the diagonalization, are shown in Fig. 13. It is quite evident from the figure that calculated values are in good agreement with the experimental data.

Using the semiclassical triaxial particle-rotor model [3,12] with irrotational-flow moment of inertia, it was shown that wobbling motion for odd systems can be categorized into longitudinal and transverse ones with angular momentum of the odd particle parallel and perpendicular to the medium axis. The main characteristic feature of longitudinal (transverse)

TABLE IV. The axial deformation parameter (ϵ), triaxial deformation parameter ϵ', and (γ) employed in the calculation for odd-A nuclei. The axial deformation ϵ is taken from Ref. [53]. The asterisk $*$ shows ϵ for positive parity in ^{183}Au nucleus.

	^{151}Eu	^{187}Au	^{135}Pr	^{133}La	^{127}Xe	^{133}Ba	^{183}Au	^{183}Au
ϵ	0.200	0.220	0.160	0.150	0.150	0.150	0.280	0.270*
ϵ'	0.110	0.100	0.110	0.110	0.100	0.100	0.110	0.100
γ^0	27	24	34	36	33	33	21	20

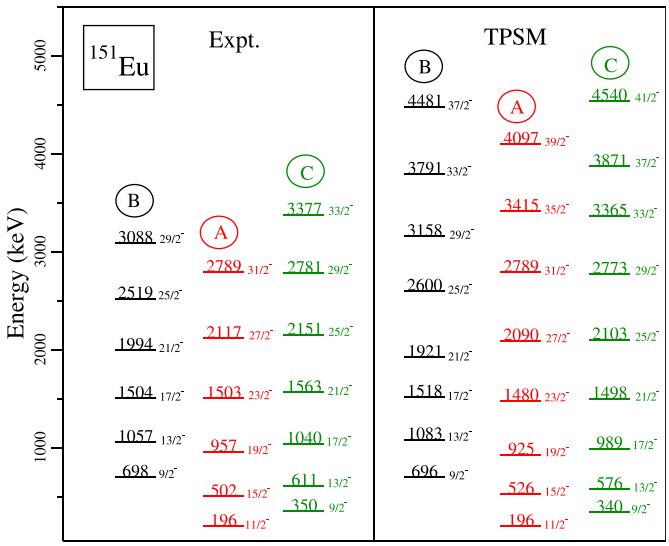


FIG. 13. Comparison of experimental levels with TPSM calculations.

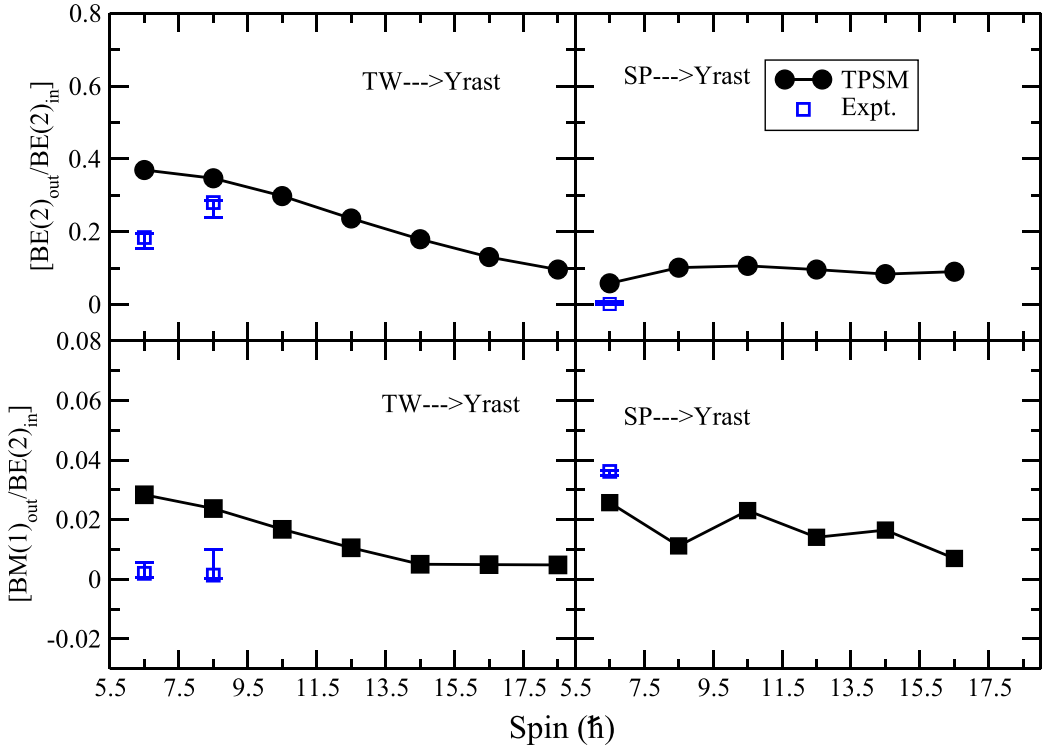


FIG. 14. $B(E2_{out})/B(E2_{in})$ and $B(M1_{out})/B(E2_{in})$ vs spin for the transverse wobbling band (TW); TW → yrast and signature partner band (SP); SP → yrast.

motion is that the wobbling frequency increases (decreases) with increasing angular momentum. In the microscopic TPSM approach, it is not possible to separate the core and the odd-particle angular momenta, and we adopt the semiclassical classification of these band structures.

The wobbling energies, E_{wobb}, defined in Eq. (6), were calculated from the level energies and are plotted in Fig. 11 as a function of spin for the $n_\omega = 1$ band. The wobbling frequency decreases with angular momentum, which suggests a transverse wobbling motion in ^{151}Eu. It is observed from this figure that the results obtained using the TPSM approach are in good agreement with the experimental wobbling frequencies. In particular, the transverse nature of wobbling observed in ^{135}Pr, ^{133}Ba, and ^{183}Au and longitudinal wobbling in ^{187}Au, ^{133}La, and ^{127}Xe is well reproduced.

We have also evaluated the transition probabilities as they are very sensitive to the nature of the collective motion. The transition probabilities in the present case have been calculated [51] using free values of g_l, while g_s was attenuated by the 0.85 factor, i.e., $g_l^\pi = 1$, $g_l^\nu = 0$, $g_s^\pi = 5.59 \times 0.85$, and $g_s^\nu = -3.83 \times 0.85$. The effective charges for the protons and the neutrons were assumed to be 1.5e and 0.5e, respectively. A comparison of the experimental and the calculated transition probabilities for ^{151}Eu is shown in Fig. 14. It is known from the semiclassical analysis that the essential feature of the wobbling bands is that $E2$ transition probability dominates for the $n_\omega = 1 \rightarrow n_\omega = 0$ connecting transitions. In Fig. 14, we present the ratios of the transition probabilities $B(E2_{out})/B(E2_{in})$ in the upper left panels and in the lower left panels $B(M1_{out})/B(E2_{in})$ for these connecting transitions. The measured as well as calculated $B(E2_{out})/B(E2_{in})$ ratios are large, indicating that the band exhibits the characteristics of wobbling motion. The results of transitions from SP → yrast are presented in the upper and lower right panels of Fig. 14 and the $B(E2_{out})/B(E2_{in})$ ratios for these transitions are much smaller than those of LW → yrast linking transitions, which supports the interpretation of this structure as a signature partner band.

VI. SUMMARY

In the present study, the excited states of the ^{151}Eu nucleus have been investigated using ^{148}Nd(^{7}Li, 4n)^{151}Eu reaction. The spin and parity of the bands are assigned using R_{DCO} and polarization measurements, respectively. Three new interconnecting transitions have been placed between the yrast band A and band B. The dominant $M1$ characteristic of the interconnecting $\Delta I = 1$, 554.5-keV transition, measured using experimental mixing ratio, along with the higher excitation energy, indicates band B to be the unfavored signature partner of the zero-phonon band A. While the dominant $E2$ behavior of the interconnecting $\Delta I = 1$ transitions between bands A and C suggests band C to be the $n_\omega = 1$ band built on the zero-phonon band A because of the first wobbling phonon excitation. Further, the decreasing wobbling excitation energy as a function of spin implies the ^{151}Eu nucleus to be the first candidate executing transverse wobbling motion in the $A \approx 150$ mass region. The experimental characteristic of the observed rotational bands was well described using the

TPSM approach. The calculated results support the transverse wobbling interpretation of bands A and C.

ACKNOWLEDGMENTS

The authors acknowledge the INGA collaboration for establishing the INGA array at IUAC, New Delhi. The authors thank the staff of the target laboratory for facilitating the preparation of the target and the Pelletron team for the smooth functioning of the accelerator at IUAC, New Delhi. A.M. and S.B. acknowledge financial support from IUAC (UFR-63314) and UGC-DAE-CSR (UGC-DAE-CSR-KC/CRS/19/NP04/0915), respectively. The authors (G.H.B., S.J., J.A.S., and N.R.) would like to acknowledge the Science and Engineering Research Board (SERB), Department of Science and Technology (Govt. of India) for providing financial assistance under Project No. CRG/2019/004960 to carry out a part of the present research work. A.K.J. acknowledges financial support from SERB Grant No. CRG/2020/000770.

[1] A. Bohr and B. R. Mottelson, *Nuclear Structure*, Vol. II (Benjamin, New York, 1975).
[2] I. Hamamoto, Phys. Rev. C **65**, 044305 (2002).
[3] S. Frauendorf and F. Donau, Phys. Rev. C **89**, 014322 (2014).
[4] N. Sensharma *et al.*, Phys. Rev. Lett. **124**, 052501 (2020).
[5] S. W. Ødegård *et al.*, Phys. Rev. Lett. **86**, 5866 (2001).
[6] P. Bringel *et al.*, Eur. Phys. J. A **24**, 167 (2005).
[7] D. R. Jensen *et al.*, Phys. Rev. Lett. **89**, 142503 (2002).
[8] G. Schönwaßer *et al.*, Phys. Lett. B **552**, 9 (2003).
[9] H. Amro *et al.*, Phys. Lett. B **553**, 197 (2003).
[10] D. J. Hartley *et al.*, Phys. Rev. C **80**, 041304(R) (2009).
[11] J. T. Matta *et al.*, Phys. Rev. Lett. **114**, 082501 (2015).
[12] N. Sensharma *et al.*, Phys. Lett. B **792**, 170 (2019).
[13] S. Biswas *et al.*, Eur. Phys. J. A **55**, 159 (2019).
[14] S. Chakraborty *et al.*, Phys. Lett. B **811**, 135854 (2020).
[15] K. Rojeeta Devi *et al.*, Phys. Lett. B **823**, 136756 (2021).
[16] S. Nandi *et al.*, Phys. Rev. Lett. **125**, 132501 (2020).
[17] J. Timar *et al.*, Phys. Rev. Lett. **122**, 062501 (2019).
[18] C. M. Petrache *et al.*, Phys. Lett. B **795**, 241 (2019).
[19] Q. B. Chen, S. Frauendorf, and C. M. Petrache, Phys. Rev. C **100**, 061301(R) (2019).
[20] F. Q. Chen and C. M. Petrache, Phys. Rev. C **103**, 064319 (2021).
[21] B. F. Lv *et al.*, Phys. Rev. C **105**, 034302 (2022).
[22] K. Tanabe and K. Sugawara-Tanabe, Phys. Rev. C **95**, 064315 (2017).
[23] E. A. Lawrie, O. Shirinda, and C. M. Petrache, Phys. Rev. C **101**, 034306 (2020).
[24] B. Qi, H. Zhang, S. Y. Wang, and Q. B. Chen, J. Phys. G: Nucl. Part. Phys. **48**, 055102 (2021).
[25] Q. B. Chen and S. Frauendorf, Eur. Phys. J. A **58**, 75 (2022).
[26] R. Budaca and C. M. Petrache, Phys. Rev. C **106**, 014313 (2022).
[27] K. Nomura and C. M. Petrache, Phys. Rev. C **105**, 024320 (2022).
[28] H. Jia, S. Y. Wang, B. Qi, C. Liu, and L. Zhu, Phys. Lett. B **833**, 137303 (2022).
[29] B. F. Lv *et al.*, Phys. Lett. B **824**, 136840 (2022).
[30] L. Hu, J. Peng, and Q. B. Chen, Phys. Rev. C **104**, 064325 (2021).
[31] J. R. Leigh *et al.*, J. Phys. G **3**, 519 (1977).
[32] J. R. Jongman *et al.*, Nucl. Phys. A **591**, 244 (1995).
[33] W. J. Vermeer *et al.*, Nucl. Phys. A **559**, 422 (1993).
[34] B. Singh, Nucl. Data Sheets **110**, 1 (2009).
[35] S. Muralithar *et al.*, Nucl. Instrum. Methods Phys. Res., Sect. A **622**, 281 (2010).
[36] R. K. Bhowmik, Ingasort Manual (private communication).
[37] D. C. Radford, Nucl. Instrum. Methods Phys. Res., Sect. A **361**, 297 (1995).
[38] D. C. Radford, Nucl. Instrum. Methods Phys. Res., Sect. A **361**, 306 (1995).
[39] R. Brun and F. Rademakers, Nucl. Instrum. Methods Phys. Res., Sect. A **389**, 81 (1997).
[40] S. Bhattacharya *et al.*, Phys. Rev. C **100**, 014315 (2019).
[41] E. S. Macias, W. D. Ruhter, D. C. Camp, and R. G. Lanier, Comput. Phys. Commun. **11**, 75 (1976).
[42] A. Mukherjee *et al.*, Phys. Rev. C **105**, 014322 (2022).
[43] P. M. Jones, Nucl. Instrum. Methods Phys. Res., Sect. A **362**, 556 (1995).
[44] O. Klein and Y. Nishina, Z. Phys. **52**, 853 (1929).
[45] C. Günther *et al.*, Phys. Rev. C **15**, 1298 (1977).
[46] G. F. Knoll, *Radiation Detection and Measurement*, 3rd ed. (Wiley, New York, 2009).
[47] J. R. Taylor, *An Introduction to Error Analysis: The Study of Uncertainties in Physical Measurements* (University Science Books Sausalito, California, 1997).
[48] S. Bhattacharya *et al.*, Phys. Rev. C **106**, 044312 (2022).
[49] G. H. Bhat, J. A. Sheikh, and R. Palit, Phys. Lett. B **707**, 250 (2012).
[50] G. H. Bhat, J. A. Sheikh, and R. Palit, Phys. Lett. B **738**, 218 (2014).
[51] S. Jehangir, G. H. Bhat, N. Rather, J. A. Sheikh, and R. Palit, Phys. Rev. C **104**, 044322 (2021).
[52] L. Hildingson, W. Klamra, T. Lindblad, C. G. Lindén, G. Sletten, and G. Sékely, Z. Phys. A **338**, 125 (1991).
[53] P. Moller, J. R. Nix, W. D. Myers, and W. J. Swiatecki, At. Data Nucl. Data Tables **59**, 185 (1995).

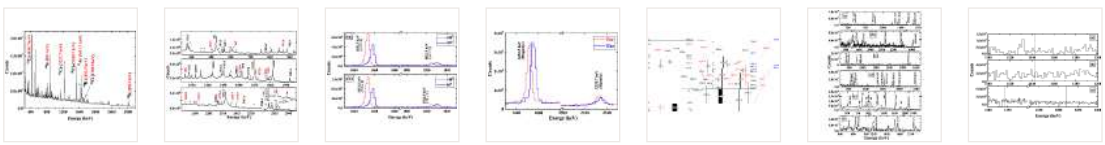
Spectroscopic study of

Rozina Rahaman, Abhijit Bisoi, Ananya Das, Y. Sapkota, Arkabrata Gupta, S. Ray, S. Sarkar, Yashraj, A. Sharma, Bharti Rohila, I. Ahmed, Kaushik Katre, S. Dutt, S. Kumar, R. P. Singh, R. Kumar, and S. Muralithar
Phys. Rev. C **109**, 024318 – Published 15 February 2024

ABSTRACT
AUTHORS
ARTICLE TEXT
INTRODUCTION
EXPERIMENTAL DETAILS AND DATA ANALYSIS
RESULT AND DISCUSSION
THEORETICAL CALCULATION
CONCLUSION
ACKNOWLEDGMENTS
REFERENCES

ABSTRACT

High spin states of populated through the (2) reaction at 68 MeV beam energy were studied using the Indian National Gamma Array (INGA) facility. Six new levels and fourteen new transitions were added to the existing level scheme. The spins and parities of most of the levels were assigned, modified, or confirmed from , , and linear polarization measurements. The multipole mixing ratios O1 for most of the transitions were measured. Large-basis shell-model calculations were performed to understand the microscopic origin of the levels. Different particle restrictions in and shell orbitals were used to explain the experimental results.



6 More

Received 31 August 2023 Revised 21 December 2023 Accepted 19 January 2024

DOI: https://doi.org/10.1103/PhysRevC.109.024318

©2024 American Physical Society

Physics Subject Headings (PhySH)

This site uses cookies. To find out more, read our Privacy Policy (https://www.aps.org/about/privacy.cfm).

Research Areas

I Agree ()

Sign up to receive regular email alerts from *Physical Review C*

Sign up (https://info.aps.org/journals-emails)

ISSN 2469-9993 (online), 2469-9985 (print). ©2024 American Physical Society. (https://www.aps.org/) All rights reserved. *Physical Review C*™ is a trademark of the American Physical Society, registered in the United States, Canada, European Union, and Japan. The *APS Physics logo* and *Physics logo* are trademarks of the American Physical Society. Information about registration may be found here (/legal). Use of the American Physical Society websites and journals implies that the user has read and agrees to our Terms and Conditions (/info/terms.html) and any applicable Subscription Agreement (https://librarians.aps.org/sitelicense.pdf).

This site uses cookies. To find out more, read our Privacy Policy (https://www.aps.org/about/privacy.cfm).

I Agree ()

Already have a manuscript?

Use our Manuscript Matcher to find the best relevant journals!

Find a Match

Refine Your Search Results

2469-9985 Search

Sort By: Title (A-Z)

Search Results

Found 1 results (Page 1) Share These Results

Exact Match Found

PHYSICAL REVIEW C

Publisher:	AMER PHYSICAL SOC , ONE PHYSICS ELLIPSE, COLLEGE PK, USA, MD, 20740-3844
ISSN / eISSN:	2469-9985 / 2469-9993
Web of Science Core Collection:	Science Citation Index Expanded
Additional *Web of Science* Indexes:	Current Contents Electronics & Telecommunications Collection | Current Contents Physical, Chemical & Earth Sciences | Essential Science Indicators

Share This Journal View profile page

** Requires free login.*

Filters Clear All

Web of Science Coverage

Open Access

Category

Country / Region

Language

Frequency

Journal Citation Reports

10

Editorial Disclaimer: As an independent organization, Clarivate does not become involved in and is not responsible for the editorial management of any journal or the business practices of any publisher. Publishers are accountable for their journal performance and compliance with ethical publishing standards. The views and opinions expressed in any journal are those of the author(s) and do not necessarily reflect the views or opinions of Clarivate. Clarivate remains neutral in relation to territorial disputes, and allows journals, publishers, institutes and authors to specify their address and affiliation details including territory.

Criteria for selection of newly submitted titles and re-evaluation of existing titles in the Web of Science are determined by the Web of Science Editors in their sole discretion. If a publisher's editorial policy or business practices negatively impact the quality of a journal, or its role in the surrounding literature of the subject, the Web of Science Editors may decline to include the journal in any Clarivate product or service. The Web of Science Editors, in their sole discretion, may remove titles from coverage at any point if the titles fail to maintain our standard of quality, do not comply with ethical standards, or otherwise do not meet the criteria determined by the Web of Science Editors. If a journal is deselected or removed from coverage, the journal will cease to be indexed in the Web of Science from a date determined by the Web of Science Editors in their sole discretion – articles published after that date will not be indexed. The Web of Science Editors' decision on all matters relating to journal coverage will be final.

Clarivate.™ Accelerating innovation.

© 2024 Clarivate Legal center Privacy notice Cookie policy
Manage cookie preferences Copyright notice Help

5

High-spin spectroscopy in ^{207}At: Evidence of a $29/2^+$ isomeric state

Khamosh Yadav,[1] A. Y. Deo,[1,*] Madhu,[1] Dhananjaya Sahoo,[1] P. C. Srivastava,[1] Saket Suman,[2] S. K. Tandel,[2] A. Sharma,[3] I. Ahmed,[4] K. Katre,[4] K. Rojeeta Devi,[4] Sunil Dutt,[4] Sushil Kumar,[4] Yashraj,[4] S. Muralithar,[4] and R. P. Singh[4]

[1]*Department of Physics, Indian Institute of Technology Roorkee, Roorkee 247667, India*

[2]*School of Physical Sciences, UM-DAE Centre for Excellence in Basic Sciences, University of Mumbai, Mumbai 400098, India*

[3]*Department of Physics, Himachal Pradesh University, Shimla 171005, India*

[4]*Inter-University Accelerator Centre, Aruna Asaf Ali Marg, New Delhi 110067, India*

(Received 17 October 2022; revised 24 March 2023; accepted 25 April 2023; published 9 May 2023)

Yrast and near-yrast states above the known $25/2^+$ isomer in ^{207}At are established for the first time. The level scheme is extended up to $47/2\hbar$ and 6.5 MeV with the addition of about 60 new γ-ray transitions. The half-life of the $25/2^+$ isomer is revisited and a value of $T_{1/2} = 107.5(9)$ ns is deduced. Evidence of a hitherto unobserved $29/2^+$ isomer in ^{207}At is presented. A systematic study of $B(E3)$ values for the transitions deexciting the $29/2^+$ isomer in the neighboring odd-A At isotopes suggests a half-life in the 2–4.5 μs range for this state in ^{207}At. The experimental results are compared with large-scale shell-model calculations performed using the KHM3Y effective interaction in the $Z = 50$–126, $N = 82$–184 model space and an overall good agreement is noted between the theory and the experiment. A qualitative comparison of the excited states and the isomers with analogous states in neighboring nuclei provides further insight into the structure of ^{207}At.

DOI: 10.1103/PhysRevC.107.054303

I. INTRODUCTION

Neutron-deficient nuclei in the region around the doubly magic ^{208}Pb nucleus reveal a large variety of structural properties and phenomena such as shape coexistence, shears bands, superdeformed bands, and various kinds of low- and high-spin isomers [1–4]. Nuclei in the vicinity of both the proton and neutron shell closures exhibit spherical or near-spherical shapes arising due to intrinsic degrees of freedom (i.e., particle-hole excitations) [5]. However, the onset of collective excitations is evident in nuclei with several valence particles or holes outside the shell closures. In this respect, Po and At isotopes offer a suitable ground for understanding the shape evolution. The level structures in the Po isotopes near the neutron shell closure ($N = 126$) have been interpreted in terms of intrinsic degrees of freedom using the shell-model approach, while the collective modes of excitation have been observed in the lighter Po isotopes [6,7]. The Po isotopes with $N \approx 112$, viz. $^{192–195}$Po [4], exhibit oblate-deformed structures, and subsequently evolve into prolate deformation as the $N = 104$ neutron midshell is approached [8]. Experimentally, the shape evolution, as one moves from the spherical to the deformed regime, is manifested in the enhancement of the $E2$ transition strengths and the energy systematics of the first excited 2^+ and 4^+ states [6,7]. A recent study on the low-lying level structures in ^{204}Po and ^{206}Po [7] isotopes reports that the transition from single-particle to collective-excitation modes with decreasing neutron number occurs below ^{206}Po. With one extra proton, the level structures in odd-A At isotopes can be interpreted in terms of an unpaired proton coupled to the even-even core of the corresponding Po isotone. Hence, the odd-A At nuclei are expected to inherit structural properties and phenomena from the corresponding Po core, which is indeed reflected in the earlier studies [9–22].

Several high-spin isomers have been reported in nuclei with $Z > 82$ and $N \leqslant 126$, which further motivates nuclear structure studies in the above near-spherical regime. The study of nuclear isomers is pivotal as it provides key inputs for understanding the structure of nuclei and to test the predictions of the shell model [23]. Among the neutron-deficient even-A Po isotopes, isomeric 8^+, 9^-, and 11^- states have been observed in $^{200–208}$Po [24–32]. The hindrance in the decay of the 8^+ state has been understood in terms of small energy difference between the 6^+ and 8^+ states of the $\pi(h^2_{9/2})$ multiplet, while the metastable nature of the 9^- and 11^- states is attributed to a change in the single-particle configuration of the isomeric state and the one to which it decays [24–32]. Similarly, several high-spin isomers have also been reported in At isotopes. An isomeric $13/2^+$ level, which originates from the $\pi(i_{13/2})$ configuration, has been observed in $^{197–203}$At isotopes [11,13,14]. In ^{197,199}At nuclei [10,11], the isomeric $13/2^+$ state is suggested to have oblate deformation and is populated by a strongly coupled rotational band, while it is known to have weak oblate deformation in ^{201}At [13]. Also, $25/2^+$ isomeric states with $T_{1/2}$ in the range of ≈14–108 ns were reported in ^{203,205,207}At [14–17]. Furthermore, an isomeric $29/2^+$ state has been observed in odd-A At isotopes with $199 \leqslant A \leqslant 211$ [13–16,18–20], except in ^{207}At [17]. The systematic presence of the $29/2^+$ isomeric level in odd-A At isotopes is one of the motivations for the detailed high-spin

*Corresponding author: ajay.deo@ph.iitr.ac.in

 ©2023 American Physical Society

study along with a search for the $29/2^+$ isomer in ^{207}At. A comprehensive spectroscopic study in ^{207}At ($Z = 85$, $N = 122$) is also needed for understanding the shape evolution along the isotopic chain in neutron-deficient odd-A At nuclei and the effect of the proton-particle and neutron-hole excitations.

In the previous high-spin study of ^{207}At [17], excited states were investigated using the ^{204}Pb(^{6}Li, $3n$)^{207}At reaction. The level scheme up to $25/2\hbar$ with 2117-keV excitation energy was established. A total of ten excited states were reported in the study by Sjoreen *et al.* [17], out of which eight levels were established with firm spin-parity. It is interesting to note that the isomeric $25/2^+$ level at 2117 keV is the only positive-parity state known in the level scheme of ^{207}At [17]. On the other hand, the level schemes of the neighboring odd-A At isotopes are known to have considerable spectroscopic information and present well-established positive- and negative-parity sequences [12–14,16]. In this paper, we propose an extended level scheme of ^{207}At with the addition of about 60 new γ-ray transitions. The excited states above the $25/2^+$ isomer are reported for the first time. We also present the first evidence of $29/2^+$ isomeric state in ^{207}At, which is known in all neighboring odd-A At isotopes [13–16,18–20].

II. EXPERIMENTAL DETAILS AND DATA ANALYSIS

High-spin states in the ^{207}At nucleus were investigated using the ^{198}Pt(^{14}N, $5n$)^{207}At heavy-ion fusion-evaporation reaction. A self-supporting ^{198}Pt target of thickness $\approx$10 mg/cm^2 and about 92% enrichment was bombarded with a DC beam of ^{14}N ions. The beam with 80-, 85-, and 87-MeV energies was delivered by the 15-UD Pelletron accelerator at Inter-University Accelerator Centre (IUAC), New Delhi. In addition to the nucleus of interest, i.e., ^{207}At, the data also had contributions from other reaction channels, viz. ^{205,206,208}At, and their β-decay products. It was also observed that the data had some degree of contamination from the Coulomb excitations of the target material and the reaction of the beam halo with the iron target frame. The γ-multiplicity trigger was set to collect the two- and higher-fold coincidence data, which was used to deduce the level scheme of ^{207}At. In addition, single-fold data were also acquired to determine the intensity of the γ-ray transitions, whenever possible. The Indian National Gamma Array (INGA) [33] was utilized to record the data, which consisted of 13 Compton-suppressed clover HPGe detectors and a low-energy photon spectrometer (LEPS) at the time of the experiment. The detectors were located at five different angles, 32°, 57°, 90°, 123°, and 148° with respect to the beam direction. The data were acquired using a VME-based data-acquisition system [34] and written to a disk in the ROOT [35] tree format. The standard ^{152}Eu and ^{133}Ba sources were used to obtain the energy calibration and relative γ-ray efficiencies of the clover Ge detectors. The data collected at the three beam energies were combined to generate various two- and three-dimensional histograms, which aid in establishing the coincidence relationships, ordering of the levels, lifetimes of the isomeric states, and the multipolarity of the γ-ray transitions. The software packages ROOT [35] and RADWARE [36] were used to analyze these histograms.

The electronic time of each γ ray was obtained from the TDC signal from the corresponding clover detector. The coincidence windows used to construct the histograms were defined by the time difference between the corresponding γ rays. To construct symmetric two- and three-dimensional histograms, the γ rays detected within 100 ns of each other were utilized. The coincidences occurring within 100–200 ns of each other were subtracted from the above histograms to account for random events. The resulting prompt histograms were utilized to establish coincidence relationships among the observed γ-ray transitions. Furthermore, an asymmetric γ-γ matrix, termed as an *early-delayed* matrix, was also constructed using the γ rays detected within 100–275 ns of each other. The *early* and *delayed* transitions for the above matrix are classified based on their relative electronic times. This matrix was utilized to investigate the isomers and the correlations between the transitions across the isomeric states. It may be noted that the useful range of the TDC was 0–275 ns.

The multipolarity of the γ-ray transitions were assigned on the basis of the directional angular correlation from the oriented states (DCO) ratio measurements [37] or intensity balance considerations. The experimental DCO ratio ($R_{\rm DCO}$) for a transition of interest was defined as the ratio of its intensities in the coincidence spectra from the detectors at 148°/32° to that at 90° with respect to the beam direction. For the present detection setup, the $R_{\rm DCO}$ value was found to be close to 1.0 (0.5) for a stretched quadrupole (dipole) transition with a gate on a stretched quadrupole transition, and a value of $R_{\rm DCO} \approx 2.0$ (1.0) was observed for a stretched quadrupole (dipole) transition in a dipole gate. More details on the procedure of the DCO ratio measurements can be found elsewhere [38,39]. The parity of the excited levels was assigned on the basis of the electric or magnetic nature of the feeding and/or depopulating γ-ray transitions. The electromagnetic nature of the γ-ray transitions, whenever possible, was confirmed from the polarization asymmetry ($\Delta_{\rm asym}$) measurements [40]. For this purpose, two asymmetric γ-γ matrices were generated with one axis comprising the energies of the γ rays scattered in the perpendicular or parallel crystals of the 90° detectors with respect to the reaction plane and the other axis corresponding to the γ-ray energies detected in the remaining detectors. Furthermore, the $\Delta_{\rm asym}$ was defined as

$$\Delta_{\rm asym} = \frac{a(E_\gamma)N_\perp - N_\parallel}{a(E_\gamma)N_\perp + N_\parallel}, \tag{1}$$

where $N_\perp$ ($N_\parallel$) are the counts recorded in the perpendicular (parallel) segments of the 90° detectors, where $a(E_\gamma)$ is a geometrical asymmetry factor which is defined as the ratio of $N_\parallel$ to $N_\perp$ for the γ rays from an unpolarized radioactive source. The experimental values of $a(E_\gamma)$ obtained using a ^{152}Eu source were plotted as a function of γ-ray energies and fit with the function $a(E_\gamma) = a_0 + a_1 E_\gamma$. The coefficients a_0 and a_1 were found to be 1.029(3) and $-7.96(363) \times 10^{-6}$, respectively. The positive and negative values of the $\Delta_{\rm asym}$ signify electric and magnetic nature of the γ-ray transitions of interest, respectively.

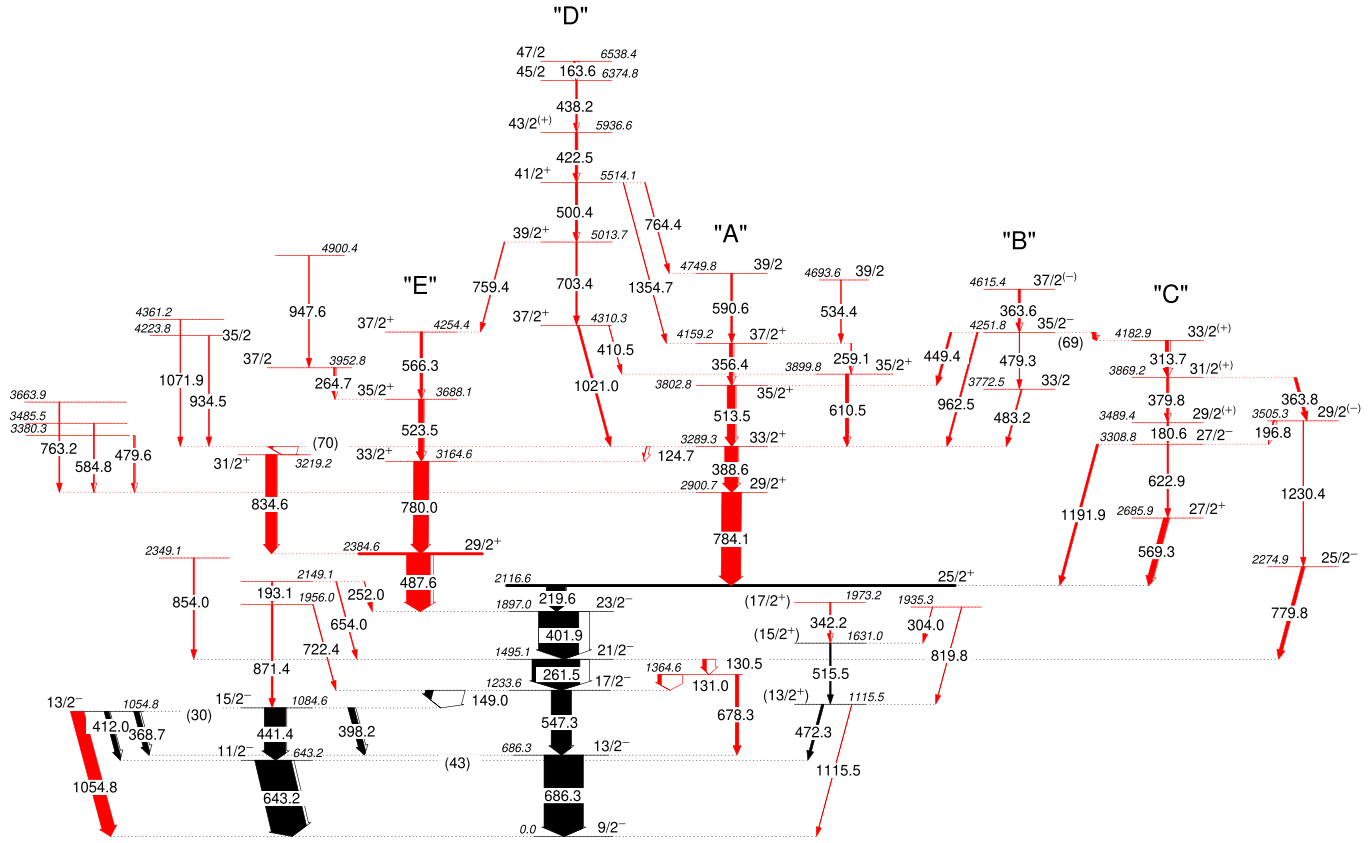


FIG. 1. The level scheme of ^{207}At established in the present work. The γ-ray transitions and levels are labeled with their energies in keV. The widths of the filled and open areas of the arrows correspond to the intensity of the γ rays and conversion electrons, respectively. The newly identified γ rays and levels are presented in red color. The transitions shown in parentheses are not observed in the present experiment, but their presence is inferred from the coincidence relationships.

III. RESULTS

Excited states in ^{207}At were studied earlier through ^{204}Pb(^{6}Li, $3n$)^{207}At heavy-ion fusion evaporation reaction [17]. This work had established a total of ten excited levels in ^{207}At including a $25/2^+$ isomer with $T_{1/2} = 108(2)$ ns at 2117 keV [17]. An extended level scheme of ^{207}At deduced from the present study is shown in Fig. 1. The level scheme below the $25/2^+$ isomer [17] is revisited and found to be consistent to the present data. Figure 2(a) illustrates the γ-ray transitions in coincidence with the 220-keV γ ray which deexcites the $25/2^+$ isomer. In addition to the known transitions, several new transitions were observed in the above coincidence spectrum. Figure 2(b) presents γ-ray transitions which precede the 220-keV γ ray within a 100-275 ns time window. The relative enhancement in the intensity of the 314-, 389-, 514-, 569-, 784-, and 1192-keV γ rays in Fig. 2(b) compared to those in Fig. 2(a) confirms the isomeric nature of the $25/2^+$ state. In addition to the above transitions, many new transitions were also observed in the *delayed* gate of the 220-keV γ ray as evident from the Fig. 2(b). It was further observed that these new transitions were also present in all the *early* coincidence spectra obtained with gates on the previously known transitions following the decay of the $25/2^+$ isomer, which unambiguously confirms their assignment to ^{207}At. The coincidence relationships of the new transitions feeding the 2117-keV isomeric level and their placement in the level scheme are discussed in Sec. III A in detail.

The half-life of the known $25/2^+$ isomer at 2117 keV was also revisited using the decay-curve analysis method as shown in Fig. 3. This method is suitable to determine lifetimes significantly greater than the full width at half-maximum (FWHM) of a prompt time distribution [41]. For the present detector system, the FWHM was found to be around 50 ns for the feeding and decaying γ-ray energies of around 500 keV. The deduced half-life, $T_{1/2} = 107.5(9)$ ns, was found to be in good agreement with the value reported earlier [17].

Several new transitions were also identified below the $25/2^+$ isomer. For example, a 1055-keV transition was found to be in coincidence with the 220-keV γ ray as shown in Fig. 2(a). It was also observed to be in coincidence with all the earlier known transitions above the 1085-keV level. Sjoreen *et al.* [17] had established a $13/2^-$ level at 1055 keV. Also, the presence of an unobserved γ ray of 30 keV between the $15/2^-$ and $13/2^-$ levels at 1085- and 1055-keV, respectively, was inferred on the basis of γ-γ coincidence relationships. The present study also supports these observations and suggests a new direct decay path to the ground state via the 1055-keV γ ray.

Furthermore, a sequence of 472-, 516-, and 342-keV γ-ray transitions was established above the $11/2^-$ level at 643 keV. It may be noticed that Sjoreen *et al.* [17] had suggested a

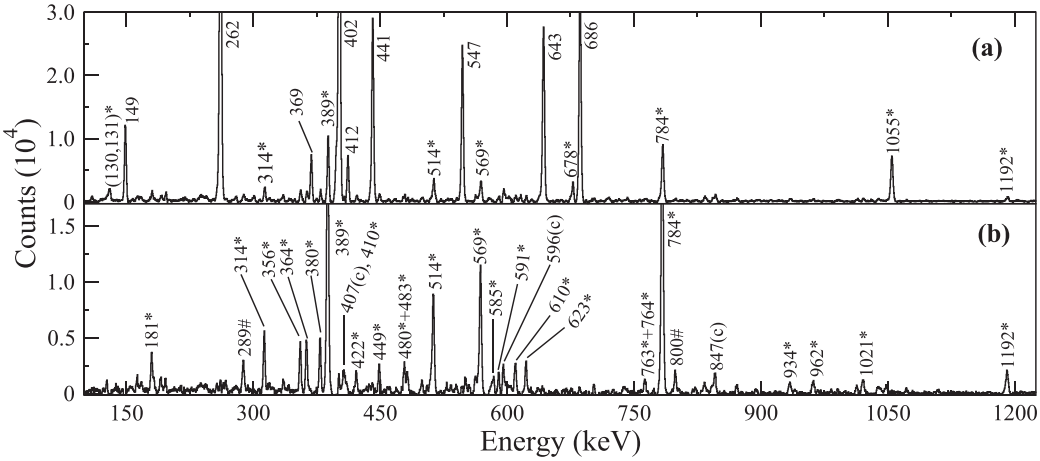


FIG. 2. The γ-ray spectra illustrating the transitions detected within (a) $\pm$100 ns prompt, and (b) 100–275 ns *early* coincidence windows of the 220-keV γ ray. The new γ rays from ^{207}At, which are firmly placed in the level scheme, are marked with an asterisk. The γ-ray transitions marked with the symbol "#" also belong to ^{207}At. However, their position in the level scheme could not be ascertained. The transitions labeled with symbol (c) are contaminant lines.

tentative 340-keV γ ray as opposed to the 342-keV one seen in this work. The γ-ray spectra presented in Fig. 4 clearly establish the coincidence relationships of the new 342-keV transition with the known 643-, 472-, and 516-keV γ rays. These spectra also confirm the placement of the new 304- and 820-keV γ-ray transitions as shown in Fig. 1. Also, a new 1116-keV γ-ray was found in coincidence with the 516- and 342-keV γ rays, but not with the 472-keV transition as illustrated in Fig. 5. The 1116-keV γ ray deexcites the associated level directly to the ground state. The spin assignment of $I = (13/2)$ and $(15/2)$ to the 1116-, and 1631-keV levels, respectively, is adopted from Ref. [17]. A spin assignment of $I = (17/2)$ to the 1973-keV level as well as positive parity for the states under consideration are proposed on the basis of similarities in their decay paths with those in the lighter odd-A At isotopes and will be discussed in detail in Sec. IV A.

The remaining level scheme below the $25/2^+$ isomer was investigated using similar γ-γ coincidence relationships, relative intensity considerations and the energy-sum technique. The procedure of the relative intensity measurements is discussed later in this section. The energy of the γ-ray transitions below the $25/2^+$ isomer and their relative γ-ray intensities are listed in Table I. The spin-parity assignments of the levels below the $25/2^+$ isomer, except for the 1115.5-, 1631.0-, and 1973.2-keV levels, are adopted from Ref. [17].

A. Level structure above the $25/2^+$ isomer

As mentioned earlier, excited states in ^{207}At were studied previously by Sjoreen *et al.* up to $25/2^+$ isomer [17]. However, no excited states were known above this isomeric

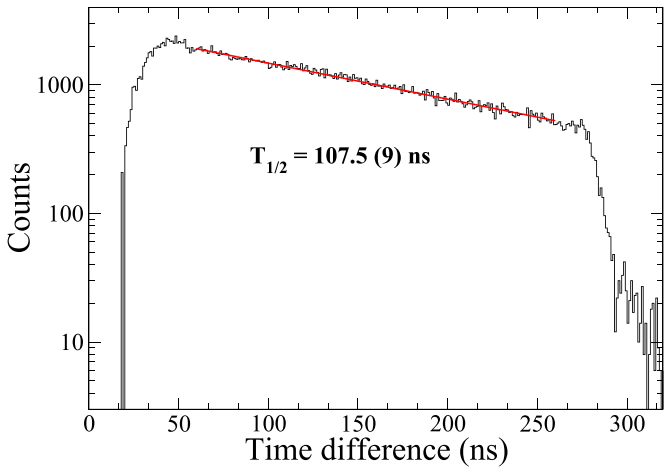


FIG. 3. Time-distribution curve (in black) to determine half-life of the $25/2^+$ state. The curve is obtained by subtracting the electronic timing of the 784-keV transition from that of the 220-keV transition. The contributions of the prompt time-distribution and background are removed from the curve. The solid line (in red) corresponds to an exponential fit to the time-distribution curve.

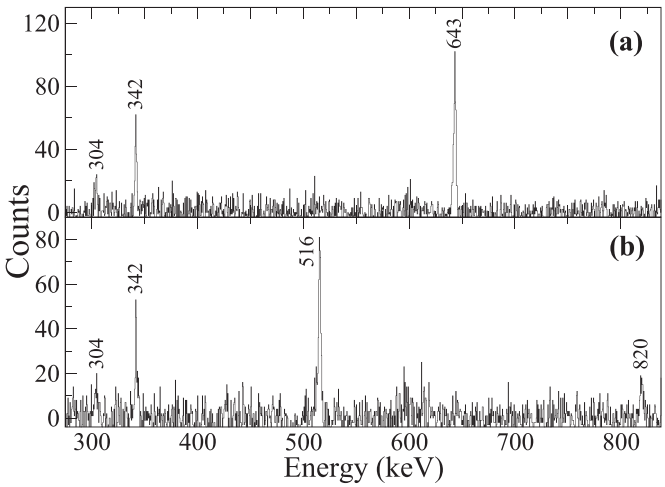


FIG. 4. The coincidence spectra with double gates on the (a) 472-, 516-keV, and (b) 472-, 643-keV transitions to illustrate evidence of the new 304-, 342-, and 820-keV γ rays.

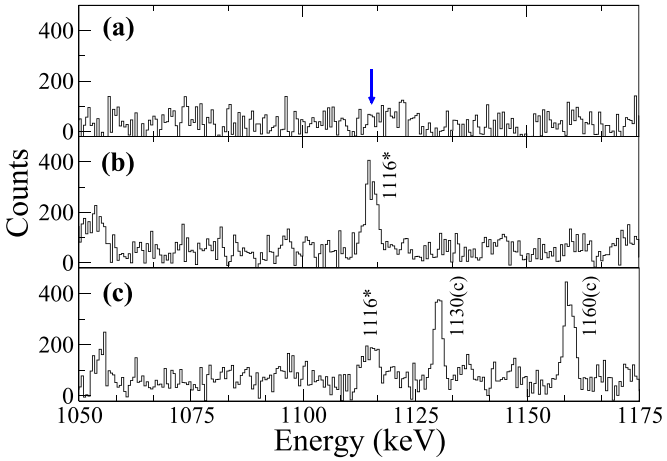


FIG. 5. The γ-ray coincidence spectra in a gate on the (a) 472-, (b) 516-, and (c) 342-keV γ-ray transitions illustrating the absence or presence of the 1116-keV γ ray in coincidence with the gating transitions. The transitions labeled with (c) in the last panel are contaminants from ^{63}Cu and ^{67}Ga produced through reactions of the beam with the Fe target frame.

level. The present study extends the level scheme beyond the $25/2^+$ isomer up to $47/2\hbar$ and $E_x \approx 6.5$ MeV. As illustrated in Fig. 2(b), many new transitions were identified which precede the 220-keV γ ray. Four new sequences consisting of about 30 new γ-ray transitions were established, which feed the known $25/2^+$ isomeric state.

The *early* γ-ray spectra obtained with gates on the γ rays following the decay of the $25/2^+$ isomer indicate that the 784- and 389-keV transitions are the strongest transitions above the isomer. These transitions were also found to be in mutual coincidence [see Fig. 6(a)], which justifies their placement above the 2117-keV isomeric level as shown in Fig. 1. A cascade of new transitions viz. 514, 356, and 591 keV, was found to be in coincidence with the above transitions. These transitions were placed above the 3289-keV level in sequence "A" in the descending order of their relative intensities as shown in Fig. 1. Another cascade of 1021-, 703-, 500-, 422-, 438-, and 164-keV transitions, labeled as sequence "D" in Fig. 1, was also identified to be in coincidence with the 784- and 389-keV γ rays. The prompt coincidence spectra illustrated in Fig. 6 support the coincidence relationships of these transitions. Furthermore, the new 483-, 479-, 449-, 962-, and 364-keV transitions were also observed in coincidence with the 389- and 784-keV γ rays. These transitions were placed in sequence "B" as shown in Fig. 1 by using their relative intensities and coincidence relationships.

The coincidence relationships and placements of the new 780-, 759-, 566-, and 524-keV transitions observed in Fig. 6(c) are discussed in the next section.

Several other new transitions, viz., 569, 1192, 623, 181, 380, and 314 keV, were also observed in *early* coincidence with the 220-keV transition [see Fig. 2(b)] as well as with the other transitions following the decay of the $25/2^+$ isomer. These transitions were not observed in coincidence with the transitions in sequences "A", "B", and "D", except the 364-keV one (see Fig. 6). Two illustrative prompt spectra with gates on the 1192- and 623-keV transitions are presented in Fig. 7. The observed new transitions were placed in sequence "C", which directly feeds the $25/2^+$ isomer.

Furthermore, some transitions were identified in the present work which bypass the $25/2^+$ isomer. Two transitions, viz. the 780- and 1230-keV ones, were observed in mutual coincidence and placed above the $21/2^-$ level at 1495 keV on the basis of their relative intensities and coincidence relationships. In addition, the presence of new 197- and 364-keV transitions and their placement in the level scheme connect the sequence "C" with the one of the bypassing transitions. Also, it was noticed that the 364-keV γ ray is a doublet and both the components are in coincidence with each other. The above coincidence relationship and coincidence of the 364-keV γ ray with all the transitions in sequence "C" suggest the

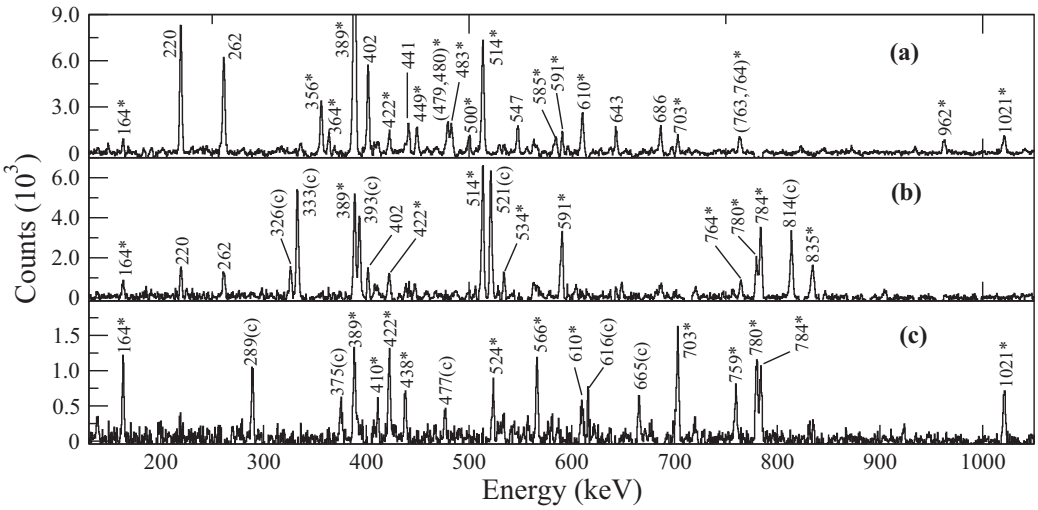


FIG. 6. The γ-ray spectra illustrating the transitions in coincidence with the (a) 784-, (b) 356-, and (c) 500-keV γ rays. The transitions marked with an asterisk are the new γ rays assigned to ^{207}At, while those marked with a symbol (c) are contaminants mainly from ^{196}Pt, ^{206,207}Po, and ^{206}At.

TABLE I. Table of γ-ray energies E_γ, corresponding level energies E_i, relative γ-ray intensity I_γ, and spin-parity of the initial (I_i^π) and final (I_f^π) levels below the $25/2^+$ isomer in ^{207}At. The relative intensities are quoted in percent by normalizing their values with respect to the intensity of the 643-keV transition, which is assumed to be 100. The listed spin-parities are adopted from Ref. [17], except for the 1115.5-, 1631.0-, and 1973.2-keV levels. See the text for their spin-parity assignments. The uncertainties in the γ-ray energies and relative intensities have contributions from both statistical and systematic factors. The systematic uncertainty in I_γ is considered to be 5% of the relative γ-ray intensity.

E_γ (keV)	E_i (keV)	I_γ	I_i^π	I_f^π
(30)[a]	1084.6(2)		$15/2^-$	$13/2^-$
(43)[a]	686.3(1)		$13/2^-$	$11/2^-$
130.5(3)	1495.1(2)	4.3(2)[b]	$21/2^-$	
131.0(5)	1364.6(5)			$17/2^-$
149.0(1)	1233.6(1)	21.3(12)	$17/2^-$	$15/2^-$
219.6(1)	2116.6(1)	53.8(31)	$25/2^+$	$23/2^-$
261.5(1)	1495.1(2)	134.7(77)	$21/2^-$	$17/2^-$
304.0(4)	1935.3(5)	<1		$(15/2^+)$
342.2(3)	1973.2(3)	2.8(2)	$(17/2^+)$	$(15/2^+)$
368.7(2)	1054.8(4)	14.3(8)	$13/2^-$	$13/2^-$
398.2(2)	1084.6(2)	16.9(10)	$15/2^-$	$13/2^-$
401.9(1)	1897.0(1)	113.4(65)	$23/2^-$	$21/2^-$
412.0(2)	1054.8(4)	13.0(7)	$13/2^-$	$11/2^-$
441.4(1)	1084.6(2)	60.5(34)	$15/2^-$	$11/2^-$
472.3(2)	1115.5(4)	6.7(4)	$(13/2^+)$	$11/2^-$
515.5(3)	1631.0(3)	3.7(2)	$(15/2^+)$	$(13/2^+)$
547.3(1)	1233.6(1)	56.1(32)	$17/2^-$	$13/2^-$
643.2(1)	643.2(1)	100.0(52)	$11/2^-$	$9/2^-$
678.3(2)	1364.6(5)	9.7(6)		$13/2^-$
686.3(1)	686.3(1)	109.6(57)	$13/2^-$	$9/2^-$
722.4(3)	1956.0(4)	1.7(1)		$17/2^-$
819.8(3)	1935.3(5)	1.2(1)		$(13/2^+)$
871.4(2)	1956.0(4)	5.2(3)		$15/2^-$
1054.8(1)	1054.8(4)	36.2(19)	$13/2^-$	$9/2^-$
1115.5(4)	1115.5(4)	<1	$(13/2^+)$	$9/2^-$

[a]Unobserved γ ray, but its presence is inferred from the coincidence relationships.
[b]Summed relative γ-ray intensity of the 130.5- and 131-keV γ rays.

presence of an unobserved 69-keV transition between the 4252- and 4183-keV levels. However, a possibility of the presence of an another 364-keV transition which may directly feed the 4183-keV level cannot be discarded.

The spin-parity of the new levels above the $25/2^+$ isomer were assigned on the basis of measured $R_{\rm DCO}$ and $\Delta_{\rm asym}$ values for the corresponding feeding and/or depopulating γ-ray transitions. As mentioned in Sec. II, the $R_{\rm DCO}$ value was found to be $\approx$1.0 when the gating transition and the γ ray of interest have the same multipolarity, while $R_{\rm DCO}$ was obtained to be $\approx$2.0 (0.5) for a stretched quadrupole (dipole) transition with a gate on a pure dipole (stretched quadrupole) one. These values were estimated from a few γ rays of known multipolarity from other nuclei populated in the same reaction. In ^{207}At, the states above the $25/2^+$ isomer are established for the first time in the present study. However, the isomeric nature of the $25/2^+$ state [$T_{1/2} = 107.5(9)$ ns] prevents the use of

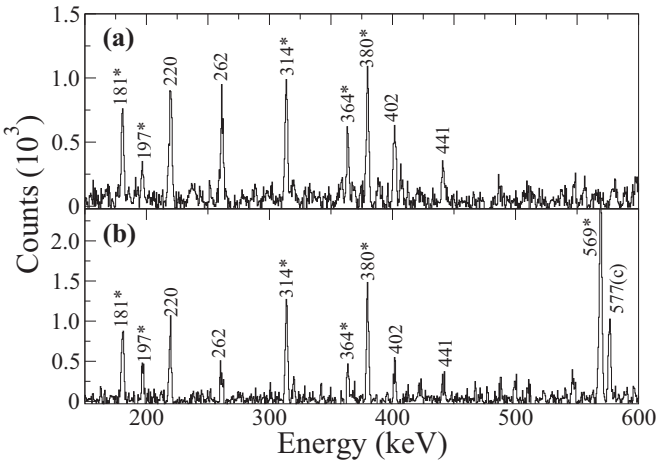


FIG. 7. The γ-ray coincidence spectra obtained with gate on the (a) 1192- and (b) 623-keV γ-ray transitions. The transitions marked with an asterisk are the new transitions from ^{207}At. The 577-keV transition marked with symbol (c) is contamination from ^{207}Po.

the transitions below the $25/2^+$ isomer to obtain the $R_{\rm DCO}$ values for the new transitions feeding the isomer. Therefore, the $R_{\rm DCO}$ values for a few new transitions of the sequence "A" viz. 784, 389, 514, and 356 keV, were determined using mutual gates and their multipolarities were assigned on the basis of consistency in their $R_{\rm DCO}$ values as discussed below. The $R_{\rm DCO}$ values for the 389-, 514-, and 356-keV transitions with a gate on the 784-keV γ ray are 1.07(8), 0.48(3), and 0.48(3), respectively. These values suggest that both the 784- and 389-keV γ-ray transitions are of the same multipolarity. Also, these $R_{\rm DCO}$ values collectively suggest that the 784- and 389-keV transitions are $\Delta I = 2$ transitions, while the 514- and 356-keV transitions are of $\Delta I = 1$ multipolarity. Furthermore, the $R_{\rm DCO}$ values for the 784-, 389-, and 514-keV transitions were determined using a gate on the 356-keV γ ray and found to be 2.00(14), 2.14(15), and 0.94(7), respectively. These values further corroborate the preceding multipolarity assignments of the 784-, 389-, 514- and 356-keV transitions. The $R_{\rm DCO}$ values for the remaining transitions in sequences "A–D" were obtained using the deduced multipolarities of the 784-, 389-, 514- and 356-keV transitions. Furthermore, the electric or magnetic nature of the new transitions were determined from the measured $\Delta_{\rm asym}$ values. The information on the γ-ray energies, relative intensities, $R_{\rm DCO}$ and $\Delta_{\rm asym}$ values for the transitions above the isomeric $25/2^+$ level are listed in Table II.

B. Evidence of a $29/2^+$ isomer at $E_x = 2385$ keV

An isomeric $29/2^+$ state is known in ^{199,201,203,205,209,211}At nuclei [13–16,18,19,19,22]. However, such a state was not known in ^{207}At [17]. In this section, we discuss the first evidence of the $29/2^+$ isomeric state in ^{207}At. Figure 8 illustrates the double-gated coincidence spectra of the (a) 402-, 262-keV, and (b) 402-, 220-keV transitions. It was observed that a strong 488-keV transition is present in Fig. 8(a) but not in Fig. 8(b). This indicates that the new 488-keV γ ray is in coincidence with the 262- and 402-keV transitions but not

TABLE II. Table of γ-ray energies E_γ, corresponding initial level energies E_i, spin-parity of the initial (I_i^π) and final (I_f^π) levels, relative γ-ray intensity I_γ, $R_{\rm DCO}$, $\Delta_{\rm asym}$ values, and assigned multipolarity of the γ-ray transitions deexciting the levels above the $25/2^+$ isomer. The relative intensities are quoted in percent by normalizing their values with respect to the intensity of the 643-keV transition, which is assumed to be 100. The uncertainties in the γ-ray energies, relative intensities and $R_{\rm DCO}$ values have contributions from both statistical and systematic factors. The systematic uncertainty in I_γ is considered to be 5% of the relative γ-ray intensity.

E_γ (keV)	E_i (keV)	I_i^π	I_f^π	I_γ	$R_{\rm DCO}$	$\Delta_{\rm asym}$	Multipolarity
(69)[a]	4251.8(4)	$35/2^-$	$33/2^{(+)}$				
(70)[a]	3289.3(2)	$33/2^+$	$31/2^+$				
124.7(3)	3289.3(2)	$33/2^+$	$33/2^+$	1.4(1)			
163.6(2)	6538.4(3)	47/2	45/2	3.7(2)	0.52(4)[b]		D
180.6(2)	3489.4(3)	$29/2^{(+)}$	$27/2^-$	4.5(3)	1.24(9)[c]		D
193.1(3)	2149.1(4)			3.8(2)			
196.8(3)	3505.3(5)	$29/2^{(-)}$	$27/2^-$	3.7(2)			
252.0(3)	2149.1(4)		$23/2^-$	1.1(1)			
259.1(4)	4159.2(5)	$37/2^+$	$35/2^+$	<1			
264.7(2)	3952.8(3)	37/2	$35/2^+$	3.8(2)	0.46(3)[b]		D
313.7(2)	4182.9(3)	$33/2^{(+)}$	$31/2^{(+)}$	9.7(5)	1.01(7)[c]	−0.112(29)	$M1$
356.4(2)	4159.2(5)	$37/2^+$	$35/2^+$	9.8(6)	0.48(3)[b]	−0.087(21)	$M1$
363.6(2)	4615.4(3)	$37/2^{(-)}$	$35/2^-$	5.4(3)	0.50(4)[b]	−0.025(35)	$(M1+E2)$
363.8(5)	3869.2(5)	$31/2^{(+)}$	$29/2^{(-)}$	7.5(6)			
379.8(2)	3869.2(5)	$31/2^{(+)}$	$29/2^{(+)}$	5.2(3)	0.94(7)[c]	−0.139(33)	$M1$
388.6(1)	3289.3(2)	$33/2^+$	$29/2^+$	36.3(20)	1.07(8)[b]	0.101(18)	$E2$
410.5(4)	4310.3(4)	$37/2^+$	$35/2^+$	<1			
422.5(2)	5936.6(3)	$43/2^{(+)}$	$41/2^+$	6.3(4)	0.54(4)[b]	−0.016(15)	$(M1+E2)$
438.2(3)	6374.8(3)	45/2	$43/2^{(+)}$	3.4(2)	0.60(5)[b]		D
449.4(2)	4251.8(4)	$35/2^-$	$35/2^+$	5.6(3)	1.17(9)[b]	−0.077(26)	$E1, \Delta I=0$
479.3(3)	4251.8(4)	$35/2^-$	33/2	1.5(1)	1.21(9)[c]		D
479.6(3)	3380.3(4)		$29/2^+$	2.4(2)			
483.2(2)	3772.5(2)	33/2	$33/2^+$	3.5(2)	0.86(6)[b]		$D, \Delta I=0$
487.6(1)	2384.6(1)	$29/2^+$	$23/2^-$	66.5(38)			
500.4(2)	5514.1(5)	$41/2^+$	$39/2^+$	6.1(4)	0.44(3)[b]	−0.045(21)	$M1$
513.5(1)	3802.8(2)	$35/2^+$	$33/2^+$	22.1(13)	0.48(3)[b]	−0.066(18)	$M1$
523.5(2)	3688.1(3)	$35/2^+$	$33/2^+$	14.3(8)	1.02(8)[c]	−0.044(21)	$M1$
534.4(3)	4693.6(3)	39/2	$37/2^+$	2.0(1)	1.03(8)[c]		D
566.3(2)	4254.4(3)	$37/2^+$	$35/2^+$	6.8(4)	1.10(8)[c]	−0.054(21)	$M1$
569.3(1)	2685.9(2)	$27/2^+$	$25/2^+$	15.1(8)	0.86(6)[c]	−0.091(32)	$M1$
584.8(3)	3485.5(4)		$29/2^+$	1.7(1)			
590.6(2)	4749.8(3)	39/2	$37/2^+$	4.8(3)	0.92(7)[c]		D
610.5(2)	3899.8(3)	$35/2^+$	$33/2^+$	8.5(5)	0.44(3)[b]	−0.072(23)	$M1$
622.9(2)	3308.8(4)	$27/2^-$	$27/2^+$	4.1(2)	2.22(16)[c]		$D, \Delta I=0$
654.0(3)	2149.1(4)		$21/2^-$	2.4(1)			
703.4(2)	5013.7(4)	$39/2^+$	$37/2^+$	3.7(2)	0.50(4)[b]	−0.040(28)	$M1$
759.4(3)	5013.7(4)	$39/2^+$	$37/2^+$	2.3(1)	0.95(7)[c]	−0.027(51)	$(M1+E2)$
763.2(3)	3663.9(4)		$29/2^+$	2.5(2)			
764.4(3)	5514.1(5)	$41/2^+$	39/2	1.9(1)	0.98(7)[c]		D
779.8(2)	2274.9(3)	$25/2^-$	$21/2^-$	9.6(5)	1.97(15)[c]	0.069(23)	$E2$
780.0(1)	3164.6(1)	$33/2^+$	$29/2^+$	42.0(24)	2.14(16)[c]	0.076(25)	$E2$
784.1(1)	2900.7(1)	$29/2^+$	$25/2^+$	54.4(30)	0.94(7)[b]	0.098(11)	$E2$
834.6(1)	3219.2(1)	$31/2^+$	$29/2^+$	31.0(18)	0.81(6)[c]	−0.029(25)	$M1$
854.0(2)	2349.1(3)		$21/2^-$	3.5(2)			
934.5(3)	4223.8(4)	35/2	$33/2^+$	2.6(2)	0.44(3)[b]		D
947.6(3)	4900.4(4)		37/2	1.9(1)			
962.5(2)	4251.8(4)	$35/2^-$	$33/2^+$	4.3(3)	0.53(4)[b]	0.188(33)	$E1$
1021.0(2)	4310.3(4)	$37/2^+$	$33/2^+$	5.7(3)	1.09(8)[b]	0.047(38)	$E2$
1071.9(3)	4361.2(4)		$33/2^+$	1.9(1)			

TABLE II. (*Continued.*)

E_γ (keV)	E_i (keV)	I_i^π	I_f^π	I_γ	R_{DCO}	Δ_{asym}	Multipolarity
1191.9(2)	3308.8(4)	$27/2^-$	$25/2^+$	6.4(4)	1.11(8)[c]	0.155(56)	$E1$
1230.4(3)	3505.3(5)	$29/2^{(-)}$	$25/2^-$	2.1(1)	1.11(8)[b]		Q
1354.7(3)	5514.1(5)	$41/2^+$	$37/2^+$	2.8(2)			

[a]Unobserved γ ray, but its presence is inferred from the coincidence relationships.
[b]R_{DCO} value is obtained with a gate on a stretched quadrupole transition.
[c]R_{DCO} value is obtained with a gate on a pure dipole transition.

with the 220-keV transition, which in turn suggests that the 488-keV transition should be placed above the 402-keV γ ray. The placement of the 488-keV γ ray introduces a new level at 2385 keV. Furthermore, Fig. 8(c) depicts the γ-ray transitions in a double gate of the 402- and 488-keV γ rays. It may be noted that only transitions below the 1495-keV level (see Fig. 1) are observed in Fig. 8(c), which further corroborates the above placement of the new 488-keV γ ray. The absence of any prompt γ ray(s) feeding the 2385-keV level indicates the presence of a long-lived isomeric state. Here, two possibilities may be considered. One could be that the 2385-keV level itself has a large half-life and therefore, the transition(s) feeding the 2385-keV level could not be observed in the prompt coincidence (100 ns) with the 488-keV transition. Another possibility could be the presence of a closely spaced higher-lying metastable state, which may deexcite to the 2385-keV level via one or more unobserved low energy and/or high multipole transitions. However, the second possibility can be discarded on the basis of the coincidence relationships of the transitions which are observed in *early* coincidence with the new 488-keV γ ray as discussed below.

Figure 9(a) illustrates the transitions which precede the 488-keV γ ray within the 100–275 ns coincidence window. It was further observed that the strongest 780- and 835-keV γ-ray transitions are not in mutual coincidence, while the 780-keV one is in coincidence with a weaker 524-keV

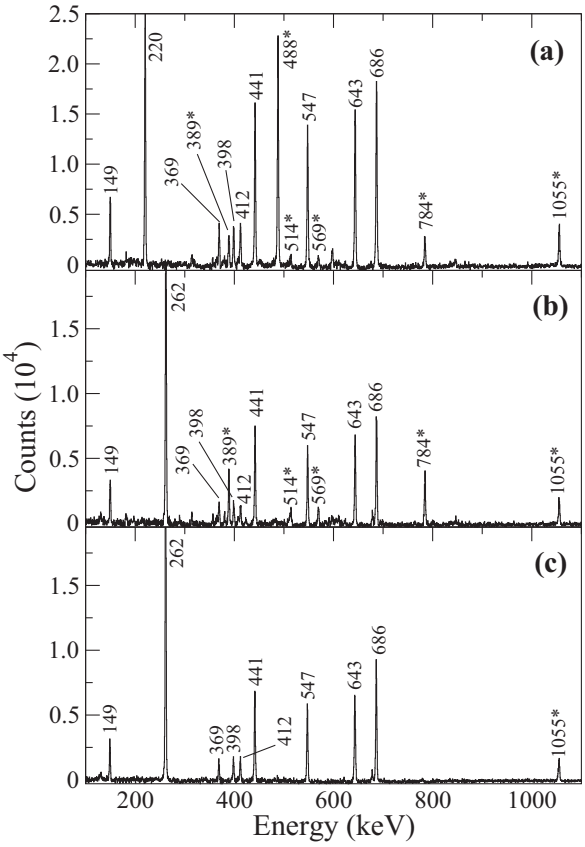


FIG. 8. Double-gated coincidence spectra illustrating γ-ray transitions in gates on the (a) 402-, 262-keV, (b) 402-, 220-keV, and (c) 402-, 488-keV γ rays within the prompt coincidence window. The new transitions are marked with asterisks.

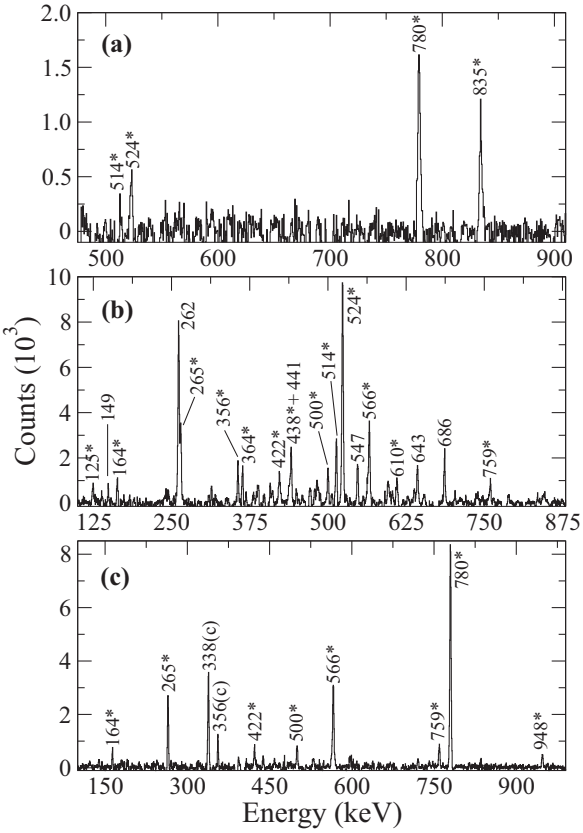


FIG. 9. Coincidence spectra illustrating γ-ray transitions in coincidence with the (a) 488-keV γ ray within a 100–275 ns *early* time window, (b) 780-, and (c) 524-keV γ rays within the prompt coincidence window. The new transitions from ^{207}At are marked with asterisks. The transitions marked with the symbol (c) are contaminants from ^{206}Bi and ^{196}Pt.

transition as evident from the two lower panels of Fig. 9. The new 780-, 524-, 265-, and 566-keV transitions were placed above the 2385-keV level as shown in Fig. 1 on the basis of their relative intensities and γ-γ coincidence relationships. In addition, a new 759-keV transition was also observed in coincidence with the 780-, 524-, and 566-keV γ rays. The placement of the 759-keV γ ray connects the sequences "D" and "E" and also corroborates the placement of the new 780-keV transition. Furthermore, the γ-ray transitions feeding the $33/2^+$ level at 3289 keV in sequence "A" are also found in coincidence with the 780- and 835-keV transitions, but not with the 524-keV one [see Figs. 9(b), 9(c), and 6(b)]. It may be noted that the presence of the 262-, 441-, 547-, 643-, and 686-keV γ-ray transitions in Fig. 9(b) is attributed to their coincidence with another 780-keV transition which is placed above the 1495-keV level, as already mentioned in Sec. III A. Also, a new 125-keV γ ray is found to be in coincidence with the 780-keV transition and with those feeding the $33/2^+$ level at 3289 keV. The placement of the new 125-keV γ ray connects the sequences "A" and "E", and hence further validates the positions of the new levels and transitions above the 2385-keV state as shown in Fig. 1. Moreover, the coincidences of the 835-keV line with the transitions feeding the 3289-keV level indicate the presence of an unobserved 70-keV transition. The placement of the transitions above the isomers in the sequences "A", "D", and "E" along with that of the 488-keV transition uniquely establishes a state at 2385 keV and the fact that it has a long half-life.

The spin-parity of the 2385-keV level is inferred based on the following considerations. The $I^\pi = 39/2^+$ for the 5014-keV level is firmly established on the basis of the $R_{\rm DCO}$ and $\Delta_{\rm asym}$ values of the 703-, 1021-, 389- and 784-keV transitions. Now, this state is connected to the 2385-keV level via three $\Delta I = 1$ transitions, viz., 759-, 566-, and 523-keV and one $\Delta I = 2$ (780-keV) transition (see Table II). These measurements suggest $I = 29/2$ for the 2385-keV level, which in turn leads to a possible $E3$ or $M3$ multipolarity for the 488-keV transition. Furthermore, intensity balance at the 1897-keV level (assuming $I = 29/2$ for the 2385-keV level, as discussed above) supports $E3$ multipolarity for the 488-keV transition, and hence $I^\pi = 29/2^+$ is proposed for the 2385-keV state. Furthermore, the $\Delta_{\rm asym}$ values for the 780-, 523-, and 566-keV transitions suggest positive parity of the 3165-, 3688-, and 4254-keV levels in sequence "E". The proposed spin-parity, $I^\pi = 29/2^+$, for the isomeric 2385-keV level is also supported by the energy systematics of the known $29/2^+$ isomeric states in the neighboring odd-A At isotopes and will be discussed in Sec. IV B in detail.

An attempt to determine the half-life of the isomeric state under consideration using the electronic timing method resulted in an almost flat time-difference distribution curve of the depopulating and feeding transitions. This suggests a significantly longer half-life as compared to the available narrow time range viz., 0–275 ns. However, a rough estimate of the half-life can be obtained as follows: The delayed gates of the 220- and 488-keV transitions were used to determine the intensities of the 784- and 780-keV transitions within the 100–275 ns *early* coincidence window, respectively. The ratio of the intensities of the 784- to 780-keV transitions was found to be 13.8(10). Now, the amount of the initial intensities (see Table II) of the 784- and 780-keV transitions which decay within the 100–275 ns were determined with the help of radioactive decay law using the known half-life [107.5(9) ns] of the $25/2^+$ state and assuming various values of $T_{1/2}$ for the $29/2^+$ state. The ratio of these intensities is to be compared with the experimental value mentioned above. Among the various values assumed for the half-life of the $29/2^+$ state, it was observed that $T_{1/2} \approx 3.5$ μs is able to reproduce the experimental ratio 13.8(10). In addition, a possible range of the half-life (2–4.5 μs) is surmised on the basis of a systematic study of the $B(E3)$ rates for the $29/2^+ \rightarrow 23/2^-$ transitions in the neighboring odd-A At isotopes and will be discussed in Sec. IV B. Finally, we note that the intensity ratios obtained using the radioactive decay law for the limits of expected half-life from the $B(E3)$ systematics viz., 2 and 4.5 μs are around 8.1 and 17.6, respectively.

C. Intensity measurements

The relative intensities of the γ-ray transitions listed in Tables I and II were determined using the data at 87 MeV. To obtain the relative intensities of the transitions below the isomers, the pure 643- and 441-keV transitions were fit in a spectrum obtained from the single-fold data. Furthermore, the deduced intensities were normalized with respect to the intensity of the 643-keV γ ray, for which the intensity of 100 units was assumed. The relative γ-ray intensities of the 686-, 1055-, and 1116-keV transitions were determined by measuring the branching ratios of all the transitions feeding directly to the ground state in the efficiency corrected summed spectrum with the gates on the relevant transitions. Furthermore, the efficiency corrected sum gate of all the transitions feeding the ground state was used to determine the intensities of the remaining transitions below the isomers. The intensities of the transitions below the isomers were normalized using the relative intensity of the 441-keV γ ray.

The relative intensities of the γ-ray transitions above the isomers were determined as follows. As discussed in the earlier sections, the 780-keV transition is a doublet; (i) $25/2^- \rightarrow 21/2^-$ transition feeding the $21/2^-$ level at 1495 keV, and (ii) $33/2^+ \rightarrow 29/2^+$ transition which feeds directly to the $29/2^+$ isomer at 2385 keV. The summed intensity of the 780-keV peak was obtained from single-fold data and normalized with respect to the relative intensity of the 643-keV transition. Furthermore, an individual relative intensity of the bypassing 780-keV [$25/2^- \rightarrow 21/2^-$] transition was deduced in a gate of the 262-keV γ ray. It may be noted that the second 780-keV transition, which populates the $29/2^+$ isomer, was not observed in the prompt coincidence (100 ns) with the transitions following the decay of the $29/2^+$ isomer (see Fig. 8). Thus, the intensity obtained with the gate on the 262-keV transition corresponds only to the relative intensity of the $25/2^- \rightarrow 21/2^-$, 780-keV transition. The relative intensity of the second 780-keV transition could then be determined by subtracting the contribution of the relative intensity of the bypassing 780-keV transition from the summed relative intensity. Furthermore, the intensity of the 835-keV transition above the $29/2^+$ isomer was determined from the ratio

of the intensities of the 780-keV and 835-keV transitions in a *delayed* gate of the 488-keV γ ray [see Fig. 9(a)]. The intensity of the 784-keV γ ray, relative to the total γ-ray intensity of the 643-keV transition, was also determined from the single-fold data. To deduce the relative intensity of the 389-keV γ-ray, the 389- and 784-keV peaks were fit in a prompt coincidence spectrum with a gate on the 220-keV γ ray. The deduced intensities of both the transitions were normalized with respect to the relative intensity of the 784-keV transition which was obtained from single-fold data as discussed above. The relative intensities of the remaining transitions in the sequences "A", "B", "D", and "E" were determined in efficiency corrected summed gates of the 780-, 784-, and 835-keV transitions and normalized with respect to the relative intensity of the 389-keV γ ray. The relative intensity of the 364-keV $[37/2^{(-)} \rightarrow 35/2^{-}]$ transition in sequence "B" is corrected for the branch which deexcites the 4252-keV level in sequence "C". Moreover, the intensity of the second 364-keV γ ray, which populates the 3505-keV level was determined by subtracting the contribution of the upper 364-keV $[37/2^{(-)} \rightarrow 35/2^{-}]$ transition from the total relative intensity of the 364-keV doublet. The total relative intensity of the doublet was determined in a efficiency corrected summed prompt spectrum obtained with gates on the 780-, 784-, 835-, 1192-, and 569-keV transitions.

Finally, the relative intensities of the 1192-, 569-, 623-, 181-, 380, and 197-keV transitions of sequence "C" were also deduced by fitting these transitions in a gate of the 220-keV γ ray. The relative intensity of the 784-keV transition (obtained from single-fold data) was used for normalization to deduce the relative intensities of the above transitions.

IV. DISCUSSION

Nuclear structure investigations in the region around the doubly-closed-shell nucleus ^{208}Pb are of immense interest because a variety of nuclear structure aspects have been observed in this region. In particular, the level structure in At isotopes with a few neutron-holes with respect to the $N = 126$ shell closure is governed by single-particle excitations [18–22]. Furthermore, shears bands have been reported in the lighter At isotopes viz., ^{201,203,204}At [13,14,42]. A similar sequence of $\Delta I = 1$ transitions had also been reported in ^{205}At [16]. However, the shear structure of the observed sequence was not confirmed [16]. On the other hand, the lighter Po and At nuclei are known to exhibit oblate and prolate deformed shapes [4,10]. Thus, a systematic study across the isotopic chain enhances the understanding of shape evolution with decreasing neutron number. In ^{207}At, which is the subject of the present work, the excited states only up to the $25/2^{+}$ isomer at 2117 keV were known [17]. The present study reports an extended level scheme of ^{207}At. In addition to several new transitions below the isomer, four new sequences are identified which feed the known $25/2^{+}$ isomer. Moreover, the new $29/2^{+}$ isomer is also established at 2385 keV, which completes the systematics of this isomer in odd-A At isotopes. The proposed level scheme is understood in the framework of the shell-model approach. The yrast and near-yrast states in ^{207}At are also compared with the systematics of the corresponding states in Po and odd-A At isotopes for a qualitative understanding, as discussed in the following sections.

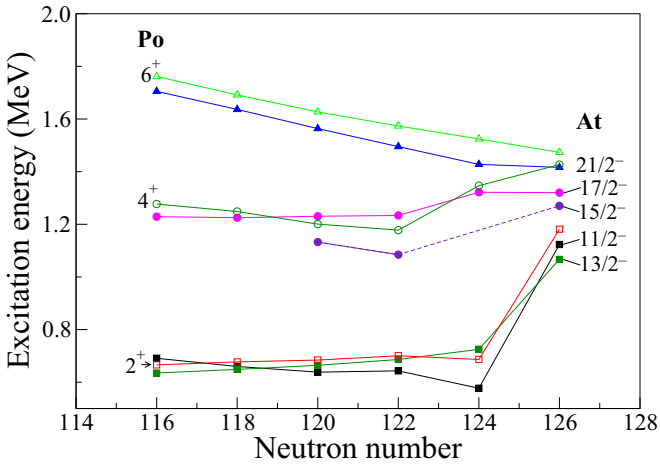


FIG. 10. Energy systematics of selected low-lying states in At (solid symbols) and Po (open symbols) isotopes. The excitation energies of the states in At and Po isotopes are taken from present work and Refs. [13–15,21,22,28,30,43,44].

Large-scale shell-model calculations have been performed with the KHM3Y effective interaction [45], which was developed for the $Z = 50$–126, $N = 82$–184 model space. The model space comprised of 24 orbitals in total; the proton orbitals include $g_{7/2}$, $d_{5/2}$, $h_{11/2}$, $d_{3/2}$, $s_{1/2}$ below the $Z = 82$ and $h_{9/2}$, $f_{7/2}$, $i_{13/2}$, $f_{5/2}$, $p_{3/2}$, $p_{1/2}$ above it, while the neutron orbitals involve $i_{13/2}$, $p_{3/2}$, $f_{5/2}$, $p_{1/2}$, $h_{9/2}$, $f_{7/2}$ below the $N = 126$ and $g_{9/2}$, $i_{11/2}$, $j_{15/2}$, $g_{7/2}$, $d_{5/2}$, $d_{3/2}$, $s_{1/2}$ above. The cross-shell two-body matrix elements (TBMEs) are based on the M3Y interaction [46]. The neutron-proton particle-particle and hole-hole TBMEs use the Kuo-Herling interaction [47] as modified in Ref. [48]. To make the calculation feasible, the proton orbitals below the $Z = 82$ shell closure were completely filled and the neutron excitations across the $N = 126$ shell were not allowed. The calculations were performed using the shell-model code NuShellX [49]. Recently, the experimental results of ^{207}Tl [50–52] and ^{208}Pb [45,52] were interpreted using the shell-model calculations which also used the same interaction as mentioned above.

A. States below the isomers

Figure 10 depicts the energy systematics of the yrast negative-parity states, viz. $11/2^{-}$, $13/2^{-}$, $15/2^{-}$, $17/2^{-}$, and $21/2^{-}$, in odd-A At isotopes, which is compared with the 2^{+}, 4^{+}, and 6^{+} states of the corresponding Po isotones. It is evident from the figure that the $(11/2^{-}, 13/2^{-})$, $(15/2^{-}, 17/2^{-})$, and $21/2^{-}$ states in odd-A At isotopes closely follow the trend in excitation energies of the 2^{+}, 4^{+}, and 6^{+} states in the corresponding Po isotones, respectively. The observed similarity in the excitation energies of the yrast states suggests that the low-lying negative-parity states in odd-A At isotopes can be understood in terms of the coupling of an unpaired proton in $h_{9/2}$ orbital to the respective states of the even-even Po core. A similar interpretation is noted to explain the low-lying negative-parity states in neighboring odd-A At isotopes

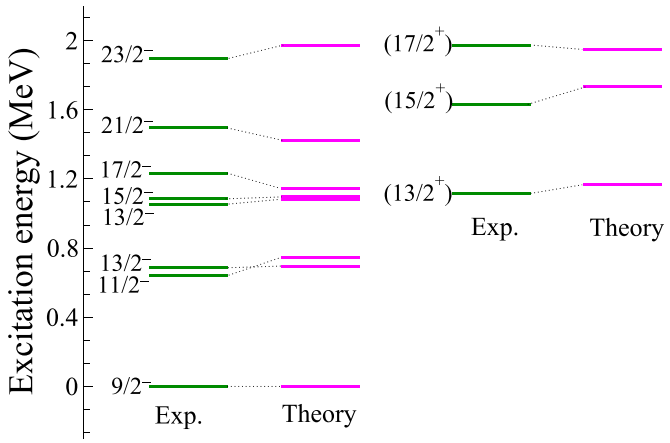


FIG. 11. Comparison of the experimental level energies of the yrast and near-yrast states below the isomers with those predicated from the shell-model calculations.

[11,13–16]. Also, a sudden increase in the excitation energy of the $11/2^-$ and $13/2^-$ $[2^+(^{210}\mathrm{Po}) \otimes \pi h_{9/2}]$ states may be noted, as opposed to the same states in the lighter isotopes where excitation energies are found to be rather constant. The marked difference in the excitation energies of the yrast states in the $N = 126$ isotones relative to those in the lighter isotopes can be attributed to the difference in their configurations. The low-lying yrast states in the closed neutron shell nuclei, viz. ^{210}Po and ^{211}At are governed by pure proton configurations, while both proton-particle and neutron-hole excitations are expected to play a role in the lighter Po and At isotopes. The yrast states in ^{211}At ($N = 126$) are well understood in terms of the $\pi(h^3_{9/2})$, $\pi(h^2_{9/2}f_{7/2})$, and $\pi(h^2_{9/2}i_{13/2})$ configurations [22].

Figure 11 shows a comparison of the experimental level energies of the yrast and near-yrast states below the isomers with those predicted from the shell-model calculations. It is evident from the figure that the experimental level energies are in good agreement (within 100 keV) with the shell-model predictions. The low-lying negative-parity states, viz. $11/2^-$, $13/2^-$, $15/2^-$, $17/2^-$, and $21/2^-$ are predicted to originate from the $\pi(h^3_{9/2}) \otimes \nu(f^{-2}_{5/2}p^{-2}_{1/2})$ configuration. The energy systematics of these states in Po and At isotopes also suggests the same configuration as discussed above. The primary configuration (with 25.6% parentage) for the $23/2^-$ state is predicated to be $\pi(h^2_{9/2}f_{7/2}) \otimes \nu(f^{-2}_{5/2}p^{-2}_{1/2})$. It may be noted that only the states with firm spin-parity assignments are compared with the shell-model calculations, except the $(13/2^+)$, $(15/2^+)$, and $(17/2^+)$ states. The positive parity of these states is suggested from the similarity in the level structures in odd-A At isotopes, as discussed below.

The $13/2^+$ state, which originates from the $\pi(i_{13/2})$ configuration, has been identified in several odd-A At isotopes [10–16,22]. Figure 12 illustrates the evolution of the $13/2^+$ state with increasing neutron number in At isotopes with $114 \leqslant N \leqslant 122$. It is observed that the excitation energy of the $13/2^+$ state increases with increasing number of neutrons. However, the excitation energy of the $11/2^-$ state remains nearly constant, as shown in Fig. 12. A similar trend in the excitation energy of the $13/2^+$ state has also been reported in odd-A Bi isotopes [53–55]. This feature is explained by the coupling of the unpaired proton in the $i_{13/2}$ orbital to the increasing number of valence neutron holes. The interaction of the $\pi\nu^{-1}$ configuration for both particles and holes in the $i_{13/2}$ orbital has the smallest repulsion, which brings the $13/2^+$ state down in energy with a decreasing number of neutrons [11,56]. In ^{199}At, the $13/2^+$ state deexcites to the ground state only via an $M2$ branch, unlike the heavier isotopes, viz. ^{201,203,205}At, where it is observed to decay via $E1$ and $M2$ transitions to the $11/2^-$ and $9/2^-$ ground states, respectively. A similar structure is also observed in ^{207}At, where the 1116-keV state deexcites via the 472- and 1116-keV γ rays to the $11/2^-$ level at 643 keV and the ground state, respectively. The observed similarities in the excitation energy and the decay paths of the 1116- and 1631-keV levels in ^{207}At with the kindred states in the neighboring At isotopes suggest that these states are also likely to have positive parity. As illustrated in Fig. 11, the excitation energies of the proposed positive-parity states viz. $(13/2^+)$, $(15/2^+)$, and $(17/2^+)$, are in very good agreement with the shell-model calculations, which suggest a dominant $\pi(h^2_{9/2}i_{13/2}) \otimes \nu(f^{-2}_{5/2}p^{-2}_{1/2})$ configuration for the states under consideration.

B. Isomers and their decay properties

The region around the doubly-magic nucleus ^{208}Pb is rich in nuclear isomerism [23]. The presence of high-j valence orbitals leads to the realization of isomeric states in this region which arise due to dominant intrinsic degrees of freedom. An isomer (38^+) in ^{212}Rn ($N = 126$) at $E_x = 12.5$ MeV is

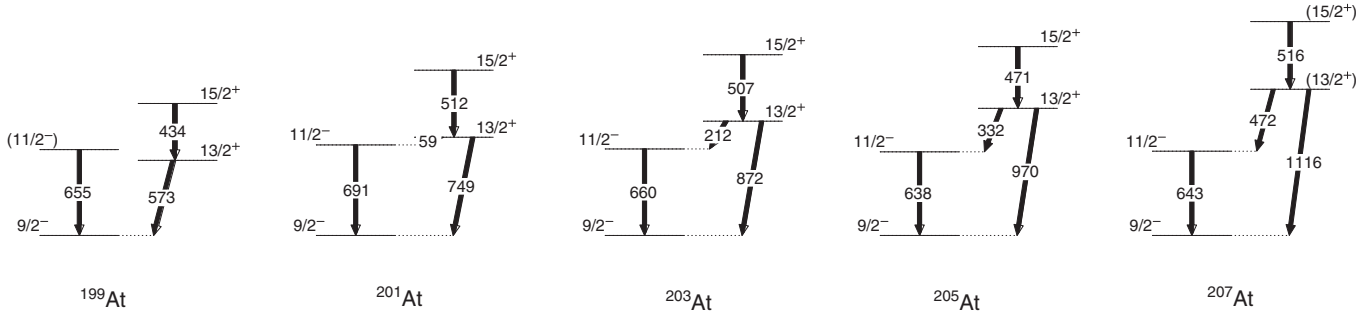


FIG. 12. Evolution of the $13/2^+$ state in odd-A At isotopes with increasing neutron number in $114 \leqslant N \leqslant 122$. The experimental information of the presented levels of the $^{199-207}$At nuclei are taken from the present work and Refs. [12–17].

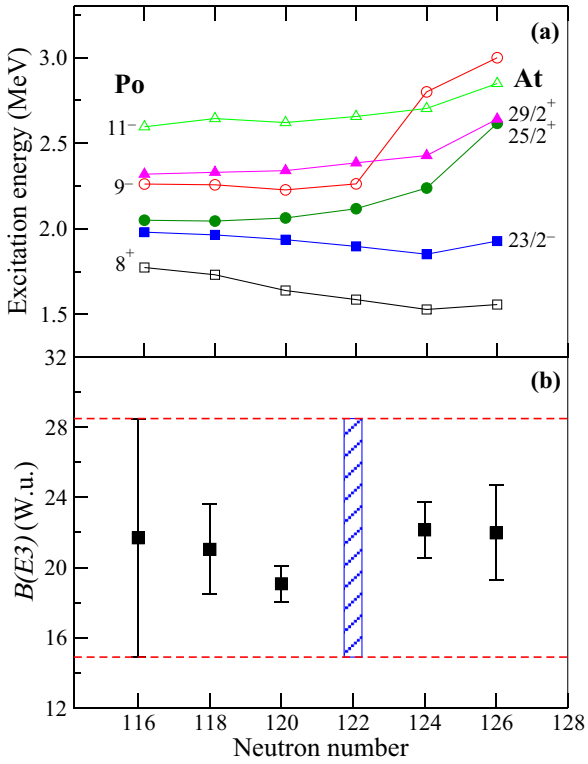


FIG. 13. (a) Energy systematics of the $29/2^+$, $25/2^+$ isomers and the $23/2^-$ state in odd-A At isotopes (solid symbols) and the 11^-, 9^-, and 8^+ states of the corresponding Po (open symbols) isotones. Panel (b) of the figure presents the variation of the experimental $B(E3)$ values for the $29/2^+ \rightarrow 23/2^-$ transition in odd-A At isotopes with increasing neutron number. The shaded area indicates the possible range of the $B(E3)$ value for the 488-keV transition in ^{207}At. The experimental information for the At and Po isotopes is taken from the present work and Refs. [28,30,43,44,59–63].

the highest-lying isomer known to date [57]. This isomer results from the triple-core excitations coupled with the aligned valence protons. Several high-spin isomeric states have been reported in Po, At, and Fr isotopes [23]. A $25/2^+$ isomer is reported in ^{203,205,207}At isotopes [14–17]. Also, a long-lived $29/2^+$ state is known in all odd-A At isotopes with $114 \leqslant N \leqslant 126$, except in ^{207}At [13–22]. As discussed in Sec. III, we have identified the long-lived $29/2^+$ isomeric state in ^{207}At at $E_x = 2385$ keV.

The high-spin isomers in odd-A At isotopes may be interpreted in terms of the coupling of an unpaired proton in specific orbitals to the even-even core of the corresponding Po isotones. The 11^- and 9^- isomeric states have been reported in even-even Po isotopes, which originate from the $\pi(h^1_{9/2}i^1_{13/2})_{11^-}$ two-quasiproton and $\nu(f^{-1}_{5/2}i^{-1}_{13/2})_{9^-}$ two-neutron-hole configurations, respectively [24,43,44,58]. Figure 13(a) illustrates the energy systematics of the 11^-, 9^-, and the subsequent 8^+ states in the even-even Po isotopes, which is compared with the corresponding $29/2^+$, $25/2^+$, and $23/2^-$ levels in the odd-A At isotones. The systematic trend in the excitation energies suggests that the structure of the $29/2^+$ and $25/2^+$ isomeric states in ^{207}At may be interpreted in terms of a weak coupling of an unpaired proton in the $h_{9/2}$ orbital to the 11^- and 9^- isomers in ^{206}Po, respectively. Similarly, the $23/2^-$ state may be realized from a weak coupling of the unpaired proton in the $f_{7/2}$ orbital to the 8^+ state of the Po core. Similar considerations have been used to explain the origin of the isomeric states in other odd-A At isotopes [11–16,18–22].

The $25/2^+$ isomer in ^{207}At deexcites to the $23/2^-$ state via the 220-keV $E1$ transition. The experimental $B(E1)$ value for the 220-keV transition is $3.6(9) \times 10^{-7}\ e^2\,\mathrm{fm}^2$, which is hindered by seven orders of magnitude with respect to the single-particle estimate. The hindrance in the decay of the $25/2^+$ state may be attributed to a considerable difference in the wave functions of the $25/2^+$ and $23/2^-$ states. In ^{203,205}At, the $25/2^+$ isomer deexcites via competing $E1$ and $E2$ transitions unlike the one in ^{207}At where only an $E1$ decay branch is observed [14–16].

The systematics of the excitation energy and the decay path for the newly identified $29/2^+$ isomer is observed to account well for its proposed spin-parity when compared with the same state in the neighboring odd-A At isotopes. In the lighter At isotopes, viz. ^{201,203,205}At, the $29/2^+$ isomer is known to deexcite via $E2$ and $E3$ transitions to the subsequent $25/2^+$ and $23/2^-$ levels, respectively [13–16], while it decays only via an $E2$ branch in ^{199}At [11]. It has been observed that the $E2$ decay-branch becomes weaker with increasing neutron number. The $29/2^+$ isomer in ^{209}At is known to decay only via an $E3$ transition [18–21]. However, in the case of ^{211}At, this isomer is reported to deexcite via an unobserved low-energy $E2$ transition, in addition to a strong $E3$ decay path [22,64]. The proposed $29/2^+$ isomeric level in ^{207}At is also observed to decay via the 488-keV $E3$ transition. However, the present data do not provide any conclusive evidence for an $E2$ decay branch.

As mentioned earlier, the direct measurement of the half-life of the $29/2^+$ isomer was not possible. However, the systematics of the $E3$ transition strengths in odd-A At isotopes can be used to determine the range of the expected half-life. Figure 13(b) depicts the variation of the $B(E3)$ values corresponding to the $29/2^+ \rightarrow 23/2^-$ transitions in odd-A At isotopes with increasing neutron number. It may be noticed that the plotted $B(E3)$ values are roughly constant. The observed striking similarities in the properties of the $29/2^+$ isomer in odd-A At isotopes as discussed above suggest that the transition strength of the 488-keV $(29/2^+ \rightarrow 23/2^-)$ $E3$ transition in ^{207}At can assume a value between the range displayed by the shaded area in Fig. 13(b). This range of $B(E3)$ values in turn suggests a half-life between 2–4.5 μs for the $29/2^+$ isomer in ^{207}At. It is worth mentioning that the rough estimate of the half-life (≈3.5 μs) for the $29/2^+$ state as outlined in the previous section is consistent with the above range.

The shell-model calculations suggest that the $29/2^+$ and $23/2^-$ levels are three quasiproton states with $\pi(h^2_{9/2}i^1_{13/2})$ and $\pi(h^2_{9/2}f^1_{7/2})$ primary configurations, respectively. The $25/2^+$ isomer is associated with the $\pi(h^3_{9/2})_{9/2^-} \otimes \nu(f^{-1}_{5/2}i^{-1}_{13/2})_{9^-}$ configuration and originates from a weak coupling of the $\pi h_{9/2}$ with two-quasineutron-hole configuration. Furthermore, it was observed that the shell-model calculations account well

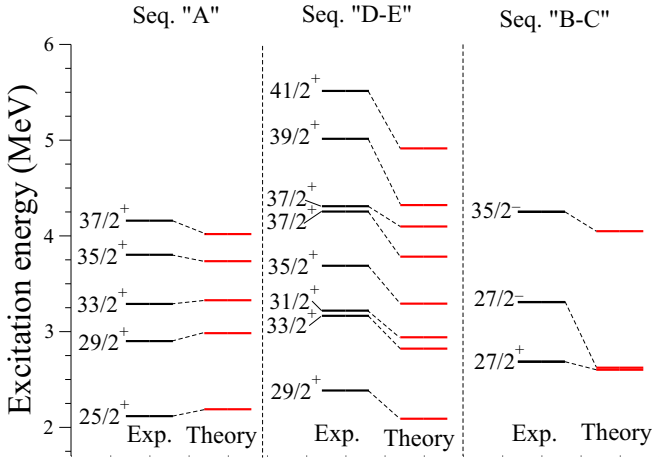


FIG. 14. Comparison of the experimental level energies of yrast and near-yrast states above the isomers with that predicted by the shell-model calculations. Only those states for which firm spin-parities are known are considered for the comparison.

for excitation energies of the $23/2^-$ and $25/2^+$ states, while an underestimation by 295 keV is observed for the $29/2^+$ isomer. It may be noted that the $29/2^+$ isomer decays via the 488-keV $E3$ transition, which corresponds to the $\pi(i_{13/2} \rightarrow f_{7/2})$ transition as suggested by the shell-model configurations for the states under consideration. In such cases, where the initial- and final-state wave-functions involve the high-j proton ($i_{13/2}$ and $f_{7/2}$) and neutron ($j_{15/2}$ and $g_{9/2}$) orbitals which differ by $\Delta j = \Delta l = 3$, the configuration of the initial state is likely to have a mixing of the 3^- octupole phonon of the ^{208}Pb coupled with the final state [65]. Therefore, the corresponding $E3$ transitions are expected to be very fast [65]. Such states have been observed in a number of nuclei around the doubly-closed ^{208}Pb [50,52,66]. The $29/2^+$ isomeric level in ^{207}At also appears to have a mixing of the octupole vibrational phonon. A recent study by Berry *et al.* reported that the states involving octupole vibrations in the region around ^{208}Pb are underestimated (≈250 keV) by the shell-model calculations performed using the KHM3Y effective interaction [50]. A similar effect is also observed in the calculations for the $29/2^+$ state in ^{207}At.

C. States above the isomers

Figure 14 shows a comparison of the excitation energies of the yrast and near-yrast states above the $25/2^+$ isomer with the shell-model calculations. The shell-model states corresponding to the experimental levels in a specific sequence are chosen on the basis of configurations. As discussed in the previous section, the isomeric $25/2^+$ state is associated with the $\pi(h^3_{9/2})_{9/2^-} \otimes \nu(f^{-1}_{5/2} i^{-1}_{13/2})_{9^-}$ configuration. The same configuration is observed to account well (within 150 keV), as shown in Fig. 14, for the higher-lying states in sequence "A" by breaking of the proton pair in the $h_{9/2}$ orbital. A similar sequence has also been reported in ^{205}At, which feeds the $25/2^+$ isomer at 2063 keV [16]. However, no such sequence was observed in ^{203}At [14].

As mentioned earlier, the $29/2^+$ isomeric level is predominantly the three quasiproton state with a maximum possible angular momentum from the $\pi(h^2_{9/2} i_{13/2})$ configuration. For the realization of the states above the $29/2^+$ isomer, the neutron-hole pairs may contribute in the angular-momentum generation. Therefore, the shell-model states originating from the $\pi(h^2_{9/2} i_{13/2})_{29/2^+} \otimes I_n$ configuration, where I_n is the contribution to the angular momentum from the neutron holes are compared with the states in sequences "D" and "E". As shown in Fig. 14, a systematic underestimation is observed in the calculated excitation energies of the states in sequences "D" and "E". It was further noticed that the deviation between the experiment and the shell-model calculations increases with excitation energy, which may be attributed to the truncation scheme adopted for the calculations, due to computational limitations. The states in sequences "B" and "C" are found to be in rather good agreement with the shell-model calculations, except the $27/2^-$ state.

Moreover, the available spectroscopic information on the states above the $29/2^+$ isomer is scarce in the neighboring odd-A At isotopes for a systematic comparison.

V. SUMMARY

Excited states above the known $25/2^+$ isomer in ^{207}At have been investigated for the first time using the ^{198}Pt(^{14}N, $5n\gamma$)^{207}At reaction. The half-life of the $25/2^+$ isomer is revisited and a value of $T_{1/2} = 107.5(9)$ ns is inferred, which is consistent with that reported by Sjoreen *et al.* [17]. The level scheme is considerably extended up to 6.5 MeV and $47/2\hbar$ with the addition of about 60 new γ-ray transitions. A long-lived $29/2^+$ isomeric state (E_x = 2385 keV) is established for the first time in ^{207}At, with a similar level having been identified earlier in the neighboring odd-A At isotopes. The half-life of the proposed $29/2^+$ isomer is estimated to be in the 2–4.5 μs range on the basis of the systematics of the $B(E3)$ values corresponding to the $E3$ transitions, which deexcite the $29/2^+$ isomer in the neighboring odd-A At isotopes. Furthermore, the 1116-keV level is suggested to originate from the $\pi(i_{13/2})$ configuration on the basis of similarities in its excitation energy and decay paths with that of the $13/2^+$ state in the neighboring odd-A At isotopes. The large-scale shell-model calculations were performed using the shell-model code NuShellX with the KHM3Y effective interaction. An overall good agreement has been observed between the experimental results and the shell-model predictions for the states below the isomers and those in sequence "A" above the $25/2^+$ isomer. However, the shell-model calculations appear to significantly underestimate the excitation energies of the remaining states. In addition, the weak coupling of an unpaired proton in the $h_{9/2}$ or $f_{7/2}$ orbitals with the states of ^{206}Po core is observed to qualitatively account for the level structure in ^{207}At. An experiment to determine half-life of the $29/2^+$ isomer is in order.

ACKNOWLEDGMENTS

The authors would like to thank the technical staff from IUAC for their support during the experiment. The financial

support by DST, India (Grant No. IR/S2/PF-03/2003-III) for the INGA project is also acknowledged. K.Y. acknowledges the financial assistance from MHRD, India. A.Y.D. and D.S. would like to acknowledge the financial support by SERB (DST), Grant No. CRG/2020/002169. Madhu acknowledges financial support from DST, India under the INSPIRE fellowship scheme (IF 180082). P.C.S. acknowledges a research grant from SERB (India), CRG/2019/000556.

[1] K. Heyde, P. Van Isacker, M. Waroquier, J. L. Wood, and R. A. Meyer, Phys. Rep. **102**, 291 (1983).
[2] J. L. Wood, K. Heyde, W. Nazarewicz, M. Huyse, and P. Van Duppen, Phys. Rep. **215**, 101 (1992).
[3] R. Julin, K. Helariutta, and M. Muikku, J. Phys. G **27**, R109 (2001).
[4] K. Helariutta *et al.*, Eur. Phys. J. A **6**, 289 (1999).
[5] M. J. A. de Voigt, J. Dudek, and Z. Szymanski, Rev. Mod. Phys. **55**, 949 (1983).
[6] T. Grahn, J. Pakarinen, L. Jokiniemi, M. Albers, K. Auranen, C. Bauer *et al.*, Eur. Phys. J. A **52**, 340 (2016).
[7] M. Stoyanova, G. Rainovski, J. Jolie, N. Pietralla, A. Blazhev, M. Beckers *et al.*, Phys. Rev. C **100**, 064304 (2019).
[8] K. Van de Vel, A. Andreyev, R. Page, H. Kettunen, P. T. Greenlees, P. Jones *et al.*, Eur. Phys. J. A **17**, 167 (2003).
[9] M. Nyman, S. Juutinen, I. Darby, S. Eeckhaudt, T. Grahn, P. T. Greenlees, U. Jakobsson, P. Jones, R. Julin, S. Ketelhut, H. Kettunen, M. Leino, P. Nieminen, P. Peura, P. Rahkila, J. Sarén, C. Scholey, J. Sorri, J. Uusitalo, and T. Enqvist, Phys. Rev. C **88**, 054320 (2013).
[10] K. Andgren, U. Jakobsson, B. Cederwall, J. Uusitalo, T. Bäck, S. J. Freeman *et al.*, Phys. Rev. C **78**, 044328 (2008).
[11] U. Jakobsson, J. Uusitalo, S. Juutinen, M. Leino, P. Nieminen, K. Andgren *et al.*, Phys. Rev. C **82**, 044302 (2010).
[12] K. Dybdal, T. Chapuran, D. B. Fossan, W. F. Piel, D. Horn, and E. K. Warburton, Phys. Rev. C **28**, 1171 (1983).
[13] K. Auranen, J. Uusitalo, S. Juutinen, U. Jakobsson, T. Grahn, P. T. Greenlees *et al.*, Phys. Rev. C **91**, 024324 (2015).
[14] K. Auranen, J. Uusitalo, S. Juutinen, H. Badran, F. Defranchi Bisso, D. Cox *et al.*, Phys. Rev. C **97**, 024301 (2018).
[15] T. P. Sjoreen, D. B. Fossan, U. Garg, A. Neskakis, A. R. Poletti, and E. K. Warburton, Phys. Rev. C **25**, 889 (1982).
[16] R. F. Davie, A. R. Poletti, G. D. Dracoulis, A. P. Byrne, and C. Fahlander, Nucl. Phys. A **430**, 454 (1984).
[17] T. P. Sjoreen, U. Garg, and D. B. Fossan, Phys. Rev. C **23**, 272 (1981).
[18] T. P. Sjoreen, G. Schatz, S. K. Bhattacherjee, B. A. Brown, D. B. Fossan, and P. M. S. Lesser, Phys. Rev. C **14**, 1023 (1976).
[19] J. Adam, A. Kuklik, A. Spalek, D. Venos, and M. J. Kuznetsova, Czech. J. Phys. B **28**, 857 (1978).
[20] V. Rahkonen and T. Lonnroth, Z. Phys. A: At. Nucl. (1975) **322**, 333 (1985).
[21] P. Mukherjee, P. Sen, I. Mukherjee, and C. Samanta, J. Phys. G **16**, L107 (1990).
[22] S. Bayer, A. P. Byrne, G. D. Dracoulis, A. M. Baxter, T. Kibédi, and F. G. Kondev, Nucl. Phys. A **694**, 3 (2001).
[23] A. K. Jain, B. Maheshwari, S. Garg, M. Patial, and B. Singh, Nucl. Data Sheets **128**, 1 (2015).
[24] H. Beuscher, D. R. Zolnowski, D. R. Haenni, and T. T. Sugihara, Phys. Rev. Lett. **36**, 1128 (1976).
[25] A. M. Baxter, A. P. Byrne, G. D. Dracoulis, R. A. Bark, F. Riess, A. E. Stuchbery, M. C. Kruse, and A. R. Poletti, Nucl. Phys. A **515**, 493 (1990).
[26] V. Rahkonen, B. Fant, and C. J. Herrlander, Phys. Scr. **34**, 720 (1986).
[27] B. Fant, T. Weckstrom, and A. Kallberg, Phys. Scr. **41**, 652 (1990).
[28] V. Rahkonen and T. Lönnroth, Nucl. Phys. A **464**, 349 (1987).
[29] R. G. Helmer and C. W. Reich, Phys. Rev. C **27**, 2248 (1983).
[30] N. Bijnens, P. Decrock, S. Franchoo, M. Gaelens, M. Huyse, H.-Y. Hwang, I. Reusen, J. Szerypo, J. von Schwarzenberg, G. Vancraeynest, P. Van Duppen, and J. Wauters, Phys. Rev. C **58**, 754 (1998).
[31] O. Häusser, T. K. Alexander, J. R. Beene, E. D. Earle, A. B. McDonald, F. C. Khanna, and I. S. Towner, Nucl. Phys. A **273**, 253 (1976).
[32] S. Nagamiya and T. Inamura, Nucl. Phys. A **182**, 84 (1972).
[33] S. Muralithar, K. Rani, R. Kumar, R. P. Singh, J. J. Das, J. Gehlot *et al.*, Nucl. Instrum. Methods Phys. Res., Sect. A **622**, 281 (2010).
[34] M. Jain, E. T. Subramaniam, and S. Chatterjee, Rev. Sci. Instrum. **94**, 013304 (2023).
[35] R. Brun and F. Rademakers, Nucl. Instrum. Methods Phys. Res., Sect. A **389**, 81 (1997).
[36] D. C. Radford, Nucl. Instrum. Methods Phys. Res., Sect. A **361**, 297 (1995).
[37] A. Krämer-Flecken, T. Morek, R. M. Lieder, W. Gast, G. Hebbinghaus, H. M. Jäger, and W. Urban, Nucl. Instrum. Methods Phys. Res., Sect. A **275**, 333 (1989).
[38] K. Yadav, A. Y. Deo, Madhu, Pragati, P. C. Srivastava, S. K. Tandel, S. G. Wahid, S. Kumar, S. Muralithar, R. P. Singh, Indu Bala, S. S. Bhattacharjee, Ritika Garg, S. Chakraborty, S. Rai, and A. K. Jain, Phys. Rev. C **105**, 034307 (2022).
[39] Pragati, A. Y. Deo, S. K. Tandel, S. S. Bhattacharjee, S. Chakraborty, S. Rai, S. G. Wahid, S. Kumar, S. Muralithar, R. P. Singh, Indu Bala, Ritika Garg, and A. K. Jain, Phys. Rev. C **97**, 044309 (2018).
[40] G. Duchêne, F. A. Beck, P. J. Twin, G. de France, D. Curien, L. Han, C. W. Beausang, M. A. Bentley, P. J. Nolan, and J. Simpson, Nucl. Instrum. Methods Phys. Res., Sect. A **432**, 90 (1999).
[41] J.-M. Régis, G. Pascovici, J. Jolie, and M. Rudigier, Nucl. Instrum. Methods Phys. Res., Sect. A **622**, 83 (2010).
[42] D. J. Hartley, E. P. Seyfried, W. Reviol, D. G. Sarantites, C. J. Chiara, O. L. Pechenaya, K. Hauschild, A. Lopez-Martens, M. P. Carpenter, R. V. F. Janssens, D. Seweryniak, and S. Zhu, Phys. Rev. C **78**, 054319 (2008).
[43] A. R. Poletti, G. D. Dracoulis, A. P. Byrne, A. E. Stuchbery, B. Fabricius, T. Kibédi, and P. M. Davidson, Nucl. Phys. A **615**, 95 (1997).
[44] L. G. Mann, K. H. Maier, A. Aprahamian, J. A. Becker, D. J. Decman, E. A. Henry, R. A. Meyer, N. Roy, W. Stöffl, and G. L. Struble, Phys. Rev. C **38**, 74 (1988), and references therein.
[45] B. A. Brown, Phys. Rev. Lett. **85**, 5300 (2000).
[46] G. Bertsch, J. Borysowicz, H. McManus, and W. G. Love, Nucl. Phys. A **284**, 399 (1977).

[47] G. H. Herling and T. T. S. Kuo, Nucl. Phys. A **181**, 113 (1972).
[48] E. K. Warburton and B. A. Brown, Phys. Rev. C **43**, 602 (1991).
[49] B. A. Brown and W. D. M. Rae, Nucl. Data Sheets **120**, 115 (2014).
[50] T. A. Berry, Z. Podolyák, R. J. Carroll, R. Lica, B. A. Brown, H. Grawe *et al.*, Phys. Rev. C **101**, 054311 (2020).
[51] E. Wilson, Z. Podolyák, H. Grawe, B. A. Brown, C. J. Chiara, S. Zhu *et al.*, Phys. Lett. B **747**, 88 (2015).
[52] Z. Podolyák, C. M. Shand, E. Wilson, B. A. Brown, H. Grawe, C. J. Chiara *et al.*, J. Phys.: Conf. Ser. **580**, 012010 (2015).
[53] T. Lönnroth, Z. Phys. A: At. Nucl. (1975) **307**, 175 (1982).
[54] W. F. Piel, Jr., T. Chapuran, K. Dybdal, D. B. Fossan, T. Lönnroth, D. Horn, and E. K. Warburton, Phys. Rev. C **31**, 2087 (1985).
[55] R. E. Stone, C. R. Bingham, L. L. Riedinger, R. W. Lide, H. K. Carter, R. L. Mlekodaj, and E. H. Spejewski, Phys. Rev. C **31**, 582 (1985).
[56] T. Lönnroth, C. W. Beausang, D. B. Fossan, L. Hildingsson, W. F. Piel, Jr., M. A. Quader, S. Vajda, T. Chapuran, and E. K. Warburton, Phys. Rev. C **33**, 1641 (1986).
[57] G. D. Dracoulis, G. J. Lane, A. P. Byrne, P. M. Davidson, T. Kibédi, P. H. Nieminen, H. Watanabe, A. N. Wilson, H. L. Liu, and F. R. Xu, Phys. Rev. C **80**, 054320 (2009).
[58] A. Maj, H. Grawe, H. Kluge, A. Kuhnert, K. H. Maier, J. Recht, N. Roy, H. Hübel, and M. Guttormsen, Nucl. Phys. A **509**, 413 (1990).
[59] F. G. Kondev, Nucl. Data Sheets **187**, 355 (2023).
[60] F. G. Kondev, Nucl. Data Sheets **177**, 509 (2021).
[61] F. G. Kondev, Nucl. Data Sheets **166**, 1 (2020).
[62] J. Chen and F. G. Kondev, Nucl. Data Sheets **126**, 373 (2015).
[63] B. Singh, D. Abriola, C. Baglin, V. Demetriou, T. Johnson, E. McCutchan, G. Mukherjee, S. Singh, A. Sonzogni, and J. Tuli, Nucl. Data Sheets **114**, 661 (2013).
[64] I. Bergström, B. Fant, C. J. Herrlander, K. Wikstrom, and J. Blomqvist, Phys. Scr. **1**, 243 (1970).
[65] I. Bergström and B. Fant, Phys. Scr. **31**, 26 (1985).
[66] M. Rejmund, K. H. Maier, R. Broda, B. Fornal, M. Lach, J. Wrzesinski, J. Blomqvist, A. Gadea, J. Gerl, M. Gorska, H. Grawe, M. Kaspar, H. Schaffner, C. Schlegel, R. Schubart, and H. J. Wollersheim, Eur. Phys. J. A **8**, 161 (2000).

APS (https://www.aps.org/)

PHYSICAL REVIEW C (/PRC/)
covering nuclear physics

Highlights (/prc/highlights) Recent (/prc/recent) Accepted (/prc/accepted) Collections (/prc/collections) Authors (/prc/authors)
Referees (/prc/referees) Search (/search) Press (/press) About (/prc/about) Editorial Team (/prc/staff) (/feeds)

Spectroscopic study of

Rozina Rahaman, Abhijit Bisoi, Ananya Das, Y. Sapkota, Arkabrata Gupta, S. Ray, S. Sarkar, Yashraj, A. Sharma, Bharti Rohila, I. Ahmed, Kaushik Katre, S. Dutt, S. Kumar, R. P. Singh, R. Kumar, and S. Muralithar
Phys. Rev. C **109**, 024318 – Published 15 February 2024

More

Article

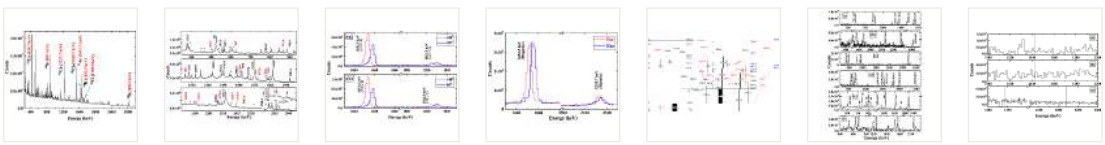
PDF (/prc/pdf/10.1103/PhysRevC.109.024318) **HTML (/prc/abstract/10.1103/PhysRevC.109.024318#fulltext)**

Export Citation (/prc/export/10.1103/PhysRevC.109.024318)

ABSTRACT
AUTHORS
ARTICLE TEXT
INTRODUCTION
EXPERIMENTAL DETAILS AND DATA ANALYSIS
RESULT AND DISCUSSION
THEORETICAL CALCULATION
CONCLUSION
ACKNOWLEDGMENTS
REFERENCES

ABSTRACT

High spin states of populated through the (2) reaction at 68 MeV beam energy were studied using the Indian National Gamma Array (INGA) facility. Six new levels and fourteen new transitions were added to the existing level scheme. The spins and parities of most of the levels were assigned, modified, or confirmed from , , and linear polarization measurements. The multipole mixing ratios O1 for most of the transitions were measured. Large-basis shell-model calculations were performed to understand the microscopic origin of the levels. Different particle restrictions in and shell orbitals were used to explain the experimental results.



6 More

Received 31 August 2023 Revised 21 December 2023 Accepted 19 January 2024

DOI: https://doi.org/10.1103/PhysRevC.109.024318

©2024 American Physical Society

Physics Subject Headings (PhySH)

This site uses cookies. To find out more, read our Privacy Policy (https://www.aps.org/about/privacy.cfm).

Research Areas

I Agree ()

Sign up to receive regular email alerts from *Physical Review C*

Sign up (https://info.aps.org/journals-emails)

ISSN 2469-9993 (online), 2469-9985 (print). ©2024 American Physical Society. (https://www.aps.org/) All rights reserved. *Physical Review C*™ is a trademark of the American Physical Society, registered in the United States, Canada, European Union, and Japan. The *APS Physics logo* and *Physics logo* are trademarks of the American Physical Society. Information about registration may be found here (/legal). Use of the American Physical Society websites and journals implies that the user has read and agrees to our Terms and Conditions (/info/terms.html) and any applicable Subscription Agreement (https://librarians.aps.org/sitelicense.pdf).

This site uses cookies. To find out more, read our Privacy Policy (https://www.aps.org/about/privacy.cfm).

I Agree ()

Already have a manuscript?

Use our Manuscript Matcher to find the best relevant journals!

Find a Match

Refine Your Search Results

2191-1649 Search

Sort By: Title (A-Z)

Search Results

Found 1 results (Page 1) Share These Results

Exact Match Found

BIONANOSCIENCE

Publisher: SPRINGER , ONE NEW YORK PLAZA, SUITE 4600 , NEW YORK, United States, NY, 10004

ISSN / eISSN: 2191-1630 / 2191-1649

Web of Science Core Collection: Emerging Sources Citation Index

Share This Journal View profile page

* Requires free login.

Filters Clear All

- *Web of Science* Coverage
- Open Access
- Category
- Country / Region
- Language
- Frequency
- Journal Citation Reports

1 – 1 of 1

Items per page: 10

Editorial Disclaimer: As an independent organization, Clarivate does not become involved in and is not responsible for the editorial management of any journal or the business practices of any publisher. Publishers are accountable for their journal performance and compliance with ethical publishing standards. The views and opinions expressed in any journal are those of the author(s) and do not necessarily reflect the views or opinions of Clarivate. Clarivate remains neutral in relation to territorial disputes, and allows journals, publishers, institutes and authors to specify their address and affiliation details including territory.

Criteria for selection of newly submitted titles and re-evaluation of existing titles in the Web of Science are determined by the Web of Science Editors in their sole discretion. If a publisher's editorial policy or business practices negatively impact the quality of a journal, or its role in the surrounding literature of the subject, the Web of Science Editors may decline to include the journal in any Clarivate product or service. The Web of Science Editors, in their sole discretion, may remove titles from coverage at any point if the titles fail to maintain our standard of quality, do not comply with ethical standards, or otherwise do not meet the criteria determined by the Web of Science Editors. If a journal is deselected or removed from coverage, the journal will cease to be indexed in the Web of Science from a date determined by the Web of Science Editors in their sole discretion – articles published after that date will not be indexed. The Web of Science Editors' decision on all matters relating to journal coverage will be final.

Clarivate.™ Accelerating innovation.

© 2024 Clarivate Legal center Privacy notice Cookie policy
Manage cookie preferences Copyright notice Help

ISSN 0975-5217
UGC-Care list (Group-I)

भैरवी

(दृश्य एवं प्रदर्शनकारी कला की शोध-पत्रिका)

(अप्रैल 2023)

(Special Volume)

मिथिलांचल संगीत परिषद्
स्नातकोत्तर संगीत एवं नाट्य विभाग
ललित कला संकाय
ललित नारायण मिथिला विश्वविद्यालय,
कामेश्वरनगर, दरभंगा 846 004

भैरवी (दृश्य एवं प्रदर्शनकारी कला की शोध-पत्रिका)

ISSN 0975-5217

UGC-Care list (Group-I)

अप्रैल-2023 (**Special Volume**)

प्रधान सम्पादक

प्रो. (डॉ.) पुष्पम नारायण

प्रकाशक : मिथिलांचल संगीत परिषद्

स्नातकोत्तर संगीत एवं नाट्य विभाग
ललित नारायण मिथिला विश्वविद्यालय,
कामेश्वरनगर, दरभंगा 846 004
मो. - 09430063265
ईमेल - npushpamji@gmail.com

मूल्य

इस अंक का मूल्य : 400/- रुपये

व्यक्तियों के लिए :

वार्षिक : 800/- रुपये / त्रैवार्षिक 2400/- रुपये

पंचवार्षिक 4000/- रुपये / आजीवन : 15000/- रुपये

संस्थाओं के लिए :

वार्षिक : 850/- रुपये / त्रैवार्षिक 2500/- रुपये

पंचवार्षिक 4500/- रुपये / आजीवन : 16000/- रुपये

(केवल मनी आर्डर / चेक / बैंक ड्राफ्ट से)
(दरभंगा से बाहर के चेक में 40 रुपये अधिक जोड़ें)

''भैरवी'' विश्वविद्यालय अनुदान आयोग नई दिल्ली द्वारा अनुमोदित एवं UGC-Care list (Group-1) में शामिल है। साथ ही यह Peer Reviewed Refereed Visual and Performing Arts Research Journal है।

सर्वाधिकार सुरक्षित
प्रकाशित सामग्री के उपयोग हेतु लेखक, प्रकाशक की अनुमति आवश्यक है।
प्रकाशित रचनाओं के विचार से सम्पादक व प्रकाशक का सहमत होना आवश्यक नहीं।
समस्त विवाद दरभंगा न्यायालय के अन्तर्गत विचारणीय।

मुद्रक : विकास कंप्यूटर एंड प्रिंटर्स, ट्रोनिका सिटी, लोनी, गाजियाबाद-201 102

Contents

1. Depicting Female Marginalization in Mamang Dai's Novel the Black Hill — *Nabanita Das, Dr. Ashutosh Thakare* — 19
2. A Sociolinguistic Study of the Marginalization Concept in Yemeni Context — *Salim Alshageri, Dr. Shailaja B. Wadikar* — 23
3. Reflection of Social Concerns and Caste Preoccupations in Premanand Gajvi's Kirvant — *Dr. Rajashri Barvekar, Shantanu Patil* — 28
4. A Critical study of Lady Chatterley's Lover from an ecofeminist approach — *Syed Abdul Quader* — 33
5. Marginalization and Social Mobility of Dalits: Study of Uchalya: The Branded — *Dhammapal Shrirang Nangare, Dr. Sunil Raosaheb Raut* — 37
6. Reading caste and Patriarchy Through Dalit Feminist Lens: A Study of Meena Kandasamy's selected poems — *Swati Niwrutirao Adode* — 42
7. Dalit, An Emblematic Study of Marginality in Aspect of Babytai Kamble's Text The Prison We Broke — *Chhoton Babu Molla* — 46
8. African American Voices An Introduction to African American Criticism — *Dr. Quadri Syeda Arshia Farooq Hussain* — 50
9. An Analysis of Sister of My Heart by Chitra Banerjee Divakaruni: Women's Struggle to find Their Identity — *Mr. Bhojraj Pandhari Shrirame, Dr. Sunil G. Chaudhari* — 54
10. Narration of Painin Baby Kamble's The Prisons We Broke — *Dr. Lahoti R.K. & Dr.Landage R.A.* — 58
11. Sexuality and Marginality : A Brief Study of Stories of Ismat Chughtai — *Dr. Abul Hasib Siddiqui* — 63

An Analysis of *Sister of My Heart* by Chitra Banerjee Divakaruni: Women's Struggle to find Their Identity

Mr. Bhojraj Pandhari Shrirame*, Dr. Sunil G. Chaudhari**

Abstract

Chitra Banerjee Divakaruni is primarily concern with how difficult it is for women in contemporary Indian society to find and preserve their identity as wife, mother and most of all as human beings. Sister of My Heart (1999) is a realistic novel enrich with myths, folktales, and fairy tales about India and Hindu religion. The story of this novel explores the struggle and sufferingof the characters go through as they skillfully negotiate between the conventional and the modern worlds and how these individual develop as a result of striking a balance between their long cherished belief and unexpectedly modern aspirations. This research article intended to examine various hegemony, patriarchy and other issues in both the eastern and western contexts. It also shows the conflict of a woman trying to find her own existence by creating her own identity.

Keywords: *Woman, hegemony, patriarchy, conflict.*

Introduction

The story of the novel *Sister of My Heart* revolves around the protagonists Anju and Sudha, born on the same day. It follows them on a ruby exploration journey to find out more about their father's death.The novel continued with the tension between the desires of mothers who hold onto traditional Indian culture and the two young girls who adopt the new western culture. The two girls, Anju and Sudhaare positioned against their mother figures, who represents normative patriarchal concepts. Divakaruni challenges the imperial and patriarchal discourses simultaneously. Through Sudha, she is introduced as being passive, rooted in tradition and unquestioningly accepting the stringent codes of conduct set by the family. Through Anju, she uses her rebellious nature to demolish the western myth of superiority and validity.

*Assistant Professor, J. M. Patel Arts, Commerce & Science College, Bhandara

**Associate Professor, N. H. College, Bramhapuri

Divakaruni's novel *The Princess in the Palace of Snakes* tells the story of a princess who lives in an underwater palace filled with snakes. In this part of the novel, both the protagonists attempt to conform to the feminine roles allocated by the male hegemonic society. She employs mythological metaphors to heighten the vividness of her characters' experiences. Sudha and Anju are cousins by birth in Calcutta, India. They were brought up together by their widowed mothers and aunt. The first part of the novel, The Princes in the Palace of Snakes, follows the theme from birth until the wedding day.Their favourite game was acting out the fairy tales Pishi told us, where Sudha was always the princess and Anju was the prince who rescued her. When we had nightmares, instead of going to our mothers for comfort, we squeezed into bed and held each other.

Anju and Sudha are two baby-girls born with "so much bad luck that they cause their fathers to die even before they are born" (SMH6). Their determination sustains them through the difficulties and deceptions they encounter as adults. Anju has more social and economic advantages than Sudha because Anju is a proud heritor of the Chatterjee family. Sudha's dream for the future is to be a wife and mother, steeped in Indian culture. Due to the good grace and dependency on Gauri Ma, Sudha is more likely to fall under the burden of the traditional Hindu-Indian gender norms. Anju's mother, Gauri Ma is the head of the Chatterjee household. Gauri Ma risks her health by managing the family bookstore. Sudha's mother, Nalini wants to lead a luxurious life. The two women are burdened by the violent and mysterious deaths of their husbands. Pishi tells the children stories and plays a pivotal role in upholding the prestige of the house.

Divakaruni explores the psyche of middle class educated Indian women, focusing primarily on Anju's dilemma of being caught between modernity and the patriarchal and traditional values that continue to permeate contemporary Indian society. Anju is determined not to follow in the footsteps of the women of the Chatterjee household. She yearns to be modern in her thinking and attitude.

Anju and Sudha get married and attempt to deal with the fluctuating undulations in the life of an immigrant woman in the US and the placid life of conformity led by a married woman back in India. "The house of marriage" turns out to be for both the women, like "many locked rooms" (SMH 166), as Sudha begins to wilt under the duress of "ownership" that her husband claims for her. Anju strives to ward off everyone who appears like "an intruder" on her freedom, including her tyrannical father-in-law.

A few days after the wedding, Mrs. Sanyal was handed over the ring of keys to Sudha with the instructions, "NutanBau, this is your home now; take charge of it". It is difficult for Mrs. Sanyal to give up responsibilities. Although circumstances different in America, the predicament remains the same for Anju and Sudha. Anju does not wish to lead a mechanical life, which according to an Indian.She dreams of a healthy, happy relationship with Sunil according to a western model of equality and respect, but the western image has actually trapped her into a conventional bond with all the associated problems. Anju presents the cultural bias of the colonised hybrid. She is an ardent admirer of western literature and constantly interrogates the validity of native culture.

Divakaruni has shown through her fiction that our tradition and myths have helped Indian immigrants to establish their roots in an alien land. It is only when Sudha tells a story based on Indian mythology to Anju over the phone that her drooping spirit is revitalized. The thematic pattern strands together the fates of Anju and Sudha, exposing them both to the daunting determinism of familial expectations, as custodians of what constitutes an authentic notion of Indians. The thematic pattern strands together the fates of Anju and Sudha, exposing them to the daunting expectations of family. Precisely, the same kind of socio-moral determinism now coils around Sudha.

Divakaruni portrays the societal norm that perpetuates female foeticide in India. Western society is so family-oriented that you give up your individual desires for the good of the family, says Sunil. In western society, people are individualistic and do not compromise with their desires. He is not bothered about Sudha when his mother compels Sudha to abort the girl child. Further, Sudha's mother, Nalini Ma, does not hesitate to sacrifice her own daughter's happiness or even her granddaughter's life, when it comes to saving face in her honor-conscious prestige and scandal-obsessed society. The upholders of the family traditions, Pishi and Gouri Ma come to the rescue of Sudha.

Once again, it's a climatic juncture that Anju imparts to Sudha the strength of her reckless decision, which encourages her to take on a hard journey. Sudha personifies much like Anju, the portrait of women who want to forge a new future that is free of the compelling need to surrender to the creed of women's denigration. Despite the clouded fear of being an alien, Sudha feels invigorated with the prospect of anonymity and solidarity that life in America would bring to her. She affirms: I am going for Anju, yes and for Dayita, but most of all I am going for me. Do I want to return? And if I do return? Will I be happy

trying myself on a man's whim again, even if he is a good man?

Divakaruni brings out the negative aspects of traditional Indian society. Through the various interactions of Sudha and Anju with their lovers, husbands and in-laws, she exposes the negative parts of society. As Anju grudgingly points out, this society wants its women to be nothing more than "good breeding stock" (SMH 98).Divakaruni has delineated both western and eastern culture in the novel. Anju, who used to complain about the noise and lack of privacy in her mother's home back in India, now ardently yearns for the din and hustle in her desolate apartment in America. Freedom and riches in the west are often bought at the expense of the extended family or the community. No doubt, America adds confidence of the Indian male, endowing him with a certain light-heartedness and ease that allows him to trust his partner's vivacity and enterprise which comes in place of family life and peacefulness.

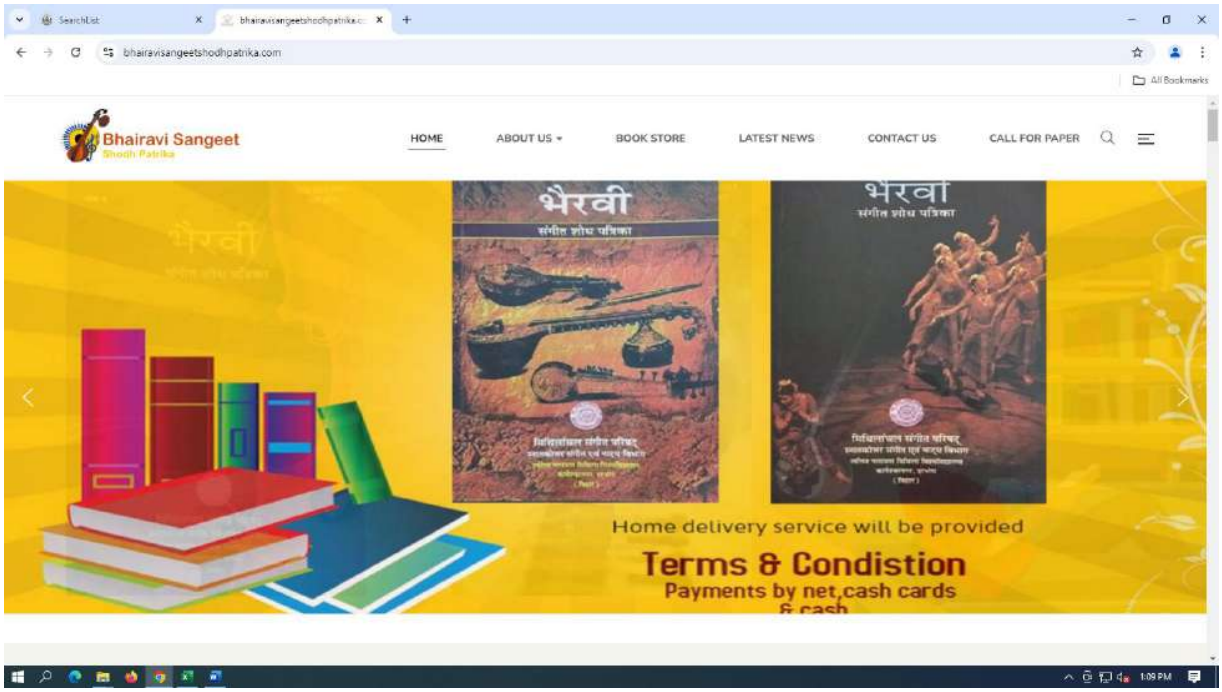
Chitra Banerjee Divakaruni's Sister of My Heart celebrates the tenuous bonds between women, tried and tested against the citadel of convention, the strife of being torn between two worlds, the traditional India and the modernized west. The novel ends not with the celebration of assimilation but with the creation of a new identity and a new home.

Conclusion:

The relationship between India and the United States is one of a hybridized sensibility as it bridges home and exile, subjectivity and agency, domination and subjugation. It exposes the slippages inherent in our construct of ethnicity, sexuality and identity against the broader framework of a transcultural experience that gravitates between Indian and American culture. In the fiction of Divakaruni, connections between women consolidate the platform from which women struggle to find their identity. It is a microcosmic representation of the lives lived by women to extricate themselves from meaningless relationships and rewrite their strategies of survival.

References:

1. Agnihotri, Neeraj. "Diasporic Consciousness in Chitra Banerjee Divakaruni's Sister of My Heart." Galaxy 3.1 (2014): 1-6. Web. 18 Feb. 2014.
2. Aldama, Frederick Luis. "Unbraiding Tradition: An Interview with Chitra Divakaruni." JSAL 35.1/2 (2000): 1- 12. JSTOR. Web. 19 Sep. 2013.
3. Alexander, Meena. The Shock of Arrival: Reflections on Postcolonial Experience. Boston: South P, 1996. Print.
4. Deshpande, Shashi. "Telling Our Own Stories." Writing From the Margin and Other Essays. India: Penguin, 2003. Print.
5. Kaur, Paramjit. "Tradition v/s Modernity in Manju Kapur's Novel – Difficult daughters." IJAR 3.6 (2013): 42-43. Print.


bhairavisangeetshodhpatrika.com
Bhairavi Sangeet
Shodh Patrika
HOME
ABOUT US
BOOK STORE
LATEST NEWS
CONTACT US
CALL FOR PAPER
भैरवी
संगीत शोध पत्रिका
भैरवी
संगीत शोध पत्रिका
Home delivery service will be provided
Terms & Condistion
Payments by net,cash cards
& cash

UGC-CARE List

You searched for "**0975-5217**". Total Journals : **1**

Search:

Sr.No.	Journal Title	Publisher	ISSN	E-ISSN	UGC-CARE coverage years	Details
1	Bhairavi (print only)	Mithilanchal Sangeet Parishad	0975-5217	NA	from October-2021 to July-2023	Discontinued from July 2023

Showing 1 to 1 of 1 entries

Previous 1 Next

Copyright © 2024 Savitribai Phule Pune University. All rights reserved. | Disclaimer

ISSN 2063-5346

ANALYSING VIRTUAL AND AUGMENTED REALITY APPLICATIONS IN DIGITAL MARKETING

Dr. ANAND MULEY,
Assistant Professor, Department of Commerce, J. M. Patel Arts Commerce and Science College Bhandara, Maharashtra.

SAKSHI PANDEY,
Assistant Professor, Faculty of Commerce and Business Management Amrapali Group of Institutes, Haldwani, Uttarakhand.

Dr. N.V.S. NATTESHAN,
Assistant Professor, Department of CSE, School of Computing, Kalasalingam Academy of Research and Education, Krishnan Koil, India.

SHARDUL SINGH CHAUHAN,
Assistant Professor, Computer Science Department, ABES Engineering College, Ghaziabad, Uttar Pradesh.

ARJUN SINGH
Associate Professor, Department of Computer and Communication Engineering, Manipal University Jaipur, India.

Article History: **Received:** 01.02.2023 **Revised:** 07.03.2023 **Accepted:** 10.04.2023

Abstract

Virtual reality (VR) and augmented reality (AR) have recently emerged as potent technologies that provide immersive experiences and make it possible for marketers to engage customers in novel ways. When it comes to digital marketing, the advantages of virtual reality (VR) and augmented reality (AR) include their capacity to deliver highly immersive experiences, establish emotional connections with users, and supply valuable data and insights. The attention of users is captured by these technologies, which also make it possible to tell interactive stories and enable personalized marketing campaigns based on users' actions. When analyzing the applications of virtual reality and augmented reality in digital marketing, several challenges and factors need to be taken into consideration. These include the availability and use of virtual reality and augmented reality technologies, the financial and time investments necessary for development, as well as the measurement and evaluation of the effectiveness of marketing campaigns. Marketers can make educated decisions about whether or not to include virtual reality and augmented reality in their digital strategies if they have a thorough understanding of the specific advantages and drawbacks of these two technologies. Marketers can take advantage of the potential of virtual reality and augmented reality to create memorable brand experiences, increase customer engagement, and accomplish their marketing goals by giving careful consideration to their target audience,

conducting cost-benefit analyses, and defining relevant key performance indicators (KPIs). The purpose of this research is to conduct an analysis of the applications of virtual and augmented reality in digital marketing in order to gain insights into how these technologies can be leveraged to improve customer engagement and brand experiences. Marketers can strategically integrate virtual reality and augmented reality technologies into their digital marketing strategies if they have a thorough understanding of the benefits and challenges associated with these technologies. This will, in the end, result in improved campaign outcomes and customer relationships. The purpose of this study is to investigate the various aspects of incorporating virtual reality and augmented reality into digital marketing strategies, including the potential benefits, potential challenges, and potential considerations.

Keywords: AR, VR, Digital Marketing, Business, Virtual

Introduction

Virtual reality (VR) and augmented reality (AR) are two powerful technologies that have emerged in recent years and have the potential to revolutionize a variety of industries, including digital marketing. Immersive experiences are offered by both virtual reality (VR) and augmented reality (AR), allowing users to interact with virtual environments or superimpose digital information onto the real world. These technologies have opened up exciting new possibilities for marketers to engage customers in novel ways and to create experiences that customers will remember for their brands.

Analyzing the applications of virtual reality and augmented reality in digital marketing entails researching the various ways in which these technologies can be successfully incorporated into marketing campaigns in order to boost customer engagement, increase brand awareness, and ultimately accomplish marketing goals. Marketers can make educated decisions about whether or not to include virtual reality and augmented reality in their digital strategies if they have a thorough understanding of the specific advantages and drawbacks of these two technologies.

Benefits of virtual and augmented reality in digital marketing

Applications that utilize virtual and augmented reality provide a number of benefits to businesses that engage in digital marketing. To begin, they deliver highly immersive experiences that seize the attention of users and leave impressions that stick with them for a long time. Virtual reality (VR) and augmented reality (AR) have the potential to offer users a sense of presence and interactivity that is difficult for traditional marketing mediums to achieve. This is because VR and AR can transport users into virtual worlds, while AR can overlay digital content onto the real world.

Second, virtual reality and augmented reality make it possible for marketers to tell emotionally engaging brand stories that engage users on a deeper level. Brands have the ability to elicit potent feelings in their target audience as well as forge deeper connections with them by utilizing techniques such as interactive experiences and storytelling. Because of this emotional resonance, increased brand loyalty and advocacy are possible outcomes.

In addition, both virtual and augmented reality have the potential to supply marketers with valuable data and insights. Marketers can gain a better understanding of customer preferences, interests, and purchasing patterns by analysing the interactions and behaviours of users within these immersive environments. This approach, which is driven by data, makes it possible to create marketing campaigns that are more personalized and targeted, which leads to higher conversion rates and a better return on investment.

Challenges and considerations

Keep in mind that despite the fact that virtual and augmented reality present digital marketers with exciting new opportunities, there are also challenges and factors to take into consideration. The availability of virtual reality and augmented reality technology presents a significant obstacle. Although in recent years these technologies have become easier to access, they still call for specialized hardware, and it is possible that they will not

be widely adopted by the general population. It is important for marketers to consider whether or not their target audience is ready and willing to participate in virtual reality and augmented reality experiences.

Another factor to take into account is the financial and time commitment necessary to create VR and AR applications of a sufficient quality. Developing experiences that are both immersive and engaging can require a significant investment of resources and the expertise of developers, designers, and content creators. When considering whether or not to include virtual reality and augmented reality in their digital marketing strategies, businesses need to conduct a thorough cost-benefit analysis. Last but not least, the measurement and evaluation of virtual reality and augmented reality campaigns can be difficult. When attempting to evaluate the significance and efficiency of immersive experiences, it is possible that traditional marketing metrics will not be directly applicable. For the purpose of tracking user engagement, conversion rates, and the overall success of a campaign, marketers need to define pertinent key performance indicators (KPIs) and make use of advanced analytics tools.

Augmented reality and digital marketing business

Within the realm of digital marketing, augmented reality, also known as AR, has emerged as a powerful tool for use by businesses. It presents one-of-a-kind opportunities to drive conversions, engage customers, and create immersive brand experiences.

Here are some highlights on how augmented reality can be integrated into digital marketing strategies:

- Augmented reality makes it possible for companies to provide their customers with interactive and interesting brand experiences. AR applications allow users to interact with products, try virtual samples, and explore brand stories in a more immersive and memorable way than was previously possible. These interactions are made possible by superimposing digital content onto the real world. Because of the interactivity, customers are more engaged, and they are more likely to remember the brand.
- Augmented reality is a tool that can be used to improve social media marketing efforts, and this tool can be activated through social media. AR filters and effects on social media platforms such as Instagram and Snapchat enable users to incorporate branded AR experiences into their content, allowing for user-generated brand advocacy and virality. Social media campaigns that are powered by augmented reality have the potential to generate buzz, increase brand visibility, and drive user participation.
- Augmented reality (AR) offers a one-of-a-kind opportunity for businesses to showcase their goods or services in a virtual environment. This gives customers the ability to visualize and customize their experiences with the goods or services being offered. AR applications allow users to virtually try on clothing, decorate their homes with virtual furnishings, and even see how cosmetics look when applied to their faces. The customer's understanding is improved, and they are better able to make decisions about their purchases as a result of this immersive product visualization.
- Augmented reality applications produce valuable data and insights that can be used to inform digital marketing strategies. Businesses are able to gain insights into customer preferences, behaviors, and purchase patterns through the analysis of user interactions within augmented reality (AR) experiences. This approach, which is driven by data, makes it possible to create marketing campaigns that are more personalized and targeted; as a result, customer engagement is improved, and conversion rates are increased.
- Before integrating augmented reality into digital marketing strategies, businesses should first define clear objectives and determine how AR aligns with their overall marketing goals. This should be done before

integrating augmented reality into digital marketing strategies. Having a clear focus will guide the development and execution of augmented reality (AR) campaigns, regardless of whether that focus is on increasing brand awareness, driving conversions, or improving customer engagement.

- To get the most out of augmented reality (AR) in digital marketing, companies need to ensure that it is seamlessly integrated with all of the different marketing channels. AR experiences may be integrated into a variety of mediums, including websites, mobile applications, social media platforms, and even physical stores. A unified and immersive experience for the customer can be achieved by maintaining consistent branding and messaging across all of these channels.
- Experts to Develop High-Quality Augmented Reality Experiences Creating high-quality AR experiences requires expertise in the development and design of Augmented Reality. Businesses should form partnerships with seasoned augmented reality (AR) professionals or agencies that can assist in the production of AR applications that are both interesting to users and technically sound. Through this collaboration, we can ensure that the augmented reality experience will deliver a seamless user experience while also aligning with marketing goals.
- The user experience in augmented reality applications is very important. The user interface needs to be straightforward, simple, and straightforward, and it needs to provide clear instructions for users on how to interact with the augmented reality content. Putting an emphasis on providing a pleasant experience for users will increase engagement as well as positive interactions with the brand.
- Integrating augmented reality into digital marketing strategies necessitates performing ongoing measurement and optimization. The performance of augmented reality (AR) campaigns should be monitored by establishing relevant KPIs for businesses to use, such as user engagement, conversion rates, and social media reach. The analysis of these data will provide insights that can be used to improve the efficiency of campaigns and optimize augmented reality strategies.

Virtual reality and digital marketing business

The game-changing technology known as virtual reality (VR) has the potential to have a significant influence on digital marketing strategies. It offers experiences that are completely encompassing, making it possible for businesses to engage customers in novel and compelling ways.

Here are some highlights on how virtual reality can be integrated into digital marketing strategies:

- ✓ Virtual reality enables companies to create experiences that are both immersive and memorable for their brands. Virtual reality (VR) applications have the ability to showcase products, services, or brand narratives in a manner that is highly engaging and interactive by transporting users to virtual environments. Customers are left with an indelible impression as a result of this immersive experience, which encourages brand loyalty and advocacy.
- ✓ VR paves the way for businesses to conduct product demonstrations conducted in a virtual environment, enabling customers to experience and interact with the products in question. Customers can explore properties, test drive virtual vehicles, or take virtual tours thanks to this capability, which is particularly useful for businesses in the real estate, automotive, and tourism industries. Customers have a better understanding of the product, more confidence in their ability to make purchasing decisions, and less need for physical prototypes when virtual product demonstrations are used.
- ✓ Virtual reality (VR) can recreate physical showrooms and retail spaces in

virtual environments. Within the virtual reality setting, consumers are able to navigate and interact with virtual shelves, look through product catalogs, and make purchases. This removes the restrictions that are imposed by the availability of physical space, broadens the market's reach, and offers customers a shopping experience that is both unique and convenient.

- ✓ Virtual reality (VR) can be used for training employees, particularly in industries that require hands-on experience or deal with complex procedures. VR is particularly useful for training employees in these types of industries. Employees are able to practice their skills, gain expertise, and improve their performance all within a setting that is safe and well-controlled thanks to the use of virtual simulations and scenarios. When compared to more conventional methods of instruction, VR-based training programs may prove to be both more efficient and cost-effective.

Review Literature

Grudzewski, Awdziej, Mazurek, and Piotrowska (2018) say that effective use of marketing communication requires not only a good understanding of social phenomena and market processes, but also an understanding of the tools and information communication technology used in the process. Hajduk (2016) says that businesses that use modern marketing communication methods and tools can talk to customers and other important people in their marketing environment in a quick and effective way. There are more and more marketing campaigns out there that use VR. In general, they can be put into two groups: those that depend on how the person sees things and those that depend on how other people see things (Pindel, 2015). When it comes to the first group of consumers, they have all the tools they need and are ready to get promotional messages at any time or place. After that, ads are usually shared through social media, such as by uploading them to YouTube or putting them on the website of a certain brand. (Jang, Hur, and Choo, 2019; Steuer, 1992) say that virtual reality (VR) creates an environment where a person can feel like they are physically present. So, VR could be a good way to make shopping the same both online and offline. The same author (Steuer, 1992) puts a lot of weight on the ideas that vividness and interactivity are the two most important things that can have a big impact on how people feel in a virtual world. More research in this area (Steuer, 1992) supports the idea that the two variables above make up telepresence, which is a key concept for understanding virtual experience. Bigné, Llinares, and Torrecilla (2016) say that test labs have already started using virtual reality as a way to gather data that can be used to predict how customers will act when they shop in traditional stores. (Lau, Lau, and Kan, 2012) Modern researchers spend a lot of time trying to figure out how virtual reality will affect customer behavior and the buying experience, which is what the customer has when they buy something. Also, the simulation showed a number of different ways to sort food, all of which were shown in a very easy-to-understand graphical format. This made it easier for the users to understand the basic ideas behind how the system worked. From inside the machines, visitors could look at the sorting processes from any angle. With the help of this strategy, Key Technology was able to show that their system was unique and very effective compared to the solutions offered by their direct competitors. The project was part of a large B2B market campaign that was meant to raise brand awareness among companies in the food industry and make the complex techniques and technologies used to process food easier to understand (Becker, 2019). The goal of the campaign was to show how the food industry uses techniques and technologies. Visitors were given virtual reality goggles and asked to look at and learn about the network's production lines (Feltham, 2016). This was done to help them build their brand and get over the idea that fast-food products are highly processed and unhealthy, which is how most people think about them. Kumar, D. (2019), observed that recent developments in virtual reality and augmented reality have resulted in the creation of several applications that are garnering increased interest from researchers

and professionals working in business enterprises. As augmented reality (AR) and virtual reality (VR) technologies advance, the number of scientific applications that can make use of them also grows. Virtual reality (VR) and augmented reality (AR) are proving their worth particularly once designing particularly planning, marketing, education, and tourist sport preservation are coming into light. The purpose of this research paper is to shed light on some of the most important technologies for use in business and social settings, particularly as they relate to AR and VR.

Problem Statement

Despite the increasing popularity and potential of VR and AR applications in digital marketing, a thorough examination of their efficacy, challenges, and considerations is required. Businesses are unable to reap the full benefits of VR and AR because they do not understand how to incorporate them into digital marketing strategies. There are no standardized metrics or evaluation frameworks for digital marketing VR and AR applications. Because VR and AR campaigns are difficult to measure, ROI and justification are difficult. VR and AR adoption is hampered by specialized hardware, high costs, and technological limitations. Due to the limited availability of VR and AR, businesses struggle to reach and engage customers. It takes time and expertise to create engaging VR and AR content. Many businesses are unsure of how to create engaging brand experiences that align with their marketing objectives. To seamlessly integrate VR and AR into digital marketing channels and platforms, careful planning and execution are required. Not all target audiences are open to VR and AR or have the necessary devices. Understanding the demographics, preferences, and technological readiness of the target audience is required for incorporating VR and AR into digital marketing strategies.

VR and AR implementations necessitate significant investments in technology, content, and expertise. Companies must evaluate cost-benefit analysis and resource allocation to ensure the success of VR and AR projects. Businesses must address these challenges and considerations in order to make informed VR and AR digital marketing decisions. To successfully implement virtual reality and augmented reality in digital marketing, you must first assess effectiveness, ROI, user adoption barriers, content creation and integration, target audience relevance, and resource allocation.

Research Methodology

This study is based both on primary & secondary data. The primary data has gathered from 04 different digital marketing-based companies located in Maharashtra. Total 220 respondents filled questionnaire for the study. Factor analysis & KMO and Bartlett's Test, reliability test has used for analysis. Secondary data has been collected from web sources, e-portals, journals etc.

Objective of the study

- To describe the concept of AR/VR applications on digital marketing.
- To investigate the various aspects of incorporating virtual reality and augmented reality into digital marketing strategies.

Hypothesis of the study

H1: There is no significant influence of VR/AR applications on digital marketing

H1: There is significant influence of VR/AR applications on digital marketing

H2: There is no significant influence of investigating the various aspects of incorporating virtual reality and augmented reality into digital marketing strategies.

H2: There is significant influence of investigating the various aspects of incorporating virtual reality and augmented reality into digital marketing strategies.

Results & Discussion

Table 1: Reliability Test

Cronbach's Alpha	Cronbach's Alpha Based on Standardized Items	N of Items	Mean	Std. Deviation
0.795	0.799	17	92.423	14.8823

Cronbach's alpha was calculated for this set of questions using SPSS, and the value was 0.795, which is excellent (a Cronbach's alpha value greater than 0.6). The mean score for the final set of 17 questions on the questionnaire was 92.423, with a standard deviation of 14.8823.

Table 2: KMO and Bartlett's Test

KMO and Bartlett's Test		
Kaiser-Meyer-Olkin Measure of Sampling Adequacy.		.897
Bartlett's Test of Sphericity	Approx. Chi-Square	1987.625
	Df	220
	Sig.	.001

Table 3: Factor Loading Matrix

Items	Factor Loadings	% Variance Explained	Factor	Alpha
Define Clear Objectives	0.772	62.716		0.909
Seamless Integration with Channels	0.667		Functional and User-Friendly Activation	
Collaborate with AR Experts	0.776			
User-Friendly Experience	0.689			
Measurement and Optimization	0.665			
Interactive Brand Experiences	0.698			
Social Media Activation	0.774			
Product Visualization and Personalization	0.678			
Data and Insights	0.779			
Enhanced Customer Engagement	0.567			
Improved Brand Awareness	0.789			
Personalized and Targeted Marketing	0.678	7.896	Transformation in Collaboration & Marketing Research to Achieve Target	0.823
Cost and Accessibility Challenges	0.779			
Audience Research and Targeting	0.765			
Strategic Integration	0.678			
Collaborate with Experts	0.713			
Measurement and Analysis	0.689			

The 17 assertions were subjected to principal component analysis to see if any factors could be extracted for further investigation. To be used for the Varimax orthogonal

rotation, significant factors had Eigen values greater than one. In the analysis of the 17-item questionnaire about the elements of AR & VR for digital marketing, only items with factor loadings of 0.5 or more were examined, and two factors were discovered, namely Functional and User-Friendly Activation, and Transformation in Collaboration & Marketing Research to Achieve Target.

Table 4: Model Summary

Model	R	R Square	Adjusted R Square	F Change	Sig. F Change
1	0.712	.398	.391	322.761	.001
2	0.710	.788	.788	74.543	.001

In regression analysis, the R, R square, and adjusted r square values were written on a table, and it was shown that the estimated value of r is always more than 30%. So, the independent variables under study have a big effect on the dependent variable of digital marketing.

Hypothesis Testing

Applications of Regression analysis, Reliability test, KMO Bartlett test & Factor loading matrix, the findings of the research stated that null hypothesis which is "there is no significant influence of VR/AR applications on digital marketing" & "there is no significant influence of investigating the various aspects of incorporating virtual reality and augmented reality into digital marketing strategies" is rejected and alternative hypothesis which is there is significant influence of VR/AR applications on digital marketing & there is significant influence of investigating the various aspects of incorporating virtual reality and augmented reality into digital marketing strategies is accepted.

Findings:

- Applications of virtual and augmented reality in digital marketing have shown the ability to significantly improve customer engagement, and this trend is expected to continue.
- Because of the immersive nature of these technologies, users' attention is easily captured, which enables brands to create experiences that are both interactive and memorable. Because users are more likely to spend more time interacting with VR and AR content, this can result in increased brand exposure as well as deeper emotional connections.
- Virtual reality (VR) and augmented reality (AR) applications provide one-of-a-kind opportunities to build brand awareness and generate buzz.
- Brands that are able to differentiate themselves from their competitors by successfully incorporating these technologies into their marketing campaigns will leave consumers with an impression that will stick with them.
- The novelty and excitement that surround virtual reality and augmented reality experiences frequently generate word-of-mouth marketing and social media sharing, which further amplifies the visibility of the brand.
- Applications that use virtual and augmented reality provide valuable data and insights that can be utilized to personalize and target marketing campaigns.
- Marketers are able to obtain a better understanding of individual consumers' preferences, interests, and behaviors through the analysis of user interactions within these immersive environments.
- This data can be used to guide the development of content that is highly targeted and relevant, which will ultimately result in improved conversion rates and a higher return on investment.
- Virtual reality (VR) and augmented reality (AR) applications in digital marketing continue to face significant challenges in terms of cost and accessibility, despite the numerous benefits they offer.
- It can be a resource-intensive process to develop and implement high-quality

virtual reality (VR) and augmented reality (AR) experiences because it requires specialized hardware and skilled professionals.

- In addition, the widespread adoption of virtual reality and augmented reality technologies among the general public is still in its infancy. As a result, it is essential for marketers to carefully evaluate the readiness and willingness of their target audience to engage with experiences that utilize these technologies.

Recommendations:

- Before marketers invest in virtual reality (VR) and augmented reality (AR) applications, they should first conduct extensive audience research to determine the interest level, demographics, and technological readiness of their target audience.
- Using this information, it will be possible to determine whether or not the incorporation of these technologies aligns with the target market and whether or not the investment is likely to result in positive outcomes.
- The use of virtual reality (VR) and augmented reality (AR) should be carefully considered by marketers in terms of how these technologies can enhance and complement existing digital marketing strategies. It is essential to determine which specific touchpoints along the customer journey these technologies can contribute to the creation of meaningful interactions and the addition of value.
- For maximum effect, strategic integration ensures that virtual reality (VR) and augmented reality (AR) experiences are seamlessly integrated into broader marketing efforts.
- Because virtual reality and augmented reality applications are both technically and creatively challenging, it is recommended that marketers work with seasoned experts in the field to develop their products.
- The production of high-quality and engaging experiences that are in line with marketing goals can be facilitated through the formation of strategic partnerships with VR and AR software developers, designers, and content creators.
- When attempting to evaluate the success of VR and AR marketing campaigns, it is essential to develop applicable KPIs and make use of sophisticated analytics tools.
- In order to assess the effect that these technologies have on marketing objectives, marketers should monitor the level of user engagement, conversion rates, and any other pertinent metrics. This approach is driven by data, which enables continuous optimization and improvement of virtual reality and augmented reality strategies.
- As virtual reality (VR) and augmented reality (AR) technologies continue to advance, it is essential for marketers to test and refine their strategies.
- Experimenting with a variety of formats, content types, and platforms enables marketers to discover what types of content and platforms are most effective with their target audiences, allowing them to adjust their strategies accordingly.
- Testing and iteration on a regular basis help refine VR and AR campaigns, which ultimately leads to improved results over time.
- By adhering to these recommendations, marketers will be able to effectively leverage virtual and augmented reality applications in digital marketing. This will allow them to capitalize on the opportunities to enhance customer engagement, increase brand awareness, and drive better marketing outcomes.

Conclusion:

Immersive experiences, interesting narrative possibilities, and invaluable consumer insights are just a few ways in which VR and AR apps have the potential to transform digital marketing. Virtual reality (VR) and augmented reality (AR) offer tremendous potential for marketers if they take the time to fully understand the tools' strengths and weaknesses. However, a

strategic and data-driven approach is necessary when incorporating VR and AR into digital marketing strategies due to the challenges of accessibility, cost, and measurement. To sum up, augmented reality has enormous potential to boost businesses' customer service, productivity, and creativity. Businesses can use AR to gain an edge in their fields by analyzing use cases, creating tailored solutions, and integrating the technology with existing systems. The potential for augmented reality to revolutionize digital marketing for businesses is exciting. Businesses can improve customer engagement, drive conversions, and gain a digital competitive edge by developing interactive brand experiences, leveraging social media activation, enabling product visualization, and making use of data-driven insights.

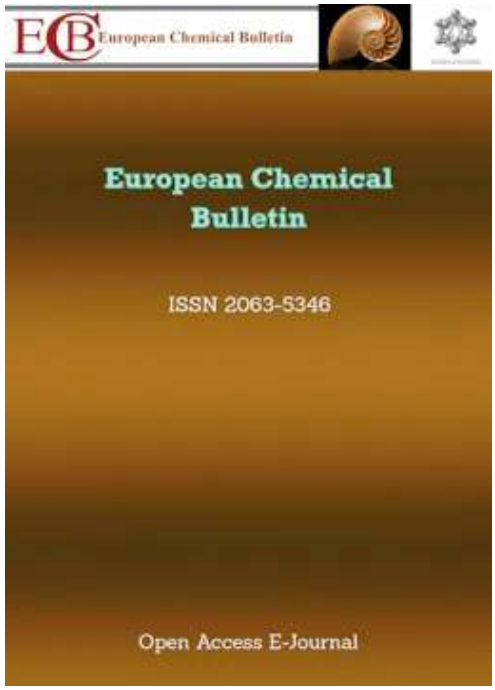
References

1. Asthana, R., & Pandey, R. (2021). The World of Virtual Reality (1st ed., pp. 141-146). Kaav Publications. https://www.kaavpublications.org/cpabstracts/the-world-of-virtual-reality
2. Becker, B. (2019). 9 VR marketing examples that you'll want to steal for 2020. Retrieved November 11, 2019 from https://blog.hubspot.com/marketing/vr-marketing-examples
3. Bigné, E., Llinares, C., and Torrecilla, C. (2016). Elapsed time on first buying triggers brand choices within a category: a virtual reality-based study. Journal of Business Research.
4. Feltham, J. (2016). McDonalds is using VR to teach people about its food production (and tractor driving). Retrieved November 21, 2019 from https://uploadvr.com/mcdonalds-using-vr-teach-peopleuk-food-production/
5. Grudzewski, G., Awdziej, M., Mazurek, G., and Piotrowska, K. (2018). Virtual reality in marketing communication – the impact on the message, technology and offer perception – empirical study. Economics and Business Review, 4(18), 3, 36-50. DOI: 10.18559/ebr.2018.3.4
6. Hajduk, G. (2016). Challenges for marketing communications in the digital age. In G. Mazurek, J. Tkaczyk (Eds.), The impact of the digital world on management and marketing (pp. 183-195). Warszawa: Poltext.
7. Jang, J. Y., Hur, H. J., and Choo, H. J. (2019). How to evoque consumer approach intention toward VR stores? Sequential mediation through telepresence and experiential value. Fashion and Textiles, 6. Kotler, Ph. (2009). Marketing management. Harlow: Pearson Education Limited.
8. Kumar, D. (2019). Virtual Reality (Vr) & Augmented Reality (Ar) Technologies. National Journal of Arts, Commerce & Scientific Research Review, 6(1), 230-235. https://www.kaavpublications.org/spiabstracts/virtual-reality-vr-augmented-reality-ar-technologies
9. Malhotra, C. (2019). Impact of Augmented Reality on Consumer Purchase Intention & Consumer Behaviour (1st ed., pp. 259-265). Kaav Publications. https://www.kaavpublications.org/cpabstracts/impact-of-augmented-reality-on-consumer-purchase-intention-consumer-behaviour
10. Pindel, D. (2015), A co by było gdyby? Wirtualnie rzeczywisty marketing. Retrieved November 21, 2019 from https://marketerplus.pl/teksty/artykuly/a-co-by-bylo-gdyby-wirtualnie-rzeczywistymarketing/
11. Steuer, J. (1992). Defining virtual reality: dimensions determining telepresence. Journal of Communication 42(4).

European Chemical Bulletin

ISSN:2063-5346

Publish Now



Chief Editor Name

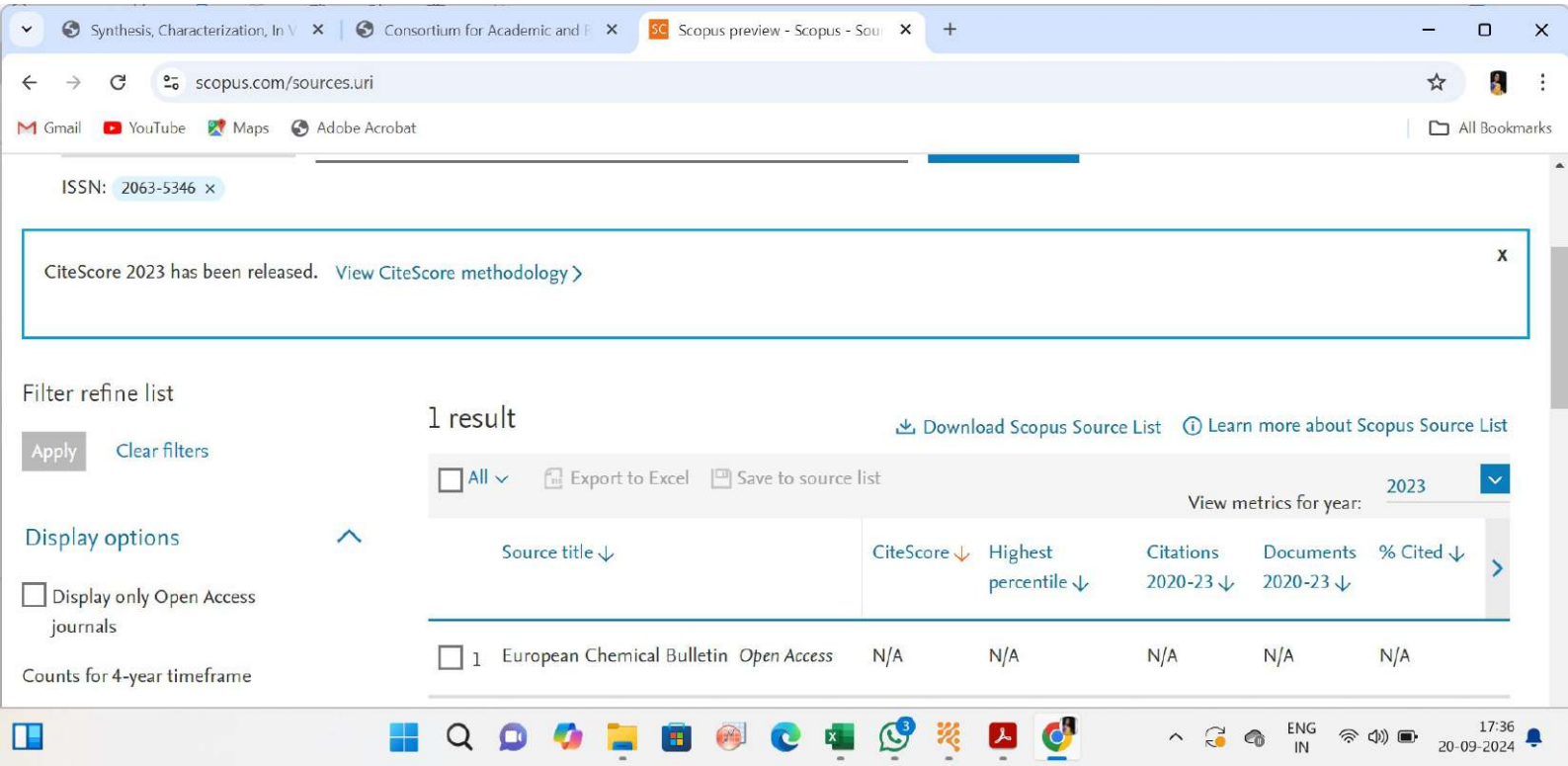
Prof. Dr. K.Krishna
Department of Chemistry, India

Publisher:

Deuton-X Ltd

European Chemical Bulletin is indexed by Chemical Abstract (CA), SciFinder, Directory of Open Access Journals (DOAJ), and Directory of Research Journals Indexing (DRJI) and is available as an Open Access Journal on the Internet. The European Chemical Bulletin was covered by Scopus inclusion for the period from 2017 to 2022. Full lengths of the articles and abstracts are available online at www.eurchembull.com European Chemical Bulletin is an open-access journal. The interesting readers can view, download, print, and redistribute our articles without a subscription, which guarantees that the author

Our Indexing Partners


Synthesis, Characterization, In
Consortium for Academic and
Scopus preview - Scopus - Sou
scopus.com/sources.uri
Gmail
YouTube
Maps
Adobe Acrobat
All Bookmarks
ISSN: 2063-5346
CiteScore 2023 has been released. View CiteScore methodology
Filter refine list
Apply
Clear filters
Display options
Display only Open Access journals
Counts for 4-year timeframe
1 result
Download Scopus Source List
Learn more about Scopus Source List
All
Export to Excel
Save to source list
View metrics for year:
2023
Source title
CiteScore
Highest percentile
Citations 2020-23
Documents 2020-23
% Cited
1
European Chemical Bulletin Open Access
N/A
N/A
N/A
N/A
N/A
ENG IN
17:36
20-09-2024

Biochem. Cell. Arch. Vol. 23, No. 1, pp. 639-646, 2023
DocID: https://connectjournals.com/03896.2023.23.639
DOI: https://doi.org/10.51470/bca.2023.23.1.639
Crossref
ISSN 0972-5075
eISSN 0976-1772

IMPACT OF HEXACONAZOLE ON HISTO-ARCHITECTURE OF LIVER AND INTESTINE OF FRESHWATER AFRICAN CATFISH, *CLARIAS GARIEPINUS* (BURCHELL, 1822)

Khomesh Hiwraj Lanjewar[1], Suresh Bapurao Zade[3], Lankesh Yashwant Bhaisare[2] and Desh Deepak Chaudhary[2]*

[1]Department of Zoology, J. M. Patel Arts, Commerce and Science College, Bhandara, Nagpur - 441 904, India.
[2]Department of Zoology, Indira Gandhi National Tribal University, Amarkantak - 484 887, India.
[3]Department of Zoology, Rashtrasant Tukadoji Maharaj Nagpur University, Nagpur - 440 033, India.
*e-mail : ddchaudhary90@gmail.com

(Received 11 February 2023, Revised 25 March 2023, Accepted 6 April 2023)

ABSTRACT : Hexaconazole is an endocrine-disrupting organic pollutant that has long-term ecotoxicological effects, posing a risk to the environment and human health. It is a broad-spectrum fungicide used for the treatment of many fungal infections in crop fields. Henceforth, the current study was conducted to investigate the effect of Hexaconazole on the liver and intestine of the African catfish *Clarias gariepinus* (Burchell, 1822). To conduct the experiment, fishes were placed into three groups: the control, the low dose (5 mg/lit), and the high dose (8 mg/lit) groups. After five days of exposure to the appropriate dosages of Hexaconazole, each group was sacrificed for the histological examination. It was noted that fish exposed to both low and high dosages of Hexaconazole displayed substantial liver damages such as disorganization of the cord, enucleated hepatocytes, hyperplasia of Kupffer cells, accumulation of a large number of the pycnotic nucleus, etc., whereas in the intestine when exposed to the low and high dose of Hexaconazole showed necrotic areas were infiltrated with lymphocytes, the disintegration of intestinal layers, dilation of lamina properia, degeneration of enterocytes, vacuolation in the epithelial cells, hypertrophy and hyperplasia of goblet cells, fusion of intestinal villi, loss of intestinal glands, etc. Thus, the present study concludes that Hexaconazole exposure causes significant alterations in the histological structure of the liver and intestine, which may impair the normal functioning of this organ in *C. gariepinus*.

Key words : EDCs, hexaconazole, histopathology, liver, intestine, pollutant.

How to cite : Khomesh Hiwraj Lanjewar, Suresh Bapurao Zade, Lankesh Yashwant Bhaisare and Desh Deepak Chaudhary (2023) Impact of hexaconazole on histo-architecture of liver and intestine of freshwater African catfish, *Clarias gariepinus* (Burchell, 1822). *Biochem. Cell. Arch.* **23**, 639-646. DOI: https://doi.org/10.51470/bca.2023.23.1.639, DocID: https://connectjournals.com/03896.2023.23.639

Check for updates

INTRODUCTION

The increased production of various substances such as drugs, petrochemicals, fertilizers, dyes, metals and pharmaceuticals lead to the release of toxic and hazardous waste into the environment in different forms such as solid, liquid, and gaseous and causing irreversible damage to the surroundings (Mishra and Pandey, 2004). Hence, the disposal of various industrial, agricultural and pharmaceutical effluents in the environment and possesses the serious problems due to its various components such as acids, alkalies, heavy metals, phenolic compounds, detergents and many other contaminants that pose a serious threat to aquatic as well as terrestrial forms of life (Ahmed *et al*, 2021). In which, agriculture effluents contain many contaminants along with different kinds of pesticides, which mixed with the water bodies.

Various types of pesticides have been used in agricultural fields to cure several harmful effects caused by the pest. Therefore, toxicological and environmental problems resulting from the widespread use of pesticides in agriculture have raised concerns, particularly with respect to the potentially toxic effects on humans and animals (Li and Randak, 2009; Bernardes *et al*, 2015; Briffa *et al*, 2020). The large-scale application of pesticides to crops and forests has contributed to the occurrence of toxic substances in the environment. These chemicals can find their way into the water reservoirs, streams and rivers thereby triggering a series of events

that directly or indirectly disturbs the aquatic life including fishes (Malik *et al*, 2020). Among these pesticides, fungicides are one of the classes of pesticides that are used in agriculture fields against the various types of fungal infections such as mancozeb (Choudhury and Das, 2020), sulfur, maneb (Rathmell and Skidmore, 1982), bordeaux mixture (Annapurneshwari *et al*, 2022), cupric salts, nickel salts (Eisler and Gardner, 1973), ketoconazole (Hontoria *et al*, 2013; Huang *et al*, 2022), etc.

Amongst the above, conazole is an azole-based fungicide that is biologically active and commonly used in agriculture and medicine to cure fungal infections (Brauer *et al*, 2019). Apart from agriculture, it is also used in horticulture to inhibit fungal growth on trees, grasses, fruits, vegetables, seeds and cereal crops (Jorgensen and Heick, 2021). There are some fungicides which are commonly used in agriculture and forestry like tebuconazole, epoxyconazole, febuconazole, penconazole, propiconazole and Hexaconazole (Mnif *et al*, 2011). Among these, Hexaconazole is a broad-spectrum systemic triazole fungicide commonly used for the treatment of numerous kinds of infections brought about by ascomycetes, basidiomycetes and blemished growths. It is especially suitable for the treatment of growth illnesses like buildup, rust, scab, earthy-colored smudge, and anthracnose brought about by the ascomycetes and basidiomycetes (Maluin *et al*, 2019).

This Hexaconazole belonging to one of the potential class of endocrine disrupting compounds interferes with the endocrine system in wildlife, humans and perhaps cause cancerous tumors, birth defects, and other developmental disorders (Mnif *et al*, 2011; Lanjewar *et al*, 2022). Hexaconazole may also interfere with the synthesis, transport, metabolism and elimination of hormones, thereby decreasing the concentration of natural hormones (Trosken *et al*, 2004). So, the anthropogenic exposure of these chemicals may cause harmful effects on the different trophic levels in the natural ecosystem. So, an experiment was performed to check the effects of fungicides on ecosystems, based on the data of knowledge on the toxicity of fungicides applications to non-target organisms such as fish. Freshwater air breathing fish, *C. gariepinus* were chosen for the current histological investigation because they are readily accessible throughout the year and are simple to transport and keep in a lab environment. Histological changes provide a rapid method to detect the effects of irritants, especially chronic ones, in various tissues and organs (Bernet *et al*, 1999).

However, among the fungicide, there is lack of knowledge of the effect of fungicide Hexaconazole, on the histological structure of liver and intestine of the fish, *C. gariepinus.* In fishes, the liver has been repeatedly proved to be an extraordinarily sensitive tool to reveal both adaptive processes and detrimental effects induced by organic pollutants. Similarly, intestine is an important organ for digestion and absorption. Although it is not mainly responsible for detoxification (Sastry and Gupta, 1979). These organs have been proven to be indicative of pollution (Hinton and Lauren, 1990). Henceforth, it was hypothesized that the fungicide Hexaconazole show harmful effect on the histological structure of the fish. Therefore, the purpose of the current study was to determine how Hexaconazole affected the histo-architecture of the liver and intestine of the African catfish *C. gariepinus*.

MATERIALS AND METHODS

Collection and maintenance

For this experiment, *C. gariepinus* with average body weights of 300±25 gm and length 33.50±05 cm were brought from the local market of Nagpur, Maharashtra (21°8'47.8788''N and 79°5'19.8960''E). The fishes were maintained in a 30 lit. of glass aquarium filled with tap water and under normal abiotic conditions of light and temperature. The fishes were fed with crushed goat liver every day and water were changed at every alternate day. All the fishes were acclimatized for one week before experimentation.

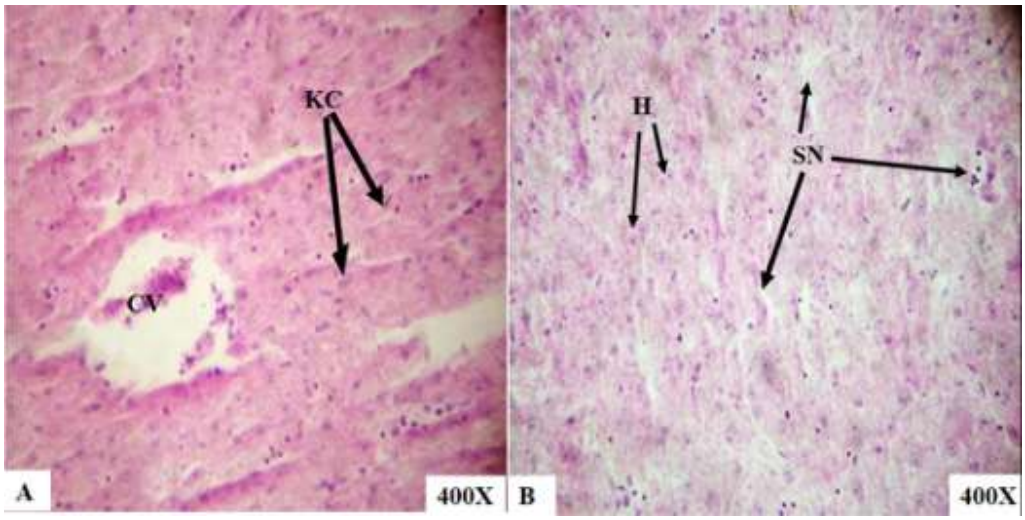
Experimental design

For the present study Hexaconazole (CAS No: 79983-71-4) was bought from Sigma-Aldrich Co. and three aquariums were taken and filled with 30 liters of tap water and labeled as control (without fungicide), low dose (5 mg/lit.), and high dose (8 mg/lit.) groups based on concentration of the Hexaconazole. Three fishes were transferred in each aquarium for 5 days with respective concentration of Hexaconazole as above. After 5 days, all of them were taken for the histological study of liver and intestine. The Bouin's fixative was promptly used for fixation of the liver and intestine. Fixed tissues underwent conventional paraffin embedding process (Robert *et al*, 2014). Tissues that had been embedded were then sectioned at a thickness of 5µ, stained with Ehrlich Hematoxylin and Eosin (H & E) and then mounted in DPX. The slides were observed under the microscope at 100X and 400X magnifications.

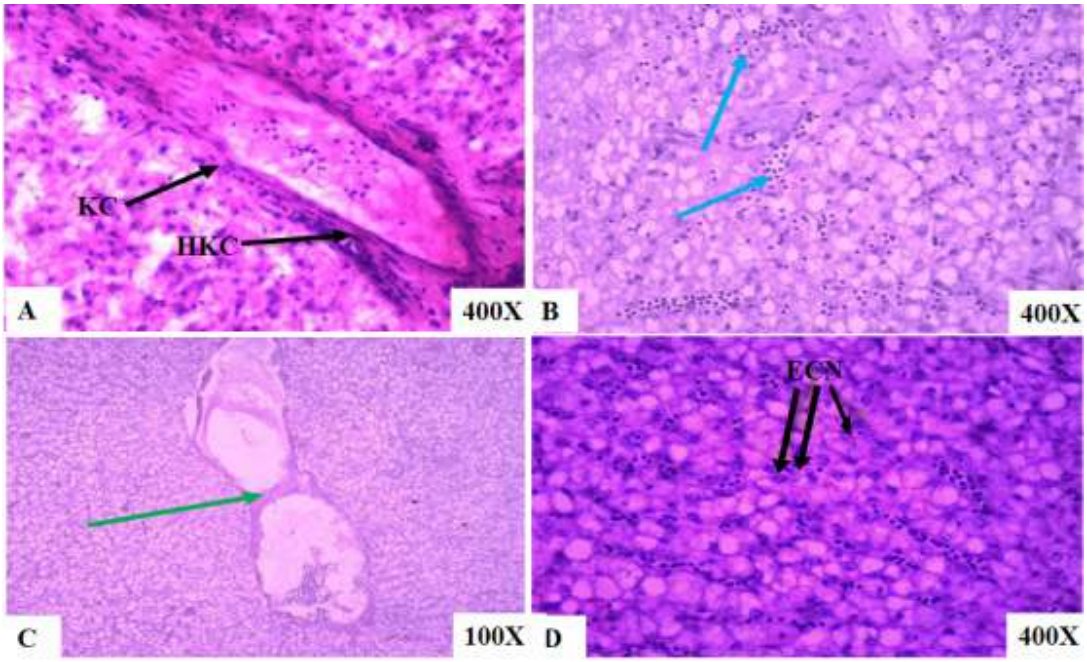
OBSERVATIONS AND RESULTS

Histopathological changes in the liver

In the histopathological observation of the liver, significant alterations were observed in experimental



Photoplate 1: Microphotograph showing histological structure of liver of a control group of fish *Clarias gariepinus* (A) continuous mass of hepatic cell, Central vein and Kupffer cell (B) The hepatocytes were large in size, polygonal in shape and sinusoid.



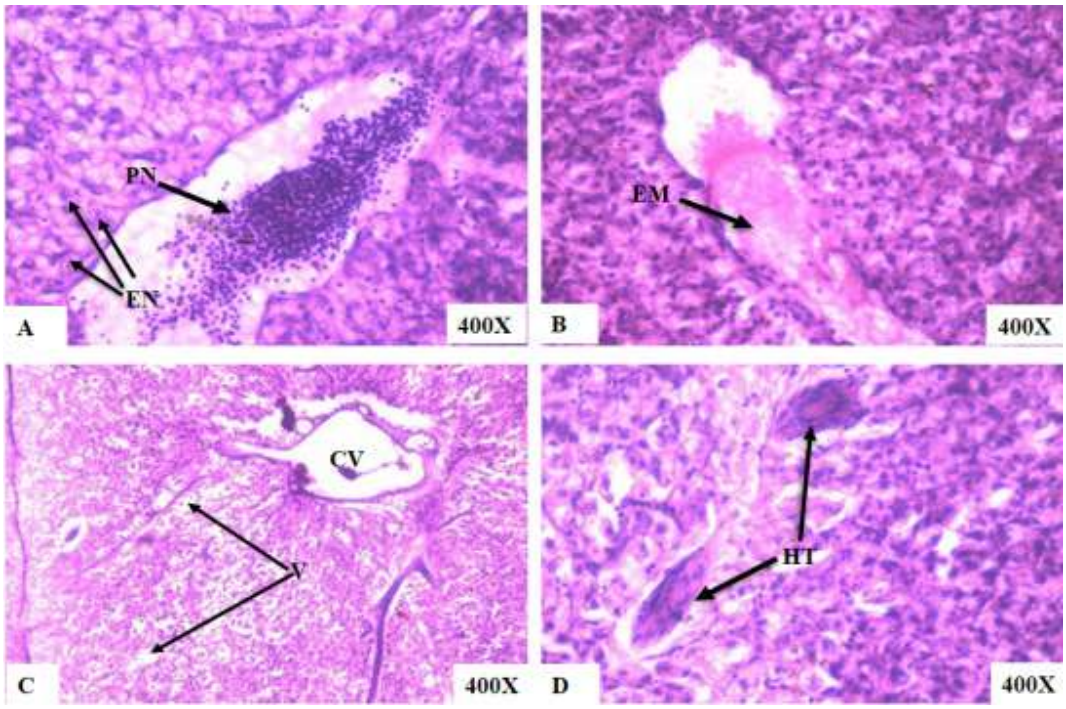
Photoplate 2: Microphotograph showing histological structure of liver of fish *Clarias gariepinus* exposed to 5 mg/lit of Hexaconazole (A) Hypertrophy of Kupffer cells (B) Pycnotic nucleus, enucleated hepatocytes (C) Green arrow show fusion of central vein (D) hepatocytes with eccentric nucleus.

fishes in compare to the control fishes. The occurrence and degree of alteration was positively correlated with the doses of Hexaconazole. The liver of the control fish, *C. gariepinus* revealed a normal histological structure like a continuous mass of a hepatic cell, hepatocytes with cord-like pattern interrupted by blood vessels and sinusoids. The hepatocytes were large in size, polygonal in shape having centrally located nuclei. The hepatocytes have homogenous eosinophilic cytoplasm. The sinusoids are communication channels occupied by blood cells with the Kupffer cell (Photoplate 1).

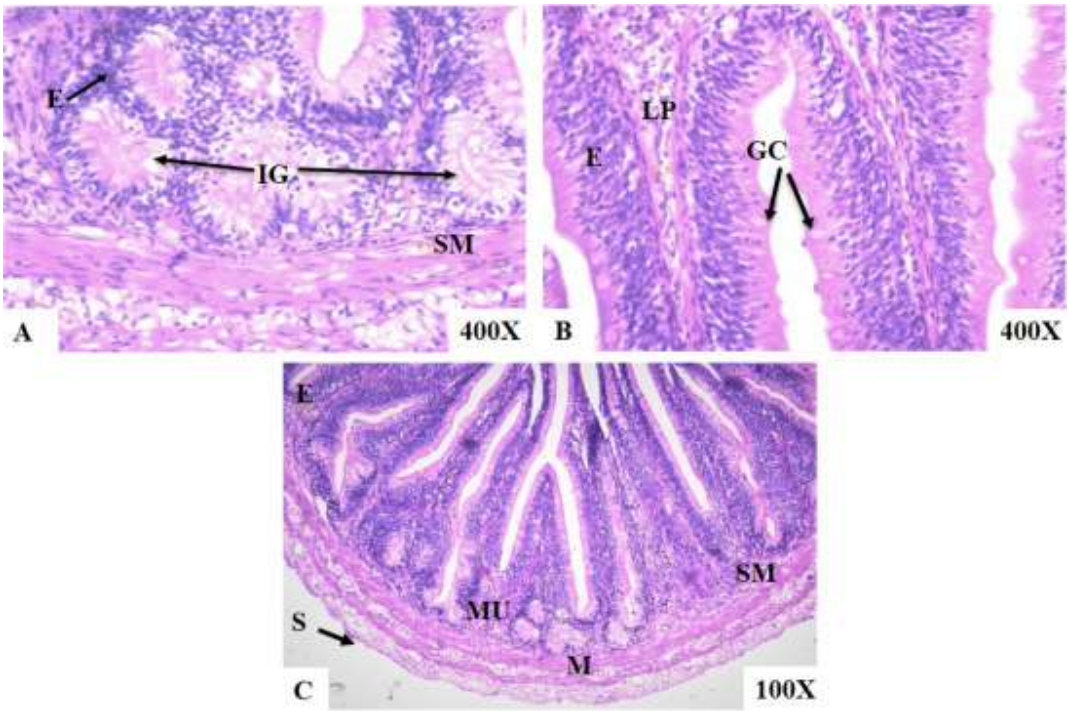
The liver of fish treated with 5mg/lit hexaconazole for 5 days showed disorganization of hepatic cord, pycnotic nucleus, hepatocytes with an eccentric nucleus, enucleated hepatocytes, a fusion of central vein, and hyperplasia of Kupffer cell (Photoplate 2). Whereas, the liver of fish exposed to the 8mg/lit hexaconazole for 5 days showed degeneration of central vein, destruction of hepatic triad, accumulation of large number of pycnotic nucleus (Photoplate 3).

Histopathological changes in the intestine

In intestine, the histological observation showed significant differences between experimental and control

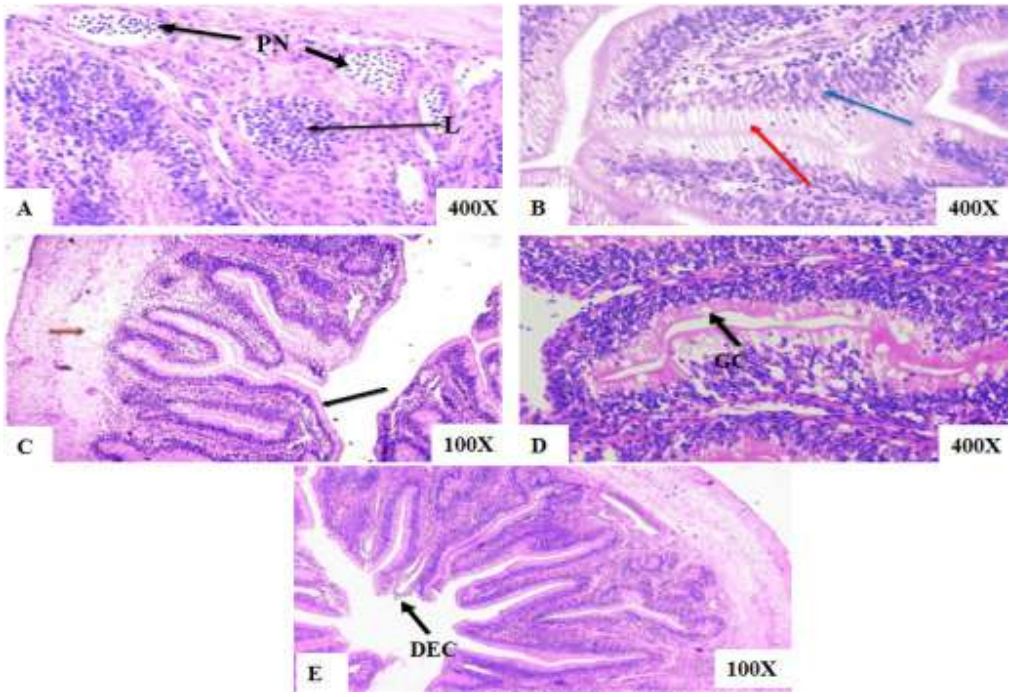


Photoplate 3: Microphotograph showing histopathological changes in experimental group of fish *Clarias gariepinus* exposed to 8mg/lit of hexaconazole (A) Accumulation of Pycnotic nucleus, Eccentric nucleus (B) Accumulation of eosinophilic material (C) Degeneration of central vein and vacuolization (D) Destruction of hepatic triad.

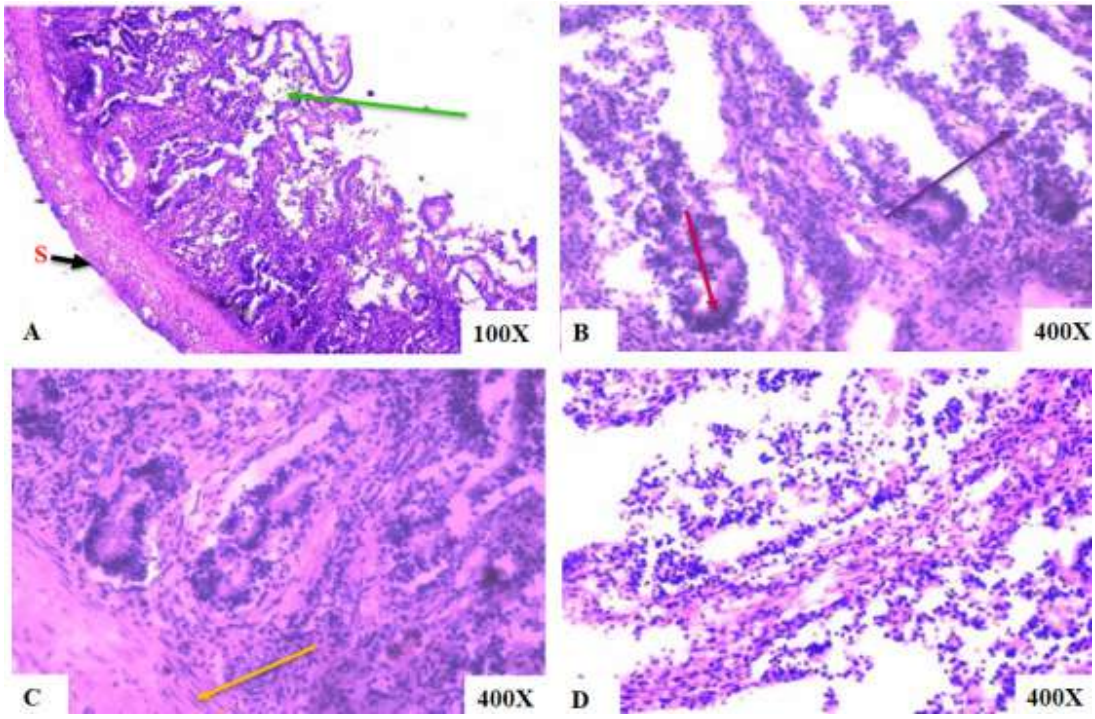


Photoplate 4 : Microphotograph showing histological structure of intestine of control group (A) Intestinal gland, muscular layers, large number of enterocyte (B) Lamina propria, Goblet cells (C) Serosa, submucosa, intestinal villi.

groups. The histological structure of intestine from control group revealed four consecutive layers: serosa, muscularis, submucosa, and mucosa. The serosa, the outermost layer is followed by a muscularis (longitudinal and circular muscle) that has grown well, which is bordered by loose connective tissue that is supplied with blood capillaries. It combines with the underlying mucosal coat's tunica propria. The mucosa is elevated into a number of longitudinal folds, and its mucous and absorptive cells make up its epithelial lining (Goblet cells)



Photoplate 5: Microphotograph showing histopathological structure of intestine of fish *Clarias gariepinus* to 5 mg/lit of hexaconazole (A) Infiltrated with lymphocytes, pycnotic nucleus with vacuolation in the epithelial cells and loss of cellular architecture of intestinal columnar epithelial cells, desquamated intestinal epithelial cells, (B) Blue arrow showed degeneration of enterocytes, red arrow showed dilation of lamina propria (C) Brown arrow showed disintegration of intestinal muscularis and sub- mucosal layer, black arrow showed necrosis in the intestinal villi.(D) Hypertrophy and hyperplasia of Goblet cells and fusion of intestinal villi (E) Disruption of epithelial cells.



Photoplate 6: Microphotograph showing histopathological structure of intestine in fish *Clarias gariepinus* group exposed to 8 mg/lit of hexaconazole (A) Green arrow showed reduction in the size of intestinal villi (B) Red arrow show loss of intestinal gland, purple arrow showed degeneration of enterocytes, reduction in the Goblet cells (C) Yellow arrow showed loss of structural integrity of mucosal folds (D) Loss of epithelial cells of intestine, destruction of intestinal villi.

(Photoplate 4).

The intestine of treated fish with 5mg/lit, hexaconazole for 5 days showed necrosis in the intestinal villi. The necrotic areas were infiltrated with lymphocytes, the disintegration of intestinal muscularis and sub- mucosal layer, dilation of lamina properia, degeneration of enterocytes, vacuolation in the epithelial cells, loss of cellular architecture of intestinal columnar epithelial cells, desquamated intestinal epithelial cells, hypertrophy and hyperplasia of goblet cells and the fusion of intestinal villi (Photoplate 5).

Whereas, the intestine of fish treated with the 8 mg/ lit. of hexaconazole for 5 days showed loss of structural integrity of mucosal folds, reduction in the size of intestinal villi, degeneration of enterocytes and loss of epithelial cells of intestine, loss of intestinal glands and reduction in the goblet cells. All these changes were more severe in the group of fishes which exposed to high concentration (Photoplate 6).

DISCUSSION

The liver is associated with the organ of detoxification and biotransformation process, which is most affected by the environmental contaminants (Camargo and Martinez, 2007). Hence, changes in the hepatic structure are utilized as an imperative biomarker of natural contamination. Intestine also plays an important role in detoxification. But the major function of the intestine is absorption, digestion and provides some immunity (Hinton and Lauren, 1990).

In the present study, histological examination of the fish liver treated with 5mg/lit. Hexaconazole for 5 days showed disorganization of the hepatic cord, pycnotic nucleus, hepatocytes with an eccentric nucleus, enucleated hepatocytes, and hyperplasia of Kupffer cell. Similar findings have been observed in the liver of *C. punctatus* exposed to Chlorpyrifos (CPF) (Devi and Mishra, 2013) and the liver of *Labeo rohita* exposed to Malathion (Karmakar *et al*, 2015). However, liver of fish treated with 8mg/lit. Hexaconazole for 5 days showed degeneration of the central vein, destruction of the hepatic triad, and accumulation of large number of pycnotic nucleus. Analogous effects also have seen by Fanta *et al* (2003) in the silluriform *Corydoras paleatus* and Bias and Lokhande (2012) in freshwater fish, *Ophiocephalus striatus* (Channa) exposed to cadmium chloride. This vacuolation of hepatocytes and other structure degeneration may have been a consequence of inhibition of protein synthesis, energy depletion, disaggregation of microtubules, or shifts in substrate utilization (Ajani and Akpoilih, 2010; Maksymiv *et al*, 2015).

Furthermore, the vacuolization of hepatocytes might indicate an imbalance between the rate of synthesis of substances in the parenchymal cells and the rate of their release into the circulatory system. Apart from this, oxygen deficiency as a result of gill degeneration is the most common cause of cellular degeneration in the liver (Gingerich, 1982). However, according to Karthigayani *et al* (2014), the pycnosis of the nucleus demonstrated the breakdown of the nucleus regulatory functions, which had an impact on how nutrients were metabolized before reaching the liver cells. This change in metabolic pathway of the essential nutrients such as glucose and amino acid may have direct or indirect influence on the other vital organ of the fish. So, by acting on the liver, Hexaconazole may alter the different metabolic pathway of fish which in turn alters the normal physiology and behavior (Jia *et al*, 2019 and Lanjewar *et al*, 2022).

Further, histological examination of the intestine of fish treated with 5mg/L hexaconazole for 5 days showed necrosis in the intestinal villi. The necrotic areas were infiltrated with lymphocytes, the disintegration of intestinal muscularis and sub- mucosal layer, dilation of lamina properia, degeneration of enterocytes, vacuolation in the epithelial cells, loss of cellular architecture of intestinal columnar epithelial cells, desquamated intestinal epithelial cells, hypertrophy and hyperplasia of goblet cells and fusion of intestinal villi. Similar findings have been observed by the Ghanbahadur and Ghanbahadur (2012) in the intestine of *Rasbora daniconius* due to the exposure of the endosulfan. Likewise, Younis *et al* (2013) and Senapati *et al* (2013) also noticed similar impact in the fish Nile tilapia *Oreochromis niloticus*, exposed to sublethal concentrations of Cadmium, and necrotic changes observed in the different intestinal layers of the studied fish *Tilapia mossambica* due to exposure of monocrotophos (Desai *et al*, 1984).

However, intestine of fish exposed to 8 mg/L hexaconazole for 5 days showed loss of structural integrity of mucosal folds, reduction in the size of intestinal villi, degeneration of enterocytes, loss of epithelial cells of the intestine, loss of intestinal glands and reduction in the goblet cells. Velmurugan *et al* (2007) reported similar histological alteration in the intestine of *C. mrigala* due to the toxicological effects of different pesticides with heavy dose. Likewise increasing the exposure of cypermethrin *Oreochromis mossambicus* had a deleterious effect on the internal epithelial lining cells and such changes in intestine, probably induce changes in biological functions of the fish that may contribute to lethargic behavioral responses. These effects also hamper the digestive and absorptive capacity of the

intestine (Karthigayani *et al*, 2014).

Thus, the present work showed various harmful effects of Hexaconazole on the histology of the liver and intestine of *C. gariepinus*. Hexaconazole has the ability to alter the fish's natural physiology by bringing about a number of detrimental alterations in the liver and intestine. In this regard, the study emphasizes the necessity of carrying out extensive, methodical research on lower Hexaconazole concentrations in natural water bodies.

CONCLUSION

The current study found that Hexaconazole had a variety of toxic effects on the histology of *C. gariepinus*'s liver and intestine. Hexaconazole has the potential to disrupt fish tissue physiology by causing several deteriorating changes in both the liver and the intestine. The study emphasizes the need for long-term, systematic studies of lower concentrations of Hexaconazole in natural water bodies. In this context, the current histological investigations show a direct relationship between fungicide exposure and histopathological changes observed in both tissues.

Author's contribution

Suresh Bapurao Zade contributed to conception and design of the study. Khomesh Hiwraj Lanjewar had performed the experiments, drafted the manuscript. Lankesh Yashwant Bhaisare helped in drafting and editing of the manuscript. Desh Deepak Chaudhary contributed to conception, select items in the drafted manuscript, critically revised manuscript and gave final approval to the manuscript.

Conflict of interest

It is verified that all authors have made substantial contributions, agree with the manuscript's contents and don't have any competing interests.

REFERENCES

Abou S, Nevine M, Abdel-Maneim A M, Khader S M and Elalkamy H (2008) Histological alterations in gonads of *Clarias lazera* (Clariidae, valencienns, 1840) after exposure to dye-stuff and chemical waste water effluent. *Egy. J. Aquac.* **34**, 351-368.

Ahmed J, Thakur A and Goyal A (2021) Industrial wastewater and its toxic effects. *Biological Ind. J. Waste Water Treat*. 1-14. https://doi.org/10.1039/9781839165399-00001

Ajani E K and Akpoilih B U (2010) Effect of chronic dietary copper exposure on hematology and histology of common carp (*Cyprinus carpio* L.). *J. Appl. Sci. Environ. Manag.* **14**(4), 39-45. DOI: 10.4314/jasem.v14i4.63254

Annapurneshwari H, Godbole M and Navya K (2022) Impact of Bordeaux mixture on behavioural, histological and some biochemical parameters of common carp (*Cyprinus carpio* L). *U. P. J. Zool.* **43**, 51-57.DOI: 10.56557/upjoz/2022/v43i243285

Bais U E and Lokhande M V (2012) Effect of cadmium chloride on histopathological changes in the freshwater fish *Ophiocephalus striatus* (Channa). *Int. J. Zool. Res*. **8**(1), 23.

Begum B H and Mithra D (2015) Effects of an organophosphate pesticide, Malathion (50% E.C) on the liver of air-breathing fish, *Heteropneustes fossilis*. *Int. J. Environ. Sci.* **4**(9), 21–24.

Berger S, El Chazli Y, Babu A F and Coste A T (2017) Azole resistance in Aspergillus fumigatus: a consequence of antifungal use in agriculture*? Front. Microbiol.* **8**, 1024.

Bernet D, Schmidt H, Meier W, Burkhardt Holm P and Wahli T (1999) Histopathology in fish: proposal for a protocol to assess aquatic pollution. *J. Fish Dis*. **22**(1), 25-34.https://doi.org/10.1046/j.1365-2761.1999.00134.x

Brauer V S, Rezende C P, Pessoni A M, De Paula R G, Rangappa K S, Nayaka S C, Gupta V K and Almeida F (2019) Antifungal agents in agriculture: Friends and foes of public health. *Biomolecules* **9**(10), 521. https://doi.org/10.3390/biom9100521

Camargo M M and Martinez C B (2007) Histopathology of gills, kidney, and liver of a neotropical fish caged in an urban stream. *Neotrop. Ichthyol.* **5**, 327-336. https://doi.org/10.1590/S1679-62252007000300013

Cardiff R D, Miller C H and Munn R J (2014) Manual Hematoxylin and Eosin staining of mouse tissue sections. *Cold Spring Harb. Protoc.* **(6)**, pdb-prot073411.

Choudhury R and Das P (2020) Histopathological studies on the liver and kidney of *Channa punctatus* (Bloch) exposed to mancozeb containing pesticide dithane m-45. *Poll. Res.* **39**, 87-91.

Cocco P (2002) Review of the scientific evidence linking occupational and environmental pesticide exposure to endocrine disruption health effects. *Cad. Saude Publica.* **18**, 379-402.

Devi Y and Mishra A (2013) Histopathological alterations in gill and liver anatomy of fresh water, air breathing fish *Channa Punctatus* after pesticide Hilban (Chlorpyrifos) treatment. *Adv. Biores.* **4**(2), 57-62.

Eisler R and Gardner G R (1973) Acute toxicology to an estuarine teleost of mixtures of cadmium, copper and zinc salts. *J. Fish Biol*. **5**(2), 131-142. https://doi.org/10.1111/j.1095-8649. 1973.tb04441.x

Fanta E, Rios F S, Romao S, Vianna A C and Freiberger S (2003) Histopathology of the fish *Corydoras paleatus* contaminated with sublethal levels of organophosphorus in water and food*. Ecotoxicol. Environ. Saf.* **54**(2), 119-130.https://doi.org/10.1016/S0147-6513(02)00044-1

Ghanbahadur A and Ghanbahadur G (2012) Histopathological effect of organochloride endosulfan on intestine and stomach of larvivorous fish *Rasbora daniconius*. *DAV Int. J. Sci.* **1**(2), 126-127.

Gingerich W H (1982) Hepatic toxicology of fishes. *Aquat. Toxicol.* (ed. Weber L J), Raven Press, New York, 55-105.

Hinton D E and Lauren D L (1990) Integrative histopathological approaches to detecting effects. *Biol. Ind. Stress Fish* **17**, 51-66.

Hontoria F, Gonzalez M A, Sitja-Bobadilla A, Palenzuela O and Alvarez-Pellitero P (2013) Ketoconazole modulates the infectivity of *Ichthyophonus* sp. (Mesomycetozoa) *in vivo* in experimentally injected European sea bass. *Dis. Aquat. Org.* **105**(3), 225-235.DOI: https://doi.org/10.3354/dao02607

Huang T, Zhao Y, He J, Cheng H and Martyniuk C J (2022) Endocrine disruption by azole fungicides in fish: A review of the evidence.

Sci. Total Environ. 153412.https://doi.org/10.1016/j.scitotenv.2022.153412

John P J and Prakash A (2003) Bioaccumulation of pesticides on some organs of freshwater catfish *Mystus vitatus*. *Bull. Environ. Contam. Toxicol*. **70**, 1013-1016. DOI:10.1007/s00128-003-0083-4

Jorgensen L N and Heick T M (2021) Azole use in agriculture, horticulture, and wood preservation. Is it indispensable? *Front. Cell Infect. Microbiol*. **11**,https://doi.org/10.3389/fcimb.2021.730297

Karmakar S, Patra K, Jana S, Mandal D P and Bhattacharjee S (2016) Exposure to environmentally relevant concentrations of Malathion induces significant cellular, biochemical and histological alterations in *Labeo rohita*. *Pestic. Biochem. Physiol*. **126**, 49-57.https://doi.org/10.1016/j.pestbp.2015.07.006

Karthigayani T, Denis M, Remy A R and Shettu N (2014) Histological study of the intestine and liver tissues in the fish *Oreochromis mossambicus* exposed to cypermethrin. *J. Modern Biotechnol*. **3**(4), 48–54.

Lanjewar K H, Zade S B, Bhaisare L Y, Nagwanshi A M and Chaudhary D D (2022) Histo-architecture of the male reproductive system of freshwater African catfish *Clarias gariepinus* (Burchell, 1822)*:* An impact of hexaconazole. *Biochem. Cell. Arch.* **22**(2), 3975-3980. DOI: https://doi.org/10.51470/bca.2022.22.2.3975

Li Z H, Zlabek V, Li P, Grabic R, Velisek J, Machova J and Randak T (2010) Biochemical and physiological responses in liver and muscle of rainbow trout after long-term exposure to propiconazole. *Ecotoxicol. Environ. Saf.* **73**(6), 1391-1396. https://doi.org/10.1016/j.ecoenv.2010.05.017

Maksymiv I V, Husak V V, Mosiichuk N M, Matviishyn T M. Sluchyk I Y, Storey J M and Lushchak V I (2015) Hepatotoxicity of herbicide Sencor in goldfish may result from induction of mild oxidative stress. *Pestic. Biochem. Phys.* **122**, 67-75.https://doi.org/10.1016/j.pestbp.2014.12.020

Malik D S, Sharma A K, Sharma A K, Thakur R and Sharma M (2020) A review on impact of water pollution on freshwater fish species and their aquatic environment. *Adv Environ Res*: *Wastewater Impacts and Treatment Technologies* **1**, 10-28.DOI: 10.26832/aesa-2020-aepm-02

Maluin F N, Hussein M Z, Yusof N A, Fakurazi S, Idris A S, Hilmi N Z and Jeffery L D (2019) A potent antifungal agent for basal stem rot disease treatment in oil palms based on chitosan-dazomet nanoparticles. *Int. J. Mol. Sci.* **20**(9), 2247.https://doi.org/10.3390/ijms20092247

Marlatt V L, Bayen S, Castaneda-Cortès D, Delbès G, Grigorova P, Langlois V S and Van Der Kraak G (2022) Impacts of endocrine disrupting chemicals on reproduction in wildlife and humans. *Environ. Res*. **208**, 112584. https://doi.org/10.1016/j.envres.2021.112584

Misra V and Pandey S D (2005) Hazardous waste, impact on health and environment for development of better waste management strategies in future in India. *Environ. Int.* **31**, 417 – 431.https://doi.org/10.1016/j.envint.2004.08.005

Mnif W, Hassine A H, Bouaziz A, Bartegi A, Thomas O and Roig B (2011) Effect of endocrine disruptor pesticides: A review. *Int. J. Environ. Hlth Res.* **8**(6), 2265–2303. https://doi.org/10.3390/ijerph8062265

Rathmell W G and Skidmore A M (1982) Recent advances in the chemical control of cereal rust diseases. *Outlook on Agriculture* **11**(1), 37-43.https://doi.org/10.1177/003072708201100107

Sakr S and Lail S M (2005) Fenvalerate induced histopathological and histochemical changes in the liver of the cat fish *Clarias gariepinus. Egypt. J. Aquat. Biol. Fish.* **6**, 103–124.

Sastry K V and Gupta P K (1979) The effect of cadmium on the digestive system of the teleost fish, *Heteropneustes fossilis*. *Environ. Res.* **19**(2), 221-230.https://doi.org/10.1016/0013-9351(79)90050-1

Sugiyama S, Shimada N, Miyoshi H and Yamauchi K (2005) Detection of thyroid system disrupting chemicals using *in vitro* and *in vivo* screening assays in *Xenopus laevis*. *Toxicol. Sci.* **88**, 367-374. https://doi.org/10.1093/toxsci/kfi330

Thayappan K, Maghil D, Remy A R A and Narayanasamy S (2014) Histological study of the intestine and liver tissues in the fish *Oreochromis mossambicus* exposed to cypermethrin. *J. Modern Biotechnol*. **3**(4), 48-54.

Trosken E E, Scholz K, Lutz R W, Volkel W, Zarn J A and Lutz W K (2004) Comparative assessment of the inhibition of recombinant human CYP19 (aromatase) by azoles used in agriculture and as drugs for humans. *Endocrine Res.* **30**, 387-394.https://doi.org/10.1081/ERC-200035093

Velmurugan B, Selvanayagam M, Cengiz E I and Unlu E (2007) Histopathology of lambda-cyhalothrin on tissues (gill, kidney, liver and intestine) of *Cirrhinus mrigala*. *Environ. Toxicol. Pharmacol.* **24**(3), 286-291.https://doi.org/10.1016/j.etap.2007.07.001

Younis E M, Abdel-Warith A A, Al-Asgah N A, Ebaid H and Mubarak M (2013) Histological changes in the liver and intestine of Nile tilapia, *Oreochromis niloticus*, exposed to sublethal concentrations of cadmium. *Pak. J. Zool*. **45**(3), 833-841.

Younis E, Abdel-Warith A W, Al-Asgah N and Ebaid H (2015) Histopathological alterations in the liver and intestine of Nile tilapia *Oreochromis niloticus* exposed to long-term sublethal concentrations of cadmium chloride. *Chin. J. Oceanol. Limnol*. **33**(4), 846-852. http://dx.doi.org/10.1007/s00343-015-4082-1

Publisher, Journal Listings, Subscription Service & Management

BIOCHEMICAL AND CELLULAR ARCHIVES



BIOCHEMICAL AND CELLULAR ARCHIVES

Subscribe Now

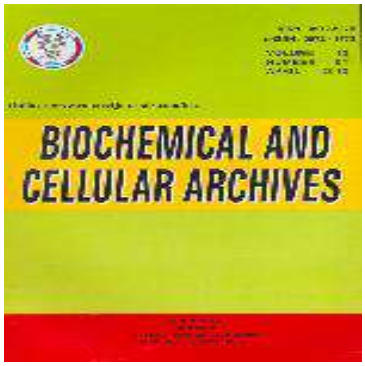
An International Journal

Publisher Name: PROF (DR.) P. R. YADAV
Chief Editor: PROF. (DR.) P. R. YADAV
Title Id: CJ-03896

General Information

Suggest an Edit
(Registered Publisher only)

Chief Editor:
PROF. (DR.) P. R. YADAV
ISSN:
0972-5075
E-ISSN:
0976-1772
Periodicity:
Half-Yearly
Publisher:
PROF (DR.) P. R. YADAV
Published since:
2001
Publishing Cycle:
April
Latest Volume:
Vol. 24 in 2024



Already have a manuscript?

Use our Manuscript Matcher to find the best relevant journals!

Find a Match

Filters Clear All

Web of Science Coverage

Open Access

Category

Country / Region

Language

Frequency

Journal Citation Reports

Refine Your Search Results

0972-5075 Search

Sort By: Title (A-Z)

Search Results

Found 1 results (Page 1) Share These Results

Exact Match Found

BIOCHEMICAL AND CELLULAR ARCHIVES

Publisher: **DR P R YADAV , 606-8 SOUTH CIVIL LINES, MUZAFFARNA, INDIA, 251-001**

ISSN / eISSN: **0972-5075 / 0976-1772**

Additional *Web of Science* Indexes: **Biological Abstracts | BIOSIS Previews**

Share This Journal View profile page

** Requires free login.*

1 – 1 of 1

Items per page: 10

Volumes I (2) 2023 **ISSN: 0972-0766**

(Established in 1804)

JOURNAL OF
THE ASIATIC SOCIETY OF MUMBAI
(A UGC - CARE Listed Journal)

International Conference on Emerging Trends & Challenges In English Language and Literature

Department of English
Navarasam Arts and Science College for Women
(An Institution affiliated to Bharathiar University)
Arachalur, Erode - 638 101.
Tamil Nadu.

Editor
Dr.S. Rajeswari,
Assistant Professor
Head of the Department of English

Published by
The Asiatic Society Of Mumbai
Town Hall, Mumbai - 400 001.
Maharashtra State (INDIA)
2023

Contents

SL.No	Articles	Page. No
1.	ACCULTURATING INTERNALISED MISOGYNY DERAILS THE EVOLUTION OF WOMENFOLK: A STUDY OF EASTERINE KIRE'S A TERRIBLE MATRIARCHY	1
2.	DECODING THE VISUAL CULTURAL SIGNS OF HOMELAND IN NIDHI CHANANI'S PASHMINA	11
3.	AGEING AS A DISABILITY: A STUDY OF INCLUSIVITY OF SEXUAL CULTURE OF THE AGEING BODY IN SLOWMAN BY J M COETZEE	25
4.	BENEFITS OF VIRTUAL LEARNING DURING COVID-19 PANDEMIC	38
5.	BIFURCATION OF CONSCIOUSNESS IN ETAF RUM'S A WOMAN IS NO MAN	56
6.	BILINGUAL METHOD AND DIRECT METHOD: IMPACT ON SPEAKING COMPETENCY IN SECONDARY SCHOOL'S ESL CLASSROOMS	62
7.	BREAKING JAYA'S SILENCE IN SHASHI DESHPANDE'S THAT LONG SILENCE	73
8.	CAROL ANN SHIELDS'THE STONE DIARIES AS AN IMITATION OF FEMININE RECON	79
9.	CONCEPTUALISING CULTURAL ROOTLESSNESS IN BHARATI MUKHERJEE'S WIFE	88
10.	CULTURAL DICHOTOMY IN RUTH PRAWER JHABVALA'S A BACKWARD PLACE	98
11.	CULTURAL RACISM AND ITS IMAPCT IN ZORA NEALE HURSTON'S THEIR EYES WERE WATCHING GOD	109
12.	THE AESTHETICS OF TAMIL LIFE: ANALYZING SOCIAL REALISM IN SELECT SHORT STORIES OF VAIRAMUTHU	114
13.	DELINEATION OF MUSICAL CULTURE AND MUSICIAN'S LIFE IN THE NOVEL "AN EQUAL MUSIC" BY VIKRAM SETH: A THEMATIC STUDY	121
14.	ENVIRONMENTAL JUSTICE : REVIVING THROUGH WOMEN IN BARBARA KINGSOLVER'S ANIMAL DREAMS	129
15.	DISENTHRALLMENT OF WOMEN IN CHITRA BANERJEE DIVAKARUNI'S SELECTED NOVELS: A REVIEW	137

DISENTHRALLMENT OF WOMEN IN CHITRA BANERJEE DIVAKARUNI'SSELECTED NOVELS: A REVIEW

Mr. Bhojraj Pandhari Shrirame

Assistant Professor

J. M. Patel Arts, Commerce & Science College, Bhandara

Email – shri100bhoj@gmail.com

Dr. Sunil G. Chaudhari

Associate Professor

N. H. College, Bramhapuri

Email – sunilchaudhari03@gmail.com

Abstract:

This research paper uses the traits of Chitra Banerjee Divakaruni's protagonist to explore how women identify both within and outside the boundaries of our society. Identity describes a person's distinctiveness, values and drive toward independence. Divakaruni skillfully captures the diasporic component of identity issues in her writings. Divakaruni's books were critically examined in an effort to investigate the identities of her female protagonists. Conflict empowers people to take control of their lives and make their own decisions, but it also makes them more indifferent and pessimistic about the world around them. In Divakaruni's works, female heroes win against adversity rather than submitting to male control. As a result, the female protagonist of Divakaruni does not fit traditional expectations. They realise, there is a brave new world out there for them to explore and that they mustmake some bold decisions in order to get there because they have done the hard thinking and seen the big picture.

Keywords: women, boundaries, pessimism, tradition, adversity.

Introduction:

Examining female consciousness in literature is a fascinating endeavor. This feminine consciousness is compelled to question and reject every belief it has acquired from its experiences, learning or exposure to the universe as it abruptly reveals the meaninglessness ofthe cosmos. Then it starts to question the purpose of its entire existence. The idea of female identity exemplifies how, generally in response to masculine paradigms of female experience, female awareness is transformed. Women's disenchantment is a process, strategy and slew of efforts by which women have sought to liberate themselves from the authority and control of men and traditional power structures, as well as to secure equal rights for women, remove gender discrimination from laws, institutions and behavioral patterns, and establish legal standards that will promote their full equality with men. (European Institute for Gender Equality, 2020).

Women's Condition:

Freedom is the birth right of all human beings, even birds and animals love freedom. It means freedom is loved by all the living beings. In early history of India man and woman had equal rights. From thousands of years ago Indians had been facing foreign invasions, which drove them in a long exile. Adopting themselves to change the environment, women passed through pardah and burning evils into the seclusion and backyard of history. The world history moved on with new concept of feminism.

This movement of feminism is divided into three phases

1. The feminine phase: In this phase the women writers try to adhere and write as male values perspective regarding the place of women in the society.

2. The feminist phase: In this phase the women writers criticize the role and oppression of women in the society.
3. The female phase: In this phase the women writers represent their authentic and valid views aboutwomen.

The concept of feminism in India is also divided into three phases. The first phase in India began during British Empire in the mid of 19th century when the European began to speak out against the social evils like Sati. The second phase of feminism was between 1915 to Indian independence. It was the period of Gandhian era where independent women organization began to emerge. The third phase of feminism included the period after independence which has focused on the fair treatment being given to women at home and in society. In contravention of the progress made by Indian feminist movement still women are facing many issues of discrimination in modern India. Literature being the mirror of society, explores the 'women's questions'. Many writers extensively and vociferously try to represent their views about women problem in front of society.

Contribution of Chitra Banerjee Divakaruni:

Chitra Banerjee Divakaruni is one of the best post-independence writers who tries to expose the tears behind the curtains of women heart. She is an award-winning Indian – American author. Her works have been published in over 50 magazines and translated in 29 languages all over the world. She was born in Kolkata, India. She completed her graduation in BA from the University of Calcutta in 1976 and for further studies she went to United States of America and received MA from Wright State University in 1985. She received Ph.D. in English from California University, Berkeley. She spent most of her life outside of India. She lives in Houston with her husband Murthy and her two sons, Anand and Abhay.

The two main families – the Boses and the Roys – represent upper-class and middle-class India. Divakaruni embraces the complexity of social class and allows the reader into a multi-layered world of money, status, education and the choices one makes as you climb the social ladder. Other issues make an appearance – religion, politics, immigration, ancestry and race – but the focus of *Oleander Girl* is very much on class. Very early in the novel,Divakaruni introduces Asif Ali, the Muslim driver for the very Hindu Bose family, and also mentions in passing the 2002 Godhra riots in India sparked by Muslims allegedly attacking a train full of Hindu pilgrims and the subsequent state-sponsored program against Muslims.

The novel, "The Forest Enchantment" related to Ramayana, one of the world's greatest epics, is also a tragic love story. In this brilliant retelling, Chitra Banerjee Divakaruni places Sita at the centre of the novel and this is Sita's version. *The Forest of Enchantments* is also a very human story of some of the other women in the epic, often misunderstood and relegated to the margins: Kaikeyi, Surpanakha, and Mandodari. A powerful comment on duty, betrayal, infidelity and honour are made. It is alsoabout women's struggle to retain autonomy in a world that privileges men, as Chitra transforms an ancient story into a gripping, contemporary battle of wills. While the Ramayana resonates even today, she makes it more relevant than ever, in the underlying questions in the novel: How should women be treated by their loved ones? What are their rights in a relationship? When does a woman need to stand up and say, 'Enough'?

Feminist literature is not new for us. It is rapidly developing critical ideology. Literature tries to represent the voice of women in our society which was usually downtrodden in patriotic culture in India. In the 21stcentury Indian society could not escape the mental enslavement of women. Even today, women are reliant on freedom, though the Indian

constitution conferred fundamental rights on women. The male dominated culture has not been exempted from the social restrictions imposed on them.

Chitra Banerjee Divakaruni offers an insightful and provocative analysis of the depth of her characters against traditional background. Her novels are written in a way to find out the truth about the social, economical, educational, political and traditional life. She elaborates the feelings and situations through her characters.

Conclusion:

My point of view in this research paper is to present all major aspects of Chitra Banerjee Divakaruni's novels, like women's value and their contribution in society, disenthrallment of women, injustice, oppression, irony and secondary treatment being given to women by patriarchal society and to bring out her contribution to the field of Indian English literature and to assert her rightful place.

Chitra Banerjee Divakaruni represents Tilo, Panchali, Sudha, Anu, Mrs. Bose etc. as female characters with unique identity in her novels. The meaning of 'self-assertion' varies from culture to culture and in different circumstances. Her work shows how women can achieve freedom openly and effectively without fear of, ridicule or guilt, lays the groundwork for full self-realization and offers proven solutions to common pitfalls that hinder women. They face any situation in their lives with the required straight, effective and positive action.

REFERENCES:

1. Divakaruni, Chitra Banerjee. *The Mistress of Spices.* Doubleday, 1997.

2. Divakaruni, Chitra Banerjee. *Sister of my Heart.* Doubleday, 1999.

3. Divakaruni, Chitra Banerjee. *The Vine of Desire.* Doubleday, 2020.

4. Divakaruni, Chitra Banerjee. *The Palace of Illusion.* Doubleday, 2008.

5. Divakaruni, Chitra Banerjee. *Oleander Girl.* Simon & Schuster, 2013Divakaruni, Chitra Banerjee. *The Forest of Enchantment.* HarperCollins, 2019

6. Divakaruni, Chitra Banerjee. *The Forest of Enchantment.* HarperCollins, 2019

1. Agrawal, Dr. Gunjan and Gunjan Kapil. *The Representation of Woman in Chitra Banerjee Divakaruni's Doors, Affairs and Meeting Mrinal*. The Criterion, Vol5, pp 77.

2. Bhattacharya, Madhumita. *Dreams and dislocation*. The Telegraph. 2005.

1. Divakaruni, Chitra Banerjee. *Divakaruni, Chitra Banerjee.* Retrieved www.chitradivakaruni.com/about/bio: www.chitradivakaruni.com/about/bio

2. *European Institute for Gender Equality*. (2020, 08 04). Retrieved from Emancipation of Women: https://eige.europa.eu/taxonomy/term/1098

3. Reddi, M. S. *Emancipation of Women*. The Hindu, 2015.

4. Dhanam,K S. *Negotiations with New Culture: A Study of Chitra Banerjee*

Divakaruni's the Mistress of Spices. Critical Essays on Diasporic Writings, edited by K. Balachandran, Arise, 2008, p. 62.

5. Divakaruni, Chitra Banerjee. *Before We Visit the Goddess*. Simon & Schuster Paperbacks, 2017.

6. Divakaruni, Chitra Banerjee. *Leaving Yuba City: New and Selected Poems.* Doubleday, 1997, p. 96.

7. Divakaruni, Chitra Banerjee. *Oleander Girl: A Novel*. Simon & Schuster Paperbacks, 2014.

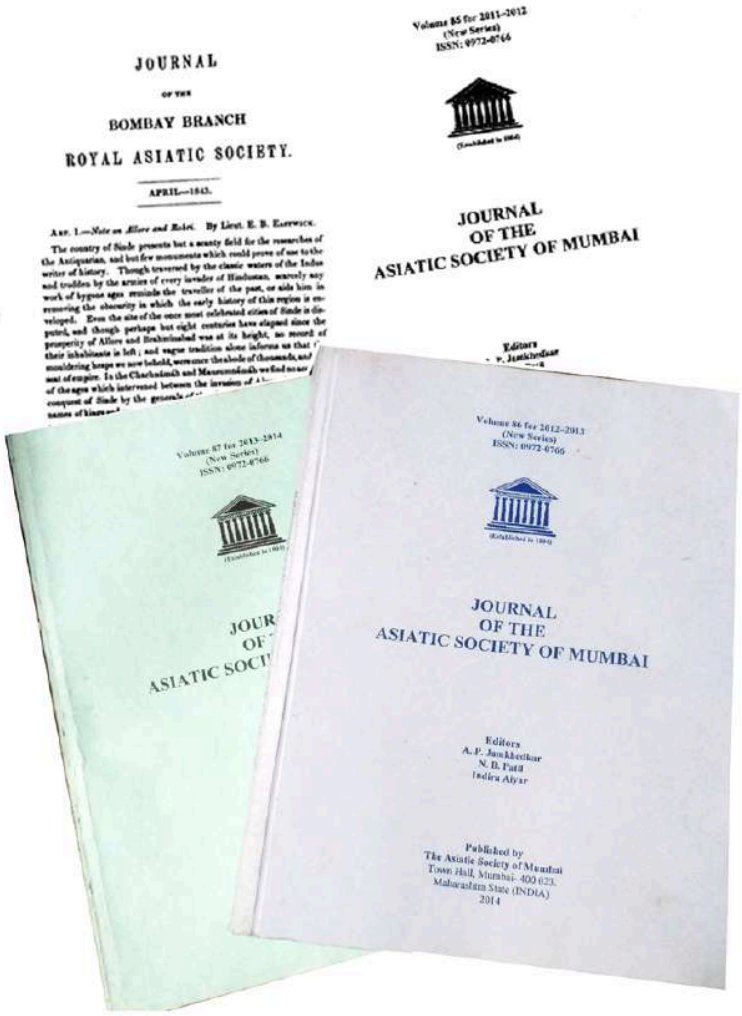
8. Parmeshwaran,Uma. *Home Is Where Your Feet Are, and May Your Heart Be There Too.* Writers of Indian Diaspora: Theory and Practice, edited by Jasbir Jain, Rawat Publications, 2011, p. 34.

9. Nimavat, Dushyant. *The Cassandras in Exile: A Study of the Diasporic Sensibility in the Poetry of Meena Alexander, Sujata Bhatt, Chitra Banerjee Divakaruni, Moniza Alvi and Jean Arasanayagam*. Saurashtra University, 2011.

10. Chitra Banerjee Divakaruni.*Wikipedia, Wikimedia Foundation*, 4 Apr. 2017, en.wikipedia.org/wiki/Chitra_Banerjee_Divakaruni. Accessed 21 Apr. 2017.

11. Divakaruni, Chitra Banerjee. *The Global Indian Family - A Talk By Chitra Banerjee Divakaruni.* Litmus 2016. Litmus 2016, New Delhi, lsrenglish.weebly.com/2016-2017.html.

About Journal (/journal/index.php/38-about-journal)



Asiatic Society of Mumbai is a pride of this city. The Society has one of the biggest treasures of different archives. One of such archives is its publication – Society's Journal. The Journal published its first issue in 1841. In 2016, the enthusiastic editors, who work on honorary basis for the Society, continue to follow the great tradition of their predecessors. It's a pride that Bharatratna MM Dr. PV Kane was once the editor of Society's Journal.

Since 1841, the Society has seen many ups and downs. It even changed its name from The Royal Asiatic Society (Bombay Branch) to Asiatic Society of Bombay, and then to Asiatic Society of Mumbai. The Journal, however, stuck to its high standards which attracted hundreds of researchers to the Society. This treasure of Journal issues in the last 172 years has always been an important source of references for the students, researchers and readers. They used to flip through the Journal's paper pages for finding the references.

- **Name of the Journal :** Journal of the Asiatic Society of Mumbai.
- **ISSN Number** : 0972-0766.
- **Nature of Publication :** Hard Copy.

- **Periodicity** : Annual.
- **Publisher :** The Asiatic Society of Mumbai.
- **City :** Town Hall, Mumbai - 400 023.
- **State :** Maharashtra.
- **Country :** India.

© 2018 The Asiatic Society of Mumbai. All Rights Reserved.

↑↑↑

UGC-CARE List

You searched for "**0972-0766"**. Total Journals : **1**

Search:

Sr.No.	Journal Title	Publisher	ISSN	E-ISSN	UGC-CARE coverage years	Details
1	Journal of the Asiatic Society of Mumbai (print only)	The Asiatic Society of Mumbai	0972-0766	NA	from June-2019 to Present	View

Showing 1 to 1 of 1 entries

Previous 1 Next

Copyright © 2024 Savitribai Phule Pune University. All rights reserved. | Disclaimer

An International Registered Peer Reviewed Bilingual Research Journal

SATRAACHEE

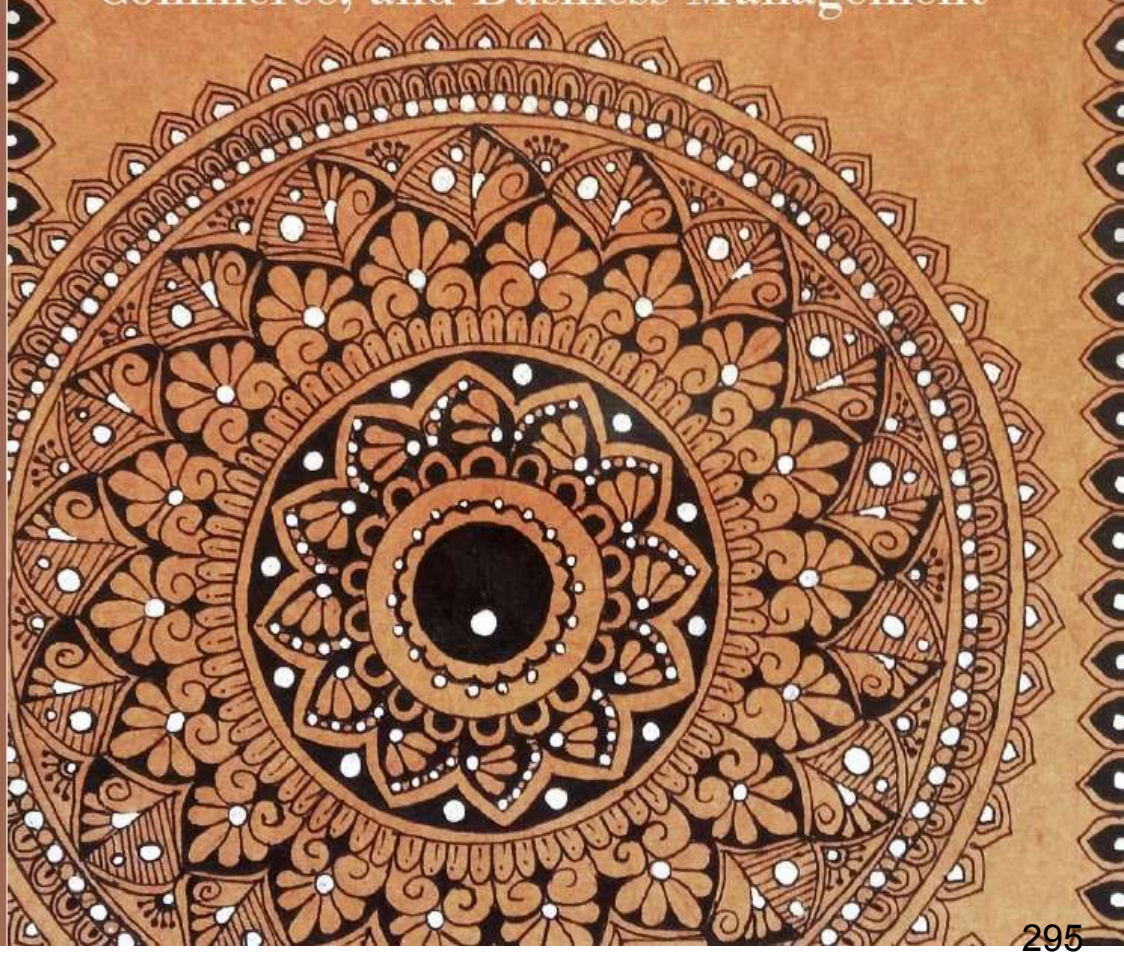
ISSN 2348-8425

सत्राची

A UGC-CARE Enlisted
Peer Reviewed Research Journal

Year 11, Issue 26,
Vol 38, No. 3.
Jan.-March, 2023

"Contemporary Issues of Social Science, Commerce, and Business Management"



ISSN : 2348-8425

SATRAACHEE

UGC Care Enlisted, Peer Reviewed research Journal

Issue 26, Vol. 38, No. 3, Jan-March, 2023

Guest Editor
Baldeo B. Kakde

Editor
Anand Bihari

Chief Editor
Kamlesh Verma

Co-Editor
Archana Gupta
Jay Prakash Singh

Review Editor
Suchita Verma
Ashutosh Partheshwar

Assistant Editor
Guntaj Kour
Shivangi

Advisory Committee and Reviewers

- *Prof. Bhupendra Kalsey, Co-Ordinator, Bhartiya Bhasha Vibhag, Nalanda Open University, Patna.*
- *Dr. Anurag Ambasta, Coordinator, Department of English, St. Xavier's College of Management and Technology, Patna*
- *Dr. Nutan Kumari, Assistant Director & Associate Professor, Amity, Institute of English Studies & Research, Amity University, Patna*
- *Dr. Shwet Nisha, Assistant Professor, Dept. of English, Amity University, Patna*
- *Dr. Pushpalata Kumari, Political Sc., Patna University, Patna.*
- *Dr. Neera Choudhury, Music, Patna University, Patna.*
- *Dr. Arvind Kumar, Music, Patna University, Patna.*
- *Dr. Raju Ranjan Prasad, History, B.B.A.Bihar University, Mujaffarpur*

❑❑

In this Issue...

07 :: A Message from the Guest Editor — *- Dr. Baldeo B. Kakde*

09 :: Unemployment: A Contemporary Issue of the Indian Economy — *- Aman A. Tirpude, Dr. C. Tembhurnekar*

15 :: Impact of Fintech on the Profitability of Public and Private Sector Banks (Indian Perspective) — *- Ashish V. Mundafale, Dr. MedhaKanetkar*

21 :: A Study Examining the Relationship between Social Media Usage and Financial Knowleldge of Working Women — *- Prof. Amol Vaze, Dr. Bhaskar L. Lengure*

30 :: Analysis of Goods and Service Tax (GST) In India — *- Dr. Ashwini S. Potphode*

33 :: A Study of the Enterpreneurial Ecosystem in India and the Factors and Challenges Affecting the Entrepreneurial Ecosystem — *- Ashwini A. Landge, Dr. Vivek S. Chavan*

39 :: Empowering Youth of Nation through Skills: An Initiative of Ministry for Skill Development & Entrepreneurship (MSDE) — *- Dr Bhavana Khapekar*

45 :: Unbanked to Banked : Role of E-Financial Inclusion in an Indian Context — *- Prof. Bhumika Shah, Dr. Vivek Nagbhidkar*

53 :: Contemporary Issues on Operating of Digital Payment Devices and Applications in India — *- Dr. C.M. Tembhurnekar*

60 :: Stress Management of College Students before and during COVID-19 Pandemic : A Literature Review — *- Divya Shrivas, Dr. Bhavesh Jasani*

65 :: Online Shopping Benefits and Challenges — *- Dr. Gajanan Babade*

69 :: A Study of Current Scenario of Digital Platform in Rural area of Nandurbar District — *- Dr. G. M. Morey*

80 :: A Study on Recent Trend in Investment in Mutual Fund in India — *- Jitendra Harichandra Raut, Dr. Aniruddha Sunil Gachak*

86 :: An Empirical Study on Investment Preferences and Awareness Level Before and After COVID-19 — *- Prof. Kaushik Save, Dr. Bhaskar L. Lengure*

94 :: Analysis of Investment Trend of People with Respect to Mutual Funds in Wardha District, Maharashtra — *- Jajodia Laxman, Dr. Mansuri A. K.*

104 :: Commercialization of Surrogacy in Contemporary India: A Legal Paradox — *- Dr. Mahendra Pachadkar*

110 :: An Analysis of Impact of Office Automation System on the Quality Improvement of College Admin Staff — *- Mr. Mangesh P. Wadhi, Dr. Pravin H. Ghosekar*

An Analysis of Impact of Office Automation System on the Quality Improvement of College Admin Staff

- Mr. Mangesh P. Wadhi *
- Dr. Pravin H. Ghosekar**

Abstract :

Office automation system is a integration of hardware, software and communication technology. This system is very helpful to the college admin staff in their various day to day task which starts from the students admission to leaving certificate, various reports related to university, government and management. The office automation system helped those admin staff to complete their task in efficient and effective manner which lead to the quality improvement in their regular work. This paper focuses on the impact of office automation system on the quality improvement of college admin staff.

Keywords: office automation, admin staff, college work

Introduction :

Office automation is a broad term which represents the use of technology and software for the profession and integration of technologies for the efficient and effective work in the office. It is mainly based on two factors: computers and communication technology. The computer technology comprises of computer, software, hardware and all peripheral devices while communication technology is the technology which facilitate transfer of data from one device to other; it comprise all the software and hardware required for the transfer of those data and information. Communication technology assimilates these devices and people. It provides an effective communications infrastructure. So, office automation is the use of different technologies (e.g. computer and telecommunication) to streamline and support routine office functions improve communication, increase office efficiency and quality improvement of admin staff. Many officeshave to perform many works including data collection, preparation of reports, correspondence, communications, file maintenance,

* Research Scholar, Radha Mahavidyalaya Nagpur

** Head, Department of Computer Science J.M. Patel Arts, Commerce & Science College, Bhandara (MS)

duplication and distribution of materials can be enabled and improved through word processing and other office automation techniques.

Objectives :

- To study the role of office automation system in college.
- To analyse the impact of office automation system on the college admin staff.

Hypothesis :

H0 : There is no significant impact of office automation system on the quality of work of college admin staff

H1 : There is a significant impact of office automation system on the quality of work of college admin staff.

Office Automation System

The system consists of both hardware and software solutions that allow the transfer of data from one device to other to minimise the human intervention. Office automation minimizes the organizational workloads by simplifying and automating different processes including accounting, data management, training, facility management, and different administrative tasks.

An office automation system doesn't mean paperless office. For example, maintaining all work product and client communication in a document management system. Yet, an office automation system facilitates organizations much more than going green by minimize the use of paper which reduces cutting trees. It is a powerful tool that can be used to eradicate manual processes, identify inefficient workflows, and enable decision-making.

Office

IT has become one of the most exciting and significant applications in the admin office of today. An office is usually referred to as a place where admin staff performs some sort of paper work on their desks. However, this definition is incomplete. An office can be described as: "A place where proper records are prepared, handled, and maintained for the purpose of controlling information and ensuring efficient and effective operations".

- A place where authorities like physicians, lawyers, or engineers conducts their business.
- It may consists of a tables, chairs, almirahs, computers, telephone, photocopier, tele printers and additional equipment like calculator, cyclostyle and Xerox machines.
- People in the office can be executives, secretaries, clerks and peons.
- It is the primary responsibility of an office to keep records of an organization - making records, using records, and preserving them for future use.
- The college admin office perform many works related to the students, university and government including admission, exam form, enrolment, mark sheet, leaving certificates, scholarships, salary and hostels administration, etc.

Function

The functions performed by an office may be divided as primary and secondary.

- Primary function of the office is to make, maintain and use records of the organization.
- The secondary functions are divided into the following categories.

(i) **Planning :** Planning is another major office function. In planning, activities are scheduled for the organization and a course of action is laid out. The performance of all office work requires prior planning. Planning is necessary to avoid waste and delay. The cost of office operations is reduced when they are planned.

(ii) **Communication :** Arranging communications within different individuals within the premises of the office through interviews, telephones and conferences, and with outsiders using letters, telephones, telegrams and personal meetings etc is a crucial work performed by the office.

(iii) **Compilation and Presentation of Statistics :** Compilation and presentation of data is also an important work of office. Collection and evaluation of prices, compilation of costs, analysis of sales and reckoning of payroll is also part of the office work.

(iv) **Systematization and Cost Reduction :** Systematization is done by analyzing the existing office routines and accepting improved ones. Office cost may be condensed by using automated technology whenever necessary. Off-line cost may also be reduced by accepting better office forms and other labour saving devices.

(v) **Creation and Management of Information :** Majority of offices of any size and kind, create and manage information that is mandatory for making decisions or providing services to people within or outside the organization.

The creation and management of information includes the following activities :

- Calculating,
- Gathering facts and figures,
- Categorizing and sorting,
- Summarizing,
- Storing and retrieving,
- Reporting.

Services

The services of an office includes :

- Drafting, typing and duplicating services : Facilitating drafting typing and duplicating letters, circulars etc.
- Mailing service :issuing, receiving and dispatching memos, letters, notices, circulars, etc.
- Oral communication service :Offering all assistance for organizinginteractions, conferences, meetings, interview and managing telephone calls.
- Accounting service : Recording and maintaining business transactions and financial accounts.
- Filing and indexing service :Preparing, maintaining, preserving and locating all

office files and account books.

- Billing service : Preparing bills and invoice, managing credit and recovery of outstanding accounts.
- Statistical service : Collection, tabulation and analysis of statistical data and preparation of graphs and reports.

Characteristics of Office Automation System

Office automation is aextensively used term from last decade. It means the use of computer and communication technology to improve the productivity of “knowledge workers".

Office automation denotes to the use of electronic equipments and communication systems to perform the “tasks electronically”.

The tasks include

- Text processing,
- Data processing,
- Information storage,
- Information retrieval and updating,
- Message distribution,
- Document transmission and reproduction,
- Teleconferencing.

√ Office automation is a process which involves people, procedure and technology.

√ Office automation technology include word processor, spreadsheets, presentation, telecommunication, reprographics, e-mail, e-filing, fax transmission, and voice technologies.

Office automation involves the use of computers, in unification with other electronic-equipment to automate the basic secretarial and adminwork of office.

√ Basic office automation consists of word processors in a network.

√ Office automation is multifunction information systems which provide executives decision support tools such as :

- o On-line access to databases,
- o Model building and forecasting,
- o Risk analysis,
- o Sophisticated graphics,
- o Integration of data and text,
- o Data communication.

√ Some office automation systems perform other important tasks along with word processing on networks.

√ Office automation supports a software packages that can be used as decision support tools which includes Word processor, Database management systems, Electronic

spreadsheets, Graphics packages, Electronic mail systems.

Benefits of Office Automation System

- Improved efficiency,
- Improved service
- Improved accuracy
- Timeliness
- Facilitates control
- Standardization of office work
- Minimizes of monotony
- Prevention of fraud
- Superior information retrieval
- Minimum operating cost
- Minimum paper work
- Better communication environment.

Improved efficiency

The large scale use of computers and other office automation technologies had minimises the cost by 10% to 30%. The use of office automation technologies increases productivity. These productivity improvements can lead to (i) a improved competitive position and (ii) improved per capita income.

Thus, office automation brings speed and competence to all types of office work. Improved efficiency leads to better profitability and creates brand image in the minds of the people.

Improved service

College admin offices use office automation technologies which helped in improvement in the services they provide to customers, clients, patients etc.

Improved accuracy

If a data processing operation is nervy to and beyond the capacity for which it was initially planned, imprecisions begin to appear and the control of official activities suffers. Online processing performs all office work accurately and efficiently. Office automation ensures better accuracy. Chances of errors are almost negligible.

Timeliness

Timeliness of information is of countless importance to all offices and organizations for decision making. Timely information helps in timely decisions making which prevents undesirable consequences. Only office automation can accomplish these and provide timely information.

Facilitates control

Office automation helps managers to exercise better degree of control over their subordinates.

Standardization of office work

Office automation helps to facilitate standardization of office work and procedures.

Standardization of office work facilitates better coordination of works.

Minimizes of monotony

Office automation reduces the monotony of carrying out boring processes which are repetitive and time consuming.

Prevention of fraud

Office automation tools are trustworthy than man. A man can cheat but a computer works on its own motion so it minimizes the fraud.

Superior information retrieval

Most information retrieval tasks clearly do not involve life or death decision; but quick computer assisted retrieval can save time and worsening for many individuals. So, office automation safeguards better information retrieval.

Minimum operating cost

Office automation technologies helps in minimizing the per hour of work which helps in reducing operating cost.

Minimum paper work

Paper based office work is costly. Office automation provides many ways for accomplishing office work through the use of office automation technologies such as computer processing, distributed data processing, e-mail, and teleconferencing etc.

Better communication

Studies reveal that a lot of office actions involve the communication of information to others. The office automation system facilitates faster communication.

Quality Improvement Strategy in College

Office automation is the use of electronic and telecommunication devices in office activities in order to increase efficiency. This increased efficiency is resulted by completion of information exchange within the office and between offices and their environment and finally could help to manager by deliverimproved information. Today automation and application of new technologies is not only considered as a need but as anacute necessity (Javadi& Safari 2013). Office automation has effects on effectiveness of human resources and his research findings indicates office automation has direct and positive effects on efficiency of human resources.The seniors and employees of colleges, prior to taking any actions in line with the application of office automation in colleges, should come to the conclusion that the continuance of the status quo is no longer conceivable and a firm determination should be felt in them respecting the application of office automation. Organizational effectiveness is affected by four types of major variables that rarely are under the control of superior. One of them is organizational feature such as structure and the technology which we are using. Thus, using tools of automation services or computerize technology like computer, Xerox, fax, printer and scanner, basis in increasing the organizational effectiveness. Thus the office automation system helps college in improving quality for admin staff.

Important features of an office automation system

There are uncountable applications and software programs that promise improved

efficiency through automation. Achieving organizational efficiency through an office automation system needs more than downloading a few apps. Rather, we need ainclusive office automation solution that offers the following features :

- **Process modelling and work flow design**

  An important advantage of an office automation system is the capability to design and improve workflows. The solution that you select should give you the ability to produce detailed workflows in a matter of minutes. Foremost solutions offer an intuitive design and comprise features like a drag and drop process modeller.

- **Mobile compatibility**

  In the age of the stay-at-home economy and the COVID-19 pandemic, mobility has utmost importance than ever. Employees must be able to accomplish their functions from anywhere. A cloud-based solution providing secure and accessible to every employee.

- **Integration**

  One of the major challenges that organizations face when endeavouring to automate their processes is integrating several third-party software or apps. Your office automation system should work effortlessly with your other tools like email marketing and other admin functions.

- **Managing tasks and deadlines**

  Task management is ansignificant feature of office automation solutions. For processes to run easily, employees must know what to do and when to do it. Your office automation system should allow us to create and view pending tasks and deadlines, as well as reallocate tasks as needed.

- **Access control and security**

  To protect the security of our systems, we need to be able to set access privileges within the organization. Cloud-based solutions offers advanced security features to protect data from being compromised.

- **Communication**

  An important feature of any automation system is the capacity to communicate flawlessly. Stakeholders should have all the information they need to accomplish each task, as well as the ability to reach out to others for added assistance. Our office automation system should offer topographies like a form builder.

- **Reporting and analytics**

  To evaluate and improve our office automation system, we need to have access to data and crucial performance indicators. Leading office automation systems have built-in reporting and analytics capabilities.

Impact of automation of College

Automation is suited to the created nations of the world which have attained a condition of full business marvel. In those nations, automation winds up fundamental in light of

shortage of labor. Computerization was not recommended for a creating nation like India on the grounds that here the condition of joblessness is intended and mechanization will expand this condition of unemployment. Be that as it may, mechanization ought to be offered in post workplaces, colleges, banks where the expanded workload requires fast and precise support of people in general. Computerization drives the additional impacts :

- Automationhelps in accomplishing college admin work more easily and efficiently.
- Office automation facilitate online admission and regular and on demand report writing.
- Office automation helps in enrolment, attendance and result management.
- The office automation system in colleges also help to manage scholarships, salary and other admin tasks.

Thus office automation improved work efficiency and quality of work of admin staff working in the colleges.

Hypothesis Testing

The hypothesis assumed during the study was

H0 : There is no significant impact of office automation system on the quality of work of college admin staff

H1 : There is a significant impact of office automation system on the quality of work of college admin staff

Testing of Hypothesis :

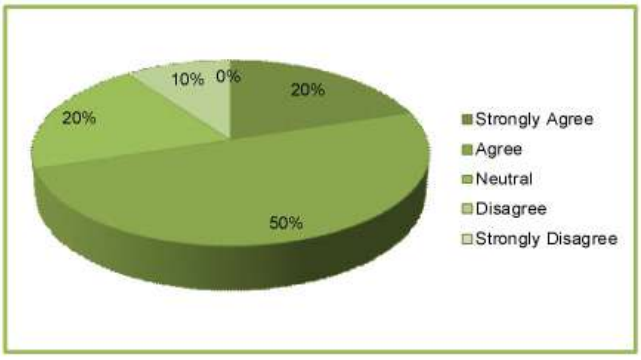
The hypothesis were tested using the graphical method. The data collected from the college 10 staff and 50 students as under.

Table 1 : Do you feel that office automation system had improved the quality of your work.

No of Respondents : 10

Strongly Agree	Agree	Neutral	Disagree	Strongly Disagree
2	5	2	1	0

Graph 1:



From the above graph it is found that out of 10 respondents 20% respondent agree about the statement "office automation system had improved the quality of your work", whereas 50% respondents agreewith the statement, 20% respondent are neutral with the statement, 10% are disagree with the statement and no respondent are strongly disagree with the statement.

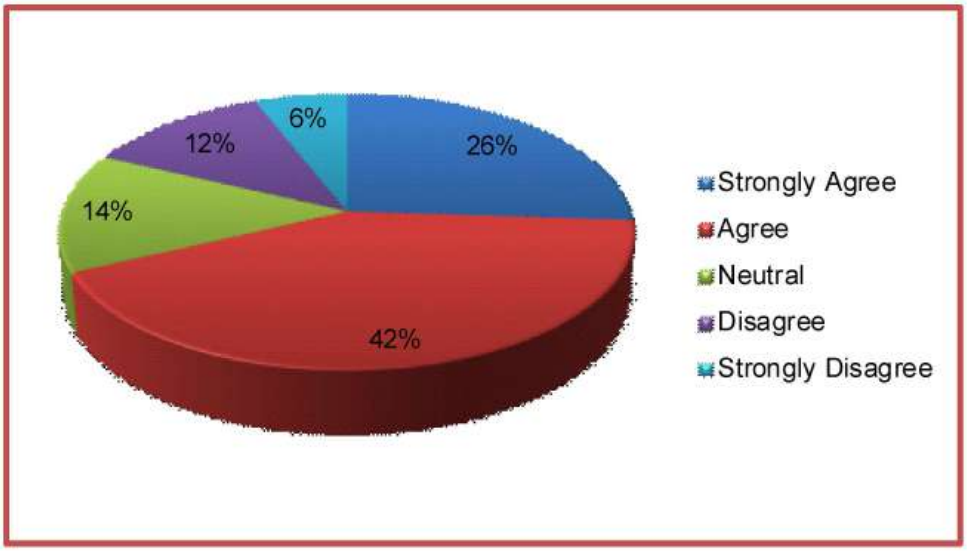
That means, it is found that office automation system had improved the quality of admin staff's work.

Table 2 : Do you feel that because of office automation system college adminstaffareable to provide proper information to students?

No of Respondents : 50

Strongly Agree	Agree	Neutral	Disagre	Strongly Disagree
13	21	7	6	3

Graph 2:



From the above graph it is found that, out of 50 respondents 26% respondent agree about the statement "Because of office automation system college admin staffare able to provide proper information to students", whereas 42% respondents agreewith the statement, 14% respondent are neutral with the statement, 12% are disagree with the statement and 6% respondent are strongly disagree with the statement.

That means, with the help of office automation system college admin staffare able to provide proper information to students.

Thus from the analysis and interpretation of above graphs it is found that the null hypothesis "There is no significant impact of office automation system on the quality of

work of college admin staff" is rejected and alternative hypothesis "There is a significant impact of office automation system on the quality of work of college admin staff" is accepted.

Thus, we can say the office automation system is positively impacts on the quality of work of college admin staff.

Conclusion

Automation in college is becoming an inevitable reality considering the number of benefits it offers to an institution. The biggest value-addition that automation brings is that it makes managing student data in most efficient and effective manner. The admin staff can monitor students and other data easily. Students also get additional support from the admin staff for any office or university related issues.It provides 360-degree automation covers to an entire college office. By analysing the data collected it is also proved that office automation system is positively impacts on the quality of work of college admin staff.

References :

- Burnes, B. (2004). Managing Change: A Strategic Approach to Organizational Dynamics (4th ed.). London: Pitman Publishing.
- Canning, Richard G. the automated office: Part I. EDP Analyzer, 16, 9 (Sept. 1978).
- Ekundayo, H.T., &Ajayi, A.I. (2009). Towards Effective Management of University Education in Nigeria. International NGO Journal, 4, 432-347.
- Hiatt, J.M. & Creasy, T.J. (2003), Change Management: The people side of change. Colorado, USA: Prosci research,
- Javadi,M.H. & Safari, H.(2013). Assessing Office Automation Effect on Performance Using Balanced Scorecard approach Case Study: Esfahan Education Organizations and Schools. International Journal of Academic Research in Business and Social Sciences 3(9).
- Kasomo, D. (2001). Research Methods in Humanities and Education. Nairobi, Kenya: Egerton University Press.
- Keshtmand, Zahra & Nowrozian, Mohammad & Hatami, Khidan. (2016). THE EFFECT OF TECHNOLOGY AND ADMINISTRATIVE AUTOMATION ON EMPLOYEES' WORK LIFE QUALITY (CASE STUDY: DEPARTMENT OF YOUTH AND SPORTS OF KERMAN SHAH PROVINCE). THE TURKISH ON LINE JOURNAL OF DESIGN, ART AND COMMUNICATION. 6. 1226-1229. 10.7456/1060AGSE/008.
- Kimutai, Kwambai (2017), Effect of Office Automation on Organizational Effectiveness of Public Universities in Kenya, International Journal of Academic Research in Business and Social Sciences, Vol. 7, No. 12 ISSN: 2222-6990
- Kothari C. R. (2004), Research Methodology. Bombay, India: New Age International Publishers.
- Mutula, S.M. and Udoto, M.O. (2002). Quality of learning facilities and learning environment: challenges for teaching and learning in Kenya's public universities. Quality Assurance in Education, 19, 20823.
- Pathak, Wankhede, Chandwani (2018). Office automation system, International Research Journal of Engineering and Technology (IRJET) , Volume: 05 Issue: 03 | Mar-2018 www.irjet.net
- Gu, Wang, XU, Dong, Liu (2012) The Design of OA System Based on B/S Structure of

Colleges and Universities, 2011 International Conference on Environmental Science and Engineering (ICESE 2011), http://www.sciencedirect.com/

- https://www.ebookbou.edu.bd/Books/Text/SST/DCSA/dcsa_1302/Unit-01.pdf
- https://mmhapu.ac.in/doc/eContent/Management/AftabAlam/OFFICE%20AUTOMATION% 20 SYSTEM%20(OAS)%20sam%204.pdf
- https://www.processmaker.com/blog/implementing-an-office-automation-system/
- https://mindfieldconsulting.com/16-examples-advantages-and-disadvantages-of-office-automation-systems/
- https://www.academiaerp.com/blog/why-is-automation-important-for-educational-institutions/

❑

SATRAACHEE, ISSN 2348-8425

आ वो होता जोहवीति सत्त: सत्राचीं रातिं मरुतो गृणान: । य ईवतो वृषणो अस्ति गोपा: सो अद्वयावी हवते व उक्थै: ।। (ऋ. 7.56.18)
उभयं शृणवच्च न इन्द्रो अर्वागिदं वच: । सत्राच्या मधवा सोमपीतये धिया शविष्ठ आ गमत् ।। (ऋ. 8.61.1)

* Editor :

Anand Bihari.
biharidot@ gmail.com
satraachee@gmail.com
09661792414, 09470738162

* Assistant Editor :

1. **Dr. Ankita Kumari**
2. **Mrs. Bhawna Mishra**

सत्राची के अंक











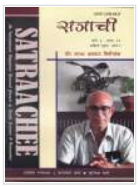


POWERED BY

Advisory Board

- **Prof. Mukteshwar Nath Tiwary.**
  Professor
  Hindi Bhawan, Vishwa Bharti,
  Shanti Niketan. West Bengal
  Mob. 09474765831
- **Dr. Kamlesh Verma.**
  Dept. of Hindi
  Rajkiya Mahila Mahavidyalya,
  Sewapuri,Varanasi, U.P.
  E-mail: kamleshvermajnu@gmail.com
  Mob. 09415256226
- **Dr. Ashutosh Partheshwar**
  Assistant Professor
  Dept. of Hindi
  Oriental College, Patna City.
  Mob. 09934260232
  E-mail: parthdot@gmail.com
- **Dr. Raju Ranjan Prasad.**
  Critic, History & Hindi Lit.
  C-19, Shreenagar,
  Ashiananagar, Patna-25
  Mob. - 08294307626
  E-mail: rajooranjan@gmail.com
- **Dr. Pushpalata Kumari.**
  Assistant Professor & H.O.D
  Political Science
  Patna University, Patna
  E-mail: drpushpalatammc@gmail.com
  Mob. 09431402736
- **Dr. Arvind Kumar.**
  Assistant Professor & H.O.D
  Music





Music
Patna University, Patna
Mob. 09835681230

POWERED BY

UGC-CARE List

You searched for **"2348-8425"**. Total Journals : **1**

Search:

Sr.No.	Journal Title	Publisher	ISSN	E-ISSN	UGC-CARE coverage years	Details
1	Satraachee	Satraachee Foundation	2348-8425	NA	from July-2022 to October- 2023	Discontinued from Oct. 2023

Showing 1 to 1 of 1 entries

Previous 1 Next

Copyright © 2024 Savitribai Phule Pune University. All rights reserved. | Disclaimer

Section A -Research paper

Impact of Converging Disruptive Technology with Business Strategies for Improved Effectiveness: An Empirical Study

Dr.Malini.T.N
Associate Professor Department of Management Studies
Nitte Meenakshi Institute of Technology
Dr. Anand Muley,
Assistant Professor, Dept of Commerce,
J. M. Patel Arts, Commerce and Science College, Bhandara.
Dr. Rashmi Yogesh Pai
Associate Professor Department of Commerce Manipal Academy of Higher Education Manipal.
Dr Jyoti Bhoj
Assistant Professor Faculty of Management and Commerce
SRM University, Delhi- NCR Sonepat, Haryana

Abstract

The convergence of disruptive technologies with business strategies has significant implications for improving organizational effectiveness. In the contemporary, swiftly progressing electronic terrain, enterprises are ceaselessly searching for ground-breaking methodologies to employ disruptive technologies to procure a competitive edge. The process of digital transformation (DX) has transformed into an omnipresent phrase that exceeds the boundaries of information technology aficionados and has garnered extensive recognition. It is not merely a fleeting subject confined to online search engines; rather, it is a phenomenon that will persist until a majority of IT companies embrace the technologies capable of liberating them from the confines of legacy IT systems. Two key technologies driving the actualization of digital transformation are convergence technology and disruptive technology. Authentic digital transformation entails a comprehensive shift in processes, transcending isolated departments and embracing enterprise-wide platforms to enhance customer experiences. In essence, true transformation necessitates the convergence of people, processes, and technology, leading to a holistic and profound change from within the organization. It is crucial to recognize that digital transformation goes beyond surface-level changes and superficial advancements. Organizations seeking a successful digital transformation must undertake a fundamental reconceptualization of their business operations. This requires the seamless integration of innovative technologies into all facets of the organization, fostering an environment that promotes agility, innovation, and customer-centricity. To accomplish this goal, businesses must overcome entrenched, traditional silos and embrace a more cross-functional approach. This means aligning personnel, streamlining processes, and leveraging advanced technologies to effectuate meaningful change, ultimately leading to new opportunities for growth and a competitive advantage.

Keywords- Business Cross-Functional Approach, Business Digital Transformation.

Introduction

The business landscape is an ever-shifting realm, characterized by constant change and turbulence. According to Lee and Trimi (2021), in today's digital age, the rate and magnitude of these changes have reached unprecedented levels, driven by factors such as the global pandemic of COVID-19. This dire situation has been particularly injurious to small and medium-sized businesses, which must now contend not with strategic long-term planning, but rather with the pressing need to formulate survival tactics for the upcoming quarter or even just the forthcoming months. The amalgamation of sundry monumental trends such as globalization, technological advancements, environmental anxieties, shifting demographics, urbanization, and the ongoing worldwide health crisis has contributed to the unpredictability that engulfs the commercial sphere.

According to Christensen, McDonald, Altman, and Palmer (2018),, these enormous trends are progressing at an increasingly accelerated pace, resulting in a greater level of intricacy. To illustrate, the concept of globalization, previously characterized exclusively by trade conflicts and nationalist ideologies, is presently undergoing significant transformations. Emerging economies such as China and India have established robust domestic markets, diminishing their reliance on global trade.

According to Evans (2020), the coronavirus crisis has had a significant impact on the technology sector With the advent of the coronavirus pandemic crisis, geopolitical divisions have deepened, supply chains have been severely disrupted, and many are questioning whether this marks the end of globalization as we know it.For example, advanced digital technologies have been extensively employed in COVID-19 testing, contact tracing, and treatment efforts, enabling the swift restructuring of disrupted supply chains, facilitating telework and remote education, and providing innovative solutions for the faltering economic and social structures. The ongoing pandemic has thrust organizations into a state of urgency, pushing them to innovate rapidly, repurpose their businesses, products, and materials, and deploy groundbreaking solutions to combat the virus's spread, alleviate material shortages, support vulnerable populations, and safely revive the economy., the competition among organizations is tough and unpredictable.

Semerikov et al., (2020) creating sustainable innovation has become a crucial requirement for all sectors, including businesses, government, and non-profit organizations, as they strive to develop flexible, adaptable, enduring, and swift capabilities. To confront emerging technologies and market conditions, organizations must adopt a comprehensive strategy that involves planning, system integration, and a culture that fosters innovation. This strategy should start with the recognition that digital transformation is not an add-on or a separate project but a necessity that permeates every aspect of the organization.

This means investing in technological infrastructure, promoting digital skills among employees, and cultivating a mindset that is receptive to change and experimentation. Furthermore, organizations must break down barriers and adopt an interdisciplinary approach that promotes cooperation and synergy among various departments. This collaborative ethos extends beyond internal stakeholders, as partnerships and ecosystems with external entities, such as startups, research institutions, and industry consortia, become crucial in leveraging emerging technologies and harnessing collective intelligence.

Literature Review

In the realm of information technology strategy, the prevalent viewpoint has traditionally held that it is a functional-level strategy that requires alignment with a company's overall business strategy. According to Bharadwaj, El Sawy, Pavlou, and Venkatraman (2013), digital business strategy is heading towards a new era of insights. even within this alignment view, the direction was established by the business strategy, with IT strategy following suit. In the last decade, the business landscape has shifted significantly as it has progressed into a digital infrastructure marked by amplified interconnectivity between products, processes, and services. Digital technologies, including information, computing, communication, and connectivity, have become the driving force behind the transformation of business strategies, processes, capabilities, products, services, and the relationships that exist between firms in vast extended business networks. In light of these developments, contend that the moment has come to reconsider the role of IT strategy.

Rather than considering it merely as a functional-level strategy subservient to the overarching business strategy, it should now be seen as a fusion between IT strategy and business strategy. This merger as "digital business strategy." To navigate this new paradigm, we suggest four essential themes that will steer our exploration of digital business strategy and assist in defining the next generation of insights. These themes encompass the magnitude, extent, rapidity, and origins of business value creation and capture within digital business strategy. In recent years, firms have been facing an increasing challenge known as "Big Data," which has emerged as a promising frontier for productivity and opportunity. The potentiality of the profound realm of Big Data analytics (BDAC) is widely acknowledged as a revolutionary impetus in the modus operandi of enterprises.

According to Akter, Wamba, Gunasekaran, Dubey, and Childe (2016), the study emphasizes the significance of enhancing firm performance through the alignment of big data analytics capability and business strategy. It is posited that Big Data analytics shall redefine the competitive terrain of industries in the forthcoming triennium, and an astonishing 89% of enterprises harbor apprehension that their failure to embrace a Big Data analytics strategy within the ensuing year may precipitate a depletion of market share and momentum. The notion of 'big data' has accrued substantial acclaim on a global scale. An exploration conducted via the Google search engine in mid-August 2014, employing the terms "big data" and "analytics," yielded an astounding 822 million and 154 million results, respectively. This

unequivocally underscores the colossal fascination and momentousness enshrouding this domain.

To estimate the constructs of BDAC, the study employs the repeated indicator approach, which allows for the simultaneous estimation of all constructs instead of separate estimates for lower-order and higher-order dimensions. The study clarifies that the measurement mode is reflective, as the first-order dimensions reflect the higher-order dimensions. Additionally, the model follows a reflective approach because the theoretical direction of causality is from constructs to items. to develop a comprehensive theory of BDAC strategy, outlining how the dimensions and sub-dimensions of BDAC can be leveraged to establish an overall BDAC climate within organizations. While previous studies have emphasized the importance of management, technology, and talent capabilities in a big data environment, this work sheds light on the role of Resource-Based Theory (RBT) and the entanglement view in proposing an integrated BDAC model and assessing its overall impact on firm performance. As the interest in the application of business analytics continues to burgeon across diverse industries, it is becoming increasingly crucial for organizations to comprehend and proficiently harness the potency of Big Data analytics. By doing so, businesses can maximize the immense potential provided by this field and attain an advantageous position in the ever-evolving business terrain.

Business models and technological innovations are intimately linked, yet a business model can be discerned from the technology itself.According to Baden-Fuller and Haefliger (2013), the relationship between business models and technological innovation is a crucial factor to consider of a business model centers on a system crafted to tackle the challenge of identifying and engaging with customers, meeting their needs, providing satisfaction, and monetizing the value derived from these interactions. In essence, the choice of a business model directly impacts how technology is monetized and the profitability of relevant firms.

Moreover, the mindset of managers, entrepreneurs, and developers regarding the business model plays a pivotal role in shaping technology development, underscoring the immense impact of these interconnections. This symbiotic relationship between business model choice and technology is intricate, multifaceted, and understudied. It is also crucial to note that technology from various domains, including information technology, can significantly impact business model creation and adaptation.

A prime example is mobile phone applications that act as process innovations for gaming or navigation purposes. Companies like Waze and Zynga heavily leverage app technology. Waze solely relies on mobile phone applications, while Zynga necessitates dependable application technology for optimal performance on tablet computers like the Apple iPad series. If performance enhancements hinge on process innovation and business model modifications, revisiting the conventional S-curve in technology management becomes necessary.

The domain of synthetic intelligence (AI) boasts a robust legacy that spans a period exceeding six decades, characterized by intervals of AI winters and springs. However, recent

strides made in the sphere of supercomputing power and Big Data technologies have infused fresh vigor into the purview of AI, lending it a forceful impetus. The advent of AI in contemporary times has engendered a veritable flurry of both excitement and polemics. Ginni Rometty, IBM's CEO, is of the opinion that AI technologies function as tools that heighten human intelligence.

According to Duan, Edwards, and Dwivedi (2019), the increasing prevalence of artificial intelligence (AI) in the era of Big Data has raised significant research questions regarding its role in decision making envisages a future wherein human beings and machines will establish a collaborative partnership, facilitating the ascension to novel heights and harnessing our sui generis human capabilities. In light of the proliferation of Big Data, advanced algorithms, and substantial improvements in computing power and storage, AI systems have metamorphosed into an integral component of digital ecosystems. AI contributes to the knowledge management and makes this task easier, efficient and effective for the staff (Mittal, et al., 2023).

These systems exert a profound influence on human decision-making mechanisms. As a result, there is a burgeoning demand for information systems researchers to scrutinize the implications of AI on decision-making processes and contribute to the progression of both theory and practice in this realm. The burgeoning popularity and prevalence of AI necessitate an understanding of its ramifications on decision-making. Researchers are tasked with revealing the intricacies of AI's effects and probing how it can be exploited to augment decision-making processes. By plumbing the theoretical underpinnings of AI and studying its pragmatic implications, researchers can play a pivotal role in propelling the field forward and ensuring the successful assimilation of AI technologies into decision-making frameworks. Effective IT-business alignment encompasses various activities, including communication activities that foster mutual understanding between the business and IT, value analytics activities that involve the use of IT and business metrics, IT governance activities such as strategic planning, reporting, and budgeting, partnership activities aimed at maintaining a strong working relationship between the business and IT organizations, IT scoping activities that promote the creation of a flexible IT infrastructure, evaluation and application of emerging technologies, driving business process change, and delivering valuable customized solutions, as well as positioning and balancing business and IT skills.

According to Luftman, Lyytinen, and Zvi (2017), the measurement of information technology (IT) business alignment and its impact on company performance These dimensions collectively contribute to IT-business alignment. Moreover, when expressed as a joint formative construct of these six alignment dimensions, the level of strategic alignment explains 15% of the overall company performance, indicating a statistically significant and reliable relationship.

While the model explains a proportion of the variability in response data, it is important to acknowledge that other factors not considered in the study, such as competition, the

effectiveness of other business activities (e.g., operations, marketing, research), likely contribute to the remaining 85% of company performance. Nonetheless, the research underscores the significance of IT-business alignment in enhancing company performance, particularly in an era where small profit margins are prevalent across industries.
By providing a comprehensive benchmark for assessing alignment status, executives can identify areas for improvement in IT-business relationships and overall performance. Evaluating alignment serves as a foundational step in formulating action plans aimed at harnessing the full potential of IT to deliver value to the business. Blockchain technology has arisen as a significant "disruptive innovation". This has seized the interest of scholars. With a multitude of disciplines. This technology serves as the bedrock for digital currencies such as Bitcoin. This technology has garnered plaudits from a diverse range of stakeholders. This includes developers, entrepreneurs, and technology enthusiasts. The capability of blockchain technology to transform the current economic, legal, political, and cultural terrain is immense. Virtual Communities connect people like never before (Kudeshia and Mittal, 2015).

Frizzo-Barker, Chow-White, Adams, Mentanko, Ha, and Green (2020) conducted a systematic review on the use of blockchain as a disruptive technology for business. this ground-breaking innovation presents a revolutionary means of storing, verifying, and transferring data that transcends traditional methods. With its decentralized architecture, the society has been lauded by these advocates. The surge of interest in this technology. This has forced business scholars to explore its impact and potential for disruption. The time period of global financial turbulence. With its enigmatic creator, Satoshi Nakamoto. Bitcoin focused to establish a decentralized digital currency. Which would circumvent the authority of governments, banks, and traditional financial institutions.

This revolutionary use of blockchain technology sparked inquisitiveness. This laid the groundwork for further exploration of its possibilities in business decisions. As researchers ventured into the realm of blockchain. Researcher discovered a landscap. The scholarly inquiry into blockchain merits attention, yet its examination remains in its incipient stage. The preponderance of ideational papers (83%) over experimental papers (17%) underscores the embryonic quality of the domain, a commonplace observation when scrutinizing unprecedented phenomena. Scholars are actively exploring various aspects of blockchain, including its potential as a disruptive force within society and its integration into the business literature. Although empirical research is still limited, the existing body of knowledge signifies the growing interest and eagerness to understand and analyze the implications of this emerging technology.Ever since the concept of disruptive technology was introduced, researchers and practitioners in the industrial business realm have been devoted to acquiring a more profound comprehension of the emergence and supremacy of these technologies.

According to Obal's (2017) disruptive technologies have been observed to conquer industries by offering novel and captivating features that set them apart from existing technologies, reminiscent of the personal computer's ascendance over minicomputers. Embracing a

disruptive technology at its early stages can present smaller firms with an opportunity to compete against larger competitors, while adhering to a declining technology can render a firm vulnerable and exposed to risks.

To ensure a comprehensive analysis, four control variables were examined in conjunction with the predictive variables of continuous adoption intention: the number of employees, buyer revenues, IT capabilities, and the length of the buyer-supplier relationship. It was hypothesized that an increase in the buying firm's efforts in searching for information would enhance the likelihood of the firm intending to persistently utilize their newly adopted disruptive technology. As anticipated, heightened searching efforts exhibited a positive influence on satisfaction.

intensified searching endeavors and a focus on efficiency-oriented motives proved to be effective drivers for sustaining intentions of continuous adoption of disruptive technology. These findings shed light on the importance of proactive information gathering and the strategic alignment of motives in facilitating the ongoing integration and utilization of disruptive technologies within organizations.

The advent of recent technological revolutions, such as social media, has ushered in an era of unprecedented data generation speed. According to Fan, Lau, and Zhao (2015), the authors examined the role of big data analytics in business intelligence, specifically focusing on marketing mix. concept of big data and its application in business intelligence has garnered significant attention in recent years, owing to its immense potential in generating profound business impacts. Big data is characterized as the volume of data that surpasses technology's capability to efficiently store, manage, and process. It encompasses three crucial dimensions: volume, velocity, and variety. In location-based advertising, customers are presented with timely advertisements or product recommendations based on their current or predicted future positions. This approach offers companies a new tool to attract more customers and enhance brand value. However, a key challenge in location-based advertising lies in accurately predicting customers' locations. This necessitates the consideration of both spatial and temporal data, including temporal moving pattern mining for location-based service.

The processing of large volumes of spatial and temporal data within a short timeframe. Before customers transition to new locations, poses a significant velocity-related challenge for location-based advertising. In light of these perspectives, the convergence of disruptive technology with business strategies presents an opportunity for improved effectiveness in leveraging the potential of big data and location-based advertising.

As disruptive technologies become increasingly prevalent, firms that possess such innovations face a strategic dilemma. Incumbent managers in established industries must grapple with the decision of whether to explore new disruptive business models or exploit existing models that have yielded past success.

According to Osiyevskyy and Dewald (2015), optimal response of contextual factors. The enthusiastic adoption of a disruptive approach can sometimes lead to detrimental consequences for incumbents. The combination of individual behavioral decision-making theories and studies on disruptive business model innovations contributes to the entrepreneurship and strategy literature by shedding light on the process of incumbent entrepreneurial adaptation to emerging industry disruptions.According to Sousa and Rocha (2019), proposed typology of responses can serve as a framework for further studies on business model evolution and disruptive innovations within descriptive and prescriptive theoretical models.

The success of strategic decision-making among UK senior managers was found to be heavily reliant on the knowledge base utilized. This knowledge base encompassed various forms of information available during a period when decision-related information was predominantly well-known, accessible through hard copy reports (explicit knowledge), or derived from managers' experience and judgment (implicit or tacit knowledge). The advent of big data, accompanied by an explosion of knowledge due to increased access, has significantly impacted how senior managers obtain and utilize information.

According to Merendino et al. (2018), the impact of big data on board level decision-making was explored the individual director level, a cognitive capability gap is identified, highlighting the need for organizations to possess the necessary cognitive abilities to effectively navigate big data. Failure to address this gap can lead to cognitive biases and information overload associated with big data. Furthermore, big data disrupts board cohesion, influencing the decision-making process itself. Directors face challenges in introducing changes within shortened timeframes brought about by big data. In terms of organizational functioning, efficient utilization of big data is contingent upon strong internal coordination, integration, and the cultivation of a shared big data culture among decision-makers. While some organizations exhibit inertia when confronted with the challenges posed by big data, there are also instances of proactive internal responses, such as building internal capabilities, and seeking external stakeholder collaborations to effectively leverage big data for decision-making processes.

Objective

To investigate the impact of converging disruptive technology with business strategies for improved effectiveness

Methodology

This research is a descriptive type that collected data from 185 participants, including CEOs, CTOs, CIOs, and other top-level executives who are responsible for making strategic decisions within their organizations. The data were analyzed using a checklist question, which required respondents to answer with either a "Yes" or a "No" for each question.

Data Analysis and Interpretations:

Table 1 Impact of Converging Disruptive Technology with Business Strategies for Improved Effectiveness

SL No.	Impact of Converging Disruptive Technology	Yes	% Yes	No	% No	Total
1	Converging disruptive technologies with business strategies can significantly improve effectiveness by enhancing efficiency and productivity.	165	89.19	20	10.81	185
2	Converging disruptive technologies with business strategies can foster accelerated innovation.	141	76.22	44	23.78	185
3	The convergence of disruptive technologies with business strategies can lead to an improved customer experience.	153	82.70	32	17.30	185
4	Converging disruptive technologies with business strategies empowers organizations with better decision-making capabilities.	173	93.51	12	6.49	185
5	Converging disruptive technologies with business strategies enables organizations to become more agile and adaptable in a rapidly changing business landscape.	137	74.05	48	25.95	185
6	The convergence of disruptive technologies with business strategies can provide organizations with a significant competitive advantage.	170	91.89	15	8.11	185

Table 1 shows the impact of converging disruptive technology with business strategies for improved effectiveness. It was found that around 93.5% respondents accept that converging disruptive technologies with business strategies empowers organizations with better decision-making capabilities. Additionally, the convergence of disruptive technologies with business strategies can provide organizations with a significant competitive advantage (91.8%). Moreover, converging disruptive technologies with business strategies can significantly improve effectiveness by enhancing efficiency and productivity (89.1%). The convergence of disruptive technologies with business strategies can lead to an improved customer experience (82.7%). However, converging disruptive technologies with business strategies can foster accelerated innovation (76.2%). Lastly, converging disruptive technologies with business strategies enables organizations to become more agile and adaptable in a rapidly changing business landscape (74.0%).

Conclusion

This empirical investigation has illuminated the consequences of merging disruptive technology with business strategies to enhance their efficacy. The outcomes have distinctly manifested that assimilating disruptive technologies, including artificial intelligence, blockchain, and the Internet of Things, into business strategies could significantly augment organizational performance.

The study has accentuated the significance of conforming business strategies with emerging technologies to exploit their transformative potential. Through adopting these disruptive technologies, entities can rationalize their operations, enrich customer experiences, and achieve a competitive advantage in the marketplace. Furthermore, the research has emphasized the necessity for proactive and strategic planning when amalgamating disruptive technologies. It is critical for enterprises to comprehend the implications, challenges, and opportunities associated with these technologies to leverage them efficiently and enhance their efficacy.

Additionally, the study has underscored the importance of an adaptable and collaborative organizational culture that embraces innovation and experimentation. Entities that cultivate an atmosphere of openness and promote cross-functional collaboration are in a better position to seamlessly execute and assimilate disruptive technologies into their business strategies.

References

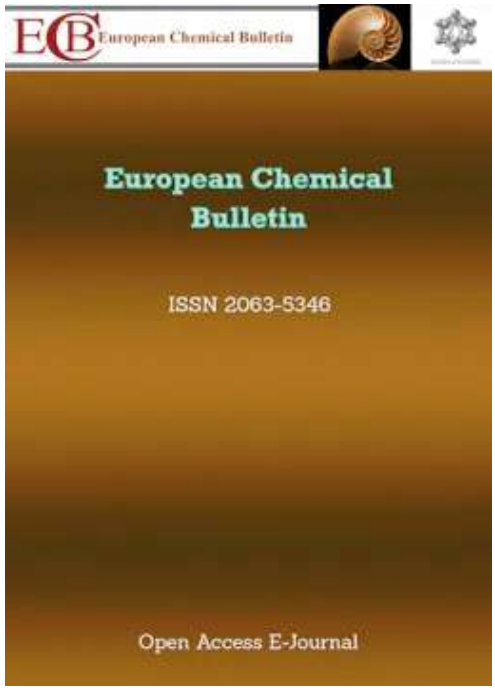
1. Lee, S. M., & Trimi, S. (2021). Convergence innovation in the digital age and in the COVID-19 pandemic crisis. *Journal of Business Research*, *123*, 14-22.
2. Christensen, C. M., McDonald, R., Altman, E. J., & Palmer, J. E. (2018). Disruptive innovation: An intellectual history and directions for future research. *Journal of management studies*, *55*(7), 1043-1078.
3. Evans, C. (2020). The coronavirus crisis and the technology sector. *Business Economics*, *55*, 253-266.
4. Semerikov, S., Chukharev, S., Sakhno, S., Striuk, A., Osadchyi, V., Solovieva, V., ... & Danylchuk, H. (2020). Our sustainable coronavirus future.
5. Bharadwaj, A., El Sawy, O. A., Pavlou, P. A., & Venkatraman, N. V. (2013). Digital business strategy: toward a next generation of insights. *MIS quarterly*, 471-482.
6. Akter, S., Wamba, S. F., Gunasekaran, A., Dubey, R., & Childe, S. J. (2016). How to improve firm performance using big data analytics capability and business strategy alignment?. *International Journal of Production Economics*, *182*, 113-131.
7. Baden-Fuller, C., & Haefliger, S. (2013). Business models and technological innovation. *Long range planning*, *46*(6), 419-426.
8. Duan, Y., Edwards, J. S., & Dwivedi, Y. K. (2019). Artificial intelligence for decision making in the era of Big Data–evolution, challenges and research agenda. *International journal of information management*, *48*, 63-71.
9. Luftman, J., Lyytinen, K., & Zvi, T. B. (2017). Enhancing the measurement of information technology (IT) business alignment and its influence on company performance. *Journal of Information Technology*, *32*(1), 26-46.

10. Frizzo-Barker, J., Chow-White, P. A., Adams, P. R., Mentanko, J., Ha, D., & Green, S. (2020). Blockchain as a disruptive technology for business: A systematic review. *International Journal of Information Management*, *51*, 102029.
11. Obal, M. (2017). What drives post-adoption usage? Investigating the negative and positive antecedents of disruptive technology continuous adoption intentions. *Industrial Marketing Management*, *63*, 42-52.
12. Fan, S., Lau, R. Y., & Zhao, J. L. (2015). Demystifying big data analytics for business intelligence through the lens of marketing mix. *Big Data Research*, *2*(1), 28-32.
13. Osiyevskyy, O., & Dewald, J. (2015). Explorative versus exploitative business model change: the cognitive antecedents of firm-level responses to disruptive innovation. *Strategic Entrepreneurship Journal*, *9*(1), 58-78.
14. Sousa, M. J., & Rocha, Á. (2019). Skills for disruptive digital business. *Journal of Business Research*, *94*, 257-263.
15. Merendino, A., Dibb, S., Meadows, M., Quinn, L., Wilson, D., Simkin, L., & Canhoto, A. (2018). Big data, big decisions: The impact of big data on board level decision-making. *Journal of Business Research*, *93*, 67-78.
16. Mittal A., Singh, S. & George R. (2023) Role of Artificial Intelligence in Knowledge Management: An Empirical Study of Industry Experts using Stepwise Multiple Regression, International Journal of Electronic Finance, DOI: 10.1504/IJEF.2023.10053587, Forthcoming.
17. Kudeshia, C., & Mittal, A. (2015). Social Media: An Eccentric Business Communication Tool for the 21st Century Marketers. International Journal of Online Marketing, 5(2), 37-57. doi: 10.4018/ijom.2015040103

European Chemical Bulletin

ISSN:2063-5346

Publish Now



Chief Editor Name

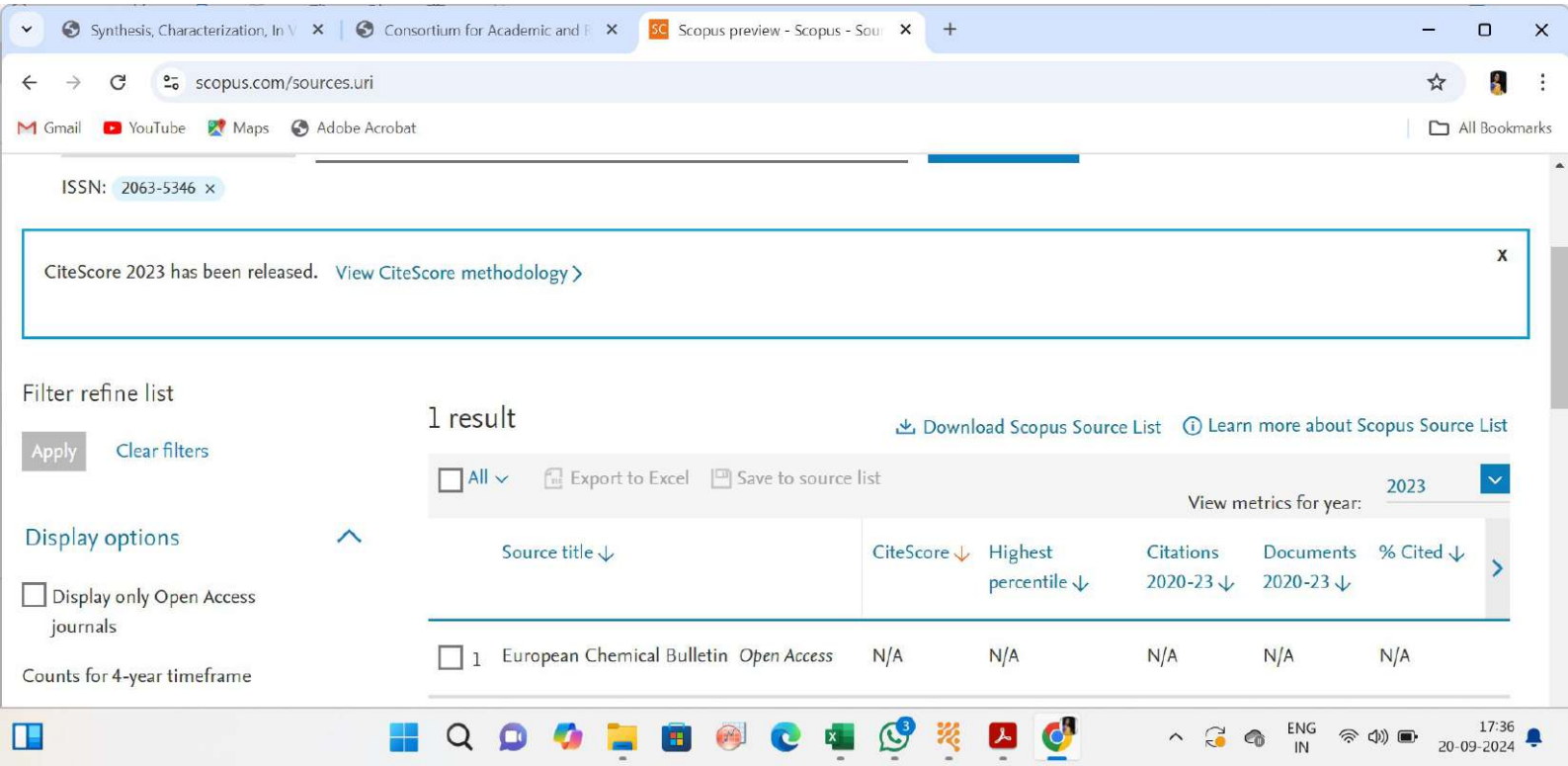
Prof. Dr. K.Krishna
Department of Chemistry, India

Publisher:

Deuton-X Ltd

European Chemical Bulletin is indexed by Chemical Abstract (CA), SciFinder, Directory of Open Access Journals (DOAJ), and Directory of Research Journals Indexing (DRJI) and is available as an Open Access Journal on the Internet. The European Chemical Bulletin was covered by Scopus inclusion for the period from 2017 to 2022. Full lengths of the articles and abstracts are available online at www.eurchembull.com European Chemical Bulletin is an open-access journal. The interesting readers can view, download, print, and redistribute our articles without a subscription, which guarantees that the author

Our Indexing Partners


Synthesis, Characterization, In
Consortium for Academic and
Scopus preview - Scopus - Sou
scopus.com/sources.uri
Gmail
YouTube
Maps
Adobe Acrobat
All Bookmarks
ISSN: 2063-5346
CiteScore 2023 has been released. View CiteScore methodology
Filter refine list
Apply
Clear filters
Display options
Display only Open Access journals
Counts for 4-year timeframe
1 result
Download Scopus Source List
Learn more about Scopus Source List
All
Export to Excel
Save to source list
View metrics for year:
2023
Source title
CiteScore
Highest percentile
Citations 2020-23
Documents 2020-23
% Cited
1
European Chemical Bulletin Open Access
N/A
N/A
N/A
N/A
N/A
ENG IN
17:36
20-09-2024

Navigating Shifting Identities: Quest for Existence in Bharati Mukherjee's *Jasmine*

Dr. Karthik Panicker
Assistant Professor
Department of English
J. M. Patel College
Bhandara - 441904

Dr. Sangita Vijay Kongre
Associate Professor
Department of English
Maharshi Dayanand College
Parel, Mumbai-12

Abstract:

An identity can be defined in a socio-cultural, economic, linguistic background. Identity cannot be framed and conceptualized in isolation. It is a gradual development of a self which gets birth, nurtures, grows in a particular supportive / hostile land with its socio-cultural values. As Karl Marx rightly remarked: it is not the consciousness of men (human beings) that determines their being, but, on the contrary, their social being that determines their consciousness.

Identity is 'conditioned' by the socio-cultural ethos in which it exists. It is never 'fixed'. It keeps changing. There is flux in identities. The flux always brings a conflict within self. The new identity comes at the cost of the previous identity. This transformation from old to new identity is never a soothing process. The research paper based on Bharati Mukherjee's *Jasmine,* intends to prove that constant flux in identity always involves psychological trauma, tension, pressure and dilemma

Key words: Indian diaspora, identity, immigrants, fluidity and fixed identity

...I sleep upon dead years.
Sometimes I dream in Chinese
I dream my father's dream.
I wake, grown up
And someone else.
I am the thin edge I sit on.
I begin to gray-white and black and in between
My hair is America.

- Diana Chang

-

An immigrant women's conflict of identities is authentically composed in the poem entitled "Second Nature" from her book of poetry *The Horizon is Definitely Speaking* by Diana Chang, a Chinese born American poet. Identity crisis is one the major facets of Diaspora discourse. Indian immigrant women writers and their female characters have certainly changed the conventional image of Indian diasporic women. Socio-cultural aspects play an important role in immigrants' lives. The pain of living 'in between' two very opposite cultural worlds creates conflict in these characters. The crisis creates a trauma in their minds, leading them to take an unusual and unexpected path in an attempt to resolve it. The concept of "fixed" identity of immigrants gets challenged by the "fluidity" of their identities in a new world. It poses risks to immigrants' ethnic identity, leading them to a crisis of identity. The pain of identity conflict is severe for the unwilling immigrants as they hardly try to accept multiplicity of identities.

Stuart Hall defines, identities as, "...the names we give to the different ways we are positioned by and position ourselves within, the narratives of the past" (225). Identity is always culture and context specific. Usually, the formation of an individual's identity initiates with self-perception. Culture plays a very significant role in identity formation. Self-perception happens in the context of cultural ambience. As a result of this, one normally conceives an identity as a fixed and stable cultural notion. The perception of an identity as something that is 'fixed' comes into confrontation when they migrate to a different geographical and cultural location. Some of the willing immigrant women try to shed off this traditional identity for the fluidity of identities. However, there are other women who don't let go their old world identity in the new land. In both the cases the

conflict of identity emerges and influences their lives in the new land. Many a times it brings them the disruption of the old identity and the feelings of frustration and failure deny them the possibilities of assimilation and the success in the new land.According to Hall:

> Cultural identity is not a fixed essence at all, lying unchanged outside history and culture…It is not a once-and-for all. It is not a fixed origin to which we can make some final and absolute Return. Of course, it is not a mere phantasm either... It has its histories—and histories have their real, material and symbolic effects. The past continues to speak to us. But it no longer addresses us as a simple, factual 'past', since our relation to it, like the child's relation to the mother, is always-already 'after the break'. It is always constructed through memory, fantasy, narrative, and myth. (230)

Hall describes Identity as something dynamic, which keeps on evolving:

> "Identity is not as transparent or unproblematic as we think. Perhaps instead of thinking of identity as an already accomplished fact, which the new cultural practices then represent, we should think, instead, of identity as a 'production', which is never complete, always in process, and always constituted within, not outside, representation" (222).

Identities are never fixed. Hall agrees the multiplicity of identities, and differentiates the way to perceive it. According to him there are at least two ways to perceive cultural identities. He writes:The first position defines 'cultural identity' in terms of one, shared culture, a sort of collective 'one true self', hiding inside the many other, more superficial or artificially imposed 'selves', which people with a shared history and ancestry hold in common…our cultural identities reflect the common historical experiences and shared cultural codes which provide us, as 'one people', with stable, unchanging and continuous frames of reference and meaning … (223)

He further adds that Cultural identity … is a matter of 'becoming' as well as of 'being'(223). Most importantly, he points out that 'Cultural identities…undergo constant transformation. Far from being eternally fixed in some essentialised past, they are subject to the continuous 'play' of history, culture and power. (225)

Bharati Mukherjee describes identity formation as a complex process as it is not created only by the agency of an individual but also by the surrounding atmosphere. Even though one tries hard to forget or get away with the former identity, still it clings to the self in the present

Identity is a major concern for Mukherjee. While most readers consider her as an Asian-American but the writer refuses this hyphenated identity. In the "American Dreamer" (1997) she

pronounces: "Call me an American, not an Asian American. My rejection of hyphenation has been called race treachery, but it is really a demand that America deliver the promises of its dream to all its citizens equally" (qtd in Shubhendu Mund, 113). Mukherjee has been criticized by the critics and scholars for her assertion of being an American and her characters' desperate willingness to adopt the American identity. They accuse her of not taking into account the sufferings of Indians in America. However, this has been wiped out by Mukherjee herself through her interviews and the writing. She clears her intention behind asserting her identity as an American. She views herself as an American writer of Indian origin. She writes in a tradition of immigrant experience rather than nostalgia and expatriation.

Mukherjee intends to make the immigrants aware about the fluidity of their identities. Jasmine's first identity is that of Jyoti at Hasnapur village. She refuses to accept the fate predicted by "a crazy old man..." *(Jasmine* 3) of her being a widow and suffering exile. This was predicted when she was only seven. This act of denial suggests Jyoti's rejection of the superstitious beliefs prevalent in India. She furiously retaliates - "You don't know what my future holds!"(*Jasmine* 3). Jasmine at the age of seven strongly believes in herself. When the old astrologer, in anger, chucked her hard in the head with a stone giving her a permanent scar on her forehead. But Jasmine, full of self-confidence, positively, calls it as her “third eye" (*Jasmine* 5). Jasmine, we realise, is quick to make things happen even out of bad situations.

Jasmine(Jyoti) dreams of getting higher education and learning English. Hence determines not to marry a Jamindar man whose proposal her grandmother brings for her. She says that"...[I] couldn’t marry a man who didn’t speak English, or at least who didn’t want to speak English. To want English was to want more than you had been given at birth; it was to want the world..." (*Jasmine* 68). Jasmine realises the importance of English language for a better future. This assertion by Jyoti hints at her willingness for acculturating in the free, liberal world. Her grandmother, a representative of the conservative Indian patriarchal system, brings a proposal for her of a widowed man having a child. Fortunately, Jyoti is saved from all this. Jyoti asserts her individuality and gets married to a man of her choice - Prakash, a man with a modern outlook. She proudly describes Prakash in the following manner: "My husband, Prakash Vijh, was a modern man, a city man. He did trash some traditions…”(*Jasmine 76*). Prakash shows her the dream of a free life in America. He wants freedom for both of them from the conservative Indian society. Jyoti suffers the conflict between the real world and the imaginary world. She was born and brought up in a strictly conservative family. She carries in her mind the image of a typical Indian

wife which Prakash wants her to throw away. "For Prakash, love was letting go. Independence, self-reliance: I learned the litany by heart. But I felt suspended between worlds"(*Jasmine* 76). Jasmine finds herself between two different worlds. Being raised in a typical patriarchal family, the patriarchal norms of behaviour are deeply ingrained in her psyche. Like any other Indian married woman, she wishes to beget a child. Prakash wants her to call him by his first name. But Jasmine hesitates to do so because "in Hasnapur wives used only pronouns to address their husbands..."(*Jasmine* 77). Jasmine suffers the dilemma - which type of behaviour to follow: "I still had a hard time calling him Prakash..."(*Jasmine*77). After the marriage, Prakash gives her a new identity and a new name, Jasmine. She tells us:

> He wanted to break down the Jyoti I'd been in Hasnapur and make me a new kind of city woman. To break off the past, he gave me a new name: Jasmine. He said, "You are small and sweet and heady, my Jasmine. You'll quicken the whole world with your perfume." Jyoti, Jasmine: I shuttled between identities (*Jasmine* 77)

Jasmine tries her best to shed off her identity of a typical Indian wife, simultaneously trying to visualise herself in the American way of life. According to Mukherjee one of the main reasons for Indians to migrate to America or to other developed countries, in addition to the greener pastures they offer, is the liberal way of life it offers, especially for women. On the day of their leaving for America, Prakash gets killed in a bomb blast. The death of Prakash is a great set back to her American dream. But soon she recovers from the shock. She realises that she should not be going back to the traditional ways: "There is no dying there is no dying there is only an ascending or a descending, a moving on to other planes. Don't crawl back to Hasnapur and feudalism. That Jyoti is dead" (*Jasmine* 96). She is determined to fulfill Prakash's dream of going to America. She is desperate to live the American dream which Prakash and she had seen together: "Later, I thought, we*had* created life. Prakash had taken Jyoti and created Jasmine, and Jasmine would complete the mission of Prakash. Vijh & Wife. A vision had formed..." (*Jasmine* 97). But the identity crisis is more at deeper level of her mind. Jasmine suffers the conflict of being in torn between the two contrasting identities. She desperately wishes to go to America and hence manages to be an illegal traveller to America. She rejects the old stories about the predicament of widows told to her by the grandmother and mother and Vimla, her friend. This assertion of self will and deliberate attempts to realise her dream make her a willing immigrant to America. Her odyssey from India to America has been described as an Indian girl "discovering American selfhood" (Carter-Sanborn 573).

The immigrant Jasmine carries a certain idealistic image of America which Prakash and the letter from Prof. Vadhera have shown her, but to her dismay as soon as she touches the shores of America, she gets raped by the Captain of the Ship, Half Face. The defilement of her body shatters her *mission.* The very responsibility of the old world's identity gets destroyed by the rape. Her long preserved identity of the chaste widow comes into the conflict with disruption of the same. The brutal incident puts her into the utter disgust of the treachery in America. Jasmine draws upon the Hindu concepts of sati and reincarnation, and links it with the self-will and resilience. Jasmine reincarnates herself as 'Kali' to give the appropriate response to the rapist. Kali, a Hindu goddess, is considered as the destroyer of evil. Jasmine cannot escape from the perception of the 'raped Jasmine'; she tries to acquire the new identity to cope up with the present, assumes the role of a destroyer, and kills the rapist, Half Face. The murder of Half-Face brings her the self-affirmation through transformation. Bharati Mukherjee aptly brings out the Indian mythology from the closet. The myth of the 'reincarnation' and the images of *Sati- Savitri* and goddesses *Kali* and *Sita*are aptly used by Mukherjee to depict the identity conflict in the context of Indian woman. Jasmine's prompt response to the situation depicts her presence of mind and it hints at her willingness to adopt the circumstances.

Jasmine tries to realize her new identity and finally seems to be controlling her destiny. The rape not only breaks her down but also builds her. The construction of new identity occurs through the destruction of the old one. Jasmine also accepts the fluidity of multiple identities. It enables her to perform various roles to suit the situation she faces. Dimri writes, "She brings death to Half-Face as Goddess Kali, she brings happiness to Duff and Taylor as a traditional, self-sacrificing Indian lover and she is offering love to Duff as a loving mother who exults in her motherhood"
(*Jasmine*75). Mukherjee asserts through Jasmine that to kill one's confined self in the conservative customs, is to achieve the personal dream of freedom. Jasmine makes herself free from all the cultural baggage to "travel light". Though Jasmine suffers through the identity conflict, she is quick to shed off the present for the possibilities of a better future.

To be free from the old identity Jasmine sets Prakash's suit and her own white sari on the fire. The act signifies her effort to shed off the old identity of being Prakash's widow. She later realizes, "My body was merely the shell, soon to be discarded. Then I could be reborn, debts and sins all paid for" (*Jasmine* 121). Jasmine believes that, one visits and revisits the world. She asserts, "Yes," I say, "I do believe you. We do keep revisiting the world. I have also travelled in

time and space. It is possible." (*Jasmine* 127). Her acceptance about the multiple identities or identity in 'flux' make her journey of adopting the American values comparatively smooth. She accepts:

> Jyoti of Hasnapur was not Jasmine, Duff's day mummy and Taylor and Wylie's *au pair* in Manhattan; that Jasmine isn't this Jane Ripplemeyer having lunch with Mary Webb at the University club today. And which of us is the undetected murderer of a half-faced monster, which of us has held a dying husband, which of us was raped and raped in boats and cars and motel rooms? (*Jasmine* 127)

Wickramagamage rightly symbolizes Jasmine's identity as, "Human identity, when it comes to Jasmine, assumes an amoeba-like consistency that can continuously reshape itself as befits its particular location..."(189). The destruction of one's old identity does not come easily. It brings shock to immigrants. It is always hard to discard the one identity for the other. It brings the unbearable pain to the immigrants. Jasmine realises this tribulation, "In the white lamplight, ghosts float toward me. Jane, Jasmine, Jyoti" (*Jasmine* 21). Moreover, the predicament is severe in Jasmine's case because, the new identity comes into existence after the violent murder of the first one. The violence at the physical and psychological level becomes the pattern in her voyage from the diasporal dream to the American dream. Jasmine travels from one identity to another identity to transform the self into the new land. The transformation reveals immigration as a platform to subvert and reformulate her identity. After shedding the old identity, Jasmine prepares herself to adapt herself into the American culture. She tells us: "I buttoned up the jacket and sat by the fire. With the first streaks of dawn, my first full American day, I walked out of the front drive of the motel to the highway and began my journey, travelling light" (*Jasmine* 121).

Mukherjee seems to suggest that, in order to deal with the dilemma of identity conflict, one must attempt deliberately to shed off the old identity. If one clings to the previous identity, it makes the crisis more painful to bear. Jasmine starts adopting the American way of living as she gets trained by Mrs. Lilian Gorden who helps her to slip into the American identity. Mrs. Gordan tells her: "Let the past make you wary, by all means. But do not let it deform you" (*Jasmine* 131). She gives her new American identity, "Jazzy" (*Jasmine* 133). Jasmine abandons her Indian identity by throwing "Hasnapuri modesty" and wears "Jazzy in a T-shirt, tight cords, and running shoes" (*Jasmine* 133). She assumesthis new identity with confidence and learns to assert herself into the American values and its culture. She begins to talk and walk like Americans. Jasmine starts adopting the American identity.

Though Jasmine being the willing immigrant, bears the internal pangs of change in identity and has to suffer the external harsh environment of the new land. For example, in America; she is considered as "dark-haired girl" in naturally blond country" (*Jasmine* 33) and with a "darkish complexion" while in India, she is "wheatish" (*Jasmine* 33). Jasmine has to undergo the pain of her identity based on the race and the skin colour in America.

To conclude, Jasmine accepts the fluidity of identities for her existence. She undergoes a painful transition from Jyoti to Jasmine to realise her American dream. She assumes multiple identities. She realizes, "We've …many selves" (*Jasmine* 214). She recalls her multiple identities, "I whisper the name, Jase, Jase, Jase, as if I am calling someone I once knew" (*Jasmine* 215).

Works Cited

Primary Source:

Mukherjee, Bharati. *Jasmine.* New York: Grove Press, Weidenfeld, 1989. Print.

Secondary Sources:

Bharati Mukherjee. "Beyond Multiculturalism," *Multi America: Essays on Cultural War and Cultural Peace*. Ed. Ishmael Reed. New York: Viking Penguin, 1997, 454-461.

Carter-Sanborn, Kristin. "We Murder Who We Were: *Jasmine* and the Violence of Identity." *American Literature* 66.3 Sept. 1994. 573-593.Print.

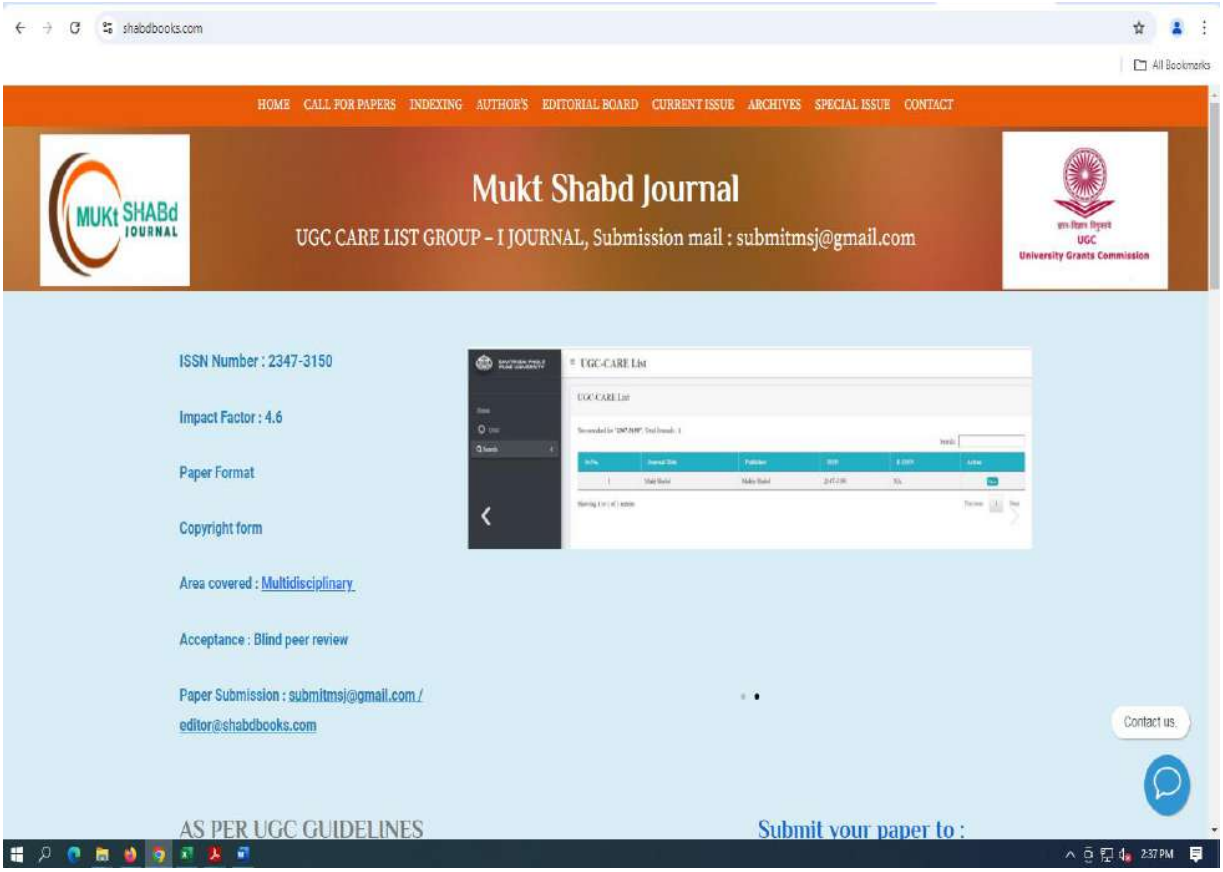
Chang, Diana. *The Horizon is Definitely Speaking.* New York: Backstreet Editions Press. 1982. Print

Dimri, Jaiwanti. "From Marriage to Murder: A Comparative Study of Bharati Mukherjee's *Wife* and *Jasmine*", *American Literature Today*. Ed. Suman Bala. New Delhi: Intellectual Publishing House.1994. 170-175. Print.

Hall, S. 'Cultural identity and diaspora', in J. Rutherford, (ed.), *Identity, Community, Culture, Difference*. London: Lawrence and Wishcraft. 1990. 222–237. Print.

Hall, S. 'Introduction: Who Needs "Identity"?', in: S. Hall and P. Du Gay (eds) Questions of Cultural Identity. London: Sage,1996. 1–17. Print.

Wickramagamage, Carmen. "Relocation as Positive Act: The Immigrant Experience in Bharati Mukherjee's Novels." *Diaspora* 2.2 (1992). 171-200. Print.


shabdbooks.com
All Bookmarks
HOME CALL FOR PAPERS INDEXING AUTHOR'S EDITORIAL BOARD CURRENT ISSUE ARCHIVES SPECIAL ISSUE CONTACT
MUKt SHABd JOURNAL
Mukt Shabd Journal
UGC CARE LIST GROUP – I JOURNAL, Submission mail : submitmsj@gmail.com
UGC
University Grants Commission
ISSN Number : 2347-3150
Impact Factor : 4.6
Paper Format
Copyright form
Area covered : Multidisciplinary
Acceptance : Blind peer review
Paper Submission : submitmsj@gmail.com / editor@shabdbooks.com
UGC-CARE List
Contact us
AS PER UGC GUIDELINES
Submit your paper to :
2:37 PM

UGC-CARE List

You searched for "**2347-3150**". Total Journals : **1**

Search:

Sr.No.	Journal Title	Publisher	ISSN	E-ISSN	UGC-CARE coverage years	Details
1	Mukt Shabd (print only)	Shabd Publication	2347-3150	NA	from June-2019 to Present	View

Showing 1 to 1 of 1 entries

Previous 1 Next

Copyright © 2024 Savitribai Phule Pune University. All rights reserved. | Disclaimer

CRITERION – III

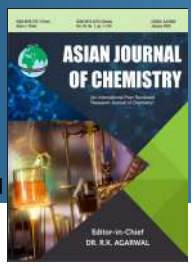
RESEARCH, INNOVATION AND EXTENSION

3.3 RESEARCH PUBLICATIONS AND AWARDS

3.3.1 NUMBER OF RESEARCH PAPERS PUBLISHED PER TEACHER IN THE JOURNALS NOTIFIED ON UGC CARE LIST DURING THE LAST FIVE YEARS

2022

Asian Journal of Chemistry; Vol. 35, No. 1 (2023), 29-38
ASIAN JOURNAL OF CHEMISTRY



A Facile Synthesis of Thiazole Derivatives bearing Imidazole Moiety, Schiff Bases and their O-Glucosides

SHITAL M. DEKATE[1], KISHOR M. HATZADE[1] and AJAY M. GHATOLE[2,*]

[1]Department of Chemistry, Dhote Bandhu Science College, Gondia-441601, India
[2]Department of Chemistry, J.M. Patel Arts, Commerce and Science College, Bhandara-441804, India

*Corresponding author: E-mail: ajay.ghatole5@gmail.com

Received: 22 September 2022; *Accepted*: 4 October 2022; *Published online*: 27 December 2022; AJC-21074

A unique approach for the synthesis of new thiazole O-glycosides is presented in this work. 2-Amino-4-hydroxy-phenyl-1,3-thiazole-5-carboxaldehyde (**3a**) was reacted with phenyl glyoxal and benzil to form 4-(4-hydroxy-phenyl)-5-(4-phenyl-1*H*-imidazol-2-yl)-thiazol-2-amine (**4a**) and 4-(4-hydroxy-phenyl)-5-(4,5-diphenyl-1*H*-imidazol-2-yl)-thiazol-2-amine (**4b**), respectively. A series of substituted Schiff bases of **4a** and **4b** were synthesized reacting with various aryl aldehyde to form 2-(imino substituted benzal)-4-(4-hydroxy-phenyl)-5-(4-phenyl-1*H*-imidazol-2-yl)-thiazoles (**5a-e**) and 2-(imino substituted benzal)-4-(4-hydroxy-phenyl)-5-(4,5-diphenyl-1*H*-imidazol-2-yl)-thiazoles (**5f-j**). Glucosylation of compounds (**5a-j**) have been done by using acetobromoglucose as glucosyl donor to afford 2-(imino substituted benzal)-4-(2,3,4,6-tetra-O-acetyl-*p*-O-β-D-glucosidoxyphenyl)-5-(4-phenyl-1*H*-imidazol-2-yl)-thiazoles (**6a-e**) and 2-(imino substituted benzal)-4-(2,3,4,6-tetra-O-acetyl-*p*-O-β-D-glucosidoxyphenyl)-5-(4,5-diphenyl-1*H*-imidazol-2-yl)-thiazoles (**6f-j**) further on deacetylation to produce 2-(imino substituted benzal)-4-(*p*-O-β-D-glucosidoxyphenyl)-5-(4-phenyl-1*H*-imidazol-2-yl)-thiazoles and 2-(imino substituted benzal)-4-(*p*-O-β-D-glucosidoxyphenyl)-5-(4,5-diphenyl-1*H*-imidazole-2-yl)-thiazoles (**7f-j**). The synthesized compounds were characterized by elemental analyses, FTIR, ^{1}H & ^{13}C NMR and electron mass spectra (EI-MS) techniques and then screened for their *in vitro* antimicrobial activity.

Keywords: Glucosylation, Imidazole, O-glucosides, Schiff bases, Thiazole.

INTRODUCTION

Penicillin and vitamin B_1 (thiamine) are two examples of natural compounds that have the structural motif of thiazole. Antibacterial, antifungal [1], anti-inflammatory [2], antiviral [3], antimalarial [4] and anti-HIV activities [5] are among the many pharmacological and biological characteristics of thiazole moiety. Analog of thiazole can bind to estrogen receptor ligands [6], neuropeptides [7] and Y5 adenosine receptors [8]. They have been shown to inhibit the human platelet aggregation factor [9], urokinase [10] and poly (ADP-ribose) polymerase-1 [11]. Thiazoles are also used in the production of pain-relieving medicines [12,13] and also work as antithrombotic fibrinogenic receptor antagonists [14], as novel bacterial DNA gyrase B inhibitors [15], *etc*.

Imidazole based compounds have implicit applications such as anticancer, antihypertensive, antihistamine, antipsychotic, hypothermic, cytotoxic, antibacterial, antioxidant *etc.* [16,17]. The highly substituted imidazole shows a high medicinal value for the chemical and biochemical processes [18] and has potential applications such as analgesic, anti-inflammatory [19], fungicidal, antibacterial [20] and anti-tumour activities [21]. O-Glucoside, which has high therapeutic potential, is abundantly dispersed across the plant world, particularly in the roots, seeds, leaves and bark of plants [22,23]. Increasing the solubility of organic molecules in water and lowering the toxicity of aglycone fraction are two of O-glucosides' most significant functions. The Koenigs Knorr method is the most favoured technique for glucosylation of compounds [24]. O-Glucosylation has been synthesized by employing the modified Michael methodology [25]. The operation activity of compounds is mostly associated with the presence of azomethine group (>C=N). These azomethines make up one of the most potent groups of molecules with a wide range of biological uses [26-28]. Therefore, it was advised to synthesize novel compounds having thiazole, imidazole, O-glucoside and azo-

This is an open access journal, and articles are distributed under the terms of the Attribution 4.0 International (CC BY 4.0) License. This license lets others distribute, remix, tweak, and build upon your work, even commercially, as long as they credit the author for the original creation. You must give appropriate credit, provide a link to the license, and indicate if changes were made.

methine moiety in one framework as persistence of our research effort and bearing in mind the numerous and important biological func-tions. In this work, 2-(imino substituted benzal)-4-(4-hydroxy-phenyl)-5-(4-phenyl-1*H*-imidazol-2-yl)thiazoles, 2-(imino substituted benzal)-4-(4-hydroxy-phenyl)-5-(4,5-diphenyl-1*H*-imidazol-2-yl)thiazoles. Moreover, the antimicrobial and antifungal activity were also evaluated since, the presence of all of the aforementioned heterocyclic rings in the same molecular framework may have a synergistic effect on the synthesized compounds.

EXPERIMENTAL

All the chemicals and solvents were bought from Himedia and Merck. Before usage, all the solvents were distilled. All melting points were measured in an open capillary tube over a liquid paraffin bath and are uncorrected. For TLC, silica gel 60 F_{254} was used (Merck). The Bruker FT-IR spectrometer was used to record the IR spectra. The Brucker AC 400 (MHz) analyzer was used to record the ^{1}H NMR and ^{13}C NMR spectra. The spectra are displayed on a scale in parts per million based on an internal standard (trimethylsilane) on the δ scale. The Perkin-Elmer 2400 CHN analyzer was used to analyze the elemental composition of the synthesized compounds.

Synthesis of 4-(4-hydroxy-phenyl)-5-(4-phenyl-1*H*-imidazol-2-yl)thiazol-2-amine (4a): Compound **4** was synthesized according to the reported method [29]. In brief, a composition of glacial acetic acid (50 mL), phenyl glyoxal (0.662 g, 5 mmol), ammonium acetate (0.77 g, 10 mmol), 2-amino-4-(4-hydroxy-phenyl)-1,3-thiazole-5-carboxaldehyde (5 mmol) and phenyl glyoxal were refluxed for 2 h. It was then added to 200 mL of ice-cold water and neutralized with NH_4OH. The resulting dark solid was filtered, washed with distilled water and recrystallized with absolute ethanol. Yield 78%, m.p.: 283 ºC. IR (KBr, ν_{max}, cm^{-1}): 3505 (OH), 3425-3255 (NH_2 *str.*), 3125 (NH *str.*), 3075 (CH-arom *str.*), 1605 (C=C arom *str.*), 1215 (C-S *str.*). ^{1}H NMR (DMSO-d_6, 400 MHz), δ ppm: 13.25 (H, s, -NH), 7.40-8.30 (9H, m, Ar-H), 7.38 (1H, s, imidazole-H), 7.15 (2H, s, -NH_2), 5.43 (1H, s, OH). ^{13}C NMR (DMSO-d_6), δ ppm: 171.2 (N=C-S), 157.3 (C=C-N), 142.1 (C=C-N) (imidazole), 132.8 (N=C-NH), 118-131 (aromatic 12C-atom), 117.9 (NH=C-C), 115.5 (C=C-S) (thiazole). EI-MS: *m/z* (%) 336 (2%), 336 (4%), 335 (22%), 334 (100%) base peak. Anal. calcd. (found) % for $C_{18}H_{14}N_4OS$: C, 64.65 (65.20); H, 4.22 (4.43); N, 16.75 (16.95); S, 9.59 (10.07); O, 4.78 (4.95).

Synthesis of 4-(4-hydroxy phenyl)-5-(4,5-diphenyl-1*H*-imidazol-2-yl)thiazol-2-amine (4b): A mixture of 2-amino-4-(4-hydroxyphenyl)-1,3-thiazole-5-carboxaldehyde (5 mmol), benzil (0.662 g, 5 mmol), CH_3COONH_4 (0.77 g, 10 mmol) and glacial acetic acid (50 mL) were refluxed for 2 h. It was then added to 200 mL of ice-cold water and neutralized with NH_4OH. The resulting dark brown solid was filtered, washed with distilled water and recrystallized with absolute ethanol. Yield 75%, m.p.: 265 ºC. IR (KBr, ν_{max}, cm^{-1}): 3515 (OH), 3440-3240 (NH_2 *str.*), 3137 (NH *str.*), 3060 (CH-arom *str.*), 1560 (C=C arom *str.*), 1240 (C-S *str.*). ^{1}H NMR δ_H (DMSO-d_6, 400 MHz): 13.12 (H, s, -NH), 7.39-8.35 (10H, m, Ar-H), 7.37 (1H, s, imidazole-H), 7.27 (2H, s, -NH_2), 5.63 (1H, s, OH). ^{13}C NMR (DMSO-d_6), δ ppm: 172.2 (N=C-S), 158.3 (C=C-N), 143.1 (C=C-N) (imidazole), 131.8 (N=C-NH), 117-131 (arom. 18C-atom), 116.2 (NH=C-C), 115.5 (C=C-S) (thiazole). EI-MS: *m/z* (%) 413 (1%), 412 (3%), 412 (5%), 411 (28%), 410 (100%) base peak. Anal. calcd. (found) % for $C_{24}H_{18}N_4OS$: C, 70.22 (70.65); H, 4.42 (4.49); N, 13.65 (13.95); S, 7.81 (8.07); O, 3.90 (4.05).

Synthesis of 2-(imino substituted benzal)-4-(4-hydroxy-phenyl)-5-(4-phenyl-1*H*-imidazol-2-yl)thiazoles (5a-e): A solution of 4-phenyl-5-(4-hydroxyphenyl-1*H*-imidazol-2-yl)thiazol-2-amine (0.1 mol) and substituted benzaldehyde (0.1 mol) was dissolved in ethanol using a catalytic amount of glacial acetic acid. The reaction mixture was refluxed with constant stirring at 50-60 ºC for 4-5 h. Then, the progress of the reaction is checked by TLC. It was cooled at room temperature and the product was filtered, dried by ether and recrystallized from hot ethanol. The product was washed with sodium bisulphite to get rid of extra aldehyde and then with cooled ethanol to get pure product.

2-(Iminobenzal)-4-hydroxy-phenyl-5-(4-phenyl-1*H*-imidazol-2-yl)thiazole (5a): Yield 75%, m.p.: 140 ºC. IR (KBr, ν_{max}, cm^{-1}): 3525 (OH), 3160 (NH atom *str.*), 3015 (CH-atom *str.*), 1612 (C=C atom *str.*), 1320 (C-S *str.*). ^{1}H NMR (DMSO-d_6, 400 MHz), δ ppm: 13.87 (H, s, NH), 8.88 (H, s, CH), 7.39 (H, s, imidazole-H), 6.90-8.32 (14H, m, Ar-H), 5.54 (1H, s, OH). ^{13}C NMR (DMSO-d_6), δ ppm: 174.4 (N=C-S), 161.2 (CH=N), 160.5 (C=C-N), 142.1 (C=C-N) (imidazole), 132.8 (N=C-NH), 129.2 (C=C-S) (thiazole), 121.9 (NH=C-C), 116-154 (arom. 18 C-atom). EI-MS: *m/z* (%) 425 (1%), 424 (4%), 424 (5%), 423 (30%), 422 (100%) base peak. Anal. calcd. (found) % for $C_{25}H_{18}N_4OS$: C, 71.07 (72.58); H, 4.29 (4.55); N, 13.26 (13.72); S, 7.56 (7.89); O, 3.79 (3.99).

2-(Imino-4-chlorobenzal)-4-hydroxy-phenyl-5-(4-phenyl-1*H*-imidazol-2-yl)thiazole (5b): Yield 75%, m.p.: 195 ºC. IR (KBr, ν_{max}, cm^{-1}): 3505 (OH), 3165 (NH atom *str.*), 3024 (CH-atom *str.*), 1618 (C=C atom *str.*), 1332 (C-S *str.*), 755 (C-Cl *str.*). ^{1}H NMR (DMSO-d_6, 400 MHz), δ ppm: 13.43 (H, s, NH), 8.76 (H, s, CH), 7.46-8.13 (13H, m, Ar-H), 7.45 (H, s, imidazole-H), 5.50 (1H, s, OH). ^{13}C NMR (DMSO-d_6), δ ppm: 173.3 (N=C-S), 161.2 (CH=N), 159.1 (C=C-N), 141.1 (C=C-N) (imidazole), 132.8 (N=C-NH), 130.2 (C=C-S) (thiazole), 127-136 (aromatic 18C-atom), 115.9 (NH=C-C). EI-MS: *m/z* (%) 460 (2%), 460 (1%), 459 (11%), 458 (4%), 458 (37%), 457 (29%), 456 (100%) base peak. Anal. calcd. (found) % for $C_{25}H_{17}N_4OSCl$: C, 65.71 (66.10); H, 3.75 (3.89); Cl, 7.76 (7.93); N, 12.26 (12.67); S, 7.02 (7.27); O, 3.50 (3.76).

2-(Imino-4-nitrobenzal)-4-hydroxyphenyl-5-(4-phenyl-1*H*-imidazol-2-yl)thiazole (5c): Yield 60%, m.p.: 159 ºC. IR (KBr, ν_{max}, cm^{-1}): 3520 (OH), 3156 (NH *str.*), 3015 (CH-atom. *str.*), 1624 (C=C atom *str.*), 1540 asymmetric, 1340 symmetric (NO_2 gp), 1338 (C-S *str.*). ^{1}H NMR (DMSO-d_6, 400 MHz), δ ppm: 13.52 (H, s, NH), 8.42 (H, s, Ar-H), 8.72 (H, s, CH), 8.29 (2H, d, Ar-H), 8.21 (H, s, imidazole-H), 6.90-8.32 (13H, m, Ar-H), 5.86 (1H, s, OH). ^{13}C NMR (DMSO-d_6), δ ppm: 171.3 (N=C-S), 162.0 (CH=N), 159.1 (C=C-N), 142.1 (C=C-N) (imidazole), 132.8 (N=C-NH), 126.2 (C=C-S) (thiazole), 124-150 (aromatic 18C-atom), 121.9 (NH=C-C). EI-MS: *m/z* (%) 470

(1%), 469 (5%), 469 (4%), 468 (27), 468 (3%), 467 (100%) base peak. Anal. calcd. (found) % for $C_{25}H_{17}O_3N_5S$: C, 64.23 (65.04); H, 3.67 (3.75); O, 10.27 (10.48); N, 14.98 (15.20); S, 6.86 (7.08).

2-(Imino-4-methoxybenzal)-4-hydroxy-phenyl-5-(4-phenyl-1*H*-imidazol-2-yl)thiazole (5d): Yield 68%, m.p.: 212 ºC. IR (KBr, ν_{max}, cm^{-1}): 3528 (OH), 3164 (NH *str.*), 3020 (CH-atom *str.*), 1615 (C=C atom *str.*), 1322 (C-S *str.*). ^{1}H NMR (DMSO-d_6, 400 MHz), δ ppm: 13.48 (H, s, NH), 8.64 (H, s, CH), 8.25 (H, s, imidazole-H), 6.90-8.60 (13H, m, Ar-H), 5.55 (1H, s, OH), 3.92 (3H, s, OCH_3). ^{13}C NMR (DMSO-d_6), δ ppm: 170.3 (N=C-S), 161.0 (CH=N), 158.1 (C=C-N), 141.1 (C=C-N) (imidazole), 131.8 (N=C-NH), 125.2 (C=C-S) (thiazole), 115-160 (aromatic 18C-atom), 121.9 (NH=C-C), 56.32 (-OCH_3). EI-MS: *m/z* (%) 455 (1%), 454 (4%), 454 (6%), 453 (30), 452 (100%) base pea. Anal. calcd. (found) % for $C_{26}H_{20}O_2N_4S$: C, 69.01 (70.04); H, 4.45 (4.75); O, 7.07 (7.48); N, 12.38 (12.60); S, 7.09 (7.50).

2-(Imino-4-methylbenzal)-4-hydroxy-phenyl-5-(4-phenyl-1*H*-imidazol-2-yl)thiazole (5e): Yield 75%, m.p.: 227 ºC. IR (KBr, ν_{max}, cm^{-1}): 3510 (OH), 3154 (NH *str.*), 3016 (CH-atom *str.*), 1605 (C=C atom *str.*), 1318 (C-S *str.*). ^{1}H NMR (DMSO-d_6, 400 MHz), δ ppm: 13.52 (H, s, NH), 8.88 (H, s, CH), 8.42 (H, s, imidazole-H), 6.90-8.30 (13H, m, Ar-H), 5.45 (1H, s, OH), 2.95 (3H, s, CH_3). ^{13}C NMR (DMSO-d_6), δ ppm: 170.8 (N=C-S), 161.7 (CH=N), 158.9 (C=C-N), 141.6 (C=C-N) (imidazole), 131.7 (N=C-NH), 125.6 (C=C-S) (thiazole), 115-160 (aromatic 18C-atom), 122.4 (NH=C-C), 21.9 (-CH_3). EI-MS: *m/z* (%) 439 (1%), 438 (5%), 438 (4.5%), 437 (29), 437 (1%), 436 (100%) base peak. Anal. calcd. (found) % for $C_{26}H_{20}ON_4S$: C, 71.54 (72.31); H, 4.62 (4.84); O, 3.67 (3.48); N, 12.83 (12.61); S, 7.35 (7.58).

General procedure for the synthesis of 2-(imino substituted benzal)-4-(4-hydroxy-phenyl)-5-(4,5-diphenyl-1*H*-imidazol-2-yl)thiazoles (5f-j): To a solution of 4,5-diphenyl-5-(4-hydroxy-phenyl-1*H*-imidazol-2-yl)thiazol-2-amines (0.1 mol) and substituted benzaldehyde (0.1 mol) were dissolved in ethanol using a catalytic amount of glacial acetic acid. The reaction mixture was refluxed with constant stirring at 50-60 ºC for 4-5 h. The progress of the reaction was checked by TLC. It was cooled at room temperature and the product was filtered, dried by ether and recrystallized from hot ethanol. The product was washed with sodium bisulphite to get rid of excess aldehyde followed by ethanol to get pure product.

2-(Iminobenzal)-4-hydroxy-phenyl-5-(4,5-diphenyl-1*H*-imidazol-2-yl)thiazole (5f): Yield 65%, m.p.: 231 ºC. IR (KBr, ν_{max}, cm^{-1}): 3520 (OH), 3435 (NH *str.*), 3045 (CH-atom *str.*), 1592 (C=C atom *str.*), 1699 (C=N), 1320 (C-S *str.*). ^{1}H NMR (DMSO-d_6, 400 MHz), δ ppm: 13.57 (H, s, NH), 8.98 (H, s, CH), 6.90-7.83 (19H, m, Ar-H), 5.54 (1H, s, OH). ^{13}C NMR (DMSO-d_6), δ ppm: 174.9 (N=C-S), 161.8 (CH=N), 159.9 (C=C-N), 132.8 (N=C-NH), 130.1 (C=C-N) (imidazole), 128.8 (C=C-S) (thiazole), 121.9 (NH=C-C), 120-138 (aromatic 24C-atom). EI-MS: *m/z* (%) 501 (1%), 500 (5%), 500 (4%), 499 (35%), 498 (100%) base peak. Anal. calcd. (found) % for $C_{31}H_{22}N_4OS$: C, 74.68 (74.98); H, 4.45 (4.86); N, 11.24 (12.02); S, 6.43 (6.89); O, 3.21 (3.98).

2-(Imino-4-chlorobenzal)-4-hydroxy-phenyl-5-(4,5-diphenyl-1*H*-imidazol-2-yl)thiazole (5g): Yield 78%, m.p.: 198 ºC. IR (KBr, ν_{max}, cm^{-1}): 3505 (OH), 3443 (NH *str.*), 3040 (CH-atom *str.*, 1585 (C=C atom *str.*), 1687 (C=N), 1317 (C-S *str.*). ^{1}H NMR (DMSO-d_6, 400 MHz), δ ppm: 13.42 (H, s, NH), 8.65 (H, s, CH), 6.46-7.58 (18H, m, Ar-H), 5.54 (1H, s, OH). ^{13}C NMR (DMSO-d_6), δ ppm: 174.5 (N=C-S), 160.9 (CH=N), 159.8 (C=C-N), 132.5 (N=C-NH), 130.1 (C=C-N) (imidazole), 129.2 (C=C-S) (thiazole), 117-138 (aromatic 24C-atom). EI-MS: *m/z* (%) 536 (2%), 536 (1%), 535 (13%), 534 (6%), 534 (37%), 533 (34%), 533 (2%), 532 (100%) base peak. Anal. calcd. (found) % for $C_{31}H_{21}N_4OSCl$: C, 69.85 (70.10); H, 3.97 (4.09); Cl, 6.65 (6.93); N, 10.51 (10.77); S, 6.02 (6.65); O, 3.00 (3.29).

2-(Imino-4-nitrobenzal)-4-hydroxy-phenyl-5-(4,5-diphenyl-1*H*-imidazol-2-yl)thiazole (5h): Yield 60%, m.p.: 159 ºC. IR (KBr, ν_{max}, cm^{-1}): 3515 (OH), 3447 (NH *str.*), 3050 (CH-atom *str.*), 1595 (C=C atom *str.*), 1675 (C=N), 1332 (C-S *str.*). ^{1}H NMR (DMSO-d_6, 400 MHz), δ ppm: 13.39 (H, s, NH), 8.41 (H, s, Ar-H), 8.72 (H, s, CH), 6.90-8.32 (18H, m, Ar-H), 5.36 (1H, s, OH). ^{13}C NMR (DMSO-d_6), δ ppm: 174.3 (N=C-S), 162.8 (CH=N), 159.8 (C=C-N), 142.1 (C=C-N) (imidazole), 133.8 (N=C-NH), 129.2 (C=C-S) (thiazole), 124-160 (aromatic 24C-atom), 120.9 (NH-C=C). EI-MS: *m/z* (%) 556 (2%), 545 (7%), 545 (4%), 544 (2%), 544 (34%), 543 (100%) base peak. Anal. calcd. (found) % for $C_{31}H_{21}O_3N_5S$: C, 68.49 (69.04); H, 3.89 (4.05); O, 8.83 (9.04); N, 12.88 (12.94); S, 5.90 (6.08).

2-(Imino-4-methoxybenzal)-4-hydroxy-phenyl-5-(4,5-diphenyl-1*H*-imidazol-2-yl)thiazole (5i): Yield 67%, m.p.: 259 ºC. IR (KBr, ν_{max}, cm^{-1}): 3507 (OH), 3433 (NH *str.*), 3032 (CH-atom *str.*), 1566 (C=C atom *str.*), 1667 (C=N), 1335 (C-S *str.*). ^{1}H NMR (DMSO-d_6, 400 MHz), δ ppm: 13.75 (H, s, NH), 8.85 (H, s, CH), 6.90-7.85 (18H, m, Ar-H), 5.58 (1H, s, OH), 3.98 (3H, s, OCH_3). ^{13}C NMR (DMSO-d_6), δ ppm: 173.9 (N=C-S), 162.5 (CH=N), 135.3 (C=C-N), 135.1 (C=C-N) (imidazole), 132.8 (N=C-NH), 129.2 (C=C-S) (thiazole), 114-165 (aromatic 24C-atom), 121.9 (NH=C-C), 56.3 (-OCH_3). EI-MS: *m/z* (%) 531 (2%), 530 (6%), 530 (5%), 529 (35%), 529 (2%), 528 (100%) base peak. Anal. calcd. (found) % for $C_{32}H_{24}O_2N_4S$: C, 72.71 (73.04); H, 4.58 (4.79); O, 6.05 (6.78); N, 10.60 (11.06); S, 6.07 (7.20).

2-(Imino-4-methylbenzal)-4-hydroxy-phenyl-5-(4,5-diphenyl-1*H*-imidazol-2-yl)thiazole (5j): Yield 65%, m.p.: 276 ºC. IR (KBr, ν_{max}, cm^{-1}): 3510 (OH), 3445 (NH *str.*), 3042 (CH-atom *str.*), 1570 (C=C atom *str.*), 1672 (C=N), 1343 (C-S *str.*). ^{1}H NMR (DMSO-d_6, 400 MHz), δ ppm: 13.82 (H, s, NH), 8.76 (H, s, CH), 6.90-7.53 (18H, m, Ar-H), 5.65 (1H, s, OH), 2.75 (3H, s, CH_3). ^{13}C NMR (DMSO-d_6), δ ppm: 170.8 (N=C-S), 161.9 (CH=N), 159.9 (C=C-N), 142.6 (C=C-N) (imidazole), 133.7 (N=C-NH), 126.6 (C=C-S) (thiazole), 115-160 (aromatic 18C-atom), 123.4 (NH=C-C), 21.9 (-CH_3). EI-MS: *m/z* (%) 515 (2%), 514 (7%), 514 (4%), 513 (36%), 513 (1%), 512 (100%) base peak. Anal. calcd. (found) % for $C_{32}H_{24}ON_4S$: C, 74.98 (75.11); H, 4.72 (5.04); N, 10.93 (11.21); O, 3.12 (3.48); S, 6.26 (6.58).

General procedure for the synthesis of 2-(imino substituted benzal)-4-(2,3,4,6-tetra-O-acetyl-*p*-O-β-D-glucosidoxyphenyl)-5-(4-phenyl-1*H*-imidazol-2-yl)thiazoles (6a-e):

A solution of 5 g of acetobromoglucose in 20 mL of dry acetone was added dropwise to a solution of 3 g of potassium salt of 2-(imino substituted benzal)-4-(4-hydroxy-phenyl)-5-(4-phenyl-1*H*-imidazol-2-yl)thiazoles in 10 mL of 5% methanolic KOH. The resulting mixture was stirred at 0 ºC for 2h. The solvent was extracted under reduced pressure after another 24 h of reaction time. TLC was used to examine the reactions. A dark syrupy mass of obtained **6a-e** was obtained.

2-(Iminobenzal)-4-(2,3,4,6-tetra-O-acetyl-*p*-O-β-D-glucosidoxyphenyl)-5-(4-phenyl-1*H*-imidazol-2-yl)thiazoles (6a): Yield 75%, m.p.: 140 ºC. IR (KBr, ν_{max}, cm^{-1}): 3154 (NH *str.*), 3055 (CH-atom *str.*), 2855 (glucosidic C–H *str.*), 1, 755 (C=O of O-acetyl group of glycone moiety), 1, 618 (C=N *str.*), 1600 (C=C atom *str.*), 1300 (C-S *str.*). ^{1}H NMR (DMSO-d_6, 400 MHz), δ ppm: 13.87 (H, s, -NH), 8.88 (H, s, CH), 7.39 (H, s, imidazole-H), 6.90-8.32 (14H, m, Ar-H), 6.43 (d, anomeric proton), 1.95-2.05 (s, 4H, OAc). ^{13}C NMR (DMSO-d_6), δ ppm: 174.4 (N=C-S), 172.2 (s, 4C, C=O), 161.2 (CH=N), 160.5 (C=C-N), 142.1 (C=C-N) (imidazole), 132.8 (N=C-NH), 129.2 (C=C-S) (thiazole), 121.9 (NH=C-C), 116-154 (aromatic 18 C-atom), 107.9 (s, anomeric C-atom), 22.0 (s, C-atom, CH_3 of acetyl group). EI-MS: *m/z* (%):755 (1%), 755 (2%), 754 (12%), 754 (4%), 753 (43%), 753 (2%), 752 (100%) base peak. Anal. calcd. (found) % for $C_{39}H_{36}N_4O_{10}S$: C, 62.22 (62.28); H, 4.82 (4.86); N, 7.44 (7.49); O, 21.25 (21.28); S, 4.26 (4.29).

2-(Imino-4-chlorobenzal)-4-(2,3,4,6-tetra-O-acetyl-*p*-O-β-D-glucosidoxyphenyl)-5-(4-phenyl-1*H*-imidazol-2-yl)thiazoles (6b): Yield 75%, m.p.: 195 ºC. IR (KBr, ν_{max}, cm^{-1}): 3140 (NH *str.*), 3044 (CH-atom *str.*), 2850 (glucosidic C–H *str.*), 1745 (C=O of O-acetyl groups of glycone moiety), 1620 (C=N *str.*), 1623 (C=C atom *str.*), 1310 (C-S *str.*). ^{1}H NMR (DMSO-d_6, 400 MHz), δ ppm: 13.43 (H, s, NH), 8.76 (H, s, CH), 7.46-8.13 (13H, m, Ar-H), 7.45 (H, s, imidazole-H), 6.33 (d, anomeric proton), 1.92- 2.04 (s, 4H, OAc). ^{13}C NMR (DMSO-d_6), δ ppm: 173.3 (N=C-S), 161.2 (CH=N), 159.1 (C=C-N), 141.1 (C=C-N) (imidazole), 132.8 (N=C-NH), 130.2 (C=C-S) (thiazole), 127-136 (aromatic 18C-atom), 115.9 (NH=C-C), 104.9 (s, anomeric C-atom), 22.5 (s, C-atom, CH_3 of acetyl group). EI-MS: *m/z* (%) 790 (4%), 790 (1%), 789 (1%), 789 (16%), 788 (11%), 788 (36%), 787 (43%), 787 (1%), 786 (100%) base peak. Anal. calcd. (found) % for $C_{39}H_{35}N_4O_{10}SCl$: C, 59.50 (59.60); H, 4.48 (4.52); Cl, 4.50 (4.57); N, 7.12 (7.18); O, 20.32 (20.35); S, 4.07 (4.11).

2-(Imino-4-nitrobenzal)-4-(2,3,4,6-tetra-O-acetyl-*p*-O-β-D-glucosidoxyphenyl)-5-(4-phenyl-1*H*-imidazol-2-yl)-thiazoles (6c): Yield 60%, m.p.: 159 ºC. IR (KBr, ν_{max}, cm^{-1}): 3147 (NH *str.*), 3049 (CH-atom *str.*), 2858 (glucosidic C–H *str.*), 1749 (C=O of O-acetyl groups of glycone moiety), 1629 (C=N *str.*), 1629 (C=C atom *str.*), 1319 (C-S *str.*). ^{1}H NMR (DMSO-d_6, 400 MHz), δ ppm: 13.52 (H, s, NH), 8.42 (H, s, Ar-H), 8.72 (H, s, CH), 8.29 (2H, d, Ar-H), 8.21 (H, s, imidazole-H), 6.90-8.32 (13H, m, Ar-H), 6.45 (d, anomeric proton), 1.92- 2.04 (s, 4H, OAc). ^{13}C NMR (DMSO-d_6), δ ppm: 171.3 (N=C-S), 162.0 (CH=N), 159.1 (C=C-N), 142.1 (C=C-N) (imidazole), 132.8 (N=C-NH), 126.2 (C=C-S) (thiazole), 124-150 (aromatic 18C-atom), 121.9 (NH=C-C), 105.9 (s, anomeric C-atom), 21.5 (s, C-atom, CH_3 of acetyl group). EI-MS: *m/z* (%) 800 (2%), 800 (2%), 799 (9%), 799 (8%), 798 (45%), 797 (100%) base peak. Anal. calcd. (found) % for $C_{39}H_{35}N_5O_{12}S$: C, 58.71 (58.74); H, 4.42 (4.45); N, 8.78 (8.20); O, 24.07 (24.10); S, 4.02 (4.08).

2-(Imino-4-methoxybenzal)-4-(2,3,4,6-tetra-O-acetyl-*p*-O-β-D-glucosidoxyphenyl)-5-(4-phenyl-1*H*-imidazol-2-yl)thiazoles (6d): Yield 68%, m.p.: 212 ºC. IR (KBr, ν_{max}, cm^{-1}): 3152 (NH *str.*), 3055 (CH-atom *str.*), 2862 (glucosidic C–H *str.*), 1756 (C=O of O-acetyl groups of glycone moiety), 1634 (C=N *str.*), 1629 (C=C atom *str.*), 1325 (C-S *str.*). ^{1}H NMR (DMSO-d_6, 400 MHz), δ ppm: 13.48 (H, s, NH), 8.64 (H, s, CH), 8.25 (H, s, imidazole-H), 6.90-8.60 (13H, m, Ar-H), 6.54 (d, anomeric proton), 3.92 (3H, s, OCH_3), 1.92- 2.04 (s, 4H, OAc). ^{13}C NMR (DMSO-d_6), δ ppm: 170.3 (N=C-S), 161.0 (CH=N), 158.1 (C=C-N), 141.1 (C=C-N) (imidazole), 131.8 (N=C-NH), 125.2 (C=C-S) (thiazole), 115-160 (aromatic 18C-atom), 121.9 (NH=C-C), 105.4 (s, anomeric C-atom), 56.32 (-OCH_3), 21.38 (s, C-atom, CH_3 of acetyl group). EI-MS: *m/z* (%) 785 (1%), 785 (2%), 784 (12%), 784 (4%), 783 (44%), 783 (1%), 782 (100%) base peak. Anal. calcd. (found) % for $C_{40}H_{38}N_4O_{11}S$: C, 61.37 (61.40); H, 4.89 (4.94); N, 7.16 (7.20); O, 22.48 (22.52); S, 4.10 (4.14).

2-(Imino-4-methylbenzal)-4-(2,3,4,6-tetra-O-acetyl-*p*-O-β-D-glucosidoxyphenyl)-5-(4-phenyl-1-H-imidazol-2-yl)thiazoles (6e): Yield 75%, m.p.: 227 ºC. IR (KBr, ν_{max}, cm^{-1}): 3160 (NH *str.*), 3065 (CH-atom *str.*), 2860 (glucosidic C–H *str.*), 1760 (C=O of O-acetyl groups of glycone moiety), 1643 (C=N *str.*), 1654 (C=C atom *str.*), 1343 (C-S *str.*). ^{1}H NMR (DMSO-d_6, 400 MHz), δ ppm: 13.52 (H, s, NH), 8.88 (H, s, CH), 8.42 (H, s, imidazole-H), 6.90-8.30 (13H, m, Ar-H), 6.60 (d, anomeric proton), 2.95 (3H, s, CH_3), 1.92-2.04 (s, 4H, OAc). ^{13}C NMR (DMSO-d_6), δ ppm: 170.8 (N=C-S), 161.7 (CH=N), 158.9 (C=C-N), 141.6 (C=C-N) (imidazole), 131.7 (N=C-NH), 125.6 (C=C-S) (thiazole), 115-160 (aromatic 18C-atom), 122.4 (NH=C-C), 104.4 (s, anomeric C-atom), 22.38 (s, C-atom, CH_3 of acetyl group), 21.9 (-CH_3). EI-MS: *m/z* (%) 769 (2%), 769 (2%), 768 (11%), 768 (5%), 767 (45%), 766 (100%) base peak. Anal. calcd. (found) % for $C_{40}H_{38}N_4O_{10}S$: C, 62.65 (62.68); H, 4.99 (5.03); N, 7.31 (7.34); O, 20.86 (20.99); S, 4.18 (4.22).

General procedure for the synthesis of 2-(imino substituted benzal)-4-(2,3,4,6-tetra-O-acetyl-*p*-O-β-D-glucosidoxyphenyl)-5-(4,5-diphenyl-imidazol-2-yl)thiazoles (6f-j): A solution of 5 g of acetobromoglucose in 20 mL of dry acetone was added dropwise to a solution of 3 g potassium salt of 2-(imino substituted benzal)-4-(4-hydroxy-phenyl)-5-(4,5-diphenylimidazol-2-yl)thiazoles in 10 mL of 5% methanolic KOH. For 2 h, the resultant mixture was stirred at 0 ºC. The solvent was extracted under reduced pressure after another 24 h of reaction time. TLC was used to evaluate the reactions. A dark syrupy mass of obtained **6f-j** was obtained.

2-(Iminobenzal)-4-(2,3,4,6-tetra-O-acetyl-*p*-O-β-D-glucosidoxyphenyl)-5-(4,5-diphenyl-1*H*-imidazol-2-yl)-thiazoles (6f): Yield 65%, m.p.: 231 ºC. IR (KBr, ν_{max}, cm^{-1}): 3156 (NH *str.*), 3065 (CH-atom *str.*), 2865 (glucosidic C–H *str.*), 1760 (C=O of O-acetyl groups of glycone moiety), 1626 (C=N *str.*), 1615 (C=C atom *str.*), 1323 (C-S *str.*). ^{1}H NMR (DMSO-d_6, 400 MHz), δ ppm: 13.57 (H, s, -NH), 8.98 (H, s, CH),

6.90-7.83 (19H, m, Ar-H), 6.54 (d, anomeric proton), 1.95- 2.05 (s, 4H, OAc). ^{13}C NMR (DMSO-d_6), δ ppm: 174.9 (N=C-S), 161.8 (CH=N), 159.9 (C=C-N), 132.8 (N=C-NH), 130.1 (C=C-N) (imidazole), 128.8 (C=C-S) (thiazole), 121.9 (NH=C-C), 120-138 (aromatic 24C-atom), 105.9 (s, anomeric C-atom), 22.9 (s, C-atom, CH_3 of acetyl group). EI-MS: *m/z* (%) 827 (1%), 827 (2%), 826 (15%), 826 (4%), 825 (49%), 825 (4%), 824 (100%) base peak. Anal. calcd. (found) % for $C_{45}H_{36}N_4O_{10}S$: C, 65.52 (65.58); H, 4.40 (4.46); N, 6.79 (6.82); O, 19.40 (19.48); S, 3.89 (3.93).

2-(Imino-4-chlorobenzal)-4-(2,3,4,6-tetra-O-acetyl-*p*-O-β-D-glucosidoxyphenyl)-5-(4,5-diphenyl-1*H*-imidazol-2-yl)thiazoles (6g): Yield 78%, m.p.: 198 ºC. IR (KBr, ν_{max}, cm^{-1}): 3140 (NH *str.*), 3043 (CH-atom *str.*), 2854 (glucosidic C–H *str.*), 1755 (C=O of O-acetyl groups of glycone moiety), 1636 (C=N *str.*), 1643 (C=C atom *str.*), 1345 (C-S *str.*). ^{1}H NMR (DMSO-d_6, 400 MHz), δ ppm: 13.42 (H, s, NH), 8.65 (H, s, CH), 6.46-7.58 (18H, m, Ar-H), 6.98 (d, anomeric proton), 1.95-2.05 (s, 4H, OAc). ^{13}C NMR (DMSO-d_6), δ ppm: 174.5 (N=C-S), 160.9 (CH=N), 159.8 (C=C-N), 132.5 (N=C-NH), 130.1 (C=C-N) (imidazole), 129.2 (C=C-S) (thiazole), 117-138 (arom. 24C-atom), 103.9 (s, anomeric C-atom), 21.9 (s, C-atom, CH_3 of acetyl group). EI-MS: *m/z* (%) 863 (1%), 862 (5%), 862 (1%), 861 (1%), 861 (19%), 860 (14%), 860 (36%), 859 (50%), 859 (1%), 858 (100%) base peak. Anal. calcd. (found) % for $C_{45}H_{35}N_4O_{10}SCl$: C, 62.90 (62.96); H, 4.11 (4.16); Cl, 4.13 (4.18); N, 6.52 (6.58); O, 18.62 (18.69); S, 3.73 (3.78).

2-(Imino-4-nitrobenzal)-4-(2,3,4,6-tetra-O-acetyl-*p*-O-β-D-glucosidoxyphenyl)-5-(4,5-diphenyl-1*H*-imidazol-2-yl)thiazoles (6h): Yield 60%, m.p.: 159 ºC. IR (KBr, ν_{max}, cm^{-1}): 3145 (NH *str.*), 3053 (CH-atom *str.*), 2865 (glucosidic C–H *str.*), 1765 (C=O of O-acetyl groups of glycone moiety), 1640 (C=N *str.*), 1654 (C=C atom *str.*), 1365 (C-S *str.*). ^{1}H NMR (DMSO-d_6, 400 MHz), δ ppm: 13.39 (H, s, NH), 8.41 (H, s, Ar-H), 8.72 (H, s, CH), 6.90-8.32 (18H, m, Ar-H), 6.77 (d, anomeric proton), 1.95- 2.05 (s, 4H, OAc). ^{13}C NMR (DMSO-d_6), δ ppm: 174.3 (N=C-S), 162.8 (CH=N), 159.8 (C=C-N), 142.1 (C=C-N) (imidazole), 133.8 (N=C-NH), 129.2 (C=C-S) (thiazole), 124-160 (aromatic 24C-atom), 120.9 (NH-C=C), 104.9 (s, anomeric C-atom), 23.9 (s, C-atom, CH_3 of acetyl group). EI-MS: *m/z* (%) 872 (3%), 872 (2%), 871 (12%), 871 (8%), 870 (51%), 869 (100%) base peak. Anal. calcd. (found) % for $C_{45}H_{35}N_5O_{12}S$: C, 62.13 (62.18); H, 4.06 (4.11); N, 8.05 (8.15); O, 22.07 (22.11); S, 3.69 (3.72).

2-(Imino-4-methoxybenzal)-4-(2,3,4,6-tetra-O-acetyl-*p*-O-β-D-glucosidoxyphenyl)-5-(4,5-diphenyl-1*H*-imidazol-2-yl)thiazoles (6i): Yield 67%, m.p.: 259 ºC. IR (KBr, ν_{max}, cm^{-1}): 3132 (NH *str.*), 3064 (CH-atom *str.*), 2832 (glucosidic C–H *str.*), 1730 (C=O of O-acetyl groups of glycone moiety), 1650 (C=N *str.*), 1675 (C=C atom *str.*), 1364 (C-S *str.*). ^{1}H NMR (DMSO-d_6, 400 MHz), δ ppm: 13.75 (H, s, NH), 8.85 (H, s, CH), 6.90-7.85 (18H, m, Ar-H), 7.07 (d, anomeric proton), 3.98 (3H, s, OCH_3), 1.95-2.05 (s, 4H, OAc). ^{13}C NMR (DMSO-d_6), δ ppm: 173.9 (N=C-S), 162.5 (CH=N), 135.3 (C=C-N), 135.1 (C=C-N) (imidazole), 132.8 (N=C-NH), 129.2 (C=C-S) (thiazole), 114-165 (aromatic 24C-atom), 121.9 (NH=C-C), 103.2 (s, anomeric C-atom), 56.3 (-OCH_3), 21.9 (s, C-atom, CH_3 of acetyl group). EI-MS: *m/z* (%) 857 (2%), 857 (1%), 856 (15%), 856 (4%), 855 (51%), 855 (1%), 854 (100%) base peak. Anal. calcd. (found) % for $C_{46}H_{38}N_4O_{11}S$: C, 64.63 (64.68); H, 4.48 (4.54); N, 6.55 (6.56); O, 20.59 (20.62); S, 3.75 (3.80).

2-(Imino-4-methylbenzal)-4-(2,3,4,6-tetra-O-acetyl-*p*-O-β-D-glucosidoxyphenyl)-5-(4,5-diphenyl-1*H*-imidazol-2-yl)thiazoles (6j): Yield 65%, m.p.: 276 ºC. IR (KBr, ν_{max}, cm^{-1}): 3140 (NH *str.*), 3032 (CH-atom *str.*), 2848 (glucosidic C–H *str.*), 1759 (C=O of O-acetyl groups of glycone moiety), 1687 (C=N *str.*), 1685 (C=C atom *str.*), 1354 (C-S *str.*). ^{1}H NMR (DMSO-d_6, 400 MHz), δ ppm: 13.82 (H, s, NH), 8.76 (H, s, CH), 6.90-7.53 (18H, m, Ar-H), 6.07 (d, anomeric proton), 2.75 (3H, s, CH_3), 1.95-2.05 (s, 4H, OAc). ^{13}C NMR (DMSO-d_6), δ ppm: 170.8 (N=C-S), 161.9 (CH=N), 159.9 (C=C-N), 142.6 (C=C-N) (imidazole), 133.7 (N=C-NH), 126.6 (C=C-S) (thiazole), 115-160 (aromatic 18C-atom), 123.4 (NH=C-C), 102.9 (s, anomeric C-atom), 21.7 (s, C-atom, CH_3 of acetyl group), 21.9 (-CH_3). EI-MS: *m/z* (%) 841 (3%), 841 (2%), 840 (14%), 840 (5%), 839 (52%), 838 (100%) base peak. Anal. calcd. (found) % for $C_{46}H_{38}N_4O_{10}S$: C, 65.86 (65.94); H, 4.57 (4.62); N, 6.68 (6.75); O, 19.07 (19.14); S, 3.82 (3.88).

General procedure for the synthesis of 2-(imino substituted benzal)-4-(*p*-O-β-D-glucosidoxyphenyl)-5-(4-phenyl-1*H*-imidazol-2-yl)thiazoles (7a-e): To a solution of 2-(imino-substituted benzal)-4-(2,3,4,6-tetra-O-acetyl-*p*-O-β-glucosidoxyphenyl)-5-(4-phenyl-1*H*-imidazol-2-yl)thiazoles (2 g) in 25 mL of dry methanol was added 1.5 mL of 5% CH_3ONa solution. A further 24 h were spent maintaining the reaction mixture at room temperature. It was filtered, concentrated *in vacuo* and neutralized using ion exchange resin to produce a thick, very hygroscopic, brown-coloured syrupy.

2-(Iminobenzal)-4-(*p*-O-β-D-glucosidoxyphenyl)-5-(4-phenyl-1*H*-imidazol-2-yl)thiazole (7a): Yield 65%, m.p.: 231 ºC. IR (KBr, ν_{max}, cm^{-1}): 3412 (broad, OH peak of carbohydrate residue), 3399 (NH *str.*), 2976 (CH-atom *str.*), 2954 (glucosidic C-H *str.*), 1565 (C=C atom *str.*), 1643 (C=N), 1364 (C-S *str.*). ^{1}H NMR (DMSO-d_6, 400 MHz), δ ppm: 13.57 (H, s, -NH), 8.98 (H, s, CH), 6.90-7.83 (14H, m, Ar-H), 5.92 (d, 1H, anomeric proton), 3.49-3.91 (m, 4H, β-D-glucopyranosyl ring). ^{13}C NMR (DMSO-d_6), δ ppm: 174.9 (N=C-S), 161.8 (CH=N), 159.9 (C=C-N), 132.8 (N=C-NH), 130.1 (C=C-N) (imidazole), 128.8 (C=C-S) (thiazole), 121.9 (NH=C-C), 120-138 (aromatic 24C-atom), 62-109 (pyranyl 5C-atom). EI-MS: *m/z* (%) 587 (1%), 587 (2%), 586 (7%), 586 (5%), 585 (34%), 584 (100%) base peak. Anal. calcd. (found) % for $C_{31}H_{28}N_4O_6S$: C, 63.69 (63.78); H, 4.83 (4.86); N, 9.58 (9.62); O, 16.42 (16.44); S, 5.48 (5.54).

2-(Imino-4-chlorobenzal)-4-(*p*-O-β-D-glucosidoxyphenyl)-5-(4-phenyl-1*H*-imidazol-2-yl)thiazole (7b): Yield 75%, m.p.: 195 ºC. IR (KBr, ν_{max}, cm^{-1}): 3400 (broad, OH peak of carbohydrate residue), 3398 (NH *str.*), 2970 (CH-atom *str.*), 2950 (glucosidic C-H *str.*), 1645 (C=C atom *str.*), 1632 (C=N), 1358 (C-S *str.*). ^{1}H NMR (DMSO-d_6, 400 MHz), δ ppm: 13.43 (H, s, NH), 8.76 (H, s, CH), 7.46-8.13 (13H, m, Ar-H), 7.45 (H, s, imidazole-H), 5.88 (d, 1H, anomeric proton), 3.51-3.98 (m, 4H, β-D-glucopyranosyl ring). ^{13}C NMR (DMSO-d_6), δ ppm: 173.3 (N=C-S), 161.2 (CH=N), 159.1 (C=C-N), 141.1 (C=C-N) (imidazole), 132.8 (N=C-NH), 130.2 (C=C-S) (thiazole), 127-

136 (aromatic 18C-atom), 115.9 (NH=C-C), 60-107 (pyranyl 5C-atom). EI-MS: *m/z* (%) 622 (2%), 622 (2%), 621 (1%), 621 (13%), 620 (37%), 619 (34%), 618 (100%) base peak. Anal. calcd. (found) % for $C_{31}H_{27}N_4O_6SCl$: C, 60.14 (60.16); H, 4.40 (4.43); Cl, 5.73 (5.76); N, 9.05 (9.08); O, 15.51 (15.54); S, 5.18 (5.27).

2-(Imino-4-nitrobenzal)-4-(*p*-O-β-D-glucosidoxyphenyl)-5-(4-phenyl-1*H*-imidazol-2-yl)thiazole (7c): Yield 60%, m.p.: 159 ºC. IR (KBr, ν_{max}, cm^{-1}): 3404 (broad, OH peak of carbohydrate residue), 3401 (NH *str.*), 2975 (CH-atom *str.*), 2955 (glucosidic C-H *str.*), 1655 (C=C atom *str.*), 1642 (C=N), 1365 (C-S *str.*). ^{1}H NMR (DMSO-d_6, 400 MHz), δ ppm: 13.52 (H, s, NH), 8.42 (H, s, Ar-H), 8.72 (H, s, CH), 8.29 (2H, d, Ar-H), 8.21 (H, s, imidazole-H), 6.90-8.32 (13H, m, Ar-H), 3.49-3.91 (m, 4H, β-D-glucopyranosyl ring).^{13}C NMR (DMSO-d_6), δ ppm: 171.3 (N=C-S), 162.0 (CH=N), 159.1 (C=C-N), 142.1 (C=C-N) (imidazole), 132.8 (N=C-NH), 126.2 (C=C-S) (thiazole), 124-150 (aromatic 18C-atom), 121.9 (NH=C-C), 58-105 (pyranyl 5C-atom). EI-MS: *m/z* (%): 632 (1%), 632 (2%), 631 (8%), 631 (4%), 630 (36%), 629 (100%) base peak. Anal. calcd. (found) % for $C_{31}H_{27}O_8N_5S$: C, 59.13 (59.17); H, 4.32 (4.36); N, 11.12 (11.20); O, 20.33 (20.48); S, 5.09 (5.13).

2-(Imino-4-methoxybenzal)-4-(*p*-O-β-D-glucosidoxyphenyl)-5-(4-phenyl-1*H*-imidazol-2-yl)thiazole (7d): Yield 68%, m.p.: 212 ºC. IR (KBr, ν_{max}, cm^{-1}): 3987 (broad, OH peak of carbohydrate residue), 3376 (NH *str.*), 2964 (CH-atom *str.*), 2932 (glucosidic C-H *str.*), 1630 (C=C atom *str.*), 1621 (C=N), 1350 (C-S *str.*). ^{1}H NMR (DMSO-d_6, 400 MHz), δ ppm: 13.48 (H, s, NH), 8.64 (H, s, CH), 8.25 (H, s, imidazole-H), 6.90-8.60 (13H, m, Ar-H), 3.92 (3H, s, OCH_3), 3.49-3.91 (m, 6H, β-D-glucopyranosyl ring). ^{13}C NMR (DMSO-d_6), δ ppm: 170.3 (N=C-S), 161.0 (CH=N), 158.1 (C=C-N), 141.1 (C=C-N) (imidazole), 131.8 (N=C-NH), 125.2 (C=C-S) (thiazole), 115-160 (aromatic 18C-atom), 121.9 (NH=C-C), 62-109 (pyranyl 5C-atom), 56.32 (-OCH_3). EI-MS: *m/z* (%) 617 (1%), 617 (2%), 616 (7%), 616 (5%), 615 (35%), 615 (2%), 614 (100%) base peak. Anal. calcd. (found) % for $C_{32}H_{30}O_7N_4S$: C, 62.53 (62.55); H, 4.92 (4.98); N, 9.11 (9.14); O, 18.22 (18.32); S, 5.22 (5.26).

2-(Imino-4-methylbenzal)-4-(*p*-O-β-D-glucosidoxyphenyl)-5-(4-phenyl-1*H*-imidazol-2-yl)thiazole (7e): Yield 75%, m.p.: 227 ºC. IR (KBr, ν_{max}, cm^{-1}): 3975 (broad, OH peak of carbohydrate residue), 3362 (NH *str.*), 2960 (CH-atom *str.*), 2923 (glucosidic C-H *str.*), 1625 (C=C atom *str.*), 1618 (C=N), 1342 (C-S *str.*). ^{1}H NMR (DMSO-d_6, 400 MHz), δ ppm: 13.52 (H, s, NH), 8.88 (H, s, CH), 8.42 (H, s, imidazole-H), 6.90-8.30 (13H, m, Ar-H), 3.49-3.91 (m, 4H, β-D-glucopyranosyl ring), 2.95 (3H, s, CH_3). ^{13}C NMR (DMSO-d_6), δ ppm: 170.8 (N=C-S), 161.7 (CH=N), 158.9 (C=C-N), 141.6 (C=C-N) (imidazole), 131.7 (N=C-NH), 125.6 (C=C-S) (thiazole), 115-160 (aromatic 18C-atom), 122.4 (NH=C-C), 62-109 (pyranyl 5C-atom), 21.9 (-CH_3). EI-MS: *m/z* (%) 601 (1%), 601 (2%), 600 (4%), 600 (2%), 600 (6%), 599 (37%), 598 (100%) base peak. Anal. calcd. (found) % for $C_{32}H_{30}O_6N_4S$: C, 64.20 (64.31); H, 5.05 (5.10); O, 16.03 (16.08); N, 9.36 (9.39); S, 5.36 (5.40).

General procedure for the synthesis of 2-(imino substituted benzal)-4-(*p*-O-β-D-glucosidoxyphenyl)-5-(4,5-diphenyl-1*H*-imidazole-2-yl)thiazoles (7f-j): To a solution of 2-(imino substituted benzal)-4-(2,3,4,6-tetra-O-acetyl-*p*-O-β-D-glucosidoxyphenyl)-5-(4,5-diphenyl-imidazol-2-yl)-thiazoles (2 g) in 25 mL of dry methanol was added 1.5 mL of 5% CH_3ONa solution. A further 24 h were spent maintaining the reaction mixture at room temperature. It was filtered, concentrated *in vacuo* and neutralized using ion exchange resin to produce a thick, very hygroscopic and brown-coloured syrupy.

2-(Iminobenzal)-4-(*p*-O-β-D-glucosidoxyphenyl)-5-(4,5-diphenyl-1*H*-imidazole-2-yl)thiazole (7f): Yield 65%, m.p.: 231 ºC. IR (KBr, ν_{max}, cm^{-1}): 3410 (broad, OH peak of carbohydrate residue), 3387 (NH *str.*), 2967 (CH-atom *str.*), 2966 (glucosidic C-H *str.*), 1664 (C=N), 1570 (C=C atom *str.*), 1354 (C-S *str.*). ^{1}H NMR (DMSO-d_6, 400 MHz), δ ppm: 13.57 (H, s, -NH), 8.98 (H, s, CH), 6.90-7.83 (19H, m, Ar-H), 3.49-3.91 (m, 4H, β-D-glucopyranosyl ring). ^{13}C NMR (DMSO-d_6), δ ppm: 174.9 (N=C-S), 161.8 (CH=N), 159.9 (C=C-N), 132.8 (N=C-NH), 130.1 (C=C-N) (imidazole), 128.8 (C=C-S) (thiazole), 121.9 (NH=C-C), 120-138 (aromatic 24C-atom), 62-109 (pyranyl 5C-atom). EI-MS: *m/z* (%): 663 (1%), 663 (2%), 662 (9%), 662 (5%), 661 (40%), 661 (2%), 660 (100%) base peak. Anal. calcd. (found) % for $C_{37}H_{32}N_4O_6S$: C, 67.26 (67.30); H, 4.88 (4.89); N, 8.48 (8.52); O, 14.53 (14.56); S, 4.85 (4.89).

2-(Imino-4-chlorobenzal)-4-(*p*-O-β-D-glucosidoxyphenyl)-5-(4,5-diphenyl-1*H*-imidazole-2-yl)thiazole (7g): Yield 79%, m.p.: 208 ºC. IR (KBr, ν_{max}, cm^{-1}): 3402 (broad, OH peak of carbohydrate residue), 3390 (NH *str.*), 2954 (CH-atom *str.*), 2975 (glucosidic C-H *str.*), 1645 (C=N), 1577 (C=C atom *str.*), 1357 (C-S *str.*). ^{1}H NMR (DMSO-d_6, 400 MHz), δ ppm: 13.50 (H, s, -NH), 8.45 (H, s, CH), 6.68-7.76 (18H, m, Ar-H), 3.49-3.91 (m, 4H, β-D-glucopyranosyl ring). ^{13}C NMR (DMSO-d_6), δ ppm: 174.5 (N=C-S), 160.9 (CH=N), 159.8 (C=C-N), 132.5 (N=C-NH), 130.1 (C=C-N) (imidazole), 129.2 (C=C-S) (thiazole), 117-138 (aromatic 24C-atom), 60-110 (pyranyl 5C-atom). EI-MS: *m/z* (%) 698 (1%), 698 (3%), 697 (1%), 697 (2%), 696 (10%), 696 (36%), 695 (40%), 695 (2%), 694 (100%) base peak. Anal. calcd. (found) % for $C_{37}H_{31}N_4O_6SCl$: C, 63.93 (63.98); H, 4.49 (4.50); Cl, 5.10 (5.13); N, 8.06 (8.07); O, 13.81 (13.85); S, 4.61 (4.67).

2-(Imino-4-nitrobenzal)-4-(*p*-O-β-D-glucosidoxyphenyl)-5-(4,5-diphenyl-1*H*-imidazole-2-yl)thiazole (7h): Yield 60%, m.p.: 159 ºC. IR (KBr, ν_{max}, cm^{-1}): 3407 (broad, OH peak of carbohydrate residue), 3398 (NH *str.*), 2962 (CH-atom *str.*), 2968 (glucosidic C-H *str.*), 1649 (C=N), 1567 (C=C atom *str.*), 1387 (C-S *str.*). ^{1}H NMR (DMSO-d_6, 400 MHz), δ ppm: 13.39 (H, s, NH), 8.41 (H, s, Ar-H), 8.72 (H, s, CH), 6.90-8.32 (18H, m, Ar-H), 3.49-3.91 (m, 4H, β-D-glucopyranosyl ring). ^{13}C NMR (DMSO-d_6), δ ppm: 174.3 (N=C-S), 162.8 (CH=N), 159.8 (C=C-N), 142.1 (C=C-N) (imidazole), 133.8 (N=C-NH), 129.2 (C=C-S) (thiazole), 124-160 (aromatic 24C-atom), 120.9 (NH-C=C), 61-109 (pyranyl 5C-atom). EI-MS: *m/z* (%) 708 (1%), 708 (2%), 707 (8%), 707 (7%), 706 (43%), 705 (100%) base peak. Anal. calcd. (found) % for $C_{37}H_{31}O_8N_5S$: C, 62.97 (63.00); H, 4.43 (4.45); O, 18.14 (18.16); N, 9.92 (9.94); S, 4.54 (4.58).

2-(Imino-4-methoxybenzal)-4-(*p*-O-β-D-glucosidoxyphenyl)-5-(4,5-diphenyl-1*H*-imidazole-2-yl)thiazole (7i):

Yield 67%, m.p.: 259 ºC. IR (KBr, ν_{max}, cm^{-1}): 3415 (broad, OH peak of carbohydrate residue), 3387 (NH *str.*), 2934 (CH-atom *str.*), 2921 (glucosidic C-H *str.*), 1634 (C=N), 1543 (C=C atom *str.*), 1358 (C-S *str.*). ^{1}H NMR (DMSO-d_6, 400 MHz), δ ppm: 13.75 (H, s, NH), 8.85 (H, s, CH), 6.90-7.85 (18H, m, Ar-H), 3.98 (3H, s, OCH_3), 3.49-3.91 (m, 4H, β-D-glucopyranosyl ring). ^{13}C NMR (DMSO-d_6), δ ppm: 173.9 (N=C-S), 162.5 (CH=N), 135.3 (C=C-N), 135.1 (C=C-N) (imidazole), 132.8 (N=C-NH), 129.2 (C=C-S) (thiazole), 114-165 (aromatic 24C-atom), 121.9 (NH=C-C), 62-109 (pyranyl 5C-atom), 56.3 (-OCH_3). EI-MS: *m/z* (%): 693 (1%), 693 (2%), 692 (10%), 692 (4%), 691 (41%), 691 (2%), 690 (100%) base peak. Anal. calcd. (found) % for $C_{38}H_{34}O_7N_4S$: C, 66.07 (66.08); H, 4.96 (4.99); O, 16.21 (16.24); N, 8.11 (8.16); S, 4.64 (4.68).

2-(Imino-4-methylbenzal)-4-(*p*-O-β-D-glucosidoxyphenyl)-5-(4,5-diphenyl-1*H*-imidazole-2-yl)thiazole (7j): Yield 65%, m.p.: 276 ºC. IR (KBr, ν_{max}, cm^{-1}): 3390 (broad, OH peak of carbohydrate residue), 3333 (NH *str.*), 2933 (CH-atom *str.*), 2937 (glucosidic C-H *str.*), 1676 (C=N), 1554 (C=C atom *str.*), 1367 (C-S *str.*). ^{1}H NMR (DMSO-d_6, 400 MHz), δ ppm: 13.82 (H, s, NH), 8.76 (H, s, CH), 6.90-7.53 (18H, m, Ar-H), 3.49-3.91 (m, 4H, β-D-glucopyranosyl ring), 2.75 (3H, s, CH_3). ^{13}C NMR (DMSO-d_6), δ ppm: 170.8 (N=C-S), 161.9 (CH=N), 159.9 (C=C-N), 142.6 (C=C-N) (imidazole), 133.7 (N=C-NH), 126.6 (C=C-S) (thiazole), 115-160 (aromatic 18C-atom), 123.4 (NH=C-C), 62-109 (pyranyl 5C-atom), 21.9 (-CH_3). EI-MS: *m/z* (%) 677 (1%), 677 (2%), 676 (8%), 676 (6%), 675 (43%), 674 (100%) base peak. Anal. calcd. (found) % for $C_{38}H_{34}O_6N_4S$: C, 67.64 (67.68); H, 5.08 (5.10); O, 3.48 (3.49); N, 8.30 (8.32); S, 4.75 (4.78).

Biological activity

Antibacterial activities: The cup plate diffusion technique was used to test the synthetic compounds **3a**, **4a-b**; **5a-j** and **7a-j** for their *in vitro* antibacterial activity against *Escherichia coli*, *Klebisilla aerogens*, *Staphylococcus aureus* and *Bacillus substilis*. Ciprofloxacin and sulfacetamide (100 µg/mL), the two most common medicines, were compared to the zone of inhibition during a 24 h incubation period at 37 ºC.

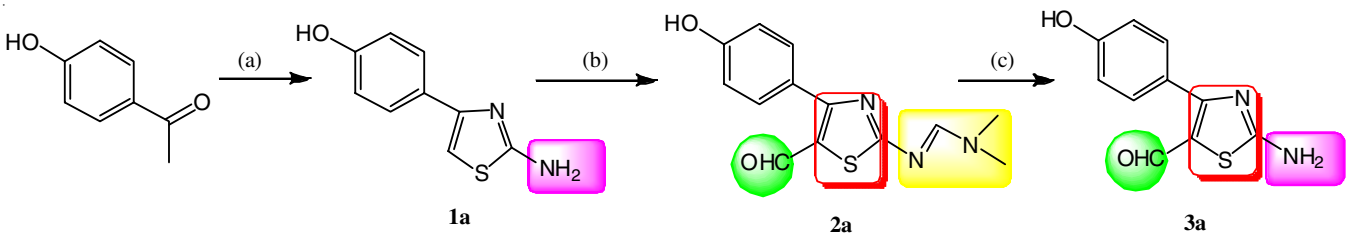
Antifungal activity: By using the cup plate diffusion technique, compounds **3a**, **4a-b**; **5a-j** and **7a-j** were further tested for their antifungal activity against *Aspergillus niger* and *Candida albicans* at a concentration of 100 µg/mL in methanol [30]. The 7 day zone of inhibition at 20 ºC was compared to 100 µg/mL doses of gentamycin and clotrimazole, as a standard drugs.

RESULTS AND DISCUSSION

Present work starts with the combination of 2-amino-4-(4-hydroxy phenyl)-1,3-thiazole (**1a**), which undergoes Vilsmeier-Haack reaction in the presence of SDS afforded intermediates **2a** and finally produce 2-amino-4-(4-hydroxy-phenyl)-1,3-thiazole-5-carboxaldehyde (**3a**). It was established that the reaction time was reduced from 4-5 h to 1-1.5 h by using a 1:1 molar concentration of SDS in the reaction medium. Sodium dodecyl sulphate is one of the least expensive, non-toxic and widely available molecules used in the Vilsmeier-Haack reaction (SDS) [31] **(Scheme-I)**.

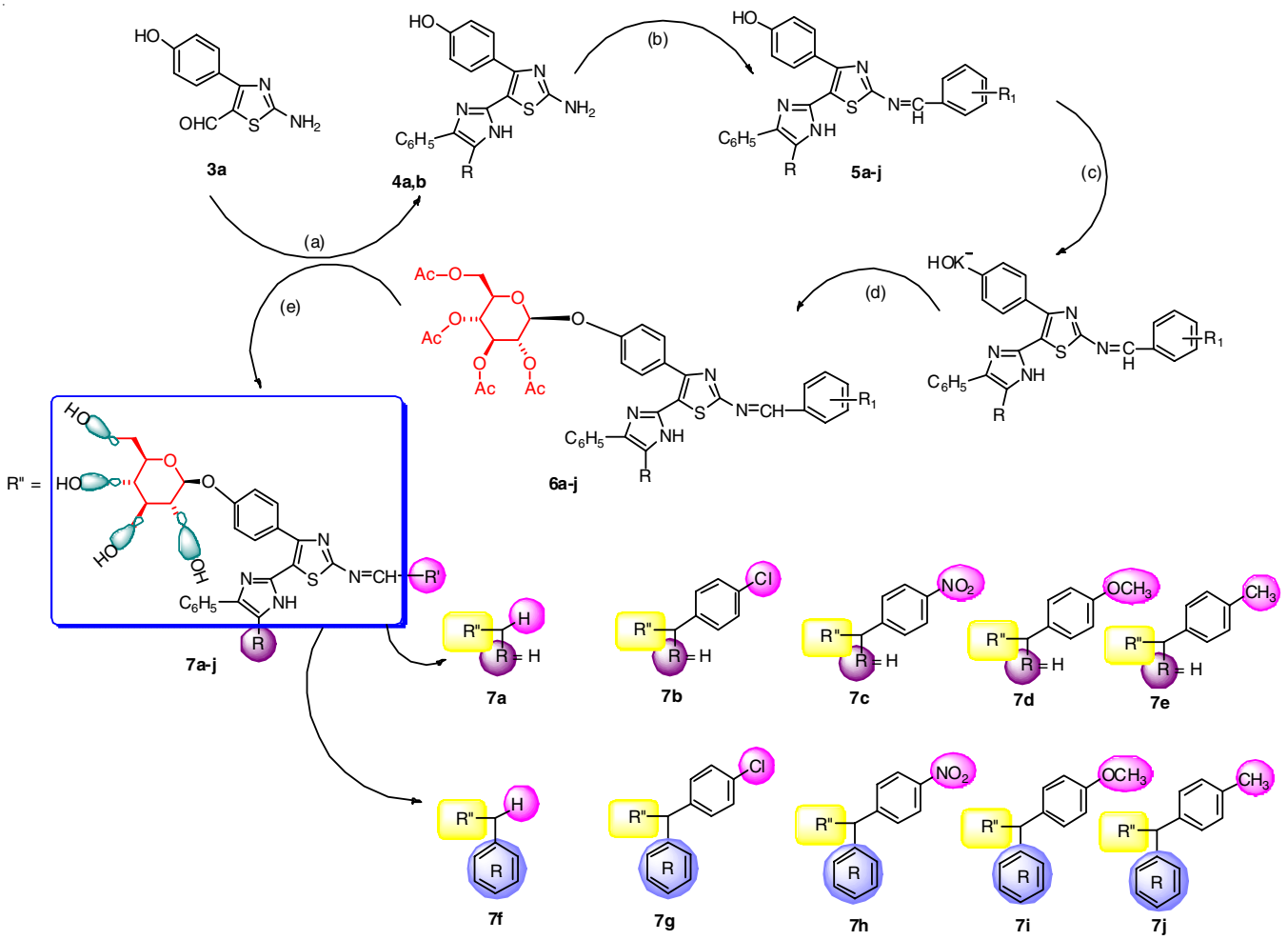
In next step, compound 4-(4-hydroxy-phenyl)-5-(4,5-substituted-1*H*-imidazol-2-yl)thiazol-2-amines (**4a-b)** [32] were synthesized by the reaction of phenyl glyoxal, ammonium acetate and glacial acetic acid with 2-amino-4-(4-hydroxy-phenyl)-1,3-thiazole-5-carboxaldehyde (**3a**). The Schiff bases were (**5a-j)** [33] synthesized from 4-(4-hydroxy-phenyl-5-(4,5-substituted-1*H*-imidazol-2-yl)thiazol-2-amine **(4a-b)** and various benzaldehydes in ethanol with a catalytic amount of glacial acetic acid. Acetobromoglucose (ACBG) was used to glucosylate 2-(imino-substituted benzal)-4-(4-hydroxy-phenyl)-5-(4,5-substituted-1*H*-imidazol-2-yl)thiazole (**5a-j**), followed by deacetylation to get the required O-glucoside with diastereoselectivity for the β-anomer. When donor's 2-hydroxyl group has an ester protecting group attached, only β-anomer by the neighbouring group participation is produced during the O-glucosylation process. Utilizing the Koeing-Knorr technique, acetobromoglucose was first made from glucose pentacetate and red phosphorus. This molecule was then reacted with potassium salts of compounds (**5a-j**) to generate 2-(imino substituted benzal) tetra-(2,3,4,6)-O-acetyl-5-(4,5-substituted-1*H*-imidazol-2-yl)thiazoles (**7a-j**). The structures of all the above synthesized molecules were confirmed by various spectroscopic analyses and a plausible mechanism is explained in **Scheme-II**.

Biological activities: As indicated in Table-1, aglycone compounds had low antimicrobial activity whereas glycosides had the maximum antibacterial activity against Gram-positive, Gram-negative bacteria and fungi. The antibacterial activity results revealed a small variance in the activities of all the glucosides against the microorganisms tested. Compounds **7a-c** and **7e-f** had the greatest antibacterial action against all the bacterial strains. Compound **7d** had low antibacterial action against all microorganisms tested. Similarly, antifungal activity data demonstrated that the glycosides had promising antifungal



1a **2a** **3a**

Scheme-I: Synthesis of 2-amino-4-(4-hydroxyphenyl)thiazole-5-carbaldehyde [Reagents and conditions: (a) thiourea, iodine, ethanol; (b) DMF, $POCl_3$, SDS, sodium carbonate; (c) NaOH/MeOH]



Scheme-II: Synthesis of 2-(imino substituted benzal)-4-(*p*-O-β-D-glucosidoxyphenyl)-5-(4-phenyl-1*H*-imidazol-2-yl)-thiazoles [Reagents and conditions: (a) phenyl glyoxal, ammonium acetate, glacial acetic acid; (b) substituted benzaldehyde, methanol, glacial acetic acid, sodium bisulphite; (c) CH_3OH, KOH; (d) acetone, α-acetobromoglucose; (e) CH_3ONa, CH_3OH]

properties against two yeast strains (*C. albicans* and *A. niger*), except for **7d**, which showed the maximum activity against *C. albicans* but low activity against *A. niger*. These findings revealed that glycosides exhibited antibacterial properties that were both efficient and selective against studied bacteria and fungi.

Conclusion

The synthesized glucosides of 2-(imino substituted benzal)-4-(4-hydroxy-phenyl)-5-(4-phenyl-1*H*-imidazol-2-yl)thiazole (**4a**) and 2-(imino substituted benzal)-4-(4-hydroxy phenyl)-5-(4,5-diphenyl-1*H*-imidazol-2-yl)thiazole (**4b**) were evaluated for *in vitro* antimicrobial activity. The *in vitro* results indicated better pharmacological significance than that of aglycone. Particularly, we suggested that the compounds **7a-c** and **7e-f** had the greatest antibacterial action against all the bacterial strains. Only, compound **7d** had low antibacterial action against all microorganisms tested. Similarly, antifungal activity data demonstrated that the glycosides had promising antifungal properties against two yeast strains (*C. albicans* and *A. niger*), except for compound **7d**, which showed the maximum activity against *C. albicans* but low activity against *A. niger*.

CONFLICT OF INTEREST

The authors declare that there is no conflict of interests regarding the publication of this article.

REFERENCES

1. S.K. Bharti, G. Nath, R. Tilak and S.K. Singh, *Eur. J. Med. Chem.*, **45**, 651 (2010); https://doi.org/10.1016/j.ejmech.2009.11.008
2. B.V. Yang, D.S. Weinstein, L.W. Doweyko, H. Gong, W. Vaccaro, T. Huynh, H. Xiao, A.M. Doweyko, L. Mckay, D.A. Holloway, J.E. Somerville, S. Habte, M. Cunningham, M. McMahon, R. Townsend, D. Shuster, J.H. Dodd, S.G. Nadler and J.C. Barrish, *J. Med. Chem.*, **53**, 8241 (2010); https://doi.org/10.1021/jm100957a
3. F.C. Spector, L. Liang, H. Giordano, M. Sivaraja and M.G. Peterson, *J. Virol.*, **72**, 6979 (1998); https://doi.org/10.1128/JVI.72.9.6979-6987.1998
4. D. González Cabrera, F. Douelle, T.S. Feng, A.T. Nchinda, Y. Younis, K.L. White, Q. Wu, E. Ryan, J.N. Burrows, D. Waterson, M.J. Witty, S. Wittlin, S.A. Charman and K. Chibale, *J. Med. Chem.*, **54**, 7713 (2011); https://doi.org/10.1021/jm201108k
5. F.W. Bell, A.S. Cantrell, M. Hoegberg, S.R. Jaskunas, N.G. Johansson, C.L. Jordan, M.D. Kinnick, P. Lind and J.M. Morin, *J. Med. Chem.*, **38**, 4929 (1995); https://doi.org/10.1021/jm00025a010

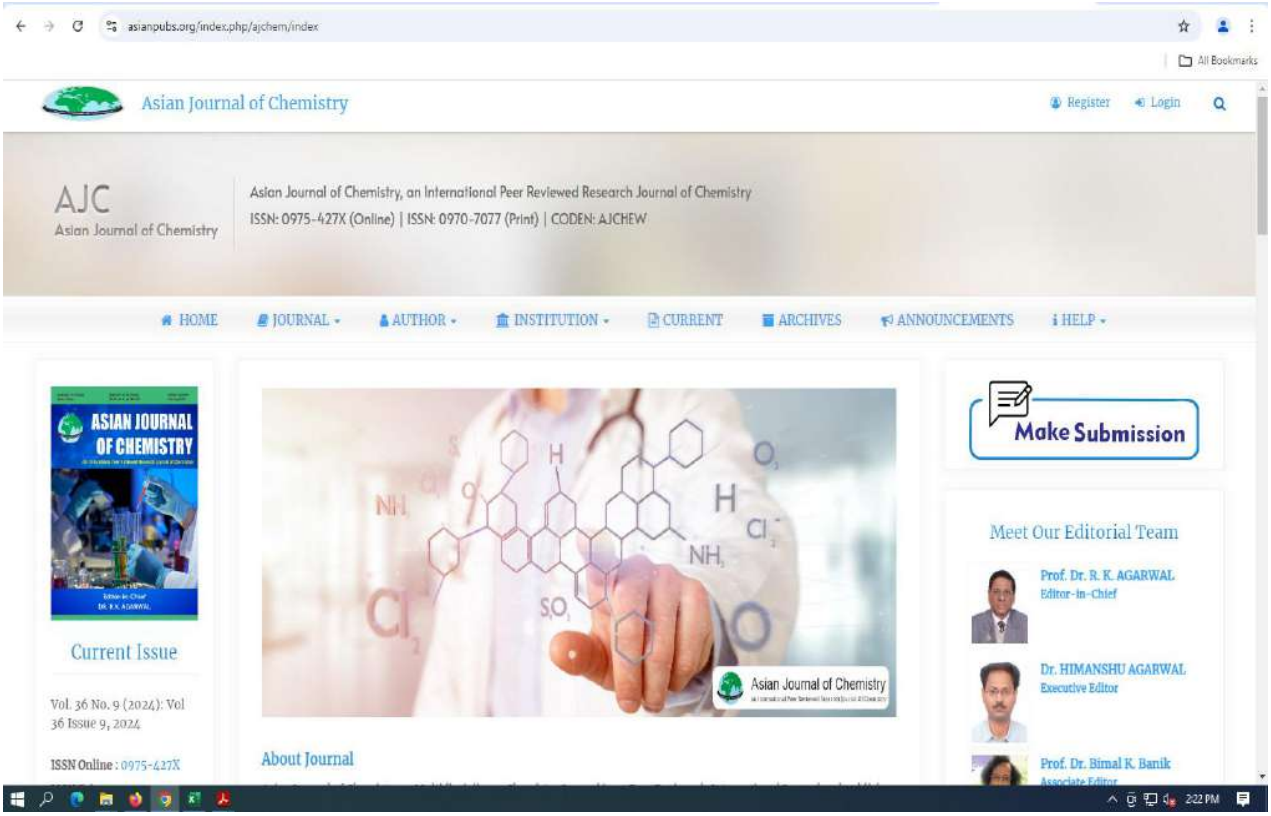
TABLE-1
ANTIMICROBIAL SCREENING RESULTS OF THE SYNTHESIZED THIAZOLE DERIVATIVES BEARING IMIDAZOLE MOIETY (**4a,b**), SCHIFF BASES (**5a-j**) AND THEIR O-GLUCOSIDES (**7a-j**)

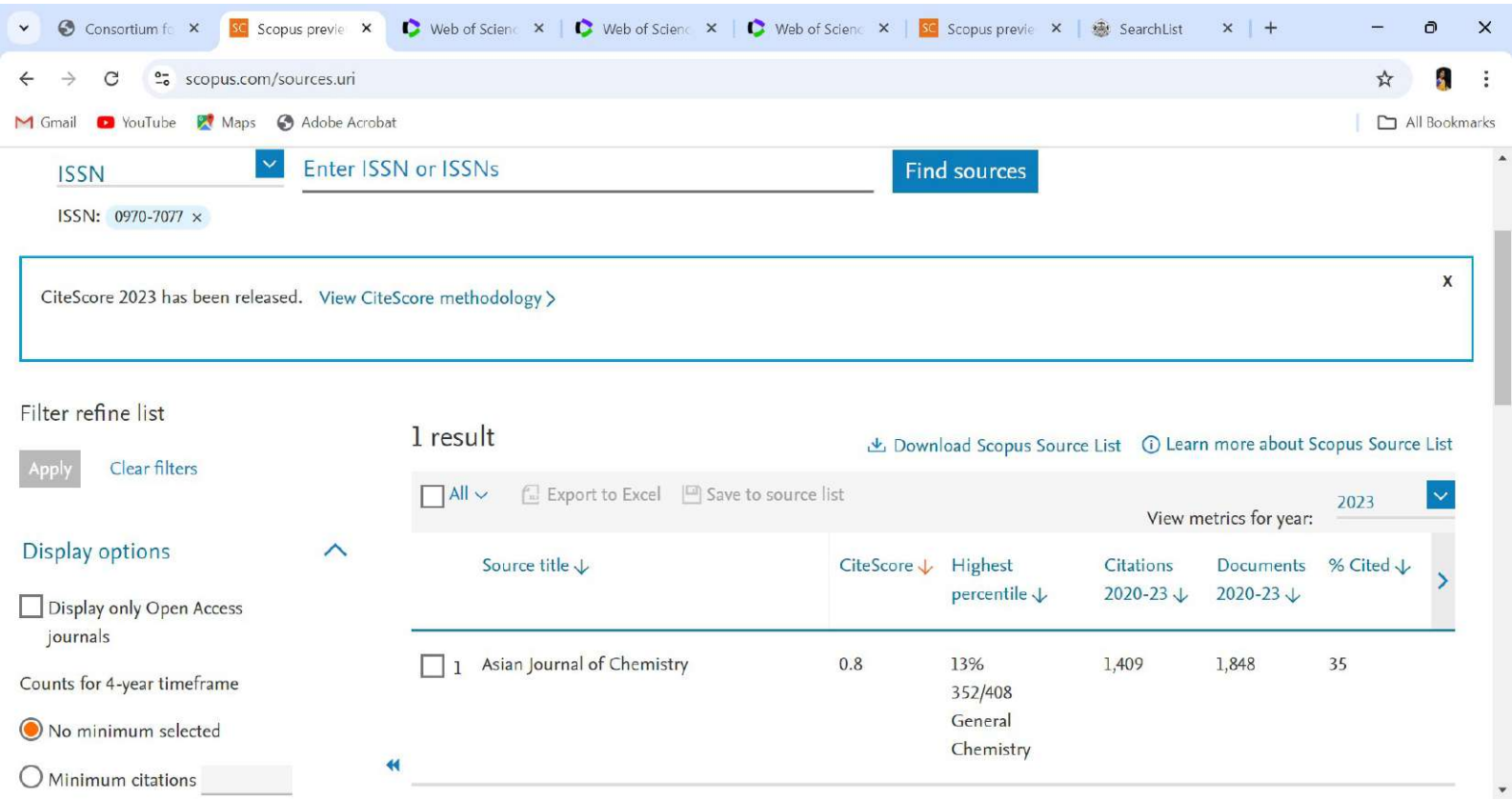
Compound No.[a]	Zone of inhibition (mm) (Activity index) std					
	Antibacterial activity				Antifungal activity	
	Gram-positive		Gram-negative			
	S. aureus	*B. substilis*	*E. coli*	*K. aerogens*	*C. albicans*	*A. niger*
3a	17 (0.53)* (0.56)#	16 (0.57)* (0.61)#	24 (0.70)* (0.85)#	08 (0.36)* (0.38)#	20 (0.95)* (0.90)#	15 (0.62)* (0.65)#
4a	20 (0.62)* (0.66)#	21 (0.75)* (0.80)#	27 (0.79)* (0.96)#	15 (0.68)* (0.71)#	21 (1.00)* (0.95)#	16 (0.66)* (0.69)#
4b	22 (0.68)* (0.73)#	23 (0.82)* (0.88)#	26 (0.76)* (0.92)#	15 (0.56)* (0.57)#	20 (0.95)* (0.90)#	14 (0.58)* (0.60)#
5a	21 (0.65)* (0.70)#	22 (0.78)* (0.84)#	27 (0.79)* (0.96)#	16 (0.72)* (0.76)#	21 (1.00)* (0.95)#	15 (0.62)* (0.65)#
5b	25 (0.78)* (0.83)#	23 (0.82)* (0.88)#	19 (0.55)* (0.67)#	17 (0.77)* (0.81)#	16 (0.76)* (0.72)#	21 (0.87)* (0.91)#
5c	24 (0.75)* (0.80)#	23 (0.82)* (0.88)#	18 (0.52)* (0.64)#	18 (0.82)* (0.86)#	19 (0.91)* (0.86)#	19 (0.79)* (0.83)#
5d	23 (0.71)* (0.76)#	21 (0.75)* (0.80)#	19 (0.56)* (0.68)#	19 (0.86)* (0.90)#	18 (0.86)* (0.82)#	18 (0.75)* (0.78)#
5e	22 (0.68)* (0.73)#	21 (0.75)* (0.80)#	17 (0.50)* (0.60)#	18 (0.82)* (0.86)#	17 (0.80)* (0.77)#	19 (0.79)* (0.83)#
5f	25 (0.78)* (0.83)#	23 (0.82)* (0.88)#	24 (0.70)* (0.86)#	19 (0.86)* (0.90)#	21 (1.00)* (0.95)#	20 (0.83)* (0.86)#
5g	23 (0.71)* (0.76)#	22 (0.78)* (0.84)#	26 (0.76)* (0.93)#	16 (0.72)* (0.76)#	18 (0.86)* (0.82)#	16 (0.66)* (0.69)#
5h	20 (0.62)* (0.66)#	19 (0.67)* (0.73)#	20 (0.58)* (0.71)#	16 (0.72)* (0.76)#	16 (0.76)* (0.72)#	19 (0.79)* (0.83)#
5i	25 (0.78)* (0.83)#	20 (0.71)* (0.76)#	22 (0.64)* (0.78)#	19 (0.86)* (0.90)#	20 (0.95)* (0.90)#	22 (0.91)* (0.95)#
5j	30 (0.93)* (1.00)#	24 (0.85)* (0.92)#	24 (0.85)* (0.92)#	17 (0.77)* (0.80)#	18 (0.86)* (0.82)#	21 (0.87)* (0.91)#
7a	25 (0.78)* (0.83)#	24 (0.86)* (0.92)#	22 (0.65)* (0.79)#	19 (0.86)* (0.90)#	20 (0.95)* (0.91)#	22 (0.92)* (0.96)#
7b	27 (0.84)* (0.90)#	22 (0.79)* (0.85)#	23 (0.68)* (0.82)#	20 (0.91)* (0.95)#	23 (1.09)* (1.04)#	18 (0.75)* (0.78)#
7c	28 (0.87)* (0.93)#	21 (0.75)* (0.80)#	24 (0.71)* (0.86)#	18 (0.82)* (0.86)#	22 (1.04)* (1.00)#	19 (0.79)* (0.83)#
7d	26 (0.81)* (0.87)#	23 (0.82)* (0.88)#	23 (0.68)* (0.82)#	18 (0.82)* (0.86)#	21 (1.00)* (0.95)#	16 (0.67)* (0.70)#
7e	25 (0.78)* (0.83)#	24 (0.86)* (0.92)#	21 (0.62)* (0.75)#	19 (0.86)* (0.90)#	24 (1.14)* (1.09)#	18 (0.75)* (0.78)#
7f	32 (1.00)* (1.06)#	27 (0.96)* (1.04)#	25 (0.74)* (0.89)#	19 (0.86)* (0.90)#	22(1.04)* (1.00)#	20 (0.83)* (0.87)#
7g	27 (0.84)* (0.83)#	23 (0.82)* (0.88)#	27 (0.79)* (0.97)#	21 (0.95)* (1.00)#	20 (0.95)* (0.91)#	19 (0.79)* (0.83)#
7h	29 (0.91)* (0.97)#	21 (0.75)* (0.80)#	23 (0.67)* (0.82)#	18 (0.81)* (0.85)#	25 (1.19)* (1.14)#	21 (0.87)* (0.91)#
7i	27 (0.84)* (0.90)#	20 (0.71)* (0.77)#	22 (0.64)* (0.78)#	18 (0.82)* (0.86)#	19 (0.91)* (0.86)#	18 (0.75)* (0.78)#
7j	26 (0.81)* (0.87)#	28 (1.00)* (1.07)#	23 (0.68)* (0.82)#	20 (0.91)* (0.95)#	23 (1.09)* (1.04)#	19 (0.79)* (0.83)#
Std. 1	32	28	34	22	21	24
Std. 2	30	26	28	21	22	23

[a]Concentration of test compounds and standard 100 µg/mL, [b]Average zone of inhibition (mm). (Activity index) = Inhibition zone of the sample/inhibition zone of the standard, *Activity index against Std. 1, #Activity index against Std. 2; For antibacterial activity: Std. 1 = Ciprofloxacin and Std. 2 = Sulphacetamide, For antifungal activity: Std. 1 = Gentamycin and Std. 2 = Clotrimazole

6. B.E. Fink, D.S. Mortensen, S.R. Stauffer, J.A. Katzenellenbogen and Z.D. Aron, *Chem. Biol.*, **6**, 205 (1999); https://doi.org/10.1016/S1074-5521(99)80037-4
7. M. Biagetti, C.P. Leslie, A. Mazzali, C. Seri, D.A. Pizzi, J. Bentley, T. Genski, R.D. Fabio, L. Zonzini and L. Caberlotto, *Bioorg. Med. Chem. Lett.*, **20**, 4741 (2010); https://doi.org/10.1016/j.bmcl.2010.06.140
8. E.W. van Tilburg, P.A.M. van der Klein, M. de Groote, M.W. Beukers and A.P. IJzerman, *Bioorg. Med. Chem. Lett.*, **11**, 2017 (2001); https://doi.org/10.1016/S0960-894X(01)00356-0
9. U. Bhoga, *Eur. J. Med. Chem.*, **42**, 1144 (2007); https://doi.org/10.1016/j.ejmech.2007.01.016
10. K.J. Wilson, C.R. Illig, N. Subasinghe, J.B. Hoffman, M.J. Rudolph, R. Soll, C.J. Molloy, R. Bone, D. Green, T. Randall, F.A. Lewandowski, M. Zhang, Z. Zhou, C. Sharp, D. Maguire, B. Grasberger, R.L. DesJarlais and J. Spurlino, *Bioorg. Med. Chem. Lett.*, **11**, 915 (2001); https://doi.org/10.1016/S0960-894X(01)00102-0
11. W.-T. Zhang, J.-L. Ruan, P.-F. Wu, F.-C. Jiang, L.-N. Zhang, W. Fang, X.-L. Chen, Y. Wang, B.-S. Cao, G.-Y. Chen, Y.-J. Zhu, J. Gu and J.-G. Chen, *J. Med. Chem.*, **52**, 718 (2009); https://doi.org/10.1021/jm800902t
12. R. Siddiqui, S. Akhter, Z.S. Saify, S. Haider, M. Ali and T.Z. Mallick, *Pak. J. Pharm. Sci.*, **32**, 2033 (2019).
13. J.S. Carter, S. Kramer, J.J. Talley, T. Penning, P. Collins, M.J. Graneto, K. Seibert, C.M. Koboldt, J. Masferrer and B. Zweifel, *Bioorg. Med. Chem. Lett.*, **9**, 1171 (1999); https://doi.org/10.1016/S0960-894X(99)00157-2
14. A. Badorc, M.-F. Bordes, P. de Cointet, P. Savi, A. Bernat, A. Lalé, M. Petitou, J.-P. Maffrand and J.-M. Herbert, *J. Med. Chem.*, **40**, 3393 (1997); https://doi.org/10.1021/jm970240y
15. J. Rudolph, H. Theis, R. Hanke, R. Endermann, L. Johannsen and F.U. Geschke, *J. Med. Chem.*, **44**, 619 (2001); https://doi.org/10.1021/jm0010623
16. H.M. Alkahtani, A.Y. Abbas and S. Wang, *Bioorg. Med. Chem. Lett.*, **22**, 1317 (2012); https://doi.org/10.1016/j.bmcl.2011.12.088
17. L. Zhang, X.-M. Peng, G.L.V. Damu, R.-X. Geng and C.-H. Zhou, *Med. Res. Rev.*, **34**, 340 (2014); https://doi.org/10.1002/med.21290
18. J.G. Lombardino and E.H. Wiseman, *J. Med. Chem.*, **17**, 1182 (1974); https://doi.org/10.1021/jm00257a011
19. S. Sondhi, S. Jain, M. Dinodia and A. Kumar, *Med. Chem.*, **4**, 146 (2008); https://doi.org/10.2174/157340608783789194
20. A.M. Ghatole, K.R. Lanjewar, M.K. Gaidhane and K.M. Hatzade, *Spectrochim. Acta A Mol. Biomol. Spectrosc.*, **151**, 515 (2015); https://doi.org/10.1016/j.saa.2015.06.035
21. K. Wittine, M. Stipkovic-Babic, D. Makuc, J. Plavec, M. Sedic, S. Kraljevic-Pavelic, K. Pavelic, P. Leyssen, J. Neyts, J. Balzarini and M. Mintas, *Bioorg. Med. Chem.*, **20**, 3675 (2012); https://doi.org/10.1016/j.bmc.2012.01.054
22. X. Zhang, M. Urbanski, M. Patel, R.E. Zeck, G.G. Cox, H. Bian, B.R. Conway, M. Pat Beavers, P.J. Rybczynski and K.T. Demarest, *Bioorg. Med. Chem. Lett.*, **15**, 5202 (2005); https://doi.org/10.1016/j.bmcl.2005.08.067
23. P. Smith, L. Brown, J. Boutagy and R. Thomas, *J. Med. Chem.*, **25**, 1222 (1982); https://doi.org/10.1021/jm00352a025
24. W. Koenigs and E. Knorr, *Chem. Ber.*, **34**, 957 (1901); https://doi.org/10.1002/cber.190103401162

25. Y.L. Garazd, M.M. Garazd and V.P. Khilya, *Chem. Nat. Compd.*, **40**, 6 (2004); https://doi.org/10.1023/B:CONC.0000025455.68950.36
26. R.M. Silverstein and F.X. Webster, Spectroscopic Identification of Organic Compound, John Wiley and Sons Inc.: New York, Edn.: 6, p. 482 (1998).
27. A. T'ang, E.J. Lien and M.M.C. Lai, *J. Med. Chem.*, **28**, 1103 (1985); https://doi.org/10.1021/jm00146a022
28. H.M. Dalloul, N.S. Al-Abadla and K.A. El-Nwairy, *Chem. Heterocycl. Compd.*, **43**, 314 (2007); https://doi.org/10.1007/s10593-007-0047-4
29. A.M. Ghatole, K.R. Lanjewar and M.K. Gaidhane, *World J. Pharm. Res.*, **3**, 4336 (2014).
30. A.M. Ghatole, K.R. Lanjewar and M.K. Gaidhane, *J. Pharm. Res.*, **5**, 2758 (2012).
31. N.J. Thumar and M.P. Patel, *Phosphorus Sulfur Silicon Rel. Elem.*, **184**, 2720 (2009); https://doi.org/10.1080/10426500802583520
32. K.M. Hatzade, J. Sheikh, V.S. Taile, A.M. Ghatole, V. Ingle, M. Genc, S. Lahsasni and T. Ben Hadda, *Med. Chem. Res.*, **24**, 2679 (2015); https://doi.org/10.1007/s00044-015-1326-8
33. Z. Hussain, E. Yousif, A. Ahmed and A. Altaie, *Org. Med. Chem. Lett.*, **4**, 1 (2014); https://doi.org/10.1186/2191-2858-4-1


asianpubs.org/index.php/ajchem/index
All Bookmarks
Asian Journal of Chemistry
Register
Login
AJC
Asian Journal of Chemistry
Asian Journal of Chemistry, an International Peer Reviewed Research Journal of Chemistry
ISSN: 0975-427X (Online) | ISSN: 0970-7077 (Print) | CODEN: AJCHEW
HOME
JOURNAL
AUTHOR
INSTITUTION
CURRENT
ARCHIVES
ANNOUNCEMENTS
HELP
ASIAN JOURNAL OF CHEMISTRY
Current Issue
Vol. 36 No. 9 (2024): Vol 36 Issue 9, 2024
ISSN Online : 0975-427X
Asian Journal of Chemistry
About Journal
Make Submission
Meet Our Editorial Team
Prof. Dr. R. K. AGARWAL
Editor-in-Chief
Dr. HIMANSHU AGARWAL
Executive Editor
Prof. Dr. Bimal K. Banik
2:22 PM


scopus.com/sources.uri
ISSN
Enter ISSN or ISSNs
Find sources
ISSN: 0970-7077
CiteScore 2023 has been released. View CiteScore methodology >
Filter refine list
Apply
Clear filters
Display options
Display only Open Access journals
Counts for 4-year timeframe
No minimum selected
Minimum citations
1 result
Download Scopus Source List
Learn more about Scopus Source List
All
Export to Excel
Save to source list
View metrics for year:
2023
Source title
CiteScore
Highest percentile
Citations 2020-23
Documents 2020-23
% Cited
1 Asian Journal of Chemistry 0.8 13% 352/408 General Chemistry 1,409 1,848 35

IJFANS INTERNATIONAL JOURNAL OF FOOD AND NUTRITIONAL SCIENCES
ISSN PRINT 2319 1775 Online 2320 7876

Research paper © 2012 IJFANS. All Rights Reserved, UGC CARE Listed (Group -I) Journal Volume 11, Iss 12, Dec 2022

ANALYSIS OF WATER QUALITY USING PHYSICO-CHEMICAL PARAMETERS OF CHULHARDOH LAKE IN TUMSAR TALUKA, BHANDARA DISTRICT, MAHARASHTRA, INDIA

Bhageshwari Arvind Thakre[1] , Sayeda Parveen Qureshi[2]

[1]Department of Botany R.T.M. Nagpur University Nagpur 440033 (M.S.) India

[2]P.G.Department of Botany J. M. Patel College Bhandara 441906 (M.S.) India

Corresponding author - **Bhageshwari Arvind Thakre**

Email: - bhageshwarithakre24@gmail.com

Abstract: - This paper present to study of the Physico-Chemical parameter of Chulhardoh Lake in Tumsar Taluka in Bhandara District Maharashtra. Monthly variation in Physico-Chemical Parameters. The Physical included Temperature, pH, Turbidity and Chemical Includes, Alkalinity, Hardness, Chloride, Phosphate. We Analyzed for Period of Pre Monsoon(April-May) Monsoon (July-August) Post Monson (Oct-Nov) in year 2022.All the Physico-Chemical Parameter for Pre Monsoon, and Post Monsoon, Season are with the maximum permissible limit. The result included the Lake is Non-Polluted and it can be used for Domestic and Irrigation Purpose.

Keyword: - ***Chulhardoh Lake, Physico - Chemical Parameter, Permissible limits, Irrigation Purpose.***

Introduction:

Water is wonder of nature. Water was useful to the people for drinking, cleaning animals and for Agriculture, plantation. " No life without water " is a common Saying depending upon the fact that water is the one of the life supporting activities. Water is most Important Component to the Ecosystem better Quality of water described by its Physical Chemical and Biological Characteristics (Muley, 2010). It is a fact that good water quality produces healthier human than one with poor Water Quality (Patil Shilpa G., 2012).Water is known to contain large number of Chemical elements, the interaction of Physical and chemical properties of water play Significant role in Composition , distribution and Abundance of aquatic community . (Sharma Riddhi, 2011)) In Todays Scenario, Unplanned urbanization, rapid industrialization, and indiscriminate use of chemicals are causing a heavy and varied pollution in aquatic environment leading to deterioration of water quality and depletion of aquatic fauna ((R.V. Bhagde, 2020). Water plays essential role in human life and its elements composition is important to life process as it provide all the essential nutrients to Organism. Water is natural resources and a basic human need .Water play essential role in human life. Although statistics, the WHO Report that approximately 36%of urban and 65% of rural

Research paper © 2012 IJFANS. All Rights Reserved, UGC CARE Listed (Group -I) Journal Volume 11, Iss 12, Dec 2022

Indians were without access to safe drinking water. (Undi Sai Nagendra Prasadu, 2020) The present work is carried out in vicinity of Tumsar area in Bhandara district in order to study the water quality. Tumsar Taluka is situated on North – Eastern Side of Maharashrta State and share the state border of Madhya Pradesh adjoining districts are Gondia on eastern side , on Northern side Bhalaghat district of Madhya Pradesh on western side Nagpur district. Tumsar it is Famous for lake.





Latitude and longitude 21.472356°-79.8175928° **Site for collection of water sample**

Fig:1 Satellite image of Chulhardoh lake with study site Latitude and longitude

Material Method:

Study area and its characteristics Chulhardoh Lake is the fresh water body in Tumsar Taluka built (Figure 1) for domestic and agricultural uses. During the rainy periods, fresh water also enters the lake as runoff.

Sampling and Analysis of water

The water samples were collected main Chulhardoh Lake in plastic bottles as possible to avoid unpredictable changes. Samples were collected from four different places (S1,S2,S3,S4.) from the Chulhardoh Lake .About 4 Water samples were collected in pre- Monsoon and post-monsoon seasons from selected side on lake. Sample was collected between 9.AM.- 11 AM From Sampling Site in pre –cleaned bottle,Sterilised Bottle Container of 1 lit. Capacity .Each side brought in Laboratory for analysis the Chemical Parameter. Water temp, Air temp, pH field, is recorded immediately on the spot. The parameter were analyzed by using standard procedure described in APHA (Rodger B.Baired, 2017)

The testing of samples was done according to the procedure prescribed by APHA. The water samples were collected and analyzed for different chemical, physical parameters and results were carefully studied and analyzed. The present study comprises of interpretation and analysis of water samples compare with the APHA recommended measurements. Various water quality parameters such

Research paper © 2012 IJFANS. All Rights Reserved, UGC CARE Listed (Group -I) Journal Volume 11, Iss 12, Dec 2022

Temperature, pH, Turbidity, Alkalinity, Hardness, Chloride, Phosphate were determined. Preservation, analysis, and interpretation are carried out in accordance APHA Method.

Results and Discussion

The water quality was analyzed by collecting samples from chulhardoh Lake. Sample S1 S2, S3, S4 was collected before and after the monsoon. The results obtained by the analysis of these samples are tabulated in table 2 and there comparison with the APHA and IS standards are tabulated in table1.

Temperature: The present study water temp was recorded 32ºC and 28ºC in pre and post respectively. The temperature is one of the important factors in aquatic environment since it regulate physic-chemicals well as biological activities (Rafiullah M.khan, 2012)

pH: The present Study pH range 6.8 to 7.10 in Both pre and post monsoon respectively . The values are found to be on the according to the APHA standards but and IS standards it will be permissible (A.R. Bhusari, 2014).

Turbidity: The turbidity recorded is 6.7 in pre monsoon and 6.8 in post monsoon. turbidity was higher which was because of rains bringing the sediment from the Adjoining areas.

Total Hardness

The hardness was found to be 68- 78.8 mg/L in pre –monsoon and 66. -76.8mg/L in post Monsoon it will be desirable limit of Hardness is 300 mg/L and it will be permissible.

Water hardness is usually due to the multivalent metal ions, which comes from minerals dissolved in the water Hardness in water is caused due to the presence of dissolved salts of calcium and magnesium. (U. G. Meshram, 2017) It was fluctuated between 68-70 mg/lit. range in pre monsoon and 76.8.mg/lit post monsoon.

Alkalinity

Alkalinity of water is described as the capacity of water to neutralize an acid. It is due to the presence of bicarbonates, carbonates and hydroxide ions in water. The alkalinity of the samples S_3 site maximum 95 and 80mg/L respectively which was found to be in post monsoon . Table2, Fig. 1 (Anima Upadhyay, 2015)

Chloride: The chloride concentration was used as an important parameter for the detection of contamination by sewage. In the present study the chloride was not found. People accustomed to higher chloride in water are subjected to laxative effects (Shahare, 2015)

Research paper © 2012 IJFANS. All Rights Reserved, UGC CARE Listed (Group -I) Journal Volume 11, Iss 12, Dec 2022

Phosphate: : In present study the value obtained were range 0.020-0.028 mg/L in pre-monsoon and 0.019-0.0.031mg/L in post-monsoon. According to IS phosphate is content in sample is less than permissible limit .Phosphates enter waterways from human and animal waste, phosphorus rich bedrock, laundry, cleaning, industrial effluents, and fertilizer runoff. (Bheemappa1, 2015)

Table 1 Water Quality Parameters and their ISI and APHA Standards

Sr. No	Parameters	IS10500-2012, APHA 2005,
1	Air Temp.(^{o}C)	---
2	Water Temp(^{o}C)	---
3	Total Hardness (mg/L)	300
4	Total Alkalinity (mg/L)	200
5	Turbidity(mg/L)	10
6	Phosphate(mg/L)	5
7	Chloride(mg/L)	600
8	pH	6.5 - 8.5

Table II

Pre- monsoon and Post monsoon variation in the physic-chemical parameter of lake.

S1, S2, S3, S4, Samples Collected From Chulhardoh lake

Sr. No.	Season	Parameter							
Site		Air Temp.	Water Temp.	Alkalinity	Hardness	Phosphate	pH	Turbidity	Chloride
S1	Pre (April-May)	32^{o}C	30^{o}C	90	68	0.025	6.76	7.10	Neg.
	Post. (Oct-Nov)	28^{o}C	28^{o}C	85	66	0.019	6.41	8	Neg.
S2	Pre (April-May)	32^{o}C	30^{o}C	95	70	0.020	7.20	6.90	Neg.
	Post. (Oct-Nov)	28^{o}C	28^{o}C	90	65	0.018	6.21	6.50	Neg.
S3	Pre (April-May)	32^{o}C	30^{o}C	90	78	0.025	7.10	6.80	Neg.
	Post. (Oct-Nov)	28^{o}C	28^{o}C	95	76.8	0.029	6,08	4.00	Neg.
S4	Pre (April-May)	32^{o}C	30^{o}C	92	68	0.028	6.80	6.70	Neg.
	Post. (Oct-Nov)	28^{o}C	28^{o}C	85	64	0.031	6.38	4.00	Neg.

Research paper © 2012 IJFANS. All Rights Reserved, UGC CARE Listed (Group -I) Journal Volume 11, Iss 12, Dec 2022

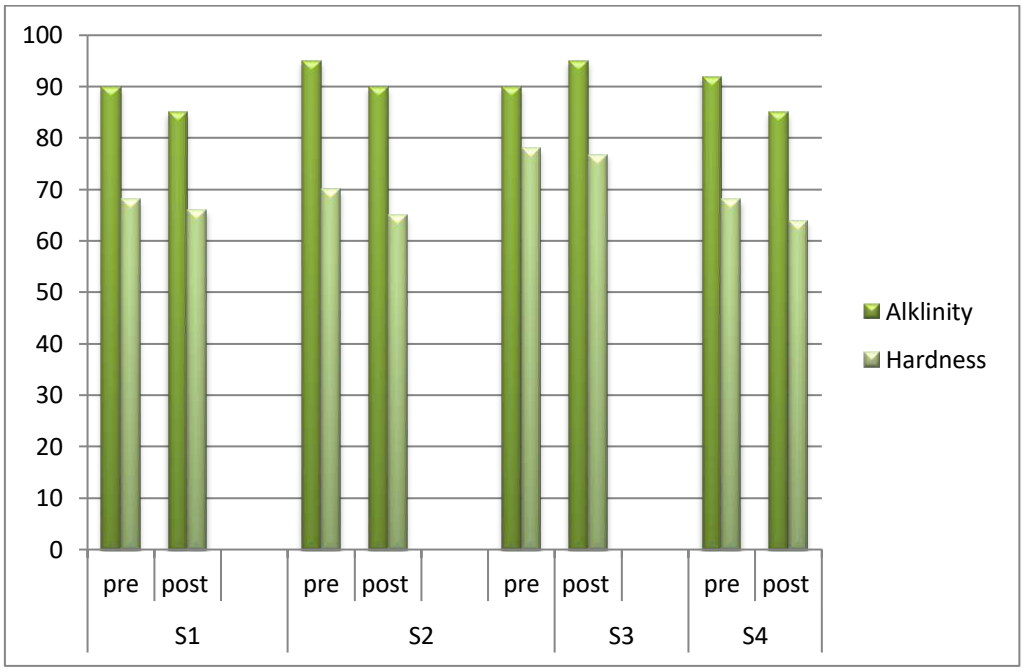


Fig2: Graph Showing Pre. and post Monsoon Variation in Alkalinity and Hardness

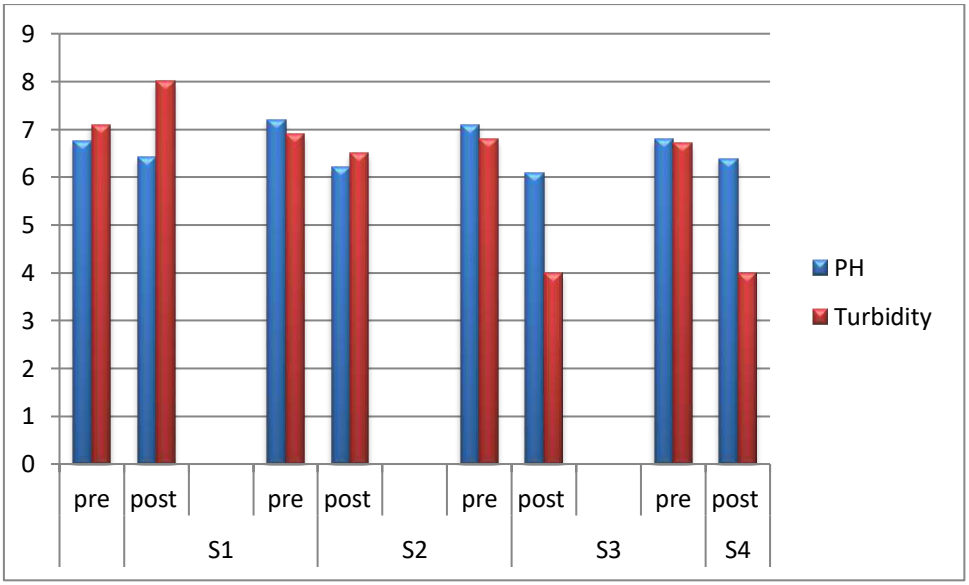


Fig3: Graph Showing Pre. and post Monsoon Variation in pH and Turbidity.

Conclusion:

The present study is Concluded that there the concentration of the investigated major ion like chloride, pH in a lake of different 4 site are within permissible limit .The present study shows that the Chulhardoh lake analysis result revealed that there was significant seasonal variation in some physicochemical parameters and most of the parameters were in the normal range and indicates better quality of water. The result indicates that the chulhardoh lake water is

Research paper © 2012 IJFANS. All Rights Reserved, UGC CARE Listed (Group -I) Journal Volume 11, Iss 12, Dec 2022

non-polluted and can be used for Domestic and Irrigation and Purposes. All the parameter is in a permissible limit.

References:

(1) A.R. Bhusari, M. R. (2014). QUALITY ASSESMENT OF WATER :A CASE STUDY OF TUMSAR AREA IN BHANDARA DISTRICT. *International Journal of Research in Bioscience , Agriculture and Technology* , 141-148.

(2) Anima Upadhyay, M. C. (2015). Pre- and Post-monsoon Study of PhysicoChemical Parameters of Ulsoor Lake Water of. *International Journal of Innovative Research in Science,,* : 2319 - 8753.

(3) Bheemappa1, K. (2015). Temporal Variation in Water Quality Parameters of Bandematta Hosakere Lake – Peri. *INTERNATIONAL JOURNALOF ADVANCED RESEARCH*, 1283-1291.

(4) Muley, S. M. (2010). ANALYSIS OF WATER QUALITY USING PHYSICO-CHEMICAL PARAMETERS TAMDALGE TANK IN KOLHAPUR DISTRICT MAHARASHTRA . *International journal of Advanceed Biotechnology and Research* , 115-119.

(5) Patil Shilpa G., C. S. (2012). Impact of Physicochemical Characterstics of shivaji university Lakes on on Phytoplankton Communities Kolhapur india . *Research Journal of Recent Sciences*, 56-60.

(6) R.V. Bhagde, S. P. (2020). A COMPARATIVE STUDY OF PHYSICO- CHEMICAL PARAMETERS OF THE FRESHWATER PONDS FROM SANGAMNER TALUKA OF AHMADNAGAR , MAHARASHTRA, INDIA . *International Journal of Biological Innovation*, 137-142.

(7) Rafiullah M.khan, M. J. (2012). PHYSICO-CHEMICAL ANALYSIS OF TRIVENI LAKE WATER OF AMRAVATI DISTRICT IN (MS) INDIA . *Bioscience Discovery* , 64-66.

(8) Rodger B.Baired, A. D. (2017). *Standaed methods for Examination of Water and Waste Water 23rd Edition.* American Public Heaith Association ,Street , NW Washington, DC 20001-3710.

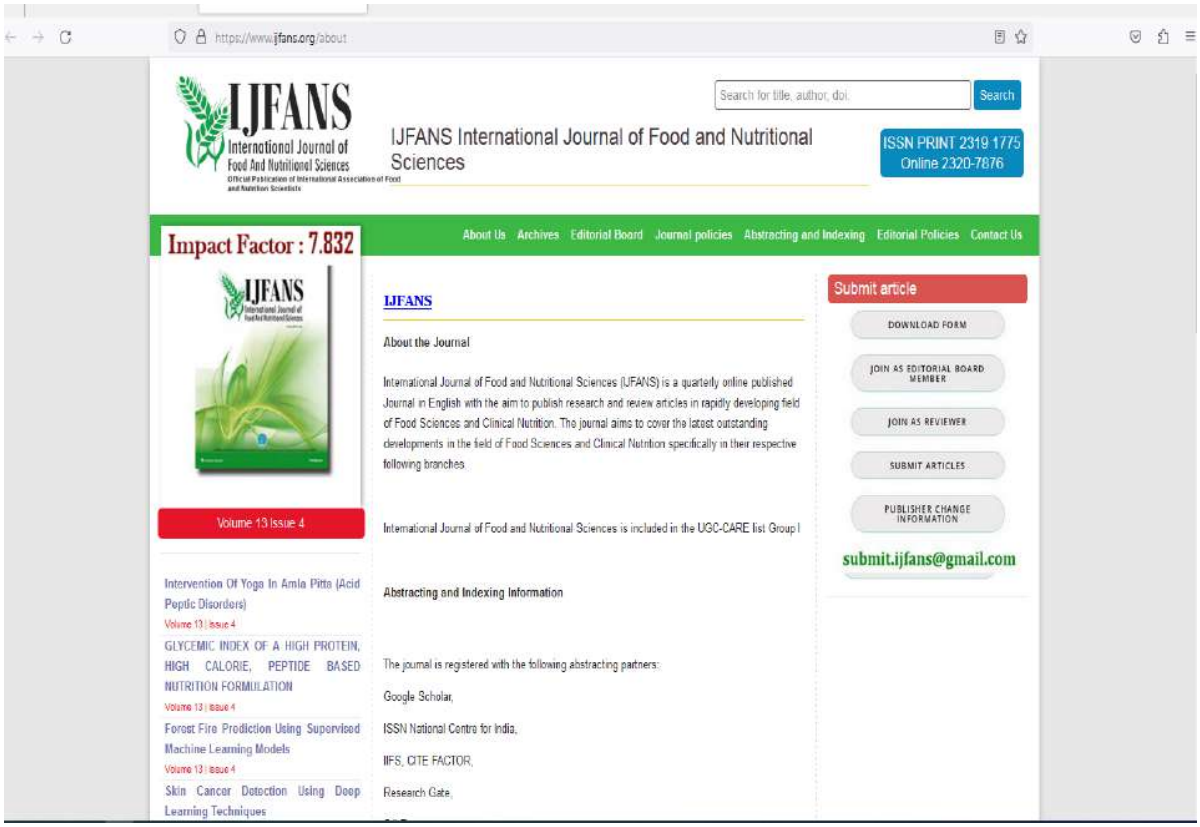
(9) Shahare, P. C. (2015). Assessment of Physico-Chemical parameters of Chulband dam in. *INTERNATIONAL JOURNAL OF RESEARCHES IN BIOSCIENCES, AGRICULTURE AND TECHNOLOGY*, 2347 – 517X.

(10) Sharma Riddhi, S. V. (2011). Studies on limnlogical Characteristic, Planktonic Diversity and Fishes (Species) in Lake Pichhola, Udaipur, Rajasthan(india). *Universal Journal of Envirnomental Reseach and Technology* , 274-285.

(11) U. G. Meshram, R. B. (2017). Study on physico-chemical parameters of kurhada Lake at Pauni, Bhandara District Mharashtra. *INTERNATIONAL JOURNAL OF RESEARCH IN BIOSCIENCE AGRICULTURE AND TECHNOLOGY*, 899-904.

(12) Undi Sai Nagendra Prasadu, G. U. (2020). pre and Post- Monsoon Variations in physico Chemical analysis of Ground water of Rural Area in East Godavari District, Andhra Pradesh ,India . *Journal of Research in Applied Chemistry* , 39-49.




https://www.ijfans.org/about
IJFANS
International Journal of Food And Nutritional Sciences
Official Publication of International Association of Food and Nutrition Scientists
Search for title, author, doi
Search
IJFANS International Journal of Food and Nutritional Sciences
ISSN PRINT 2319 1775
Online 2320-7876
Impact Factor : 7.832
About Us
Archives
Editorial Board
Journal policies
Abstracting and Indexing
Editorial Policies
Contact Us
Volume 13 Issue 4
Intervention Of Yoga In Amla Pitta (Acid Peptic Disorders)
Volume 13 | Issue 4
GLYCEMIC INDEX OF A HIGH PROTEIN, HIGH CALORIE, PEPTIDE BASED NUTRITION FORMULATION
Volume 13 | Issue 4
Forest Fire Prediction Using Supervised Machine Learning Models
Volume 13 | Issue 4
Skin Cancer Detection Using Deep Learning Techniques
IJFANS
About the Journal
International Journal of Food and Nutritional Sciences (IJFANS) is a quarterly online published Journal in English with the aim to publish research and review articles in rapidly developing field of Food Sciences and Clinical Nutrition. The journal aims to cover the latest outstanding developments in the field of Food Sciences and Clinical Nutrition specifically in their respective following branches.
International Journal of Food and Nutritional Sciences is included in the UGC-CARE list Group I
Abstracting and Indexing Information
The journal is registered with the following abstracting partners:
Google Scholar,
ISSN National Centre for India,
IIFS, ICTE FACTOR,
Research Gate,
Submit article
DOWNLOAD FORM
JOIN AS EDITORIAL BOARD MEMBER
JOIN AS REVIEWER
SUBMIT ARTICLES
PUBLISHER CHANGE INFORMATION
submit.ijfans@gmail.com

UGC-CARE List

You searched for "**2320-7876"**. Total Journals : **1**

Search:

Sr.No.	Journal Title	Publisher	ISSN	E-ISSN	UGC-CARE coverage years	Details
1	International Journal of Food and Nutritional Sciences	Global E smart Technologies	2319-1775	2320-7876	from January-2021 to January- 2023	Discontinued from Jan 2023

Showing 1 to 1 of 1 entries

Previous 1 Next

Copyright © 2024 Savitribai Phule Pune University. All rights reserved. | Disclaimer

ISSN PRINT 2319 1775 Online 2320 7876

Research paper © 2012 IJFANS. All Rights Reserved, UGC CARE Listed (Group -I) Journal Volume 11, Iss 11, Dec 2022

INVESTIGATION ON ENDANGERED NUTRITIONAL MEDICINAL VALUE PLANTS OF BHANDARA DISTRICT AND THEIR CONSERVATION.

Dr. Sayeda Parveen Qureshi

P.G. Department of Botany ,J. M. Patel College Bhandara (M.S.)
Email-drsdprvnqureshi17@gmail.com

Abstract
The present report has been conducted in Bhandara District ,of Maharashtra . Bhandara is well known for its natural diverse Flora and Fauna .Bhandara covered the area about 3,717 square kilometre .The natural vegetation of this District includes the most of the plant species of medicinal and nutritional importance, which were regularly being used by the tribal peoples to cure various diseases and for nutritional objectives .The paper includes important nutritional medicinal plants, which is under endangered and threatened categories.

Key Words- Flora , Nutritional ,Medicinal ,Endangered ,Threatened.

Introduction

In the present study, we choose some plants currently used in the folk medicine in our region, small rural place in Bhandara, a rich fauna and a good source of medicinal plants. Bhandara , the district of lakes and also called as the 'rice bowl of Maharashtra' is situated in the Nagpur division (21.09 N latitude and 79.42 E longitude). It is surrounded by Balaghat district (Madhya Pradesh) in the North, Gondia in the East, Chandrapur in the South, and Nagpur in the West. The area is flat or undulating, broken by the isolated hillocks and ranges of low hills. The district is covered by Ambagad hills, Ballahi range and Pauni ranges. The forest is tropical dry deciduous type and consists of sub-types, teak forest and mixed forests. Gond people are quite aware of the uses of plant species having ethno botanical values .In the past few decades there has been an ever increasing global inclination towards herbal medicine, followed by a belated growth in International awareness about the dwinding supply of worlds medicinal plants (Bodekar 2002).The plants used in the Phyto pharmaceutical preprations are obtained mainly from the natural growing areas .The genetic diversity of medicinal plants pharmaceutical preprations are obtained mainly from the naturally growing areas .The genetic diversity of medicinal plants in the world is getting endangered at alarming rate because of ruinous harvesting practices and overharvesting for production of medicines, with little or no regard to the future .Also, extensive destruction of the plant rich habitat as a result of forest degradation ,agricultural encroachment ,urbanization etc. Is other factor ,thus challenging their existence (Gupta et al.1998).In view of the tremendously growing world population ,increasing anthropogenic activities rapidly eroding natural ecosystem , etc. The natural habitat for a great number of herbs and trees are dwindling and

of per captia consumption has resulted in unsustainable exploitation of earth's biological diversity exacerbated by climate change ,Ocean acidification , and other anthropogenic environmental impact (Rands et.al. 2010).The nutritionally rich medicinal plants and their value added product will overcome the weakness , malnutrition ,underweight and nutritional disorders in all age groups of person. The Seven threatened nutritionally rich medicinal plants and their conservation are given below

Materials and Method

A Survey of the area was conducted during 2021-22. The ethno botanical information was gathered from the various tribal communities of the Bhandara district. The valuable information was also collected from the tribal communities. The plant specimen is collected and preserved in the form of a herbarium. The herbarium specimens are deposited in the Botany Department, J.M.Patel Arts, Commerce and Science College, Bhandara. The identification and authentification were made with the help of flora and Subject experts.

Result-

This need not only to conserve threatened nutritional value medicinal plants but also used to be protected in terms to provide a sustainable source. The seven threatened plants studied were discussed in detail

1.*Rauvolfia Serpentina (L.)*

Common name- Sarpgandh

ISSN PRINT 2319 1775 Online 2320 7876

Research paper © 2012 IJFANS. All Rights Reserved, UGC CARE Listed (Group -I) Journal Volume 11, Iss 11, Dec 2022

Family-*Apocynaceae*

Sarpagandha are glabrous undershrub's, un-branched or with few branches, up to 1 m. high. Leaves are whorled, 3 at each node, simple, elliptic lanceolate, acuminate, entire; up to 17 cm. long and 5.5 cm. broad, dark green and shinning above, pale beneath; petiole up to 1 cm. long.Inflorescence a terminal umbelliform cyme, often appearing as lateral due to the growth of the shoot Flowers hermaphrodite, actinomarphic, short pedicelled, bracteate Calyx 5-fid, bright scarlet; segments 2 mm. long.Corolla salver-shaped, densely hairy inside, pink or rose; tube slender, slightly dilated at the middle, 1-1.5 cm. long; lobes 5; elliptic oblong, 3-4 mm. long, imbricate, stamens 5, inserted at the swollen portion of the corolla tube, included.Disc cup shaped, membranous; obscurely lobed. Carpels 2, connate; ovules 2 in each carpel, style filiform, stigma broad, calyptriform at base and 2-fid at the tip. Fruit a single drupe or didymous and connate, about 5 mm. in daim, purplish black when ripe.

Medicinal Uses of Sarpagandha: The root is purgative, anthelmintic, a sedative and hypotensive and is an antidote for snake and insect-bite; now mostly used in hypertension.The root contains many alkaloids the most important of which is reserpine which is a specific remedy in hypertension and certain neuro psychiatric disorders.

2 *Cissus quadrangularis*

Common name- Hadjod

Family- *Vitaceae*

Cissus quadrangularis belongs to the family *Vitaceae* . The *Cissus quadrangularis* tree grows up to a height of 1.5 m, with branches splitting into four parts or a quadrangular arrangement. The leaves are bright green, with sharp edges and three lobes. This plant bears white or jade flowers and red berries when ripened. All parts of *Cissus quadrangularis* are edible, with the stem and leaves being used traditionally for cooking and therapeutic purposes.

Medicinal uses of *Cissus quadrangularis*

Cissus quadrangularis portrays powerful traits in mending fractures of the bones as well as being an excellent natural remedy for flatulence, indigestion, weight loss,epilepsy and haemorrhoids

3.*Terminalia arjuna*

Common name-Arjuna

Family-*Combretaceae*

Terminalia arjuna, commonly Known as *Arjuna* belongs to the family of *Combretaceae Arjuna* tree is about 60-80 ft in height ,leaves are sub-opposite coriaceous ,oblong/elliptic, dull green from the upper side and pale brown on the lower side, often unequal sided with 10-15 pairs of nerves.The tree bears white sessile bisexsual flowers in short auxillary spikes or in a terminal panicle arrangement.Fruits of *Terminalia arjuna* are drupe,ovoid,fibrous-woody and smooth skinned with five hard wings or angles which are oblique and curved upwards.Stem bark is simple,smooth and pinkish grey in colour in external view.An internal view, the bark is soft and reddish in colour

Medicinal uses of *Terminalia arjuna*

The bark has been described as an astringent ,demulcent ,expectorant ,cardio tonic ,styptic antidy senteric ,urinary astringent ,and has shown to be useful in fracture ,ulcers ,leukorrheae diabetes , anemia ,cardiopathy ,and cirrhosis . Decotation of the bark has been used as ulcer wash, while bark ashes have been prescribed fot snakebite and scorpion sting. Fresh leaf juice is used for the treatment of ear ache

4. *Tinospora cordifolia*

Common name- Gulvel (Giloy)

Family : Menispermaceae

Tinospora cordifolia is a large, deciduous, extensively spreading and climbing shrub with several elongated twining branches. The dried aerial roots are light grey –brown or creamy white in colour, which arises from the mature branches. Stem of this plant is rather succulent with long, filiform, fleshy and climbing in nature. Leaves of this plant are membranous, simple, alternate, with long petiole approximately 15cmwhich is round, pulvinate, heart shaped, twisted partially and half way round .Leaves are seen in bulk intensely green in colour but over mature leaves are yellowish green to yellow colour. Leaves are bitter and have an indistinct odour. Lamina is ovatecordate, 10-20 cm long, 8-15cm broad . Flowers are small and unisexual which are greenish yellow in colour. Male flowers are clustered and female flowers exist in solitary. Fruits are fleshy and single seeded which are aggregates of one to three. These are drupelets on thick stalk with a sub terminal style scars .The shape of the fruit is ovoid with smooth texture and Scarlet or orange red in colour .

ISSN PRINT 2319 1775 Online 2320 7876

Research paper © 2012 IJFANS. All Rights Reserved, UGC CARE Listed (Group -I) Journal Volume 11, Iss 11, Dec 2022

Medicinal Uses of *Tinospora cordifolia*

Tinospora cordifolia is useful in the treatment of helminthiasis , heart diseases, leprosy rheumatoid arthritis, support the immune system, the body's resistance to infections, supports standard white blood cell structure, function and levels. It also helps in digestive aliments such as hyper acidity , colitis, worm infestations, loss of appetite ,abdominal pain, excessive thirst and vomiting ,and even liver disorders like hepatitis.

5.*Sterculia urens Roxb*

Common name- Gullar

Family- *Malvaceae*

Sterculia urens Roxb is from the family *Malvaceae ,* Commonly called "karaya". It is recognized as gum karaya tree' for the globally significant gum ,known as 'Indian Tragcanth, found chiefly in India .Deciduous trees, to 15m high, bark 10-12mm, white or greenish-grey, smooth, exfoliating in large, thin papery flakes ;blaze red; exudation yellowish –white ,sticky ;branches horizontal; branchlets pubescent .leaves simple , palmetely 3-5 lobed ,alternate clustered at the tips of branchlets; stipules free ,lateral, cauducous petiole 8-18 cm long ,stout ,pubescent ;lamina 15-30x 18-30cm,orbicular ,base cordate or sagittate ,lobe apex acuminate or caudate acuminate ,margin entire ,glabrous above ,velvety pubescent beneath ,coriaceous ;3-5 ribbed from base, palmate ,prominent ,lateral nerves 5-7 pairs, pinnate ,prominent intercostae subscalariform , faint. Flowers polygamous ,greenish yellow ,in axillary panicles, covered with sticky tomentose of glandular ,stellate hairs.

Medicinal uses of *sterculia urens Roxb*

It is best used as laxatives. Its characteristic makes this very popular product. It forms a mucilaginous gel when it gets in contact with water.Our body does not digest and absorb Gum Karaya Granules. It swells in the intestine, makes it dilate, and works as laxative. Adhesive for dental implant**s.**Gum karaya has some antibacterial and anti-inflammatory characteristics by which it is an effective remedy in sore throat. It also maintains normal blood sugars. Many anti-diabetic medicines contain Gum karaya.

6.*Acacia Catechu*

Common name- Khair –Kattha

Family -*Fabaceae*

Acacia catechu is a small or medium-sized, thorny tree up to 15 m tall; bark dark grey or greyish-brown. . It is commonly known as catechu, kattha and black cutch. Leaves bipinnately compound with 9-30 pairs of pinnae, glabrous or pubescent.Flowers in 5-10 cm long axillary spikes, pentamerous, white to pale yellow in colour , .Fruit a strap-shaped flat, tapering at both ends, shining brown, dehiscent, 3-10-seeded.

Medicinal uses of *Acacia catechu* It is used for medicinal purposes, especially for the treatment of cough, asthma, bronchitis and sore throat.The gummy extract of the wood called black catechu, is used as an anodyne, astringent and bactericide. The heartwood extract is also used in, colic, diarrhea, boils, skin afflictions. The bark shows anti-helmintic, antipyretic and anti-inflammatory properties. It is also used in the treatment of ulcers, anaemia and gum troubles

7. *Aegle marmelos*

Common name- Bael

Family -*Rutaceae*

Aegle marmelos is a slow-growing, medium sized tree, up to 12-15 m tall with short trunk. Its bark is thick, soft, flaking and spreading. The leaves are deciduous, alternate, borne singly or in 2's or 3's oval, pointed, shallowly toothed leaflets, 4-10 cm long, 2-5 cm wide and the terminal one with a long petiole. Flowers are fragrant having sweet aroma and blooms in clusters of 4 to 7 along the young branchlets . Each flower has 4 curved fleshy petals which are green outside and yellowish inside, and 50 or more greenish-yellow stamens. Shapes of the fruits can vary with varieties and can have round, pyriform , oval, or oblong shapes having 5-20 cm diameter. Fruit may have a thin, hard, woody or soft rind. It is dotted with minute oil glands which are aromatic. Inside the fruit, there is a hard central core and 8 to 20 faintly defined triangular segments, with thin, dark orange walls. Seeds are flattened-oblong, about 1 cm long, bearing woolly hairs.

Medicinal uses of *Aegle marmelos*

Aegle marmelos(L.) Corr.) is an important medicinal plantwhich has an enormous traditional value against various diseases. The different parts Aegle marmelos are used for various therapeutic purposes, such as for treatment of Asthma, Anemia, Fractures, Healing of Wounds, Swollen Joints, High Blood Pressure, Jaundice, Diarrhoea Healthy Mind and Brain. *Aegle marmelos* has been used as a herbal

ISSN PRINT 2319 1775 Online 2320 7876

Research paper © 2012 IJFANS. All Rights Reserved, UGC CARE Listed (Group -I) Journal Volume 11, Iss 11, Dec 2022

medicine for the management of diabetes. The unripe dried fruit is an astringent, digestive, stomachic and used to cure diaorrhea and dysentery. The leaves are made into a poultice and used in the treatment of ophthalmic. The roots and the bark of the tree are used in the treatment of fever by making a decoction of them.

Conclusion

The normal health care practice is typically structured on medicinal vegetation gathered from the wild. In spite of this, the Medicinal and Nutritional plant biodiversity is being depleted due to man-made and natural calamities. Moreover, the indigenous information related with the conservation and use of medicinal flora is also disappearing at an alarming rate. The purpose of conservation is to aid sustainable improvement through defending and the usage of biological sources in ways that do not scale down the world's range of genes and species or damage important habitats and ecosystems. In general, it entails things to do such as collection, propagation, characterization, evaluation, disease indexing and elimination, storage and distribution. The overall conclusion of the find out about is to initiate and aid for conservation, management and sustainable utilization of medicinal and nutritional vegetation for human and livestock fitness care and to promote in-situ conservation,ex-situ conservation and sustainable makes use of of medicinal plants life in and around site of global significance.

Refrences

1.Bodeker, G.(2002). Medicinal plants: towards sustainability and security. http://source.bellanet.org/medplant/docs/ssong/MEDPLANT_Discussion_Paper1.Doc

2 . Chopra, R.N.(1932). The Indigenous Drugs of India. Calcutta .

3 .Cooke, T. The Flora of the Presidency of Bombay, I-II, Londan , 1901-1908

4 . Ramteke ,D.D. , Zade ,S.B. & .khune , C.J. (2007). Conservation practices and utilization Strategies of Medicinal plants in Bhandara district of vidarbha region M.S. India. Environment conservation Journal, 8 (3)63-65 (ISSN 0972-3099)

5.Gupta , R. (1998) . Genetic Resources of medicinal plants .Indian Journal Plant Genetic Resources, 1.98 :102

6 . https://www.researchgate.net/publication/291274163

7 . https://www.researchgate.net/publication/280009975

8 . Jain, S. K.,(1991) . Dictionary of Indian Folk Medicine and Ethnobotany. Deep publications, New Delhi.

9 . Patil , K. J., Patil , S.V . , (2012) . Biodiversity of Vulnerable and endangered plants from Jalgaon district of North Maharashtra . Asian Journal of pharmacy and Life science, ISSN 2231-4423 vol.2 (2)

10 . Sunil ,M A., Sunita,Y.S. , Radhakrishnan , E. K. & Jyothis , M. (2019). Journal of Ayurveda and Integreative Medicine ,Vol 10 Issue 3 , ,Pg 185-191

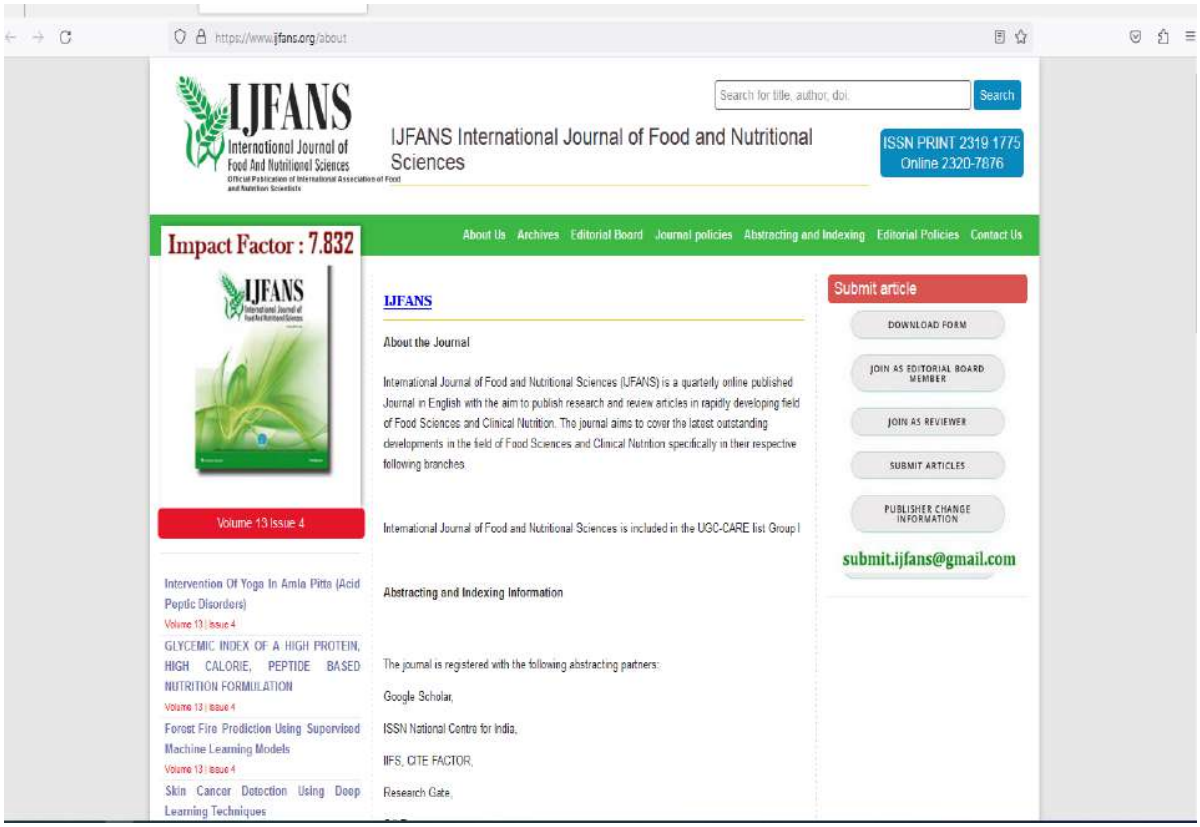
11. Gupta , R. , Vairale ,M.G., Chaudhari ,P.R. & Wate , S.R. (2009) . Ethnomedicinal Plants used by Gond Tribe of Bhandara District Maharashtra in the Treatment of Diarrhoea and Dysentery , Ethnobotanical Leaflets 13: 900-09.

12. Rands, M.R.W., Adams, W.M., & Bennun, , L. (2010) .Biodiversity conservation: challenges beyond , *Sci*., **329**:1298–03.

13 . Kadam , S. T. & Pawar , A. D.(2020) . Conservation of Medicinal Plants: A Review , International Ayurvedic Medical Journal ,ISSN 2320 5091 Pg 3890-3895

14 . Sharma, S. & Thokchom , R. (2014) . A review on endangered medicinal plants of India and their conservation . Journal of Crop and Weed , 10(2):205-218

15 . Venkata ,N. K. & Karumuri , S. S. (2011). Conservation of Medicinal Plants (Past ,Present & Future Trends). et al /J. Pharm. Sci. & Res. Vol.3(8), 1378-1386


https://www.ijfans.org/about
IJFANS
International Journal of Food And Nutritional Sciences
Official Publication of International Association of Food and Nutrition Scientists
Search for title, author, doi
Search
IJFANS International Journal of Food and Nutritional Sciences
ISSN PRINT 2319 1775
Online 2320-7876
Impact Factor : 7.832
About Us
Archives
Editorial Board
Journal policies
Abstracting and Indexing
Editorial Policies
Contact Us
Volume 13 Issue 4
Intervention Of Yoga In Amla Pitta (Acid Peptic Disorders)
Volume 13 | Issue 4
GLYCEMIC INDEX OF A HIGH PROTEIN, HIGH CALORIE, PEPTIDE BASED NUTRITION FORMULATION
Volume 13 | Issue 4
Forest Fire Prediction Using Supervised Machine Learning Models
Volume 13 | Issue 4
Skin Cancer Detection Using Deep Learning Techniques
IJFANS
About the Journal
International Journal of Food and Nutritional Sciences (IJFANS) is a quarterly online published Journal in English with the aim to publish research and review articles in rapidly developing field of Food Sciences and Clinical Nutrition. The journal aims to cover the latest outstanding developments in the field of Food Sciences and Clinical Nutrition specifically in their respective following branches.
International Journal of Food and Nutritional Sciences is included in the UGC-CARE list Group I
Abstracting and Indexing Information
The journal is registered with the following abstracting partners:
Google Scholar,
ISSN National Centre for India,
IIFS, ICTE FACTOR,
Research Gate,
Submit article
DOWNLOAD FORM
JOIN AS EDITORIAL BOARD MEMBER
JOIN AS REVIEWER
SUBMIT ARTICLES
PUBLISHER CHANGE INFORMATION
submit.ijfans@gmail.com

UGC-CARE List

You searched for "**2320-7876"**. Total Journals : **1**

Search:

Sr.No.	Journal Title	Publisher	ISSN	E-ISSN	UGC-CARE coverage years	Details
1	International Journal of Food and Nutritional Sciences	Global E smart Technologies	2319-1775	2320-7876	from January-2021 to January- 2023	Discontinued from Jan 2023

Showing 1 to 1 of 1 entries

Previous 1 Next

Copyright © 2024 Savitribai Phule Pune University. All rights reserved. | Disclaimer

Journal
of the
Oriental Institute
M.S. University of Baroda

ISSN: 0030-5324
UGC CARE Group 1

USE AND USER STUDY OF COLLEGE LIBRARIES IN BHANDARA CITY.(MAHARASHTRA)

Mona Shambhau Yeole
Librarian, J. M. Patel Arts, Commerce and Science College, Bhandara

Dr. Prince Ajaykumar T. Aagashe
Librarian, Matru Sewa Sangh Institute of Social Work, Nagpur

ABSTRACT
The library provides a variety of services to meet the requirements of the scholarly institution, which helps it play an essential role in achieving the overall aims of its parent organization.
This study focused on five college library user surveys in Bhandara city under R.T.M.Nagpur University, Nagpur.
A university library's performance must be evaluated since it is a service organisation
in order to ascertain whether it achieves its particular goals and to support library spending.A well-structured questionnaire was used for collecting opinions of the library users about the uses of the collections and services. Out of 750 users, only 517 questionnaires were collected from the respondents and selected for analysis of data. The present study demonstrates and elaborates on the various aspects of library collection uses within the available resources, frequency and purposes of visit, adequacy of library hours, use of library services & collections, ways of document searching and user satisfaction with the overall performance of the library.
Keywords: Performance assessment, Expectations, User Study, College library, User satisfaction

Introduction:
This is the era of Information Explosion. Users of libraries now have different requirements and expectations due to the development of information and the digital revolution. Users want correct information in a quick way. The availability and usability of information resources, services delivered, professional experience and conduct, and facilities that come close to users' expectations and perceptions. As a result, libraries must give their customers outstanding service and enhance their standing as service organizations.This study helps to know the user's expectations and needs in academic
libraries. The study helps to identify Problems for providing best practices and get solutions for improving library resources and services.
The primary objective of a library is to satisfy the increasing needs and demands of its users engaged in academic pursuit and research (Mohindra and Kumar, 2015). Always good service organisation identifying user's desired expectations and library management to
identify priorities andprovide a precise and timely supply of information resources and services besides infrastructure facilities. For many years a different types of surveys organized in different

types of libraries for measuring the usefulness of their services. The most popular example of measurement usefulness of the practice is the Information retrival system.

1. Objectives

i. To study the use of library collections and services of the ;

ii. To find out the purpose of the information search;

iii. To find out the overall user satisfaction with the resources and services facilities provided in the five college libraries.

Availability and Use of Information Resources in University Libraries:

All libraries have both printed and non-printed resources available, including books, journals, e-resources, e-books, e-journals, CD ROMs, DVDs, magazines, internet access, audio-visual materials, atlases and maps, subscribed online databases, as well as bibliographic databases and other resources that can be used to their effective utilization in a library.

Significance and scope of the Study

This study is try to find out the use of the resource and services of the libraries by students in the undergraduate colleges in Bhandara City under R.T.M. Nagpur University, Nagpur, Maharashtra. The scope of the study is confined to the following five colleges, namely

1) J.M.Patel Arts, Commerce and Science College Bhandara.
2) Smt. Rewaben Manoharbhai Patel Mahila Kala Mahavidyalaya, Bhandara.
3) Pragati Mahila Mahavidylaya, Bhandara.
4) Athawale College of Social Work, Bhandara.
5) Government College of Education, Bhandara

2. Distribution of Questionnaire

Name of the Colleges	Number of questionnaires distributed	Number of responses	Number of responses Percentage
J.M.Patel Arts,Commerce and Science College, Bhandara	150	140	93.3
Smt.Rewaben Manoharbhai Patel Mahila Kala Mahavidyalaya, Bhandara	150	110	73.3
Pragati Mahila Mahavidyalay, Bhandara	150	88	58.66
Athawale College of Social Work, Bhandara	150	98	65.3
Government College of Education, Bhandara	150	81	54
	750	**517**	**344**

3. Methodology

In this study, a questionnaire-based survey was conducted. The data was gathered using a well-designed and user-friendly questionnaire. Consequently, a suitable sample technique has been applied.750 questionnaires, carefully chosen from the five college libraries under investigation, were given to the users. As a result, 517 questionnaires in all were returned. The gathered data were then tabulated and appropriately analysed. The results of the findings were accessible in tables using percentages.

4. Data Analysis

Table 5.1: Visitor Frequency in libraries

Visitor frequency is obviously influenced by the type of library, its holdings, services, organisation, upkeep, and most importantly, its patrons. However, the behaviour of library staff members can also serve to boost visitor frequency.

The table shows that everyday user is 12.76%, most of the users visit the library 2 days in week 31.14, as well as users come 25.72% once a week. Once in 2-week users is 17.60%. Monthly users are 11.60% and occasionally very fewerusers visited the library i.e 3.67%.

Table 5.1:

Frequency Number of	responses	Percentage
Everyday	66	12.76
2 day in a week	161	31.14
Once in week	120	25.72
Once in 2 week	91	17.60
Monthly	60	11.60
Occasionally	19	3.67
Not at all visited	00	00

(Fig-1)

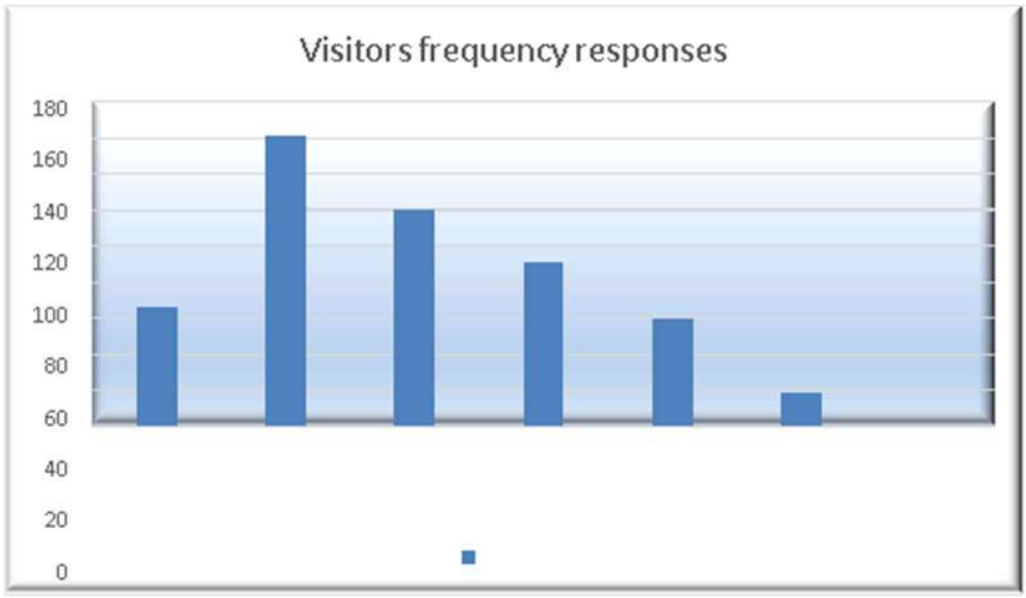


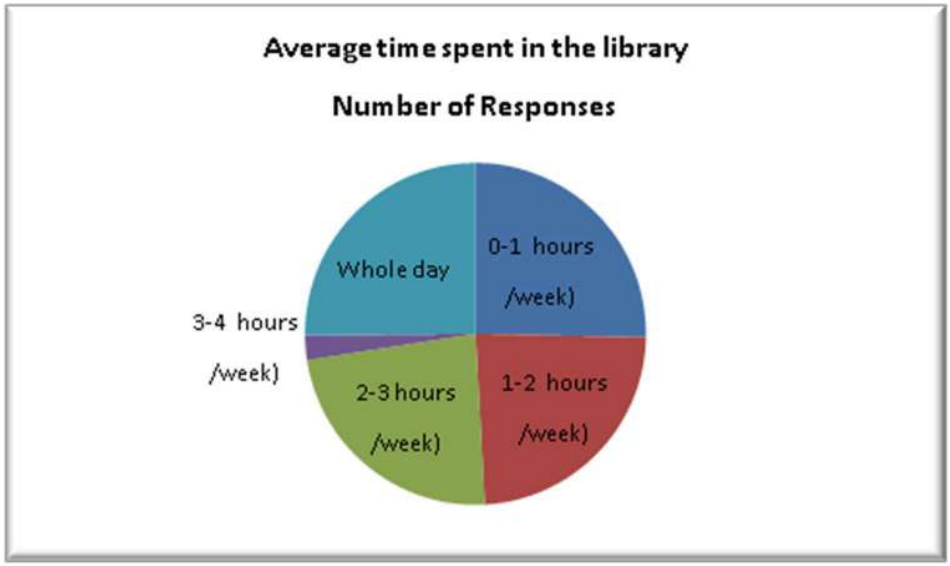
Table 5.2: Average time spent in the library

Table 5.2,(fig.2) Average number of hours each week that students spend at the library. It is remarked that half of the total respondents (25.33%) spend less than one hour per week, while 23.79% spend '1-2hrs', 23.40% spend '2-3hrs' and 2.32% spend '3-4hrs'. However, only 25.14% of students spend the whole day in the library.

Table 5.2: Average time spent in the library

Average Time spent	Number of Responses	Percentages
0-1 hours /week	131	25.33
1-2 hours /week	123	23.79
2-3hours /week	121	23.40
3-4 hours /week	12	2.32
Whole day	130	25.14

(Fig-2)



5.3 : Visitor's Purpose for using Library Resources

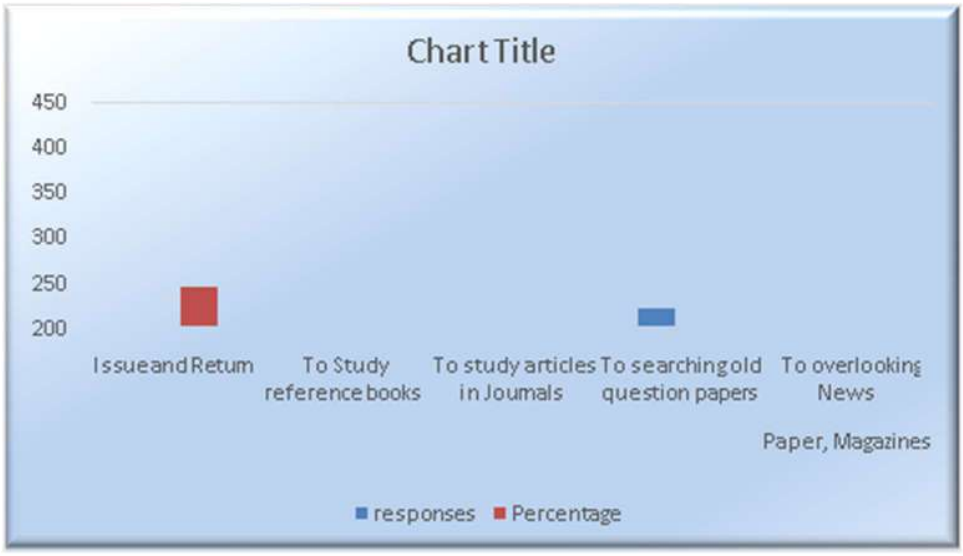
In the library different types of resources are available and users use it with the help of library staff indicates that 75.24% of the students use/visit the library for 'Issue and Return of textbooks', followed by 6.38% for 'searching old question papers and 5.22% for 'To overlooking newspaper, magazines, etc.for improving general awareness of11.21% student's visit library to study reference books and 1.9% user visit library to study articles in
Journals.

Table 5.3: Visitor's Purpose for using Library Resources

Purpose Number of	responses	Percentage

Issue and Return of Books	389	75.24
To Study reference books	58	11.21
To study articles in Journals	10	1.9
To searching old question papers	33	6.38
To overlooking News Paper, Magazines for G.K	27	5.22

(fig-3)



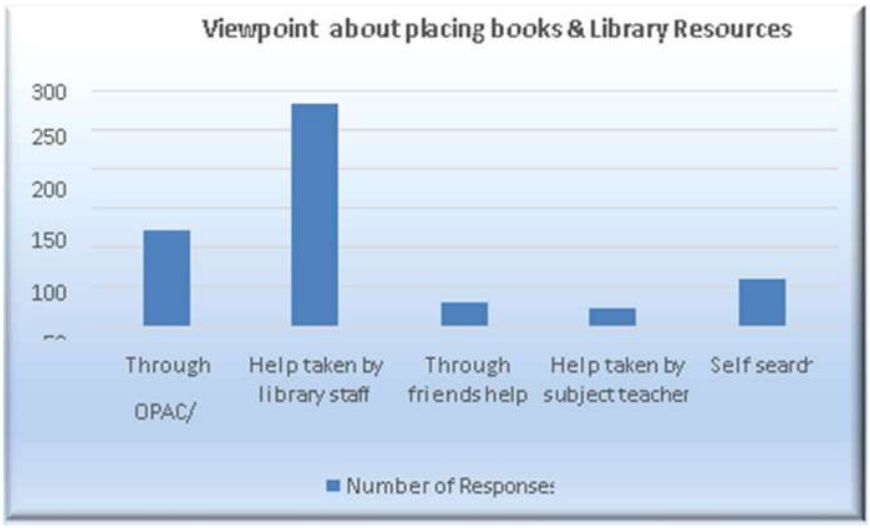
5.4 : Viewpoint about placing books & Library Resources

In a search, 54.93 percent of students find or obtain their information resources "with the assistance of the library staff.", followed by 23.40% and 5.80% of the respondents get theirdesired information resources through 'browsing the card catalogue and OPAC' andwith the help of friend respectively. 11.60% students took self- help for search.

Table 5.4:

Viewpoint	**Number of Responses**	**Percentages**
Through OPAC/ Catalogue	121	23.40
Help taken by library staff	284	54.93
Through friends help	30	5.80
Help taken by subject teacher	22	4.25
Self search	60	11.60

(fig-4)



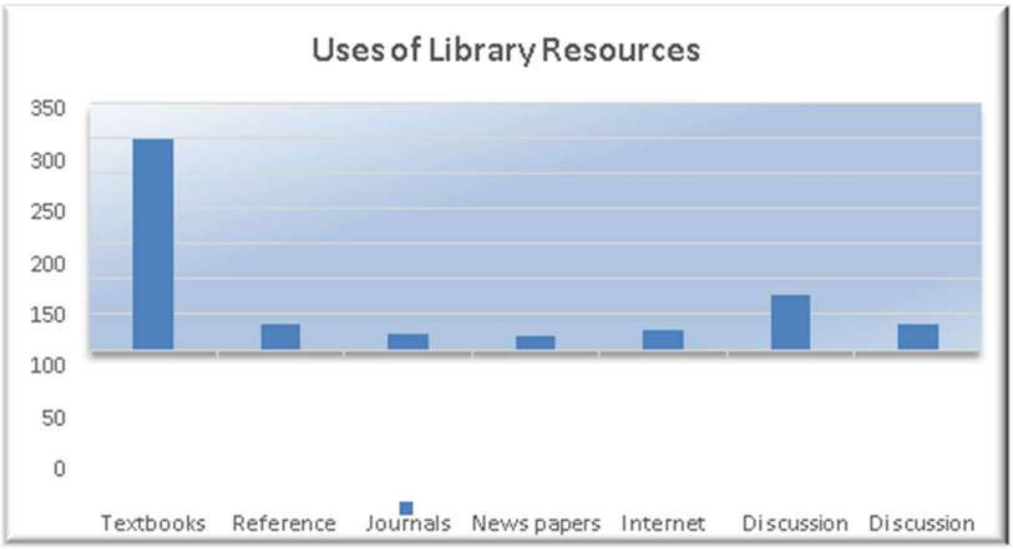
5.5.: Uses of Library Resources

Table 5(fig. 5) Express that majority of the students i.e. 57.67% replied on the textbooks is very needful. About 15.08% of the respondent's consult 'human sources' such as faculty, librarian, etc. as one of their resource of information. About 7.15% of the respondents replied on books and books'and 3.67% of the respondents indicate the use of newspaper, magazines. Besides, these sources about 4.06% of the respondents opted for other sources of information such as internet and journals.

Table 5- Uses of Library Resources

Type of information resources	Number of responses	Percentage
Textbooks	298	57.67
Reference Book	37	7.15
Journals	21	4.06
Newspapers, magazine's	19	3.67
Internet	27	5.22
Discussion with Faculty	78	15.08
Discussion with Library Staff	37	7.15

(fig-5)



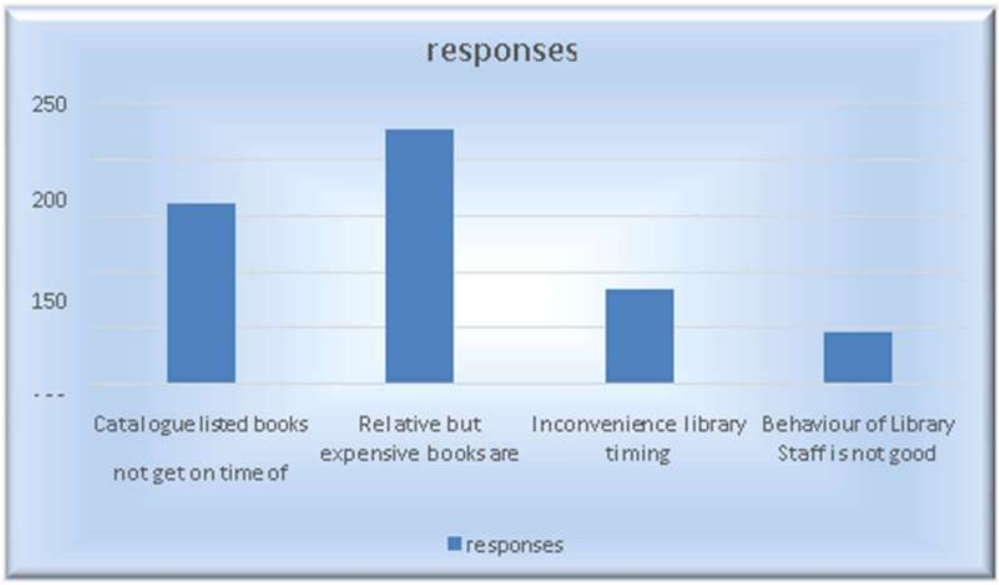
5.6 : Problems faced by students in searching information

When students search information in the library some problems faced by them i.e.30.94% students told that 'Catalogue listed books not get on time the of borrowing, whereas 43.90% students gave opinion was 'Expensive relative books are kept for reference' reveals that
30%, About 16.24% students not use library properly because library timing is inconvenient for them. Only 8.89% students said that the did not like behaviour of Library Staff so its effects on using library sources.

Table - 6

Opinion	**responses**	**Percentage**
Catalogue listed books not get on time of borrowing	160	30.94
Relative but expensivebooks are kept for reference	227	43.90
Inconvenience library timing	84	16.24
Behaviour of Library Staff is not good	46	8.89

(fig-6)



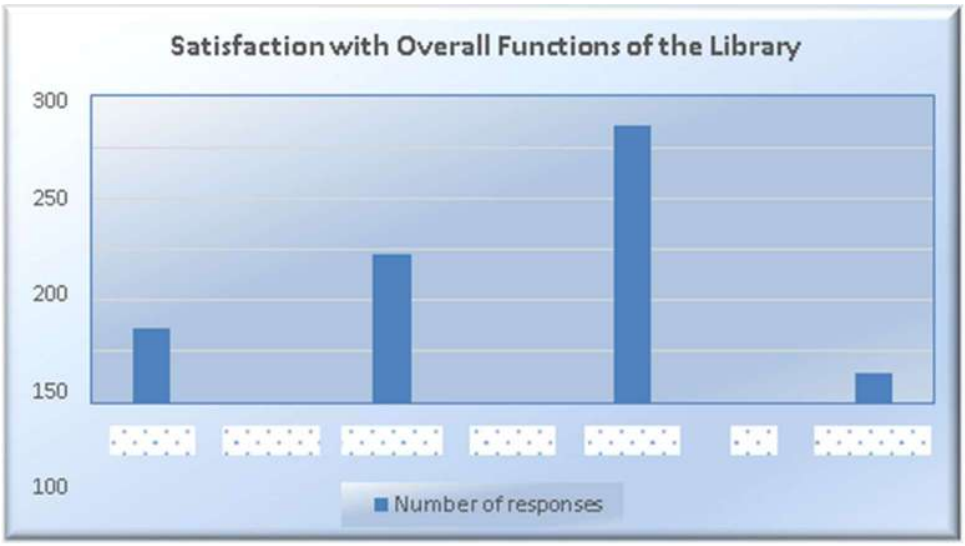
5.7 : Satisfaction with Academic requirements

The respondents were asked to comment on how well they felt the information resources met their demands for academic research.In accordance with Table 7's (Fig. 7), more than half (55%) of the respondents reported being happy in the range of "25 to 50%," with 52.41% and 14.11% of respondents reporting outstanding satisfaction, respectively.Only 5.41% of those surveyed reported being very unsatisfied.

Table 7- Satisfaction with the library's Functions

Satisfaction	*Number of responses*	*Percentage*
Excellent (80-100)%	*73*	*14.11*
Very Good (50-80)%	*145*	*20.04*
Good (25-50)%	*271*	*52.41*
Poor (<25)%	*28*	*5.41*

(fig-7)



6. RECOMMENDATIONS

These suggestions and recommendations are given in the context of the following findings:

i. The library collection should be increased valuable books. Except J.M. Patel college library. This library is good collection.

ii. Reading materials should be organised on the shelves in the correct order using classification schemes like D.D.C./C.C.

iii. User orientation programme is must for all libraries. Programme should be conducted from time to time. J.M.Patel college conduct Orientation and awareness Programme.

iv. Give practical demonstration in searching of information sources through catalogue(Card/OPAC).

v. Personal computers should be made available so that users can access the Library's collection of information.

vi. The timing of the library services should be extended to round the clock. Some Colleges not issued book everyday.

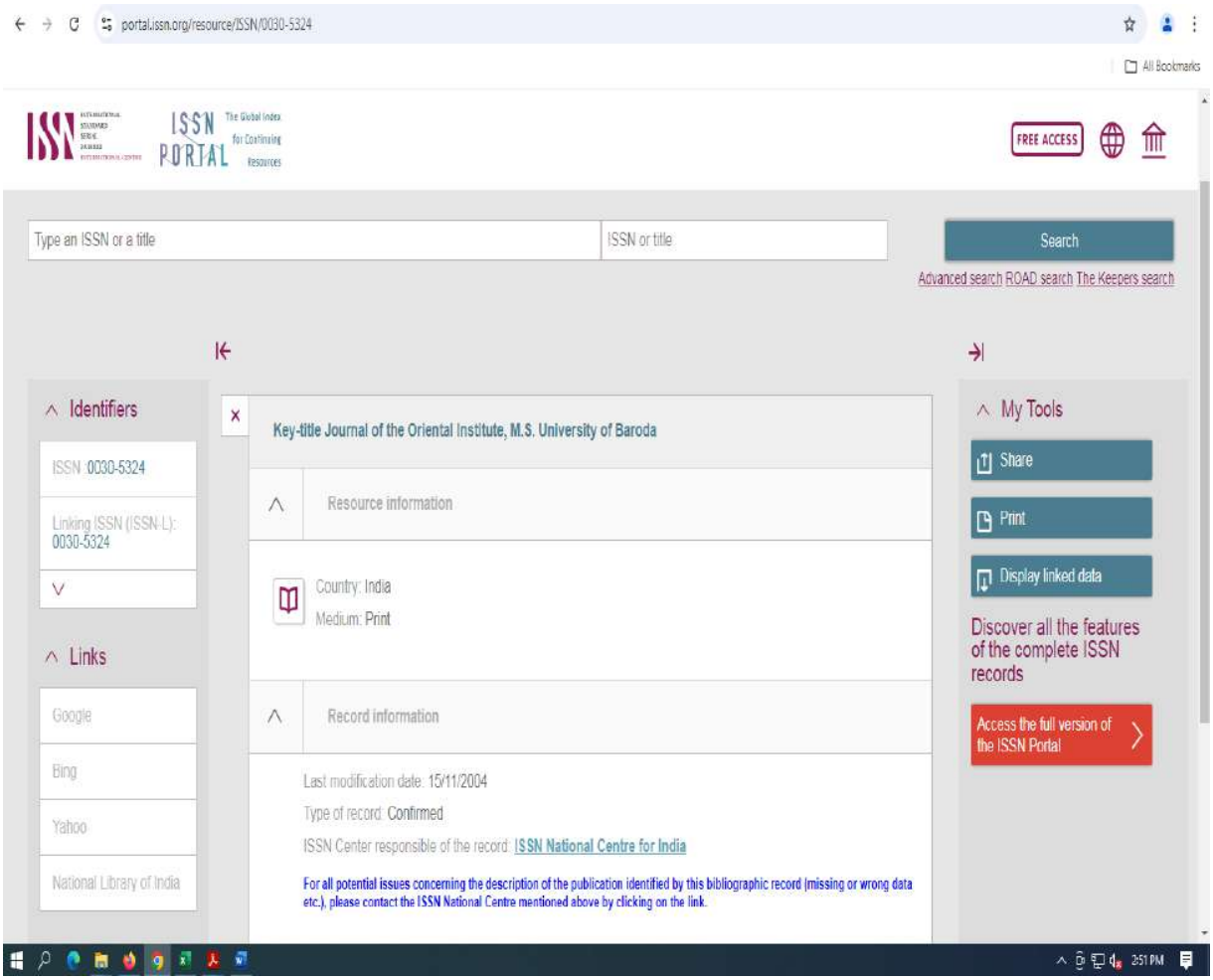
7. CONCLUSIONS

This study provided a precise imageof the use of college libraries in Bhandara City, Maharashtra. The utilisation of college libraries by their potential users canbe increased by adopting advance facilities. To deal with the current situation, automation of libraries using modern technology is too important.There are many issues that make it difficult to provide information services to users, including user education, a shortage of professional and non- professional employees, issues with policies, a lack of autonomy for library professionals, etc.Therefore, the authority is requested to provide this concern their immediate attention.It is quite challenging to provide users with access to all the needed documents, but it is somewhat manageable by keeping user demand in mind while buying new books, magazines, and other print and non-print information items.To address the

needs of the user community, the library should therefore include additional books, periodicals, and other print and non-print information resources.

REFERENCES

1. Babu, A. D. (1994), Information generation and library use by university libraries, Gyan Publishing House, New Delhi.
2. Callinan, J. E. (2005) ,Information seeking behaviour of undergraduate biology students: A comparative analysis of first year and final year student in university college Dublin', Library Review, Vol. 54 No.2, pp.86-99.
3. Fizdani, B. T. (1998) ,Information needs and information seeking behaviour of graduate students at the University of Botswana', Library Review, Vol. 47No.7, pp.329-40.
5. Mittal R.L. (2001), Library administration: Theory and practices, New Delhi metropolitan Book Co. Ltd., PP. 112
6. Nath Amar (2006), Pattern of Usage of Information Resources by Research scholars in Punjab Agricultural University Library: A study, 4th International caliber, Information and Library Network Center, P.P. 290-297
7. Veer D.K. and Pawar Rameshwar(2011), Public library in Maharashtra: Yesterday, Today and Tomorrow, Modernization public and Academic Libraries: Issues and solution, seminar paper's, state level workshop, edited by Jadhav R.N. and other's, parbhani, Pratibhas Prakashan, P.P. 34-47
8. Siddiqui, A. F. (2001)'Use of library collections in the Jawaharlal Nehru University library, New Delhi', IASLIC Bulletin, Vol. 46 No. 4, pp. 184-196. Follow us on: IRJLIS, Facebook, Twitter


portal.issn.org/resource/ISSN/0030-5324
All Bookmarks
ISSN PORTAL
The Global Index for Continuing Resources
FREE ACCESS
Type an ISSN or a title
ISSN or title
Search
Advanced search ROAD search The Keepers search
Identifiers
ISSN 0030-5324
Linking ISSN (ISSN-L): 0030-5324
Links
Google
Bing
Yahoo
National Library of India
Key-title Journal of the Oriental Institute, M.S. University of Baroda
Resource information
Country: India
Medium: Print
Record information
Last modification date: 15/11/2004
Type of record: Confirmed
ISSN Center responsible of the record: ISSN National Centre for India
For all potential issues concerning the description of the publication identified by this bibliographic record (missing or wrong data etc.), please contact the ISSN National Centre mentioned above by clicking on the link.
My Tools
Share
Print
Display linked data
Discover all the features of the complete ISSN records
Access the full version of the ISSN Portal
2:51 PM

UGC-CARE List

You searched for "**Journal of the Oriental Institute"**. Total Journals : **1**

Search:

Sr.No.	Journal Title	Publisher	ISSN	E-ISSN	UGC-CARE coverage years	Details
1	Journal of the Oriental Institute (print only)	Oriental Institute, Maharaja Sayajirao University of Baroda	0030-5324	NA	from January-2020 to Present	View

Showing 1 to 1 of 1 entries

Previous 1 Next

Copyright © 2024 Savitribai Phule Pune University. All rights reserved. | Disclaimer

Check for updates

Review Article

Entrepreneurial Ecosystem: A Systematic Literature Review

Vision
1–14
© 2022 MDI
Reprints and permissions:
in.sagepub.com/journals-permissions-india
DOI: 10.1177/09722629221093866
journals.sagepub.com/home/vis
SAGE

Rahul Krushnaji Wadichar[1], Prashant Manusmare[1] and Mukul Abasaheb Burghate[2]

Abstract

Entrepreneurial ecosystems (EEs) is a relatively new concept that has piqued the curiosity of legislators, researchers and professionals. Despite the fact that research on EES is growing, their inputs are still dispersed. No studies have attempted to combine the available research on EES because the literature is fragmented. As a result, the goal of this study is to perform a systematic literature review on EES. This assessment of the literature looks at research included in the Scopus and web of science indexed journals publication like Emerald, Science Direct (Elsevier), JSTOR, SAGE and Google Scholar. The purpose of this research is to uncover research gaps and flaws in the field of entrepreneurial ecosystem (EE). The results reveal that the emergence of EEs is poorly understood, with conceptual research dominating in recent years. By recognizing research gaps in the current literature, we provide a road map for future entrepreneurial environment research. Cooperation, knowledge exchange and innovation at the higher levels are more likely to produce favourable entrepreneurship environments. It identifies present gaps in theories and empirical studies as well as potential research directions in EEs.

Key Words

Entrepreneurship, Entrepreneurial Ecosystems, Systematic Literature Review (SLR), Entrepreneurs, Conceptual Framework

Introduction

Multi-dimensional research has brought together a multidisciplinary approach to entrepreneurship, such as entrepreneurship economics, urban economics and economic geography (Acs et al., 2014; Atiase et al., 2017; Sambo, 2018; Ucbasaran et al., 2001; Welter, 2011). According to the European Commission, entrepreneurship is a process of increasing economic growth by taking chances, being innovative and creative, and having a well-organized and competent management structure in place. Social capital, according to Chinese entrepreneurs, is crucial in the development of start-ups, attracting more investment, and gaining a larger market share (Yue & Rivera, 2021). Entrepreneurial activities and entrepreneurs originate from a highly interwoven and complicated system with various actors rather than in isolation (Cowell et al., 2018). As a result, the phrase 'entrepreneurship ecosystem' was established to characterize and express the structures that regulate how start-ups and entrepreneurs interact with other stakeholders. Entrepreneurship is a critical component of economic development (Audretsch et al., 2007). Being an entrepreneur is not hereditary, according to one important stream of past entrepreneurship writings (Alum & Drucker, 1986). According to Isenberg and Global (2011), the entrepreneurial ecosystem (EE) was created to address some of the policy flaws that have arisen as a result of how methods are perceived and implemented, including the following:

- A lack of governmental support for entrepreneurship,
- Inadvertent sabotage of entrepreneurship goals,
- Uncertainty in the goals of entrepreneurial strategies,
- Skewed outcomes of disordered programmes, such as a brain drain educational plan.

The involvement of other participants in supporting the entire innovation process is more prominent in EEs and start-ups and in entrepreneurs, who are considered the

[1] J. M. Patel College (RTMNU Nagpur University), Bhandara, Maharashtra, India
[2] Dr. Panjabrao Deshmukh Institute of Management Technology & Research, Nagpur, Maharashtra, India

Corresponding author:
Rahul Krushnaji Wadichar, J. M. Patel College of Arts Commerce and Science, Near Civil Line, MSEB Colony, Bhandara, Maharashtra 441904, India.
E-mail: rahulwadichar@gmail.com

system's core actors (Giudice et al., 2016). Maroufkhani et al. (2018) presented a descriptive study of EE research, including the methodology used and the sources where they were published. A citation-based analysis of the literature on EEs was given, emphasizing the scope and campus-based EEs (Malecki, 2018). Although there is a large body of knowledge on EEs, it has only finally caught scholars' interest (Kshetri, 2014; Stam, 2015; Zahra & Nambisan, 2011, 2012); none of the research has given enough thought to incorporating the existing literature studies on the EE. Hence, there is still a scarcity of studies on the EE. As a result, utilizing a thorough literature analysis, this study aims to address this gap by categorizing the many concepts that exist in the EE sector. Modern entrepreneurship systematic review research, for example (Liñán & Fayolle, 2015; Mary George et al., 2014; Schmitz et al., 2016), have not paid attention to the EE.

The fundamental aim for reviewing the entrepreneurship literature from an ecosystem viewpoint is to benefit both academic researchers and executives from a comprehensive study of the topic of EEs, aside from the ease of condensing the scholarly publications' literature summary sections. This study offers a thorough examination of EE research. The research aim of this study is to add to the body of knowledge: First, by offering a synthesis of EE research and associated ideas. Second, by undertaking a comprehensive textual analysis to highlight how many components of the EE have been researched and argued over time, we hope to complement previous evaluations and add to the current state of research in this study. Third, by identifying gaps and flaws in the current research, we offer a study path for future studies on the EE. The following research questions are formulated following the study's goal: (a) What are the most important conceptual and theoretical frameworks for the EE? (b)How has the study of the EE progressed over time? (c) What are the new research pathways for EEs that are emerging?

This article is organized as follows: The methodology used in the second section is described in full, including data gathering and analysis. The descriptive results and the conceptual framework are presented in the third and fourth sections. Finally, we provide future research directions based on the findings of our review.

Methodology

According to the nature (mature or emerging) of the issue under research, systematic literature reviews (SLRs) disclose different characteristics (namely, the total number of articles under consideration, their aims and their contributions to the literature; Kraus et al., 2020; Snyder, 2019; Torraco, 2005). When employing literature sources, we conducted a systematic literature evaluation utilizing the who furnished criteria to ensure that the analysis was transparent and replicable (Tranfield et al., 2003). Researchers can employ a complete literature review to map existing ideas and guide their research subjects toward expertise development and manufacturing (Cook, 1997; Tranfield et al., 2003).

Sampling and Data Collection

This review of the literature looks at research that is included in the Scopus and web of science indexed journals publication like Emerald, Science Direct (Elsevier), JSTOR, SAGE and Google Scholar (search engine). A list of relevant papers was evaluated to aid in the identification of articles that met the reference criteria.

We used the following important search phrases within the topic: **entrepreneurial ecosystem* or *entrepreneurship ecosystem* or *ecosystem for entrepreneurship**, *and entrepreneur** AND *ecosystem**. To represent relationships between search phrases and retrieve relevant articles, Boolean logic (i.e., AND or OR) was used (* Represents the key search terms within topic, title and abstract. It gives idea about search phrases within different paper related to entrepreneurial ecosystem).

Furthermore, we limited our research to peer-reviewed papers that have been published up to 2022 to have solid and informative articles. We retrieved 423 articles from Emerald, Science Direct (Elsevier), JSTOR, SAGE and Google Scholar (search engine) at that first stage. We arrived at 83 common items by deleting overlapping entries. The study includes empirical publications written in English peer-reviewed journals and studies that looked at the links between the ideas under consideration. We carefully scrutinized abstracts and weeded out studies that did not specifically address the topic of EEs, such as pieces about ecosystems in the natural world (Brown et al., 2015; Dedehayir et al., 2018). Articles about topics apart from entrepreneurship were omitted. Articles were eliminated from consideration if they did not include the phrases 'entrepreneurial/entrepreneurship ecosystem'. Contributions to the ecosystem that did not have a clear emphasis on entrepreneurship topics were also disqualified. The benefits of a comprehensive corpus minimization are self-evident. The information on the screening procedure is shown in Figure 1 using the preferred reporting items for systematic review (PRISMA Flowchart) and meta-analysis (Moher et al., 2009). This resulted in a sampling size of 57 relevant articles, resulting in a further 26 items being removed from our analysis.

Entrepreneurial Ecosystems Research Articles-Descriptive Analysis

Publication Year

The publication year was not restricted in any way. During the research study, a descriptive analysis was used to grasp the meaning of the literature on EE (Brito & Leitão, 2020). As a result, we divided the 57 papers into various descriptive categories. The graph in Figure 2 shows the

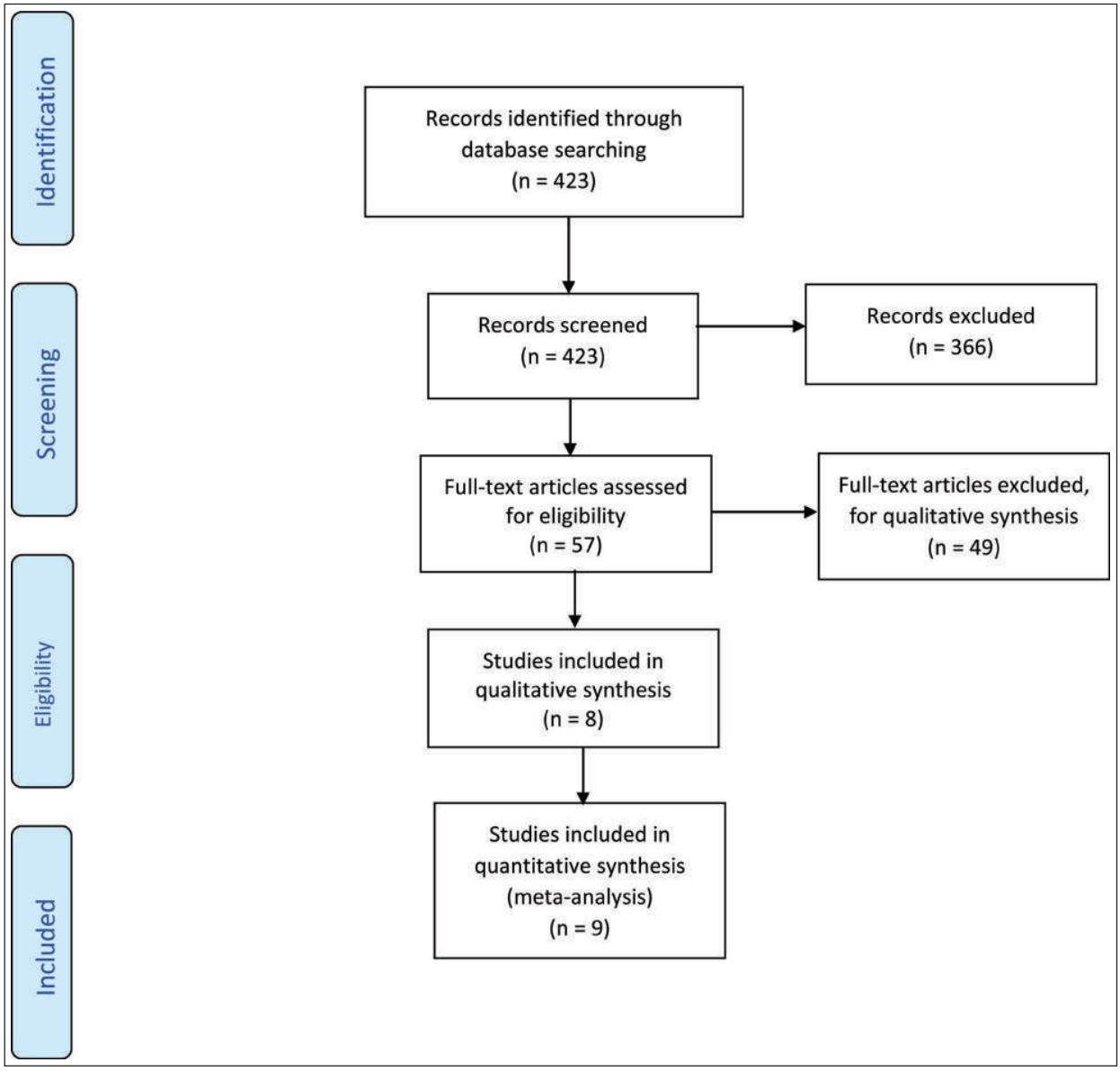


Figure 1. The PRISMA Flow Chart

Source: Moher et al., (2009).

sequence of data gathered and the number of articles discovered from 2005 to 2020. Between 2005 and 2011, just one or two articles were published; however, seven articles were published in 2017, followed by nine pieces in 2020. In 2020, the topic of the EE drew more attention, but in 2008 and 2010, there was a distinct lack of publication pressure. Although the number of publications in 2017 has not yet been completed, there is an overall growing trend, indicating the topic's increased promise in recent years (Malecki, 2018; Maroufkhani et al., 2018). The overall publishing frequency in the field of EEs appears to have increased in recent years, as indicated in Figure 2, that is, in 2020. The trendline in Figure 2 shows that in recent years, a greater emphasis has been placed on the EEs.

Entrepreneurial Ecosystems Research Article Classification

Figure 3 depicts the distribution of papers. As previously stated, the Emerald, Science Direct (Elsevier), JSTOR, SAGE and Google Scholar (search engine) were utilized to classify the papers. As shown in Figure 3, 11 of the 57 publications are connected to business, management and accounting, while the rest are devoted to other technical elements of study (Cho et al., 2021; Maroufkhani et al., 2018). The findings show that there is a noticeable lack of scholarly articles relating to specific business tasks such as psychology and marketing. Business, management and accounting, energy, environmental science and agriculture

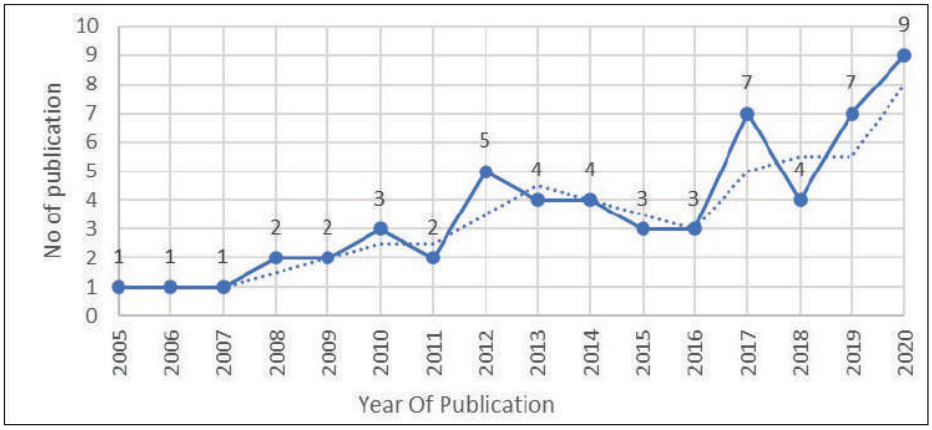


Figure 2. Publication Year and Frequency

Source: The authors.

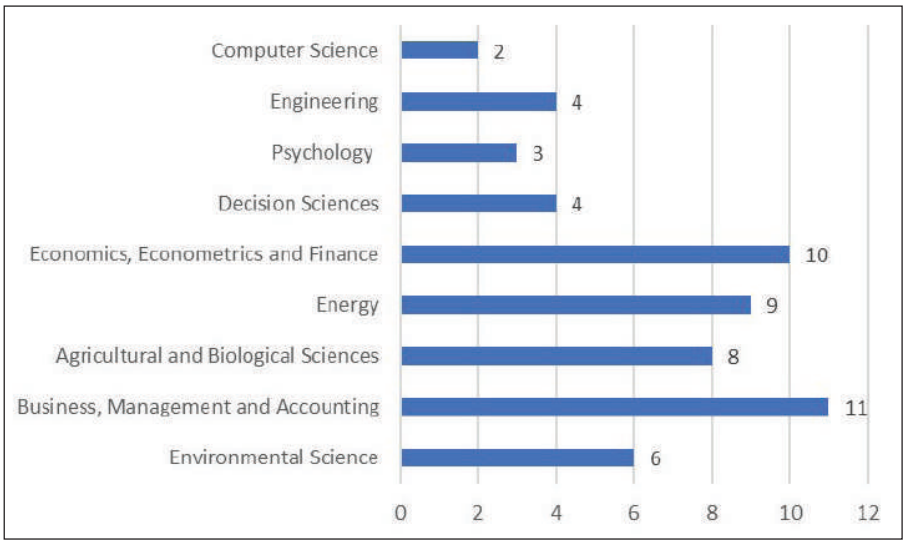


Figure 3. The Distribution of Papers

Source: The authors.

and biological sciences, on the other hand, show a semblance of technological domination. The majority of papers in the EE are divided into categories such as business, management, accounting, economics and econometrics.

Article Type in Entrepreneurial Ecosystems Research

The majority of the articles chosen for this systematic literature assessment of the EE are review articles, book chapters, research articles, encyclopaedia entries, case studies, discussions, book reviews, short communications, conference abstracts and editorials. Figure 4 shows the article type in EEs research. Eleven out of the 57 publications that contributed to the EE intended to use report review articles in their research. The researchers' second most popular article type is book chapters, which was used in 10 studies. Of course, some publications employ both book chapters and case report study methodologies. The encyclopaedia comes in third place for research in the EE. In their investigation, 7 out of the 57 articles that contributed to the EE aimed to employ a research article.

Country and Industry Focus

Due to the absence of empirical backing for several theoretical concepts, the bulk of them seem to have a similar focus rather than focusing on specific industries

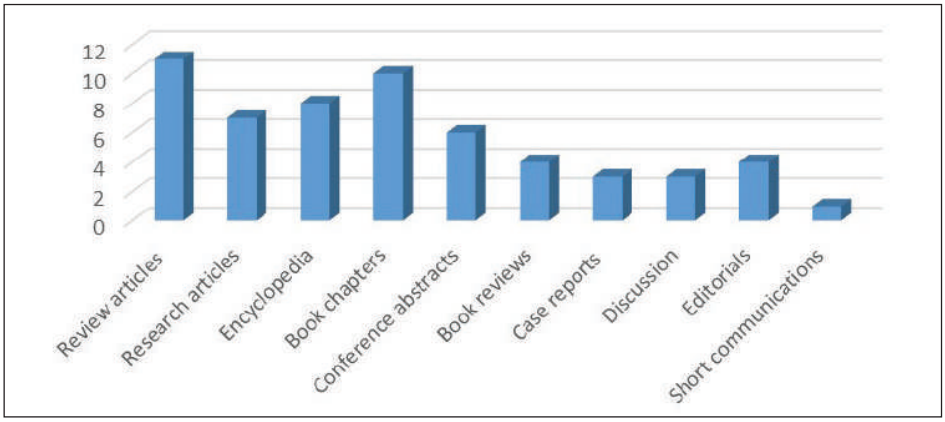


Figure 4. Article Type in Entrepreneurial Ecosystems Research

Source: The authors.

(Maroufkhani et al., 2018). Recent empirical studies concentrating on R&D activities and also the education system looked into the function of institutions in supporting entrepreneurial activity within EEs (Kansheba & Wald, 2020). In the technological industry, just a few researches have been done. Furthermore, as shown in Figure 5 and according to a SLR done by the country, numerous recent researches on the EE (Out of 57 articles) have been undertaken in Europe (23%) and the United States (28%), the performance of EEs varies from one area to the next and between nations. As a result, more empirical research on EEs in other businesses, notably non-tech enterprises, as well as in varied country settings, like Asia (10%) and Africa (9%), is required. Gustafsson et al. (2015) emphasize that emerging industries are in the early stages of development, which means there are more prospects for entrepreneurs.

Source of Entrepreneurial Ecosystems Articles

Due to the large number of articles identified, this SLR only includes journals with ten or even more publications (Brito & Leitão, 2020). Figure 6 shows the final results of this collection, highlighting the following journals: *The Journal of Entrepreneurship* (21%), *International Journal of Entrepreneurship and Innovation* (19%) and *Entrepreneurship Theory and Practice* (18%). Because more than ten papers were published in these journals, three journals appear to be the most relevant in our corpus. The remaining papers have appeared in journals such *as Journal of Enterprising Communities: People and Places in the Global Economy*, *Journal of Entrepreneurship and Public Policy*, *Research Policy*, *Small Business Economics*,

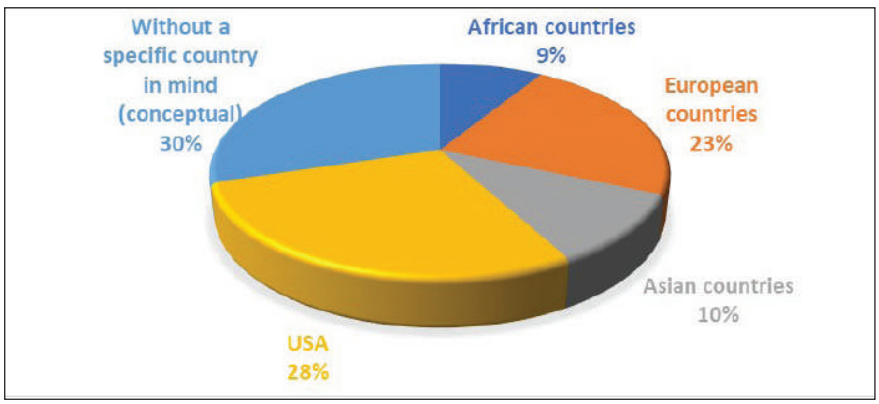


Figure 5. Country Focus Entrepreneurial Ecosystem Research

Source: The authors.

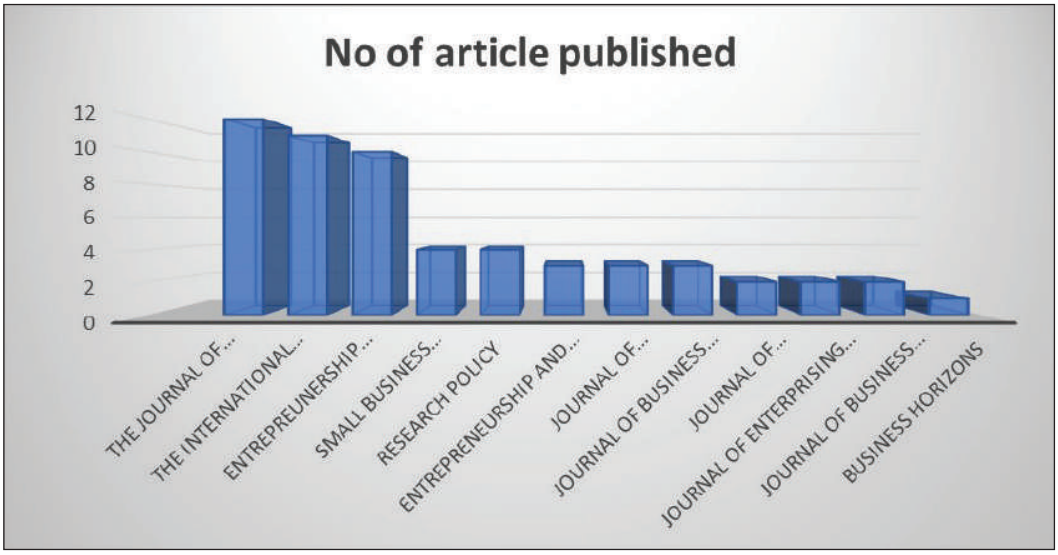


Figure 6. Journals with a More Significant Number of Publications

Source: The authors.

Entrepreneurship, *Regional Development*, *Journal of Business Research*, *Journal of Entrepreneurship and Innovation in Emerging Economies* and *Journal of Business Venturing and Business Horizons*.

Methodology Used in Entrepreneurial Ecosystems Articles

We looked at the many methods that were used. Table 1 shows that a case study technique was utilized in the majority of studies (23) on EEs (Kansheba & Wald, 2020; Maroufkhani et al., 2018). The second place goes to conceptual work, which includes submissions that lack empirical data but do not necessarily include an apparent theoretical grounding (13 publications). Mixed method, qualitative and quantitative approaches are used in the remaining empirical publications. The predominance of conceptual work implies a scarcity of empirical research on the subject. Furthermore, because most publications are conceptual studies, the results suggest that the majority of them lack a specific unit of analysis. Around nine papers looked at entrepreneurs as a unit of analysis. Several articles (8) do, however, look into the role of educational institutions and development and research organizations in EEs. Only four papers examine the role of incubators in EEs. Because the focus should be on the system's key actors, this sampling unit is especially important for researching EEs (Entrepreneurs, both individual and corporate; Acs et al., 2017; Audretsch et al., 2007; Isenberg, 2010).

Table 1. Analysis of Methodology and Theoretical Foundation Entrepreneurial Ecosystems Papers

Analysis	No. of Articles
Methodology used	
Case study	23
Conceptual	13
Quantitate	9
Qualitative	8
Mixed mode	4
Theoretical foundation.	
Social capital theory	5
Social network theory	11
Stakeholder theory	4
Field theory	3
Institutional theory	7
Without specified theory	27

Source: The authors.

Theoretical Underpinning

Much research on EEs lacks a clear theoretical underpinning, with 27 papers mentioning no theory at all. Table 1 shows the various theoretical underpinnings. Theories at the macro level—primarily theories of social media, capital, and institutions—are used in a few research (Apa et al., 2017; Neumeyer et al., 2018). These concepts have been applied to the interpersonal characteristics and connections that exist within specific elements of EEs (e.g., between institutions and business angels; Kansheba & Wald, 2020).

Recent Entrepreneurial Ecosystems Research Works Findings

A cohesive ecosystem may improve the likelihood of entrepreneurs from various professions meeting, discussing

ideas and eventually agreeing to collaborate on a new business (Spigel, 2022). Understanding the essential factors behind the development of EEs will help policymakers make choices that will boost their local economy's competitiveness (Cho et al., 2021). The idea of a sustainable EE is a new approach in terms of EEs that promote long-term growth (Bischoff, 2019). Start-up companies and accelerators operate as a bridge between EE players and fintech entrepreneurs (Alaassar et al., 2021). The lifecycle model of the EE can be used to compare EEs in various stages of development in the same or other industries across the globe (Cantner et al., 2020). EEs are moulded by the country's economic growth, and high-growth companies have a stronger influence on the EE than young enterprises in general (Martínez-Fierro et al., 2019). Different types of connectivity enable the growth of the EE in smaller, outlying areas, as well as the formation of industries (Yamamura & Lassalle, 2019). Diverse regional institutions (the many characteristics of economic liberty) have different effects on regional entrepreneurship levels (Bennett, 2020). Despite significant government backing, the context makes innovation entrepreneurship tough (Biru et al., 2020).

An entrepreneurial culture, along with specialized stakeholder support and participation, are major key elements for a robust, long-term EE (Bischoff & Volkmann, 2018). As the ecosystem expands, governance shifts from hierarchical to relational; consequently, the responsibility of various players and support organizations shifts as well (Colombelli et al., 2017). Cultural aspects, government assistance programmes and domestic market dynamics are the most important EE variables that enable the development and operations of high-growth start-ups (Corrente et al., 2018). Within EEs, there are societal clusterings that specialize in specific sorts of entrepreneurship (Neumeyer et al., 2018). Many EE elements benefit women more than men globally, although depending on the level of economic growth, men may benefit more in specific circumstances (Hechavarría & Ingram, 2018).

Conceptual Framework

Entrepreneurial Ecosystems

Scholars and others involved in corporate practice and policy have yet to agree on a definition of EE. This is due in part to the fact that EE is expressed differently in different dimensions, research data and projects.

There are various explanations available, which allows for reviewing a limited number of EE definitions in chronological order (Table 2). EEs are a method aimed at boosting economic development by encouraging entrepreneurship, small business growth and innovation (Meshram & Rawani, 2019). The majority of the ideas expressed earlier emphasize the interaction or synthesis of factors, often through networks, to establish similar values

Table 2. Entrepreneurial Ecosystems: Conceptual Definitions

Author	Definition
Cohen (2005)	Sustainable EEs is defined as a network of players in a particular geographic community who are devoted to long-term development by supporting and fostering new sustainable ventures.
Isenberg (2010)	EEs are made up of elements that fall into six categories: (a) a favourable culture; (b) policy and leadership facilitation; (c) specific financing availability; (d) applicable human capital; (e) product-friendly markets; and (f) a comprehensive variety of infrastructure and institutional support.
Isenberg and Global (2011)	EEs are made up of 12 elements organized into six domains that, while distinctive because of their intricate interactions, must always be present if entrepreneurship is self-sustaining. As a result, while each combination is unique, proper regulations, markets, capital, people skills, culture and support are required for self-sustaining entrepreneurship.
Mason and Brown (2014)	EEs are a collection of interconnected entrepreneurial actors, organizations, institutions and processes.
Stam (2015)	An EE is a collection of interconnected players and circumstances that work together to enable fruitful entrepreneurship. As a result, entrepreneurship takes place in a community of autonomous actors, with the ecosystem's heart being formed by networks of entrepreneurs, leadership, funding, talent, information and support services. The ecosystem's success is determined by the presence of certain constituents and their interactions.
Audretsch and Belitski (2016)	The entrepreneurial system is defined by institutional and organizational players, as well as other systemic elements, which interact and impact the identification and commercialization of entrepreneurial possibilities.
Spigel (2017)	EEs are a collection of localized cultural perspectives, social networks, investment capital, universities and active economic policies that foster innovative ventures.
Theodoraki and Messeghem (2017)	EEs can be defined as a broad framework aimed at encouraging entrepreneurship in a specific region. As a result, both horizontal and vertical networks are covered by them. They also include public and private funding institutions, support groups, research organizations and corporate consortia that assist businesspeople. Physical and nonphysical elements appear to combine to generate EEs. Entrepreneurial regulation and culture, for example, are tied to geographical specificities.
Meshram and Rawani (2019)	EEs are a method aimed at boosting economic development by encouraging entrepreneurship, small business growth and innovation.

Source: The authors.

of the culture that support entrepreneurial activity. Cohen (2005) defines EE as a network of interrelated players committed to long-term development through the assistance and stimulation of sustainable future ventures in a certain geographic region. This emphasizes the relevance of formal and informal contacts in the local business environment as performance enablers. The emerging concept of a sustainable ecosystem and entrepreneurial innovative system proposed by (Brito & Leitão, 2020). Sustainable ecosystem is created by natural surroundings and the bodies live in them engaging with one another and with the surroundings. An EE, which is usually displayed as a diagram or list, includes several players or stakeholders, as well as several components that are required for the EE to function (Erina et al., 2017). The government's role in public policy is to feed the ecosystem (Stam, 2015), ensuring that the prerequisites for entrepreneurship to thrive are met (Brown et al., 2015; Isenberg & Global, 2011). In emerging economies, entrepreneurship orientation improves small and medium enterprises' financial and non-financial performance significantly (Khan et al., 2020).

EEs are a collection of interconnected entrepreneurial actors, organizations, institutions and processes (Mason & Brown, 2014). It is also the responsibility of the government to ensure that there are no unnecessary hurdles to entrepreneurship. Financial independence and specialized competency have the biggest impact on the venture's overall performance, followed by an entrepreneurial mentality and a supportive atmosphere (Matharu & Juneja, 2021a). The simplicity and administration of tax issues, the security of shareholders from lenders, and the creation and modernization of capital markets are all things that need to be addressed, and the streamlining of the termination of labour contracts, as well as support for the unemployed, are among the initiatives with this goal (Autio et al., 2014; Isenberg, 2010, Isenberg & Global, 2011;). Entrepreneurial competence has a considerable impact on a company's financial performance but has little impact on its non-financial performance (Kovid et al., 2021). Pickernell et al. (2013) state that entrepreneurial training is fundamental for providing information about the market and international situations, and that entrepreneurial leadership is becoming more widely used to assist communities in creating a more sustainable ecology (Emami, 2018; Packham et al., 2010). These EEs create an environment that supports the training of a skill set and flexible attitude (Jones & Jones, 2014). Because the contributions of entrepreneurs to the formation of an EE are not inevitable, capable businesspeople are necessary. Market and organizational factors were the most crucial predictor of e-commerce adoption by new firms (Mishra & Gupta, 2020). Local entrepreneurs serve as mentors and educators, resulting in a stream of entrepreneurs who create new things and expand their enterprises over time. When confronted with a critical situation (COVID–19), entrepreneurial skills such as creativity, adaptability, networking and consistency have a substantial and favourable impact on establishing the resilient mindset of women entrepreneurs (Matharu & Juneja, 2021b). Training is vital in the early stages of a business (Clarysse & Bruneel, 2007; Ramaciotti et al., 2016). Government organizations should encourage social media as a business model by creating faith in the system, in the hopes of encouraging students to engage in entrepreneurial activity on social media (Nawi et al., 2019). Physical and nonphysical elements appear to combine to generate EEs. Entrepreneurial regulation and culture, for example, are tied to geographical specificities (Theodoraki & Messeghem, 2017).

The Entrepreneurial Ecosystem's Composition and Relationships

Figure 7 displays a mash-up of characteristics of real worth, entrepreneurial actions and experiences (Stam, 2015). It is a structural representation of the EE's properties, as well as a social platform and organizational viewpoints (Alvedalen & Boschma, 2017). Entrepreneurial behaviour is defined as actions that benefit entrepreneurship and are generated from a critical component of the entrepreneurial mindset (Krueger, 2007). Scale-up, market development, opportunity recognition, start-up, economic development and entrepreneurial employees are all examples of entrepreneurial behaviour (Audretsch & Belitski, 2016). Entrepreneurship is a vehicle for creating economic, societal, and personal benefits through value creation (Neck & Greene, 2010). These elements, when combined with the ecosystem's interdependent actors, illustrate the wide range of interactions and relationships that occur in these systems(Stam, 2015). Spigel (2017) defines investment capital, historical perspectives of entrepreneurship, universities, cultural attitudes, networks, dealmakers and mentors, worker talent, physical infrastructure, support services regulations, markets and governance as qualities (social, cultural and material). Entrepreneurs gain from these characteristics since they supply them with resources and benefits, whereas relationships offer them with resources. Between the elements, EE is complemented by a variety of arrangements. Institutional viewpoints are introduced as collaboration and as additional layers relevant to the framework, to investigate the dynamics that occur inside these systems. This is to broaden our horizon and provide a better grasp of the ecosystem's composition and interrelationships.

Entrepreneurial Ecosystems, Elements, Actors, and Assets

Entrepreneurs are the players and components of the Entrepreneurial ecosystem (Isenberg, 2010); firms attract skilled workers and plan programs for their development (Brown et al., 2015). An entrepreneurial spirit is one in which institutions encourage entrepreneurial activities and positive feelings toward businesses, hence shaping entrepreneurship

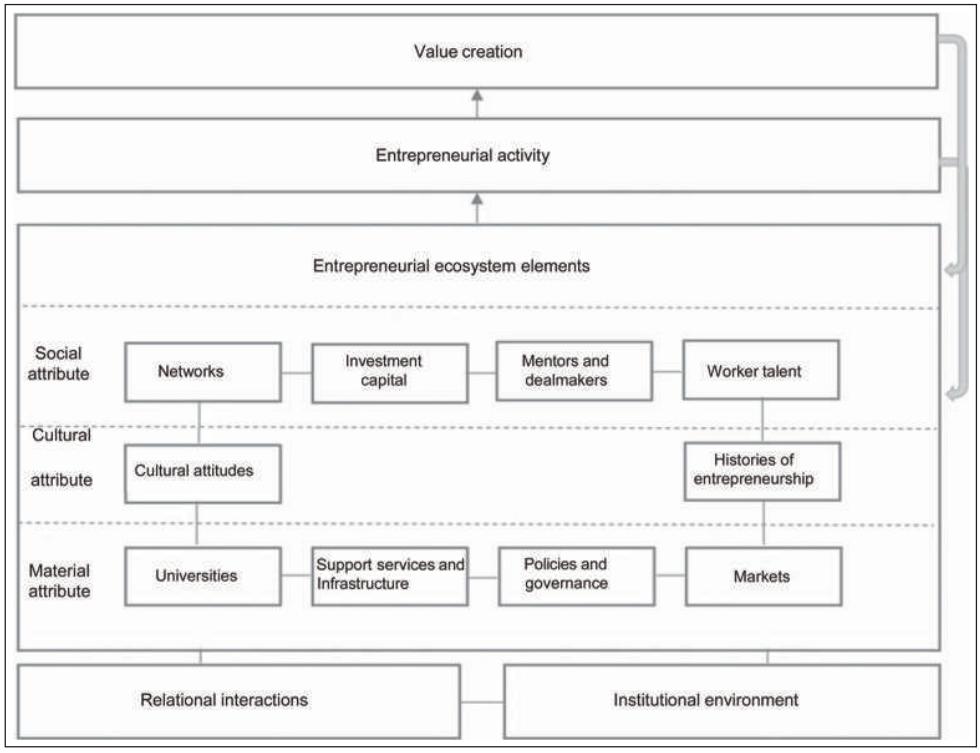


Figure 7. The Entrepreneurial Ecosystem's Composition and Relationships

Source: Adapted from Stam (2015) and Spigel (2017).

(Krueger et al., 2013; Liñán et al., 2015). Finance includes venture capital, accelerators and crowdfunding (Drover et al., 2017).

Financing is essential for entrepreneurship's success (Schwarzkopf, 2016). Supporting organizations can be found both inside and outside of colleges. Technology Transfer Offices (TTOs), scientific parks, accelerators and incubators within universities provide facilities and assistance for academicians and practitioners to create spin-offs as well as start-ups, allowing them to interface with the industry, organizations and government bodies (Bliemel et al., 2018; Wright et al., 2017). Other supportive institutions that assist to provide a lot of technical and business help include dealmakers, finance and professional associations (Connor et al., 2017). It was revealed that the process of new enterprise formation has typically relied substantially on a knowledge strategy in terms of resource generation and mobilization, as well as their link to EE (Kor et al., 2007).

Gaps in Theory and Practice of Entrepreneurial Ecosystems

Despite its widespread application in entrepreneurship policy, practice and study, the notion of EEs remains hampered by a lack of empirical research and a solid theoretical basis (Spigel & Harrison, 2017). There is a scarcity of reliable data on key ecosystem activities such as entrepreneurial relationships, information flows and cultural aspects like risk-taking and trust. Spigel and Harrison (2017) argued that the suggested procedure's viewpoint allows for good knowledge of how EEs work and affect entrepreneurial processes, allowing for more efficient policy actions. They also advocate empirical investigation to support the framework and ideas they provide. The formation of rules and practices that are not well-informed being targeted at supporting entrepreneurial growth has resulted from an absence of logical consistency that is conceptually motivated (Stam, 2015). These ideas are often used to describe the related characteristics and linkages that exist among specific EE components (e.g., business incubators and universities).

A more comprehensive theoretical framework is required to describe and explain how EEs emerge and function from an entrepreneur-centric perspective. The uniqueness of the EE and the related idea has received little attention (Cao & Shi, 2020). Regional actors build and develop EEs, resulting in just winners. The structure may be lacking in governance, and the interplay of the elements may be ineffective (Hakala et al., 2019). There is a lack of EEs theory linking the regional, social and political context to company outcomes, including development, existence, globalization and invention (Autio et al., 2018).

Furthermore, the majority of the articles assessed were conceptual-based research, which are contributions that lack empirical backing (Colombo et al., 2017; Roundy, 2017). More studies are required to study how the various parts of EEs contribute to entrepreneurship (Alvedalen & Boschma, 2017).

The few empirical studies on innovation enterprises in global markets are limited (Apa et al., 2017; Audretsch et al., 2007). EEs are notorious for having a deficit of high-quality entrepreneurship-supporting firms. Private actors, in particular, can be scarce in certain nations and can perform a critical role in the development of EEs (Sheriff & Muffatto, 2015). Another flaw is that EEs are primarily concerned with start-ups (Isenberg & Global, 2011). Previous research has concentrated on identifying elements without taking into account their interrelationships. Understanding ecological dynamics is difficult due to a complete lack of knowledge of how EEs elements interact (Motoyama & Knowlton, 2017). Another issue is the evaluation and performance of EEs (Spigel, 2017). Within the EEs, the significance of interactions between individual components has not been fully investigated (Motoyama & Watkins, 2014). The significance of networks within EEs has still not been adequately investigated (Wal & Boschma, 2011).

Conclusion

We extensively examined the literature on the growing notion of EEs in this review. Because there is no commonly agreed definition of EE, more investigation is needed to obtain better knowledge that was previously explored and even to suggest a brand new idea of the EE. As a result, this SLR concentrates on already published research, locating flaws that have to be filled explored in any future study that will be conducted in addition to building a better comprehension of the literature's impact on invention in several ways, particularly clusters and open innovation in developing an integrated approach to the EE. Furthermore, we have emphasized that conceptualizing the concept of EEs is still required. EEs are a little-understood phenomenon, according to the study, with recent research dominated by conceptual studies.

This work also contributes to knowledge development and provides more suggestions for future studies by using systematic literature methodologies, conceptual framework analysis and descriptive analysis. This review paper addresses a gap in EE research by enhancing knowledge of the concerns and obstacles that entrepreneurs face. The literature was organized into five stages: (a) constructing the SLR research questions and defining the standards for study inclusion and exclusion; (b) seeking proof; (c) evaluating and choosing articles and collecting evidence; (d) assessing the studies' research quality; and (e) displaying the findings. When it comes to the first research question, the conceptualization of an EE can be done in the following terms: an EE is a collection of individual actors and elements that work together to promote entrepreneurship in a certain area. Regarding the second SLR research question, academicians and researchers have been interested in the notion since 2000, with a large number of articles published between 2017 and 2021. Because of the start-up community, the EE has grown in prominence in recent years. Many studies of the EE have progressed over time in terms of industry focus, country focus, theory focus and methodology focus.

The third SLR question identifies new research pathways for EEs. Encouraging EEs in the agriculture industry, service sector, oil and industries could have a substantial impact on economic development and growth. Another topic of a future research direction that should be looked into is the necessity of assessing the diversity, transparency and quality of organizations and their governance for the long-term growth of EEs.

Future Research Directions

The notion of EEs is still understudied, according to our findings. The majority of the contributions are intellectual, demonstrating an awareness of the various aspects that contribute to the creation of favourable business ecosystems. As a result, we believe that further empirical study is needed, particularly in regard to potential causal relationships between EE features, context factors, outputs and outcomes. Future research should look into how and in what ways industrial change benefits firms in having productive entrepreneurs. This can be accomplished by concentrating more on technical studies, as our data reveal a scarcity of such articles. In most underdeveloped nations, agriculture is one of the most important economic sectors (Kansheba, 2020). Agricultural entrepreneurship obtains little emphasis in studies despite its importance to the economy. As a result, we advise that more research be done on how to build agricultural entrepreneurship ecosystems. More research is needed to better understand how EEs evolve through several phases of the lifecycle at the macro, meso and micro levels. Another area of future research that might be explored is the significance of evaluating the diversity, transparency and quality of organizations and their governance for the EE's long-term growth.

Promoting entrepreneurial growth in the primary sector is one of the best and most productive strategies (Parlee, 2015). To achieve efficient entrepreneurial growth in the gas and oil industry, countries must first gain a better knowledge of how the sector's various entrepreneurial individuals and processes interact. Encouragement of EEs in the gas and oil industry could have a significant economic impact. Platform innovations are frequently unintentional and unplanned, depending instead on market conditions. This means that entrepreneurs have the freedom to explore their ideas but might be coerced into making certain

investments that result in innovative products and services. As a result, more research into how platform technologies enable new types of entrepreneurship to emerge is required. The service industry accounts for up to 70% of GDP in industrialized economies, according to the flagship report of the World Bank. Even in developing economies, the service industry is critical; it accounts for approximately 50% of GDP in Sub-Saharan Africa. As a result, encouraging EEs in this industry could have a substantial impact on economic development and growth. Investors, academia, universities, accelerators and incubators are the primary ecosystem entities in emerging economies. More research is required on how other stakeholders, such as chambers of commerce, industry groups, and non-profit and private organizations, can help to build strong EEs.

Future research direction in EEs should focus on how diverse emotional characteristics, such as assertiveness or submissiveness, influence an EE. More research is needed in the EE to link the debate over social responsibilities and duties to an actor's position in the EE. We want to encourage more research on how to quantify the effectiveness of EEs and their influence on the establishment and long-term viability of sustainable businesses. Future studies should focus on determining whether ecosystems that are successful in encouraging traditional entrepreneurship are also important in encouraging a sustainable EE.

Declaration of Conflicting Interests

The authors declared no potential conflicts of interest concerning this article's research, authorship, and/or publication.

Funding

This research received no specific grant from any funding agency in the public, commercial, or not-for-profit sectors. The authors received no financial support for the research, authorship and/or publication of this article.

ORCID iD

Rahul Krushnaji Wadichar https://orcid.org/0000-0001-5539-5183

References

Ács, Z. J., Autio, E., & Szerb, L. (2014). National systems of entrepreneurship: measurement issues and policy implications. *Research Policy*, *43*(3), 476–494. https://doi.org/10.1016/j.respol.2013.08.016

Acs, Z. J., Stam, E., Audretsch, D. B., & O'Connor, A. (2017). The lineages of the entrepreneurial ecosystem approach. *Small Business Economics*, *49*(1), 1–10. https://doi.org/10.1007/s11187–017–9864–8

Alaassar, A., Mention, A. L., & Aas, T. H. (2021). Ecosystem dynamics: Exploring the interplay within fintech entrepreneurial ecosystems. *Small Business Economics*, *58*(4), 2157–2182. https://doi.org/10.1007/s11187–021–00505–5

Alum, R. A., & Drucker, P. F. (1986). Innovation and entrepreneurship: Practice and principles. *Public Productivity Review*, *10*(1), 105. https://doi.org/10.2307/3380320

Alvedalen, J., & Boschma, R. (2017). A critical review of entrepreneurial ecosystems research: Towards a future research agenda. *European Planning Studies*, *25*(6), 887–903. https://doi.org/10.1080/09654313.2017.1299694

Apa, R., Grandinetti, R., & Sedita, S. R. (2017). The social and business dimensions of a networked business incubator: The case of H-Farm. *Journal of Small Business and Enterprise Development*, *24*(2), 198–221. https://doi.org/10.1108/jsbed–07–2016–0103

Atiase, V. Y., Mahmood, S., Wang, Y., & Botchie, D. (2017). Developing entrepreneurship in Africa: Investigating critical resource challenges. *Journal of Small Business and Enterprise Development*, *25*(4), 644–666. https://doi.org/10.1108/jsbed–03–2017–0084

Audretsch, D. B., & Belitski, M. (2016). Entrepreneurial ecosystems in cities: Establishing the framework conditions. *The Journal of Technology Transfer*, *42*(5), 1030–1051. https://doi.org/10.1007/s10961–016–9473–8

Audretsch, D. B., Grilo, I., & Thurik, A. R. (2007). Explaining entrepreneurship and the role of policy: A framework. In *Handbook of research on entrepreneurship policy*. https://doi.org/10.4337/9781847206794.00005

Autio, E., Kenney, M., Mustar, P., Siegel, D., & Wright, M. (2014). Entrepreneurial innovation: The importance of context. *Research Policy*, *43*(7), 1097–1108. https://doi.org/10.1016/j.respol.2014.01.015

Autio, E., Nambisan, S., Thomas, L. D. W., & Wright, M. (2018). Digital affordances, spatial affordances, and the genesis of entrepreneurial ecosystems. *Strategic Entrepreneurship Journal*, *12*(1), 72–95. https://doi.org/10.1002/sej.1266

Bennett, D. L. (2020). Local institutional heterogeneity & firm dynamism: Decomposing the metropolitan economic freedom index. *Small Business Economics*, *57*(1), 493–511. https://doi.org/10.1007/s11187–020–00322–2

Biru, A., Gilbert, D., & Arenius, P. (2020). Unhelpful help: The state of support programmes and the dynamics of entrepreneurship ecosystems in Ethiopia. *Entrepreneurship & Regional Development*, *33*(1–2), 108–130. https://doi.org/10.1080/08985626.2020.1734267

Bischoff, K. (2019). A study on the perceived strength of sustainable entrepreneurial ecosystems on the dimensions of stakeholder theory and culture. *Small Business Economics*, *56*(3), 1121–1140. https://doi.org/10.1007/s11187–019–00257–3

Bischoff, K., & Volkmann, C. K. (2018). Stakeholder support for sustainable entrepreneurship—A framework of sustainable entrepreneurial ecosystems. *International Journal of Entrepreneurial Venturing*, *10*(2), 172. https://doi.org/10.1504/ijev.2018.092714

Bliemel, M., Flores, R., de Klerk, S., & Miles, M. P. (2018). Accelerators as start-up infrastructure for entrepreneurial clusters. *Entrepreneurship & Regional Development*, *31*(1–2), 133–149. https://doi.org/10.1080/08985626.2018.1537152

Brito, S., & Leitão, J. (2020). Mapping and defining entrepreneurial ecosystems: A systematic literature review. *Knowledge Management Research & Practice*, *19*(1), 21–42. https://doi.org/10.1080/14778238.2020.1751571

Brown, R., Gregson, G., & Mason, C. (2015). A post-mortem of regional innovation policy failure: Scotland's intermediate technology initiative (ITI). *Regional Studies*, *50*(7), 1260–1272. https://doi.org/10.1080/00343404.2014.985644

Cantner, U., Cunningham, J. A., Lehmann, E. E., & Menter, M. (2020). Entrepreneurial ecosystems: A dynamic lifecycle

model. *Small Business Economics*, *57*(1), 407–423. https://doi.org/10.1007/s11187–020–00316–0

Cao, Z., & Shi, X. (2020). A systematic literature review of entrepreneurial ecosystems in advanced and emerging economies. *Small Business Economics*, *57*(1), 75–110. https://doi.org/10.1007/s11187–020–00326-y

Cho, D. S., Ryan, P., & Buciuni, G. (2021). Evolutionary entrepreneurial ecosystems: A research pathway. *Small Business Economics*, *58*(4), 1865–1883. https://doi.org/10.1007/s11187–021–00487–4

Clarysse, B., & Bruneel, J. (2007). Nurturing and growing innovative start-ups: The role of policy as integrator. *R&D Management*, *37*(2), 139–149. https://doi.org/10.1111/j.1467–9310.2007.00463.x

Cohen, B. (2005). Sustainable valley entrepreneurial ecosystems. *Business Strategy and the Environment*, *15*(1), 1–14. https://doi.org/10.1002/bse.428

Colombelli, A., Paolucci, E., & Ughetto, E. (2017). Hierarchical and relational governance and the life cycle of entrepreneurial ecosystems. *Small Business Economics*, *52*(2), 505–521. https://doi.org/10.1007/s11187–017–9957–4

Colombo, M. G., Dagnino, G. B., Lehmann, E. E., & Salmador, M. (2017). The governance of entrepreneurial ecosystems. *Small Business Economics*, *52*(2), 419–428. https://doi.org/10.1007/s11187–017–9952–9

Cook, D. J. (1997). Systematic reviews: Synthesis of best evidence for clinical decisions. *Annals of Internal Medicine*, *126*(5), 376. https://doi.org/10.7326/0003–4819–126–5–199703010–00006

Connor, A., Stam, E., Sussan, F., & Audretsch, D. B. (2017). Entrepreneurial ecosystems: The foundations of place-based renewal. In A. O'Connor, E. Stam, F. Sussan, & D. B. Audretsch (Eds), *Entrepreneurial ecosystems* (International Studies in Entrepreneurship Series Vol. 18, 1–21. https://doi.org/10.1007/978–3–319–63531–6_1

Corrente, S., Greco, S., Nicotra, M., Romano, M., & Schillaci, C. E. (2018). Evaluating and comparing entrepreneurial ecosystems using SMAA and SMAA-S. *The Journal of Technology Transfer*, *44*(2), 485–519. https://doi.org/10.1007/s10961–018–9684–2

Cowell, M., Lyon-Hill, S., & Tate, S. (2018). It takes all kinds: Understanding diverse entrepreneurial ecosystems. *Journal of Enterprising Communities: People and Places in the Global Economy*, *12*(2), 178–198. https://doi.org/10.1108/jec–08–2017–0064

Dedehayir, O., Mäkinen, S. J., & Roland Ortt, J. (2018). Roles during innovation ecosystem genesis: A literature review. *Technological Forecasting and Social Change*, *136*, 18–29. https://doi.org/10.1016/j.techfore.2016.11.028

Drover, W., Busenitz, L., Matusik, S., Townsend, D., Anglin, A., & Dushnitsky, G. (2017). A review and road map of entrepreneurial equity financing research: Venture capital, corporate venture capital, angel investment, crowdfunding, and accelerators. *Journal of Management*, *43*(6), 1820–1853. https://doi.org/10.1177/0149206317690584

Emami, A. (2018). [Review of the book *Entrepreneurial Universities: Collaboration, Education, and Policies* by J. Ferreira, A. Fayolle, V. Ratten & Mario Raposo, Eds. *International Entrepreneurship and Management Journal*, *14*(4), 1131–1133. https://doi.org/10.1007/s11365–018–0535–2

Erina, I., Shatrevich, V., & Gaile-Sarkane, E. (2017). Impact of stakeholder groups on development of a regional entrepreneurial ecosystem. *European Planning Studies*, *25*(5), 755–771. https://doi.org/10.1080/09654313.2017.1282077

Giudice, M., Nicotra, M., Romano, M., & Schillaci, C. E. (2016). Entrepreneurial performance of principal investigators and country culture: Relations and influences. *The Journal of Technology Transfer*, *42*(2), 320–337. https://doi.org/10.1007/s10961–016–9499-y

Gustafsson, R., Jääskeläinen, M., Maula, M., & Uotila, J. (2015). Emergence of industries: A review and future directions. *International Journal of Management Reviews*, *18*(1), 28–50. https://doi.org/10.1111/ijmr.12057

Hakala, H., O'Shea, G., Farny, S., & Luoto, S. (2019). Re-storying the business, innovation and entrepreneurial ecosystem concepts: The model-narrative review method. *International Journal of Management Reviews*, *22*(1), 10–32. https://doi.org/10.1111/ijmr.12212

Hechavarría, D. M., & Ingram, A. E. (2018). Entrepreneurial ecosystem conditions and gendered national-level entrepreneurial activity: A 14-year panel study of GEM. *Small Business Economics*, *53*(2), 431–458. https://doi.org/10.1007/s11187–018–9994–7

Isenberg, D. J. (2010). How to start an entrepreneurial revolution. *Harvard Business Review*, *88(6)*, 40–50. https://hbr.org/2010/06/the-big-idea-how-to-start-an-entrepreneurial-revolution

Isenberg, D., & Global. (2011). The Entrepreneurship ecosystem strategy as a new paradigm for economic policy: Principles for cultivating entrepreneurship. *Institute of International and European Affairs, Dublin, Ireland,* 1–13. http://www.innovationamerica.us/images/stories/2011/The-entrepreneurship-ecosystem-strategy-for-economic-growth-policy-20110620183915.pdf

Jones, P., & Jones, A. (2014). Attitudes of sports development and sports management undergraduate students towards entrepreneurship. *Education + Training*, *56*(8/9), 716–732. https://doi.org/10.1108/et–06–2014–0060

Kansheba, J. M. P. (2020). Small business and entrepreneurship in Africa: The nexus of entrepreneurial ecosystems and productive entrepreneurship. *Small Enterprise Research*, *27*(2), 110–124. https://doi.org/10.1080/13215906.2020.1761869

Kansheba, J. M. P., & Wald, A. E. (2020). Entrepreneurial ecosystems: A systematic literature review and research agenda. *Journal of Small Business and Enterprise Development*, *27*(6), 943–964. https://doi.org/10.1108/jsbed–11–2019–0364

Khan, R. U., Salamzadeh, Y., Kawamorita, H., & Rethi, G. (2020). Entrepreneurial orientation and small and medium-sized enterprises' performance: Does 'access to finance' moderate the relation in emerging economies? *Vision: The Journal of Business Perspective*, *25*(1), 88–102. https://doi.org/10.1177/0972262920954604

Kor, Y. Y., Mahoney, J. T., & Michael, S. C. (2007). Resources, capabilities and entrepreneurial perceptions. *Journal of Management Studies*, *44*(7), 1187–1212. https://doi.org/10.1111/j.1467–6486.2007.00727.x

Kovid, R. K., Bhati, B., & Sharma, G. M. (2021). Entrepreneurial competencies, institutional voids and performance of small and medium enterprises: Evidence from an emerging economy. *Vision: The Journal of Business Perspective*, 097226292110588. https://doi.org/10.1177/09722629211058809

Kraus, S., Breier, M., & Dasí-Rodríguez, S. (2020). The art of crafting a systematic literature review in entrepreneurship research. *International Entrepreneurship and Management Journal*, *16*(3), 1023–1042. https://doi.org/10.1007/s11365–020–00635–4

Krueger, N. F. (2007). What lies beneath? The experiential essence of entrepreneurial thinking. *Entrepreneurship Theory and Practice*, *31*(1), 123–138. https://doi.org/10.1111/j.1540–6520.2007.00166.x

Krueger, N., Liñán, F., & Nabi, G. (2013). Cultural values and entrepreneurship. *Entrepreneurship & Regional Development*, *25*(9–10), 703–707. https://doi.org/10.1080/08985626.2013.862961

Kshetri, N. (2014). Developing successful entrepreneurial ecosystems. *Baltic Journal of Management*, *9*(3), 330–356. https://doi.org/10.1108/bjm–09–2013–0146

Liñán, F., & Fayolle, A. (2015). A systematic literature review on entrepreneurial intentions: Citation, thematic analyses, and research agenda. *International Entrepreneurship and Management Journal*, *11*(4), 907–933. https://doi.org/10.1007/s11365–015–0356–5

Liñán, F., Jaén, I., & Ortega, F. J. (2015). Understanding the role of culture and economic conditions in entrepreneurship. *Entrepreneurship, Regional Development and Culture*, 53–73. https://doi.org/10.1007/978–3–319–15111–3_4

Malecki, E. J. (2018). Entrepreneurship and entrepreneurial ecosystems. *Geography Compass*, *12*(3), e12359. https://doi.org/10.1111/gec3.12359

Maroufkhani, P., Wagner, R., & Wan Ismail, W. K. (2018). Entrepreneurial ecosystems: A systematic review. *Journal of Enterprising Communities: People and Places in the Global Economy*, *12*(4), 545–564. https://doi.org/10.1108/jec–03–2017–0025

Martínez-Fierro, S., Biedma-Ferrer, J. M., & Ruiz-Navarro, J. (2019). Impact of high-growth start-ups on entrepreneurial environment based on the level of national economic development. *Business Strategy and the Environment*, *29*(3), 1007–1020. https://doi.org/10.1002/bse.2413

Mary George, N., Parida, V., Lahti, T., & Wincent, J. (2014). A systematic literature review of entrepreneurial opportunity recognition: Insights on influencing factors. *International Entrepreneurship and Management Journal*, *12*(2), 309–350. https://doi.org/10.1007/s11365–014–0347-y

Mason, B., & Brown, R. (2014). *Entrepreneurial ecosystems and growth-oriented entrepreneurship*. OECD LEED Programme and the Dutch Ministry of Economic Affairs. https://www.oecd.org/cfe/leed/Entrepreneurial-ecosystems.pdf

Matharu, S. K., & Juneja, D. (2021a). Factors impacting resilience of women entrepreneurs in India in the face of COVID–19. *Vision: The Journal of Business Perspective*. https://doi.org/10.1177/09722629211043299

Matharu, S. K., & Juneja, D. (2021b). The influence of perceived motivational factors on success of women-driven ventures and their contribution in economic development. *Vision: The Journal of Business Perspective*. https://doi.org/10.1177/09722629211008268

Meshram, S. A., & Rawani, A. M. (2019). Understanding entrepreneurial ecosystem. *International Journal of Social Ecology and Sustainable Development*, *10*(3), 103–115. https://doi.org/10.4018/ijsesd.2019070107

Mishra, O. N., & Gupta, S. (2020). Antecedents and impact of e-commerce adoption among new venture firms: Evidence from tourism and hospitality industry. *Vision: The Journal of Business Perspective*, *24*(4), 431–440. https://doi.org/10.1177/0972262920927940

Moher, D., Liberati, A., Tetzlaff, J., & Altman, D. G. (2009). Preferred reporting items for systematic reviews and meta-analyses: The PRISMA statement. *Journal of Clinical Epidemiology*, *62*(10), 1006–1012. https://doi.org/10.1016/j.jclinepi.2009.06.005

Motoyama, Y., & Knowlton, K. (2017). Examining the connections within the startup ecosystem: A case study of St. Louis. *Entrepreneurship Research Journal*, *7*(1). https://doi.org/10.1515/erj–2016–0011

Motoyama, Y., & Watkins, K. K. (2014). Examining the Connections within the startup ecosystem: A case study of St. Louis. https://doi.org/10.2139/ssrn.2498226

Nawi, N. C., Mamun, A. A., Nasir, N. A. M., & Muniady, R. (2019). Factors affecting the adoption of social media as a business platform: A study among student entrepreneurs in Malaysia. *Vision: The Journal of Business Perspective*, *23*(1), 1–11. https://doi.org/10.1177/0972262918821200

Neck, H. M., & Greene, P. G. (2010). Entrepreneurship education: Known worlds and new frontiers. *Journal of Small Business Management*, *49*(1), 55–70. https://doi.org/10.1111/j.1540–627x.2010.00314.x

Neumeyer, X., Santos, S. C., & Morris, M. H. (2018). Who is left out: Exploring social boundaries in entrepreneurial ecosystems? *The Journal of Technology Transfer*, *44*(2), 462–484. https://doi.org/10.1007/s10961–018–9694–0

Packham, G., Jones, P., Miller, C., Pickernell, D., & Thomas, B. (2010). Attitudes towards entrepreneurship education: A comparative analysis. *Education + Training*, *52*(8/9), 568–586. https://doi.org/10.1108/00400911011088926

Parlee, B. L. (2015). Avoiding the resource curse: Indigenous communities and Canada's oil sands. *World Development*, *74*, 425–436. https://doi.org/10.1016/j.worlddev.2015.03.004

Pickernell, D., Senyard, J., Jones, P., Packham, G., & Ramsey, E. (2013). New and young firms. *Journal of Small Business and Enterprise Development*, *20*(2), 358–382. https://doi.org/10.1108/14626001311326770

Ramaciotti, L., Muscio, A., & Rizzo, U. (2016). The impact of hard and soft policy measures on new technology-based firms. *Regional Studies*, *51*(4), 629–642. https://doi.org/10.1080/00343404.2016.1255319

Roundy, P. T. (2017). 'Small town' entrepreneurial ecosystems. *Journal of Entrepreneurship in Emerging Economies*, *9*(3), 238–262. https://doi.org/10.1108/jeee–09–2016–0040

Sambo, W. (2018). A conceptual study of an intrapreneurship ecosystem at South African universities. *Problemy Zarzadzania*, *2018*(73), 192–215. https://doi.org/10.7172/1644–9584.73.12

Schmitz, A., Urbano, D., Dandolini, G. A., de Souza, J. A., & Guerrero, M. (2016). Innovation and entrepreneurship in the academic setting: A systematic literature review. *International Entrepreneurship and Management Journal*, *13*(2), 369–395. https://doi.org/10.1007/s11365–016–0401-z

Schwarzkopf, C. (2016). *Fostering innovation and entrepreneurship: Entrepreneurial ecosystem and entrepreneurial fundamentals in the USA and Germany*. https://doi.org/10.1007/978–3–658–13512–6

Sheriff, M., & Muffatto, M. (2015). The present state of entrepreneurship ecosystems in selected countries in Africa. *African Journal of Economic and Management Studies*, *6*(1), 17–54. https://doi.org/10.1108/ajems–10–2012–0064

Snyder, H. (2019). Literature review as a research methodology: An overview and guidelines. *Journal of Business Research*, *104*, 333–339. https://doi.org/10.1016/j.jbusres.2019.07.039

Spigel, B. (2017). The relational organization of entrepreneurial ecosystems. *Entrepreneurship Theory and Practice*, *41*(1), 49–72. https://doi.org/10.1111/etap.12167

Spigel, B. (2022). Examining the cohesiveness and nestedness entrepreneurial ecosystems: Evidence from British FinTechs. *Small Business Economics*. https://doi.org/10.1007/s11187–021–00589-z

Spigel, B., & Harrison, R. (2017). Toward a process theory of entrepreneurial ecosystems. *Strategic Entrepreneurship Journal*, *12*(1), 151–168. https://doi.org/10.1002/sej.1268

Stam, E. (2015). Entrepreneurial ecosystems and regional policy: A sympathetic critique. *European Planning Studies*, *23*(9), 17591769. https://doi.org/10.1080/09654313.2015.1061484

Theodoraki, C., & Messeghem, K. (2017). Exploring the entrepreneurial ecosystem in the field of entrepreneurial support: A multi-level approach. *International Journal of Entrepreneurship and Small Business*, *31*(1), 47. https://doi.org/10.1504/ijesb.2017.083847

Torraco, R. J. (2005). Writing integrative literature reviews: Guidelines and examples. *Human Resource Development Review*, *4*(3), 356–367. https://doi.org/10.1177/1534484305278283

Tranfield, D., Denyer, D., & Smart, P. (2003). Towards a methodology for developing evidence-informed management knowledge by means of systematic review. *British Journal of Management*, *14*(3), 207–222. https://doi.org/10.1111/1467–8551.00375

Ucbasaran, D., Westhead, P., & Wright, M. (2001). The focus of entrepreneurial research: contextual and process issues. *Entrepreneurship Theory and Practice*, *25*(4), 57–80. https://doi.org/10.1177/104225870102500405

Wal, A. L. J., & Boschma, R. (2011). Co-evolution of firms, industries and networks in space. *Regional Studies*, *45*(7), 919–933. https://doi.org/10.1080/00343400802662658

Welter, F. (2011). Contextualizing entrepreneurship—Conceptual challenges and ways forward. *Entrepreneurship Theory and Practice*, *35*(1), 165–184. https://doi.org/10.1111/j.1540–6520.2010.00427.x

Wright, M., Siegel, D. S., & Mustar, P. (2017). An emerging ecosystem for student start-ups. *The Journal of Technology Transfer*, *42*(4), 909–922. https://doi.org/10.1007/s10961–017–9558-z

Yamamura, S., & Lassalle, P. (2019). Proximities and the emergence of regional industry: Evidence of the liability of smallness in Malta. *European Planning Studies*, *28*(2), 380–399. https://doi.org/10.1080/09654313.2019.1668915

Yue, L., & Rivera, J. P. R. (2021). Probing Chinese perception on the importance of social capital in entrepreneurial success. *Vision: The Journal of Business Perspective*, 097226292110025. https://doi.org/10.1177/09722629211002573

Zahra, S. A., & Nambisan, S. (2011). Entrepreneurship in global innovation ecosystems. *AMS Review*, *1*(1), 4–17. https://doi.org/10.1007/s13162–011–0004–3

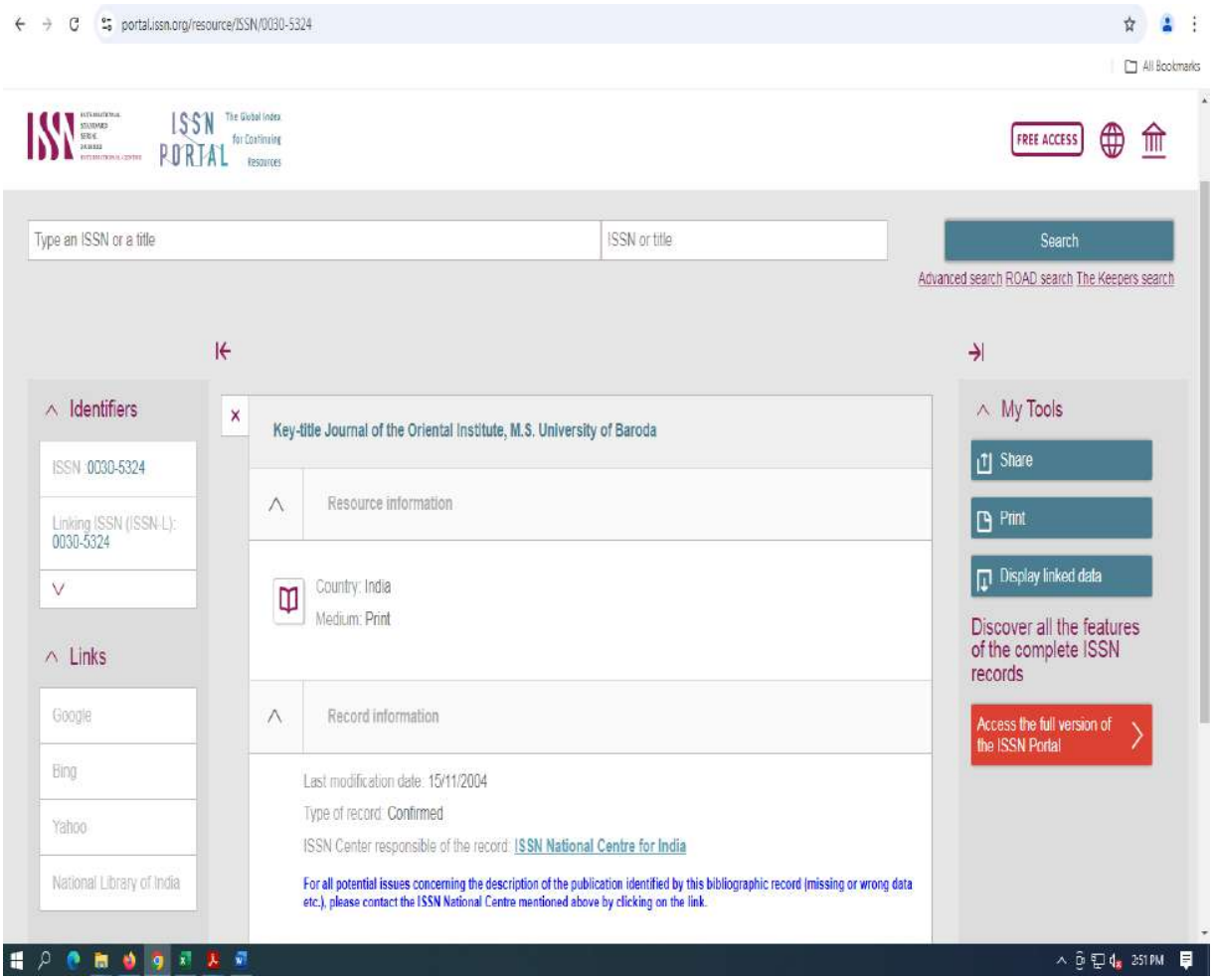
Zahra, S. A., & Nambisan, S. (2012). Entrepreneurship and strategic thinking in business ecosystems. *Business Horizons*, *55*(3), 219–229. https://doi.org/10.1016/j.bushor.2011.12.004

About the Authors

Rahul Krushnaji Wadichar (rahulwadichar@gmail.com) is a PhD Scholar at the Department of Management Science & Research J.M Patel College, Bhandara, Maharashtra (India). His main research topics are related to the entrepreneurship development and impact of government policies and initiatives on start-up growth and development.

Prashant Manusmare (dmsr.4103@gmail.com) is an Assistant Professor of Management faculty of Department Management science & Research J.M Patel College, Bhandara, Maharashtra (India). His primary research interests focus on entrepreneurship financing, international business networks, marketing and social entrepreneurship. He has published many research papers in referred journal like International Journal of Commerce and Management Studies, Radix international journal of research in marketing.

Mukul Abasaheb Burghate (mukulburghate@gmail.com) is an Associate Professor of Management faculty Department of Business Management & Research, Dr. Punjabrao Deshmukh Institute of Management Technology and Research, Nagpur, Maharashtra (India). He has published many research papers in referred journal like international journal of social sciences & interdisciplinary research, International Journal of Commerce and Management Studies, International Journal of Management.


portal.issn.org/resource/ISSN/0030-5324
All Bookmarks
ISSN PORTAL
The Global Index for Continuing Resources
FREE ACCESS
Type an ISSN or a title
ISSN or title
Search
Advanced search ROAD search The Keepers search
Identifiers
ISSN 0030-5324
Linking ISSN (ISSN-L): 0030-5324
Links
Google
Bing
Yahoo
National Library of India
Key-title Journal of the Oriental Institute, M.S. University of Baroda
Resource information
Country: India
Medium: Print
Record information
Last modification date: 15/11/2004
Type of record: Confirmed
ISSN Center responsible of the record: ISSN National Centre for India
For all potential issues concerning the description of the publication identified by this bibliographic record (missing or wrong data etc.), please contact the ISSN National Centre mentioned above by clicking on the link.
My Tools
Share
Print
Display linked data
Discover all the features of the complete ISSN records
Access the full version of the ISSN Portal
2:51 PM

Already have a manuscript?

Use our Manuscript Matcher to find the best relevant journals!

Find a Match

Refine Your Search Results

0972-2629 Search

Sort By: Title (A-Z)

Search Results

Found 1 results (Page 1) Share These Results

Exact Match Found

VISION-THE JOURNAL OF BUSINESS PERSPECTIVE

Publisher: SAGE PUBLICATIONS INDIA PVT LTD , B-1-I-1 MOHAN CO-OPERATIVE INDUSTRIAL AREA, MATHURA RD, POST BAG NO 7, NEW DELHI, INDIA, 110 044

ISSN / eISSN: 0972-2629 / 2249-5304

Web of Science Core Collection: Emerging Sources Citation Index

Share This Journal View profile page

** Requires free login.*

Filters Clear All

Web of Science Coverage

Open Access

Category

Country / Region

Language

Frequency

Journal Citation Reports

1 – 1 of 1

Items per page: 10

Materials Today: Proceedings xxx (xxxx) xxx

Contents lists available at ScienceDirect

Materials Today: Proceedings

journal homepage: www.elsevier.com/locate/matpr

Synthesis of copolymer and its composites with carbon and their photoluminescence studies

Yashpal U. Rathod [a], Vikram U. Pandit [b], Devidas S. Bhagat [c], Wasudeo B. Gurnule [d,*]

[a] Department of Chemistry, J. M. Patel College, Bhandara 441904, M. S., India
[b] Department of Chemistry, H. V. Desai College, Pune 04, M. S., India
[c] Department of Forensic Chemistry and Toxicology, Government Institute of Forensic Science, Aurangabad 431004, M. S., India
[d] Department of Chemistry, Kamla Nehru Mahavidyalaya, Nagpur 440024, M. S., India

ARTICLE INFO

Article history:
Available online xxxx

Keywords:
Copolymer
Composites
Photoluminescence
Morphology
NMR
FTIR

ABSTRACT

The photoluminescence study of a copolymer and its copolymer/ carbon composite was studied using a novel comparative account. 8-hydroxyquinoline5-sulphonic acid and phthalic acid with formaldehyde were used to prepare the new composite. Various characterization techniques, such as elemental analysis, FTIR, UV–Visible, NMR (^{13}C and ^{1}H), and SEM, were used to examine the structure and characteristics of the copolymer and copolymer/carbon composite. The photoluminescence residences of lately included copolymer composites was measured on RF-501 (PC) S CE (LVD) MODEL. The factor of this present research is to supply the cooperative help amongst design and photoluminescence via new and essential commitments from dynamic specialists within the area.
Copyright © 2022 Elsevier Ltd. All rights reserved.
Selection and peer-review under responsibility of the scientific committee of the Polymer & Mediterranean Fiber International Conference2021.

1. Introduction

As of late, there has been apparent advancement in the improvement of polymeric substances showing the capacity of iridescence. The photoluminescent materials utilized so far are being supplanted with a lot less expensive natural mixtures which do not emit harmful radiation, especially hydrocarbon subordinates of naphthalene. These mixtures with one of kind glowing properties are researched and utilized as fluorophores [1–2]. Preparation of polymer composites containing nano-sized particles of silver sulphide involves extraordinary logical and functional interest. Magerrmov et al. [3] prepared polymer nanocomposites based on polypropylene pp+ Ag_2S. It is expected that critical reduction in the intensity of the luminescence at high concentrations might be because of the phenomenon of concentration quenching and decline of the particular surface of the nanoparticles in a polymer matrix. The research centered on the phenomenon of photoluminescence present in the monomer 2,7-NAF.DM and its copolymers with different commercial monomers [4–5]. Posudievsky and colleagues concentrated on the improved and tuneable photoluminescence of polyphenylenevinylenes confined in nanocomposite films [6].

Jamaludin et al. [7] prepared photoluminescent carbon specks (CD), one of the nanomaterial family members with a size of <10 nm, have become progressively famous in the previous decade because of its remarkable optical and electric properties. Gurnule et al. [8] reports Synthesis, spectral and photoluminescence investigations of organic copolymer gum. The pre-arranged copolymer gum shows high photoluminescence properties. Dhobale and collaborators [9] orchestrated europium (Eu) doped magnesium pyrophosphate ($Mg_2P_2O_7$) nanopowders utilizing gamma light in the portion scope of 0.1 to 3 kGyby compound co-precipitation blend route. TL examination of integrated examples were performed after the illumination of $Mg_2P_2O_7$:Eu with cobalt-60 (60Co) gamma beams.

Photoluminescent supra atomic design has as of late pulled in much interest on account of their possible applications in photoelectronic gadgets or as fluorescence sensors and probes. Polymers have begun to discover use in making LEDs, liquid crystals and as sensors for metal particle fighting specialists, microorganisms and biomolecules. The photoluminescence (PL) properties of composites received with the aid of implanting green-transmitting semiconductor nanocrystals (NCs) of two distinct types (thiol-included CdTe and CdSe/ZnS) into chitosan-based biopolymer deb-

* Corresponding author.
E-mail address: wbgurnule@gmail.com (W.B. Gurnule).

https://doi.org/10.1016/j.matpr.2021.12.422
2214-7853/Copyright © 2022 Elsevier Ltd. All rights reserved.
Selection and peer-review under responsibility of the scientific committee of the Polymer & Mediterranean Fiber International Conference2021.

ris had been investigated. The gotten biocompatible composites with NCs randomly disseminated internal a biopolymer molecule confirmed a higher PL resistance to the answer acidity that expands the applicability range of thiol-capped NCs [10]. The researchers created a series of platinum-acetylide copolymers containing thiophene, selenophene, and tellurophene. Polymers undergo intersystem crossing to triplet states, according to photoluminescence investigations leading to phosphorescence. The found phosphorescence decreases in intensity shifting down the group [11]. The polymer nanoclay adjusted structure showed upgraded solvency contrasted with the first polymers and worked on warm dependability, alongside higher corrosion inhibition productivity and accumulation instigated outflow with radiance reliant upon the total design [12]. Gurnule and et al. reported the combination, characterization and photo radiant property of polymer got from 2,2′- dihydroxybiphenyl, formaldehyde and ethylenediamine [13].

The objective of this work is to synthesize copolymer 8-hydroxyquinoline-5-sulphonic acid-phthalic acid-formaldehyde and its composites. The synthesized copolymer was characterized by UV–Visible, FTIR, ^{1}H and ^{13}C NMR Spectral methods. The morphology of copolymer and its composites was examined by scanning electron microscopy. In this article, we discuss the physical science that underlies light-emitting polymer conduct and clarify the procedures and experiments that is the reason we used to study our synthesized copolymers.

2. Experimental

2.1. Synthesis of 8-hydroxyquinoline-5-sulphonic acid copolymer

The copolymer 8-hydroxyquinoline-5-sulphonic acid copolymer (8-HQ-5SAPF) was formed by combining Phthalic acid, 8-hydroxyquinoline-5-sulphonic acid and methanol in a 1:1:2 M ratio with intermittent shaking in an oil bath in the presence of 2 M hydrochloric acid as a catalyst. Then the reaction combos were then refluxed for 5 h at a temperature 124 °C ± 2 °C. The yellow shade strong compound turned into obtained and rinsed with hot water. After a period of time, the product was extracted using diethyl ether from unreacted starting materials and corrosive monomers that may be present in the eight-HQ-5SAPF copolymer. It was also cleaned by soaking it in 8% NaOH for a few minutes and then separating it. The yields of the copolymer were found to be 84% and the reaction series for the preparation is revealed in Fig. 1.

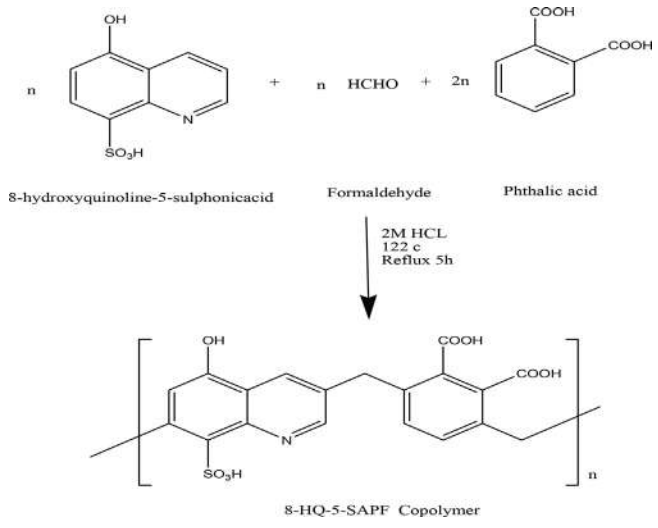


Fig. 1. Reaction for Synthesis of 8-HQ-5SAPF copolymer.

2.2. Preparation of copolymer composites with nano carbon

The new copolymer/activated charcoal composite had been organized with the aid of polymer (0.5 g) and activated charcoal (Sd Fine Chem Limited) (1.0 g) in 1:2 ratios. The copolymer dissolved in 25 mL of dimethyl sulfoxide (DMSO) was taken in a round bottomed flask and activated charcoal become delivered into it and the combination was subjected to ultrasonication for 3 h with regular stirring for twenty-four h at room temperature. After the specific time, the black color composite turned into received and separated, washed with ethanol and acetone to take away the impurities, the composite was filtered and dried at 70 °C for 24 h

3. Results and discussion

3.1. Elemental analysis

Elemental quantitative analysis is used to determine the content of these elements in the molecule of an organic compound. This facts is critical to assist determine the shape and purity of a newly synthesized copolymer. In the present work 8-HQ5-SAPF copolymer have been examined for C, H, N, and S at Indian Institute of Technology (IIT) Mumbai.

The empirical formula was derived using the elemental analysis data. The estimated values and observed outcomes are found to be in good agreement. The empirical weights of a single repeating unit were determined using the empirical formula and are included in Table 1.

3.2. UV spectra of copolymer 8-HQ5-SAPF

Fig. 2 shows the ultraviolet–visible spectra of 8-HQ5-SAPF copolymer recorded into pure dimethylsulfoxide at wavelength ranging from 190 to 800 nm. At 211 nm and 380 nm, the range revealed two retention groups. The existence of the preceding band may be express as π-π* transition, while latter weak band could be expected n-π* transition. The π-π* transition in a benzene ring is acceptable transition, whereas the n-π* transition accounted for phenolic-OH group (auxochrome) [14].

3.3. FTIR spectra of copolymer 8-HQ5-SAPF

The FTIR spectrum of a copolymer is shown in Fig. 3. A broad band visible in the copolymer spectrum about 3508 cm^{-1} can be attributed to the phenolic hydroxy (–OH) structure stretching frequency, indicating intermolecular hydrogen bonding [15]. The peak at 3102–3080 cm^{-1} is probably accounted for by stretching vibrations of the –CH linkage [20]. It's possible that the sharp band at 2789 cm^{-1} is due to aromatic –CH stretching. The quinoline ring stretching frequency of –C=C is responsible for the band's performance in the 1626–1413 cm^{-1} range. The signal at 1229 cm^{-1} indicates the presence of methylene bridges within the polymeric chain [16]. The tetra substitution moiety 2,5,6,8 in quinoline ring are shown at 775, 1046, 1137 and1191 cm^{-1}.

The prepared 8-HQ5-SAPF-C compounds FTIR spectra are depicted in Fig. 4. The strong band assigned at 3402 cm^{-1} respectively is confirmed to the –OH group appeared from the copolymer [17].The presence of –NH bending vibrations can be attributed to the band at 1498 &1555 cm^{-1} respectively. In addition, the aromatic ring stretching also caused from copolymer, the band appeared at 3099 & 3080 cm^{-1} respectively. The band appeared at 1387 & 1329 cm^{-1} respectively which may be due to the C-N

Table 1
Micro analysis and empirical formula of copolymer.

Copolymer	% of C observed (Cal.)	% of H observed (Cal.)	% of N observed (Cal.)	% of S observed (Cal.)	Empirical formula of repeated unit	Empirical formula Weight
8-HQ5-SAPF	42.44 (43.07)	4.0 (4.30)	4.96 (5.11)	8.37 (9.12)	$C_{20}H_{16}NO_8S$	459.46

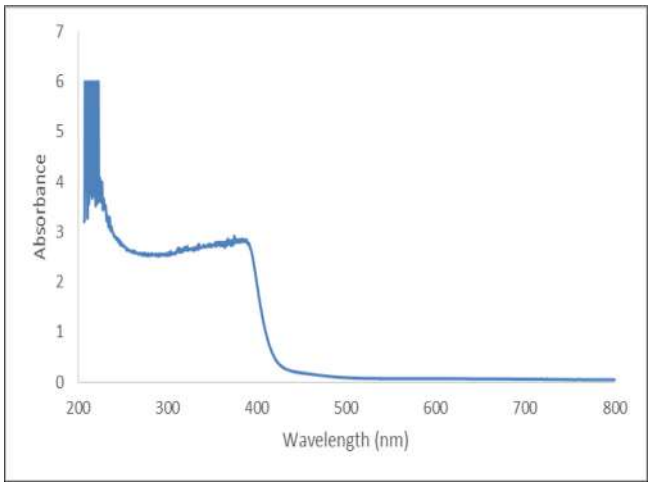


Fig. 2. UV–Visible Spectra of 8-HQ5-SAPF copolymer.

stretching vibration shifted from copolymer. This obviously indicates the formation of composites and the composites have been observed different absorption bands which is confirmed the copolymer has interface with carbon. Taking the above confirmation, the formation of composites are clearly established by copolymer and activated charcoal.

3.4. Proton (^1H) NMR spectra of copolymer 8-HQ5-SAPF

Fig. 5 shows the proton NMR spectra of the copolymer 8-HQ5-SAPF. The ^1H NMR spectra of the 8-HQ5-SAPF copolymer was obtained in $DMSOd_6$. The protons in the aromatic ring receive an unsymmetrical multiplet signal in the range of 7.3–8.0 (δ) ppm. The phenolic hydroxyl group is attributed with a sharp and solid peak at 9.1 ppm, indicating intramolecular hydrogen bonding. $-CH_2$ bridging could be assigned to a sharp signal found at 2.5 (δ) ppm [18]. The $-SO_3H$ group was assigned a triplet signal in the range 9.8 (δ) ppm [19].

3.5. Carbon (^{13}C) NMR spectra of copolymer 8-HQ5-SAPF

Fig. 6 shows ^{13}C NMR spectra of the typical copolymer 8-HQ5-SAPF. On the basis of the literature, the detected chemical shifts are allocated. The Ar–CH_2 bridge in the copolymer [20] is responsible for the peak appeared at 40.00 ppm. The quinoline rings C1 to C9 peaks were found in the copolymer at 145.90, 144.66, 135.88, 133.32, 131.35, 129.97, 128.88, 126.67 and 123.05 ppm, respectively.

3.6. SEM micrograph of copolymer 8-HQ5-SAPF

The surface character of the copolymer and its composite was studied using scanning electron microscopy. Figs. 7a, 7b & 7c shows SEM micrographs of the copolymer and its composite. According to the image, the copolymer and its composite have larger pore structures, which can operate as a more active site for enhanced heavy metal ion adsorption. Figs. 7a, 7b shows that the copolymer's structure has a large void volume on the surface, indicating that metals can easily be adsorbed on the surface. The copolymer structure was formed by combining the big dimple with the reinforcing particles.

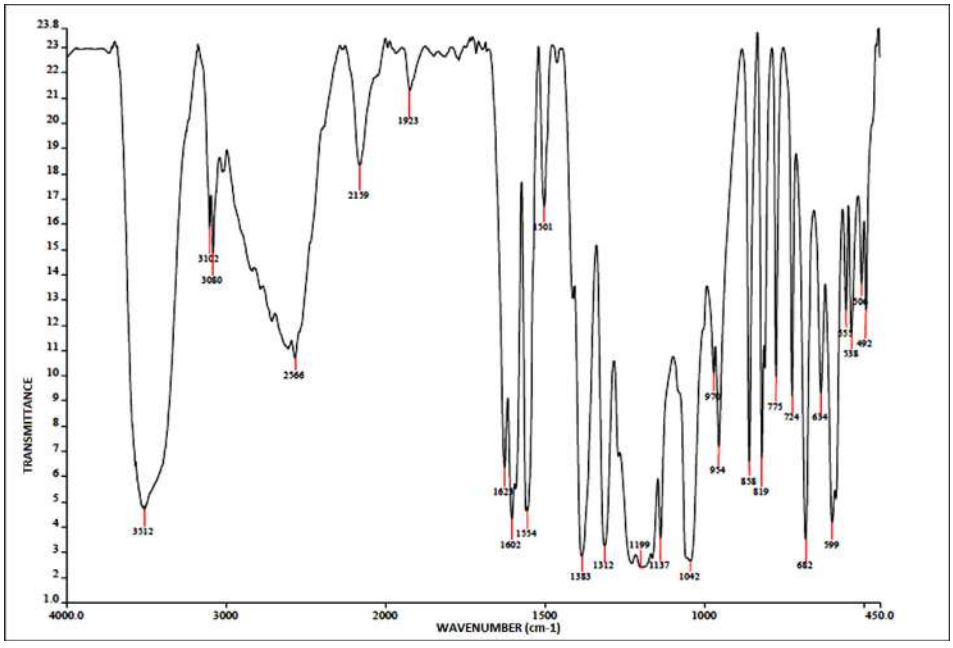


Fig. 3. FTIR Spectra of 8-HQ5-SAPF copolymer.

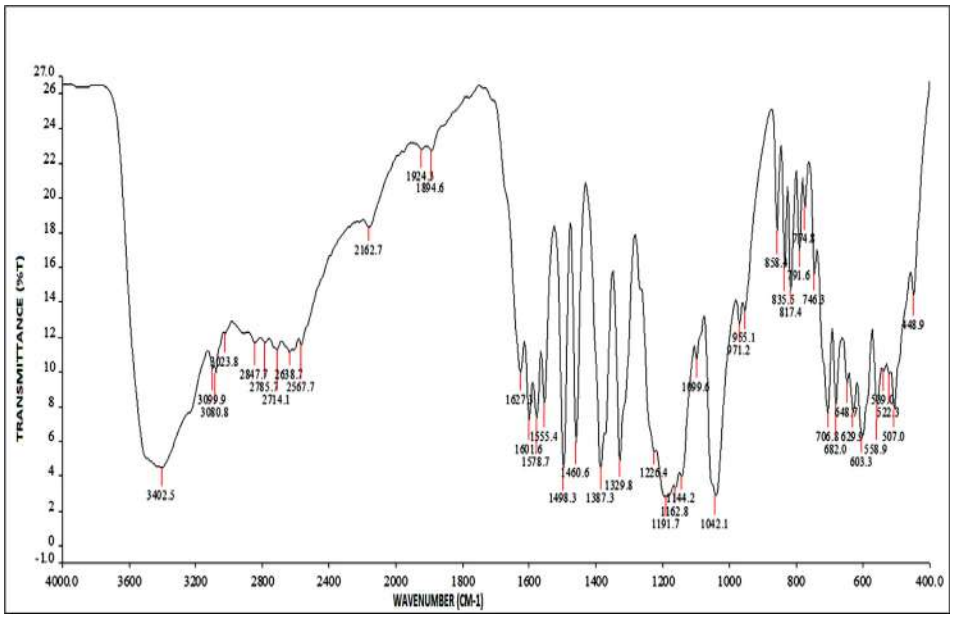


Fig. 4. FTIR Spectra of 8-HQ5-SAPF Composites.

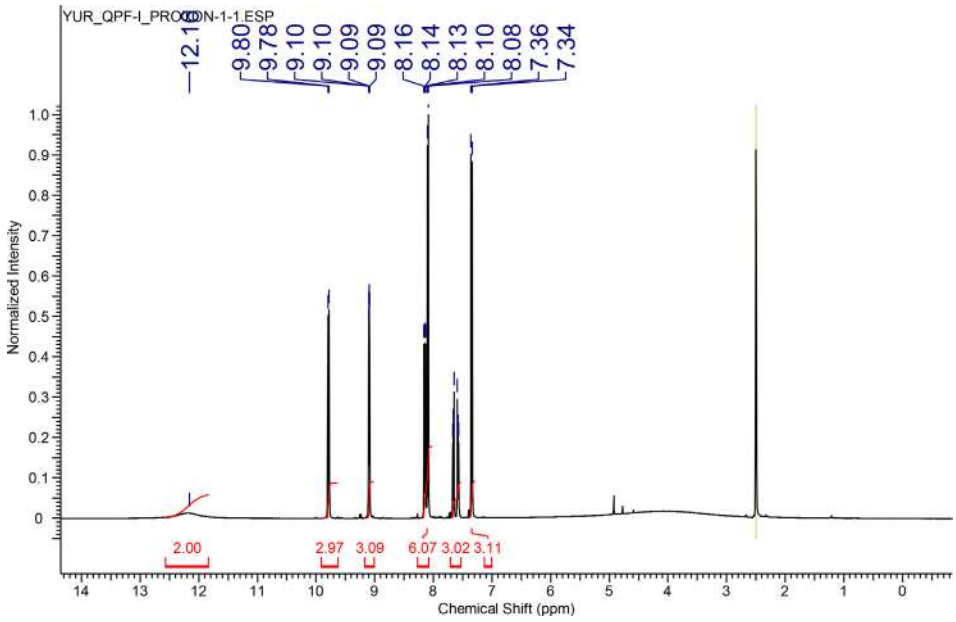


Fig. 5. ^{1}H NMR Spectra of 8-HQ-5SAPF Copolymer.

The surface microstructure of the copolymer has a high porosity and permeability [21]. The composite contains a wide range of pores. The micrograph reveals a new active site adhesive on the surface in a sputter cluster, indicating that the copolymer and carbon have been joined. The surface area of the composite increases more than that of the copolymer.

3.7. Photoluminescence studies

The photoluminescence properties of lately incorporated copolymer composite samples have been recorded on RF-501 (PC) S CE (LVD) LS55 Shimadzu MODEL spectrophotometer in Kamla Nehru College, Nagpur, end result of photoluminescence evaluation for copolymer 8-HQ5-SAPF composites are proven in Figs. 8 and 9. In these way PL spectra of this copolymer composite with carbon show that the brought material has sufficient great to be applied within the exploration of semiconductor gadgets. The results find that the readied co-appointment copolymer may be utilized for image luminescent fluid precious stone exhibit (PLLCD) and sturdy country lights applications as a assisting material [22].

Figs. 8 and 9 Shows the PL spectral plots of 8-HQ5-SAPF copolymer composites. Figs. 8 and 9 suggests emission band at 456 nm along excitation peak approximately 407 nm (blue), 369 (nm) wavelengths. Fundamental issue of this look at is to speak about the photo luminescent behaviour of the characterized copolymer composites. In these way PL spectra of this copolymer composites display that the introduced material has sufficient quality to be utilized inside the exploration of semiconductor gadgets. The results find that the readied co-appointment copolymer can be applied for mild emitting devices like supporting material for solid king-

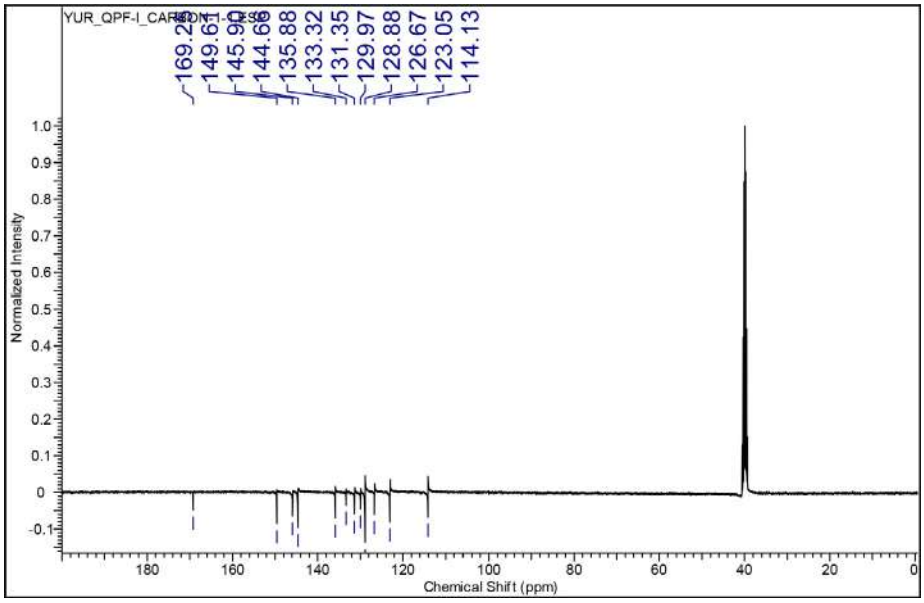


Fig. 6. ^{13}C NMR Spectra of 8-HQ-5SAPF Copolymer.

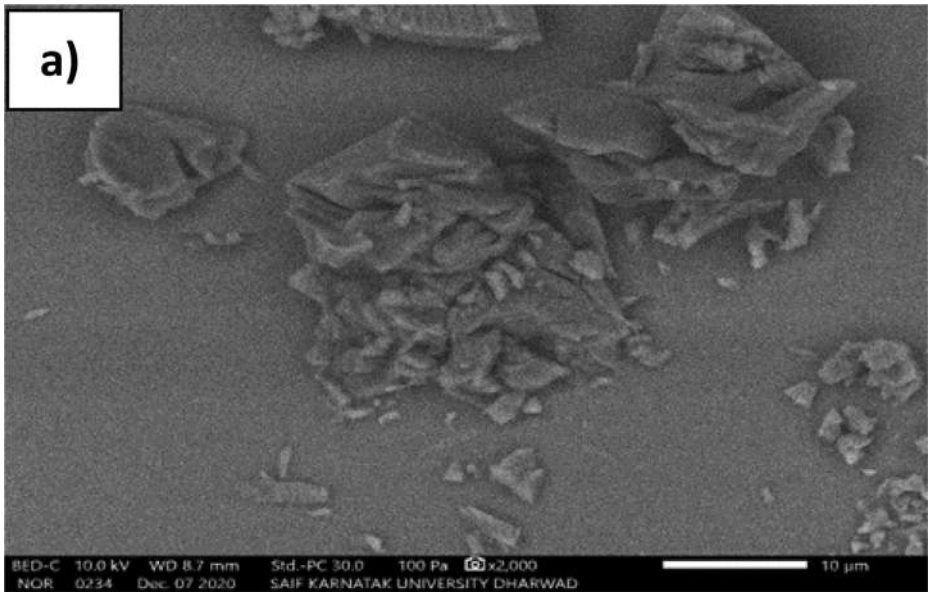


Fig. 7a. SEM Images of 8-HQ5-SAPF Copolymer.

dom lights programs and liquid crystal display (PLLCD). In nutshell we accept as true with that based on our studies revel in and understanding within the area of nanomaterials and their copolymer/ polymer composite substances will also play an vital position in the mild emitting materials [23–27].

4. Conclusion

The copolymers were made by combining 8-hydroxyquinoline-5-sulphonic acid, phthalic acid, and formaldehyde in the presence of 2 M HCl. Based on spectral and physico-chemical analysis, the structure of the copolymer and its composites was confirmed. The PL spectral plots of 8-HQ5-SAPF copolymer composites suggests emission band at 456 nm along excitation peak approximately 407 nm (blue), 369 (nm) wavelengths. The photoluminescence analysis of the 8-HQ5-SAPF copolymer reveals that it has various properties that could be useful in the testing of semiconductor devices and light emitting materials. The surface character of the copolymer and its composite was studied using scanning electron microscopy. SEM micrograph of the copolymer composite contains a wide range of pores. The micrograph reveals a new active site adhesive on the surface in a sputter cluster, indicating that the copolymer and carbon have been joined. The surface area of the composite increases more than that of the copolymer.

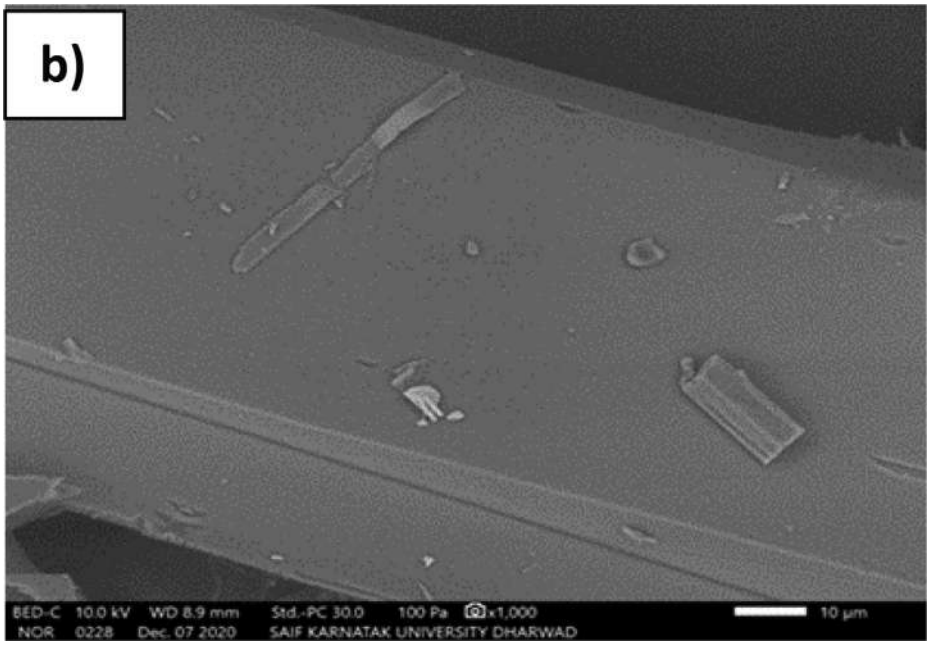


Fig. 7b. SEM Images of 8-HQ5-SAPF Copolymer.

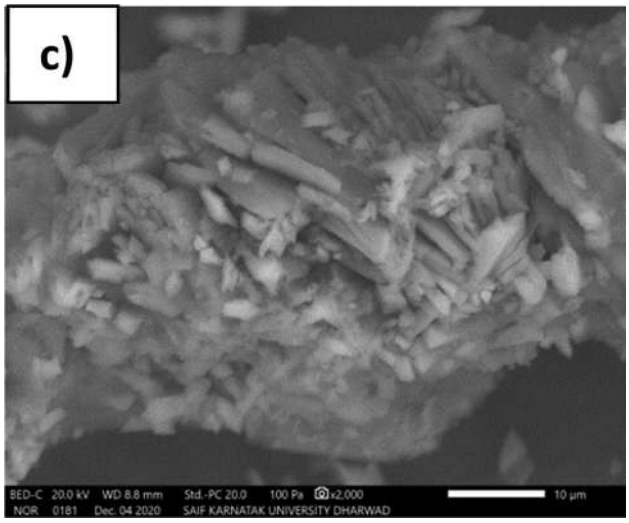


Fig. 7c. SEM Images of 8-HQ5-SAPF Copolymer composites.

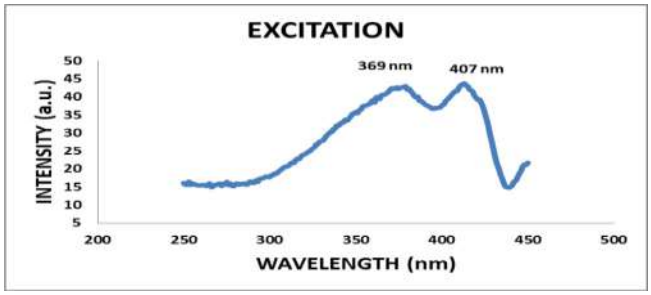


Fig. 8. PL Spectra (Excitation) for 8-HQ5-SAPF-C copolymer Composites.

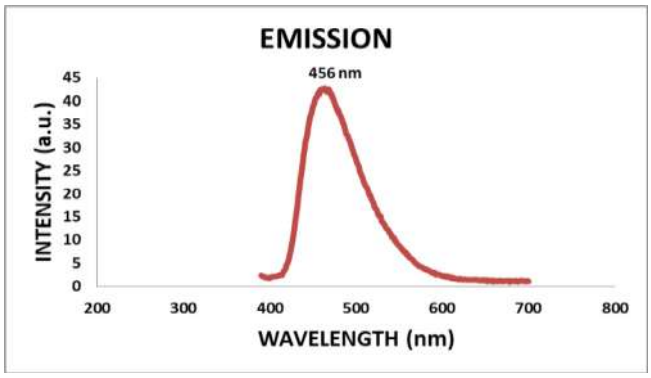


Fig. 9. PL Spectra (Emission) for 8-HQ5-SAPF-C copolymer Composites.

Declaration of Competing Interest

The authors declare that they have no known competing financial interests or personal relationships that could have appeared to influence the work reported in this paper.

References

[1] T. Mori, M. Kijima, Eur. Polym. J. 45 (2009) 1149–1157.
[2] J. Feng, X. Chen, Q. Han, H. Wang, P. Lu, Y. Wang, J. Lumin. 131 (2011) 2775–2783.
[3] A.M. Maggermov, M.A. Ramazanov, S.G. Nuriyeva, F.V. Hajiyeva, U.A.J. Hasanova, Opto Biom Mater 7 (2) (2015) 39–45.
[4] B. Podkoscielna, Pat. 2015; PL 402734.
[5] B. Podkoscielna, A. Lipke, B. Gawdzik, M. Majdan, Polym. Adv. Technol. 26 (2015) 176–181.
[6] O.Y. Posudievsky, M.S. Papakin, O.P. Boiko, V.G. Koshechko, V.D. Pokhodenko, Nanoscale Res. Lett. 10 (2015) 118.
[7] J. Norhanisah, A.R. Suraya, T. Tongling, Syn. Tech. Appl. Carbon Nanomater. (2019) 109–134.
[8] C.G. Kohad, W.B. Gurnule, Mater. Today: Proc. 15 (3) (2019) 438–446.
[9] K.K. Gupta, N.S. Dhoble, K.D. Burghate, S.J. Dhobale, Luminescence 33 (5) (2018) 947–953.
[10] N. Slyusarenko, M. Gerasimova, A. Plotnikov, N. Gaponik, Slyusareva, Phys. Chem. Chem. Phys. 9 (2019).

[11] A.K. Mahrok, E.I. Carrera, A.J. Tilley, S. Ye, D.S. Sefros, Chem. Comm. 51 (2015) 5475.
[12] K.I. Aly, O. Younis, M.H. Mahross, O. Tsutsumi, G. Mohamed, M.M. Sayed, Polym. J. 51 (2019) 77–90.
[13] S.P. Chakole, K.A. Nandekar, W.B. Gurnule, J. Phys. Conf. Ser. 1913 (2021) 012062.
[14] W.B. Gurnule, Y.U. Rathod, Curr. Appl. Polym. Sci. 4 (2020) 1–8.
[15] M.A.R. Ahamed, R.S. Azarudeen, D. Jeyakumar, A.R. Burkanudeen, Int. J. Polym. Mater. 60 (2011) 124–143.
[16] M.M. Yeole, A.S. Shrivastav, W.B. Gurnule, Der Pharma Chem. 7 (5) (2015) 124–129.
[17] G. Velmurugan, K.R. Ahmed, R.S. Azarudeen, Iran Polym. J. 24 (3) (2015) 229–242.
[18] W.B. Gurnule, Y.U. Rathod, A.D. Belsare, N.C. Das, Mater. Today Proc. 29 (4) (2020) 1044–1049.
[19] Y.U. Rathod, S.B. Zanje, W.B. Gurnule, J. Phys. Conf. Ser. 1913 (2021) 012061.
[20] R.S. Azarudeen, A. Mohamed, M.A.R. Ahamed, A.R. Burkanudeen, Desalination 268 (2011) 90–96.
[21] G. Velmurugan, R.K. Ahmed, R.S. Azarudeen, M. Thirumarimurugan, Sep. Sci. Technol. 52 (12) (2017) 1946–1958.
[22] W.B. Gurnule, K.S. Vajpai, R.V. Mankar, C.G. Kohad, 29 (4) (2020) 974–980.
[23] V. Pandit, S. Arbuj, Y. Pandit, S. Naik, S. Rane, U. Mulik, S. Gosavi, B. Kale, RSC Adv. 5 (2015) 10326–11033.
[24] V. Pandit, S. Arbuj, U. Mulik, B. Kale, Environ. Sci. Technol. 7 (2014) 4178–4183.
[25] V. Pandit, S. Arbuj, R. Hawaldar, P. Kshirsagar, U. Mulik, S. Gosavi, C. Park, B. Kale, J. Mater. Chem. 3 (2015) 4338–4344.
[26] V. Jawale, G. Gugale, M. Chaskar, S. Pandit, R. Pawar, S. Suryawanshi, V. Pandit, G. Umarji, S. Arbuj, J. Mater. Res. 36 (2021) 1573–1583.
[27] V.U. Pandit, S.S. Arbuj, R.R. Hawaldar, P.V. Kshirsagar, J.D. Ambekar, U.P. Mulik, S.W. Gosavi, B.B. Kale, RSC Adv. 5 (2015) 13715–13721.

ScienceDirect

4.9
CiteScore

Submit your article | Guide for authors

Menu Search in this journal

About the journal

Materials Today: Proceedings provides the materials science community with a fast and flexible route to the publication of research presented at national and international scientific conferences in the field of materials science.
Guest Editors are responsible for quality control, the peer review ...

View full aims & scope

$200 ⓘ
Article publishing charge for open access

14 days
Time to first decision

44 days
Review time

81 days
Submission to acceptance

View all insights

Articles

Latest published | Articles in press | Top cited | Most downloaded

Most popular

Online ISSN: 2214-7853

Copyright © 2024 Elsevier Ltd. All rights are reserved, including those for text and data mining, AI training, and similar technologies.

For authors

Resources for authors ↗

Track your accepted paper ↗

Journal Finder ↗

Researcher Academy ↗

Rights and permissions ↗

Journal Article Publishing Support Center ↗

For editors

Resources for editors ↗

Publishing Ethics Resource Kit ↗

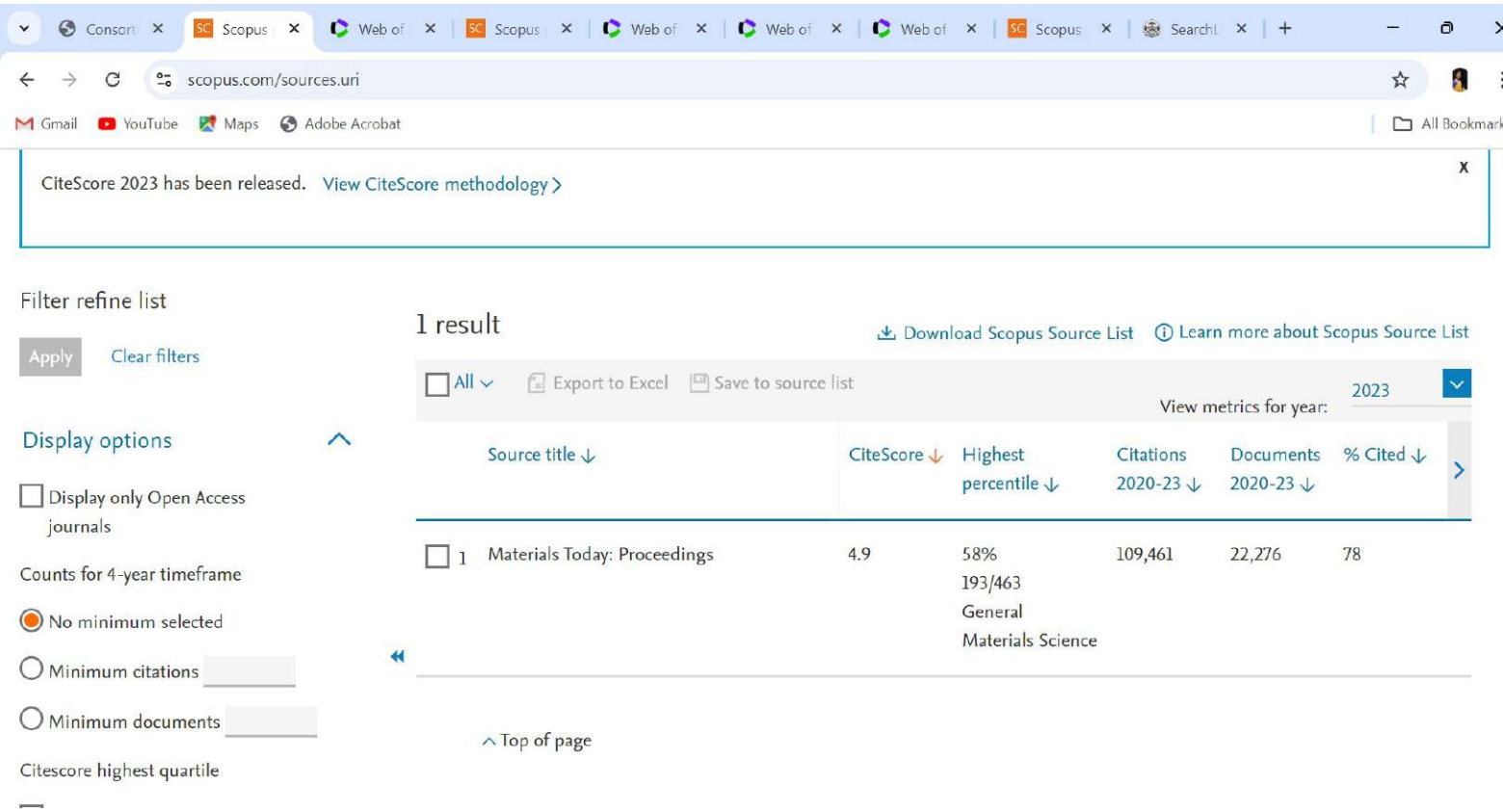
Guest editors ↗

For reviewers

Resources for reviewers ↗

Reviewer recognition ↗

All content on this site: Copyright © 2024 Elsevier B.V., its licensors, and contributors. All rights are reserved, including those for text and data mining, AI training, and similar technologies. For all open access content, the Creative Commons licensing terms apply.


scopus.com/sources.uri
Gmail
YouTube
Maps
Adobe Acrobat
All Bookmarks
CiteScore 2023 has been released. View CiteScore methodology >
Filter refine list
Apply
Clear filters
Display options
Display only Open Access journals
Counts for 4-year timeframe
No minimum selected
Minimum citations
Minimum documents
Citescore highest quartile
1 result
Download Scopus Source List
Learn more about Scopus Source List
All
Export to Excel
Save to source list
View metrics for year:
2023
Source title
CiteScore
Highest percentile
Citations 2020-23
Documents 2020-23
% Cited
1 Materials Today: Proceedings 4.9 58% 193/463 General Materials Science 109,461 22,276 78
Top of page

Materials Today: Proceedings xxx (xxxx) xxx

Contents lists available at ScienceDirect

Materials Today: Proceedings

journal homepage: www.elsevier.com/locate/matpr

Thermal degradation studies of 2-hydroxy-4-methoxy acetophenone, guanidine and formaldehyde copolymer

Preeti A. Mishra [a], Yashpal U. Rathod [b], Vikram U. Pandit [c], Wasudeo B. Gurnule [a,*]

[a] Department of Chemistry, Kamla Nehru Mahavidyalaya, Nagpur-440024, M. S., India
[b] Department of Chemistry, J. M. Patel College, Bhandara-441904, M. S., India
[c] Department of Chemistry, H. V. Desai College, Pune-04, M. S., India

ARTICLE INFO

Article history:
Available online xxxx

Keywords:
Synthesis
Polycondensation
Conductometry
Spectral methods
Thermal methods.

ABSTRACT

The 2-hydroxy 4-methoxyacetophenone-guinidine-formaldehyde (HMAGF) copolymer was synthesized by the using monomers of 2-hydroxy-4-methoxyacetophenone, guanidine and formaldehyde in 2M hydrochloric acid medium at 124 °C in 1:1:2M proportions of the three reactants. The characterization of the newly synthesized HMAGF copolymer was confirmed by basic investigation and different spectral techniques like UV-Visible, FTIR, and ^{1}H NMR spectroscopy. The warm debasement investigations of the copolymer were done by thermogravimetric examination (TGA). Sharp Wentworth and Freeman Carroll methods were utilized to calculate thermodynamic parameters like activation energy (Ea), Change in entropy (ΔS), change in free energy (ΔF), change in entropy (S^*), the frequency factor. (Z). The activation energy determined by the Sharp Wentworth and Freeman Carroll methods are almost same. The order of reaction is found to be 0.8.
Copyright © 2022 Elsevier Ltd. All rights reserved.
Selection and peer-review under responsibility of the scientific committee of the Polymer & Mediterranean Fiber International Conference2021.

1. Introduction

Copolymers are an incredibly fundamental and flexible class of materials having really first rate applications and have been totally changing ourselves for a significant long time with various applications in the discipline which incorporates wastewater treatment [1,2], molecule exchanger [3–5], drug [6,7], planning [8], cultivating [9] and semiconductor [10] due to their exorbitant warm and electrical solidness. Copolymer materials are used for the preparation of functional nanostructures due to their escellent thermal charactristics. Thus, thermal stability and thermal degradation kinetics may be significant for the production and application of copolymer based materials. TGA data have been used to determine the thermal degradation kinetics and therml stability of copolymer. Copolymer of 4-hydroxybenzoic acid, thiourea with formaldehyde and 8-hydroxyquinoline, formaldehyde with pyrogallol have been examined by Ahmad and coworkers [11,12]. Electrical conductivity and thermal studies have been carried out by using salicylic acid, hexamethylenediamine, and formaldehyde Masram [13]. Dhote and coworkers have performed thermal degradation and thermokinetic examination of copolymer obtained from salicylaldehyde, melamine, and formaldehyde [14]. The examination of non-isothermal method and kinetic parameters of 2, 4-Dihydroxybenzoic acid, melamine and formaldehyde copolymer Butoliya [15]. Similar thermodynamic examination of copolymeric materials from p-hydroxy acetophenone, resorcinol and glycerol have been represented [16].

The present research article discuss the synthesis and characterization of the copolymer derived from 2-hydroxy-4-methoxyacetophenone, guanidine hydrochloride and formaldehyde. The thermal behaviour of the copolymer was evaluated by TGA mthod, and the kinetic and thermodynamic parameters such as activation energy (Ea), order of the reaction (n), entropy change, free energy change, apparent entropy ad frequency factor (Z) were evauated by FC and SW methods [16,17].

2. Experimental

2.1. Synthesis of HMAGF copolymer resin

The new copolymer HMAGF was synthesized by using 2-hydroxy-4-methoxyacetophenone (0.1 mol), guanidine (0.1 mol)

* Corresponding author.
E-mail address: wbgurnule@gmail.com (W.B. Gurnule).

https://doi.org/10.1016/j.matpr.2021.12.383
2214-7853/Copyright © 2022 Elsevier Ltd. All rights reserved.
Selection and peer-review under responsibility of the scientific committee of the Polymer & Mediterranean Fiber International Conference2021.

ScienceDirect

4.9
CiteScore

Submit your article | Guide for authors

Menu Search in this journal

About the journal

Materials Today: Proceedings provides the materials science community with a fast and flexible route to the publication of research presented at national and international scientific conferences in the field of materials science.
Guest Editors are responsible for quality control, the peer review ...

View full aims & scope

$200 ⓘ
Article publishing charge for open access

14 days
Time to first decision

44 days
Review time

81 days
Submission to acceptance

View all insights

Articles

Latest published | Articles in press | Top cited | Most downloaded

Most popular

Online ISSN: 2214-7853

Copyright © 2024 Elsevier Ltd. All rights are reserved, including those for text and data mining, AI training, and similar technologies.

For authors

Resources for authors ↗

Track your accepted paper ↗

Journal Finder ↗

Researcher Academy ↗

Rights and permissions ↗

Journal Article Publishing Support Center ↗

For editors

Resources for editors ↗

Publishing Ethics Resource Kit ↗

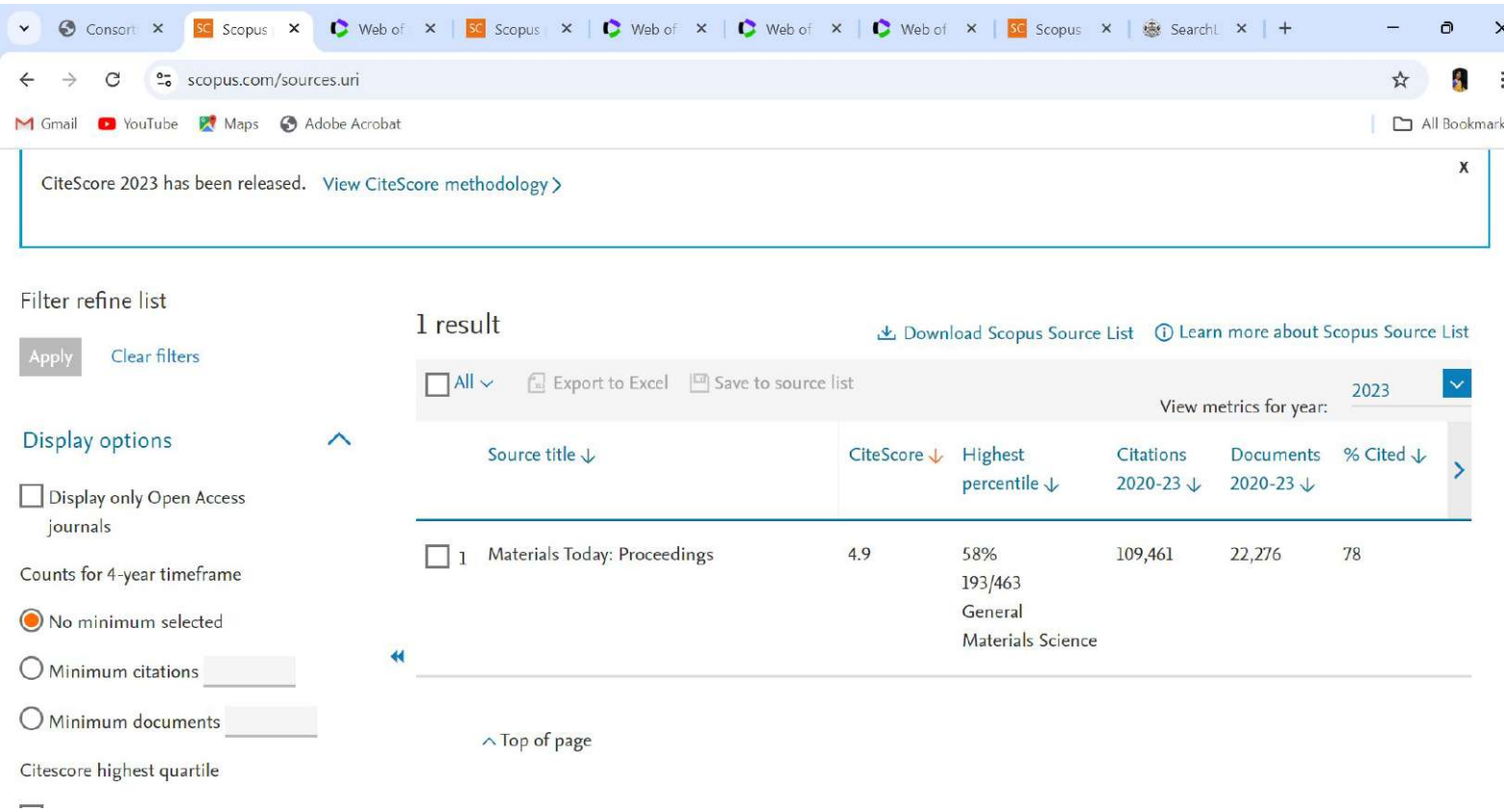
Guest editors ↗

For reviewers

Resources for reviewers ↗

Reviewer recognition ↗

All content on this site: Copyright © 2024 Elsevier B.V., its licensors, and contributors. All rights are reserved, including those for text and data mining, AI training, and similar technologies. For all open access content, the Creative Commons licensing terms apply.


scopus.com/sources.uri
Gmail
YouTube
Maps
Adobe Acrobat
All Bookmarks
CiteScore 2023 has been released. View CiteScore methodology >
Filter refine list
Apply
Clear filters
Display options
Display only Open Access journals
Counts for 4-year timeframe
No minimum selected
Minimum citations
Minimum documents
Citescore highest quartile
1 result
Download Scopus Source List
Learn more about Scopus Source List
All
Export to Excel
Save to source list
View metrics for year:
2023
Source title
CiteScore
Highest percentile
Citations 2020-23
Documents 2020-23
% Cited
1 Materials Today: Proceedings 4.9 58% 193/463 General Materials Science 109,461 22,276 78
Top of page

Materials Today: Proceedings xxx (xxxx) xxx

Contents lists available at ScienceDirect

Materials Today: Proceedings

journal homepage: www.elsevier.com/locate/matpr

Thiamine hydrochloride (vitamin B1) catalyzed greener synthesis of thiazolidin-4-one derivatives

Devidas S. Bhagat [a,*], Wasudeo B. Gurnule [b], Yashpal U. Rathod [c], Mahipal S. Sankhla [d], Vikram U. Pandit [e]

[a] Department of Forensic Chemistry and Toxicology, Government Institute of Forensic Science, Aurangabad 431 004, MS, India
[b] Department of Chemistry, Kamla Nehru Mahavidyalaya, Nagpur 440024, MS, India
[c] Department of Chemistry, J.M. Patel College, Bhandara 441904, MS, India
[d] Department of Forensic Science, Vivekananda Global University, Jaipur, Rajasthan 303012, India
[e] Department of Chemistry, H.V. Desai College, Pune, MS, India

ARTICLE INFO

Article history:
Available online xxxx

Keywords:
One-pot synthesis
Biodegradable catalyst
Thiamine hydrochloride (VB1)
Thiazolidin-4-one derivatives

ABSTRACT

Eco-friendly synthesis of thiazolidin-4-one scaffolds has been accomplished by the one-pot protocol. Thiazolidin-4-one scaffolds were obtained by multicomponent cyclo condensation of aromatic amine, a carbonyl compound, and a thioglycolic acid in thiamine hydrochloride (vitamin B1) as a biodegradable catalyst in acetonitrile solvent. The structure of the synthesized thiazolidin-4-one was elucidated by FT-IR, Proton nuclear magnetic resonance, and HR-MS spectral techniques. The reported route possesses outstanding features includes; efficient, cost-effective, easy work-up procedure, high yield, and biodegradable catalyst.
Copyright © 2022 Elsevier Ltd. All rights reserved.
Selection and peer-review under responsibility of the scientific committee of the Polymer & Mediterranean Fiber International Conference2021.

1. Introduction:

One-pot synthesis is one of the parts of the multicomponent reactions (MCRs) which are useful in synthetic organic chemistry for designing and synthesis new heterocyclic scaffolds in chemical libraries. The MCRs are used for the synthesis of simple to complex molecules with a high degree of molecular diversity, due to the number of benefits over multistep reactions [1]. The five-membered heterocyclic compound thiazolidine (**1**) contains nitrogen and sulfur heteroatom. 1,3-thiazolidin-4-ones (**2**) possess (>C=O) carbonyl functional group. Thiazolidine is a type five-membered ring that contains a thioether group (—S—) and an amine group (—NH—) in the 1 and 3 positions. The 1,3-thiazolidin-4-ones are present in well-known drugs such as Pioglitazone (**3**) and Penicillin (**4**). Pioglitazone is an antihyperglycemic, antidiabetic drug and it decreases blood sugar for the treatment of diabetes disease. Penicillin is a broad-spectrum antibiotic that is used to control gram-positive and gram-negative bacteria [2]. The structure of these bioactive scaffolds is given in Fig. 1.

In the last three decades, the scientific community focused on the creation of bioactive heterocyclic motifs. Synthesized heterocycles have great importance in medicinal chemistry which provides the solution to numerous diseases. Nitrogen and sulfur-containing five members and six members heterocycles are building blocks of the numerous drug scaffolds [3]. Few significant thiazolidines containing heterocyclic scaffolds include; (*Z*)-3-(2-aminoethyl)-5-(4-ethoxybenzylidene)thiazolidine-2,4-dione (**5**) show greater selectivity for inhibiting the proliferation of melanoma cells bearing active ERK signaling activity [4], *N*-(5-Methyl-4-oxo-thiazolidin-3-yl)-nicotinamide (**6**) derivatives showed excellent antibacterial activity [5]. 2-imino-3-(4-arylthiazol-2-yl)-thiazolidin-4-ones (**7**) possess excellent fungicidal activity obtained from acetophenone and thiourea [6]. 2-aryl-3-(4,5,6-trimethylpyrimidin-2-yl)thiazolidin-4-one derivatives (**8**) show HIV-RT inhibitory activity [7]. 2-(4-fluorophenyl)thiazolidin-4-one (**9**) shows antioxidant activity [8]. The of the bioactive motifs are provided in Fig. 2.

The bio-heterocycles containing N, O, F, and S are among the most frequently encountered candidates in drug and pharmaceutical fields. Thiazolidinones are an important class of heterocyclic compounds that possess five-membered heterocyclic rings containing nitrogen and sulfur heteroatom. It has been considered an important building block that shows a wide range of biological activity. The derivatives of thiazolidine show pharmacological activities such as antiproliferative [9], antimicrobial [10], anti-

* Corresponding author.
E-mail address: devidas.bhagat@gov.in (D.S. Bhagat).

https://doi.org/10.1016/j.matpr.2021.12.292
2214-7853/Copyright © 2022 Elsevier Ltd. All rights reserved.
Selection and peer-review under responsibility of the scientific committee of the Polymer & Mediterranean Fiber International Conference2021.

ScienceDirect

4.9
CiteScore

Submit your article | Guide for authors

Menu Search in this journal

About the journal

Materials Today: Proceedings provides the materials science community with a fast and flexible route to the publication of research presented at national and international scientific conferences in the field of materials science.
Guest Editors are responsible for quality control, the peer review ...

View full aims & scope

$200 ⓘ
Article publishing charge for open access

14 days
Time to first decision

44 days
Review time

81 days
Submission to acceptance

View all insights

Articles

Latest published | Articles in press | Top cited | Most downloaded

Most popular

Online ISSN: 2214-7853

Copyright © 2024 Elsevier Ltd. All rights are reserved, including those for text and data mining, AI training, and similar technologies.

For authors

Resources for authors ↗

Track your accepted paper ↗

Journal Finder ↗

Researcher Academy ↗

Rights and permissions ↗

Journal Article Publishing Support Center ↗

For editors

Resources for editors ↗

Publishing Ethics Resource Kit ↗

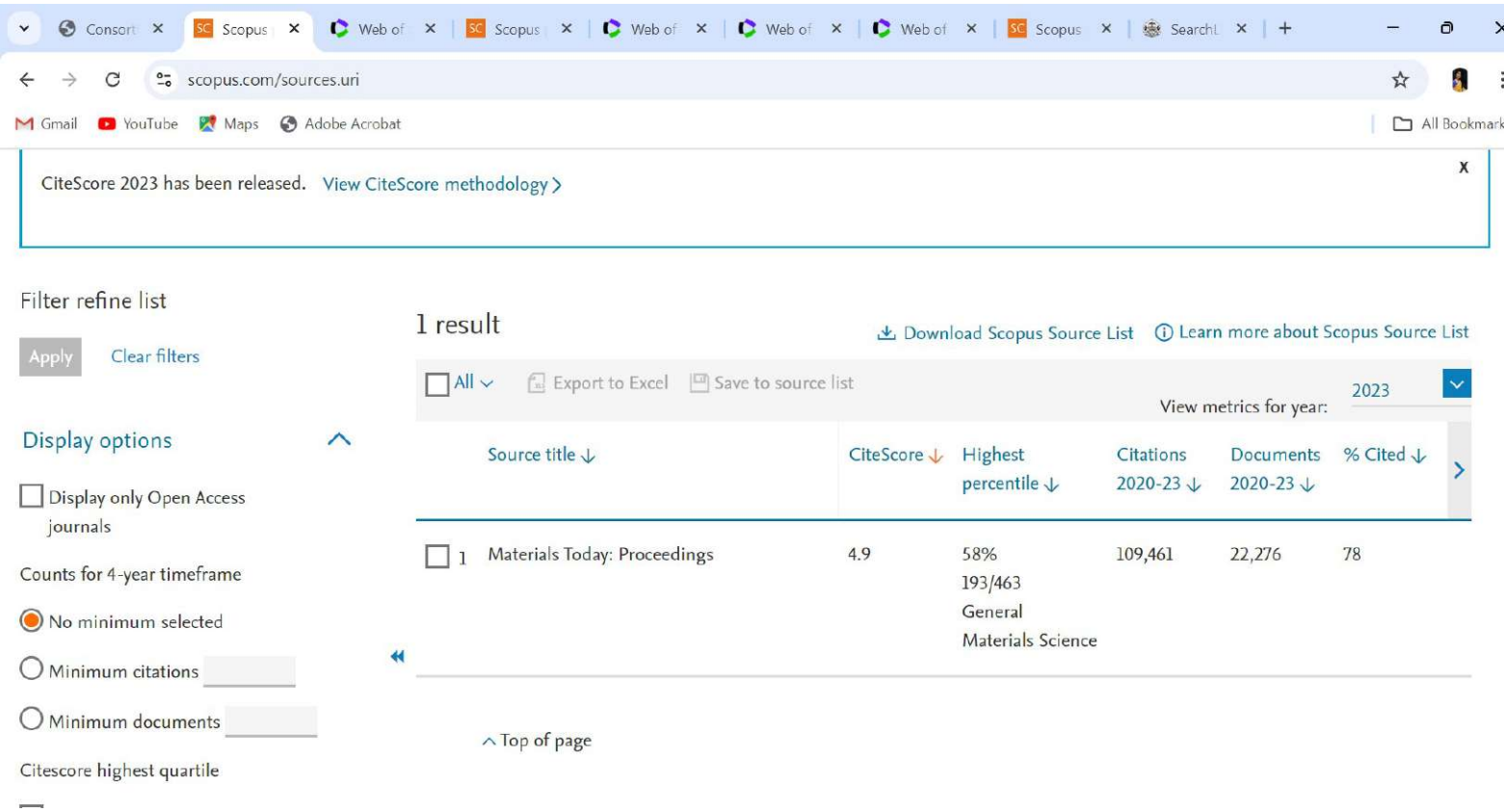
Guest editors ↗

For reviewers

Resources for reviewers ↗

Reviewer recognition ↗

All content on this site: Copyright © 2024 Elsevier B.V., its licensors, and contributors. All rights are reserved, including those for text and data mining, AI training, and similar technologies. For all open access content, the Creative Commons licensing terms apply.


scopus.com/sources.uri
Gmail
YouTube
Maps
Adobe Acrobat
All Bookmarks
CiteScore 2023 has been released. View CiteScore methodology >
Filter refine list
Apply
Clear filters
Display options
Display only Open Access journals
Counts for 4-year timeframe
No minimum selected
Minimum citations
Minimum documents
Citescore highest quartile
1 result
Download Scopus Source List
Learn more about Scopus Source List
All
Export to Excel
Save to source list
View metrics for year:
2023
Source title
CiteScore
Highest percentile
Citations 2020-23
Documents 2020-23
% Cited
1 Materials Today: Proceedings 4.9 58% 193/463 General Materials Science 109,461 22,276 78
Top of page

Materials Today: Proceedings xxx (xxxx) xxx

Contents lists available at ScienceDirect

Materials Today: Proceedings

journal homepage: www.elsevier.com/locate/matpr

Synthesis, characterization and thermal behavior of 2,2′-dihydroxybiphenyl-formaldehyde-phenylenediamine copolymer

Santosh P. Chakole [a], Yashpal U. Rathod [b], Vikram U. Pandit [c], Wasudeo B. Gurnule [a,*]

[a] Department of Chemistry, Kamla Nehru Mahavidyalaya, Nagpur 440024, M.S., India
[b] Department of Chemistry, J.M. Patel College, Bhandara 441904, M.S., India
[c] Department of Chemistry, H.V. Desai College, Pune 04, M.S., India

ARTICLE INFO

Article history:
Available online xxxx

Keywords:
Synthesis
Polycondensation
Conductometric
Disintegration
Thermal behaviour
Activation energy
Free energy change
Order of reaction

ABSTRACT

Polymer 2,2′-BPPHDF-III was synthesized by polycondensation of the monomers 2,2′-dihydroxybiphenyl (BP), phenylenediamine (PH) and formaldehyde (F) is in the molar proportion [3:1:5] in an acidic medium. Copolymer syntheses and structure have been controlled by elemental analysis, Number average atomic weight of copolymer was controlled by conductometric titration in non-aqueous medium, FTIR, ^{1}H NMR and the SEM studies of copolymer was examined by scanning electron microscopy (SEM). The studies have been additionally reached out to TGA for assurance of their method of disintegration and relative thermal behaviour. Actuation energy (Ea), order of reaction (n), and frequency factor (z) were determined by Sharp-Wentworth and Freeman-Carroll techniques. Actuation energy determined by Sharp Wentworth and Freeman-Carroll techniques are in close concurrence with one another.
Copyright © 2022 Elsevier Ltd. All rights reserved.
Selection and peer-review under responsibility of the scientific committee of the Polymer & Mediterranean Fiber International Conference2021.

1. Introduction

Investigation of warm examination includes a gathering of strategies wherein an actual study of material is estimated as a component of temperature when the substance is exposed to a controlled temperature. Since the advanced history of TGA, warm debasement of polymers and the investigation of their energy have been at the focal point of warm examination. Numerous scientists attempted to work on the warm security at raised temperature by change of the monomer creation in polymer synthesis [1].

The investigation of copolymer has turned into a subject of late revenue, being a significant property, which essentially chooses warm dependability and processability. A wide assortment of thermally stable polymers have been integrated and contemplated their TGA property and finds numerous applications, for example, particle exchangers [2–5], semiconductors [6], high dielectric steady for energy stockpiling capacitors [7], bundling, glues and coatings in electrical sensors, activators, impetuses and thermally stable materials [8–10]. Michael et al. done warm debasement of terpolymers integrated from salicylic corrosive/8-hydroxyquinoline and guanidine with formaldehyde [11–13]. Phenolic tars are known for their wide applications in different regions in view of their warm security, simple accessibility, cost adequacy, and a portion of their fantastic properties [14]. The warm steadiness of copolymers has been widely concentrated by utilizing the technique for thermogravimetric investigation (TGA) by a few creators. Thermo scientific and dynamic investigations of terpolymer pitches got from 8-hydroxyquinoline-5-sulphonica cid/p-cresol, oxamide/melamine with formaldehyde have been revealed by Singru et al. [15–18]. 2-hydroxy, 4-metoxybezophenone, 1,5-diaminonapthalene, formaldehyde by Das [19] has been concentrated exhaustively. Techniques for the assessment of active boundaries from thermogravimetric examinations are by and large dependent with the understanding that the Arrhenius condition is substantial with warm and dissemination obstructions being irrelevant. Different examinations on union, portrayal and thermogravimetric investigation of a few new polymeric pitches have been accounted for [20-21]. Thus, in the current examination, it has been arranged to consider the TGA investigation of terpolymer got from 2,2′-dihydroxybiphenyl, phenylenediamine and formaldehyde which has not been accounted for so far.

* Corresponding author.
E-mail address: wbgurnule@gmail.com (W.B. Gurnule).

https://doi.org/10.1016/j.matpr.2021.12.395
2214-7853/Copyright © 2022 Elsevier Ltd. All rights reserved.
Selection and peer-review under responsibility of the scientific committee of the Polymer & Mediterranean Fiber International Conference2021.

ScienceDirect

4.9
CiteScore

Submit your article | Guide for authors

Menu Search in this journal

About the journal

Materials Today: Proceedings provides the materials science community with a fast and flexible route to the publication of research presented at national and international scientific conferences in the field of materials science.
Guest Editors are responsible for quality control, the peer review ...

View full aims & scope

$200 ⓘ
Article publishing charge for open access

14 days
Time to first decision

44 days
Review time

81 days
Submission to acceptance

View all insights

Articles

Latest published | Articles in press | Top cited | Most downloaded

Most popular

Online ISSN: 2214-7853

Copyright © 2024 Elsevier Ltd. All rights are reserved, including those for text and data mining, AI training, and similar technologies.

For authors

Resources for authors ↗

Track your accepted paper ↗

Journal Finder ↗

Researcher Academy ↗

Rights and permissions ↗

Journal Article Publishing Support Center ↗

For editors

Resources for editors ↗

Publishing Ethics Resource Kit ↗

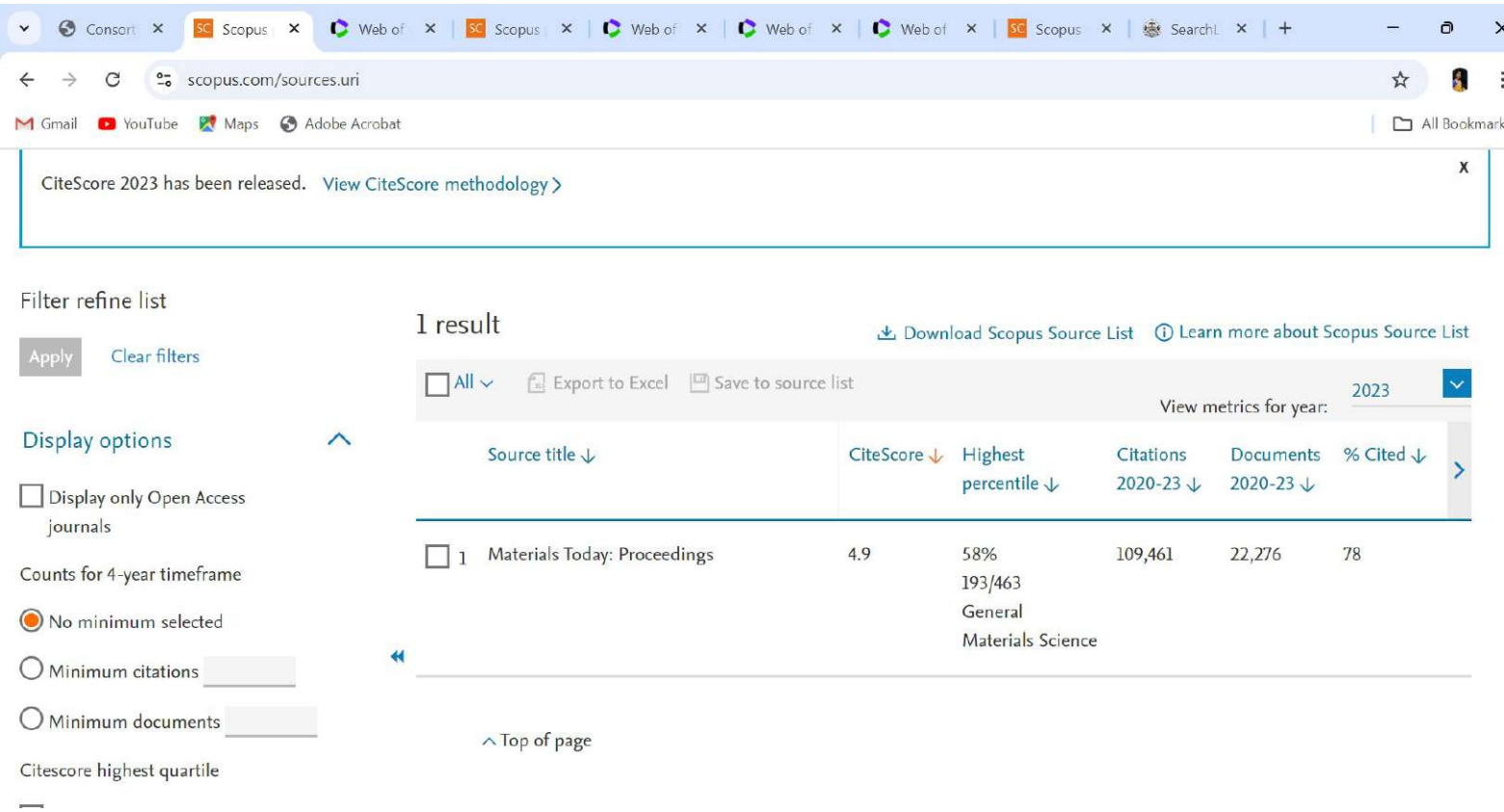
Guest editors ↗

For reviewers

Resources for reviewers ↗

Reviewer recognition ↗

All content on this site: Copyright © 2024 Elsevier B.V., its licensors, and contributors. All rights are reserved, including those for text and data mining, AI training, and similar technologies. For all open access content, the Creative Commons licensing terms apply.


scopus.com/sources.uri
Gmail
YouTube
Maps
Adobe Acrobat
All Bookmarks
CiteScore 2023 has been released. View CiteScore methodology >
Filter refine list
Apply
Clear filters
Display options
Display only Open Access journals
Counts for 4-year timeframe
No minimum selected
Minimum citations
Minimum documents
Citescore highest quartile
1 result
Download Scopus Source List
Learn more about Scopus Source List
All
Export to Excel
Save to source list
View metrics for year:
2023
Source title
CiteScore
Highest percentile
Citations 2020-23
Documents 2020-23
% Cited
1 Materials Today: Proceedings 4.9 58% 193/463 General Materials Science 109,461 22,276 78
Top of page

Materials Today: Proceedings xxx (xxxx) xxx

Contents lists available at ScienceDirect

Materials Today: Proceedings

journal homepage: www.elsevier.com/locate/matpr

Non-isothermal decomposition study of copolymer derived from 2-amino 6-nitrobenzothiazole, melamine, and formaldehyde

Punam M Gupta [a], Yashpal U. Rathod [b], Vikram U. Pandit [c], Rajesh H. Gupta [d], Wasudeo B. Gurnule [a,*]

[a] Department of Chemistry, Kamla Nehru Mahavidyalaya, Nagpur 440024, M. S., India
[b] Department of Chemistry, J. M. Patel College, Bhandara 441904, M. S., India
[c] Department of Chemistry, H. V. Desai College, Pune 04, M. S., India
[d] Department of Chemistry, K. Z. S. Science College, Kalmeshwar 441501, Nagpur, India

ARTICLE INFO

Article history:
Available online xxxx

Keywords:
Melamine
Spectroscopy
Activation energy
Frequency factor
Synthesis
Thermal

ABSTRACT

2-Amino 6-nitrobenzohiazole, melamine, and formaldehyde were utilized as a monomer in 2:1:4 M proportions to form BMF-II copolymer using polycondensation polymerization technique in presence of 2 M HCl as catalyst. In light of the essential assessment and spectrical technique like UV–Visible, FT-IR, and ^{1}H NMR spectroscopy, the construction of the integrated copolymer not really set in stone. A non-aqueous conductometric titration approach were used to evaluate the copolymer's number average molecular weight. The surface morphology of a copolymer was concentrated on utilizing scanning electron microscopy. The The energy of activation have been evaluated from thermal methods. The four disintegration steps of the warm crumbling bend are inspected. Utilizing the Sharp-Wentworth, and Freeman-Carroll techniques the activation energy (Ea) and thermodynamic parameters were assessed. based on information from the Freeman-Carroll technique, kinetic and order of reaction, for example, entropy change (ΔS), free energy change (ΔF), evident entropy change (S^*) and recurrence factor (Z) were additionally assessed. The Activation energy calculated by these methods are good in agreement with each other. It is found that the order of reaction (n) is 1.16.
Copyright © 2022 Elsevier Ltd. All rights reserved.
Selection and peer-review under responsibility of the scientific committee of the Polymer & Mediterranean Fiber International Conference2021.

1. Introduction

Copolymers are amorphous, crystalline, or resinous polymers that have a wide range of applications. Because of the simplicity of processing, chemical and heat resistance, high thermal stability, electrical insulation capabilities, diverse properties, and cost-effectiveness, phenolic resins have been the workhorse as matrix resins in composites and therefore used in a variety of applications such as ion exchangers [1], semiconductors [2], insulating materials [3], activators [4], protective adhesives [5], and catalysts [6]. The disintegration properties of polymeric properties have long been studied by the thermogravimetric analysis methods, and many researchers have altered the monomer compositions to improve the copolymer's thermal stability at high temperatures [7,8]. Many researchers are interested in studying warm deteoriation behavior and computing kinetic parameters using modern evolving thermal degradation kinetic methodologies [9,10]. The importance of kinetics is well established since it is linked to the decomposition mechanisms that occur during thermal degradation [11,12].

Gurnule and coworkers examined the thermal decomposition of a copolymer derived from 1,5-diaminonaphthalene, 2- hydroxy, 4-methoxybenzophenone, with formaldehyde. [13]. The warm disintegration energy of copolymer blended from eight-hydroxyquino line-five-sulphonic corrosive, guanidine, and formaldehyde had been tried through Rathod and coworkers [14]. The copolymer HMBPDANF-II has been incorporated by utilizing buildup of 2-hydroxy, four-methoxybenzophenone, and 1, 5-diaminonaphthalene with formaldehyde and studied seperation of toxic metal ions from waste water by S. S. Rahagdale and coworkers [15]. Burkanudeen et al. incorporated copolymer from anthranilic corrosive, and salicylic corrosive with formaldehyde and inspected the warm corruption energy, and tried their inhibitory activity against pathogenic microbes and parasites [16]. Mujafarkani and Ahamed coordinated and concentrated on the warm

* Corresponding author.
E-mail address: wbgurnule@gmail.com (W.B. Gurnule).

https://doi.org/10.1016/j.matpr.2021.12.396
2214-7853/Copyright © 2022 Elsevier Ltd. All rights reserved.
Selection and peer-review under responsibility of the scientific committee of the Polymer & Mediterranean Fiber International Conference2021.

ScienceDirect

4.9
CiteScore

Submit your article | Guide for authors

Menu Search in this journal

About the journal

Materials Today: Proceedings provides the materials science community with a fast and flexible route to the publication of research presented at national and international scientific conferences in the field of materials science.
Guest Editors are responsible for quality control, the peer review ...

View full aims & scope

$200 ⓘ
Article publishing charge for open access

14 days
Time to first decision

44 days
Review time

81 days
Submission to acceptance

View all insights

Articles

Latest published | Articles in press | Top cited | Most downloaded

Most popular

Online ISSN: 2214-7853

Copyright © 2024 Elsevier Ltd. All rights are reserved, including those for text and data mining, AI training, and similar technologies.

For authors

Resources for authors ↗

Track your accepted paper ↗

Journal Finder ↗

Researcher Academy ↗

Rights and permissions ↗

Journal Article Publishing Support Center ↗

For editors

Resources for editors ↗

Publishing Ethics Resource Kit ↗

Guest editors ↗

For reviewers

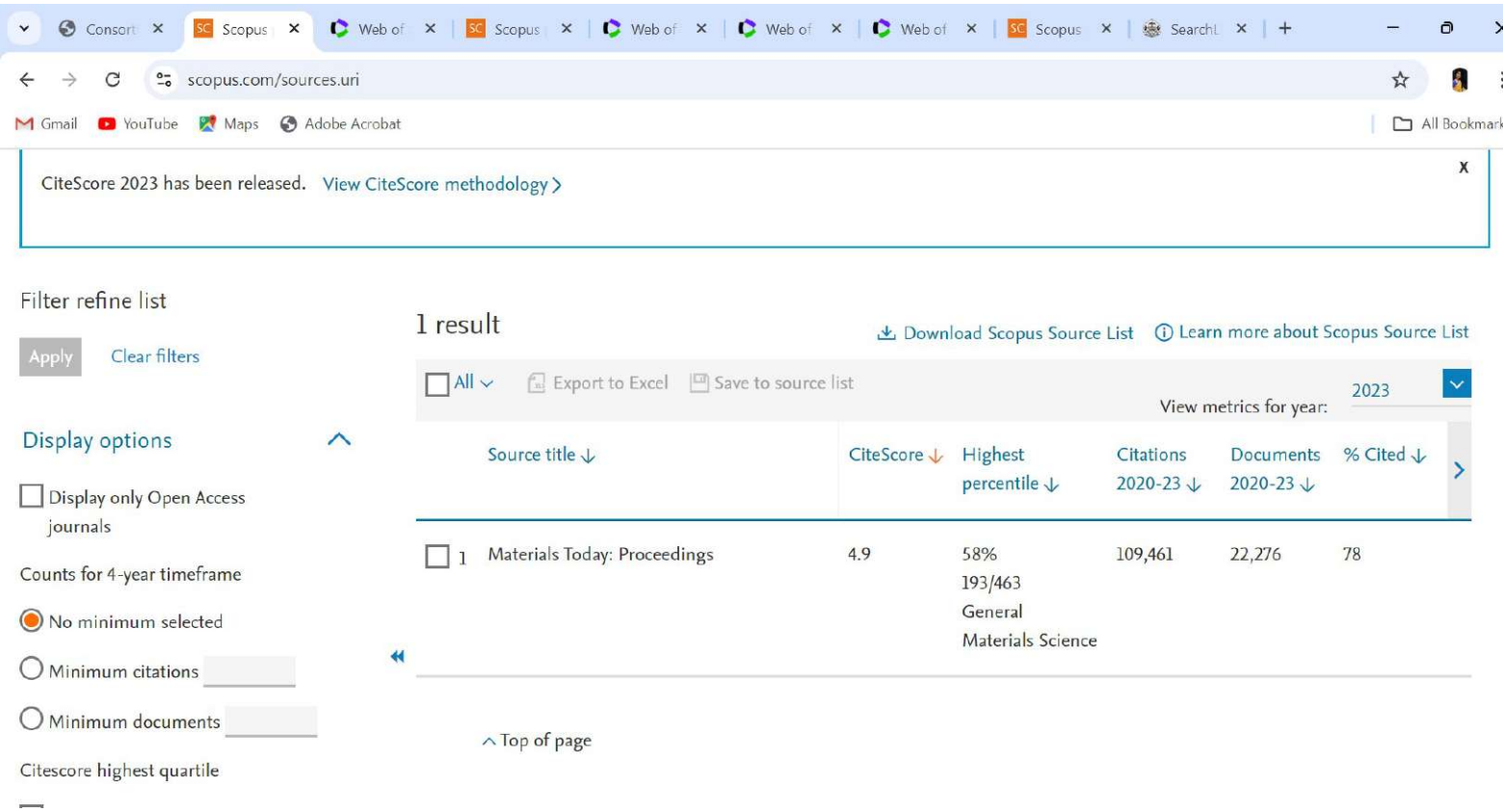
Resources for reviewers ↗

Reviewer recognition ↗

ELSEVIER

All content on this site: Copyright © 2024 Elsevier B.V., its licensors, and contributors. All rights are reserved, including those for text and data mining, AI training, and similar technologies. For all open access content, the Creative Commons licensing terms apply.

RELX™


scopus.com/sources.uri
Gmail
YouTube
Maps
Adobe Acrobat
All Bookmarks
CiteScore 2023 has been released. View CiteScore methodology >
Filter refine list
Apply
Clear filters
Display options
Display only Open Access journals
Counts for 4-year timeframe
No minimum selected
Minimum citations
Minimum documents
Citescore highest quartile
1 result
Download Scopus Source List
Learn more about Scopus Source List
All
Export to Excel
Save to source list
View metrics for year:
2023
Source title
CiteScore
Highest percentile
Citations 2020-23
Documents 2020-23
% Cited
1 Materials Today: Proceedings
4.9
58% 193/463 General Materials Science
109,461
22,276
78
Top of page

CRITERION – III

RESEARCH, INNOVATION AND EXTENSION

3.3 RESEARCH PUBLICATIONS AND AWARDS

3.3.1 NUMBER OF RESEARCH PAPERS PUBLISHED PER TEACHER IN THE JOURNALS NOTIFIED ON UGC CARE LIST DURING THE LAST FIVE YEARS

2021

Indian Journal of Chemistry
Vol. 60B, February 2021, pp. 303-320

In vitro anticancer activity of thiazole based β-amino carbonyl derivatives against HCT116 and H1299 colon cancer cell lines; study of pharmacokinetics, physicochemical, medicinal properties and molecular docking analysis

Ajay Manohar Ghatole*[a,b], Mahesh Krishanarao Gaidhane[c], Kushal Radhesham Lanjewar[d] & Kishor Manohar Hatzade[b]

[a] Department of Chemistry, Gov. Institute of Science, Civil line, Nagpur 441 001, India

[b] Department of Chemistry, Dhote Bandhu Science College, Gondia 441 614, India

[c] Department of Chemistry, Shri Lemdeo Patil Mahavidyalaya, Mandal, Kuhi, India

[d] Department of Chemistry, Mohsin Bhai Zawer College, Wadsa, Desaigang, India

E-mail: ajay.ghatole5@gmail.com; kishorhatzade@gmail.com

Received 1 December 2019; accepted (revised) 19 January 2021

The present study describes the synthesis and anticancer evaluation of certain substituted rac-(2S)-2-[(R)-[(4-substitutedphenyl){[4-(4-substitutedphenyl)-1,3-thiazol-2-yl]amino}methyl]cyclohexanone derivatives. The *in vitro* anti-cancer assay indicating substituted β-amino carbonyl derivatives **4g** and **4r** are particularly active in both tests (HCT116 and H1299). The **4f, 4o**, and **4t** are the least functioning; **4m** and **4n** are marginally active; **4b** and **4c** are more cytotoxic when the growth inhibition percent is compared with standard drugs Camptothecin (CPT.), Acyclovir (ACV), Cisplatin (CDDP.), Vinblastine (VBL) and Trichothecene (TCT.). Among them, 2-((4-*p*-tosylthiazol-2-ylamino)(4-hydroxyphenyl)methyl) cyclohexanone **4u** exhibits selective cytotoxicities for IC_{50} µg/mL against HCT116 and H1299, respectively. Simulation of virtually designed 21 compounds has been studied for active binding sites of Crystal Structure of the Cancer Genomic DNA Mutator APOBEC3B (PDB ID- 5CQD) enzyme using molecular modelling of protein-ligand interactions. The in-depth sequencing studies reveal that the involvement of APOBEC3B in cancer mutagenesis. For comparison, the binding behaviour of known standard drugs has also studied. The new SwissADME web utensil that gives free access to a pool of quick yet reliable analytical models is presented for physicochemical properties, pharmacokinetics, drug-likeness, and medicinal chemistry. Among them, in-house capable technique, for example, BOILED-Egg, iLOGP, and Bioavailability Radar, are readily available on the web.

Keywords: Thiazole derivatives, HCT116, H1299, APOBEC3B (PDB ID- 5CQD), SwissADME, BOILED-Egg, bioavailability radar

The principal aim of our effort is the discovery of novel cytotoxic and anticancer agents with fewer side effects of standard drugs (Figure 1). The three main treatments of neoplastic diseases comprise surgery, radiotherapy, and chemotherapy; this last one is the most limited, with a rate value of 5-10% of total healing. There is numeral difficulty with the safety profile and efficacy of chemotherapeutic agents. The attempts to create a new drug, which can be used further in the treatment of any disease is a formidable challenge. Many failures accompany development. It is always necessary to have a lot of creativity, intelligence, and overall good team work for better results[1].

Cytotoxic primarily affects the rapidly dividing cells, so it does not target the cancer cells, which specified in the resting phase. Finally, cytotoxic are associated with a high incidence of adverse effects. The typical examples consist of bone marrow suppression, alopecia, mucositis, nausea, and vomiting. Several publications reported on Mannich ketones as potential cytotoxins[2-5].

Some Mannich bases synthesized from thiazole or its derivatives containing aromatic or heterocyclic rings. It was estimated that at least 35% of β-amino carbonyl derivatives related articles are published in pharmaceutical journals. They are known through use in polymers, resins, the surface at active agents[6], detergent additives[7] antioxidants, and diuretic[8]. They have a broad range of biological activities, including antipsychotic[9], oxytocin[10], anticonvulsant[11], centrally acting muscle relaxant[12], anticancer[13,14], antimalarial[15], antiviral[16], anti-tubercular, anti-bacterial and anti-fungal[17]. Furthermore, β-amino

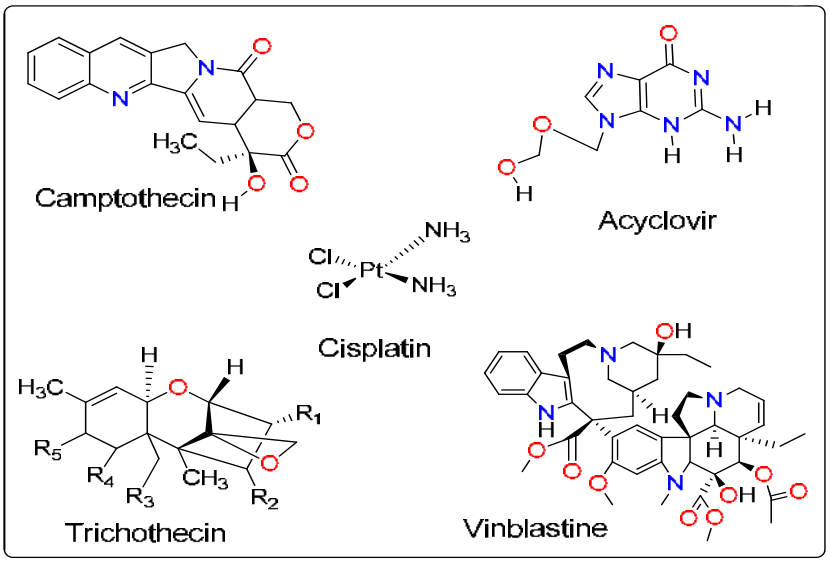


Figure 1 — Molecular structure of the standard drugs

carbonyl derivatives of various bioactive compounds have been prepared as prodrugs utilizing overwhelming some boundaries.

The synthesis of asymmetric Mannich reaction is one of the most critical results in the formation of C-C bonds in the simulated organic chemistry used during the construction of enantiomerically augmented nitrogenous molecules and their derivatives. The development of asymmetric Mannich reaction has been encouraged by a wide variety of natural products and drugs possessing optically active, nitrogen-containing molecules, which have attracted attention from synthetic chemists and the pharmaceutical industry[18-23]. To support the above study, we have to carry out the *in vitro* anticancer activity of the synthesized compounds against HCT116 and H1299 cancer cell lines with the help of Dr D. P. Manivasakam, Director, Biology Indus Pharmaceuticals 25 Olympia Avenue Suite K-600, Woburn, MA, USA.

For the additional support to study, we have carried out the computational docking against the Cancer Genomic DNA Mutator APOBEC3B (PDB ID-5CQD). A few years ago, scientists discovered a distinctive mutagen that poses in our cells: APOBEC, a protein that habitually functions as a preserving agent against viral infection. APOBEC3B is a member of the astronomical family of zinc-dependent DNA deaminases that to adherent the cytosine that works typically as a nuclear-localized restriction factor of DNA-based pathogens bases into uracil in single-stranded DNA and RNA[24,25]. APOBEC is a useful yet fatal, intrinsic cellular protein. Typically meant to fight viruses, it has only the power of modifying single-stranded DNA. Human double-stranded DNA, therefore, should not be altered. But scientists observed that mutations brought by APOBEC found in many tumorous cells, throughout the genome[26]. The APOBEC3B mutagenesis accounts for the most clustered and dispersed cytosine deamination that causes mutation in cancer. The cause of the disease is because of abnormal cell growth, which docks DNA mutations, electrifying during the DNA replication process. If the regular miscue takes place without having any deadly effect on the organism, a specific part of the genome may be affected by which causes the accumulation of the mutant cell, which then enters the body. Today geneticist has conceived how APOBEC takes supremacy of a weakness in our DNA approximation process to check mutations in our genome[27].

Notwithstanding the above computational examination, we additionally utilize advance and new methodology, *i.e.*, Swiss absorption, distribution, metabolism, and excretion study. Swiss ADME is an excellent and exhaustive site kept running by the Swiss foundation of bioinformatics (SIB), which gives bioinformatics administrations and assets to researchers around the world. SIB has more than 65 bioinformatics research gatherings and 800 researchers from the real Swiss schools of advanced education and research institute. Swiss ADME

empowers the appraisal of ADME parameters of medication applicants and small molecules and gives data that permits early hazard evaluation in the drug improvement process. Eminently, swissADME provides a stage to evaluate Lipinski's rule of five[28] for medication resemblance of oral bioavailability. Drug-likeness is an unpredictable equalization of molecular properties and structural features that decide if an unfamiliar molecule resembles the known drug. These molecular properties incorporate hydrophobicity, electronic dispersion, and hydrogen bonding attributes molecular size and adaptability. SwissADME includes the 'BOILED-Egg' assessment[29] that foresee gastrointestinal captivation (HIA) and efflux/maintenance by P-glycoprotein (Pgp). Also, the blood-brain barrier (BBB) infiltration and Cytochrome P450 (CYP) enzyme substrate-restraint expectation can make.

Overall, these *in vitro* and computational studies provide a framework for further mechanistic studies and the development of novel anti-cancer drugs to inhibit this enzyme. Among these methods, docking has been used widely in drug designing for cancer[30,31] dampen tumour evolution, and minimize adverse outcomes such as drug resistance and metastasis. So, it better to limit the present study to some selected cancer macromolecules. The role of these macromolecules well studied by different scientists from time to time[32,33], and their inhibition justifies the role in anticancer potential.

Furthermore, there are increasing concerns about environmental effects, which require synthetic manipulation that minimize the use of hazardous chemicals. Many strategies have devised and investigated, mainly by replacing the traditional organic with other non-toxic solvents. Recently, ionic liquids have attracted broad interest as excellent alternatives to organic solvents, due to there desirable properties, such as non-flammability, no measurable vapour pressure, low toxicity, reusability, low-cost and high thermal stability[34-38]. In addition to the polar properties of ionic liquids, they are non-coordinating, which avoids any undesired solvent binding in pre-transition states, and hence offers excellent advantages for asymmetric synthesis. As a result, ionic liquids considered promising alternative solvents for organic reactions. Over the past few years, these liquids have generated a significant amount of interest[39-49].

Result and Discussion

In this study, we observed that substituted thiazole-based β-amino carbonyl derivatives**4d**, **4g**, **4i**, **4k**, **4l**, **4r**, **4s**, and **4u** are more cytotoxic than the growth inhibition% compared with standard drug's CPT., ACV., CDDP., VBL., and TCT. Indifferent human cancer cell lines with several p53 statuses. Besides, asymmetric synthesis of various functional molecules is one of the essential tasks in modern organic synthesis[50]. Therefore, it is crucial to develop efficient a symmetric C-C bond forming reactions.

The IR spectra of compounds **4a-u** showed a peak at 3098-3150 cm^{-1} due to –NH function. A sharp band observed at 1680-1720 cm^{-1} corresponding to the carbonyl (-C=O) function derived from cyclohexanone structure.

The ^{1}H NMR spectra of compounds **4a-u** displayed an additional signal at 6.53 ppm due to the –NH linkage derived from a thiazole moiety with aldehyde and cyclohexanone, while the sign due to the $–NH_2$ group of thiazole structure did not appear. The singlet for $–OCH_3$ observed at 3.6 ppm integrated for three protons in ^{1}H NMR spectra of compounds **4a-h**. The ^{1}H NMR spectra of compounds **4i-p** and **4q-u** revealed singlets at 9.1 ppm and 1.3 ppm integrating for a single proton of –OH group and three protons of $–CH_3$ group, respectively. Also, $-OCH_3$ group of compound**4b** resonated at 3.84 ppm integrating for three protons as a singlet in the ^{1}H NMR spectrum. Moreover, the signals derived from two $–CH_3$ groups in compound **4c** and **4j** were recorded at 2.3 ppm integrating for three protons. A singlet at 9.1 ppm observed for the Ar –OH group of compound **4u**.

The ^{13}C NMR spectrum of compound **4a** showed aromatic resonances at 126.0, 129.4, and 151.7 for aromatic carbon atoms. Aromatic resonance's signals for -Cl carbon appears at 162.32 for $–OCH_3$, -OH, $-CH_3$ substitution and fused aldehydic aromatic carbon of compound 4a appears at 139.54, 134.14, 130.44, 129.23, 126.51 and 115.48. The carbon of cyclohexanone ring found at 57.22, 39.52, 27.92, 25.65, 23.65, respectively. The peak corresponding to the $–OCH_3$ at 61.9 and the peaks at 62.9 and 64.6 indicated the attachment of cyclohexanone ring *via* aromatic aldehyde with the formation of diastereomer arising from two unresolved chiral centres. The compounds **4a-u** revealed peaks at 211.0-217.3, suggesting the presence of -C=O of cyclohexanone ring.

In this paper, we demonstrate an asymmetric Mannich-type reaction in ionic liquids (Scheme I).

The elemental analysis and molecular ion peaks of compounds **4a-u** were consistent with the assigned structure. The yield and melting point reported in Table I.

Table I — Synthesis of compounds **4a-u**

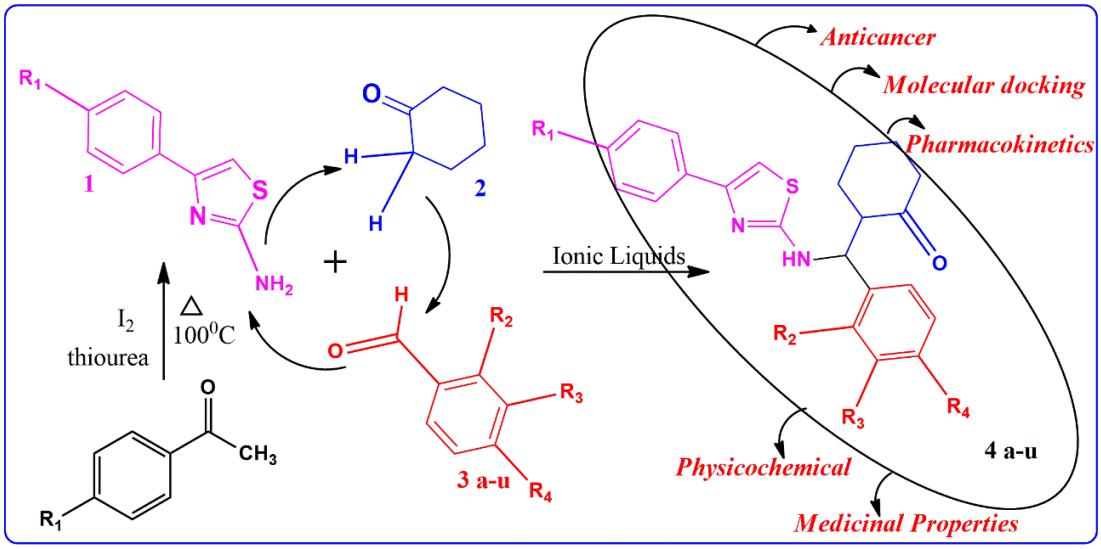
S. No.	R_1	R_2	R_3	R_4	Time (hr.)	m.p. (°C)	% Yield
4a	OCH_3	Cl	H	H	6	217	85
4b	OCH_3	H	H	OCH_3	6	190	89
4c	OCH_3	H	H	$N(CH_3)_2$	6	185	87
4d	OCH_3	H	H	F	6	188	85
4e	OCH_3	H	H	Cl	6	195	84
4f	OCH_3	H	Cl	H	6	245	84
4g	OCH_3	H	NO_2	H	6	190	84
4h	OCH_3	H	H	H	6	194	83
4i	OH	H	H	OCH_3	6	232	92
4j	OH	H	H	$N(CH_3)_2$	6	212	86
4k	OH	H	H	F	6	232	90
4l	OH	H	H	Cl	6	235	90
4m	OH	H	Cl	H	6	254	91
4n	OH	H	NO_2	H	6	230	89
4o	OH	H	H	OH	6	230	90
4p	OH	H	H	H	6	258	82
4q	CH_3	H	H	OCH_3	6	130	85
4r	CH_3	H	H	Cl	6	124	84
4s	CH_3	H	Cl	H	6	125	83
4t	CH_3	H	NO_2	H	6	125	84
4u	CH_3	H	H	OH	6	126	83

Biological activity of the target molecules

All compounds, as well as the standard drugs (Figure 1), were evaluated *in vitro* against a 2-cell line panel consisting of HCT116 and H1299 colon cancer cell lines, respectively. Results of all the substituted 2-((4-phenyl)(4-(4-phenyl)thiazol-2-ylamino)methyl)-cyclohexanone derivatives **4a-u** are active, out of which most of the methoxy; hydroxy-phenylthiazole (**4a-c**, **e-f**, **h**, **j**, **m)** and methyl-phenylthiazole unit of substituted Mannich derivatives (**4q**, **4t)** exhibited a weak inhibitory activity on the growth of HCT116. The H1299 cell line, all the compounds, shows promising activity. 2-(((4-(4-methoxyphenyl) thiazol-2(3H)-ylidene)amino)(3-nitrophenyl)methyl) cyclohexanone (**4g)** and 2-((4-chlorophenyl)((4-(p-tolyl)thiazol-2(3H)-ylidene)amino)methyl)cyclohexanone (**4r)** were particularly active in both assays; 2-((3-chlorophenyl)((4-(4-methoxyphenyl)thiazol-2(3H)-ylidene)amino)methyl)cyclohexanone (**4f**) and 2-((4-hydroxyphenyl)((4-(4-hydroxyphenyl)thiazol-2(3H)-ylidene)amino)methyl)cyclohexanone (**4o**) were the least functioning; **4m** and **4n** are marginally active. The effect of all new compounds on colon cancer cell lines HCT116 and H1299 was observed, and results depicted in Figures 2-5. Growth inhibition % compared with standard drugs Camptothecin, Acyclovir, Cisplatin, Vinblastine, and Trichothecene. (Table II, Table III and Figures 6-7).

Geometrical conformation

The possible existence of the prepared compounds in various tautomeric forms represented in (Figure 8).



Scheme I — One pot synthesis of thiazole based β-amino carbonyl derivatives

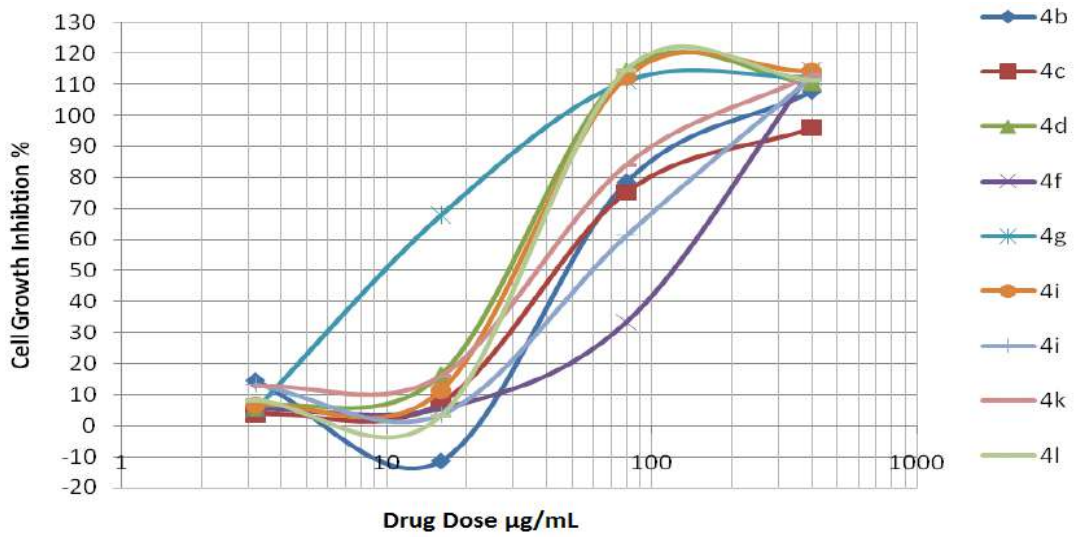


Figure 2 — Colon Cancer Cell (HCT116) growth inhibition against compounds **4b-l**

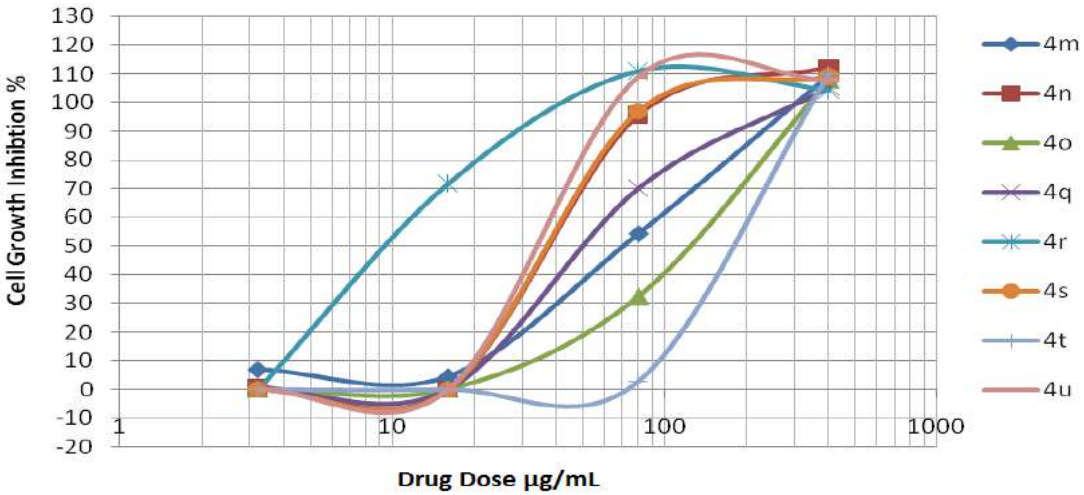


Figure 3 — Colon Cancer Cell (HCT116) growth inhibition against compounds **4m-u**

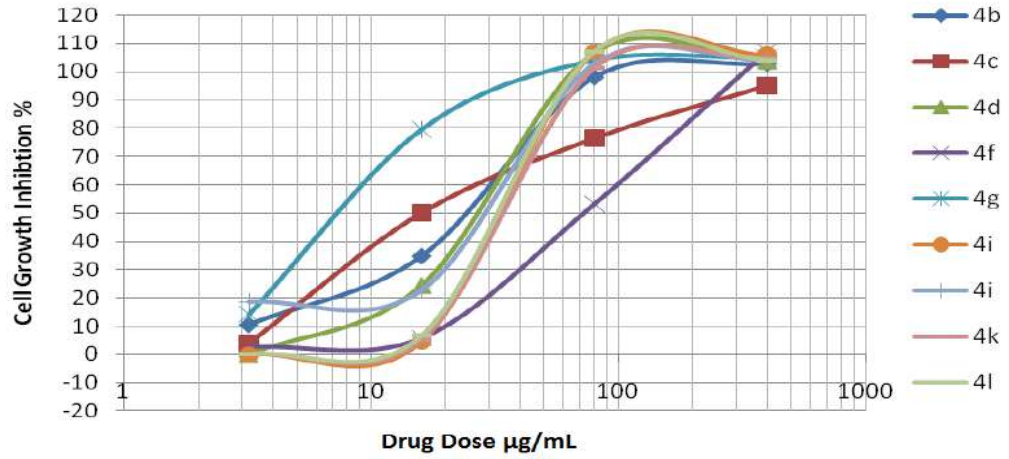


Figure 4 — Colon Cancer Cell (H1299) growth inhibition against compounds **4b-l**

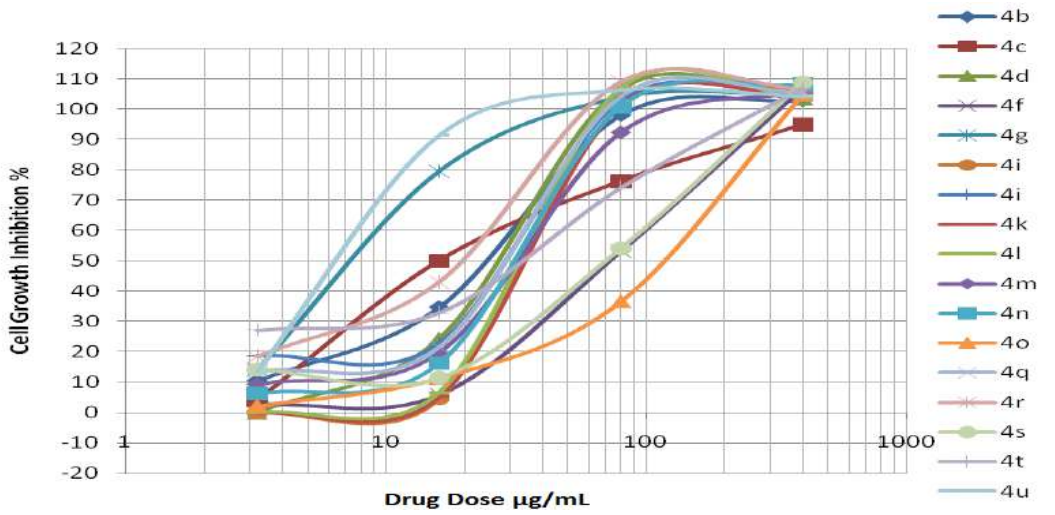


Figure 5 — Colon Cancer Cell (H1299) growth inhibition against compounds **4b-u**

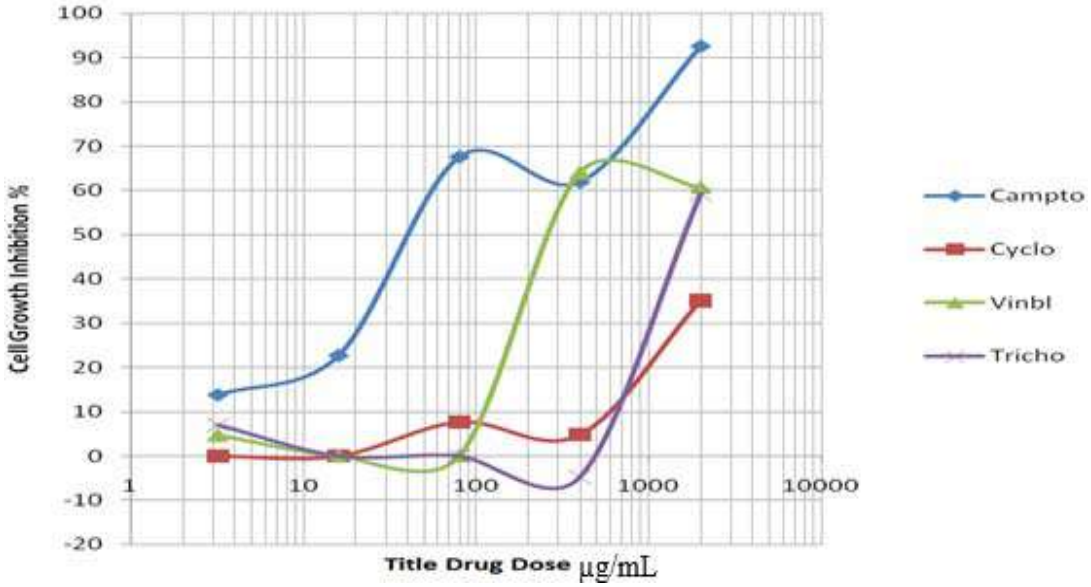


Figure 6 — Colon Cancer Cell (HCT116) growth inhibition against standard anticancer drugs

Table II — IC_{50} µg/mL of all synthesized compounds **4b-u**

	4b	**4c**	**4d**	**4f**	**4g**	**4i**	**4j**	**4k**	**4l**	**4m**	**4n**	**4o**	**4q**	**4r**	**4s**	**4t**	**4u**
HCT116	50	50	30	120	10	30	70	40	30	60	40	150	50	10	40	200	35
H1299	25	20	40	80	8	30	40	40	30	30	35	150	30	20	70	35	5.5

Table III — Docking score (kcal/mole) of various anticancer drugs with APOBEC3B (PDB ID: 5QCD)

S. No.	Ligand	Docking score (kcal/mole)
1.	Camptothecin	- 5.9
2.	Acyclovir	- 4.9
3.	Cisplatin	- 2.8
4.	Trichothecin	- 4.8
5.	Vinblastine	- 7.0

In order to achieve better insight into the molecular structure of the most bioactive stereoisomer or tautomeric forms for compounds **4a-u**, conformational analysis of the target compounds has been proposed (Figure 8).

The tautomeric equilibrium clearly reveals that the central amino residue is in interaction with the keto group of cyclohexanone moiety. So, a significant impact on the binding energies and binding process

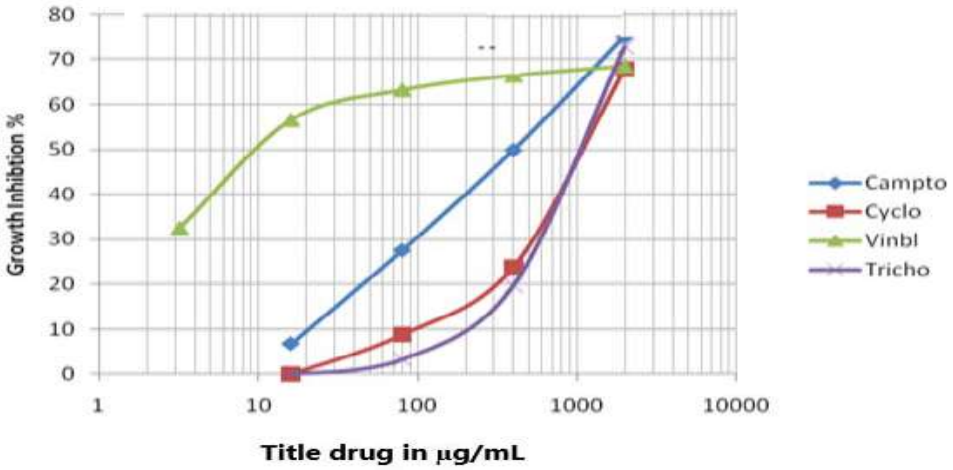


Figure 7 — Colon Cancer Cell (H1299) growth inhibition against standard anticancer drugs

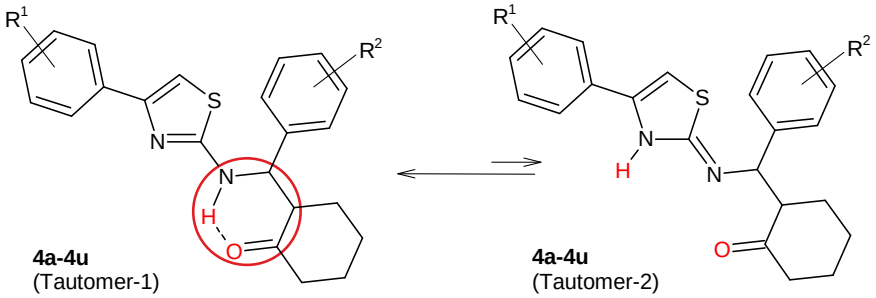


Figure 8 — Proposed tautomer structures of most stable stereoisomer compound

interaction with bio target were observed (Table II). This could probably be due to the presence of opening/closing pseudo-ring in the synthesized compounds **4a-u**.

Molecular modelling

Docking of the known anticancer drug in the active site of APOBEC3B (PDB ID: 5QCD) enzyme

A comparative study involving the interaction of known anticancer *viz*. Camptothecin, Acyclovir, Cisplatin, Trichothecin, and Vinblastine ion the active site pocket of APOBEC3B made for a better understanding of there anticancer action. Docking score of these depicted in Table III

In the case of APOBEC3B selective Vinblastine (Figure 9), the negative binding energies (-7.0 kcal/mol) are in agreement with its APOBEC3B selectivity as reported in several kinds of literature. Binding of Vinblastine in the binding pocket of APOBEC3B resulted from the conformational placement of amino acid residues in the active site and through hydrophobic interactions.

There is a weak hydrogen bond of 2.88, 3.18, 3.19, and 3.22Å between the vinblastine carbonyl and three amino acid *viz*. Arg212, Trp281, and Gln213, as well as they, show hydrophobic interaction. The distal carbonyl oxygen and carbon of vinblastine show aromatic as well as allyl interaction with Tyr215, Arg211, and Phe237.

Complexation of the docked ligand **4a-u** and standard drugs with APOBEC3B enzyme was interpreted by looking at the H-bonding or hydrophobic interaction of the ligand with the amino acid residues in the active site. The results are summarized in Table IV.

Docking of the synthesized ligand into APOBEC3B (PDB ID: 5CQD) active site

All the twenty-one synthesized β-amino carbonyl derivatives showed binding in the 5CQD active site with binding scores between -5.8 and -6.6 kcal/mol, as shown in Table IV. The compelling data can be utilized further to develop potent anti-cancer heterocycles.

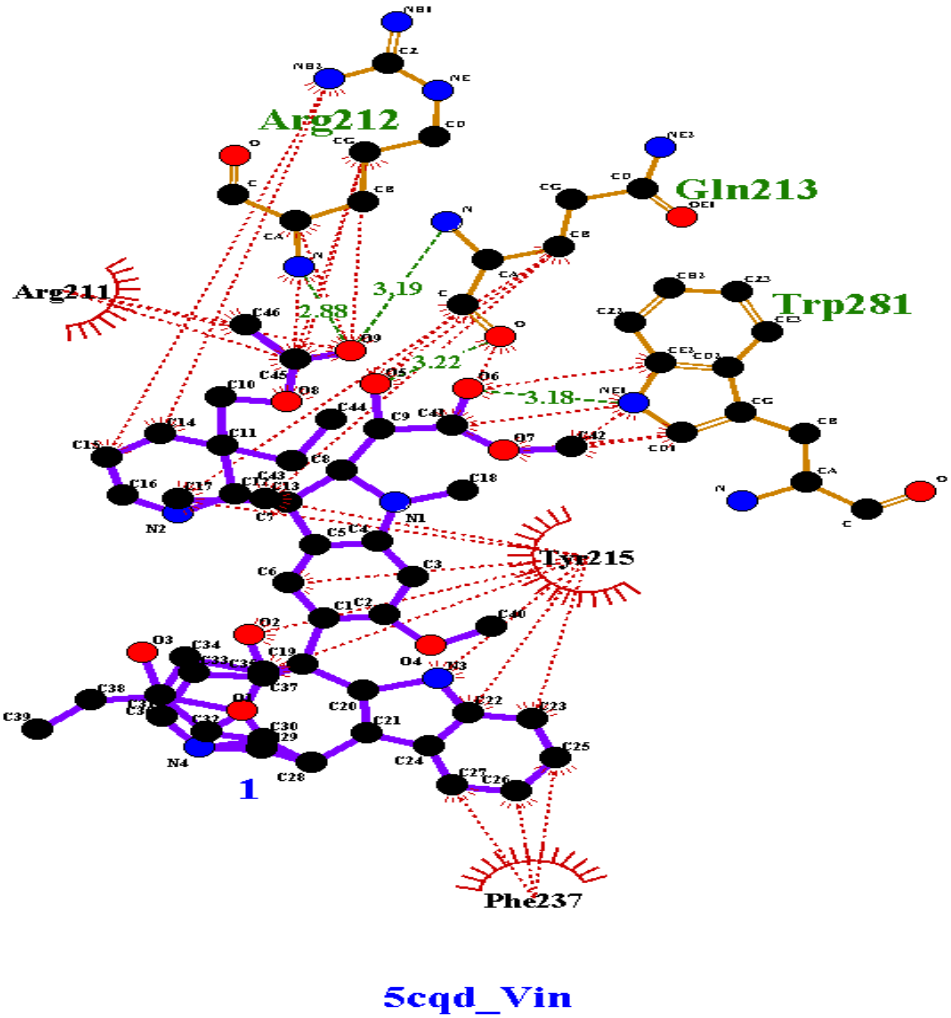


Figure 9 — LIGPLOT Ligand (Vinblastine)-protein PDB ID- 5CQD interaction diagram

Table IV — Docking score (kcal/mole) of different β-amino carbonyl analogue ligands **4a-u** with APOBEC3B (PDB ID: 5CQD)

S. No.	Ligand	Docking score (kcal/mol)	S. No.	Ligand	Docking score (kcal/mol)
1.	**4a**	-5.8	12.	**4l**	-5.9
2.	**4b**	-5.9	13.	**4m**	-5.9
3.	**4c**	-5.9	14.	**4n**	-6.2
4.	**4d**	-6.0	15.	**4o**	-6.1
5.	**4e**	-5.9	16.	**4p**	-5.9
6.	**4f**	-5.9	17.	**4q**	-6.3
7.	**4g**	-6.2	18.	**4r**	-6.4
8.	**4h**	-5.8	19.	**4s**	-6.5
9.	**4i**	-6.0	20.	**4t**	-6.6
10.	**4j**	-5.9	21.	**4u**	-6.3
11.	**4k**	-6.0			

Detailed 4t-5CQD structural interaction having the highest binding score among the other synthesized β-amino carbonyl derivatives

From a consideration of the stereo view of **4t** complexed inside the active-site gorge of 5CQD together with the LIGPLOT diagrams displayed in Figure 10, the following assignments can be made for protein-inhibitor interactions.

The carbonyl oxygen of Gln213 shows hydrophobic interaction with the sulfur and carbon atoms of the thiazole ring along with this sulfur from thiazole interact with the aromatic ring of Tyr215. On top of communication, there is a weak hydrogen bond of 3.07Å between the carbonyl oxygen of the cyclohexanone chain with the primary amine of Gln213. Near the top of the gorge, the distal nitro group of **4t** makes interaction with Tyr215

and a herringbone interaction with Gln213. At the bottom of the canyon and side amino acid, there is an aromatic-aromatic interaction between the proximal phenyl ring of **4t** and Trp281 and the carbon and nitrogen atom of nitro-substituted aromatic carbon ring interact with Tyr215. The Arg211 and Arg212 show electrostatic interaction between the cationic *meta* carbon of nitrobenzene ring and cyclohexanone ring.

The LIGPLOT diagrams in Figure 10 show atoms-atoms contacts of ≤ 3.09Å made by the three inhibitors, *viz*. **4r**, **4s**, and **4t** having the highest negative value compare with the other amino-acid residues lining the active site. The inhibitors show hydrophobic interaction with nearby side chains, as shown in red dashed. The red circles and ellipses in each plot designate protein residue that are corresponding 3D positions to the residues in the plot. The hydrogen bond is shown as green dotted lines, while the spoked arcs signify residues making nonbonded contact with the ligand. The highlighted equivalent side-chain residue has red underly beneath

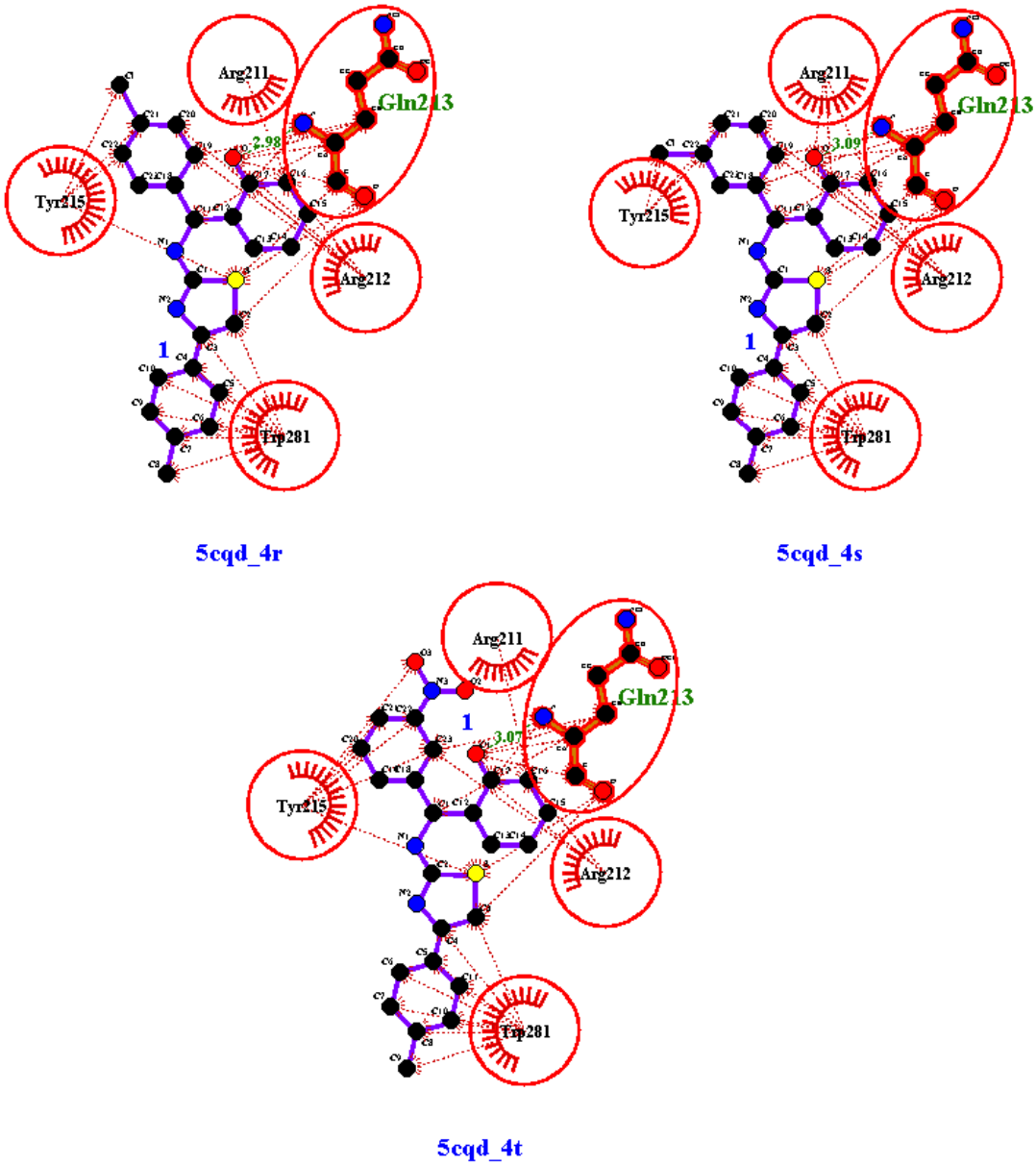


Figure 10 — Ligand-protein interaction diagrams for binding sites of the same protein APOBEC3B (PDB ID- 5CQD) each with a different ligand molecule having maximum negative binding value

there bond and atoms. Equivalent waste engaged in hydrophobic interaction shown in thicker lines.

Detailed study of Pharmacokinetics, Physicochemical, and Medicinal Properties by SwissADME online screening

The operational highlights of these molecules entered in the SwissADME site (http://swissadme.ch) utilizing the ChemAxon's Marvin JS structure drawing instrument. Auxiliary highlights of a pharmacophore impact the conduct of a unit in people, including bioavailability, transport properties, empathy to proteins, reactivity, poisonous quality, and metabolic steadiness. Incomparable to swissADME is the bioavailability radar [51] that gives a graphical preview of the medication similarity parameters of an orally available bioactive drug. The drug resemblance diagram displayed as a hexagon (Figure 11) with each of the vertices speaking to a setting that characterizes a bioavailable drug. The pink region inside the

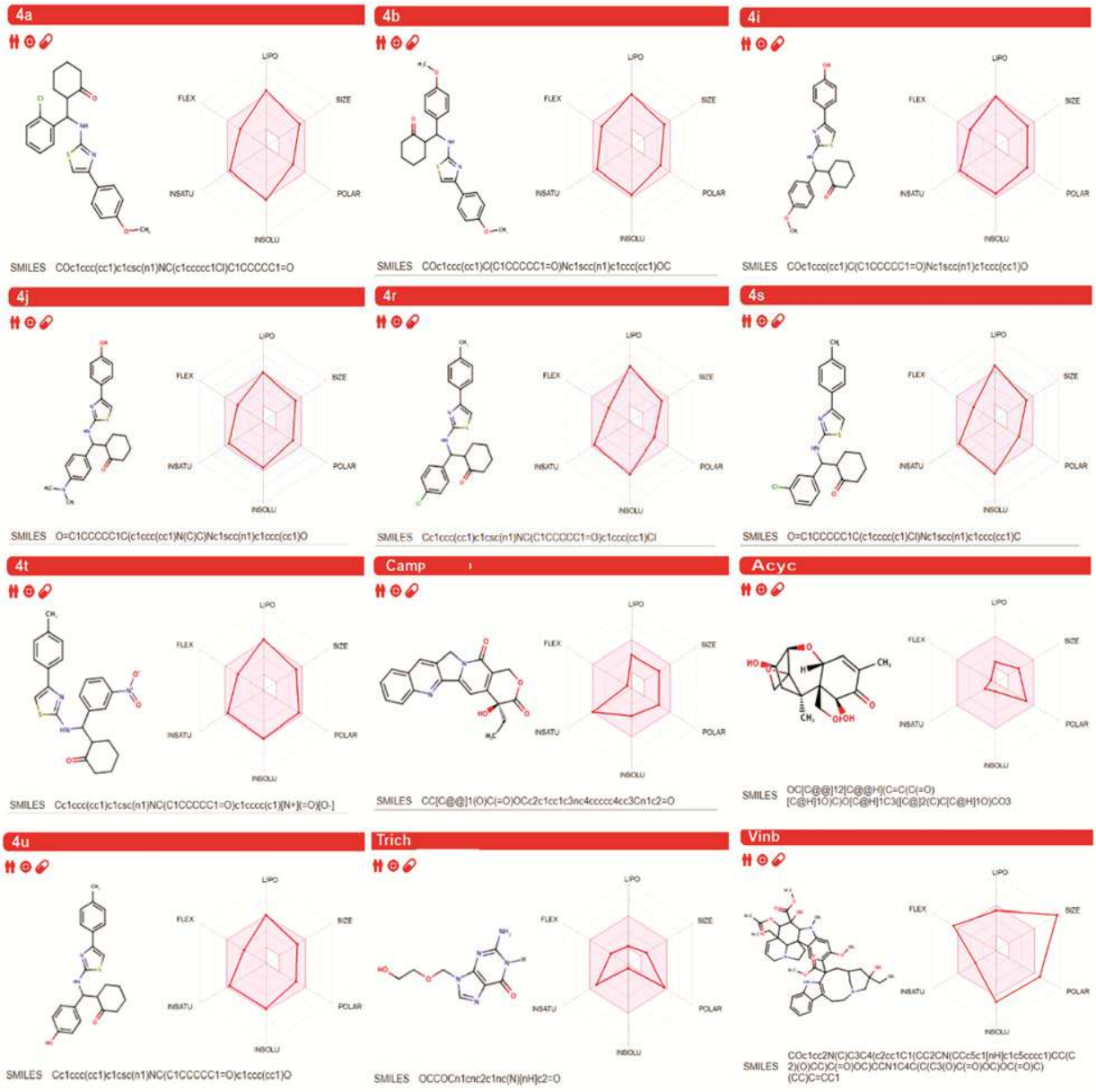


Figure 11 — The bioavailability radar of the synthesized molecules (**4a-u**) and standard drugs (Camp., Acyc., Trich., Vinb.) evaluating using the swissADME web tool

hexagon speaks to the ideal range for every property (lipophilicity: XLOGP3 between − 0.7 and + 5.0, size: polarity: TPSA somewhere in the range of 20 and 130 Å, MW somewhere in the range of 150 and 500 g/mol, solubility: log S not higher than 6, flexibility: close to 9 rotatable bonds, and saturation: part of carbons in the sp3 hybridization at least 0.25) Table V.

Drug-likeness

The drug resemblance properties of the fused compound and standard drug are articulated to by the red mutilated hexagon inside the pink shade (Figure 11). The **4b-d**,**g-k**,**n-p**,**t-u** molecules fall within the drug-likeness parameter of a bioavailable drug. While **4a**,**r**,**s** shows outside parameters describe for lipophilicity and insolubility for bioavailability parameter and **4e**,**f**,**l**,**m** have slightly outside the optical range of lipophilicity. (Figure 11). SwissADME likewise has computational channels that incorporate Ghose[52], Egan[53], Veber[54], and Muegee[55] created by top pharmaceutical organizations and cheminfomaticians to assess the drug resemblance of molecules.

The Ghose screen quantitatively describes molecules dependent on figured physicochemical property profiles that incorporate log P, molar refractivity (MR), molecular weight (MW), and several atoms. The passing scope of determined log P (ClogP) is between -0.4 and 5.6. For MW, the moving extent is somewhere in the range of 160 and 480. For MR, the passing reach is somewhere in the range of 40 and 130, and for the total number of atoms, the moving extent is between 20 and 70 atoms in a small molecule. Our compounds **4b,c, g-q, t-u**, and out of four standard drugs tested only camptothecin qualify the Ghose qualifying criteria, but the molecule **4a,e,f,r**, and **4s** out of the qualifying range (Table VI).

Veber (GSK filter) model represents molecules as druglike on the off chance that they have ten or less rotatable bonds and a PSA equivalent to or under 140 Å2 with 12 or less H-bond donors and acceptors.

Egan (Pharmacia) filter gives an expectation of drug assimilation dependent on physical procedures engaged with film absorbency of a molecule. Significantly, the Egan computational model for human passive intestinal absorption (HIA) of

Table V — Physicochemical properties of the synthesized molecules **(4 a-u)** and standard drugs(MW: Molecular weight; HA: Heavy atoms; AHA: Aromatic heavy atom; FCsp3: Fraction Csp3; RTB: Rotatable bonds; HBA: H-bond acceptors; HBD: H-bond donors; MR: Molar refractivity; TPSA: Total polar surface area).

Sr. No.	MW	HA	AHA	FCsp3	RTB	HBA	HBD	MR	TPSA
4a	426.96	29	17	0.3	6	3	1	119.77	79.46
4b	422.54	30	17	0.33	7	4	1	121.25	88.69
4c	435.58	31	17	0.36	7	3	1	128.97	82.7
4d	410.5	29	17	0.3	6	4	1	114.72	79.46
4e	426.96	29	17	0.3	6	3	1	119.77	79.46
4f	426.96	29	17	0.3	6	3	1	119.77	79.46
4g	437.51	31	17	0.3	7	5	1	123.58	125.28
4h	392.51	28	17	0.3	6	3	1	114.76	79.46
4i	408.51	29	17	0.3	6	4	2	116.79	99.69
4j	421.56	30	17	0.33	6	3	2	124.5	93.7
4k	396.48	28	17	0.27	5	4	2	110.25	90.46
4l	412.93	28	17	0.27	5	3	2	115.3	90.46
4m	412.93	28	17	0.27	5	3	2	115.3	90.46
4n	423.48	30	17	0.27	6	5	2	119.12	136.28
4o	394.49	28	17	0.27	5	4	3	112.32	110.69
4p	378.49	27	17	0.27	5	3	2	110.29	90.46
4q	406.54	29	17	0.33	6	3	1	119.73	79.46
4r	410.96	28	17	0.3	5	2	1	118.25	70.23
4s	410.96	28	17	0.3	5	2	1	118.25	70.23
4t	421.51	30	17	0.3	6	4	1	122.06	116.05
4u	392.51	28	17	0.3	5	3	2	115.26	90.46
Camp	348.35	26	16	0.25	1	5	1	95.31	81.42
Acyc	296.32	21	0	0.8	1	6	3	70.66	99.52
Trich	225.2	16	9	0.38	4	5	3	55.68	119.05
Vinb	810.97	59	15	0.59	10	11	3	232.52	154.1

molecule represents dynamic carriage and efflux components and is, in this way, vigorous in foreseeing adaptation of drugs. The Egan violation only observed in **4n**,**r**,**s**, and standard vinblastine drugs (Table VI).

Muegge (Bayer filter) model is a database-free pharmacophore point screen that separates between drug-like and nondrug-like matter. It depends on the perception that non-drugs are frequently less functionalized. Four purposeful themes are characterized to be significant in drug-like molecules and incorporate hydroxyl, amine, ketone, and sulfonyl groups. In this manner, a base check of well-characterized pharmacophore focuses is required to pass the screen. The manifestation of these efficient themes ensures hydrogen-holding capacities that are basic for explicit drug cooperation with its objectives. These serviceable groups can consolidate to what Muegge model alludes to as pharmacophore points. The pharmacophore emphases incorporate amine, amide, alcohol, ketone, sulfone, sulfonamide, carboxylic acid, carbamate, guanidine, amidine, urea, and active ester groups. These pharmacophore efforts in molecules possibly give critical communications with the objective protein. From the screening data, the synthesized compound **4a-h**,**l**,**m**,**q**,**r**,**s**,**t**, and **u** that they don't have the recommended functional group for the interaction with the target protein suggested by the Muegge.

PAINS, Break and Leadlikeness screening

PAINS (pan-assay interference screening) that often gives false favourable chemical properties results in high-throughput screens. PAINS tend to react non-specifically with numerous biological targets rather than specifically affecting one anticipated goal.

PAINS (pan-assay interference screening) that regularly give false favourable synthetic properties bring about high-throughput screens. PAINS will, in general, respond non-specifically with various biological targets as opposed to explicitly influencing one anticipated objective. SwissADME evaluation did not post any PAINS alert except **4c** and **4j** molecules (Table VII).

In another choice model, Brenk[56] considered composites that are smaller and less hydrophobic and

Table VI — Drug-likeness evaluation of synthesized compounds (**4 a-u**) using swissADME

Sr. No.	Lipinski #violations	Ghose #violations	Veber #violations	Egan #violations	Muegge #violations
4a	0	1	0	0	1
4b	0	0	0	0	1
4c	0	0	0	0	1
4d	0	1	0	0	1
4e	0	1	0	0	1
4f	0	1	0	0	1
4g	0	0	0	0	1
4h	0	0	0	0	1
4i	0	0	0	0	0
4j	0	0	0	0	0
4k	0	0	0	0	0
4l	0	0	0	0	1
4m	0	0	0	0	1
4n	0	0	0	1	0
4o	0	0	0	0	0
4p	0	0	0	0	0
4q	0	0	0	0	1
4r	0	1	0	1	1
4s	0	1	0	1	1
4t	0	0	0	0	1
4u	0	0	0	0	1
Camp	0	0	0	0	0
Acyc	0	1	0	0	0
Trich	0	1	0	0	0
Vinb	2	3	1	1	4

Table VII — Medicinal chemistry evaluation of the synthesized compounds

Sr. No.	PAINS #alerts	Brenk #alerts	Leadlikeness #violations	Synthetic Accessibility
4a	0	0	2	3.97
4b	0	0	2	4.01
4c	2	0	2	4.13
4d	0	0	2	3.89
4e	0	0	2	3.87
4f	0	0	2	3.91
4g	0	2	2	4.06
4h	0	0	2	3.86
4i	0	0	2	3.9
4j	2	0	2	4.03
4k	0	0	2	3.79
4l	0	0	2	3.78
4m	0	0	2	3.82
4n	0	2	2	3.97
4o	0	0	2	3.81
4p	0	0	2	3.77
4q	0	0	2	3.98
4r	0	0	2	3.93
4s	0	0	2	3.96
4t	0	2	2	4.11
4u	0	0	2	3.89
Camp	0	0	0	3.84
Acyc	0	1	0	5.42
Trich	0	0	1	2.47
Vinb	0	2	3	9.65

not those characterized by "Lipinski's standard of 5" to enlarge open doors for lead streamlining. That was after the prohibition of compounds with possibly mutagenic, reactive, and unfavourable groups, for example, nitro, sulfates, phosphates, 2-halopyridines, and thiols. Brenk model confines the ClogP/ClogD to sandwiched between zero and four, the quantity of hydrogen-bond donors and acceptors to less than 4 and 7, individually, and the number of substantial atoms to in the range of 10 and 27. Furthermore, just compounds with restricted entanglement characterized as less than eight rotatable bonds, less than five ring structures, and no ring structures with more than two fused rings are considered medicinal. The **4g**,**n**, and **4t** flouted two break rules by the presence of one nitro group, and standard Vinblastine also had two breaks.

Leadlikeness tests are proposed to furnish leads with great kinship in high-throughput screens that take into account the detection and manipulation of new exchanges in the lead advancement stage (Table VII). The standard drugs camptothecin and acyclovir passed all the leadlikness criteria, while the synthesized compound with the standard trichothecene and vinblastine fail in leadlikness.

P-glycoprotein and CYP enzyme activity prediction

SwissADME additionally empowers the estimation for a compound to be a substrate of p-glycoprotein (P-gp) or inhibitor of the cytochrome p450 isoenzymes (CYP isoenzymes). P-gp is broadly dispersed and communicated in the intestinal epithelium where it thrusts xenobiotics, for example, medicates over into the intestinal lumen and in the delicate endothelial cells making the blood-brain barrier where it propels them once again into the vessels. CYP isoenzymes are in charge of the biotransformation of drugs[57]. Drug digestion through CYP isoenzymes is a significant determinant of drug connections that can prompt to drug toxicities and diminished pharmacological impact. The models return "Yes" or "No" if the molecule under examination has a higher likelihood to be substrate or non-substrate of P-gp or inhibitor or non-inhibitor of a given CYP. The screening results are tabulated in Table VIII.

Table VIII — Pharmacokinetic evaluation of the synthesized compounds (GI: gastro-intestinal absorption; BBB: blood-brain barrier; CYP: Cytochromes, P-gp: P-glycoprotein)

Sr. No.	GI absorption	BBB permeant	Pgp substrate	CYP1A2 inhibitor	CYP2C19 inhibitor	CYP2C9 inhibitor	CYP2D6 inhibitor	CYP3A4 inhibitor
4a	High	No	Yes	No	Yes	Yes	Yes	Yes
4b	High	No	Yes	No	Yes	Yes	Yes	Yes
4c	High	No	Yes	No	Yes	Yes	Yes	Yes
4d	High	No	Yes	No	Yes	Yes	Yes	Yes
4e	High	No	Yes	No	Yes	Yes	Yes	Yes
4f	High	No	Yes	No	Yes	Yes	Yes	Yes
4g	Low	No	No	No	Yes	Yes	No	Yes
4h	High	No	Yes	Yes	Yes	Yes	Yes	Yes
4i	High	No	Yes	Yes	Yes	Yes	Yes	Yes
4j	High	No	Yes	Yes	Yes	Yes	Yes	Yes
4k	High	No	Yes	Yes	Yes	Yes	Yes	Yes
4l	High	No	Yes	Yes	Yes	Yes	Yes	Yes
4m	High	No	Yes	Yes	Yes	Yes	No	Yes
4n	Low	No	Yes	Yes	Yes	Yes	No	Yes
4o	High	No	Yes	Yes	Yes	Yes	Yes	Yes
4p	High	No	Yes	Yes	Yes	Yes	Yes	Yes
4q	High	No	Yes	No	Yes	Yes	Yes	Yes
4r	High	No	Yes	Yes	Yes	Yes	No	Yes
4s	High	No	Yes	Yes	Yes	Yes	No	Yes
4t	Low	No	No	Yes	Yes	Yes	No	Yes
4u	High	No	Yes	Yes	Yes	Yes	Yes	Yes
Camp	High	No	Yes	Yes	No	Yes	No	Yes
Acyc	High	No	Yes	No	No	No	No	No
Trich	High	No	No	No	No	No	No	No
Vinb	Low	No	Yes	No	No	No	No	Yes

HIA and BBB prediction

Appropriate to P-gp and CYP protein energy is human gastrointestinal ingestion (HIA) and blood-brain barrier infiltration (BBB). SwissADME 'BOILED-Egg' (Figure 12) permits for assessment of HIA as an element of the situation of the molecules in the WLOGP-*versus*-TPSA referential. The white section of the 'BOILED-Egg' is for a high possibility of reflexive adaptation by the gastrointestinal tract, and the yellow area (yolk) is for a high probability of cerebrum entrance. Yolk and white zones are not fundamentally unrelated. With this, the points are shaded in blue whenever anticipated as effectively effluxed by P-gp (PGP+) and in red projected as non-substrate of P-gp (PGP−). All the synthesized compound shows high GI absorption and no BBB prediction except **4g**,**t** (red dot) and **4n** they have the low GI and no BBB prediction. (Figure 12).

HIA and BBB are subject to water solubility and lipophilicity of the drug. Two topological approaches to foresee water solubility comprised of SwissADME. The first is an execution of the ESOL[58] model, and the subsequent one modified from Ali *et al*.[59]. Swiss ADME third indicator for solubility was created by SILICON-IT. All anticipated qualities are the decimal logarithm of the molar solubility in water (log S).

The Ali and Silicoms IT screening show poor solubility of all the synthesized compound while in ESOL solubility analysis most of the compounds are moderately soluble except **4a**,**f**,**r** and **s** they show poor solubility (Table IX). Even the standard drugs are in the range of poor solubility to very soluble. Consensus Log p is the average value of all Log P evaluated with various lipophilicity criteria (Table X).

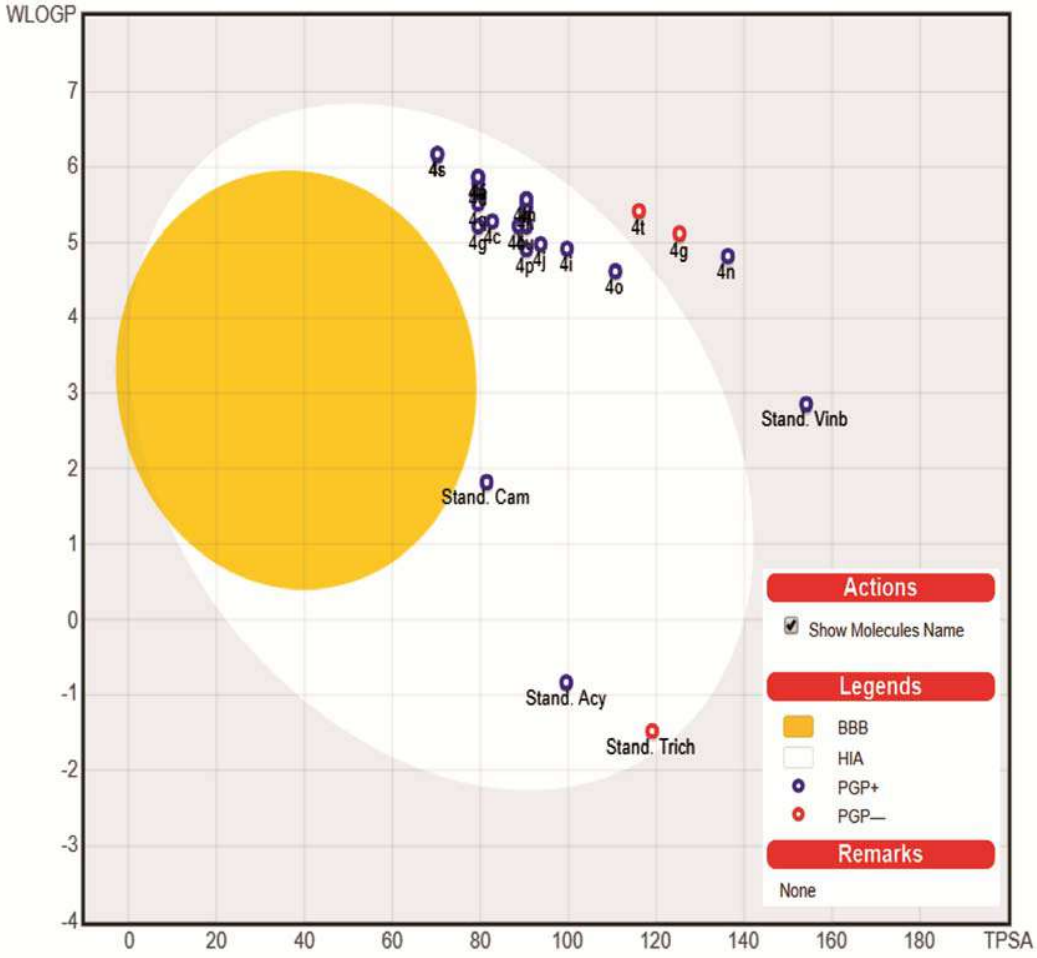


Figure 12 — The BOILED-Egg allows for evaluation of passive gastrointestinal absorption (HIA), brain penetration (BBB) and P-glycoprotein in the presence of the molecule (P-gp)

Table IX — Water solubility evaluation of the synthesized compounds (Solu.: Solubility; PS: Poorly soluble; MS: Moderately soluble; S: soluble; VS: Very soluble)

Sr. No.	ESOL				Ali				Silicon-IT			
	Log S	Solu. (mg/mL)	Solu. (mol/L)	Class	Log S	Solu. (mg/mL)	Solu. (mol/L)	Class	LogSw	Solu. (mg/mL)	Solu. (mol/L)	class
4a	-6.18	2.83E-04	6.62E-07	PS	-7.24	2.47E-05	5.77E-08	PS	-8.39	1.72E-06	4.03E-09	PS
4b	-5.66	9.21E-04	2.18E-06	MS	-6.76	7.38E-05	1.75E-07	PS	-7.91	5.19E-06	1.23E-08	PS
4c	-5.82	6.54E-04	1.50E-06	MS	-6.79	7.10E-05	1.63E-07	PS	-7.88	5.72E-06	1.31E-08	PS
4d	-5.75	7.31E-04	1.78E-06	MS	-6.7	8.21E-05	2.00E-07	PS	-8.07	3.47E-06	8.45E-09	PS
4e	-6.18	2.83E-04	6.62E-07	PS	-7.24	2.47E-05	5.77E-08	PS	-8.39	1.72E-06	4.03E-09	PS
4f	-6.18	2.83E-04	6.62E-07	PS	-7.24	2.47E-05	5.77E-08	PS	-8.39	1.72E-06	4.03E-09	PS
4g	-5.65	9.73E-04	2.22E-06	MS	-7.38	1.82E-05	4.16E-08	PS	-7.15	3.10E-05	7.10E-08	PS
4h	-5.59	1.01E-03	2.57E-06	MS	-6.6	9.97E-05	2.54E-07	PS	-7.81	6.09E-06	1.55E-08	PS
4i	-5.45	1.46E-03	3.57E-06	MS	-6.65	9.22E-05	2.26E-07	PS	-7.22	2.46E-05	6.01E-08	PS
4j	-5.61	1.04E-03	2.47E-06	MS	-6.68	8.88E-05	2.11E-07	PS	-7.19	2.71E-05	6.43E-08	PS
4k	-5.54	1.15E-03	2.91E-06	MS	-6.59	1.03E-04	2.59E-07	PS	-7.38	1.64E-05	4.14E-08	PS
4l	-5.97	4.41E-04	1.07E-06	MS	-7.14	3.01E-05	7.29E-08	PS	-7.71	8.14E-06	1.97E-08	PS
4m	-5.97	4.41E-04	1.07E-06	MS	-7.14	3.01E-05	7.29E-08	PS	-7.71	8.14E-06	1.97E-08	PS
4n	-5.44	1.55E-03	3.65E-06	MS	-7.27	2.28E-05	5.38E-08	PS	-6.46	1.47E-04	3.48E-07	PS
4o	-5.24	2.27E-03	5.75E-06	MS	-6.55	1.12E-04	2.85E-07	PS	-6.53	1.16E-04	2.95E-07	PS
4p	-5.38	1.58E-03	4.19E-06	MS	-6.48	1.24E-04	3.28E-07	PS	-7.12	2.88E-05	7.62E-08	PS
4q	-5.89	5.25E-04	1.29E-06	MS	-6.97	4.37E-05	1.07E-07	PS	-8.19	2.66E-06	6.53E-09	PS
4r	-6.41	1.59E-04	3.86E-07	PS	-7.46	1.43E-05	3.47E-08	PS	-8.67	8.81E-07	2.14E-09	PS
4s	-6.41	1.59E-04	3.86E-07	PS	-7.46	1.43E-05	3.47E-08	PS	-8.67	8.81E-07	2.14E-09	PS
4t	-5.88	5.57E-04	1.32E-06	MS	-7.59	1.08E-05	2.56E-08	PS	-7.42	1.59E-05	3.78E-08	PS
4u	-5.68	8.29E-04	2.11E-06	MS	-6.86	5.45E-05	1.39E-07	PS	-7.49	1.26E-05	3.21E-08	PS
Camp	-3.49	1.14E-01	3.27E-04	S	-3.07	2.99E-01	8.58E-04	S	-5.83	5.20E-04	1.49E-06	MS
Acyc	-1.16	2.06E+01	6.96E-02	VS	-0.89	3.78E+01	1.28E-01	VS	-0.81	4.59E+01	1.55E-01	S
Trich	-0.41	8.85E+01	3.93E-01	VS	-0.43	8.32E+01	3.69E-01	VS	-1.28	1.19E+01	5.28E-02	S
Vinb	-6.84	1.17E-04	1.44E-07	PS	-6.81	1.25E-04	1.54E-07	PS	-8.46	2.80E-06	3.45E-09	PS

Experimental Section

Every one of the reactions was conveyed under the stipulated conditions, utilizing freshly prepared thiazole, ionic liquid, and pure solvents. The open capillary technique was utilized to decide the dissolving purpose of the compound and are uncorrected. The refined dissolvable was utilized to perform TLC on silica gel G. All the synthetic compounds were bought from S.D. Fine synthetic substances of AR grade. ^{1}H NMR and ^{13}C NMR spectra recorded from DMSO-d_6 arrangements on a Brucker AC 400 (MHz). TMS as an inward standard for detailing the substance move in ^{1}H NMR. KBr plates strategy used to IR spectra on a Perkin Elmer 1800 spectrophotometer and mass spectra interpretation finished with a GC-MS (70ev). All tertiary alkyl amines concentrated H_2SO_4, cyclohexanone, and aromatic aldehydes obtained from S.D. Fine chemicals of AR grades.

Procedure for 2-amino-4-(4-methoxyphenyl) thiazole2a[49]

The title compound was set up by the expansion of resublimed iodine (0.01 moles) to 1-(4-methoxyacetophenone (0.01 mol) and thiourea (0.02 mol), trailed by warming of the blend on a water bath at 100°C. The cooled reaction mixture was triturated with diethyl ether to evacuate any unreacted iodine and acetophenone. The solid residue was placed in cold water (250 mL) and treated with aqueous ammonium hydroxide. The precipitated thiazole was gathered and cleansed by crystallization from ethanol. The yield was 88%.

General procedure for preparation of rac-(2S)-2-[(R)-[(4-substituted phenyl){[4-(4-substitutedphenyl) - 1,3-thiazol-2-yl]amino}methyl]cyclohexanone(4a-4u)[17]

The preparation of substituted β-amino carbonyl derivatives investigated in several ionic liquids. The

Table X — lipophilicity evaluation of the synthesized compounds

Sr. No.	iLOGP	XLOGP3	WLOGP	MLOGP	Silicos-IT Log P	Consensus Log P
4a	3.67	5.8	5.87	3.54	6.45	5.07
4b	3.67	5.15	5.22	2.71	5.88	4.53
4c	3.85	5.3	5.28	2.92	5.5	4.57
4d	3.68	5.28	5.78	3.44	6.24	4.88
4e	3.82	5.8	5.87	3.54	6.45	5.1
4f	3.74	5.8	5.87	3.54	6.45	5.08
4g	3.32	5.01	5.12	2.1	3.65	3.84
4h	3.65	5.18	5.22	3.06	5.82	4.59
4i	3.28	4.82	4.92	2.5	5.33	4.17
4j	3.25	4.97	4.98	2.71	4.96	4.17
4k	3.2	4.95	5.47	3.23	5.7	4.51
4l	3.11	5.48	5.57	3.33	5.92	4.68
4m	3.3	5.48	5.57	3.33	5.92	4.72
4n	2.75	4.68	4.82	1.89	3.1	3.45
4o	2.82	4.5	4.62	2.29	4.8	3.81
4p	3.02	4.85	4.91	2.85	5.29	4.18
4q	3.96	5.54	5.52	3.28	6.34	4.93
4r	4.01	6.2	6.17	4.13	6.92	5.49
4s	3.95	6.2	6.17	4.13	6.92	5.47
4t	3.23	5.4	5.42	2.63	4.11	4.16
4u	3.14	5.21	5.22	3.06	5.8	4.49
Cam	2.49	1.74	1.82	1.64	3.29	2.2
Acy	1.78	-0.72	-0.84	-0.74	0.8	0.06
Tric	0.48	-1.56	-1.48	-1.43	-0.57	-0.91
Vin	5.06	3.88	2.85	2.35	4.72	3.77

choices of ionic liquids were motivated by there being the most widely used, and therefore the most widely available[50].

Biological Assay

In vitro anticancer assays

In this assay, the viability of chemically treated cells measured by a dye, Resazurin, or Alamar blue (AB). AB, a non-fluorescent marker colour, is changed over to brilliant red– fluorescent resorufin employing the reduction reactions of metabolically dynamic cells. The quantity of living cells is legitimately corresponding to the measure of fluorescence delivered.

Protocol:

1 Trypsinize the cell and dilute with RPMI medium (with 5% serum)
2 Count the cells and dilute them in the same RPMI medium.
3 Add 100,000 cells per well in 40 µL. Use 384 well black plates.
4 Make a 2X solution for each dilution in the RPMI medium and add 50µL per well. Use appropriate positive and negative controls.
5 Add 10 µL Alamar blue and incubate ON.
6 Measure Fluorescence. (560nm / 590 nm Ex/Em). The contrast in fluorescence intensity estimates the counter cancer impact of that compound.

Sample (5 mg) was dissolved in 250 µL DMSO to achieve a concentration of 20 mg/mL. In each well, 100 µL medium with cells was added and allowed to grow overnight so that cells attained a limit of 10.000 cells / well. Two cell lines HCT116 (Mismatched DNA repair deficiency) and H1299 (P53 deficient). The supernatant medium discarded, and 100 µL of fresh medium added. The top of the well had 125 µL of the solution; 2.5 µL of stock solution added. The net concentration of the cells was 400 µg/mL. The material was inserted into the second row of the microtiter plates and sequentially diluted to 1/5: a total of six dilutions made. The 7^{th} and 8^{th} rows used as controls. The plates incubated for 48 hours, and the supernatant discarded. Fresh medium containing 2% Alomar Blue added. Further incubation of 2 hours was followed by a reading of the fluorescence intensity. The active cells released the fluorescence; the intensity was directly proportional to the number

of cells. Both HCT116 and H1299 are colon cancer cell lines obtained from ATCC. HCT116 is a mismatch repair-deficient cell line, and H1299 has a p53 mutation.

In vitro anti-cancer activity

Standard Alamar Blue Assay protocol for Cell viability assay used. Coherently developed cells were trypsinized, and around 10,000 cells seeded in each well of 96 well plates. The next day the medium was supplanted with medium containing suitable centralization of the drug. Compounds were suspended in 250 µL DMSO, and 2.5 µL added to each well in 125 µL, 1/5 dilution up to 5 dilutions for HCT116/H1299 Cancer cell line. The maximum concentration of each drug is 400 µg/mL, 1/5 dilution used for each drug. The cells treated for 48 hours and 2 µL of Alamar blue was added to each well and brooded for two hours. Fluorescence intensity read with a plate reader. The IC_{50} value was calculated from the graph.

Computational Details

All the ligand used was made using ChemDraw 3D [60]. Before the docking calculation of the ligands, the structure was lower in energy and then docked by using PyRx[61]. The crystal structure for the complex with an inhibitor downloaded from Protein Data Bank (http://www.rscb.org/) as a PDB file. The active site of the docked protein was found out by Argus Lab 4.0[62], which used for the docking in the PyRX.

The downloaded protein of the Cancer Genomic DNA Mutator APOBEC3B (PDB ID- 5CQD) contain chain A and C with Glycerin; Propane-1,2,3-triol and zinc ion as interacting ligand. The selected chain A contains 185 residues having twenty-six active site *viz*. Arg211, Arg212, Arg257, Asn240, Asp346, Cys239, Cys284, Cys289, Gln213, Glu241, Glu255, Glu342, His253, Leu238, Leu318, Met186, Phe237, Phe285, Pro283, Ser286, Thr214, Trp281, Trp287, Tyr191, Tyr215 and Tyr313. The chain A and C with the residues, water, and hetero group within a radius of 2.08A° refined for further cleaned by ascertaining the hybridization and introducing the H-atoms to the protein residue with the removal of water molecules. The cleaned structure of the Cancer Genomic DNA Mutator APOBEC3B (PDB ID- 5CQD) chain A carried no charge, 1356 valence electron, and 496 atoms. The docking with PyRx (Autodock) was conducted vina search space of dimension size x = 45.9667083596, y = 33.1205244125, z = 34.2302049496; center x = 73.3676401887, y = 4.22414666002, z = 0.401404471846 with nine exhaustiveness. The best conformational binding energy reported in Table VI. The LIGPLOT+ version V.1.4.5[63] was used to find the multiple ligand-protein interaction diagram.

Conclusion

All compounds were evaluated *in vitro* against a two-cell line panel consisting of HCT116 and H1299, respectively. Results indicate that all the substituted 2-((4-phenyl)(4-(4-phenyl)thiazol-2-ylamino)methyl) cyclohexanone derivatives **4a-u** are active.

From the graphical representation, it can conclude that the compounds **4b**,**c** and **q** moderate repressive while the **4j**,**m** weak inhibitory activity, and **4f**,**o** and **t** have very less action against but out of which **4g**, **r** shows proposing an operation against a cancer cell line HCT116. In case activity against H1299 cell lines,**4g** shows excellent activity while the others are moderate activity. The compound **4r**, **4s**, and **4t** show comparable binding energy score with the standard drug-like Vinblastine (-7.0kcal/mol) and higher as compare to Camptothecin (-5.9 kcal/mol).

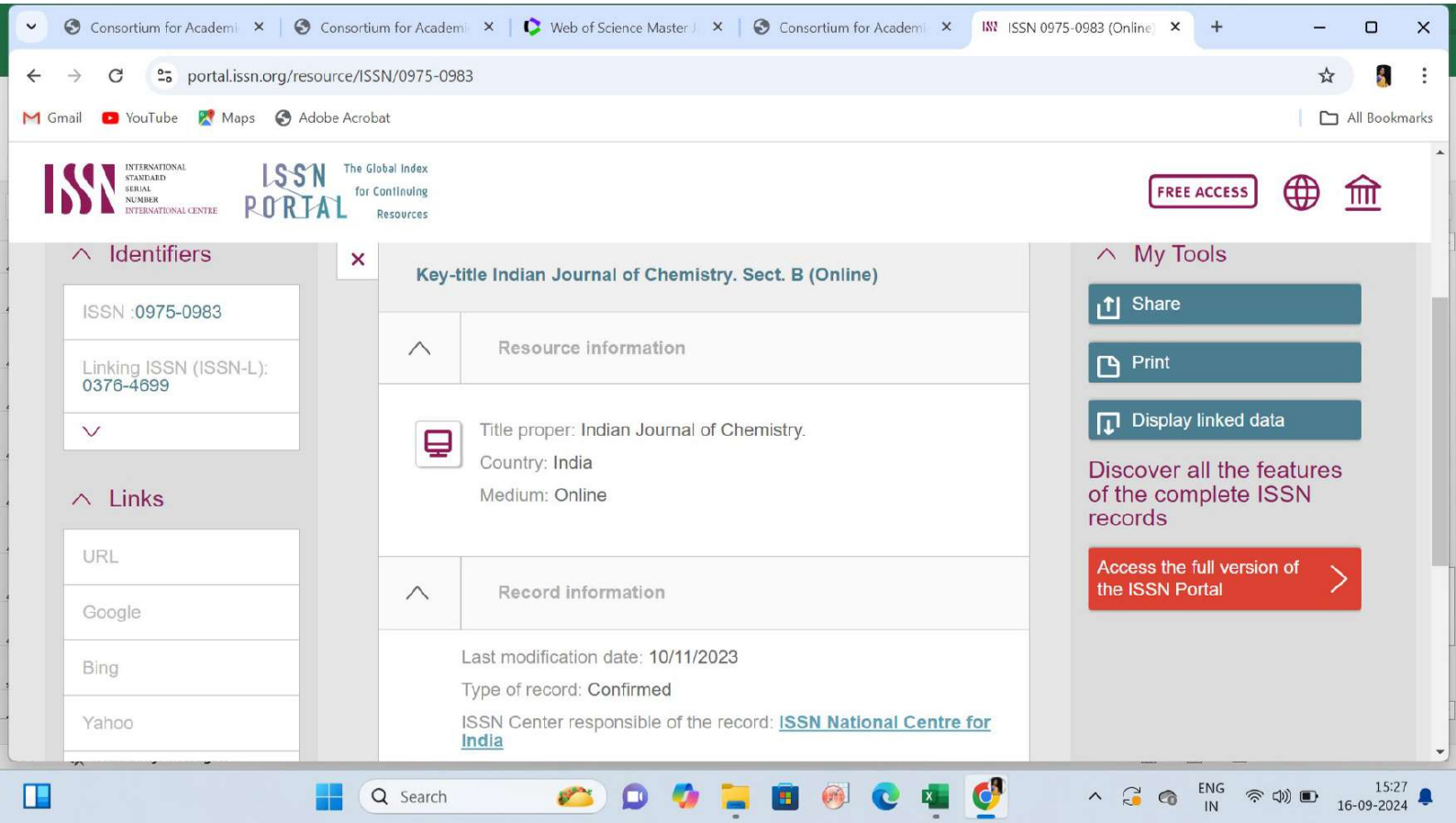
Acknowledgements

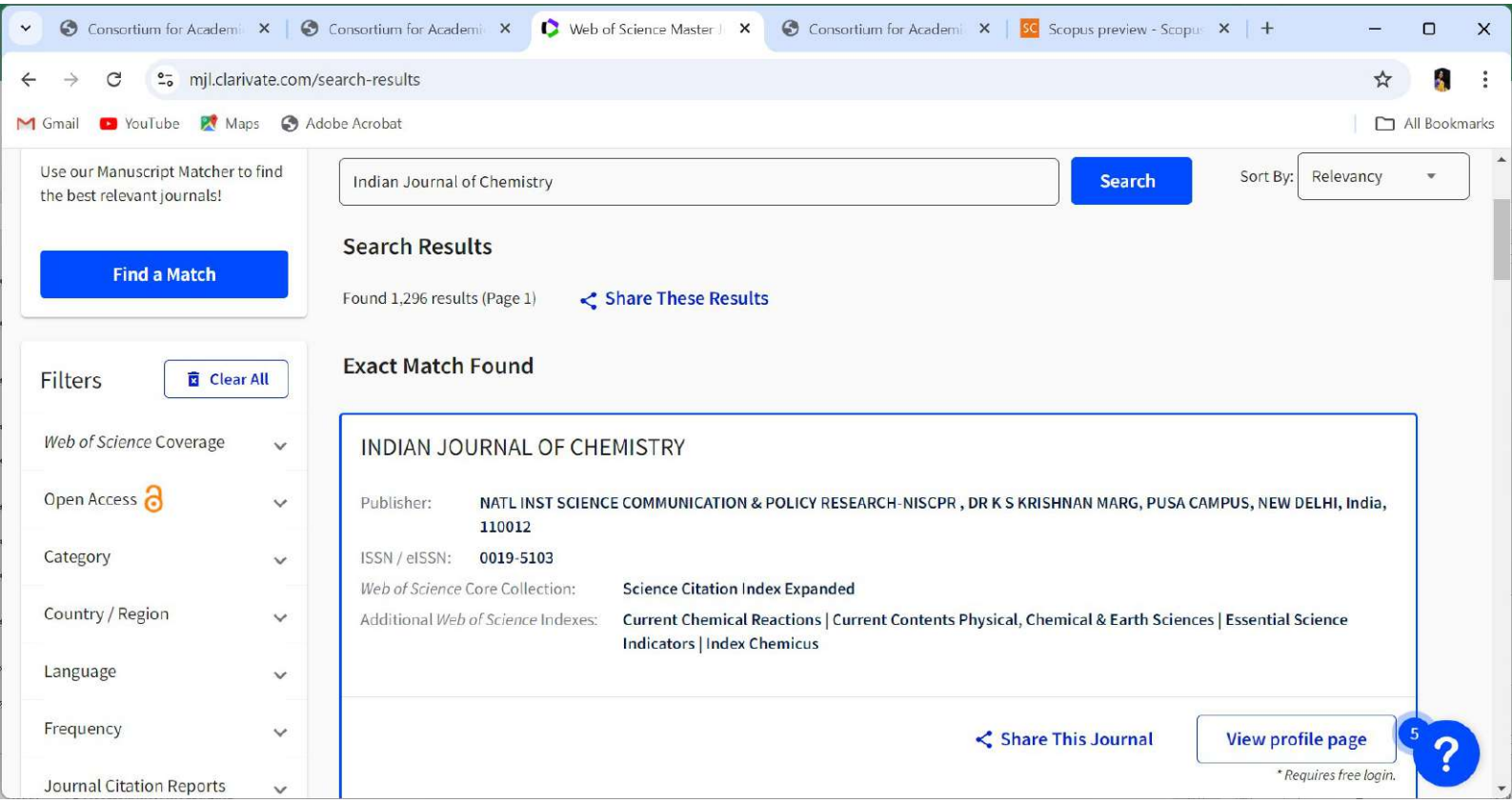
We express our gratitude to SAIF, Chandigarh, for spectral analysis. We pay special thanks to Dr D. Palaniyandi Manivasakam, Director, Biology Indus Pharmaceuticals 25 Olympia Avenue Suite K-600, Woburn, MA 01801, for anticancer screening.

References

1 Brana M F & Migallon A S, *Clinical and Translational Oncology*, 8(10) (2006) 717.
2 Hieu B T, Thuy L T, Thuy V T, Tien H X & Chinh L V, *Bulletin Korean Chem Soc*, 33 (2012) 1586.
3 Gul H I, Yerdelen K O, Gul M, Das U & Pandit B, *Arch Pharm Chem Life Sci*, 340 (2007) 195.
4 Gul H I, Yerdelen K O, Gul M, Das U & Pandit B, *Chem Pharm Bull*, 56 (2008) 1675.
5 Dimmock J M, Kandepu N M, Hetherington M, Quail J W & Pugazhenthi U, *J Med Chem*, 41 (1998) 1014.
6 Karll R E & Lee R J, *US Patent*, US 4,384,138 (1983).
7 Otto F P, *US Patent*, US 3, 649,229 (1972).
8 Horodysky A G & Kaminski J M, *US Patent*, US4, 394, 278 (1983).
9 Scott M K, Martin G E, DiStefano D L, Fedde C L & Kukla M J, *J Med Chem*, 35 (1992) 552.
10 Cohen A, Hall R A, Heath-Brown B, Parkes M W & Rees A H, *British J Pharm Chemother*, 12 (1957) 194.

11 Borenstein M R & Doukas P H, *J Pharm Sci*, 76 (1987) 300.
12 Shiozawa A, Narita K, Izumi G, Kurashige S & Sakitama K, *Eur J Med Chem*, 30 (1995) 85.
13 Barlin G B & Jiravinja C, *Australian J Chem*, 43 (1990) 1175.
14 Barlin G B, Jiravinja C & Yan J H, *Australian J Chem*, 44 (1991) 677.
15 (a) Edwards M L, Ritter H W, Stemerick D M & Stewart K T, *J Med Chem*, 26 (1983) 431; (b) Ghatole A M, Lanjewar K R & Gaidhane M K, *J Pharm Res*, 5 (2012) 2758; (c) Ghatole A M, Lanjewar K R & Gaidhane M K, *Int J Res Biosciences*, *Agriculture & Technology*, 1 (2015) 89.
16 Dimmock J R & Kumar P, *Curr Med Chem*, 4, 1997, 1.
17 (a) Ghatole A M, Lanjewar K R, Gaidhane M K & Hatzade K M, *Spectrochim Acta Part A: Molecular and Biomolecular Spectroscopy*, 151 (2015) 515; (b) Ghatole A M, Lanjewar K R, Gaidhane M K & Hatzade K M, *Bulgarian J Science Education*, 29 (2020) 206.
18 Cordova A, *Accts Chem Res*, 37 (2004) 102.
19 Kleinmann E F, in *Comprehensive Organic Synthesis*. edited by Trost B M, Flemming T, Vol. 2. (Pergamon Press, New York) (1991).
20 Arend M, Westermann B & Risch N, *Angew Chem Int Ed*, 37 (1998) 1044.
21 Tramontini M & Angiolini L, *Tetrahedron*, 46 (1990) 1791.
22 Denmark S & Nicaise O J C, in *Comprehensive Asymmetric Catalysis*, edited by Pfaltz A, Jacobsen E N, Yamamoto H. (Verlag Berlin Heidelberg: Springer), 2 (1999) 93.
23 Kobayashi S & Ishitani H H, *Chem Rev*, 99 (1999) 1069.
24 Conticello S G, *Genome Biology*, 9(6) (2008) 229.
25 Refsland E W & Harris R S, *Curr Top Microbiol Immunol*, 371 (2013) 1.
26 Krejci A, Hupp T R, Lexa M, Vojtesek B & Muller P, *Bioinformatics*, 32(1) (2016) 9.
27 Seplyarskiy V B, Soldatov R A, Popadin K Y, Antonarakis S E & Bazykin G A, *Genome Res*, 26(2) (2016) 174.
28 Lipinski C A, Lombardo F, Dominy B W & Feeney P G, *Adv Drug Deliv Rev*, 46(1-3) (2001) 3.
29 Daina A & Zoete V A, *Chem Med Chem.*, 11(11) (2016) 1117.
30 Zahra S N E, Khattak N A & Mir A, *Theoretical Biology & Medical Modelling*, 10 (2013) 1.
31 Tabassum S, Zaki M, Afzal M & Arjmand A, *Eur J Med Chem*, 74 (2014) 509.
32 Shi K, Demir O, Carpenter M A, Wagner J & Kurahashi K, *Scientific Reports*, 7(1) (2017) 17415.
33 Yang B Li, Xiaosa L & Liqun C, *J Genet Genomics*, 44(9), 2017, 423.
34 Gordon C M, *Appl Catal A*: *General*, 222 (2001) 101.
35 Holbrey J D & Seddon K R, *Clean Product Processes*, 1 (1999) 223.
36 Wasserscheid P & Keim W, *Angew Chem*, 39(21) (2000) 3772.
37 Sheldon R A, *Chem Commun*, 2399 (2001).
38 Welton T, *Chem Rev*, 99 (1999) 2071.
39 Wenzel A & Jacobsen J E N, *J Am Chem Soc*, 124 (2002) 12964.
40 Katritzky A R, Qiu G, He H Y & Yang B J, *J Org Chem*, 65 (2000) 3683.
41 Manabe K, Mori Y, Wakabayashi T & Nagayama S, *J Am Chem Soc*, 122 (2000) 7202.
42 Manabe K, Mori Y & Kobayashi S, *Tetrahedron*, 57 (2001) 2537.
43 Cozzi P G, Simone B D & Umani-Ronchi A, *Tetrahedron Lett*, 37 (1996) 1691.
44 Kobayashi S. Araki M & Yasuda M, *Tetrahedron Lett*, 36 (1995) 5773.
45 Kobayashi S, Iwamoto S & Nagayama S, *Synlett*, 1099 (1997).
46 Kobayashi S, Busujima T & Nagayama S, *Synlett*, 545 (1999).
47 Akiyama T, Takaya J & Kagoshima H, *Synlett*, 1426 (1999).
48 Loh T P & Wei L L, *Tetrahedron Lett*, 39 (1998) 323.
49 Loh T P, Liung S B K W, Tan K L & Wei L L, *Tetrahedron*, 37 (2000) 3227.
50 Ojima I, *Catalytic Asymmetric Synthesis*, 2nd Edn. edited by I Ojima (Wiley-VCH, New York) (http:// www.wiley.com/). (2000), Pages: XIV, 864 Pages, Hardcover. Price: 169.- Euro / 330.54 DM / 294- SFR. ISBN: 0-471-29805-0, *Molecules: A Journal of Synthetic Chemistry and Natural Product Chemistry*, 6(12) (2001) 1013.
51 Daina A, Michielin O & Zoete V, *Sci Rep*, 7 (2017) 42717.
52 Ghose A K, Viswanadhan V N & Wendoloski J J, *J Comb Chem*, 1(1) (1999) 55.
53 Egan W J, Jr Merz K M & Baldwin J J, *J Med Chem*, 43(21) (2000) 3867.
54 Veber D F, Johson S R, Cheng H Y, Smith B R & Ward K W, *J Med Chem.*, 45(12) (2002) 2615.
55 Muegge I, Heald S L & Brittelli D, *J Med Chem.*, 44(12) (2001) 1841.
56 Brenk R, Schipani A, James D, Krasowski A & Gilbert I H, *Chem Med Chem.*, 3(3) (2008) 435.
57 Ogu C C & Maxa J L, *Proc* (*Bayl Univ Med Cent*), 13(4) (2000) 421.
58 Delaney J S, *J Chem Inf Comput Sci*, 44(3) (2004) 1000.
59 Fagerberg J H, Kaarlsson E, Ulander J, Hanisch G & Bergström C A, *Pharm Res*, 32(2) (2015) 578.
60 Chem Draw 3D Ultra Software.
61 Trott O & Olson A J, *J Comput Chem*, 31 (2010) 455.
62 Argus Lab 4.0.1 docking software.
63 Laskowski R A & Swindells M B, *J Chem Inf Model*, 51 (2011) 2778.


Consortium for Academi
Consortium for Academi
Web of Science Master J
Consortium for Academi
ISSN 0975-0983 (Online)
portal.issn.org/resource/ISSN/0975-0983
Gmail
YouTube
Maps
Adobe Acrobat
All Bookmarks
ISSN INTERNATIONAL STANDARD SERIAL NUMBER INTERNATIONAL CENTRE
ISSN PORTAL The Global Index for Continuing Resources
FREE ACCESS
Identifiers
ISSN :0975-0983
Linking ISSN (ISSN-L): 0376-4699
Links
URL
Google
Bing
Yahoo
Key-title Indian Journal of Chemistry. Sect. B (Online)
Resource information
Title proper: Indian Journal of Chemistry.
Country: India
Medium: Online
Record information
Last modification date: 10/11/2023
Type of record: Confirmed
ISSN Center responsible of the record: ISSN National Centre for India
My Tools
Share
Print
Display linked data
Discover all the features of the complete ISSN records
Access the full version of the ISSN Portal
Search
ENG IN
15:27
16-09-2024


Consortium for Academi
Consortium for Academi
Web of Science Master
Consortium for Academi
Scopus preview - Scopus
mjl.clarivate.com/search-results
Gmail
YouTube
Maps
Adobe Acrobat
All Bookmarks
Use our Manuscript Matcher to find the best relevant journals!
Find a Match
Indian Journal of Chemistry
Search
Sort By: Relevancy
Search Results
Found 1,296 results (Page 1)
Share These Results
Exact Match Found
Filters
Clear All
Web of Science Coverage
Open Access
Category
Country / Region
Language
Frequency
Journal Citation Reports
INDIAN JOURNAL OF CHEMISTRY
Publisher: NATL INST SCIENCE COMMUNICATION & POLICY RESEARCH-NISCPR , DR K S KRISHNAN MARG, PUSA CAMPUS, NEW DELHI, India, 110012
ISSN / eISSN: 0019-5103
Web of Science Core Collection: Science Citation Index Expanded
Additional Web of Science Indexes: Current Chemical Reactions | Current Contents Physical, Chemical & Earth Sciences | Essential Science Indicators | Index Chemicus
Share This Journal
View profile page
* Requires free login.

Journal of Applied Biological Sciences
E-ISSN: 2146-0108 15(1): 64-74, 2021
Research Article

BUTEA MONOSPERMA BARK EXTRACT TO ITS GREEN SYNTHESIS OF SILVER NANOPARTICLES AND THEIR ANTIOXIDANT, TOTAL FLAVONOID CONTENT AND ANTIMICROBIAL ACTIVITIES

Gunwant P. Gadekar[1], Kalpana P. Ghoshal[2], Ajay M. Ghatole[3*]

[1]*Dept. of Zoology, Dhote Bandhu Science College, Gondia (MS), India*
[2]*Dept. of Botany, Dhote Bandhu Science College, Gondia (MS), India*
[3]*Dept. of Chemistry, Dhote Bandhu Science College, Gondia (MS), India*

**Corresponding Author:*
E-mail: ajay.ghatole5@gmail.com

(Received 31st August 2020; accepted 22nd December2020)

ABSTRACT. Biological methodologies utilizing microorganisms and plants or plant extracts for metal nanoparticles union have been recommended as important options in contrast to concoction strategies. The utilization of plant materials for the preparation of nanoparticles could be more worthwhile, in light of the fact that it doesn't require expound procedures, for example, intracellular amalgamation and numerous purging advances or the maintenance of microbial cell societies. An endeavor has been made to build up a straightforward quick method for bioreduction of silver nanoparticles (AgNPs) using bark concentrate of *Butea monosperma* and to assess the antimicrobial action of prepared silver nanoparticles against different microorganisms. Characterization was determined by using UV-VIS spectroscopy and the antimicrobial activities of the produced Ag nanoparticles were resolute using the disc diffusion assay method. UV-Vis range of the aqueous medium holding silver nanoparticles revealed an absorption peak at 478 nm. The formed silver nanoparticles revealed profound antimicrobial drive against different microorganisms like Escherichia coli, Bacillus subtilis, Pseudomonas aeruginosa and Streptococcus pneumonia. Present examination shows *Butea monosperma* has solid potential for the synthesis of silver nanoparticles by quick reduction of silver particles (Ag^+ to Ag^o). Present investigation suggests strong proof for basic, fast and prudent course to integrate AgNPs using aqueous bark concentrate of *Butea monosperma*. The formed AgNPs showed strong antimicrobial potential. The results were compared with the effect of antibiotics. And were found to be more potent than antibiotics. It was observed that the growth rate was strongly inhibited by the presence of small concentration of nanoparticles.

Keywords: *Antioxidant activity, Antimicrobial activity, Butea monosperma, Silver nanoparticles,*

INTRODUCTION

Nanotechnology concept is in the use since ancient times without actually defining the science. But nowadays nanotechnology is expected to be the basis of many technological innovations in the 21st century. Nowadays, noble metal nanoparticles have been the subject of centered exploration because of their novel optical, electronic, mechanical, magnetic and chemical properties that are fundamentally not quite the same as those of mass materials [1]. These special and unique properties could be attributed to their small sizes and large surface areas. For these reasons, metallic nanoparticles have found uses in many applications in different fields, such as catalysis, photonics, and electronics.

Preparation of silver nanoparticles has fascinated particularly substantial attention due to their various properties and uses like electrical conductivity [2] antimicrobial and antibacterial activities [3,4], DNA sequencing [5] and Surface-Enhanced Raman Scattering (SERS) [6]. Numerous strategies of integrating silver nanoparticles, for example, chemical reduction of silver particles in aqueous arrangements with or without balancing agents [7], thermal deterioration in organic solvents [8] chemical photoreduction and reduction in turn around micelles [9,10] and radiation chemical reduction[11,12] has been recorded previously. Majority of these techniques are very costly and, furthermore, utilizes poisonous, risky synthetic concoctions, indicating natural and biological dangers. Since noble metal nanoparticles are broadly applied to zones of human contact [13] there is a growing need to develop environmentally responsive procedures for nanoparticle amalgamation that are not destructive to the nature. Biological strategies for nanoparticle union utilizing microorganisms [14 -16], chemicals [17], growth [18] and plants or plant have been proposed as conceivable eco-friendly options in contrast to substance and physical strategies. Late exploration announced that silver nanoparticles prepared utilizing different natural products like green tea Camellia sinensis [19], Azadirachta indica leaf broth [20] natural rubber [21], Aloe vera plant extract [22] Latex of Jatropha cureas [23]etc. *Butea monosperma* (Lam) Taub (Butea frondosa) commonly known as Palas in Sanskrit belonging to family Fabaceae is a traditionally used medicinal plant. Seeds, leaves bark, flowers all have medicinal properties. Besides it has been reported to have antibacterial, antifungal properties also. In the present examination, we have reported the union of silver nanoparticles, reducing the silver ions present in the arrangement of silver nitrate by the fluid bark concentrate of *B. monosperma.* Further these green synthesized silver particles were explored for their potential against different pathogenic bacteria.

MATERIALS AND METHODS

All chemicals used in the experiment were of maximum purity and gained from Merk and Hi-media laboratories Pvt Ltd Mumbai, India. The bacterial culture of Streptococcus pneumonia, Escherichia coli, Pseudomonas aeruginosa and Bacillus subtilis were bought from National Center for cell science (NCCS) Pune. Anti-infection agents (Vancomycin and Erythromycin) were bought from Hi-media Mumbai, India. Bark of *B. monosperma* was collected locally from Gondia City, Maharashtra.

Collection of specimens

The bark for the current investigation were gathered in the early daytime throughout the late spring season in March 2020 from a *B. monosperma* tree close to Mundipar forest region, Dist.- Gondia, Maharashtra. The 1 kg of bark were collected and dried under shade and pummeled utilizing a mechanical processor and coming about force was put away in an impenetrable holder for the further examination.

Preparation of Bark Extract

Bark extract was prepared by mixing 10 g dried powder with 100 mL sterile distilled water and filtered through Whatman filter paper No. 1 (pore size 0.45 µm) and was further filtered through 0.22 µm filters. The extract was boiled for 10 min and stored at 4°C for

further experiments.

Synthesis of Silver Nanoparticles

The aqueous solution of 0.1 mM silver nitrate ($AgNO_3$) was arranged and utilized for the union of silver nanoparticles. Ten milliliters of *B. mon*osperma bark extract was mixed to 90 mL of 0.1 mM of $AgNO_3$ and then heated at 80°C for 15 min for the reduction of Ag^+ ions. A shading change from yellowish earthy colored to rosy earthy colored was observed.

Procedure for total flavonoid contain

The 2 mL of plant extract of difference concentrated solution was taken in a test tube to each test tube 2 ml aluminium chloride (2 %) and 3 mL of sodium acetate (5 %) was added to get 1000 µg/mL (1mg/mL) concentrated extract solution. The incubation of test solution was done at room temperature for 150 min. Blank consists of all the reagent, except for the extract solution is substituted with 2 mL of methanol. The stock solution was prepared by dissolving 1 mg quercetin in 1 mL distilled water, so the concentration of the solution is 1 mg/mL (1000 µg/mL). Then serial dilution was performed in order to prepare different concentrated solution 10 µg/mL, 50 µg/mL, 100 µg/mL, and 200 µg/mL. Then the absorbance of each test tube measured at 440 nm using spectrophotometer (Shimadzu UV-2450, Japan) against blank.

Procedure for antioxidant activity

The 2 mL of methanol solution of plant extract at different concentration was taken in a test tube to that 3 mL methanol solution of DPPH was added. The incubation was conducted for 30 min at room temperature in dark place so as to complete the reaction. Then the absorbance of the solution was measured at 517 nm using spectrophotometer against blank. Then % inhibition wear plotted against concentration and from the graph IC50 was calculated [24]**.**

RESULTS AND DISCUSSION

The response blend, bark concentrate of *B. monosperma* with watery arrangement of the silver nitrate, began to change its shading from yellowish earthy colored to rosy earthy colored (Fig. 1). Which demonstrated the formation of AgNPs with the reduction of silver particles. The characteristic surface plasmon absorption bands were observed at 478 nm. UV spectra of silver nano particle synthesis from $AgNO_3$ were shown in Fig. 3. Biosynthesized silver nanoparticles were studied for antimicrobial activity (Fig.5) against pathogenic microorganisms by using standard zone of inhibition. The effect of different concentrations such as 0.2 mM, 0.4 mM and 0.8 mM of silver nanoparticles on bacteria were performed. A clear inhibition zone treated with silver nanoparticles was observed. (Table 1.) The standard antibiotics like vancomycin, erythromycin shows smaller zone of inhibition as compared to the nanoparticles treated discs. (Plate. 1)



A-Before **B- After**

Fig. 1. *Colour changes before (A) and after (B) the process of reduction of Ag^+ to Ag nanoparticles.*

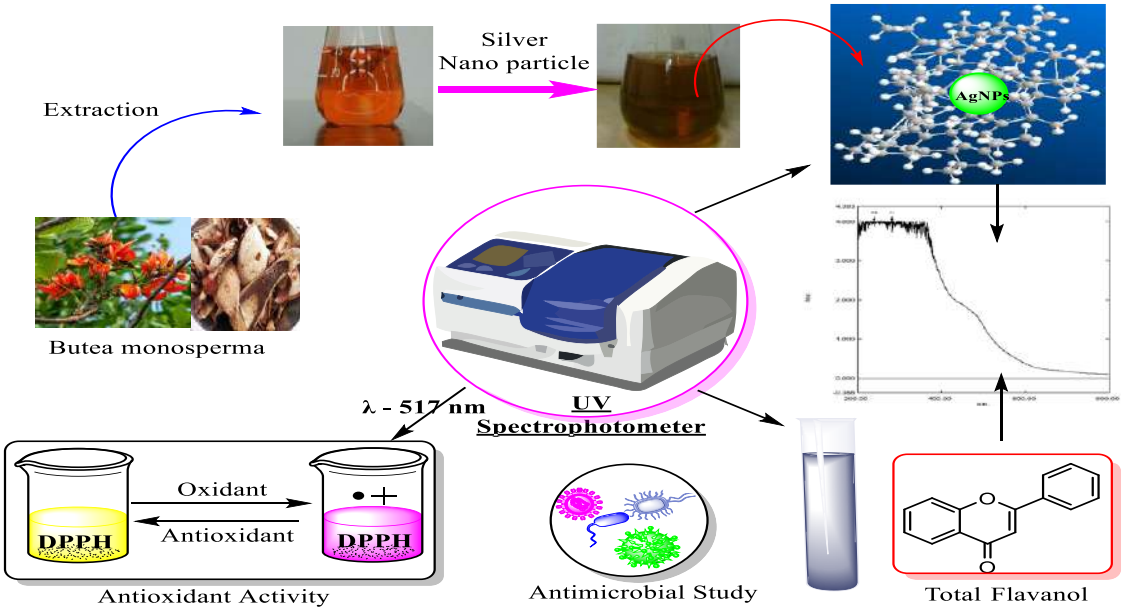


Fig. 2. *Butea monosperma extraction, analysis and testing.*

UV-VIS spectra analysis

The UV-VIS unearthly examination was carried out by utilizing UV-VIS spectrophotometer (Shimadzu UV-2450, Japan). The decrease of unadulterated Ag^+ particles was observed by estimating the UV-VIS range of the response medium at room temperature worked at a goal of 1 nm. The reduction of silver particles was affirmed by subjective testing of supernatant got after centrifugation with a spot of NaCl.

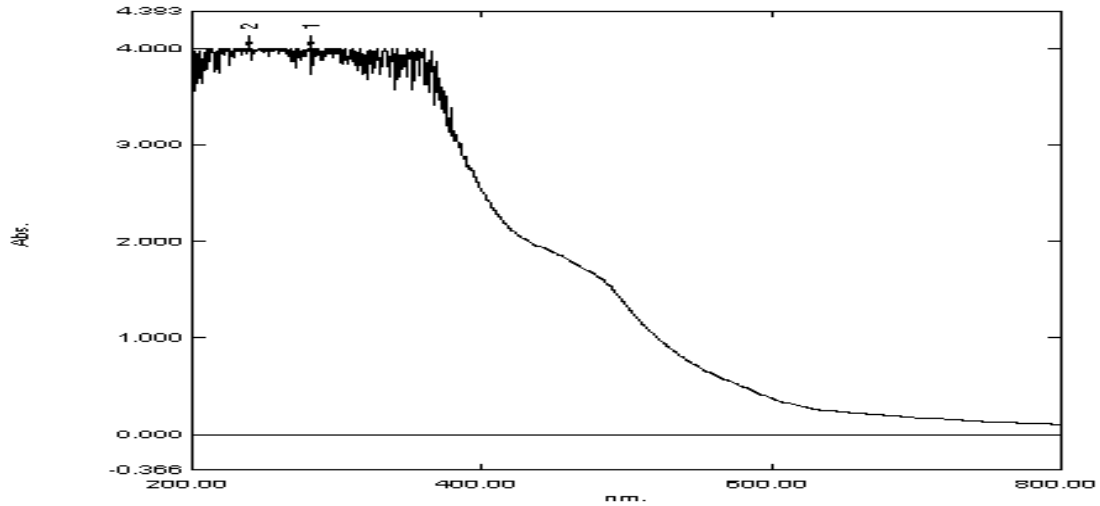


Fig. 3. *UV-VIS absorption spectra of silver nanoparticles (478 nm) synthesized from B. Monosperma*

Total flavonoid content

The flavonoids content of *Butea monosperma* was determined according to the Aluminium chloride method performed by Kumaran and Karunakaran [25]. Flavonols are a class of flavanoids that have 3-hydroxy flavanone. Flavonols are present in the wide variety of fruits and vegetables. Flavanoids shows strong oxidative ability in laboratory studies. In the study, flavonols content of the *Butea monosperma* extract was measured using 5% $AlCl_3$. Table 1 shows the total flavonoid content of sample tested quercetin equivalent by reference of a standard curve Y=25.5 x, R^2 = 0.9812, x is the observance, Y is the quercetin equivalent. The total flavonols content of in *Butea monosperma* was 69.144±0.14 mg quercetin equivalence/g of extract which was shown in the table 1.

The concentration of quercetin in samples were determined by using an equation that was obtained from standard quercetin graph. The equation is given below.

$$y = 25.5\ x$$

Eqn. 1

Where,
x is the absorbance
C is the Intersection = Zero
m is the slope = 25.5
y is the quercetin concentration µg/mL
Now, the total flavonols content in sample was determined as milligrams of quercetin equivalent by using the following equation 2.

$$A = (C \times v)/m$$

Eqn. 2

Where,
A is a total flavonoid content (mg/g quercetin equivalent)
C is X/1000 = Concentration of quercetin mg/mL
V is volume of extract
m is mass of the extract (g)

Table 1. *Total flavanols content of Butea monosperma silver nanoparticle***.**

Sample solution (µg/mL)	Weight of dry extract/mL m(g)	Absorbance (x)	QE conc. 'C'(y = 25.5 x µg/mL)	QE conc. 'C' (mg/mL)	TFLAC as QE, A= (C x v)/m (µg/mL)	Mean ± SEM
1000	0.001	1.361	34.705	0.0347	69.41	
1000	0.001	1.354	34.527	0.0345	69.05	**69.14±0.14**
1000	0.001	1.352	34.476	0.0344	68.95	

Antioxidant Activity

The 0.004 % w/v DPPH solution was prepared by dissolving 4 mg DPPH in 100 mL methanol (95%) in a dark room. The standard stock solution asorbic acid solution (800 µg/mL) was prepared by dissolving 2 mg asobic acid in 2.5 mL distilled water. The further dilution was prepared to get 400 µg/mL, 200 µg/mL, 100 µg/mL, 50 µg/mL, 25 µg/mL concentrated solution. The 3 mL DPPH solution was used as a negative control. The blank for the solution is ethanol. The absorbance of the test solution was measured at 517 nm using UV spectrophotometer (Shimadzu UV-2450, Japan) against blank [26-28].

The percentage (%) inhibition activity was calculated from the following equation 3.

$$\% I = \{(A_o - A_l)/A_o\} X 100$$

Eqn. 3

Where, A_o is the absorbance of the control, and
A_l is the absorbance of the extract / standard.

Table 2. *IC50 calculations of Butea monosperma silver nanoparticle.*

Concentration µg/mL	Absorbance	% SCV	IC50 (µg/mL)
12.5	0.861	23.125	
25	0.805	28.125	
50	0.712	36.42857143	**112.724296**
100	0.35	68.75	
200	0.251	77.58928571	
400	0.191	82.94642857	
Blank	1.12		

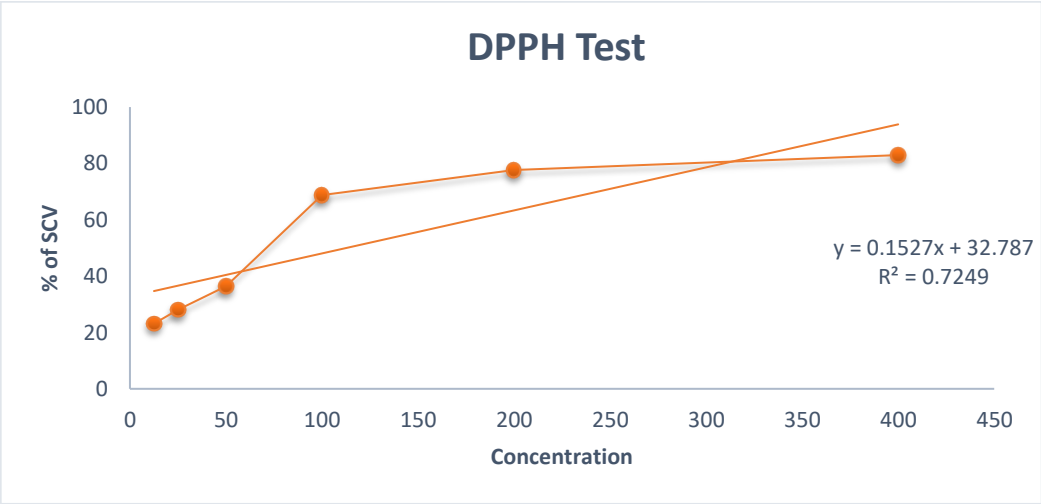


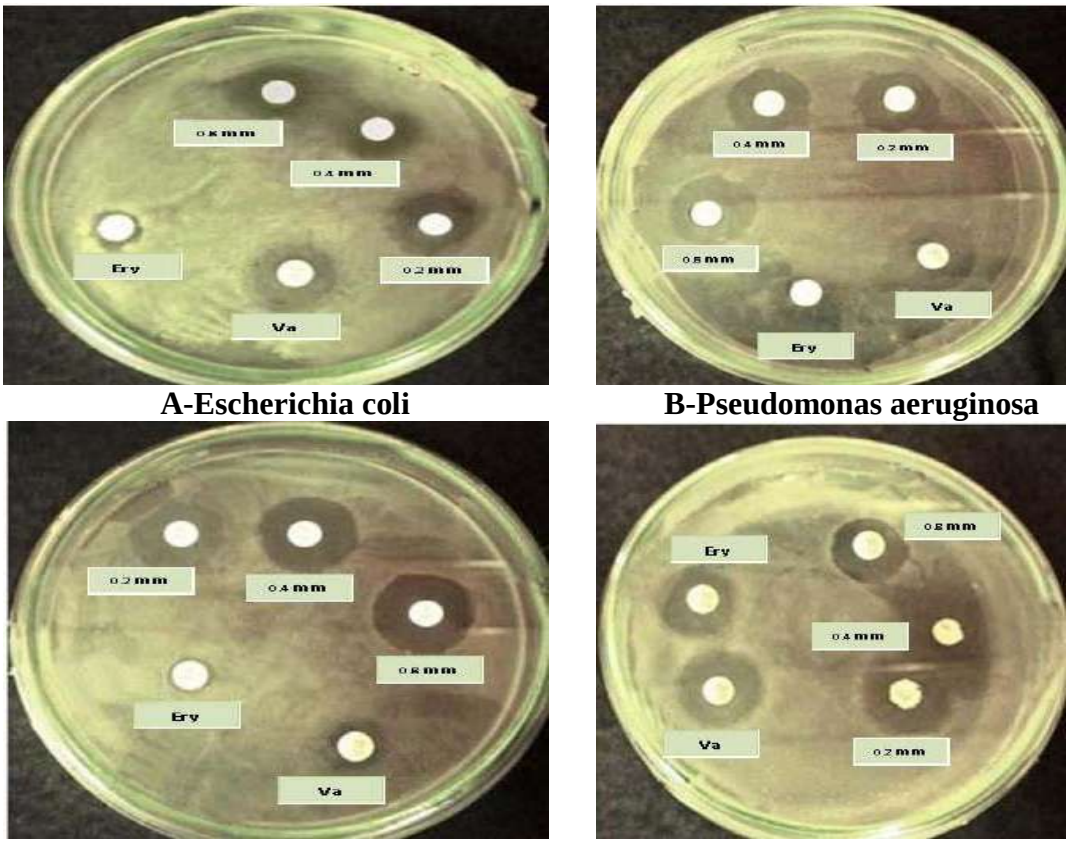
Fig. 4. *IC50 graph for various concentration.*

Antibacterial Activity

The antibacterial test [29] was performed by standard plate dissemination strategy. Supplements were used to cultivate microscopic organisms. The media was autoclaved and cooled. The media was poured in Petri circles and was kept for 30 minutes for hardening. Following 30 minutes, the new short-term societies of inoculum (100 µL) of four distinct living beings were spread on supplement agar plates. Sterile paper discs made of Whatman filter paper, 5 mm diameter dipped in different concentrations of aqueous solution of silver nanoparticles such as 0.2 mM, 0.4 mM, and 0.8 mM along with two standard antibiotics containing discs were placed in each plate. The cultured agar plates were incubated at 37 °C for 24 hr. After 24 hr of incubation, the zone of inhibition was measured in millimeters.

Table 2. *Antimicrobial activity.*

Bioactive agent	**Conc.**	**Zone of inhibition (diameter, mm)**			
		E. coli	***Bacillus subtilis***	***Pseudomonas aeruginosa***	***Streptococcus pneumonia***
Ag nanoparticle	0.2 mM	2.5	3.2	3.1	3.2
	0.4 mM	3.4	4.2	3.3	3.4
	0.8 mM	4.5	4.4	4.3	3.8
Erythromycin (10 mcg/disc)		nil	nil	0.6	4.1
Vancomycin (10 mcg/disc)		0.8	nil	0.8	3.8



A-Escherichia coli **B-Pseudomonas aeruginosa**

C- Bacillus subtilis **D- Streptococcus pneumonia**

Fig. 5. *Antibacterial activities of discs of different concentrations of Ag nanoparticles (0.2 mM, 0.4 mM and 0.8 mM, Va-Vancomycin, Ery-Erythromycin) and other antibiotics.*

The union of nanoparticles is in the lime light of present-day nanotechnology scenario. Biosynthesis of nanoparticles by plant removes is now under abuse. The advancement of organically motivated exploratory procedures for the blend of nanoparticles has developed as significant part of nanotechnology. The current investigation manages the amalgamation of silver nanoparticles using bark concentrate of *B. monosperma* and watery Ag^+ particles. Comparative investigations were carried out to examine the pace of bioreduction of silver particles. The methodology described here in the investigation reveals a financially savvy option in contrast to traditional techniques for preparing silver nanoparticles. Arrangement and strength of silver nanoparticles in fluid colloidal arrangement were affirmed utilizing UV-VIS otherworldly investigation. It is notable that silver nanoparticles show yellowish earthy colored shading in fluid arrangement because of excitation of surface plasmon vibration in silver nanoparticles [30,31]. As the *B. monosperma* bark extract was blended in with watery arrangement of the silver nitrate, it began to change the shading from yellowish earthy colored to dim rosy earthy colored due to reduction of silver particles, which showed the development of silver nanoparticles. It is commonly perceived that UV-VIS spectroscopy is utilized to observe size and shape-controlled nanoparticles in watery suspension [32]. Retention spectra of silver nanoparticles framed in the response media has a solid absorbance top at 478 nm and widening of pinnacles demonstrated that the particles are polydispersed.

Silver nitrate which is readily soluble in water has been exploited as an antiseptic agent

for many decades. It is being used as a safe inorganic antibacterial agent since centuries and is capable of killing about 650 microorganisms that causes diseases. Silver has been depicted as being 'oligodynamic' that is, its particles are fit for causing a bacteriostatic (development restraint) or even a bactericidal (antibacterial) sway. i.e., likewise having capacity to apply a bactericidal impact at minute focus. The specific instrument of the counter-bacterial impact of silver particles was somewhat comprehended. Writing overview uncovers that the bactericidal practice of nanoparticles is credited to the nearness of electronic impact that is achieved because of progress in neighborhood electronic structure of the surface because of littler sizes.

These impacts are viewed as contributing towards improvement of reactivity of silver nanoparticles surface. Silver in ionic structure unequivocally associate with thiol gathering of fundamental protein and inactivates them. Shrivastava [33] considered antibacterial action against E. Coli, S. aureus and S. typhi. They have reported that the impact was portioned dependent and was more articulated against gram-negative life forms than gram-positive ones.

They have found that the major mechanisms through which silver nanoparticles manifest antibacterial property was either by anchoring or penetrating the bacterial cell wall or modulating cellular signaling by dephosphorylating putative key peptide substrates on tyrosine residues.

The antibacterial efficacy of the biogenic silver nanoparticles revealed in the current investigation might be credited to the system depicted above, however, it despite everything stays to explain the specific impact of the nanoparticles on significant cell digestion like DNA, RNA and protein blend. A basic need in the field of nanotechnology is the improvement of a dependable and eco-accommodating procedure for the amalgamation of silver nanoparticles. We have shown first time the blend of silver nanoparticles utilizing bark concentrate of *B. monosperma* through effective green procedure, evading the nearness of risky and harmful solvents. The green synthesized silver nanoparticles using bark extract of *B. monosperma* shows profound antimicrobial activity in table 2. The present investigation reveals simple, rapid and economical route to synthesize silver nanoparticles.

Acknowledgement. The authors are thankful to the Department of Biotechnology, Shri Shivaji Science College, Nagpur and D.B. Science College, Gondia for providing the facilities to carry out the experimental works. We also extend our thanks to Dr. S.R. Thakare and Sandip Gawande for their valuable guidance.

REFERENCES

[1] Mazur, M. (2004): Electrochemically prepared silver nanoflakes and nanowires. Electrochemistry Communications, 6: 400-403.

[2] Chang, L., & Yen, C. (1995): Studies on the preparation and properties of conductive polymers. VIII. Use of heat treatment to prepare metallized films from silver chelate of PVA and PAN. Journal of Applied Polymer Science, 55(2): 371-374. doi:https://doi.org/10.1002/app.1995.070550219

[3] Baker, C., Pradhan, A., Pakstis, L., Pochan, D., & Shah, S. (2005): Synthesis and antibacterial properties of silver nanoparticles. Journal of Nanoscience and Nanotechnology, 4: 224-249.

[4] Shahverdi, A., Mianaeian, S., Shahverdi, H., Jamalifar, H., & Nohi, A. (2007): Rapid synthesis of silver nanoparticles using culture supernatants of Enterobacteria: A novel biological approach. Process Biochemistry, 42: 919-923.

[5] Cao, Y., Jin, R., & Mirkin, C. (2001). DNA-modified core-shell Ag/Au nanoparticles. Journal of American Chemical Society, 123, 7961-7962.
[6] Matejka, P., Vlckova, B., Vohlidal, J., Pancoska, P., & Baumuruk, V. (1992): The Role of Triton X-100 as an adsorbate and a molecular spacer on the surface of silver colloid: A surface-enhanced Raman scattering study. The Journal of Physical Chemistry, 96: 1361-1366.
[7] Liz-Marzan, L., & Lado-Tourino, I. (1996): Reduction and stabilization of silver nanoparticles in ethanol by nonionic surfactant. Langmuir, 12(15): 3585-3589. doi:https://doi.org/10.1021/la951501e
[8] Esumi, K., Tano, T., Torigoe, K., & Meguro, K. (1990): Preparation and characterization of biometallic Pd-Cu colloidsby thermal decomposition of their acetate compounds in organic solvents. Chemistry of Materials, 2(5): 564-567. doi:https://doi.org/10.1021/cm00011a019
[9] Pileni, M. (2000): Fabrication and physical properties of self-organized silver nanocrystals. Pure Appliyed Chemistry, 72: 53-65.
[10] Sun, Y., Atorngitjawat, P., & Meziani, M. (2001): Preparation of silver nanoparticles via rapid expansion of water in carbondioxide microemulsion into reductant solution. Langmuir, 17: 5707-5710.
[11] Henglein, A. (1993): Physicochemical properties of small metal particles in solution:'Microelectrode' reactions, chemisorption, composite metal particles, and the atom-to- metal transition. The Journal of Physical Chemistry, 97: 5457-5471.
[12] Henglein, A. (2001) Reduction of Ag(CN)2 on silver and platinum colloidal nanoparticles. Langmuir, 17, 2329-2333.
[13] Jae, Y., & Beom, S. (2009): Rapid biological synthesis of silver nanoparticles using plant leaf extracts. Bioprocess and Biosystems Engineering volume, 32: 79-84.
[14] Klaus, T., Joerger, R., Olsson, E., & Granqvist, C. (1999): Silver-based crystalline nanoparticles, microbially fabricated. Proceedings of the National Academy of Sciences of the United States of America, 96(24): 13611-13614. doi: https://doi.org/10.1073/pnas.96.24.13611
[15] Nair, B., & Pradeep, T. (2002): Coalescence of nanoclusters and formation of submicron crystallites assisted by Lactobacillus strains. Crystal Growth & Design, 2(4): 293-298.
[16] Konishi, Y., Ohno, K., Saitoh, N., Nomura, T., Nagamine, S., Hishida, H., Uruga, T. (2007): Bioreductive deposition of platinum nanoparticles on the bacterium Shewanella algae. Journal of Biotechnology, 128(3): 648-653.
[17] Willner, I., Baron, R., & Willner, B. (2006): Growing metal nanoparticles by Enzymes. Advanced Materials, 18(9): 1109-1120.
[18] Vigneshwaran, N., Ashtaputre, N., Varadarajan, P., Nachane, R., Paraliker, K., & Balasubramanya, R. (2007): Biological synthesis of silver nanoparticles using the fungus Aspergillus flavus. Materials Letters, 61(6): 1413-1418.
[19] Vilchis-Nestor, A., Sanchez, M., Camacho-Lopez, M., & Gomez-Espinoza, R. (2008): Solventless synthesis and optical properties of Au and Ag nanoparticles using Camellia sinensis extract. Material Letter, 62: 3103-3105.
[20] Shankar, S., Rai, A., Ahmad, A., & Sastry, M. (2004): Rapid synthesis of Au, Ag and bimetallic Au core-Ag shell nanoparticles using neem(Azadirachta indica) leaf broth. Journal of Colloid Interface Science, 275: 496-502.
[21] Abu-Bakar, N., Ismail, J., & Abu-Bakar, M. (2007): Synthesis and characterization of silver nanoparticle in natural rubber. Material Chemistry and Physics, 104(2-3): 276-283.
[22] Chandran, S., Chaudhary, M., Pasricha, R., Ahmad, A., & Sastry, M. (2006): Synthesis of gold and silver nanoparticles using Aloe Vera plant extract. Biotechnology Progress, 22: 577-583.
[23] Bar, H., Bhui, D., Sahoo, G., Sarkar, P., De, S., & Misra, A. (2009): Green synthesis of silver nanoparticles using latex of Jatropha curcas. Colloids and Surfaces A: Physicochemical and Engineering Aspects, 339: 134-141.

[24] Kumaran, A., & R., K. (2007): In vitro antioxidant activities of methanol extracts of five Phyllanthus species from India. LWT. Food Science and Technology, 40: 344-352.
[25] Gaidhane, M., Ghatole, A., & Lanjewar, K. (2016): Antioxidant and biological evoluation of syntesized oxaazetidin-1-yl quinoline 3-carbaldehyde analogous. Gurukul International Multidisciplinary Research Journal, 206-215.
[26] Gaidhane, M., Ghatole, A., & Lanjewar, K. (2020): Synthesis of Chromone Functionalized Chitosan Polymer: Application/Screening of Its Physical Parameters. Polymer Science, Series B, 62(3): 206-217.
[27] Ghatole, A., Gaidhane, M., & Lanjewar, K. (2020): Pharmacokinetics, drug-likeness, medicinal properties, molecular docking analysis of substituted B-lactams synthesized via [Bmim][PF6]/[ET3NH]+[HSO4]- catalyzed coupling reaction. Chemistry: Bulgarian Journal of Science Education, 29(2): 206-244.
[28] Ghatole, A., Lanjewar, K., Hatzade, K., & Gaidhane, M. (2015): A Comparative Synthesis of Ring-Substituted 3-(3-Bromo-4-Oxo-4h-Chromen-2-Yl)-4h-Chromen-4-One. International Journal of Research In Biosciences, Agriculture & Technology, 89-99.
[29] (a) Ghatole, A., Lanjewar, K., Hatzade, K., & Gaidhane, M. (2014): Synthesis and anti-microbial activity of some substituted bis[2-((e)-2-(4-benzylideneamino)thiazol-4-yl)-4-methylphenol] metal complexes. International Journal of Pharmacy and Pharmaceutical Sciences, 6(2): 142-146; (b) Gaidhane, M., Ghatole, A., Narule, M., Gaidhane, P., Lanjewar, K., & Gadekar, G. (2020): Synthesis of Substituted Phenothiazines derivatives, Antioxidant, P-Glycoprotein, Cyp Enzyme Activity, HIA and BBB Prediction, Der Pharma Chemica, 12(7) 1-11.
[30] Ghatole, A., Lanjewar, K., & Gaidhane, M. (2014): Antimicrobial activities; ionic liquid and microwave assistend synthesis of ring-substituted3-(3-bromo-4-oxo-4H-chromen-2-yl)-4H-chromen-4-one . World Journal of Pharmaceutical Research, 3(3): 4336-4350.
[31] Nogmov, M., Zhu, G., Bahoura, M., Adegoke, J., Amall, C., & Ritzo, B. (2007): The effect of grain and absorption on surface plasmon in metal nanoparticles. Applied Physics B, 86: 455-460.
[32] Shrivastava, S., & Dash, D. (2009): Applying nanotechnology to human health. Journal of Nanotechnology, 12: 240-243.
[33] Shrivastava, S., Bera, T., Roy, A., Singh, G., Ramchandrarao, P., & Dash, D. (2007): Characterization of enhanced antibacterial effect of novel silver nanoparticles. Nanotechnology, 18: 225103.

JOURNAL of APPLIED BIOLOGICAL SCIENCES

E-ISSN: 2146-0108

International, Peer-Reviewed and Open-Access Journal Publishing by Anatolia Science Academy

New !!!!

2022-01-06

Articles to be published in the Journal of Applied Biological Sciences (JABS) will be given a DOI number starting from 2022.

The Journal of Applied Biological Sciences (JABS) is indexed in Open AIRE from 2022.

All of the received manuscripts are checked with software for originality. The manuscripts having reported for **a similarity below 20%** would be accepted for a peer-review process.

- Publication Fees/Charges: No submission and publication fees or page charges

Read More ›

Current Issue

Vol. 18 No. 2 (2024): 2024-2



Published: 2024-06-12

Full Issue

Products

Master Journal List | Search Journals | Match Manuscript | Downloads | Help Cent

Already have a manuscript?

Use our Manuscript Matcher to find the best relevant journals!

Find a Match

Filters | Clear All

Web of Science Coverage

Open Access

Category

Country / Region

Language

Frequency

Journal Citation Reports

ine Your Search Results

7-1130 Search

y: Title (A-Z)

rch Results

d 1 results (Page 1) Share These Results

ct Match Found

URNAL OF APPLIED BIOLOGICAL SCIENCES-
BS

blisher: ANATOLIA ACAD SCIENCES , SELCUK UNIV TECH DEV ZONE, ACADEMY ST, NO 67 , KONYA, Turkiye, 00000

N / eISSN: 1307-1130 / 2146-0108

ditional *Web of Science* Indexes: Zoological Record

Share This Journal View profile page

* Requires free login.

1 – 1 of 1

Items per page: 10

Kala : The Journal of Indian Art History Congress
ISSN : 0975-7945

ISSUES AND CHALLENGES OF QUALITY EDUCATION – AN INDIAN PERSPECTIVE.

Dr. Anand Ashok Muley
Department Of Commerce, J. M. Patel Arts, Commerce and Science College,Bhandara-441904 (M.S), muleyanand21@gmail.com

ABSTRACT:-

This paper focuses on the concept of Issues and Challenges of quality education an Indian perspective. In modern times while providing quality education we faces challenges and issues that are going on this topic. The paper gives an overview of the quality education as the UNESCO's sustainable development goal number four. In India the progress of our society has made over the centuries is because of education. In this paper author assesses that no innovation or change can be implemented without education. The quality & efficiency of education depends on quality of education.

KEYWORDS:- Quality education, Issues, challenges, Indian perspective.

INTRODUCTION:-

Quality is an extract word which comes from the 'Latin' word 'Qualitas' (value, characteristic, feature, property, ability).According to the place, people & time it is vary as per its meaning, scale and measurement. Education is also a vast word independence numerous dimension of life in this world. Hence, when quality education is referred to it has a wide range of aspects and facets while being relative in nature. It is relative in the sense that by a good quality what is meant in India may be of a very good or high quality in the African countries and likely what is good for the civilized world may not be good for the native tribes of the Andaman. Now, the question is who will decide this scale and measurement what is good quality education and what is bad quality education. Can there be a general rule for the whole world to determine the quality of education. Though it seems tough in the common perspective but UNESCO can be of a great help in this regard. After achieving the target of quantity by providing education to the maximum number of beneficiaries through its education for all programme UNESCO now has the job in hands to provide quality education for all because it is found with great concern that almost 35 to 50 percent of the students of the under developed and developing countries do not poses the basic reading writing or numeracy skills. But there are several challenges to reach the target of providing quality education to all.

Whatever progress our society has made over the centuries is because of education. Being the foundation stone of society, education brings reforms, helps in progress and paves way for innovation. The importance of quality education cannot be undermined in a society, which is why great personalities have extensively written on its need in a civilized society. It is because of education, humans have been able to explore the vastness of the universe and the mystery of its existence in atoms. The concepts like gravity, cognitive dissonance, laser-guided surgical procedures and millions of more would not exist if education were not there to unleash our potential. In the 21st century, there are countries that are lagging behind in the race for quality education.

OBJECTIVE:-

- To ensure that there is free primary and secondary education for girls and boys for effective learning outcomes.
- To ensure that both girls and boys have access to quality early development and pre-primary education by 2030.
- To Ensure equal access to affordable and quality technical, vocational and tertiary education.
- To Increase the number of people, both youth and adults who have relevant skills for employment, jobs and entrepreneurship.
- To Eliminate all discrimination in education

RESEARCH METHODOLOGY:-

This paper is basically descriptive and analytical in nature. In this paper an attempt has been taken to analyses Issues and Challenges of quality education. Here, the data from various research journals, websites and articles are collected in order to understand the Indian education system & the data used in it is purely from secondary sources according to the need of this study.

ISSUES OF QUALITY EDUCATION:-

Indian education is being divided into two parts private and government education, the ratio is 5:7 respectively. Government education has failed to give a good quality of education. The education received from the government schools is hugely insufficient. This is also because of the lack of teachers and no proper check on them, particularly in rural areas. Therefore, urban areas have a much higher literacy rate than rural areas. Public schools have weak infrastructure and poor academic attention which is very terrible for the overall development of an individual. Better facilities must be given to students in academic, sports, cultural, technical, media, arts, music, religious, social, and political areas which would aid them to discover their areas of interest. Government schools lack a lot in this kind of aspect.

Whereas, the private schools which give all such facilities are too expensive for the lower class families. Above 37% of the Indian population is living below the poverty line. And they cannot afford education even at a primary level. India being a country of morals and beliefs, people are still traditionalistic and apprehend modern education. The performance of the workers depends on several important factors like health and nutrition, education and training, etc. These are regarded as a significant determinant of quality of life. Sufficient investment in these fields will increase the productivity and efficiency of the manpower. The body of knowledge is achieved by the population and capacity of the population to use the knowledge effectively.

- **Lack of money**

The absence of sufficient assets is a fundamental issue in the improvement of education. Because of poor economics, most instructive institutions need the framework, science gear and libraries, and so on. Because of this, the desired outcomes can't be achieved. Every year there

is a separate budget for the Education sector but it needs to be well directed through the appropriate pipeline so that it reaches every sector, where it's needed the most.

- **Costly higher education**

College and specialized institutions have turned out to be expensive in India. The expense structure of specific and able institutions. Privatization of advanced education has helped the development of benefit greedy business people. Now advanced education is a much expensive undertaking.

- **Neglect of Indian languages**

The medium of teaching especially is English because of the focus on education in English, students are not developing foundational literacy and numerical skills.

- **No practical knowledge**

In educational institutions, lots of attention is provided to theory and books, and practical knowledge is completely neglected. When these students pass the exam, they forget all the things they have studied due to a lack of practical experience. In India, parents and teachers expect their students to score high in the exam rather than getting quality knowledge. Due to that reason students unable to get practical knowledge.

- **The problem of brain drain**

Whenever smart, capable, and meriting candidates don't get reasonable positions in the nation. They need to travel to another country to look for employment. So our nation is denied good ability. This wonder is called 'Brain Drain'. Because of that, we lost so many talents that could be utilized in our nation for the betterment of education as well as the overall development of the country.

- **Mass illiteracy**

Still, we are not capable of getting 100 percent education. Even now most of the individuals stay uneducated. In India, the quantity of illiterate individuals is approximately 33 percent of the aggregate uneducated people. Propelled nations are almost 100 percent educated, and the situation in India is very unfavorable.

- **Wastage of resources**

Our education system depends on General Education. The dropout percentage is high in the essential and auxiliary dimensions. The huge majority of the understudies in the 7-14 age group leave the school before completing their studies. It implies the wastage of financial and Human Resources.

- **General education structure:**

Our education structure is of General Education in nature. The advancement of specialized and professional education is very unacceptable. So our way of instruction is ineffective.

- **Problems of primary education**

Our primary education is performed with an extreme number of issues. A huge number of primary schools have no structures, basic facilities like drinking water, furniture and study materials, urinals and power, and many more. Large quantities of grade schools are single educator schools and many schools are even without teachers.

- **Outdated syllabus**

There is an urgent requirement to modify the present system of higher education in the country. We are required to ensure quality in education as well as quantity. Students are acquiring knowledge from the outdated syllabus. Lots of technological and scientific advancements are taking place in India. And hence the courses are Graduate and postgraduates need to be updated as per the modern and technological development.

CHALLENGES OF INDIAN EDUCATION:-

It is the main challenge to provide quality education to all. To provide quality education it must have to be known what quality education is. If it is known what to provide then it becomes easier to answer the question how to provide. From the UNESCO's vision 2030 it can be easily found as to what it means by quality education. It is the number four goal of UNESCO's sustainable development goals of vision 2030. According to the world Education Forum, 2015 "quality education fosters creativity and knowledge, and ensures the acquisition of the foundational skills of literacy and numeracy as well as analytical, problem-solving and other high-level cognitive, interpersonal and social skills. It also develops the skills, values and attitudes that enable citizens to lead healthy and fulfilled lives, make informed decisions, and respond to local and global challenges through Education for Sustainable Development (ESD) and global citizenship education (GCED)".

There is some challenges of Indian education system -

- **Proper assessment for quality education**

The first and foremost challenge to provide quality education is to properly assess the present quality of the education to find out the dimensions where there is a need of improvement and which sector needs to be emphasized. Once the assessment is done then a plan can be implemented for providing quality education

- **High- dropout rates**

The other major challenge in the education system is the high dropout rate in public schools or government schools. It is all due to several factors such as poverty, lack of toilets, long distance to school, child marriages, patriarchal mindset, and cultural factors etc.

- **Poor governance and lack of responsibility**

Due to, the absence of teachers in government schools and poor management in these schools is also another major problem as these school management committees are barely

functional. Also, the parents are unaware of their rights and do not know whom to address in such conditions.

- **Lack of infrastructure**

One of the major challenges faced by public schools is the lack of drinking water facilities, electricity, toilets, and poor hygiene, etc.

- **Quality of teachers**

Lack of trained and skilled teachers is another problem mostly faced by our education system. Besides this lack of skilled teachers, they are also burdened with a non-academic workload which diverse their focus from teaching.

- **Use of ICT, Artificial Intelligence and other modern technologies for the development quality of education.**

To provide quality education the thinking process must have to be innovative .The innovation in the field of technology with the advent of artificial intelligence is a great boon for the education sector. Artificial intelligence and the other technological innovations like app based learning, virtual learning and augmented reality used for the educational purpose. With the help of this we can improve the education system.

- **Proper Inspection, monitoring and overall governance for quality education.**

One of the major issues is the lack of proper governance in the overall education sector. It is one of the crucial challenges for providing quality education in current scenario. Proper inspection with required guidance for the educational institution along with the parental monitoring is the need of the hour.

INDIAN PERSPECTIVE:-

Indian perspective for the quality education is not different from the world. The purpose of universalizing primary education has almost been achieved. Yet, there is not a single Indian University in the top 100 list of the world top University ranking by 'Times Higher Education World Reputation Rankings',2017. Therefore, in India the focus has been put on quality education. "Sarva Shiksha Abhiyan" is a footstep towards this goal. Indian government scheme will help to develop the whole education sector from primary to higher studies along with the skill development and the appropriate teacher education and orientation. By 2030 the scheme targets to eliminate gender and other disparities in education, provide opportunities for the youth to acquire adequate literacy, numeracy, technical skill and knowledge for sustainable development and lifestyle by providing ample scholarships and qualified teachers.

CONCLUSION:-

This study outline the Educating possesses a good position in the society. If we provide proper training of quality education to the teachers then it will helps the teacher to refresh the new information, abilities to utilize the new computerized apparatuses and assets. Its concluded that quality education is the need of the hour which encompasses economic, social, cognitive and cultural aspects of education in India.

Quality education is an essential factor for the economic, social and psychological development in this 21st century which can only be achieved by adopting innovative measures and developing unique systems which are flexible as well as accountable, which can adjust quickly to the changes and are capable of self learning for proper adaptation to face the new challenges while providing quality education to the humankind for its betterment, peace and above all for its existence.

REFERENCES:-

- International Journal of Educational Research and Technology ,Volume 7, December 2016 by Harsangeet Kaur.
- Journal of Research & Development, April 2021, Volume II, by Dr. S. Tephillah Vasantham.
- http://www.unesco.org/education/gmr_download/chapter1.pdf
- https://unesdoc.unesco.org/ark:/48223/pf0000146641_eng
- https://www.aflatoun.org/goals/quality-of-education/?gclid=EAIaIQobChMIpuqEl7Ox9AIVgJlmAh3R7wafEAAYASAAEgJzTvD_BwE
- https://asq.org/education/why-quality/common-issues.html
- https://www.saralstudy.com/blog/issues-and-challenges-in-indian-education/
- www.wikipedia.com
- www.google.com

Share | QR Code

Back To Results

Kala: The Journal of Indian Art History Congress

Publisher: Guwahati Indian Art History Congress 2004

Description: x, 131p.

Subject(s): Journal

DDC classification: 070.175

MARC View

ISBD View

Holdings

000 -LEADER	
fixed length control field	00487nam a2200193Ia 4500
003 - CONTROL NUMBER IDENTIFIER	
control field	RRL
040 ## - CATALOGING SOURCE	
Transcribing agency	RRL
041 ## - LANGUAGE CODE	
Language code of text/sound track or separate title	eng
260 ## - PUBLICATION, DISTRIBUTION, ETC.	
Place of publication, distribution, etc.	Guwahati
Name of publisher, distributor, etc.	Indian Art History Congress
Date of publication, distribution, etc.	2004
300 ## - PHYSICAL DESCRIPTION	
Extent	x, 131p.
650 ## - SUBJECT ADDED ENTRY--TOPICAL TERM	
Topical term or geographic name entry element	Journal
044 ## - COUNTRY OF PUBLISHING/PRODUCING ENTITY CODE	
MARC country code	ii
082 ## - DEWEY DECIMAL CLASSIFICATION NUMBER	
Edition number	
Classification number	070.175
Item number	T42K

UGC-CARE List

You searched for "**0975-7945**". Total Journals : **1**

Search:

Sr.No.	Journal Title	Publisher	ISSN	E-ISSN	UGC-CARE coverage years	Details
1	Kala: The Journal of Indian Art History Congress (print only)	Indian Art History Congress	0975-7945	NA	from June-2019 to July- 2023	Discontinued from July 2023

Showing 1 to 1 of 1 entries

Previous 1 Next

Copyright © 2024 Savitribai Phule Pune University. All rights reserved. | Disclaimer

Materials Today: Proceedings xxx (xxxx) xxx

Contents lists available at ScienceDirect

Materials Today: Proceedings

journal homepage: www.elsevier.com/locate/matpr

Studies of chelation ion-exchange properties of copolymer resin derived from 1,5-diaminonaphthalene, 2,4-dihydroxy- propiophenone and formaldehyde

Narayan C. Das [a], Yashpal U. Rathod [b], Vikram U. Pandit [c], Wasudeo B. Gurnule [d,*]

[a] Department of Chemistry, Dr. Ambedkar College of Arts, Commerce and Science, Chandrapur 442404, India
[b] Department of Chemistry, J. M. Patel College, Bhandara 441904, M. S., India
[c] Department of Chemistry, H. V. Desai College, Pune 04, M. S., India
[d] Department of Chemistry, Kamla Nehru Mahavidyalaya, Nagpur 440024, M. S., India

ARTICLE INFO

Article history:
Available online xxxx

Keywords:
Copolymer
Ion-exchange properties
Batch equilibrium
Chelatin
Concentration

ABSTRACT

The copolymer 2,4-DHP-1,5-DANF-I has been synthesized by the condensation of 2, 4-dihydroxypropiophenone, 1,5-diaminonaphthalene and formaldehyde in the presence of 2 molar HCl as a catalyst with 1:1:2 molar proportion of reactants. The resin has been characterized by various spectral techniques such as elemental analysis, FT-IR, ^{1}H NMR. The ion-exchange properties of the copolymer resin for specific metal ions viz. Ni^{2+}, Cu^{2+}, Co^{2+}, Zn^{2+} and Pb^{2+} ions was evaluated by a batch equilibrium method. The study was extended to three variations: evaluation of metal ion uptake in the presence of different electrolytes at different concentrations; evaluation of metal ion uptake at different pH; and evaluation of metal ion uptake at different times. From the results it was observed that the copolymer resin acts as an effective chelting ion-exchanger. Copolymer shows a higher selectivity for Cu^{2+} and Ni^{2+} ion than for Co^{2+}, Zn^{2+} and Pb^{2+} ions.
© 2021 Elsevier Ltd. All rights reserved.
Selection and peer-review under responsibility of the scientific committee of the Polymer & Mediterranean Fiber International Conference' 2021

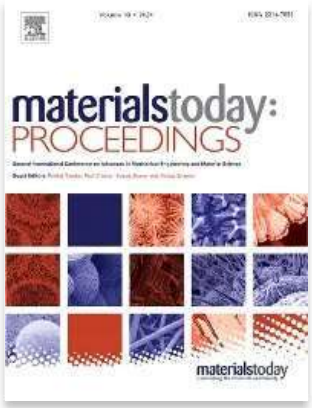
1. Introduction

The toxicity of heavy metal ions has increased rapidly and strongly because of many industries catalyst contains metal ions. Techniques have been developed for the removal of metal ions such as solid liquid extraction, electro-deposition and co-precipitation. To remove the undesired metal ions from aqueous solution chelating resins have been widely used for this purpose. Toxic heavy metal ions are well known for their harmful effect to human health. The energy and material require of the waste water treatment process can be simple if the toxic metal ion can be recovered. The use of chelating resins for the removal of metal ions is the method used due to its high efficiency separation, high loading capacity, high degree of selectivity [1].

An ion exchange resin have been prepared from 4-hydroxybenzophenone and melamine with formaldehyde which was characterized by elemental analysis other spectral methods and chelating nature of resin was studied with Ni^{2+}, Cu^{2+}, Cd^{2+}, Zn^{2+}, and Pb^{2+} metal ions [2]. Copolymeric chelating ion-exchange resin was synthesized from phallic acid - melamine - formaldehyde copolymer and characterized by FT-IR, ^{1}H NMR spectra and elemental analysis [3]. Metal ion uptake capacity of synthesized copolymer has been carried out by Batch equilibration method for different metal ions at different concentrations. Comparative study of strong anion exchange poly (Styrene-co-EGDMA-co-VBC) and strong anion exchange hypercrosslinked poly (HEMA-co-EGDMA-co-VBC) was carried out [4]. Synthesis, antimicrobial and ion-exchange studies of copolymer resin derived from substituted resorcinol, biuret and formaldehyde have been studied [5]. Copolymer resin have been synthesized from salicylic acid and diaminobenzoic acid with formaldehyde and the batch equilibrium method was used to study the chelating ion-exchange properties. The resin was found to be, selectivity for Fe^{*3}, Cu^{2+} and Ni^{2+} ion than for Zn^{2+}, Co^{2+} and Pb^{2+} ions [6]. Copolymer resin by condensation of salicylic acid, semicarbazide and formaldehyde in presence of acid catalyst and studied its ion-exchange properties for Co^{2+}, Zn^{2+}, Cu^{2+}, Ni^{2+}, and Pb^{2+} ions. The study was carried out at different shak-

* Corresponding author.
E-mail address: wbgurnule@gmail.com (W.B. Gurnule).

https://doi.org/10.1016/j.matpr.2021.12.370
2214-7853/© 2021 Elsevier Ltd. All rights reserved.
Selection and peer-review under responsibility of the scientific committee of the Polymer & Mediterranean Fiber International Conference' 2021



Materials Today: Proceedings

Volume 24 • Issue 24 • ISSN: 2214-7853

Materials Today: Proceedings provides the materials science community with a fast and flexible route to the publication of research presented at national and internati... Read more ↓

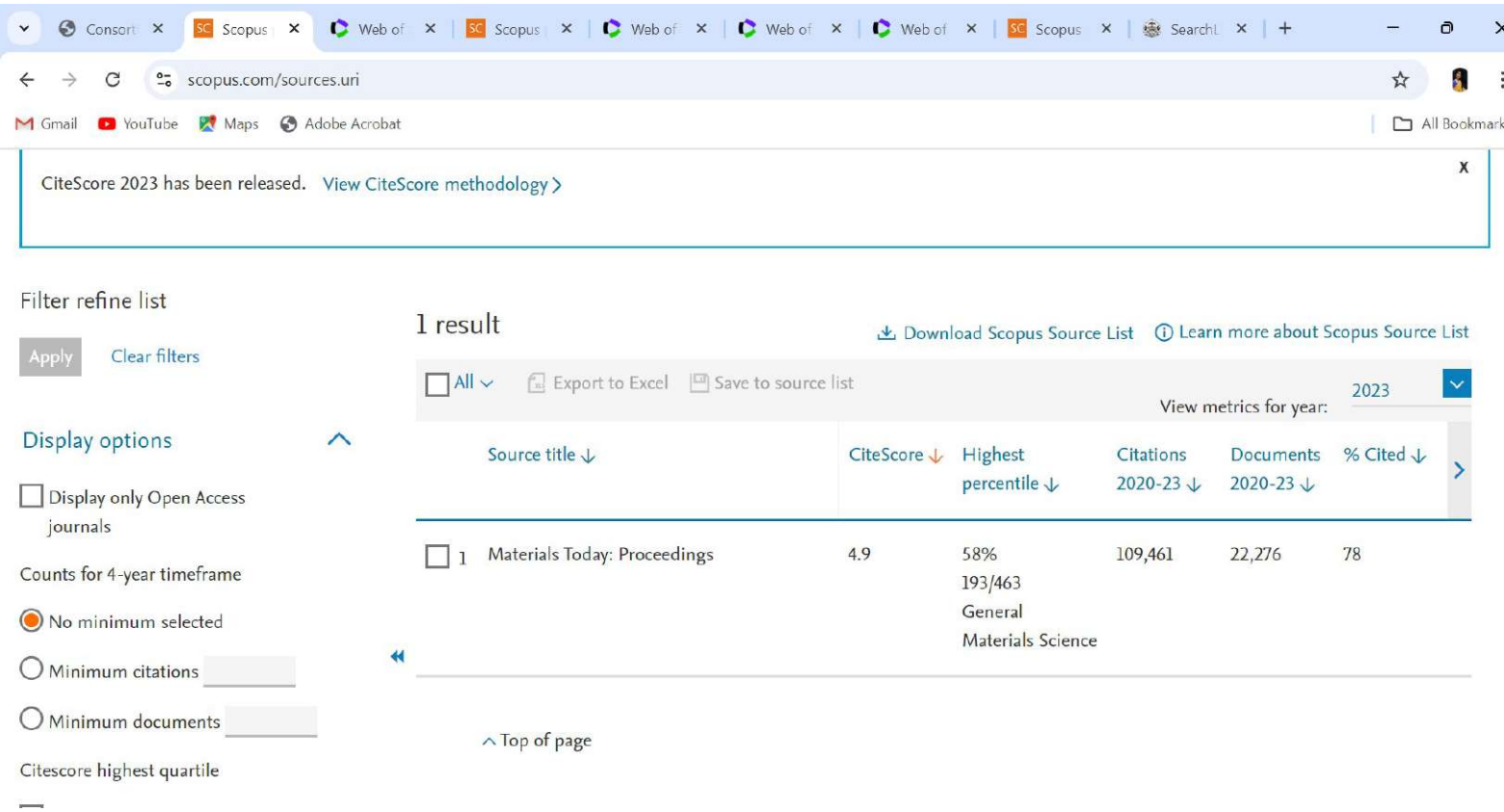
Subscription options

Sorry, this title is not available for purchase in your country/region.

Institutional subscription on ScienceDirect

Request a sales quote ↗

Description


scopus.com/sources.uri
Gmail
YouTube
Maps
Adobe Acrobat
All Bookmarks
CiteScore 2023 has been released. View CiteScore methodology >
Filter refine list
Apply
Clear filters
Display options
Display only Open Access journals
Counts for 4-year timeframe
No minimum selected
Minimum citations
Minimum documents
Citescore highest quartile
1 result
Download Scopus Source List
Learn more about Scopus Source List
All
Export to Excel
Save to source list
View metrics for year:
2023
Source title
CiteScore
Highest percentile
Citations 2020-23
Documents 2020-23
% Cited
1 Materials Today: Proceedings 4.9 58% 193/463 General Materials Science 109,461 22,276 78
Top of page

Publications

Available Online

J. Sci. Res. **13** (3), 971-978 (2021)

JOURNAL OF SCIENTIFIC RESEARCH

www.banglajol.info/index.php/JSR

An Efficient Carbonized Sugar Catalyzed Entry to 7,8-dihydro-2*H*-Chromen-5(6*H*)-ones

T. Siddiqui[1], P. Kulkarni[2], G. Tiwari[3], Z. Pudukulathan[1*]

[1]School of Chemical Sciences, Swami Ramanand Teerth Marathwada University, Nanded– 431606, Maharashtra, India

[2]Department of Chemistry, Hutatma Rajguru Mahavidyalaya, Pune - 410505, Maharashtra, India

[3]Department of Chemistry, J. M. Patel Arts, Commerce & Science College, Bhandara - 441904, Maharashtra, India

Received 25 March 2021, accepted in final revised form 17 June 2021

Abstract

The present paper describes a facile entry to various substituted 7,8-dihydro-2*H*-chromen-5-ones under neat conditions using simple carbonized sugar as a catalyst. The reaction was promoted by visible light under neat or in acetic acid as a solvent with a catalyst to afford the desired products in good to excellent yield. Mild conditions coupled with ease of operation make the protocol synthetically attractive and may find widespread application for the synthesis of chromenone scaffold.

Keywords: Carbonized sugar; Chromenones; Nano; Visible light; Photochemical reaction.

© 2021 JSR Publications. ISSN: 2070-0237 (Print); 2070-0245 (Online). All rights reserved.
doi: http://dx.doi.org/10.3329/jsr.v13i3.52614 J. Sci. Res. **13** (3), 971-978 (2021)

1. Introduction

Chromanes are represented by a fused core tetrahydropyran ring or pyran unit to a six-membered ring. This basic unit represents a principal synthon for many organic transformations and is entrenched in numerous natural products [1-3]. In recent years, chromenone derivatives have attracted significant interest to organic chemists due to their growing biological and pharmaceutical applications [4-8]. Several graceful synthetic methods exist for these intermediates from α, β-unsaturated iminium salts [9-11] under acidic conditions [12], and by employing tandem Stille-oxa-electrocyclization reaction [13-15]. Also, several synthetic strategies have been reported to construct these skeletons *via* [3+3] cycloaddition of α, β-unsaturated aldehydes and 1,3-dicarbonyl compounds employing different catalysts such as Indium (III) chloride [16], EDDA [17,18], Lewis acid [19], Bronsted acid [20,21], or EDDA/$ZnCl_2$ co-catalysts [22], Iodine [23], biocatalyst [24], sulfated tin oxide [25].

1,3-Dicarbonyl compounds are versatile synthons for the incorporation of electrophilic and nucleophilic units [26-28]. Further, these derivatives can be converted to

* *Corresponding author*: zubaidhapk@gmail.com

Bangladesh Journals Online

Journal of Scientific Research



Published by the Faculty of Sciences, University of Rajshahi. Full-text articles available from ARCHIVES.

Journal of Scientific Research is included on DOAJ.

Submission of Paper, Author Guidelines

2009-01-05

The Editorial Board invites papers from the researchers for future issues of JSR.

See details for modest publication charge (Go to next line and Click More...)

Read More ›

Current Issue

Vol. 16 No. 3 (2024)

Published: 2024-09-09

Section A: Physical and Mathematical Sciences

Leveraging AdaBoost and CatBoost to Classify the Likelihood of Brain Stroke

P. Nandal, S. Malik

637-646

pdf

Established by INASP in 2007. Managed by Bangladesh Academy of Sciences.

Bangladesh Journals Online (BanglaJOL) is a service to provide online publication of Bangladeshi journals. For more information about BanglaJOL and how to join the service, see the About page.

Information

For Readers

For Authors

Journal of Scientific Research
ISSN 2070-0237 eISSN 2070-0245

UGC-CARE List

You searched for "**2070-0245**". Total Journals : **1**

Search:

Sr.No.	Journal Title	Publisher	ISSN	E-ISSN	UGC-CARE coverage years	Details
1	Journal of Scientific Research	Faculty of Sciences, Rajshahi University	2070-0237	2070-0245	from June-2019 to Present	View

Showing 1 to 1 of 1 entries

Previous 1 Next

Copyright © 2024 Savitribai Phule Pune University. All rights reserved. | Disclaimer

Journal of Radioanalytical and Nuclear Chemistry
https://doi.org/10.1007/s10967-021-07828-3

Liquid–liquid extraction of uranium(VI) from weak sodium acetate medium using 2-octylaminopyridine: real sample analysis

Gurupad D. Kore[1,2] · Sunil B. Zanje[3] · Arjun N. Kokare[1] · Vishal J. Suryavanshi[1] · Mansing A. Anuse[1] · Sanjay S. Kolekar[1]

Received: 8 April 2021 / Accepted: 7 June 2021
© Akadémiai Kiadó, Budapest, Hungary 2021

Abstract
The analytical technique has been developed for the extraction and determination of uranium(VI). This process is based on the ion-pair complex formation of uranium(VI) with 2-octylaminopyridine in xylene. Uranium(VI) is quantitatively extracted by optimizing the parameters of solvent extraction in presence of sodium acetate, such as pH, concentration of weak organic acids, strippant, shaking period, solvent study, and concentration of extractant. A mechanism of extraction was proposed based on the slope ratio analysis method. The interference of various cations and anions was also investigated. The versatility of the developed method was investigated by employing it to binary and ternary mixtures. The robustness of the method was demonstrated by determining uranium(VI) in the bone sample.

Keywords Solvent extraction · Uranium(VI) · 2-octylaminopyridine · Sodium acetate · Bone sample

Introduction

Uranium is the most vital element for nuclear energy [1]. It is universal that uranium is toxic and is being radioactive; thus the safety profiles for uranium compounds are well established [2]. Hence it is one of the elements for which world health organization (WHO) norms are most stringent (30 µg/L) in drinking water. This is because uranium is a relatively contaminating element in many surface or near-surface environments, its geological exploration requires the measurement of trace quantities of metal ions in water and other samples [3–5]. The natural source for uranium is monazite which contains a sizeable amount of uranium. Consequently, the separation purification of uranium is of great practical importance. The methodology adopted for extraction and purification from ore and nuclear fuel reprocessing has always attracted the attention of separation scientists. The efficient and selective extraction of uranium from aqueous solution has been a subject of significant interest because of the global shortage of uranium sources and radioactive contaminants in the environment, soil, water in which versatile new materials that can separate efficiently desired ore [6–8].

A large number of modern analytical tools have been available for the determination of uranium in a wide variety of samples, The increasing availability of powerful instrumental techniques such as neutron activation analysis (NAA), energy dispersive X-ray fluorescence (EDXRF), inductively coupled plasma atomic emission spectrometry (ICP-AES); inductively coupled plasma emission mass spectrometry (ICP-MS) has enabled the analysis of complex mixtures with high accuracy and precision [9–14]. Even though these techniques provide high sensitivity and favorable detection limit, their application requires rather expensive equipment and leads to higher running cost [15]. Generally, solvent extraction and spectrophotometric technique are widely used to separate and determine uranium(VI) [16–20].

In this context, attentions have been given for the development of soft donor complexing agents as extractants for Ln/An separation. Relatively soft donor atom such as nitrogen prefers 5f elements than 4f elements, providing the higher selectivity than harder oxygen atoms. Concerning this high molecular weight, amines act as better extractant

✉ Gurupad D. Kore
gdkore1027@gmail.com

[1] Analytical Chemistry Research Laboratory, Department of Chemistry, Shivaji University, Kolhapur 416004, India

[2] Department of Chemistry, Padmabhushan Vasantraodada Patil Mahavidyalaya, Kavathemahankal, MS 416405, India

[3] Department of Chemistry, J. M. Patel Arts, Commerce and Science College, Bhandara, MS 441904, India

Published online: 24 June 2021

SPRINGER LINK

Log in

Menu Search Cart

Home Journal of Radioanalytical and Nuclear Chemistry



Journal of Radioanalytical and Nuclear Chemistry

An International Journal Dealing with All Aspects and Applications of Nuclear Chemistry

Publishing model

Hybrid

Submit your manuscript

AKADÉMIAI KIADÓ

Editorial board

Aims and scope

Journal updates

Overview

Journal of Radioanalytical and Nuclear Chemistry is an international journal covering a wide range of topics in the field of nuclear chemistry.

Open for submissions in all fields of radiopharmaceuticals
Coverage includes nuclear chemistry, radiochemistry, radiation chemistry, radiobiological chemistry, environmental radiochemistry, production and control of radioisotopes and labeled compounds nuclear power plant chemistry, nuclear fuel chemistry, radioanalytical chemistry, radiation detection and measurement, nuclear instrumentation and automation, and more.
Presents original papers, letter, review papers and short communications

Editor-in-Chief
Zsolt Révay

Journal Impact Factor
1.5 (2023)

5-year Journal Impact Factor
1.5 (2023)

Submission to first decision (median)
8 days

Downloads
631,201 (2023)

Societies and partnerships

AKADÉMIAI KIADÓ

Akadémiai Kiadó

Latest issue

September 2024

CAB Abstracts
CLOCKSS
CNKI
CNPIEC
Chemical Abstracts Service (CAS)
Chimica
Current Contents/Physical, Chemical and Earth Sciences
Dimensions
EBSCO
EI Compendex
EMBASE
Gale
Google Scholar
IFIS Publishing
INIS Atomindex
INSPEC
INSPIRE
Japanese Science and Technology Agency (JST)
Naver
OCLC WorldCat Discovery Service
Portico
ProQuest
Reaction Citation Index
Reaxys
SCImago
SCOPUS
Science Citation Index Expanded (SCIE)
Semantic Scholar
TD Net Discovery Service
UGC-CARE List (India)
Wanfang

Copyright information
Rights and permissions
Editorial policies

© Akadémiai Kiadó, Budapest, Hungary

For authors

Products

Master Journal List | Search Journals | Match Manuscript | Downloads | Help Cent

Already have a manuscript?

Use our Manuscript Matcher to find the best relevant journals!

Find a Match

Filters | Clear All

- *Web of Science* Coverage
- Open Access
- Category
- Country / Region
- Language
- Frequency
- Journal Citation Reports

ine Your Search Results

6-5731 Search

y: Title (A-Z)

rch Results

d 1 results (Page 1) Share These Results

ct Match Found

URNAL OF RADIOANALYTICAL AND NUCLEAR HEMISTRY

blisher: SPRINGER , VAN GODEWIJCKSTRAAT 30, DORDRECHT, NETHERLANDS, 3311 GZ

N / eISSN: 0236-5731 / 1588-2780

b of Science Core Collection: Science Citation Index Expanded

ditional *Web of ence* Indexes: Current Contents Physical, Chemical & Earth Sciences | Essential Science Indicators

Share This Journal | View profile page

** Requires free login.*

1 – 1 of 1

Items per page: 10

5

Journal of Molecular Structure 1247 (2022) 131293

Contents lists available at ScienceDirect

Journal of Molecular Structure

journal homepage: www.elsevier.com/locate/molstr

The transition metal complexes of Fe(II), Ni(II) and Cu(II) derived from phthalazine based ligands: Synthesis, crystal structures and biological activities

Smita S. Patil[a], Samina K. Tadavi[b], Amol Dikundwar[c], Ratnamala S. Bendre[d,*]

[a] School of Chemical Sciences, Kavayitri Bahinabai Chaudhari North Maharashtra University, Jalgaon, Maharashtra 425001, India
[b] Department of Chemistry, J. M. Patel Arts, Commerce and Science College, Bhandara, Maharashtra 441904 India
[c] Solid State and Structural Chemistry Unit, Indian Institute of Science, Bangalore 560 012, India
[d] School of Chemical Sciences, Kavayitri Bahinabai Chaudhari North Maharashtra University, Jalgaon, Maharashtra 425001, India

ARTICLE INFO

Article history:
Received 7 May 2021
Revised 25 July 2021
Accepted 11 August 2021
Available online 14 August 2021

Keywords:
Phthalazine derivatives
Metal complexes
Single crystal structures
Antimicrobial activity
Antioxidant activity and DNA cleavage activity

ABSTRACT

Twelve metal complexes of Iron(II), Nickel(II) and Copper(II) have been synthesized in 1:1 and 1:2 molar ratio from new phthalazine based ligands (E)-2-(phthalazin-1-yl)-1-(1-(pyridin-2-yl)ethylidene)hydrazine (L1) and (E)-2-(phthalazin-1-yl)-1-((pyridin-2-yl)methylene)hydrazine (L2). The compounds have been characterized by UV-Visible, FT-IR, ^{1}H-NMR, LC-MS/ESI-MS spectroscopic techniqueas well as conductivity measurements and finally structures of some of the compounds have been confirmed through single crystal X-ray crystallographic technique. Crystal data for [Cu(II)L1Cl](2) complex: $C_{15}H_{12}ClCuN_5$, triclinic, Space group *P*-1, a = 10.5114(11) Å, b= 10.7962(11) Å, c = 13.7510(14) Å, α = 74.206(9)°, β = 71.981(9)°, γ = 84.122(8)° and Z = 1, final R_1 was 0.0553($I > 2\sigma(I)$) and wR_2 was 0.1892(all data). Crystal data for $[Ni(II)(L1)_2](ClO_4)_2$(7) complex: $C_{30}H_{26}Cl_2N_{10}NiO_8$, monoclinic, Space group $P2_1/n$, a = 13.0740(7) Å, b = 19.1326(10) Å, c = 14.5808(9) Å, α = 90°, β = 104.511(6)°, γ = 90°, V = 3530.9(4) Å^3, Z = 4, final R_1 was 0.0778 ($I > 2\sigma(I)$) and wR_2 was 0.2226 (all data). Crystal data for $[(L2)_2(\mu\text{-}Cl)Cu_2(II)]Cl$(10) complex: $C_{28}H_{22}Cl_2Cu_2N_{10}$, triclinic, Space group *P*-1, a = 7.7441(15) Å, b = 14.954(3) Å, c = 15.004(3) Å, α = 92.458(11)°, β = 96.234(11)°, γ = 96.291(12)° and Z = 2, final R_1 was 0.0576($I > 2\sigma(I)$) and wR_2 was 0.1671(all data). Crystal data for $[Ni(II)(L2)_2](ClO_4)_2$(14) complex: $C_{28}H_{22}N_{10}O_8Cl_2Ni$, monoclinic, Space group $P2_1/c$, a = 13.1220(12) Å, b = 11.3216(10) Å, c = 23.982(2) Å, α = 90°, β = 104.621(4)°, γ = 90° and Z = 4, final $R_1$was 0.0931($I > 2\sigma(I)$) and wR_2 was 0.3083 (all data). The compounds were investigated for their antimicrobial, antioxidant and DNA cleavage activities.

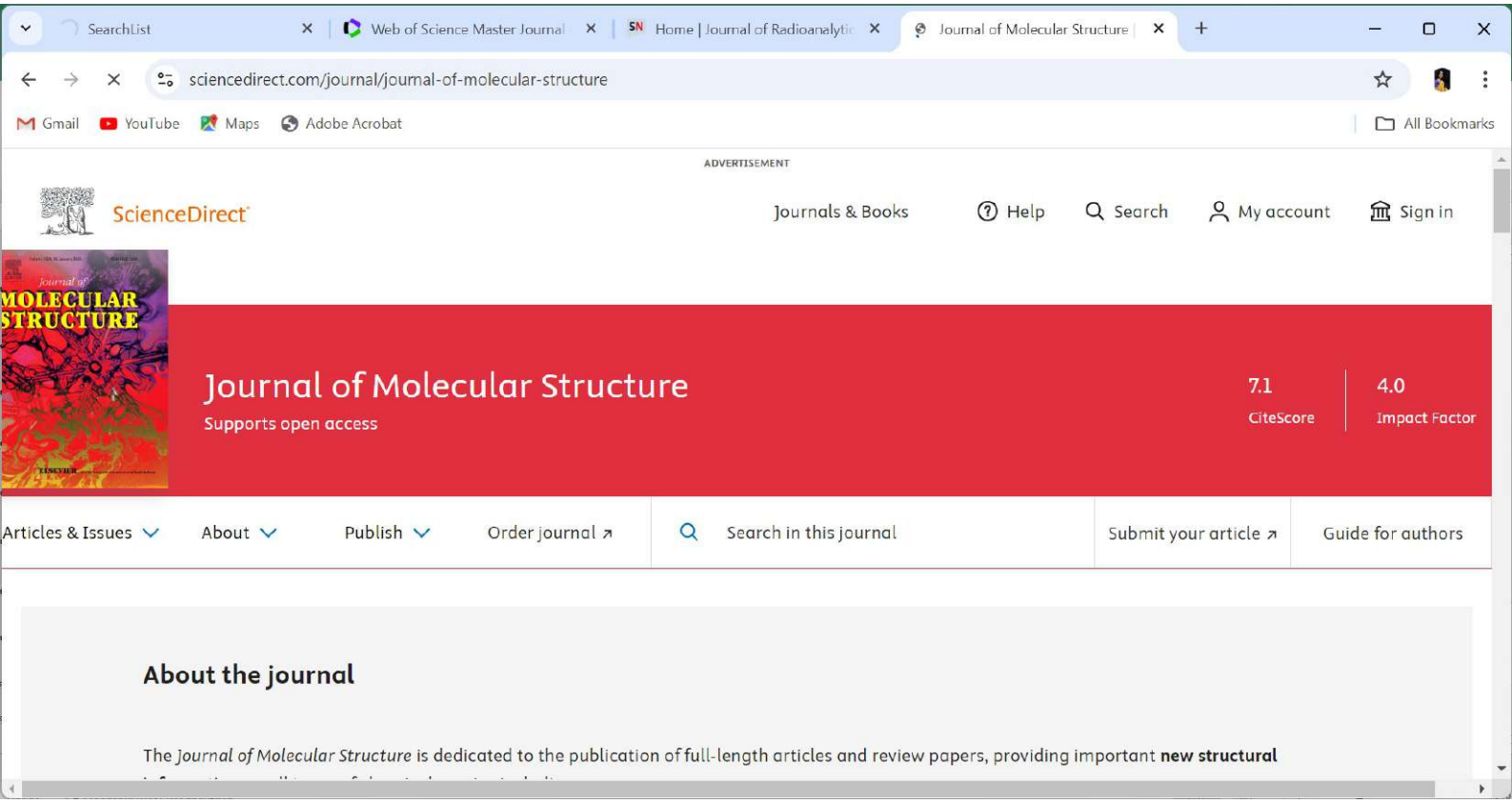
© 2021 Published by Elsevier B.V.

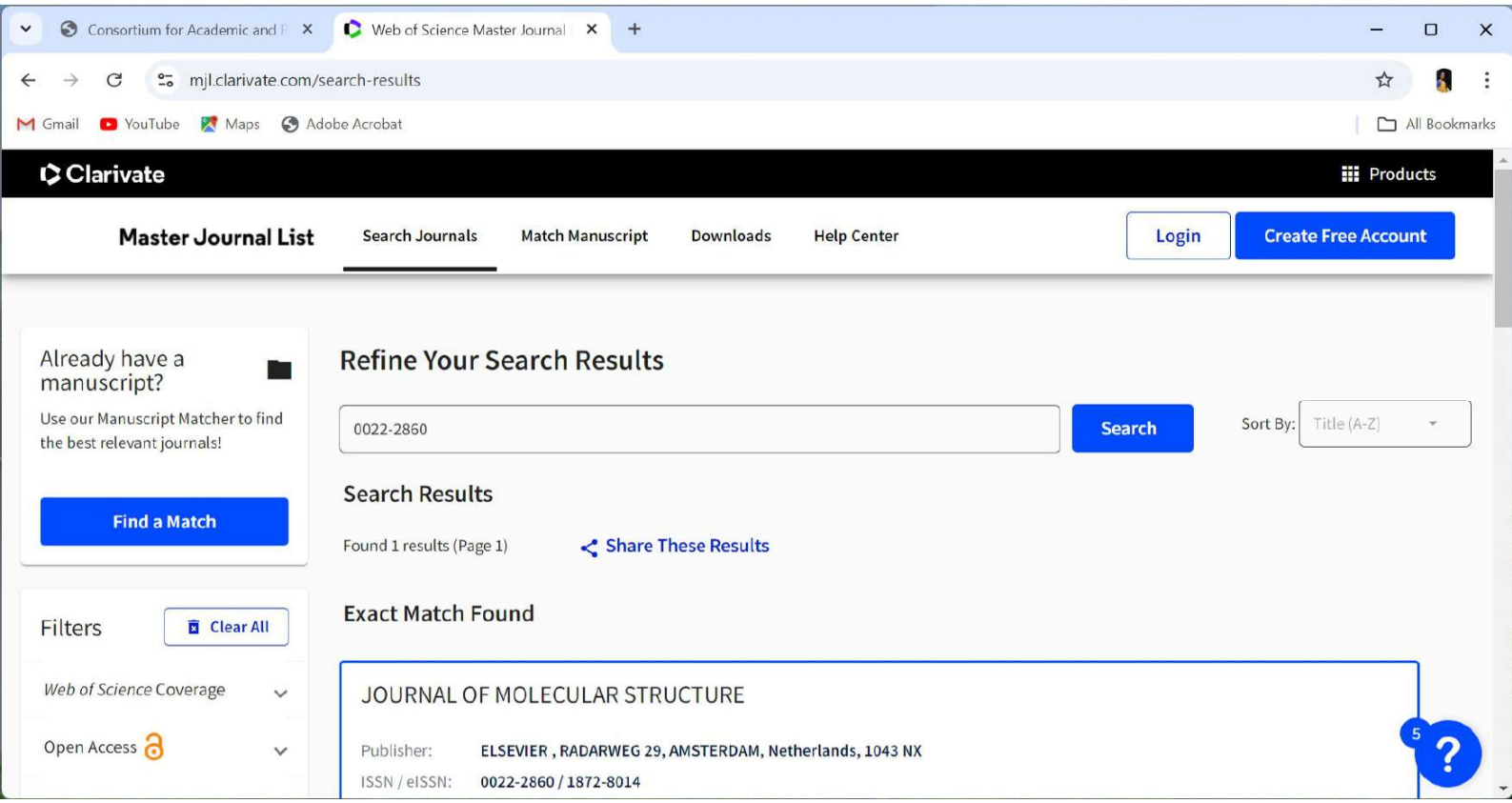
1. Introduction

The demand for new metal-based antibacterial and antifungal compounds is the rising area of research which is being fulfilled by metal-organic chemistry [1]. Also, the development of resistance towards available drugs is rapidly becoming a major global concern and hence the major goal of drug development projects is to synthesize new compounds and assess their biological and pharmacological activities. Hydrazone is a versatile moiety having the basic structure $R_1R_2C = NNH_2$ that exhibits broad spectrum biological activities [2]. Among the most numerous types of hydrazones, particularly nitrogen-containing heterocyclic hydrazones have received much attention as stipulated by the several studies published on their applicability in different areas, especially as drugs; and due to their wide-ranging pharmacological properties such as hypotensive, antituberculous, antitumoral, antiviral, antibacterial, anti-inflammatory [3], antihypertensive [4] and psychotropic [5]. Hydrazones and their complexes are widely applied in particular as catalysts, dyes, analytical reagents, and pesticides [5]. In the world of organic compounds, heterocyclic derivatives seem to be an important class for the development of novel drugs and phthalazine a heterocyclic weak base shows multifarious biological activities through exhaustive studies in modern coordination chemistry, in bioorganic and medicinal chemistry by application in drug discovery. Phthalazine is one of the most important heterocyclic moieties, comprising of pyridazine ring fused with a benzene ring, it possesses numerous applications and there are several reports in the literature related to phthalazine representing that the presence of this bicyclic ring system is beneficial structural profile for biological properties [6]. Phthalazine compounds have been syn-

* Corresponding author.
E-mail address: bendrers@gmail.com (R.S. Bendre).

https://doi.org/10.1016/j.molstruc.2021.131293
0022-2860/© 2021 Published by Elsevier B.V.


SearchList
Web of Science Master Journal
Home | Journal of Radioanalytic
Journal of Molecular Structure
sciencedirect.com/journal/journal-of-molecular-structure
Gmail
YouTube
Maps
Adobe Acrobat
All Bookmarks
ADVERTISEMENT
ScienceDirect
Journals & Books
Help
Search
My account
Sign in
Journal of Molecular Structure
Supports open access
7.1
CiteScore
4.0
Impact Factor
Articles & Issues
About
Publish
Order journal
Search in this journal
Submit your article
Guide for authors
About the journal
The Journal of Molecular Structure is dedicated to the publication of full-length articles and review papers, providing important new structural


Consortium for Academic and
Web of Science Master Journal
mjl.clarivate.com/search-results
Gmail
YouTube
Maps
Adobe Acrobat
All Bookmarks
Clarivate
Products
Master Journal List
Search Journals
Match Manuscript
Downloads
Help Center
Login
Create Free Account
Already have a manuscript?
Use our Manuscript Matcher to find the best relevant journals!
Find a Match
Refine Your Search Results
0022-2860
Search
Sort By:
Title (A-Z)
Search Results
Found 1 results (Page 1)
Share These Results
Exact Match Found
Filters
Clear All
Web of Science Coverage
Open Access
JOURNAL OF MOLECULAR STRUCTURE
Publisher:
ELSEVIER , RADARWEG 29, AMSTERDAM, Netherlands, 1043 NX
ISSN / eISSN:
0022-2860 / 1872-8014

Kalyan Bharati

ISSN No. 0976-0822
(UGC-CARE List Group I)

EFFECT OF SELECTED PRANAYAMA TECHNIQUES ON CARDIOVASCULAR ENDURANCE OF DIFFERENT COLLEGE STUDENTS OF RASHTRASANT TUKADOJI MAHARAJ NAGPUR UNIVERSITY, NAGPUR

Romi Bisht
Department of Physical Education, J.M. Patel College, Bhandara-441904, (MS), India.

Madhavi Mardikar
Department of Physical Education, Institute of Science, Nagpur-440001, (MS), India.

Chandra Mohan Singh
Department of Physical Education, T.G Mahavidyalya, Ramtek-441106, (MS), India.

Abstract
The purpose of the study was to know the effect of selected pranayama techniques on cardiovascular endurance of different college students of Rashtrasant Tukadoji Maharaj Nagpur University, Nagpur. 60 subjects were selected randomly from the Post Graduate Training Department of Physical education, Rashtrasant Tukadoji Maharaj Nagpur University, Nagpur and Hislop college, Nagpur. 30 subjects from each colleges were selected. All the subjects were between the age range from 22 to 25 years. Two groups consisting of 30 subjects each was formed by random sampling method. 30 subjects from Post Graduate Training Department of Physical education, Rashtrasant Tukadoji Maharaj Nagpur University, Nagpur were selected in experimental group and 30 subjects from Hislop college, Nagpur were selected in control group. The study was divided into three phases i.e. pre test, implementation of training, post test. In pre test, the data was collected from both the groups. In implementation of training, practice of selected pranayama was done by all subjects daily for 30 minutes for six weeks and control group was given no training. In post test, the data was collected from both groups. The data was collected by measuring fitness index of subjects using Harvard step test. After collection of data, it was subjected to statistical treatment in which the comparison was done on the basis of scoring. The level of significance was set at 0.05. There is no significant difference in cardio-vascular endurance of control group between pre and post test. There is significant difference in cardio-vascular endurance of experimental group between pre and post test. Six week pranayama training programme shows positive effect on cardio-vascular endurance. There is no significant difference in cardio vascular endurance of pre test between experimental and control group. There is significant difference in cardio-vascular endurance of post test between experimental and control groups.

Keywords: Yoga; Pranayama; Cardio-vascular Endurance; Fitness.

Introduction:

Yoga science of breathing is called pranayama. Oxygen is the most vital nutrient to our body. It is essential for the integrity of brain, nerves, glands and internal organs. It is a systematic exercise of respiration, which makes the lungs stronger, improves blood circulation, makes the man healthier and bestows upon him the boon of a long life. It aids the respiratory system function at its best whereby the life force can be activated and regulated in order to go beyond one's normal boundaries or limitations and attain a higher state of vibratory energy. Pranayama is the fourth step of Ashtang Yoga.

It is scientific way of controlling the breath leading towards better health for both mind and body. Pranayama is the breathing exercise to boost individuals cardiovascular endurance. Cardiovasucular endurance may be defined as the ability of hearts and lungs to take in and to transport adequate amount of oxygen to the working muscles for activities to be performed over a long period of time. For example – running, walking, swimming and bicycling, activities which involves large muscles. Cardiovascular endurance is also frequently called as cardio respiratory endurance, aerobic endurance and broadly may be also called endurance – although endurance may also refer to the ability of the muscle to do repeated work without fatigue. It is also one of five components of physical fitness. **Jaykishan Santoshi** conducted a study on the effect of Pranayama on status of cardio respiratory endurance. The study was conducted on 120 male students between the age group of 13 to 17 years. 4 groups consisting of 30 students each word formed. The study examined which type of Pranayama group had the maximum effect on the physiological fitness of subjects. Results showed that every type of pranayams improves the physiological fitness but training of Ujjayi and Bhastrika Pranayama can collectively provide the best result. **Thakur** conducted a study to see the effects of kapalbhati or cardio respiratory variables. He found that there were significant increase in vital capacity (F = 5.29 against requied value 4.08), maximum possible breath holding capacity (F = 45.23 against 4.08), cardio vascular efficiency (F = 4.53 against required value of 4.08), total body fat percent (F = 71.5 against the required value 4.08) whereas blood pressure and air flow rate showed no significant charge by practice of kapalbhati kriya.

Methodology:

Selection of Subjects: 60 subjects were selected randomly from the P.G.T.D. of Physical education and hislop college. 30 subjects from each college. All the subjects were between the age range 22 to 25 years.

Selection of variables: Selected Pranayama techniques are Anulom-Vilom, Sitkari Pranayama, Shitali Pranayama, Kapalbhati

Formation of experimental and control group: Two groups consisting of 30 subjects each was formed by random sampling method. 30 subjects from Post Graduate Training Department of Physical education, Rashtrasant Tukadoji Maharaj Nagpur University, Nagpur were selected in experimental group and 30 subjects from Hislop college, Nagpur were selected in control group.

The study was carried in three phases:-

Phase I – PRE TEST

Phase II – IMPLEMENTATION OF TRAINING

Phase III – POST TEST

Pre – Test: Cardiovascular endurance of both the groups was measured by administrating Harvard Step Test.

Implementation of Training: Experimental group was doing Pranayama for at least half hour daily for six weeks. No training was given to control group. Experimental group followed the training schedule as given in Table no. 1.

Post – Test: Cardiovascular measurement was done by administrating the same test as in pre – test phase.

ISSN No. 0976-0822
(UGC-CARE List Group I)

Table No. 1 : Training Schedule

Day	Name of Pranayama	Duration
Monday To Saturday	Om kar jaap	5 minutes
	Rest	30 seconds
	Kapalbhati	5 minutes
	Rest	30 seconds
	Anulom - Vilom	5 minutes
	Rest	30 seconds
	Sheetali	5 minutes
	Rest	30 seconds
	Sitkari	5 minutes
	Yognidra	3 minutes
Total Duration		30 minutes

Method of cardio vascular endurance measurement

Cardiovascular endurance of all the subjects of both groups was measured by administrating them with Harvard step test and calculating their fitness index.

The data pre-test and post-test was compared by using 't' test and as per the result was analyzed. The level of significance was kept at 0.05 to test the hypothesis.

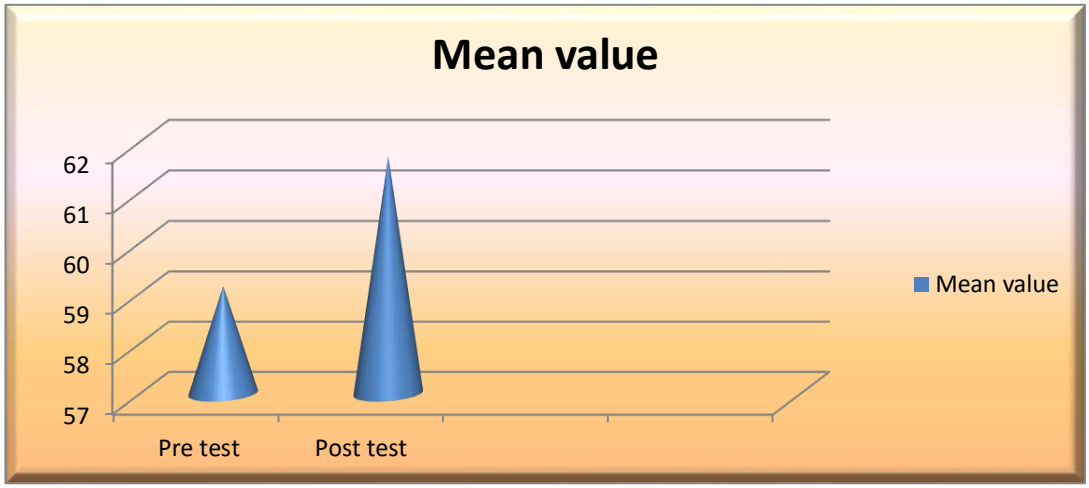
Findings and Discussions:

Table 2: Comparison of cardio – vascular endurance between pre and post test of control group

Group	Test	Mean	SD	SE	MD	O 't'	T 't'
Control group	Pre	59.14	6.22	1.54	2.57	1.66	2.02
	Post	61.71	5.73				

From the Table No. 2 it is clear that, there is insignificant difference in cardio- vascular endurance of control group between pre and post test as obtained 't' value is less than the table value.

Graph No. 1 Mean value of pre and post cardio vascular endurance of control group



ISSN No. 0976-0822
(UGC-CARE List Group I)

Table No. 3 Comparison of cardio-vascular endurance between pre and post test of experimental group.

Group	Test	Mean	SD	SE	MD	O 't'	T 't'
Experimental group	Pre	61.79	5.62	1.43	5.93	4.15	2.02
	Post	67.72	5.52				

From the Table No. 3, it is clear that there is significant difference in cardio-vascular endurance of experimental group between pre and post test as the obtained 't' value of 4.15 is more than the table value of 2.02.

Graph No. 2 Mean value of pre and post test cardio-vascular endurance of Experimental group

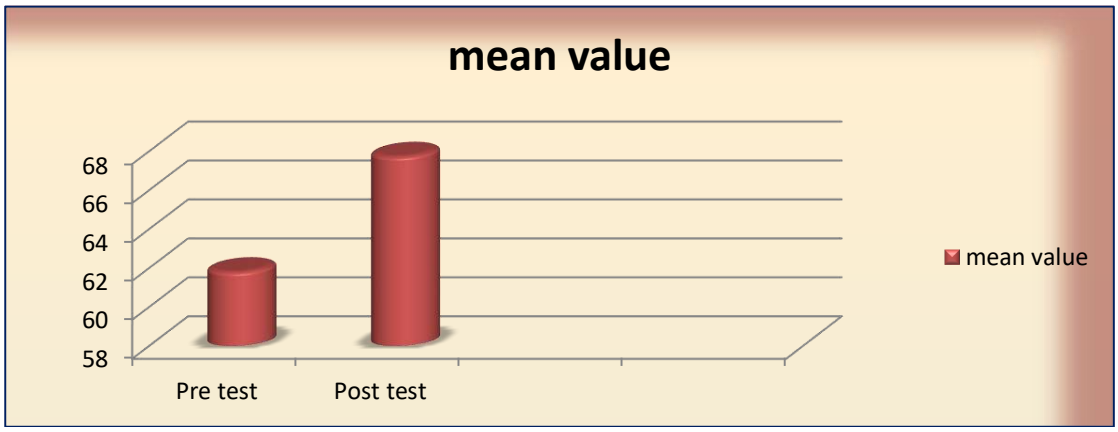
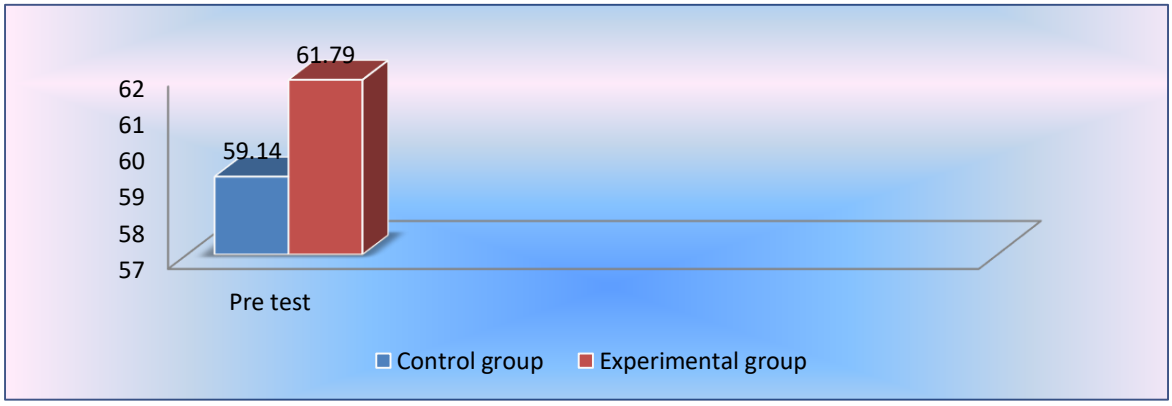


Table No. 4 Comparison of cardio-vascular endurance between control and experimental group of pre test.

Group	Test	Mean	SD	SE	MD	O 't'	T 't'
Control	Pre	59.14	6.22	1.53	2.65	1.73	2.02
Experimental	Pre	61.79	5.62				

From the table, it is clear that there is insignificant difference in cardio-vascular endurance of pre test between control and experimental group as the obtained 't' value of 1.73 is less than the table value of 2.02.

Graph No. 3 Mean value of cardio-vascular endurance of control and experimental group in pre test.



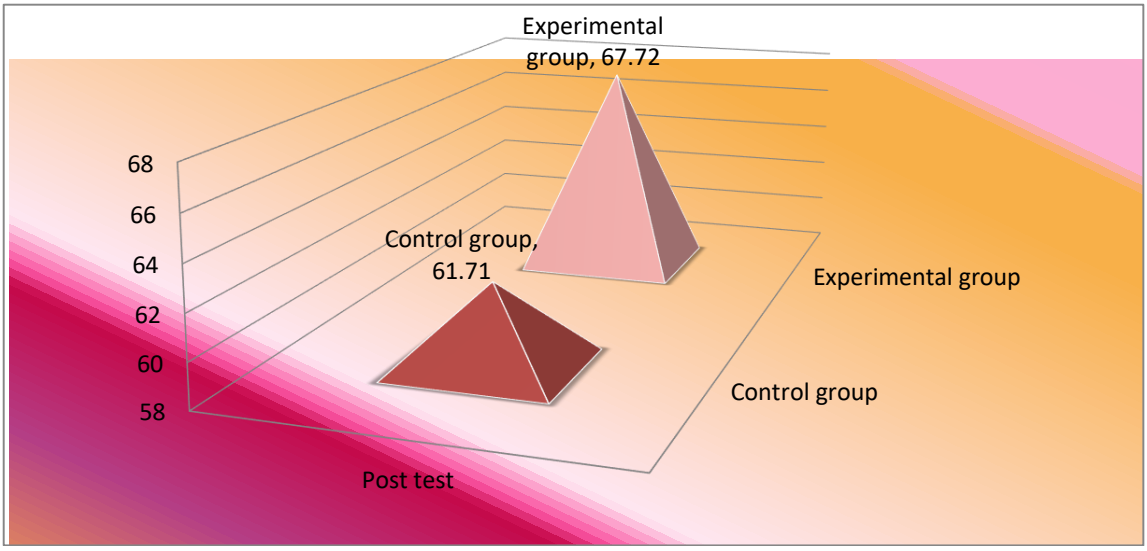
ISSN No. 0976-0822
(UGC-CARE List Group I)

Table no. 5 Comparison of cardio-vascular endurance between experimental and control group of post test.

Group	Test	Mean	SD	SE	MD	O 't'	T 't'
Control	Post	61.71	5.73	1.45	6.01	4.14	2.02
Experimental	Post	67.72	5.52				

From the table, it is clear that there is significant difference in cardio-vascular endurance of post test between control and experimental group as the obtained 't' value of 4.14 is more than the table value of 2.02.

Graph No. 4 Mean value of cardio-vascular endurance of control and Experimental group in post test.



Discussion of Hypothesis

For the study it was hypothesized that Pranayama will bring significantly more difference in cardio-vascular endurance. So the overall numerical and statistical analysis and comparison of pre test and post test of experimental and no change in control group, shows that there is significantly more difference in cardiovascular endurance after the practice of pranayama.

Conclusions

- There is no significant difference in cardio-vascular endurance of control group between pre and post test.
- There is significant difference in cardio-vascular endurance of experimental group between pre and post test. Six week pranayama training programme shows positive effect on cardio-vascular endurance.
- There is no significant difference in cardio vascular endurance of pre test between experimental and control group.
- There is significant difference in cardio-vascular endurance of post test between experimental and control groups.

Recommendations

- To compare the effects of pranayama and yoga on premenstrual syndrome.
- To compare the effect of pranayama and Suryanamaskar on cardiovascular fitness.
- Similar study may be conducted on the players of different games.
- Impact of pranayama on Cardio-vascular in relation to adolescence health.
- Effect of pranayama on psycho-physical health of college students during covid-19.

References:

1. Chavhan SP Effects of yoga training on low level physical fitness secondary school boys. International Journal of physical education, Sports and health2015;1(5)37- 40.

2. D.Shaktignanavel, "Effect of pranayama with aerobic exercise on aerobic fitness", Yoga mimasa,32:4,(January 1998), page no.1-12.

3. http://www.about.com

4. http://www.answerfitness.com

5. http://www.ashtangayoga.info/philosophy/source-texts-and-mantra/yoga-sutra/chapter-2/

6. http://www.yogiclogic.com/Yoga-articles/pranayama-in-yoga.php

7. Iyengar BKS. Light on Yoga: Unwin Paperbacks c.1986,21.

8. Jaykishan Santoshi, "Effect of pranayama on status of cardio respiratory endurance", International Journal of physical education,Vol.3No.1&2(April & October,2010):31-33

9. Kansal Devinder k., "Textbook of applied measurement evaluation and sports selection" P. 272

10. Santosh Bapurao Yawale, "Effect of Pranayama on cardiovascular endurance",International Journal of physical education, Sports and health 2016:3(3):573-577

11. Sharma Dr. Sudhir Kumar, "Journal of physical education sports management and yogic sciences"vol.2,No.1 January-march2012:P. 1.

12. Sharama Dr. Sudhir Kumar, "Journal of physical education sports management and yogic sciences"Vol.2No.1(2012):p.41

13. Shodhganga.inflibnet.ac.in

14. Singh, Ajmer. Others. Essential of physical education. Kalyani Publisher, New Delhi, 3rd edition, 2008, 517-519.

ISSN INTERNATIONAL STANDARD SERIAL NUMBER INTERNATIONAL CENTRE
ISSN PORTAL The Global Index for Continuing Resources

FREE ACCESS

PUBLISHERS' AREA

DISCOVER ISSN SERVICES

SEARCH OPEN ACCESS RESOURCES

KEEPERS REGISTRY

ISSN INTERNATIONAL CENTER

Home Record

Type an ISSN or a title | ISSN or title | Search

Advanced search ROAD search The Keepers search

Identifiers

ISSN :0976-0822
Linking ISSN (ISSN-L): 0976-0822

Links

Google
Bing

Key-title	**Kalyan Bharati : journal of Indian history and culture**
Identifiers	
ISSN :0976-0822 Linking ISSN (ISSN-L): 0976-0822	
	Resource information

My Tools

Share

Print

Display linked data

Discover all the features of the complete ISSN records

Access the full version of the ISSN Portal

ISSN INTERNATIONAL STANDARD SERIAL NUMBER INTERNATIONAL CENTRE ISSN PORTAL The Global Index for Continuing Resources

FREE ACCESS

Medium: Print

Record information

Last modification date: 28/12/2011

Type of record: Confirmed

ISSN Center responsible of the record: **ISSN National Centre for India**

For all potential issues concerning the description of the publication identified by this bibliographic record (missing or wrong data etc.), please contact the ISSN National Centre mentioned above by clicking on the link.

Links

Google

Bing

Yahoo

National Library of India

GTU | Licence | Contact | Newsletter | FAQ | Data sources | ISSN © 2024

UGC-CARE List

You searched for **"0976-0822"**. Total Journals : **1**

Search:

Sr.No.	Journal Title	Publisher	ISSN	E-ISSN	UGC-CARE coverage years	Details
1	Kalyan Bharati (print only)	Kalyan Kumar Dasgupta Memorial Committee	0976-0822	NA	from September-2019 to October- 2021	Discontinued from Oct. 2021

Showing 1 to 1 of 1 entries

Previous 1 Next

Copyright © 2024 Savitribai Phule Pune University. All rights reserved. | Disclaimer

Journal of Radioanalytical and Nuclear Chemistry
https://doi.org/10.1007/s10967-021-07698-9

Facile extractive separation studies of uranium(VI) assisted by dicyclohexano-18-crown-6 through green approach

Shivaji H. Burungale[1] · **Sunil B. Zanje**[2]

Received: 5 January 2021 / Accepted: 26 March 2021
© Akadémiai Kiadó, Budapest, Hungary 2021

Abstract
A reliable precise analytical method has been developed for the extraction of uranium(VI) from 1 M ammonium thiocyanate and 1 M acetic acid with 0.001 M dicyclohexano-18-crown-6 in nitrobenzene. Various parameters like ammonium thiocyanate concentration, acetic acid concentration, reagent study, solvent study, strippant study and loading capacity were studied. Uranium(VI) were selectively extracted and separated from diverse ion and ternary mixture. The proposed method was also used for the determination of uranium(VI) from rock and monazite sand sample.

Keywords Analysis of rock sample · Extraction · Uranium(VI) · Dicyclohexano-18-crown-6

Introduction

Uranium is a naturally occurring significant radioactive metal. Nowadays uranium is used as a nuclear fuel in nuclear power generation. Uranium is a significant strategic resource [1]. Uranium resources are broadly employed in medicine, scientific research, national defence, industry, and other fields [2, 3]. The quick growth of nuclear technology has steadily increased the requirement of uranium mining and smelting products, resulting in a huge quantity of uranium tailings [1, 4]. Therefore time requires that it should be extracted and lastly in pure form.

It is significant to extract uranium from natural resources by environmental friendly approaches. Different strategies for the separation of uranium have been investigated. Along with solvent extraction is most often employed strategy. Different extractants have been used for the extraction of uranium such as dibenzo-24-crown-8 [5], dibenzo-18-crown-6 [6], trioctylphosphine oxide (TOPO), triphenylphosphine-oxide (TPPO), tri *iso*-octylamine [7], tributylphosphate [8], KROPHOS-18 [9]. Cyanex-272 [10], Tri-n-dodecylamine [11], 2-ethylhexylphosphonic acid (PC88A) [12], UTEVA [13], didodecylphosphoric acid (DDPA) [14], N,N,N′,N′-tetrabutylmalonamide [15], N,N-dialkylamide [16].

Calcium chloride ($CaCl_2$) roasting and nitric acid (HNO_3) leaching were used for the extraction of uranium [17]. Wen-Jiwang studied the distribution of Dicyclohexano-18-crown-6 in 1, 2-dichloroethane at two phases [18]. The potential analytical abilities of dicyclohexano-18-crown-6 is high, therefore it was used for extraction of U(VI) through solid-phase extraction [19], also, it was employed for extraction of U(VI) from mixed aqueous-organic solutions [20], its fate was applied for extraction of U(VI) with Re(VII) [21]. The N, N, N, N-tetra octyl diglycomide (TODGA) has been investigated for extraction of uranium in nitric acid medium [22].

According to the robustness of the work is concerned, in the former work, U(VI) was extracted with different extractants as given in Table 1. However, those necessitate a high concentration of mineral acid media, maximum concentration of extractant and more time of extraction etc. Whereas, in the projected system, the extraction was carried out in a mixture of 1 M acetic acid and 1 M ammonium thiocyanate medium, dicyclohexano-18-crown-6 concentration was 1×10^{-3} M, demonstrating the system is comparatively eco-friendly and a step ahead in the direction of green chemistry.

The goal of the present study was to extend a more specific and greener method for the extraction of U(VI). The extraction scheme has been optimized by studying various parameters. The uniqueness of the scheme lies in a smaller

✉ Shivaji H. Burungale
shivajiburungale777@gmail.com

[1] Laboratory of Analytical Chemistry, PG Department of Chemistry, Yashwantrao Chavan College of Science, Karad, MS 415124, India

[2] Department of Chemistry, J. M. Patel Arts, Commerce and Science College, Bhandara, MS 441904, India

Published online: 27 April 2021

Table 1 Comparison of the current method with previous reported solvent extraction systems for extraction of uranium

Extractant	Solvent	Acidity	Strippant	Method of determination	Equilibrium time	References
Dibenzo-24-crown-8	Nitrobenzene	0.5–8.0 M HBr	2 M HNO_3	Spectrophotometry	10 min	[5]
Dibenzo-18-crown-6	Nitrobenzene	0.1–5.0 M NH_4SCN	1 M HNO_3	Spectrophotometry	10 min	[6]
Tributyl phosphate	Dodecane	3 M HNO_3	–	Spectrophotometry	10 min	[8]
KROPHOS-18	Kerosene	8 M HCl	10 M H_3PO_4	–	2 min	[9]
Cyanex-272	Xylene	2 M HNO_3	0.5 M Na_2CO_3	ICP-AES	5 min	[10]
Tri-n- dodecylamine	n-Hexane	7 M HCl	–	Spectrophotometry	24 h	[11]
PC88A	Dodecane	0.1 M Oxalic acid	3 M HNO_3	FTIR	30 min	[12]
Didodecylphosphoric acid	Toluene	1–7 M HNO_3/$HClO_4$	–	Spectrophotometry	3 h	[14]
N,N,N',N'- tetrabutyl-malonamide	Toluene	1 M HNO_3	$LiNO_3$	Spectrophotometry	10 min	[15]
N,N-dialkylamide	Toluene	4 M HNO_3	–	Spectrophotometry	30 min	[16]
DC-18-C-6	1,2-DCE	4 N HCl	Picric acid	–	–	[18]
DC-18-C-6	Toluene	7 M HNO_3	–	Spectrophotometry	40 min	[20]
DC-18-C-6	$CHCl_3$	3–8 M HNO_3	–	–	10 min and 30 min contact time	[21]
Dicyclohexano-18-crown-6	Nitrobenzene	1 M CH_3COOH	1 M HCl	Spectrophotometry	5 min	Proposed method

amount use of extractant concentration and utilizing of greener weak acid. The prettiness of the system is a recovery of solvent and does not need too much instrumentation.

Experimental

Equipments

A systronic spectrophotometer, digital pH meter (Model LI-120, Elico, India) and separating funnel were used for experimental work.

Reagents and solutions

The U(VI) solution was prepared by dissolving 2.166 g of uranyl nitrate hexahydrate (Anala R, BDH) in 1000 ml double distilled water and standardized gravimetrically [23]. The 100 µg/ml of U(VI) solution was equipped by suitable dilution of standard stock solution. Solution of dicyclohexano-18-crown-6 (Aldrich, USA) without further purification.

Extraction procedure

To an aliquot of solution containing 100 µg of U(VI) was mixed with 1 M acetic acid and 1 M ammonium thiocyanate in a total volume of 10 ml and then transferred to 125 cm^3 separating funnel. 10 ml of 0.001 M Dicyclohexano-18-crown-6 in nitrobenzene was added as an extractant and equilibrated for 5 min. The two phases were allowed to settle down and separate. Uranium(VI) from the organic phase was back-extracted with 1 M HCl as a strippant (3 × 10 ml) solution. The stripped solution containing U(VI) was concentrated to moist dryness and diluted with water. U(VI) in the aqueous phase was quantitatively calculated spectrophotometrically with PAR [24] at 530 nm using a calibration graph.

Results and discussion

Effect of Ammonium thiocyanate on extraction of uranium(VI)

The influence of ammonium thiocyanate concentration on the extraction of uranium(VI) assisted by dicyclohexano-18-crown-6 in nitrobenzene was studied. In this study, the concentration of ammonium thiocyanate was differed over the range 0.1–5 M, while 0.001 M dicyclohexano-18-crown-6 in nitrobenzene was kept constant and extraction of uranium(VI) was performed. The extraction of uranium(VI) was initiated at 0.1 M NH_4SCN and becomes quantitative at 0.8 M. From the range of 0.8–5 M NH_4SCN concentrations, extraction remains quantitative as shown in Fig. 1. Ammonium thiocyanate acts as a salting out effect which reduce free water molecule in the system, which increases the activity of the extracted species to increase the distribution ratio. There is no dissociation of complexed

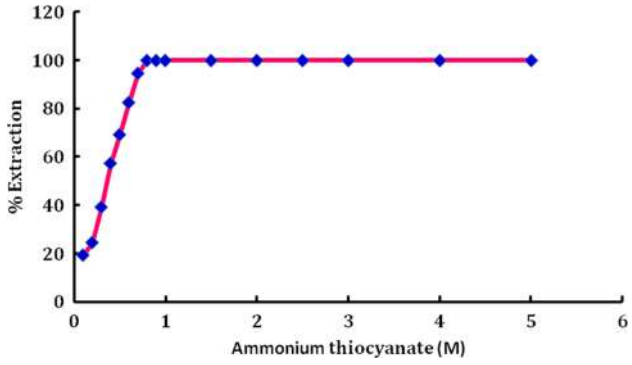


Fig. 1 Ammonium thiocyanate concentration

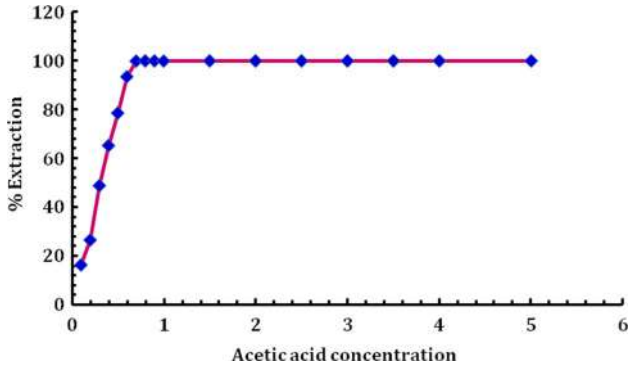


Fig. 2 Acetic acid concentration

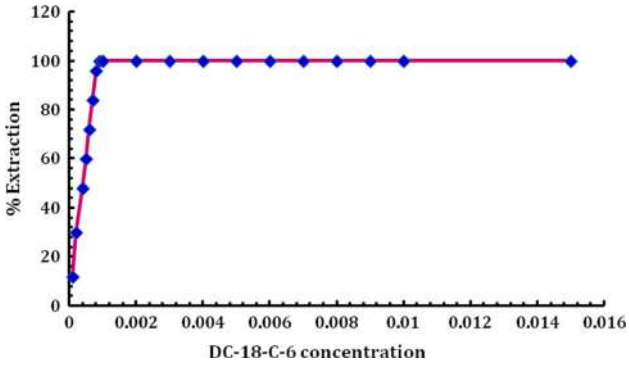


Fig. 3 Reagent concentration

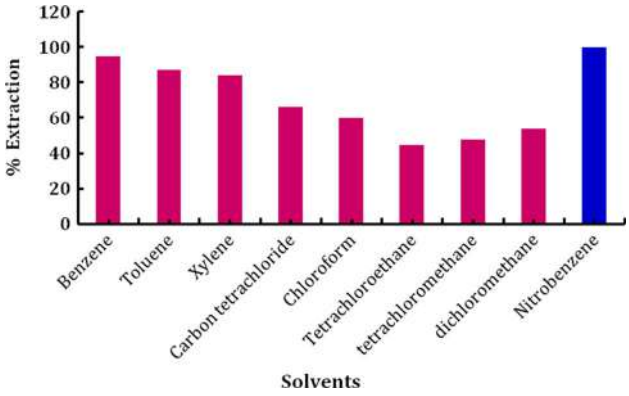


Fig. 4 Solvent study

ions in a higher concentration of NH_4SCN. Consequently, for further extraction study, 1 M NH_4SCN was used.

Impact of acetic acid concentration on the extraction of uranium(VI)

The extraction of uranium(VI) was studied from acetic acid in the range of 0.1–5 M as shown in Fig. 2. Acetic acid was used as a medium which helps to formation of uranium-dicyclohexano-18-crown-6 complex. It was examined that the extraction of uranium(VI) increases with an increase in acetic acid concentration in the range of 0.1–0.7 M and remains quantitative in the range of 0.7–5 M. Therefore, 1 M concentration of acetic acid was used throughout work.

Effect of dicyclohexano-18-crown-6 concentration

The concentration of dicyclohexano-18-crown-6 was varied in the range between 1×10^{-4} to 2×10^{-2} M in nitrobenzene to optimize extraction conditions of uranium(VI) at 1 M acetic acid and 1 M ammonium thiocyanate. The study showed that extraction of uranium(VI) increases from 1×10^{-4} to 9×10^{-4} M and becomes quantitative in the range of 9×10^{-4} to 2×10^{-2} M. Therefore based on study, we illustrate that 1×10^{-3} M of dicyclohexano-18-crown-6 was sufficient to getting quantitative extraction of uranium(VI). Therefore 10 mL of 1×10^{-3} M dicyclohexano-18-crown-6 in nitrobenzene was used in an actual experiment (Fig. 3).

Effect of solvents on extraction of uranium(VI)

The selectivity and extractability for the extraction of uranium(VI) by organic extractant are greatly influenced by the nature of the diluents. Thus the influence of nature of solvents viz. Tetrachloroethane, tetrachloromethane, dichloromethane, chloroform, carbon tetrachloride, xylene, toluene, benzene, and nitrobenzene (Fig. 4) was examined. The 0.001 M dicyclohexano-18-crown-6 dissolved in the above solvents and used for the extraction of uranium(VI). The study showed that the nitrobenzene diluents shows clear cut phase separation due to solubility of species and gives quantitative extraction of uranium(VI) while other solvents show incomplete extraction of uranium(VI). However, for further experimental study nitrobenzene was adopted as a solvent.

Effect of shaking time on extraction of uranium(VI)

The effect of contact time on the extraction of uranium(VI) was observed by using 0.001 M dicyclohexano-18-crown-6 in nitrobenzene and the aqueous solution of 100 µg of uranium(VI) in 1 M CH_3COOH and 1 M NH_4SCN. The equilibrium time has differed from 15 s to 30 min (Fig. 5). The results showed that the quantitative extraction of uranium was achieved in 5 min. Moreover, the prolonged contact time does not affect on quantitative extraction of uranium(VI). Therefore, for further study 5 min contact time was selected to ensure complete extraction of uranium(VI).

Strippant study

In the solvent extraction technique, the back extraction is the contrary phenomenon of extraction and it is the most significant step for uranium(VI) extraction in the organic phase. To back extract uranium(VI) from dicyclohexano-18-crown-6 in nitrobenzene organic phase. We have employed various stripping agents viz. HCl, HNO_3, NaOH, and NH_3. The study shows that uranium(VI) was extracted with dicyclohexano-18-crown-6 in nitrobenzene and was completely back-extracted with 0.5–1.5 M HCl and 2–3.5 M HNO_3 (Fig. 6). There was no complete back extraction with ammonia and sodium hydroxide solution. Hence, for the experimental study 1 M HCl was used as a strippant.

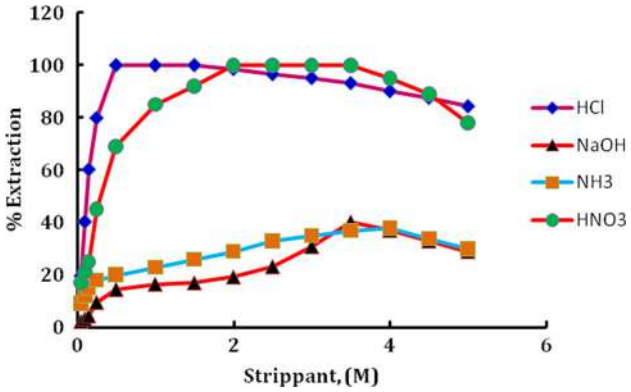


Fig. 6 Strippant study

Effect of uranium(VI) loading capacity on 0.001 M dicyclohexano-18-crown-6

The solvent extraction behaviour of uranium(VI) as a function of uranium(VI) loading capacity was examined at different concentrations of uranium(VI) between 100 and 1500 µg (Fig. 7). The examination showed that the quantitative extraction takes place between 100 and 1200 µg. It means that up to 1200 µg of uranium(VI) was tolerable in 10 mL of 0.001 M dicyclohexano-18-crown-6. After 1200 µg extraction decreases this indicates that there is a deficiency of dicyclohexano-18-crown-6. The results showed that 1200 µg of uranium(VI) was a loading capacity of 10 mL dicyclohexano-18-crown-6.

Probable mechanism of uranium(VI) extraction

Stock solution of uranyl nitrate forms aquo complex of uranium nitrate. In the presence weak acid medium salting out agent substituted the nitrate. Uranium forms complex species with crown ether as a neutral uncharged species, which was extracted in organic solvent.

$$UO_2(NO_3)_{2\ (aq)} + 2H_2O \rightleftharpoons \left[UO_2(NO_3)_2(H_2O_2)\right]_{aq}$$

$$\left[UO_2(NO_3)_2(H_2O)_2\right]_{(aq)} + 2NH_4SCN \xrightarrow{CH_3COOH} \left[UO_2(SCN)_2(H_2O)_2\right]_{(aq)} + 2NH_4NO_3$$

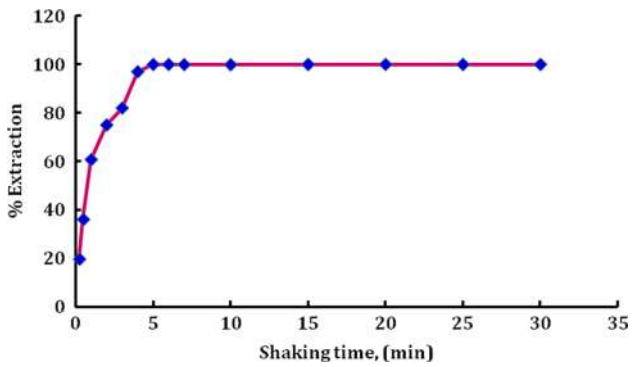


Fig. 5 Effect of shaking time

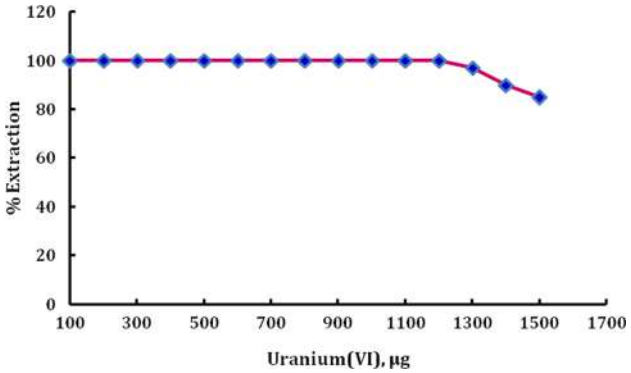


Fig. 7 Loading capacity

$$\mathrm{DC\text{-}18\text{-}C\text{-}6_{(org)} + \left[UO_2(SCN)_2 \cdot (H_2O)_2\right]_{(aq)} \xrightarrow{CH_3COOH} \left[DC\text{-}18\text{-}C\text{-}6 \cdot UO_2(SCN)_2\right]_{org} + 2H_2O\ (aq)}$$

Applications

Foreign ion study

To observe the versatility and applicability of the proposed uranium(VI) extraction method. The effect of foreign ions was checked. The uranium(VI)-dicyclohexano-18-crown-6 method is free from a large number of anions and cations. In the proposed method uranium(VI) was extracted with 0.001 M reagent concentration in nitrobenzene from 1 M NH_4SCN in the presence of a broad range of ions (Table 2). The extraction and determination of uranium(VI) from diverse ions were achieved by taking the benefit of the variation in the extraction conditions of the metal ions. Those metal ions showed interference in the extraction and determination of uranium(VI), they were masked with appropriate sequestering agents. The amount of added ions that gives an error less than ± 2% in the recovery of uranium(VI) known as the tolerance limit.

In this study solution of 100 µg of uranium(VI) was taken, another anion/cation was mixed and followed by the proposed methods procedure. Firstly the diverse ions mixed to uranium(VI) solution in large excess i.e. 100 mg for anions and 50 mg for cations. For finding the interference, the practical procedure was repeated with successively lesser amounts of added ion. Interference of very few Cu(II), Ni(II), Zn(II), Mn(II), Pb(II) and Th(IV) ions was registered and they were masked with respective masking agents as shown in Table 2.

Separation of uranium(VI) from multicomponent mixtures

To extend the applicability of the uranium(VI)-dicyclohexano-18-crown-6 extraction method. It was applied for the multicomponent mixture separation. Multicomponent mixture of uranium(VI) along with Fe(III), K(I), Li(I), Mg(II), Ca(II) were carried out. The extraction of uranium(VI) from added metal ion was quantitative as given in Table 3.

Table 3 Separation of uranium(VI) from multicomponent mixtures

Composition (µg)	Average recovery, %	R. S. D., %
U(VI) 100; Fe(III) 100;K(I) 100	99.91	0.04
U(VI) 100; Fe(III) 100;Li (I) 100	99.95	0.03
U(VI) 100; Fe(III) 100;Mg(II) 100	99.96	0.04
U(VI) 100; Fe(III) 100;Ca(II) 100	99.98	0.04
U(VI) 100; Fe(III) 100;Ba(II) 100	99.95	0.02
U(VI) 100; Fe(III) 100;Zn(II)[c] 100	99.92	0.04

[c]Masked by 10 mg of thiocyanate

Table 2 Separation of uranium(VI) from foreign ions

Ions	Added as	Tolerance limit (mg)	Ions	Added as	Tolerance limit (mg)
Na(I)	NaCl	25	Ce(III)	$CeCl_3 \cdot 6H_2O$	40
Rb(I)	RbCl	20	Sb(III)	$SbCl_3$	20
Cs(I)	CsCl	20	Y(III)	$Y(NO_3)_3$	30
Be(II)	$BeSO_4 \cdot 4H_2O$	25	Zr(IV)	$Zr(NO_3)_4 \cdot 4H_2O$	5
Mg(II)	$MgCl_2 \cdot 6H_2O$	40	V(IV)	$VOSO_4 \cdot 4H_2O$	5
Ca(II)	$CaCl_2$	25	Th(IV)[d]	$Th(NO_3)_4$	0.5
Sr(II)	$Sr(NO_3)_2$	30	Cr(VI)	$K_2Cr_2O_7$	5
Ba(II)	$Ba(NO_3)_2$	25	Mo(VI)	$(NH_4)_6Mo_7O_{24} \cdot 4H_2O$	5
Cu(II)[a]	$CuCl_2 \cdot 2H_2O$	0.5	W(VI)	$Na_2WO_4 \cdot 4H_2O$	30
Ni(II)[c]	$NiCl_2 \cdot 6H_2O$	5	La(III)	$LaCl_3$	0.1
Mn(II)[b]	$MnCl_2 \cdot 4H_2O$	0.3	Al(III)	$Al(NO_3)_3 \cdot 9\ H_2O$	5
Zn(II)[c]	$ZnCl_2$	0.3	SCN^-	NaSCN	75
Pb(II)[a]	$Pb(NO_3)_2$	0.5	ClO_4^-	$HClO_4$	10
Fe(III)	$FeCl_3 \cdot 6H_2O$	5	CH_3COO^-	CH_3COOH	35
Cr(III)	$Cr(NO_3)_3 \cdot 9\ H_2O$	5	Tartrate	Tartaric acid	25

[a]Masked by 10 mg tartrate, [b]Masked by 10 mg citrate, [c]Masked by 10 mg of thiocyanate, [d]Masked by 10 mg fluoride

Table 4 Analysis of uranium(VI) in rock and sand sample

Sr. no	Sample	Certified value of uranium taken	Uranium found by proposed method	Relative standard deviation %
1	Syenite rock	280 ppm	278 ppm	0.71
2	Monazite sand	0.29%	0.285%	0.54

Extraction of uranium(VI) in syenite rock sample and monazite sand sample

The proposed method was applied to the measurement of uranium(VI) in real samples viz. Syenite rock sample and monazite sand. The rock and sand samples were brought in solution by the procedure [25]. An aliquot of rock and sand sample solution was separated and determined with 0.001 M dicyclohexano-18-crown-6 in nitrobenzene from 1 M NH_4SCN and 1 M CH_3COOH. The quantity of uranium getting in syenite rock was 278 ppm as against the reported value of 280 ppm and monazite sand was 0.285% as against the standard value of 0.29% as shown in Table 4.

Conclusions

1. The proposed method permits the separation of uranium(VI) at micro level concentration.
2. The concentration of dicyclohexano-18-crown-6 required is very low.
3. The method permits the separation of uranium(VI) from Fe(III), K(I), Li(I), Ba(II) and Ca(II) effectively.
4. The proposed system was employed for the analysis of uranium(VI) in different sand and rock samples.
5. The recommended method is reliable, rapid and simple for the separation of uranium(VI).

Author's contributions S B carried out the experimental studies, analysis, data interpretation. SZ wrote the manuscript under the supervision of SB. Authors read and approved the final manuscript.

Funding Not applicable.

Declaration

Conflict of interest The authors declare that they have no conflict of interest.

References

1. Zhou Z, Yang Z, Sun Z, Chen G, Xu L, Liao Q (2019) Optimization of bioleaching high-fluorine and low-sulfur uranium ore by response surface method. J Radioanal Nucl Chem 322:781–790. https://doi.org/10.1007/s10967-019-06712-5
2. Li M, Huang C-M, Zhang X-W, Gao F-Y, Wu X-Y, Fang Q, Tan W-F, Zhang D (2018) Extraction mechanism of depleted uranium exposure by dilute alkali pretreatment combined with acid leaching. Hydrometallurgy 180:201–209. https://doi.org/10.1016/j.hydromet.2018.07.021
3. Singh DK, Hareendran KN, Sreenivas T, Kain V, Dey GK (2017) Development of a phosphate precipitation method for the recovery of uranium from lean tenor alkaline leach liquor. Hydrometallurgy 171:228–235. https://doi.org/10.1016/j.hydromet.2017.05.021
4. Wang X, Liu Y, Sun Z, Li J, Chai L, Min X, Guo Y, Li P, Zhou Z (2017) Heap bioleaching of uranium from low-grade granite type ore by mixed acidophilic microbes. J Radioanal Nucl Chem 314:251–258. https://doi.org/10.1007/s10967-017-5406-8
5. Mohite BS, Burungale SH (1999) Liquid-liquid extraction separation of uranium(VI) from associated elements using dibenzo-24-crown-8 from hydrobromic acid medium. J Radioanal Nucl Chem 241:589–593. https://doi.org/10.1007/BF02347217
6. Sawant SM (2001) Solvent extraction of uranium(VI) using dibenzo-18-crown-6 in nitrobenzene from ammonium thiocyanate medium. J Radioanal Nucl Chem 249:613–616. https://doi.org/10.1023/A:1013206517457
7. Biswas S, Basu S (1997) Synergic extraction of uranium(VI) by combination of tri-iso-octylamine and neutral donors. J Radioanal Nucl Chem 220:267–269. https://doi.org/10.1007/BF02034871
8. Alibrahim M, Shlewit H (2007) Solvent extraction of uranium(VI) by tributyl phosphate/dodecane from nitric acid medium. Period Polytechn Chem Eng J 51:57–60. https://doi.org/10.3311/pp.ch.2007-2.09
9. Sanghani R (2014) Novel technique for purification of fertilizer phosphoric acid with simultaneous uranium extraction. Procedia Eng 83:225–232. https://doi.org/10.1016/j.proeng.2014.09.042
10. Rajeswari B, Dhawale B, Bangia T (2002) Role of cyanex-272 as an extractant for uranium in the determination of rare earths by ICP-AES. J Radioanal Nucl Chem 254:479–483. https://doi.org/10.1023/A:1021633920249
11. Metwally E, Saleh A, El-Naggar H (2005) Extraction and separation of uranium(VI) and thorium(IV) using Tri-n-dodecylamine impregnated resins. J Nucl Radiochem Sci 6:119–126. https://doi.org/10.14494/jnrs2000.6.2_119
12. Mapara P, Godbole A, Swarup R (1999) Extraction of uranium and plutonium from oxalate bearing solutions using phosphonic acid: Solvent extraction, extraction chromatography and infrared studies. J Radioanal Nucl Chem 240:631–635. https://doi.org/10.1007/BF02349424
13. Casacuberta N, Lehritani M, Mantero J, Masque P, Garcia-Orellana J, Garcia-Tenorio R (2012) Determination of U and Th α-emitters in NORM samples through extraction chromatography by using new and recycled UTEVA resins. Appl Radiat Isot 70:568–573. https://doi.org/10.1016/j.apradiso.2011.11.063
14. Nazal M, Albayyari M, Khalili F (2014) Effect of high ionic strength on the extraction of uranium(VI) ions. J Saudi Chem Soc 18:59–67. https://doi.org/10.1016/j.jscs.2011.05.014
15. Sh Y, Wang G, Sun X, Bao B (1997) N, N, N′, N′-tetrabutylmalonamide as a new extractant for extraction of

nitric acid and uranium(VI) in toluene. J Radioanal Nucl Chem 224:151–153. https://doi.org/10.1007/BF02034629
16. Sun G, Han J, Bao B, Sun S (1998) Structural effect of N, N-dialkylamide in toluene on the extraction of uranium(VI). J Radioanal Nucl Chem 232:245–247. https://doi.org/10.1007/BF02383748
17. Yubo G, Zhongkui Z, Jiamin L, Guanchao L, Chao L, Zhanxue S, Lili Z, Zhihui Y, Rao M (2020) Combined use of $CaCl_2$ roasting and nitric acid leaching for the removal of uranium and radioactivity from uranium tailings. J Radioanal Nucl Chem 325:657–665. https://doi.org/10.1007/s10967-020-07272-9
18. Wang W, Sun Q, Chen B (1987) Further study of extraction equilibrium of uranium(VI) with dicyclohexano-18-crown-6 and its application to separating uranium and thorium. J Radioanal Nucl Chem 11:227–233. https://doi.org/10.1007/BF02055025
19. Preetha C, Prasada Rao T (2006) Preconcentration of uranium(VI) by solid phase extraction onto dicyclohexano-18-crown-6 embedded benzophenone. J Radioanal Nucl Chem 267:265–270. https://doi.org/10.1007/s10967-006-0042-8
20. Shukla J, Kumar A, Singh R (1993) Solvent extraction of uranium(VI) into toluene by dicyclohexano-18-crown-6 from mixed aqueous-organic solutions. Talanta 40:1261–1266. https://doi.org/10.1016/0039-9140(93)80196-X
21. Favre-Réguillona A, Drayeb M, Cotec G, Czerwinskyd K (2019) Insights in uranium extraction from spent nuclear fuels using dicyclohexano-18-crown-6—fate of rhenium as technetium homolog. Sep Purif Technol 209:338–342. https://doi.org/10.1016/j.seppur.2018.07.034
22. Liu X, Sun G, Cai X (2015) Extraction of U(VI) with N, N, N′, N′-tetraoctyl diglycolamide from nitric acid solution. J Radioanal Nucl Chem 306:549–553. https://doi.org/10.1007/s10967-015-4101-x
23. Vogel A (1975) A Textbook of Quantitative Inorganic Analysis, 3rd edn. Longmans, London
24. Pollard F, Hanson P, Geary W (1959) 4-(2-Pyridylazo)-resorcinol as a possible analytical reagent for the colorimetric estimation of cobalt, lead and uranium. Anal Chim Acta 20:26–31. https://doi.org/10.1016/0003-2670(59)80004-0
25. Mohite B, Patil J, Zambare D (1993) Solvent extraction separation of uranium(VI) with dibenzo-24-crown-8. J Radioanal Nucl Chem 170:215–224. https://doi.org/10.1007/BF02134593

Publisher's Note Springer Nature remains neutral with regard to jurisdictional claims in published maps and institutional affiliations.

SPRINGER LINK

Log in

Menu Search Cart

Home Journal of Radioanalytical and Nuclear Chemistry



Journal of Radioanalytical and Nuclear Chemistry

An International Journal Dealing with All Aspects and Applications of Nuclear Chemistry

Publishing model

Hybrid

Submit your manuscript

AKADÉMIAI KIADÓ

Editorial board

Aims and scope

Journal updates

Overview

Journal of Radioanalytical and Nuclear Chemistry is an international journal covering a wide range of topics in the field of nuclear chemistry.

Open for submissions in all fields of radiopharmaceuticals
Coverage includes nuclear chemistry, radiochemistry, radiation chemistry, radiobiological chemistry, environmental radiochemistry, production and control of radioisotopes and labeled compounds nuclear power plant chemistry, nuclear fuel chemistry, radioanalytical chemistry, radiation detection and measurement, nuclear instrumentation and automation, and more.
Presents original papers, letter, review papers and short communications

Editor-in-Chief
Zsolt Révay

Journal Impact Factor
1.5 (2023)

5-year Journal Impact Factor
1.5 (2023)

Submission to first decision (median)
8 days

Downloads
631,201 (2023)

Societies and partnerships

AKADÉMIAI KIADÓ

Akadémiai Kiadó

Latest issue

September 2024

View all articles →

This journal has 527 open access articles →

Journal updates

Manuscript Template

To make manuscript preparation easier for you, we provide you with a Word template which you can download here.

Akadémiai Kiadó

Akadémiai Kiadó, founded in 1828 by the Hungarian Academy of Sciences (HAS), is Hungary's oldest continuously operating publishing house. Their mission is to promote Hungarian and international science, that is, to publish the new discoveries in various areas of science, to effectively support information exchange amongst scientists on a global level, and to make scientific results a public property for all who seek valuable and reliable knowledge.

View all updates →

Journal information

Electronic ISSN 1588-2780

Print ISSN 0236-5731

Co-Publisher information

Co-publication with Akadémiai Kiadó, Budapest, Hungary

Visit Co-Publisher Site: Link to Akadémiai Kiadó

Abstracted and indexed in

ANVUR

Astrophysics Data System (ADS)

BFI List

Baidu

CAB Abstracts
CLOCKSS
CNKI
CNPIEC
Chemical Abstracts Service (CAS)
Chimica
Current Contents/Physical, Chemical and Earth Sciences
Dimensions
EBSCO
EI Compendex
EMBASE
Gale
Google Scholar
IFIS Publishing
INIS Atomindex
INSPEC
INSPIRE
Japanese Science and Technology Agency (JST)
Naver
OCLC WorldCat Discovery Service
Portico
ProQuest
Reaction Citation Index
Reaxys
SCImago
SCOPUS
Science Citation Index Expanded (SCIE)
Semantic Scholar
TD Net Discovery Service
UGC-CARE List (India)
Wanfang

Copyright information
Rights and permissions
Editorial policies

© Akadémiai Kiadó, Budapest, Hungary

For authors

Products

Master Journal List | Search Journals | Match Manuscript | Downloads | Help Cent

Already have a manuscript?

Use our Manuscript Matcher to find the best relevant journals!

Find a Match

Filters | Clear All

- *Web of Science* Coverage
- Open Access
- Category
- Country / Region
- Language
- Frequency
- Journal Citation Reports

ine Your Search Results

6-5731 Search

y: Title (A-Z)

rch Results

d 1 results (Page 1) Share These Results

ct Match Found

URNAL OF RADIOANALYTICAL AND NUCLEAR HEMISTRY

blisher: SPRINGER , VAN GODEWIJCKSTRAAT 30, DORDRECHT, NETHERLANDS, 3311 GZ

N / eISSN: 0236-5731 / 1588-2780

b of Science Core Collection: Science Citation Index Expanded

ditional *Web of ence* Indexes: Current Contents Physical, Chemical & Earth Sciences | Essential Science Indicators

Share This Journal | View profile page

** Requires free login.*

1 – 1 of 1

Items per page: 10

5

CRITERION – III

RESEARCH, INNOVATION AND EXTENSION

3.3 RESEARCH PUBLICATIONS AND AWARDS

3.3.1 NUMBER OF RESEARCH PAPERS PUBLISHED PER TEACHER IN THE JOURNALS NOTIFIED ON UGC CARE LIST DURING THE LAST FIVE YEARS

2020

Available online at www.derpharmachemica.com

ISSN 0975-413X
CODEN (USA): PCHHAX

Der Pharma Chemica, 2020, 12(7): 1-11
(http://www.derpharmachemica.com/archive.html)

Synthesis of Substituted Phenothiazines derivatives, Antioxidant, P-Glycoprotein, Cyp Enzyme Activity, HIA and BBB Prediction

Mahesh K Gaidhane[1], Ajay M Ghatole[2]*, Meghasham N Narule[3], Pravin K Gaidhane[4], Kushal R lanjewar[5] and Gunwant P Gadekar[6]

[1]*Shri Lemdeo Patil Mahavidyalaya, Department of Chemistry, Mandhal, India*
[2]*Dhote Bandhu Science College, Department of Chemistry, Gondia*
[3]*Vidya Vikas Arts, Commerce & Science College, Samudrapur*
[4]*Govindrao Wanjari Engineering and Technology, Hudkshwar Road, Nagpur*
[5]*Mohsinbhai Zaweri Mahavidyalaya, Desaiganj, Wadsa, MS, India,*
[6]*Dhote Bandhu Science College, Department of Zoology, Gondia*

***Corresponding author:** Ajay M Ghatole, Department of Chemistry, Dhote Bandhu Science College, Gondia, India,*
E-mail: ajay.ghatole5@gmail.com

ABSTRACT

As of late, there is an enormous increment of medication safe pathogens, prompting the plan and advancement of more current antibacterial specialists. Different epic subbed phenothiazines derivatives have arranged to concentrate based on pharmacological exercises in drugs revelation. Phenothiazine derivatives subbed in the 2, 3 and 4 positions have a place with a major gathering of tricyclic aromatic combinations. They are in broad use in psychiatry as tranquillizers and neuroleptics. Because of their trademark structure, they show numerous important scientific properties. A short easy synthesis of 8- [2/-(3//, 5//- dimethyl-4//- ethoxy carbonyl pyrrolyl) hydrazine] subbed phenothiazines ***(5a-j)*** *from 2-arylaminbenzal-2-(3',5'-dimethyl-4'-ethoxycarbonyl pyrrole) hydrazines (4) in the imminence of sulfur and iodine. These combinations show antibacterial and antifungal drills when contrasted and standard drug Norfloxacin and Griseofulvine against Bacterial cultures, for example, Escherichia coli, Pseudomonas aeruginosa, Staphylococcus aureus, Proteus Vulgaris and fungal cultures, such as Aspergillus niger and Candida albicans. And also, these compounds screened for their antioxidant activity. The synthesized compounds characterized by FTIR, 1H NMR, elemental and chemical properties. The modern Swiss ADME web tool that stretches free admittance to a pool of hasty yet solid clarifying models for physicochemical properties, pharmacokinetics, and therapeutic science.*

Keywords: Antioxidant active, Antifungal activity, Pyrrolyl, Phenothiazines

INTRODUCTION

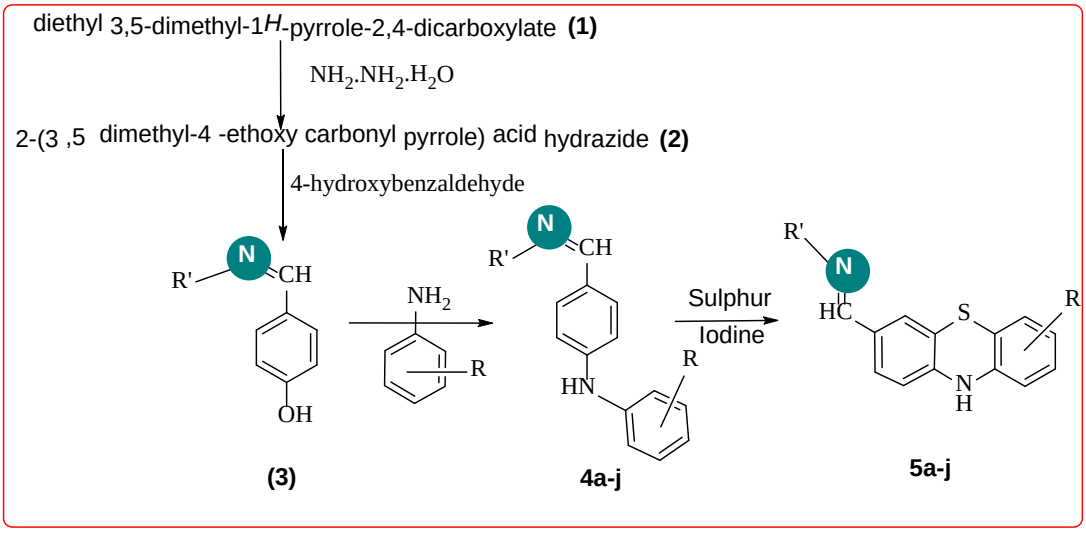
We survey the proof to propose that phenothiazines claim characteristic antibacterial and efflux inhibitory properties empowering them to battle drug resistance. We likewise talk about that understanding their mode of action is basic to facilitate the structure of new phenothiazine derivatives or novel specialists for use as an antibiotic adjuvant [1]. Phenothiazine derivatives incorporate compounds described by a tricyclic aromatic ring with sulfur and nitrogen atoms and substituents in the 2 and 10 or 3 and 7 positions. Phenothiazine positions are anticholinergic derivatives substituted in the 2 and 10 known as anti-psychotropic and antihistaminic drugs. They have been studied in many fields of chemical, biological and medical research owing to their pharmacological activity [2]. Studies right now uncovered that numerous compounds, having a place with various pharmacological families, bear huge nanocarriers on antibacterial movement. Instances of such "non-antibiotics" incorporate antihistamines, for example, promethazine and fluphenazine antipsychotic compounds, for example, promazine, chlorpromazine thioridazine, trifluoperazine and triflupromazine, anti-inflammatory specialists, for example, diclofenac and even antihypertensive operators, such as methyl-DOPA and propranolol [3]. Few drugs such as orlistat, lorcaserin, qsymia, contrave, phentermine etc. have approved by Food and Drug Administration as anti-obesity agents while some others such as sibutramine and rimonabant have withdrawn due to their serious side effects [4]. Pyrroles exhibit interesting biological properties1-3. Besides, Phenothiazines are well known CNS depressant compounds and have emerged as an important area of research for the biological activities like antiparkinsonian [5], anticonvulsant [6], New job growing extraneously dynamic of phenothiazine derivatives as incidentally acting CB1 receptor threatening enemy of obesity agent [7]. Antihelmatic [8], antiviral, anti-parasitic activities [9,10]. Anti-proliferative and anti-MDR activities [11], synthetic antipsychotic drugs [12] Antitubercular, antimalarial and analgesic activities [13]. Heterocycles are the biggest class of organic compounds [14] Among them, pyrroles have a recognized situation in the chemistry of living organisms because of their nearby biogenetic association with the porphyrins, the chlorins, and the corrins. Besides, they viewed as advantaged structures by synthetic chemists on account of widespread applications in therapeutic chemistry and materials science [15]. Until this point, antipsychotic and antihistamine

specialists from the gathering of phenothiazines have recited most for their antimicrobial activity both in vitro and in vivo [16,17]. Impact of novel phenothiazine derivatives on brain dopamine in Wistar rodents [18]. Swiss ADME permits the review of ADME restrictions of medication aspirants and small molecules and gives statistics that authorizations early hazard calculation in the drug enhancement progression [19]. Exceptionally, swiss ADME affords a point to estimate Lipinski's rule of five [20] for medication semblance of oral bioavailability.

Interpretation of these annotations it thought worthwhile to synthesized and investigate the compounds in which pyrrole derivative have linked with phenothiazine moiety. We report in this paper, the synthesis and pharmacological investigation of 8-[2′-(3″,5″-dimethyl-4″-ethoxy carbonyl pyrrolyl) hydrazine] substituted phenothiazines **(5a-j) (Scheme-I).**

RESULTS AND DISCUSSIONS

The required starting material 3′,5′-dimethyl-2′,4′-diethoxy carbonyl pyrrole (1) has prepared by the reported method. The compound (1) refluxed with hydrazine hydrate to yield 2-(3′,5′ dimethyl-4′-ethoxy carbonyl pyrrole) acid hydrazide (2). The compound (2) which reacts with 4-hydroxy benzaldehyde in the presence of ethanol for 8 hr to get the desired isosemicarbazide (3). The compound (3) was condensed with different aryl amines by refluxing in ethanol to get Substituted 2-arylamin benzal-2-(3′,5′-dimethyl-4′-ethoxy carbonyl pyrrole) hydrazine (4a-j). The compound (4a-j) treated with sulphur and iodine to yield 8-[2′-(3″, 5″-dimethyl-4″-ethoxy carbonyl Pyrrolyl) hydrazine] substituted Phenothiazines (5a-j) in the scheme I (Figure 1).



Scheme-1

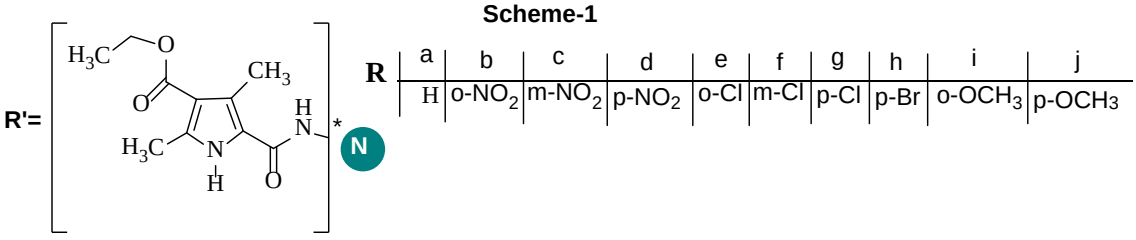


Figure 1: Synthesis and pharmacological investigation of 8-[2′-(3″,5″-dimethyl-4″-ethoxy carbonyl pyrrolyl) hydrazine] substituted phenothiazines.

Antioxidant activity

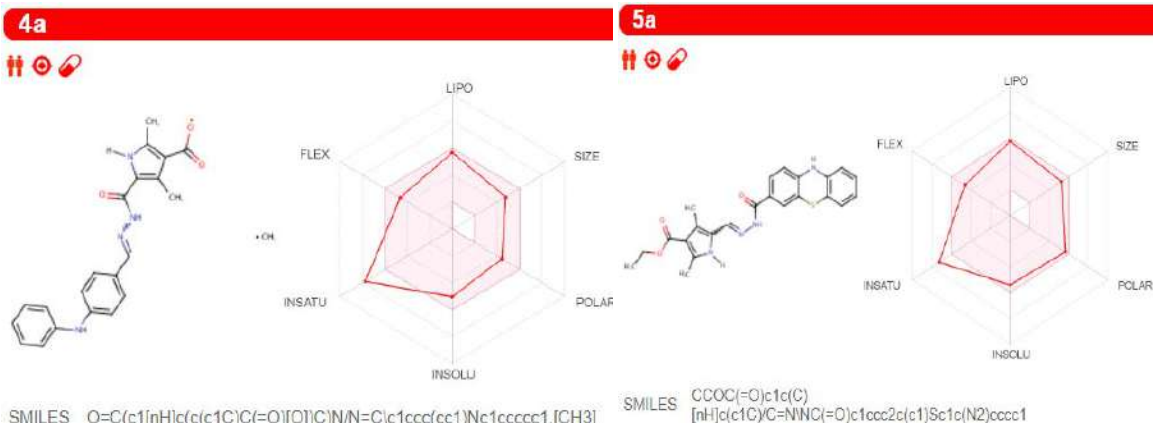
Free radical scavenging activity of the test mixes 4a-j and 5a-j were controlled by the 1,1-diphenyl picryl hydrazyl (DPPH) test strategy. Drug stock arrangement (1 mg/mL) was weakened to definite concentrations of 2, 4, 6, 8 and 10 mg mL^{-1} in methanol. DPPH methanol arrangement (1 mL, 0.3 mmol) was added to 2.5 mL of drug arrangements of various concentrations and permitted to respond at room temperature. After 30 min the absorbance esteems were estimated at 518 nm and changed over into the rate antioxidant activity. Methanol was utilized as the solvent and ascorbic corrosive as the standard. The level of hindrance extrapolated against fixation is delineated. Results are introduced in Table 1. The standard drug utilized was ascorbic acid [21].

Table 1: Antioxidant activity of the compounds 4a-j and 5a-j.

% Inhibition					
Comp.	**20 µg/mL**	**40 µg/mL**	**60 µg/mL**	**80 µg/mL**	**100 µg/ml**
4a	12	16	22	27	34
4b	15	14	19	23	31
4c	16	21	25	28	32
4d	14	16	16	22	28
4e	12	18	20	24	28
4f	13	16	22	24	26
4g	14	17	20	22	25
4h	15	15	18	20	24
4i	18	25	28	32	36
4j	20	26	29	34	36
5a	18	22	26	30	34
5b	18	27	30	36	39
5c	25	29	34	37	41
5d	24	28	33	38	45
5e	23	28	34	39	46
5f	28	35	39	46	52
5g	27	40	46	48	52
5h	18	36	41	44	46
5i	28	33	42	48	54
5j	25	29	38	45	48
	2 µg/mL	4 µg/mL	6 µg/mL	8 µg/mL	10 µg/mL
Ascorbic acid	10	15	20	33	56

Swiss ADME Pharmacokinetics, Physicochemical, Medicinal Properties study

The functioning highlights of these molecules entered in the Swiss ADME site (http://swissadme.ch) using the Chem Axon's Marvin JS structure drawing instrument. Assistant highlights of a pharmacophore sway including bioavailability, transport properties, sympathy to proteins, reactivity, poisonous quality, and metabolic steadiness. Unique to swiss ADME is the bioavailability radar [22] that gives a graphical assessment of the prescription resemblance parameters of an orally accessible bioactive drug. The drug impression chart exhibited as a hexagon (Figures 2) with every one of the vertices dialogues to a restriction that symbolizes a bioavailable drug.



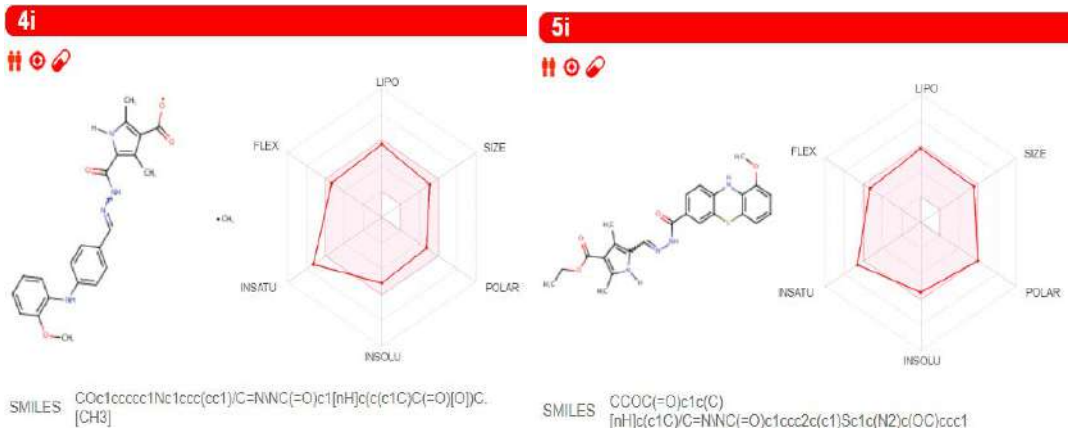


Figure 2: The bioavailability radar comparison between the synthesized molecules 4a, and 4i vs 5a, and 5i evaluating using swiss ADME web tool.

The pink location inside the hexagon speaks to the perfect range for each property (lipophilicity: XLOGP3 somewhere in the array of −0.7 and +5.0, size: extremity: TPSA (Topological Polar Surface Area) somewhere in the field of 20 and 130 Å2, MW somewhere in the scope of 150 and 500 g/mol, solubility: log S not higher than 6, adaptability: close to 9 rotatable bonds, and saturation: some portion of carbons in the sp3 hybridization at any rate 0.25). The near recommended run for the compound to go about as bioavailable medication is portrayed in Tables 2 and 3.

Table 2: The drug-likness ideal range for every property of a bioavailable drug.

Sr. No.	Flex	Lipo	Size	Polar	Insolu.	Insatu.
4a	IN	IN	IN	IN	IN	OUT
4b	OUT	BOU	IN	OUT	IN	OUT
4c	OUT	IN	IN	OUT	IN	OUT
4d	OUT	IN	IN	OUT	IN	OUT
4e	BOU	BOU	IN	IN	IN	OUT
4f	BOU	BOU	IN	IN	IN	OUT
4g	BOU	BOU	IN	IN	IN	OUT
4h	BOU	BOU	BOU	IN	IN	OUT
4i	IN	IN	IN	IN	IN	OUT
4j	OUT	IN	IN	IN	IN	OUT
5a	IN	IN	IN	IN	IN	OUT
5b	IN	IN	BOU	OUT	IN	OUT
5c	IN	IN	BOU	OUT	IN	OUT
5d	IN	IN	BOU	OUT	IN	OUT
5e	IN	BOU	IN	IN	BOU	OUT
5f	IN	BOU	IN	IN	BOU	OUT
5g	IN	BOU	IN	IN	BOU	OUT
5h	IN	BOU	BOU	IN	OUT	OUT
5i	IN	IN	IN	BOU	IN	OUT
5j	IN	IN	IN	BOU	IN	OUT

(Lipo- lipophilicity; Insolu.- Insolubility; Insatu.- Insaturation, IN- Inside the hexagon speaks; OUT- Outside the hexagon speaks, BOU- Boundary of the hexagon speaks).

Table 3: Physicochemical properties of the synthesized molecules 4a-j and 5a-j.

Sr. No.	MW	HA	AHA	FCsp3	RTB	HBA	HBD	MR	TPSA
4a	390.44	29	17	0.14	7	4	3	112.32	86.35
4b	449.46	33	17	0.17	10	6	3	126.35	141.4
4c	449.46	33	17	0.17	10	6	3	126.35	141.4
4d	449.46	33	17	0.17	10	6	3	126.35	141.4
4e	438.91	31	17	0.17	9	4	3	122.53	95.58
4f	438.91	31	17	0.17	9	4	3	122.53	95.58
4g	438.91	31	17	0.17	9	4	3	122.53	95.58
4h	483.36	31	17	0.17	9	4	3	125.22	95.58
4i	420.46	31	17	0.17	8	5	3	118.81	95.58
4j	434.49	32	17	0.21	10	5	3	124.02	104.81
5a	434.51	31	17	0.17	7	4	3	124.58	120.88
5b	479.51	34	17	0.17	8	6	3	133.4	166.7
5c	479.51	34	17	0.17	8	6	3	133.4	166.7
5d	478.5	34	17	0.17	8	7	2	132.44	163.8
5e	468.96	32	17	0.17	7	4	3	129.59	120.88
5f	468.96	32	17	0.17	7	4	3	129.59	120.88
5g	468.96	32	17	0.17	7	4	3	129.59	120.88
5h	513.41	32	17	0.17	7	4	3	132.28	120.88
5i	464.54	33	17	0.21	8	5	3	131.07	130.11
5j	464.54	33	17	0.21	8	5	3	131.07	130.11

(MW: Molecular weight; HA: Heavy atoms; AHA: Aromatic heavy atom; FCsp3: Fraction Csp3; RTB: Rotatable bonds; HBA: H-bond acceptors; HBD: H-bond donors; MR: Molar refractivity; TPSA: Topological polar surface area).

Drug-likeness

The drug resemblance properties of the fused compound are articulated to by the red mutilated hexagon inside the pink shade (Figure 1). Swiss ADME likewise has computational channels that incorporate Ghose [23], Egan [24], Veber [25], and Muegee [26] created by top pharmaceutical organizations and cheminfomaticians to assess the drug resemblance of molecules. The values maintained in Table 4 indicated the violation of the prescribed range for the molecule to act as a drug.

Table 4: Drug-likeness evaluation of synthesized compounds using swiss ADME.

Sr. No.	Lipinski #violations	Ghose #violations	Veber #violations	Egan #violations	Muegge #violations
4a	0	0	0	0	0
4b	0	0	1	1	0
4c	0	0	1	1	0
4d	0	0	1	1	0
4e	0	0	0	0	1
4f	0	0	0	0	1
4g	0	0	0	0	1
4h	0	1	0	0	1
4i	0	0	0	0	0
4j	0	0	0	0	0
5a	0	0	0	0	0
5b	0	1	1	1	1
5c	0	1	1	1	1
5d	0	1	1	1	1
5e	0	0	0	0	1
5f	0	0	0	0	1

5g	0	0	0	0	1
5h	1	2	0	0	1
5i	0	1	0	0	0
5j	0	1	0	0	0

PAINS, Break and Lead likeness screening

PAINS (pan-assay interference screening) that regularly gives bogus positive chemical properties bring about high-throughput screens. PAINS will, in general, respond vaguely with various biological targets as opposed to explicitly influencing one foreseen objective. Swiss ADME evaluation did not post any PAINS alert (Table 5). In additional verdict model, Brenk [27] measured combinations that are smaller and less hydrophobic and not those described by "Lipinski's standard of 5" to augment open doors for lead streamlining. Lead likeness tests are projected to provide primes with extraordinary kinship in high-throughput screens that consider the recognition and control of new exchanges ahead of the pack headway stage (Table 5). All the synthesized compound 4a-j and 5a-j drifted the break alert and lead likeness criteria.

Table 5: Medicinal chemistry evaluation of the synthesized compounds.

Sr. No.	PAINS #alerts	Brenk #alerts	Lead likeness #violations	Synthetic Accessibility
4a	0	1	2	3.27
4b	0	3	3	3.74
4c	0	3	3	3.74
4d	0	3	3	3.62
4e	0	1	3	3.49
4f	0	1	3	3.49
4g	0	1	3	3.47
4h	0	1	3	3.52
4i	0	1	3	3.39
4j	0	1	3	3.57
5a	0	1	2	3.83
5b	0	3	3	4.05
5c	0	3	3	4.03
5d	0	3	3	4
5e	0	1	2	3.86
5f	0	1	2	3.83
5g	0	1	2	3.84
5h	0	1	2	3.88
5i	0	1	3	4.04
5j	0	1	3	4.01

P-glycoprotein and CYP enzyme activity prediction

Swiss ADME furthermore permits the valuation for a compound to be a substrate of p-glycoprotein (P-gp) or inhibitor of the cytochrome p450 isoenzymes (CYP isoenzymes). P-gp is largely spread and linked in the intestinal epithelium where it drives xenobiotics [28]. The generations return "Yes" or "No" if the particle under assessment has a higher probability to be substrate or non-substrate of P-gp or inhibitor or non-inhibitor of a given CYP. The screening results classified (Table 6).

Table 6: Pharmacokinetic evaluation of the synthesized compounds.

Sr. No.	GI abs.	BBB per.	P-gp sub.	CYP1A2 inhibitor	CYP2C19 inhibitor	CYP2C9 inhibitor	CYP2D6 inhibitor	CYP3A4 inhibitor
4a	High	No	No	Yes	No	No	No	No
4b	Low	No	No	No	Yes	Yes	No	Yes
4c	Low	No	No	No	Yes	Yes	No	Yes
4d	Low	No	No	No	Yes	Yes	No	Yes
4e	High	No	No	No	Yes	Yes	No	Yes
4f	High	No	No	No	Yes	Yes	No	Yes
4g	High	No	No	No	Yes	Yes	No	Yes

4h	High	No	No	No	Yes	Yes	No	Yes
4i	High	No	No	No	No	No	No	No
4j	High	No	No	No	Yes	Yes	No	Yes
5a	High	No	No	No	Yes	Yes	No	Yes
5b	Low	No	No	No	Yes	Yes	No	Yes
5c	Low	No	No	No	Yes	Yes	No	Yes
5d	Low	No	Yes	No	Yes	No	No	No
5e	Low	No	No	No	Yes	Yes	No	Yes
5f	Low	No	No	No	Yes	Yes	No	Yes
5g	Low	No	No	No	Yes	Yes	No	Yes
5h	Low	No	No	No	Yes	Yes	No	Yes
5i	Low	No	No	No	Yes	Yes	Yes	Yes
5j	Low	No	No	No	Yes	Yes	Yes	Yes

(GIabs.: gastrointestinal absorption; BBBper.: blood-brain barrier permeant; CYP: Cytochromes, P-gp sub.: P-glycoprotein substrate)

HIA and BBB prediction

Suitable to P-gp and CYP protein vitality is human gastrointestinal ingestion (HIA) and blood-brain barrier infiltration (BBB). Swiss ADME 'BOILED egg' (Figure 3) grants for appraisal of HIA as a component of the circumstance of the molecules in the WLOGP-versus-TPSA referential.

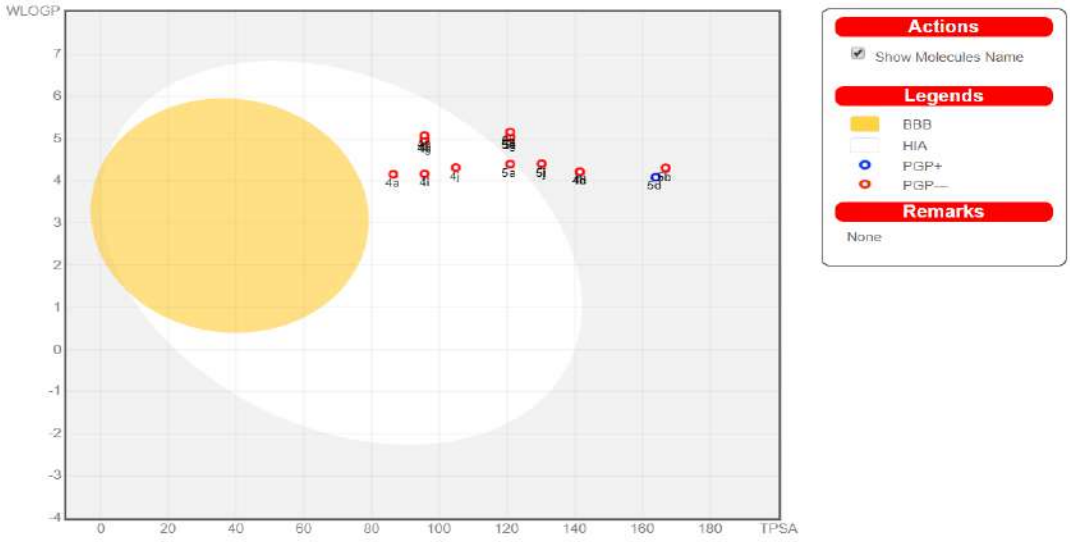


Figure 3: The BOILED-Egg allows for evaluation of passive gastrointestinal absorption (HIA), brain penetration (BBB) and P-glycoprotein in the presence of the molecule (P-gp)

The white segment of the 'BOILED egg' is for a high chance of reflexive adjustment by the gastrointestinal tract, and the yellow region (yolk) is for a high prospect of cerebrum entrance, Some of the blended particle 4a, e,g, i,j, and 5a under the white segment. With this, the focuses are concealed in blue at whatever point foreseen as adequately effluxes by P-gp (PGP+) and in red anticipated as non-substrate of P-gp (PGP−). HIA and BBB are responsible for water solvency and lipophilicity of the medication. Two topological ways to deal with predict water solvency contained Swiss ADME. The first is an implementation of the ESOL (Delaney, 2004) model, and the resulting one improved from Ali et al. [29,30]. SILICON-IT made Swiss ADME third pointer for solvency. Every single foreseen quality are the decimal logarithm of the molar solvency in water (log S) portrayed in Table 7. Agreement Log p is the normal estimation of all Log P assessed with different lipophilicity criteria (Table 8).

Table 7: Water solubility evaluation of the synthesized compounds.

Sr. No.	ESOL				Ali				Silicos			
	Log S	Solu. (mg/ml)	Solu. (mol/l)	Class	Log S	Solu. (mg/ml)	Solu. (mol/l)	Class	Log S	Solu. (mg/ml)	Solu. (mol/l)	Class
4a	-5.03	3.65E-03	9.34E-06	MS	-5.97	4.16E-04	1.07E-06	MS	-6.88	5.18E-05	1.33E-07	PS
4b	-5.41	1.75E-03	3.89E-06	MS	-7.56	1.23E-05	2.73E-08	PS	-7.3	2.26E-05	5.04E-08	PS
4c	-5.06	3.89E-03	8.65E-06	MS	-6.99	4.57E-05	1.02E-07	PS	-7.3	2.26E-05	5.04E-08	PS

4d	-5.06	3.89E-03	8.65E-06	MS	-6.99	4.57E-05	1.02E-07	PS	-7.3	2.26E-05	5.04E-08	PS
4e	-5.59	1.12E-03	2.56E-06	MS	-6.86	6.04E-05	1.38E-07	PS	-8.54	1.25E-06	2.85E-09	PS
4f	-5.59	1.12E-03	2.56E-06	MS	-6.86	6.04E-05	1.38E-07	PS	-8.54	1.25E-06	2.85E-09	PS
4g	-5.59	1.12E-03	2.56E-06	MS	-6.86	6.04E-05	1.38E-07	PS	-8.54	1.25E-06	2.85E-09	PS
4h	-5.91	6.01E-04	1.24E-06	MS	-6.92	5.77E-05	1.19E-07	PS	-8.73	8.90E-07	1.84E-09	PS
4i	-5.1	3.32E-03	7.89E-06	MS	-6.13	3.08E-04	7.33E-07	PS	-6.98	4.40E-05	1.05E-07	PS
4j	-5.07	3.69E-03	8.50E-06	MS	-6.37	1.85E-04	4.27E-07	PS	-8.06	3.78E-06	8.69E-09	PS
5a	-5.39	1.75E-03	4.03E-06	MS	-6.89	5.54E-05	1.28E-07	PS	-8.04	3.99E-06	9.18E-09	PS
5b	-5.46	1.64E-03	3.43E-06	MS	-7.68	1.00E-05	2.09E-08	PS	-7.37	2.04E-05	4.26E-08	PS
5c	-5.46	1.64E-03	3.43E-06	MS	-7.68	1.00E-05	2.09E-08	PS	-7.37	2.04E-05	4.26E-08	PS
5d	-5.35	2.16E-03	4.52E-06	MS	-7.43	1.77E-05	3.70E-08	PS	-7.37	2.04E-05	4.26E-08	PS
5e	-5.99	4.77E-04	1.02E-06	MS	-7.55	1.33E-05	2.83E-08	PS	-8.62	1.13E-06	2.41E-09	PS
5f	-5.99	4.77E-04	1.02E-06	MS	-7.55	1.33E-05	2.83E-08	PS	-8.62	1.13E-06	2.41E-09	PS
5g	-5.99	4.77E-04	1.02E-06	MS	-7.55	1.33E-05	2.83E-08	PS	-8.62	1.13E-06	2.41E-09	PS
5h	-6.31	2.54E-04	4.94E-07	PS	-7.61	1.26E-05	2.45E-08	PS	-8.8	8.04E-07	1.57E-09	PS
5i	-5.47	1.57E-03	3.38E-06	MS	-7.06	4.07E-05	8.77E-08	PS	-8.13	3.40E-06	7.33E-09	PS
5j	-5.47	1.57E-03	3.38E-06	MS	-7.06	4.07E-05	8.77E-08	PS	-8.13	3.40E-06	7.33E-09	PS

MATERIALS AND METHODS

The synthesized compounds are first purified by re-crystallization using appropriate solvents. Melting points were resolved in an open capillary tube and are uncorrected. The IR spectra were recorded on ABB BOMEM FTIR Spectrometer utilizing KBr plate method. The NMR spectra were recorded as Bruker 400MHz NMR Spectrometer in DMSO utilizing TMS as an inner standard. Chemical shift is given in δ ppm. Mass spectra were recorded on GCMS QP 5000 Shimadzu. Thin-layer chromatography was made using pre-coated aluminium plates, coated with silica gel GF254 [E. Merck]. ethyl acetate–acetone (6:4) for 5a, 5b, 5c, 5e; ethyl acetate – chloroform (8:2) for 5d, 5f, 5g, 5h, 5i, 5j Solvent for crystallization; aq. ethanol for (5a –j). The spots were visualized in the iodine chamber. Characterization data of compounds are given in Table 9.

Table 9: Characterization of data of newly synthesized compounds.

Compound	Molecule Formula	RF Value	Yield (%)	Analysis (Cal) (found)		
				C	H	N
5a	$C_{23}H_{22}O_3N_4S$	0.36	80%	65.7	5	12.9
				-65.8	(5.95	-12
5b	$C_{23}H_{21}O_5N_5S$	0.24	65%	56.61	4.3	14.6
				-56.9	(4.20	-14.7
5c	$C_{23}H_{21}O_5N_5S$	0.91	62%	56.61	4.3	18.7
				-56.9	(4.20	-18.7
5d	$C_{23}H_{21}O_5N_5S$	0.71	68%	56.61	4.3	18.7
				-56.9	(4.20	-18.7
5e	$C_{23}H_{21}O_3N_4SCl$	0.37	70%	58.9	4.4	11.9
				-58.7	-4.3	-11.4
5f	$C_{23}H_{21}O_3N_4SCl$	0.48	58%	58.9	4.4	11.9

				-58.7	-4.3	-11.4
5g	$C_{23}H_{21}O_3N_4SCl$	0.36	55%	58.9	4.4	11.9
				-58.7	-4.3	-11.4
5h	$C_{24}H_{23}O_4N_4S$	0.87	66%	62.1	4.9	12.09
				-62	-4.9	-12.6
5i	$C_{24}H_{23}O_4N_4S$	0.11	92%	62.1	4.9	12.09
				-62	-4.9	-12.6
5j	$C_{23}H_{20}O_3N_4SBr$	0.92	71%	53.9	3.9 (3.4)	10.9 (10.7)
				-53.6		

2-(3',5'-Dimethyl-4'-ethoxy carbonyl pyrrole) acid hydrazide (2)
3,5-Dimethyl-2,4-diethoxy carbonyl pyrrole **(1)** (0.05 mole), hydrazine hydrate (1.0 mL, 99%), and ethanol (20 mL) were taken in a 100 mL round base flask. The response blend was refluxed for 4hr. on the water bath. The response was checked by thin-layer chromatography. The mixture was dissipated to its half and left-over night. The product precipitated was sieved, washed with water, desiccated and crystallized from ethanol. Yield 70%: M.P.216°C: IR (KBr, cm^{-1}): 3153(NH), 1621(CONH), 1712 ($COOC_2H_5$), 1322($-CH_3$):[1] ^{1}H-NMR (DMSO, δ in ppm): (m, 3H $CONHNH_2$), 8.9 (s,1H, Pyrrole-NH).

4-Hydroxybenzal-2-(3′, 5′dimethyl-4′ ethoxy carbonyl pyrrolyl) hydrazines (3)
A mixture of 2-(3′,5′-dimethyl-4′-ethyl carbonyl pyrrole) acid hydrazide (**2)** (0.01 mole) and p-hydroxy aldehyde in appropriate amounts in excess of DMF was magnetically stirred for 8 hours. The resulting mix was permitted to stand for 1 hour keeping the internal temperature between 5–10 °C. The mixture was refluxed for 3 hours. The solvent was detached under vacuum to obtain the crude product which was swept away with water followed by ethanol (10ml) and crystallized from appropriate solvents (70% aqueous ethanol).M.P. 187°, yield 72%. ; IR (KBr, cm^{-1}): 3393.0 (OH), 3306.3 (N-H), 1693.8 (C=O, ester), 1682 (C=N, azomethine), 1573.5 (-CONH). ^{1}H-NMR (DMSO, δ in ppm): 2.10 (s, 6H, 2 x CH_3), 3.31(m, 5H, COO CH_2CH_3), 3.42 (s, 1H, CH=N), 8.93(s, 1H, 2-OH), 8.1(4H, ArH); ^{13}C NMR (300MHz, DMSO-d_6) 36.93, 39.20, 39.48, 39.76, 40.03, 77.74, 78.18, 78.62, 116.13, 117.4, 118.9, 131.09, 132.51, 158.60, 163.02.

General Procedure for (4a-j)
Substituted 2-Arylaminebenzal-2-(3′, 5′dimethyl-4′ethoxycarbonylpyrrolyl) hydrazines (4a-j)
A mixture of 4-hydroxy benzal-2-(3′, 5′dimethyl-4′ ethoxy carbonyl pyrrolyl) hydrazines **(3)** (0.05mole) and substituted aromatic primary amine (0.05mole) in absolute ethanol (100ml) was heated under reflux in the presence of anhydride $ZnCl_2$ (0.5g) for 3 hr. on a water bath. On cooling a solid mass parted out which was wash away repeatedly with acidified water to remove inorganic materials. It was filtered off, dried and crystallized from ethanol. (M. P. 170° yield 72 %.). IR (KBr, cm^{-1}): 3342.6 (N–H-pyrrole), 1792.9 (CONH), 1712 ($COOC_2H_5$), 1650 (-C=O, ester). 1649 (N-H-Bridge) 1322($-CH_3$); ^{1}H-NMR (DMSO, δ in ppm): 2.56(s, 6H, 2 x CH_3), 4.28 (q, 5H, $COOCH_2CH_3$), 3.54 (s, 1H, -CONH); ^{13}C NMR (300MHz, DMSO-d_6), 11.3, 13.4, 13.9, 27.0, 38.9, 39.2, 39.5, 39.7, 40.0, 40.3, 58.5, 76.8, 77.2, 77.6, 111.8, 119.1, 126.2, 137.3, 162.2, 165.0.

8-[2′-(3″, 5″-dimethyl-4″-ethoxy carbonyl pyrrolyl) hydrazine] phenothiazines (5a)
A mixture of **(4)** (0.01mole) sulphur (0.1 moles) and Iodine (0.5 g) was rapidly heated at 180^0c in an oil bath and this temperature was maintained for 2 hr. The hot melt was rapidly poured into a mortar and crushed to a fine powder. It was washed with water dried and crystallized from ethanol containing animal charcoal. (M. P. 215° yield 80%.). IR (KBr, cm^{-1}): 3344.6 (N–H-pyrrole), 3320 (N-H-phenothiazine), 2967 (C-H-Aromatic stretch), 1792.9 (CONH), 1714 ($COOCH_2CH_3$), 1650 (-C=O, ester), 1332 ($-CH_3$), 785 (C-S); ^{1}H-NMR (DMSO, δ in ppm): 2.56 (s, 6H, 2 x CH_3), 4.28 (q, 5H, COO CH_2CH_3), 3.54(s, 1H, -CONH); ^{13}C NMR(300MHz, DMSO-d_6) 12.3, 13.4, 13.9, 27.0, 38.9, 39.2, 39.5, 39.7, 40.0, 40.3, 58.5, 76.8, 77.2, 77.6, 111.8, 119.1, 126.2, 137.3

8-[2′-(3″, 5″-dimethyl-4″-ethoxy carbonyl pyrrolyl) hydrazine] 2-nitro phenothiazines 5b
(M. P. 224° yield 65%.). IR (KBr, cm^{-1}): 3342.6 (N – H-pyrrole), 3323 (N-H-phenothiazine), 2965 (C-H-Aromatic stretch), 1792.9 (CONH), 1714 (COO CH_2CH_3), 1650 (-C=O, ester), 1555 ($-NO_2$), 1514 ($-NO_2$), 1332 ($-CH_3$), 785 (C-S); ^{1}H-NMR (DMSO, δ in ppm): 2.56 (s, 6H, 2 x CH_3), 4.28 (q, 5H, COO CH_2CH_3), 3.54 (s, 1H, -CONH); ^{13}C NMR(300MHz, DMSO-d_6) 14.3, 13.5, 13.6, 22.0, 37.9, 38.2, 34.5, 39.4, 40.0, , 58.5, 76.8, 77.2, 77.6, 111.8, 159.1, 126.2, 137.3, 162.2, 162.1.

8-[2′-(3″, 5″-dimethyl-4″-ethoxy carbonyl pyrrolyl) hydrazine] 3-nitro phenothiazines 5c
(M. P. 212° yield 62%). IR (KBr, cm^{-1}): 3342.6 (N – H-pyrrole), 3324 (N-H-phenothiazine), 2967 (C-H-Aromatic stretch), 1792.9 (CONH), 1714 ($COOC_2H_5$), 1650 (-C=O, ester), 1552 ($-NO_2$), 1332 ($-CH_3$), 785 (C-S); ^{1}H-NMR (DMSO, δ in ppm): 2.56 (s, 6H, 2 x CH_3), 4.28 (q, 5H, COO CH_2CH_3), 3.54 (s, 1H, -CONH); ^{13}C NMR (300MHz, DMSO-d_6), 11.3, 13.4, 13.9, 27.0, 38.9, 39.2, 39.5, 39.7, 40.0, 40.3, 58.5, 76.8, 77.2, 77.6, 111.8, 119.1, 126.2, 137.3, 162.2, 165.0.

8-[2′-(3″, 5″-dimethyl-4″-ethoxy carbonyl pyrrolyl) hydrazine] 4-nitro phenothiazines 5d
(M. P. 267° yield 68%.). IR (KBr, cm^{-1}): 3346.(N – H-pyrrole), 3324 (N-H-phenothiazine), 2967 (C-H-Aromatic stretch), 1792.9 (CONH), 1714 (COO CH_2CH_3), 1650(-C=O, ester), 1553 (-NO2), 1336 ($-CH_3$), 785 (C-S); ^{1}H-NMR (DMSO, δ in ppm): 2.56 (s, 6H, 2 x CH_3), 4.28 (q, 5H, COO CH_2CH_3), 3.54 (1H, s, -CONH); ^{13}C NMR (300MHz, DMSO-d_6) 11.3, 13.4, 13.9, 27.0, 38.9, 34.2, 39.5, 39.7, 40.0, 40.3, 58.5, 76.8, 77.2, 77.6, 111.8, 119.1, 126.2, 137.3, 162.2, 164.6.

8-[2′-(3″, 5″-dimethyl-4″-ethoxy carbonyl pyrrolyl) hydrazine] 2-chloro phenothiazines 5e (M. P. 238° yield 70%.). IR (KBr, cm^{-1}): 3442.6 (N – H-pyrrole),3327 (N-H-phenothiazine), 2967 (C-H-Aromatic stretch), 1792.9 (CONH), 1714 ($COOC_2H_5$), 1650 (-C=O, ester), 1332 ($-CH_3$), 785 (C-

S), 706 (-Cl); ^{1}H-NMR (DMSO, δ in ppm): 2.56 (s, 6H, 2 x CH_3), 4.28 (q, 5H, COO CH_2CH_3), 3.54 (s,1H, -CONH); ^{13}C NMR(300MHz, DMSO-d_6), 11.3, 13.4, 13.9, 27.0, 38.9, 34.2, 39.5, 39.7, 40.0, 40.3, 58.5, 76.8, 77.2, 77.6, 111.8, 119.1, 126.2, 137.3, 162.2, 165.3.

8-[2′-(3″, 5″-dimethyl-4″-ethoxy carbonyl pyrrolyl) hydrazine] 3-chloro phenothiazines 5f (M. P. 245° yield 58%.). IR (KBr, cm^{-1}): 3342.6 (N – H-pyrrole),3320 (N-H-phenothiazine), 2960 (C-H-Aromatic stretch), 1792.9 (CONH), 1714 (COO CH_2CH_3), 1650 (-C=O, ester), 1332 (-CH_3), 785 (C-S) 736 (-Cl); ^{1}H-NMR (DMSO, δ in ppm): 2.56 (s, 6H, 2 x CH_3), 4.28 (q, 5H, COO CH_2CH_3), 3.54 (s, 1H, -CONH); ^{13}C NMR(300MHz, DMSO-d_6), 11.3, 13.4, 13.9, 27.0, 38.9, 39.2, 39.5, 39.7, 40.0, 40.3, 58.5, 76.8, 77.2, 77.6, 111.8, 119.1, 126.2, 137.3, 162.2, 165.1.

8-[2′-(3″, 5″-dimethyl-4″-ethoxy carbonyl pyrrolyl) hydrazine] 4-chloro phenothiazines 5g (M. P. 217° yield 55%.). IR (KBr, cm^{-1}): 3348.6(N – H-pyrrole),3326 (N-H-phenothiazine), 2967 (C-H-Aromatic stretch), 1792.9 (CONH), 1714 (COO CH_2CH_3), 1650 (-C=O, ester), 1332 (-CH_3), 785 (C-S),726 (-Cl); ^{1}H-NMR (DMSO, δ in ppm): 2.56 (s, 6H, 2 x CH_3), 4.28 (q, 5H, COO CH_2CH_3), 3.54 (s, 1H, -CONH); ^{13}C NMR(300MHz, DMSO-d_6), 11.3, 13.4, 12.9, 25.0, 38.9, 39.2, 39.5, 39.7, 40.0, 40.3, 58.5, 76.8, 77.2, 77.6, 111.8, 119.1, 123.2, 137.3, 164.2, 165.3.

8-[2′-(3″, 5″-dimethyl-4″-ethoxy carbonyl pyrrolyl) hydrazine] 2-methoxy phenothiazines 5h (M. P. 209° yield 66%.). IR (KBr, cm^{-1}): 3452.6 (N – H-pyrrole), 3352 (N-H-phenothiazine), 2969 (C-H-Aromatic stretch), 1792.9 (CONH), 1714 (COO CH_2CH_3), 1650 (-C=O, ester), 1332 (-CH_3), 785 (C-S); ^{1}H-NMR (DMSO, δ in ppm): 2.56 (s, 6H, 2 x CH_3), 4.28 (q, 5H, $COOCH_2CH_3$), 3.54 (s, 1H, -CONH); ^{13}C NMR(300MHz, DMSO-d_6), 11.3, 13.4, 13.9, 27.0, 38.9, 39.2, 39.5, 39.7, 40.0, 40.3, 58.5, 76.8, 77.2, 77.6, 111.8, 119.1, 126.2, 137.3, 162.2, 165.0.

8-[2′-(3″, 5″-dimethyl-4″-ethoxy carbonyl pyrrolyl) hydrazine] 4-methoxy phenothiazines 5i
(M. P. 251° yield 92%.). IR (KBr, cm^{-1}): 3362.6 (N – H-pyrrole),3390 (N-H-phenothiazine), 2967 (C-H-Aromatic stretch), 1792.9 (CONH), 1714 (COO CH_2CH_3), 1650 (-C=O, ester), 1339 (-CH_3), 785 (C-S). ^{1}H-NMR (DMSO, δ in ppm): 2.56 (s, 6H, 2 x CH_3), 4.28 (q, 5H, COO CH_2CH_3), 3.54 (s, 1H, -CONH), ^{13}CNMR(300MHz,DMSOd_6), 11.3, 13.4, 13.9, 27.0, 38.9, 39.2, 39.5, 39.7, 40.0, 40.3, 58.5 ,6.8, 77.2, 77.6, 111.8, 119.1, 126.2, 137.3, 162.2.

8-[2′-(3″, 5″-dimethyl-4″-ethoxy carbonyl pyrrolyl) hydrazine] 2-bromo phenothiazines 5j
(M. P. 218^0 yield 71%.). IR (KBr, cm^{-1}): 3362.6 (N – H-pyrrole), 3332 (N-H-phenothiazine), 2961 (C-H-Aromatic stretch), 1792.9 (CONH), 1714 (COO CH_2CH_3), 1650 (-C=O, ester), 1332 (-CH_3), 785 (C-S), 518 (-Br); ^{1}H-NMR (DMSO, δ in ppm): 2.56 (s, 6H, 2 x CH_3), 4.28 (q, 5H, COO CH_2CH_3), 3.54 (s, 1H, CONH); ^{13}CNMR(300MHz,DMSOd_6), 11.3, 13.4, 13.9, 37.09, 38.9, 39.5, 39.7, 40.0, 40.3, 58.5, 76.8, 77.2, 77.6, 111.8, 119.1, 126.2, 137.

CONCLUSION

A series of 8-[2/-(3//, 5//-dimethyl-4//-ethoxy carbonyl pyrrolyl) hydrazine] substituted phenothiazines (5a-j) from 2-arylamin benzal-2-(3′,5′-dimethyl-4′-ethoxy carbonyl pyrrole) hydrazines (4a-j) in presence of sulphur and iodine. These compounds were screened for their Antioxidant Activity.

ACKNOWLEDGEMENT

I am highly thankful to the principal, VVACSC, Samudrapur for providing the necessary facility for the completion of this research work. The authors are also thankful to the Head, Department of Pharmaceutical Science Nagpur University for screening activities, Head RSIC, CDRI, Lucknow for providing the spectral data of the compounds.

REFERENCES

[1] JV Alvar. Leishmaniasis Worldwide and Global Estimates of Its Incidence. **2012**, Plos one.
[2] JS Arpinskat. Medical research owing to their pharmacological activity. **1996,** p. 12.
[3] R. Brenk, D Schipani, James et al., Chem. Med. Chem., 3(3): p. 435-44.
[4] AP Chamoun-Emanuelli. Agents and Chemotherapy, **2013**, 57(6): 2571-2581.
[5] YC Chen. Acta Anaesthesiol Taiwan. **2010,** 48(1): p. 3-7.
[6] A Daina, O Michielin & V Zoete. Sci Rep. **2017**. 7: p. 42717.
[7] J Delaney. J. Chem. Inf. Comput. Sci. **2004,** 44(3): p. 1000-1005.
[8] W Egan, K Merz and J Baldwin. Journal of Medicinal Chem., **2000.** 43(21): p. 3867-3877.
[9] J Fagerberg, E Karlsson, J. Ulander et al., Pharmaceutical Research. **2015.** 32(2): p. 578-589.
[10] MG Gaidhane. Gurukul Int. Multidisci. Res. J. **2016.** p. 206-215.
[11] AL Garcia. PLoS One. **2014.** 9(11).
[12] A. Ghatole, M Gaidhane, K Lanjewar et al., Bulg. J. sci. edu. 29(2): p. 206-244.
[13] A Ghatole, K Lanjewar and M Gaidhane. J. Pharm. Res. **2012.** 5(5): p. 2758-2762.
[14] A Ghatole, A., Lanjewar, K., & Gaidhane, M. (2014). Antimicrobial Activities; Ionic Liquid And Microwave Assisted Synthesis Of Ring-Substituted 3-(3-Bromo-4-Oxo-4h-Chromen-2-Yl)-4h-Chromen-4-One. World Journal of Pharmaceutical Research, 3(3), 4336-4350.
[15] A Ghatole, K Lanjewar and M Gaidhane. Int. J. Pharm Sci, **2012.** 6(2): p. 142-146.
[16] A Ghose, V Viswanadhan and J Wendoloski. J Comb Chem. **1999,** 1(1) 55-68.
[17] CS Gopi. J. Chem. **2019,** 9(4): p. 255-289.
[18] MG Gracio. Int J Antimicrob Agents. **2003,** 22(3): p. 347-51. doi:10.1016/s0924-8579(03)00204-8
[19] FP Grimsey. FEMS Microbiology Reviews. **2019**, 43(6): p. 577–590.
[20] SC Hibinoa. Natural Products Reports. **2001,** 18: p. 66-81.
[21] MF Kucukdisli. Beilstein J. Org. Chem. **2014,** 10: p. 466-470.
[22] C. Lipinski, F Lombardo, B. Dominy et al., Adv Drug Deliv Rev. **2001**, 46: p. 3-26.
[23] JA McGee. American J. Hosp. Pharm. 36(5): p. 633-640.
[24] I Muegge, S Heald and D Brittelli. J. Med. Chem. **2001,** 44(12): p. 1841-1846.
[25] G Ogu and J Maxa. Proc Bayl Univ Med Cent. **2000,** 13(4): p. 421-423.

[26] IJ Onakpoya. BMC Med. **2016,** 14: p. 1-11.
[27] MM Sharma. Scientific Report. **2018,** 8(1650): p. 1-18.
[28] SP Sinha. Chem Inform. **2012,** 2(4): p. 1130-1137.
[29] R Sundberg. New York, USA: Academic Press. **1997.**
[30] D Veber, S Johnson, H Cheng et al., J Med Chem. **2002,** 45(12): p. 2615-2623.

DER PHARMA CHEMICA

JOURNAL FOR MEDICINAL CHEMISTRY, PHARMACEUTICAL CHEMISTRY, PHARMACEUTICAL SCIENCES AND COMPUTATIONAL CHEMISTRY

ISSN: 0975-413X

All submissions of the EM system will be redirected to **Online Manuscript Submission System**. Authors are requested to submit articles directly to Online Manuscript Submission Systemof respective journal.



Journal h-index : 48
Journal Impact Factor : 3.2
Average acceptance to publication time (5-7 days)
Average article processing time (30 - 45 days)

Select your language of interest to view the total content in your interested language

Select Language
Powered by Google Trans

GET THE APP

30+ Million Reac

Social

Welcome

The primary mission of the **Der Pharma Chemica** is to become the premier source of high quality research from whole of the world. All authors not only receive fast and comprehensive peer-review but also the article promotion to researchers working in the same field.

Der Pharma Chemica A is peer-reviewed and is published in electronic version. The language of the *Der Pharma Chemica* is English.

Der Pharma Chemica publishes research and review articles, rapid and short communication and book reviews. The current emphasis of the journal includes (but is not limited to) the following areas: medicinal chemistry,pharmaceutical chemistry and computational chemistry.

Der Pharma Chemica is a peer-reviewed journal that is devoted to the dissemination of new and original knowledge in all branches of Chemistry and Pharmacy. The chemistry theme may include Electrochemistry, Computational chemistry, Phytochemistry, Synthetic Drug chemistry, Nano chemistry, Instrumentation analysis; Spectroscopic methods, Chromatographic techniques and the pharmacy theme may include Pharmaceutical analysis, Biopharmaceutics, Industrial Pharmacy etc. Accepted articles may be theoretical or they may report experimental results especially in chemistry and pharmaceutical knowledge. The journal meets analytical operations including samplings, measurements, data analysis and data interpretation of all the experimental results.

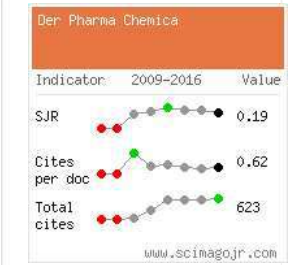
The journal Der Pharma Chemica, which deals with traditional analytical procedures, must provide unique applications of the most recent, approaches in the major fields of chemistry and pharmacy sector. The main objective of this journal is to provide a wide range of knowledge in chemical and pharmaceutical sciences to all over the world. Der pharma Chemica is gladly invite the researchers to submit their respective manuscripts who are dealing with chemistry and pharmacy discipline.

OPEN ACCESS POLICY

Der Pharma Chemica publishes all its articles in full open access format which are easily accessible for scientific community.Researchers have free and unlimited access to the full-text of articles published in Scholars Research Library Journals ie Readers can access the published articles freely without login and password. It gives the authors research high visibility, availability and more citations.

You can send your submission online here :- www.scholarscentral.org/submissions/der-pharma-chemica.html

Journal Der Pharma Chemica is Abstracted/Indexed in:



Google Scholar citation report

Citations : 15261

Der Pharma Chemica received 15261 citations as per Google Scholar report



Der Pharma Chemica peer review process verified at publons



CNKI
Chemical Abstract Services (USA),
SCOPUS
EMBASE
SCIMAGO
Indian Science Abstract,
HINARI
DOAJ
Open J Gate
Genomics Journalseek
Google scholar

h-index

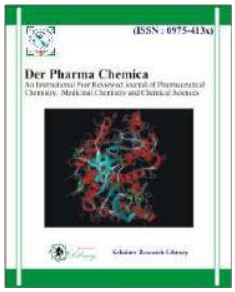
Articles published in **Der Pharma Chemica** have been cited by esteemed scholars and scientists all around the world. **Der Pharma Chemica** has got h-index 48 , which means every article in Der Pharma Chemica has got 48 average citations.

Posts from @derpharmachemi1 Follow

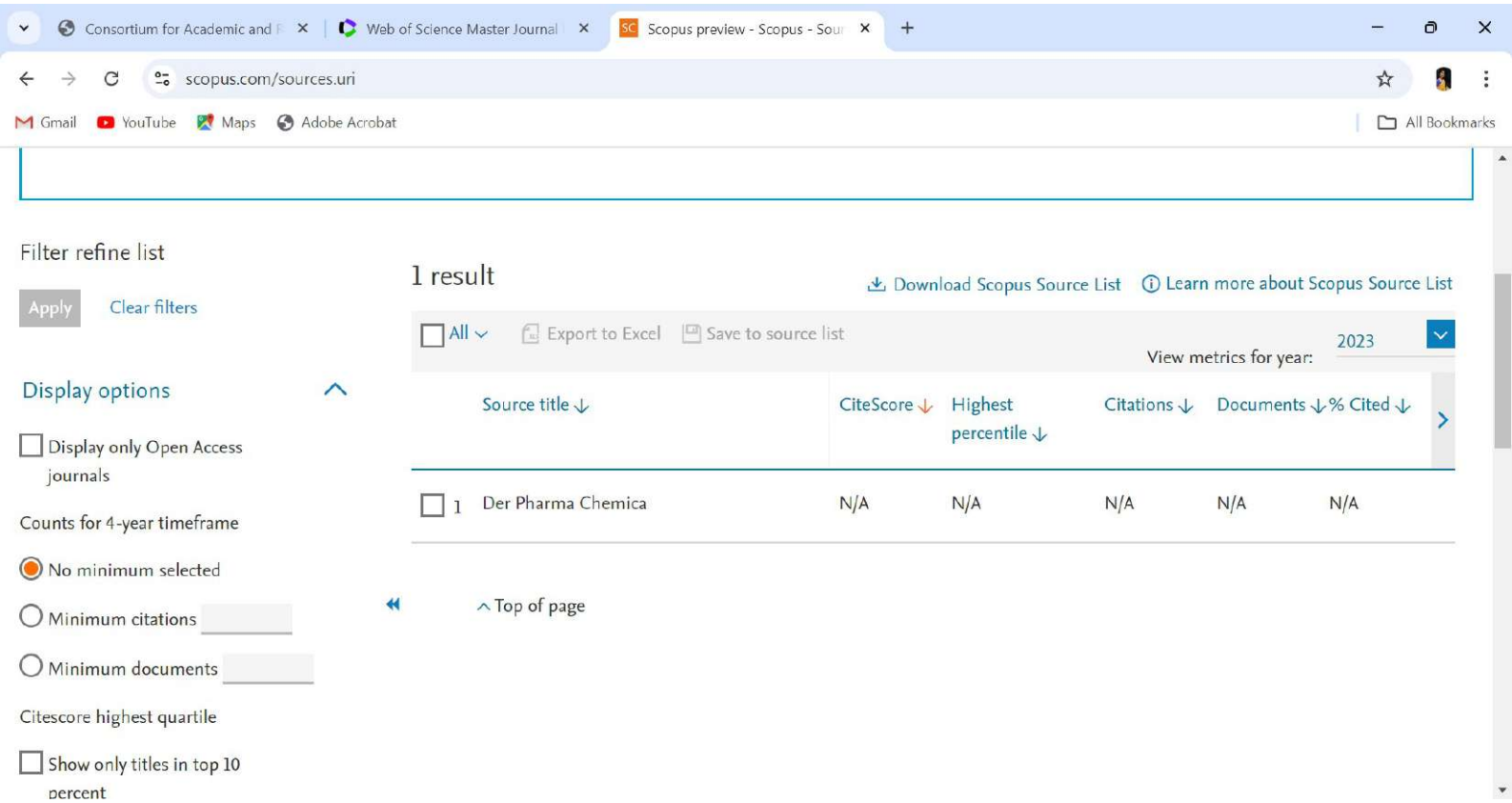
Nothing to see here - yet

DOWNLOADS

- Copyright Form
- Editorial / Advisory Board Form
- Author's Guideline
- Publication Ethics



Copyright © 2024 [Last updated: September 16, 2024]


Consortium for Academic and
Web of Science Master Journal
Scopus preview - Scopus - Sour
scopus.com/sources.uri
Gmail
YouTube
Maps
Adobe Acrobat
All Bookmarks
Filter refine list
Apply
Clear filters
Display options
Display only Open Access journals
Counts for 4-year timeframe
No minimum selected
Minimum citations
Minimum documents
Citescore highest quartile
Show only titles in top 10 percent
1 result
Download Scopus Source List
Learn more about Scopus Source List
All
Export to Excel
Save to source list
View metrics for year:
2023
Source title
CiteScore
Highest percentile
Citations
Documents
% Cited
1 Der Pharma Chemica N/A N/A N/A N/A N/A
Top of page

TÜBİTAK

Turkish Journal of Chemistry

http://journals.tubitak.gov.tr/chem/

Research Article

Turk J Chem
(2020) 44: 1495-1514
© TÜBİTAK
doi:10.3906/kim-2006-13

Innovational combination of hetero-bifunctional N-PEG quinoline scaffolds derivatives with improved anticancer activity against breast and colon cancer cell lines and P-glycoprotein, cytochrome p450 enzyme activity prediction

Mahesh GAIDHANE[1], Ajay GHATOLE[2,*], Kushal LANJEWAR[3], Kishor HATZADE[2]

[1]Department of Chemistry, Shri Lemdeo Patil Mahavidyalaya, RTMNU, Mandal, MS, India
[2]Department of Chemistry, Dhote Bandhu Science College, RTMNU, Gondia, MS, India
[3]Department of Chemistry, Mohsinbhai Zaweri Mahavidyalaya, Desaiganj, Wadsa, MS, India

Received: 05.06.2020 • **Accepted/Published Online:** 20.10.2020 • **Final Version:** 16.12.2020

Abstract: Polyethylene glycol (PEG) is a polymer that is widely used as a carrier for drug delivery systems (DDS). A library of N-PEGylated quinoline derivatives of PEG molecular weight 200 was prepared rapidly after the activation of PEGs using maleic anhydride. Quinoline with a polymer backbone is essential as new material. PEG is a water-soluble nonionic polymer approved by food and drug organizations for medicine applications. Because of its nontoxic grapheme, it is widely utilized in numerous biochemical, cosmetic, pharmaceutical, and industrialized applications. The modern SwissADME is a web tool that stretches free admittance to a pool of hasty, yet solid, clarifying models for physicochemical properties, pharmacokinetics, and therapeutic science. The present facile synthetic strategy can be a practical approach for incorporating polymeric carriers conjugated with drug moieties, either in the backbone of the polymer or as a terminal and pendant group on the polymer chains.

Key words: PEGylated quinoline, breast, colon cancer, P-glycoprotein, cytochrome P450 enzyme

1. Introduction

A library of N-polyethylene glycol(PEG)ylated quinoline derivatives of PEG molecular weight 200 was prepared rapidly after the activation of PEGs using maleic anhydrides. Quinoline with a polymer backbone is essential as new material. In 1995, Zalipskyet al.[1] and Herman et al. [2] reported the functionalization of polyethylene glycol for the preparation of biologically-relevant conjugates along with some reactive end groups. Polyethylene glycol conjugation chemistry represents an emerging trend for the generation of potential therapeutic agents. Woodle et al. [3] and Allen et al. [4] have demonstrated that PEG-modified biological molecules can benefit from extended plasma lifetimes, induced by reducing the uptake by the reticuloendothelial system and more generally, from a decrease of the undesired consequences of electrostatic and van der Waals interactions. A future direction towards nonviral gene therapy is the use of PEG-grafted synthetic vectors as long-circulating carriers for receptor-mediated gene delivery [5]. PEG has been used as a solvent medium for regioselective Heck reaction with elementary recyclability of solvents [6]. The incomparable ability of PEG to be soluble in both aqueous solution and organic solvents makes it eligible for end grouping derivatization and chemical conjugation to biological molecules under insignificant physiological conditions. The PEG-modified drug has been used widely as an antitumor drug carrier because of its excellent water solubility and biocompatibility [7]. Norfloxacin, one of the fluoroquinolone antibiotics, was conjugated to mannosylated dextrin to increase the intake of the drug by cells, enabling faster access to microorganisms, [8,9]. The backbone of polyurethanes and other ordinary low-density polyethylenes with antimicrobial Norfloxacin drugs were investigated by Yang et al. [10] against several gram-positive, and gram-negative bacteria, and displayed excellent antimicrobial activities. Recent advances in tumor therapy has demonstrated that successful anticancer strategies could be developed by employing proper carrier systems able to deliver probes, drugs, or genes to tumors targets [11]. Quinoline derivatives have been widely used for their biological [12–14], antibacterial, and antimalarial actions and in addition, for their cardiovascular, antineoplastic, and receptor agonist actions [15]. PEG, a water-soluble, nonionic polymer, which has a nontoxic character, is widely used as a carrier for drug delivery systems, and in many biochemical, cosmetic, pharmaceutical, and business applications [16]. The novel facile synthesis of a family of N-PEGylated quinoline

* Correspondence: ajay.ghatole5@gmail.com

This work is licensed under a Creative Commons Attribution 4.0 International License.

by coupling $PEG_{200(n)}$ with 2-formyl, 3-chloro, 6-amino quinoline via maleic anhydride as an activator was presented herein. Antimicrobial activities of the quinoline-PEG polymer and quinoline were tested against gram-positive and gram-negative bacteria. The results indicated that the new polymers had potential as potent antimicrobial agents. Since these polymers were comparatively stable at high temperatures, they can be used for medical and biomaterial applications with prior thermal sterilization. SwissADME permits the review of absorption, distribution, metabolism, and excretion (ADME) restrictions of medication aspirants and small molecules and provides statistics that authorize the early hazard calculation in drug enhancement progression. Exceptionally, SwissADME affords a point to estimate Lipinski's rule of five [17] for medication semblance of oral bioavailability. The present facile synthetic strategy can be a practical approach for incorporating the polymeric carriers conjugated with drug moieties, either in the backbone of the polymer or as a terminal and pendant group on the polymer chains.

PEG is the covalent link of nonpoisonous, hydrophilic polyethylene glycol (PEG) to dynamic pharmaceutical constituents [18]. The technology established from revolutionary work was conducted in the 1950s and 1960s on the coupling of polymers to protein. The amendment of a biopharmaceutical with polyethylene glycol increases its hydrodynamic area and reduces its immunogenicity and antigenicity. Other achievements included braked renal evacuation, enhanced stability in the direction of proteolysis, and increased solubility of the biopharmaceutical in aqueous solution [19]. The synthesis of macromolecules with different functional groups in 2 ends is a promising field of research. A lot of useful materials can be designed from the macromolecules. However, due to the difficulty of separation of the reacted mixture, significant achievements have not yet been made. Pozzo et al. reported that some monofunctional derivatives of PEG could be prepared and separated using excess PEG, but the molecular weight of the monosubstituted PEGs was no more than 1000. It was evident that the higher the molecular weight of the starting PEG, the more difficult it was for the isolation of monosubstituted PEG from the reacted mixture. This is because there was no sharp difference between monosubstituted, disubstituted, and raw PEGs in the chemical and physical properties [20–22].Heterocyclic mixes have increased gigantic significance as a result of their low reverberation vitality and solid hydrogen-bonding capacities [23]. A recent investigation reported the fruitful synthesis of new heterocyclic-like ester and amide under water as a solvent and the surface of silica-coated $CoFe_2O_4$ magnetic nanoparticles for the synthesis of 3-pyrrolin-2-ones [24], as well as for the preparation of 2-amino-4,6-diarylnicotinonitrile under microwave irradiation [25].

2. Result and discussion

An extension of PEG-supported chemistry was linked in the arena of functionalized polymers as reagent supports. Prepared was novel PEG N-terminal quinoline substituted derivatives and it was shown that, when related to a heterogeneous commercially-existing counterpart, they held promising reaction kinetics equal to the Staudinger and Mitsunobu etherification reactions. They were evaluated for their in vitro anticancer, antibacterial, and antifungal activities. The present study expanded on those preliminary investigations to explore the synergistic effects of such pharmacophores.

The PEGylation chemistry successfully demonstrated at the amino group was situated at C-7 of the quinoline hybrids. To couple a PEG to a quinoline molecule, it is first necessary to activate the polymer by converting the hydroxyl terminus to some functional group proficient reacting with the functional group situated on quinoline molecule. Herein, it was opted to activate the PEG by turning it to its acid derivative and coupling it with an amino group of quinoline molecules. This PEGylation methodology involved the conjugation of quinoline onto hetero-bifunctional PEG derivatives that had -OH on one terminus and -COOH on the other for covalent attachment of the amino group. The free carboxyl group of compounds was used for conjugation through an amine connection. It was determined that this conjugation proceeded through the formation of amide linkage between the PEG chain and quinoline under mild reaction conditions.

In its most common form, PEG is a linear or branched polyether terminated with hydroxyl groups and has the general structure as shown below:

$HO\text{-}(CH_2CH_2O)_n\text{-}CH_2CH_2\text{-}OH$.

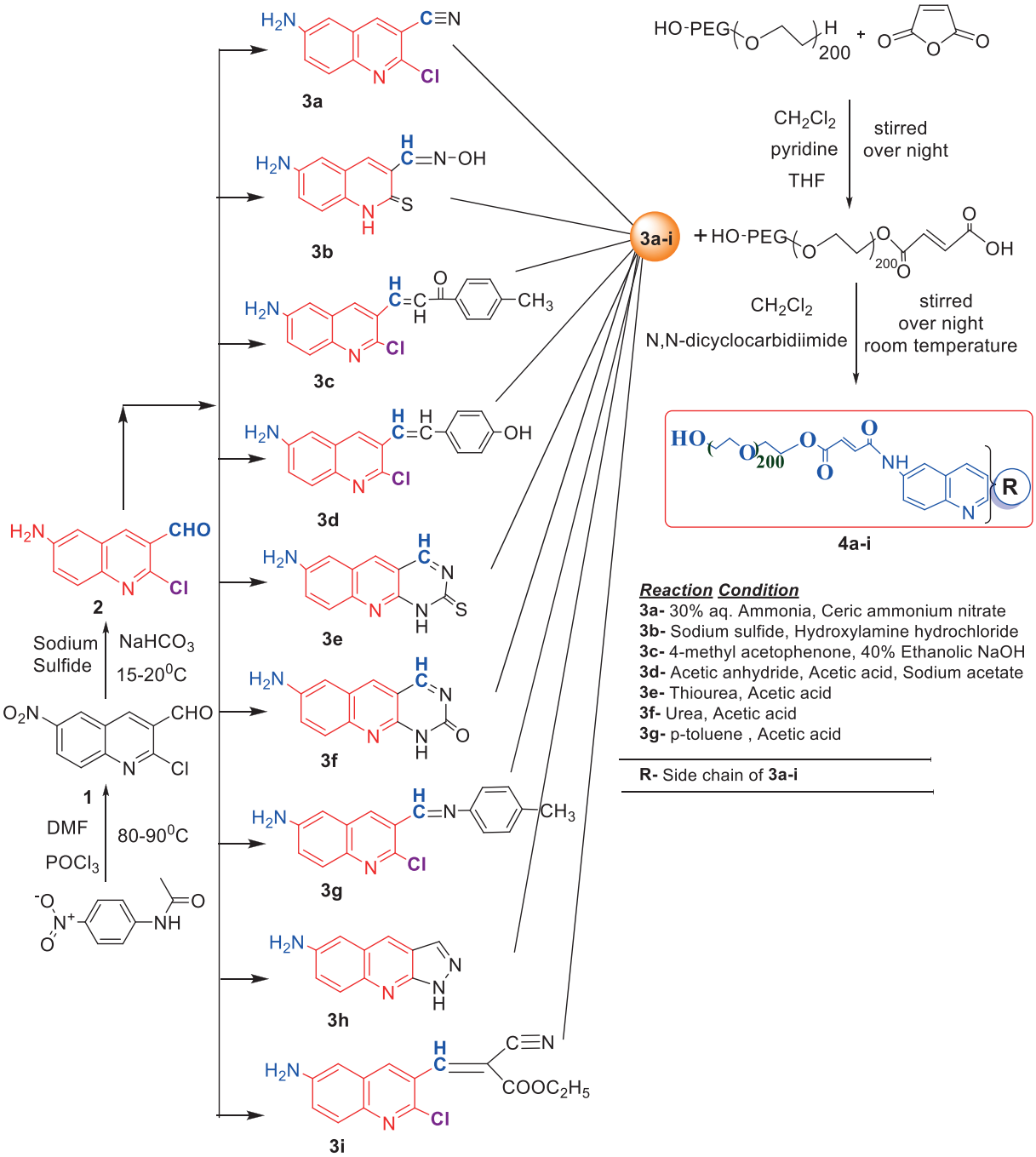
PEG is synthesized by anionic ring-opening polymerization of ethylene oxide initiated by the nucleophilic attack of a hydroxide ring.

$PEG_{200(n)}$ (5 mL, 0.028 moles, 200 g/mole) was dissolved in 20 mL of dry CH_2Cl_2. Added to this solution was tetrahydrofuran (THF) containing maleic anhydride (0.056 mol, 0.54 mg) and pyridine (0.056 mol, 0.46 mL). After stirring overnight at room temperature, the reaction was completed, as indicated by thin-layer chromatography (TLC) (methanol:ethyl acetate, 7:3) (no anhydride left and the detection of a single polar PEG compound). The monoacid derivative of the poly (ethylene glycol)$_{200(n)}$ was used without purification. The most useful for polypeptide modification is monoacid PEG, which has the general structure:

$HO\text{-}(CH_2CH_2O)_n\text{-}CH_2CH_2\text{-}O\text{-}COOH$.

Now, for this monoacid derivative of PEG coupled to a 6-amino-2-chloroquinoline-3-carbonitrile (**3a**), it was necessary to activate the PEG by maleic anhydride. In the present study, the solution synthesis of a novel family of PEGylating reagent was presented, which contained a free -COOHterminus. Conditions were developed for the coupling of this novel PEGylating reagents to the -NH_2function of model quinoline to illustrate their general utility. Together, this study demonstrated that these PEGylating reagents were well-suited for conjugation peptide and protein containers, either free -COOH or -NH_2 functions. These reagents might have wide utility in therapeutic expansion, as branched PEGylation has been observed to deliver more effective protection of proteins from proteolysis by protecting the protein surface approaching the macromolecules.

The synthesis of quinoline compounds **3a**–**3i** (Scheme) was accomplished, starting with 6-amino-2-chloroquinoline-3-carbaldehyde (**2**). The treatment of compound **2** with ceric ammonium nitrate (CAN) in 30% aq. ammonia at 0–2 °C with constant stirring for 2–3 h gave 6-amino-2-chloroquinoline-3-carbonitrile (**3a**). However, the reaction of compound



Scheme. Hetero-bifunctional N-PEG quinoline scaffold derivatives.

2 with fused sodium sulfide in dry dimethylformamide (DMF), followed by hydroxyl amination, afforded 6-amino-2-mercaptoquinoline-3-carbaldehydeoxime (**3b**). Next, 3-(6-amino-2-chloroquinoline-3-yl)-1-p-tolylprop-2-en-1-one (**3c**) was prepared by the reaction of compound **2** with 4-methyl acetophenone in 40% ethanolic NaOH. Moreover, 4-(2-(6-amino-2-chloroquinoline-3-yl) vinyl phenol (**3d**) was synthesized by treating a mixture of compound **2** and p-cresol in AcOH/Ac_2O under reflux for 6–7h. Additionally, compound **2** was treated with thiourea and urea in AcOH under reflux for 15–16h and produced 7-aminopyrimido(4,5-b)quinoline-2(1H)thione(**3e**) and 7-aminopyrimido(4,5-b) quinoline-2(1H)one (**3f**), respectively. Furthermore, 3-(*P*-tolylimino) methyl-2-chloroquinoline-6 amine (**3g**) was prepared by condensation of compound **2** with p-toludiene in acidic methanol. A noteworthy ring annulation was observed when compound **2** was condensed with hydrazine hydrate in ethanol under reflux for 5–6h, which afforded *1-H*-pyrazolo (**3** and **4b**), and quinolin-6-amine (**3h**). The synthesis of (Z)-ethyl 3-(6 amino-2-chloroquinoline-3-yl)-2-cyanoacrylate (**3i**) was accomplished by condensation of compound **2** with ethyl cyanoacetate (Table 1).

The monoacid derivative of hydroxycarboxy PEG (HO-PEG_{200}COOH) (28.0mmol) was activated with a 1:2molar equivalent of 6-amino-2-chloroquinolin-3-carbonitrile (**2a**) (46.0mmol) and N, N dicyclocarbidiimide (46.0mmol) dissolved in dichloromethane. The solution was stirred for 24 h at room temperature. A syrupy resin was obtained and dried under a vacuum. The syrupy resin was dissolved in 15 mL of acetone. A white precipitate of dicyclohexylurea (DCU) appeared and was discarded, and the filtrate was collected. The final filtrate was evaporated to afford the product. TLC (methanol:ethyl acetate, 7:3) was performed to check the existence ofDCU, which exposed a negative outcome that was confirmed by the infrared spectroscopy (IR) spectra. A negative dye test indicated complete amino group capping.

The resin was dehydrated in a vacuum for IR, ^{1}HNMR, ^{13}CNMR, and mass spectral analysis. At this point, the adhesive did not stick to the glass wall anymore. The IR spectrum of the resin showed the characteristic absorption band of the PEG ether backbone (1120 cm^{-1}) and absorption bands (1760 and 1685 cm^{-1})for the ester and amide bond, respectively (C=O) (Table 2).

3. Experimental

All of the recorded melting points were taken in open capillary tubes and were uncorrected. The IR spectra were recorded with a FTIR PerkinElmer Rx-I instrument (PerkinElmer, Inc., Waltham, MA, USA) using Nujol.^{1}HNMR spectra were recorded on 400 MHz Bruker AC-300 F instrument (Bruker BioSpin Corp., Billerica, MA, USA) using tetramethylsilane as the internal standard and deuterated chloroform as the solvent, and the mass spectra were recorded on a VG.70 S instrument at SAIF Chandigarh. The TLC technique was used to check the purity of the compound using silica gel G.

3.1. Biological assay

3.1.1. In vitro anticancer assays

A library of 24 compounds was tested using the Alamar blue (AB) assay (in the case of leukemia cells) for their antiproliferative activity in vitro against 2 cancer cell lines: SW620, MD468, and MD468-2 were all colon cancer cell lines obtained from the American Tissue Culture Collection (ATCC, Manassas, VA, USA). MD468 is a mismatched repair-deficient cell line, and MD468-2 has a p53 mutation. The results of the cytotoxic activity in vitro were expressed as an ID_{50} (nM/mL), i.e. the concentration of the compound that inhibited the proliferation of 50% of the tumor cells when compared to the untreated control cells. Camptothecin (10 nM), Paclitaxel (10 nM), Doxorubicin (250 nM), and Oxaliplatin (2000 nM) were applied as referential cytotoxic agents (positive test controls). A value of less than 10 nM/mL was considered as an antiproliferative activity criterion for synthetic compounds. The results of the cytotoxicity studies are summarized in Table 3.

3.1.2.Antiproliferative activity

All 24 compounds were tested via AB assay (in the case of leukemia cells) for their antiproliferative activity in vitro against 2 cancer cell lines: SW620, MD468, and MD468-2 were all colon cancer cell lines obtained from the ATCC. MD468 is a mismatched repair-deficient cell line, and MD468-2 has a p53 mutation. The results of the cytotoxic activity in vitro were expressed as an ID_{50} (nM/mL), as stated above. Camptothecin (10nM), Paclitaxel (10 nM), Doxorubicin (250 nM), and Oxaliplatin (2000 nM) were applied as referential cytotoxic agents (positive test controls). A value of less than 10 nM/mL was considered as an antiproliferative activity criterion for synthetic compounds. The results of the cytotoxicity studies are summarized in Table 3.

In general, compounds **3a**–**4i** did not display any anticancer activity, whereas compounds **4a**–**4i** exhibited potent antiproliferative activity against theSW620, MD468, and MD468-2 colon cancer cell lines. This implied that after PEGylation, the anticancer activity enormously increased in multiples of 469- to 11896-fold. PEGylated 1-H-pyrazol (**3** and **4b**) and quinolin-6-amine (**4h**) exhibited the highest activity against the SW620, MD468, and MD468-2 colon cancer

Table 1. Physical characterization data of substituted quinoline derivatives **1**, **2**, and **3a**–**3i**.

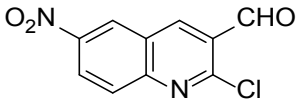
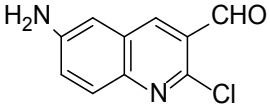
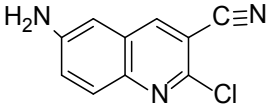
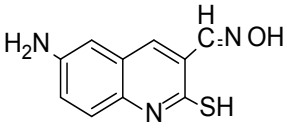
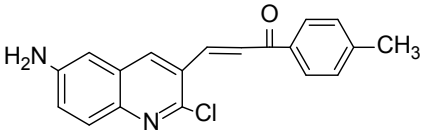
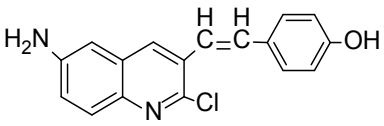
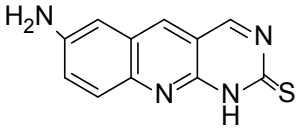
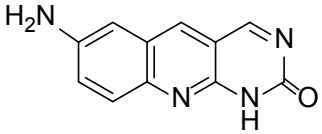
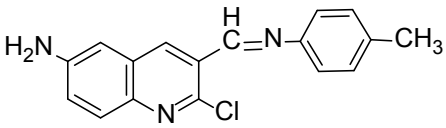
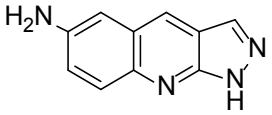
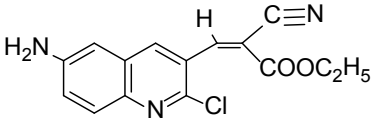
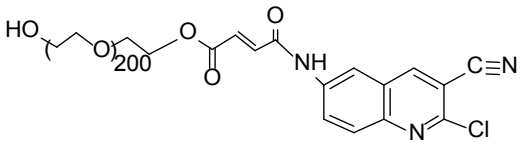
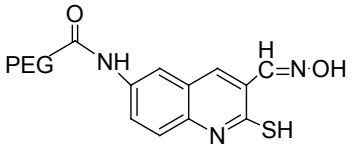
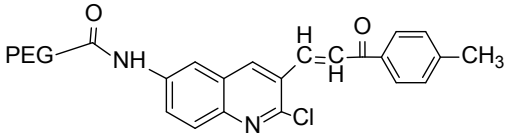
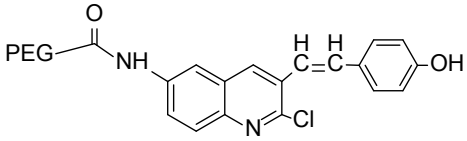
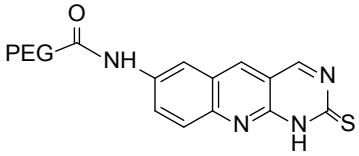
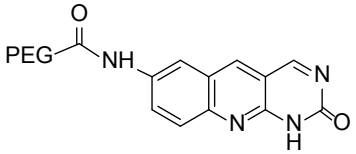
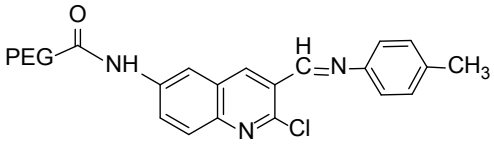
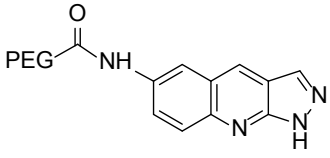
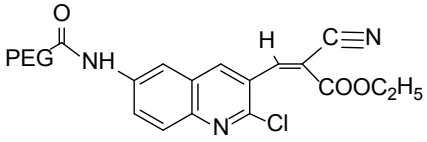
Entry	Product	Temperature	Yield (%)	m.p. (°C)	Molecularformula
1		90 °C Heating	86	260	$C_{10}H_5ClN_2O_3$
2		Refluxed	82	208	$C_{10}H_7ClN_2O$
3a		Stirring/RT	83	162	$C_{10}H_6ClN_3$
3b		Stirring/RT	78	168	$C_{10}H_9N_3OS$
3c		Stirring/RT	84	240	$C_{19}H_{15}ClN_2O$
3d		Refluxed	83	168	$C_{17}H_{13}ClN_2O$
3e		Refluxed	82	272	$C_{11}H_8N_4S$
3f		Refluxed	78	247	$C_{11}H_8N_4O$
3g		Refluxed	86	176	$C_{17}H_{14}ClN_3$
3h		Refluxed	76	288	$C_{10}H_8N_4$
3i		Refluxed	86	122	$C_{15}H_{12}ClN_3O_2$

Table 2. Structures of the PEGylated quinolines (**4a**–**4i**).

S. No.	Structures of the PEGylated quinolines	Density (d) in cm^3
4a		1.012
4b		1.126
4c		1.058
4d		1.158
4e		1.038
4f		1.038
4g		1.152
4h		1.008
4i		1.102

cell lines and had IC_{50} values of 8.5 nM/mL and 9.3 nM/mL, respectively, for the corresponding cell lines. Compound **4i** had an IC_{50} value of 7.8 nM/mL and also possessed the highest anticancer activity against the SW620 colon cancer cell line. Compounds **4g** and **4b** showed lower activity among compounds **4a**–**4i** against MD468, MD468-2, and SW620, respectively, with IC_{50} values of 49.8 nM/mL and 39.3 nM/mL. However, compounds **4a**–**4f** displayed moderate activity

Table 3. Comparative IC50 nM of compounds **3a**–**3i** and **4a**–**4i**.

Sr No.	MDA MD 468 (breast cancer cell line)					SW480 (colon cancer cell)				
	Before PEGylating (**3a**–**3i**)		After PEGylating (**4a**–**4i**)		Improvement in efficacy (fold)	Before PEGylating (**3a**–**3i**)		After PEGylating (**4a**–**4i**)		Improvement in efficacy (fold)
1	17514	**3a**	37.3	**4a**	469	23839	**3a**	34.9	**4a**	682
2	77690	**3b**	22.6	**4b**	3430	98317	**3b**	39.3	**4b**	2499
3	12478	**3c**	20.8	**4c**	600	9077	**3c**	33.0	**4c**	275
4	82492	**3d**	28.2	**4d**	2921	72731	**3d**	24.1	**4d**	3014
5	97473	**3e**	39.5	**4e**	2469	83269	**3e**	29.5	**4e**	2823
6	102107	**3f**	20.9	**4f**	4876	108894	**3f**	33.0	**4f**	3297
7	102593	**3g**	49.8	**4g**	2061	135575	**3g**	19.1	**4g**	7114
8	100639	**3h**	8.5	**4h**	11896	86233	**3h**	9.3	**4h**	9256
9	20253	**3i**	7.8	**4i**	2607	56723	**3i**	27.4	**4i**	2068

IC_{50} values of the anticancer agents (controls).
Camptothecin: 10 nM, Paclitaxel: 10 nM, Doxorubicin: 250 nM, Oxaliplatin: 2000 nM.

when the IC_{50} values of all of the compounds were compared with those of standard drugs like Camptothecin (IC_{50}:10 nM) and Paclitaxel (IC_{50}: 10 nM). Doxorubicin (IC_{50}: 250 nM) and Oxaliplatin (IC_{50}: 2000 nM) were also suited as reference cytotoxic agents. A comparative investigation of the IC_{50} concentrations of compounds **4a**–**4i** with those of Doxorubicin (IC_{50}: 250nM) and Oxaliplatin (IC_{50}: 2000nM) was conducted. The anticancer activity displayed at an IC_{50} concentration ranging from 7.8 nM/mL to 49.8 nM/mL indicated that all of the synthesized compounds exhibited incredibly higher potency than those of Doxorubicin (IC_{50}: 250 nM) and Oxaliplatin (IC_{50}: 2000 nM). The results summarized in Table 3 suggested that the potency of each compound as an anticancer agent was irrespective of its substituents and showed high selectivity and more specificity towards the binding targeted sites. Compound **4h** proved to be a highly-potent candidate against the SW620, MD468, and MD468-2 colon cancer cell lines than the existing armory of anticancer drugs attributable to the ring annulations with fused pyrazole nucleus.

3.1.3. Assay principle

In this assay, the viability of chemically-treated cells were measured by a dye, Resazurin or Alamar blue (AB). AB, a nonfluorescent pointer dye, changed to bright red-fluorescent resorufin through the reduction reactions of metabolically active cells. The quantity of fluorescence produced was directly proportional to the number of living cells.

Cells: For the initial screen of A549, the lung cancer cells were used. Positive hits were then used to screen 7 other cell lines used in the NIH assays.

Protocol: Standard AB assay protocol for cell viability assay was used. Confluently-grown cells were trypsinzed, and around 10,000 cells were seeded in each well of a 96-well plate. The next day, the medium was replaced with medium containing the appropriate concentration of the drug. The maximum concentration of each drug was 400μg/mL, and a one-quarter dilution was used for each drug. The cells were treated for 48 h and 2μL of AB was added to each well and incubated for 2 h. Fluorescence intensity was read with a plate reader. From the graph, the IC_{50} value was calculated. SW620, MD468, and MD468-2 were all colon cancer cell lines obtained from the ATCC. MD468 is a mismatched repair-deficient cell line, and MD468-2 has a p53 mutation. The effects of all of the new compounds on colon cancer cell lines SW620, MD468, and MD468-2, were observed and the results are depicted in Figures 1and 2. The growth inhibition percentages were compared with those of standard drugs Camptothecin, Paclitaxel, Doxorubicin, and Oxaliplatin (Table 3, Figures 1 and 2). For the rows, alcohol was added to generate killed cells.

3.1.4. In vitro antibacterial and antifungal activity

All of the newly synthesized compounds were screenedin vitrofor their antimicrobial activity and antifungal activity against a variety of bacterial and fungal strains, such as *Staphylococcus Aureus* (gram +ve), *Escherichia Coli* (gram –ve), *Pseudomonas Aeruginosa* (Gram –ve), and *Candida Albicans* using the disc diffusion method. The nutrient agar broth was prepared by aseptic inoculation with 0.5 mL of 24-h-old subcultures of *S. Aureus*, *E. Coli*, and *C. Albicans* in separate flasks at 40–50 °C and mixing well by gentle shaking.

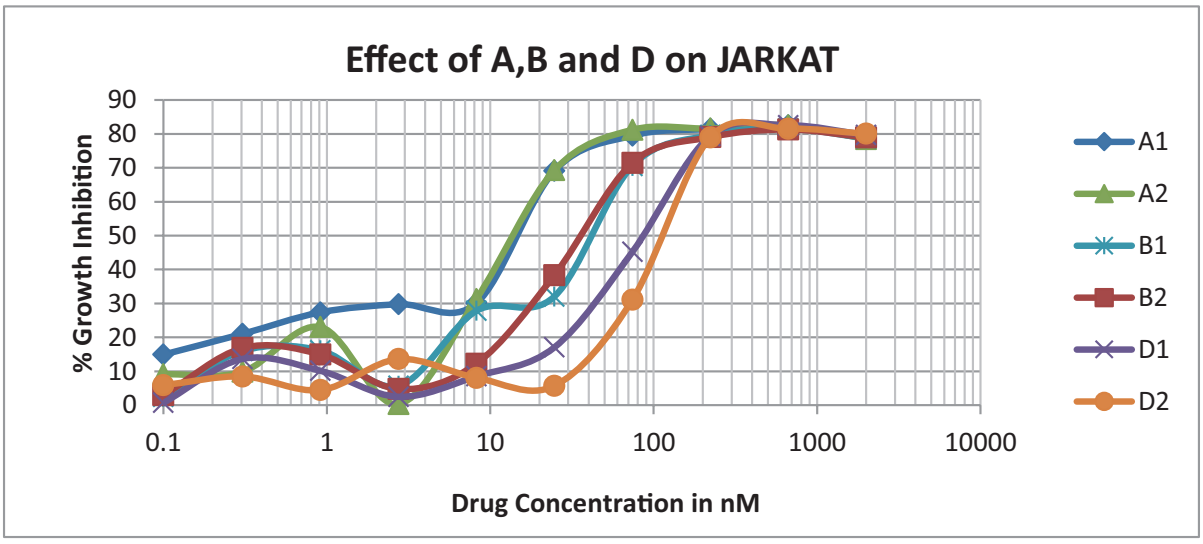


Figure 1. Effect of compounds **4a**–**4i** in colon cancer line (SW620).

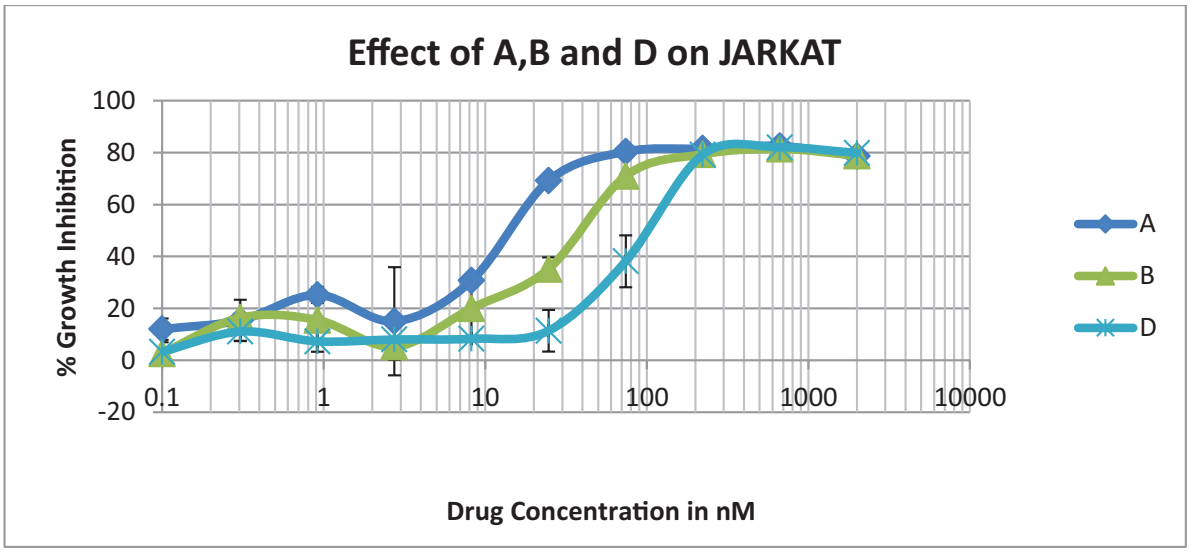


Figure 2. Effect of control standard anticancer drugs in SW620 cells.

About 25 mL of the contents of the flask were poured and evenly spread in a Petri dish (13 cm in diameter) and allowed to set for 2h. Each test compound (20 mg) was dissolved in 2 mL of dimethyl sulfoxide (DMSO), which was used as a sample solution. A concentrated (100 µg/mL) solution was prepared using the dilution method. The sample size for all of the compounds was fixed as 10 µL.

The plates were incubated at 37 °C for 24 h, the control was similarly maintained with 1 mL of DMSO, and the zones of inhibition of the bacterial growth were measured in mm using a zone reader.

3.1.5. In vitro antibacterial and antifungal activity

The newly synthesized compounds (**3a**–**3i** and **4a**–**4i**) were tested for theirin vitro antimicrobial activity against clinical isolates of gram-positive bacteria *S.Aureus*, gram-negative bacteria *E.coli* and *P. Aeruginosa*, and the fungus *C. Albicans*. For all of the compounds, along with the standards for the bacteria, doxycycline, ampicillin, and fungi, fluconazole was used at a concentration of 100 µg/mL in DMSO as the solvent control and nutrient agar was used as the culture method [26–29]. After 24h of incubation at 37 °C, the zones of inhibition were measured in mm.

All of the synthesized compounds exhibited good to moderate activity against all of the microbes. No zone of inhibition was observed against the strains of *P. Aeruginosa* with compounds **3c**, **3h**, and **4c**, while all of the compounds displayed significant activity against the strains of *C. Albicans*, *E. Coli*, and *S. Aureus*.

The toxicity increased with the increase in the concentration of the test solution containing new compounds, suggesting a maximum tolerated dose. Some compounds did not meet the conventional bacteriostatic standards at lower concentration levels. The variance in the efficiency of compounds in contradiction ofdiverse organisms depends on either the impenetrability of the cell microorganisms or dispersion in the ribosomes of microbial cells. The results obtained after screening the synthesized compounds against various microorganisms are shown in Table 4.

4. SwissADME pharmacokinetics, physicochemical, and medicinal properties study [30]

The functioning highlights of these molecules were entered into the SwissADME site (http://swissadme.ch) using the ChemAxon's Marvin JS structure drawing instrument (Budapest, Hungary). Assistant highlights of the pharmacophore sway included bioavailability, transport properties, sympathy to proteins,reactivity, poisonous quality, and metabolic steadiness. Unique to SwissADME is the bioavailability radar [31], which gives a graphical assessment of the prescription resemblance parameters of an orally-accessible bioactive drug. The drug impression chart is exhibited as a hexagon (Figure 3) with every one of the vertices dialogs to a restriction that symbolizes a bioavailable drug.

The pink location inside the hexagon speaks to the perfect range for each property (lipophilicity: XLOGP3 somewhere in the array of −0.7 and +5.0, size: extremity: topological polar surface area (TPSA) somewhere in the field of 20 and 130 Å2, MW somewhere in the scope of 150 g/mol and 500g/mol, solubility: log S not higher than 6, adaptability: close to 9 rotatable bonds, and saturation: some portion of carbons in the sp3 hybridization at any rate 0.25). The recommended run for the compound as bioavailable medication is portrayed in Table 5.

Table 4. Antibacterial and antifungal activity of the synthesized compounds.

Comp.	E. Coli	P. Aeruginosa	S. Aureus	C. Albicans
1	10	8	10	9
2	11	7	12	10
3a	10	9	11	9
3b	10	7	8	8
3c	8	-	9	10
3d	10	8	10	8
3e	10	7	7	10
3f	8	8	8	8
3g	10	7	7	8
3h	8	-	9	8
3i	8	8	10	7
4a	12	10	12	11
4b	10	9	11	9
4c	10	-	10	11
4d	10	9	10	9
4e	10	9	11	12
4f	09	8	11	9
4g	10	9	10	8
4h	09	8	11	10
4i	12	8	9	9
SA	35	13	-	-
SD	18	15	23	-
SF	-	-	-	33

*100 µg/mL: drug concentration; SA: standard Ampicillin; SD: standard doxycycline; SF: standard fluconazole.

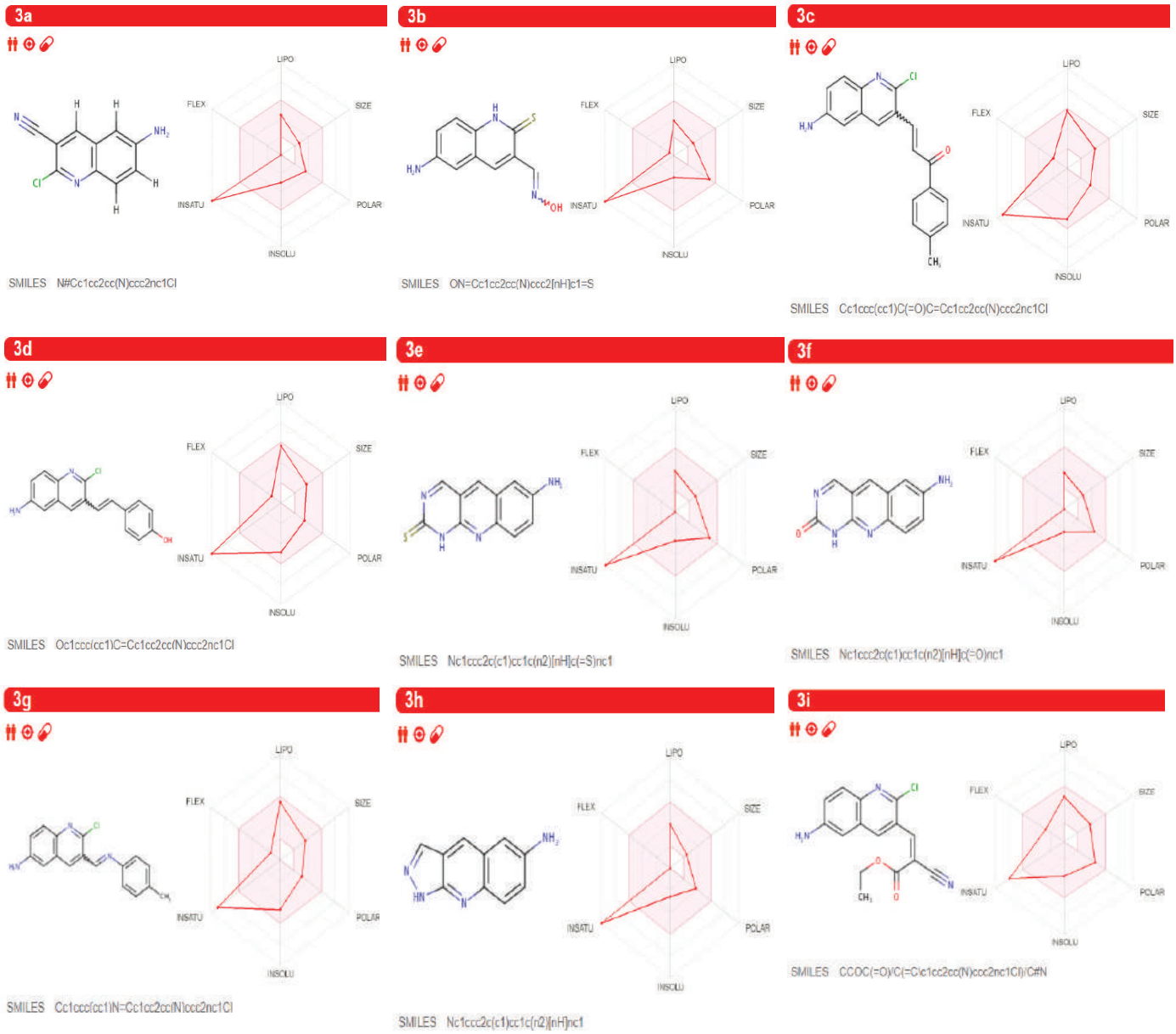


Figure 3. Bioavailability radar of the synthesized molecules **3a**–**3i** evaluating using SwissADME web tool.

4.1. Drug-likeness

The drug resemblance properties of the fused compound are indicated by the red mutilated hexagon inside of the pink shade (Figure 3). SwissADME, likewise, has computational channels that incorporate Ghose [32], Egan [33], Veber [34], and Muegee [35], created by top pharmaceutical organizations and cheminfomaticians to assess the drug resemblance of molecules. The values maintain in Table 6 indicated the violation of the prescribed range for the molecule to act as a drug.

4.2. PAINS, break, and leadlikeness screening

Pan-assay interference compound (PAINS) screening, which regularly gives bogus positive chemical properties, brings about high-throughput screens. PAINS will in general respond vaguely with various biological targets as opposed to explicitly influencing one foreseen objective. The SwissADME evaluation did not post any PAINS alert (Table 7). In additional to the verdict model, Brenk [36] measured combinations that were smaller and less hydrophobic, and not those described by Lipinski's standard of 5 to augment open doors for lead streamlining. Leadlikeness tests have been projected to provide primes with extraordinary kinship in high-throughput screens that consider the recognition and control of new exchanges ahead of the pack headway stage (Table 7). All of the synthesized compounds (**3a**–**3i**) drifted the break alert and leadlikeness criteria.

Table 5. Physicochemical properties of synthesized molecules **3a**–**3i**.

Sr. No.	MW	HA	AHA	FCsp3	RTB	HBA	HBD	MR	TPSA
3a	203.63	14	10	0	0	2	1	55.87	62.7
3b	219.26	15	10	0	1	2	3	62.92	106.49
3c	322.79	23	16	0.05	3	2	1	95.93	55.98
3d	296.75	21	16	0	2	2	2	88.55	59.14
3e	228.27	16	14	0	0	2	2	66.63	99.68
3f	212.21	16	14	0	0	3	2	62.07	84.66
3g	295.77	21	16	0.06	2	2	1	89.82	51.27
3h	184.2	14	13	0	0	2	2	55.8	67.59
3i	301.73	21	10	0.13	4	4	1	81.51	89

MW: molecular weight, HA: heavy atoms, AHA: aromatic heavy atom, FCsp3: fraction Csp3, RTB: rotatable bonds, HBA: H-bond acceptors, HBD: H-bond donors, MR: molar refractivity, TPSA: topological polar surface area.

Table 6. Drug-likeness evaluation of the synthesized compounds using SwissADME.

Sr. No.	Lipinski #violations	Ghose #violations	Veber #violations	Egan #violations	Muegge #violations
3a	0	0	0	0	0
3b	0	0	0	0	0
3c	0	0	0	0	0
3d	0	0	0	0	0
3e	0	0	0	0	0
3f	0	0	0	0	0
3g	0	0	0	0	0
3h	0	0	0	0	1
3i	0	0	0	0	0

Table 7. Medicinal chemistry evaluation of the synthesized compounds.

Sr. No.	PAINS #alerts	Brenk #alerts	Leadlikeness #violations	Synthetic accessibility
3a	0	2	1	1.71
3b	0	5	1	2.1
3c	0	3	1	2.88
3d	0	2	1	2.39
3e	0	3	1	1.63
3f	0	2	1	1.55
3g	0	3	1	2.65
3h	0	1	1	1.64
3i	0	4	0	2.76

4.3. P-glycoprotein and CYP enzyme activity prediction

SwissADME, furthermore, permits the valuation for a compound to be a substrate of p-glycoprotein (P-gp) or inhibitor of the cytochrome p450 isoenzymes (CYP isoenzymes). P-gp is largely spread and linked in the intestinal epithelium where

it drives xenobiotics [37]. The generations return Yes or No if the particle under assessment has a higher probability to be a substrate or nonsubstrate of P-gp or inhibitor or noninhibitor of a given CYP. The screening results were classified in Table 8.

4.4. Human intestinal absorption and blood-brain barrier prediction

Suitable for P-gp and CYP protein vitality is human intestinal absorption (HIA) and blood-brain barrier (BBB) infiltration. SwissADME BOILEDegg (Figure 4) grants the appraisal of HIA as a component of the circumstance of the molecules in the WLOGP-versus-TPSA referential.

The white segment of the BOILEDegg is for a high chance of reflexive adjustment by the gastrointestinal tract, and the yellow region (yolk) is for a high prospect of cerebrum entrance, and it can be seen that some of the blended particles (**3b**,**3e**,**3f**, and **3i**) are under the white segment. With this, the focuses are concealed in blue at whatever point was foreseen as adequately effluxed by P-gp (PGP+), shown by **3h** and in red, anticipated as a nonsubstrate of P-gp (PGP−) by **3a**, **3b**, **3c**, **3d**, and **3g**. HIA and the BBB are responsible for the water solvency and lipophilicity of the medication. There are 2 topological ways to deal with the predicted water solvency contained in the SwissADME. The first was an implementation

Table 8. Pharmacokinetic evaluation of the synthesized compounds.

Sr. No.	GIabs.	BBB per.	P-gp sub.	CYP1A2 inhibitor	CYP2C19 inhibitor	CYP2C9 inhibitor	CYP2D6 inhibitor	CYP3A4 inhibitor
3a	High	Yes	No	Yes	No	No	No	No
3b	High	No	No	Yes	Yes	No	No	No
3c	High	Yes	No	Yes	Yes	Yes	No	Yes
3d	High	Yes	No	Yes	Yes	No	Yes	Yes
3e	High	No	No	Yes	No	No	No	No
3f	High	No	No	Yes	No	No	No	No
3g	High	Yes	No	Yes	Yes	Yes	No	Yes
3h	High	Yes	Yes	Yes	No	No	No	No
3i	High	No	No	Yes	Yes	Yes	No	No

GIabs: gastrointestinal absorption,BBBper: blood-brain barrier permeant, P-gp sub: P-glycoprotein substrate, CYP: cytochromes.

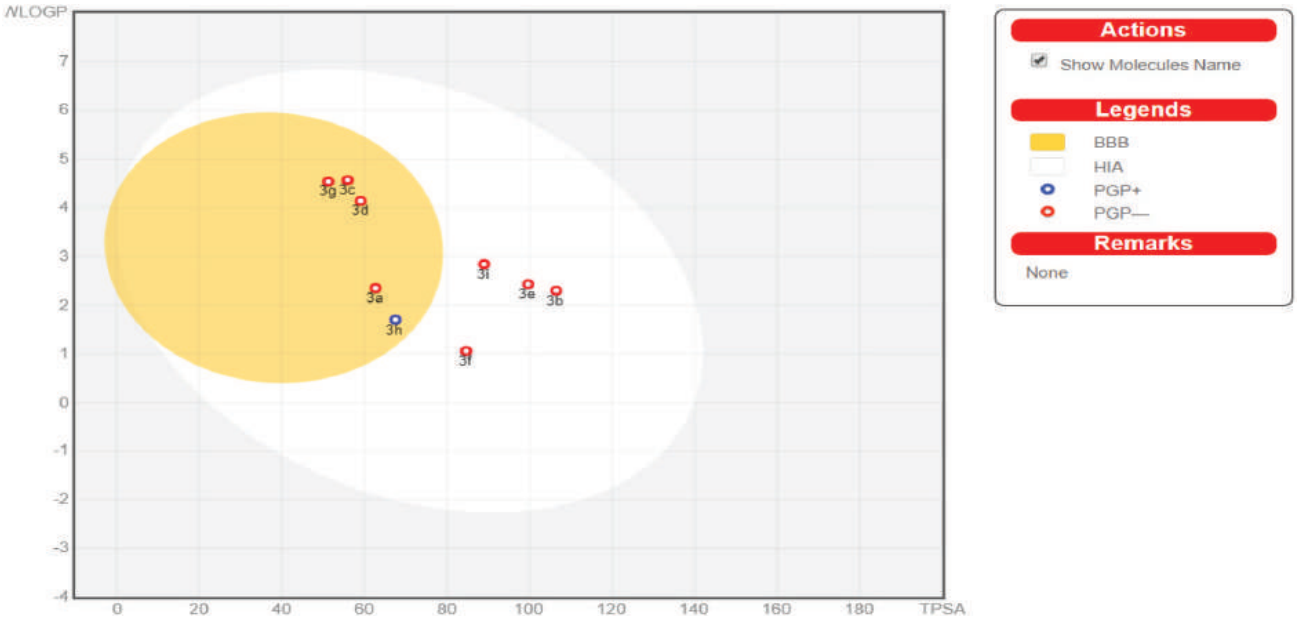


Figure 4. BOILED-Egg allows for evaluation of passive gastrointestinal absorption (HIA), brain penetration (BBB), and P-glycoprotein in the presence of the molecule (P-gp).

of the estimated solubility (ESOL) [38] model, and the resulting one was improved by Ali et al. [39]. Silicos-IT made SwissADME third pointer for molar solvency. Every single foreseen quality is the decimal logarithm of the molar solvency in water (log S) portrayed in Table 9. Agreement Log p is the normal estimation of all Log P assessed with different lipophilicity criteria (Table 10).

5. Structure-activity relationship

Depending upon the structural features, the newly synthesized molecules (**4a**–**4i**) could be divided into 3 discrete segments, as the diversely substituted central core quinoline ring A PEGylation center, ring B, and substitution at C-2/C-3 (Figure 5).

The exceptionally high anticancer activity of PEGylated quinoline derivatives is suggestive of the fact that the enhanced efficacy of molecules maybe because of the high mobility of the end terminal of the tethered PEG molecules, and due to the presence of inter-repulsive forces exerted between the hydrated PEG chains. There is a strong possibility of single PEG molecule conjugation with the approaching protein.

The data evident in Table 3 led to another noteworthy deduction, that the molecules with unsaturated centers at C-3 position exhibited good to moderate anticancer activity against the cancer cell lines. In contrast, the quinoline scaffold that amalgamated with the fused pyrazole and pyrimidine ring structures showed excellent anticancer activity against the SW620, MD468, and MD468-2 colon cancer cell lines. However, the imine derivatives of the PEGylated quinoline did

Table 9. Water solubility evaluation of the synthesized compounds.

Sr. No.	ESOL				Ali				Silicos			
	Log S	Solu. (mg/mL)	Solu. (mol/L)	Class	Log S	Solu. (mg/mL)	Solu. (mol/L)	Class	Log S	Solu. (mg/mL)	Solu. (mol/L)	Class
3a	–3.01	1.99E-01	9.76E-04	S	–3.14	1.47E-01	7.24E-04	S	–4.05	1.82E-02	8.93E-05	MS
3b	–2.37	9.35E-01	4.26E-03	S	–3.01	2.13E-01	9.73E-04	S	–2.98	2.31E-01	1.05E-03	S
3c	–5.06	2.84E-03	8.79E-06	MS	–5.5	1.02E-03	3.16E-06	MS	–6.88	4.27E-05	1.32E-07	PS
3d	–4.87	3.99E-03	1.35E-05	MS	–5.34	1.36E-03	4.59E-06	MS	–5.98	3.11E-04	1.05E-06	MS
3e	–2.68	4.79E-01	2.10E-03	S	–2.92	2.74E-01	1.20E-03	S	–4.39	9.28E-03	4.06E-05	MS
3f	–2.2	1.34E+00	6.31E-03	S	–1.98	2.21E+00	1.04E-02	VS	–4.19	1.38E-02	6.50E-05	MS
3g	–4.71	5.80E-03	1.96E-05	MS	–4.91	3.61E-03	1.22E-05	MS	–6.95	3.35E-05	1.13E-07	PS
3h	–2.6	4.68E-01	2.54E-03	S	–2.5	5.88E-01	3.19E-03	S	–3.85	2.57E-02	1.40E-04	S
3i	–3.71	5.83E-02	1.93E-04	S	–4.57	8.03E-03	2.66E-05	MS	–4.6	7.51E-03	2.49E-05	MS

Solu.: solubility; PS: poorly soluble; MS: moderately soluble; S: soluble; VS: very soluble.

Table 10. Lipophilicity evaluation of the synthesized compounds.

Sr. No.	iLOGP	XLOGP3	WLOGP	MLOGP	Silicos-IT Log P	Consensus Log P
3a	1.5	2.19	2.35	1.09	2.3	1.89
3b	1.4	1.18	2.3	0.41	3.13	1.68
3c	2.81	4.6	4.57	3.05	4.87	3.98
3d	2.48	4.38	4.14	2.93	3.95	3.58
3e	1.41	1.23	2.43	1.12	3.25	1.89
3f	1.03	0.63	1.06	1.11	1.8	1.13
3g	2.66	4.13	4.54	2.93	4.75	3.8
3h	0.98	1.47	1.7	1.35	1.78	1.46
3i	2.44	3.04	2.84	1.39	2.89	2.52

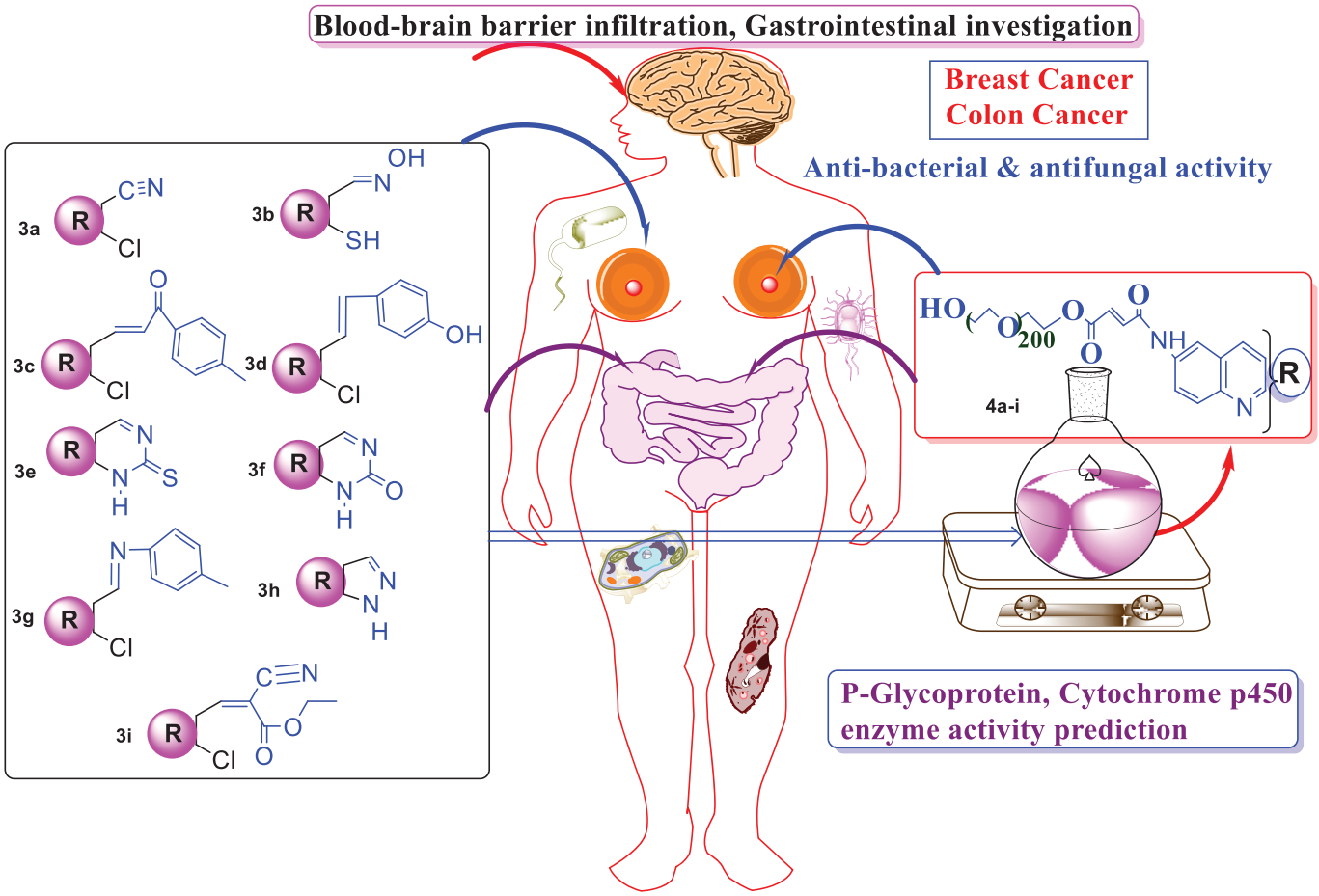


Figure 5. N-PEG quinoline scaffold derivatives.

not display significant activity. These annotations proposed that C-2 and C-3 played a vital role in the structure-activity relationship of compounds **4a**–**4i**.

Compounds **4a** and **4i** were found to be most potent amongst the synthesized compounds against the microbial strains of *E. Coli*. The rest of these compounds showed moderate to potent activities against *S. Aureus*. All of the compounds screened against *S. Aureus* showed moderate to potent activities, confirming the fact that the substituted quinoline, with an adjacent ring C like the cyano group and pyrazole, played a vital role in enhancing the efficacy of the compounds, thus modulating the antibacterial activity.

All of the compounds screened as antifungals showed moderate to potent activities. The synthesized PEGylated quinoline was found to possess moderate antifungal activity against *C. Albicans*.

6. Synthesis of 2- chloro-6-nitro-3-formilquinoline (1):[40]

To the solution of p-nitro acetanilide (5 mmol) in dry DMF (15 mmol) at 0–5 °C, $POCl_3$ (35 mmol) was added dropwise and stirred, and then the mixture was stirred at 80–90 °C for 16–19 h. The mixture was poured on to crushed ice, stirred for 5 min, and the resulting solid was filtered, washed well with water, and dried. The compound recrystallized from ethyl acetate and methanol m.p. 260–262 °C. Yield 86%. Color: brownish yellow.

IR (KBr, cm^{-1}); 1685, 1675, 1640.^{1}HNMR (DMSO-d_6); δ 7.90–7.91 (1H, q), 7.50–7.53 (1H, d, J= 14.24), 7.70–7.72 (1H, d, J = 8.96), 8.15 (1H, s), 9.74 (1H, s, CHO). ^{13}CNMR (DMSO-d_6); δ122.82, 123.25, 124.23, 125.13, 126.91, 142.33, 144.56, 146.33, 153.95, 190.26. MS (*m/z*): 236. Elemental analysis: ($C_{10}H_5ClN_2O_3$): calculated C: 50.76, H: 2.13, Cl: 14.98, N: 11.84, O: 20.29; found: C: 50.64, H: 2.8, Cl: 14.85, N: 11.73, O: 20.18.

6.1. Reduction of -NO_2 quinoline

Synthesis of 6-amino-2-chloroquinoline-3-carbaldehyde (2):

Dissolve sodium sulfide (2 g) in water (5–6 mL) was added to $NaHCO_3$ (0.7 g) in small portions and stirred. When the added $NaHCO_3$had dissolved, methanol (5–6 mL) was added and the reaction mixture was cooled to below 20 °C. Filtering

off of the precipitated sodium carbonate was performed with pump. The precipitate was then washed with a small amount of methanol. The filtrate was then used for further reactions.

Next, 2-chloro-6-nitro-3-formilquinoline (0.75 g) was dissolved in hot methanol (6 mL), added to the above solution containing sodium hydrogen sulfide, and shaken. The reaction mixture refluxed for 2 h. The reaction mixture was then allowed to cool and was then placed into ice water (20–40 mL) to filter the reduced compound, and it was then recrystallized from methanol. m.p.208–210 °C. Yield: 82%. Color: dark brown.

IR (KBr, cm^{-1}); 3458, 1675, 1620.^{1}HNMR (DMSO-d_6); δ 4.92 (2H, s, -NH_2), 7.52–7.53 (1H, d, J= 7.28), 7.64–7.66 (1H, d, J = 7.56), 7.80–7.84 (1H, q), 8.10 (1H, s), 9.51 (1H, s, CHO). ^{13}CNMR (DMSO-d_6); δ122.82, 123.25, 124.23, 125.13, 126.91, 142.33, 144.56, 146.33, 153.95, 190.26. MS (*m/z)*:206. Elemental analysis: ($C_{10}H_7ClN_2O$): calculated C: 58.13, H: 3.41, Cl: 17.16, N: 13.56, O: 7.74; found: C: 58.5, H: 3.30, Cl: 17.11, N: 13.43, O: 7.65.

6.2. Synthesis of 6-amino-2-chloroquinoline-3-carbonitrile (3a)

A suspension of 6-amino-2-chloroquinoline-3-carbaldehyde (1 mol) in 30% aq. ammonia was stirred for 15–25 min at room temperature, to this CAN was added at 0–2 °C, andthe reaction mixture was stirred for 2–3 h at 0–2 °C (after completion of the reaction monitored by TLC, the disappearance of the reddish-brown color of the reaction mixture in 30–40 min was observed), extracted with chloroform-ethyl acetate (7:3), dried over Na_2SO_4,and evaporated under reduced pressure to obtain the solid product of 6-amino-2-chloroquinoline-3-carbonitrile (**3a**). The solid product was crystallized with ethanol. m.p. 162 °C. Yield: 83%.Color: brown.

IR (KBr, cm^{-1}); 4365, 2115, 1650. ^{1}HNMR (DMSO-d_6); δ 4. 68 (2H, s, NH_2), 7.23–7.26 (1H, d, J= 12.4), 7.64 (1H, s), 7.80–7.84 (1H, q), 8.10–8.13 (1H, d, J = 9.56). ^{13}CNMR (DMSO-d_6); δ43.57, 105.36, 116.82, 123.25, 129.23, 131.13, 133.51, 138.56, 143.33, 153.95.MS (*m/z)*:203. Elemental analysis: ($C_{10}H_6ClN_3$): calculated C: 58.98, H: 2.97, Cl: 17.41, N: 20.64; found: C: 58.85, H: 2.9, Cl: 17.32, N: 20.58.

6.3. Synthesis of 6-amino-3-hydroxyiminomethylquinoline-2(1H)-thione (3b)

To the solution of 6-amino-2-chloro quinoline-3-carbaldehyde (1.5mmol) in dry DMF, fused sodium sulfide was added and stirred for 3–4 h at room temperature. Hydroxylamine hydrochloride and sodium acetate were further added with continued stirring for 4–5 h. On completion, the reaction mixture was poured into ice-cold water and the crude product of 6-amino-3-hydroxyiminomethylquinoline-2(1*H*)-thione (**3b**) was achieved, and purified by recrystallization from aq. ethanol. m.p. 168 °C.Yield: 78%. Color: yellow.

IR(KBr, cm^{-1}); 3465, 3455, 2725, 1675, 1215.^{1}HNMR (DMSO-d_6); δ3.76 (1H, SH), 4.87 (2H, s, NH_2), aromatic reg.: 6.40–6.80 (4H, m), 7.28 (1H, s, CH=N), 10.58 (1H, s, OH).^{13}CNMR(DMSO-d_6); δ113.36, 116.86, 123.35, 125.66, 134.29, 136.95, 145.63, 155.95, 185.45.MS (*m/z)*:219. Elemental analysis: ($C_{10}H_9ClN_3OS$): calculated C: 54.78, H: 4.14, N: 19.16, O: 7.30, S: 14.62; found: C: 54.60, H: 4.8, N: 19.12, O: 7.24, S: 14.53.

6.4. Synthesis of 3-(6-amino-2-chloroquinoline-3-yl)-1-p-tolylprop-2-en-1-one (3c)

A mixture of 6-amino-2-chloroquinoline-3-carbaldehyde (0.01 mol, 1.91 g) and4-methyl acetophenone in 40% ethanolic NaOH was stirred vigorously for 2 h and kept overnight at room temperature. The reaction mixture was poured onto crushed ice and acidified with 1:1 HCl. The solid 3-(6-amino-2-chloroquinoline-3-yl)-1-*p*-tolylprop-2-en-1-one (**3c**) was isolated. It was recrystallized using acetic acid and ethanol. m.p. 240 °C.Yield: 84%. Color: yellowish-white.

IR(KBr, cm^{-1}); 3435, 3015, 2980, 1685.^{1}HNMR (DMSO-d_6);δ 2.51 (3H, s, CH_3), 5.25 (2H, s, NH_2), 7.24–7.26 (1H, d, J= 9.12), 7.53–7.58 (3H, m), 7.84–7.86 (1H, d, J= 9.16), 8.04 (1H, s), (4H, m, Ben.), ^{13}CNMR(DMSO-d_6); δ24.53, 119.15, 123.35, 125.39, 129.15–129.33, 134.16, 136.94, 139.15, 141.13, 144.62, 148.15, 151.59, and 192.16 ppm, MS (*m/z)*:322. Elemental analysis: ($C_{19}H_{15}ClN_2O$): calculated C: 70.70, H: 4.68, Cl: 10.98, N: 8.68, O: 4.96: found: C: 70.62, H: 4.57, Cl: 10.88, N: 8.58, O: 4.91.

6.5. Synthesis of 4(2-(6-amino-2-chloroquinoline-3-yl)vinylphenol (3d)

A mixture of 6-amino-2-chloroquinoline-3-carbaldehyde (0.01 mol), p-cresol (0.01 mol), freshly distilled acetic anhydride (10 mL), acetic acid (10 mL), and sodium acetate (2 g) was heated and refluxed in an oil bath at 145 °C for 6–7 h. After cooling, the reaction mixture was poured onto crushed ice and left overnight. The precipitated product was filtered, dried, and crystallized from ethyl acetate-methanol. m.p. 168 °C. Yield: 83%. Color: brown.

IR(KBr, cm^{-1});3480, 3425, 3015. ^{1}HNMR (DMSO-d_6);δ 3.25 (2H, s, NH_2), 6.53–6.54 (1H, d, J= 3.64), 6.68–6.69 (1H, d, J= 2.00), 7.77–7.83 (2H, m, Ben.), 7.95–7.97 (1H, 1H, d, J= 8.96), 8.12–8.20 (2H, m, Ben.), 8.40–8.43 (1H, d, J= 8.96), 8.68 (1H, s), 10.29 (1H, s, OH). ^{13}CNMR (DMSO-d_6); δ118.23, 123.05, 127.51, 129.03, 131.13, 133.51, 135.29, 141.31, 143.33, 148.38, 159.35. MS (*m/z)*:296. Elemental analysis: ($C_{17}H_{13}ClN_2O$): calculated C: 68.81, H: 4.42, Cl: 11.95, N: 9.44, O: 5.39: found: C: 68.74, H: 4.36, Cl: 11.86, N: 9.37, O: 5.31.

6.6. Synthesis of 7-aminopyrimido(4,5-b)quinoline-2(1H)thione (3e)

6-amino-2-chloroquinoline-3-carbaldehyde (0.002 mol) and (0.002 mol) were dissolved in 15 mL of glacial acetic acid and refluxed for 15 h. On completion, the reaction mixture was poured onto crushed ice and neutralized with diluted NaOH. The solid product, 7-aminopyrimido-(4,5-b)-quinoline-2(1 H)thione (**3e**), was separated out. m.p. 272 °C.Yield: 82%. Color: yellowish-brown.

IR (KBr, cm^{-1}); 3396, 3440, 1655, 1235. ^{1}HNMR(DMSO-d_6); δ 5.49 (2H, s, NH_2), 7.83–8.50 (aromatic reg. 5H, m), 11.50 (1H, s, NH).^{13}CNMR (DMSO-d_6;115.12, 120.36, 122.15, 129.13, 132.23, 135.55, 142.13, 159.56, 161.59, 182.25. MS (*m/z)*:228. Elemental analysis: ($C_{11}H_8N_4S$): calculated C: 57.88, H: 3.53, N: 24.54, S: 14.05: found: C: 57.79, H: 3.46, N: 24.48, S: 13.95.

6.7. Synthesis of 7-aminopyrimido(4,5-b)quinoline-2(1H)one (3f)

6-amino-2-chloroquinoline-3-carbaldehyde (0.002 mol) and urea were dissolved in 15 mL of glacial acetic acid and refluxed for 15 h. On completion (inferred through TLC), the mixture was poured onto crushed ice and neutralized with diluted NaOH. The solid product, 7-aminopyrimido (4, 5-b) quinoline-2(1 H)one (**3f**), was separated. m.p. 247 °C. Yield: 78%. Color: brownish-yellow.

IR (KBr, cm^{-1}); 3485, 3440, 1735, 1640. ^{1}HNMR (DMSO-d_6); δ 6.62 (2H, s, NH_2), 7.46–8.83 (aromatic reg. 5H, m), 11.32(1H, s, NH).^{13}CNMR (DMSO-d_6); 115.02, 118.62, 121.81, 128.11, 133.53, 135.65, 149.64, 156.95, 161.55, 181.52. MS (*m/z)*:212. Elemental analysis: ($C_{11}H_8N_4O$): calculated C: 62.26, H: 3.80, N: 26.40, O: 7.54: found: C: 62.18, H: 3.71, N: 26.32, O: 7.48.

6.8. Synthesis of 3-(P-tolylimino)methyl-2-chloroquinoline-6-amine (3g)

To the solution of 6-amino-2-chloroquinoline- 3-carbaldehyde (1mol) and p-toluene in 15 mL methanol was added 1 mL of acetic acid. The reaction mixture was refluxed for 5–6 h. Completion of the reaction was inferred through TLC, after which, it was cooled, the precipitate formed, and the product of 3-(*P*-tolylimino)methyl-2-chloroquinoline-6 amine (**3g**) separated. It was filtered off, dried, and crystallized with ethanol. m.p. 176 °C. Yield: 86%. Color: darkbrown.

IR (KBr, cm^{-1}); 3460, 1650, 1635. ^{1}HNMR (DMSO-d_6); δ 2.50 (3H, s, CH_3), 5.24 (2H, s, NH_2), 6.06–9.27 (aromatic reg. 9H, m), ^{13}CNMR (DMSO-d_6); 24.35, 118.12, 120.05, 122.35, 125.15, 129.03, 131.13, 134.23, 136.95, 142.13, 144.62, 146.15, 148.56, 195.16. MS (*m/z)*:296. Elemental analysis: ($C_{17}H_{14}ClN_3$): calculated C: 69.03, H: 4.77, Cl: 11.99, N: 14.21: found: C: 68.97, H: 4.69, Cl: 11.91, N: 14.18.

6.9. Synthesis of 1H-pyrazolo(3,4-b)quinoli-6-amine (3h)

6-amino-2-chloroquinoline-3-carbaldehyde (0.02 mol) was refluxed with 5 mL (excess) of NH_2-NH_2 in ethanol for 5–6h. Their action mixture was then cooled and poured into ice-cold water. The solid that formed was filtered, washed with water, and dried. It was crystallized with ethyl acetate. m.p. 288 °C.Yield: 76%. Color: yellowish-brown.

IR (KBr, cm^{-1}); 3475, 3318–3325, 1650. ^{1}HNMR (DMSO-d_6); δ 3.87 (2H, s, NH_2), 6.32 (1H, s), 6.87 (1H, s), 6.60–6.62 (2H, m), 7.93 (1H, s), 10.43 (1H, s, NH). ^{13}CNMR (DMSO-d_6); 120.13–120.32, 122.25, 130.31–131.23, 132.95, 135.13, 139.23–139.59, 141.11, 142.55, 154.13, 182.25.MS (*m/z)*:184. Elemental analysis: ($C_{10}H_8N_3$): calculated C: 65.21, H: 4.38, N: 30.40: found: C: 65.13, H: 4.28, N: 30.31.

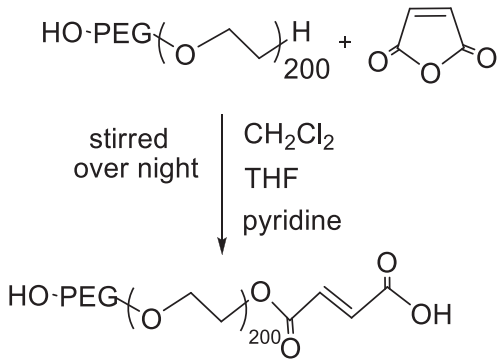
6.10. Synthesis of (Z)-ethyl-3-(6-amino-2-chloroquinoline-3-yl)-2-cyanoacrylate (3i)

To the solution of 6-amino-2-chloroquinoline-3-carbaldehyde (0.005 mol) and ethyl cyanoacetate in 30 mL ethanol, triethylamine was added. The reaction mixture was refluxed for 3 h. On completion of the reaction, the solution was poured into ice-cold water, and a solid product of (Z)-ethyl-3-(6-amino-2-chloroquinoline-3-yl)-2-cyanoacrylate (**3i**) was separated. It was washed with cold water and dried, and then recrystallized with methanol. m.p.122 °C. Yield: 86%. Color: white.

IR(KBr, cm^{-1}); 3505, 3022, 2985, 2115, 1720.^{1}HNMR(DMSO-d_6); δ 1.21–1.38 (3H, m, CH_3), 3.09–3.14 (2H, m, CH_2), 4.20 (2H, s, NH_2), 6.34 (1H, s, CH=C), 6.59–8.40 (aromatic reg. 4H, m), ^{13}CNMR (DMSO-d_6);18.51, 96.24, 114.24, 120.51, 128.11, 130.23, 132.85, 141.53, 143.35, 149.64, 156.91, 168.52. MS (*m/z)*:302. Elemental analysis: ($C_{15}H_{12}ClN_3O_2$): calculated C: 59.71, H: 4.01, Cl: 11.75, N: 13.93, O: 10.61: found: C: 59.63, H: 3.93, Cl: 11.68, N: 13.85, O: 10.54.

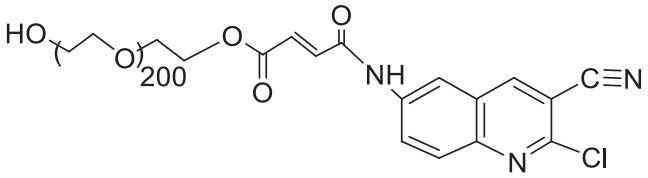
7. Synthesis of hydroxy carboxy polyethylene glycol (HO-PEG200COOH)

Polyethylene glycol (5 mL, 0.028 mol, 200 g/mol) was dissolved in 20 mL of dry CH_2Cl_2. To this solution was added THF containing maleic anhydride (0.056 mol, 0.54 mg) and pyridine (0.056 mol, 0.46 mL). After stirring overnight at room temperature, the reaction was completed, as indicated by TLC (methanol:ethyl acetate, 7:3) (no anhydride was left and there was the detection of a single polar PEG compound). The monoacid derivative of $(polyethylene\ glycol)_{200}$ was used without purification.



7.1. Synthesis of resin via N-terminal of PEGylated-6-amino-2-chloroquinoline-3-carbonitrile (4a) like syrupy material
The monoacid derivative of hydroxy carboxy polyethylene glycol (HO-PEG_{200}COOH) (0.028 mol) was activated with a 1:2 molar equivalent of 6-amino-2-chloroquinoline-3-carbonitrile (**3a**) (0.046 mol) and N, N-dicyclocarbidiimide (0.046 mol) was dissolved in dichloromethane. The solution was stirred over night at room temperature. This reaction mixture appeared like a resin when dried under a vacuum. This syrupy resin was dissolved in 15 mL of acetone. Later the white precipitate of DCU that appeared was discarded and the filtrate was collected. The final filtrate was evaporated to afford compound **4a**. TLC in (methanol:ethyl acetate 7:3) was performed to check for the presence of DCU. It showed a negative result. The IR spectra confirmed this negative result. A negative dye test indicated complete amino group capping.

The resin was dried in a vacuum for IR, H^1NMR, C^{13}NMR, and mass spectral analysis. At this stage, the resin did not stick to the glass wall anymore. The IR spectrum of the resin showed the characteristic absorption band of the PEG ether backbone (1120 cm^{-1}) and absorption bands at 1760 and 1685 cm^{-1} for the ester and amid bond, respectively (C=O).



Color: yellow syrupy material, IR (KBr, cm^{-1}); 3475, 2115, 1685.^{1}HNMR (DMSO-d_6);δ 3.04–3.67 (m, PEG)δ 4.72 (1H, s, -NH), 6.56 (1H, s),6.85–6.87 (1H, q), 7.25 (1H, s),7.50–7.52 (1H, d, J= 8.36), ^{13}CNMR (DMSO-d_6); δ47.57, 55.11, 55.53, 63.52, 68.53, 107.80, 116.12, 123.59, 126.33, 131.16, 132.26, 138.65, 143.36, and 149.53: MS (*m/z)*:485.

7.2. Synthesis of PEGylated-6-amino-3-hydroxyiminomethylquinoline-2(1H)-thione (4b).
Color: dark yellow syrupy material, IR (KBr, cm^{-1}); 3440, 2735, 1655, 1230.^{1}HNMR (DMSO-d_6);δ 3.49–3.76 (m, PEG), δ 4.01 (1H, s -SH), 5.27 (1H, s, -NH), 6.25(1H, s), 6.63 (1H, s),7.25–7.28 (1H, q), 8.56 (1H, s),8.042–8.047 (1H, d, J= 2.08):^{13}CNMR (DMSO-d_6); δ41.37, 46.23–46.57, 54.23–55.33, 61.21, 64.55, 112.12, 116.36, 123.11, 125.13, 134.45, 136.21, 136.25, 145.13, 152.24, and 185.51: MS (*m/z)*:497.

7.3. Synthesis of PEGylated-3-(6-amino-2-chloroquinoline-3-yl)-1-p-tolylprop-2-en-1-one (4c)
Color: yellowish-white syrupy material, IR (KBr, cm^{-1}); 3025. 2965. 1655.^{1}HNMR (DMSO-d_6);δ 2.22 (3H, s, -CH_3), 3.52–4.33 (m, PEG), δ 5.29 (1H, s, -NH), 6.59–6.61 (1H, d, J= 9.72), 6.82 (2H, s), 7.28–7.31 (4H, m, Ben.), 7.67–7.71 (2H, m), 8.01–8.03 (1H, d, J= 10.36). ^{13}CNMR (DMSO-d_6); δ28.34, 45.65, 46.93–50.54, 53.39, 62.55, 119.13, 124.35, 126.43, 129.15–129.63, 143.11, 136.90, 138.55, 140.13, 144.32, 148.15, 153.21, and 190.41: MS (*m/z)*:602.

7.4. Synthesis of PEGylated-4(2-(6-amino-2-chloroquinoline-3-yl)vinyl phenol (4d)
Color: yellowish-brown syrupy material, IR (KBr, cm^{-1}); 3465, 3020, 1635.^{1}HNMR (DMSO-d_6); δ 3.31–4.42 (m, PEG), δ 5.27 (1H, s, -NH), 6.26 (1H, s), 6.70 (1H, s), 7.28–7.31 (2H, m), 7.66–7.78(4H, m, Ben.), 8.57–8.59 (1H, d, J= 10.48),8.11–8.13 (1H, d, J= 9.12), 10.67 (1H, s, -OH).^{13}CNMR (DMSO-d_6); δ25.51, 29.93, 33.77, 41.03–45.90, 46.37, 118.73, 121.15, 127.51, 129.03, 131.13, 134.57, 137.22, 140.13, 142.39, 153.81, and 159.45: MS (*m/z)*:576.

7.5. Synthesis of PEGylated-7-aminopyrimido(4,5-b)quinoline-2(1 H)thione (4e)
Color: brownish-yellow syrupy material, IR (KBr, cm^{-1}); 3425, 1665, 1245.^{1}HNMR (DMSO-d_6); δ 3.04–3.67 (m, PEG), 4.72 (1H, s, -NH), 6.26 (1H, s), 6.73–6.78 (2H, m), 7.26 (1H, s), 7.57 (1H, s), 10.67 (1H, s, -OH). ^{13}CNMR (DMSO-d_6); δ29.65, 32.61–36.45, 42.93, 46.55, 115.62, 120.61, 122.52, 129.33, 132.93, 136.55, 142.43, 159.65, 164.49, and 185.15: MS (*m/z)*:544.

7.6. Synthesis of PEGylated-7-aminopyrimido(4,5-b)quinoline-2(1 H)one (4f)
Color: brownish-yellow syrupy material, IR (KBr, cm^{-1}); 3420, 1720, 1650. ^{1}HNMR (DMSO-d_6); δ 3.04–3.65 (m, PEG), 5.25 (1H, s, -NH), 6.51 (1H, s), 6.78–6.78 (2H, q),7.12 (1H, s), 7.40 (1H, s), 10.26 (1H, s, -OH). ^{13}CNMR (DMSO-d_6); δ28.68, 32.63–36.48, 44.35, 46.85, 114.32, 120.61, 122.50, 128.13, 132.53, 146.93, 195.65, 161.51, and 181.52: MS (*m/z)*:528.

7.7. Synthesis of PEGylated-3-((P-tolylimino)methyl-2-chloroquinoline-6-amine (4g)
Color: brownish-yellow syrupy material, IR (KBr, cm^{-1}); 1655, 1640.^{1}HNMR (DMSO-d_6); δ 2.09 (3H, s, -CH_3), 3.51–4.27 (m, PEG), 4.81 (1H, s, -NH), 6.98–7.49 (9H, m, aromatic reg.). ^{13}CNMR (DMSO-d_6); δ24.35, 35.34, 39.27, 44.03–49.90, 55.43, 116.26, 120.65, 122.35, 126.15, 129.63, 131.19, 136.23, 144.69, 146.42, 148.61, and 159.11: MS (*m/z)*:606.

7.8. Synthesis of PEGylated-1H-pyrazolo(3,4-b)quinoli-6-amine (4h)
Color: brownish-yellow syrupy material, IR (KBr, cm^{-1}); 3445, 3325, 1665.^{1}HNMR (DMSO-d_6); δ 3.42–4.31 (m, PEG), 5.28 (1H, s, -NH),6.27 (1H, s) 6.59–8.02 (4H, m, aromatic reg.), 10.31 (1H, s, -NH). ^{13}CNMR (DMSO-d_6); δ29.91, 36.65, 39.91–43.45, 49.39, 52.54, 120.31–120.39, 122.52, 130.35–131.33, 132.91, 135.53, 139.32–139.55, 141.18, 142.55, 156.53, and 182.25: MS (*m/z)*:463.

7.9. Synthesis of PEGylated-(Z)-ethyl 3-(6-amino-2-chloroquinoline-3-yl)-2-cyanoacrylate (4i)
Color: yellow syrupy material, IR (KBr, cm^{-1}); 3025, 2975, 2130, 1690.^{1}HNMR (DMSO-d_6);δ 1.68 (3H, -CH_3), 3.07 (2H, -CH_2), 3.52–4.33 (m, PEG), δ 5.29 (1H, s, -NH), 6.82 (1H, s, CH=C),7.28–8.03 (4H, m, aromatic reg.). ^{13}CNMR (DMSO-d_6); δ18.15, 34.36, 36.54–40.35, 43.85, 46.50, 55.98, 90.85, 114.42, 120.21, 128.12, 139.23, 136.89, 141.53, 143.38, 151.64, 154.45, and 168.52: MS (*m/z)*:581.

Acknowledgments
The authors are thankful to the Department of Pharmacy, Nagpur for the IR spectral analysis, and SAIF, Chandigarh, for the ^{1}H NMR spectral analysis. We are grateful to SAIF, Pune University, for the mass spectral analysis of all of the newly synthesized compounds. We extend special thanks to Dr. Sandhya Saoji for the microbial analysis.

References

1. Herman S, Hoofman G, Schacht E. Polyethylene glycol with reactive endgroups: I. Modification of Protein. Journal of Bioactctive and Computible Polymers 1995; 10: 145-187.
2. Zalipsky S. Chemistry of polyethylene glycol conjugates with biologically active molecules. Bioconjugate Chemistry 1995; 16 (2-3): 157-182.
3. Allen TM. The use of glycolipids and hydrophilic polymers in avoiding rapid uptake of liposomes by the mononuclear phagocyte system. Advance Drug Delivery Review 1994; 13 (3): 285-309.
4. Woodle MC, Lasic DD. Sterically stabilized liposomes. Biochimica et Biophysica (BBA) Acta- Reviews on Biomembranes 1992; 1113: 171-199.
5. Blume G, Cevc G, Crommelin MD, Bakker-Woudenberg IA, Kluft C et al. Specific targeting with poly (ethylene gycol)-modified liposomes: coupling of homing devices to the end of the polymeric chains combines effective target binding with long circulation times. Biochimica et Biophysica (BBA) Acta-Reviews on Biomembranes1993; 1149: 180-184.
6. Chandrasekhar S, Narsihmulu C, Sultana SS, Reddy NR. Poly(ethylene glycol) (PEG) as a reusable solvent medium for organic synthesis. Application in the Heck reaction. Organic Letters 2002; 4: 4399-4401.
7. Jia Z, Zhang H, Huang J. Synthesis of poly(Ethylene glycol) with sulfadiazine and chlorambucil end groups and investigation of its antitumor activity. Bioorganic & Medicinal Chemistry Letters 2003; 13 (15): 2531-2534.
8. Coessens V, Schacht EH, Domurado D. Synthesis and in vitro stability of macromolecular prodrugs of norfloxacin. Journal of Controlled Release 1997; 47: 283-291.
9. Roseeuw E, Coessens V, Schacht E, Vrooman B, Domurado D et al. Polymeric prodrugs of antibiotics with improved efficiency. Journal of Materials Science: Materials in Medicine 1999; 10: 743-746.
10. Yang M, Santerre P. Utilization of quinolone drugs as monomers: characterization of the synthesis reaction products for poly(norfloxacin diisocyanatododecane polycaprolactone). Biomacromolecules 2001; 2 (1): 134-141.
11. Caliceti P, Salmaso S, Semenzato A, Carofiglio T, Fornasier R et al. Synthesis and physicochemical characterization of folate-cyclodextrin bioconjugate for active drug delivery. Bioconjugate Chemistry 2003; 14 (5): 899-908.
12. Dube D, Blouin M, Brideau C, Chan CC, Desmarais S et al. Quinolines as potent 5-lipoxygenase inhibitors: synthesis and biological profile of L-746,530. Bioorganic and Medicinal Chemistry Letters 1998; 8 (10): 1255-1260.

13. Gupta R, Gupta AK, Paul S, Somal P. Microwave-assisted synthesis and biological activities of some 7/9-substituted-4-(3-alkyl/aryl-5,6-dihydro-s-traizolo[3,4-b][1,3,4]thiadiazol-6-yl)-tetrazolo[1,5-a]quinolines. Indian Journal of Chemistry Section-B 2000; 39B: 847-852.

14. Gupta R, Gupta AK, Paul S, Kachroo PL. Synthesis of 3, 4-dihidropyrimidin-2 (1H)-ones. Indian Journal of Chemistry Section-B. 1998; 37B: 1211-1213.

15. Leenders F. PEGylation technology and biopharmaceuticals. Biopharmaceuticals 2006; 39-40.

16. Veronese F, Mero A. The impact of PEGylation on biological therapies. BioDrugs 2008; 22 (5): 315-329.

17. Lipinski CA, Lombardo F, Dominy BW, Feeney PJ. Experimental and computational approaches to estimate solubility and permeability in drug discovery and development settings. Advance Drug Delivery Review 2001; 46 (1-3): 3-26.

18. Gaidhane MK, Ghatole AM, Lanjewar KR. Synthesis of chromone functionalized chitosan polymer: application/screening of its physical parameters. Polymer Science Series B 2020; 62(3): 1-12.

19. Roberts MJ, Bentley MD, Harris JM. Chemistry for peptide and protein PEGylation. Advance Drug Delivery Review 2002; 54 (4): 459-476.

20. Harris JM, Liu Y, Chai S, Andrews MD, Vederas JC. Modification of the Swern oxidation: use of a soluble polymer-bound, recyclable, and odorless sulfoxide. The Journal of Organic Chemistry 1998; 63 (7): 2407-2409.

21. Wipf P, Venkatraman S. An improved protocol for azole synthesis with PEG-supported Burgess reagent. Tetrahedron Letters 1996; 37: 4659-4662.

22. Wentworth JP, Vandersteen AM, Janda KD. Poly(ethylene glycol) (PEG) as a reagent support: the preparation and utility of a PEG–triarylphosphine conjugate in liquid-phase organic synthesis (LPOS). Chemical Communications 1997; 8: 759-760.

23. Aghahosseini H, Ramazani A, Taran J, Slepokura K, Lis T. Heteroaromatic aldehydes with unprecedented catalytic performance in selective radical reactions: synthesis of α-aminophosphonate scaffolds. Asian Journal of Organic Chemistry 2019; 8 (8): 1519-1527.

24. Hosseinzadeh Z, Razzaghi-Asl N, Ramazani A, Aghahosseini A, Ramazani A. Synthesis, cytotoxic assessment, and molecular docking studies of 2,6-diaryl-substituted pyridine and 3,4- dihydropyrimidine-2(1H)-one scaffolds. Turkish Journal of Cemistry 2020; 44 (1): 194-213.

25. Hosseinzaedeh Z, Ramazani A, Razzaghi-Asl NKS, Lis T. Boric acid as an efficient and green catalyst for the synthesis of 2-amino-4,6-diarylnicotinonitrile under microwave irradiation in solvent-free conditions. Turkish Journal of Chemistry 2019; 43 (2): 464-474.

26. Ghatole AM, Lanjewar KR, Gaidhane MK. Antimicrobial activities; ionic liquid and microwave assisted synthesis of ring-substituted 3-(3-bromo-4-oxo-4h-chromen-2-yl)-4h-chromen-4-one. World Journal of Pharmaceutical Research 2014; 3 (3): 4336-4350.

27. Ghatole AM, Lanjewar KR, Gaidhane MK, Hatzade KM. Evaluation of substituted methyl cyclohexanone hybrids for anti-tubercular, anti-bacterial and anti-fungal activity: Facile syntheses under catalysis by ionic liquids. Spectrochimica Acta Part A: Molecular and Biomolecular Spectroscopy 2015; 151: 515-524.

28. Ghatole AM, Lanjewar KR, Hatzade KM, Gaidhane MK. A comparative synthesis of ring-substituted 3-(3-bromo-4-oxo-4h-chromen-2-yl)-4h-chromen-4-one. International Journal of Researches in Biosciences, Agriculture & Technology 2015; 1: 89-99.

29. Ghatole AM, Lanjewar KR, Gaidhane MK. Synthesis and anti-microbial activity of some substituted bis[2-((e)-2-(4- benzylideneamino) thiazol-4-yl)-4-methylphenol] metal complexes. International Journal of Pharmacy and Pharmaceutical Sciences. 2014; 6 (2): 142-146.

30. Ghatole AM, Gaidhane MK, Lanjewar KR, Hatzade KM. Pharmacokinetics, drug-likeness, medicinal properties, molecular docking analysis of substituted β-lactams synthesized via [Bmim][PF_6]/[Et_3NH]$^+$[HSO_4]$^-$ catalyzed coupling reaction. Chemistry: Bulgarian Journal of Science Education 2020; 29 (2): 206-244.

31. Daina A, Michielin O, Zoete V. SwissADME: a free web tool to evaluate pharmacokinetics, drug-likeness and medicinal chemistry friendliness of small molecules. Scientific Reports 2017; 7: 42717.

32. Ghose AK, Viswanadhan VN, Wendoloski JJ. A knowledge-based approach in designing combinatorial or medicinal chemistry libraries for drug discovery. 1. A qualitative and quantitative characterization of known drug databases. Journal of Combinatorial Chemistry 1999; 1 (1): 55-68.

33. Egan WJ, Merz KM, Baldwin JJ. Prediction of drug absorption using multivariate statistics. Journal of Medicinal Chemistry 2000; 43 (21): 3867-3877.

34. Veber DF, Johnson SR, Cheng HY, Smith BR, Ward KW et al. Molecular properties that influence the oral bioavailability of drug candidates. Journal of Medicinal Chemistry 2002; 45 (12): 2615-2623.

35. Muegge I, Heald SL, Brittelli D. Simple selection criteria for drug-like chemical matter. Journal of Medicinal Chemistry 2001; 44 (12): 1841-1846.

36. Brenk R, Schipani A, James D, Krasowski A, Gilbert IH et al. Lessons learnt from assembling screening libraries for drug discovery for neglected diseases. ChemMedChem 2008; 3 (3): 435-44.

37. Ogu GC, Maxa JL. Drug interaction due to cytochrome P450. Baylor University Medical Center Proceedings. 2000; 13 (4): 421-423.

38. Delaney JS. Esol: Estimating aqueous solubility directly from molecular structure. Journal of Chemical Information and Computer Sciences 2004; 44 (3): 1000-1005.

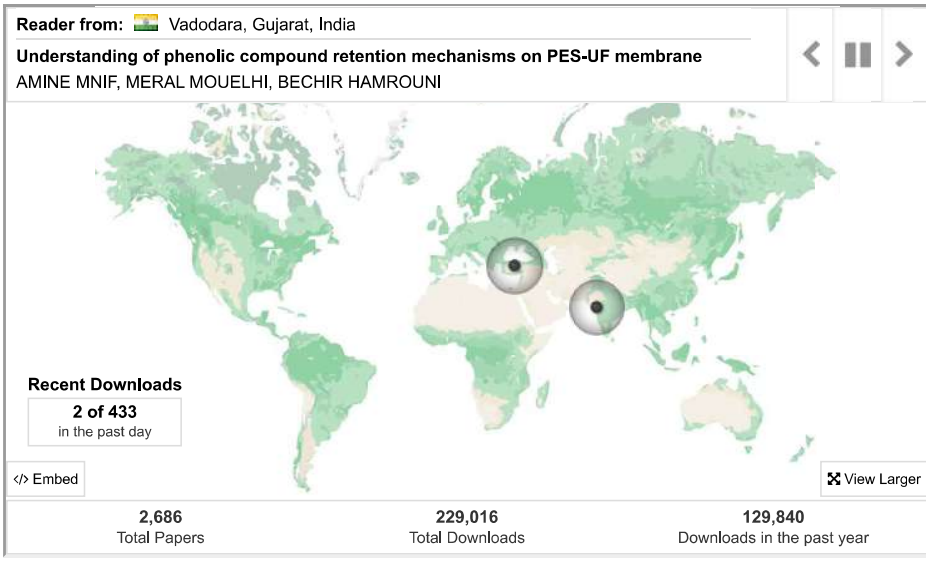
39. Fagerberg JH, Karlsson E, Ulander J, Hanisch G, Bergstrom CAS. Computational prediction of drug solubility in fasted simulated and aspirated human intestinal fluid. Pharmaceutical Research 2015; 32 (2): 578-589.

40. Gaidhane MK, Ghatole AM, Lanjewar KR. Novel synthesis and antimicrobial activity of novel schiff base derived quinoline and their β-lactam derivatives. International Journal of Pharmacy Pharmaceutical Sciences 2013; 5 (3): 421-426.

ACADEMIC JOURNALS
Published by the Scientific and Technological Research Council of Turkey

Turkish Journal of Chemistry (https://journals.tubitak.gov.tr/chem)

(https://journals.tubitak.gov.tr) (https://www.tubitak.gov.tr/en)
Follow (https://network.bepress.com/api/follow/subscribe?publication=ZWI1N2I1YWE1MGE5NDg2MTZlMzk1MzkwZDE1NjEzZDE%3D&format=html)



The Turkish Journal of Chemistry *is an international, bi-monthly, peer-reviewed, diamond* open-access journal by the Scientific and Technological Research Council of Turkey (TUBITAK) - Turkish Academic Network and Information Center (ULAKBIM). ***Turk J Chem*** publishes manuscripts on various fields of research in chemistry and chemical engineering. The journal is published in February, April, June, August, October, and December. The journal has been indexed in **Scopus since 1996 and in PMC since 2020.**

ISSN: 1300-0527

EISSN: 1303-6130

Journal Metrics

Impact Factor (2023) 1.3

5-Year Impact Factor 1.2

The Turkish Journal of Chemistry is pleased to announce its support to the United Nations Sustainable Development Goals (UN SDGs) (https://sdgresources.relx.com/) ; the journal explicitly concentrates on three out of 17 goals: affordable and clean energy, industry, innovation and infrastructure, clean water and sanitation.

Current Issue: Volume 48, Number 4 (2024)

Cover and Contents

Cover and Contents (https://journals.tubitak.gov.tr/chem/vol48/iss4/1)

Research Articles

LaCoO3 is a promising catalyst for dry reforming of benzene used as a surrogate of biomass tar (https://journals.tubitak.gov.tr/chem/vol48/iss4/10)
BAŞAR ÇAĞLAR and DENİZ ÜNER
Pages 643-658

Synthesis and Characterization of New Hexahydroquinoline Derivatives, Evaluation of Their Cytotoxicity, Intracellular ROS Production and Inhibitory Effects on Inflammatory Mediators (https://journals.tubitak.gov.tr/chem/vol48/iss4/11)
EZGİ PEHLİVANLAR, DENİZ ARCA ÇAKIR, SONIA SANAJOU, HÜLYA TEZEL YALÇIN, TERKEN BAYDAR, PINAR ERKEKOĞLU, HANİFE AVCI, and RAHİME ŞİMŞEK
Pages 659-675

Identification of blood at simulated crime scenes using silver nanoparticles with SERS (https://journals.tubitak.gov.tr/chem/vol48/iss4/12)
UĞUR KÖROĞLU, NECDET SAĞLAM, UĞUR TAMER, RAMAZAN AKCAN, İSMAİL HAKKI BOYACI, and EYLÜL EVRAN
Pages 676-690

Synthesis and photooxygenation of 3-(p-substituted phenyl)-3a,8a-dihydro-4H-cyclohepta[d]isoxazoles: Facial selectivity (https://journals.tubitak.gov.tr/chem/vol48/iss4/13)
MAHİRE EMEL OLGUN, ABDULLAH MENZEK, ERTAN ŞAHİN, and YASİN ÇETİNKAYA
Pages 691-700

Preparation of a chiral hyperbranched polymer based on cinchona alkaloids and investigation of its catalytic activity in asymmetric reactions (https://journals.tubitak.gov.tr/chem/vol48/iss4/2)
RAFIQUL ISLAM, MOHAMMAD SHAHID ULLAH, ABDUS SALAM, and SHINICHI ITSUNO
Pages 512-523

Synthesis, characterization, and physico-chemical aspects of a new PVC-based quaternary triethanol ammonium chloride anionite for tungsten recovery (https://journals.tubitak.gov.tr/chem/vol48/iss4/3)
BAHIG ATIA
Pages 524-549

Exploring the efficiency of nitrogenated carbon quantum dots/TiO2 S-scheme heterojunction in photodegradation of ciprofloxacin in aqueous environments (https://journals.tubitak.gov.tr/chem/vol48/iss4/4)
YILMAZ ATEŞ, ZAFER EROĞLU, ÖZKAN AÇIŞLI, ÖNDER METİN, and SEMRA KARACA
Pages 550-567

Liquefaction optimization of grape pulp using response surface methodology for biopolyol production and bio-based polyurethane foam synthesis (https://journals.tubitak.gov.tr/chem/vol48/iss4/5)
FURKAN ÇOLAKOĞLU, EMRE AKDOĞAN, and MURAT ERDEM
Pages 568-581

New imidazolidindionedioximes and their Pt(II) complexes: Synthesis and investigation of their antitumoral activities on breast cancer cells (https://journals.tubitak.gov.tr/chem/vol48/iss4/6)
EMRAH KARAHAN, TUĞBA GENÇOĞLU KATMERLİKAYA, EMEL ÖNAL, AYDAN DAĞ, AYŞE GÜL GÜREK, and VEFA AHSEN
Pages 582-596

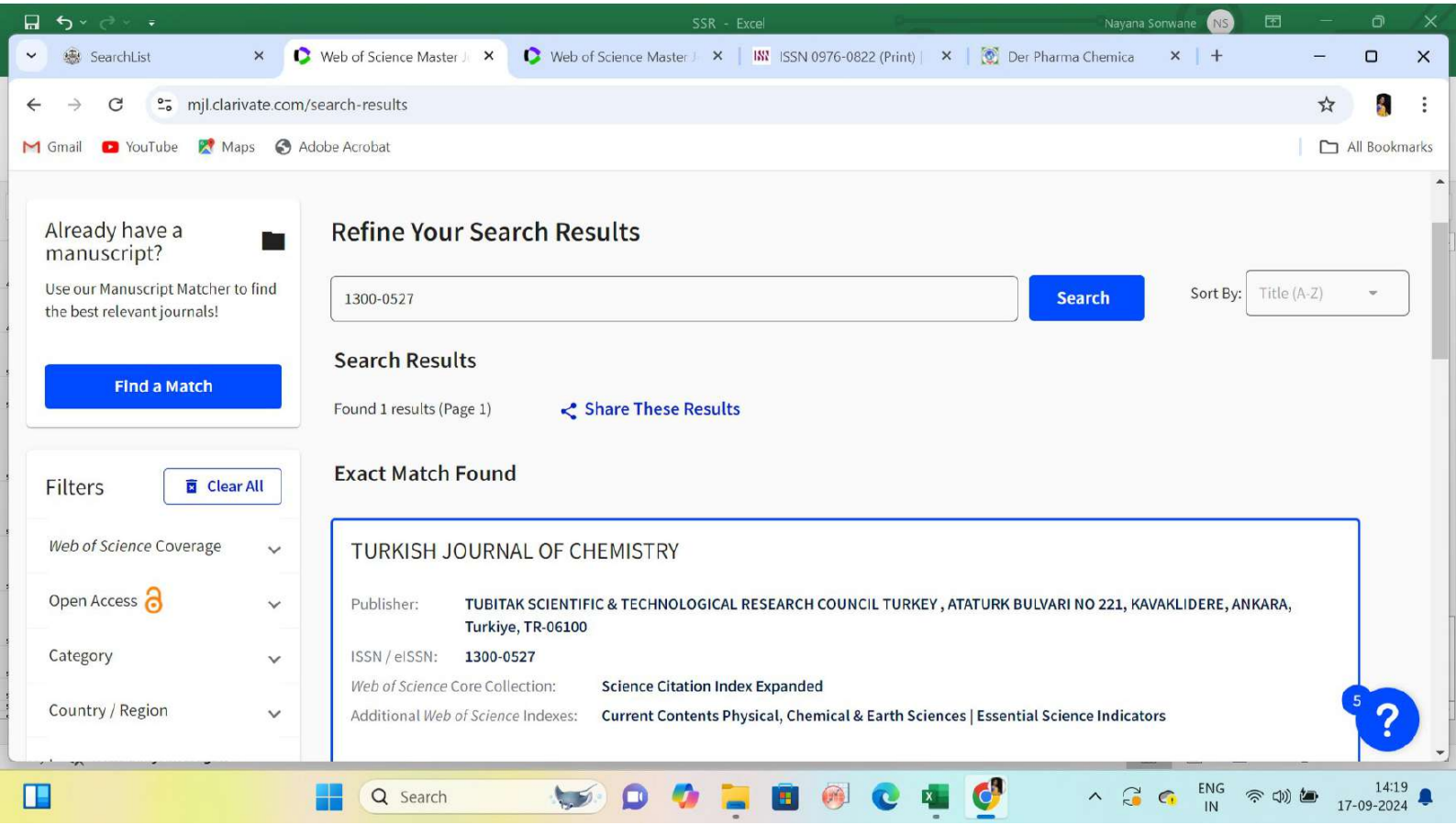
Synthesis of 3-Methyl-3-Buten-1-Ol by Supercritical CO2 in Coordination with HZSM-5 Catalyzed Formaldehyde-Isobutene Prins Reaction (https://journals.tubitak.gov.tr/chem/vol48/iss4/7)
HANG YUAN, GUI-PING CAO, and HUI LV
Pages 597-619

Magnetic solid-phase extraction technique based on Fe3O4@coPPy-PTH nanocomposite for extraction of cobalt, chromium, and nickel prior to determination by micro-sample injection system-flame atomic absorption spectrometry in alcoholic and nonalcoholic beverages (https://journals.tubitak.gov.tr/chem/vol48/iss4/8)
MELİKE KÜÇÜKSAKALLI, QAMAR SALAMAT, BUKET TİRELİ, and ŞÜKRÜ GÖKHAN ELÇİ
Pages 620-630

β-Ketoenamine-Linked Covalent Organic Framework for Efficient Iodine Capture (https://journals.tubitak.gov.tr/chem/vol48/iss4/9)
ONUR BÜYÜKÇAKIR
Pages 631-642

Corrigendum

Corrigendum to “Polybrominated methoxy- and hydroxynaphthalenes” [Turkish Journal of Chemistry 40 (2) 2016 332-346] (https://journals.tubitak.gov.tr/chem/vol48/iss4/14)
KIYMET BERKİL AKAR, Osman Çakmak, and TUNCAY TUNÇ
Pages 701-702


SSR - Excel
Nayana Sonwane
SearchList
Web of Science Master J
Web of Science Master J
ISSN 0976-0822 (Print) |
Der Pharma Chemica
mjl.clarivate.com/search-results
Gmail
YouTube
Maps
Adobe Acrobat
All Bookmarks
Already have a manuscript?
Use our Manuscript Matcher to find the best relevant journals!
Find a Match
Refine Your Search Results
1300-0527
Search
Sort By:
Title (A-Z)
Search Results
Found 1 results (Page 1)
Share These Results
Exact Match Found
Filters
Clear All
Web of Science Coverage
Open Access
Category
Country / Region
TURKISH JOURNAL OF CHEMISTRY
Publisher:
TUBITAK SCIENTIFIC & TECHNOLOGICAL RESEARCH COUNCIL TURKEY , ATATURK BULVARI NO 221, KAVAKLIDERE, ANKARA, Turkiye, TR-06100
ISSN / eISSN:
1300-0527
Web of Science Core Collection:
Science Citation Index Expanded
Additional Web of Science Indexes:
Current Contents Physical, Chemical & Earth Sciences | Essential Science Indicators
Search
ENG
IN
14:19
17-09-2024

Author's personal copy

Medicinal Chemistry Research (2021) 30:163–181
https://doi.org/10.1007/s00044-020-02649-7

MEDICINAL CHEMISTRY RESEARCH

ORIGINAL RESEARCH

A facile synthesis of some new pyrimidine-2,4,6-triones analogs and their *O*-β-D-glucosides P-glycoprotein and antioxidant, antimicrobial study, blood–brain barrier, cytochrome p450 enzyme activity prediction

Kishor M. Hatzade[1] · Ajay M. Ghatole[1] · Pravin K. Gaidhane[2] · Mahesh K. Gaidhane[3] · Gunwant P. Gadekar[4]

Received: 19 June 2020 / Accepted: 7 October 2020 / Published online: 22 October 2020
© Springer Science+Business Media, LLC, part of Springer Nature 2020

Abstract

The condensation of several 1,3-disubstitutedpyrimidine-2,4,6(1*H*,2*H*,3*H*)-triones **2a**–**g** by 3-formyl-4*H*-chromen-4-one **1** has resulted in the formation of new 5-[(7-hydroxy-4-oxo-4*H*-chromen-3-yl)methylene]-1,3-disubstitutedpyrimidine-2, 4, 6 (1*H*, 2*H*, 3*H*)-triones **3a**–**g**. These compounds have used for the synthesis of medicinally important 5-[(7-*o*-β-D-glucopyranosyloxy-4-oxo-4*H*-chromen-3-yl)methylene]-1,3-disubstitutedpyrimidine-2,4,6(1*H*,2*H*,3*H*)-triones **6a**–**g** using α-acetobromoglucose (ACBG) as a glucosylating agent in the presence of dodecyltrimethylammonium bromide (DTMAB) as a phase transfer catalyst. The structures of the product have confirmed based on ^{1}H NMR, ^{13}C NMR, ES-MS, optical activity, and elemental analysis. The mixes were assessed for their in vitro biological action. Among all the incorporated exacerbates, nobody is foreseen devoured and not blood–brain barrier permeant considering the way that outside of the extent of the plot with the exclusion of the standard medication clotrimazole. By considering the medicinal chemistry assessment all the incorporated molecule violet the PAINS, Brenk, and Leadlikness except for clotrimazole. The modern SwissADME web tool that stretches free admittance to a pool of hasty yet solid clarifying models for physicochemical properties, pharmacokinetics, and therapeutic science.

Keywords α-Acetobromoglucose · Chromones · Deacetylation · Glycosylating agent · Pyrimidine-2,4,6(1*H*,2*H*,3*H*)-triones · ADME

Introduction

The synthesis of organic compounds containing pyrimidine (a keto form) has attracted a current interest in the organic synthesis because of their pharmacological activities such as sedatives and hypnotics, antitumour, antiviral, anti-inflammatory, bacteriostatic, antineoplastic, cardiovascular, antidepressant, antituberculosis, antihypertensives, hypothermic, and herbicidal activities [1–3]. In the most recent decades, carbohydrate drugs increased much consideration since they are in charge of their capacity in different biological processes [4–6] incorporating especially cellular recognition on account of resistant response [7, 8] tumor metastasis [9] inflammation [10–12], and bacterial and viral infections [4]. Often, the carbohydrate serves as a carrier of a known pharmacophore group. The carbohydrate carrier may change an aspect of absorption, distribution, metabolism, or excretion of the drugs. Remembering the above certainties and in continuation of our studies [13–17] is considered significant to incorporate hybrid molecules as new synthetic substances comprising of chromone, pyrimidine and glucose moiety [18, 19]. Herein, we account an effective synthesis of new compounds comprising pyrimidine, viz., 5-[(7-hydroxy-4-oxo-4*H*-chromen-3-yl) methylene]-1,3-disubstitutedpyrimidine-2,4,6 (1*H*, 2*H*, 3*H*)-triones **3a**–**g** by the interaction of 7-hydroxy-3-formyl-

✉ Ajay M. Ghatole
ajay.ghatole5@gmail.com

[1] Department of Chemistry, Dhote Bandhu Science College, Gondia 441614, India

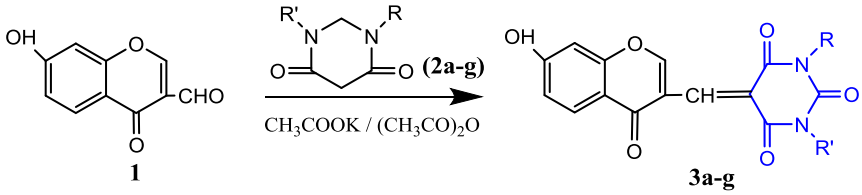
[2] Department of Chemistry, GWCOET, RTMNU, Nagpur, India

[3] Department of Chemistry, Shri Lemdeo Patil Mahavidyalaya, Mandal, Kuhi, India

[4] Department of Zoology, Dhote Bandhu Science College, Gondia 441614, India

Author's personal copy

Scheme 1 Synthesis of 5-[(7-hydroxy-4-oxo-4*H*-chromen-3-yl)methylene]-1,3-disubstitutedpyrimidine-2,4,6 (1*H*,2*H*,3*H*)-triones (**3a**–**g**)



	R-	R'-	Yield
a)	H	H	92%
b)	C_6H_5	H	89%
c)	C_6H_5	C_6H_5	75%
d)	2-$CH_3C_6H_4$	H	68%
e)	2-$CH_3C_6H_4$	2-$CH_3C_6H_4$	77%
f)	2-$OCH_3C_6H_4$	H	86%
g)	2-$OCH_3C_6H_4$	2-$OCH_3C_6H_4$	79%

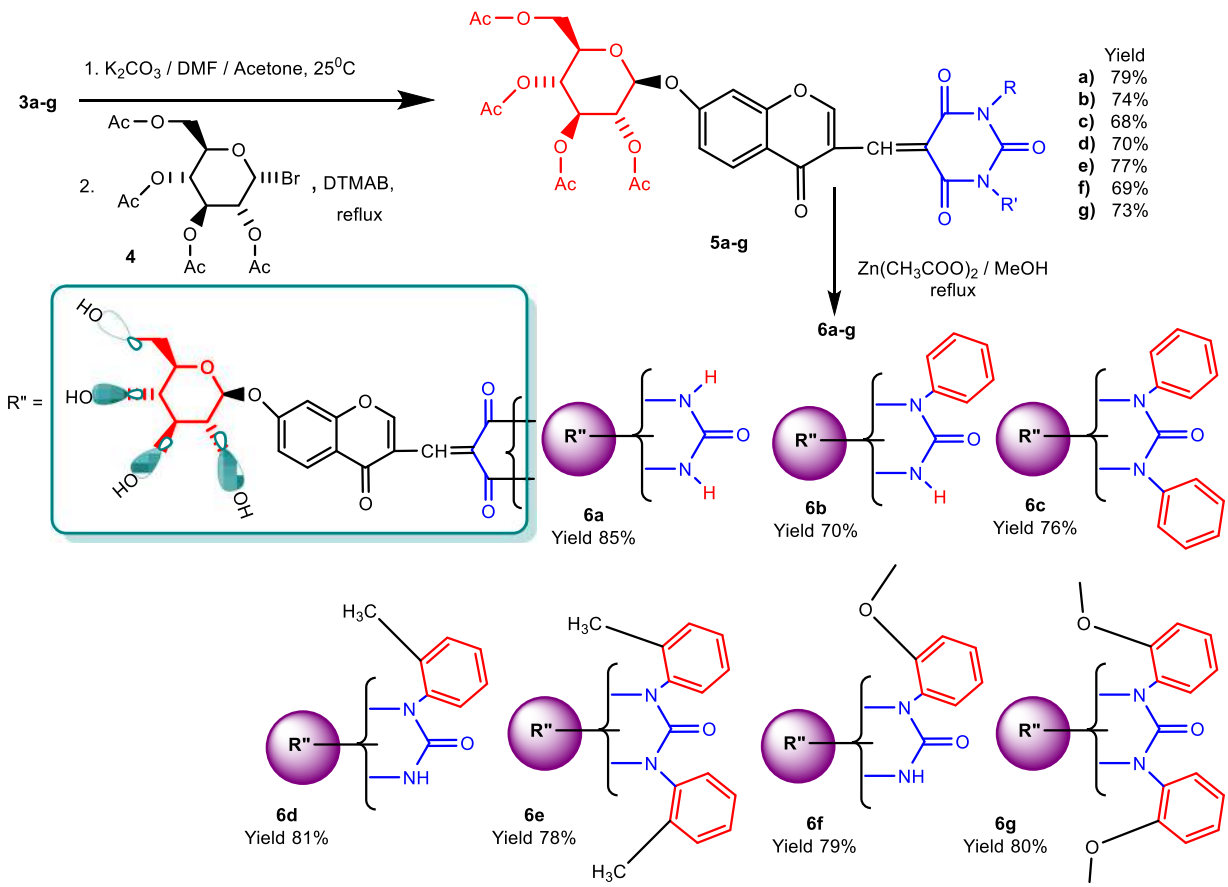
4*H*-chromen-4-one **1** and 1, 3-disubstitutedpyrimidine-2,4,6 (1*H*,2*H*,3*H*)-triones **2a**–**g**. *o*-Glucosylation of hydroxy compounds **3a**–**g** afforded corresponding 7-*o*-β-D-glucosides **6a**–**g**. Hydroxy compounds **3a**–**g** and their glucosides **6a**–**g** screened against *Escherichia coli, Klebisilla aerogens, Staphylococcus aureus* and *Bacillus substilis* and *Candida albicans* and *Aspergillus niger* for their antibacterial and antifungal action. Besides, these compounds were additionally contemplated for their antioxidant action. Nowadays drug revelation includes an assessment of the productivity of penetrating molecule and their capacity to attain in bioactive structure. This includes cellular, animal, and human clinical groundwork that is normally overpriced and weighed down with dangers. At present, computer-assisted evaluation of absorption, distribution, metabolism, and excretion of medications (ADME) has added up power to alleviate these concerns [20]. Prominently, computer models give prescient and dependable quick information and thus accolade investigational tactics. These computer models forecast pharmacokinetic, physicochemical, and therapeutic properties of small molecules and aid the advancement of lead molecules to persistent medications. SwissADME is a current and comprehensive website run by the Swiss foundation of bioinformatics which delivers bioinformatics facilities and properties to researchers around the world. SwissADME empowers evaluation of ADME parameters of medication competitors and small molecules and gives data that permits early hazard appraisal in the medication improvement process. Patently, swissADME gives a stage to evaluate Lipinski's standard of five [21] for medicating similarity of oral bioavailability. Medication resemblance is an unpredictable equalization of molecular properties and basic highlights which decide if a mysterious molecule resembles the known medications. These molecular properties incorporate hydrophobicity, electronic distribution, and hydrogen-holding appearances, molecule size and adaptability. SwissADME incorporates, 'BOILEDegg' assessment [22] that anticipate gastrointestinal ingestion (HIA) and efflux/preservation by P-glycoprotein (Pgp). Furthermore, the blood–brain barrier (BBB) infiltration and cytochrome P450 (CYP) enzyme substrate-restraint forecast can be made. Significantly, bogus positive outcomes normally observed in biochemical tests of small molecules are anticipated with a reasonable level of inevitability [23].

Results and discussion

Throughout our present research work, 7-Hydroxy-3-formyl-4*H*-chromen-4-one **1** produced from 2,4-dihydroxyacetophenone [24]. The 1,3-disubstitutedpyrimidine-2,4,6 (1*H*,2*H*,3*H*)-triones (barbiturates) **2a**–**g** prepared by the condensation of malonic acid with various areas [25]. The substitution of N-hydrogen by aryl bunches builds the dissolvability of disubstituted pyrimidine triones in organic solvents. The reaction of **1** with 1,3-disubstitutedpyrimidine-2,4,6(1*H*,2*H*,3*H*)-triones **2a**–**g** in the presence of fused potassium acetate [26] in dry $(CH_3CO)_2O$ at 110–120 °C for about 2 h afforded 5-[(7-hydroxy-4-oxo-4*H*-chromen-3-yl)methylene]-1,3-disubstitutedpyrimidine-2,4,6(1*H*,2*H*,3*H*)-triones **3a**–**g** [Scheme 1]. The IR spectrum of **3a** showed the presence of characteristic absorption peaks at 3406 (Br, OH), 2924 (s, NH), 1719 (vs, C=O), 1439 (C=C), 1018 (m, C–O–C) cm^{-1}. In the ^1H NMR range, **3a** compound displayed a singlet for NH at δ 11.11 and 11.05 ppm while the ^{13}C NMR range demonstrated signs at 164.55 (C-4′, C=O), 162.92 (C-6′, C=O), 149.45 (C-2′, C=O), 120.44 (C-5′, C=CH). The negative test for –CHO group, the absence of –CHO absorption band in the IR spectrum and also no signal in ^1H NMR spectrum at δ 3.07 due to CH_2 group confirm the development of compound **3a**.

o-Glucosydations [27] of **3a**–**g** carried out under anhydrous condition with α-acetobromoglucose (ACBG) **4** as glucosyl donor in the presence of dodecyl

Author's personal copy



Scheme 2 Synthesis of 5-[(2,3,4,6-tetra-*o*-acetyl-7-*o*-β-D-glucopyranosyloxy-4-oxo-4*H*-chromen-3-yl-)methylene]-1,3-disubstitutedpyrimidine-2,4,6(1*H*, 2*H*, 3*H*)-triones (**5a**–**g**)

trimethylammonium bromide (DTMAB) as a phase transfer catalyst, anhydrous K_2CO_3 in DMF-acetone mixture (3:2 v/v) to give 5-[(2,3,4,6-tetra-*o*-acetyl-7-*o*-β-D-glucopyranosyloxy-4-oxo-4*H*-chromen-3-yl)methylene]-1,3-disubstitutedpyrimidine-2, 4, 6(1*H*, 2*H*, 3*H*)-triones (**5a**–**g** β-anomer: 95% by column chromatography). The nonattendance of IR band at 3406 cm^{-1} because of OH extend and the solid band at 1033 cm^{-1} for C–O–C extend is showing the arrangement of product **5a**. Further, the crests at 2363 and 2924 cm^{-1} were because of the Ar–CH and NH extends. The C=O extends top observed to move to 1727 cm^{-1}. A solid absorption at 1754 cm^{-1} allotted to C=O stretch of O-acetyl gatherings of glucose moiety. A sharp top at 2854 cm^{-1} allotted to glucosidic –CH extend. The ^{1}H NMR range of **5a** indicated signs at δ 9.69 and 9.68 (s, 1H, NH), 4.79 (d, H-1″, anomeric proton) while the ^{13}C NMR range demonstrated signs at δ 171.70, 171.03–171.24 (C-particles of 3Acetyl C=O), 163.66 (C-4′, C=O), 162.43 (C-6′, C=O), 149.46 (C-2′, C=O), 111.24 (C-5′, C=CH), 97.86 (C-1″, anomeric C-molecule), 73.23 (C-3″), 72.48 (C-5″), 71.33 (C-2″), 69.00 (C-4″), 62.62 (C-6″), 21.03–21.34 (C-particles, 3CH_3 of Acetyl group), 20.65 (C-particle, CH_3 of Acetyl group). Deacetylation of mixes **5a**–**g** with anhydrous zinc acetate in dry methanol achieved the desired 5-[(7-O-β-D-glucopyranosyloxy-4-oxo-4H-chromen-3-yl) methylene]-1,3-disubstitutedpyrimidine-2,4,6(1H,2H,3H)-triones **6a**–**g** [Scheme 2].

The IR spectrum of **6a** showed the presence of characteristic absorption peaks at 3374 (broad, OH), 2927 (s, NH), 2854 (s, glucosidic-CH), 1627 (s, C=O), 1032 (m, C–O–C) cm^{-1} indicating the formation *o*-β-D-glucoside of **3a**. This was also confirmed by its ^{1}H, ^{13}C NMR, and ES-MS data. The ^{1}H NMR information demonstrates the nearness of carbohydrate moiety. The chemical shifts of the anomeric proton show β-linkage at δ 5.82 (d, 1H, C–H) indicating the linkage of carbohydrate unit to the C-7 position of the aglycone. Compound **6a** exhibited N–H at δ 10.40 and 10.35 ppm, aromatic protons at δ 6.66–7.64 and the characteristic pyranosyl ring protons at δ 3.42–4.24. Signals of protons of the carbohydrate of the hydroxyl group were not watched as a result of the quick exchange of all non-hydrogen bonded OH groups. In the ^{13}C NMR spectrum, **6a** compound showed signals at 101.31 (C-1″, anomeric C-atom), 77.98 (C-5″), 77.61 (C-3″), 73.87 (C-2″), 71.11 (C-4″), 62.15 (C-6″). In ES-MS studies the

Author's personal copy

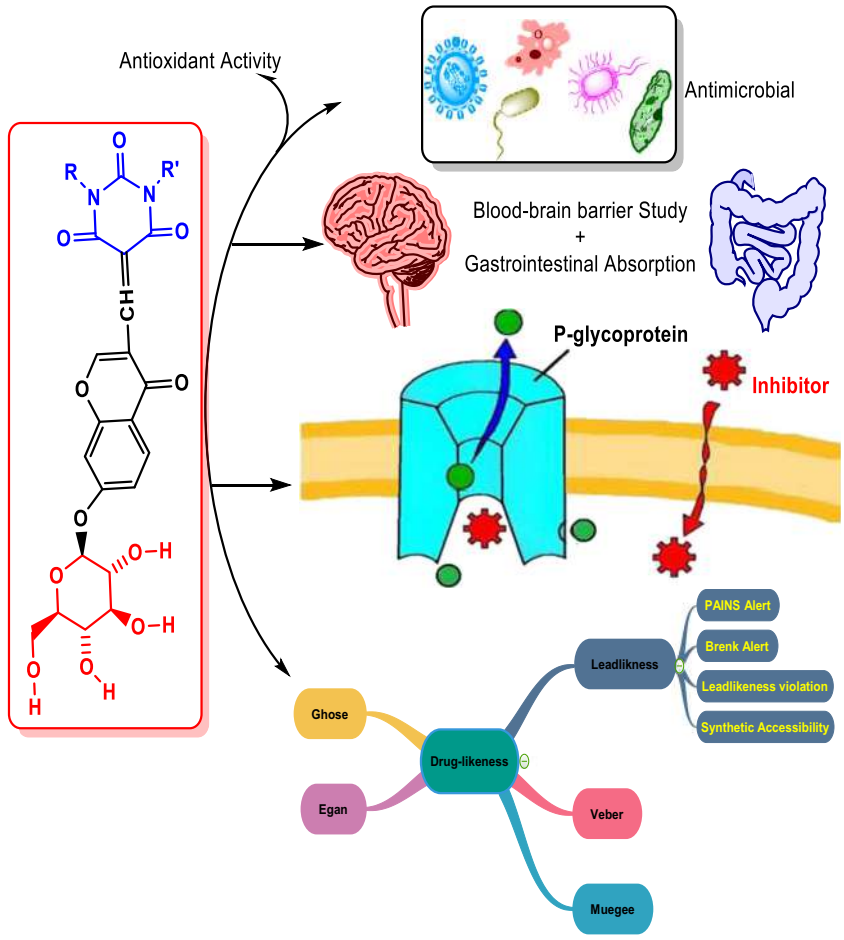


Fig. 1 The biological study includes antioxidant, antimicrobial, BBB, gastrointestinal absorption, drug-likeness study

molecular ion peak at *m/z* 463 $[M + 1]^+$ dominated by *m/z* 300 (100 %) with the loss of 163 amu corresponding to the loss of an intact anhydro-sugar moiety. This rupture design is qualities for *o*-glucosidically connected sugar. The molecular ion at m/z 463 $[M + H]^+$ affirms the subatomic recipe $C_{20}H_{18}N_2O_{11}$ of the glucoside. The mixes gave agreeable C, H, and N examination Fig. 1.

Biological activity

Blended mixes **3a–g** and **6a–g** assessed for their in vitro antibacterial, antifungal, and antioxidant exercises (Tables 1 and 2).

In vitro antibacterial and antifungal activity

In vitro antibacterial action of the said mixes assessed against bacterial strains viz., *E. coli*, *K. aerogens*, *S. aureus*, and *B. substilis* utilizing the supplement agar plate dissemination strategy. To propose approaches for screening the antimicrobial activity, we examined the parts of the microdilution technique utilized for the assurance of minimum inhibitory concentration.

Agar plate diffusion method

The bacterial inoculum was consistently spread utilizing sterile cotton swab on a sterile Petri dish MH agar. Five sequential dilutions yielded 100, 80, 60, 40, and 20 mg/mL of concentration for synthesized compounds and *Ciprofloxacin* and *Sulphacetamide* as standard in DMSO. The 50 µL of each were added to each of the five wells (7 mm diameter holes cut in the agar gel; 20 mm separated from each other). The zone of embarrassment after 24 h of growth at 37 °C contrasted *Ciprofloxacin* and *Sulphacetamide* (standard medications). The outcomes demonstrated that every one of the mixes showed a noticeable degree of action against microscopic organisms in contrast with standard medications. The in vitro antifungal movement of the mixes was likewise determined against *C. albicans* and *A. niger* growths by this strategy: The compounds dissolved in DMSO at 100, 80, 60, 40, and 20 mg/mL of and incubated for 7 days at 20 °C. The zones of inhibition estimated and contrasted with zones of *Gentamycin* and *Clotrimazole*. Every one of the compounds exhibited remarkable action against the strains tried [Table 1].

Author's personal copy

Table 1 The in vitro antimicrobial activity of compounds (3a–g and 6a–g)

Compd No.	The diameter of zone of inhibition (mm) (activity index)[std]					
	Antibacterial activity				Antifungal activity	
	S. aureus	*B. substilis*	*E. coli*	*K. aerogens*	*C. albicans*	*A. niger*
3a	18 (0.56)[a] (0.58)[b]	20 (0.69)[a] (0.76)[b]	10 (0.29)[a] (0.34)[b]	07 (0.32)[a] (0.33)[b]	19 (0.90)[a] (0.90)[b]	11 (0.44)[a] (0.46)[b]
3b	19 (0.56)[a] (0.61)[b]	16 (0.55)[a] (0.62)[b]	16 (0.46)[a] (0.55)[b]	11(0.50)[a] (0.52)[b]	13 (0.62)[a] (0.57)[b]	9 (0.36)[a] (0.37)[b]
3c	14 (0.41)[a] (0.45)[b]	10 (0.34)[a] (0.38)[b]	13 (0.37)[a] (0.45)[b]	10 (0.45)[a] (0.48)[b]	19 (0.90)[a] (0.83)[b]	11(0.44)[a] (0.46)[b]
3d	09 (0.26)[a] (0.29)[b]	08 (0.28)[a] (0.30)[b]	12 (0.34)[a] (0.41)[b]	09 (0.41)[a] (0.43)[b]	10 (0.48)[a] (0.43)[b]	10 (0.40)[a] (0.42)[b]
3e	14 (0.41)[a] (0.45)[b]	11(0.38)[a] (0.42)[b]	13 (0.37)[a] (0.45)[b]	12 (0.55)[a] (0.57)[b]	18 (0.86)[a] (0.78)[b]	13 (0.52)[a] (0.54)[b]
3f	11(0.32)[a] (0.35)[b]	15 (0.52)[a] (0.58)[b]	16 (0.46)[a] (0.55)[b]	10 (0.45)[a] (0.48)[b]	14 (0.66)[a] (0.60)[b]	12 (0.48)[a] (0.50)[b]
3g	18 (0.56)[a] (0.58)[b]	20 (0.69)[a] (0.76)[b]	10 (0.29)[a] (0.34)[b]	07 (0.32)[a] (0.33)[b]	19 (0.90)[a] (0.90)[b]	11 (0.44)[a] (0.46)[b]
6a	31(0.91)[a] (1.00)[b]	23(0.79)[a] (0.88)[b]	30(0.86)[a] (1.03)[b]	18(0.81)[a] (0.86)[b]	19(0.90)[a] (0.83)[b]	17 (0.68)[a] (0.71)[b]
6b	29 (0.85)[a] (0.94)[b]	21 (0.72)[a] (0.81)[b]	25 (0.71)[a] (0.86)[b]	17 (0.77)[a] (0.81)[b]	32 (1.52)[a] (1.39)[b]	16 (0.64)[a] ((0.66)[b]
6c	25 (0.73)[a] (0.81)[b]	20 (0.69)[a] (0.77)[b]	27 (0.77)[a] (0.93)[b]	15 (0.68)[a] (0.71)[b]	30 (1.43)[a] (1.30)[b]	20 (0.80)[a] (0.83)[b]
6d	30 (0.88)[a] (0.97)[b]	22 (0.76) (0.85)[b]	24 (0.69)[a] (0.83)[b]	20 (0.91)[a] (0.95)[b]	25 (1.19)[a] (1.09)[b]	18 (0.72)[a] (0.75)[b]
6e	28 (0.82)[a] (0.90)[b]	21 (0.72)[a] (0.81)[b]	29 (0.83)[a] (1.00)[b]	17 (0.77)[a] (0.81)[b]	27 (1.29)[a] (1.17)[b]	20 (0.80)[a] (0.83)[b]
6f	25 (0.74)[a] (0.81)[b]	34 (1.17)[a] (1.31)[b]	20 (0.57)[a] (0.69)[b]	20 (0.91)[a] (0.95)[b]	31 (1.48)[a] (1.35)[b]	21 (0.84)[a] (0.88)[b]
6g	29 (0.85)[a] (0.94)[b]	24 (0.83)[a] (0.92)[b]	21 (0.60)[a] (0.72)[b]	19 (0.86)[a] (0.90)[b]	30 (1.43)[a] (1.30)[b]	22 (0.88)[a] (0.92)[b]
Std.1	34	29	35	22	21	25
Std. 2	31	26	29	21	23	24

For antibacterial activity: Std. 1 = Ciprofloxacin and Std. 2 = Sulfacetamide.; for antifungal activity: Std. 1 = Gentamycin and Std. 2 = Clotrimazole

Activity index inhibition zone of the sample/Inhibition zone of the standard

[a]Activity index against Std. 1

[b]Activity index against Std. 2

Table 2 Data for antioxidant activity of compounds (3a–g and 6a–g)

Compd No.	% Inhibition Antioxidant DPPH	Compd No.	% Inhibition Antioxidant DPPH
3a	69.15 (0.70)[a]	**6a**	90.01 (0.92)[a]
3b	66.35 (0.68)[a]	**6b**	89.24 (0.91)[a]
3c	58.56 (0.60)[a]	**6c**	85.88 (0.88)[a]
3d	69.45 (0.71)[a]	**6d**	76.56 (0.78)[a]
3e	64.12 (0.65)[a]	**6e**	82.34 (0.84)[a]
3f	69.89 (0.71)[a]	**6f**	84.45 (0.86)[a]
3g	69.15 (0.70)[a]	**6g**	78.12 (0.80)[a]
Std. 1	98.03		

Std. 1 = Ascorbic acid

[a]Activity index against Std. 1

Antioxidant activity

In vitro, free radical scavenging activities of compounds assessed DPPH measure technique [28]. This technique depends on the decrease of a methanolic solution of the shaded DPPH radical: To a set of test tubes containing 3 mL of methanol, 50 µL of DPPH reagent (2 mg/mL) included. The primary absorbance assessed. To these test tubes, a methanolic solution of various test solution (1 mg/mL) included (10–50 µL). Ascorbic acid (0.5 mg/mL) included in the array of 10–25 µL. After 20 min, absorbance recorded at 516 nm. The test made in triplicate. The percentage reduction in absorbance calculated from the initial and final absorbance of each solution. The percentage rummaging of DPPH radical determined utilizing the equation: % Scavenging of DPPH = [(Control − Test)/Control] × 100. The aglycones exposed weak activity, yet the consistent glycosides had the highest antimicrobial activity against bacteria and fungi. The glucosides also offered more promising antioxidant activities than that of aglycones [Table 2].

ADME analysis of compounds [29]

Material and strategies

The comparative study of the ADME was done on the website http://www.swissadme.ch between the standard drugs with the synthesized quinoline chalcone. The information zones itself include molecular sketcher dependent on ChemAxon's Marvin JS (http://www.chemaxon.com) that permit the client to draw and alter 2D chemical structures.

Author's personal copy

The structures are displayed on one side on the screen on the other side of the page we can input the define simplified molecular-input line-entry system and results are introduced for every molecule in tables, graphically and as an exceed expectations spreadsheet.

Pharmacology

Auxiliary highlights of a pharmacophore impact the performance of a molecule in people, including bioavailability, transport properties, liking to proteins, reactivity, poisonousness, and metabolic steadiness. Interesting to swissADME is the bioavailability radar [30] that gives a graphical depiction of the medication resemblance limitations of an orally accessible bioactive medication. The hexagon (Fig. 2) graph represents the medication similarity with every one of the vertices speaking to a parameter that characterizes a bioavailable medication. The ideal range for every property is represented by pink region inside the hexagon speaks (The ranges are decided for lipophilicity: XLOGP3 = −0.7 to +5.0, size: MW = 150 and 500 g/mol, polarity: TPSA = 20 and 130 A2, solubility: log S = Not higher than 6, saturation: a segment of carbons in the sp3 hybridization at least 0.25, and flexibility: close to 9 rotatable bonds) (Table 3).

Drug-likeness

The drug-likeness properties of all the compounds including standard drugs are represented by the red distorted hexagon within the pink shade (Fig. 2). Particularly, synthesized compound (**6a**) fall within parameters of a bioavailable drug except its polarity indicated by an off-shoot of the vertices. While among the four standard drugs only ciprofloxacin falls within the range Fig. 2. The Ghose [31], Egan [32], Veber [33], and Muegee [34] screens developed by the driving pharmaceutical organizations and cheminfomaticians used by swissADME to assess the medication resemblance of small molecules. The Ghose screen quantitatively portrays small molecules dependent on processed physicochemical property profiles that incorporate logP, molar refractivity (MR), subatomic weight (MW), and several atoms. Furthermore, the Ghose [31], riddle incorporate a qualitative portrayal dependent on the existence of functional groups and significant substructures. The passing scope of determined log *P* (ClogP) is between −0.4 and 5.6. For MW, the passing reach is in the range of 160 and 480. For MR, the passing reach is amongst in the range of 40 and 130 and for the entire quantity of atoms; the passing extent is somewhere in the range of 20 and 70 atoms in a small molecule (Table 4). Our targeted molecule **6a**–**g** along with the standard drugs gentamicin does not meet the while only clotrimazole, ciprofloxacin and sulfacetamide met the Ghose qualifying models.

The molecule to act as medication the Veber (GSK filter) [33] model describe parameters are the molecule have 10 or less rotatable bond and a polar surface area (PSA) equal to or less than 140 A2 with 12 or less H-bond donors and acceptors. All the synthesized molecules with the standard does not meet the Veber rules except clotrimazole, ciprofloxacin, and sulfacetamide standard (Tables 3 and 4).

Drug absorption prediction based on physical methods tangled in membrane permeability of a small molecule screening used by Egan (Pharmacia) [32]. The descriptors in the Egan model are PSA and AlogP98v with the elimination of excess descriptors, for example, MW. PSA is a reference point for AlogP98 [35] since the last descriptor is a proportion of lipophilicity to hydrophilicity which not contains data on the supreme proportion of either factor. Significantly, the Egan computational model for human submissive intestinal absorption (HIA) of small molecules represents dynamic passage and efflux components and is in this way vigorous in anticipating retention of medications. Avoidance of excess descriptors permitted by clotrimazole, ciprofloxacin, and sulfacetamide standard excluding all the small molecule **6a**–**g** and standard gentamicin not comply with the Egan rules (Table 4).

Muegge (Bayer filter) model is a database-free pharmacophore point screen that separates between drug-like and nondrug-like matter. It relies upon the recognition that nondrugs are as often as possible less functionalized. Four intentional topics are portrayed to be noteworthy in drug-like molecules and incorporate hydroxyl, amine, ketone, and sulfonyl gatherings. As such, a base check of well-described pharmacophore centers is required to pass the screen. The indication of these productive subjects guarantees hydrogen-holding limits that are essential for express drug participation with its targets. These workable gatherings can be united to what Muegge model insinuates as pharmacophore focuses. The pharmacophore accentuations incorporate amine, amide, liquor, ketone, sulfone, sulfonamide, carboxylic corrosive, carbamate, guanidine, amidine, urea, and ester proficient gatherings. These pharmacophore endeavors in molecules conceivably give key interchanges with the goal protein Muegge (Bayer filter) [34] model is a database-free pharmacophore point screen that segregates between drug-like and nondrug-like substance matter. Muegge screen is based on the molecules often having less functionalized they observed as nondrugs. Four functional groups like ketone, hydroxyl, sulfonyl, and amine are important for a molecule to have drug-likeness. Consequently, for a molecule to have well-defined pharmacophore these are the minimum required to pass the screen. The event of these useful themes ensures hydrogen-bonding capacities that are basic for explicit medication associations with its objectives. These useful gatherings can be consolidated to what Muegge model [34] alludes to as

Author's personal copy

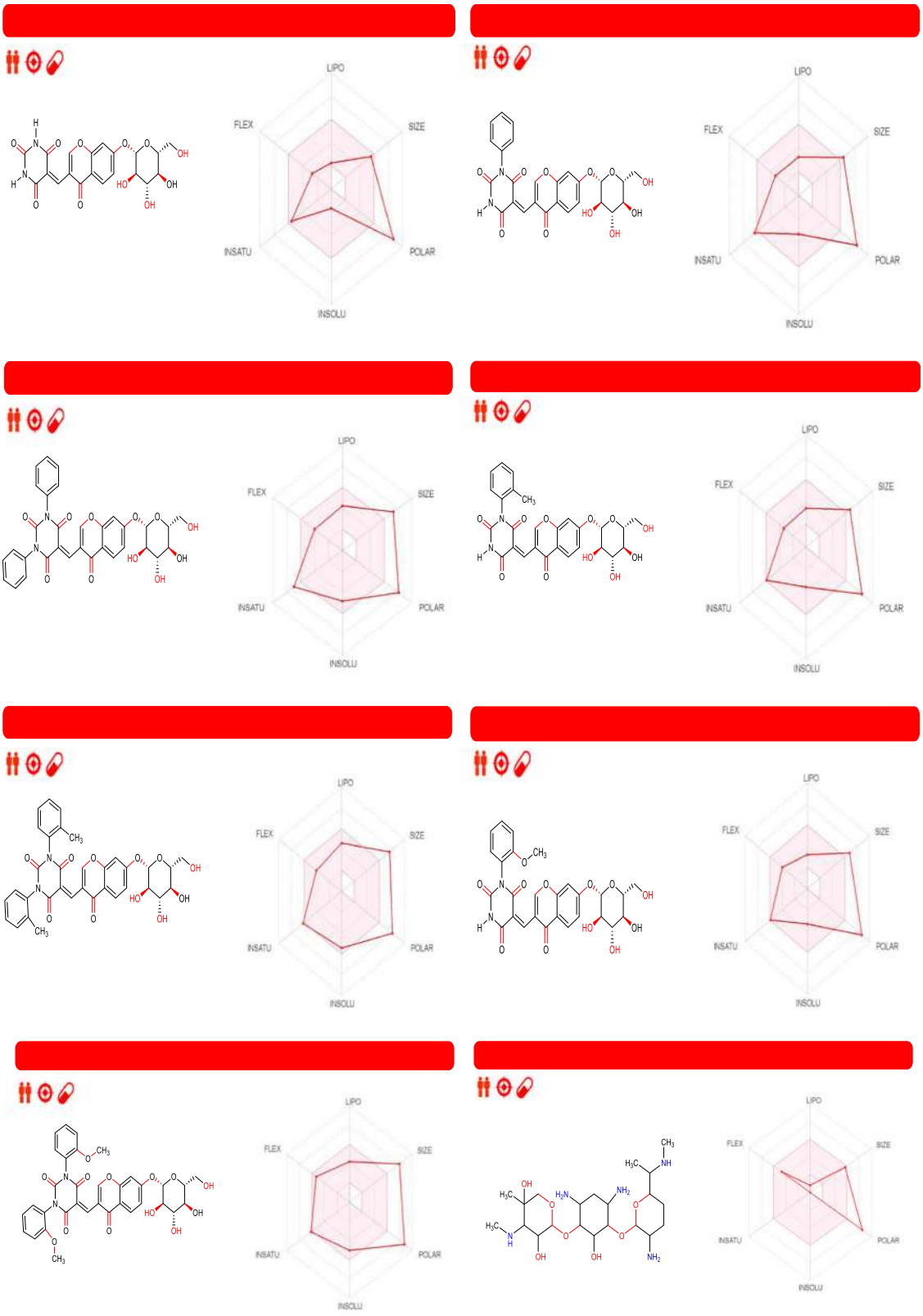


Fig. 2 The bioavailability radar of the synthesized molecules (6a–g) and standard drugs (gentamicin; clotrimazole; ciprofloxacin; sulfacetamide) evaluating using swissADME web tool

Author's personal copy

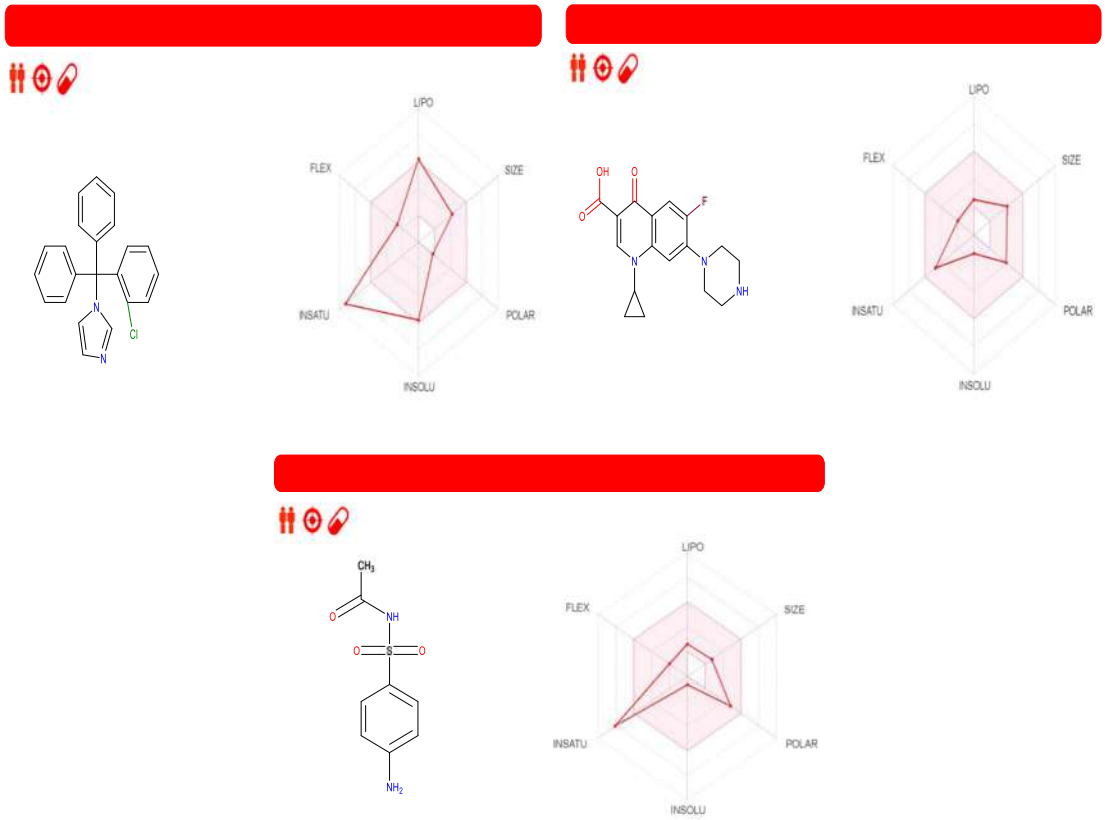


Fig. 2 (Continued)

Table 3 Physicochemical properties of the synthesized molecules (6a–g) and standard drugs

Sr. No.	MW	HA	AHA	FCsp3	RTB	HBA	HBD	MR	TPSA
6a	462.36	33	10	0.3	4	11	6	113.45	204.86
6b	538.46	39	16	0.23	5	11	5	138.59	196.07
6c	614.56	45	22	0.19	6	11	4	163.73	187.28
6d	552.49	40	16	0.26	5	11	5	143.55	196.07
6e	642.61	47	22	0.24	6	11	4	173.66	187.28
6f	568.49	41	16	0.26	6	12	5	145.08	205.3
6g	674.61	49	22	0.24	8	13	4	176.71	205.74
SD1	477.6	33	0	1	7	12	8	118.31	199.73
SD2	344.84	25	23	0.05	4	1	0	101.84	17.82
SD3	331.34	24	10	0.41	3	5	2	95.25	74.57
SD4	214.24	14	6	0.12	3	3	2	51.75	97.64

MW molecular weight, *HA* heavy atoms, *AHA* aromatic heavy atom, *FCsp3* fraction Csp3, *RTB* rotatable bonds, *HBA* H-bond acceptors, *HBD* H-bond donors, *MR* molar refractivity, *TPSA* total polar surface area, *SD1* gentamicin, *SD2* clotrimazole, *SD3* ciprofloxacin, *SD4* sulfacetamide

pharmacophore focuses. The pharmacophore focuses on incorporate sulfonamide, amine, alcohol, amide, carboxylic acid, ketone, carbamate, sulfone, urea, guanidine, amidine, and ester functional group. These pharmacophore points in small molecules conceivably give key communications with the objective protein. All the synthesized molecule contains most commonly one functional group i.e., hydroxy as described by the Muegge.

PAINS, break, and leadlikeness screening

The motivation behind this segment is to help restorative physicists in their everyday medicate disclosure attempts. Two corresponding example acknowledgement strategies take into consideration recognizable proof of possibly risky pieces. PAINS (for pan assay interference compounds) are molecule comprising bases indicating strong reaction in

Author's personal copy

Table 4 Drug-likeness evaluation of synthesized compounds (6a–g) using swissADME

Sr. No.	Lipinski #violations	Ghose #violations	Veber #violations	Egan #violations	Muegge #violations
6a	2	1	1	1	3
6b	2	3	1	1	2
6c	2	3	1	1	3
6d	2	3	1	1	2
6e	2	3	1	1	3
6f	2	3	1	1	2
6g	2	3	1	1	3
SD1	2	2	1	1	4
SD2	1	0	0	0	1
SD3	0	0	0	0	0
SD4	0	0	0	0	0

SD1 gentamicin, *SD2* clotrimazole, *SD3* ciprofloxacin, *SD4* sulfacetamide

Table 5 Medicinal chemistry evaluation of the synthesized compounds (6a–g) and standard

Sr. No.	PAINS #alerts	Brenk #alerts	Leadlikeness #violations	Synthetic accessibility
6a	1	2	1	5.01
6b	1	2	1	5.34
6c	1	2	1	5.74
6d	1	2	1	5.47
6e	1	2	1	6
6f	1	2	1	5.54
6g	1	2	2	6.11
SD1	0	0	1	6.51
SD2	0	0	1	2.7
SD3	0	0	0	2.51
SD4	0	1	1	1.85

SD1 gentamicin, *SD2* clotrimazole, *SD3* ciprofloxacin, *SD4* sulfacetamide

tests independent of the protein target. Such sections, yielding bogus positive biological yield, have been distinguished by Baell et al. [36] in dissecting six orthogonal tests and separating the molecules dynamic on at least 2 measures into 481 intermittent sections, potentially leading to promiscuous compounds. SwissADME evaluation did not post any PAINS alert except the all the standard drugs (Table 5).

Plus, we actualized structural alert, which comprises in a rundown of 105 fragments recognized by Brenk et al. [37] to be putatively toxic, metabolically unbalanced, chemically reactive, or to tolerate properties liable for poor pharmacokinetics. Brenk considered exacerbates that are smaller and less hydrophobic and not those characterized by "Lipinski's standard of 5" to broaden openings for lead improvement. This was after avoidance of mixes with conceivably mutagenic, receptive, and hostile groups, for example, phosphates, nitro, 2-halopyridines, sulfates, and thiols. In SwissADME, it is conceivable to have a compound depiction of the tricky segments found in a given molecule by flying over the "question mark" symbol showing up after the section list. This is actualized for the PAINS and Brenk screens. By applying these and other physicochemical screens to configuration screening libraries, Brenk et al. [37] saw that the majority of the rest of the compounds fulfill standards for "lead likeness". This idea is like medication resemblance, yet concentrating on physicochemical limits characterizing a decent lead, for example, a molecular entity reasonable for enhancement. By definition, leads are exposed to concoction changes that will probably expand size and lipophilicity [38].

Brenk model limits the ClogP/ClogD to zero and four, the number of hydrogen-bond acceptors and donor 7 and less than 4, individually, and the number of overwhelming atoms to somewhere in the range of 10 and 27 [37]. Moreover, compounds with constrained intricacy characterized as fewer than eight rotatable bonds, less than five-ring frameworks, and no ring frameworks with more than two fused rings are considered medicinal [37].

All the synthesized molecules had two Brenk rule, while the standard gentamicin, clotrimazole, and ciprofloxacin no Brenk but a Sulfacetamide ridiculed 1 Brenk rule (Table 5). On the other hand, Teague [39] and others recommend that there are a lot of points of reference to propose that libraries comprising of atoms with MW in the range 100 ± 350 and ClogP in the range 1 ± 3.0 are enormously better than those considered medications like mixes and are along these lines lead-like [39]. Considering the above measures all molecules with standard violet the leadlikeness except ciprofloxacin (Table 5). Leadlikeness tests are planned to furnish leads with a high liking in high-throughput screens that take into consideration the revelation and misuse of extra cooperation ahead of the pack streamlining stage (Table 5).

Author's personal copy

Table 6 Pharmacokinetic evaluation of the synthesized compounds (6a–g) and standard

Sr. No.	GI absorption	BBB permeant	Pgp substrate	CYP1A2 inhibitor	CYP2C19 inhibitor	CYP2C9 inhibitor	CYP2D6 inhibitor	CYP3A4 inhibitor
6a	Low	No	No	No	No	No	No	No
6b	Low	No	No	No	No	No	No	No
6c	Low	No	No	No	No	No	No	No
6d	Low	No	Yes	No	No	No	No	No
6e	Low	No	No	No	No	No	No	No
6f	Low	No	Yes	No	No	No	No	No
6g	Low	No	No	No	No	No	No	No
SD1	Low	No	Yes	No	No	No	No	No
SD2	High	Yes	Yes	Yes	Yes	Yes	Yes	Yes
SD3	High	No	Yes	No	No	No	No	No
SD4	High	No	No	No	No	No	No	No

GI gastrointestinal absorption, *BBB* blood–brain barrier, *CYP* cytochromes, *P-gp* P-glycoprotein, *SD1* gentamicin, *SD2* clotrimazole, *SD3* ciprofloxacin, *SD4* sulfacetamide

Pgp and CYP enzyme activity prediction

SwissADME additionally empowers the estimation for a compound to be a substrate of p-gp or inhibitor of the cytochrome p450 isoenzymes (CYP isoenzymes). P-gp is broadly dispersed and communicated in the intestinal epithelium where it drives xenobiotics, for example, medicates again into the intestinal lumen and in the vessels endothelial cells making the blood–mind barrier where it drives them once more into the vessels. CYP Isoenzymes are liable for the biotransformation of drugs [40]. Medication digestion through CYP isoenzymes is a significant determinant of medication connections that can prompt medication poison levels and diminished pharmacological impact. The models return "Yes" or "No" if the molecule under scrutiny has a higher likelihood to be substrate or non-substrate of P-gp or inhibitor or non-inhibitor of a given CYP. All the small molecules restored "No" for P-gp substrate and "No" for most CYP isoenzymes. The screening results are arranged (Table 6).

HIA and BBB prediction

The BBB is a term used to portray one of a kind property of the microvasculature of the central nervous system (CNS). CNS vessels are nonstop non penetrated vessels, yet besides containing a progression of extra properties that permit them to firmly manage the development of ions, molecules, and cells between the blood and the CNS [41, 42]. This intensely limiting hindrance limit permits BBB ECs to firmly manage CNS homeostasis, which is basic to consider appropriate neuronal occupation, just as shield the CNS from injury, poisons, inflammation, pathogens, and sickness. Relevant to P-gp and CYP catalyst energy is human gastrointestinal ingestion (HIA) blood–brain barrier entrance (BBB). SwissADME 'BOILEDegg' (Fig. 3) takes into consideration the assessment of HIA as a component of the situation of the small molecules in the WLOGP-versus-TPSA referential.

The white locale is for a high likelihood of inactive assimilation by the gastrointestinal tract, and the yellow location (yolk) is for a high likelihood of brain entrance. Yolk and white regions are not equally limited. Furthermore, the focuses are highlighted in blue whenever anticipated as effectively effluxed by P-gp (PGP+) and in red whenever anticipated as non-substrate of P-gp (PGP−). In this model, Lapatinib is anticipated as not captivated and not brain penetrant (outside the Egg), Omeprazol is anticipated very much ingested yet not getting to the brain (in the white) and PGP+ (blue spot), Sunitinib is anticipated as inactively crossing the BBB (in the yolk), yet pumped out from the brain (blue spot), and Palonosetron is anticipated as mind penetrant (in the yolk) and not expose to dynamic efflux (red spot).

Among all the synthesized compounds, no one is anticipated not consumed and not BBB permeant because outside of the scope of the plot except the standard drug clotrimazole (Fig. 3). Ciprofloxacin and sulfacetamide are only two drugs are anticipated as consumed by gastrointestinal (white district) however do not mind penetrant (yolk) (Fig. 3) in that clotrimazole own the race compared with all the synthesized and standard compound.

All the blended molecules and sulfacetamide assessed are PGP negative and are not dependent upon dynamic efflux (red dab) (Fig. 3).

Both gastrointestinal absorption (HIA) and BBB are reliant on water solubility and lipophilicity of the medication. Having a soluble molecule incredibly encourages many medication improvements exercises, principally the simplicity of taking care of and formulation [43]. Two topological strategies to foresee water dissolvability are involved for SwissADME. The first is a usage of the ESOL model and

Author's personal copy

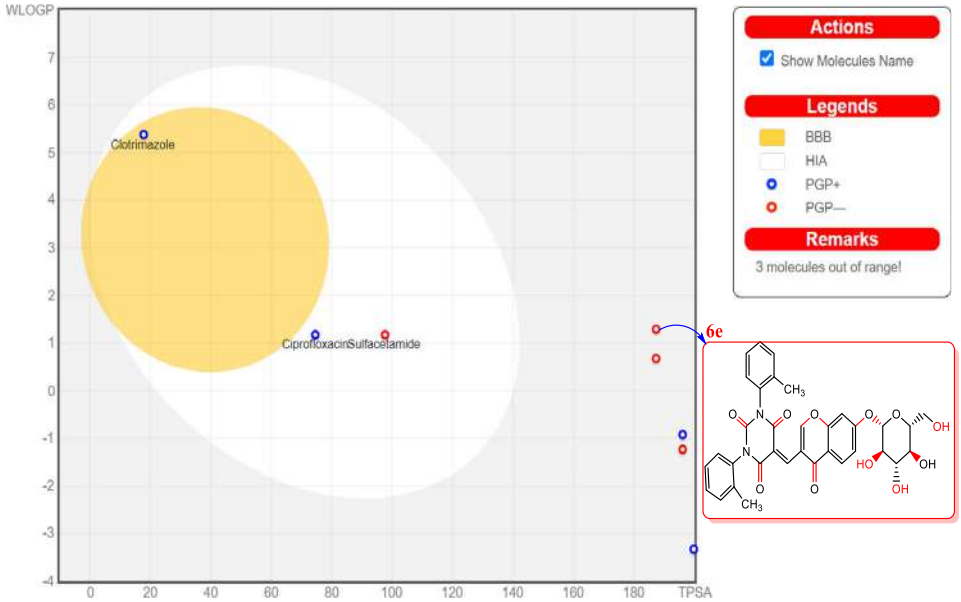


Fig. 3 The BOILED-Egg allows for evaluation of passive gastrointestinal absorption (HIA), brain penetration (BBB), and P-glycoprotein in the presence of the molecule (P-gp)

the subsequent one is modified from Ali et al. [44]. SwissADME third indicator for solubility was created by SILICOS-IT. All anticipated qualities are the decimal logarithm of the molar solubility in water (log S). Water solubility [45] of Table 7: Water solubility assessment of the small molecules extended from very soluble (**6a**) to soluble utilizing the ESOL [45] and other criteria [44] (Table 7).

Alternately, lipophilicity assessed among the synthesized compounds as Consensus Log *P* showed **6e** to be the most lipophilic (Consensus Log $P = 1.75$) though **6a** was the least lipophilic (Consensus Log $P = -1.72$). Accord Log *P* is the normal estimation of all Log *P* assessed with different lipophilicity rules (Table 8). The Ali and Silicoms IT screening show moderately soluble to poor solubility of all the incorporated compound while in ESOL solvency examination the greater part of the mixes is modestly dissolvable (Table 8). Indeed, even the standard medications are in the scope of poor solvency to highly soluble.

Experimental

The melting points assessed in an open capillary tube in paraffin bath uncorrected. FT-IR spectra noted on Perkin-Elmer range Rx-I spectrophotometer utilizing KBr plates. ^{1}H NMR and ^{13}C NMR spectra attained on a Bruker II-400 NMR spectrophotometer (^{1}H, 400 MHz and ^{13}C, 100 MHz); applying TMS as an internal standard in DMSO-d_6, chemical shifts (δ) estimated in ppm. Mass spectra resolved on Hitachi Perkin-Elmer RMU 6D mass spectrometer. Optical rotations were recorded at the sodium D line and ambient temperature with a JASCO computerized polarimeter. Immaculateness of the compounds checked on silica gel plates utilizing iodine vapor as an envisioning agent. Elemental studies resolved using the Perkin-Elmer 2400 CHN analyzer. Different substituted urea was synthesized utilizing strategies portrayed in literature [45].

5-[(7-hydroxy-4-oxo-4*H*-chromen-3-yl)methylene]-1,3-disubstitutedpyrimidine-2,4,6(1*H*,2*H*,3*H*)-triones (3a–g)

Equimolar mixture of 7-hydroxy-3-formyl-4*H*-chromen-4-one **1** (2.87 mmol) and 1, 3-disubstituted pyrimidine-2, 4, 6 (1*H*, 2*H*, 3*H*)-triones **2** (2.87 mmol) and 4 mL dry acetic anhydride was heated in the existence of recently fused potassium acetate at 110–120 °C for around 2 h. The reaction mixture cooled at room temperature and product got was filtered off and crystallized from solvents.

5-(7-Hydroxy-4-oxo-4*H*-chromen-3-yl) methylenepyrimidine-2,4,6(1*H*,2*H*,3*H*)-trione (3a)

Yield 92 %, m.p. 295 °C (Dioxane), IR (KBr): 3406 (br, OH), 2924 (s, NH), 1719 (vs, C=O), 1018 (m, C–O–C). ^{1}H NMR (400 MHz, DMSO-d_6): δ 11.11 (s, 1′-H, NH), 11.05 (s, 3′-H, NH), 8.73 (s, 2-H, CH), 7.97 (s, CH=), 7.56 (s, 1H, Ar–H), 7.38 (s, 1H, OH), 6.55–6.60 (m, 2H, Ar–H). ^{13}C NMR (100 MHz, DMSO-d_6): δ 170.19 (s, C-4, C=O), 164.55 (s, C-4′, C=O), 162.92 (s, C-6′, C=O), 162.67 (s, C-7), 156.76 (s, C-9), 154.97 (s, C-2), 149.45 (s, C-2′,

Author's personal copy

Table 7 Water solubility evaluation of the synthesized compounds (6a–g) and standard

Sr. No.	ESOL				Ali				Silicos-IT			
	Log S	Solu. (mg/ml)	Solu. (mol/l)	Class	Log S	Solu. (mg/ml)	Solu. (mol/l)	Class	Log S	Solu. (mg/ml)	Solu. (mol/l)	Class
6a	−1.68	9.71E+00	2.10E−02	VS	−2.22	2.76E+00	5.97E−03	S	−2.21	2.88E+00	6.24E−03	S
6b	−3.26	2.96E−01	5.51E−04	S	−3.85	7.69E−02	1.43E−04	S	−3.92	6.47E−02	1.20E−04	S
6c	−4.83	9.18E−03	1.49E−05	MS	−5.48	2.05E−03	3.34E−06	MS	−5.62	1.46E−03	2.38E−06	MS
6d	−3.57	1.48E−01	2.68E−04	S	−4.23	3.26E−02	5.90E−05	MS	−4.29	2.83E−02	5.13E−05	MS
6e	−5.44	2.35E−03	3.65E−06	MS	−6.22	3.84E−04	5.98E−07	PS	−6.36	2.81E−04	4.38E−07	PS
6f	−3.35	2.53E−01	4.45E−04	S	−4.02	5.45E−02	9.59E−05	MS	−4.01	5.54E−02	9.75E−05	MS
6g	−5	6.77E−03	1.00E−05	MS	−5.8	1.06E−03	1.58E−06	MS	−5.79	1.08E−03	1.60E−06	MS
SD1	0.24	8.37E+02	1.75E+00	HS	0.51	1.54E+03	3.23E+00	HS	0.52	1.56E+03	3.27E+00	S
SD2	−5.8	5.43E−04	1.57E−06	MS	−5.54	9.96E−04	2.89E−06	MS	−8.59	8.88E−07	2.58E−09	PS
SD3	−1.32	1.57E+01	4.74E−02	VS	0	3.34E+02	1.01E+00	HS	−3.5	1.04E−01	3.13E−04	S
SD4	−0.68	4.45E+01	2.08E−01	VS	−0.61	5.31E+01	2.48E−01	VS	−2.36	9.40E−01	4.39E−03	S

Solu solubility, *PS* poorly soluble, *MS* moderately soluble, *S* soluble, *VS* very soluble, *HS* highly soluble, *SD1* gentamicin, *SD2* clotrimazole, *SD3* ciprofloxacin, *SD4* sulfacetamide

C=O), 144.89 (s, CH=), 129.71 (s, C-3), 127.29 (s, C-5), 120.44 (s, C-5′, C=CH), 117.50 (s, C-10), 116.57 (s, C-6), 102.18 (s, C-8). Anal. Calcd for $C_{14}H_8N_2O_6$: C, 56.01; H, 2.69; N, 9.33. Found: C, 55.89; H, 2.55; N, 9.25 (%).

5-[(7-Hydroxy-4-oxo-4*H*-chromen-3-yl)methylene]-1-phenylpyrimidine-2,4,6(1*H*,2*H*,3*H*)-trione (3b)

Yield 89 %, m.p. 304 °C (Toluene), IR (KBr): 3433 (br, OH), 2952 (vs, NH), 1724 (vs, C=O), 1089 (s, C–O–C). ^{1}H NMR (400 MHz, DMSO-d_6): δ 11.06 (s, 3′-H, NH), 8.03 (s, 2-H, CH), 7.95 (s, CH=), 7.58 (s, Ar–H, 1H), 7.02–7.32 (m, 5H, Ar–H), 7.37 (s, 1H, OH), 6.52–6.55 (m, 2H, Ar–H). ^{13}C NMR (100 MHz, DMSO-d_6): δ 170.21 (s, C-4, C=O), 164.52 (s, C-4′, C=O), 162.90 (s, C-6′, C=O), 162.65 (s, C-7), 156.71 (s, C-9), 154.89 (s, C-2), 149.39 (s, C-2′, C=O), 144.91 (s, CH=), 135.76 (s, C-1″), 129.75 (s, C-3), 128.41-129.13 (s, aromatic 5C-atom), 127.25 (s, C-5), 120.41 (s, C-5′, C=CH), 117.49 (s, C-10), 116.52 (s, C-6), 102.11 (s, C-8). Anal. Calcd for $C_{20}H_{12}N_2O_6$: C, 63.83; H, 3.21; N, 7.44. Found: C, 63.71; H, 3.14; N, 7.32 (%).

5-[(7-Hydroxy-4-oxo-4*H*-chromen-3-yl)methylene]-1,3-diphenylpyrimidine-2,4,6(1*H*,2*H*,3*H*)-trione (3c)

Yield 75 %, m.p. 289 °C (Toluene), IR (KBr): 3415 (br, OH), 1729 (vs, C=O), 1045 (s, C–O–C). ^{1}H NMR (400 MHz, DMSO-d_6): δ 8.11 (s, H-2, CH), 7.87 (s, CH=), 7.86 (s, 1H, Ar–H), 7.39–7.47 (m, 6H, Ar–H), 7.38 (s, 1H, OH), 7.23–7.36 (m, 4H, Ar–H), 6.48–6.51 (d, 2H, Ar–H). ^{13}C NMR (100 MHz, DMSO-d_6): δ 170.18 (s, C-4, C=O), 157.16 (s, C-4′, C=O), 159.76 (s, C-6′, C=O), 162.66 (s, C-7), 156.72 (s, C-9), 154.91 (s, C-2), 150.21 (s, C-2′, C=O), 145.69 (s, CH=), 135.36 (s, C-1″), 135.35 (s, C-1‴), 129.74 (s, C-3), 128.31–129.24 (s, aromatic 10C-atom), 127.26 (s, C-5), 123.31 (s, C-5′, C=CH), 117.46 (s, C-10), 116.53 (s, C-6), 102.17 (s, C-8). Anal. Calcd for $C_{26}H_{16}N_2O_6$: C, 69.02; H, 3.56; N, 6.19. Found: C, 68.90; H, 3.44; N, 6.07 (%).

5-[(7-Hydroxy-4-oxo-4*H*-chromen-3-yl-)methylene]-1-(o-tolyl)-pyrimidine-2,4,6(1*H*,2*H*,3*H*)-triones (3d)

Yield 69 %, m.p. 279 °C (Dioxane + Toluene), IR (KBr): 3422 (br, OH), 2933 (s, NH), 1710 (vs, C=O), 1040 (m, C–O–C). ^{1}H NMR (400 MHz, DMSO-d_6): δ 10.93 (s, 3′-H, NH), 8.56 (s, 2-H, CH), 7.87 (s, CH=), 7.48 (s, 1H, Ar–H), 7.38 (s, 1H, OH), 7.12–7.14 (m, 3H, Ar–H), 6.50–6.96 (m, 3H, Ar–H), 2.23 (s, 3H, CH_3). ^{13}C NMR (100 MHz, DMSO-d_6): δ 170.18 (s, C-4, C=O), 164.02 (s, C-4′, C=O), 162.64 (s, C-7), 158.11 (s, C-6′, C=O), 156.73 (s, C-9), 154.92 (s, C-2), 153.62 (s, C-2′, C=O), 144.51 (s, CH=), 132.96 (s, C-1″), 129.72 (s, C-3), 128.39–129.09

Author's personal copy

Table 8 Lipophilicity evaluation of the synthesized compounds (6a–g) and standard

Sr. No.	iLOGP	XLOGP3	WLOGP	MLOGP	Silicos-IT Log *P*	Consensus Log *P*
6a	0.1	−1.57	−3.15	−3.08	−0.91	−1.72
6b	1.64	0.17	−1.23	−1.75	0.05	−0.23
6c	3.8	1.92	0.68	−0.52	1.01	1.38
6d	2.25	0.54	−0.92	−1.55	0.58	0.18
6e	2.86	2.64	1.3	−0.15	2.09	1.75
6f	2.3	0.15	−1.22	−2.02	0.13	−0.13
6g	3.23	1.86	0.7	−1.09	1.18	1.18
SD1	3.17	−4.1	−3.33	−2.92	−3.56	−2.15
SD2	3.07	5.41	5.38	4.38	4.98	4.64
SD3	2.24	−1.08	1.18	1.28	1.9	1.1
SD4	0.5	−0.96	1.18	−0.12	−0.46	0.03

SD1 gentamicin, *SD2* clotrimazole, *SD3* ciprofloxacin, *SD4* sulfacetamide

(s, aromatic 5C-atom), 127.24 (s, C-5), 123.16 (s, C-5′, C=CH), 117.47 (s, C-10), 116.51 (s, C-6), 102.10 (s, C-8), 17.23 (s, CH_3). Anal. Calcd for $C_{21}H_{14}N_2O_6$: C, 64.62; H, 3.62; N, 7.18. Found: C, 64.51; H, 3.49; N, 7.07 (%).

5-[(7-Hydroxy-4-oxo-4*H*-chromen-3-yl-)methylene]-1,3-di(p-tolyl)-pyrimidine-2,4,6(1*H*,2*H*,3*H*)-triones (3e)

Yield 77 %, m.p. 299 °C (Dioxane), IR (KBr): 3455 (br, OH), 1701 (vs, C=O), 1034 (m, C–O–C). ^{1}H NMR (400 MHz, DMSO-d_6): δ 8.46 (s, 2-H, CH), 7.86 (s, CH=), 7.51 (s, 1H, Ar–H), 7.42 (s, 1H, OH), 6.94–7.17 (m, 8H, Ar–H), 6.41–6.52 (m, 2H, Ar–H), 2.22 (s, 6H, CH_3). ^{13}C NMR (100 MHz, DMSO-d_6): δ 170.16 (s, C-4, C=O), 162.63 (s, C-7), 159.02 (s, C-4′, C=O), 156.74 (s, C-9), 156.51 (s, C-6′, C=O), 154.91 (s, C-2), 148.62 (s, C-2′, C=O), 145.61 (s, CH=), 132.97 (s, C–N), 132.95 (s, C–N), 131.15 (s, C–CH_3), 131.14 (s, C–CH_3), 129.73 (s, C-3), 127.77–129.65 (s, aromatic 8C-atom), 127.25 (s, C-5), 123.31 (s, C-5′, C=CH), 117.49 (s, C-10), 116.52 (s, C-6), 102.11 (s, C-8), 17.21 (d, CH_3). Anal. Calcd for $C_{28}H_{20}N_2O_6$: C, 69.99; H, 4.20; N, 5.83. Found: C, 69.88; H, 4.07; N, 5.76 (%).

5-[(7-Hydroxy-4-oxo-4*H*-chromen-3-yl-)methylene]-1-(o-anisyl)-pyrimidine-2,4,6 (1*H*,2*H*,3*H*)-triones (3f)

Yield 86 %, m.p. 301 °C (Dioxane), IR (KBr): 3339 (br, OH), 2901 (vs, NH), 1688 (s, C=O), 1120 (m, C–O–C). ^{1}H NMR (400 MHz, DMSO-d_6): δ 10.11 (s, 3′-H, NH), 8.59 (s, 2-H, CH), 7.83 (s, CH=), 7.41–7.45 (s, 2H, Ar–H), 7.36 (s, 1H, OH), 6.80–6.98 (m, 3H, Ar–H), 6.47–6.54 (m, 2H, Ar–H), 3.70 (s, 3H, OCH_3). ^{13}C NMR (100 MHz, DMSO-d_6): δ 170.15 (s, C-4, C=O), 164.01 (s, C-4′, C=O), 162.62 (s, C-7), 158.09 (s, C-6′, C=O), 156.77 (s, C-9), 155.54 (s, C–OCH_3), 154.94 (s, C-2), 153.64 (s, C-2′, C=O), 144.49 (s, CH=), 129.73 (s, C-3), 127.35–129.43 (s, aromatic 5C-atom), 127.25 (s, C-5), 123.17 (s, C-5′, C=CH), 117.46 (s, C-10), 116.50 (s, C-6), 102.12 (s, C-8), 56.79 (s, OCH_3). Anal. Calcd for $C_{21}H_{14}N_2O_7$: C, 62.07; H, 3.47; N, 6.89. Found: C, 61.99; H, 3.37; N, 6.73 (%).

5-[(7-Hydroxy-4-oxo-4*H*-chromen-3-yl-)methylene]-1,3-di(p-anisyl)-pyrimidine-2,4,6(1*H*,2*H*,3*H*)-triones (3g)

Yield 79 %, m.p. 294 °C (Toluene), IR (KBr): 3391 (br, OH), 1703 (vs, C=O), 1123 (m, C–O–C). ^{1}H NMR (400 MHz, DMSO-d_6): δ 8.48 (s, 2-H, CH), 7.79 (s, CH=), 7.49 (s, 1H, Ar–H), 7.39 (s, 1H, OH), 6.89–7.16 (m, 8H, Ar–H), 6.47–6.55 (m, 2H, Ar–H), 3.83 (s, 6H, OCH_3). ^{13}C NMR (100 MHz, DMSO-d_6): δ 170.11 (s, C-4, C=O), 162.66 (s, C-7), 159.03 (s, C-4′, C=O), 156.71 (s, C-9), 156.61 (s, C-6′, C=O), 155.04 (s, C–OCH_3), 155.02 (s, C–OCH_3), 154.95 (s, C-2), 148.72 (s, C-2′, C=O), 145.63 (s, CH=), 129.75 (s, C-3), 127.71–129.69 (s, aromatic 10C-atom), 127.26 (s, C-5), 123.30 (s, C-5′, C=CH), 117.45 (s, C-10), 116.50 (s, C-6), 102.17 (s, C-8), 56.79 (d, OCH_3). Anal. Calcd for $C_{28}H_{20}N_2O_8$: C, 65.62; H, 3.93; N, 5.47. Found: C, 65.51; H, 3.83; N, 5.40 (%).

5-[(2,3,4,6-tetra-*o*-acetyl-7-*o*-*β*-D-glucopyranosyloxy-4-oxo-4*H*-chromen-3-yl-)methylene]-1,3-disubstitutedpyrimidine-2,4,6(1*H*,2*H*,3*H*)-triones (5a–g)

In a 25 mL round-bottomed flask, anhydrous K_2CO_3 (6.3 mmol) was added to the blend of DMF (9 mL) and acetone (6 mL), at that point 5-[(7-hydroxy-4-oxo-4H-chromen-3-yl-)methylene]-1,3-disubstitutedpyrimidine-2,4,6(1H,2H,3H)-triones (0.30 mmol) **3**, DTMAB (10 mg) and ACBG (0.60 mmol) **4** were added under mixing, the reaction mixture was refluxed for 5–6 h (monitored by TLC). At that moment acetone was

Author's personal copy

evacuated under vacuum, water (20 mL) was added to the flask. The blend was extricated with ethyl acetate (5 × 10 mL), the organic layer was washed by 20 mL water and brine, dried over anhydrous $MgSO_4$, then removed the solvent to give the residue which was purified by silica gel flash chromatography (ethyl acetate: petroleum ether 1: 2 v/v) to give a brown syrup semisolid.

5-[(2,3,4,6-Tetra-*o*-acetyl-7-*o*-β-D-glucopyranosyloxy-4-oxo-4*H*-chromen-3-yl) methylene]-pyrimidine-2,4,6(1*H*,2*H*,3*H*)-triones (5a)

Yield 79 %, $[\alpha]_D^{25} = -8.9$ (*c* 0.1, DMSO), IR (KBr): 2924 (s, NH), 2854 (s, glucosidic CH), 2363 (s, Ar–CH), 1754 (vs, C=O of *o*-acetyl gps of glycone moiety), 1727 (s, C=O), 1033 (m, C–O–C). ^{1}H NMR (400 MHz, DMSO-d_6): δ 9.69 (s, 1′-H, NH), 9.68 (s, 3′-H, NH), 8.64 (s, 2-H, CH), 7.87 (s, CH=), 6.85–7.72 (m, 3H, Ar–H), 4.86–5.02 (3H, m, 2″, 3″, 4″-H), 4.79 (1H, d, 1″-H, anomeric proton), 4.41 (1H, dd, 5″-H), 3.89–4.10 (2H, m, 6″-H), 2.02, 2.00, 1.99, 1.91 (m, 3H, 4OAc). ^{13}C NMR (100 MHz, DMSO-d_6): δ 171.70, 171.03–171.24 (s, C-atoms of 3Acetyl C=O), 170.61 (s, C-4, C=O), 163.66 (s, C-4′, C=O), 163.25 (s, C-7), 162.43 (s, C-6′, C=O), 156.73 (s, C-9), 155.97 (s, C-2), 149.46 (s, C-2′, C=O), 145.22 (s, CH=), 130.01 (s, C-3), 126.60 (s, C-5), 121.66 (s, C-10), 118.11 (s, C-6), 111.24 (s, C-5′, C=CH), 103.18 (s, C-8), 97.86 (s, C-1″, anomeric C-atom), 73.23 (s, C-3″), 72.48 (s, C-5″), 71.33 (s, C-2″), 69.00 (s, C-4″), 62.62 (s, C-6″), 21.03–21.34 (s, C-atom, $3CH_3$ of Acetyl group), 20.65 (s, C-atom, CH_3 of Acetyl group). Anal. Calcd for $C_{28}H_{26}N_2O_{15}$: C, 53.34; H, 4.16; N, 4.44. Found: C, 53.23; H, 4.07; N, 4.36 (%).

5-[(2,3,4,6-Tetra-*o*-acetyl-7-*o*-β-D-glucopyranosyloxy-4-oxo-4*H*-chromen-3-yl) methylene]-1-phenyl pyrimidine-2,4,6(1*H*,2*H*,3*H*)-triones (5b)

Yield 74 %, $[\alpha]_D^{25} = -7.4$ (*c* 0.1, DMSO), IR (KBr): 2956 (s, NH), 2851 (s, glucosidic CH), 2360 (s, Ar–CH), 1748 (vs, C=O of *o*-acetyl gps of glycone moiety), 1717 (s, C=O), 1133 (m, C–O–C). ^{1}H NMR (400 MHz, DMSO-d_6): δ 10.56 (s, 3′-H, NH), 8.10 (s, 2-H, CH), 7.88 (s, CH=), 6.55–7.32 (m, 8H, Ar–H), 4.89–5.03 (3H, m, 2″, 3″, 4″-H), 4.81 (1H, d, 1″-H, anomeric proton), 4.35 (1H, dd, 5″-H), 3.85–4.13 (2H, m, 6″-H), 2.01, 2.00, 1.98, 1.91 (m, 3H, 4OAc). ^{13}C NMR (100 MHz, DMSO-d_6): δ 171.71, 171.06–171.25 (s, C-atoms of 3Acetyl C=O), 170.64 (s, C-4, C=O), 163.23 (s, C-7), 163.14 (s, C-4′, C=O), 157.37 (s, C-6′, C=O), 156.70 (s, C-9), 155.96 (s, C-2), 154.53 (s, C-2′, C=O), 144.87 (s, CH=), 136.22 (s, C–N), 130.05 (s, C-3), 128.42–129.15 (s, aromatic 5C-atom), 126.63 (s, C-5), 121.61 (s, C-10), 118.14 (s, C-6), 114.04 (s, C-5′, C=CH), 103.19 (s, C-8), 97.85 (s, C-1″, anomeric C-atom), 73.25 (s, C-3″), 72.46 (s, C-5″), 71.35 (s, C-2″), 69.04 (s, C-4″), 62.65 (s, C-6″), 21.05–21.35 (s, C-atom, $3CH_3$ of Acetyl group), 20.63 (s, C-atom, CH_3 of Acetyl group). Anal. Calcd for $C_{34}H_{30}N_2O_{15}$: C, 57.79; H, 4.28; N, 3.96. Found: C, 57.69; H, 4.13; N, 3.85 (%).

5-[(2,3,4,6-Tetra-*o*-acetyl-7-*o*-β-D-glucopyranosyloxy-4-oxo-4*H*-chromen-3-yl) methylene]-1,3-diphenylpyrimidine-2,4,6 (1*H*,2*H*,3*H*)-triones (5c)

Yield 68 %, $[\alpha]_D^{25} = -7.9$ (*c* 0.1, DMSO), IR (KBr): 2868 (s, glucosidic CH), 2361 (s, Ar–CH), 1755 (vs, C=O of *o*-acetyl gps of glycone moiety), 1708 (s, C=O), 1073 (m, C–O–C). ^{1}H NMR (400 MHz, DMSO-d_6): δ 8.08 (s, 2-H, CH), 7.81 (s, CH=), 6.58-7.28 (m, 13H, Ar–H), 4.86–5.00 (3H, m, 2″, 3″, 4″-H), 4.88 (1H, d, 1″-H, anomeric proton), 4.37 (1H, dd, 5″-H), 3.86–4.15 (2H, m, 6″-H), 2.02, 2.00, 1.95, 1.94 (m, 3H, 4OAc). ^{13}C NMR (100 MHz, DMSO-d_6): δ 171.69, 171.04–171.24 (s, C-atoms of 3Acetyl C=O), 170.66 (s, C-4, C=O), 163.21 (s, C-7), 159.86 (s, C-4′, C=O), 156.71 (s, C-9), 155.97 (s, C-2), 155.61 (s, C-6′, C=O), 149.31 (s, C-2′, C=O), 146.07 (s, CH=), 135.74–135.95 (s, 2C–N), 130.01 (s, C-3), 128.13–129.13 (s, aromatic 10C-atom), 126.61 (s, C-5), 121.65 (s, C-10), 118.15 (s, C-6), 114.09 (s, C-5′, C=CH), 103.15 (s, C-8), 97.88 (s, C-1″, anomeric C-atom), 73.26 (s, C-3″), 72.43 (s, C-5″), 71.31 (s, C-2″), 69.02 (s, C-4″), 62.67 (s, C-6″), 21.02–21.31 (s, C-atom, $3CH_3$ of Acetyl group), 20.63 (s, C-atom, CH_3 of Acetyl group). Anal. Calcd for $C_{40}H_{34}N_2O_{15}$: C, 61.38; H, 4.38; N, 3.58. Found: C, 61.25; H, 4.30; N, 3.49 (%).

5-[(2,3,4,6-Tetra-*o*-acetyl-7-*o*-β-D-glucopyranosyloxy-4-oxo-4*H*-chromen-3-yl) methylene]-1-(o-tolyl)-pyrimidine-2,4,6(1*H*,2*H*,3*H*)-triones (5d)

Yield 70 %, $[\alpha]_D^{25} = -5.3$ (*c* 0.1, DMSO), IR (KBr): 2938 (s, NH), 2851 (s, glucosidic CH), 2362 (s, Ar–CH), 1734 (vs, C=O of *o*-acetyl gps of glycone moiety), 1708 (s, C=O), 1073 (m, C–O–C). ^{1}H NMR (400 MHz, DMSO-d_6): δ 10.71 (s, 3′-H, NH), 8.17 (s, 2-H, CH), 7.82 (s, CH=), 6.51–7.27 (m, 7H, Ar–H), 4.81–4.99 (3H, m, 2″, 3″, 4″-H), 4.82 (1H, d, 1″-H, anomeric proton), 4.37 (1H, dd, 5″-H), 3.90–4.11 (2H, m, 6″-H), 2.25 (s, 3H, CH_3), 2.01, 2.00, 1.97, 1.92 (m, 3H, 4OAc). ^{13}C NMR (100 MHz, DMSO-d_6): δ 171.69, 171.05–171.22 (s, C-atoms of 3Acetyl C=O), 170.65 (s, C-4, C=O), 163.27 (s, C-7), 163.14 (s, C-4′, C=O), 156.57 (s, C-6′, C=O), 156.75 (s, C-9), 155.98 (s, C-2), 153.38 (s, C-2′, C=O), 144.82 (s, CH=), 133.08 (s, C–N), 131.29 (s, C–CH_3), 130.09 (s, C-3), 127.90–129.83 (s, aromatic 4C-atom), 126.65 (s, C-5), 121.65 (s, C-10),

Author's personal copy

118.12 (s, C-6), 114.07 (s, C-5′, C=CH), 103.15 (s, C-8), 97.83 (s, C-1″, anomeric C-atom), 73.21 (s, C-3″), 72.42 (s, C-5″), 71.33 (s, C-2″), 69.00 (s, C-4″), 62.64 (s, C-6″), 21.02–21.31 (s, C-atom, $3CH_3$ of Acetyl group), 20.61 (s, C-atom, CH_3 of Acetyl group), 17.42 (s, Ar–CH_3). Anal. Calcd for $C_{35}H_{32}N_2O_{15}$: C, 58.33; H, 4.48; N, 3.89. Found: C, 58.22; H, 4.34; N, 3.78 (%).

5-[(2,3,4,6-Tetra-*o*-acetyl-7-*o*-β-D-glucopyranosyloxy-4-oxo-4*H*-chromen-3-yl-) methylene]-1,3-di(o-tolyl)-pyrimidine-2,4,6 (1*H*,2*H*,3*H*)-triones (5e)

Yield 77 %, $[\alpha]_D^{25} = -6.2$ (*c* 0.1, DMSO), IR (KBr): 2851 (s, glucosidic CH), 2366 (s, Ar–CH), 1744 (vs, C=O of *o*-acetyl gps of glycone moiety), 1709 (s, C=O), 1063 (m, C–O–C). ^{1}H NMR (400 MHz, DMSO-d_6): δ 8.07 (s, 2-H, CH), 7.82 (s, CH=), 6.56–7.25 (m, 11H, Ar–H), 4.82–5.01 (3H, m, 2″, 3″, 4″-H), 4.77 (1H, d, 1″-H, anomeric proton), 4.38 (1H, dd, 5″-H), 3.87–4.14 (2H, m, 6″-H), 2.28 (s, 6H, CH_3), 2.02, 2.01, 1.98, 1.92 (m, 3H, 4OAc). ^{13}C NMR (100 MHz, DMSO-d_6): δ 171.67, 171.05–171.22 (s, C-atoms of 3Acetyl C=O), 170.67 (s, C-4, C=O), 163.28 (s, C-7), 159.13 (s, C-4′, C=O), 156.75 (s, C-9), 155.98 (s, C-2), 155.05 (s, C-6′, C=O), 147.81 (s, C-2′, C=O), 146.08 (s, CH=), 133.09 (s, C–N), 133.02 (s, C–N), 131.15 (s, C–CH_3), 131.01 (s, C–CH_3), 130.09 (s, C-3), 127.81–128.98 (s, aromatic 8C-atom), 126.67 (s, C-5), 121.61 (s, C-10), 118.16 (s, C-6), 114.19 (s, C-5′, C=CH), 103.16 (s, C-8), 97.83 (s, C-1″, anomeric C-atom), 73.21 (s, C-3″), 72.46 (s, C-5″), 71.35 (s, C-2″), 69.01(s, C-4″), 62.61 (s, C-6″), 21.05–21.36 (s, C-atom, $3CH_3$ of Acetyl group), 20.65 (s, C-atom, CH_3 of Acetyl group), 17.20–17.60 (s, 2Ar–CH_3). Anal. Calcd for $C_{42}H_{38}N_2O_{15}$: C, 62.22; H, 4.72; N, 3.46. Found: C, 62.11; H, 4.61; N, 3.34 (%).

5-[(2,3,4,6-Tetra-*o*-acetyl-7-*o*-β-D-glucopyranosyloxy-4-oxo-4*H*-chromen-3-yl-) methylene]-1-(p-anisyl)-pyrimidine-2,4,6(1*H*,2*H*,3*H*)-triones (5f)

Yield 69 %, $[\alpha]_D^{25} = -6.6$ (*c* 0.1, DMSO), IR (KBr): 2935 (s, NH), 2851 (s, glucosidic CH), 2361 (s, Ar–CH), 1728 (vs, C=O of *o*-acetyl gps of glycone moiety), 1708 (s, C=O), 1089 (s, C–O–C); ^{1}H NMR (400 MHz, DMSO-d_6): δ 10.51 (s, 3′-H, NH), 8.19 (s, 2-H, CH), 7.84 (s, CH=), 6.50–7.21 (m, 7H, Ar–H), 4.79–4.98 (3H, m, 2″, 3″, 4″-H), 4.84 (1H, d, 1″-H, anomeric proton), 4.39 (1H, dd, 5″-H), 3.94–4.14 (2H, m, 6″-H), 3.65 (s, 3H, OCH_3), 2.01, 2.00, 1.95, 1.94 (m, 3H, 4OAc). ^{13}C NMR (100 MHz, DMSO-d_6): δ 171.67, 171.06–171.21 (s, C-atoms of 3Acetyl C=O), 170.62 (s, C-4, C=O), 163.23 (s, C-7), 163.13 (s, C-4′, C=O), 159.72 (s, C–OCH_3), 157.56 (s, C-6′, C=O), 156.74 (s, C-9), 155.95 (s, C-2), 154.57 (s, C-2′, C=O), 144.82 (s, CH=), 130.02 (s, C-3), 129.48 (s, C–N), 127.45–129.13 (s, aromatic 4C-atom), 126.63 (s, C-5), 121.61 (s, C-10), 118.09 (s, C-6), 114.05 (s, C-5′, C=CH), 103.17 (s, C-8), 97.84 (s, C-1″, anomeric C-atom), 73.22 (s, C-3″), 72.45 (s, C-5″), 71.31 (s, C-2″), 69.02 (s, C-4″), 62.63 (s, C-6″), 56.02 (s, Ar–OCH_3), 21.01–21.32 (s, C-atom, $3CH_3$ of Acetyl group), 20.62 (s, C-atom, CH_3 of Acetyl group). Anal. Calcd for $C_{35}H_{32}N_2O_{16}$: C, 57.07; H, 4.38; N, 3.80. Found: C, 56.87; H, 4.25; N, 3.73 (%).

5-[(2,3,4,6-Tetra-*o*-acetyl-7-*o*-β-D-glucopyranosyloxy-4-oxo-4*H*-chromen-3-yl-) methylene]-1,3-di(p-anisyl)-pyrimidine-2,4,6 (1*H*,2*H*,3*H*)-triones (5g)

Yield 73 %, $[\alpha]_D^{25} = -4.8$ (*c* 0.1, DMSO), IR (KBr): 2864 (s, glucosidic CH), 2360 (s, Ar–CH), 1748 (vs, C=O of *o*-acetyl gps of glycone moiety), 1719 (s, C=O), 1102 (m, C–O–C). ^{1}H NMR (400 MHz, DMSO-d_6): δ 8.07 (s, 2-H, CH), 7.82 (s, CH=), 6.56–7.25 (m, 11H, Ar–H), 4.82–5.01 (3H, m, 2″, 3″, 4″-H), 4.78 (1H, d, 1″-H, anomeric proton), 4.40 (1H, dd, 5″-H), 3.84–4.15 (2H, m, 6″-H), 3.69 (s, 6H, OCH_3), 2.01, 2.00, 1.97, 1.94 (m, 3H, 4OAc). ^{13}C NMR (100 MHz, DMSO-d_6): δ 171.69, 171.02–171.23 (s, C-atoms of 3Acetyl C=O), 170.64 (s, C-4, C=O), 163.29 (s, C-7), 159.83 (s, C-4′, C=O), 159.56–159.72 (s, 2C–OCH_3), 156.77 (s, C-9), 155.95 (s, C-2), 155.65 (s, C-6′, C=O), 149.31 (s, C-2′, C=O), 146.06 (s, CH=), 130.10 (s, C-3), 128.65–128.79 (s, 2C–N), 127.41–128.48 (s, aromatic 8C-atom), 126.65 (s, C-5), 121.63 (s, C-10), 118.11 (s, C-6), 114.13 (s, C-5′, C=CH), 103.17 (s, C-8), 97.84 (s, C-1″, anomeric C-atom), 73.20 (s, C-3″), 72.44 (s, C-5″), 71.32 (s, C-2″), 68.97 (s, C-4″), 62.59 (s, C-6″), 21.06–21.37 (s, C-atom, $3CH_3$ of Acetyl group), 20.61 (s, C-atom, CH_3 of Acetyl group), 56.02–56.23 (s, 2Ar–OCH_3). Anal. Calcd for $C_{42}H_{38}N_2O_{17}$: C, 59.86; H, 4.54; N, 3.32. Found: C, 59.75; H, 4.39; N, 3.21 (%).

5-[(7-*o*-β-D-glucopyranosyloxy-4-oxo-4*H*-chromen-3-yl-)methylene]-1,3-disubstitutedpyrimidine-2,4,6 (1*H*,2*H*,3*H*)-triones (6a–g)

The mixture of 5-[(2,3,4,6-tetra-*o*-acetyl-7-*o*-β-D-glucopyranosyloxy-4-oxo-4*H*-chromen-3-yl-)methylene]-1,3-disubstitutedpyrimidine-2,4,6(1*H*,2*H*,3*H*)-trione (0.109 mmol) **5**, dry methanol (2 mL) and, anhydrous zinc acetate (0.126 mmol) was refluxed for 7–8 h (checked by TLC). After chilled off at room temperature, it was filtered through cation traded resin; the solvent was evacuated under vacuum. The residue was cleaned by silica gel chromatography ($CHCl_3$, MeOH, 12:1 v/v) to get viscous, strongly hygroscopic titled compound as brown syrup.

Author's personal copy

5-[(7-*o*-β-D-Glucopyranosyloxy-4-oxo-4*H*-chromen-3-yl-)methylene]-pyrimidine-2,4,6(1*H*,2*H*,3*H*)-trione (6a)

Yield 85 %, $[\alpha]_D^{25} = -16.2$ (*c* 0.1, DMSO), IR (KBr): 3374 (br, –OH peak of carbohydrate residue), 2927 (s, NH), 2854 (s, glucosidic CH), 2363 (s, Ar–CH), 1627 (s, C=O), 1032 (m, C–O–C). ^{1}H NMR (400 MHz, DMSO-d_6): δ 10.40 (s, 1′-H, NH), 10.35 (s, 3′-H, NH), 7.77 (s, CH=), 7.64 (s, 1H, Ar–H), 7.19 (s, 2-H, CH), 6.66–6.69 (d, 2H, Ar–H), 5.82 (d, 1H,1″-H, anomeric proton), 4.24 (dd, 1H, 2″-H), 3.50 (dd, 1H, 4″-H), 3.47 (d, 2H, 6″-H), 3.43 (dd, 1H, 3″-H), 3.42 (ddd, 1H, 5″-H). ^{13}C NMR (100 MHz, DMSO-d_6): δ 170.58 (s, C-4, C=O), 163.63 (s, C-6′, C=O), 163.21 (s, C-7), 162.46 (s, C-4′, C=O), 156.69 (s, C-9), 155.94 (s, C-2), 149.45 (s, C-2′, C=O), 145.20 (s, CH=), 130.02 (s, C-3), 126.56 (s, C-5), 121.62 (s, C-10), 118.08 (s, C-6), 111.21 (s, C-5′, C=CH), 103.17 (s, C-8), 101.31 (s, C-1″, anomeric C-atom), 77.98 (s, C-5″), 77.61 (s, C-3″), 73.87 (s, C-2″), 71.11 (s, C-4″), 62.15 (s, C-6″). MS (EI, 70 eV): *m/z* (%) 463 (28) $[M + 1]^+$, 300 (100), 163 (32), 161 (28), 139 (10), 127 (12). Anal. Calcd for $C_{20}H_{18}N_2O_{11}$: C, 51.95; H, 3.92; N, 6.06. Found: C, 51.83; H, 3.81; N, 5.97 (%).

5-[(7-*o*-β-D-Glucopyranosyloxy-4-oxo-4*H*-chromen-3-yl-)methylene]-1-phenylpyrimidine-2,4,6(1*H*,2*H*,3*H*)-triones (6b)

Yield 70 %, $[\alpha]_D^{25} = -19.6$ (*c* 0.1, DMSO), IR (KBr): 3398 (br, –OH peak of carbohydrate residue), 2954 (s, NH), 2867 (s, glucosidic CH), 2360 (m, Ar–CH), 1678 (vs, C=O), 1087 (m, C–O–C). ^{1}H NMR (400 MHz, DMSO-d_6): δ 10.65 (s, 3′-H, NH), 8.55 (s, 2-H, CH), 7.79 (s, CH=), 6.51–7.42 (m, 8H, Ar–H), 5.77 (d, 1H,1″-H, anomeric proton), 4.24 (dd, 1H, 2″-H), 3.50 (dd, 1H, 3″-H), 3.49 (dd, 1H, 4″-H), 3.45 (d, 2H, 6″-H), 3.40 (ddd, 1H, 5″-H). ^{13}C NMR (100 MHz, DMSO-d_6): δ 170.58 (s, C-4, C=O), 163.16 (s, C-7), 163.12 (s, C-4′, C=O), 157.32 (s, C-6′, C=O), 156.69 (s, C-9), 155.94 (s, C-2), 154.51 (s, C-2′, C=O), 144.83 (s, CH=), 136.19 (s, C–N), 130.01 (s, C-3), 128.74–129.96 (s, aromatic 5C-atom), 126.61 (s, C-5), 121.63 (s, C-10), 118.12 (s, C-6), 114.01 (s, C-5′, C=CH), 103.16 (s, C-8), 101.29 (s, C-1″, anomeric C-atom), 77.96 (s, C-5″), 77.61 (s, C-3″), 73.95 (s, C-2″), 71.14 (s, C-4″), 62.21 (s, C-6″). MS (EI, 70 eV): *m/z* (%) 539 (18) $[M + 1]^+$, 376 (100), 215 (11), 203 (35), 163 (32), 161 (24). Anal. Calcd for $C_{26}H_{22}N_2O_{11}$: C, 57.99; H, 4.12; N, 5.20. Found: C, 57.89; H, 4.07; N, 5.06 (%).

5-[(7-*o*-β-D-Glucopyranosyloxy-4-oxo-4*H*-chromen-3-yl-)methylene]-1,3-diphenylpyrimidine-2,4,6 (1*H*,2*H*,3*H*)-triones (6c)

Yield 76 %, $[\alpha]_D^{25} = -21.3$ (*c* 0.1, DMSO), IR (KBr): 3399 (br, –OH peak of carbohydrate residue), 2849 (s, glucosidic CH), 2360 (s, Ar–CH), 1698 (vs, C=O), 1059 (m, C–O–C). ^{1}H NMR (400 MHz, DMSO-d_6): δ 7.84 (s, CH=), 7.33–7.58 (m, 5H, Ar–H), 7.22 (s, 2-H, CH), 6.61–7.19 (m, 8H, Ar–H), 5.75 (d, 1H,1″-H, anomeric proton), 4.18 (dd, 1H, 2″-H), 3.51 (dd, 1H, 4″-H), 3.47 (d, 2H, 6″-H), 3.42 (dd, 1H, 3″-H), 3.41 (ddd, 1H, 5″-H). ^{13}C NMR (100 MHz, DMSO-d_6): δ 170.65 (s, C-4, C=O), 163.23 (s, C-7), 159.81 (s, C-6′, C=O), 156.69 (s, C-9), 155.94 (s, C-2), 155.66 (s, C-4′, C=O), 149.30 (s, C-2′, C=O), 146.09 (s, CH=), 135.71–135.93 (s, 2C–N), 130.03 (s, C-3), 128.15–129.25 (s, aromatic 10C-atom), 126.65 (s, C-5), 121.61 (s, C-10), 118.12 (s, C-6), 114.15 (s, C-5′, C=CH), 103.19 (s, C-8), 101.39 (s, C-1″, anomeric C-atom), 77.93 (s, C-5″), 77.64 (s, C-3″), 73.91 (s, C-2″), 71.12 (s, C-4″), 62.17 (s, C-6″). MS (EI, 70 eV): *m/z* (%) 616 (19) $[M + 1]^+$, 453 (100), 291 (23), 279 (27), 163 (18), 161 (28). Anal. Calcd for $C_{32}H_{26}N_2O_{11}$: C, 62.54; H, 4.26; N, 4.57. Found: C, 62.38; H, 4.15; N, 4.41 (%).

5-[(7-*o*-β-D-Glucopyranosyloxy-4-oxo-4*H*-chromen-3-yl-)methylene]-1-(o-tolyl)-pyrimidine-2,4,6 (1*H*,2*H*,3*H*)-triones (6d)

Yield 81 %, $[\alpha]_D^{25} = -17.8$ (*c* 0.1, DMSO), IR (KBr): 3394 (br, –OH peak of carbohydrate residue), 2957 (s, NH), 2862 (s, glucosidic CH), 2361 (s, Ar–CH), 1674 (vs, C=O), 1082 (m, C–O–C). ^{1}H NMR (400 MHz, DMSO-d_6): δ 10.90 (s, 3′-H, NH), 8.59 (s, 2-H, CH), 7.81 (s, CH=), 6.60–7.59 (m, 7H, Ar–H), 5.77 (d, 1H,1″-H, anomeric proton), 4.22 (dd, 1H, 2″-H), 3.47 (d, 2H, 6″-H), 3.46 (dd, 1H, 4″-H), 3.43 (dd, 1H, 3″-H), 3.39 (ddd, 1H, 5″-H), 2.19 (s, 3H, CH_3). ^{13}C NMR (100 MHz, DMSO-d_6): δ 170.67 (s, C-4, C=O), 163.23 (s, C-7), 163.12 (s, C-4′, C=O), 156.73 (s, C-9), 156.54 (s, C-6′, C=O), 155.95 (s, C-2), 153.32 (s, C-2′, C=O), 144.84 (s, CH=), 133.01 (s, C–N), 131.22 (s, C–CH_3), 130.05 (s, C-3), 127.92–129.74 (s, aromatic 4C-atom), 126.62 (s, C-5), 121.64 (s, C-10), 118.11 (s, C-6), 114.04 (s, C-5′, C=CH), 103.25 (s, C-8), 101.29 (s, C-1″, anomeric C-atom), 77.91 (s, C-5″), 77.62 (s, C-3″), 73.83 (s, C-2″), 71.10 (s, C-4″), 62.14 (s, C-6″), 17.40 (s, Ar–CH_3). MS (EI, 70 eV): *m/z* (%) 554 (21) $[M + 1]^+$, 391 (100), 229 (18), 217 (17), 163 (32), 161 (28). Anal. Calcd for $C_{27}H_{24}N_2O_{11}$: C, 58.70; H, 4.38; N, 5.07. Found: C, 58.59; H, 4.24; N, 4.97 (%).

Author's personal copy

5-[(7-*o*-β-D-Glucopyranosyloxy-4-oxo-4*H*-chromen-3-yl-)methylene]-1,3-di(o-tolyl)-pyrimidine-2,4,6 (1*H*,2*H*,3*H*)-triones (6e)

Yield 78 %, $[\alpha]_D^{25} = -19.7$ (*c* 0.1, DMSO), IR (KBr): 3377 (br, –OH peak of carbohydrate residue), 2848 (s, glucosidic CH), 2366 (s, Ar–CH), 1687 (vs, C=O), 1072 (m, C–O–C). ^{1}H NMR (400 MHz, DMSO-d_6): δ 7.82 (s, CH=), 7.21 (s, 2-H, CH), 6.63–7.19 (m, 11H, Ar–H), 5.79 (d, 1H, 1″-H, anomeric proton), 4.18 (dd, 1H, 2″-H), 3.71 (d, 2H, 6″-H), 3.68 (dd, 1H, 3″-H), 3.34 (dd, 1H, 4″-H), 3.23 (ddd, 1H, 5″-H), 2.31 (s, 6H, CH_3). ^{13}C NMR (100 MHz, DMSO-d_6): δ 170.64 (s, C-4, C=O), 163.27 (s, C-7), 159.11 (s, C-4′, C=O), 156.71 (s, C-9), 155.94 (s, C-2), 155.07 (s, C-6′, C=O), 147.85 (s, C-2′, C=O), 146.02 (s, CH=), 133.01–133.11 (s, 2C–N), 131.11–131.21 (s, 2C–CH_3), 130.03 (s, C-3), 127.62–128.88 (s, aromatic 8C-atom), 126.61 (s, C-5), 121.64 (s, C-10), 118.13 (s, C-6), 114.15 (s, C-5′, C=CH), 103.18 (s, C-8), 101.34 (s, C-1″, anomeric C-atom), 77.96 (s, C-5″), 77.61 (s, C-3″), 73.85 (s, C-2″), 71.11(s, C-4″), 62.16 (s, C-6″), 17.25–17.55 (s, 2Ar–CH_3). MS (EI, 70 eV): *m/z* (%) 644 (18) $[M + 1]^+$, 481 (100), 319 (24), 307 (18), 163 (29), 161 (31). Anal. Calcd for $C_{34}H_{30}N_2O_{11}$: C, 63.55; H, 4.71; N, 4.36. Found: C, 63.41; H, 4.63; N, 4.25 (%).

5-[(7-*o*-β-D-Glucopyranosyloxy-4-oxo-4*H*-chromen-3-yl-)methylene]-1-(p-anisyl)-pyrimidine-2,4,6 (1*H*,2*H*,3*H*)-triones (6f)

Yield 79 %, $[\alpha]_D^{25} = -19.1$ (*c* 0.1, DMSO), IR (KBr): 3384 (br, –OH peak of carbohydrate residue), 2974 (s, NH), 2871 (s, glucosidic CH), 2360 (s, Ar–CH), 1624 (vs, C=O), 1089 (m, C–O–C). ^{1}H NMR (400 MHz, DMSO-d_6): δ 10.81 (s, 3′-H, NH), 8.57 (s, 2-H, CH), 7.75 (s, CH=), 6.59–7.42 (m, 7H, Ar–H), 5.77 (d, 1H,1″-H, anomeric proton), 4.24 (dd, 1H, 2″-H), 3.71 (d, 2H, 6″-H), 3.70 (dd, 1H, 3″-H), 3.77 (s, 3H, CH_3), 3.31 (dd, 1H, 4″-H), 3.17 (ddd, 1H, 5″-H). ^{13}C NMR (100 MHz, DMSO-d_6): δ 170.60 (s, C-4, C=O), 163.27 (s, C-7), 163.11 (s, C-4′, C=O), 159.71 (s, C–OCH_3), 157.36 (s, C-6′, C=O), 156.71 (s, C-9), 155.94 (s, C-2), 154.51 (s, C-2′, C=O), 144.84 (s, CH=), 130.03 (s, C-3), 129.42 (s, C–N), 127.25–129.02 (s, aromatic 4C-atom), 126.61 (s, C-5), 121.64 (s, C-10), 118.07 (s, C-6), 114.07 (s, C-5′, C=CH), 103.15 (s, C-8), 101.34 (s, C-1″, anomeric C-atom), 77.92 (s, C-5″), 77.62 (s, C-3″), 73.91 (s, C-2″), 71.16 (s, C-4″), 62.17 (s, C-6″), 56.01 (s, Ar–OCH_3). MS (EI, 70 eV): *m/z* (%) 570 (15) $[M + 1]^+$, 407 (100), 245 (16), 233 (21), 163 (22), 161 (35). Anal. Calcd for $C_{27}H_{24}N_2O_{12}$: C, 57.04; H, 4.26; N, 4.93. Found: C, 56.97; H, 4.14; N, 4.80 (%).

5-[(7-*o*-β-D-Glucopyranosyloxy-4-oxo-4*H*-chromen-3-yl-)methylene]-1,3-di(*p*-anisyl)-pyrimidine-2,4,6 (1*H*,2*H*,3*H*)-trione (6g)

Yield 80 %, $[\alpha]_D^{25} = -20.0$ (*c* 0.1, DMSO), IR (KBr): 3394 (br, –OH peak of carbohydrate residue), 2857 (s, glucosidic CH), 2360 (s, Ar–CH), 1698 (s, C=O), 1078 (m, C–O–C). ^{1}H NMR (400 MHz, DMSO-d_6): δ 7.79 (s, CH=), 7.31–7.60 (m, 5H, Ar–H), 7.21 (s, 2-H, CH), 6.63–6.85 (m, 6H, Ar–H), 5.79 (d, 1H, 1″-H, anomeric proton), 4.22 (dd, 1H, 2″-H), 3.49 (dd, 1H, 4″-H), 3.41 (dd, 1H, 3″-H), 3.45 (d, 2H, 6″-H), 3.36 (ddd, 1H, 5″-H), 3.79 (s, 6H, OCH_3). ^{13}C NMR (100 MHz, DMSO-d_6): δ 170.59 (s, C-4, C=O), 163.21 (s, C-7), 159.82 (s, C-4′, C=O), 159.45–159.62 (s, 2C–OCH_3), 156.71 (s, C-9), 155.97 (s, C-2), 155.61 (s, C-6′, C=O), 149.33 (s, C-2′, C=O), 146.01 (s, CH=), 130.04 (s, C-3), 128.27–128.66 (s, 2C–N), 127.39–128.41 (s, aromatic 8C-atom), 126.62 (s, C-5), 121.65 (s, C-10), 118.09 (s, C-6), 114.11 (s, C-5′, C=CH), 103.18 (s, C-8), 101.31 (s, C-1″, anomeric C-atom), 77.94 (s, C-5″), 77.60 (s, C-3″), 73.89 (s, C-2″), 71.17 (s, C-4″), 62.19 (s, C-6″), 56.23–56.83 (s, 2Ar–OCH_3). MS (EI, 70 eV): *m/z* (%) 676 (11) $[M + 1]^+$, 513 (100), 351 (25), 339 (18), 163 (17), 161 (19). Anal. Calcd for $C_{34}H_{30}N_2O_{13}$: C, 60.53; H, 4.48; N, 4.15. Found: C, 60.41; H, 4.31; N, 4.04 (%).

Conclusions

The condensation of 7-hydroxy-3-formyl-4*H*-chromen-4-one with 1,3-disubstituted pyrimidine-2,4,6(1*H*,2*H*,3*H*)-triones in the existence of recently fused potassium acetate in dehydrated acetic anhydride followed by glucosydation of resulting aglycones with ACBG afforded 5-[(7-*o*-β-D-glucopyranosyloxy-4-oxo-4*H*-chromen-3-yl)methylene]-1,3-disubstitutedpyrimidine-2,4,6(1*H*,2*H*,3*H*)-triones **6a**–**g** in decent yield. These aglycones and glucosides assessed in vitro antimicrobial and antioxidant activity. *o*-β-D-Glucosides **6a**–**g** exhibited moderate to outstanding biological activity.

Acknowledgements The inventors are appreciative to the Director, SAIF, Chandigarh and the Head, Department of Chemistry, IIT-Pawai, Mumbai for giving essential spectral examination, the Head, Department of Pharmaceutical Sciences, R T M Nagpur University, Nagpur for biological activity and the Head, Department of Chemistry, R T M Nagpur University, Nagpur for giving fundamental research facility workplaces.

Compliance with ethical standards

Conflict of interest The authors declare that they have no conflict of interest.

Author's personal copy

Publisher's note Springer Nature remains neutral with regard to jurisdictional claims in published maps and institutional affiliations.

References

1. Sing P, Paul K. Simple synthesis of 5-spirobarbituric acids and transformations of spirocyclopropanobarbiturates to 5-substituted barbiturates. Indian J Chem. 2006;45B:247–51.
2. Padmavathi V, Reddy B, Subbaiah V, Padmaja A. Michael adducts-Synthons for a new class of 1,4-dispirocyclohexane derivatives. Indian J Chem. 2006;45B:808–12.
3. Sokmen B, Ugras S, Sarikaya H, Ugras H, Yanardag R. Antibacterial, antiurease, and antioxidant activities of some arylidene barbiturates. Appl Biochem Biotechnology. 2013;171:2030–9.
4. Varki A. Biological roles of glycans. Glycobiology. 2017;27:3–49.
5. Sears P, Wong C. Enzyme action in glycoprotein synthesis. Cell Mol Life Sci. 1998;54:223–52.
6. Bertozzi C, Kiessling L. Chemical glycobiology. Chem Glycobiol. 2001;291:2357–64.
7. Ryan C. Oligosaccharides signals: from plant defence to parasite offence. Proc Natl Acad Sci U Sate Am. 1994;91:1–2.
8. Rudd P, Elliott T, Cresswell P, Wilson I, Dwek R. Glycosylation and the immune system. Science. 2001;291:2370–6.
9. Feizi T. Oligosaccharides that mediate mammalian cell-cell adhesion. Curr Opin Struct Biol. 1993;3:701–10.
10. Phillips M, Nudelman E, Gaeta F, Perez M, Singhal A, Kakomori S. et al. ELAM-1 mediates cell adhesion by recognition of a carbohydrate ligands, Sialyl-Lex. Science. 1990;250:1130–2.
11. Giannis A. The Sialyl lewisx group and its analogues as ligands for selectins: chemoenzymatic syntheses and biological functions. Angew Chem Int Ed Engl. 1994;33:178–80.
12. Yuen CT, Bezouska K, O′Brien J, Stoll M, Lemoine R, Lubineau A. et al. Sulfated blood group Lewisa-A superior oligosaccharide ligand for human E-selectin. J Biol Chem. 1994;269:1595–8.
13. Hatzade K, Taile V, Gaidhane P, Ingle V. Synthesis, structural determination and biological activity of new 7-hydroxy-3-pyrazolyl-4H-chromen-4-ones and their O-D-glucosides. Turkish J Chem. 2010;34:241–54.
14. Hatzade K, Taile V, Ingle V. Synthesis of O-β-D-Glucosides of 7-Hydroxy-3-(disubstituted imidazol-2-yl)-4H-chromen-4-ones, Macroheterocycles. Med Chem Res. 2013;6:192–8.
15. Hatzade K, Sheikh J, Taile V, Ghatole A, Ingle V, Genc M. et al. Antimicrobial/antioxidant activity and POM analyses of novel 7-O-D-glucopyranosyloxy-3-(4, 5-disubstituted imidazol-2-yl)-4H-chromen-4-ones. Med Chem Res. 2015;24:2679–93.
16. Taile VS, Ingle VN, Hatzade KM. Synthesis of 2-(substituted benzylideneamino)-4-(4'-hydroxyphenyl)-thiazoles and their O-glucosides. J Carbohydr Chem. 2010;29:207–21.
17. Taile V, Hatzade K, Umare V, Ingle V. Synthesis of 2-Aryl-4, 5-diphenyl-1-(N-β-D-glucopyranosyl)-imidazoles. Macroheterocycles. 2010;3:157–60.
18. Ghatole A, Lanjewar K, Gaidhane M. Antimicrobial activities; ionic liquid and microwave assistend synthesis of ring-substituted3-(3-bromo-4-oxo-4H-chromen-2-yl)-4H-chromen-4-one. World J Pharm Res. 2014;3:4336–50.
19. Ghatole A, Lanjewar K, Gaidhane M. Synthesis and antimicrobial activity of some substituted bis[2-((E)-2-(4-benzylideneamino) thiazol-4-yl)-4-methylphenol]metal complex. International Journal of Pharmacy and Pharmaceutical Sciences. 2014b;6:142–6.
20. Sliwoski G, Kothiwale S, Meiler J, Lowe E. Computational methods in drug discovery. Pharm Rev. 2014;66:334–95.
21. Lipinski C, Lombardo F, Dominy B, Feeney P. Experimental and computational approaches to estimate solubility and permeability in drug discovery and development settings. Adv Drug Deliv Rev. 2001;46:3–26.
22. Daina A, Zoete V. BOILED-Egg to predict gastrointestinal absorption and brain penetration of small molecules. Chem Med Chem. 2016;11:1117–21.
23. Matlock M, Hughes T, Dahlin J, Swamidass S. Modeling small molecule reactivity identifies promiscuous bioactive compounds. J Chem Inf Model. 2018;26:1483–500.
24. Lacova M, Loos D, Furdik M, Matulova M, El-Shaaer H. Synthesis and reactions of new 4-oxo-4H-benzopyran-3-carboxaldehydes containing hydroxy groups or 2-oxopyran cycles. Molecules. 1998;3:149–58.
25. Cope C, Heyl D, Eide C, Arrova A. 1,3-dimethyl-5-alkyl barbituric acids. J Am Chem Soc. 1941;63:356–8.
26. Lacova M, Gasparova R, Loos D, Liptay T, Pronayova N. Effect of microwave irradiation on the condensation of 6-substituted 3-formylchrononones with some five-membered heterocyclic compounds. Molecules. 2000;5:167–78.
27. Wang Y, Li L, Wang Q, Li Y. An improved phase transfer catalysed synthetic method for ononin and rothindin. Synth Commun. 2001;31:3423–7.
28. Gaidhane M, Ghatole A, Lanjewar K. Synthesis of chromone functionalized chitosan polymer: application/screening of its physical parameters. Polym Sci, Ser B. 2020;62:206–17.
29. Ghatole A, Gaidhane M, Lanjewar K. Pharmacokinetics, drug-likeness, medicinal properties, molecular docking analysis of substituted β-lactams synthesized via [Bmim][PF_6]/[ET_3NH]$^{+}$[HSO_4]$^{-}$ catalyzed coupling reaction. Chem Bulgarian J Sci Educ. 2020;29:206–44.
30. Daina AMO. SwissADME: a free web tool to evaluate pharmacokinetics, drug-likeness and medicinal chemistry friendliness of small molecules. Sci Rep. 2017;7:42717.
31. Ghose A, Viswanadhan V, Wendoloski J. A knowledge-based approach in designing combinatorial or medicinal chemistry libraries for drug discovery. 1. A qualitative and quantitative characterization of known drug databases. J Comb Chem. 1999;1:55–68.
32. Egan W, Merz K, Baldwin J. Prediction of drug absorption using multivariate statistics. J Med Chem. 2000;43:3867–77.
33. Veber D, Johnson S, Cheng H, Smith B, Ward KK. Molecular properties that influence the oral bioavailability of drug candidates. J Med Chem. 2002;45:2615–23.
34. Muegge I, Heald S, Brittelli D. Simple Selection Criteria for Drug-like Chemical Matter. J Med Chem. 2001;44:1841–6.
35. Ghose A, Viswanadhan V. Prediction of hydrophobic (lipophilic) properties of small organic molecules using fragmental methods: an analysis of ALOGP and CLOGP methods. J Phys Chem. 1998;102:3762–72.
36. Baell J, Holloway G. New substructure filters for removal of pan assay interference compounds (PAINS) from screening Baell JB, Holloway GA. New substructure filters for removal of pan assay interference compounds (PAINS) from screening. J Med Chem. 2010;53:2719–40.
37. Brenk RS, James D, Krasowski A, Gilbert I, Frearson J. Lessons learnt from assembling screening libraries for drug discovery for neglected diseases. Chem Med Chem. 2008;3:435–44.
38. Hann M, Keseru G. Finding the sweet spot: the role of nature and nurture in medicinal chemistry. Nat Rev Drug Discov. 2012;11:355–65.
39. Teague S, Davis A, Leeson P, Oprea T. The design of leadlike combinatorial libraries. Angew Chem Int Ed Engl. 1999;38:3743–8.
40. Ogu C, Maxa J. Drug interactions due to cytochrome P450. Proc (Bayl Univ Med Cent). 2000;13:421–3.
41. Zlokovic B. The blood–brain barrier in health and chronic neurodegenerative disorders. Neuron. 2008;57:178–201.

Author's personal copy

42. Daneman R. The blood–brain barrier in health and disease. Ann Neurol. 2012;72:648–72.
43. Ritchie T, Macdonald S, Peace S, Pickett S, Luscombe C. Increasing small molecule drug developability in suboptimal chemical space. Med Chem Commun. 2013;4:673.
44. Fagerberg J, Karlsson E, Ulander J, Hanisch G, Bergstrom C. Computational prediction of drug solubility in fasted simulated and aspirated human intestinal fluid. Pharm Res. 2015;32:578–89.
45. Delaney J. Esol: Estimating aqueous solubility directly from molecular structure. J Chem Inf Comput Sci. 2004;44:1000–5.
46. Furniss BS, Hannaford AN, Smith P, Tatechell A. Vogel's Text Book of Practical Organic Chemistry. 5 ed. EL/BS, London: Wiley; 1989.

SPRINGER LINK

Log in

Menu Search Cart

Home Medicinal Chemistry Research



Medicinal Chemistry Research

Publishing model
Hybrid

Submit your manuscript

Editorial board

Aims and scope

Journal updates

Overview

Medicinal Chemistry Research is a journal focused on the publication of novel findings in drug design, drug discovery, and mechanisms of action of biologically active compounds.

Offers prompt publication of experimental achievements.
Covers chemical biological relationships, especially on: structure–activity relationships, investigations of biochemical and pharmacological targets of drug action, and correlations of structure with mode of action.
Increases understanding of biochemical interactions.

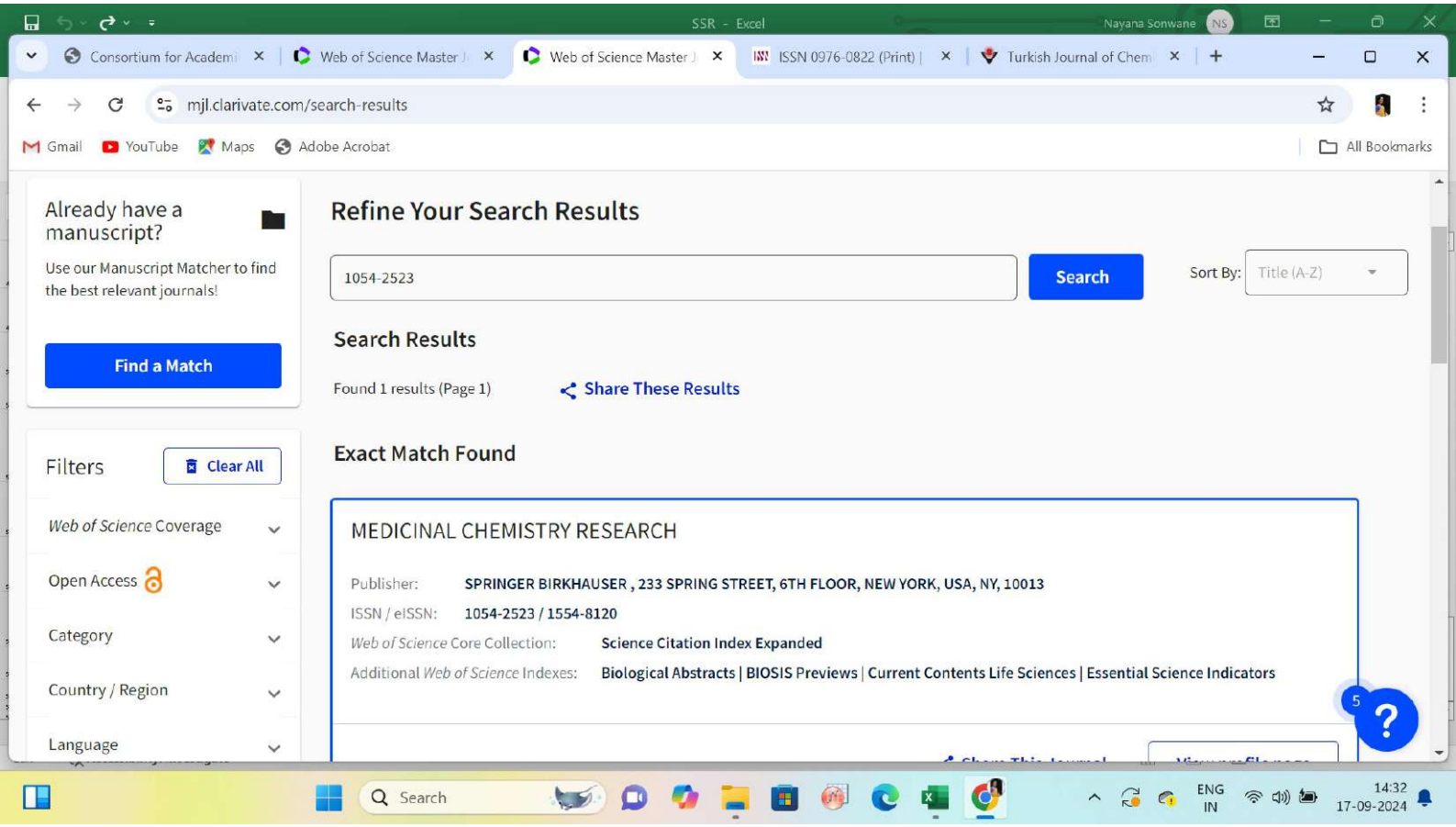
Electronic ISSN **Print ISSN**
1554-8120 1054-2523

Abstracted and indexed in

AGRICOLA
BFI List
BIOSIS
Baidu
Biological Abstracts
CAB Abstracts
CLOCKSS
CNKI
CNPIEC
Chemical Abstracts Service (CAS)
Chimica
Current Contents/Life Sciences
Dimensions
EBSCO
EMBASE
Google Scholar
INIS Atomindex
Japanese Science and Technology Agency (JST)
Meta
Naver
Norwegian Register for Scientific Journals and Series
OCLC WorldCat Discovery Service
Portico
ProQuest
Reaxys
SCImago
SCOPUS
Science Citation Index Expanded (SCIE)
TD Net Discovery Service
UGC-CARE List (India)
Wanfang

Copyright information

Rights and permissions
Editorial policies


SSR - Excel
Nayana Sonwane
Consortium for Academi
Web of Science Master J
Web of Science Master J
ISSN 0976-0822 (Print) |
Turkish Journal of Chem
mjl.clarivate.com/search-results
Gmail
YouTube
Maps
Adobe Acrobat
All Bookmarks
Already have a manuscript?
Use our Manuscript Matcher to find the best relevant journals!
Find a Match
Refine Your Search Results
1054-2523
Search
Sort By:
Title (A-Z)
Search Results
Found 1 results (Page 1)
Share These Results
Exact Match Found
Filters
Clear All
Web of Science Coverage
Open Access
Category
Country / Region
Language
MEDICINAL CHEMISTRY RESEARCH
Publisher: SPRINGER BIRKHAUSER , 233 SPRING STREET, 6TH FLOOR, NEW YORK, USA, NY, 10013
ISSN / eISSN: 1054-2523 / 1554-8120
Web of Science Core Collection: Science Citation Index Expanded
Additional Web of Science Indexes: Biological Abstracts | BIOSIS Previews | Current Contents Life Sciences | Essential Science Indicators
Search
ENG
IN
14:32
17-09-2024

ISSN (Online): 2349-1183; ISSN (Print): 2349-9265
TROPICAL PLANT RESEARCH
The Journal of the Society for Tropical Plant Research
7(2): 484–490, 2020
DOI: 10.22271/tpr.2020.v7.i2.057

Research article

Digitaria and *Setaria* species of subfamily- Panicoideae, Tribe- Paniceae (Poaceae) from Bhandara District of Maharashtra, India

Vijay J. Tiwari* and Chandan R. Sakharkar

Department of Botany, J. M. Patel College, Bhandara 441 904, Maharashtra, India

*Corresponding Author: vijaysstiwari@gmail.com

[Accepted: 16 August 2020]

Abstract: The present paper deals with the taxonomic study of four species of *Digitaria* and three species of *Setaria* grasses. The reports species are *viz.*, *Digitaria ciliaris*, *D. stricta*, *D. radicosa*, *D. sangunalis*, *Setaria intermedia*, *S. Verticillata* and *S. pumila* collected from Bhandara district of Maharashtra State.

Keywords: Digitaria spp. - Setaria spp. - Bhandara district.

[Cite as: Tiwari VJ & Sakharkar CR (2020) *Digitaria* and *Setaria* species of subfamily- Panicoideae, Tribe- Paniceae (Poaceae) from Bhandara District of Maharashtra, India. *Tropical Plant Research* 7(2): 484–490]

INTRODUCTION

The genus *Digitaria* Heist., is commonly known as digit grass because of its radiating inflorescence like fingers of palm. Heister (1748) gave the name *Digitaria*. There are 218 species of genus all around the world (Vega *et al.* 2009). Veldkamp (1973) reported 27 species from Malaysia. Diego (2005) and Valdés-Reyna *et al.* (2015) have reported species diversity from Mexico and Columbia respectively. Boonsuk *et al.* (2016) carried out a taxonomic revision of the *Digitaria* in Myanmar, Peninsular Malaysia, Thailand and Vietnam. Vega *et al.* (2009) carried out studies on morphology-based cladistics analysis of the genus. In India work on *Digitaria* started when Bor (1960) reported 29 species of the genus from Burma, Ceylon, India and Pakistan. Deshpande & Singh (1986) reported 10 species. Singh & Deshpande (1978) reported *Digitaria abludens* (Roem. & Schult.) Veldkamp *D. bicornis* (Lam.) Roem and Schult., *D. ciliaris* (Retz.) Koel., *D. compacta* (Roth.) Veldkamp, *D. longiflora* (Retz.) Pers., *D. radicosa* (J.Presl.) Miq. and *D. setigera* Roth. Shukla (1978) reported 14 species of genus from Eastern India. Recently Singh & Srivastava (2016) carried out taxonomic study of six species of genus *Digitaria abludens* (Roem. & Schult.) Veldkamp, *D. ciliaris* (Retz.) Koel., *D. griffithii* (Hook.f.) Henrard., *D. longiflora* (Retz.) Pers. *D. ternate* (A.Rich.) Stapf., and *D. violascens* Link., collected from Vindhayan region of Uttar Pradesh, India. E-flora published by Botanical Survey of India have species *viz.*, *Digitaria abludens* (Roem. & Schult) Veldkamp, *D. bicornis* (Lam.) Roem & Schult., *D. ciliaris* (Retz.) Koel. *D. cruciata* (Nees ex Steud.) A.Camus., *D. griffithii* (Hook.f) Henrard, *D. longiflora* (Retz.) Pers., *D. radicosa* (J.Presl.) Miq. and *D. setigera* Roth. (eflora of India 2007)

Setaria P. Beauv., is a cosmopolitan genus of with 114 species (Webster 1987). Species of this genus are growing commonly as a weed in paddy fields and open grassland (Rominger 1962, PrasadRao *et al.* 1987, Pensiero 1999). The Old World species are concentrated largely in tropical regions of Africa, including several species endemic to Madagascar (Stapf & Hubbard 1930), whereas in the New World the center of diversity is Brazil (Rominger 1962). The genus is of economic importance because some species are cultivated for grains or perennial forage grass (Rominger 1962, PrasadaRao *et al.* 1987). *Seteria sphacelata* (Schumach.) Stapf & C.E.Hubb. is extensively collected as wild cereals in African savannas in times of scarcity (Delziel 1937) and *S. italica* (L.) P.Beauv., is known as foxtail millet, is cultivated in Asia and other regions as a cereal for humans (Naciri *et al.* 1992). In India Malik (2015) reported *S. glauca*, *S. homogyna*, *S. italica* (L.) P.Beauv., *S. verticillata* (L.) P. Beauv. *S. viridis* (L.) P.Beauv., and e-flora published by Botanical Survey of India reported *Setaria barbata* (Lam.)Kunth., *S. faberim* Herrm., *S. glauca* (L.) P.Beauv. *S. intermedia* Roem. & Schult., *S. italica* (L.) P.Beauv. *S. paliniflora* (K D Koenig) Stapf., *S.poiretiana* (Schult.) Kunth. *S. pumila* (Poir.) Roem. &

Received: 18 March 2020 Published online: xx xxxx 2020
https://doi.org/10.22271/tpr.2020.v7.i2.057

Schult., *S. sphacelata*, (Schumach.) Stapf & C E Hubb., *S.verticillata* (L.) P.Beauv. *S. virdis* (L.) P.Beauv. (eflora of India 2007).

In Maharashta State there are 415 species belonging to 125 genera of grasses (Potdar *et al.* 2012). The history of botanical exploration in the Bhandara district and its adjoining regions reveals that Witt (1911) published a list of fodder grasses found in Central Province and Berar regions. He draw beautiful quarto-atlas depicting the habit sketches of 39 grasses and compiled a list of 80 grass species which he collected from adjoining districts of Bhandara. Later on Graham (1913) enumerated 48 grasses in his descriptive list from adjoining districts *viz.*, Wardha, Naour and Chandrapur. The pioneer work on the grasses in the adjoining Nagpur district was started by Ugemuge (1985). He reported 133 species belonging to 66 genera of grasses. Purekar (1985) in his thesis work reported six species of *Digitaria* and four species of *Setaria* and 197 species distributed among 81 genera of grasses. Later on Tiwari (2013) reported the biodiversity of nine species of *Eragrostis* from the Bhandara district. Tiwari & Deshmukh (2019) four species of *Sporobolus* and 27 species of *Andropogonae* and 56 species of *Paniceae* from Bhandara district. There still exist a number of areas in Bhandara district which are yet to be explored for the study of grasses and hence the present investigation have been undertaken.

MATERIALS AND METHOD

Area under study

Latitude and Longitude - Bhandara district	21º 38′ and 79º 27′
Total Area	3717 km^2
Cultivated Area	1718.63 km^2
Forest Area	1343 km^2
Total major and minor lakes in the district	1254
Maximum Temperature	45ºC
Minimum Temperature	06ºC
Grassland Area	20.370 km^2
Non Agriculture Land	430 km^2
Barren Land	390 km^2
Average Rainfall	1250–1500 mm per annum
Average Elevation	357 meters
Rivers	Wainganga, Chulband, Sur, Godra, Bawanthadi
Adjoining Districts	Nagpur, Chandrapur, Gadchiroli, Balaghat, Gondia

Method adopted

Several field visits were conducted during the year 2018–2019 in various localities for the collection of grasses. 2 or 3 specimens of material is collected for the preparation of herbarium sheets. The morphological study of specimen was carried out with the help of dissecting microscope of Olympus Magnus MSZ – TR Model with binocular eye pieces of SWF10X/22 magnification. Field data was noted in the field book. The plant specimens were pressed, dried, preserved and mounted on standard size of herbarium sheets. The herbarium sheets are deposited in herbarium of J M Patel College, Bhandara. The botanical identification was confirmed by using floras and monographs. The Nikon Cool Pix L810; 26X Zoom 16.1 Mp Camera is used for photography. The taxonomic key is prepared based on easily observable morphological characters in the field.

RESULTS

Enumeration of species

1. *Digitaria ciliaris* (Retz.) Koeler., Descr. Gram. 27. 1802. Bor in Towns., Guest & Al- Rawi, Fl. Iraq 9: 478. 1968; Blake in Proc. R. Soc. Queensland 81: 10. 1969; Bor in Rech.F., Fl. Iran.70: 490.1970; Tzvelev, Poaceae URSS 671. 1976; Calyton in Tutinet. al., Fl. Eur. 5: 262. 1980. **[Fig. 1A]**

Clums erect and decumbent, 30–100 cm. Nodes and pubescent. Leaf shape is linear-lanceolate, upper surface pilose. Ligule present. Inflorescence is raceme, digitate, 5–17 cm, branches 3–10. Spikelet elliptic-acute, 2.50–3.45 mm. Rachis triquetlous. Upper glume ovate, 7 veined. Lower glume triangular. Lower lemma 7 nerved. Stamen 3, Lodicules absent. Caryopsis ellipsoid, light brown.

Flowering and Fruiting: August to December

Habitat: growing as a weed in open grassland.

Locality: Wakeshwar

Collectors Name and Herbarium Sheet Number: VJT- 1751



Figure 1. A, *Digitaria ciliaris* (Retz.) Koeler.; **B**, *Digitaria sanguinalis* (L.) Scopoli; **C**, *Digitaria stricta* Roth ex Roemer & Schultes.; **D**, *Digitaria radicosa* (J. Presl) Miquel.

2. *Digitaria sanguinalis* (L.) Scopoli, Fl. Carinol., ed. 2. 1: 52. 1771. **[Fig. 1B]**

Panicum sanguniale Linnaeus, Sp. Pl. 1: 57. 1753; *Paspalum sanguinale* (L.) Lamarck.

Clums decumbent, 20–70 cm, nodes glabrous. Leaf shape linear lanceolate.Leaf surface pilose. Keel present in leaf sheath, Ligule membranous. Inflorescence receme, digitate, 5–18 cm, branches 4–12, rachis winged. Spikelets are lanceolate –ovate, 3.0–3.5 mm. Upper glumes lanceolate, pubescent and 3–5 nerved. Lower glume is triangular and veinless. Lower lemma is leathery, 7-nerved. Lodicules present. Anthers-3. Caryopsis light green.

Fruiting: October to November

Habitat: Growing on roadsides

Locality: Kesalwada

Collectors Name and Herbarium Sheet Number: VJT- 1762

3. *Digitaria stricta* Roth ex Roemer & Schultes. **[Fig. 1C]**

Agrostis pilosa Retzius; *Digitaria puberula* Link; *D. royleana* (Nees ex J. D. Hooker) Prain; *Paspalum royleanum* Nees ex J. D. Hooker; *Setaria stricta* (Roth ex Roemer & Schultes) Kunth.

Clums ascending, 20–40 cm. Nodes and glabrous. Leaves are linear-lanceolate. Leaf surface hirsute, apex acuminate. Leaf-sheath keel present. Leaf-sheath keel present. Ligule membrances. Inflorescence raceme, digitate, 4–147 cm, 3–6. Rachis winged. Spikelet elliptic-oblong. Sterile florets are basal. Spikelets are 1.2–1.4 mm, pedicillate, three florets in cluster. Upper glume elliptic, glabrous, 3 veined, apex acute. Lower glume isobscure. Lemma of sterile florets, 3–5 nerved, hairy lines between the veins. Lemma of fertile floret is elliptic,

3 nerved, apex is apiculate, cartilaginous. Stamens 3. Lodicules absent. Caryopsis is light brown.

Flowering and Fruiting: July to December

Habitat: growing on open grasslands and roadsides on dry sandy soil.

Locality: Mujbhi

Collectors Name and Herbarium Sheet Number: VJT- 1755

4. *Digitaria radicosa* (J. Presl) Miquel, Fl. Ned. Ind. 3:437. 1837. [**Fig. 1D]**

Panicum radicosum J. Presl, Reliq. Haenk.1: 297. 1830; *Digitaria chinensis* Hornemann var. *hirusta* (Honda) Ohwi; *D. formosana* Rendle; *D. formosana* var. *hirsute* (Honda) Henrard*; D. radicosa* var. *hirsute* (Honda) C.C. Hsu; *D. tenuispica* Rendle; *D. timorensis* (Kunth) Balansa; *Panicum formosanum* (Rendle) Makino &Nemoto: *P. timorense* Kunth; *Syntherisma formosana* (Rendle) Honda; *S. formosana* var. *hirsute* Hond.

Clums trailing, 30–50 cm. Nodes glabrous leaves linear lanceolate. Ligule present. Raceme digitate, branches 2–4, 4–10 cm. Rachis triquetrous. Spikelet with fertile and sterile floret. Sterile floret on lower side. Sterile floret on lower side. Spikelet 2.8–3.0 mm, pedicillate, 2 florets in pair. Upper glume ovate 1–3 veined. Lower glume triangular, apex obtuse. Lower lemma 5–7 veined. Upper lemma is yellow. Palea is cartilaginous. Stames 3. Lodicules absent. Caryopsis yellow.

Habitat: Growing as a weed in wasteland

Locality: Bhilewada

Collectors Name and Herbarium Sheet Number: VJT- 1772

5. *Setaria pumila* (Poiret) Roemer & Schultes, Syst. Veg, 2: 891 1817. **[Fig. 2A]**

Panicum pumilum Poir.; Encycl (suppl.) 4:273, 1816 *Setaria pallidefusca* (Schumach.) Stapf & C.E. HUbb., Bull. Misc. Inform. 1939, 259, 1930; C.Fischer, Fl. Madras 3:1789 (1239) 1934; Bor Grass India 363; 1960; Matthew Mat Fl. Tamilnadu Carnatic 400 1982. *Panicum pallidefuscum* Schum. Beskr Giun. Pl. 58, 1827. Steriaglauca Brot.3:135, 1884, non P. Beauv. 1812: Hooker. F. Fl. Brit India 7, 78, 1896. Rangachari and Tadulingam Handb.5 S. Indian Grasses 110, f, 109, 1921.

Clums tall and erect, 20–90 cm. Leaf blade linear, ligulate. Inflorescence panicle, cylindrical, 3–17 cm, Spikelets ovate, 2.5–3.5mm, bristles 5–10. Upper glume ovate, 5-veined. Lower glume acute 3 veined. Upper lemma ovate, rugose. Lower palea hyaline, keels winged.

Flowering and Fruiting: July to December

Habitat: growing as a weed in paddy field

Locality: Kardha

Collectors Name and Herbarium Sheet Number: VJT- 1750

6. *Setaria verticillata* (L.) P. Beauvois, Ess, Agrostogr. 51. 1812. **[Fig. 2B]**

Panicum verticillatum Linnaeus, Sp. Pl., ed. 2, 1: 82. 1762; *Chaetochloa brevispica* Scribner & Merrill; *C. vertici-llata* (L.) Scribner; *Chamaraphis italic* (L.) Kuntze var. *verticillata* (L.) Kuntze; *C. verticillata* (L.) Porter; *Panicum asperum* Lamarck; *Pennisetum verti-cillatum* (L.) R. Brown; *Setaria brevispica* (Scribner & Merrill) K. Schumann.

Clums tufted, 30–100 cm. Leaves are linear lanceolate. Leaf sheath puberulous, margin ciliate.Leaf blade linear lanceolate.Ligulate. Inflorescence panicled, dense 4–15 cm. Bristles 1–4. Spikelets elliptic, 1.5–2.5mm.Upper glume boat shape, 7-veined.Lower glume obtuse. Upper lemma compressed, rugose.

Flowering and Fruiting: August to October

Habitat: on dry sandy soil roadsides

Locality: Mohadi

Collectors Name and Herbarium Sheet Number: VJT- 1752

7. *Setaria intermedia* Roemer & Schultes, Syst. Veg. 2:489.1817. **[Fig. 2C]**

Panicum tomentosum Roxb.; *Setaria tomentosa* (Roxb.) Kunth.

Clum descubent, 40–60 cm. Leaves are linear lanceolate, liguate as line of hairs. Inflorescence panicle, contracted, narrow lanceolate 3–12 cm. Spikelets elliptic-ovate, acute, 1.5–2.0 mm. Glume elliptic, obtuse.

Lower glume 1-nerved. Upper glume elliptic, obtuse, 5-veined. Palea ovate, second lemma ovate, coracious. Palea faintly rugose.

Flowering and Fruiting: August to December

Habitat: growing as a weed in paddy field

Locality: Tavepar

Collectors Name and Herbarium Sheet Number: VJT- 1749



Figure 2. A, *Setaria pumila* (Poiret) Roemer & Schultes; **B**, *Setaria verticillata* (L.) P. Beauvois; **C**, *Setaria intermedia* Roemer & Schultes.

Taxonomic keys

Digitaria

(1a) Nodes pubescent, upper glume 7 nerved, caryopsis light yellow ……..…….. *D. ciliaris*

(1b) Nodes glabrous, upper glume 3–5 nerved, caryopsis light green/light green ….…….….. (2)

(2a) Lodicules present ……..……. *D. sangunalis*

(2b) Lodicules absent ……..……..…….. (3)

(3a) Raceme 3–6, single spikelet consists of cluster of 3florets ……..…….... *D. stricta*

(3b) Raceme 2–4, single spikelet in pairs of 2 florets ……..……...……. *D. radicosa*

Setaria

(1a) Spikelet ovate 2.5 mm to 3.5 mm ……..…….. *S. pumila*

(1b) Spikelet elliptic 1.5 mm to 2.5 mm ……..……..…… (2)

(2a) Upper glume boat shaped, 7 veined ……..…….. *S. verticillata*

(2b) Upper glume elliptic, obtuse shaped, 5 veined ……..……..... *S. intermedia*

DISCUSSION AND CONCLUSION

Digitaria is extremely variable in inflorescence structure relative length of spikelet scales, and spikelets appressed pubescence, glassy bristles and marginal cilia possible within the same species or even between the two members of a spikelet pair. The morphological study of *Setaria* indicates that species can be differentiated based on node, lead blade, ligule, inflorescence, spikelets and seeds. The authors have pointed out morphological similarities and dissimilarities while dissecting the florets under the microscope to identify these species, The present study plays a significant role in the preparation of taxonomic keys of species of both the genera.

ACKNOWLEDGEMENTS

This second author (CRS) is a student of M Sc. Final year. He worked without any financial support under the guidance of first author. The critical reading and suggestions for improvements of manuscript by Dr. P. N. Purekar, Retd. Principal and Head, Agrostologist, Department of Botany, Shivaji Science College, Nagpur is very much appreciated. The authors are thankful to Dr Vikas Dhomne, Principal, J. M. Patel College, Bhandara for providing basic infrastructure.

REFERENCES

Boonsuk BPC & Hodkinson TR (2016) A taxonomic revision of the genus *Digitaria* (Panicoideae: Poaceae) in mainland Southeast Asia. *Phytotaxa* 246 (4): 248–280.

Bor NL (1960) *The Grasses of Burma, Ceylon, India and Pakistan*. International Book Distributors, Dehradun, pp. 292–397.

Delziel JM (1937) *The Useful Plants of West Tropical Africa*. Crown Agents, London.

Deshpande UR & Singh NP (1986) *Grasses of Maharashtra: Annotated Inventory*. Mittal Publ., Delhi, India, pp. 49–50.

Diego GC (2005) Las Especies Colombianas Del Género Digitaria (Poaceae: Panicoideae: Paniceae) The Colombian species of the genus *Digitaria* (Poaceae: Panicoideae: Paniceae). *Caldasia* 27(1): 25–87.

eflora of India (2007) Database of Indian Plants. Available from: https://sites.google.com/site/efloraofindia/species/m---z/po/poaceae/setaria (accessed: 13 Mar. 2020).

Graham RJD (1913) *List of Grasses and Sedges found on the Nagpur and Telankheri Farms*. Govt. Press., Nagpur.

Heister L (1748) *Systema Plantarum*. Generale ex Fructificatione

Malik V (2015) A Checklist of Grasses (Poaceae) of Saharanpur Forest Division. *Indian Journal of Fundamental and Applied Life Sciences* 5(2): 74–80.

Naciri Y, Darmency H., Belliard J., Dessiant F & Perne's J (1992) Breeding strategy in foxtail millet, *Setaria italica* (L.) P. Beauv. Following interspecific hybridization. *Euphytica* 60: 97–103.

Pensiero JF (1999) Las species sudamericanas del ge'nero Setaria (Poaceae, Paniceae). *Darwiniana* 37: 37–151.

Potdar GG, Salunkhe CB & Yadav SR (2012) *Grasses of Maharashtra*. Shivaji University Publication, Kolhapur.

PrasadaRao KE, de Wet, JET, Brink DE & Mengesha MH (1987) Interspecific variation and systematic of cultivated *Setaria italica*, foxtail millet (Poaceae). *Economic Botany* 41: 108–116.

Purekar PN (1985) Grasses of Nagpur District Taxonomy and Palynology, (Ph.D. Thesis). RTM Nagpur University, Nagpur.

Rominger JM (1962) Taxonomy of *Setaria* (Gramineae) in North America. *III Biology Monograph* 29: 1–132.

Shukla U (1978) Notes on the Grasses of Eastern India. *Indian Journal of Forestry* 1(4): 293–296.

Singh AK & Srivastava MK (2016) Taxonomy and Seedling Morphology of Six species of *Digitaria* (Poaceae) from Vindhyan region, Uttar Pradesh, India. *International Journal of Advanced Research* 4(8): 464–472.

Singh NP & Deshpande UR (1978) A note on the nomenclatural changes in the Indian species of *Digitaria*

Hailer. *Annals of Arid Zone* 17(3): 332–333.

Stapf O & Hubbard OE (1930) *Setaria*. In: D Oliver (ed) *Flora of tropical Africa, Vol, 9 - Gramineae (Maydeae-Paniceae)*. Reeve, Ashford, pp. 768–866.

Tiwari VJ & Deshmukh RN (2019) New Records of Species of *Sporobolus* (Poaceae: Chloridoideae: Cynodontae: Zoysieae) from Bhandara District of Maharashtra State, India *Journal of Emerging Technologies and Innovative Research* 6(6): 954–999.

Tiwari VJ (2013) Biodiversity of Genus *Eragrostis* Wolf. Of Family Poaceae. In: Kapgate DK & Saha RC (eds) *UGC Seminar Biodiversity- A Global Need*. Department of Botany, J. M. Patel College, Bhandara, pp. 109–113.

Ugemuge NR (1985) *Flora of Nagpur district*. Shree Prakashan, Nagpur, M.S., India, pp. 412–413.

Valdés-Reyna J, Villaseñor JL, Encina-Domínguez JA & Enrique O (2015) The Grass Family (Poaceae) in Coahuila, Mexico: Diversity and Distribution. *Botanical Sciences* 93(1): 119–129.

Vega AS, Rua GH, Fabbri LT & Rúgolo ZE (2009) A morphology-based cladistics analysis of *Digitaria* (Poaceae, Panicoideae, Paniceae). *Systematic Botany* 34(2): 312–323.

Veldkamp JF (1973) A revision of *Digitaria Haller* (Gramineae) In Malaysia. Notes on Malaysian Grasses VI. *Blumea* 21: 1–80.

Webster RD (1987) *The Australian Paniceae (Poaceae)*. J. Kramer, Berlin.

Witt DO (1911) *List of Fodder Grasses Found in the Berar Forest Circle of the Central Provinces*. Pioneer Press, Allahabad.


Consortium for Ac
Web of Science M
Web of Science M
ISSN 0976-0822
Home | Medicinal
Tropical Plant Res
tropicalplantresearch.com
Gmail
YouTube
Maps
Adobe Acrobat
All Bookmarks
Tropical Plant Research
An International Journal by Society for Tropical Plant Research
ISSN (E): 2349-1183
ISSN (P): 2349-9265
HOME
INSTRUCTIONS
EDITORIAL BOARD
ARCHIVES
SOCIETY
CONTACT US
WEBMAIL
SEARCH
Journal is inviting manuscripts for its coming issue. Contac
NAVIGATION BAR
Home
Instructions
Editorial Board
Fellows of Society
Library Subscription
USEFUL LINKS
About Journal
Tropical Plant Research is an International, Open Access, Triannual, Peer Reviewed Journal by the Society for Tropical Plant Research. The aim of the Journal is to publish articles related to the current trends of Plant Research in Tropical and Sub-tropical regions of the globe. The Journal provides the platform for motivating the students and research personnel working in the area of Algae, Bryophytes, Pteridophytes, Gymnosperms, Angiosperms and lichenised as well as non lichenised fungi.
Tropical Plant Research considers original research articles, review and short communications related to: Taxonomy, Diversity assessment, Ecology, Environment, Climate Change, GIS/Remote
ONLINE SUBMISSION
Login
Sign Up
ISSUE BAR
Online Issues
Current Issue
Previous Issue
https://www.tropicalplantresearch.com/webmail
Search
ENG
IN
14:57
17-09-2024

UGC-CARE List

You searched for **"2349-1183"**. Total Journals : **1**

Search:

Sr.No.	Journal Title	Publisher	ISSN	E-ISSN	UGC-CARE coverage years	Details
1	Tropical Plant Research	Society for Tropical Plant Research	2349-9265	2349-1183	from June-2019 to January-2020	Discontinued from Jan. 2020

Showing 1 to 1 of 1 entries

Previous 1 Next

Copyright © 2024 Savitribai Phule Pune University. All rights reserved. | Disclaimer

Materials Today: Proceedings xxx (xxxx) xxx

Contents lists available at ScienceDirect

Materials Today: Proceedings

journal homepage: www.elsevier.com/locate/matpr

Thermal degradation and antibacterial study of transition metal complexes derived from novel terpolymer ligand

Wasudeo B. Gurnule [a,*], Yashpal U. Rathod [b], Amoli D. Belsare [c], Narayan C. Das [d]

[a] Department of Chemistry, Kamla Nehru Mahavidyalaya, Nagpur 440024, India
[b] Department of Chemistry, J. M. Patel College, Bhandar 441904, India
[c] Department of Electronics and Telecommunication Engineering, Yaswantrao Chavan College of Engineering, Nagpur, India
[d] Department of Chemistry, Dr. Ambedkar College, Chandrapur 442404, India

ARTICLE INFO

Article history:
Received 5 April 2020
Received in revised form 24 April 2020
Accepted 25 April 2020
Available online xxxx

Keywords:
Metal complexes,
Terpolymer
Antimicrobial activity
Thermogravimetric analysis
FTIR
Morphology

ABSTRACT

Metal complexes are prepared by the buildup of 8-hydroxyquinoline-5-sulphonic acid, formaldehyde and guanidine with 2 M HCl acid is required as a catalyst for polymerization with different feed ratio (3:1:5) of monomers. The structure of metal complexes and ligand were elucidated by NMR, FTIR and elemental analysis. Thermogravimetric analysis was used for the investigation of thermal stability of the terpolymer ligand metal complexes. Additionally, Freeman-Carroll method was utilized for the calculation of activation energy with the help of TGA data. The surface morphology of terpolymer ligand was examined by scanning electron microscopy. The antimicrobial activities of metal complexes and its ligand were tested against *S. aureus*, *E. coli*, and *K. Pneumoniae Klebseilla* bacteria.
© 2020 Elsevier Ltd. All rights reserved.
Selection and peer-review under responsibility of the scientific committee of the International Conference on Advanced Functional Materials (Innovations in Chemical, Physical and Biological Sciences).

1. Introduction

In the recent past synthesis of coordination polymers attracted great enthusiasm owing to their fascinating characteristics such as ability to bind toxic metal ions, thermal stability, act as a catalyst, photoluminescence properties [1–4]. Due to its features as high thermal stability and antimicrobial behavior, the synthesis of polymer-metal complexes attracted researchers [5]. Saeed and co-workers synthesized new thermally stable epoxy polymers containing copper and nickel ions using diglycidal bisphenol A ether with metal complexes in aminothiourea [6]. Azarudeen et al. synthesized new terpolymer ligand and metal chelates derived from anthranilic acid aminopyridine, formaldehyde anthranilic acid, phenyl hydrazine and the complex were studied for thermal stability and antibacterial screening. The results reveals that all the complexes are highly thermally stable and more potent antibacterial agents than their corresponding ligands [7,8]. Some divalent transition metal complexes of 8-hydroxquinoline were prepared and described for their warm air stability and antibacterial activities [9].

The organic copolymer resin and their metal complexes were prepared from hexametylenediammine, formaldehyde and 8-hydroxyquinoline-5-sulfonic acid [10]. Nanosized 8-hydroxyquino-late complexes were synthesized by utilizing simple and layer-by-layer chemical deposition method and contemplated [11]. Terpolymeric ligands and its metal complexes were synthesized involving salisaldehyde, phenylthiourea with glutaraldehyde and investigated for thermal stability and antibacterial properties [12]. Chelation properties of new chelating polymer were investigated and X-ray diffraction data indicates that the incorporation of the metal ions significantly improved the degree of crystallinity [13]. R. Chitra et al synthesized 7-Acryloyloxy-4-methylcoumarin monomer with N-cyclohexyl-Acrylamide in different feed ratio using Azobis isobutyl nitrite as initiator in DMF. The synthesized copolymer were tested for their antibacterial activity and was carried out by using Escherichia coli, Salmonella typhi and bacillus cereus [14].

Recently, however, 2-(N-phthalimido) ethyl methyacrylate and p-chlorophenyl methacrylate homo and copolymers have been prepared in DMF solution at 70 °C using 2,2 azobisisobutyronitrile as initiator, the synthesized copolymer has been evaluated on different microorganisms and these polymers enable bacteria, fungi and yeast to grow by 10–52, 20–58, and 18–56 percent respec-

* Corresponding author.
E-mail address: wbgurnule@gmail.com (W.B. Gurnule).

https://doi.org/10.1016/j.matpr.2020.04.708
2214-7853/© 2020 Elsevier Ltd. All rights reserved.
Selection and peer-review under responsibility of the scientific committee of the International Conference on Advanced Functional Materials (Innovations in Chemical, Physical and Biological Sciences).

ScienceDirect

4.9
CiteScore

Submit your article | Guide for authors

Menu Search in this journal

About the journal

Materials Today: Proceedings provides the materials science community with a fast and flexible route to the publication of research presented at national and international scientific conferences in the field of materials science.
Guest Editors are responsible for quality control, the peer review ...

View full aims & scope

$200 ⓘ
Article publishing charge for open access

14 days
Time to first decision

44 days
Review time

81 days
Submission to acceptance

View all insights

Articles

Latest published | Articles in press | Top cited | Most downloaded

Most popular

Online ISSN: 2214-7853

Copyright © 2024 Elsevier Ltd. All rights are reserved, including those for text and data mining, AI training, and similar technologies.

For authors

Resources for authors ↗

Track your accepted paper ↗

Journal Finder ↗

Researcher Academy ↗

Rights and permissions ↗

Journal Article Publishing Support Center ↗

For editors

Resources for editors ↗

Publishing Ethics Resource Kit ↗

Guest editors ↗

For reviewers

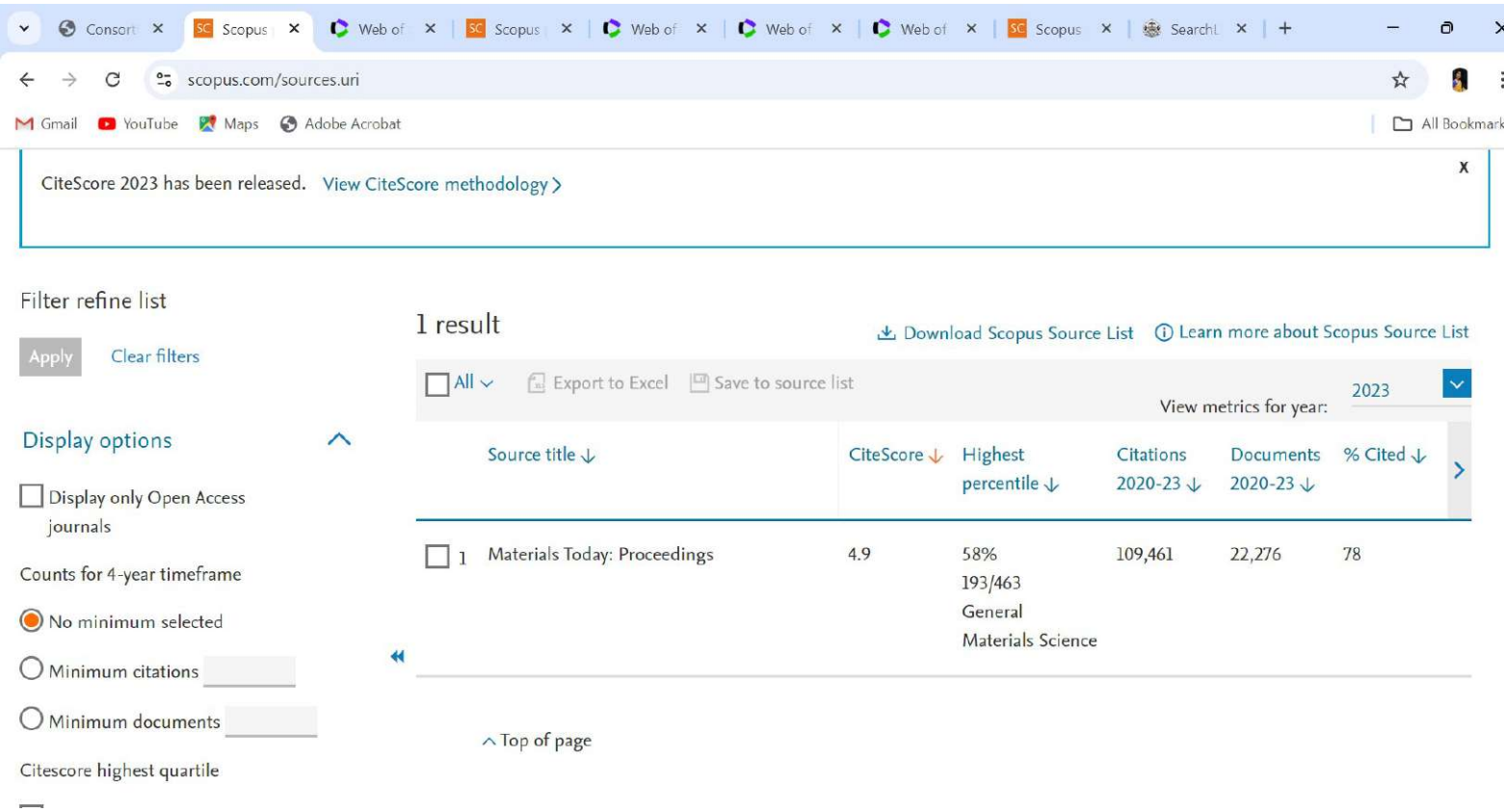
Resources for reviewers ↗

Reviewer recognition ↗

ELSEVIER

All content on this site: Copyright © 2024 Elsevier B.V., its licensors, and contributors. All rights are reserved, including those for text and data mining, AI training, and similar technologies. For all open access content, the Creative Commons licensing terms apply.

RELX™


scopus.com/sources.uri
Gmail
YouTube
Maps
Adobe Acrobat
All Bookmarks
CiteScore 2023 has been released. View CiteScore methodology >
Filter refine list
Apply
Clear filters
Display options
Display only Open Access journals
Counts for 4-year timeframe
No minimum selected
Minimum citations
Minimum documents
Citescore highest quartile
1 result
Download Scopus Source List
Learn more about Scopus Source List
All
Export to Excel
Save to source list
View metrics for year:
2023
Source title
CiteScore
Highest percentile
Citations 2020-23
Documents 2020-23
% Cited
1 Materials Today: Proceedings 4.9 58% 193/463 General Materials Science 109,461 22,276 78
Top of page

Materials Today: Proceedings xxx (xxxx) xxx

Contents lists available at ScienceDirect

Materials Today: Proceedings

journal homepage: www.elsevier.com/locate/matpr

Synthesis, characterization and thermal degradation study of copolymer resin

Wasudeo B. Gurnule [a,*], Narayan C. Das [b], Sharad Vajpai [c], Yashpal U. Rathod [d]

[a] Department of Chemistry, Kamla Nehru Mahavidyalaya, Nagpur 440024, India
[b] Department of Chemistry, Dr. Ambedkar College, Chandrapur 442402, India
[c] Department of Chemistry, Chaitanya College, Pangarh, Janjgir-Champa 495554, CG, India
[d] Department of Chemistry, J. M. Patel College, Bhandara 441906, India

ARTICLE INFO

Article history:
Received 5 April 2020
Received in revised form 25 April 2020
Accepted 28 April 2020
Available online xxxx

Keywords:
Copolymer
Thermal degradation
Kinetics
Thermal stability
Sharp-Wentworth and Freeman-Carroll methods

ABSTRACT

The copolymer 2-H,4-MBP-1,5-DANF-III has been synthesized by the condensation polymerization of 2-hydroxy, 4-methoxybenzophenone (2-H,4-MBP) and 1,5-diaminonaphthalene (1,5-DAN) with formaldehyde (F) in an acidic medium with 3:1:5 M ratio of reactants. Copolymer resin has been characterized by elemental analysis, Ultraviolet, infrared (IR) and nuclear magnetic resonance (NMR) spectroscopy. The morphology of copolymer was studied by scanning electron microscopy (SEM). The thermogravimetric analysis (TGA) has been performed to evaluate the thermal degradation characteristics and to ascertain its thermal stability. Freeman-Carroll and Sharp-Wentworth methods have been used for the evaluation of kinetic parameters. Thermal activation energy Ea determined by Freeman-Carroll and Sharp-Wentworth methods are in close agreement with each other.
© 2020 Elsevier Ltd. All rights reserved.
Selection and peer-review under responsibility of the scientific committee of the International Conference on Advanced Functional Materials (Innovations in Chemical, Physical and Biological Sciences).

1. Introduction

Study of thermal degradation behaviour and computation of kinetic parameters by implementing modern developing thermal degradation kinetic techniques is the subject of interest for many investigators. The interest is fully recognized because the kinetics is related with the decomposition mechanisms in which the thermal degradation takes place [1]. Phenolic resins have a wide number of applications in ion exchangers, semiconductors, insulating materials, activators, protective adhesive, catalysts etc. because of their chemical and heat resistance, high thermal stability and electrical insulation properties [2–4]. To improve the thermal stability at elevated temperature, many researchers have synthesized the copolymer by changing the monomer compositions. Thermogravimetric analysis (TGA) method was applied to study the thermal stability of wide variety of copolymers by several authors [5–9].

Thermal degradation study of copolymer derived from 2,4-dihydroxypropiophenone, 4-pyridylamine with formaldehyde was carried out by Rahangdale et al. [10]. Niley et al. have studied the thermal degradation and electrical conductivity of 4-hydroxyacetophenone, ethylenediamine and formaldehyde terpolymer resin [11]. Gurnule and co-worker studied the non-isothermal degradation of copolymer resin derived from 1,5-diaminonaphthalene, 2,4-dihydroxypropiophenone and formaldehyde [12]. Thermal degradation of 2,4-dihydroxyacetophenone - propylenediamine - formaldehyde terpolymer has been reported by Jiwatode et al. [13]. Dontulwar and coworkers have been studied the kinetics of thermal decomposition of resin resulted from 1-naphthol-4-sulphonic acid, hexamethylenediamine and formaldehyde [14]. Nandekar K. and Mandavgade S. have synthesized copolymer by condensation of salicylic acid and thiosemicarbazide with formaldehyde and TGA method was applied to study the non-isothermal kinetics [15].

The present communication deals with the synthesis, characterization and thermal degradation study of 2-H, 4-MBP-1,5-DAF-III copolymer. The Sharp-Wentworth and Freeman-Carroll methods have been used for the evaluation of activation energy and kinetic parameters such as entropy change (ΔS), free energy change (ΔF), apparent entropy change (S*), frequency factor (Z) and order of reaction (n).

* Corresponding author.
E-mail address: wbgurnule@yahoo.co.in (W.B. Gurnule).

https://doi.org/10.1016/j.matpr.2020.04.828
2214-7853/© 2020 Elsevier Ltd. All rights reserved.
Selection and peer-review under responsibility of the scientific committee of the International Conference on Advanced Functional Materials (Innovations in Chemical, Physical and Biological Sciences).

ScienceDirect

4.9
CiteScore

Submit your article | Guide for authors

Menu Search in this journal

About the journal

Materials Today: Proceedings provides the materials science community with a fast and flexible route to the publication of research presented at national and international scientific conferences in the field of materials science.
Guest Editors are responsible for quality control, the peer review ...

View full aims & scope

$200 ⓘ
Article publishing charge for open access

14 days
Time to first decision

44 days
Review time

81 days
Submission to acceptance

View all insights

Articles

Latest published | Articles in press | Top cited | Most downloaded

Most popular

Online ISSN: 2214-7853

Copyright © 2024 Elsevier Ltd. All rights are reserved, including those for text and data mining, AI training, and similar technologies.

For authors

Resources for authors ↗

Track your accepted paper ↗

Journal Finder ↗

Researcher Academy ↗

Rights and permissions ↗

Journal Article Publishing Support Center ↗

For editors

Resources for editors ↗

Publishing Ethics Resource Kit ↗

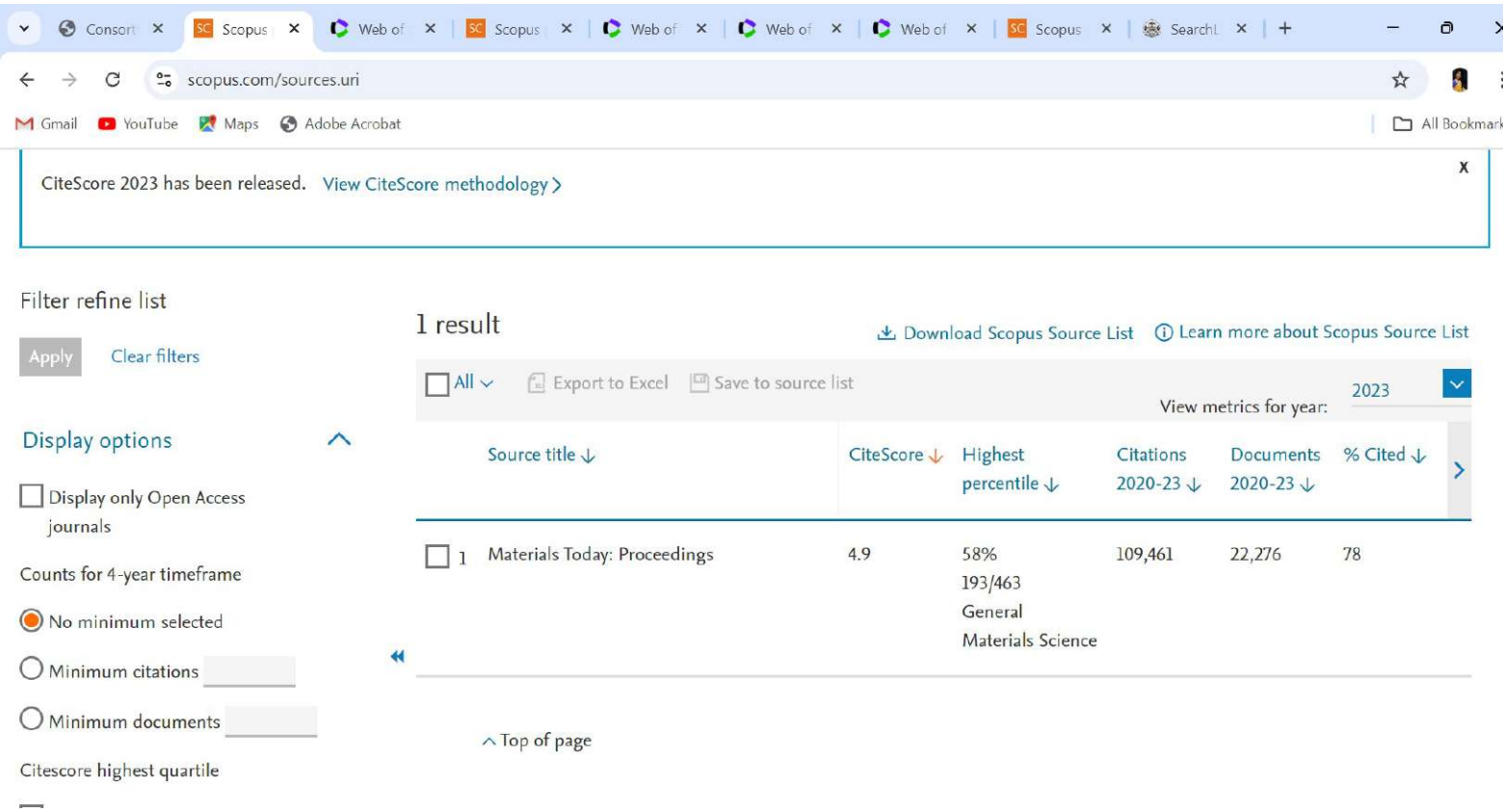
Guest editors ↗

For reviewers

Resources for reviewers ↗

Reviewer recognition ↗

All content on this site: Copyright © 2024 Elsevier B.V., its licensors, and contributors. All rights are reserved, including those for text and data mining, AI training, and similar technologies. For all open access content, the Creative Commons licensing terms apply.


scopus.com/sources.uri
Gmail
YouTube
Maps
Adobe Acrobat
All Bookmarks
CiteScore 2023 has been released. View CiteScore methodology >
Filter refine list
Apply
Clear filters
Display options
Display only Open Access journals
Counts for 4-year timeframe
No minimum selected
Minimum citations
Minimum documents
Citescore highest quartile
1 result
Download Scopus Source List
Learn more about Scopus Source List
All
Export to Excel
Save to source list
View metrics for year:
2023
Source title
CiteScore
Highest percentile
Citations 2020-23
Documents 2020-23
% Cited
1 Materials Today: Proceedings 4.9 58% 193/463 General Materials Science 109,461 22,276 78
Top of page